Methods of Cancer Diagnosis, Therapy, and Prognosis

Volume 2
General Methods and Overviews,
Lung Carcinoma and Prostate Carcinoma

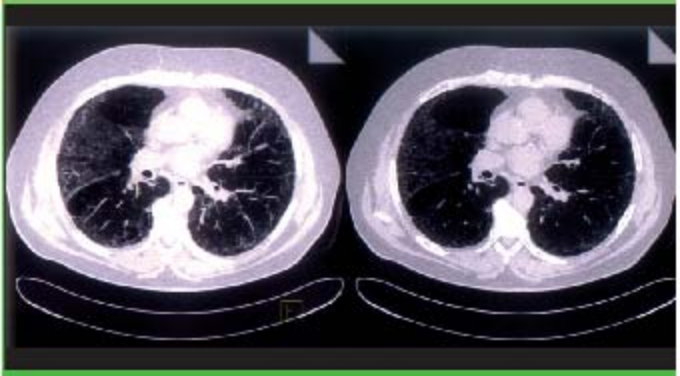

M.A. Hayat
Editor

Springer

General Methods and Overviews, Lung Carcinoma and Prostate Carcinoma

Methods of Cancer Diagnosis, Therapy, and Prognosis

Volume 2

For other titles published in this series, go to
www.springer.com/series/8172

Methods of Cancer Diagnosis, Therapy, and Prognosis

Volume 2

General Methods and Overviews, Lung Carcinoma and Prostate Carcinoma

Edited by

M.A. Hayat
Department of Biological Sciences,
Kean University, Union, NJ, USA

Springer

Editor
M.A. Hayat
Department of Biological Sciences
Kean University
Union, NJ
USA

ISBN 978-1-4020-8441-6 e-ISBN 978-1-4020-8442-3

Library of Congress Control Number: 2008930172

Printed on acid-free paper

9 8 7 6 5 4 3 2 1

springer.com

New technology, for better or for worse, will be used, as that is our nature.

Lewis Thomas

You have been given the key that opens the gates of heaven; the same key opens the gates of hell.

Writing at the entrance to a Buddhist temple

Authors and Co-Authors of Volume 2

Naglaa F. Abbas
Medical Division, National Research Center, Al-Tahrir Street, Dokki Giza, Egypt

Imran Ahmad
Saskatoon Cancer Center, University of Saskatchewan, 20 Campus Drive, University of Saskatchewan, Saskatoon, SK, Canada S7N 4H4
E-mail: sahmed@scf.sk.ca

Shahid Ahmed
Saskatoon Cancer Center, University of Saskatchewan, 20 Campus Drive, University of Saskatchewan, Saskatoon, SK, Canada S7N 4H4

Annette Altmann
Clinical Cooperation Unit Nuclear Medicine, German Cancer Research Center, Im Neuenheimer Feld 280, FRG-69120 Heidelberg, Germany
E-mail: a.altmann@dkfz-heidelberg.de

Samuel G. Armato III
Department of Radiology- MC 2026, The University of Chicago, 5841 S. Maryland Ave., Chicago, IL 60637
E-mail: s-armato@uchicago.edu

Florence Arnold
Saskatoon Cancer Center, University of Saskatchewan, 20 Campus Drive, University of Saskatchewan, Saskatoon, SK, Canada S7N 4H4

Armando Bartolazzi
Department of Oncology-Pathology, Cellular and Molecular Pathology, Cancer Center Karolinska, CCK R8:04 Karolinska Hospital, 17176 Stockholm, Sweden
E-mail: Armando.Bartolazzi@cck.ki.se

Susana Benlloch
Research Unit, Alicante University General Hospital, Avda Pintor Baeza 12, Alicante 03010, Spain
E-mail: benlloch_sus@gva.es

Heinrich Bulzebruck
IT-Abteilung der Thoraxklinik am Universitatsklinikum, Heidelburg, Amalienstrasse 5, D-69126 Heidelberg, Germany

Loren E. Clarke
Penn State Milton S. Hershey Medical Center-M.C. H179, P. O. Box 850, 500 University Drive, Hershey, PA 17033

Philip Clewer
Medical Physics and Bioengineering, Southampton General Hospital, Tremona Road Southampton, SO16 6YD, United Kingdom
E-mail: Philip.Clewer@suht.swest.nhs.uk

Gaetano Compagnone
Department of Medical Physics, S. Orsola-Malpighi Hospital, Azienda Ospedaliero-Universitaria di Bologna, Via Massarenti, 9 40138 Bologna, Italy
E-mail: gcompa@orsola-malpighi.med.unibo.it

Leslie C. Costello
Department of Biomedical Sciences, Dental School and the Greenbaum Cancer Center, University of Maryland, 650 West Baltimore, MD 21201
E-mail: lcostello@umaryland.edu

Juanita Crook
University of Toronto/Princess Margaret Hospital, 610 University Avenue, Toronto M5G 2M9
E-mail: Juantia.Crook@rmp.uhn.on.ca

Gabriel D. Dakubo
Genesis Genomics, Inc., 290 Munro Street, Ste. 1000, Thunder Bay, ON P7A 7T1, Canada
E-mail: Gabriel.dakubo@genesisgenomics.com

Marco Das
Hochschule Aachen University, Rheinisch-Westfalische Technische, Department of Diagnostic Radiology, Pauwelsstrasse 30, Aachen 52074, Germany
E-mail: das@rad.rwth-aachen.de

Henndrik Dienemann
Chirurgische Abteilung der Thoraxklinik am Universitatsklinikum, Heidelburg, Amalienstrasse 5, D-69126 Heidelberg, Germany

David Dingli
Harvard University, Program for Evolutionary Dynamics, One Brattle Sq. Suite 6, Cambridge, MA 02138
E-mail: dingli.david@mayo.edu

Vikram S. Dogra
University of Rochester, School of Medicine, Department of Imaging Sciences, 601 Elmwood Avenue, Box 648, Rochester, NY 14642
E-mail: vikram_dogra@urmc.rochester.edu

Nadia G. EL-Hefnawy
Pathology Department, Faculty of Medicine, Ain-Shams University, Cairo, Egypt

Sonia L. El-Sharkawy
Medical Division, National Research Center, Al-Tahrir Street, Dokki Giza, Egypt
E-mail: elsharkawy60@hotmail.com

Renty B. Franklin
Department of Biomedical Sciences, Dental School and the Greenbaum Cancer Center, University of Maryland, 650 West Baltimore, MD 21201

José Marcelo Galbis-Caravajal
Medical Oncology, Alicante University General Hospital, Avda Pintor Baeza 12, Alicante 03010, Spain

Christian Görg
Department of Internal Medicine, Philipps-University Marburg, Baldingerstraße, D-35033 Marburg, Germany
E-mail: Christian.Goerg@med.uni-marburg.de

Peter Grandics
A-D Research Foundation, 5922 Farnsworth Ct., Carlsbad, CA 92008
E-mail: pgrandics@earthlink.net

Cesare Gridelli
Division of Medical Oncology, S.G. Moscati Hospital, Contreds Amorette, 83100 Avellino, Italy
E-mail: cgridelli@libero.it

Olli H.J. Grohn
Department of Biochemistry, University of Cambridge, Old Addenbrookes Site, 80 Tennis Court Road, CB2 1GA Cambridge, United Kingdom

S.J. Gwyther
East Surrey Healthcare NHS Trust, Redhill, Canda Avenue, Surrey, United Kingdom
E-mail: GwytherSJ@aol.com

Uwe Haberkorn
Clinical Cooperation Unit Nuclear Medicine,German Cancer Research Center, Im Neuenheimer Feld 280, FRG-69120 Heidelberg, Germany

Kamal Haider
Saskatoon Cancer Center, University of Saskatchewan, 20 Campus Drive, University of Saskatchewan, Saskatoon, SK, Canada S7N 4H4

Kristie Harding
Saskatoon Cancer Center, University of Saskatchewan, 20 Campus Drive, University of Saskatchewan, Saskatoon, SK, Canada S7N 4H4

M.A. Hayat
Kean University, 1000 Morris Avenue, Union, NJ 07083
E-mail: ehayat@cougar.kean.edu

Rui Henrique
Department of Pathology, Portugese Oncology Institute – Porto, Rua Dr. Antonio, Bernardino de Almeida, 4200-072 Porto, Portugal

Kenzo Hiroshima
Kenzo Hiroshima, Department of Diagnostic Pathology, Graduate School of Medicine, Chiba University, 1-8-1 Inohana, Chuo-ku, Chiba 260-8670, Japan
E-mail: kenzo@faculty.chiba-u.jp

Angelique Holland
Department of Internal Medicine, Philipps-University Marburg, Baldingerstraße, D-35033 Marburg, Germany

John P. Jakupciak
National Institute of Standards and Technology, Biochemical Science Division, Gaithersburg, MD 20899

Samer Kalakish
Comprehensive Cancer Center, Wake Forest University, School of Medicine, Winston Salem, NC 27157
E-mail: kalakish@wfubmc.edu

Mikko I. Kettunen
Department of Biochemistry, University of Cambridge, Old Addenbrookes Site, 80 Tennis Court Road, CB2 1GA Cambridge, United Kingdom
E-mail: mik21@mole.bio.cam.ac.uk

Katsuyuki Kiura
Department of Respiratory Medicine, Okayama University Hospital, Graduate School of Medicine, Okayama 700-8558, Japan

Shan Lu
Department of Pathology, University of Cincinnati, College of Medicine, 231 Albert Sabin Way, Cincinnati, OH 45267
E-mail: shan.lu@uc.edu

Charles M. Ludgate
Radiation Oncology Program, BC Cancer Agency - Vancouver Island Centre, 2410 Lee Ave., Victoria, BC, Canada, V8R 6V5

Edmond S.K. Ma
Division of Molecular Pathology, Department of Pathology and Cancer Genetics Center, Hong Kong Sanatorium and Hospital, 2 Village Road, Happy Valley, Hong Kong
E-mail: eskma@hksh.com

Paolo Maione
Division of Medical Oncology, S.G. Moscati Hospital, Contreds Amorette, 83100 Avellino, Italy

Stephen Man
Department of Medical Biochemistry and Immunology, Health Park, Cardiff, CF14 4XN, School of Medicine, Cardiff University, U.K

Bartomeu Massutí
Thoracic Surgery, Hospital de La Ribera, Alzira, Valencia, Spain

Luca Moscetti
Medical Oncology Department, Centreal Hospital of Outcome, Research Network for Evaluation of Treatment, Results in Oncology, Belcolle-ASL di Viterbo, Strada Sammartinese snc, 01100 Viterbo, Italy
E-mail: f.nelli@asl.vt.it

Fabrizio Nelli
Medical Oncology Department, Centreal Hospital of Outcome, Research Network for Evaluation of Treatment, Results in Oncology, Belcolle-ASL di Viterbo, Strada Sammartinese snc, 01100 Viterbo, Italy

Brad H. Nelson
Trev and Joyce Deeley Research Centre, BC Cancer Agency – Vancouver Island Centre, 2410 Lee Ave., Victoria, BC, Canada, V8R 6V5
E-mail: bnelson@bccancer.bc.ca

Nancy J. Nesslinger
Trev and Joyce Deeley Research Centre, BC Cancer Agency – Vancouver Island Centre, 2410 Lee Ave., Victoria, BC, Canada, V8R 6V5

Hiroaki Nomori
Department of Thoracic Surgery, Graduate School of Medicine, Kumamoto University, 1-1-1 Honjo, Kumamoto 860-8556, Japan
E-mail: hnomori@qk9.so-net.ne.jp

Jorge M. Pacheco
Harvard University, Program for Evolutionary Dynamics, One Brattle Sq., Suite 6, Cambridge, MA 02138

Howard H. Pai
Radiation Oncology Program, BC Cancer Agency - Vancouver Island Centre, 2410 Lee Ave., Victoria, BC, Canada, V8R 6V5

Klaus Pantel
Institute of Tumor Biology, University Medical Center, Hamburg-Eppendorf, Martinistrasse 52, D-20246 Hamburg, Germany
E-mail: pantel@uke.uni-hamburg.de

Ryan L. Parr
Genesis Genomics, Inc., 290 Munro Street, Ste. 1000, Thunder Bay, ON P7A 7T1, Canada

Joachim Pfannschmidt
Chirurgische Abteilung der Thoraxklinik am Universitatsklinikum, Heidelburg, Amalienstrasse 5, D-69126 Heidelberg, Germany
E-mail: joachim.pfannschmidt @thoraxklinik-heidelberg.de

David Popkin
Saskatoon Cancer Center, University of Saskatchewan, 20 Campus Drive, University of Saskatchewan, Saskatoon, SK, Canada S7N 4H4

Garth Powis
Department of Experimental Therapeutics, University of Texas, M.D. Anderson Cancer Center, 1400 Holcombe Blvd., FC6. 3044, Unit 422, Houston, TX 77030
E-mail: gpowis@mdanderson.org

Franclim R. Ribeiro
Department of Genetics, Portuguese Oncology Institute - Porto, Portugal Rua Dr. Antonio Bernardino de Almeida, Porto, 4200-072, Portugal
E-mail: frsr@netcabo.pt

Amer Sami
Saskatoon Cancer Center, University of Saskatchewan, 20 Campus Drive, University of Saskatchewan, Saskatoon, SK, Canada S7N 4H4

Heidi Schwarzenbach
Institute of Tumor Biology, University Medical Center, Hamburg-Eppendorf, Martinistrasse 52, D-20246 Hamburg, Germany

Yoshihiko Segawa
Department of Medicine and Thoracic Oncology, National Hospital Organization, Shikoku Cancer Center, 160 Kou-Minami-Umemoto-cho, Matsuyama, Ehime 791-0288, Japan
E-mail: ysegawa@shikoku-cc.go.jp

William F. Sensakovic
Department of Radiology- MC 2026, The University of Chicago, 5841 S. Maryland Ave., Chicago, IL 60637

Rabia K. Shahid
Saskatoon Cancer Center, University of Saskatchewan, 20 Campus Drive, University of Saskatchewan, Saskatoon, SK, Canada S7N 4H4

Rolf I. Skotheim
Department of Cancer Prevention, Institute for Cancer Research, Rikshospitalet-Radiumhospitalet Medical Center, NO-0310 Oslo, Norway

Zsuzsanna Tabi
Department of Oncology and Palliative Medicine, Velindre Hospital, Whitchurch, CF14 2TL Cardiff, United Kingdom
E-mail: zsuzsanna.tabi@velindre-tr.wales.nhs.uk

Nagio Takigawa
Department of Respiratory Medicine, Okayama University Hospital, Graduate School of Medicine, Okayama 700-8558, Japan
E-mail: ntakigaw@md.okayama-u.ac.jp

Manuel R. Teixeira
Department of Genetics, Portuguese Oncology Institute - Porto, Portugal Rua Dr. Antonio Bernardino de Almeida, Porto, 4200-072, Portugal

Franck Toledo
Institut Curie, Centre de Recherche, UMR CNRS 7147, 26 rue d'Ulm 75248, Cedex 05 Paris, France
E-mail: franck.toledo@curie.fr

Frank M. Torti
Comprehensive Cancer Center, Wake Forest University, School of Medicine, Winston-Salem, NC 27157

Ahmet T. Turgut
Department of Radiology, Ankara Training and Research Hospital, 25. Cadde 362. Sokak Hüner Sitesi No: 18/30 Karakusunlar, Ankara, TR-06530 Turkey

Sarah J. Welsh
University of Oxford, Harris Manchester College, Manchester Road, Oxford, OX1 3 TD, UK

Chris L.P. Wong
Division of Molecular Pathology, Department of Pathology and Cancer Genetics Center, Hong Kong Sanatorium and Hospital, 2 Village Road, Happy Valley, Hong Kong

Sunil Yadav
Saskatoon Cancer Center, University of Saskatchewan, 20 Campus Drive, University of Saskatchewan, Saskatoon, SK, Canada, S7N 4H4

Dani S. Zander
Penn State Milton S. Hershey Medical Center-M.C. H179, P. O. Box 850, 500 University Drive, Hershey, PA 17033
E-mail: dzander@hmc.psu.edu

Pat Zanzonico
Room Z 2002 (Zuckerman Research Center), Memorial Sloan-Kettering Cancer Center, 1275 York Avenue, New York, NY 10021
E-mail: zanzonip@mskcc.org

Preface

Cancer is the leading cause of death, after cardiovascular diseases, in the United States. A total of ~ 1,399,790 new cancer cases and ~ 564,830 deaths were reported in the year 2006 in the country. Approximately, one in every two men and one in every three women in the country will have some type of cancer during their lifetime. Healthcare costs exceed 1.7 trillion dollars per year in the United States, which is ~ 15% of the country's gross domestic product.

Tobacco use is the most serious preventable cause of cancer. Tobacco use causes cancer of the lung, throat, mouth, pancreas, urinary bladder, stomach, liver, kidney, and other types. Passive smoking causes lung cancer. In 2007, ~ 168,000 cancer deaths were expected to be caused by tobacco use (Am. Cancer Society, 2007).

The most important risk factor for the development of cancer is increasing age. This factor and epidemiologic shifts have resulted in a marked increase in the number of older patients with cancer. This fact will result in marked increased burden of cancer to the world, including the United States. The fastest-growing segment of the United States population comprises persons of 65 years and older, and an increase in the number of older cancer patients is expected. Approximately, 77% of all types of cancers are diagnosed in persons of 55 years and older. It was estimated that one-third of the 559,650 cancer deaths in 2007 in the United States were related to overweight or obesity, physical inactivity, and nutrition, and thus could also be prevented (Am. Cancer Society, 2007). However, in developed countries, including United States, the average person of 65 years can expect to live another 15 years in a fairly good health. Persons of 75 or 85 years old have an average expectancy of 10 and 6 years, respectively.

During the last three decades, intensive clinical research has resulted in reduced cancer incidence, side effects of treatments, and death rates and increased survival rates. As a result, there are ~ ten million cancer survivors in the United States; some of them are cancer-free, while others may still have cancer and may be undergoing treatment.

It is recognized that scientific journals facilitate exchange of information, resulting in rapid progress. In this endeavor, the main role of scientific books is to present information in more detail after careful, additional evaluation of the investigational

results, especially those of new or relatively new methods, and their potential side-effects.

Although subjects of diagnosis, therapy assessment, and prognosis of various types of cancers, cancer recurrence, and resistance to chemotherapy are scattered in a vast number of journals and books, there is need of combining these subjects in single volumes. An attempt has been made to accomplish this goal in these volumes. A constructive evaluation of commonly used methods for elucidating primary and secondary cancer initiation, progression, relapse, and metastasis is presented.

In the era of cost-effectiveness, my opinion may be a minority prospective, but it needs to be recognized that the potential for false-positive or false-negative interpretation on the basis of a single laboratory test in clinical pathology does exist. Interobservor or intraobservor variability in the interpretation of results in pathology is not uncommon. Interpretive differences often are related to the relative importance of criteria being used.

Generally, no test always performs perfectly. Although there is no perfect remedy to this problem, standardized classifications with written definitions and guidelines will help. Standardization of methods to achieve objectivity is imperative in this effort. The validity of a test should be based on the objective interpretation of the photomicrographs or tomographic images. The interpretation of the results should be explicit rather than implicit. To achieve accurate diagnosis, and correct prognosis, the use of molecular criteria is important. Indeed, molecular medicine has arrived.

This volume discusses in detail all aspects of lung cancer and prostate cancer, including diagnosis using molecular genetics, various imaging modalities, and tumor markers. Treatments such as chemotherapy, radiation, chemoradiation, hormonal therapy, immunotherapy, and surgery; and prognosis. The side effects of the treatments are also pointed out. Both primary and secondary cancers, and risk of cancer survivors developing other cancers are explained. An attempt is also made to translate molecular genetics into clinical practice. Evidence-based therapy is included.

Role of metabolism in malignancy and cancer stem cells are discussed in detail. Methods of cancer diagnosis discussed include various modalities of imaging (e.g., MRI, PET, Whole-Body PET, Multidetector-Row Computed Tomography, Transcutaneous Contrast-Enhanced Sonography, and Transrectal Sonography), and Histology and Immunohistochemistry. Other methodologies, such as Array-Based Comparative Genomic Hybridization and Polymerase Chain Reaction Analysis, are also included.

Prognostic biological markers such as mitochondrial mutations and circulating DNA in blood for prostate cancer are described. Treatment of NSCLC with docetaxel, platinum-based chemotherapy, and gefitinib is discussed. Chemotherapy with vinorelbine, doxorubicin, and prednisone, and radiotherapy for prostate cancer are discussed. Overexposure of patients to radiology is included.

Each chapter is written by distinguished, practicing clinicians/surgeons/oncologists. Their practical experience highlights their writings, which should build and further the endeavors of the readers. This volume was written by 75 scientists representing 14 countries. It is my hope that these handbooks would assist in more complete

understanding of at least some of the globally-encountered cancer problems. Successful cancer treatment, cure, and prevention are areas of immediate concern of and demand by the public.

I am grateful to the contributors for their promptness in accepting my suggestions, and appreciate their dedication and hard work in sharing their invaluable knowledge with the readers. Each chapter provides unique individual, practical knowledge based on the expertise and practical experience of the authors. The chapters contain the most up-to-date practical as well as theoretical information. It is my hope that the book will be published expeditiously.

I am thankful to the Board of Trustees, Dr. Dawood Farahi, and Dr. Kristie Reilly for recognizing the importance of scholarship in an institution of higher education and providing the resources for completing this important project. I am thankful to Ayesha Muzaffar and Lina Builes for their expert help in preparing this volume.

M.A. Hayat
February 2008

Contents

Contents of Volume 1

1
Metabolic Transformations of Malignant Cells: An Overview

Leslie C. Costello and Renty B. Franklin

INTRODUCTION

It is generally considered that the hallmark studies of Otto Warburg and colleagues reported in 1926 (Warburg *et al*., 1926) sparked the era of tumor cell metabolism. From that time until around 1980, and especially from 1940–1970, studies of intermediary metabolism of normal and malignant cells were dominant areas of research and graduate and post-graduate training in biomedical sciences. Pursuant to ~ 1980, the advent, development, and subsequent dominance of molecular genetics, proteomics, and molecular technology in clinical and experimental biomedical application was accompanied by the nearly complete submersion of interest and training in areas of intermediary metabolism and tumor cell metabolism. (The contemporary consequences of this transition are discussed in a following section.) Now a resurging interest in intermediary metabolism along with the development of metabolomics in relation to cancer and other diseases has emerged. This provides a timely reason to revisit some of the important issues of tumor cell metabolism with a perspective of the contemporary associations of genomics/proteomics/metabolomics, coupled with molecular technology; none of which existed during the days of the outstanding biochemists and mitochondriacs of earlier times.

The following overview will present some important considerations that relate to the intermediary energy metabolic requirements of tumor cells. However, one must also recognize that differing metabolic pathways exist for different malignant cells *in situ*; therefore, generalizations of metabolic transformations are not likely to be uniformly applicable to all malignant cells. Also, as authors, we take license to present some concepts of malignancy that might be challenged by others. Nevertheless, this presentation will serve as "food for thought" that might stimulate interest and further studies in the exciting field of metabolism of malignancy.

AXIOMS OF RELATIONSHIPS OF CELLULAR ACTIVITY, CELLULAR METABOLISM, AND MALIGNANCY

The following are important generalizations that we consider to be axiomatic and applicable to all cells.

1. The existing cellular intermediary metabolism of a cell provides the bioenergetic/synthetic/catabolic requirements that are essential for the manifestation of the cell's current activities (function, growth, and proliferation).
2. When the activity of a cell changes, its metabolism must also be adjusted consistent with any newly established bioenergetic/synthetic/catabolic requirements.
3. Malignant cells exhibit a parasitic existence. They have no specialized function other than the activities essential for their generational propagation (growth and proliferation), which occur at the expense of their host.
4. Malignant cells are derived from normal cells that have undergone a genetic transformation to a neoplastic cell phenotype that is endowed with malignant potential.
5. Manifestation of the malignant potential of the neoplastic cell necessitates alterations in its metabolism (i.e., a metabolic transformation) to provide the bioenergetic/synthetic requirements of malignancy.
6. In the absence of the metabolic transformation, the neoplastic cell will not progress to complete malignancy. Conversely, the metabolic transformation, in the absence of the genetic transformation to a neoplastic malignant cell, will not cause malignancy.
7. Common to all malignant cells is the metabolic requirement for *de novo* lipogenesis/cholesterogenesis for membraneogenesis that is essential for their proliferative existence.

These axioms define a relationship (represented in Figure 1.1) that we propose is applicable to all malignancies.

DEFINING A MALIGNANT CELL: A PARASITIC EXISTENCE

An understanding of the "purpose" of the existence of a cell at any point in time in its life provides information of the requirement

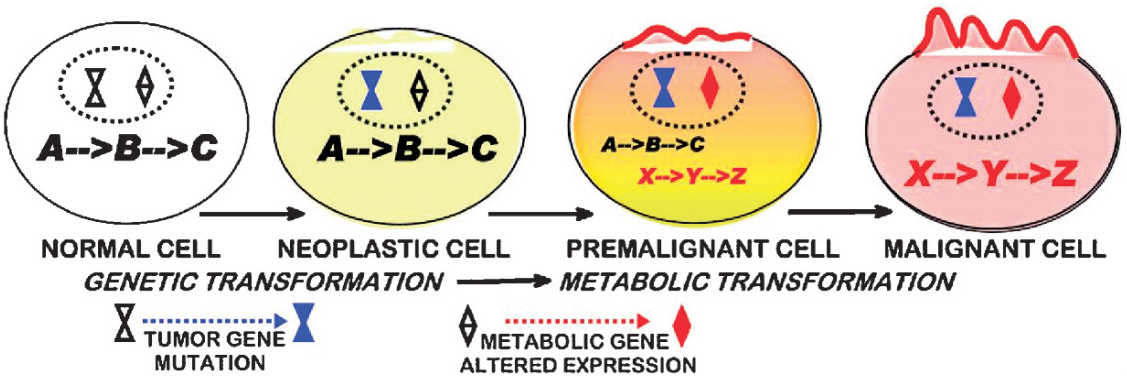

FIGURE 1.1. The role of altered intermediary metabolism in the process of the development of malignancy. Malignancy begins with the genetic transformation of a normal cell to a neoplastic malignant phenotype. The neoplastic cell undergoes genetic expression changes involved in the metabolic transformation from the normal cell metabolism of A→B→C to the malignant cell metabolism of X→Y→Z to fulfill the energetic and synthetic metabolic requirements of malignancy. The neoplastic cell can then fulfill its malignant potential

for and role of its intermediary metabolism. Malignant cells are "parasitic" cells. They exist for one purpose, that is, to grow and to proliferate to ensure their generational propagation. They do so at the expense and destruction of the host. These are the criteria that define a parasitic life-style. Except for the relevance to clinical identification, it is an error (in our view) to consider or to describe tumor cells as "dedifferentiated" or "undifferentiated" cells. To do so places tumor cells in the same category as normal undifferentiated cells (e.g., stem cells, basal cells, mesenchyme cells and others that we will refer to collectively as "stem" cells). Stem cells, like tumor cells, also exist to grow and proliferate, but they do so for the purpose of differentiating into specialized cells that perform specific functions. Stem cells proliferate to maintain a continual population of cells for further differentiation. However, unlike the parasitic tumor cells, these cells grow/proliferate in harmony with the host tissue, i.e., they exhibit a symbiotic life-style. In this sense these are "sane" cells, while tumor cells are "insane" cells. The malignant cells exhibit two essential activities for their progression and propagation: (1) growth and proliferation; (2) invasion and motility. The latter are life-cycle activities in support of the former. The intermediary metabolism of the malignant cells must provide the bioenergetic and synthetic requirements for these activities.

THE *IN SITU* ENVIRONMENT OF THE MALIGNANT CELL DICTATES ITS METABOLISM

Especially for solid tumors, the malignant cells are subjected to a changing environment as they grow and progress. Most notable is the influence of the availability of oxygen and micronutrients derived from circulation. The former is of paramount importance in relation to the intermediary metabolism of the malignant cell. The initiation of the malignant cell activity is followed by growth and proliferation that results in an increasing mass of malignant cells. This subjects the population of malignant cells to different gradients of oxygen ranging from normoxia through hypoxia toward anoxia. One can visualize a solid ball of cells in which the outside layer of cells is in apposition to the air, and each inner layer of cells progressively is more distant from the air. Thus, the intermediary metabolism of the malignant cells comprising the tumor mass cannot be expected to be uniform at any one time, and the intermediary metabolism of the malignant cells can be expected to change as the availability of oxygen changes. As the environment becomes more hypoxic leading to anoxia, the continued malignant proliferation and other activities will become compromised and ultimately arrested. This is due to the inability of the major population of malignant cells to derive their metabolic bioenergetic and biosynthetic requirements. The lack of available oxygen and nutrients, such as glucose, from circulation prevents the malignancy from progressing. This is best illustrated by the requirements for lipogenesis/cholesterogenesis and even the accelerated glycolysis, neither of which can be sustained under such conditions. One must not forget that the "waste products" of the metabolism of the malignant cells also need to be eliminated, which also requires the availability of circulation. In other words, a refurbished perfusate is an essential environmental condition for tumor progression. Indeed, the successful

evolution of malignant cells has resulted from adaptive capabilities to confront and to overcome this adversity. For example, they upregulate hypoxia inducible factor and stimulate angiogenesis to create the circulation and environment that allows their further progression.

Therefore, the cycle of malignancy involves periods of growth and proliferation and periods of arrest to "refuel" the environment; all of which accommodate the metabolic requirements of the malignant cells. To optimize their parasitic existence, some malignant cells will vacate the primary site of their development and seek other host tissue sites to invade and continue their parasitic existence. Thus, the capability and stages of metastasis are invoked. The vascularization and distant tissue site invasion provide different environmental conditions that likely affect the metabolism of the metastatic cells. Very little is known concerning the *in situ* metabolic relationships of these cells. The understanding of all of these relationships (and other relationships not described herein) dictate that any studies of tumor cell metabolism must be extrapolated and related to the realities of the *in situ* environment of the malignant cells.

TUMOR CELL PROLIFERATION AND INVOLVED METABOLIC PATHWAYS FOR ITS ACHIEVEMENT

The propagation of a cell-type requires its ability for cell proliferation. This is the dominant activity of parasitic cells. To achieve this, the intermediary metabolism of the malignant cell is dominated by the bioenergetic and biosynthetic requirements of cell proliferation. For this reason, we will focus our discussion on such requirements, with recognition that many other areas of intermediary metabolism are critical to the development and propagation of tumor cells. A hallmark metabolic activity of proliferating cells is the pathway to *de novo* lipogenesis/cholesterogenesis that is essential for the membraneogenesis requirement of cell growth and proliferation. (While we focus on this, one must also be cognizant that protein and polysaccharide synthesis are also involved.) Therefore, a major metabolic transformation in malignancy is the "switch" from the functional metabolism of their parental normal cell to the *de novo* lipogenesis/cholesterogenesis requirement of the tumor cell.

The purpose of this overview presentation is not to detail the pathway(s) to *de novo* lipogenesis/cholesterogenesis, but to highlight some relationships for consideration. *De novo* lipogenesis/cholesterogenesis begins with the availability of cytosolic acetyl CoA (acetyl coenzyme A), the common carbon skeleton for fatty acid synthesis (lipogenesis) and lanesterol synthesis (cholesterogenesis). Therefore, tumor cells must direct their attention to providing a source and pathway for cytosolic acetyl CoA synthesis. In mammalian cells, the major source of cytosolic acetyl CoA is derived from the mitochondrial production of citrate (Figure 1.2), which is exported into the cytosol *via* a mitochondrial citrate transporter protein (CTP). Normally, in most mammalian cells CTP expression is low, so that citrate is retained predominantly within the mitochondria mainly to be oxidized *via* the Krebs cycle for energy production and also to provide intermediates for associated metabolic pathways.

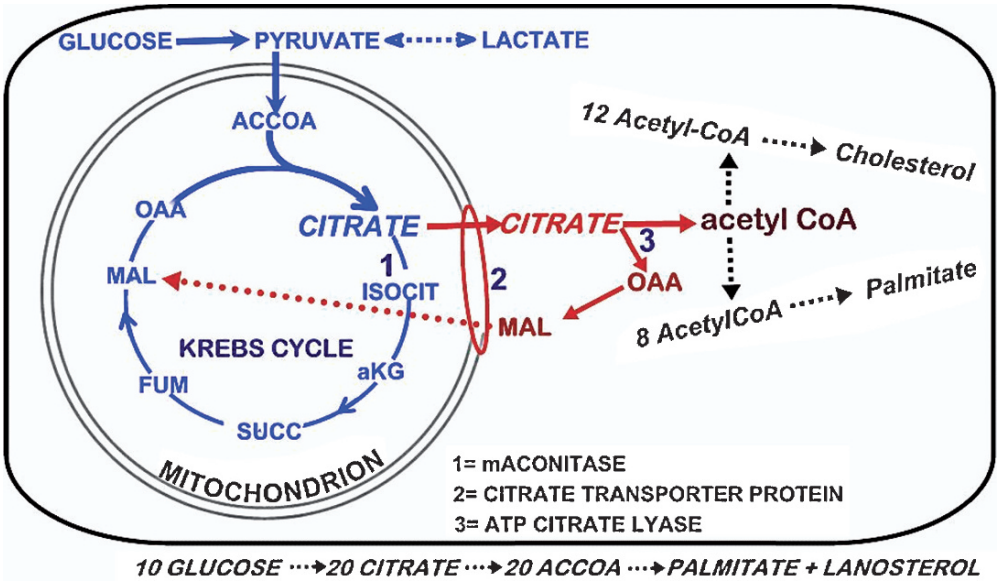

FIGURE 1.2. The glucose-citrate pathway to de novo lipogenesis/cholesterogenesis in malignant cells. Glucose is utilized for the mitochondrial synthesis and production of citrate. Citrate transporter protein is up-regulated, which permits the export of some citrate to the cytosol while some citrate is oxidized via the Krebs cycle. The cytosolic citrate is converted to acetyl CoA for lipogenesis/cholesterogenesis

Tumor cells exhibit an upregulation of CTP which permits an increased export of citrate to cytosol where it is converted by ATP citrate lyase to acetyl CoA + oxalacetate. Therefore, in the absence of alternative sources of cytosolic acetyl CoA, proliferating tumor cells must direct their metabolism to optimize the mitochondrial production of citrate.

THE COUPLING OF GLYCOLYSIS VIA CITRATE TO *DE NOVO* LIPOGENESIS/ CHOLESTEROGENESIS

Glycolysis is coupled with *de novo* lipogenesis/cholesterogenesis because glucose generally provides the carbon source for acetyl CoA production in most tumor cells and other lipogenic/cholesterogenic cells. As shown in Figure 1.2, it takes a prolific amount of glucose conversion to fulfill the lipogenic/cholesterogenic requirements of growing/proliferating tumor cells. This brings us to the consideration of the "hallmark" characterization of tumor cell metabolism as being a transformation to "high aerobic glycolysis"; a characterization that has dominated the studies of tumor cell metabolism both directly and indirectly. In its strictly defined metabolic end-point, which is lactic acid, a high aerobic glycolysis would be inconsistent with the requirements for proliferating tumor cells, unless an alternative pathway to mitochondrial citrate synthesis exists (described below). In the absence of alternative sources, the 'high aerobic glycolysis" could provide energy for sustaining the cells in a non-proliferating condition, which is

an energy-inefficient process that produces only 2 mols ATP/mol glucose under anaerobic (anoxic) conditions; or possibly 8 mols ATP/mol glucose under aerobic conditions if NADH is shuttled to mitochondria for re-oxidation to NAD. This is contrasted with the generation of 38 mols ATP/mol glucose that is completely oxidized. This inefficiency is somewhat compensated by the rapidity of glycolysis and by the large host plasma pool of glucose that is available to the parasitic tumor cells.. On the other hand, an "accelerated aerobic glycolysis" is likely to exist for the increased production of lactate → pyruvate → citrate as the end-point in the following pathway:

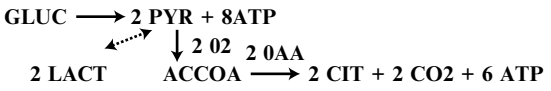

This pathway requires oxygen and results in the production of citrate along with 14 ATP molecules/glucose.

Then, the increased availability of a mitochondrial pool of citrate will provide for an increased export of citrate for cytosolic acetyl CoA production along with the continued oxidation of citrate via the Krebs cycle for energy production (Figure 1.2). Consequently, those tumor cells *in situ* that are exposed to physiological anoxia (i.e., insufficient oxygen availability to sustain aerobic oxidative metabolism) cannot proliferate and are in an arrested/dormant state. Neither anoxic glycolysis that produces only lactic acid nor normoxic glycolysis that completely oxidizes glucose, regardless of the bioenergetic consequences of each, is compatible with the *de novo* lipogenic/cholesterogenic requirements of tumor cells, unless an alternative pathway exists (presented below).

To establish the operation of this pathway of glucose utilization in cells, one must conduct a stoichiometric analysis of the utilization of glucose and its major products. Typically, in anaerobic glycolysis essentially all of the glucose utilized will be balanced by the production of lactate + pyruvate (assuming minimal accumulation of other glycolytic intermediates). However, the utilization of glucose under aerobic conditions will likely result in the oxidation of pyruvate which can lead to citrate production. In this case, the level of lactate + pyruvate will be significantly less than the glucose utilized. One must then incorporate the analysis of CO_2 production and citrate levels. Since some portion of the latter will be swept into the lipogenic/cholesterogenic pathway, the incorporation of citrate into this pathway must be considered. In a practical sense, one can use fluoroacetate to inhibit m-aconitase activity and citrate oxidation. Then the sum of lactate, pyruvate, CO_2, and citrate should approximate the glucose utilized. If it does not, then the incorporation of citrate into lipogenesis/cholesterogenesis must be pursued. The use of ATP citrate lyase inhibitor such as hydroxycitrate can also be incorporated, in which case most of the citrate that is produced will be accumulated. One must be cautious in using inhibitors to ensure that appropriate and effective concentrations are employed. These are representative of some of the types of metabolic studies that must be employed. The important point to be recognized is that simply accounting for "most" (whatever that means) of the glucose utilized as residing in the accumulation of lactate does not negate the role of glucose as the precursor for citrate production leading to lipogenesis/cholesterogenesis.

THE OPERATION OF THE KREBS CYCLE IN TUMOR CELLS

The preceding discussion raises the important issue regarding the operation of the Krebs cycle in tumor cells. Most studies indicate that the enzymes and reactions of the Krebs cycle remain operational in tumor cells. An important issue is the concept of a "truncated Krebs cycle" in tumor cells (Parlo and Coleman, 1986), which suggests that an increased rapid export of citrate, due to the upregulation of CTP (Parlo and Coleman, 1984), depletes citrate availability for oxidation by the Krebs cycle. A contemporary understanding of the m-aconitase reaction makes this concept untenable. It is well established that the Krebs cycle downstream reactions from isocitrate to oxalacetate are operational in tumor cells (Costello and Franklin, 2005). However, the critical reaction is m-aconitase, about which little is known in tumor cells. Studies of hepatoma cells indicate the existence of a complete Krebs cycle including citrate oxidation (Kelleher *et al*., 1987; Dietzen and Davis, 1993); while another study (Hernanz and de la Fuente, 1988) reports that the Krebs cycle is truncated. In malignant prostate cells, m-aconitase activity and a functional Krebs cycle exist (Costello and Franklin, 2001, 2006; Costello *et al*., 2005; Singh *et al*., 2006). The important consideration is that under conditions of the presence of uninhibited m-aconitase and downstream oxidation, it is not possible for the rate of citrate export to deplete the citrate pool so that no citrate oxidation would occur. The kinetic relationships of citrate export versus m-aconitase activity dictate that, in the presence of a sufficient intramitochondial pool of citrate that would support high citrate export, m-aconitase activity and citrate oxidation will prevail. Therefore, m-aconitase activity must be decreased and become rate-limiting in the tumor cells if citrate oxidation is truncated while high citrate export occurs. In our view, it is plausible to expect that the upregulation of CTP in tumor cells will provide for export of citrate concurrently with citrate oxidation as long as the source of citrate production for increased citrate utilization exists (Figure 1.2).

GLUTAMINOLYSIS AS AN ALTERNATIVE OR ADDITIONAL PATHWAY IN TUMOR CELLS

Although a high rate of glycolysis has been presented as a prominent pathway in issues of altered intermediary metabolism in tumor cells, increased glutaminolysis is also associated with tumor cell metabolism. Mazurek et al. (1999) concluded, "… that a special metabolic feature (increased glycolysis and glutaminolysis) is a general characteristic of tumor cells…" Moreadith and Lehninger (1984) observed, "In fact, many malignant cell lines, as well as some normal cells, do not have an absolute requirement for glucose per se…" They further stated, "The two major products of the [glutamate oxidation] pathway described here, citrate and alanine, have important roles in tumor metabolism. Citrate is required as the major source of cytosolic acetyl-coA for fatty acid and cholesterol biosynthesis." McKeehan (1982) proposed the utilization of glutaminolysis as a source

of pyruvate in tumor cells. The following is a modified representation of the pathway of glutaminolysis through citrate to lipogenesis in the absence of glucose utilization or in tumor cells that exhibit a high aerobic glycolysis:

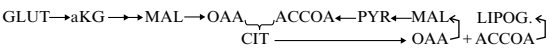

These descriptions are presented as illustrations of the energetic/synthetic metabolic alterations and requirements that are implicated in the development and progression of malignant cells. While we emphasize the generalized requirement of *de novo* lipogenesis/cholesterogenesis and the bioenergetic requirement of all tumor cells for their proliferation; no "universal" metabolic pathway for all tumor cells to achieve this end exists. The metabolism of each "species" of tumor cell in relation to its true environment must be established. A "one-size fits all" pathway is not applicable to tumor cell metabolism.

THE APPLICATION OF MOLECULAR GENETICS AND PROTEOMICS TO TUMOR CELL INTERMEDIARY METABOLISM

In view of the current issues that arise from the contemporary application of molecular technology/genomics/proteomics to studies of intermediary metabolism, we must add the 8th axiom to the preceding list of seven axioms: Genetic transformations and proteomic alterations will have little relevancy to tumor metabolism and other disease processes if the genetic/proteomic alterations are not manifested in altered and impaired cellular and metabolic function. We mentioned in the Introduction that, pursuant to ~ 1980, molecular genetics, proteomics, and molecular technology have become contemporary focal and dominant areas of biomedical research, training, and teaching. These technologies now provide potential new approaches to the study of the cellular intermediary metabolism of tumor cells, which will provide new insights and revelations concerning the metabolic relationships and transformations in malignancy. These developments provide for an exciting and revealing era of rejuvenated interest in intermediary metabolism to address the critical issues, "What are the essential adaptive metabolic requirements of malignant cells, and how is the altered metabolism achieved?" However, this molecular biology/molecular technology dominance and emphasis (perhaps over-emphasis) has created problems and issues that did not exist in the past. Simultaneously, the training of young investigators with a focus and expertise in biochemistry, intermediary metabolism, enzymology, and enzyme kinetics during the past 25 years has been widely diminished or eliminated from the didactic, methodology, and seminar components of pre- and post-doctoral training programs.

In prior times, the study of cellular intermediary metabolism was conducted by those who were trained in the principles and methodology of biochemistry, enzymology, cellular physiology, metabolic pathways, and related areas. As the molecular biology era evolved, this generation became trained in the developing areas of molecular genetics, proteomics, and molecular technology. With this

capability, these researchers identified the pathways of metabolism and the activities of the enzymes involved through the application of substrate analysis and enzyme kinetic studies. To state that this was difficult, tedious, and time-consuming work is a gross understatement. For this group of investigators, the developing molecular approaches were added to their fundamental strength in biochemistry and metabolism. The view of this generation is that the cellular enzyme activities and operation of pathways are the critical events that need to be established. The role of gene expression and enzyme protein biosynthesis are viewed as critical tools to understanding the factors that are associated with alterations of cellular metabolism. They fully understand that molecular genetics and proteomics cannot identify the operation of cellular pathways of metabolism and/or specific enzyme activities, and can only be established by the traditional methods of substrate analysis and enzyme kinetics. This group of researchers is a generation that is reaching extinction.

This group is being replaced by the younger generation of researchers who have been trained in the events of molecular genetics and proteomics that are associated with the expression and biosynthesis of proteins, including enzymes. The principles of molecular genetics and proteomics are then applied similarly and generally to proteins, among which enzymes of intermediary metabolism are included. These molecular events are then extrapolated to cellular metabolic events. The weakness of this group is the absence of training in and understanding of the principles of biochemistry and enzymology, the factors that affect cellular enzyme activity, and the relationships of sequential enzyme activities in metabolic pathways. This is the evolving dominant group in contemporary biomedical research associated with intermediary metabolism.

One must recognize that intermediary metabolism reactions and pathways are governed by regulatory enzymes. The rate of an enzymatic reaction is the product of the level and the specific activity of the enzyme. The level of the enzyme is established by its gene expression and its subsequent biosynthesis to its active form. The specific activity of the enzyme is dependent upon the enzyme kinetic properties, cellular environmental conditions of the reaction (such as pH, ionic conditions, product inhibition, and substrate concentration), enzyme activation-deactivation reactions and other conditions. One cannot presume that altered expression and biosynthesis of an enzyme is manifested by a corresponding change in the reaction rate within the cell. Conversely, one cannot presume that the absence of a change in the expression and level of an enzyme provides evidence that the specific enzyme activity alteration is not associated with a cellular metabolic change. This is exemplified by our identification that m-aconitase expression and level are unchanged in malignant vs nonmalignant glandular epithelial cells (Costello and Franklin, 2006; Costello *et al*., 2005; Singh *et al*., 2006). However, the enzyme activity is markedly inhibited by zinc in normal prostate epithelial cells, which results in inhibition of citrate oxidation and truncation of the Krebs cycle. In contrast, the malignant cells do not accumulate zinc so that m-aconitase activity is not inhibited, and these cells oxidize citrate *via* a functional Krebs cycle. This is a major and critical metabolic transformation that is essential for the development

and progression of prostate malignancy. Genetic and proteomic studies in the absence of metabolism studies would have lead to an erroneous conclusion regarding a major factor for this important metabolic transformation. The employment of gene and protein microarrays would dismiss m-aconitase as an essential factor in prostate malignancy!

The contemporary literature contains numerous instances in which gene expression studies (e.g., RT-PCR) and protein abundance studies (e.g., Western blot analysis) have lead to conclusions that the changes in the expression and level of specific enzymes are evidence of corresponding changes in the cellular enzyme activity and associated pathway. Conversely, the absence of changes in expression has lead to conclusions that the enzyme-associated activity and pathway are not involved in altered metabolism in a tumor cell or a disease process. Notably absent from such reports are the essential cellular metabolic studies that are required to determine the relationship of genetic/proteomic observations to the cellular metabolic events. Such circumstances reveal the absence of an essential understanding of fundamental cellular metabolic relationships. The only circumstance in which a genetic/proteomic alteration can be directly related to a corresponding cellular enzyme effect is the complete down regulation of the gene with the absence of the enzyme, so that cellular enzyme activity cannot exist.

In any series of reactions that comprises a metabolic pathway, the activity rate of the pathway is governed by the slowest reaction within the pathway (the 'master reaction'). The following exemplifies a sequence of enzymes comprising a metabolic pathway leading to the following product:

Enzyme activities 1,2,4 are in excess, and enzyme 3 is rate limiting. The product of the pathway 'E' is low despite the fact that enzyme 4 is in excess. Reaction 4 is low because the substrate D concentration is lower than the Km for the reaction 4 enzyme. Therefore, the up regulation of enzyme 4 gene expression will have little, if any, effect on increasing the pathway for conversion of substrate 'A' to product 'E'. Moreover, the accumulation of intermediate C could induce a product inhibition of reaction 2, which would then decrease product C, even if enzyme 2 is in excess. In such an example, the identification of altered expression of metabolic genes and of changes in the level of the corresponding enzymes does not establish changes in the cellular activity of the enzyme or the associated metabolic pathway. Conversely, the identification of altered enzyme activity of metabolic pathways does not identify the factors and cause of the altered metabolism. This is when the genetic/proteomic approach becomes a critical tool for understanding mechanisms of regulation of cellular metabolism.

One must also recognize an important distinction between regulatory enzymes of intermediary metabolism and other enzymes/proteins. We classify genes that are involved in the expression of enzymes of intermediary metabolism as "metabolic" genes to differentiate from the genes that are involved in the expression of other proteins such as structural/skeletal proteins and secretory/digestive enzymes. The latter group can be classified as "abundant" proteins that require increased expression level over a many-fold range. Enzymes of intermediary metabolism are not abundant proteins and exist in micro-abundant levels. In many instances the alterations in the level of regulatory enzymes of

intermediary metabolism in the range of 1–2 fold will exhibit significant changes in the cellular enzyme activity. In fact, it makes no sense for such regulatory enzymes to be increased several-fold above the level required for its cellular maximal activity.

Consequently, the statistical requirements of microarray analysis or gene expression changes will tend to eliminate small, but metabolically important, changes in the expression of "metabolic" genes. The statistical parameters applied to microarrays and to RT-PCR for identification of significant changes in the expression of a gene are of serious consequence for "metabolic genes." The statistical stringency that is applied to the analysis of typical microarray data is somewhat arbitrary and designed to separate signal from noise. In order to reduce the rate at which significant differences in expression are falsely identified, the threshold for designating differences as being significant is often set higher (e.g., 2-fold or greater) than might be expected for significant functional differences in metabolic enzyme activity. Thus, the potential for "false-negative" results is more probable for metabolic genes than for other genes.

If we apply the aforementioned conditions and principles to the relationship between gene expression and intermediary metabolism, two distinct approaches can be identified, i.e., the geneticist approach and the biochemist approach (Figure 1.3).

1. *The "Geneticist" Approach:* This approach (Figure 1.3) focuses initially on the identification of changes in gene expression by microarray analysis (step A) and/or specific gene expression analysis (step B). If a "significant" difference in a gene expression is revealed, studies proceed to the proteomic identification of corresponding changes in the relative level of the enzyme protein (step C). Very often demonstrable alterations in the gene expression and the relative protein level become presumptive evidence of a corresponding change in the cellular enzyme activity and associated pathway of metabolism. This presumption leads to the geneticist approach ending at step C, and eliminates the most critical step D. If step D were to reveal an alteration in the cellular specific enzyme activity and/or the associated pathway due to the cellular kinetic conditions, the geneticist approach in the absence of step D would have elicited a "false-positive" interpretation. Conversely, if steps A and/or B and/or C reveal no significant change in the expression of a gene, the presumption is made that its associated enzyme and/or metabolic pathway is not involved in a metabolic transformation, and step D

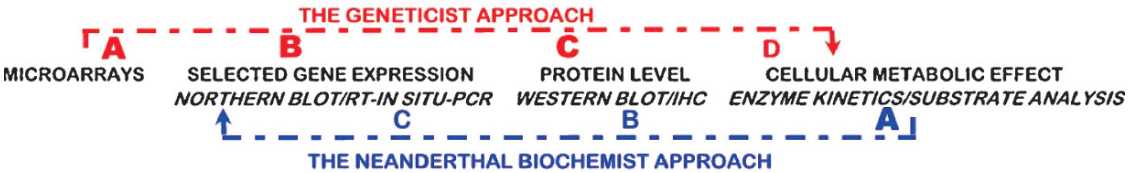

FIGURE 1.3. The geneticist and biochemist approaches to establishing cellular enzyme activities and associated metabolic pathways in tumor cells

is eliminated. However, further study that involves step D could reveal cellular changes in the enzyme activity and associated pathway. Thus, a false-negative result would have been reported.

2. The "Biochemist" Approach: This approach (Figure 1.3) first seeks to identify the alteration in the cellular intermediary metabolism (step A) such as a change in the specific enzyme activity and/or the operation of a metabolic pathway. If an alteration in the cellular enzyme activity and/or associated metabolic pathway is not identified, its involvement in a metabolic transformation is unlikely. The need to proceed with genetic and proteomic studies (steps B and C), seemingly becomes unnecessary. However, pursuant genetic/proteomic studies might reveal altered expression and level of the enzyme. Then an important issue is revealed. "What are the cellular conditions that prevent the change in the activity of the altered enzyme level?" This would dictate the need for further investigation.

Alternatively, Step A might reveal a cellular alteration in the enzyme activity and associated metabolic pathway. Then, the issue becomes the identification of the mechanism of altered enzyme and metabolic activity. The application of the contemporary molecular tools of proteomics and gene expression are then applied, with biochemical examination of cellular conditions that can alter the activity of an enzyme. For example, a kinetic change in the enzyme Vmax with no change in the substrate Km value would suggest that the level of enzyme is altered. This could correlate with a corresponding change in the gene expression and/or protein level (steps C and B), and define a critical role of altered gene expression in the metabolic transformation. Conversely, the enzyme kinetic change might not be mimicked by genetic/proteomic changes. Then one must consider alternative reasons for the change in Vmax as described above. There are other scenarios that exist. However, the "biochemist" approach is essentially devoid of potential false-positive and false-negative results relative to defining the involvement of specific enzymes in metabolic transformations. The application of genetic/proteomic studies is essential for the elucidation of the mechanisms of altered enzyme activity and the regulation of metabolic transformations.

These relationships are also applicable to mutations in the mitochondrial (mt) DNA genome. Mutated mtDNA is a common occurrence in malignant cells *in situ*. For example, mutations in the cytochrome c oxidase subunit (COX1 gene) have been widely reported in malignant prostate cells. However, important information concerning the effects of specific mutations on the mitochondrial cytochrome c oxidase activity and terminal oxidation often does not exist. Mutations that do not have any metabolic implications become irrelevant.

These issues in the marriage of molecular genetics/proteomics with cellular intermediary metabolism raise the important question, "What should be done to alleviate the problems?" Hopefully, awareness of these issues and principles by the contemporary biomedical researchers will provide some immediate resolution in forthcoming studies and reports. The more permanent and meaningful resolution resides in the pre-and post-doctoral training programs. Cellular biochemistry, intermediary metabolism, enzyme kinetics,

and enzymology must be reinstituted into the didactic and seminar components of training of biomedical researchers; particularly in the molecular genetics training programs. Practical laboratory training and experience in the biochemical/metabolic methodologies along with the molecular technology methodologies would be extremely beneficial for those involved in studies of the regulation of cellular intermediary metabolism of tumor cells and other diseases. Such programs would provide the most capable generation of biomedical scientists to address and resolve the critical issues of altered intermediary metabolism in malignancy and in other areas of biology and medicine.

In conclusion, a new era of tumor cell metabolism is evolving. Critical issues of the role of altered intermediary metabolism in the development and progression of malignancy can now be addressed. The factors and mechanisms involved in the regulation and alteration of intermediary metabolism in malignant cells can be addressed. This new frontier of cancer research (and other diseases) requires the appropriate marriage of genetics/proteomics/molecular technology with the principles and methodology of enzyme relationships and intermediary metabolism. A hybrid of the geneticist approach and the biochemist approach is essential. New insights into the importance and mechanism of the metabolic transformations required for the development and progression of malignancy altered are at hand. The understanding of the genetic/molecular/metabolic basis of malignancy is critical to the issues of diagnosis, treatment, and prevention of the various types of cancers. This provides for an exciting and revealing future for clinical and experimental studies in which tumor cell metabolism will be an indispensable and critically important component in the effort to eliminate cancer as a significant human disease.

Acknowledgement. The cited studies of LCC and RBF described in this review were supported in part by NIH grants CA71207, CA21097, CA79903. and CA93443.

REFERENCES

Costello, L.C., and Franklin, R.B. 2001. The intermediary metabolism of the prostate: A key to understanding the pathogenesis and progression of prostate malignancy. *Oncology 59*: 269–282.

Costello, L.C., and Franklin, R.B. 2005. "Why Do Tumor Cells Glycolyze?": From glycolysis through citrate to lipogenesis. *Mol. Cell. Biochem. 280*: 1–8.

Costello, L.C., and Franklin, R.B. 2006. The clinical relevance of the metabolism of prostate cancer; zinc and tumor suppression: connecting the dots. *Mol. Cancer 5*: 17.

Costello, L.C., Feng, P., and Franklin, R.B. 2005. Mitochondrial function, zinc, and intermediary metabolism relationships in normal prostate and prostate cancer. *Mitochondrion 5*: 143–153.

Dietzen, D.J., and Davis, E.J. 1993. Oxidation of pyruvate, malate, citrate, and cytosolic reducing equivalents by AS-30D hepatoma mitochondria. *Arch. Biochem. Biophys. 305*: 91–102.

Hernanz, A., and de la Fuente, M. 1988. Characterization of aconitate hydratase from mitochondria and cytoplasm of ascites tumor cells. *Biochem. Cell Biol. 66*: 792–795.

Kelleher, J.K., Bryan, B.M. 3rd, Mallet, R.T., Holleran, A.L., Murphy, A.N., and Fiskum, G. 1987. Analysis of tricarboxylic acid-cycle metabolism of hepatoma cells by comparison of 14CO2 ratios. *Biochem. J. 246*: 633–639.

Mazurek, S., Eigenbrodt, E., Failing, K., and Steinberg, P. 1999. Alterations in the glycolytic and glutaminolytic pathways after malignant transformation of rat liver oval cells. *J. Cell. Physiol. 181*: 136–146.

McKeehan, W.L. 1982. Glycolysis, glutaminolysis and cell proliferation. *Cell Biol. Int. Rep. 6*: 635–650.

Moreadith, R.W., and Lehninger, A.L. 1984. The pathways of glutamate and glutamine oxidation by tumor cell mitochondria. Role of mitochondrial NAD(P)+-dependent malic enzyme. *J. Biol. Chem. 259*: 6215–6221.

Parlo, R.A., and Coleman, P.S. 1984. Enhanced rate of citrate export from cholesterol-rich hepatoma mitochondria. *J. Biol. Chem. 259*: 997–1003.

Parlo, R.A., and Coleman, P.S. 1986. Continuous pyruvate carbon flux to newly synthesized cholesterol and the suppressed evolution of pyruvate-generated CO2 in tumors: further evidence for a persistent truncated Krebs cycle in hepatomas. *Biochim. Biophys. Acta 886*: 169–176.

Singh, K.K., Desouki, M.M., Franklin, R.B., and Costello, L.C. 2006. Mitochondrial aconitase and citrate metabolism in malignant and non-malignant human prostate tissues. *Mol. Cancer 5*: 14, 4.

Warburg, O., Wind, F., and Negelein E. 1926. Uber den Stoffwechsel von Tumoren im Korper. *Klin. Woch. 5*: 829–832.

2
Detection of Recurrent Cancer by Radiological Imaging

S.J. Gwyther

INTRODUCTION

Diagnosis of cancer is often viewed by the general population as a life changing event that will inevitably lead to an early death after treatment with unpleasant and noxious side effects. Whilst there have been improvements in treatment and prolonged survival in many types of cancers in recent years, cancer has remained common. It has been estimated that one in three people develop some form of cancer at some point during their life and one in four will die as a result of it (Seddon and Workman, 2003). The overall number of patients will inevitably rise as the overall world population not only increases in number but becomes more aged. This is borne out by the fact that in the year 2000 ~10 million new cases of cancer were diagnosed worldwide, and this number is expected to rise to 15 million by the year 2020 (Stewart and Kleihuer, 2003). Table 2.1 gives the estimated figures for the number of patients who will develop the major cancers and Table 2.2 the estimated number of patients who will die of various cancers in the United States during 2006 (NCI, Common Cancer types, 2006; American Cancer Society, 2006). The best chance of long term survival is early detection of disease when a curative procedure can be undertaken, usually by complete surgical excision, though curative chemotherapy and/or radiotherapy are effective in some situations such as early stage Hodgkin's lymphoma and seminoma of the testis.

Those who die of their disease or as a result of their disease can be divided into two groups. Firstly, those patients who always have evidence of disease from the time of diagnosis. When conventional treatment strategies fail they may enter clinical trials using new agents or combinations and are likely to achieve, at best, a partial response to treatment, defined as a predetermined reduction in tumor bulk, usually based on the reduction in size of well-defined lesions seen on anatomical imaging. The most common imaging modality used is computerised tomography (CT), though magnetic resonance imaging (MRI) is also used but in specific anatomical sites, such as the diagnosis of spinal cord compression. Should the disease relentlessly continue to progress during treatment, the patient is defined as having progressive disease and the ineffective treatment is withdrawn.

The second group comprises those patients who have been treated by curative

TABLE 2.1. Estimated number of new cases of cancer in the USA for 2006.

Male	Female
All sites: 720,280 (100%)	All sites: 679,520 (100%)
Prostate: 244,460 (33%)	Breast: 212,920 (212,920 (31%)
Lung: 92,700 (13%)	Lung: 81,770 (12%)
Colon/rectum: 72,800 (10%)	Colon/rectum: 75,810 (11%)
Bladder: 44,690 (6%)	Uterus: 41,200 (6%)
Melanoma: 34,260 (5%)	NHL: 28,190 (4%)
NHL: 30,680 (4%)	Melanoma: 27,930 (4%)
Kidney: 24,650 (3%)	Thyroid: 22,590 (3%)
Oral cavity: 20,180 (3%)	Ovary: 20,180 (3%)
Leukaemia: 20.000 (3%)	Bladder: 16,730 (2%)
Pancreas: 17,150 (2%)	Pancreas: 16,850 (2%)

TABLE 2.2. Estimated deaths for cancer patients by tumor type in the USA for 2006.

Male	Female
All sites: 291,270 (100%)	All sites: 273,560 (100%)
Lung: 90,330 (31%)	Lung: 72,130 (26%)
Colon/rectum: 27,870 (10%)	Breast: 40,970 (15%)
Prostate: 27,350 (9%)	Colon/rectum: 27,300 (10%)
Pancreas: 16,090 (6%)	Pancreas: 16,210 (6%)
Leukaemia: 12,470 (4%)	Ovary: 15,310 (6%)
Liver & bile ducts: 10,840 (4%)	Leukaemia: 9,810 (4%)
Esophagus: 10,730 (4%)	NHL: 8,840 (3%)
NHL: 10,000 (3%)	Uterus: 7,350 (3%)
Bladder: 8,900 (3%)	Myeloma: 5,630 (2%)
Kidney: 8,130 (3%)	Brain & CNS: 5,560 (2%)

means, by whatever procedure and who initially have no evidence of disease, only for it to recur at some later time. The term recurrent disease is a misnomer. The disease has not disappeared and somehow mysteriously returned, but these patients have always harbored disease from the time of diagnosis, and although all macroscopic disease appeared to have been excised with clear margins, small foci of cancer cells obviously persist in the body which are beyond the resolution of current imaging modalities or biochemical strategies, implying the disease process was systemic at the time of diagnosis and therefore not localized. These cells either grow incessantly until they become evident or appear to lie dormant until some phenotypic switch activates them to become frankly malignant and invasive, hence the apparent "recurrence." This chapter deals with the latter group of patients.

Until ~ 30 years ago, plain radiographs were the mainstay of any imaging department in terms of detection of recurrent cancer. Major advances in imaging modalities which have become available during this time need to be placed in context. Historically, patients who attended radiological investigations tended to be symptomatic, presenting with either bone pain or pathological fractures, in which case plain radiographs of the relevant bones were indicated or they presented with chest symptoms, in which case a chest radiograph (CXR) may detect abnormal soft tissue masses projected over the lung fields. The CXR is relatively insensitive and to detect a mass it has to be in the order of 1 cm in diameter, though retrospective analysis of prior films may demonstrate the mass was present at an earlier time. The CXR also suffers from "hidden areas," such as the cardiac contour, the hemi-diaphragms, and the lung apices. Detection of bony lesions is even more insensitive. To detect a lytic bone lesion on a plain X-ray, 70% of the bone needs to be destroyed before it becomes radiologically apparent, so it is not surprising that patients present with symptoms prior to the examination. Before the 1980s there was little else in the way of imaging, but it is surprising how often even now plain radiographs

are employed to confirm the presence of recurrent disease.

Two other simple and relatively inexpensive imaging modalities frequently employed are isotope bone scans and ultrasound examinations. Isotope bone scans use radioactive technetium methylene diphosphonate (^{99}Tc MDP) which is an indicator of osteoblastic activity and therefore new bone formation. This detects both the more common lytic lesions as seen commonly in lung and breast cancer and sclerotic lesions as seen typically in metastatic prostate cancer. Isotope bone scans are significantly more sensitive than plain films and detect lesions often before clinical symptoms ensue, though they rarely detect myeloma, which is an osteoclastic process in all but ~3% of cases. Ultrasound examinations continue to play a major role in the detection of recurrent disease. Visceral lesions are detected within the abdominal and pelvic organs, though lesions generally have to be >0.7 cm in diameter in organs such as liver and spleen and appear as being hypoechoic (darker) or hyperechoic (brighter) with respect to the normal echogenicity of the given organ. Lymph nodes, subcutaneous nodules, and intramuscular lesions can also be detected. Ultrasound is a subjective imaging modality, so it is operator-dependent as well as patient-dependent. The ultrasound beam is not able to penetrate large distances, so obese patients and those with ascites are less suitable, and the ultrasound beam is not able to penetrate gas. Patients in pain often swallow air, so it may be impossible to demonstrate deep abdominal structures such as the pancreas or paraaortic lymph nodes due to gas in the overlying bowel. Similarly, the lungs are not amenable to ultrasound assessment due to normal aeration. However, ultrasound has the great advantages of being readily available, inexpensive, easy to perform, and abnormal masses can be readily biopsied, using either fine needle aspiration or core biopsies.

True cross sectional imaging has revolutionised radiological imaging. This encompasses both CT and MRI. CT became commonly available in the early 1980s but imaging protocols specific for cancers were not developed for several years. However, many lesions not previously suspected were readily detected using CT, i.e., the thorax. Paratracheal, anterior and subcarinal lymph nodes are readily apparent, as are lesions at the costophrenic angles, lung apices, and in positions posterior to the cardiac contour. Moreover, when different imaging parameters, such as "lung windows" are employed, small intraparenchymal metastases of only ~3 mm are reliably demonstrated. Intravenous (IV) contrast agents accentuate the difference between normal visceral enhancement and tumor enhancement. Liver and other visceral metastases rely on differences in attenuation coefficients between metastases and normal tissue during intravenous contrast enhanced examinations. Most metastases are hypovascular and are of decreased attenuation (density) with respect to the normal tissue. However, some metastases are hypervascular and therefore of increased attenuation, such as those from carcinoid and some colorectal carcinomas. Lytic bone metastases are demonstrated on "bone windows" before they are reliably visible on plain radiographs, thereby increasing the overall sensitivity.

Further technological changes in the 1990s saw the advent of helical (spiral) CT. This led to the development of rapid scanning through a whole body part such as the

thorax in a single breath hold. This enabled misregistration of small lung nodules to be largely eliminated and also enabled different phases after the injection of an IV contrast agent to be scrutinized. Three distinct phases are recognized: (1) the arterial phase, which occurs ~ 20 – 30 sec after the injection of a contrast agent into a peripheral upper limb vein; (2) the intermediate phase which occurs ~ 40 – 50 sec after injection; and (3) the portal venous phase, which occurs ~ 70 – 80 sec after the injection. This is important when hypervascular and hypovascular metastases are considered, as they are more obvious at the relevant maximal contrast difference between the lesion and normal tissue enhancement.

The advent of multislice CT (MSCT) in the last 8 years followed by the inevitable technological improvements resulting in state of the art 64 slice scanners (compared with the original four slice scanners and the imminent arrival of 256 slice scanners) has resulted in further improvements in scanning, so that an examination of the entire thorax, abdomen, and pelvis can be undertaken in < 8 sec. The data acquired from such an examination enable high definition reconstruction films in any anatomical plane to be made available. Computer software programs have further enhanced detection of tumors with CT colonography, virtual bronchoscopy, and volumetric studies, the latter being particularly useful in sequential follow up of solitary pulmonary nodules. Small lung nodules can be followed on successive CT examinations and even though on axial imaging there may appear to be no significant difference in size, the software accurately determines whether there has been a change in overall volume.

Magnetic resonance imaging plays a significant role in cancer detection and management. It has become more widely available during the last 20 years, and is particularly sensitive to detecting central nervous system tumors, both in the brain and spinal cord. Imaging sequences demonstrating abnormalities within the bone marrow, such as T1-weighted sequences are exquisitely sensitive for detecting bone metastases, significantly more so than traditional isotope scans. MRI is also particularly useful in detecting the extent of the disease in prostatic and bladder tumors, whether the disease has spread beyond the capsule and similarly in gynaecological tumors, particularly those of the cervix and endometrium. Single breath hold sequences and contrast-enhanced scans enable the liver to be imaged with accurate detection of malignancy. The introduction of liver specific contrast agents, such as manganese based agents and superparamagnetic iron oxide particles (SPIOS) have increased sensitivity in the detection of liver metastases. Diffusion and perfusion studies are being developed to demonstrate early changes in pathophysiology to reflect angiogenesis and the effects of anti-angiogenesis agents and changes in tumor metabolism and function.

Dynamic studies using principally CT and MRI but also ultrasound show changes in tumor function by demonstrating changes in blood flow, volume and permeability before and during cancer therapy to help determine whether there has been an early response to treatment.

All anatomical imaging requires a true anatomical abnormality to be present. Therefore, lymph nodes must be enlarged before tumors may be detected. Lymph nodes under 1 cm in size using anatomical criteria

are generally assumed to be disease free, which is not necessarily the case. Positron emission tomography (PET) scanning is used to measure function rather than size, though lesions do have to be of a minimum size, ~ 0.7 – 1.0 cm in size before enough tracer is reliably detectable. Certain isotopes emit positrons during their decay. 18 Fluorine (^{18}F) is such a positron emitter and has a half-life of ~ 110 min ^{18}F can be incorporated into 2-[fluoro-18] fluoro-deoxy-D-glucose (FDG) which is a glucose analogue and enters cells actively metabolizing glucose. Unlike glucose, it is not metabolised, so it is trapped in the cells and can be detected by measuring the activity from the isotope. It is the physiological or pathophysiological process that is being measured, in this case glucose metabolism and not simply an anatomical size change. However, the sensitivity of PET to detect small lesions, $<0.5 - 1.0$ cm in size is more limited (25–43%) for detection of metastatic lesions less than 1 cm in diameter (Fukai *et al*., 2005), but a positive FDG PET may help characterize lesions of this size, which are generally too small to be accurately characterized with CT. It must be remembered that FDG PET detects any cause of increased glucose metabolism. It is, therefore, not specific for malignancy, and infective and inflammatory processes also show increased activity. However, in the appropriate settings, it is a very powerful tool. The spatial resolution is poor compared to anatomical imaging but during the last 5 years, scanners have been developed so CT and PET are linked together as one machine allowing the PET scan to be accurately superimposed over the CT image. This is important to determine whether a focus of abnormal activity represents real pathology or whether it is likely to represent one of the many pitfalls, such as increased activity in the masseter muscles if the patient has been repeatedly clenching his/her teeth or the vocal cords if the patient has been talking immediately prior to the examination.

One study of 1,750 patients with suspected or proven cancer showed a frequency of unexpected findings on FDG PET scans to be 3.3% (58 of 1,750 patients) and the incidence of proven malignancy as a result of FDG PET to be 1.7% (30 of 1,750) in patients who were otherwise well, had no abnormality on physical examination and a normal CT scan (Agress and Cooper, 2004). Neither anatomical nor functional imaging gives histological diagnosis, but they do localize the area of interest so that a biopsy of the relevant structures may be undertaken. One study using FDG PET-CT for detection of bony metastases compared the CT component with the FDG PET component. 179 lesions were detected in 55 patients on the FDG PET component as highly suggestive of metastases and 133 lesions in 33 patients were confirmed histologically. Of these 133 lesions, the CT examination showed osteolytic changes in 41 patients (33%), osteoblastic changes in 21 (16%), no apparent change in 49 (37%) and nonspecific changes in 22 (17%). This demonstrates that CT detected only approximately half the lesions suggested by the FDG PET component. In fact, of 46 lesions that were false-positives on FDG PET, 38 were in fact metastases in adjacent structures, such as the pleura, which emphasises the importance of having both the functional and anatomical data together to make an accurate assessment. PET-CT is not a panacea that will detect all tumor types. Many tumors are simply not well demonstrated at PET, such as gastric cancer.

This may be due to relatively low glucose metabolism or reflect the number and activity of GLUT receptors responsible for glucose transport into cells, or may represent relatively slow growing and hypocellular tumors or any combination thereof.

The above brief description of the current major imaging techniques gives some sense of the importance and predominance of cross-sectional imaging and the rapid and significant improvements which have occurred in these imaging modalities during the last 15 years added to the recent introduction of functional imaging which has revolutionised medical imaging in oncology. Recurrent disease is now increasingly being diagnosed before it is clinically apparent. The important question is, does this matter? If there is no effective treatment available to alter the course of the disease, we are doing nothing more than increasing the lead time. Fortunately, newer chemotherapy regimens and newer specific anti-angiogenesis agents and enzyme target agents show promise in several tumor types such as gastrointestinal stromal tumors (GIST) and chronic lymphatic leukaemia (CLL). In many cases appropriate treatment strategies with second and third line therapy options are available when first line treatment fails. This inevitably mandates the continued surveillance of patients to detect early treatment failure and evidence of early recurrent disease. Although the history, physical examination, and biochemistry are important; imaging, particularly CT, plays a major role in detection of recurrent disease. The relative value of these various imaging modalities currently in use will be discussed for the major tumor types and a few other selected tumor types.

Lung Cancer

Lung cancer is the leading cause of cancer mortality in the United States in both men and women, and is the second most common cancer in terms of the number of new cases. It is estimated that in 2006 > 90,000 men and 72,000 women will die as a result of the disease in the United States, accounting for 31% and 26%, respectively, of all cancer deaths (NCI, Common cancer types, 2006; American Cancer Society, 2006). Although the rate is falling slightly in men, it is rising in women. More than 80% of cases are due to non-small cell lung cancer (NSCLC). Of the many factors which influence prognosis, staging at diagnosis is considered the most important. CT is accurate in determining the size of tumors and assessing whether there is infiltration into adjacent structures, but it is less accurate at assessing mediastinal lymph node involvement; PET scanning is more sensitive.

PET-CT is more sensitive than CT or PET alone at assessing the primary tumor (T), the mediastinal lymph nodes (N) and distant metastases (M), and leads to a change in therapy in ~ 25 – 30% of patients and FDG PET detects ~ 10% of unsuspected metastatic disease when the CT scan shows no convincing evidence of metastatic disease (Antoch *et al*., 2003; Kostakoglu *et al*., 2003). In the same study the sensitivity, specificity, and accuracy of detecting metastases in the mediastinal nodes for PET-CT were 89%, 94% and 93%, for PET alone they were 89%, 89% and 89% and for CT alone they were 70%, 59% and 66%, respectively (Antoch *et al*., 2003). PET alone does not demonstrate the tumor size well nor infiltration into adjacent structures due to

its limited spatial resolution, whereas this is less of a problem with CT, though anatomical imaging often cannot differentiate between viable tumor and atelectasis, whereas PET can. Hence, the importance of accurately evaluating the PET and CT components is obvious. The N stage is entirely determined by anatomical size using CT criteria. The assumption is that nodes greater than 10 mm in their short axis are likely to contain metastases, but up to 21% of nodes < 10 mm have been shown to contain metastases, whereas ~ 40% of nodes > 10 mm are benign.

PET-CT also accurately demonstrates nodal position, so N2 disease may be diagnosed rather than N1. The demonstration of small volume but nonetheless N or M stage disease has a profound effect on patient management and precludes futile curative surgery, though the converse is also true. Bulky but benign nodes should not prevent a curative procedure, which would otherwise have been the case should CT alone have been used. However, the resolution for PET-CT detection is in the order of 5–6 mm, so very small nodes or micro-metastatic disease may still not be detected at presentation by PET-CT. The CT technique should commence the scan at least 3 cm above the lung apices so as to include the supraclavicular lymph nodes and extend inferiorly to include the adrenal glands, as these are well known sites for metastatic disease.

With reference to the supraclavicular lymph nodes, one study showed 22 out of 55 patients (40%) had enlarged but non-palpable supraclavicular nodes on CT or ultrasound, of whom 17 had malignancy, emphasising the need for biopsy at initial presentation to accurately stage the patient, otherwise these patients may be misstaged as having developed recurrent disease when the disease was stage N3 and, therefore, irresectable at the time of diagnosis. A further study showed that supraclavicular nodes were palpated in 15 patients, detected by CT in 34 and by ultrasound in 38 of 117 patients, and ultrasound-guided fine needle aspiration of all 38 nodes demonstrated tumor in 30 (26%). The sensitivities for detection were 0.33 (10 out of 30) for palpation, 0.83 (25 of 30) for CT and 1.0 (30 of 30) for ultrasound (van Overhagen *et al.*, 2004).

Conflicting reports regarding the role of PET in detecting bony metastases rather than conventional isotope scans have been tabled. One study showed PET to be 96% accurate in detecting bony metastases compared with 66% for isotope scans, whereas another showed a lower sensitivity for PET (73%) compared to isotope scans (81%), but greater specificity, giving an overall accuracy of 90% for PET compared to 78% for bone scans (Gayed *et al.*, 2003).

Tumors that have high FDG uptake both before and after radiotherapy are much more likely to relapse than those where the FDG activity drops after treatment, and another study showed that lack of uptake of FDG after radical radiotherapy or chemoradiation correlates with reduced relapse (MacManus *et al.*, 2005). In the post-surgical setting, FDG PET and PET-CT are playing an ever-increasing role. One study in 17 patients post pneumonectomy who were either at high risk of recurrent disease or had suspected recurrent disease underwent PET which changed the patient management in > 50% of patients by demonstrating a different pattern or disease distribution compared to CT alone. For those with no evidence of increased FDG

uptake there was a favorable outcome (Roberts *et al*., 2005). Another study of 63 post operative patients who had undergone curative surgery but who were suspected of relapse showed that the presence and extent of disease were prognostic factors, and the treatment was altered in > 60% of cases (Hicks *et al*., 2001).

A further recent study of 62 post-surgical patients found that PET-CT showed a sensitivity of 93%, specificity of 89% and accuracy of 92% in the detection of recurrent tumor. It also identified those who may benefit from further surgery and showed that a raised standardized uptake value (SUV) correlated inversely with prognosis (Hellwig *et al*., 2006). MRI and CT, however, are more accurate in detecting brain metastases than FDG PET due to the high glucose metabolism by normal brain which makes detection of small metastases difficult to identify. In the early post-radiotherapy period, it must be remembered that FDG uptake occurs in infective and inflammatory processes, so infection, radiotherapy and other inflammatory changes such as tuberculosis and sarcoid should be considered. Some tumors, such as bronchioalveolar cell carcinoma, are not FDG avid, so reliance on cross-sectional imaging, particularly CT, remains the most sensitive imaging modality. Recurrent disease in previously irradiated areas may manifest as a convex bulge in the border of fibrosis, a discrete mass extending into adjacent structures or as filling in of bronchiectatic tissue.

Breast Cancer

Breast cancer is the most prevalent tumor in women accounting for 31% of cancers detected, and is the second most lethal tumor in women, after lung cancer, accounting for >40,000 cancer related deaths in the USA. Ninety-nine percent of breast cancers occur in women (NCI, Common Cancer Types, 2006; American Cancer Society, 2006). Following mastectomy, the local chest wall recurrence rate in women is 0.2–1.0% per year, and for those undergoing breast conserving treatment with lumpectomy and radiotherapy the local recurrence rate is 1–2% per year, which is similar to that for patients who undergo mastectomy and transverse abdominis musculocutaneous (TRAM) flap reconstruction, though different management paradigms exist for these different groups. Routine mammography is undertaken annually for the breast conserving treatment group, but not for the TRAM flap patients, who only receive clinical examination. A recent study of 106 screening mammograms in patients with TRAM flaps detected two cancers in 2 years (1.9%) before they were clinically palpable, suggesting that mammography should be undertaken in this group (Helvie *et al*., 2002).

A major problem in breast cancer is the assessment in previously irradiated fields and scarring versus recurrent disease. Mammography detects only 66% of cases of recurrences in post-lumpectomy patients. Cross-sectional imaging (CT and MRI) is less sensitive than PET scanning for detection of locoregional lymph node involvement and metastatic disease to the lungs, liver, and bones. With increased use of breast conserving surgery, locoregional recurrence is an issue and the isolated lymph node recurrence rate at 5 years is 3%. Patients with thoracic and internal mammary node metastases have a worse outcome than patients with axillary nodal disease alone. CT has been the most

widely used imaging tool to detect thoracic node recurrence, but relies on size as the main indicator of disease and so suffers from poor sensitivity (Jing *et al*., 2004). One study of 73 patients with recurrent or metastatic breast cancer showed that the prevelance of thoracic and internal mammary recurrence was much higher on FDG PET than on CT, 40% versus 23%, upstaging 10 patients (30%), again demonstrating the poor sensitivity of CT which relies on size alone to detect disease.

Moreover, patients with mediastinal and internal mammary nodal disease are much more likely to develop ipsilateral intraparenchymal and pleural disease, suggesting a lymphatic course of spread. Bony metastases are the most common site of distant metastases in breast cancer, occurring in 31% of cases of patients with metastases, and FDG PET is more sensitive than isotope bone scanning in lytic metastases or those predominantly involving the marrow, though isotope scans are more sensitive in detecting osteoblastic metastases. Breast cancer is the commonest cause of spinal cord compression in women, particularly the thoracic and lumbar spine, for which MRI is the imaging modality of choice (Jing *et al*., 2004).

After bone, lung metastases are the most common site and tend to be multiple, peripherally sited, variable in size, and oval shaped. Lymphangitis is the most common manifestation of thoracic disease in metastatic breast cancer and is best demonstrated by CT, particularly high resolution studies (Jing *et al*., 2004). Pleural disease is common and the usual manifestation is a unilateral pleural effusion, which can be demonstrated by CXR, ultrasound or CT, though the latter modality will show nodules, suggesting metastases. Solitary pulmonary nodules in breast cancer patients may represent recurrence, but one study found that was in a minority of cases, 43%, whilst 52% has a new primary lung cancer and 5% had benign conditions such as sarcoid and TB. Histological analysis, therefore, is vital in this setting (Jing *et al*., 2004).

Colorectal Cancer

Colorectal cancer is the second leading cause of cancer related death in the United States, accounting for >55,000 deaths, surpassed only by lung cancer in both men and women and also by breast cancer in women, and is the third most prevalent tumor in both sexes (NCI, Common Cancer Types, 2006; American Cancer Society, 2006). Following curative surgery, the risk of recurrence is ~ 10% and recurrence is predominantly local recurrence or liver metastases. Approximately 70% of patients will eventually develop liver metastases and 30–40% of these patients have disease restricted to the liver, though potentially curative surgery is possible in a minority of cases due to the size and location of these metastases. CT is the main imaging modality employed, but relies on size changes and comparison with normal anatomy, which may be altered after surgery. MRI is of help in specific situations such as rectal tumors and in determining whether presacral masses represent recurrence or fibrosis, using T2 weighted sequences, where tumors have a higher water content than fibrosis, and, therefore, a higher signal. However, improvements in MRI techniques and liver specific contrast agents have improved the sensitivity.

In one study of 79 patients, 159 (87%) lesions were detected by liver specific MR contrast agents and intra-operative ultrasound

(IOUS) detected an extra 12 (9.4%) lesions in 10 patients, but this only altered the management in 3 (4%) patients. However, 9 lesions (6%) remained undetected by IOUS and were only detected at histology. Transabdominal ultrasound is a useful screening tool as diffuse metastatic disease within the liver can be detected, in which case further imaging may not be required. FDG PET is more sensitive than CT. The overall sensitivity for detection of recurrent disease is 87% for FDG PET and 66% for CT and the specificity 68% and 59%, respectively, though the sensitivity of FDG PET is lower in mucinous tumors, probably due to the hypocellularity of the tumor. The sensitivity of FDG PET in detecting local recurrence and extrahepatic disease is 90% whilst for CT it is 71%, and for hepatic disease it is 89% and 71%, respectively. Bipat *et al*. (2005) reported a metaanalysis regarding imaging modalities for detection of hepatic metastases from colorectal cancer from 61 articles from the period 1990–2003 and found that the sensitivity estimates per patient for non-helical CT, helical CT, 1.5T MRI and FDG PET were 60.2%, 64.7%, 75.4%, and 94.6%, respectively. On a per lesion basis the sensitivity estimates for non-helical CT, helical CT 1.0T MRI, 1.5T MRI and FDG PET were 52.3%, 63.8%, 66.1%, 64.4% and 75.9%, respectively (Bipat *et al*., 2005). FDG PET is the most sensitive method per patient, and contrast enhanced MRI is superior to CT. FDG PET detected unsuspected extra-hepatic disease in 25% of patients in one study of 43 patients, thereby preventing unwarranted surgery in these cases, though survival was improved in those who were eligible for hepatic resection. The 5-year survival after hepatic resection varies between 22–60%, compared to 0% in those who do not undergo resection.

IOUS remains the gold standard in terms of lesion detection prior to hepatic resection, but is necessarily invasive. Accurate detection is, however, necessary in those patients with apparently localized disease within the liver for whom potentially curative hepatic resection is planned. It is this group of patients who require contrast enhanced MRI and FDG PET (Bipat *et al*., 2005). Multiple studies have found MRI to be more accurate than CT in the prediction of organ and pelvic wall invasion and bone marrow invasion (Beets-Tan and Beets, 2004). A recent study compared FDG PET with dynamic MRI in patients with suspected liver metastases and found a negative correlation between tumor to nontumor FDG uptake and the rate constant for contrast uptake within tumors (using gadopentate dimeglumine) at dynamic MRI. This suggests a reduced oxygen supply in tumors necessitating a higher glucose uptake to maintain tumor energy. Moreover, hypoxia is known to stimulate angiogenesis and upregulate membrane bound glucose transport proteins, thereby, aiding glucose transport into tumor cells *via* various factors, e.g., hypoxia inducible factor alpha 1.

There was a positive correlation between vascular density and rate constant, but not between tumor to nontumor ratio of FDG uptake, indicating a potential method of measuring tumor vascularity *in vivo* (and more importantly the functioning vasculature) and its relationship to FDG uptake (van Laarhoven *et al*., 2005). Dynamic contrast enhanced MRI can be used to construct signal intensity time curves, which give a “type 3” curve, typical of malignancy (Kuhl *et al*., 1999). This effectively shows rapid uptake of the contrast agent by the tumor, followed by rapid washout, reflecting increased

vascularity and increased permeability due to abnormal, immature, "leaky" vessels which allow the contrast agent to diffuse back into the intravascular space.

Lymphomas

Lymphoma is the 7th most common cause of cancer related deaths in the United States, accounting for >18,000 deaths per annum (NCI, Common Cancer Types, 2006; American Cancer Society, 2006). Over 80% are non-Hodgkin lymphoma. Currently contrast enhanced CT is the imaging modality of choice for both Hodgkin and non-Hodgkin lymphoma. The criteria used are structural changes in lymph node size and changes in contrast enhancement within organs. However, residual disease in the nodes of normal size, the spleen and the bone marrow cannot be assessed. FDG PET and particularly FDG PET-CT detects active disease with increased sensitivity at these sites compared to CT, though there is no significant difference in extra-nodal disease detection in Hodgkin and high grade non-Hodgkin lymphoma.

Schaefer *et al*. (2004) reported the sensitivity for lymph node involvement to be 94% for FDG PET-CT and 88% for contrast enhanced CT and the specificity to be 100% and 86% respectively. For organ involvement the sensitivity was 88% and 50% and the specificity was 100% and 90%, respectively. They also found that increased activity in nodes of any size at FDG PET-CT represented active disease, but for CT alone several false-positives were obtained due to the lag in morphological response where large nodes without disease were detected, though they did eventually return to normal size. After treatment, Hodgkin disease often leaves residual soft tissue masses representing scar tissue or necrosis, and reliance is based on serial CT scans showing no change in the size of the mass on sequential examinations (Kazama *et al*., 2005; Spaepen *et al*., 2001). A further study suggested similar sensitivities for detection of residual disease between FDG PET and CT (88% and 84%, respectively), but FDG PET was far more specific (83% and 31%, respectively), CT being limited by size criteria alone (Kostakoglu *et al*., 2003).

FDG PET and FDG PET-CT show evidence of recurrence much earlier than CT, which is important, so further treatment may be instituted early. This study suggests that FDG PET-CT could replace contrast enhanced CT, but caution has to be exercised. False-negatives do occur with FDG PET-CT, when small foci of disease beyond the resolution of the scanner are present. Early FDG PET scans are of value after only 1–2 courses of treatment as a sharp fall in activity is suggestive of successful treatment, whereas residual activity indicates treatment failure. In this respect lymphomas are different from "solid" tumors in that any residual activity on FDG PET suggests residual active disease, and further therapy or autologous bone marrow transplant is required for successful treatment (Kazama *et al*., 2005). The sensitivity of PET in low grade lymphomas is variable, though most low grade lymphomas such as follicular lymphoma are detected. However, peripheral T-cell lymphomas are not clearly seen and gastrointestinal lymphomas may be obscured by physiological uptake (Kazama *et al*., 2005).

Pancreatic Cancer

More than 32,000 people died of pancreatic cancer in the USA in 2006. Approximately 50% of patients have metastatic disease

at presentation, a further 40% will have irresectable locally-advanced disease, so <10% are eligible for curative surgery, which itself constitutes major surgery with a 4% mortality rate and an overall 5 year survival rate of 4%. Detection of recurrent disease is, therefore, not such an issue as accurately staging the disease at presentation. CT and MRI are the main imaging modalities used, including CT or MR angiographic studies. The sensitivity of CT in detecting liver metastases has been estimated at 0.73, for detecting peritoneal metastases 0.54 and 0.80 for local extension. The specificity was estimated at 0.84 for liver metastases, 0.91 for peritoneal metastases and 0.84 for local extension. The sensitivity of fast MR imaging was estimated at 0.82 for liver metastases, 0.84 for peritoneal metastases and 0.62 for local extension. The specificity was estimated at 0.92 for liver metastases, 0.87 for peritoneal metastases and 0.67 for local extension. Endoscopic ultrasound plays a role in those patients still potentially eligible for surgery and has a sensitivity for detecting local unresectable cancer of 0.89 and a specificity of 1.00. Laparoscopic ultrasound has an estimated sensitivity of 0.89 for detecting local extension and 1.00 for detecting liver metastases. The specificity is 1.00 for both liver metastases and local extension (McMahon *et al*., 2001). FDG PET-CT may be of benefit in determining whether a pancreatic lesion is benign or malignant and guiding the operator to a suspicious area to biopsy and demonstrate distant metastases. However, the small size of tumors and the low metabolic activity in mucinous tumors are causes of false-negatives, while pancreatitis and infection can lead to false-positives (von Schulthess *et al*., 2006).

Prostate Cancer

Prostate cancer is responsible for the deaths of more than 27,000 patients in the USA, accounting for 9% of all cancer deaths in men. Approximately 20% are treated with radiation and hormonal therapy but the recurrence rate is ~50% in 5 years, with either local recurrence or distant metastatic spread primarily to the bones (Coakley *et al*., 2004). Transrectal ultrasound is only likely to be positive for locally recurrent disease when it is relatively advanced and similarly for isotope bone scintigraphy with advanced bony metastatic disease. CT lacks sensitivity for detecting local recurrence, though it may be of use in the subset of patients with lymphadenopathy. MRI of the prostate is of limited value after irradiation, as the gland shrinks, tends to have a diffuse low signal on T2-weighted images, and loss of the normal zonal anatomy. However, MR spectroscopy which detects abnormal metabolism may play a role. Normal prostate secretes citrate, but cancer cells do not. Choline, a cell membrane constituent, is secreted in tumors, presumably due to increased cell turnover and a rise in the spectral pattern of choline with a fall in citrate is suggestive of local recurrent disease, whilst absence of both choline and citrate on the spectral pattern suggests no recurrence (Coakley *et al*., 2004). FDG PET-CT does not play a role in prostatic cancer, but fluorocholinefluoromethyl-dimethyl-2-hydroxyethylammonium (^{18}F FCH), a positron emitting choline analogue does show promise in the detection of locally recurrent and metastatic disease.

In one small study, nine patients with suspected recurrence were correctly diagnosed, four with evidence of local recurrence, four with pelvic lymph node recurrence and one with multiple bony metastases (Schmid *et al*., 2005).

Esophageal Cancer

Esophageal cancer killed > 11,000 patients in the USA in 2006 (NCI, Common Cancer Types, 2006; American Cancer Society, 2006). CT is generally regarded as the best imaging modality for detecting recurrent disease, but in one meta-analysis comparing response to therapy *versus* endoscopic ultrasound and FDG PET scanning, CT was significantly inferior in sensitivity, 54%, whereas for endoscopic ultrasound it was 84% and 85% for FDG PET. CT was always possible, but endoscopic ultrasound was not possible in 6% and of limited value in a further 14% of patients where esophagitis and luminal stricture precluded the examination. The low accuracy of CT is due to the fact that CT is not able to reliably distinguish between active tumor and scar or inflammatory tissue, but this is also a feature of endoscopic ultrasound. FDG PET is a sensitive indicator of patient response after therapy. Those showing a reduction in FDG uptake after only two courses of treatment showed overall improved response to therapy (Kostakoglu *et al*., 2003; Westerterp *et al*., 2005). Care has to be taken when interpreting FDG PET scans within 4 weeks of surgery when postoperative inflammatory changes may cause false-positive appearances, as can examinations performed 8–12 weeks after radiotherapy when radiotherapy induced esophagitis can cause increased uptake of FDG (Westerterp *et al*., 2005).

Melanoma

The overall incidence of melanoma is rising rapidly, partly due to increased awareness and associated successful curative wide local excision procedures. However, the death rate has doubled in the last 35 years, partly due to increased exposure to bright sunlight related in part to inexpensive vacations in the sun with inadequate protection to the suns ultraviolet rays. For the most part, CT is utilized as the main imaging modality, but suffers from relying on size changes in assorted structures, as melanoma can and does metastasize to almost any site in the body without any apparent motive. However, FDG PET is more accurate, sensitive, and specific than CT scanning in detecting recurrence and follow up of melanoma patients. The sensitivity is 92% versus 58% and the specificity is 94% versus 45%, respectively. CT provides many more false-positives and false-negatives in recurrent melanoma patients than PET (Kostakoglu *et al*., 2003). Figure 2.1 demonstrates the increased sensitivity of PET over CT alone and also how the lesions can be accurately localized when the PET and the CT images are fused.

Gynecological Cancers

Ovarian Cancer

Epithelial ovarian cancer is the most common gynecological cancer and the 5th most common cause of malignancy related death in women in the USA (NCI, Common Cancer Types, 2006; American Cancer Society, 2006). Recurrent disease is often difficult to detect by imaging due to the multiple small, miliary-like peritoneal metastases typical of this disease. However, hematogenous and lymphatic

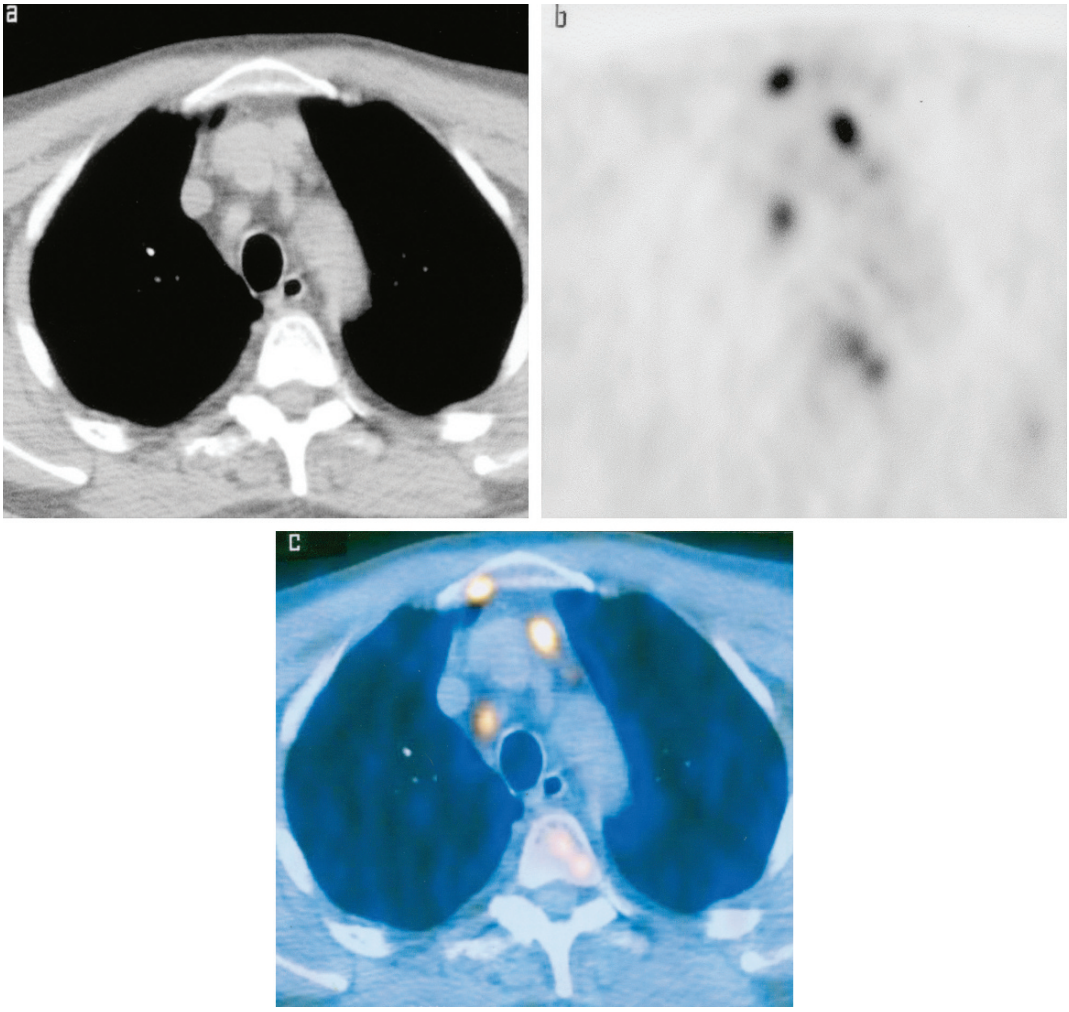

FIGURE 2.1. FDG PET-CT scan of the thorax at the level of the aortic arch in a patient with recurrent melanoma. (a) CT component demonstrates small lymph nodes less than 1 cm in the anterior mediastinum and anterior carinal region which would not be regarded as suspicious for recurrence using anatomical criteria alone. No other significant abnormality is seen. (b) Corresponding PET component (attenuation corrected image) shows increased abnormal FDG uptake in the lymph nodes of normal size, and also in the sternum on the right. Moderate increased uptake in the vertebral body represents marrow activity. (c) Fused image accurately confirms the anatomical site of the increased FDG uptake in the lymph nodes and the bone metastasis in the right sternum despite the apparently normal CT appearances

spread occurs less commonly. CT is the usual modality used in the follow-up of patients with ovarian cancer. The sensitivity for detecting peritoneal metastases using CT is ~ 85 – 93%, but for lesions < 1 cm falls to 25–50%, the small bowel mesentry is particularly difficult to assess due to partial volume effects, again demonstrating the size constraints inherent in anatomical imaging (Pannu *et al.*,

2004; Coakley *et al*., 2002). CT and non-contrast enhanced MRI are of equal value in detecting peritoneal metastases, with sensitivities of 92% and 95%, respectively, for lesions > 1 cm (Pannu *et al*., 2004). Newer multislice CT scanners using thin section imaging of 1–2 mm can generate images that can be reconstructed in multiplanar formats on a workstation, thereby making identification of small peritoneal metastases easier (Pannu *et al*., 2003).

In one study of 68 patients, gadolinium-enhanced MRI detected residual or recurrent tumor equivalent to laparotomy, the sensitivity for contrast enhanced MRI was 90%, specificity 88%, and accuracy 89% and for laparotomy 88%, 100%, and 89%, respectively, when patients were followed clinically for 1 year. This included the assessment of small peritoneal metastases. Gadolinium was given as a double dose and imaging was delayed by 5 min for optimal visualization of small enhancing peritoneal metastases (Low *et al*., 2005). PET-CT can be of benefit as recurrence in nodes of normal size containing tumor can be detected and correlation between the anatomy and PET scan can accurately direct biopsy of any suspicious area. PET is more sensitive in patients with suspected recurrence than those with no disease, the sensitivity ranging from 80% to 100%, though small lesions, < 5 mm may not be detected even with PET-CT (Pannu *et al*., 2004). In one study PET-CT correctly identified 32 of 41 recurrent lesions, all of the 9 remaining lesions not demonstrating recurrence were < 0.5 cm (Sironi *et al*., 2004). The combination of PET-CT with CT and MRI does improve the sensitivity, specificity, and overall accuracy (Pannu *et al*., 2004; Subhas *et al*., 2005).

Endometrial Cancer

MRI plays a major role but FDG PET can be important. Uptake of FDG is abnormal in post-menopausal women, although it is a normal finding during the ovulatory phase and menstruation in pre-menopausal women. Up to 18% of fibroids show FDG uptake, so care should be taken not to assume all uptake represents malignancy. However, in the detection of recurrent endometrial cancer most patients will have undergone hysterectomy at the time of diagnosis, so CT or MRI will be used to detect evidence of local recurrence in the pelvis and CT to detect distant metastatic disease. FDG PET increases the sensitivity and accuracy compared to CT and/or MRI. One study of 21 patients with endometrial cancer who had undergone therapy showed a sensitivity of 85%, specificity of 86%, and accuracy of 85% for conventional CT and/or MRI, but when FDG PET was added the sensitivity rose to 100%, the specificity was 82% and accuracy 93% (Saga *et al*., 2003). FDG PET readily demonstrated increased uptake in lymph nodes, so biopsy of specific lymph nodes may be undertaken, if necessary (Subhas *et al*., 2005).

Cervical Cancer

This is the third most common gynecological malignancy. CT is the usual imaging modality in detecting recurrent disease, as distant metastases in the thorax and lymph node chains can be demonstrated, assuming there is an enlargement of the involved structures. However, it is often difficult to differentiate between recurrent disease and post-operative or post-radiotherapy fibrosis. MRI is better at detecting recurrent disease in the pelvis and assessing vaginal

and pelvic floor infiltration, particularly on T2-weighted sequences. MRI is also more accurate in detecting bladder and rectal infiltration, and provides better soft tissue contrast than CT. Recurrence most commonly occurs in the pelvis, and lymph node involvement is based on size criteria. A node >1 cm in its short axis is assumed to contain metastatic disease. CT is slightly less accurate than MRI in detecting pelvic node involvement (73–83% and 76–100%, respectively), but only has an accuracy of 40–60% in the paraaortic regions (Jeong *et al*., 2003). Central necrosis within a node has a positive predictive value of 100% for malignancy. FDG PET is more sensitive than CT or MRI in detecting lymph node metastases. In one study where the CT was negative for paraaortic lymphadenopathy, FDG PET detected disease with a sensitivity of 86%, specificity of 94%, and accuracy of 92% (Lin *et al*., 2003). A similar study with negative MRI of the paraaortic lymph nodes showed a sensitivity of 83%, specificity of 97% and accuracy of 93% for FDG-PET (Yeh *et al*., 2002). A further study using FDG PET in restaging patients with cervical cancer demonstrated a sensitivity of 82% and 100% for detection of local and distant disease, respectively, and a specificity of 97% and 90%, respectively (Wong *et al*., 2004). Cervical lesions which after radiotherapy and chemotherapy show persisting or new FDG uptake are the most significant predictor of metastatic disease and death from cervical cancer (Grigsby *et al*., 2004).

Head and Neck Cancers

Head and neck tumors affect >30,000 patients in the USA annually. Recurrent disease tends to show little response to treatment, but the best chance, as with most other solid tumors, is early detection. CT and MRI are relatively insensitive at detecting recurrent disease, partly due to post-surgical or radiotherapy changes where normal anatomical landmarks are lost. The sensitivity and specificity for CT alone is 67–82% and 25–56%, respectively, and for PET-CT it is 86–100% and 69–87%, respectively (Fukai *et al*., 2005). Metabolic changes in tumors precede the anatomical changes and FDG PET utilizes this fact, but there are many normal variants for FDG uptake in the neck, ranging from normal lymphoid tissue to muscular activity and brown fat, so fusion of the FDG PET with the anatomical image is important. In one study 155 lesions from head and neck cancers identified by FDG PET alone showed improved anatomic localization in 98 (63%) when the FDG PET image was fused with the corresponding CT examination, especially in patients who had been previously treated, 42 of 56 patients (74%) for previously treated patients and 58 of 101 (58%) for untreated patients. Fusion of FDG PET with CT led to a change in clinical management in 12 of 68 (18%) patients (Schoder *et al*., 2004). Another study involving 143 patients with squamous cell carcinoma of the neck showed a sensitivity of 96% and specificity of 72% for detection of recurrent disease by FDG PET-CT (Wong *et al*., 2002).

FDG PET-CT enables suspicious tissue to be accurately located and biopsied, which is helpful in patients where post-radiotherapy scarring makes anatomical assessment difficult. One study showed increased FDG uptake in two patients who underwent a negative biopsy, but the FDG uptake remained high, so repeat biopsy was performed which

confirmed tumor, illustrating potential sampling problems associated with biopsy (Lowe *et al*., 1997). If anatomical imaging alone is available, necrosis within lymph nodes is a reliable indicator of malignancy in squamous cell cancer. Between 56–63% of nodes > 1.5 cm show necrosis, while 10–33% of nodes < 1 cm also show necrosis. In one study with 89 lymph nodes positive for tumor, 43 showed some degree of necrosis. CT and MRI were similar in detecting necrosis, with an accuracy, sensitivity and specificity of 92%, 91% and 93%, respectively for CT, 91%, 93% and 89% for MRI and 85%, 77% and 93% for ultrasound (US), indicating that CT and MRI are similar and both are superior to US (King *et al*., 2004).

Thyroid Cancer

Detection of recurrent thyroid cancer using FDG PET is dependent to some degree on the extent of differentiation; the less well-differentiated, the greater the FDG uptake by the tumor. PET can help detect recurrent disease suspected on the basis of a rising thyroglobulin level despite a negative iodine 131 isotope scan, and PET-CT can help detect recurrence and localize the lesion to allow accurate biopsy to be undertaken, which is helpful when postsurgical changes distort the anatomy (Wong *et al*., 2002). In a study of 33 patients with recurrent papillary carcinoma FDG PET-CT provided additional useful information in 22 of 33 (67%) patients and the FDG PET-CT findings correlated with histology in 25 of 36 lesions, demonstrating an accuracy of 70%, a specificity of 100%, and a negative predictive value of 27%, suggesting that FDG PET-CT is not very accurate at excluding recurrent disease, but is effective at detecting recurrent disease (Nahas *et al*., 2005).

Renal and Bladder Tumors

Renal cell tumors tend to recur within the first 2 years after nephrectomy and the lung is the most likely site of recurrence. Up to 40% of patients who undergo curative surgery experience recurrence. Prognosis depends on tumor burden, the less the burden the better the prognosis and tumor size and grade. One study of 194 patients who had undergone a curative nephrectomy, 41 (21%) demonstrated recurrent disease. Of these patients, 81% recurred within 2 years with most in the lungs, suggesting that follow up should consist of CT scans of the thorax, abdomen and pelvis at 6 month intervals for the first 2 years followed by annual screening (Chae *et al*., 2005). Bone is the second most common site of metastatic spread, accounting for 20–60% of metastases and for 10% of all pathological fractures. MRI and isotope bone scans are, therefore, of use in this setting. FDG PET imaging has a limited role due to the low sensitivity. For example, one study of 66 patients who underwent 90 FDG PET examinations, showed an overall sensitivity of only 60% (Kang *et al*., 2004).

Urothelial tumors are best assessed by CT and MRI. FDG PET scanning is limited for detection of local recurrence due to excretion of the isotope in the urine. Recurrent urothelial lymph node metastases tend to be larger than in prostatic cancer, which explains a higher sensitivity for lymph node metastases than for prostatic cancer (76%) but USPIO-enhanced MR imaging has a significantly higher sensitivity of 96% for detection of nodal disease between 8–10 mm, a specificity of 95%, and negative predictive value of 98% (Deserno *et al*., 2004). PET imaging may play a role in detection of distant disease, though other isotopes such as ^{14}C methionine may

be more appropriate (Wong-You-Cheong *et al*., 2006).

Primary Intracranial Tumors

Primary intracranial tumors can be relatively easily diagnosed on conventional MRI, which is the favored modality, though CT is often more readily available and easier to perform (Al-Okaili *et al*., 2006). Progressive disease is based on an increase in tumor size, but there are newer means of detecting changes before size changes become apparent. Perfusion and diffusion-weighted MR imaging studies can be utilized for this purpose. Relative tumor and cerebral blood volume tends to increase with tumor grade on perfusion studies which correlates with leaky vessels in tumor angiogenesis. Also, cerebral blood flow correlates with both microvessel density (MVD), which is a surrogate for tumor angiogenesis and tumor grade. Therefore, a response to antiangiogenesis treatment can be detected by measuring a decrease in relative cerebral blood flow, which correlates with a reduction in MVD, and thus a decrease in tumor angiogenesis (Al-Okaili *et al*., 2006; Provenzale *et al*., 2006). The converse is true for any evidence of progressive disease, before any tumor size changes are evident. Diffusion-weighted studies are of potential benefit and they suggest that successful treatment is accompanied by an increase in water diffusion within a few weeks of successful treatment, thereby allowing successful treatment to be predicted early, before changes in tumor size occur; nonresponders show no such changes in diffusion. Those with recurrent disease show a decrease in water diffusion compared to the prior examination. The distinction between tumor recurrence and tumor necrosis can be difficult with both conventional CT and MRI, but perfusion MR imaging and FDG PET scanning can differentiate between the two, as necrosis shows areas of no uptake. Provenzale *et al*. (2006) describe the principles of diffusion and perfusion MR imaging and provide a good overview of the subject. FDG PET is not the ideal isotope with which to image the brain because it almost exclusively metabolises glucose, so early recurrent disease may be masked by the high uptake within normal brain tissue. Therefore either carbon (^{11}C) methionine or ^{18}F fluorothymidine (FLT) can be used instead, though ^{11}C has a shorter half life of ~ 20 min. The former reflects new protein synthesis and the latter DNA synthesis.

Conclusions

Detection of recurrent cancer comprises imaging designed to detect an abnormality associated with clinical symptoms. However, modern treatment regimens mandate that patients should be monitored during treatment to determine efficacy of the therapy, so if the disease is progressing with treatment then it can be replaced by a different and hopefully more effective regimen, or if none exists but experimental drugs are available, the patient may be eligible to participate in a clinical trial. Evidence of an increase in anatomical size of lesions or the appearance of new lesions indicates progressive disease and CT is the primary imaging modality of choice. MRI is appropriate in many settings, particularly the central nervous system and to answer specific queries. The above brief summary illustrates the impact newer functional imaging techniques play in the

detection of early recurrent disease. This is becoming increasingly important as newer anti-cancer agents target specific receptors within cells preventing the action of specific enzymes, such as anti-angiogenesis agents and tyrosine kinase inhibitors. These agents prevent growth of cells and do not necessarily kill the cells, so traditional anatomical changes in tumor size may not be an appropriate surrogate. If there is an increase in tumor size it will inevitably have been preceded by physiological changes and the best chance of instituting effective treatment is at the earliest opportunity. These are exciting times but as yet we are still far from determining which patients will go on to develop progressive disease compared to those who have truly been cured of their disease. However, the combination of functional and anatomical imaging in conjunction with immunohistochemistry, specific serum tumor markers and the development of specific targeted anti-cancer treatment may herald the age of patients with apparent progressive disease and tumor burdens living for significantly longer periods.

REFERENCES

Agress, H., and Cooper, B.Z. 2004. Detection of clinically unexpected malignant and premalignant tumors with whole body FDG PET: histopathologic comparison. *Radiology 230*: 417–422.

Al-Okaili, R.N., Krejza, J., Wang, S., Woo, J.H., and Melhem, E.R. 2006. Advanced MR imaging techniques in the diagnosis of intra-axial brain tumors in adults. *Radiographics 26*: S173–S189.

American Cancer Society: Cancer Facts and Figures. 2006. Atlanta, GA: American Cancer Society, 2006. Accessed online at: www.cancer.org/downloads/stt/CAFF06EsCsMcLd.pdf. Last accessed 29 Oct 2006.

Antoch, G., Stattaus, J., Nemat, T., Marnitz, S., Beyer, T., Kuehl, H., Bockisch, A., Debatin, J.F., and Freudenberg, L.S. 2003. Non-Small Cell Lung Cancer: dual-modality PET/CT in preoperative staging. *Radiology 229*: 526–533.

Beets-Tan, R.G.H., and Beets, G.L. 2004. Rectal cancer: review with emphasis on MR imaging. *Radiology 232*: 335–346.

Bipat, S., van Leeuwen, M.S., Comans, E.F.I., Pijl, M.E.J., Bossuyt, P.M.M., Zwinderman, A.H., and Stoker, J. 2005. Colorectal liver metastases: CT, MR imaging and PET for diagnosis – meta-analysis. *Radiology 237*: 123–131.

Chae, E.J., Kim, J.K., Kim, S.H., Bae, S.J., and Cho, K.S. 2005. Renal cell carcinoma: analysis of postoperative recurrence patterns. *Radiology 234*: 189–196.

Coakley, F.V., Choi, P.H., Gougoutas, C.A., Pothuri, B., Venkatramen, E., Chi, D., Bergman, A., and Hricak, H. 2002. Peritoneal metastases: Detection with spiral CT in patients with ovarian cancer. *Radiology 223*: 495–499.

Coakley, F.V., The, H.J., Qayyum, A., Swanson, M.G., Lu, Y., Roach, M., Pickett, B., Shinohara, K., Vigeron, D.B., and Kurhanewicz, J. 2004. Endorectal MR imaging and MR spectroscopic imaging for locally recurrent prostate cancer after external beam radiation therapy: Preliminary experience. *Radiology 233*: 441–448.

Deserno, W.M.L.L.G., Harisinghani, M.G., Taupitz, M., Jager, G.J., Witjes, J.A., Mulder, P.F., Hulsberger, van de Kaa, C.A., Kaufmann, D., and Barentsz, J.O. 2004. Urinary bladder cancer: preoperative nodal staging with ferumoxtran-10-enhanced MR imaging. *Radiology 233*: 449–456.

Fukai, M.B., Blodgett, T.M., Snyderman, C.H., Johnson, J.J., Myers, E.N., Townsend, D.W., and Meltzer, C.C., 2005. Combined PET-CT in the head and neck. *Radiographics 25*: 913–930.

Gayed, I., Vu, T., Johnson, M., Macapinlac, H., and Podoloff, D. 2003. Comparison of bone and 2-deoxy-2-[18F] fluoro-D-glucose positron emission tomography in the evaluation of bony metastases in lung cancer. *Mol. Imaging Biol. 5*: 26–31.

Grigsby, P.W., Siegel, B.A., Dehdashti, F., Rader, J., and Zoberi, I. 2004. Posttherapy [18F] fluorodeoxyglucose positron emission tomography in carcinoma of the cervix: response and outcome. *J. Clin. Oncol. 22*: 2167–2171.

Hellwig, D., Groschel, A., Graeter, T.P., Hellwig, A., and Nestle, U. 2006. Diagnostic performance and prognostic impact of FDG-PET in suspected recurrence of surgically treated non-small cell lung cancer. *Eur. J. Nucl. Med. Mol. Imaging 33*: 13–21.

Helvie, M.A., Bailey, J.E., Roubidoux, M.A., Pass, H.A., Chang, A.E., Pierce, L.J., and Wilkins, E.G. 2002. Mammographic screening of TRAM flap breast reconstruction for detection of nonpalpable recurrent cancer. *Radiology 224*: 211–216.

Hicks, R.J., Kalff, V., MacManus, M.P., Ware, R.E., McKenzie, A.F., Matthews, J.P., and Ball, D.L. 2001.The utility of [18] F-FDG PET for suspected recurrent non-small cell lung cancer after potentially curative therapy: impact on management and prognostic stratification. *J. Nucl. Med. 42*: 1605–1613.

Jeong, Y.Y., Kang, H.K., Chung, T.W., Seo, J.J., and Park, J.G. 2003. Uterine cervical carcinoma after therapy: CT and MR Imaging after therapy. *Radiographics 23*: 969–981.

Jing, J.J., Kim, H.H., Park, S.H., Song, S.W., Chung, M.H., Kim, H.S., Kim, K.J., Ahm, M.I., Seo, S.B., and Hahn, S.T. 2004. Thoracic manifestations of breast cancer and its therapy. *Radiographics 24*: 269–1285.

Kang, D.E., White, R.L. Jr., Zuger, J.H., Sasser, H.C., and Teigland, C.M. 2004. Clinical use of fluorodeoxyglucose F 18 positron emission tomography for detection of renal cell carcinoma. *J. Urol. 171*: 1806–1809.

Kazama, T., Faria, S.C., Varavithya, V., PhongkitKarun, S., Ito, H., and Macapinlac, H.A. 2005. FDG PET in the evaluation of treatment for lymphoma: clinical usefulness and pitfalls. *Radiographics 25*: 191–207.

King, A.D., Tse, G.M.K., Ahuya, A.T., Yuen, E.H.Y., Vlantis, A.C., To, E.W.H., and van Hasselt, A.C. 2004. Necrosis in metastatic neck nodes: diagnostic accuracy of CT MR imaging and US. *Radiology 230*: 720–726.

Kostakoglu, L., Agress, H., and Goldsmith, J. 2003. Clinical role of FDG PET in evaluation of cancer patients. *Radiographics 23*: 315–340.

Kuhl, C.K., Mielcareck, P., Klaschik, S., Leutner, C., Wardelman, E., Gieseke, J., and Schild, H.H. 1999. Dynamic breast MR imaging: are signal intensity time course data useful for differential diagnosis of enhancing lesions? *Radiology 211*: 101–110.

Lin, W.C., Hung, Y.C., Yeh, L.S., Kao, C.H., Yen, R.F., and Shen, Y.Y. 2003. Usefulness of [18]F-fluorodeoxyglucose positron emission tomography to detect para-aortic lymph nodal metastasis in advanced cervical cancer with negative computed tomography findings. *Gynecol. Oncol. 89*: 73–76.

Low, R.N., Duggan, B., Barone, R.M., Saleh, F., and Song, S.Y.T. 2005. Treated ovarian cancer: MR imaging, laparotomy reassessment and serum CA-125 values compared with clinical outcome at 1 year. *Radiology 235*: 918–926.

Lowe, V., Dunphy, F., Varvares, M., Kim, H., Wittry, M., Dunphy, C.H., Dunleavy, T., McDonough, E., Minster, J., Fletcher, J.W., and Boyd, J.H. 1997. Evaluation of chemotherapy response in patients with advanced head and neck cancer using [F-18] fluorodeoxyglucose positron emission tomography. *Head Neck 19*: 666–674.

MacManus, M.P., Hicks, R.J., Matthews, J.P., Wirth, A., Rischin, D., and Ball, D.L. 2005. Metabolic (FDG-PET) response after radical radiotherapy/chemoradiotherapy for non-small cell lung cancer correlates with patterns of failure. *Lung Cancer 49*: 95–108.

Nahas, Z., Goldenberg, D., Fakhry, C., Ewertz, M., Zeiger, M., Ladenson, P.W., Wahl, R., and Tufano, R.P. 2005. The role of positron emission tomography/computed tomography in the management of recurrent papillary thyroid carcinoma. *Laryngoscope 115*: 237–243.

National Cancer Institute: Common Cancer Types. 2006. Washington. Accessed online at: www.cancer.gov/cancertopics/commoncancers. Last accessed 29 Oct 2006.

Pannu, H.K., Bristow, R.E., Montz, F.J., and Fishman, E.K. 2003. Multidetector CT of peritoneal carcinomatosis from ovarian cancer. *Radiographics 23*: 681–701.

Pannu, H.K., Bristow, R.E., Cohade, C., Fishman, E.K., and Wahl, R.L. 2004. PET-CT in recurrent ovarian cancer: initial observations. *Radiographics 24*: 209–223.

Provenzale, J.M., Mukundan, S., and Barboriak, D.P. 2006. Diffusion-weighted and perfusion MR imaging for brain tumor characterization and assessment of treatment response. *Radiology 239*: 632–649.

Roberts, K.B., MacManus, M.P., and Hicks, R.J. 2005. PET imaging for suspected residual tumour

or thoracic recurrence of non-small cell lung cancer after pneumonectomy. *Lung Cancer 47*: 49–57.

Saga, T., Higashi, T., Ishimori, T., Mamede, M., Nakamoto, Y., Mukai, T., Fujita, T., Togashi, K., Yura, S., Higuchi, T., Kita, M., Fujii, S., and Konishi, J. 2003. Clinical value of FDG-PET in the follow up of post-operative patients with endometrial cancer. *Ann. Nucl. Med. 17*: 197–203.

Schaefer, N.G., Hany, T.F., Taverne, C., Seifert, B., Stumpe, K.D.M., von Schulthess, G.K., and Goerres, G.W. 2004. Non-Hodgkin Lymphoma and Hodgkin Disease: Coregistered FDG-PET and CT at stagging and Ristaging: Do we need contrast-enhanced CT? *Radiology 232*: 823–829.

Schmid, D.T., John, H., Zweiful, R., Cservenyak, T., Westera, G., Goerres, G.W., von Schulthess, G.K., and Hany, T.F. 2005. Fluorocholine PET/CT in patients with prostate cancer: initial experience. *Radiology 235*: 623–628.

Schoder, H., Yeung, H.W.D., Gonen, M., Kraus, D., and Larson, S.M. 2004. Head and neck cancer: clinical usefulness and accuracy of PET/CT image fusion. *Radiology 231*: 65–72.

Seddon, B.M., and Workman, P. 2003. The role of functional and molecular imaging in cancer drug discovery and development. *Brit. J. Radiol. 76*: S128–38.

Sironi, S., Messa, C., Mangili, G., Zangheri, B., Aletti, G., Garavaglia, E., Vigano, R., Picchio, M., Taccagni, G., Del Maschio, A., and Fazio, F. 2004. Integrated FDG PET-CT in patients with persistent ovarian cancer: correlation with histologic findings. *Radiology 233*: 433–440.

Spaepen, K., Stroobants, S., Dupont, P., van Steenweghen, S., Thomas, J., Vandenberghe, P., Vanuytsel, L., Bormans, G., Balzarini, J., deWolf-Peeters, C., Mortelmans, L., and Verhoef, G. 2001. Prognostic value of positron emission tomography (PET) with fluorine-18 fluorodeoxyglucose ([18F]FDG) after first-line chemotherapy in non-Hodgkin's lymphoma: is [18F]FDG-PET a valid alternative to conventional diagnostic methods? *J. Clin. Oncol. 19*: 414–419.

Stewart, B.W., and Kleihuer, P. 2003.World Cancer Report. World Health Organisation. *International Agency for Research on Cancer*.

Subhas, N., Patel, P.V., Pannu, H.K., Jacene, H.A., Fishman, E.K., and Wahl, R.L. 2005. Imaging of pelvic malignancies with in-line FDG PET-CT: case examples and common pitfalls of FDG PET. *Radiographics 25*: 1031–1043.

van Laarhoven, H.W.M., de Guis-Oei, L-F., Wiering, B., Lok, J., Rijpkema, M., Kaanders, J.H.A.M., Krabbe, P.F.M., Ruers, T., Punt, C.J.A., van der Kogel, A.J., Oyen, W.J.G., and Heerschap, A. 2005. Gadopentate dimeglumine and FDG uptake in liver metastases of colorectal carcinoma determined with MR imaging and PET. *Radiology 237*: 181–188.

van Overhagen, H., Brakel, K., Heijenbok, M.W., van Kasteran, J.H.L.M., van de Moosdijk, C.N.F., Roldaan, A.C., van Gils, A.P., and Hansen, B.E. 2004. Metastases in supraclavicular lymph nodes in lung cancer: assessment with palpation US and CT. *Radiology 232*: 75–80.

von Schulthess, G.K., Steinert, H.C., and Hany, T.I. 2006. Integrated PET/CT: current applications and future directions. *Radiology 238*: 405–422.

Westerterp, M., von Westreenen, H.L., Reitsma, J.B., Hoekstra, O.S., Stoker, J., Fockens, P., Jager, P.L., Van Eck-Smit, B.L.F., Plukker, J.T.M., van Lanschott, J.J.B., and Sloof, G.W. 2005. Esophageal cancer: CT, endoscopic US, and FDG PET for assessment of response to neoadjuvant therapy-systematic review. *Radiology 236*: 841–851.

Wong, R.J., Lin, D.T., Schoder, H., Patel, S.G., Gronen, M., Wolden, S., Pfister, D.G., Shah, J.P., Larson, S.M., and Kraus, D.H. 2002. Diagnostic and prognostic value of ([18]F) fluorodeoxyglucose positron emission tomography for recurrent head and neck squamous cell carcinoma. *J. Clin. Oncol. 20*: 4199–4208.

Wong, T.Z., Jones, E.L., and Coleman, R.E. 2004. Positron emission tomography with 2-deoxy-2-[18F]fluoro-D-glucose for evaluating local and distant disease in patients with cervical cancer. *Mol. Imaging Biol. 6*: 55–62.

Wong-You-Cheong, J.J., Woodward, P.J., Manning, M.A., and Sesterhenm, I.A. 2006. Neoplasms of the urinary bladder: radiologic pathologic correlation. *Radiographics 26*: 553–580.

Yeh, L.S., Hung, Y.C., Shen, Y.Y., Kao, C.H., Lin, C.C., and Lee, C.C. 2002. Detecting para-aortic lymph nodal metastasis by positron emission tomography of 18F-fluorodeoxyglucose in advanced cervical cancer with negative magnetic resonance imaging findings. *Oncol. Rep. 9*: 1289–1292.

3
Tumor Gene Therapy: Magnetic Resonance Imaging and Magnetic Resonance Spectroscopy

Mikko I. Kettunen and Olli H.J. Gröhn

INTRODUCTION

Tumor gene therapy is rapidly approaching the stage where it is tested in clinical settings. To gain the full potential of therapy and minimize patient suffering, one has to be able to assess the efficacy of therapy as early as possible. Imaging methods that can assess early treatment response are critical in achieving this goal. Modern imaging technologies such as positron emission tomography (PET), single photon emission computed tomography (SPECT), computed tomography (CT), ultrasound, optical imaging, and nuclear magnetic resonance (NMR) offer a range of methods to assess different stages of therapy from transgene delivery to the final tumor eradication (Shah *et al*., 2004). This chapter focuses on the use of magnetic resonance imaging (MRI) and magnetic resonance spectroscopy (MRS) for the assessment of individual steps in gene therapy process in tumors. It should be noted, that several recent reviews have also covered molecular imaging of tumor gene therapy (Bhakoo *et al*., 2004; Kettunen and Gröhn, 2005; Massoud and Gambhir, 2003; Shah *et al*., 2004).

TUMOR GENE THERAPY

While a thorough review of the current state of tumor gene therapy is beyond the scope of this chapter (for more details see for example (Lawler *et al*., 2006)), a brief summary of the subject is given from a point of view of diagnostic imaging. Tumor gene therapy models are often used to target gliomas and other brain tumors. Several factors make gliomas good models for experimental therapy. While gliomas are usually very malignant with poor prognosis, they rarely metastasize and usually form relatively stable, albeit heterogenous, tumors that are amenable to surgical resection. This makes the application of transgene carriers more straightforward (Lawler *et al*., 2006). Tumor gene therapies usually target cells that undergo active cell division. The cells in brain tissue have very low regeneration rates so the normal tissue is only slightly susceptible to its effects.

Several potential targets for transgenes have been tested. These include transgenes that make tumors more sensitive to prodrugs, alter their cell cycle regulation, stimulate the immune response, or inhibit the formation of vasculature through angiogenesis. All these approaches have

shown variable success both alone and in combination with different therapies. The most used approaches have been based on "suicide genes" that convert prodrug into cytotoxic forms. Examples of such systems include herpes simplex virus thymidine kinase/ganciclovir (HSV-TK/GCV) and cytosine deaminase/5-fluorocytosine (CD/5-FC). As the selected transgene is not present in normal tissue, the therapy affects transfected tumor cells only.

Successful tumor gene therapy strategy requires several crucial steps that could benefit from imaging. Firstly, the transgene needs to be delivered to tumor tissue. In gliomas, gene therapy approaches are usually used in combination with surgery, so the transgene carriers can be delivered directly to the remaining tumor tissue. Alternatively, systemic delivery of transgene could be used. Several potential carrier approaches have been tested so far, the most successful being viral-based (Lawler *et al.*, 2006). Both retrovirus and adenovirus have shown success in effectively transfecting tumor cells, yet their use requires careful study of possible side effects from the viral genome. Other systems include HSV, liposome based carriers and stem cells. Secondly, expression of transgene and synthesis of the protein product is required. Thirdly, for suicide genes, this should lead to the conversion of the prodrug to the cytotoxic drug. Finally, the result of therapy is increased cell death in the tumor. A large part of therapy response is due to the "bystander" effect, where the actions of the transgene are spread to neighboring non-transfected cells. However, this can make therapy response potentially heterogeneous. Consequently, the follow-up studies should provide spatial information on tumor response. Most importantly, they should be able to reliably detect successful therapy response as early as possible to minimize patient morbidity due to inefficient therapy.

MAGNETIC RESONANCE IMAGING

Magnetic resonance imaging (MRI) has proven to be a powerful tool to non-invasively study anatomy, function and metabolism with high spatial resolution (less than 100 μm in experimental settings) and relatively high temporal resolution, which makes it a useful method to follow the effects of gene therapy. In the following, the basic ideas and concepts of MRI contrasts and MRS are briefly summarized. The applications of these methods to gene therapy are then described in the remaining chapter.

Magnetic resonance imaging is based on principles of nuclear magnetic resonance (NMR), and it exploits magnetic properties of certain nuclei (most typically that of a proton, ^{1}H, but other nuclei with non-zero spin quantum number can also be used, these nuclei are often called 'spins'). In the presence of external magnetic field, the spins align themselves in discrete orientations relative to the external field. These orientations have different energy states with an energy difference that depends on the external magnetic field strengths (for proton and other spin-1/2 nuclei, this gives rise to two energy states). As in all equilibrium systems in nature, slight excess of spins choose to be in the lower energy state, creating small net magnetization in the sample or tissue containing ^{1}H. MR signal is detected after

applying a radio frequency (RF) pulse, which disturbs the equilibrium state of nuclei by inducing changes in populations between their energy states. Following the pulse, spins return to their equilibrium state through so-called relaxation processes. During this time, they emit energy, which can be detected with a receiver coil. As the energy difference and subsequently frequency of the NMR signal are dependent on external magnetic field, signal can be localized using additional magnetic field gradients. Because of the frequency range used (MHz), MR methods have excellent tissue penetration, and are not significantly limited by the amount of radiation that can be safely administered. On the other hand, the difference between energy states is small leading to very small population difference between energy states and small net magnetization, which renders MR methods inherently insensitive as compared to many other imaging methods. This means that molecules present at millimolar concentrations and with a molecular weight of tens of kiloDalton can be detected using proton MR, and the concentration limit is even higher for other nuclei. Fortunately, MRI signal most often originates from hydrogen in water, the great abundance of which in tissue easily compensates the inherent insensitivity of the method making the modern MRI a high signal-to-noise approach capable of rapidly providing high-resolution data from living systems.

Endogenous Magnetic Resonance Imaging Contrast

The appearance of MRI signal depends on the way tissue water interacts with macromolecules as it moves around. These interactions affect the relaxation properties of water. Relaxation occurs through two major pathways, longitudinal and transversal, the time courses of which are described by T_1 and T_2 relaxation times, respectively. The longitudinal relaxation involves exchange of energy between the excited spin and its surroundings, usually called the "lattice". This leads to return of the original equilibrium state where net magnetization is lying along the main magnetic field. T_1 relaxation in tissue is induced by magnetic fluctuations at the resonance frequency of the hydrogen, which is in Megahertz range. These fluctuations are created by other rapidly rotating molecules with magnetic properties, mostly other "free" or slightly hydrogen bonded water molecules. The transversal relaxation is caused be locally changing magnetic fluctuations that are slow if compared to ones that induce T_1 relaxation (MHz), still rapid if compared to MRI measurement time scale (Hz-kHz). These are typically associated with interactions between water and macromolecular pool in the tissue, and lead individual spins to end up with different phases (so-called dephasing or loss of phase coherence) creating smaller detectable magnetization. In addition, T_2 relaxation is sensitive to many apparent relaxation effects arising from diffusion and exchange of hydrogen atoms between sites of different magnetic susceptibilities or chemical shifts in the pulse sequence and magnetic field strength-dependent manner.

Processes similar to longitudinal relaxation can also occur along the RF field that is rotating perpendicular to the main field. In this case, the excited spins are effectively locked together in transverse plane so the contrast is called spin-lock contrast

and is mainly governed by $T_{1\rho}$ relaxation time, or T_1 in the rotating time. The used spin-lock fields are in the order of 100 μT (kHz range), so $T_{1\rho}$ is therefore expected to be sensitive to low-frequency interactions between water and macromolecules and can be modulated by changing the spin-lock amplitude. Transverse relaxation also occurs in the rotating frame, $T_{2\rho}$, with different sensitivity to some dynamic phenomena such as exchange.

All relaxation pathways are sensitive to tissue water content and the water environment, which influence the rotational mobility of the molecules. The latter is more pronounced for relaxation times that are sensitive to low-frequency interactions, i.e., T_2, $T_{2\rho,}$ and $T_{1\rho}$. Low-frequency processes such as dipolar interactions of slowly tumbling molecules and proton exchange between water and macromolecules are of particular interest since they are more sensitive to alterations in cellular protein pools, which are expected to undergo changes, for example, during cell-death processes.

In addition to direct relaxation contrast, MRI also offers other endogenous contrasts. Probably the most important of these is based on the diffusion, or Brownian motion, of water. While diffusion plays an important role in the relaxation processes described above, the sensitivity to it can be further increased by applying a pair of strong magnetic field gradients. These amplify the effect of movement on the loss of phase coherence of the excited spins. Apparent diffusivity (termed apparent diffusion coefficient, ADC) of the molecules can be quantified by varying the amplitude of the diffusion gradients as well as the delay between them leading to different levels of diffusion weighting described often by so-called 'b-value'. Further information can be obtained through analysis of diffusion in different directions (anisotropy) using diffusion tensor analysis. *In vivo* diffusion is complicated due to cell organelles, semi-permeable cell membranes and other structures causing restrictions in the diffusion. Magnetic resonance imaging offers a powerful tool to the non-invasive study of the size of these restricting structures.

Another potentially interesting source of endogenous MRI contrast is based on chemical exchange saturation transfer (CEST) of magnetization (Zhou and van Zijl, 2006). This is based on the fact that exchangeable protons in the surface, for example, of macromolecules interact with water molecules, which leads to alterations in the water signal intensity when they are excited. Recently suggested amide proton transfer (APT) contrast is one example of such contrasts, and is based on exchange of water protons with amide protons in mobile proteins. The contrast is expected to be sensitive to changes in pH and the amount of amide groups in the tissue.

From an experimental point of view, the possibility of obtaining several different forms of endogenous contrast by simply altering the imaging parameters in a single imaging session allow flexible imaging possibilities. Conversely, endogenous contrasts are usually affected by a host of different processes, so the interpretation of the observed changes in biological terms can be difficult particularly *in vivo*.

Exogenous Contrast Agents

Magnetic resonance imaging contrast can also be generated with the aid of exogenous contrast agents. Recent advantages in molecular biology have also allowed

new MR contrast agents to be aimed towards specific cellular targets. Two major classes of contrast agents are used, the first enhancing T_1 relaxation and the other T_2 relaxation. The contrast agents in the first class are usually based on paramagnetic Gd^{3+}-chelates that increase the longitudinal relaxation rates (Aime *et al*., 2002). The reduction in T_1 relaxation times can be detected as bright regions on T_1-weighted images. While relatively small in molecule size and therefore more efficient at penetrating the tissue, Gd-based contrast agents usually have relatively low sensitivity due to their low relaxitivies (for example, Gd-DTPA has relaxivity of approximately $4\,s^{-1}mM^{-1}$). The local contrast agent concentration needed for MRI has been estimated to be 10^{-3}–10^{-5} M (Massoud and Gambhir, 2003), that is, several orders of magnitude higher than for example detection limit of radionuclei in PET (10^{-11}–10^{-12} M). The problem can be partially solved by creating molecules that can carry larger Gd-loads (Aime *et al*., 2002). The increased relaxivity is due to both the increased number of Gd and improved relaxation properties of the larger molecule size. Still, the use of these contrast agents is limited by the relatively high concentration needed to be present. A further limitation of Gd-based contrast agents is that the move to higher main magnetic fields usually leads to a degradation of their relaxitivity. It should be noted, that Gd^{3+} and other lanthanides can also be used as CEST-based contrast agents (Zhou and van Zijl, 2006), and the performance of CEST-agents is expected to improve with increasing magnetic fields.

The sensitivity is slightly less of a problem with the second class of contrast agents that are usually based around iron oxide particles (Modo *et al*., 2005). These create local microscopic distortions in the magnetic fields, which lead to significant reductions in T_2 relaxation times manifested as dark regions on T_2-weighted images. However, the use of iron oxide based contrast agents is complicated by several facts. Several effects can lead to signal dropouts and dark regions in T_2-weighted images, and identification of the contrast agent from other effects is not always straightforward. An additional challenge with iron oxide based contrast agents is that one cannot easily change the size of the relaxation effect, so it is difficult to create molecules that could, for example, show response to enzyme-activation. The greatest limitation of T_2-based contrast agents is their relatively large size (tens of nanometers to micrometers), which can severely limit their tissue penetration. In general, the problem with all exogenous contrast agents is the estimation of the molecule distribution *in vivo*, which can greatly affect the interpretation of the results.

MAGNETIC RESONANCE SPECTROSCOPY

Unlike most other imaging methods, that cannot easily separate between different marker molecules, magnetic resonance spectroscopy (MRS) offers the possibility to non-invasively follow the metabolism of molecules of interest. This feature is based on the fact that the resonance frequency ("chemical shift") of MR-visible signal varies depending on the chemical structure of the molecule. The appearance of new peaks or shift of peaks can be directly used to follow the metabolism. MR spectra can

therefore reveal the metabolism through the patterns of peaks present and detect a range of metabolites in a single scan. In addition to protons, other nuclei (e.g., ^{13}C, ^{19}F, ^{31}P, ^{23}Na) can also be used to study metabolism either using endogenous metabolites or exogenous marker molecules. Furthermore, MRS can be extended to reveal spatial distribution of metabolites through MRSI approaches.

The chemical shift range can vary from tens to hundreds of part-per-millions of the main magnetic field (ppm) for different nuclei. From a practical point of view, it is unfortunate that the most sensitive nucleus, ^{1}H, has a narrow chemical shift range of approximately 10 ppm. This leads to significant overlap of the peaks from different metabolites, making the analysis complex. Another technical challenge for ^{1}H MRS is the dominant water signal that needs to be suppressed while minimally disturbing the other metabolites. Both of these are dependent on magnetic field homogeneity, and can therefore be problematic for *in vivo* approaches where lower spectral resolution is usually achieved. Recent developments in automatic shimming techniques and onset of new high field magnets have greatly improved the spectral quality. For other nuclei the situation with spectral overlap is less problematic as chemical shift ranges are broader. However, the most serious limitation of all MRS methodologies is their relative insensitivity due to low polarization levels at currently used magnetic fields. While ^{1}H and ^{31}P MRS is feasible *in vivo* without exogenous contrast agents, for most other nuclei, specifically labeled compounds are needed. It should be noted that in some cases this could make the detection easier because there is less background signal, particularly in the case of ^{19}F spectroscopy. Despite the high relative sensitivity and natural abundance of ^{19}F, there is very little naturally occurring NMR-visible fluorine *in vivo*, which allows the detection of ^{19}F labeled compounds with virtually no background. Low signal levels make MRS relatively slow, especially for MRSI applications. This severely limits the spatial resolution achieved, which can lead to blurring of signal and contamination of signal between voxels. For example, in ^{1}H studies of brain gliomas, contamination from subcutaneous lipid signals can dominate the spectra completely and needs to be suppressed during spectroscopy.

DETECTION OF TRANSGENE DELIVERY AND EXPRESSION USING MAGNETIC RESONANCE IMAGING AND SPECTROSCOPY

The first step of a successful gene therapy approach is the delivery and transfection of a transgene into the target tissue. Direct imaging of both of these targets is very challenging due to the low concentration and high molecular weight of a transgene and its transcription products. However, several proof-of-principle works have shown that in some cases it is possible to image transgene carriers mostly for nonviral systems (for more details see for example Bhakoo *et al*., 2004; Kettunen and Gröhn, 2005). Recent progress in using stem cells as transgene carriers is of particular interest because MR labeling of cells is becoming a routine experimental tool (Modo *et al*., 2005). Iron oxide beads measuring up to a micron in size can be

used to label the cells, and in some cases it is already possible to detect single cells *in vivo* (Heyn *et al*., 2006). However, in most practical situations higher concentration of cells is required. Interestingly, a recent study showed that ^{19}F-containing compounds could also be used to label cells, potentially improving the identification of labeled cells due to minimal background (Ahrens *et al*., 2005). Yet at the moment, no proven means to follow transgene delivery using MR methods is widely available. It should also be noted that as these methods usually target the carrier rather than DNA plasmid itself, these methods do not directly reveal DNA distribution and transfection efficacy.

Magnetic resonance imaging follow-up of transgene expression *in vitro* and *in vivo* has also been demonstrated. Because the direct detection of the transgene product is not usually possible, current MRI and MRS methods for transgene expression are mostly indirect using a reporter gene and a subsequently administered exogenous marker compound that is metabolized into MR-visible form. The aim is to encode the reporter gene at the same time as the actual transgene, so that the production of the MR-label corresponds to transgene expression. The reporter gene can encode for example an intracellular enzyme or cell-surface receptor. Recent studies show that one can target transgene activity using both T_1 and T_2 contrast agents that undergo conformational changes due to enzyme activation, and accumulate to the tissue due to increased uptake or target specific antigens on the cell surface (Kettunen and Gröhn, 2005).

The enzyme-activated contrast agents suffer from a major challenge of delivering the marker molecule to intracellular space in high concentrations. On the other hand, the accumulation of iron-containing molecules such as transferrin has shown success, and has already been applied to gene therapy (Ichikawa *et al*., 2002). Because all these approaches are based on proton MRI, one can get high-resolution images of enzyme activity. An interesting approach to detect β-galactosidase activity using ^{19}F-based compounds was recently demonstrated (Yu *et al*., 2006). In this approach, the changes in chemical shift reveal the enzyme activity. Finally, some interesting approaches based on the use of endogenous contrasts have recently been suggested. This circumvents the potential problem of the distribution of exogenous target molecules. The simplest approach would be to have the reporter gene encode an enzyme that is normally not present in the system so that the presence of metabolite will indicate the gene activity. The challenge of this approach is the identification of suitable metabolite. For example, the production of phosphocreatine (PCr) has been demonstrated in the liver (Li *et al*., 2005), yet its usefulness in the brain would be limited due to high endogenous PCr levels. Probably the most promising approach so far is based on the iron storage protein ferritin (Cohen *et al*., 2005; Genove *et al*., 2005). The system closely resembles that using transferrin, yet it can potentially harvest endogenous iron from the body and therefore does not need an external marker molecule. The use of APT contrast to detect transgene activity through production of a highly aminated endogenous marker protein has also been proposed (Gilad *et al*., 2007) although it could be technically very challenging *in vivo*.

The limitation of all reporter gene approaches is that in principle, transgene

activity can differ from the reporter gene. A more direct method would be to monitor conversion of the prodrug to a cytotoxic drug, which would give the indication of both the prodrug distribution and enzyme activity. Recent studies using CD/5-FC therapy model with the ^{19}F labeled 5-fluorocytosine have shown that such experiments are possible *in vivo* (Hamstra *et al*., 2004). The deamination of 5-FC to 5-fluorouracil and the production of cytotoxic fluorinated nucleotides can be followed using MRS where the appearance of the peaks gives an indication of enzyme activity within the tumor. In theory, one could create similar approaches for other prodrugs using ^{19}F, ^{13}C, or other MR-visible nuclei if suitable nuclei are present.

DETECTION OF GENE THERAPY RESPONSE USING MAGNETIC RESONANCE IMAGING AND SPECTROSCOPY

The end result of successful gene therapy is the death of remaining tumor cells. Cell death is manifested by a variety of different metabolic, cellular and structural alterations that can be potentially detected using MR methods. Cell death progresses through several different pathways, the most important ones are apoptosis and necrosis. The hallmarks of apoptosis include caspase activation, cell shrinkage and a concomitant increase of the extracellular space, and membrane blebbing into apoptotic bodies. Finally macrophages and the neighboring cells remove the apoptotic cells without inflammatory reaction. In contrast, necrosis usually leads to cell swelling and inflammation. Both of these processes offer several targets for MR approaches (Kettunen and Brindle, 2005).

Volumetric Imaging

The simplest and most widely used MRI approach for response follow-up is the measurement of the tumor volume from multi-slice images. High spatial resolution and versatile contrast offered by MRI usually allow a clear delineation of tumor borders. The contrast can be further enhanced with Gd-based contrast agents. While easy to perform and giving quantitative volume information, the tumor mass is usually slow to respond to therapy, so volumetric approaches often cannot be used to give an early indication of successful therapy.

Endogenous Contrasts

Diffusion-weighted MRI is the most promising MRI approach for the early detection of gene therapy induced cell-death. The apparent diffusion coefficient increases shortly after the start of tumor therapy and often precedes the changes in volume (Ross *et al*., 2003). Similar changes have been observed in a number of therapy models, and in fact it appears that the increase in apparent diffusion is a relatively universal marker of successful cell-death inducing therapy. Both the HSV-TK/GCV (Valonen *et al*., 2004) (Figure 3.1) and the CD/5-FC (Hamstra *et al*., 2004) gene therapy models show increased diffusion during successful therapy. Recently, diffusion-MRI was combined with ^{19}F-MRS detection of 5-FC conversion to cytotoxic drug, providing a comprehensive MRI diagnosis system for gene therapy studies using CD/5-FC model (Hamstra *et al*., 2004). The amplitude of diffusion appears to

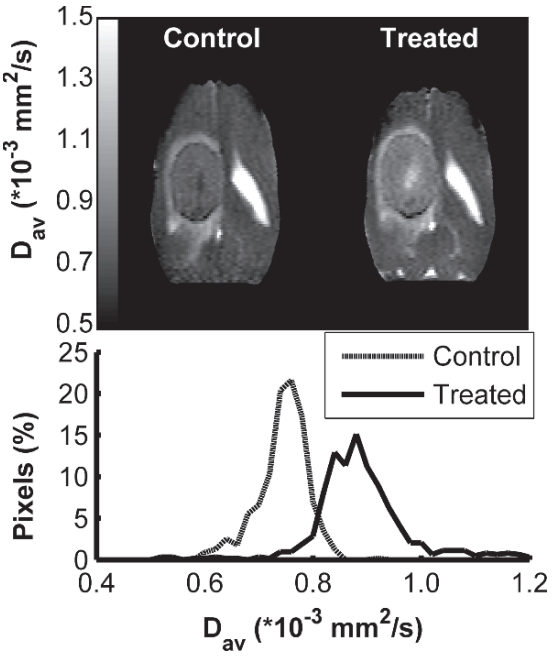

FIGURE 3.1. Diffusion-weighted MRI is a sensitive marker for gene therapy induced cell death as seen in HSV-tk model in BT4C rat gliomas. Four days after the start of ganciclovir therapy, apparent diffusion coefficient (1/3 of the trace of the diffusion tensor, D_{av}) has increased due to loss of cells and increased extracellular space; thus, indicating successful therapy. Diffusion-MRI also allows the detection of spatially heterogeneous therapy response. Changes induced by the treatment are best seen in the histogram analysis of tumor pixels shown in the panel below the diffusion maps. (Data obtained by Alexandra Sierra, at the University of Kuopio, Finland)

correlate with the therapy success, although further work is needed to establish the connection move clearly and to estimate its usefulness for diagnosis (Rehemtulla *et al*., 2002; Valonen *et al*., 2004). This is important since high-resolution diffusion MRI could be used to reveal the heterogenous response of tumor tissue and identify regions where further therapy is needed. The increase in diffusion is associated with reduced cellularity and an increase in the extracellular space (Ross *et al*., 2003). Further details on diffusion restrictions may be obtained using diffusion tensors, higher b-values and more sophisticated data analysis, or through the diffusion of intracellular metabolites.

Diffusion-MRI is already widely used in the clinics for the diagnosis of cerebral ischemia, so its implementation for tumor studies should not be technically challenging. In fact, diffusion-MRI has already been applied in patients receiving therapy (Ross *et al*., 2003). However, there are some limitations for its use. The biggest challenge for diffusion imaging is its sensitivity to motion artifacts due to the strong magnetic field gradients needed. While generally not a problem in the brain, it can limit the use of diffusion-MRI in other tumors. Unlike in stroke diagnosis, where diffusion-weighted images can be used to reveal the extent of ischemia, the measurement of apparent diffusion coefficient is usually needed for tumor therapy follow-up. This makes the approach slightly slower as several images need to be acquired. Furthermore, the normal value of diffusion coefficient can vary slightly from one tumor model to another and needs to be assessed on a tumor-by-tumor basis.

Other endogenous MRI contrast methods have not proven as successful in the detection of early therapy response as both T_1 and T_2 relaxation times usually show relatively modest changes that occur close to the time point when tumors have already started to shrink (Hakumäki *et al*., 2002). Furthermore, the use of quantitative relaxation values is slightly complicated by the fact that relaxation times depend on the strength of the main magnetic field. $T_{1\rho}$ relaxation time appears more promising as reported $T_{1\rho}$ increases resemble diffusion in their time course and precede those seen

in T_2 and T_1 (Gröhn *et al*., 2003; Hakumäki *et al*., 2002). While the mechanism for these early changes is still unknown, it is likely to resemble those affecting diffusion. The biggest limitations for spin-lock contrasts are the potential problems with heating caused by long RF pulses and the lack of pulse sequences in clinical environment. Interestingly, (Gröhn *et al*., 2003) recently reported that Carr-Purcell T_2 using adiabatic RF pulses, which is conceptually close to spin-lock experiment, showed similar early changes, and could potentially circumvent some of these problems by reducing the used RF power. The pulse sequences required are also not currently widely available, although the implementation of the pulse sequences into clinical scanners is possible. The usefulness of endogenous contrast is slightly limited by their non-specificity. A range of different processes can influence the contrast and correlating them with biological alterations is not always straightforward. This does not, however, mean that they could not be used as surrogate markers for successful therapy.

Sodium Magnetic Resonance Imaging

An interesting approach to detect cell death through sodium (^{23}Na) MRI has recently gained interest as increased sodium signals have been observed during tumor chemotherapy (Schepkin *et al*., 2006). The increase in signal is likely to reflect the alteration of sodium distribution between extra- and intracellular spaces, possibly due to loss of function of cell membrane ion channels and/or destruction of cellular membranes. The time course of the increased sodium signal in a drug-treated tumor is very similar to the changes observed in water diffusion suggesting that it would be an early marker for therapy (Schepkin *et al*., 2006). Sodium imaging could be potentially transferable to clinical settings if the issues with low sensitivity can be solved.

Molecular Imaging

More specific detection of cell death could be achieved using exogenous contrast agents targeted against specific markers of cell death. Such targets could, for example, be intracellular enzyme activities or alterations in the cell surface (Kettunen and Brindle, 2005). For the former, molecules sensitive to caspase and other protease activity would be particularly interesting. The use of these approaches is currently limited by similar problems as with detection of transgene activation, namely low sensitivity and problems with the internalization of marker molecules. A more viable target is the detection of alterations of cell surface composition. A particularly interesting target is externalized phosphatidylserine that is commonly associated with apoptotic cell death (Corsten *et al*., 2006). In healthy cells, phosphatidylserine is present predominantly on the inner leaflet of the plasma membrane. Upon cell death it may be transferred to the cell surface, so neighboring macrophages will phagocytose the dying cell. Annexin V and other similar molecules can be used to target phosphatidylserine, and they have been successfully used to detect cell death using several different imaging methods including MRI. Similarly, one could target reduced angiogenesis in the responding tumor either using targeted contrast agents or more straightforward angiography or perfusion MRI experiments.

However, the development of specifically targeted MR contrast agents has been relatively slow. The reasons for this are partially due to problems of identifying specific cellular targets, but the biggest limitation is the afore-mentioned low sensitivity of MR contrast agents. On the other hand, the approaches to improve the sensitivity are likely to lead to increased molecule size and non-specificity, so the creation of MR contrast agents is a balance between molecule size, specificity, and sensitivity. It may not therefore be surprising that none of the other proof-of-principle works have been tested in gene therapy models.

Magnetic Resonance Spectroscopy of Metabolic Alterations

Cellular metabolism can be significantly affected by cell death. Detection of altered metabolism forms the basis of the use of ^{18}F-fluorodeoxyglucose (FDG) uptake as PET marker to cell death (Jacobs *et al.*, 2002). The possibility of detecting several metabolites allows similar studies using MRS, albeit with much lower sensitivity. Energy metabolism can be studied directly using either phosphorus (^{31}P) or carbon (^{13}C) MRS (Gillies and Morse, 2005). The former detects alterations in adenosinetriphosphate (ATP) and free phosphate levels, which can be used as a marker for cell death. Additionally, ^{31}P can give an indication of cellular acidity. The latter approach can be used to follow the fate of ^{13}C-labeled molecules, such as (1-^{13}C)-glucose, as they are metabolized in the cell (Gruetter *et al.*, 2003). This could allow the direct detection of compromised metabolism, although the use of carbon is severely limited due to its low sensitivity. Interestingly, recent developments in the use of hyperpolarized marker molecules (Ardenkjaer-Larsen *et al.*, 2003) could significantly improve the sensitivity of ^{13}C detection, yet currently the usefulness of this approach is still unknown. Employing these direct markers of energy metabolism is limited, because energy metabolism may not always be disturbed by early events of cell death, and the high background from healthy cells may hide the therapy response. The latter is particularly a problem due to low spatial resolution achievable. From this point of view it is not surprising that no universal, *in vivo* compatible marker for cell death has yet been identified using ^{31}P and ^{13}C MRS.

A potentially more viable approach is to use ^{1}H spectroscopy to follow alterations in lipid metabolism. Lipids in tissue are largely found in cellular membranes, which renders their resonances nearly invisible in normal ^{1}H spectra. For example, although brain tissue contains relatively high levels of lipids, one does not detect large lipid resonances from brain tissue. However, a secondary pool of more mobile lipids can be detected using MRS. Tumors often exhibit high levels of mobile lipids that produce several prominent signals on spectra. Most important of these are methylene (1.3 ppm, -$CH_2C\mathbf{H_2}CH_2$-) and methyl (0.9 ppm, -$CH_2C\mathbf{H_3}$) signals as well as those from polyunsaturated fats at 2.8 ppm (=CHC$\mathbf{H_2}$CH=) and 5.4 ppm (-C**H**=C**H**-) (Figure 3.2). Importantly, increases in several of these resonances have been observed following successful therapy in tumors (Kettunen and Brindle, 2005). Increased signal intensities in the 0.9–1.3 ppm region have been reported in HSV-tk gene therapy model of 9 L gliosarcoma and BT4C gliomas. The studies in the

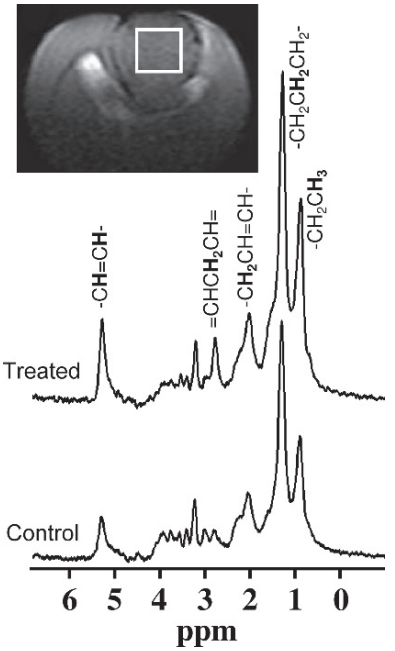

FIGURE 3.2. Magnetic Resonance Spectroscopy (MRS) data obtained from a localized voxel inside the tumor before and after 8 days of HSV-tk mediated gene therapy. Significant increase both in saturated (-$CH_2C\mathbf{H_2}CH_2$-, -$CH_2C\mathbf{H_3}$) and unsaturated (-$C\mathbf{H_2}CH$=CH-, =CHC$\mathbf{H_2}$CH=, -C**H**=C**H**-) lipid signal are typically detected during the apoptotic response to the treatment. Data are obtained using short echo time STEAM-type pulse sequence and spectra are shown with exponential filtering of 5 Hz. (Data obtained by Kimmo Lehtimäki and Timo Liimatainen, University of Kuopio, Finland)

latter model also reported the appearance of prominent signals from polyunsaturated fatty acids due to therapy. The accumulation of these lipids appears to occur in the early stage of therapy. Polyunsaturated fats in particular are interesting since their appearance in BT4C gliomas appears to correlate with the presence of apoptosis, and could therefore provide more detailed information on therapy response. Furthermore, MRS approaches can be extended to assess spatial distribution of lipids so the heterogeneity of response during therapy can be potentially studied.

Associated with lipid metabolism are the changes in choline-containing metabolites (choline, glycerophosphocholine, phosphocholine, as well as taurine and myo-inositol) that have a prominent resonance at 3.2 ppm (Gillies and Morse, 2005). These signals show alterations following therapy, but the low spectral resolution achievable *in vivo* does not allow the separation of different metabolites forming the signals, so its usefulness as a marker may be somewhat limited.

The appearance of lipid signals was initially associated with tiny microdomains located in cellular membranes. Further evidence suggests that the majority of the signal change reflects the accumulation of mobile lipids, mostly triacylglycerols and cholesterol esters, into larger lipid droplets (0.5–10 μm) in the cytosol and the extracellular space (Kettunen and Brindle, 2005). This view is supported by the histological evidence that shows a close association between the appearance of lipid droplets and lipid signals, as well as diffusion experiments, which suggest that the lipids are located in compartments with sizes very similar to lipid droplets. However, the mechanism of lipid accumulation is not yet fully understood. This accumulation could reflect increased catabolism of membrane lipids, decreased synthesis of membrane phospholipids, or increased uptake of extracellular lipids. Several studies suggest that increased phospholipase activation occurs during cell death. This will break membrane phospholipids, including those of mitochondria, to free fatty acids that can then be converted to triacylglycerols. Phospholipase A_2 activity in particular has been tentatively linked to increased lipid signals. On the other hand, inhibited synthesis of phosphatidylcholine, which is part

of the phospholipid synthesis pathway, has also been reported, suggesting that this route is likely to be affected by cell death leading to the accumulation of diacylglycerols and triacylglycerols. It is, therefore, conceivable that all pathways could contribute to the formation of lipid bodies, possibly in a cell line-dependent fashion.

Despite several appealing features, the wider applicability of lipid spectroscopy as a therapy marker may be limited by both biological and technical problems. Lipid metabolism is sensitive to various alterations in the cellular status, and the inherent lipids levels can vary significantly independently of cell death. Furthermore, an increase in lipid signals following therapy can be relatively modest compared to lipid signals initially present. This can make the accurate detection of cell death more difficult and so quantitative approaches are needed. A further problem arises from the limited spectral resolution, which leads to significant overlap of lipids and other metabolites, such as lactate at 1.3 ppm. The appearance of the 5.4 ppm lipid signal that would otherwise be the most promising marker may be similarly compromised by inefficient water suppression. This can be particularly problematic for MRSI approaches where homogeneous magnetic field over the whole volume is difficult to obtain. One also has to be careful to avoid the contamination of spectra with lipids outside of the tumor, particularly outside the brain. These may be present at much higher concentrations than those within the tumor, and can therefore dominate spectra unless these signals can be thoroughly suppressed. Finally, as with all other MRS approaches, lipid spectroscopy suffers from long acquisition times that can limit its use in clinical settings.

SUMMARY

The current state of MR approaches for detection of tumor gene therapy looks promising. While the imaging of transgene expression remains a challenging task for MR approaches and is probably better served by other imaging modalities such as PET, several MR approaches can improve the detection of successful therapy response. Diffusion-weighted MRI in particular with its combination of sensitivity to early therapy response with high spatial resolution is likely to prove to be useful for studies of heterogeneous therapy response. Importantly, previous experience with cerebral ischemia means that diffusion-MRI methodology is already available in clinical settings. For other endogenous contrasts, more work is required and especially novel relaxation-based contrasts may improve the situation in the future. The detection of altered lipid metabolism through ^{1}H-MRS remains a potential candidate for response marker. Particularly, its association with apoptosis makes it an interesting approach. High magnetic field systems (3T or more) are also becoming more common in clinical use, which will increase the importance of this kind of approach.

Current exogenous molecular imaging approaches suffer from the relatively low sensitivity of the current generation of MR contrast agents. This limits both the detection of initial transgene expression and cell death response. It is likely that further advances in molecular biology can identify more readily available targets and improve the sensitivity of contrast agents. However, the development of MRI based molecular imaging has been slow, and currently there are only a few readily available MRI approaches.

An attractive approach to partially avoid some of the problems with low sensitivity would be CEST-type contrast agents that allow the contrast to be turned on and off. This would allow better comparison between background and activated signal, which could be combined with more sophisticated data analysis methods.

Currently available MRI and MRS techniques already provide insights into several different aspects related to gene therapy process and treatment response. Future developments in the fields of engineering, NMR physics, molecular biology and contrast agent chemistry are likely to provide even more broad and detailed views into process taking place during gene therapy and will facilitate efficient, tailored treatment of the patients.

REFERENCES

Ahrens, E.T., Flores, R., Xu, H., and Morel, P.A. 2005. In vivo imaging platform for tracking immunotherapeutic cells. *Nat. Biotechnol. 23*: 983–987.

Aime, S., Cabella, C., Colombatto, S., Geninatti Crich, S., Gianolio, E., and Maggioni, F. 2002. Insights into the use of paramagnetic Gd(III) complexes in MR-molecular imaging investigations. *J. Magn. Reson. Imaging 16*: 394–406.

Ardenkjaer-Larsen, J.H., Fridlund, B., Gram, A., Hansson, G., Hansson, L., Lerche, M.H., Servin, R., Thaning, M., and Golman, K. 2003. Increase in signal-to-noise ratio of > 10,000 times in liquid-state NMR. *Proc. Natl. Acad. Sci. U.S.A. 100*: 10158–10163.

Bhakoo, K.K., Bell, J.D., Cox, I.J., and Taylor-Robinson, S.D. 2004. The application of magnetic resonance imaging and spectroscopy to gene therapy. *Methods Enzymol. 386*: 303–313.

Cohen, B., Dafni, H., Meir, G., Harmelin, A., and Neeman, M. 2005. Ferritin as an endogenous MRI reporter for noninvasive imaging of gene expression in C6 glioma tumors. *Neoplasia 7*: 109–117.

Corsten, M.F., Hofstra, L., Narula, J., and Reutelingsperger, C.P. 2006. Counting heads in the war against cancer: defining the role of annexin A5 imaging in cancer treatment and surveillance. *Cancer Res. 66*: 1255–1260.

Genove, G., Demarco, U., Xu, H., Goins, W.F., and Ahrens, E.T. 2005. A new transgene reporter for in vivo magnetic resonance imaging. *Nat. Med. 11*: 450–454.

Gilad, A.A., McMahon, M.T., Walczak, P., Winnard Jr., P.T., Raman, V., van Laarhoven, H.W., Skoglund, C.M., Bulte, J.W., and van Zijl, P.C.M. 2007. Artificial reporter gene providing MRI contrast based on proton exchange. *Nat. Biotechnol. 25*: 217–219.

Gillies, R.J., and Morse, D.L. 2005. In vivo magnetic resonance spectroscopy in cancer. *Annu. Rev. Biomed. Eng. 7*: 287–326.

Gröhn, O.H., Valonen, P.K., Lehtimäki, K.K., Väisänen, T.H., Kettunen, M.I., Ylä-Herttuala, S., Kauppinen, R.A., and Garwood, M. 2003. Novel magnetic resonance imaging contrasts for monitoring response to gene therapy in rat glioma. *Cancer Res. 63*: 7571–7574.

Gruetter, R., Adriany, G., Choi, I.Y., Henry, P.G., Lei, H., and Oz, G. 2003. Localized in vivo ^{13}C NMR spectroscopy of the brain. *NMR Biomed. 16*: 313–338.

Hakumäki, J.M., Gröhn, O.H., Tyynelä, K., Valonen, P., Ylä-Herttuala, S., and Kauppinen, R.A. 2002. Early gene therapy-induced apoptotic response in BT4C gliomas by magnetic resonance relaxation contrast T_1 in the rotating frame. *Cancer Gene Ther. 9*: 338–345.

Hamstra, D.A., Lee, K.C., Tychewicz, J.M., Schepkin, V.D., Moffat, B.A., Chen, M., Dornfeld, K.J., Lawrence, T.S., Chenevert, T.L., Ross, B.D., Gelovani, J.T., and Rehemtulla, A. 2004. The use of ^{19}F spectroscopy and diffusion-weighted MRI to evaluate differences in gene-dependent enzyme prodrug therapies. *Mol. Ther. 10*: 916–928.

Heyn, C., Ronald, J.A., Mackenzie, L.T., MacDonald, I.C., Chambers, A.F., Rutt, B.K., and Foster, P.J. 2006. In vivo magnetic resonance imaging of single cells in mouse brain with optical validation. *Magn. Reson. Med. 55*: 23–29.

Ichikawa, T., Hogemann, D., Saeki, Y., Tyminski, E., Terada, K., Weissleder, R., Chiocca, E.A., and Basilion, J.P. 2002. MRI of transgene expression: correlation to therapeutic gene expression. *Neoplasia 4*: 523–530.

Jacobs, A.H., Dittmar, C., Winkeler, A., Garlip, G., and Heiss, W.D. 2002. Molecular imaging of gliomas. *Mol. Imaging 1*: 309–335.

Kettunen, M.I., and Brindle, K.M. 2005. Apoptosis detection using magnetic resonance imaging

and spectroscopy. *Prog. Nucl. Mag. Res. Sp. 47*: 175–185.

Kettunen, M.I., and Gröhn, O.H. 2005. Tumour gene therapy monitoring using magnetic resonance imaging and spectroscopy. *Curr. Gene Ther. 5*: 685–696.

Lawler, S.E., Peruzzi, P.P., and Chiocca, E.A. 2006. Genetic strategies for brain tumor therapy. *Cancer Gene Ther. 13*: 225–233.

Li, Z., Qiao, H., Lebherz, C., Choi, S.R., Zhou, X., Gao, G., Kung, H.F., Rader, D.J., Wilson, J.M., Glickson, J.D., and Zhou, R. 2005. Creatine kinase, a magnetic resonance-detectable marker gene for quantification of liver-directed gene transfer. *Hum. Gene Ther. 16*: 1429–1438.

Massoud, T.F., and Gambhir, S.S. 2003. Molecular imaging in living subjects: seeing fundamental biological processes in a new light. *Genes Dev. 17*: 545–580.

Modo, M., Hoehn, M., and Bulte, J.W. 2005. Cellular MR imaging. *Mol. Imaging 4*: 143–164.

Rehemtulla, A., Hall, D.E., Stegman, L.D., Prasad, U., Chen, G., Bhojani, M.S., Chenevert, T.L., and Ross, B.D. 2002. Molecular imaging of gene expression and efficacy following adenoviral-mediated brain tumor gene therapy. *Mol. Imaging 1*: 43–55.

Ross, B.D., Moffat, B.A., Lawrence, T.S., Mukherji, S.K., Gebarski, S.S., Quint, D.J., Johnson, T.D., Junck, L., Robertson, P.L., Muraszko, K.M., Dong, Q., Meyer, C.R., Bland, P.H., McConville, P., Geng, H., Rehemtulla, A., and Chenevert, T.L. 2003. Evaluation of cancer therapy using diffusion magnetic resonance imaging. *Mol. Cancer Ther. 2*: 581–587.

Schepkin, V.D., Chenevert, T.L., Kuszpit, K., Lee, K.C., Meyer, C.R., Johnson, T.D., Rehemtulla, A., and Ross, B.D. 2006. Sodium and proton diffusion MRI as biomarkers for early therapeutic response in subcutaneous tumors. *Magn. Reson. Imaging 24*: 273–278.

Shah, K., Jacobs, A., Breakefield, X.O., and Weissleder, R. 2004. Molecular imaging of gene therapy for cancer. *Gene Ther. 11*: 1175–1187.

Valonen, P.K., Lehtimäki, K.K., Väisänen, T.H., Kettunen, M.I., Gröhn, O.H., Ylä-Herttuala, S., and Kauppinen, R.A. 2004. Water diffusion in a rat glioma during ganciclovir-thymidine kinase gene therapy-induced programmed cell death in vivo: correlation with cell density. *J. Magn. Reson. Imaging 19*: 389–396.

Yu, J., Liu, L., Kodibagkar, V.D., Cui, W., and Mason, R.P. 2006. Synthesis and evaluation of novel enhanced gene reporter molecules: detection of beta-galactosidase activity using ^{19}F NMR of trifluoromethylated aryl beta-D-galactopyranosides. *Bioorg. Med. Chem. 14*: 326–333.

Zhou, J., and van Zijl, P.C.M. 2006. Chemical exchange saturation transfer imaging and spectroscopy. *Prog. Nucl. Mag. Res. Sp. 48*: 109–136.

4
Assessment of Gene Transfer: Magnetic Resonance Imaging and Nuclear Medicine Techniques

Annette Altmann and Uwe Haberkorn

INTRODUCTION

The recent progress in basic science has delivered a better understanding of the mechanisms of carcinogenesis, tumor progression, and the patient's immune response towards the tumor. Moreover, the characterization of tumor cell-specific properties allows the design of new treatment modalities such as gene therapy, which circumvent resistance mechanisms towards conventional chemotherapeutic drugs. Currently, five different gene therapy approaches are being evaluated in experimental and clinical studies. These approaches are primarily based on the transduction of modulating or cytotoxic genes into tumor cells:

1. Improvement of the tumor-specific immune response by genetically modifiying tumor cells and/or tumor-infiltrating immune competent cells. The transduction of genes coding for immunogeneic determinants on the tumor cell surface may elicit an immune response leading to the elimination of genetically modified as well as of nonmodified tumor cells. If tumor-infiltrating lymphocytes or tumor cells are transduced by genes coding for cytokines, enhanced recruitment and activation of immune competent cells are expected due to elevated intratumoral cytokine concentrations.
2. Protection of non-malignant tissue such as the bone marrow from chemotherapeutic effects. This may be achieved by the transfer of a gene coding for the drug efflux pump glycoprotein p into bone marrow progenitor cells. The expression of glycoprotein p leads to a reduction of the intracellular concentration of chemotherapeutic drugs to lower nontoxic levels.
3. Reversion of the malignant phenotype, either by introducing tumor suppressor genes or by suppressing oncogene expression. The inactivation of oncoproteins can be achieved by using antisense oligonucleotides and ribozymes, or by transduction of genes coding for oncogene specific intracellular antibodies (intrabodies).
4. Direct killing of tumor cells by introducing cytotoxic or prodrug-activating genes (suicide genes, Table 4.1).
5. Induction of radioiodide uptake by transduction of the Na^+/I^- symporter (NIS) gene into tumor cells.

With regard to the clinical application of the gene therapeutic approaches, a tight control of both the spatial and temporal

TABLE 4.1. Suicide systems used for gene therapy.

Enzyme	Prodrug	Active drug
E. coli purine nucleoside phosphorylase (DeoD)	6-methylpurine-2′-deoxyribonucleoside	6-methylpurine
E. coli thymidine phosphorylase	5′-deoxy-5′-fluorouridine, tegafur	5-fluorouracil
E. coli guanosine-xanthine phosphoribosyltransferase (gpt)	6-thioxanthine, 6-thioguanine	6-thioxantine-MP, 6-thioguanine-MP
Xanthine oxidase	Xantine, hypoxanthine	H_2O, OH and O_2 radicals
Carboxypeptidase G2	Benzoic acid mustards-glumatic acid	Benzoic acid mustards
Alkaline phosphatase	Etoposide phosphate, doxorubicin phosphate, mitomycin phosphate	Etoposide, doxorubicin, mitomycin phenol mustard
Cassava linamarase	Linamarin	Aceto cyanohydrin, HCN
Carboxypeptidase A	Methotrexate-alanine	Methotrexate
Cytosine deaminase	5-Fluorocytosine (5FC)	5-Fluorouracil (5FU)
Cytosine deaminase + uracil phosphoribosyltransferase	5-Fluorocytosine	5-Fluorouracil + 5-fluorouridine-5′monophosphate
Penicillin amidase	Doxorubicin-phenoxyacetamide	Doxorubicin
	Melphalan-phenoxyacetamide	Melphalan
	Palytoxin-4	Palytoxin
	Hydroxyphenoxyacetamide	
ß-glucosidase	Amygdalin	Cyanide
ß-glucoronidase	Epirubicin-glucoronide, phenol mustard-glucuronide, daunomycin-glucoronide, adrimycin-glucoronide	Epirubicin, phenol mustard, daunomycin, adriamycin
ß-lactamase	Phenylenediamine mustard cephalosporin	Phenylenediamine mustard
E. coli Nitroreductase	CB1954 (5-aziridin 2,4-dinitrobenzamidine)	5-Aziridin 2,4-hydroxyamino 2-nitrobenzamidine
Cytochrome P450 2B1	Cyclophosphamide	Phosphoramide mustard
Rabbit hepatic carboxylesterase	Irinotecan	SN38 (7-ethyl-10-hydroxycamptothecin)
Human deoxycytidine kinase	Cytosine arabinoside (Ara C), fludarabine	Ara-CMP, fludarabine-MP
Dm-deoxyribonucleoside Kinase	Pyrimidine and purine analogs	Phosphorylated metabolites
HSV thymidine kinase	Ganciclovir (GCV), Aciclovir (AVC)	Phosphorylated metabolites
VZV thymidine kinase	6-methoxypurine arabinonucleoside (araM)	Phosphorylated metabolite

expression of the therapeutic transgene is required, and information concerning gene expression is necessary for therapy planning, and follow up studies in treated tumors and also for prognosis. Recent progress in molecular imaging (MI) techniques enables one to directly or indirectly monitor and record the spatiotemporal distribution of molecular or cellular processes for biochemical, biological, diagnostic, or therapeutic applications (Table 4.2). Based on the application of specific radioactive probes or contrast agents, either direct or indirect evaluation of gene expression is allowed. Direct evaluation is possible with, for example, ligands that directly bind to a specific target (e.g., receptor). Indirect evaluation may be achieved by using specific substrate probes for a target enzyme. By employing reporter genes for molecular imaging of gene expression in gene therapy, direct visualization may be achieved by optical detection of the respective gene product (e.g., green fluorescent protein). Indirect visualization is possible as a result of accumulation of an image probe because

TABLE 4.2. Genes and imaging methods used for the monitoring of successful gene transfer.

Gene	Principle	Imaging method	Tracer/contrast agent
Enzymes			
Cassava linamarase	Therapeutic effects	MRI	Ga-DTPA
CD	Therapeutic effects	MRI	Ga-DTPA
CD	Enzyme activity	MRS, PET	5-fluorocytosine
CD/uracil phosphoribosyltransferase	Therapeutic effects	MRI	Ga-DTPA
HSVtk	Therapeutic effects	MRI, MRS, PET, SPECT	FDG, HMPAO, misonidazole
HSV tk	Enzyme activity	SPECT, PET	Specific substrates
HSVtk mutant	Enzyme activity	PET	Specific substrates
Tyrosinase	Metal scavenger	MRI,SPECT, scintigraphy	^{111}In
Non-suicide reporter genes			
SSTR2	Receptor expression	SPECT, scintigraphy	Radiolabeled ligand
D2R	Receptor expression	PET	Radiolabeled ligand
Transferrin receptor	Receptor expression	MRI	Radiolabeled ligand
CEA antigen	Antigen expression	Scintigraphy	Radiolabeled antibody
Modified green fluorescence protein	Transchelation	SPECT, scintigraphy	^{99m}Tc-glucoheptonate
Human sodium iodide transporter	Transport activity, therapy	Scintigraphy	^{131}I
Various therapeutic genes			
EGFR-Antisense	Therapeutic effects	MRI	Ga-DTPA
IL1-alpha	Therapeutic effects	MRI	Ga-DTPA
IL-2	Therapeutic effects	MRI	Ga-DTPA
IL-4	Therapeutic effects	MRI	Ga-DTPA
Interferon gamma	Therapeutic effects	MRI	Ga-DTPA
Human transforming growth factor beta	Therapeutic effects	MRI	Ga-DTPA

of enzymatic action or transporter function of the reporter gene product (e.g., iodine accumulation due to the action of the Na(+)/I(−) symporter). The reporter gene may not have a therapeutic role itself but by coupling it to a therapeutic gene, expression of the reporter gene reports on the expression of the therapeutic gene.

Molecular Imaging Modalities for Gene Expression

Among the wide range of imaging modalities allowing for *in vivo* studies in animal models, such as mice up to whole body imaging in humans; magnetic resonance imaging (MRI), and magnetic resonance spectroscopy (MRS) and positron emission tomography (PET) are often performed. Based on the interaction of nuclear spins with a strong external magnetic field, magnetic resonance imaging has the advantage of high spatial resolution but offers low sensitivity. Optical imaging is limited concerning the visualization of deeper tissue structures. MRI allows for differentiation between tissues with different absorbtion or scatter properties and for the measurement of tissue-specific biomarkers (Weissleder *et al.*, 1999). Compared to MRI imaging and MRS, nuclear medicine procedures offer a greater sensitivity which is located in the picomolar range. Labelling of substrates with radioactive isotopes and administration of very low amounts of these tracers allow the assessment of

biochemical or physiological processes without any interference. PET is used to detect decaying isotopes such as ^{11}C or ^{18}F. Depending on the tracer used, different cellular processes may be visualized, such as cell proliferation in tumors. In addition, new therapeutic strategies using radioactive isotopes can be developed in the future.

Molecular Imaging of Suicide Gene Transfer and Therapeutic Effects

The transfer and expression of suicide genes into malignant tumor cells represent an attractive approach for human gene therapy. Suicide genes typically code for nonmammalian enzymes which convert nontoxic prodrugs into highly toxic metabolites. Consequently, after the systemic application of the nontoxic prodrug, the active drug will only be produced at the tumor site. Although a broad range of suicide principles has been described, mainly two suicide systems are applied in most studies: the cytosine deaminase (CD) and Herpes Simplex Virus thymidine kinase (HSVtk). Cytosine deaminase is expressed in yeasts and bacteria and converts the antifungal agent 5-fluorocytosine (5-FC) to the highly toxic 5-fluorouracil (5-FU). In mammalian cells, however, the enzyme is not expressed and 5-FC is incorporated into the nucleic acid fraction. Therefore, gene therapeutic approaches based on the transfection of CD in tumor cells are associated with moderate pharmacological effects in nontransfected cells and allow the application of high therapeutic doses. 5-FU exerts its toxic effect by interfering with DNA and protein synthesis due to substitution of uracil by 5-FU in RNA and inhibition of thymidilate synthetase by 5-fluorodeoxy-uridine monophosphate, resulting in impaired DNA biosynthesis (Myers, 1981). Nishiyama *et al*. (1985) implanted CD-containing capsules into rat gliomas and subsequently treated the animals with systemic application of 5-FC. In these experiments significant amounts of 5-FU in the tumors as well as a decrease in tumor growth rate and systemic cytotoxicity were observed. In order to apply this approach in patients with disseminated tumor diseases, Wallace *et al*. (1994) used monoclonal antibody (mAb)-enzyme conjugates to achieve a selective activation of 5-FC. They obtained a 7-fold higher level of 5-FU in the tumor after administration of mAb-CD and 5-FC compared to the systemic application of 5-FU. Recently, *in vitro* and *in vivo* studies have further demonstrated the potency of the CD suicide system. Tumor cells which had been infected with a retrovirus carrying the cytosine deaminase gene showed a strict correlation between 5-FC sensitivity and CD enzyme activity (Huber *et al*., 1993; Mullen *et al*., 1994).

The expression of the herpes simplex virus thymidine kinase (HSVtk) as suicide gene has been studied in a variety of tumor models *in vitro* and *in vivo* after viral as well as nonviral transfer of the gene (Barba *et al*., 1994). In contrast to the human thymidine kinase, HSVtk is less specific and phosphorylates nucleoside analogs such as acyclovir and ganciclovir to their monophosphate metabolites, which are subsequently phosphorylated by cellular kinases to the di- and triphosphates. After integration of the triphosphate metabolites into DNA, chain termination occurs, followed by cell death. Encouraging results have been initially obtained in rat gliomas

using a retroviral vector system for transfection of the HSVtk gene (Culver *et al*., 1992; Ram *et al*., 1993). In addition, it was shown that the complete tumor regression does not require the HSVtk expression in every tumor cell, but tumor cells in close proximity of HSVtk-expressing cells become sensitive to GCV ('bystander effect') (Culver *et al*.,1992; Ram *et al*., 1993). However, often a sufficient therapeutic response after GCV or 5-FC application is not achieved due to low infection efficiency of the respective recombinant retrovirus. For planning and application of suicide gene therapy, molecular imaging has to be performed to decide if repeated injections of the recombinant viruses may be necessary to reach a therapeutic level of enzyme activity in the tumor and to find a therapeutic window of maximum gene expression and consecutive prodrug administration (Haberkorn *et al*., 1996). Because both 5-FC and GCV can be labeled with ^{18}F with sufficient *in vivo* stability (Alauddin and Conti, 1998), PET may be applied to assess the enzyme activity *in vivo*. In addition, by employing tracers of tumor metabolism and PET, the effect of suicide gene therapy at an early stage of the treatment can be measured, facilitating the prediction of therapy efficacy in a variety of tumors and therapeutic regimens (Haberkorn *et al*., 1993, 1994a).

By employing MRI and PET, the effect of different suicide gene therapeutic approaches with regard to morphology, metabolism, and perfusion in individual tumors has been evaluated and different vector systems used for transfection of the suicide gene were investigated with respect to their toxicity towards non-malignant tissues. Early effects of gene therapy have been shown to be more efficiently assessed by the determination of the metabolic changes within the tumor tissue instead of morphological changes. Studies concerning the glucose metabolism or thymidine incorporation into the cellular DNA have been performed with PET employing the respective tracers. In malignant tissues treated with the HSV-tk/GCV suicide system, DNA chain termination will be expected to occur in tumor cells leading to changes in thymidine incorporation into tumor cell DNA. These may be assessed by PET using [^{11}C]thymidine as tracer (Shields *et al*., 1990). In addition, malignant tumors are usually characterized by an enhanced glucose metabolism. Clinical and experimental studies performed on osteosarcomas, rat prostate adenocarcinoma or gliomas revealed an increased ^{18}F-fluorodeoxyglucose (FDG) and ^{14}C-FDG uptake, respectively, early after conventional treatment with chemotherapeutic drugs (Haberkorn *et al*., 1994a, b, 1997a). By employing rat prostate adenocarcinoma cells for investigation, the enhanced FDG uptake was associated with an increased glucose transport in cell culture systems (Haberkorn *et al*., 1997a), which might be due to a redistribution of the glucose transport protein from intracellular pools to the plasma membrane in response to cellular stress (Wertheimer *et al*., 1991). Dynamic PET measurements of ^{18}FDG uptake were performed in rats transplanted with HSVtk-expressing Morris hepatoma cells (Haberkorn *et al*., 1998a). 2 days and 4 days after the onset of therapy with 100 mg GCV/kg body weight as well as after administration of sodium chloride, the arterial FDG plasma concentration was measured dynamically in an extracorporeal loop and the rate constants

for FDG transport (K_1, k_2), and FDG phosphorylation (k_3) were calculated using a three-compartment model modified for heterogeneous tissues. In addition, the thymidine incorporation into the tumor DNA was determined after i.v. administration of ^{3}H-thymidine. After 2 days of GCV treatment, an uncoupling of 2-fluoro-2-deoxyglucose transport and phosphorylation was found with enhanced K_1 and k_2 values and a normal k_3 value. The increase in FDG transport normalized after 4 days, whereas the phosphorylation rate increased. In contrast, the thymidine incorporation into the tumor cellular DNA declined to 10.5% of the controls after 4 days of treatment with GCV.

In order to assess metabolic changes in tumor cells *in vitro*, uptake experiments can be performed employing ^{14}C-labeled and ^{3}H-labeled molecules, respectively. In a HSVtk-expressing rat hepatoma cell line, the uptake of ^{14}C-fluorodeoxyglucose (FDG), ^{14}C-aminoisobutyric acid (AIB), ^{3}H-labeled 3-O-methylglucose, and ^{3}H-thymidine was measured in the presence of different concentrations of GCV (Haberkorn *et al*., 1997b, c). In the HSVtk-expressing cell line an increased (up to 250%) thymidine uptake in the acid-soluble fraction and a decrease to 5.5% in the acid-insoluble fraction was found. The decrease of radioactivity in the nucleic acid fraction occurs early (4 h) after exposure of the cells to GCV and represents DNA chain termination induced by the HSVtk/ganciclovir system. The phenomenon of a posttherapeutic increase of thymidine or its metabolites in the acid-soluble fraction was observed in former studies after chemotherapy (Haberkorn *et al*., 1994a). This effect may be explained by an increase in the activity of salvage pathway enzymes, e.g., of host thymidine kinase activity during repair of cell damage.

During GCV treatment the uptake for FDG and 3-O-methylglucose increased up to 195% after 24 h incubation with GCV. An HPLC analysis revealed a decline of the FDG-6-phosphate fraction after 48 h incubation with GCV. Consequently, a normalization of FDG uptake was observed after this incubation period, whereas the 3-O-methylglucose uptake was still increased. Experiments performed with different amounts of HSVtk-expressing cells and control cells showed that these effects are dependent on the percentage of HSVtk-expressing cells (Haberkorn *et al*., 1997b). The AIB uptake decreased to 47%, while the methionine uptake in the acid-insoluble fraction decreased to 17%. The amino acid uptake experiments are evidence of an inhibition of protein synthesis as well as of the neutral amino acid transport.

To evaluate the effect of adenoviral mediated HSVtk gene transfer and GCV therapy of intracerebral 9L gliosarcomas in rats, Ross *et al*. (1995) used MRI and *in vivo* localized H MRS. Significant variation in therapeutic response has been evaluated after the MRI quantitation of changes in 9L tumor doubling times. Localized H MRS of treated 9L tumors revealed a significant increase in the resonance intensity at 0.9–1.3 ppm, corresponding to mobile lipids and/or lactate. The changes in the tumor doubling times correlated with changes in H tumor magnetic resonance spectra. Therefore, changes in tumor metabolite levels may be predictive of the effectiveness of this gene therapeutic approach.

MRI has been performed to assess morphological changes in different tumor models in response to cytosine deaminase gene transfer and 5-fluorocytosine

administration (Adachi *et al*., 2000; Ichikawa *et al*., 2000; Stegman *et al*., 2000). After infection with an adenovirus carrying the CD gene the 5-FC sensitivity in 9L cells was increased 1,700-fold compared to the control cells (Ichikawa *et al*., 2000). MRI demonstrated remarkable inhibition of tumor growth correlated with a survival of 70% of the rats for more than 90 days. Moreover, the mean tumor diffusion increased by 31% within 8 days after the onset of 5-FC treatment preceding tumor growth arrest and tumor regression (Stegman *et al*., 2000). A complete regression of the intracranial tumor was observed in four of five treated animals, and the recurrent tumor in the remaining animal showed a water diffusion behavior which was similar to primary, untreated tumors. In rats bearing chemically induced hepatocellular carcinoma, C6 glioblastomas, as well as in patients suffering from glioblastoma, significant tumor necrosis or growth retardation and regression after induction of HSVtk expression followed by GCV application were observed in the MR examination (Gerolami *et al*., 2000; Namba *et al*., 2000). After gene therapy of rat C6 glioma using adenovirus-mediated transfer of the HSVtk gene, an initial response to GCV application was 90% and a complete regression in 70% of the treated animals, but recurrence was also found (Maron *et al*., 1996). A more clinical relevant experimental protocol was designed by Bouali-Benazzouz *et al*. (1999) consisting of late GCV delivery on large glioma formations in rats. In long-term experiments, the survival of treated rats was improved by 60% compared to that of the control animals, and a complete regression of the tumor was demonstrated by MRI imaging in those animals responding to the treatment. In these experiments stably HSVtk-expressing glioma cells had been used for transplantation avoiding difficulties associated with gene transfer which, however, often arise in the course of clinical application in patients. The importance of efficient gene transfer was further demonstrated in the rat BT4C glioma, which had been treated by injection of HSVtk-producing PA317 packaging cells and intraperitoneal ganciclovir application (Sandmair *et al*., 1999). Obviously, due to low gene transfer efficiency and limited life span of the injected packaging cell inside the malignant tissues, these tumors did not respond to gene therapy.

Poptani *et al*. (1998) employed high resolution MRI to quantify the tumor volume, the transverse relaxation time (T2), and the apparent diffusion constant (ADC) of water in rat gliomas and in the contralateral brain after HSVtk/GCV therapy. Following GCV application, a regional increase in T2 and ADC was observed at day 4 of the treatment, even though the tumor volume was still increasing. According to the image obtained by MR and the histological examination, a local necrosis developed in the area of the tumor. In a group of five tumor bearing rats, retrovirus-producing packaging cell injections were given intratumorally to mimic clinically relevant gene therapy. In these cases, only small and short-lasting T2 and ADC elevations were found following GCV treatment without an effect on the overall tumor growth and outcome. Therefore, quantitative MRI, including the evaluation of T2 and ADC, is considered to be superior to volume measurements as far as the prediction of an early response to retrovirus-mediated gene therapy *in vivo* is concerned.

In clinical studies elevating the effect of HSVtk suicide system in patients with recurrent glioblastoma multiforme (GBM), transient neurological disorders were found after the ganciclovir treatment, which were associated with MRI enhancement (Shand *et al*., 1999). Deliganis *et al*. (1997) describe an increase in volume of MRI contrast enhancement in three of seven GBM patients treated with the HSVtk/ganciclovir suicide system early (between 40 and 80 days) after therapy followed by a decrease or plateau which might reflect an inflammatory response to the local injection of the viral vector. Goodman *et al*. (1996) performed toxicity studies in adult baboons who had received intracerebral injections of either high dose of adenoviral vectors bearing the HSVtk with or without GCV administration or low doses of a control adenovirus and ganciclovir. MRI of the brain was obtained prior to and 3 and 6 weeks after treatment. Animals having received the recombinant vector at high doses followed by ganciclovir treatment developed coagulative necrosis at the sites of injection and died during the first week. In contrast, animals treated by the high vector dose without ganciclovir showed no clinical symptoms of damage, but necrosis was detected at the site of injection with MRI. Animals having received a low dose of control adenoviral vector and ganciclovir were clinically normal, exhibited small MRI abnormalities, and microscopic foci of necrosis at autopsy.

Because recombinant retroviral vectors used for the transduction of the suicide gene occasionally integrate into the genome of endothelial cells lining the tumor blood vessels, tumor vascularization might be effected by ganciclovir treatment. Studies performed to investigate the effect of HSVtk transduction and ganciclovir therapy on morphological changes and growth of 9L glioma in rats, revealed a decrease of the tumor vasculature after application of the prodrug (Ram *et al*., 1994). In the presence of vector-producer cells continuously releasing infectious recombinant viral particles, diffuse and multifocal hemorrhages occurred after treatment with ganciclovir (Ram *et al*., 1997). When the tumor cells had been transfected by the HSV thymidine kinase gene before transplantation, no hemorrhages were observed during ganciclovir therapy, indicating that endothelial cells had not been transduced. To investigate whether tumor regression is partly due to tumor ischemia caused by the destruction of endothelial cells after HSVtk-transduction *in vivo* and subsequent treatment with ganciclovir, Doppler color-flow and ultrasound imaging were performed on the subcutaneous 9L gliosarcoma tumors in rats. The intratumoral injection of virus producing cells without ganciclovir administration did not influence the tumor growth or the intratumoral vasculature. In contrast, administration of ganciclovir caused a decrease of vessel density in the HSVtk-expressing tumors and early necrotic changes associated with ultrasonographic signs of scattered intratumoral hemorrhage occurred. Evidence for changes in tumor vasculature and tumor volume was also observed after transfer of the genes coding for interleukin-4, interleukin-12, interleukin 1-alpha (IL1-alpha), mouse interferon gamma (IFN-gamma), human transforming growth factor beta (TGF-beta), and antisense epidermal growth factor receptor (EGFR) cDNA into rat gliomas (Benedetti *et al*., 1999, 2000; DiMeco *et al*., 2000; Su *et al*., 2000). In

the case of tumors modified by the mouse IL-1alpha gene, an increase of the vascular volume was observed, which correlated with the continuing growth in tumor size, and the decrease in vascular volume was predictive of the onset of tumor regression (Su *et al.*, 2000).

Tumor perfusion, as measured in HSVtk-expressing KBALB tumors after intravenous administration of [^{99m}Tc]hexa methylpropyleneamine oxime (HMPAO), increased by 206% at day 2 after the onset of ganciclovir treatment (Morin *et al.*, 2000). In the same animals, the accumulation of the hypoxia tracer [^{3}H]misonidazole decreased to 34% at day 3 indicating that the tumor tissue had become less hypoxic during ganciclovir treatment.

Molecular Imaging of Suicide Gene Therapy by the Uptake of Specific Substrates

Imaging based on the accumulation of a radiolabeled substrate as a result of enzymatic activity of the suicide gene product was first demonstrated by Saito *et al.* (1982) for the visualization of HSV encephalitis. Since then a variety of experiments concerning the uptake of specific substrates have been performed *in vitro* and *in vivo* with scintigraphy or PET and an enhanced accumulation of 5-iodo-2′-fluoro-2′deoxy-1-b-D-arabinofuranosyluracil (FIAU), fluorodeoxycytidine (FCdR), 5-fluoro-1-(2′-deoxy-fluoro-ß-D-ribofuranosyl)uracil (FFUdR), ganciclovir, 8-[^{18}F]fluoroganciclovir (PGCV), 9-(4-[^{18}F]-fluoro-3-hydroxymethylbutyl)-guanine ([^{18}F]FHBG) or 9-[(3-^{18}F-fluoro-1-hydroxy-2-propoxy)methyl]-guanine ([^{18}F]-FHPG) in tumor cells genetically modified by HSVtk have been found (Alauddin *et al.*, 1999; De Vries *et al.*, 2000; Gambhir *et al.*, 1999; Haberkorn *et al.*, 1998b; Haubner *et al.*, 2000; Hospers *et al.*, 2000; Hustinx *et al.*, 2001). Furthermore, the uptake of ganciclovir, FFUdR, and FIAU was highly correlated to the percentage of HSVtk-expressing cells and to the growth inhibition as measured in bystander experiments (Germann *et al.*, 1998; Tjuvajev *et al.*, 1998). In rats infected with adenovirus particles, there was a significant positive correlation between the percent injected dose of 8-[^{18}F]fluoroganciclovir FGCV retained per gram of liver and the levels of hepatic HSVtk expression (Gambhir *et al.*, 1999).

The nucleoside transport in mammalian cells is known to be heterogeneous with two classes of nucleoside transporters: the equilibrative, facilitated diffusion systems and the concentrative, sodium-dependent systems. To elucidate the transport mechanism of the HSVtk specific substrate, ganciclovir inhibition/competition experiments were performed in rat hepatoma and human mammary carcinoma cells. In these experiments, competition for all concentrative nucleoside transport systems and inhibition of the ganciclovir transport by the equilibrative transport systems was observed, whereas the pyrimidine nucleobase system showed no contribution to the ganciclovir uptake (Haberkorn *et al.*, 1997c, 1998b). In human erythrocytes, acyclovir has been shown to be transported mainly by the purine nucleobase carrier (Mahony *et al.*, 1988). Due to a hydroxymethyl group on its side chain, ganciclovir has a stronger similarity to nucleosides and, therefore, may also be transported by a nucleoside transporter. Moreover, the 3′hydroxyl moiety of nucleosides was shown to be important for their interaction with the nucleoside transporter (Gati *et al.*, 1984).

In rat hepatoma cells as well, as in human mammary carcinoma cells, the ganciclovir uptake was shown to be much lower than the thymidine uptake (Haberkorn *et al.*, 1997c, 1998b). Therefore, in addition to low infection efficiency of the current viral delivery systems, slow transport of the substrate and also its slow conversion into the phosphorylated metabolite is limiting for the therapeutic success of the HSVtk/ganciclovir system. Cotransfection with nucleoside transporters or the use of other substrates for HSVtk with higher affinities for nucleoside transport and phosphorylation by HSVtk may improve therapy outcome.

Retroviral transfer of the gene for the *Drosophila melanogaster* multisubstrate deoxyribonucleoside kinase (DMdNK) was done to evaluate this gene as a new potential suicide and *in vivo* reporter gene (Altmann *et al.*, 2004). Thereafter, uptake measurements were performed in wild type and HSVtk-expressing and DMdNK-expressing cell lines using different radiolabeled potential substrates: thymidine, fluorodeoxyuridine, iododeoxyuridine, bromodeoxyuridine, fluorodeoxycytidine, chlorodeoxyadenosine, FIAU, ganciclovir, bromovinyldeoxyuridine (BVDU), iododeoxycytidine and gemcitabine. DMdNK-expressing cells showed an enhanced uptake of different radiolabeld nucleoside analogs with a different pattern as compared to HSVtk. Furthermore, the enzyme confers enhanced uptake of gemcitabine and enhanced sensitivity against the drug.

The effects of cytosine deaminase (CD) gene transfer were evaluated in human glioblastoma cells. When exposed to ^{3}H-fluorocytosine (5-FC), these cells produced ^{3}H-5-FU, whereas in the control cells only ^{3}H-5-FC was detected (Haberkorn *et al.*, 1996). Moreover, significant amounts of 5-FU were found in the medium of cultured cells, which may account for the bystander effect observed in previous experiments. However, uptake studies revealed only a moderate and nonsaturable accumulation of radioactivity in the tumor cells and lack of inhibition by hypoxanthine or uracil suggesting that 5-FC enters the cells only via diffusion. Although a significant difference in 5-FC uptake was seen between CD-positive cells and control cells after 48 h incubation, no difference was observed after 2 h incubation. Furthermore, a rapid efflux could be demonstrated. Therefore, 5-FC transport and 5-FU efflux may be limiting factors for this therapeutic procedure and quantitation with PET has to rely on dynamic studies and modelling, including HPLC analysis of the plasma rather than on nonmodelling approaches (Haberkorn *et al.*, 1996). To evaluate the 5-FC uptake *in vivo*, a rat prostate adenocarcinoma cell line was transfected with a retroviral vector bearing the E. coli CD gene. The cells were found to be sensitive to 5-FC exposure, but lost this sensitivity with time. This may be due to inactivation of the viral promoter (CMV) used in this vector. *In vivo* studies with PET and ^{18}FC showed no preferential accumulation of the tracer in CD-expressing tumors although HPLC analysis revealed a production of 5-fluorouracil which was detectable in tumor lysates as well as in the blood of the animals (Haberkorn, 1999). A comparison of the functional properties of bacterial CD and yeast CD expressed in COS-1 cells revealed that both recombinant enzymes utilized cytosine with equal efficacy, but 5-FC was a poor substrate for the bacterial CD, with an apparent catalytic efficiency

280-fold lower than that observed for the yeast CD (Hamstra *et al*., 1999). Furthermore, after infection of tumor cell lines with retroviruses bearing different CD genes, the IC50 of 5-FC was found to be 30-fold lower in yeast CD-infected cells compared to those cells expressing the bacterial CD gene. In subcutaneous human colorectal carcinoma xenografts in nude mice, *in vivo* MRS was done to measure yeast CD transgene expression in genetically modified tumors by direct detection of CD-catalyzed conversion of 5-fluorocytosine to 5-fluorouracil (Stegman *et al*., 1999). A three-compartment model revealed a first-order kinetics, suggesting that the yeast CD was not saturated *in vivo* in the presence of measured intratumoral 5-FC concentrations above the *in vitro* determined affinity (K_m) values.

Noninvasive Imaging of Reporter Gene Transfer

Gene therapy is occasionally based on the transduction of non-suicide genes such as cytokines that stimulate an anti-tumor specific immune response. For the noninvasive imaging of these approaches, bicistronic viral vector systems or fusion genes are required that simultanously transfer both the therapeutic gene and an *in vivo* reporter gene into the tumor cells and allow for the evaluation of gene expression by MRI imaging or techniques based on the accumulation of radiolabeled tracers. In addition, combining specific promoter elements with an *in vivo* reporter gene promoter, regulation involved in signal transduction and gene regulation during changes of the physiological environment and pharmacological intervention may be characterized. *In vivo* reporter genes normally include those genes encoding for enzymes, receptors, antigens and transporters. Enzyme activity can be assessed by the accumulation of the metabolites of radiolabeled specific substrates, receptors by binding and internalization of ligands, antigens by binding of antibodies and transporters by the uptake of their specific substrates. For instance, HSVtk phosphorylates the specific substrate leading to the accumulation of the corresponding negatively charged metabolite in the tumor tissue (De Vries *et al*., 2000; Gambhir *et al*., 1999; Haberkorn 1998b, 1999; Haubner *et al*., 2000; Hospers *et al*., 2000; Hustinx *et al*., 2001). However, due to the low affinity of the HSVtk-specific substrate for the nucleoside transport system on the one hand and for the enzyme on the other hand, the cellular accumulation of radioactivity is rather limited (Haberkorn and Altmann, 2001). Therefore, imaging based on the HSVtk transduction needs to be improved by either the identification of substrates with different biochemical properties increasing the affinity of the radiolabeled tracer for the transport system and the enzyme or the use of an HSVtk mutant. Despite low transduction efficiency of the *in vivo* reporter gene Gambhir *et al*. (2000) performed imaging by PET employing a mutant herpes simplex virus type 1 thymidine kinase (HSV1-sr39tk). In C6 rat glioma cells transduced by the mutant gene, the uptake of the specific substrates [8-^{3}H]penciclovir, and 8-[^{18}F]fluoropenciclovir was enhanced and the accumulation of the tracer increased twofold when compared to the tumor cells transfected by the wild type HSVtk.

Tyrosinase catalyzes the hydroxilation of tyrosine to DOPA and the oxidation of DOPA to DOPAquinone, which after

cyclization and polymerization results in melanin production. Melanins are scavengers of metal ions such as iron and indium through ionic binding. In a variety of cells transfected by the tyrosinase gene, melanins are synthesized, which provides the possibility for imaging of gene transfer using NMR or the ^{111}In-detection by a gamma camera. Cells transfected by the tyrosinase gene were shown to stain positively for melanin. In addition, when compared to wild type cells, tyrosinase-expressing cells were characterized by a higher ^{111}In binding capacity dependent on the amount of the vector used for transfection (Weissleder *et al*., 1997). However, imaging based on the transduction of the tyrosinase gene is often hampered by the low expression of the enzyme associated with low amounts of melanin and the cytotoxicity of melanin produced in modified cells. These problems may be encountered by the construction of chimeric tyrosinase proteins characterized by increased enzymatic activity and by positioning of the enzyme at the outer side of the membrane. Using a human transferrin receptor engineered to be highly overexpressed in transfected cells and a MRI reporter construct which consisted of monocrystalline iron oxide nanoparticles (MION) conjugated to human holo-transferrin, Weissleder *et al*. (2000) showed that even modest increases in the receptor level lead to changes in MR imaging signals. Alternatively, individual molecules of a recently developed class of gadolinium chelates can be enzymeatically converted by the reporter gene β-galactosidase leading to changes in their relaxation properties (Hüber, 1998). However, due to the less efficient delivery of these contrast agents to intact cells and tissues, imaging is limited (Bell and Taylor-Robinson, 2000). To circumvent this problem, coupling of the chelate complex to biological macromolecules might be necessary.

The reporter genes coding for an extracellular receptor or transporter that binds or transports a radiolabelled probe are the human dopamine 2 receptor (hD2R) gene, the human somatostatin receptor subtype-2 (hSSTR2) gene (MacLaren *et al*., 1999; Rogers *et al*., 1999), the sodium iodide symporter (Altmann and Haberkorn, 2003) and the norepinephrine transporter, which has been used to image a liver metastasis model (Altmann *et al*., 2003). The dopamine D2 receptor gene is encoded by an endogenous gene, and ectopic expression should not induce an immune response. The positron-labeled reporter probe 3-(2′-[^{18}F]-fluoroethyl)spiperone (FESP) rapidly crosses the blood-brain-barrier, can be produced at high specific activity and is currently used in humans (Barrio *et al*., 1989; Bahn *et al*., 1989). Employing an adenoviral-directed D2R gene delivery system and a D2R expressing tumor model, the ability of the D2R/FESP reporter system to image reporter gene expression was investigated in mice, and the tracer uptake was found to correlate with the hepatic FESP accumulation, dopamine receptor ligand binding, and the D2 receptor mRNA (MacLaren *et al*., 1999). Moreover, tumors genetically modified to express the D2 receptor significantly accumulated more FESP than wild type tumors. The human type 2 somatostatin receptor was transferred into non-small cell lung cell lines, and imaging of the hSSTR2 gene was achieved using a radiolabeled somatostatin-avid peptide (P829), which was radiolabeled to high specific activity with ^{99m}Tc or ^{188}Re. In

the genetically modified tumors in mice a 5–10-fold higher accumulation of both radiolabeled P829 peptides as compared to the control tumors was observed (Zinn *et al*., 2000).

The human sodium iodide symporter (hNIS) gene has been transferred into a variety of tumor models for gene therapeutic and imaging purposes (Haberkorn *et al*., 2001, 2003). Thyroid follicular cells are characterized by their ability to accumulate iodide, which is a fundamental step in the synthesis of thyroid hormones. The complex process of iodide metabolism in the thyroid primarily depends on the active transport of the ion into the cells against an electrochemical gradient mediated by the human sodium iodide symporter (hNIS) and the activity of the thyroperoxidase. Consequently, benign thyroid diseases and differentiated thyroid carcinomas can be successfully treated with radioiodide therapy. In undifferentiated thyroid carcinomas, however, a reduced radioiodide concentrating activity or even a failure to accumulate iodide is often observed, which can be attributed to a decreased expression of the NIS and other proteins involved in iodide metabolism (Cho *et al*., 2000; Venkataraman *et al*., 1999). With regard to the treatment of undifferentiated thyroid carcinomas or even nonthyroid tumors by radioiodine therapy, strategies based on the transduction of the NIS gene regulated by constitutive promoter elements have been developed. Uptake experiments performed after hNIS gene transduction into Morris hepatoma cells revealed a significant increase in iodide accumulation in the tumor cells (a factor of 84–235) after 1 h incubation (Haberkorn *et al*., 2001). Experiments performed on rats bearing wild type and hNIS-expressing Morris hepatoma revealed a maximum ^{131}Iodide uptake after 1 h followed by a continuous disappearance of the radioactivity out of the body as well as of the hNIS-expressing tumors (Haberkorn *et al*., 2001, 2003; Sieger *et al*., 2003). *In vitro* a rapid efflux of iodide occurred with 80% of the radioactivity released into the medium after 20 min (Haberkorn *et al*., 2001, 2003). Although the NIS activity favors the iodide influx, the intracellular iodide will drop proportionally to the external iodide concentration in thyroid-unrelated cells that do not organify iodide by coupling to tyrosine residues. Therefore, a definitive proof of therapeutically useful absorbed doses *in vivo* after transfer of the NIS gene is still lacking. In order to prevent the efflux of radioiodide from tumor tissues and to achieve a therapeutic effect, further studies concerning pharmacological modulation may be performed. With respect to its function as a reporter, however, NIS seems to be promising. Employing a bicistronic vector for coexpression of the NIS gene a gene of interest and ^{121}I and ^{124}I or ^{99m}Tc-pertechnetate as reporter probe for the transporter, noninvasive imaging of gene expression may be performed with PET or a γ camera. In addition, because iodide is not metabolized in most tissues and no adverse effects of the sodium influx have been observed to date (Haberkorn *et al*., 2002), the sodium iodide symporter presents the advantage of not interacting with underlying cell biochemistry. In contrast, the HSVtk gene may alter the cellular behavior towards apoptosis by changes in the deoxynucleotide (dNTP) pool (Oliver *et al*., 1997), antigens may cause immunoreactivity and receptors may result in second messenger activation such as triggering signal transduction pathways.

A similar approach for targeted radiotherapy is provided by the uptake of I-meta-Iodobenzylguanidine (MIBG), a metabolically stable false analog of norepinephrine, which has been primarily used for the treatment of patients suffering from neural crest derived tumors such as neuroblastoma or pheochromocytoma. The mechanism of MIBG uptake, which is qualitatively similar to that of norepinephrine, has been studied in a variety of cellular systems and a non-specific, non-saturable diffusion process in most tissues as well as an active uptake of the tracer mediated by the noradrenalin (norepinephrine) transporter (NET) in cells of the neuroadrenergic tissues and malignant tumors derived thereoff has been postulated (Mairs *et al*., 1994; Lode *et al*., 1995).

In a variety of experiments performed *in vitro* on COS-1 cells, HeLa cells, glioblastoma cells or rat hepatoma cells transfected by the hNET and *in vivo* on nude mice transplanted by hNET-expressing tumors, a significant increase of radioiodinated MIBG was demonstrated (Boyd *et al*., 1999; Altmann *et al*., 2003).When compared to previous studies concerning the efflux of ^{131}I from hNIS-expressing rat hepatoma cells (Haberkorn *et al*., 2001) a longer retention of MIBG in the hNET-transfected cells was observed (Altmann *et al*., 2003). The clinical use of the MIBG radiotherapy is so far restricted to neural crest derived malignancies, and due to insufficient ^{131}I-MIBG uptake therapy in these tumor patients is not curative. In order to achieve therapeutically sufficient doses of radioactivity in the genetically modified tumor cells of non-neuroectodermal origin, an intracellular trapping of the tracer is required. With respect to its function as an *in vivo* reporter, the recombinant hNET gene product seems to be less promising than NIS because the images showed high background and relatively faint appearance of the genetically modified tumor (Altmann *et al*., 2003).

In conclusion, clinical gene therapy requires the targeting of therapeutic genes to malignant or non-malignant tissues by the use of recombinant viral vectors and tissue-specific or tumor-specific regulatory sequences. The success of this promising therapeutic modality depends on the efficient gene transduction including infection efficiency of the recombinant virus and expression of the therapeutic gene. Molecular imaging methods based on specific probes or contrast agents that allow either direct or indirect spatio-temporal evaluation of gene expression deliver information which may be used for therapy planning, follow up studies in treated tumors, and as an indicator of prognosis. For instance, using radiolabeled ligands, antigens or substrates, the successful transfer of the genes coding for the respective receptors, antigens, transport proteins or enzymes may be assessed. The monitoring of gene therapy effects is performed by the evaluation of the morphological changes of the tumor employing MRI or by the measurement of tumor-associated metabolic variations with PET using tracers of tumor metabolism and proliferation. The uptake of ^{18}FDG has been demonstrated to be a useful parameter for the assessment of the glucose metabolism, and the tumor growth can be evaluated by the uptake of (^{11}C)thymidine or other proliferative markers. Finally, enhancement of radioactive isotope accumulation in tumors by transfer of the appropriate genes may be used for the treatment of malignant tumors.

REFERENCES

Adachi, Y., Tamiya, T., Ichikawa, T., Terada, K., Ono, Y., Matsumoto, K., Furuta, T., Hamada, H., and Ohmoto, T. 2000. Experimental gene therapy for brain tumors using adenovirus-mediated transfer of cytosine deaminase gene and uracil phosphoribosyltransferase gene with 5-fluorocytosine. *Hum. Gene Ther. 11*: 77–89.

Alauddin, M.M., and Conti, P.S. 1998. Synthesis and preliminary evaluation of 9-(4-[^{18}F]-fluoro-3-hydroxymethylbutyl)guanine ([^{18}F]FHBG): a new potential imaging agent for viral infection and gene therapy using PET. *Nucl. Med. Biol. 25*: 175–180.

Alauddin, M.M., Shahinian, A., Kundu, R.K., Gordon, E.M., and Conti, P.S. 1999. Evaluation of 9-[(3-^{18}F-fluoro-1-hydroxy-2-propoxy)methyl]guanine ([^{18}F]-FHPG) *in vitro* and *in vivo* as a probe for PET imaging of gene incorporation and expression in tumors. *Nucl. Med. Biol. 26*: 371–376.

Altmann, A., and Haberkorn, U. 2003. Assessment of gene transfer using imaging methodology. *Curr. Genom. 4*: 167–184.

Altmann, A., Kissel, M., Zitzmann, S., Kübler W, Mahmut M, Peschke P, and Haberkorn, U. 2003. Increased MIBG uptake after transfer of the human norepinephrine transporter gene in rat hepatoma. *J. Nucl. Med. 44*: 973–980.

Altmann, A., Eisenhut, M., Mier, W., Karlsson, A., and Haberkorn, U. 2004. The Drosophila melanogaster deoxyribonucleoside kinase gene induces enhanced gemcitabine sensitivity in rat hepatoma cells. *Eur. J. Nucl. Med. 31*(2): S 357.

Bahn, M.M., Huang, S.C., Hawkins, R.A., Satyamurthy, N., Hoffman, J.M., Barrio, J.R., Mazziotta, J.C. and Phelps, M.E. 1989. Models for *in vivo* kinetic interactions of dopoamine D_2 neuroreceptors and 3-(2′-[^{18}F]Fluoroethyl)spirone examined by positron emission tomography. *J. Cerebral. Blood Flow Metab. 9*: 840–849.

Barba, D., Hardin, J., Sadelain, M., and Gage, F.H. 1994. Development of anti-tumor immunity following thymidine kinase-mediated killing of experimental brain tumors. *Proc. Natl. Acad. Sci. USA 91*: 4348–4352.

Barrio, J.R., Satymurthy, N., Huang, S.C., Keen, R.E., Nissenson, C.H., Hoffman, J.M., Ackermann, R.F., Bahn, M.M., Mazziotta, J.C. and Phelps, M.E. 1989. 3-(2′-[^{18}F]Fluoroethyl)spirone: *in vivo* biochemical and kinetic characterization in rodents, nonhuman primates, and humans. *J. Cerebral. Blood Flow Metab. 9*: 830–839.

Bell, J.D., and Taylor-Robinson, S.D. 2000. Assessing gene expression *in vivo*: magnetic resonance imagung and spectroscopy. *Gene Ther. 7*: 1259–1264.

Benedetti, S., Bruzzone, M.G., Pollo, B., DiMeco, F., Magrassi, L., Pirola, B., Cirenei, N., Colombo, M.P., and Finocchiaro, G. 1999. Eradication of rat malignant gliomas by retroviral-mediated, *in vivo* delivery of the interleukin 4 gene. *Cancer Res. 59*: 645–652.

Benedetti, S., Pirola, B., Pollo, B., Magrassi, L., Bruzzone, M.G., Rigamonti, D., Galli, R., Selleri, S., Di-Meco, F., De-Fraja, C., Vescovi, A., Cattaneo, E., and Finocchiaro, G. 2000. Gene therapy of experimental brain tumors using neural progenitor cells. *Nat. Med. 6*: 447–450.

Bouali-Benazzouz, R., Laine, M., Vicat, J.M., Boisseau, S., Remy, C., Fouilhe, N., Thomas, F., Nissou, M.F., Benabid, A.L., and Berger, F. 1999. Therapeutic efficacy of the thymidine kinase/ganciclovir system on large experimental gliomas: a nuclear magnetic resonance imaging study. *Gene Ther. 6*: 1030–1037.

Boyd, M., Cunningham, S.H., Brown, M.M., Mairs, R.J., Wheldon, T.E. 1999. Noradrenaline transporter gene transfer for radiation cell kill by ^{131}I meta-iodobenzylguanidine. *Gene Ther. 6*: 1147–1152.

Cho, J.Y., Xing S, Liu X, Buckwalter TL, Hwa L, Sferra TJ, Chiu IM, Jhiang SM. 2000. Expression and activity of human Na+/I- symporter in human glioma cells by adenovirus-mediated gene delivery. *Gene Ther. 7*: 740–749.

Culver, K.W., Ram, Z., Walbridge, S., Ishii, H., Oldfiled, E.H., and Blaese, R.M. 1992. *In vivo* gene transfer with retroviral vector-producer cells for treatment of experimental brain tumors. *Science 256*: 1550–1552.

Deliganis, A.V., Baxter, A.B., Berger, M.S., Marcus, S.G., and Maravilla, K.R. 1997. Serial MR in gene therapy for recurrent glioblastoma: initial experience and work in progress. *Am. J. Neuroradiol. 18*: 1401–1406.

De Vries, E.F., van Waarde, A., Harmsen, M.C., Mulder, N.H., Vaalburg, W., and Hospers, G.A. 2000. [^{11}C]FMAU and [^{18}F]FHPG as PET tracers for herpes simplex virus thymidine kinase

enzyme activity and human cytomegalovirus infections. *Nucl. Med. Biol. 27*: 113–119.

DiMeco, F., Rhines, L.D., Hanes, J., Tyler, B.M., Brat, D., Torchiana, E., Guarnieri, M., Colombo, M.P., Pardoll, D.M., Finocchiaro, G., Brem, H., and Olivi, A. 2000. Paracrine delivery of IL-12 against intracranial 9L gliosarcoma in rats. *J. Neurosurg. 92*: 419–427.

Gambhir, S.S., Barrio, J.R., Phelps, M.E., Iyer, M., Namavari, M., Herschmann, H.R. 1999. Imaging adenoviral-directed reporter gene expression in living animals with positron emission tomography. *Proc. Natl. Acad. Sci. USA 96*: 2333–2338.

Gambhir, S.S., Bauer, E., Black, M.E., Liang Q., Kokoris M.S., Barrio, J.R., Iyer M., Namavari, M., Phelps M., and Herschmann H.R. 2000. A mutant herpes simplex virus type 1 thymidine kinase reporter gene shows improved sensitivity for imaging reporter gene expression with positron emission tomography. *Proc. Natl. Acad. Sci. USA 97*: 2785–2790.

Gati, W.P., Misra H.K., Knaus E.E., and Wiebe L.E. 1984. Structural modifications at the 2′ and 3′ positions of some pyrimidine nucleosides as determinants of their interaction with the mouse erythrocyte nucleoside transporter. *Biochem. Pharmacol. 33*: 3325–3331.

Germann, C., Shields, A.F., Grierson, J.R., Morr, I., Haberkorn, U. 1998. 5-Fluoro-1-(2′-deoxy-2′-fluoro-ß-D-ribofuranosyl)uracil trapping in Morris hepatoma cells expressing the Herpes Simplex Virus thymidine kinase gene. *J. Nucl. Med. 39*: 1418–1423.

Gerolami, R., Cardoso, J., Lewin, M., Bralet, M.P., Sa-Cunha, A., Clement,O., Brechot, C., and Tran, P.L. 2000. Evaluation of HSV-tk gene therapy in a rat model of chemically induced hepatocellular carcinoma by intratumoral and intrahepatic artery routes. *Cancer Res. 60*: 993–1001.

Goodman, J.C., Trask, T.W., Chen, S.H., Woo, S.L., Grossman, R.G., Carey, K.D., Hubbard, G.B., Carrier, D.A., Rajagopalan, S., Aguilar-Cordova, E., and Shine, H.D. 1996. Adenoviral-mediated thymidine kinase gene transfer into the primate brain followed by systemic ganciclovir: pathologic, radiologic, and molecular studies. *Hum. Gene Ther. 7*: 1241–1250.

Haberkorn, U. 1999. Monitoring of gene transfer for cancer therapy with radioactive isotopes. *Ann. Nucl. Med. 13*: 369–377.

Haberkorn, U., and Altmann, A. 2001. Imaging methods in gene therapy of cancer. *Curr. Gene Ther. 1*: 163–182.

Haberkorn, U., Strauss, L.G., Dimitrakopoulou, A., Seiffert, E., Oberdorfer, F., Ziegler, S., Reißer, C., Doll, J., Helus, F., and Kaick G. van 1993. Fluorodeoxyglucose imaging of advanced head and neck cancer after chemotherapy. *J. Nucl. Med. 34*: 12–17.

Haberkorn, U., Oberdorfer, F., Klenner, T., Strauss, L.G., Stöhr, M., Wallich, R., Altmann, A., and Kaick, G. van 1994a. Metabolic and transcriptional changes in osteosarcoma cells treated with chemotherapeutic drugs. *Nucl. Med. Biol. 21*: 835–845.

Haberkorn, U., Morr, I., Oberdorfer, F., Bellemann, M.E., Blatter, J., Altmann, A., Kahn, B., and Kaick, G. van 1994b. Fluorodeoxyglucose uptake *in vitro*: aspects of method and effects of treatment with gemcitabine. *J. Nucl. Med. 35*: 1842–1850.

Haberkorn, U., Oberdorfer, F., Gebert, J., Morr I., Haack K., Weber K., Lindauer M., Kaick G. van, and Schackert H.K. 1996. Monitoring of gene therapy with cytosine deaminase: *in vitro* studies using ^{3}H-5-fluorocytosine. *J. Nucl. Med. 37*: 87–94.

Haberkorn, U., Bellemann, M.E., Altmann, A., Gerlach, L., Morr, I., Oberdorfer, F., Brix, G., Doll, J., Blatter, J., and Kaick, G. van 1997a. F-18-fluoro-2-deoxyglucose uptake in rat prostate adenocarcinoma during chemotherapy with 2′,2′-difluoro-2′-deoxycytidine. *J. Nucl. Med. 38*: 1215–1221.

Haberkorn, U., Altmann, A., Morr, I., Germann, C., Oberdorfer, F., and Kaick, G. van 1997b. Multi tracer studies during gene therapy of hepatoma cells with HSV thymidine kinase and ganciclovir. *J. Nucl. Med. 38*: 1048–1054.

Haberkorn, U., Altmann, A., Morr, I., Knopf, K.W., Germann, C., Haeckel, R., Oberdorfer, F., and Kaick, G. van 1997c. Gene therapy with Herpes Simplex Virus thymidine kinase in hepatoma cells: uptake of specific substrates. *J. Nucl. Med. 38*: 287–294.

Haberkorn, U., Bellemann, M.E., Gerlach, L., Morr, I., Trojan, H., Brix, G., Altmann, A., Doll, J., and Kaick, G. van 1998a. Uncoupling of 2-fluoro-2-deoxyglucose transport and phosphorylation in rat hepatoma during gene therapy with HSV thymidine kinase. *Gene Ther. 5*: 880–887.

Haberkorn, U., Khazaie, K., Morr, I., Altmann, A., Müller, M., and Kaick, G. van 1998b. Ganciclovir uptake in human mammary carcinoma cells expressing Herpes Simplex Virus thymidine kinase. *Nucl. Med. Biol. 25*: 367–373.

Haberkorn, U., Henze, M., Altmann, A., Jiang, S., Morr, I., Mahmut, M., Peschke, P., Kübler W., Debus J., and Eisenhut M. 2001. Transfer of the human sodium iodide symporter gene enhances iodide uptake in hepatoma cells. *J. Nucl. Med. 42*: 317–325.

Haberkorn, U., Altmann, A., and Eisenhut, M. 2002. Functional genomics and proteomics - the role of nuclear medicine. *Eur. J. Nuc. Med. 29*: 115–132.

Haberkorn, U., Kinscherf, R., Kissel, M., Kübler W., Mahmut, M., Sieger, S., Eisenhut M, Peschke P, and Altmann A. 2003. Enhanced iodide transport after transfer of the human sodium iodide symporter gene is associated with lack of retention and low absorbed dose. *Gene Ther. 10*: 774–780.

Hamstra, D.A., Rice, D.J., Pu, A., Oyedijo, D., Ross, B.D., and Rehemtulla, A. 1999. Enzyme/prodrug therapy for head and neck cancer using a catalytically superior cytosine deaminase. *Hum. Gene. Ther. 10*: 1993–2003.

Haubner, R. Avril, N., Hanzopoulos, P.A., Gansbacher, B., and Schwaiger, M. 2000. *In vivo* imaging of herpes simplex virus type 1 thymidine kinase gene expression: early kinetics of radiolabelled FIAU. *Eur. J. Nuc. Med. 27*: 283–291.

Hospers, G.A., Calogero A., van Waarde A., Doze, P., Vaalburg, W., Mulder, N.H., and de Vries, E.F. 2000. Monitoring of herpes simplex virus thymidine kinase enzyme activity using positron emission tomography. *Cancer Res. 60*: 1488–1491.

Huber, B.E., Austin, E.A., Good, S.S., Knick, V.C., Tibbels, S., and Richards, C.A. 1993. *In vivo* antitumor activity of 5-fluorocytosine on human colorectal carcinoma cells genetically modified to express cytosine deaminase. *Cancer Res. 53*: 4619–4626.

Hüber, M.M. 1998. Fluorescently detectable magnetic resonance imaging agents. *Bioconjug. Chem. 9*: 242–249.

Hustinx, R., Shiue, C.Y., Alavi, A., McDonald, D., Shiue, G.G., Zhuang, H., Lanuti, M., Lambright, E., Karp, J.S., and Eck, S. 2001. Imaging *in vivo* herpes simplex virus thymidine kinase gene transfer to tumour-bearing rodents using positron emission tomography and (^{18}F)FHPG. *Eur. J. Nucl. Med. 28*: 5–12.

Ichikawa, T., Tamiya, T., Adachi, Y., Ono, Y., Matsumoto, K., Furuta, T., Yoshida, Y., Hamada, H., and Ohmoto, T. 2000. *In vivo* efficacy and toxicity of 5-fluorocytosine/cytosine deaminase gene therapy for malignant gliomas mediated by adenovirus. *Cancer Gene Ther. 7*: 74–82.

Lode, H.N., Bruchelt, G., Seitz, G., Gebhard, S., Gekeler, V., Niethammer, D., Beck, J. 1995. Reverse transcriptase-polymerase chain reaction (RT-PCR) analysis of monoamine transporters in neuroblastoma cell lines: correlations to meta-iodobenzylguanidine (MIBG) uptake and tyrosine hydroxylase gene expression. *Eur. J. Cancer 31A*: 586–590.

MacLaren, D.C., Gambhir, S.S., Satyamurthy, N., Barrio, J.R., Sharfstein, S., Toyokuni, T., Wu, L., Berk, A.J., Cherry, S.R., Phelps, M.E., and Herschman, H.R. 1999. Repetitive non-invasive imaging of the dopamine D2 receptor as a reporter gene in living animals. *Gene Ther. 6*: 785–791.

Mahony, W.B., Domin, B.A., McConnel, R.T., and Zimmerman, T.P. 1988. Acyclovir transport into human erythrocytes. *J. Biol. Chem. 263*: 9285–9291.

Mairs, R.J., Livingstone, A., Gaze, M.N., Wheldon, T.E., Barrett, A. 1994. A Prediction of accumulation of ^{131}I-labelled meta-iodobenzylguanidine in neuroblastoma cell lines by means of reverse transcription and polymerase chain reaction. *Br. J. Cancer 70*: 97–101.

Maron, A., Gustin, T., Le-Roux, A., Mottet, I., Dedieu, J.F., Brion, J.P., Demeure, R., Perricaudet, M., and Octave, J.N. 1996. Gene therapy of rat C6 glioma using adenovirus-mediated transfer of the Herpes Simplex Virus thymidine kinase gene: long-term follow up by magnetic resonance imaging. *Gene Ther. 3*: 315–322.

Morin, K.W., Knaus, E.E., Wiebe, L.I., Xia, H., and McEwan, A.J. 2000. Reporter gene imaging: effects of ganciclovir treatment on nucleoside uptake, hypoxia and perfusion in a murine gene therapy tumour model that expresses herpes simplex type-1 thymidine kinase. *Nucl. Med. Commun. 21*: 129–137.

Mullen, C.A., Coale, M.M., Lowe, R., and Blaese, R.M. 1994. Tumors expressing the cytosine

deaminase suicide gene can be eliminated *in vivo* with 5-fluorocytosine and induce protective immunity to wild type tumor. *Cancer Res. 54*: 1503–1506.

Myers, C.E. 1981. The pharmacology of the fluoropyrimidines. *Pharmacological Reviews 33*: 1–15. Namba, H., Tagawa, M., Miyagawa, T., Iwadate, Y., and Sakiyama, S. 2000. Treatment of rat experimental brain tumors by herpes simplex virus thymidine kinase gene-transduced allogeneic tumor cells and ganciclovir. *Cancer Gene Ther. 7*: 947–953.

Namba, H., Tagawa, M., Miyagawa, T., Iwadate, Y., and Sakiyama, S. 2000. Treatment of rat experimental brain tumors by herpes simplex virus thymidine kinase gene-transduced allogeneic tumor cells and ganciclovir. *Cancer Gene Therap. 7*: 947–953.

Nishiyama, T., Kawamura, Y., Kawamoto, K., Matsumura, H., Yamamoto, N., Ito, T., Ohyama, A., Katsuragi, T., and Sakai, T. 1985. Antineoplastic effects of 5-fluorocytosine in combination with cytosine deaminase capsules. *Cancer Res. 45*: 1753–1761.

Oliver, F.J., Collins, M.K.L., and Lopez-Rivas, A. 1997. Overexpression of a heterologous thymidine kinase delays apoptosis induced by factor deprivation and inhibitors of deoxynucleotide metabolism. *J. Biol. Chem. 272*: 10624–10630.

Poptani, H., Puumalainen, A.M., Grohn, O.H., Loimas, S., Kainulainen, R., Yla-Herttuala, S., and Kauppinen, R.A. 1998. Monitoring thymidine kinase and ganciclovir-induced changes in rat malignant glioma *in vivo* by nuclear magnetic resonance imaging. *Cancer Gene Ther. 5*: 101–109.

Ram, Z., Culver, W.K., Walbridge, S., Blaese, R.M., and Oldfield E.H. 1993. In situ retroviral-mediated gene transfer for the treatment of brain tumors in rats. *Cancer Res. 53*: 82–88.

Ram, Z., Walbridge, S., Shawker, T., Culver, K.W., Blaese, R.M., and Oldfield, E.H. 1994. The effect of thymidine kinase transduction and ganciclovir therapy on tumor vasculature and growth of 9L gliomas in rats. *J. Neurosurg. 81*: 256–260.

Ram, Z., Culver, K., Oshiro, E.M., Viola, J.J., DeVroom, H.L., Otto, E., Long, Z., Chiang, Y., McGarrity, G.J., Muul, L.M., Katz, D., Blaese, R.M., and Oldfield, E.H. (1997) Therapy of malignant brain tumors by intratumoral implantation of retroviral vector-producing cells. *Nature Med. 3*: 1354–1361.

Rogers, B.E., McLean, S.F., Kirkman, R.L., Della Manna, D., Bright, S.J., Olsen, C.C., Myracle, A.D., Mayo, M.S., Curiel, D.T., and Buchsbaum, D.J. 1999. *In vivo* localization of [(111)In]-DTPA-D-Phe1-octreotide to human ovarian tumor xenografts induced to express the somatostatin receptor subtype 2 using an adenoviral vector. *Clin. Cancer Res. 5*: 383–393.

Ross, B.D., Kim, B., and Davidson, B.L. 1995. Assessment of ganciclovir toxicity to experimental intracranial gliomas following recombinant adenoviral-mediated transfer of the herpes simplex virus thymidine kinase gene by magnetic resonance imaging and proton magnetic resonance spectroscopy. *Clin. Cancer Res. 1*: 651–657.

Saito, Y., Price, R., Rottenberg, D.A., Fox, J.J., Su, T.L., Watanabe, K.A., and Philipps, F.A. 1982. Quantitative autoradiographic mapping of herpes simplex virus encephalitis with radiolabeled antiviral drug. *Science 217*: 1151–1153.

Sandmair, A.M., Loimas, S., Poptani, H., Vainio, P., Vanninen, R., Turunen,M., Tyynela, K., Vapalahti, M., and Yla-Herttuala, S. 1999. Low efficacy of gene therapy for rat BT4C malignant glioma using intra-tumoural transduction with thymidine kinase retrovirus packaging cell injections and ganciclovir treatment. *Acta Neurochir. Wien 141*: 867–872.

Sieger, S., Jiang, S., Schönsiegel, F., Eskerski H., Kübler W., Altmann A., and Haberkorn U. 2003. Tumour specific activation of the Sodium/Iodide Symporter Gene under Control of the Glucose Transporter Gene 1 Promoter (GTI-1.3). *Eur. J. Nucl. Med. 30*: 748–756.

Shand, N., Weber, F., Mariani, L., Bernstein, M., Gianella-Borradori, A., Long, Z., Sorensen, A.G., and Barbier, N. 1999. A phase 1–2 clinical trial of gene therapy for recurrent glioblastoma multiforme by tumor transduction with the herpes simplex thymidine kinase gene followed by ganciclovir. GLI328 European-Canadian Study Group. *Hum. Gene Ther. 10*: 2325–2335.

Shields, A.F., Lim, K., Grierson, J., and Krohn, K.A. 1990. Utilization of labelled thymidine in DNA sythesis : Studies for PET. *J. Nucl. Med. 31*: 337–342.

Stegman, L.D., Rehemtulla, A., Beattie, B., Kievit, E., Lawrence, T.S., Blasberg, R.G., Tjuvajev,

J.G., and Ross, B.D. 1999. Noninvasive quantitation of cytosine deaminase transgene expression in human tumor xenografts with *in vivo* magnetic resonance spectroscopy. *Proc. Natl. Acad. Sci. USA 96*: 9821–9826.

Stegman, L.D., Rehemtulla, A., Hamstra, D.A., Rice, D.J., Jonas, S.J., Stout, K.L., Chenevert, T.L., and Ross, B.D. 2000. Diffusion MRI detects early events in the response of a glioma model to the yeast cytosine deaminase gene therapy strategy. *Gene Ther. 7*: 1005–1010.

Su, M.Y., Taylor, J.A., Villarreal, L.P., and Nalcioglu, O. 2000. Prediction of gene therapy-induced tumor size changes by the vascularity changes measured using dynamic contrast-enhanced MRI. *Magn. Reson. Imaging 18*: 311–317.

Tjuvajev, J.G., Avril, N., Oku, T., Sasayama, T., Miyagawa, T., Joshi, R., Safer, M., Beattie, B., DiResta, G., Daghighian, F., Augensen, F., Koutcher, J., Zweit, J., Humm J, Larson SM, Finn R, Blasberg R. 1998. Imaging herpes virus thymidine kinase gene transfer and expression by positron emission tomography. *Cancer Res. 58*: 4333–4341.

Venkataraman, G.M., Yatin, M., Marcinek, R., and Ain, K.B. 1999. Restoration of iodide uptake in dedifferentiated thyroid carcinoma: relationchip to human Na+/I-symporter gene methylation status. *J. Clin. Endocrinol. Metab. 84*: 2449–2457.

Wallace, P.M., MacMaster, J.F., Smith, V.F., Kerr, D.E., Senter, P.D., and Cosand, W.L. 1994. Intratumoral generation of 5-fluorouracil mediated by an antibody-cytosine deaminase conjugate in combination with 5-fluorocytosine. *Cancer Res. 54*: 2719–2723.

Weissleder, R., Simonova, M., Bogdanova, A., Bredow, S., Enochs, W.S., and Bogdanov, A. Jr. 1997. MR imaging and scintigraphy of gene expression through melanin induction. *Radiology 204*: 425–429.

Weissleder, R., Tung, C.H., Mahmood, U., and Bogdanov, A. Jr. 1999. *In vivo* imaging of tumors with protease-activated near-infrared fluorescent probes. *Nature Biotechnol. 17*: 375–378.

Weissleder, R., Moore, A., Mahmood, U., Bhorade, R., Benveniste, H., Chiocca, E.A., and Basilion, J.P. 2000. *In vivo* magnetic resonance imaging of transgene expression. *Nature Med. 6*: 351–354.

Wertheimer, E., Sasson, S., Cerasi, E., and Ben-Neriah, Y. 1991. The ubiquitous glucose transporter GLUT-1 belongs to the glucose-regulated protein family of stress-inducible proteins. *Proc. Natl. Acad. Sci. USA 88*: 2525–2529.

Zinn, K.R., Buchsbaum, D.J., Chaudhuri, T.R., Mountz, J.M., Grizzle, W.E., and Rogers, B.E. 2000. Noninvasive monitoring of gene transfer using a reporter receptor imaged with a high-affinity peptide radiolabeled with ^{99m}Tc or ^{188}Re. *J. Nucl. Med. 41*: 887–895.

5
Role of *TP53* Mutations in Cancer (An Overview)

Franck Toledo

INTRODUCTION

p53 was discovered in 1979 as a cellular protein that forms a complex with the SV40 large T antigen in SV40-transformed cells, which first suggested that p53 was an oncoprotein. Ten years later, however, several studies led to the conclusion that p53 is a tumor suppressor protein. Among these was the seminal study by Baker *et al*. (1989), which reported colorectal cancer cell lines containing one mutated *TP53* allele and missing the other allele, an observation consistent with the theoretical hallmark of tumor suppressors (Knudson, 1985). The mutation/deletion of *TP53* was soon demonstrated in many common tumor types (Nigro *et al*., 1989), and the cancer-prone Li-Fraumeni Syndrome, which is characterized by a familial clustering of early (<45 years) onset tumors, was found to be caused by germline mutations in the *TP53* gene (Malkin *et al*., 1990).

Since then, thousands of studies have reported mutations in the *TP53* gene, and the International Agency for Research on Cancer (IARC) *TP53* mutation database (Olivier *et al*., 2002) contains >23,000 somatic and close to 400 germline mutations in its latest release (R11, October 2006). We now know that *TP53* is mutated in ~50% of all human cancers, and that alterations of regulators or targets of p53 occur in the remainder, which demonstrates the crucial role of the p53 pathway in tumor suppression. This review aims to summarize what *TP53* mutations may reveal regarding p53 function or cancer development, and to address whether data on *TP53* mutations may have prognostic and predictive values, or can be used to design new therapeutic strategies.

IMPACT OF *TP53* MUTATIONS ON P53 TRANSACTIVATION CAPACITY

Human p53 is a 393-amino acids transcription factor that responds to various stresses including DNA damage and oncogene activation to regulate target genes involved in cell cycle arrest, apoptosis, senescence or DNA repair, preventing cells with a damaged genome to proliferate (Vogelstein *et al*., 2000). Recent reports disclosed new p53 target genes involved in various processes including glycolysis, autophagy, cell motility, mRNA maturation, and suntanning, which may also participate in p53

tumor suppressive functions. In addition, p53 has been proposed to induce apoptosis through non-transcriptional cytoplasmic mechanisms (Mihara *et al*., 2003), but such mechanisms may also rely on p53 target gene products (Chipuk *et al*., 2005).

Because of its cytostatic and cytotoxic functions, p53 is tightly regulated, essentially at the protein level, so that it becomes active and stable in response to stress. The related proteins Mouse Double Minute 2 (MDM2) and MDM4 (also known as MDMX) are essential inhibitors in this regulation, as demonstrated by the p53-dependent death of MDM2-deficient and MDM4-deficient mouse embryos (Toledo and Wahl, 2006). Recent *in vivo* studies concluded that MDM2 and MDM4 have complementary roles in p53 regulation; MDM2 is the major regulator of p53 stability, as it ubiquitinates p53 to trigger its degradation by the proteasome, whereas MDM4 acts a major regulator of p53 activity, probably by occluding the p53 transactivation domain. But, the regulation of p53 is extremely complex, as >160 additional proteins are thought to interact with p53 to affect its activity and stability (Toledo and Wahl, 2006). p53 is a modular protein with 5 proposed domains: an N-terminal transactivation domain (TAD), a proline-rich domain (PRD), a core DNA binding domain (DBD), a tetramerization domain (4D) and a C-terminal regulatory domain (CTD) (Figure 5.1A). According to *in vitro* and transfection studies, many p53-interacting proteins would modify residues in the TAD, the PRD, and the CTD, and these post-translational modifications would provide on or off switches for p53 function. The phosphorylation of serines and threonines in the TAD, the PRD, and the CTD, the isomerization of prolines in the PRD, and the ubiquitinylation or acetylation of lysines in the CTD were proposed to be critical determinants of p53 stability and activity (Toledo and Wahl, 2006).

The distribution of *TP53* somatic mutations in human cancers, however, does not support this model (Figure 5.1B). More than 70% of the reported *TP53* mutations are missense mutations, which allow the evaluation of phenotypic consequences of mutating a single residue. Strikingly, mutations of modified residues in the TAD, the PRD, and the CTD are extremely rare, and most missense mutations cluster in the core DNA-binding domain (Figure 5.1B). This distribution suggests that the mutation of a single modified residue in the TAD, the PRD or the CTD does not alter p53 function sufficiently to engender a selective advantage. In support of this conclusion, mouse models expressing targeted mutations of modified residues were recently shown to have modest phenotypes: p53 mutants of serines in the TAD, threonines and prolines in the PRD, or serines and lysines in the CTD, are still able to suppress tumors, often as efficiently as wild-type p53 (Toledo and Wahl, 2006).

The distribution of *TP53* mutations in tumors does not suggest that N-terminal and C-terminal modified residues act as on or off switches of p53 function, but rather emphasizes that an alteration of the p53 core DNA binding domain promotes tumor formation. As the DBD is essential for the recognition of specific consensus sequences in the promoters of target genes, most mutations in this domain are expected to decrease p53 DNA binding capacity and its transactivation activity. Clear evidence for this has been obtained. The crystal structure of the p53 DBD bound to DNA has been characterized by X-ray

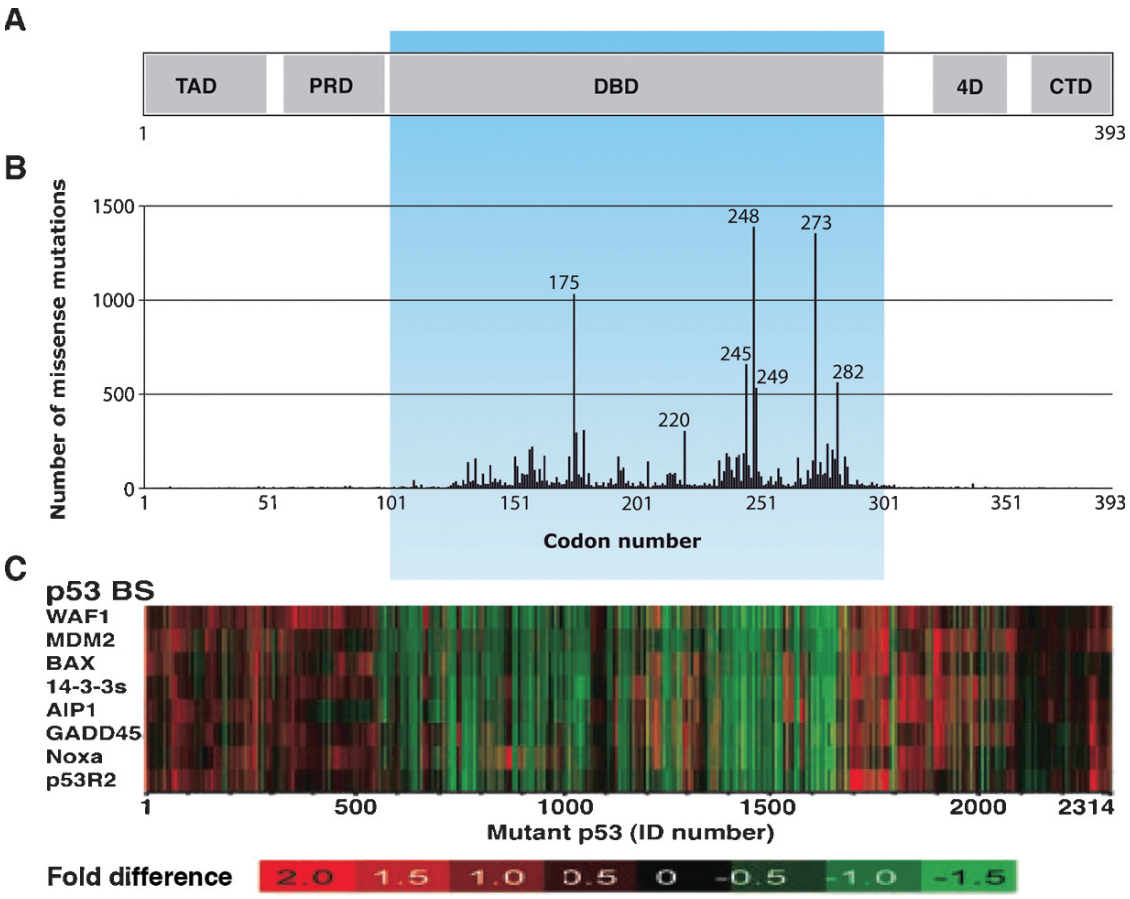

FIGURE 5.1. *TP53* missense mutations are clustered in the DNA binding domain, and affect p53 transactivation capacity. A simplified map of Human p53 is shown **(A)**. Human p53 consists of 393 amino acids, with 5 proposed domains: the transactivation domain (residues 1–40), required for transcriptional activation; the proline-rich domain (61–94) proposed to enable protein-protein interactions; the DNA binding domain (100–300) that specifically binds to target promoters; the tetramerization domain (324–355); and a C-ter regulatory domain (360–393). Below the map **(B)**, the number of missense somatic mutations in human cancers for each codon, according to the IARC *TP53* mutation database R10 (July 2005), was plotted against the p53 map. Data are from a total of 15,911 tumors. The 7 most frequently mutated residues are indicated. Below **(C)**, the transactivation activity of 2,314 missense mutants was assayed in yeast and plotted against the map. The capacity of mutants to transactivate 8 target genes (p21/WAF1, MDM2, Bax, 14-3-3σ, AIP1, GADD45, Noxa, p53R2), relative to that of wild-type p53, is shown. (Adapted from Toledo and Wahl, 2006.)

crystallography, and in its free form in solution by NMR. The p53 DNA binding domain consists of a central β-sandwich that acts as a scaffold for the DNA binding surface, which is composed of two large loops (L2, residues 163–195; and L3, residues 236–251), stabilized by a Zinc ion and a loop-sheet-helix motif (Figure 5.2). Compared to the DBDs of its paralogs p63 and p73, the p53 DBD has evolved to be dynamic and unstable, with a melting temperature of ≈ 42°C. Out of the 7 residues

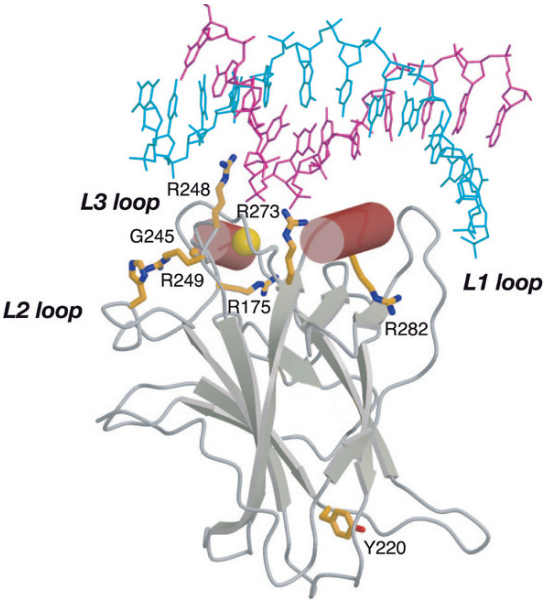

FIGURE 5.2. Structure of the p53 DNA binding domain bound to DNA. The two strands of bound consensus DNA are shown in blue and magenta. The bound Zinc ion is shown as a golden sphere, and the 7 residues for which missense mutations are frequently observed in human cancers (see Figure 5.1) are highlighted in orange. (Adapted from Joerger *et al*. 2006.)

most frequently mutated in human tumors (Figure 5.1B), 6 are located in or very close to the DNA binding surface (Figure 5.2). Mutants of these residues can be subdivided into two classes. In the first class, «contact mutants» directly affect DNA binding, because a DNA-contacting residue is lost: the cancer hotspot mutations R248Q, R248W, R273H, and R273C belong to this class. The second class includes mutants R175H, G245S, R249S, and R282W, which are «structural mutants», because they alter the structure of the core domain, thereby affecting DNA binding indirectly (Joerger *et al*., 2006). As for mutation Y220C, it is the most frequent mutation in human cancers that does not affect the DNA binding surface. It was recently shown to cause a loss of hydrophobic interactions, which reduce the core thermodynamic stability (Joerger *et al*., 2006). Thus, the 9 most frequent *TP53* mutations directly affect DNA binding or alter the structure of the DBD. Furthermore, a systematic analysis of the activity of all (2,314) possible missense mutations produced by single-nucleotide substitution in the entire *TP53* sequence revealed that mutations in the TAD, PRD, or CTD have little effect on the transactivation of 8 tested target genes, whereas mutations in the DBD more dramatically affect transactivation (Kato *et al*., 2003 and Figure 5.1C). Strikingly, with this assay, the above mentioned 9 mutations most frequently observed in human cancers have lost all capacity to transactivate target genes. Together, the present data lead to the conclusion that loss of p53 transactivation capacity is strongly selected for the development of human cancers.

The analysis of *TP53* germline mutations strengthens this conclusion. *TP53* germline mutations are mainly associated with Li-Fraumeni and Li-Fraumeni-like syndromes (LFS and LFL, respectively). The clinical definition of LFS includes a proband with early (<45 years of age) onset sarcoma, a first degree relative with early onset cancer, and another first or second degree relative with early onset sarcoma. LFL corresponds to a less severe phenotype, as it includes families with one of two tumors at a later age. Families with germline *TP53* mutations that do not fulfill LFS and LFL definitions are designated FH (Family History); these are associated with an even less severe phenotype, as they usually correspond to a familial clustering of later onset tumors. Importantly, in LFS families 92% of *TP53* missense mutations abolish all transactivation capacity, whereas only 70% in LFL and 65% in FH families do

so, suggesting a direct correlation between the frequency of transactivation loss and the severity of the phenotype. In addition, carriers of a germline mutation that abolish transactivation develop breast or colorectal cancers 10–15 years earlier than carriers of a mutation that maintains some transactivation capacity (Petitjean *et al*., 2007). Together, the data indicate that loss of transactivation capacity is a key factor in the selection of missense mutations, and that it may also accelerate cancer development. However, this may not be the only factor involved, as both wild-type and mutant p53 may have additional functions discussed below.

OTHER EFFECTS OF *TP53* MUTATIONS

While crystallography and NMR studies of p53 mutants indicate that DNA binding by the DBD is essential to transactivate target genes, the DBD is also known to be involved in protein-protein interactions that may alter transactivation by p53. For example, the interaction of the SV40 large T-antigen with the p53 DBD stabilizes p53 but inhibits its transactivation activity. The apoptosis stimulating proteins of p53 (ASPP) were also shown to interact with the p53 DBD to promote apoptosis rather than cell cycle arrest, presumably by selectively inducing the transactivation of pro-apoptotic genes. The p53 DBD is also proposed to be involved in protein-protein interactions mediating transcription-independent apoptotic processes (Mihara *et al*., 2003). Upon stress, cytoplasmic p53 would bind anti-apoptotic BclXL (Bcl2-related protein, long isoform), leading to mitochondrial outer membrane permeabilization and cytochrome c release. Mihara *et al*. (2003) observed that p53 mutants R175H, L194F, R273H and R280K have a decreased ability to bind BclXL, and proposed that p53 mutations occurring in human tumors select against the transcriptional and non-transcriptional activity of p53 concomitantly. However, the rather rare L194F mutant retains some transcriptional activity while it is completely unable to bind BclXL. Transcriptional activation is dramatically reduced in the other mutants, R175H, R273H, and R280K, which are more frequently found in human cancers (Kato *et al*., 2003), yet R280K retains some capacity to bind BclXL (Mihara *et al*., 2003). Taken together, the present data suggest that the frequency of a mutation in human tumors correlates well with a loss of transactivation activity, but not with a loss of BclXL binding. A more stringent selection against transactivation activity than against BclXL binding in tumorigenesis is also consistent with data indicating that PUMA, the product of a pro-apoptotic p53 target gene, is essential for transcription-independent apoptotic processes (Chipuk *et al*., 2005). Indeed, the analysis of 179 missense p53 mutants suggests a good correlation between the capacity to transactivate PUMA and that to induce apoptosis (Toledo and Wahl, 2006).

In addition to the loss of p53 wild-type functions, some mutants may gain new, oncogenic functions. Most p53 mutations in human cancers are missense mutations encoding full-length p53 mutants that often accumulate in the nucleus of tumor cells. The mechanisms underlying mutant p53 accumulation are not completely understood, but decreased MDM2 levels are a likely important factor. As *MDM2* is a p53 target gene, a mutant p53 with reduced transactivation capacity will

lead to less MDM2 in the cell to target for its degradation. However, mouse studies revealed that p53 mutants that accumulate in tumors are less abundant in normal tissues, indicating that additional events during tumorigenesis are required for mutant p53 to accumulate (Olive *et al*., 2004). Recent data suggest what the additional events might be, as cancer cells appear to have constitutive ARF activation (Ventura *et al*., 2007) or an activated DNA damage signaling (Brummelkamp *et al*., 2006). Thus, mutant p53 might accumulate more in tumor cells because the limited amount of MDM2 in these cells is inhibited by ARF (Sherr, 2006) or DNA damage signaling induces MDM2 auto-ubiquitination (Toledo and Wahl, 2006). Accumulated mutant p53 may gain oncogenic functions, as it engages in new protein-protein interactions and/or alters the expression of genes not regulated by WT p53. The DBD of mutant p53 was found to interact with family members p73 and p63 to inhibit their activities. These interactions would promote tumorigenesis; for example, the interaction of mutant p53 DBD with p73 may inhibit apoptosis (Stiewe, 2007). Recently, the interaction of R273H and R248W p53 mutants with Mre11 (homolog of *S. Cerevisiae* Meiotic Recombination 11) was also shown to impair ATM (*Ataxia Telangectasia* Mutated)-dependent cellular responses to double strand breaks (Song *et al*., 2007). Mutant p53 may also transactivate new genes, to promote cancer development (e.g., the transactivation of *NFKB2* [*Nuclear Factor Kappa-B2*]) or cancer chemoresistance (e.g., the transactivation of *MDR1* [*Multi-Drug Resistance 1*]), through mechanisms that remain poorly understood. Importantly, the comparison of the transcriptional programs of different p53 mutants show that they share some, but not all transcriptional targets, suggesting that they may possess distinct gain-of-function phenotypes. In addition, mouse models suggest that a mutant p53 may have tissue-specific gain-of-function. A gain-of-function for mouse mutant R270H (equivalent to the hot-spot human mutation R273H) was shown to promote sinonasal carcinomas, but neither lung adenocarcinomas nor skin tumors (Wijnhoven *et al*., 2007). Evidence that mutant p53 gain-of-function may participate in cancer development has thus been obtained. However, the present database of somatic p53 mutations in human cancers does not suggest that gain-of-function is strongly selected during cancer development (Petitjean *et al*., 2007).

p53 transcriptional activity relies on the formation of tetramers. Mutant proteins may interfere with wild-type p53 by forming hetero-tetramers less competent for specific DNA binding. The capacity of mutant proteins to interfere with the wild type form, often called dominant-negative effect (DNE), has been studied using transactivation assays in yeast or human cells (Dearth *et al*., 2007). These studies led to the proposal that most of the mutations frequently found in tumors have lost p53 transactivation capacity and are, in addition, able to interfere with WT p53 (Dearth *et al*., 2007). As mentioned earlier, a hallmark of tumor suppressor genes is the observation of tumors with a mutated allele of the gene and the loss of the other allele, i.e., a loss of heterozygosity (LOH). Importantly, a p53 mutant that would exert a strong DNE would alleviate the need for LOH at *TP53* in tumors because p53 heterotetramers would be nonfunctional. Unfortunately, most of the studies reported

in the IARC *TP53* mutation database did not include LOH analyses. Data on LOH for p53 missense mutations in the DBD are available for only 159 tumors; LOH was found in 94 of the tumors, but not in the remainder 65 cancers (41%) (Dearth *et al*., 2007). Likewise, earlier studies indicated that 38% of 150 tumors in germline *TP53* mutation carriers do not show LOH at *TP53*, and that most tumors in germline carriers of the hotspot mutation R248Q do not show LOH at *TP53*. Mouse models also reveal that a R270H mutant (equivalent to human R273H) exerts DNE in both skin cancer and advanced lung cancer. However, the DNE is only partial in lung tumors because all lung cancers show LOH at *TP53*, whereas most skin tumors retain the WT allele, indicating a stronger DNE in this tumor site (Wijnhoven *et al*., 2007). Together, the data indicate that DNE is likely an important factor in the development of some cancers. Because the dogma for tumor suppressor genes is that LOH is required for tumor development, the DNE of p53 mutants was probably underestimated for many years. More studies are thus required to identify the p53 mutants with strong DNE *in vivo*, and to characterize possible tissue-specific requirements for LOH for any given *TP53* mutation.

TP53 MUTATIONS AND THE ETIOLOGY OF HUMAN CANCERS

The distribution of *TP53* missense mutations in all human cancers correlates with their functional impact, as the most frequent mutations severely impair sequence-specific DNA binding and transactivation (Figures 5.1 and 5.2). Importantly, however, the mutation hotspots in *TP53* may reflect not only the selective growth advantage they confer to mutated cells, but also the mutability of a particular codon to endogenous metabolites or exogenous carcinogens. For instance, the hypermutability of methylated CpG dinucleotides is well documented: the 5′-methylated cytosine undergoes spontaneous deamination at a higher rate than the unmethylated base, leading to a C - > T transition. CpG dinucleotides in *TP53* are highly methylated, apparently in all human tissues (Tornaletti and Pfeifer, 1995). The 23 methylated CpGs located between codons 120 and 290 of the p53 DBD represent ~8% of the DBD sequence, but 33% of all mutations in this region. Furthermore, out of the 7 hotspots for missense mutations (Figure 5.1), 5 contain methylated CpGs (codons 175, 245, 248, 273, and 282), and a hotspot for a truncating mutation (codon 213) also contains a methylated CpG. Importantly however, transversions at guanines adjacent to a methylated cytosine also account for mutations at some of these residues (codons 248 and 273), confirming that a strong biological selection contributes to the frequency of these *TP53* mutation hotspots in the IARC database.

While the deamination of methylated cytosines is an endogenous mutagenic process, strong evidence that exogenous carcinogens may alter the distribution of *TP53* mutations has been shown in some cancers. For example, the incidence rates of hepatocellular carcinoma (HCC) reflects the prevalence of two main etiologic factors: hepatitis B or C infections and exposure to aflatoxins in the diet. In high incidence areas, such as Mozambique, Senegal, and Gambia (Africa) or the

Qidong county (China), the most frequent mutation in *TP53* is R249S, whereas this mutation is uncommon in HCC from other geographic areas, or in other cancers worldwide. High incidence areas for HCC are regions where the molds *Aspergillus flavis* and *Aspergillus parasiticum* contaminate maize and peanuts. These molds produce aflatoxins that, once metabolized by the liver, may generate DNA adducts at several guanines in *TP53*, leading to G to T transversions. Interestingly, as aflatoxin adducts are found at codon 249 but also at a few other codons, the high frequency of the R249S (AG*G* -> AG*T*) mutation also results from its clonal selection during hepatocellular carcinogenesis (Denissenko *et al*., 1998).

Cigarette smoking was also shown to cause distinctive mutations in the *TP53* gene. In a recent study, *TP53* mutations were found in >75% of lung cancers from current smokers, but less than half of lung cancers from patients who never smoked (Le Calvez *et al*., 2005). Furthermore, the *TP53* mutational spectrum in all cancers is dominated by C -> T transitions, whereas transversions are found in most lung cancers from smokers (Le Calvez *et al*., 2005). Particularly, G -> T transversions are considered as mutagen fingerprints of cigarette smoking, as they are 5 times more frequent in lung cancers from smokers than that from non smokers (Le Calvez *et al*., 2005). These transversions often occur in methylated CpG sequences at codons 157, 158, 245, 248 and 273, which have been experimentally shown to be preferred sites of adduct formation by benzo(a)pyrene metabolites, a polycyclic aromatic hydrocarbon found in tobacco smoke. Codon 156 was also experimentally shown to be a preferred site for benzo(a)pyrene adduct formation, but it is not selected for in tumors, as in this case the G -> T transversion leads to a silent mutation. Interestingly, most G -> T transversions found in lung cancers are attributed to guanines on the non transcribed strand of the *TP53* gene, consistent with experimental evidence that benzo(a)pyrene adducts in the transcribed strand are more efficiently repaired. Thus, the distribution of *TP53* mutations in lung cancers from smokers apparently results from the combined effects of site preference for adduct formation, differential DNA strand repair efficiencies, and clonal selection of the mutations that most affect p53 function.

Evidence that preferential sites for adduct formation and DNA repair efficiency contribute to the spectrum of *TP53* mutations was also obtained for sun-induced skin cancers. In non-melanoma skin cancers such as basal cell carcinomas, an increased frequency of C -> T transitions is observed, including tandem CC -> TT transitions in 6% of all mutations, a type of mutation never observed in tumors unrelated to Ultra-Violet (UV) irradiation. Furthermore, the *TP53* mutation hotspots in skin cancers are distinctive, as they map to codons including 151, 177, 178, and 278. The tandem CC -> TT transitions would result from UV-induced pyrimidine dimers that escape nucleotide excision repair (NER). In support of this, in skin tumors from *Xeroderma pigmentosum* patients, who present defects in NER, ~50% of *TP53* mutations, and 65% of mutations in *PTCH1* (Homolog of *Drosophila* Patched 1, another gene implicated in basal cell carcinomas) are CC-> TT transitions (Bodak *et al*., 1999). Furthermore, *TP53* mutations hotspots in skin cancers were found to be sites of slow repair of

UV-induced lesions. Such a clear association raises the question of skin cancers due to occupational exposure. Indeed farmers, fishermen or forestry workers, whose work exposes them to many hours of UV irradiation each day, are at considerable risk of developing basal cell carcinomas. Evidence for this was obtained by comparing the frequency of C -> T or CC -> TT transitions in *TP53* from sun exposed areas (head, neck, arms, and hands) and unexposed areas from 12 patients with UV-induced basal cell carcinomas suspected to be work-related. CC-> TT transitions were found only in samples from sun-exposed areas, and only in these samples was a predominance of C -> T transitions observed (Weihrauch *et al*., 2002). Possible work-related cancers are also suggested by the observation of distinctive *TP53* mutation spectra in the lung cancers of uranium miners or chromium workers, or in liver angiosarcomas of workers exposed to vinyl chloride. A strong correlation between a specific spectrum of *TP53* mutations and occupational exposure to a suspected carcinogen might have legal implications, as it could be used as evidence in court for work-related cancer cases.

PROGNOSTIC AND PREDICTIVE VALUE OF *TP53* MUTATIONS

The tumor node metastasis (TNM) histopathological system for cancer staging and grading classifies tumors according to their growth and dissemination. First proposed in the 1940s and constantly updated to integrate improvements in diagnosis and treatment, this system is the one of choice for prognosis, i.e., to estimate the outcome – survival or disease-free survival – of cancer patients at the time of diagnosis. The prognostic value of a classification system or a molecular marker thus reflects its capacity to inform on tumor aggressiveness. Also clinically important, a molecular marker may have predictive significance if it helps in evaluating the response to a specific therapeutic treatment. In the late 1980s and early 1990s, when it was found that *TP53* was mutated in ~50% of human cancers, p53 appeared to be a good candidate marker with prognostic and/or predictive value. Since then, hundreds of studies have been carried out to test the prognostic and predictive relevance of mutant p53, but results have often been inconsistent. Reasons for this are likely to include the methodology to detect mutants (e.g. DNA sequencing vs the identification of accumulated mutant proteins by immunohistochemistry), small sample size, or the use of variable adjuvant therapies. Meta-analyses of reports relying only on DNA sequencing to identify p53 mutants have suggested modest but significant increases in risk of death (1.3–2.2 fold) for patients with breast or colorectal cancers carrying *TP53* mutations (Pharoah *et al*., 1999; Munro *et al*., 2005). Also, in most studies *TP53* mutations were associated with poor response to various chemotherapeutic or radiotherapeutic regimens. However, even large-scale analyses present limitations, as they do not integrate the distinct phenotypic consequences of different *TP53* mutations. As mentioned earlier, some p53 mutants may retain partial tumor suppressive functions, whereas others may gain oncogenic functions or exert dominant negative effects. These differences

should translate into dramatic variations in tumor aggressiveness, or in responses to therapeutic agents. Direct evidence for this was obtained when the response to doxorubicin in breast tumors carrying different *TP53* mutations was analyzed (Aas *et al*., 1996) or, as mentioned earlier, when tumor onset in Li-Fraumeni families with different *TP53* mutations were compared (Petitjean *et al*., 2007). Some large-scale prognostic or predictive studies tried to integrate these parameters by including a classification of *TP53* mutations with regard to their position in the protein (e.g., in the L2 loop of the DBD). However, distinct mutations of a single codon may also have different properties. For instance, the R175H mutation is frequently found in human tumors, and the homologous murine mutant protein $p53^{R172H}$ has gained oncogenic, prometastatic functions (Olive *et al*., 2004). In striking contrast, the R175P mutation is rare in human cancers, consistent with the observation that the murine $p53^{R172P}$ mutant retains partial tumor-suppressive functions (Liu *et al*., 2004). Furthermore, we now also know that a large fraction of tumors with intact *TP53* may present other alterations in the p53 pathway, such as the amplification or overexpression of the p53 inhibitors MDM2 and MDM4 (Toledo and Wahl, 2006). Together, these factors contribute to limit the value of *TP53* mutations in prognostic and predictive studies. Nevertheless, as *TP53* mutations can be detected in circulating free DNA in various body fluids of cancer patients, it remains possible that they will prove useful to detect early relapse during post-treatment follow-up of patients with defined *TP53* mutations in the primary lesion (Fleischhacker and Schmidt, 2007).

CORRECTION OF P53 PATHWAY IN TUMORS

The frequent finding that tumors with *TP53* mutations are associated with a poor response to various therapeutic treatments (such as doxorubicin, fluorouracil, and tamoxifen) is consistent with the notion that these anticancer strategies often rely on p53-dependent anti-proliferative responses to be effective. An alternative is to develop strategies that directly attempt to restore p53 function in tumors (Figure 5.3). The potential of such strategies has been demonstrated *in vivo* in mouse models: the restoration of p53 function in various tumors leads to their regression due to p53-dependent apoptosis or senescence (Ventura *et al*., 2007). In the 50% of cancers that express a mutant p53, gene therapy, i.e. the introduction of a WT *TP53* allele, is a possible approach. A recombinant adenovirus carrying a *TP53* gene has been commercialized in China since 2004 under the name of Gendicine, and Phase III clinical trials of a similar product, Advexin, are presently being carried out in the USA. The use of such vectors in conjunction with classical radiotherapeutic or chemotherapeutic regimens is apparently successful for the treatment of head and neck squamous cell cancers, but the treatments are expensive, the therapeutic efficiency for other cancers is not firmly established, and the potential hazard of adenoviral vectors is still an issue (Jia, 2006).

Another strategy specifically targets mutant p53 in tumors. As mentioned above, many *TP53* mutations lead to an altered structure of the DNA binding domain, and thus to p53 misfolding and possibly aggregating. Mutations leading to protein misfolding are at the root of many other

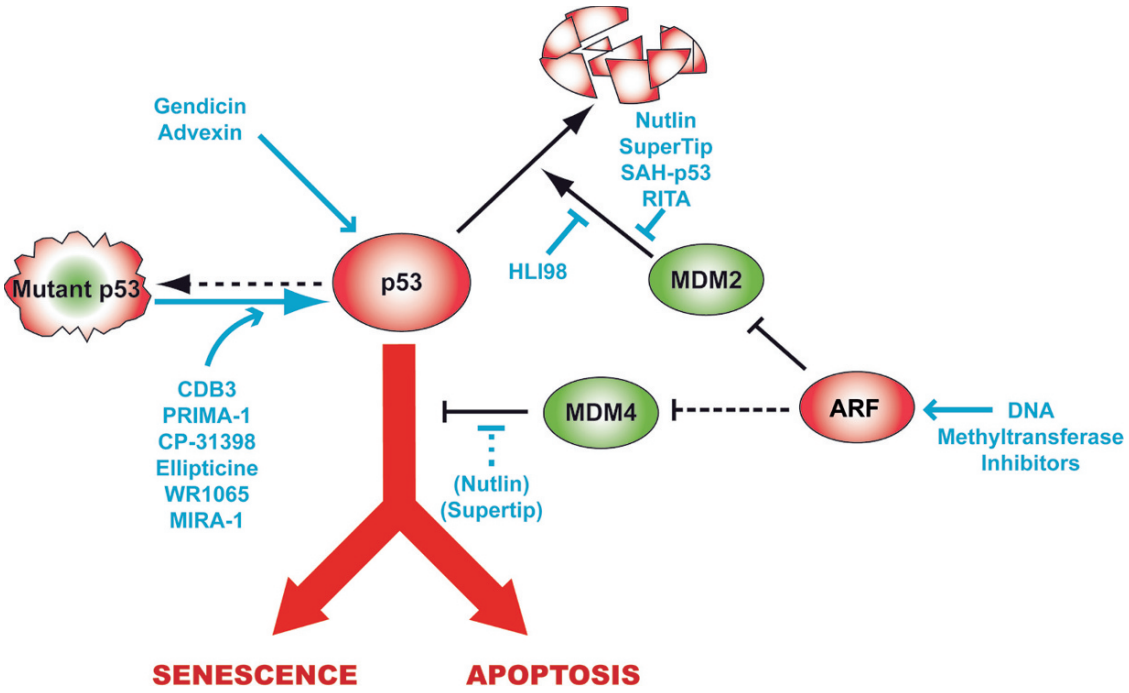

FIGURE 5.3. Strategies to reactivate p53 in tumors. The core components of the p53 pathway are shown, with oncogenes in green, tumor suppressors in red, and candidate therapeutic molecules in blue. Note that *TP53* mutations have various consequences, so that «mutant p53» may retain some tumor suppressive capacity, be inert, or acquire oncogenic properties. On the left, in about 50% of cancers, p53 is mutated. In these tumor cells, if wild-type p53 is absent (loss of heterozygosity), it can be reintroduced using gene therapy (Gendicine, Advexin). Alternatively, as many p53 mutations lead to a structural change affecting DNA binding, molecules (CDB3, etc…) that may restore a wild-type p53 conformation to mutant p53 can be considered, particularly for mutants that have a strong dominant negative effect. On the right: in the remaining cancers, a wild-type p53 is maintained, but its stability or activity is altered, often due to an amplification/overexpression of MDM2 or MDM4, or the inactivation of ARF. In these tumors, DNA methyl transferase inhibitors may reactivate ARF, and HLI98 may inhibit MDM2 ubiquitin-ligase activity. In addition, Nutlins or SuperTips may efficiently prevent p53-MDM2 interactions, but are inefficient to antagonize p53-MDM4 interactions. Importantly, molecules like Nutlins could also be used for tumors with hypomorphic p53 mutants, or in conjunction with gene therapy. All of these approaches aim to restore a wild-type p53 function in the tumor cell, to induce senescence or apoptosis. (Adapted from Toledo *et al*. 2007.)

human diseases, such as amyloidoses, cystic fibrosis and lysosomal storage diseases. A strategy for the treatment of such diseases is to develop small molecules, termed chemical chaperones, that will assist in protein refolding and reactivation. A similar strategy can be considered to restore a wild-type conformation to p53 mutants: destabilized p53 mutants would undergo a folding-unfolding equilibrium, involving numerous states ranging from native or native-like structures, through distorted structures, to globally unfolded states. A chemical chaperone that binds the

native, but not the denatured state, would result in a shift of the equilibrium towards the native state, leading to a restoration of activity (Bullock and Fersht, 2001). The structure of the complex between the p53 DBD and the protein ASPP2 was used as the starting point to design p53-specific chemical chaperones. This led to the identification of CDB3 (core domain binding peptide 3), a 9 amino-acid residue peptide that binds loop L1 of the p53 DBD (Friedler *et al*., 2002). Subsequent studies showed that the fluoresceinated derivative FL-CDB3 is 50 times more active than CDB3, and that it can restore the transactivation of the *p21* and *MDM2* genes by the hotspot p53 mutants R175H and R273H. These studies demonstrate that the rational design of a chemical chaperone may rescue p53 function. Alternatively, several recent studies have relied on the random screening of chemical libraries to identify small molecules that can restore a native conformation and/or DNA binding activity to mutant p53 proteins. These screens led to the discovery of molecules including ellipticine, CP-31398, PRIMA-1 and its methylated derivative PRIMA-1MET, WR-1065, and MIRA-1. Among these, PRIMA-1MET appears very promising, as it was shown to limit human tumor xenograft growth in SCID mice, and to synergize with traditional chemotherapeutic agents such as cisplatin (Bykov *et al*., 2005). A major inconvenience of random screens, however, is that the mode of action and/or specificity of the identified molecules remain obscure. For instance, CP-31398 was shown to inhibit tumor growth *in vivo* and alter the conformation of a mutant p53, but it does not interact with the p53 DBD, and it appears to induce both p53-dependent and p53-independent cell death, indicating that it also targets proteins other than p53 (Wischhusen *et al*., 2003).

In tumors expressing wild-type p53, p53 function is often lost due to an amplification/overexpression of its inhibitors MDM2 and MDM4, or due to the inactivation of ARF, a tumor suppressor that acts as an inhibitor of MDM2, and possibly MDM4. As ARF is often inactivated in tumors due to the methylation of its promoter, inhibitors of DNA methyltransferases, presently in clinical trials, can be considered. For those tumors that express wild-type p53 but have amplified the *MDM2* gene, inhibiting MDM2 activity has been considered an attractive anticancer strategy for many years. Analysis of the MDM2-p53 interface by crystallography indicated that only 3 residues in the p53 TAD (F19, W23, and L26) are essential for MDM2-p53 interactions, suggesting that small peptides or molecules that efficiently disrupt this interaction could be found. The first series of experiments using p53 TAD-derived peptides (called SuperTips) validated this approach, as SuperTips were found to specifically disrupt p53-MDM2 interactions (Bottger *et al*., 1997). The efficiency of these peptides was reduced, however, because they could form a helical structure when bound to MDM2, but adopted several conformations in solution. More recently, hydrocarbon stapling has been used to stabilize the helical structure of such peptides, leading to the design of SAH-p53, a peptide that more efficiently disrupts p53-MDM2 interactions, although its efficacy remains to be tested *in vivo* (Bernal *et al*., 2007). A similar approach has consisted of the screening for chemical molecules that mimic p53 TAD peptides, and several promising molecules have

been described in the past 3 years. Among them, Nutlin 3a was shown to induce the regression of human tumors xenografted in nude mice without any apparent toxicity for the mice (Vassilev, 2007). Another approach involved searching for molecules that inhibit the ubiquitin ligase activity of MDM2. Compounds such as HLI98 inhibit MDM2-dependent p53 degradation, but also exhibit p53-independent effects and were not tested *in vivo*. Finally, a cellular-based screen led to the identification of RITA, which was proposed to bind p53 in such a way to antagonize MDM2 binding, though this remains to be proven (Krajewski *et al*., 2005).

In recent years, MDM4 was shown to be frequently overexpressed in tumors, and to be an important regulator of p53 activity, suggesting that it could also be an interesting target in anticancer strategies (Toledo and Wahl, 2006). Importantly however, a screening for specific MDM4 antagonists remains to be reported. Despite the similarity of p53-MDM2 and p53-MDM4 interfaces, SuperTips and Nutlins were found to be poor antagonists of MDM4-p53 interactions. Finding specific MDM4 antagonists thus appears to be an important goal, because genetic approaches in the mouse (Toledo *et al*., 2006), or the combined use of Nutlin and MDM4 small interfering RNAs (Patton *et al*., 2006), indicate that MDM2 and MDM4 antagonists should cooperate to induce strong p53 activation in tumors. Importantly, MDM2 and MDM4 antagonists could also be important for the treatment of tumors expressing hypomorphic p53 mutants, i.e. mutants that remain partially functional.

Further studies are required to evaluate the feasability of these approaches in a clinical setting. The recent estimate that MDM2 and MDM4 antagonists could be used in the treatment of 2–3 millions patients diagnosed with cancer each year (Toledo and Wahl, 2006) provides a strong incentive for the search for p53-based anticancer strategies. Conceptually, this number could even be higher, if the combined use of Nutlins and a p53 adenovirus was shown to improve the effect of p53 gene therapy. In addition, synthetic chaperone molecules like CDB3, by correcting R175H and R273H mutants, might be useful in therapeutic regimens for millions of patients. Clearly, the ability to obtain diverse p53-activating strategies opens up exciting opportunites for the development and implementation of broadly applicable therapeutic regimens.

FUTURE PERSPECTIVES

The earlier sections have presented a general overview of the main p53 functions selected during cancer development, the potential use of *TP53* mutations to deduce the etiology of carcinogen-induced cancers or for prognostic and predictive studies, and strategies to reactivate p53 in cancer cells for therapeutic purposes. However, a few studies have revealed new notions in p53 regulation that are likely to impact on all of these aspects, providing additional layers of complexity that may take years to explore.

Among these is the evidence that the *TP53* gene encodes 9 (or possibly 10) different isoforms, which appear to have very distinct biological functions. Evidence that *TP53* encodes several isoforms was first observed for the mouse gene, with an alternative splicing between exons 10 and 11 that generates p53as, a p53 isoform with a variant C-terminus. However, p53as

was later shown to be mouse-specific, and instead, an alternative splicing between exons 9 and 10 in human *TP53* was found to generate the isoform p53i9, later called p53β (Bourdon *et al*., 2005). Another human p53 isoform with an N-terminal truncation of 39 amino-acids (due to an alternative splicing in intron 2 or alternate translation initiation in exon 4) was later found, and called p44, p47, ΔNp53 or Δ40p53 (Bourdon *et al*., 2005). Intra-exons splicing of exons 7–9 was also proposed to generate Δp53, an isoform with a partial deletion of the DBD (Rohaly *et al*., 2005), but this isoform remains controversial (Bourdon, 2007).

The most comprehensive study of human p53 isoforms was recently performed by Bourdon *et al*. (2005), who found an additional alternative splice site between exons 9 and 10 leading to isoform p53γ. In addition, they established that, similarly to the *TP63* and *TP73* genes, *TP53* has a dual gene structure, as it contains an alternative promoter in intron 4. This alternative promoter is conserved in evolution and leads to isoforms with an alternate translation start site at codon 133. Together, the combination of the different alternative splice sites and translation start sites would generate 9 isoforms, called p53, p53β, p53γ, Δ40p53, Δ40p53β, Δ40p53γ, Δ133p53, Δ133p53β, and Δ133p53γ, expressed in several human tissues in a tissue-dependent manner (Bourdon *et al*., 2005). Some of these isoforms were shown to have an impact on p53 transcriptional activity, e.g., apoptosis is slightly induced by the co-transfection of p53 and p53β, but strongly inhibited by the co-transfection of p53 and Δ133p53 (Bourdon *et al*., 2005). These findings, together with the abnormal expression of p53 isoforms observed frequently in breast cancers, acute myeloid leukemia, or head and neck squamous cell carcinomas, suggest that the balance and interactions between p53 isoforms may play a role in cancer development (Bourdon, 2007). Variations in the ratios of MDM2 or MDM4 isoforms might also modulate the p53 DNA damage response (Chandler *et al*., 2006). In fact, altered gene splicing has emerged as a common and likely major feature in human cancers.

The potential importance of p53 isoforms raises a series of questions regarding the biological, prognostic, and predictive significance of the *TP53* mutations reported in the IARC database. First, 39 missense somatic mutations at Methionine 133 are found in the IARC database (R11): whether these are primarily selected in tumors because they prevent the expression of the Δ133p53, Δ133p53β, and Δ133p53γ isoforms, or rather because they alter the DBD of all other p53 isoforms, remains to be determined. Second, 364 missense mutations affect the donor or acceptor splicing sites of regular exons. These represent ~1.5% of all missense mutations in the database. The proportion of tumors carrying missense mutations affecting splice sites of alternative exons, however, remains unknown, because most studies were not designed to detect them. Third, as the alternative promoter in intron 4 was found only recently, information is also lacking on possible mutations that would specifically affect this promoter. Fourth, chemotherapy of acute myeloid leukemia patients was shown to alter the ratio between p53 and one or several shorter isoforms *in vivo*. This suggests that better knowledge of the expression of p53 isoforms in different cancers, as well as of the effects of various therapeutic regimens on these isoforms,

might also prove useful for prognostic and predictive studies.

The biological importance of polymorphisms in the p53 pathway has also emerged in the past few years. By definition, a polymorphism has a minor allele frequency of >1% in at least one population. According to the IARC database, 42 polymorphisms have been described in the human *TP53* gene. All but one are single nucleotide polymorphisms (SNPs). Out of 41 SNPs, 7 are in exons, including 4 that change the p53 amino acid sequence: P/S at residue 47, R/P at residue 72, V/M at residue 217 and G/A at residue 360. The biological consequences of the latter two exonic SNPs are unknown. The serine polymorphic variant at codon 47 is found in <5% of African-Americans and undetectable in Caucasians. This variant was proposed to be a poorer substrate for the phosphorylation of serine 46, apparently correlating with a decrease in the transactivation of the *PUMA* and *p53AIP1* proapoptotic genes. However, the effects of the S47 polymorphism on cancer risk or therapy, if any, are presently unknown. The SNP at codon 72, initially identified because it gives rise to variants of distinct electrophoretic mobility, has been more extensively studied. This SNP occurs in the p53 PRD (Figure 5.1), a domain thought to be important for p53 regulation and function, through mechanisms that remain poorly understood. The R72 variant has been found to induce apoptosis more efficiently than the P72 variant, and this was proposed to result from an enhanced nuclear export of R72 that would favor the mitochondrial pathway of cell death (Dumont *et al*., 2003). Interestingly, the frequency of the P72 allele was found to vary from 17% in a population of Swedish Saamis to 63% in Nigerian Blacks. In fact, P72 allele frequency increases in a linear manner as populations near the equator (Sjalander *et al*., 1996). The recent finding that this polymorphism impacts on the suntan response provides a likely interpretation for such a geographical selective pressure (Cui *et al*., 2007). Furthermore, a number of studies suggest that the P72 variant correlates with an earlier tumor onset in head and neck squamous cell carcinomas and colorectal cancers, and that the R72 variant associates with a better survival after chemo- or radiotherapy of breast, lung, and head and neck cancers (Pietsch *et al*., 2006). Moreover, among the 35 polymorphisms in intronic *TP53* sequences, at least 2 appear to impact on cancer development: a 16 bp polymorphism in intron 3 and a SNP in intron 6 (Pietsch *et al*., 2006).

The seminal work of Bond *et al*. (2004) has recently demonstrated that polymorphisms in other genes in the p53 pathway may also impact on cancer development. These authors identified a SNP in the promoter of the *MDM2* gene (SNP309, with T/G alleles) and proposed that the G allele would increase the DNA binding affinity of the transcriptional activator Sp1, leading to increased MDM2 levels attenuating p53 responses. In agreement with this, the G allele associates with accelerated tumor formation in both hereditary and sporadic cancers (Bond *et al*., 2004). Interestingly, SNP309 is located in a region of the MDM2 promoter that is regulated by estrogens, and recent data suggest that an active estrogen-signaling pathway is needed for the G allele to accelerate tumor formation in humans, so that SNP309 affects cancer development in a gender-specific manner (Bond *et al*., 2006). These find-

ings indicate that a better understanding of the biological impact of SNPs in the p53 pathway is required to improve the relevance of prognostic and predictive studies of *TP53* mutations in cancer. Likewise, the combined sequencing of *TP53* and other genes frequently mutated in cancer, or the development of methods facilitating the discovery of multiple somatic mutations in cancer tissues, are likely to improve the clinical relevance of such studies. Indeed, sequence variations in SNPs or multiple genes in the p53 pathway probably account for the fact that p53-specific transcript profiles in cancer cells are better prognostic and predictive indicators than *TP53* mutations (Miller *et al*., 2005). In the future, the characterization of SNPs and multiple mutated genes in cancers should contribute to the development of optimal therapeutic strategies specifically designed to integrate both the genetic background of the patient and the somatic alterations in the tumor.

Acknowledgements. This work was supported by Grant #4046 from the Association pour la Recherche sur le Cancer. I would like to thank Iva Simeonova and Olivier Bluteau for comments on the manuscript.

REFERENCES

Aas, T., Borresen, A. L., Geisler, S., Smith-Sorensen, B., Johnsen, H., Varhaug, J. E., Akslen, L. A., and Lonning, P. E. 1996. Specific P53 mutations are associated with de novo resistance to doxorubicin in breast cancer patients. *Nat. Med. 2*: 811–814.

Baker, S. J., Fearon, E. R., Nigro, J. M., Hamilton, S. R., Preisinger, A. C., Jessup, J. M., vanTuinen, P., Ledbetter, D. H., Barker, D. F., Nakamura, Y., White, R., and Vogelstein, B. 1989. Chromosome 17 deletions and p53 gene mutations in colorectal carcinomas. *Science 244*: 217–221.

Bernal, F., Tyler, A. F., Korsmeyer, S. J., Walensky, L. D., and Verdine, G. L. 2007. Reactivation of the p53 tumor suppressor pathway by a stapled p53 peptide. *J. Am. Chem. Soc. 129*: 2456–2457.

Bodak, N., Queille, S., Avril, M. F., Bouadjar, B., Drougard, C., Sarasin, A., and Daya-Grosjean, L. 1999. High levels of patched gene mutations in basal-cell carcinomas from patients with xeroderma pigmentosum. *Proc. Natl. Acad. Sci. U.S.A. 96*: 5117–5122.

Bond, G. L., Hu, W., Bond, E. E., Robins, H., Lutzker, S. G., Arva, N. C., Bargonetti, J., Bartel, F., Taubert, H., Wuerl, P., Onel, K., Yip, L., Hwang, S. J., Strong, L. C., Lozano, G., and Levine, A. J. 2004. A single nucleotide polymorphism in the MDM2 promoter attenuates the p53 tumor suppressor pathway and accelerates tumor formation in humans. *Cell 119*: 591–602.

Bond, G. L., Hirshfield, K. M., Kirchhoff, T., Alexe, G., Bond, E. E., Robins, H., Bartel, F., Taubert, H., Wuerl, P., Hait, W., Toppmeyer, D., Offit, K., and Levine, A. J. 2006. MDM2 SNP309 accelerates tumor formation in a gender-specific and hormone-dependent manner. *Cancer Res. 66*: 5104–5110.

Bottger, A., Bottger, V., Sparks, A., Liu, W. L., Howard, S. F., and Lane, D. P. 1997. Design of a synthetic Mdm2-binding mini protein that activates the p53 response in vivo. *Curr. Biol. 7*: 860–869.

Bourdon, J. C. 2007. p53 and its isoforms in cancer. *Br. J. Cancer 97*: 277–282.

Bourdon, J. C., Fernandes, K., Murray-Zmijewski, F., Liu, G., Diot, A., Xirodimas, D. P., Saville, M. K., and Lane, D. P. 2005. p53 isoforms can regulate p53 transcriptional activity. *Genes Dev. 19*: 2122–2137.

Brummelkamp, T. R., Fabius, A. W., Mullenders, J., Madiredjo, M., Velds, A., Kerkhoven, R. M., Bernards, R., and Beijersbergen, R. L. 2006. An shRNA barcode screen provides insight into cancer cell vulnerability to MDM2 inhibitors. *Nat. Chem. Biol. 2*: 202–206.

Bullock, A. N., and Fersht, A. R. 2001. Rescuing the function of mutant p53. *Nat. Rev. Cancer 1*: 68–76.

Bykov, V. J., Zache, N., Stridh, H., Westman, J., Bergman, J., Selivanova, G., and Wiman, K. G. 2005. PRIMA-1(MET) synergizes with cisplatin

to induce tumor cell apoptosis. *Oncogene 24*: 3484–3491.

Chandler, D. S., Singh, R. K., Caldwell, L. C., Bitler, J. L., and Lozano, G. 2006. Genotoxic stress induces coordinately regulated alternative splicing of the p53 modulators MDM2 and MDM4. *Cancer Res. 66*: 9502–9508.

Chipuk, J. E., Bouchier-Hayes, L., Kuwana, T., Newmeyer, D. D., and Green, D. R. 2005. PUMA couples the nuclear and cytoplasmic proapoptotic function of p53. *Science 309*: 1732–1735.

Cui, R., Widlund, H. R., Feige, E., Lin, J. Y., Wilensky, D. L., Igras, V. E., D'Orazio, J., Fung, C. Y., Schanbacher, C. F., Granter, S. R., and Fisher, D. E. 2007. Central role of p53 in the suntan response and pathologic hyperpigmentation. *Cell 128*: 853–864.

Dearth, L. R., Qian, H., Wang, T., Baroni, T. E., Zeng, J., Chen, S. W., Yi, S. Y., and Brachmann, R. K. 2007. Inactive full-length p53 mutants lacking dominant wild-type p53 inhibition highlight loss of heterozygosity as an important aspect of p53 status in human cancers. *Carcinogenesis 28*: 289–298.

Denissenko, M. F., Koudriakova, T. B., Smith, L., O'Connor, T. R., Riggs, A. D., and Pfeifer, G. P. 1998. The p53 codon 249 mutational hotspot in hepatocellular carcinoma is not related to selective formation or persistence of aflatoxin B1 adducts. *Oncogene 17*: 3007–3014.

Dumont, P., Leu, J. I., Della Pietra, A. C., 3rd, George, D. L., and Murphy, M. 2003. The codon 72 polymorphic variants of p53 have markedly different apoptotic potential. *Nat. Genet. 33*: 357–365.

Fleischhacker, M., and Schmidt, B. 2007. Circulating nucleic acids (CNAs) and cancer–a survey. *Biochim. Biophys. Acta 1775*: 181–232.

Friedler, A., Hansson, L. O., Veprintsev, D. B., Freund, S. M., Rippin, T. M., Nikolova, P. V., Proctor, M. R., Rudiger, S., and Fersht, A. R. 2002. A peptide that binds and stabilizes p53 core domain: chaperone strategy for rescue of oncogenic mutants. *Proc. Natl. Acad. Sci. U.S.A. 99*: 937–942.

Jia, H. 2006. Controversial Chinese gene-therapy drug entering unfamiliar territory. *Nat. Rev. Drug. Discov. 5*: 269–270.

Joerger, A. C., Ang, H. C., and Fersht, A. R. 2006. Structural basis for understanding oncogenic p53 mutations and designing rescue drugs. *Proc. Natl. Acad. Sci. U.S.A. 103*: 15056–15061.

Kato, S., Han, S. Y., Liu, W., Otsuka, K., Shibata, H., Kanamaru, R., and Ishioka, C. 2003. Understanding the function-structure and function-mutation relationships of p53 tumor suppressor protein by high-resolution missense mutation analysis. *Proc. Natl. Acad. Sci. U.S.A. 100*: 8424–8429.

Knudson, A. G., Jr. 1985. Hereditary cancer, oncogenes, and antioncogenes. *Cancer Res. 45*: 1437–1443.

Krajewski, M., Ozdowy, P., D'Silva, L., Rothweiler, U., and Holak, T. A. 2005. NMR indicates that the small molecule RITA does not block p53-MDM2 binding in vitro. *Nat. Med. 11*: 1135–1136; author reply 1136–1137.

Le Calvez, F., Mukeria, A., Hunt, J. D., Kelm, O., Hung, R. J., Taniere, P., Brennan, P., Boffetta, P., Zaridze, D. G., and Hainaut, P. 2005. TP53 and KRAS mutation load and types in lung cancers in relation to tobacco smoke: distinct patterns in never, former, and current smokers. *Cancer Res. 65*: 5076–5083.

Liu, G., Parant, J. M., Lang, G., Chau, P., Chavez-Reyes, A., El-Naggar, A. K., Multani, A., Chang, S., and Lozano, G. 2004. Chromosome stability, in the absence of apoptosis, is critical for suppression of tumorigenesis in Trp53 mutant mice. *Nat. Genet. 36*: 63–68.

Malkin, D., Li, F. P., Strong, L. C., Fraumeni, J. F., Jr., Nelson, C. E., Kim, D. H., Kassel, J., Gryka, M. A., Bischoff, F. Z., Tainsky, M. A., and Friend, S. H. 1990. Germ line p53 mutations in a familial syndrome of breast cancer, sarcomas, and other neoplasms. *Science 250*: 1233–1238.

Mihara, M., Erster, S., Zaika, A., Petrenko, O., Chittenden, T., Pancoska, P., and Moll, U. M. 2003. p53 has a direct apoptogenic role at the mitochondria. *Mol. Cell 11*: 577–590.

Miller, L. D., Smeds, J., George, J., Vega, V. B., Vergara, L., Ploner, A., Pawitan, Y., Hall, P., Klaar, S., Liu, E. T., and Bergh, J. 2005. An expression signature for p53 status in human breast cancer predicts mutation status, transcriptional effects, and patient survival. *Proc. Natl. Acad. Sci. U.S.A. 102*: 13550–13555.

Munro, A. J., Lain, S., and Lane, D. P. 2005. P53 abnormalities and outcomes in colorectal cancer: a systematic review. *Br. J. Cancer 92*: 434–444.

Nigro, J. M., Baker, S. J., Preisinger, A. C., Jessup, J. M., Hostetter, R., Cleary, K., Bigner, S. H., Davidson, N., Baylin, S., Devilee, P., Glover, T., F.S., C., Weslon, A., Modali, R., Harris, C. C., and Vogelstein, B. 1989. Mutations in the p53 gene occur in diverse human tumour types. *Nature 342*: 705–708.

Olive, K. P., Tuveson, D. A., Ruhe, Z. C., Yin, B., Willis, N. A., Bronson, R. T., Crowley, D., and Jacks, T. 2004. Mutant p53 gain of function in two mouse models of Li-Fraumeni syndrome. *Cell 119*: 847–860.

Olivier, M., Eeles, R., Hollstein, M., Khan, M. A., Harris, C. C., and Hainaut, P. 2002. The IARC TP53 database: new online mutation analysis and recommendations to users. *Hum. Mutat. 19*: 607–614.

Patton, J. T., Mayo, L. D., Singhi, A. D., Gudkov, A. V., Stark, G. R., and Jackson, M. W. 2006. Levels of HdmX expression dictate the sensitivity of normal and transformed cells to Nutlin-3. *Cancer Res. 66*: 3169–3176.

Petitjean, A., Mathe, E., Kato, S., Ishioka, C., Tavtigian, S. V., Hainaut, P., and Olivier, M. 2007. Impact of mutant p53 functional properties on TP53 mutation patterns and tumor phenotype: lessons from recent developments in the IARC TP53 database. *Hum. Mutat. 28*: 622–629.

Pharoah, P. D., Day, N. E., and Caldas, C. 1999. Somatic mutations in the p53 gene and prognosis in breast cancer: a meta-analysis. *Br. J. Cancer 80*: 1968–1973.

Pietsch, E. C., Humbey, O., and Murphy, M. E. 2006. Polymorphisms in the p53 pathway. *Oncogene 25*: 1602–1611.

Rohaly, G., Chemnitz, J., Dehde, S., Nunez, A. M., Heukeshoven, J., Deppert, W., and Dornreiter, I. 2005. A novel human p53 isoform is an essential element of the ATR-intra-S phase checkpoint. *Cell 122*: 21–32.

Sherr, C. J. 2006. Divorcing ARF and p53: an unsettled case. *Nat. Rev. Cancer 6*: 663–673.

Sjalander, A., Birgander, R., Saha, N., Beckman, L., and Beckman, G. 1996. p53 polymorphisms and haplotypes show distinct differences between major ethnic groups. *Hum. Hered. 46*: 41–48.

Song, H., Hollstein, M., and Xu, Y. 2007. p53 gain-of-function cancer mutants induce genetic instability by inactivating ATM. *Nat. Cell. Biol. 9*: 573–580.

Stiewe, T. 2007. The p53 family in differentiation and tumorigenesis. *Nat. Rev. Cancer 7*: 165–168.

Toledo, F., and Wahl, G. M. 2006. Regulating the p53 pathway: in vitro hypotheses, in vivo veritas. *Nat. Rev. Cancer 6*: 909–923.

Toledo, F., Krummel, K. A., Lee, C. J., Liu, C. W., Rodewald, L. W., Tang, M., and Wahl, G. M. 2006. A mouse p53 mutant lacking the proline rich domain rescues Mdm4 deficiency and provides insight into the Mdm2-Mdm4-p53 regulatory network. *Cancer Cell 9*: 273–285.

Toledo, F., Bluteau, O., and Simeonova, I. 2007. [The activation of p53 in tumors: a promising strategy against cancer.]. *Med. Sci.* (Paris) *23*: 565–567.

Tornaletti, S., and Pfeifer, G. P. 1995. Complete and tissue-independent methylation of CpG sites in the p53 gene: implications for mutations in human cancers. *Oncogene 10*: 1493–1499.

Vassilev, L. T. 2007. MDM2 inhibitors for cancer therapy. *Trends Mol. Med. 13*: 23–31.

Ventura, A., Kirsch, D. G., McLaughlin, M. E., Tuveson, D. A., Grimm, J., Lintault, L., Newman, J., Reczek, E. E., Weissleder, R., and Jacks, T. 2007. Restoration of p53 function leads to tumour regression in vivo. *Nature 445*: 661–665.

Vogelstein, B., Lane, D., and Levine, A. J. 2000. Surfing the p53 network. *Nature 408*: 307–310.

Weihrauch, M., Bader, M., Lehnert, G., Wittekind, C., Tannapfel, A., and Wrbitzky, R. 2002. Carcinogen-specific mutation pattern in the p53 tumour suppressor gene in UV radiation-induced basal cell carcinoma. *Int. Arch. Occup. Environ. Health 75*: 272–276.

Wijnhoven, S. W., Speksnijder, E. N., Liu, X., Zwart, E., vanOostrom, C. T., Beems, R. B., Hoogervorst, E. M., Schaap, M. M., Attardi, L. D., Jacks, T., van Steeg, H., Jonkers, J., and de Vries, A. 2007. Dominant-negative but not gain-of-function effects of a p53.R270H mutation in mouse epithelium tissue after DNA damage. *Cancer Res. 67*: 4648–4656.

Wischhusen, J., Naumann, U., Ohgaki, H., Rastinejad, F., and Weller, M. 2003. CP-31398, a novel p53-stabilizing agent, induces p53-dependent and p53-independent glioma cell death. *Oncogene 22*: 8233–8245.

6
Personalized Medicine for Cancer

Sarah J. Welsh and Garth Powis

Summary Personalized medicine is a model of the way medicine will evolve through the use of specific treatments and therapies best suited to an individual's genotype and is driven by patient demand for safer and more effective medicines and therapies. This chapter focuses on the role of personalized medicine in cancer and explores its use in current clinical practice, its likely application in the future and the challenges which need to be overcome in order to achieve this goal. Economic, social, and ethical considerations relating to personalized medicine are also discussed.

INTRODUCTION

Personalized medicine is a model of the way medicine will evolve through the use of specific treatments and therapies best suited to an individual's genotype, and is driven by patient demand for safer and more effective medicines and therapies. However, the concept of individualizing treatment is not new, and the study of hereditary influences on the response to drugs (pharmacogenetics) is reflected in the scientific literature from the 1960s (Yong *et al*., 2006). The number of new articles published remained constant until 1996 when technical developments and new insights into the highly complex nature of many diseases resulted in the advent of pharmacogenomics (Watters and McLeod, 2003). Pharmacogenomics is closely related to pharmacogenetics but the emphasis is on the influence of a whole set or complement of genes on the response to drugs, with the aim of improving drug efficacy rather than simply being concerned with drug safety. Subsequent growth in the new field of pharmacogenomics-based personalized medicine has been exponential, particularly in the area of cancer therapy.

The term 'personalized medicine' is mainly used in the context of pharmacogenomics, and although pharmacogenomics is one of the main drivers of this new area, it is important to realize that this view can be rather narrow. Personalized medicine also includes areas such as disease susceptibility in addition to the molecular traits and mechanisms underlying individual characteristics. Applications of personalized medicine range from personal risk profiles leading to personal preventative measures, such as vaccination and personalized health planning leading to early diagnosis, to genetic counseling, databases, and decision support tools. This chapter focuses on

the role of personalized medicine in cancer therapy and explores its use in current clinical practice, its likely application in the future, and the challenges needing to be overcome to achieve this goal.

Why Is Personalized Medicine Important in Cancer?

Personalized medicine is more important for cancer patients than for those with other diseases for several reasons. Firstly, cancer is a highly heterogeneous disease with significant molecular differences in the expression and distribution of tumor cell markers among patients with the same type and grade of tumor. Secondly, cellular mutations tend to accumulate as cancer progresses, further increasing tumor heterogeneity. Thirdly, currently used cancer therapies at the doses employed are often toxic to normal cells resulting in sometimes severe side effects rarely seen in other diseases. Finally, cancer patients have limited time to try one kind of treatment and, if it does not work, to try others until the right medicine is found. Therefore, cancer therapy presents a unique example of personalized medicine in which an individual's genotype not only determines the therapeutic and toxic responses to a drug (the pharmacogenotype), but also that of the tumor.

To What Extent Is Cancer Medicine Already Personalized?

During the past 20 years, a large amount of the fine detail of the basic biological processes that become disturbed in cancer has been amassed. We now know the key elements of growth factor binding, signal transduction, gene transcription control, cell cycle checkpoints, apoptosis, angiogenesis and metastasis, and more than 350 mutated genes have been causally implicated in cancer development (Futreal, 2004). Indeed, systematic sequencing of DNA corresponding to the coding exons of 518 protein kinase genes in 210 diverse human cancers recently showed that ~120 of the genes screened are estimated to carry mutations which drive the development of cancer by conferring growth advantage on the cell in which they occur (Greenman *et al*., 2007). The new paradigm for cancer therapy is to develop agents that target the precise molecular pathology driving the progression of individual cancers. Investment in genomics, genetics, and automation has already resulted in a large number of rationally designed anticancer drugs with a record number of novel compounds currently in clinical trials (Collins and Workman, 2006). High profile drugs such as imatinib (Gleevec) (Capdeville *et al*., 2002), trastuzumab (Herceptin) (Morris and Carey, 2006), erlotinib (Tarceva) (Cohen *et al*., 2005) and bevacizumab (Avastin) (Hadj Tahar, 2004) specifically target underlying molecular lesions and are in widespread clinical use. We are able to identify patients with precise molecular lesions that respond to the agents and these agents have provided important proof-of-principle evidence for the benefits of targeted therapy in cancer and represent a significant advance towards achieving personalized medicine.

A consequence of having molecularly targeted drugs is a move to target rather than disease-based therapy because it is frequently found that a molecular target occurs in more than one type of cancer. An example among the newly approved agents for targeted therapy in cancer is the use of imatinib (Capdeville

et al., 2002)). Imatinib was originally developed to target the BCR/ABL receptor tyrosine kinase, which is formed from a reciprocal chromosomal translocation between the long arms of chromosomes 9 and 22. This process fuses the body of the Abelson tyrosine kinase (abl) gene on chromosome 9 with the breakpoint cluster region (bcr) gene on chromosome 22 to generate an oncogene that encodes the chimeric BCR-ABL protein. The BCR/ABL protein is a constitutively active, cytoplasmic form of the ABL kinase which transforms primary myeloid cells to leukemic cells *via* its ABL receptor tyrosine kinase activity. This characteristic genetic abnormality, known as the Philadelphia chromosome, is present in the marrow cells of >90% of all patients with chronic myelogenous leukemia (CML) and in 15–30% of patients with acute lymphoblastic leukaemia (ALL). Imatinib selectively inhibits BCR-ABL by occupying the ABL adenosine triphosphate binding site, maintaining the protein in an inactive conformation, thereby inhibiting its tyrosine kinase activity, resulting in 89% overall survival of patients after 5 years. Subsequent analysis has also revealed activity against the tyrosine kinases associated with the c-Kit protein (stem cell factor receptor) and platelet-derived growth factor receptor (PDGFR).

Constitutive activation of the c-Kit tyrosine kinase has been shown to be critical in the pathogenesis of gastrointestinal stromal tumor (GIST), a rare neoplasm for which there had been no effective systemic therapy (Hirota *et al*., 1998). Indeed, activating mutations of c-Kit and/or PDGFR have been found in 88% and 5% of GISTs, respectively (Heinrich *et al*., 2003), with 100% of GIST tumor specimens demonstrating positive immunostaining for the KIT protein (Sihto *et al*., 2005). Clinical trials subsequently demonstrated imatinib to be an effective therapy in GIST with a 53.3% overall efficacy rate (complete response + partial response), and a 84.3% rate for disease-control (complete response + partial response + stable disease) with 1 year survival rates of 88% (Kubota, 2006). Imatinib is now approved for treatment of GIST, demonstrating the importance of a target, rather than disease-based approach for future clinical drug development.

To achieve the goal of personalized medicine, in addition to developing drugs with defined molecular specificities, it is essential to have biomarker and imaging tests to identify the molecular targets in a patient's tumor and the patient's pharmacogenotype. Biomarkers act as molecular signposts of the physiological state of a cell and are determined by the genes, proteins, and other organic chemicals synthesized by the cell. The advantage of using biomarkers to identify patients likely to benefit from a particular treatment is demonstrated by the success of the humanized murine monoclonal antibody trastuzumab (Herceptin) in breast cancer (reviewed in (Morris and Carey, 2006)). Trastuzumab targets the human epidermal growth factor receptor 2 (HER-2) which belongs to a family of four transmembrane receptor tyrosine kinases that mediate cell growth, differentiation and survival of cells. Over-expression of the HER-2 protein, amplification of the *HER-2* gene, or both, occur in 15–30% of breast cancers and are associated with increased proliferation, decreased cell death and increased metastasis. HER-2 over-expression is a marker of poor prognosis in node-positive breast cancer patients and has also been suggested to be a predictor for resist-

ance to endocrine therapy. Trastuzumab therapy significantly improves response rates in women with HER-2-over-expressing breast cancer either alone or in combination with chemotherapy (35% and 50% respectively). However, trastuzumab therapy shows poor response rates in tumors expressing lower levels of HER-2 (35% in HER-2 over-expressing tumors versus 0% in those expressing lower levels of HER-2). Given its implications for prognosis and treatment, and also the costly nature of trastuzumab, the accurate identification of HER-2 over-expression is of considerable importance. Patients likely to benefit from trastuzumab are selected using immunohistochemistry test kits or fluorescence in situ hybridization (FISH) assays which detect the presence of the HER-2 protein. Patients whose tumors do not express HER-2/*neu* are spared futile treatment and potential treatment-related side-effects; such patients should be offered alternative therapy saving precious time and resources.

A related objective of using biomarker tests is to enable monitoring of the effect of a defined drug on its molecular target and to assess early response so that a non-responding patient can be spared unnecessary treatment and be offered alternative therapies. An example is the use of imatinib for treatment of chronic myeloid leukemia (CML) reviewed in (Capdeville *et al*., 2002). Although clinical trials showed that imatinib was particularly effective in newly diagnosed chronic-phase CML, patients with advanced CML are less sensitive to imatinib with 24% and 66% of patients in accelerated and blastic phases respectively, failing to achieve hematologic remission despite treatment with high doses of imatinib. Additionally, responses to imatinib in patients with advanced disease are often transient, generally lasting less than 6 months (Druker *et al*., 2001; Silver *et al*., 2004; Talpaz *et al*., 2003). Consequently, patients are regularly monitored using a number of parameters including measurements of the levels of Philadelphia chromosome positive cells. Failure to achieve hematologic response after 3 months of therapy, cytogenetic response after 6 months, major cytogenetic response (Philadelphia chromosome positive cells reduced to $<35\%$) after 12 months, or complete cytogenetic response after 18 months constitutes an indication for modifying imatinib therapy (Baccarani *et al*., 2006). This includes treatment with higher doses of imatinib, imatinib combinations, new tyrosine kinase inhibitors (dasatinib) (Talpaz *et al*., 2006) or nilotinib (Weisberg *et al*., 2006), allogeneic stem-cell transplantation, or investigational therapies. For patients who achieve complete cytogenetic response, hematologic and cytogenetic assessment is continued, with regular molecular monitoring of BCR-ABL versus ABL transcript levels as increasing levels of BCR-ABL transcripts are associated with the emergence of BCR-ABL mutants and resistance to imatinib (Branford *et al*., 2004; Mauro and Deininger, 2006).

Biomarkers can also provide essential information regarding how much drug is needed to inhibit a particular molecular target in a tumor and whether there is a benefit to giving more drug. Ideally these tests should be noninvasive as biopsy of solid tumors is expensive and subjects patients to additional invasive procedures with associated risks. Although traditional sources such as serum or plasma are currently in routine use, recent advances in

noninvasive techniques such as molecular imaging show the potential to provide detailed functional and metabolic information (Workman *et al*., 2006). During the past few years, there has been a major increase in the use of positron emission spectroscopy (PET) which allows dynamic, noninvasive measures of the three-dimensional distribution of a positron-labelled compound within the living body. By labelling molecules of interest (such as drugs, metabolic substrates, peptides, and antibodies) with positron-emitting isotopes such as ^{11}C, ^{18}F, ^{124}I or ^{13}N, pharmacokinetic and pharmacodynamic measurements can be performed in addition to evaluating the effect of novel therapeutics on both generic and specific biologic endpoints.

In the case of studies that employ generic endpoints, PET has been used to monitor changes in cellular proliferation using ^{11}C –thymidine, tissue perfusion with ^{15}O-H_2O, glucose utilisation with ^{18}FDG and DNA synthesis using 18-fluorothymidine. Specific biologic endpoints have the potential to provide proof of principle for a proposed mechanism of action for existing or novel therapies. Examples include the detection of thymidylate synthase inhibition with ^{11}C–thymidine, detection of hypoxia using ^{18}fluoro-misonidazole and other ^{18}F-labeled 2-nitroimidazoles, imaging of apoptosis using ^{124}I-annexin V, and visualization of the pharmacodynamics of HER-2 degradation due to heat shock protein 90 inhibition. Positron-labelled antibodies or peptides also offer the potential for noninvasive monitoring of receptor expression such as the detection of overexpression of Erb-B2 receptors with ^{68}Ga-labelled anti-Erb-B2 antibody.

However, although PET imaging has enormous potential advantages for use in drug development, not all compounds can be radio-labelled and each compound must be considered on an individual basis. Additionally, PET images have low anatomic resolution as well as a lack of chemical resolution being unable to distinguish between the parental radio-tracer and its labelled, or unlabelled, metabolites. Radiation exposure is also a potential limitation of PET radioisotopes, particularly if studies are performed on multiple occasions. Alternative methods include magnetic resonance imaging (MRI) and magnetic resonance spectroscopy (MRS) (Workman *et al*., 2006). MRI is routinely used in the initial evaluation of tumor size, shape, and anatomic appearance, and changes in these parameters can be used to assess and quantify the pharmacodynamic effects of a drug. In addition, dynamic contrast-enhanced MRI (DCE-MRI) is proving increasingly useful for assessing pharmacodynamic endpoints, especially for changes related to the vasculature. Importantly, almost all major hospitals in the developed world have access to MRI for routine use.

MRS is the only noninvasive *in vivo* method for chemically distinguishing between, and measuring concentrations of drugs and their metabolites (Kurhanewiez *et al*., 2002). Although MRS does not provide an anatomic image, data are visualized in the form of a spectrum, in which the peaks correspond to different cellular constituents. Thus, MRI can be used to define a volume in a tumor or normal tissue, and can be used to measure the concentration of endogenous biochemical compounds or drugs in that volume in real time. The advantage of this approach is that nothing (other than the drug) is administered, no samples are taken, and no ionizing radiation is used. MRS has been shown to

increase the level of diagnostic confidence in a number of situations in which conventional MRI may be unhelpful (Sibtain *et al*., 2007). Additionally, studies have shown that MRS can be used to monitor response to chemotherapy in lymphoma, germ cell tumors, and glioma (Murphy *et al*., 2000, 2004; Schwarz *et al*., 2002). To date, pharmacokinetic studies using MRS in patients have been restricted to fluorine-containing drugs such as 5-fluorouracil (5FU), its prodrug, capecitabine, and gemcitabine using ^{19}F-MRS, and to ifosfamide and cyclophosphamide using ^{31}P-MRS (Workman *et al*., 2006). The elimination rate of 5FU from tumors in patients is associated with response, allowing an early prediction of the likely success or failure of a treatment regime (Wolf *et al*., 1998). However, the value of MRS data is highly dependent on expert spectroscopists for acquisition, analysis, and interpretation of MR spectra. Therefore, MRS is not generally used in routine clinical practice outside specialist centers, but due to the logistic and ethical issues associated with invasive measurements, looks well-placed to fulfill the increasing requirement for minimally invasive assays to measure PK, PD, and target modulation in the future.

The newly emerging area of cancer phenomics can be used as a practical illustration of how genetic studies can be successfully integrated with phenotypic data to improve the specificity of personalized medicine (Zbuk and Eng, 2007). Cancer phenomics refers to the systematic and detailed collection, objective documentation, and cataloguing of phenotypic data at many levels, including clinical, molecular and cellular phenotype. Data are most mature for germline mutations in the receptor tyrosine kinase RET (rearranged during transfection). RET plays a crucial role in transducing growth and differentiation signals in tissues derived from the neural crest (Nakamura *et al*., 1994; Takahashi, 1988). Germline mutations in RET, which lead to a constitutively active receptor tyrosine kinase or decreased specificity for its substrate, predispose to the cancer-associated syndrome multiple endocrine neoplasia-2 (MEN2) (Eng and Mulligan, 1997). MEN2 is a clinical syndrome involving predisposition to medullary thyroid cancer and phaeochromocytoma in addition to other endocrine, mucocutaneous, and skeletal features. MEN2-asociated tumors are more often bilateral and multifocal, and occur at a much younger age than their sporadic counterparts. Meticulous characterization of RET phenomics at the clinical and biochemical levels has revolutionized management of families with MEN2 (Zbuk and Eng, 2007). When a mutation is identified in an individual, predictive testing can be performed on family members, and only those who carry the mutation require further MEN2 management. The correlation between genotype and phenotype in MEN2 has lead experts to suggest individualized recommendations for the timing of prophylactic thyroidectomy (surgical removal of the thyroid gland) on the basis of the RET mutation genotype. For other mutations in RET, phenomics has suggested a specific routine surveillance program for early detection, which is a more appropriate management route. Recent advances in noninvasive sampling techniques, such as the use of buccal cell isolates as a source of DNA, offer a more acceptable sample collection method for such surveillance programs (King *et al*., 2002). Knowledge of the molecular pathways that are deregulated as a result of RET

mutations will enable targeted therapies to be explored that might prove useful in treating tumors arising as a result of RET mutations.

The Future of Personalized Medicine in Cancer

The Human Genome Project, and its successor the Cancer Genome Project and related activities are expected to identify the majority of genes in most of the common human cancers during the next 5 years. Together these projects will provide a vast repository of comparative information regarding normal and malignant cells. Instead of licensing drugs for empirical use in different types of cancers with relatively poor response, new therapies will require the identification of specific molecular lesions resulting in improved response rates. Reduced toxicity due to increased selectivity will allow new therapies to be given during prolonged periods of time, in some cases for the rest of the patients' life, a concept unthinkable with current cytotoxic therapy. More complete knowledge of tumor biology and the role of target pathways in normal physiology will reduce the likelihood of unexpected toxicities that can limit or even curtail the usefulness of a drug. The recent unexpected cardiotoxicity in some patients treated with imatinib is an example (Kerkela *et al*., 2006).

Detailed analysis of the differences between normal and malignant cells also allows the possibility of individual cancer risk assessment, leading to tailored prevention programs and specific screening programs to detect early cancer. Although cancer prevention currently absorbs only 2% of the total current funding of cancer care and research, this percentage is likely to increase in the postgenomic era (Bosanquet and Sikora, 2006). Currently, it is accepted that over 120 genes are associated with the development of a range of cancers (Greenman *et al*., 2007). However, the detection of polymorphisms in low-penetrance cancer-related genes or a combination of changed genes will allow identification of people at increased risk, and demand for prevention strategies will increase. It is predicted that within 20 years most people will be genetically mapped with the information easily stored on a smart card. Thus, predisposition to some cancers will be found in early adult life with potential for correction well before manifestation of the disease.

Multiple technologies exist to achieve the goal of personalized treatment in cancer, and molecular diagnosis can be established at multiple levels where molecular differences can be found between individuals with identical clinical manifestations. Currently, available diagnostic procedures are insufficient to determine which patients will primarily benefit from rational tumor therapy. In the future, gaining information on the morphology, genetic, proteomic, and epigenetic alterations will be essential to provide clinicians with relevant information for individualized medicine to be prescribed.

DNA microarrays are the first approach close to being used in routine diagnosis (Dietel and Sers, 2006). These consist of a solid support, such as a silicon chip or glass slide, with thousands of immobilized complementary DNA molecules specific for individual genes (up to 20,000) or oligonucleotide probes (up to 65,000) arranged in a defined order. To analyze gene expression, target nucleic acids are

extracted from tissue, and most commonly labelled with fluorescent dye. A genetic expression profile indicating over-expression, under-expression, no change, or complete absence for each gene in the tissue sample is obtained by monitoring the amount of label that has hybridized to each location on the microarray. Patterns of gene changes or novel genes associated with disease development or clinical outcome of an individual tumor can then be identified by specialist bioinformatic programs that use statistical methods to evaluate the complex information, and translate molecular information into clinically relevant data.

For example, microarray analysis has been used to classify acute leukemias (Golub *et al*., 1999). By analyzing gene expression profiles in 38 acute leukaemia samples, 1,100 genes were identified that were differentially expressed between acute lymphoid leukaemia (ALL; reviewed in Volume 3) and acute myeloid leukaemia (AML; reviewed in Volume 3). By focusing on the 50 genes whose expression was correlated most closely with disease type, a classification scheme was developed that was able to accurately identify new ALL or AML samples, as well as B-lineage or T-lineage ALL within the ALL group samples. Subsequent work using oligonucleotide microarrays to analyze gene expression patterns of >12,600 genes in leukemic blasts from 360 pediatric ALL patients identified all known prognostically significant leukaemia subgroups (Yeoh *et al*., 2002). Additionally, the study identified distinct expression profiles that predicted relapse with high accuracy within specific subtypes (no single gene could be used to predict the risk of relapse).

Microarrays can also be used to identify patients likely to benefit from a particular therapy, and those who should be given additional therapies to increase their chances of survival. In a recent breast cancer study, microarrays were used to analyze 25,000 genes in 78 primary breast tumors from young women who were node-negative at the time of diagnosis (van't Veer *et al*., 2002). Seventy representative genes were identified which accurately predicted the subsequent metastatic status in 83% of patients. The set of 70 genes was then shown to accurately predict future metastatic status in 17 out of 19 additional independent breast tumors, showing that the predictive power of this prognosis indicator for clinical metastasis in node-negative breast cancer is much greater than that of current approaches. In fact, using current criteria, 70–91% of breast cancer patients treated with surgery and radiotherapy would be unnecessarily advised to receive adjuvant chemotherapy (Caldas and Aparicio, 2002). This approach was also able to identify women who appeared to need more aggressive therapy for their breast cancer.

Similar analysis of proteins as proteomic patterns also appears on the horizon (Kolch *et al*., 2005). It is estimated that our 40,000 genes may generate ~1 million distinguishable functional entities at the protein level, due to differential splicing and translation, and numerous post-translational modifications. Therefore, although complex, the proteome offers a much richer source for the functional description of cancers and the discovery of diagnostic therapeutic targets, especially given the dynamic nature of cancer. The main current applications of proteomics include protein expression profiling of tumors, tumor fluids and

tumor cells; protein microarrays; mapping of cancer signalling pathways; pharmacoproteomics; identification of biomarkers for diagnosis, staging and monitoring of the disease and therapeutic response; and profiling the immune response to cancer. The most clinically advanced of these applications is the use of protein microarrays that are mainly employed for functional studies with antibodies which recognise posttranslational modifications. For example, screening of ovarian tumor cell lysates with phospho-specific antibodies for extracellular-signal-regulated kinase 1/2 (ERK 1/2), Akt and glycogen synthase kinase 3β (GSK-3β), suggested that in ovarian cancer signalling pathways may be activated in a patient-specific rather than type- or stage-specific pattern (Wulfkuhle *et al*., 2003). Thus, proteomic technologies, particularly when combined with genomic analyses, offer enormous potential for the delivery of personalized medicine, although their implementation in routine clinical medicine remains a challenge.

An alternative strategy for delivering personalized management of cancer via proteomics is phage display (Samoylova *et al*., 2006). Phage display technology utilizes combinatorial libraries of proteins expressed on phage particles that can be selected for specific binding to cancer cells. Although phage display has yet to reach its potential in research and clinics, it carries great promise for a variety of applications including identification of cell-specific targeting molecules, identification of cell surface biomarkers, profiling cell-specific delivery of cytotoxic agents, identification of cancer biomarkers, profiling of tumor specimens, and design of peptide-based anticancer therapeutics for personalized treatments. Importantly, phage display does not require any prior knowledge about cell surface targets for identification of cell-targeting molecules, nor does the target have to be immunogenic. Unlike traditional approaches applied to individualized cancer medicine, phage display offers the parallel development of anticancer therapeutics with companion diagnostics. Unfortunately, currently only low numbers of samples can be processed, and a high through-put solution lies in the development of instrumentation for automation of key steps in the process. However, phage display has the necessary prerequisites to find a unique niche for improving personalized medicine in the future.

The development of high throughput methods for investigation of the methylation status of DNA provides a further level of information. Epigenetic modification of DNA by the addition of a methyl group to cytosine residues in CpG dinucleotides is one of the most important mechanisms of tumor suppressor gene inactivation known today (Baylin *et al*., 2001; Jones and Baylin, 2002). Although a multitude of publications on high-throughput analysis of DNA methylation in tumor samples already exist, this technology needs further development to enter routine clinical practice (Dietel and Sers, 2006). Nevertheless, it is clear that individually neither genomic, proteomic nor epigenomic analysis will provide all the information required for an efficient individualized approach. Therefore, a ‘multiplex’ approach combining the different biological levels of DNA, RNA, and protein, may be necessary to functionally classify malignant tumors with the highest relevance for prognosis and therapy.

The Challenges for Achieving Personalized Medicine

One of the major limitations to achieving personalized medicine is incomplete knowledge of tumor biology. Our understanding will continue to be supplemented by data from The Human Genome Project and The Cancer Genome Project and their related activities. However, continued investment in technical developments and bioinformatics is necessary to develop special methods capable of detecting the entire spectrum of rate-limiting oncogenic pathways in tumors, before and after therapy, to identify those patients who will benefit from novel therapies. These include the broad profiling of human tissue for morphology, genetic, proteomic, and epigenetic alterations as described above. Before establishment of such an integrated approach into daily routine can occur, extensive development is necessary to allow a firm prediction on the activation of a certain pathway in clinical material.

More insidious challenges stem from the way cancer drugs are currently developed. The simplest being that currently drugs frequently enter clinical trials without a 'validated' biomarker or imaging test to select patients most likely to respond to treatment. 'Validated' means that the test is standardized and has been shown to be reproducible across institutions, if not in patients then at least in animal models. Instead of being an after-thought, these tests need to be developed early in the development of a drug and be ready for use in clinical trials. Additionally, current requirements for disease-specific drug trials mean that responding patients must be identified by separate trials for each disease group. A move to target rather than disease-based drug clinical development will require a paradigm shift in the way cancer drugs are developed.

We are still in the era of "one drug fits all" mentality, and it is upon this notion that the success of the pharmaceutical industry has been developed and thus will be hard to break. With the continuing focus on the search for "blockbuster" drugs having annual sales of $1 billion, there is a natural disinclination to subdivide the market, which is what personalized medicine, too often, appears to do. If only 10% of patients with a particular cancer can be shown to respond to a particular agent because only they posses the molecular target, then the market has been reduced by 90%. Of course, the patients are likely to take the agents for a longer time, but this is not seen as compensating for the decrease in market size. The drug may also be active in subsets of patients with other cancer types so that the total market could eventually reach that of a "blockbuster drug". An example is imatinib, discussed previously, which is active in several small cancer types. However, this is by no means certain during the early stages of a drug development when important strategic decisions are being made. So, for the time being, there is a perceived commercial risk in personalizing cancer therapy and testing patients for molecular targets.

What if we are wrong regarding the target, and what if there are other targets responsible for or contributing to therapeutic effect? These are legitimate concerns but without well designed studies with validated tests we will not know the answer. The increasing tendency to conduct clinical trials at multiple institutions also increases the need to have properly

validated tests that can be conducted by all institutions. This requires that test validation is built early into the development of a drug. In a risk averse market it is safer to stick to "one drug fits all" and attempt to develop alternate strategies such as combinations, which it is hoped will make an inactive drug active in more patients, but still treat all patients with the disease with the drug. There is a danger in that obscuration is the real goal in order to maintain market share. One answer is to treat the molecular target not the disease and have clinical trails across tumor types; thus, reducing the financial burden of testing a drug in essentially repetitive multiple disease specific trials. This, of course, will require a paradigm shift in the way we think about and organize the treatment of cancer. However, personalized medicine is proving its value in other diseases and has begun to do so in cancer. The ethics and cost to society and cancer patients who are treated with drugs to which they have little likelihood of response cannot be ignored.

A further challenge for drug development results from the likely need to use the newer molecularly targeted drugs (which are nearly all cytostatic, arresting tumor growth), in combination with more conventional cytotoxic drugs that cause tumor shrinkage. This approach, of course, retains the toxic effects of current therapy. It may be that in the future we will accept as a first step time to disease progression rather than tumor shrinkage as the goal of therapy, if patients are able to live with their cancer under control, in the same way that individuals live with diabetes controlled by antidiabetic drugs. The ultimate goal for cancer therapy, however, is cure with complete eradication of all traces of a patient's tumor. A rational way to develop molecularly targeted cancer drugs is to use combinations that attack different points in the same or parallel signalling pathways. However, the reluctance of pharmaceutical companies to test their experimental agents in combination with a competitor's agent is a frustration for many clinical investigators. A framework for providing intellectual property protection to companies that test drugs in combination has recently been provided by the US National Cancer Institute Cancer Therapy Evaluation Program (CTEP) with a number of CTEP-sponsored drug combination studies underway. This type of model will need to be extended and made more readily available in the future.

Other challenges for drug development include the widespread frustration with the cost and time that it takes to bring a new cancer drug to trial. Initiatives are in place to help to speed up the drug development process, both in the drug discovery pipeline and in the design of clinical trials. The implementation of chemical biology, which provides experimental techniques for linking together elements from all stages of what was previously viewed as a linear pathway from gene to drug, may help to speed up the drug development process. To encourage the more rapid introduction of drugs into clinical trial, the Federal Drug Agency recently introduced the concept of phase 0 or microdose trials at less than one-one hundredth of the dose calculated to yield a pharmacologic effect, thus allowing the collection of human pharmacokinetic and bioavailability data earlier in the drug development process. These human data can then be combined with preclinical data to select the best

candidates to advance to more expensive and extensive clinical development. However, much work needs to be done in this area to ensure personalized medicine to become a reality.

Finally, there has been much discussion of the economic, social, and ethical considerations of personalized medicine. Inevitably, there will be conflicting demands on resources, particularly given the possibility that cancer could become a chronic disease within the next 20 years due to advances in understanding the fundamental biology of cancers and translation of this knowledge into impressive therapies. The costs of treating a cancer patient is expected to quadruple by 2025, compared to that spent in 2005 (Sikora, 2007). The only way to reduce cancer care costs will be to ensure that expensive medicines are only given to patients who are predicted to really benefit from them and to confirm their response as soon as possible.

As with all health issues, the question of access will be determined by cost and political will. Politicians will be forced to consider the alignment between patients' requirements, and tax-payers' and voters' wishes. Fewer than 50% of voters in the United Kingdom currently pay tax, and the percentage of tax-payers is likely to fall as the population ages. The interests of voters may be very different from the interests of tax-payers. Additionally, whatever system is put in place to pay for cancer-related care, there is the prospect of a major socio-economic division in cancer care. A small proportion of the elderly population will have made suitable provision for their retirement, both in terms of health and welfare, but the vast majority will not be properly prepared. Policy makers need to start planning now. The most productive way to move forward is to start involving cancer patients and health advocacy groups in the debate to ensure that difficult decisions are reached by consensus.

Although the tools of genetic and molecular medicine are powerful, so are the social and ethical risks. Several personal values are at stake: privacy, protection of minorities, and prevention of discrimination. Early in the Human Genome Project it was recognized that the Project also had ethical, legal, and social implications (ELSI), and so the ELSI program was established. It remains a key objective in the vision for the future of genomics research. One proposal of how to safe-guard privacy advocates three major pillars on which to base protection for pharmacogenetic testing (Robertson, 2001; Robertson *et al*., 2002): informed consent, trusted intermediaries, and legal protection. Informed consent is well known from clinical studies and is based on the assertion that the decision to carry out, continue or stop an investigation rests exclusively with the patient. The patient should also decide whether and to what extent he/she wishes to be informed, and to draw conclusions from the result of the investigation. Trusted intermediaries are proposed to act as 'firewalls' between genetic tests and medical records by holding DNA samples and test results. The intermediary would release genetic information regarding a person only to those who need access to it and only when that person specifically has requested it. Legal protection has the aim of protecting human dignity and personality, of preventing improper genetic testing and improper use of genetic data, and of guaranteeing the quality of genetic tests and interpretation of their results. The basic principles of this legislation are: prohibition

of discrimination, informed consent, right of not knowing, protection of genetic data, and licensing of genetic testing.

A further important social concern is the protection of genetic minorities. Although, they might strongly benefit from future drugs tailored to their specific genetic make-up, they have been under-privileged in the current 'one drug fits all' era. However, they also risk becoming therapeutic orphans as it may be difficult to recruit sufficient patient numbers for trials, and it may not be profitable for industry to develop special drugs for them.

Finally, a critical issue for the social acceptance of personalized medicine is the danger of discrimination on the grounds of genetic testing. This may result from decision making based on faulty or incomplete data, or misinterpretation of the implications of genetic test results for morbidity or mortality (irrational discrimination), or that based on scientifically sound and empirically supported discrimination (rational discrimination) (Anderlik and Rothstein, 2001). Although it is likely that irrational discrimination will be banned, rational discrimination is already commonly used by insurers to classify risk based on age, sex, occupation, personal and family medical histories, serum cholesterol, and alcohol and tobacco use. Personal genetic profiles are an extension of this risk evaluation, with profiling likely to become more precise in the future. However, it is often difficult to differentiate between rational and irrational discrimination, and the misuse of personal risk profiles is a real danger for the success of personalized medicine which needs legal regulation.

In conclusion, we are at one of the most exciting times in modern cancer therapy due to the development of rational therapy and the move towards personalized treatment for cancer. The concepts to be tested are well established, the drugs are becoming available, and new emerging technologies in target identification, drug discovery, molecular markers, and imaging can finally make the goal a reality: personalized health planning, early diagnosis, the right drugs for the right patient, with predictable side effects.

REFERENCES

Anderlik, M.R., and Rothstein, M.A. 2001. Privacy and confidentiality of genetic information: what rules for the new science? *Annu. Rev. Genom. Hum. Genet. 2*: 401–433.

Baccarani, M., Saglio, G., Goldman, J.M., Hochhaus, A., Simonsson, B., Appelbaum, F., Apperley, J.F., Cervantes, F., Cortes, J., Deininger, M.W., Gratwohl, A., Guihot, F., Horowitz, M., Hughes, T., Kantarjian, H., Larson, R.A., Niederwieser, D., Silver, R.T., and Hehlmann, R. 2006. Evolving concepts in the management of chronic myeloid leukemia: recommendations from an exert panel on behalf of the European Leukemia Net. *Blood 108*: 1809–1820.

Baylin, S.B., Esteller, M., Rountree, M.R., Bachman, K.E., Schuebel, K., and Herman, J.G. 2001. Aberrant patterns of DNA methylation, chromatin formation and gene expression in cancer. *Hum. Mol. Genet. 10*: 687–692.

Bosanquet, N., and Sikora, K. 2006. The Economics of Cancer Care. Cambridge University Press, Cambridge.

Branford, S., Rudzki, Z., Parkinson, I., Grigg, A., Taylor, K., Seymour, J.F., Durrant, S., Browett, P., Schwarer, A.P., Arthur, C., Catalano, J., Leahy, M.F., Filshie, R., Bradstock, K., Hermann, R., Joske, D., Lynch, K., and Hughes, T. 2004. Real time quantitative PCR analysis can be used as a primary screen to identify patients with CML treated with imatinib who have BCR-ABL kinase domain mutations. *Blood 104*: 2926–2932.

Caldas, C., and Aparicio, S.A. 2002. The molecular outlook. *Nature 415*: 484–485.

Capdeville, R., Buchdunger, E., Zimmerman, J., and Matter, A. 2002. Glivec (ST571,imatinib),

a rationally developed, targeted anticancer drug. *Nature Rev. Drug Discov. 1*: 493–502.

Cohen, M.H., Johnson, J.R., Chen, Y.F., Sridhara, R., and Pazdur, R. 2005. FDA approval summary: erlotinib (Tarceva) tablets. *Oncologist 10*: 461–466.

Collins, I., and Workman, P. 2006. New approaches to molecular cancer therapeutics. *Nature Chem. Bio. 2*: 689–700.

Dietel, M., and Sers, C. 2006. Personalized medicine and development of targeted therapies: the upcoming challenge for diagnostic molecular pathology. A review. *Virchows Arch. 448*: 744–755.

Druker, B.J., Talpaz, M., Resta, D.J., Peng, B., Buchdunger, E., Ford, J.M., Lydon, N.B., Kantarjian, H., Capdeville, R., Ohno-Jones, S., and Sawyers, V.L. 2001. Efficacy and safety of a specific inhibitor of the BCR-ABL tyrosine kinase in chronic myeloid leukemia. *N. Engl. J. Med. 344*: 1031–1037.

Eng, C., and Mulligan, L.M. 1997. Mutations of the RET proto-oncogene in multiple endocrine neoplasia type 2 related sporadic tumors and Hirschsprung disease. *Hum. Mutat. 9*: 97–109.

Futreal, P.A. 2004. A consensus of human cancer genes. *Nature Rev. Cancer. 4*: 177–183.

Golub, T.R., Slonim, D.K., Tamayo, P., Huard, C., Gaasenbeek, M., Mesirov, J.P., Coller, H., Loh, M.L., Downing, J.R., Caligiuri, M.A., Bloomfield, C.D., and Lander, E.S. 1999. Molecular classification of cancer: class discovery and class prediction by gene expression monitoring. *Science 286*: 531–537.

Greenman, C., Stephens, P., Smith, R., Dalgliesh, G.L., Hunter, C., and Stratton, M.R. 2007. Patterns of somatic mutation in human cancer genomes. *Nature 446*: 153–158.

Hadj Tahar, A. 2004. Bevacizumab for advanced colorectal cancer. *Is. Emerg. Hlth. Technol. 63*: 1–4.

Heinrich, M.C., Corless, C.L., Demetri, G.D., Blanke, C.D., von Mehren, M., Joensuu, H., McGreevey, L.S., Chen, C.J., Van den Abbeele, A.D., Druker, B.J., Kiese, B., Eisenberg, B., Roberts, P.J., Singer, S., Fletcher, C.D., Siberman, S., Dimitrijevic, S., and Fletcher, J.A. 2003. Kinase mutations and imatinib response in patients with gastrointestinal stromal tumors. *J. Clin. Oncol. 21*: 4342–4349.

Hirota, S., Isozaki, K., Moriyama, Y., Hashimoto, K., Nishida, T., Ishiguro, S., Kawano, K., Hanada, M., Kurata, A., Takeda, M., Muhammad Tunio, G., Matsuzawa, Y., Kanakura, Y., Shinomura, Y., and Kitamura, Y. 1998. Gain-of-function mutations of c-kit in human gastrointestinal stromal tumors. *Science 279*: 577–580.

Jones, P.A., and Baylin, S.B. 2002. The fundamental role of epigenetic events in cancer. *Nature Rev. Gene. 3*: 415–428.

Kerkela, R., Grazette, L., Yacobi, R., Iliescu, C., Patten, R., Beahm, C., Walters, B., Shevtsov, S., Pesant, S., Clubb, F.J., Rosenzweig, A., Salomon, R.N., Van Etten, R.A., Alroy, J., Durand, J.B., and Force, T. 2006. Cardiotoxicity of the cancer therapeutic agent imatinib mesylate. *Nature Med. 12*: 908–916.

King, I.B., Satia-Abouta, J., Thornquist, M.D., Bigler, J., Patterson, R.E., Kristal, A.R., Shattuck, A.L., Potter, J.D., and White, E. 2002. Buccal cell DNA yield, quality, and collection costs: comparison of methods for large scale studies. *Cancer Epidemiol. Biomarkers Prev. 11*: 1130–1133.

Kolch, W., Mischak, H., and Pitt, A.R. 2005. The molecular make-up of a tumor: proteomics in cancer research. *Clin. Science 108*: 369–383.

Kubota, T. 2006. Gastrointestinal stromal tumor (GIST) and imatinib. *Intern. J. Clin. Oncol. 11*: 184–189.

Kurhanewiez, J., Swanson, M.G., Nelson, S.J., and Vigeron, D.B. 2002. Combined magnetic resonance imaging and spectroscopic imaging approach to molecular imaging of prostate cancer. *J. Magn. Reson. Imag. 16*: 451–463.

Mauro, M.J. and Deininger, M.W. 2006. Chronic myeloid leukemia in 2006: a perspective. *Haematologica 91*: 152.

Morris, S., and Carey, L. 2006. Trastuzumab and beyond: new possibilities for the treatment of HER2-positive breast cancer. *Oncology 20*: 1763–1771.

Murphy, P.S., Dzik-Jurasz, A., Baustert, I., Leach, M.O., and Rowland, I.J. 2000. Choline signal correlates with vascular permeability in human gliomas. *Proc. Intern, Soc. Magn. Reson. Med. 8*: 393.

Murphy, P.S., Viviers, L., Abson, C., Rowland, I.J., Brada, M. and Leach, M. 2004. Monitoring temozolamide treatment of low-grade glioma with proton magnetic resonance spectroscopy. *Brit. J. Cancer 90*: 781–786.

Nakamura, T., Ishizaka, Y., Nagao, M., Hara, M., and Ishikawa, T. 1994. Expression of the RET proto-oncogene product in human normal and neoplastic tissues of neural crest origin. *J. Patho. 172*: 255–260.

Robertson, J.A. 2001. Consent and privacy in pharmacogenetic testing. *Nat. Genet. 28*: 207–209.

Robertson, J.A., Brody, B., Buchanan, A., Kahn, J., and McPherson, E. 2002. Pharmacogenetic challenges for the health care system. *Health Aff. (Millwood) 21*: 155–167.

Samoylova, T.I., Morrison, N.E., Globa, L.P., and Cox, N.R. 2006. Peptide phage display: opportunities for development of personalized anti-cancer strategies. *Anti-cancer Agents Med. Chem. 6*: 9–17.

Schwarz, A.J., Maisey, N.R., Collins, D.J., Cunningham, D., Huddart, R., and Leach, M.O. 2002. Early in vivo detection of metabolic response: a pilot study of 1H MR spectroscopy in extracranial lymphoma and erm cell tumors. *Brit. J. Radio. 75*: 959–966.

Sibtain, N.A., Howe, F.A., and Saunders, D.E. 2007. The clinicalvaue of proton magnetic resonance spectroscopy in adult brain tumors. *Clin. Radio. 62*: 109–119.

Sihto, H., Sarlomo-Rikala, M., Tynninen, O., Tanner, M., Andersson, L.C., Franssila, K., Nupponen, N.N., and Joensuu, H. 2005. KIT and platelet-derived growth factor receptor alpha tyrosine kinase gene mutations and KIT amplifications in human solid tumors. *J. Clin. Oncol. 23*: 49–57.

Sikora, K. 2007. Personalized medicine for cancer: from molecular signature to therapeutic choice. *Adv. Cancer Res. 96*: 345–369.

Silver, M., Talpaz, M., Sawyers, C.L., Druker, B.J., Hochhaus, A., and Schiffer, C.A. 2004. Four years follow up of 1027 patients with late chronic phase (L-CP), accelerated phase (AP), or blast crisis (BC) chronic myeloid leukemia (CML) treated with imatinib in three large phase II trials [Abstract number 23]. *Blood 104*: 10a.

Takahashi, M. 1988. Cloning and expression of the RET oncogene encoding a receptor tyrosine kinase with two potential transmembrane domains. *Oncogene 3*: 571–578.

Talpaz, M., Goldman, J.M., Sawyers, C.L., Hochhaus, A., Silver, R.T., and Douglas-Smith, B.D. 2003. High dose imatitinib (STI571,Gleevec) provides durable long-term outcomes for patiens (pts) with chronic myeloid leukemia (CML), in accelerated phase (AP) or myeloid blast crisis (BC): follow up of the phase II studies [Abstract]. *Blood 102*: 905a–906a.

Talpaz, M., Shah, N.P., Kantarjian, H., Donato, N., Nicoll, J., Paquette, R., Cortes, J., O'Brian, S.G., Nicaise, C., Bleickardt, E., Blackwood-Chirchir, M.A., Iyer, V., Chen, T.T., Huang, F., Decillis, A.P., and Sawyers, C.L. 2006. Dasatinib in imatinib-resistant Philadelphia chromosome-positive leukemias. *N. Engl. J. Med. 354*: 2531–2541.

van't Veer, L.J., Dai, H., van de Vijer, M.J., He, Y.D., Hart, A.A., Mao, M., Peterse, H.L., van der Kooy, K., Marton, M.J., Witteveen, A.T., Schreiber, G.J., Kerkhoven, R.M., Roberts, C., Linsley, P.S., Bernards, R., and Friend, S.H. 2002. Gene expression profiling predicts clinical outcome in breast cancer. *Nature 415*: 530–536.

Watters, J.W., and McLeod, H.L. 2003. Cancer pharmacogenomics: current and future applications. *Biochim. Biophys. Acta 1603*: 99–111.

Weisberg, E., Manley, P., Mestan, J., Cowan-Jacob, S., Ray, A., and Griffin, J.D. 2006. AMN107 (nilotinib): a novel and selective inhibitor of BCR-ABL. *Brit. J. Cancer 94*: 1765–1769.

Wolf, W., Waluch, V., and Presant, C.A. 1998. Non-invasive 19F-MRS of 5-fluorouracil in pharmacokinetics and pharmacodynamics. *NMR Biomed. 11*: 380–387.

Workman, P., Aboagye, E.O., Chung, Y.-L., Griffiths, J.R., Hart, R., Leach, M., Maxwell, R.J., McSheehy, P.M.J., Price, P., and Zweit, J. 2006. Minimally invasive pharmacokinetic and pharmacodynamic technologies in hypothesis testing clinical trials of innovative therapies. *J. Nat. Cancer Instit. 98*: 580–598.

Wulfkuhle, J.D., Auino, J.A., Calvert, V.S., Fishman, D.A., Coukos, G., Liotta, L.A., and Petricoin, E.F. 2003. Signal pathway profiling of ovarian cancer from human tissue specimens using reverse-phase protein microarrays. *Proteomics 3*: 2085–2090.

Yeoh, E.J., Ross, M.E., Shurtleff, S.A., Williams, W.K., Patel, D., Mahfouz, R., Behm, F.G., Raimondi, S.C., Relling, M.V., Patel, A., Cheng, C., Campana, D., Wilkins, D., Zhou, X., Li, J., Lui, H., Pui, C.H., Evans, W.E., Naeve, C., Wong, L., Wong, L., and Downing, J.R. 2002. Classification, subtype discovery, and prediction of outcome in pediatric acute lymphoblastic leukemia by gene expression profiling. *Cancer Cell 1*: 133–143.

Yong, W.P., Innocenti, F., and Ratain, M.J. 2006. The role of pharmacogenetics in cancer therapy. *Br. J. Clin. Pharmacol. 62*: 35–46.

Zbuk, K.M., and Eng, C. 2007. Cancer phenomics: RET and PTEN as illustrative models. *Nature Rev. Cancer 7*: 35–45.

7
Radiation Doses to Patients Using Computed Radiography, Direct Digital Radiography, and Screen-Film Radiography

Gaetano Compagnone

INTRODUCTION

Medical use of ionizing radiation now represents >95% of all man-made radiation exposures and is the largest single radiation source after natural background radiation. Therefore, it is important to quantify the amount of radiation received by a patient during a radiological examination for many reasons:

To optimize radiological procedures because the operators can improve remarkably their performances by identifying the examination protocols that maximize image quality (when patient dose is kept constant) or minimize patient dose (when image quality is kept constant).

To establish the approximate risk from a particular examination and to measure the risk to an individual patient (for example in the case of an unsuspected pregnancy).

To compare doses in different examinations or departments and to ensure compatibility with recommended standards, because it is well known that doses can be unnecessarily high (for example, due to inattention or too much work pressure), and those comparisons can promote changes in working procedures by showing what is possible in other centres.

To document the adequacy of the dosimetric aspects of a quality assurance program.

To study medical doses with respect to man-made exposures and natural background.

Because of all these reasons there is a need for fully investigating radiation doses to patients undergoing radiographic examinations, of course by paying careful attention at the same time to the image quality. In the next paragraphs radiation quantities are firstly defined, then screen-film radiography, computed radiography (CR) and direct digital radiography (DR) are described in terms of both the basic operating principles and the mutual relationships between patient dose and image quality.

RADIATION QUANTITIES USED IN PATIENT DOSIMETRY

An X-ray examination is usually associated with a benefit, which originates from the capability to obtain suitable clinical information from the image, and with a risk because ionizing radiations have harmful effects on living tissues. A higher radiation dose to the image detector, and therefore to the patient, reduces the noise levels in the final image and consequently can be strictly related to image quality and at last to the benefit of the examination to the patient; a higher patient dose can therefore potentially increase both the benefit and the risk of the examination. Frequent evaluations of radiological procedures, systems performance, and patient dose are necessary to ensure that

optimal conditions are achieved. In order to accomplish this task it is necessary to first define some quantities useful in characterizing the "dose" concept.

The radiation generated by an X-ray tube can be quantified by the radiated energy fluence, but is most conveniently expressed by measuring the amount of charge produced by ionization in a volume of air placed in the X-ray beam. Therefore, a quantity called "exposure" (X) has been defined as the charge "dQ" (in Coulomb, C) produced per unit mass of air "dm" (in kg):

$$X = dQ/dm. \quad (7.1)$$

In the SI unit system, exposure is measured in [C/kg], and in the non-SI system exposure is measured in Roentgen (R), where $1\,R = 2.58 \times 10^{-4}$ C/kg. The exposure is directly related to the intensity of a radiation source, and it is independent of any material that may be situated in the radiation beam.

Conversely, another radiation quantity called "absorbed dose" (D) generally depends on which material is placed into an X-ray beam: for a given exposure, a high atomic number material will absorb more radiation energy than a low atomic number material. Therefore, it is possible to define the absorbed dose as the mean energy imparted ($d\varepsilon$) by ionizing radiation to material of mass dm:

$$D = d\varepsilon/dm. \quad (7.2)$$

In the SI unit system, absorbed dose is measured in gray (Gy), where 1 Gy = 1 J/kg, and in the non-SI system absorbed dose is measured in rad, where 1 rad = 10 mGy = 100 erg/g.

When a given mass of air receives an exposure of 1 R it is possible to calculate by definition how many electrons have been released: since the mean energy required to produce an ion pair in air is 33.97 eV, an exposure of 1 R corresponds to an air dose of 8.76 mGy (= 0.876 rad). Air dose is thus an alternative to exposure for quantifying the intensity of an X-ray beam, and measures the energy deposited in the air.

In order to characterize the intensity of an X-ray beam, the quantity "air kerma" (Kinetic Energy Released per unit Mass) is also used, and it measures the kinetic energy transferred from the X-ray beam to electrons in air. Air dose and air kerma are expressed in the same units (i.e., Gy or rad), and for most practical purposes these quantities may be thought as interchangeable in diagnostic X-ray dosimetry because the differences between them are very small at the low energies used in diagnostic radiology. The reason for this is that, in the strict sense, kerma only applies to initial photon interactions with medium, i.e., the transfer of energy from the primary photons to the secondary electrons as kinetic energy, differently from absorbed dose which is affected by subsequent interactions, i.e., secondary electrons arriving from a finite mass of material surrounding the point of interest. Therefore, if charged particle equilibrium could not be ensured, very accurate D measurements would require strictly defined experimental conditions and the use of a certain number of small correction factors. However, at the relatively low energy photons used in diagnostic radiology, this equilibrium is readily achieved and bremsstrahlung production is negligible, and in this situation D and kerma are equal when both are expressed in Gy.

Another important radiation quantity to monitor and to record the total X-ray beam intensity incident on the patient,

which takes into account both D and X-ray beam area, is the "dose-area product" (DAP): for example, a uniform air dose of 100 mGy over an area of $5 \times 5\,cm^2$ would result in a DAP reading of $100 \times 5 \times 5 = 2{,}500\,mGy\,cm^2$.

In order to determine the biological effect to organs from the absorbed ionizing radiation energy it is important to measure the rate at which energy is transferred to the medium and, therefore, the density of ionization along the track of the radiation. This is a complex concept to apply in the strict sense, and a quantity called "linear energy transfer" (LET) has been defined as the energy transferred to the medium per unit track length. Linear energy transfer is measured in [keV μm^{-1}] and from definition follows that radiations which are easily stopped will have a high LET (e.g. the LET values for 5 MeV neutrons and α-particles are ~20 keV μm^{-1} and 50 keV μm^{-1}, respectively), whereas those which are penetrating will have a low LET (e.g., the LET values for 100 kVp X-rays and 20 keV β-particles are ~6 keV μm^{-1} and 10 keV μm^{-1}, respectively).

Following this characterization of the beams of ionizing radiation in terms of their LET, a quantity called "equivalent dose" (H) has been defined as:

$$H = D \times w_r, \qquad (7.3)$$

where w_r is the radiation weighting factor, whose value basically depends on the radiation LET value. Radiations used in diagnostic radiology (i.e., X-rays) are low LET radiations and have w_r equal to 1, other radiations (e.g., alpha particles) are high LET radiations and can have w_r up to 20: therefore, for a given absorbed dose, high LET radiations are much more damaging than X-rays.

In the SI system, the unit of equivalent dose is the sievert (Sv). In the non-SI system the unit is the rem, where 1 rem = 10 mSv. It is important to differentiate physical quantities "exposure" (related to beam intensity), "absorbed dose" (related to what the tissue will absorb) and "equivalent dose" (related to the biological consequences of a given dose), although there could be a close numerical correspondence between them.

The above mentioned biological effects of ionizing radiations on human beings can be distinguished into two classes: "stochastic effects" and "deterministic effects".

Stochastic effects are those whose probabilities of occurrence instead of their severity increase with dose with no apparent threshold (e.g., carcinogenesis and the induction of genetic effects that appear in the descendants of irradiated individuals). Deterministic effects are those whose severity is directly related to dose and for which a threshold exists (e.g., cataracts of the lens, dermatitis, epilation).

Generally, a diagnostic examination results in a nonuniform dose distribution: exit dose is ~1% of the entrance dose, and higher doses are imparted to tissues within the direct X-ray beam than to those outside the X-ray field. The skin dose is a useful descriptor for predicting the possibility of deterministic effects: however, it has a threshold of ~ 2 Gy, and, therefore, are very rare in diagnostic radiology, while the patient risks in the rest of the cases are the stochastic processes.

Therefore, the skin dose (that does not account for the penetrating power of the X-ray beam, the size of X-ray field, the radiosensitivity of the organs and tissues that are irradiated) is not a significant dose indicator for patient risk. The total amount of radiation

received by a patient is best quantified by another quantity, the "effective dose" (E), which measures the stochastic risk of the induction of cancer and genetic effects in future generations, accounting for the irradiated organs and tissues, and their relative radiosensitivity. It has been defined as:

$$E = \Sigma_i H_i \times w_i, \qquad (7.4)$$

where H_i is the equivalent dose to organ i, w_i is the relative radiosensitivity of this organ, and the summation is over all the organs and tissues that were irradiated for any specific examination.

Use of E allows all radiological procedures using ionizing radiations to be directly compared. For example, if an abdomen CT scan has an effective dose of 8 mSv, whereas the E of a chest examination ("posteroanterior + lateral" projections) is 0.05 mSv, it is possible to state that, from a patient risk point of view, that abdomen CT scan is equivalent to 160 chest examinations.

Effective doses can also be directly compared with exposures from natural background (~3 mSv/year), as well as with regulatory dose limits for members of the public.

Moreover, it is possible to convert E into approximate values of stochastic risk: for a whole population the International Commission on Radiation Protection (ICRP) recommends a risk factor for total detriment of 0.073/Sv. However, nominal risk coefficients are associated with very large uncertainties at the low doses normally used in diagnostic radiology. For the sake of completeness it is added that the situation could change in the near future because the ICRP suggested in a draft of forthcoming recommendations that effective dose should only be utilized as prospective radiation protection guidance, and not at low doses in retrospective situations for assessing risks of stochastic effects.

CONVENTIONAL SCREEN-FILM SYSTEMS

In a screen-film system the emulsion is the sensitive part of the detector, and is composed of crystals of silver and bromide ions arranged in a cubic lattice (a transparent base material, usually polyester, is used to preserve stiffness and support the emulsion).

The use of radiographic film alone as an image receptor for X-rays in the diagnostic energy range provides very low imaging speed (see below for "speed" definition) and low image contrast because only a very small fraction of X-rays is absorbed in the film. On the other hand, films can show high speed and contrast when exposed to light photons because the absorption coefficient of the film for light of suitable wavelength is very high. As a consequence of that, intensifying screens that absorb X-rays efficiently and convert their energy into light are typically used for medical diagnostic imaging. The film, in contact with the screens, then efficiently absorbs the light emitted from the screens to produce a latent image that corresponds to the X-ray image pattern absorbed by the screens.

When a film, after being exposed, developed and fixed, is placed in front of an uniformly illuminated light box it is possible to define a quantity called "optical density" (OD) as:

$$OD = \log_{10} (B_0/B), \qquad (7.5)$$

where B_0 is the brightness of the light beam from the light box and B is the amount of transmitted light.

The most critical disadvantage of screen-film system is the incapability to optimize independently the image-recording and image-display functions, because its sensitometric response curve determines the image recording latitude as well as the display contrast and the dynamic range: therefore, with screen-film systems one can use either wide exposure recording latitude or high contrast sensitivity, but not both at the same time. Other disadvantages of this technology are as follows: problems related to the storage, retrieval and possible loss of images on film; incapability to quickly transfer images for review at remote locations; technical and environmental problems associated with wet chemical film processing solutions. As a result, screen-film systems are less and less used in favour of digital technologies (except in some special practices, e.g., mammography).

Dose measurements are very important in quantifying the amount of radiation received by a patient when using screen-film systems (or digital techniques, see below): a very detailed review of the dosimetry physical aspects and techniques in diagnostic radiology has been given by Wall *et al.* (1988). The absorbed dose on the surface of the patient (or of a phantom simulating the patient) can be measured directly with a suitable dosimeter (e.g., thermoluminescent dosimeters, see below) or can be calculated from the exposure or absorbed dose measured in free air. As stated above, D is related to the absorbing material, and, therefore, the exact composition of the medium should be always clearly defined when absorbed dose measurements are quoted. Generally, for measurements on the surface of a patient, the absorbing medium is assumed to be soft tissue or water: D_{mus} in muscle is related to D_{air} in air by the ratio of the mass energy absorption coefficients of muscle and air, $(\mu_{en}/\rho)_{mus}$ and $(\mu_{en}/\rho)_{air}$ respectively:

$$D_{mus} = D_{air} \times (\mu_{en}/\rho)_{mus}/(\mu_{en}/\rho)_{air}. \quad (7.6)$$

Mass energy absorption coefficients depend on photon energy, while average values weighted for typical X-ray spectra do not vary considerably from one spectrum to another: D_{mus} can consequently be assumed to differ from D_{air} by a factor of 1.06 for all typical diagnostic X-ray qualities (with uncertainty $< \pm 1\%$).

The dose measured on the surface of the patient at the point of entry of the X-ray beam includes a contribution from photons scattered back from deeper tissues, which is not present when measurements are made in free air. More precisely, the backscatter factor (BSF) is the ratio of the entrance surface dose in air at the position corresponding to the surface of the patient, when the patient is present, to that at the same point when the patient is absent. Therefore, entrance surface dose (ESD) at the focus-to-surface distance FSD, calculated from free-in-air measurements made at a distance "d" from the focus, needs to be corrected both for BSF and for the inverse square law:

$$ESD = D \times (d/FSD)^2 \times BSF\,, \quad (7.7)$$

where D is the absorbed dose at distance d from the tube focus.

Typical values for the BSF vary between ~1.2 and 1.4 and depend for the most part on the X-ray quality and the beam area, and to a lesser extent on the thickness of the part of the patient being irradiated and the composition of the underlying tissues.

The process of monitoring doses from diagnostic radiology procedures should

be based on experimental beam output measurements made in each radiographic room at a wide spread of kilovoltages settings. The output can be measured with a cavity ionization chamber calibrated in terms of absorbed dose to air or air kerma: it should be held in a scatter free support on the X-ray beam central-axis at a known distance from the tube focus (e.g., 75 cm or 100 cm). It should be also ensured that electronic equilibrium in the walls surrounding the cavity, whose thickness must be equal or exceed the maximum electron range, is established. The ESD for a specific examination can thus be estimated from knowledge of the actual exposure factors used in the clinical protocol (kVp, mAs, d, …) and from Equation (7.7), where the output has to be calculated as a function of the exposure factors.

Usually, for practical reasons, it is not possible to measure outputs for all exposure factors used in the actual clinical procedures, and therefore, it is necessary to use some mathematical model for calculating a specific tube output from the experimental outputs measured in each radiographic room. Many mathematical models have been proposed to calculate the dependence of the output of a diagnostic X-ray unit on kVp, mAs and d over the clinical range. A phenomenological relation has been described by Harpen (1996) as a function of kVp_{pro}, mAs_{pro} and d_{pro} (kilovoltage, mAs and focus-to-surface distance, respectively, used in the actual clinical procedures) by taking only two X-ray tube output measurements at two different kilovoltages (D_0 at kVp_0, and D_1 at kVp_1) at fixed mAs_{fix} and at a fixed distance FSD_{fix} from the tube focus:

$$ESD = \alpha \times (kVp_{pro})^{\beta} \times mAs_{pro} \times BSF, \quad (7.8)$$

where α and β parameters depend on the type of X-ray generator, anode material, and filtration and are defined as:

$$\alpha = D_0 \times (d_{pro}/FSD_{fix})^2 / ((kVp_0)^{\beta} \times mAs_{fix}) \quad (7.9)$$

$$\beta = \ln (D_0/D_1)/\ln(kVp_0/kVp_1)\,. \quad (7.10)$$

In order to measure the DAP, by integrating the absorbed dose over the whole beam area, large area ionization chambers are available which can be mounted on the X-ray tube diaphragm housing to intercept the entire X-ray beam: their response is independent of the distance from the tube focus.

Direct measurements of ESD in diagnostic radiology are most readily performed by small, independently calibrated, thermoluminescent dosimeters (TLD) attached directly to the skin of the patient at a point coincident with the center of the incident X-ray beam. The advantages of TLD are as follows: low atomic number so they are almost tissue equivalent; unlikelihood of masking diagnostic information; not a cause of discomfort to the patient. On the other hand, thermoluminescent dosimeters have also some disadvantages: delay between exposure and readout; possibly slowing patient throughput in a busy department; need of expensive TLD read out equipment.

Usually, evaluating the effective dose for a specific examination is not an easy task because this needs an explicit knowledge of the doses to all irradiated organs and tissues. It is possible that direct demanding E measurements are replaced by using mathematical anthropomorphic phantoms and Monte Carlo techniques, in order to provide the pattern of energy deposition in a patient for a specific examination, where ESD or DAP is already known. Thus, E to patients may be obtained by measuring or

calculating the ESD (or DAP), and using Monte Carlo-generated conversion factors E/ESD (or E/DAP) to estimate the corresponding effective doses.

PATIENT DOSE AND IMAGE QUALITY WITH CONVENTIONAL SCREEN-FILM SYSTEMS

The X-ray photon energy used for a specific radiographic imaging procedure is to a great degree imposed by the anatomical features of clinical interest and the image contrast required. The photon energy must be sufficiently high so that a certain reasonable fraction of the incident X-ray beam is transmitted through the anatomy to convey the information to the image detector. On the other hand, the photon energy must be sufficiently low so that a suitable fraction of the photons are attenuated due to either scattering or absorption by the anatomical features being imaged to produce a differential pattern of X-ray distribution corresponding spatially to those anatomical features.

For obtaining high contrast images, it is advisable that the fraction of photons attenuated by the anatomical features are highly relative to the fraction that is transmitted without attenuation. Consequently, lower energy X-ray photons would be chosen for high contrast. On the other hand, to minimize dose to patient, one would choose higher X-ray photon energy thus reducing the fraction of photons absorbed in the patient. Consequently, a proper settlement must be made for a specific diagnostic imaging task to account for both the need for high image contrast and the wish to minimize patient radiation dose.

The speed of a screen-film system is usually defined as the reciprocal of the dose in mGy required to produce an image density of 1.0 above the basic fog. The higher the speed class, the more sensitive the screen-film combination (i.e., faster screen-film speeds are associated with lower patient doses): very high resolution and high contrast combinations are likely to have a speed class of ~100–200, whereas very fast combinations will have less resolution and possibly contrast. The most frequently used speed classifications are the 200 and 400 classes: 400-speed screen-film systems are generally used for a range of routine examinations (e.g., abdomen, lumbar spine, etc.) because they offer a good compromise between speed and image spatial resolution, 200-speed systems are often utilized for examinations where greater spatial resolution is required (e.g., extremities). Many standards are available to manufacturers to measure the speed of a given screen-film system, for example, those provided by American National Standards Institute (ANSI), Deutsches Institut fur Normung (DIN), and International Standards Organization (ISO). Each of these employs different protocols for calculating absolute speed by using various beam energies, focus to film distances, and filtration thickness and types.

Therefore, special attention should be paid to the reliability of absolute system speed classifications. Thus, the "relative" speed is more useful because it gives the relative difference in speed between systems. For example, if one radiological department uses a 200-speed system and another department employs a 400-speed system, all other factors remaining constant,

the first department uses approximately twice the amount of radiation to produce its radiographs compared with the second department.

For a specific film, the speed of a screen is determined by the screen thickness (besides its composition), which is a key element that contributes to determining the amount of blurring in the image: fast screens are thick and have poor spatial resolution characteristics, whereas slow screens are thin and have superior resolution performance.

With pediatric patients, more frequently than with adults, a lower level of image quality may be acceptable for some clinical indications, but this limitation can be justified only if it has been deliberately planned by the radiologist and if it is associated with a lower dose to patient. Higher speed classes of screen-film systems are a very important factor with respect to dose reduction and, moreover, they have the potential of allowing shorter exposure times that reduce motion unsharpness, which is the most significant cause of blurring in pediatric imaging (in this case, the reduced spatial resolution of those systems can be comparatively less important for most of clinical indications).

In a radiology department the most important imaging requirement is detection of abnormalities, but most evaluations of medical image quality must be based on visualization of normal anatomy because most images are normal. Guidelines to achieve adequate image quality and reasonably low radiation dose per radiograph were presented by the European Union (1996). Anatomical criteria are used to concentrate on the visibility of predefined anatomic features as evaluation criteria. According to this philosophy, diagnostic requirements are proposed as the image quality criteria, which must be fulfilled when specific clinical questions are asked. Thus, image quality criteria are a list, which in most cases defines important anatomical structures that should be visible on a radiograph to help accurate diagnosis. The level of visibility can be described by the following.

Visualization: characteristic features are detectable but details are not fully reproduced, features are barely visible.

Reproduction: details of anatomical structures are visible but not necessarily clearly defined; details are barely emerging.

Visually sharp reproduction: anatomical details are clearly defined; details are clear.

Important image details: these define the minimum limiting dimensions in the image at which specific normal or abnormal anatomical details should be recognised.

Diagnostic reference levels (DRLs) were introduced as a practical tool for management of patient doses in radiology. They can be defined as dose levels in medical radiodiagnostic practices for typical examinations, for groups of standard-sized patients or standard phantoms, and for broadly defined types of equipment. These levels should not be exceeded for standard procedures when good and normal practice regarding diagnostic and technical performance is carried out. A value lower than a reference level for a given medical imaging task may not necessarily be an optimal value, but it shows that the procedure delivers a patient dose within the current local practice for the procedure. The reference levels can be considered a ceiling from which advance should be pursued to lower dose levels in line with the ALARA (as low as reasonably achievable) principle. A value consistently higher than a reference level may require review to determine if it is necessary to change the protocol for the imaging procedure in regards to the aspects

that affect patient dose. However, DRLs do not represent a dividing line between the acceptable and unacceptable practice of radiology.

COMPUTED RADIOGRAPHY

In contrast to intrinsic digital techniques such as CT or MRI modalities, all digital projection radiography techniques result from the continuous evolution of conventional, analogue, screen-film systems. The first development was the computed radiography also known as storage phosphor or photostimulable phosphor radiography. It is a system of producing digital radiographic images that utilizes a storage-phosphor plate (instead of film) in a cassette and a conventional radiographic acquisition geometry. The X-ray energy incident upon the detector is deposited into a photostimulable phosphor with delayed luminescence properties. After the plate is exposed, a laser beam scans it to produce the digital data that are converted into an image. In order to do that, the deposited energy is released as visible light that is captured by a light detector, translated into digital signals, and registered with the location on the screen from which it has been released. The digital data are then postprocessed for appropriate display, and are sent to a hard-copy printer or a soft-copy display monitor in order to be clinically evaluated.

In contrast to conventional screen-film radiography, CR offers the inherent feature that the detection of the X-ray image is completely divided from processing and display, and therefore, the look of a CR image is not solely determined by the radiation exposure and the detector response because it can be adjusted through image post-processing and display. Indeed, image processing can modify the numerical values of pixels, and therefore, the contrast in particular regions of an image which can be adapted to the needs of specific clinical examinations. For example, in chest examinations the latitude of film is a limitation for screen-film systems because of the largely varying tissue attenuations in the chest. Computed Radiography has much more latitude than screen-film systems, and therefore, the contrast in the low-density mediastinum region can be increased without overenhancing the lung fields.

An excellent review of the physics and technology of computed radiography systems has been given by Task Group 10 of the American Association of Physicists in Medicine (2006). Many compounds have the feature of being photostimulable phosphor, but only few possess properties advisable for radiography: stimulation-absorption peak at a wavelength generated by normal lasers; stimulated emission peak easily absorbed by normal photomultiplier tubes input phosphors; storing of the latent image without significant signal loss due to phosphorescence. The materials that most closely fulfil these conditions are alkali-earth halides (e.g., BaFBr:Eu). Photostimulable phosphor frequently requires greater exposure to attain similar image quantum statistics compared with a 400-speed rare-earth detector. In addition, storage phosphors show high absorption probability of X-rays below 50 keV, where a significant fraction of lower energy scattered radiation occurs, and thus they have a greater sensitivity to scatter compared with the rare-earth screen.

Photostimulated luminescence is emitted in all directions from the phosphor screen:

an optical collection system captures a fraction of the emitted light, and transmits it to the photocatode of the photomultiplier tube of the reader assembly.

For screen-film systems, which are used as both the acquisition and the display medium, it is necessary to adjust the detector contrast and radiographic speed to a restricted exposure range to obtain images with optimal contrast and minimal noise properties, because film is optimally sensitive to a limited range of exposures. Digital systems are not compelled by the same demands because the acquisition and display media are separated, and compensation for under- and overexposures is possible by proper processing of the digital data. However, because under- and overexposed images can go unnoticed by the system, a method to mark the exposure incident on each image is necessary to identify those cases that exceed the expected or target exposure range so that action can be taken to settle any difficulties. Most important is the broad range of overexposures, which can lead to a slight or steady and potentially unperceived increase in exposure when digital detectors are used, and therefore an unnecessary radiation dose to the patient.

In computed radiography equipment the X-ray detector has to comply with many requirements. The pixel size must be small enough to allow sufficient spatial resolution, and at the same time the field size must be large enough for all radiographic examinations. The sensitivity must be high enough to allow low-dose procedures. The dynamic range must be large enough to cover a wide range of X-ray beam intensities. Internal noise sources must be small enough to retain image quality, and the readout time must be quick enough to allow efficient workflow.

The easiest way to improve the X-ray absorption efficiency of an imaging plate is to increase its thickness, but this method has two weaknesses: the lateral diffusion of the light in the phosphor layer (for both the stimulating laser light and the emitted light) will increase proportionally to the layer thickness, affecting the resolution; the signal intensity will rise almost negligibly when the layer exceeds a certain thickness because most of the light stimulated at greater depth will not arrive to the surface and therefore, will not be able to be detected. The idea of overcome the latter weakness is to make the substrate of the imaging plate transparent and to detect the stimulated light emerging both from the front and from the back side of the plate. This needs two light-collection systems, but still only one stimulating laser beam. A detective quantum efficiency (DQE, that can be defined as the ratio of the signal-to-noise at the output of the system to that at the input of the system, all squared) improvement of ~30–50% compared with single-side reading can be achieved with only secondary effect on the contrast of detailed structures.

The fundamental readout principle of CR systems is the flying spot scanner, as described above: i.e., a finely focused laser beam is moved over the imaging plate in a raster-like way in order to stimulate the luminescence from each pixel individually. This principle has a basic weakness in read out time, and consequently in throughput. Because of the decay time of the phosphor luminescence, the necessary stimulation time per pixel cannot be much less then 4 μs; therefore, the read out of a high resolution 4,000 × 4,000 pixel image requires $\sim 4 \times 10^{-6} \times 4{,}000^2 = 64$ s.

A technological evolution of CR systems that prognosticates improvements in this

situation is known as "parallel reading" or "line scanning": a full-line of pixels is addressed and readout is produced at each point instead of a single pixel. This needs a linear laser light source and a linear detector array over the full-width of the imaging plate. Both the laser source and the linear detector are integrated into a compact unit, which is then moved in one direction over the imaging plate. An increase in readout speed seems possible because line scanning reads several thousands pixels in parallel; however, this new technological approach is not free from problems as there are other limitations, for example, the disposable power of laser stimulation light and some mechanical restrictions. Still, it seems achievable to decrease the scanning time for a large area, producing a high resolution image in less than 10 s. Other advantages of the line scanning technology are: a more efficient readout process because the detectors can be brought closer to the imaging plate, and a more compact reader unit that can be combined with radiographic stands or tables.

With nonstructured phosphors both excitation laser and stimulated light are scattered strongly and isotropically in imaging plates. On the other hand, it is well known that phosphor needles act as light guides, transmitting the luminescence light preferentially along their axes. Therefore, another technological development in CR systems will make needle phosphor layers thick without loosing too much spatial resolution, and with high packing density. The difficulties in using structured phosphors for the CR systems are: it is not easy to find materials that can be grown in needle shape and at the same time offer adequate photostimulation properties, and needle crystalline phosphors tend to be breakable and hygroscopic, which makes their use in a cassette-based system difficult.

PATIENT DOSE AND IMAGE QUALITY WITH COMPUTED RADIOGRAPHY

Computed radiography systems can produce suitable image luminance even for under- or overexposures because of their wide latitude response and capability to scale the signal, as reported earlier. Therefore, it is very important to have an indicator of the average incident exposure on the imaging plate to verify appropriate radiological techniques. Each CR manufacturer has a specific approach to yield this indicator, and a very good review of different methods has been reported by Frey and Sprawls (1997).

Fuji uses a "sensitivity number", which is an indication of how much amplification is required to set the image information to the correct digital range (it is inversely related to the incident exposure). Under normal processing conditions for the standard resolution plates, the system sensitivity number S is given as:

$$S = 200/(\text{exposure in mR}) \quad (7.11)$$

It follows that a large sensitivity number shows a low average X-ray exposure incident on the imaging plate. When the system sensitivity number is equal to 200, an average incident exposure within the area scanned by the CR reader can be estimated equal to 1 mR (at 80 kVp, no object, no added filtration: Fuji does not filter the beam to calibrate the system).

Carestream Health (previously Kodak) provides an "exposure index" (EI), which

is a value directly proportional to the average exposure incident on the imaging plate and is computed as:

$$EI = 1000 \times \log(\text{exposure in mR}) + 2000 \quad (7.12)$$

In these CR systems, an exposure of 1 mR (at 80 kVp, 0.5 mm Cu+1 mm Al added filtration) will provide an exposure index of 2,000, an exposure of 10 mR will provide an exposure index of 3,000, and an exposure of 0.1 mR will provide an exposure index of 1,000. Doubling the screen exposure provides an increase of approximately 300 in the exposure index value.

Agfa uses "lgM", a value indicating the actual exposure to the imaging plate by a mathematical relationship to the Scanned Average Level (SAL), which is the average grayscale value. For each examination, projection, and cassette size, an average value of lgM is either computed over 50 examinations or set manually.

Konica provides REX (relative exposure) value, which is generated as follows:

$$S = QR \times E_1/E \quad (7.13)$$

where QR is the preset quantization range, E is the average exposure in the region of the imaging plate utilised for calculating S, and E_1 is the plate exposure in mR that provides a digital value of 1,535. For a QR = 200, the system is calibrated to produce the 1,535 code value with an exposure of 1 mR at 80 kVp. Consequently, an exposure equal to 1 mR provides an S = 200, and an exposure equal to 2 mR provides an S = 100.

Whichever computed radiography system is used, a calibration of the exposure indicator is compulsory for carrying out accurate results: it is sensitive to many parameters, e.g., effective energy of the beam, positioning of the patient relative to the phosphor, delay between exposure and readout, segmentation algorithms, source-to-image distance. This number is a very important element of quality assurance, patient care and training issues: keeping the exposure incident on the imaging plates approximately the same from patient to patient should make the amount of noise in the images consistent.

As soon as a radiology department changes from screen-film systems to computed radiography an increase in patient doses can be noticed, due to the lack of both specific training in the new digital technique and well-established methods for checking patient radiation exposures. If staff has limited experience with digital techniques, high mAs settings for avoiding noisy images (i.e., higher than necessary for good image quality) or low kVp for increasing contrast could be used. Therefore, the importance of an appropriate choice of technical parameters for exposure is never over-emphasized, especially in digital radiology.

A summary of typical figures of merit describing the image quality has been reported by ICRP (2004): spatial resolution limit; contrast of coarse structures; contrast of detailed structures (sharpness); noise perception (graininess, small area fluctuations); homogeneity (large area signal fluctuations); artefacts (due to defects or scratches, pixel drop-outs). The assessment of image quality should be undertaken before new digital systems are used in clinical practice.

Image compression can be an important element affecting the quality of stored images in the picture archiving and communications systems (PACS) and it can also alter the time required to have the images available (transmission speed

through networks). It is possible to suffer loss of image quality if the images have been overly digitally compressed. In consequence of that, some examinations may have to be repeated, and thus the patient will receive an additional dose of radiation. The level of compression consistent with required image quality is very dependent on modality (i.e., CR or flat-panel imagers, see below), the medical imaging tasks, and the type of examination. Therefore, the suitable level of compression should be fixed for each modality at each institution, taking into account the network infrastructure and the hardware available across the institution.

Dosimetry techniques when using CR systems are similar to those described above for screen-film radiography. Reevaluation of local DRLs should be undertaken when computed radiography replaces conventional screen-film, because DRLs for analogue systems do not necessarily apply to similar CR imaging procedures. It is not difficult to measure patient entrance dose for a computed radiography equipment, but at present there is no established international agreement on the DRLs that should be set for definite digital examinations.

The Digital Imaging and Communications in Medicine (DICOM) standard is the industry standard for transferral of digital radiology images and other medical information between computers. The DICOM standard allows digital information exchange between medical imaging equipment and systems from different manufacturers. Such connectivity is important for cost-effectiveness in healthcare, and permits users to supply radiology services within facilities as well as for distant access. Therefore, for the field of medical communication, all new medical products should fulfill its requirements. However, due to the fast evolution of new technologies and techniques, the connectivity and compatibility of equipment from different manufacturers is still not an easy task. Because the X-ray equipment and read out device are not usually linked in the CR systems, exposure parameters (e.g., kVp, mAs, etc.) cannot be recorded automatically as element of the image description data (e.g., in the DICOM header).

When using digital equipment, and in particular computed radiography systems, many actions can affect image quality and patient dose: they can be described by the following.

Improvement in the use of tools of the workstation to visualise images decreases dose to patient because that permits more information to be obtained from the same image.

Use of different post-processing techniques could sometimes reduce retakes and consequently decrease the dose to the patient, at the same time getting better image quality or diagnostic information.

Permitting easy access to the PACS and use of teleradiology to look at previous images decreases patient dose and improves diagnostic information.

Workstation accessibility for post-processing (also for radiographers) to avoid some retakes decreases patient dose and improves diagnostic information.

Supplying the console of the X-ray system with dose indication has no influence on image quality or diagnostic information, but decreases patient dose because it can reduce retakes and helps to optimise radiographic techniques.

Presence of false lesions or pathologies due to artefacts generated by inaccurate digital post-processing has no effect on patient dose but can produce loss of information and need for retakes.

Permitting inadequate conditions in the use of visualisation monitor increases patient dose with a potential loss of diagnostic information.

Using deteriorated storage-phosphor imaging plates increases patient dose because of retakes and can be the cause of loss of image quality.

Post-processing problems, faults in electrical power supply or problems in the network during the archiving of the images, and problems in printer and local hard disk increase patient dose with potential loss of images or retakes.

Deletion of image files at the viewing station or workstation of seemingly non-useful images increases patient dose due to possible loss of some useful information and difficult to control repeated exposures.

DIRECT DIGITAL RADIOGRAPHY

Direct digital radiography systems are based upon active matrix flat-panel imaging (AMFPI) technology: large area integrated circuits ("active-matrix arrays") allow the deposition of semiconductors across large area substrates in a well controlled way such that the physical and electrical properties of the resulting structures, coupled with traditional phosphors or photoconductors, can detect the transmitted X-ray fluence through a patient. Consequently, the X-ray energy is captured and converted to a latent image as locally deposited charge, and the latent image is then converted directly to a digital image dataset without further system interaction by the operator. Flat-panel X-ray imaging devices are currently divided into "indirect detection" (i.e., when an X-ray is detected a phosphor produces visible wavelength photons) and "direct detection" (i.e. when a X-ray is detected a photoconductor produces electrical charges).

In the indirect detection strategy, a phosphor layer (e.g., a structured scintillator such as CsI:Tl) is placed in close contact with an active-matrix array. The amount of the light emitted from a specific location of the phosphor is a measure of the intensity of the X-ray beam incident on the surface of the detector at that point. Each pixel on the active-matrix array has a photosensitive element that produces an electrical charge whose magnitude is proportional to the light intensity emitted from the phosphor in the location close to the pixel. This charge is stored in the pixel until the active-matrix array is read out. The magnitude of the signal charge from the different pixels holds the imaging information inherent in the intensity variations of the incident X-ray beam.

Thus, a hydrogenated amorphous silicon (a-Si:H), coupled to a phosphor screen, operates as individual photodiodes which convert the light emitted by the phosphor layer to charge. This charge is then stored as pixel capacitance, and finally it is read out through an active thin-film transistor switch integrated into each pixel. This detection process is called "indirect" because the image information is transmitted from the X-rays to visible-light photons and then lastly to electrical charge.

In the direct detection approach, the X-ray detection is carried out with a thick layer of photoconductor material, for example amorphous selenium (a-Se) photoconductive layer in direct electrical contact with an underlying flat-panel array. The pixels incorporate a conductive electrode to collect the charge and a capacitor element to store it (different from a photosensitive element as used in the indirect approach). When X-rays incide on the surface of the detector, charge is generated in the photoconductor. This charge is then shared between the pixel-storage capacitance and the inherent capacitance of the photoconductive layer. This detection process is called "direct" since the image information is transferred from X-rays directly to electrical charge with no middle stage.

The terms "direct" and "indirect" are therefore, most attributable to the nature of the initial X-ray detection process rather than the features of the flat-panel array

configuration. In both strategies, the flat-panel detector integrates the incoming signal over a finite period of time, therefore operating as an X-ray fluence detector rather than an individual X-ray photon detector. However, a two-dimensional array of imaging pixels is incorporated into both indirect and direct AMFPI systems. Each pixel is usually composed of a switching element and a sensing/storage element. Other components of the device are as follows: various metallic lines utilised to control the readout of the imaging information from the array of pixels; peripheral circuitry that amplifies, digitizes and synchronizes the readout of the image; a computer that processes and distributes the image for the final presentation as softcopy or hardcopy.

All the switches along a specific row on an active-matrix array are connected together with a single control line. In this way the external circuitry is able to change the state of all the switching elements along the row with a single controlling voltage. Each row of pixels needs a separate switching control line. The signal outputs of the pixels down a specific column are connected to a single signal line, and each column of pixels has its own read out amplifier. This arrangement allows the imager to be read out one horizontal line at a time. Consequently, active-matrix arrays transmit signal from the pixel element directly to the read out amplifier.

Many of the advantages reported for CR can be applied to DR equipment because both are based upon the digital technology: wide exposure latitude; linear signal response; flexibility in image display, processing and printing; possibility of interfacing to a PACS; monitor (softcopy) reading of clinical images. However, CR and direct digital radiography differ from each other in a few peculiar features: CR systems are less expensive than DR, are portable and usually are more flexible in achieving proper patient positioning for particular projections. Direct digital radiography has a much faster image readout (the image is available within a few seconds after the exposure, and then the detector is ready for the next image acquisition) and better performances of physical parameters, for example a higher DQE. The DQE of DR equipment is superior to both conventional screen-film radiography and CR systems, and this efficiency results in a superior contrast-detail performance with the potential of reducing radiation dose to patient.

The performance characteristics show differences between commercially available direct (a-selenium) or indirect (caesium iodide and a-silicon) DR equipment. Indeed, the electric field in the selenium layer, necessary to separate the charges that are produced by the absorbed X-ray photons, restrains the lateral diffusion of the charge cloud, in this way retaining a high spatial resolution (definitely higher than both the indirect detector and CR systems). On the other hand, the only moderate X-ray absorption efficiency of selenium (resulting from its low Z-value) and the noise aliasing provide a DQE for the direct detector lower than for indirect detector, although still better than that of computed radiography systems. Other photoconductors are extensively investigated for their use as direct X-ray converters: at the present time, it is possible to have materials showing a much better photon absorption efficiency than selenium for a given layer of thickness and also a higher charge yield (i.e., a higher signal per absorbed photon), but

unfortunately further technology progress is necessary to have layers of these materials that are highly homogeneous, stable, and defect-free.

Differently from a CR imaging plate, a DR detector has a fixed pixel size which is determined by the configuration of the readout array. Typical pixel dimensions for active matrix arrays are in the range of 100–200 μm. This results in limiting spatial resolutions of 2.5–5 lp mm^{-1}, according to the Nyquist theorem (the Nyquist frequency is the minimum frequency that will exactly sample an analogue signal, and this is twice the maximum frequency of the signal to be sampled), and although these resolutions seem to be sufficient for general radiography, there is a trend toward smaller pixel sizes, particularly for mammographic applications. However, smaller pixels reduce the fill-factor of the sensor array, that is, the proportion of the sensitive pixel area to the area of the pixel electronics (switching elements and readout lines). The fill-factor reduction may lead to DQE losses, and because of this reason, a practical pixel size not much less than 100 μm seems to be an unavoidable lower limit for DR equipment.

PATIENT DOSE AND IMAGE QUALITY WITH DIRECT DIGITAL RADIOGRAPHY

In order for digital radiography to replace the conventional radiography, it should ideally provide doses that are no greater than, and possibly smaller than, those provided by screen-film systems. Many authors have investigated doses associated with screen-film systems, computed radiography and direct digital radiography, but not all of their results are in agreement each other, even if there is an universal consent in DR being the lowest dose-imparting technology. For example, it was found by Compagnone *et al.* (2006) that effective doses to patients undergoing standard radiographic examinations (abdomen, chest, lumbar spine, pelvis, and skull) were approximately 29% and 43% lower for DR equipment than those for screen-film radiography and CR systems, respectively. In particular, lumbar spine examination showed the most prominent differences, because DR effective dose was 179 μSv compared with 309 μSv and 476 μSv delivered by screen-film and CR, respectively; in skull examination the lowest differences were found, because DR effective dose was 22 μSv compared with 27 μSv and 29 μSv delivered by screen-film and CR, respectively.

Direct digital radiography systems provide a considerable dose reduction compared with CR without significant loss of diagnostic information, although the degree of possible dose reduction is quite variable, because differences in doses depend on the level of acquisition dose, the reference technique used for comparison, the statistical analysis utilised, and the type of lesions studied. For example, a dose reduction of 50% for chest radiography using a flat-panel detector without loss of diagnostic information was demonstrated by Herrmann *et al.* (2002).

From a complementary point of view, it is also possible to assert that DR performs better than other imaging modalities with regard to overall image quality when images are obtained with about same doses. As an extreme example of this, a dose reduction of 50% for chest imaging with a flat-panel detector in comparison with a conventional

screen-film system with a speed of 200 was reported by Fink *et al*. (2002). Moreover, in this study the image quality and the conspicuity of almost all anatomical structures of interest in the images produced by DR equipment were rated significantly superior to those produced by conventional screen-film system.

Because chest radiography is the most diffused examination, it is of great interest to compare doses to patients undergoing this specific diagnostic radiographic procedure and to examine using screen-film, CR and DR equipment. An important and significant reduction in both entrance skin dose and effective dose with DR system for three comparable patient groups was reported by Bacher *et al*. (2003). Indeed for "posteroanterior + lateral" projections the effective dose decreased from 100.2 μSv with screen-film system to 62.3 μSv with CR equipment to 36.7 μSv with DR system. Similar conclusions could be made for entrance skin dose: in lateral projection ESD decreased from 1286.2 μGy with screen-film system to 733.6 μGy with CR equipment to 346.7 μGy with DR system. Moreover, image quality produced by amorphous silicon flat-panel detector was significantly better than image quality produced by screen-film or computed radiography systems, that is, the reduction in dose can be not detrimental to image quality.

A comparison between two commercially available DR systems based on direct conversion (amorphous selenium) or indirect conversion (amorphous silicon with a needle-structured CsI:Tl scintillator) with regard to radiation dose and image quality of digital chest examinations was performed by Bacher *et al*. (2006), and a significantly lower effective dose with amorphous silicon equipment was found. In particular, for the posteroanterior view the effective doses were 9.6 μSv and 22.6 μSv with amorphous silicon and amorphous selenium systems, respectively; for the lateral view the effective doses were 27.1 μSv and 79.2 μSv with amorphous silicon and amorphous selenium systems, respectively. Moreover, the quality of the images produced by indirect conversion based flat-panel was equal or even superior to that of the images produced by direct conversion based system.

Direct radiography permits various levels of image quality (of course using different patient doses) that can be matched to the different clinical tasks; for example, the follow-up of a fracture does not need the same level of image quality as that necessary for its diagnosis, and it was reported by Strotzer *et al*. (1998) that a radiation dose reduction of up to 75% with digital techniques in comparison with conventional screen-film systems can be achieved.

When a radiology department begins to use direct digital radiography equipment (or at regular frequencies when the DR systems are already in use), surveys of dose and image quality should be implemented and they should use quality criteria, as described above for CR systems. Some criteria include visualization of several anatomical details and these should be scored independently by radiologists. Evaluation should be undertaken for a random selection of equipment and patients of average size (~70 kg), and exposure factors and dose values should be recorded for each examination. At least two radiologists should examine each radiograph, fill up questionnaires where image quality criteria (which should be met) are listed, and

then scores should be averaged. The cause of any consistent non-compliance with image quality criteria should be researched and corrective action undertaken where this is considered necessary.

Introduction of the process of audit for both dose and image quality is one of the most important elements for improving performance in an imaging department. Regular evaluations are an incentive to evaluate technical aspects of equipment performance and how these are correlated with image quality and patient dose. Significant progress can often be made with regard to radiation dose and image quality in those institutions where performance is carefully checked. When a quality control audit of both radiation dose and image quality is implemented and results provided back to users, a significant reduction in radiation dose is usually achieved with no measurable degradation of image quality.

In consequence, local diagnostic reference levels should be reviewed when new DR systems are introduced in a certain institution, as already stated above for computed radiography. Accomplishing this task is easier with direct digital systems because, in contrast to CR equipment, they can yield automatic recording and storing of the DAP value together with the image data: indeed the recorded DAP values should be part of the image description data (e.g. in the DICOM header).

Even if examinations are carried out properly, with digital techniques there can be an increase in the number of radiographs requested by the referring physicians, probably due to the ease and convenience of obtaining the images and results. The number of exposures (i.e., acquired images) should be limited to the number required for the medical imaging task (and no more): that means the number of radiographs per examination should be kept at a number equal to (or lower than) that for conventional screen-film systems. The advantage of post-processing is that more information can be extracted from the modification of numerical data, use of magnification, and grey-scale inversion. Therefore, post-processing has the potential of avoiding the extra projections often required in some screen-film radiology.

CONCLUSIONS

Patient radiation doses and image quality are both very important in the present radiology and medical physics, and it is essential to keep in mind that reducing dose indefinitely is not possible without image suffering: therefore, the primary goal should be achieving the proper level of image quality. Computed radiography and flat-panel imaging have a large dynamic range and therefore, it is relatively easy to inadvertantly overexpose the patient. On the other hand, digital radiography, particularly when DR systems are used, has the potential of delivering doses to patient lower than screen-film systems provided that dose management programs for digital techniques (e.g. patient dose surveys, and specific training for operators) are implemented in the clinical routine.

Differences between the digital detector types primarily concern their efficiency as dose receptors, their physical parameters performance and workflow integration. The introduction of digital flat-panel systems represents important progress in imaging that potentially offers improved

image quality coupled with a significant reduction in the patient radiation dose compared with both screen-film systems and computed radiography equipment. More technology developments that will improve the performance of both the CR and DR systems can be expected and future research will try to improve the practical issues of using the digital detectors in a clinical environment. Indeed at the present time most CR systems are cassette-based while flat-panel detectors usually are integrated. However, portable flat-panel detectors (cassette-like) are already available, as well as some CR readers which can be integrated into the examination systems. Therefore, it can be expected that both digital imaging modalities will coexist in the near future.

To date, digital radiology is more expensive than film-based radiology. These higher costs are legitimated if all advantages of the new digital techniques are explored and integrated into the daily routine: better image quality or less patient dose; substantial decrease of archive space; increased speed and improved workflow; shorter patient examination times or increased patient comfort; possibility of teleradiology and remote expert consultation.

Digital technology is advancing rapidly as the natural evolution of screen-film radiography and will soon concern several millions of patients. If accurate consideration is not given to the radiation protection aspects of digital radiology, medical exposures of patients will increase considerably and without accompanying benefit. On the contrary, if the radiation protection aspects are dealt with properly, patient doses may be lowered without decreasing the diagnostic benefits.

REFERENCES

American Association of Physicists in Medicine, Task Group 10. 2006. Acceptance testing and quality control of photostimulable storage phosphor imaging systems. *American Association of Physicists in Medicine*, College Park, Maryland: AAPM Report No.93.

Bacher, K., Smeets, P., Bonnarens, K., De Hauwere, A., Verstraete, K., and Thierens, H. 2003. Dose reduction in patients undergoing chest imaging: digital amorphous silicon flat-panel detector radiography versus conventional film-screen radiography and phosphor-based computed radiography. *Am. J. Roentgenol. 181*: 923–929.

Bacher, K., Smeets, P., Vereecken, L., De Hauwere, A., Duyck, P., De Man, R., Verstraete, K., and Thierens, H. 2006. Image quality and radiation dose on digital chest imaging: comparison of amorphous silicon and amorphous selenium flat-panel systems. *Am. J. Roentgenol. 187*: 630–637.

Compagnone, G., Casadio Baleni, M., Pagan, L., Calzolaio, F.L., Barozzi, L., and Bergamini, C. 2006. Comparison of radiation doses to patients undergoing standard radiographic examinations with conventional screen-film radiography, computed radiography and direct digital radiography. *Br. J. Radiol. 79*: 899–904.

European Commission. 1996. European guidelines on quality criteria for diagnostic radiographic images. *Office for Official Publications of the European Communities*, Luxembourg: EUR 16260EN.

Fink, C., Hallscheidt, P.J., Noeldge, G., Kampschulte, A., Radeleff, B., Hosch, W.P., Kauffmann, G.W., and Hansmann, J. 2002. Clinical comparative study with a large-area amorphous silicon flat-panel detector: image quality and visibility of anatomic structures on chest radiography. *Am. J. Roentgenol. 178*: 481–486.

Frey, G.D., and Sprawls P. (Editors). 1997. The expanding role of medical physics in diagnostic imaging. *Advanced Medical Publishing*, Madison, Wisconsin.

Harpen, M.D. 1996. A mathematical spread sheet application for production of entrance skin exposure nomograms. *Med. Phys. 23(2)*: 241–242.

Herrmann, A., Bonel, H., Stabler, A., Kulinna, C., Glaser, C., Holzknecht, N., Geiger, B., Schatzl, M., and Reiser, F. 2002. Chest imaging

with flat-panel detector at low and standard doses: comparison with storage phosphor technology in normal patients. *Eur. Radiol. 12(2)*: 385–390.

International Commission on Radiological Protection. 2004. Managing patient dose in digital radiology. *Elsevier Ltd*, Oxford, UK: Annals of the ICRP Publication 93.

Strotzer, M., Gmeinwieser, J., Volk, M., Frund, R., Seitz, J., Manke, C., Albrich, H., and Feuerbach, S. 1998. Clinical applications of a flat-panel X-ray detector based on amorphous silicon technology: image quality and potential for radiation dose reduction in skeletal radiography. *Am. J. Roentgenol. 171(1)*: 23–27.

Wall, B.F., Harrison, R.M., and Spiers, F.W. 1988. Patient dosimetry techniques in diagnostic radiology. *The Institute of Physical Sciences in Medicine*, York, England: IPEM Report No.53.

8
Cancer Vaccines and Immune Monitoring (An Overview)

Zsuzsanna Tabi and Stephen Man

INTRODUCTION

The successful development of vaccines to prevent infectious diseases has made a major impact on public health. Global vaccination campaigns have eradicated or controlled once deadly diseases such as smallpox and polio. During the last decade, intense research into vaccines has continued with attempts to develop vaccines against globally important diseases such as malaria, tuberculosis and AIDS, and emerging infectious organisms with the potential to cause pandemics. Another area of human health that has been targeted for vaccine development is cancer, with 10 million new cases of cancer per annum worldwide. The World Health Organisation (2003) has predicted that this figure will rise to 15 million per annum by 2020. Despite advances in diagnosis and treatment, the prognosis for advanced, recurrent or metastatic disease is poor. In developing countries, incidence of cancer usually equates to mortality. Therefore, new approaches are needed, and this has driven the development of cancer vaccines to prevent or treat cancers.

Prophylactic cancer vaccines aim to prevent infection by infectious organisms that cause cancer. This is achieved by inducing strong and sustained antibody responses by activating specific B-lymphocytes. There are currently two licensed prophylactic cancer vaccines; one to prevent Hepatitis B virus infection that is associated with development of liver cancer, and the other to prevent human papillomavirus infection that is associated with the development of cervical cancer.

Therapeutic cancer vaccines aim to treat established disease by predominantly inducing a strong cell-mediated immune response. The potential power of this immune response is illustrated by the speed with which transplanted organs from unrelated donors are rejected. Therapeutic cancer vaccines aim to induce large numbers of T cells that specifically recognise and destroy tumor cells while leaving normal healthy cells unharmed. In contrast with prophylactic cancer vaccines that clearly target infectious organisms, the selection of target antigens for therapeutic vaccines is more difficult, as the majority of proteins expressed by cancer cells will be shared with normal tissue.

The earliest human cancer vaccines sought to induce strong cytotoxic T lymphocyte (CTL) responses with the rationale that such

cells would have a direct effector action against cancer cells. However, these CTL, which usually have the $CD8^+$ phenotype, are only the end-product of immune responses that depend on the coordinate action of T helper cells ($CD4^+$) and antigen presenting cells such as dendritic cells (DCs). These important cells have only recently been appreciated, and in hindsight the failure of vaccine designers to incorporate agents that activate $CD4^+$ T cells and DCs may account for the poor success rate of early vaccines. A review by Rosenberg *et al*. (2004) on cancer vaccines, including 1,306 patients, concluded that the overall objective response rate was only 3.3%. This indicates that the elements necessary for immune-mediated tumor rejection still need to be optimized.

Many cancers may fail to develop because of "silent" immunosurveillance mechanisms that eliminate cells with aberrant growth patterns before they become transformed. However, if this early elimination fails, equilibrium between small tumors and the immune system may be established. If the immune system is unable to maintain this equilibrium, tumors may escape and it is this last phase when they become symptomatic. Therapeutic cancer vaccines have the difficult job of changing the balance back towards the immune system, breaking the "tolerance" that the host has established to the tumor. It should also be noted that the transformed cells will be genetically unstable, and may generate mutations that favor immune escape. A plethora of immune evasion mechanisms have been described, but one of the most common is the loss of either the target tumor antigens or the MHC class I molecules recognized by T cells.

The development of therapeutic cancer vaccines in particular is a very challenging field. In this chapter, we review several types of cancer vaccines in development for solid tumors, discuss the methods used to monitor immune responses in cancer vaccine trials, and outline promising developments for the future.

PROPHYLACTIC CANCER VACCINES

Cancer vaccines have been the subject of much media coverage recently. This is largely due to the large scale testing and subsequent licensing of a vaccine to prevent infection by human papillomaviruses, the major causative agents of cervical cancer. This vaccine has been called a cancer vaccine because its long term aim is to prevent the development of cervical cancer. However, it is important to distinguish this vaccine, which is really a conventional prophylactic anti-viral vaccine, from the many other cancer vaccines aimed at treating established cancers.

A recent global survey by Parkin (2006) estimated that > 17% of cancers were caused by infectious agents, with nearly two thirds being attributable to three types of viruses, human papillomavirus (HPV) and Hepatitis B and C viruses. Thus, development of prophylactic vaccines against cancer-causing viruses could lead to substantial reduction in the global burden of cancer.

VACCINES TO PREVENT HPV INFECTION AND CERVICAL CANCER

Human papillomaviruses (HPV) are a large family of DNA viruses that infect epithelial cells at cutaneous or mucosal

sites. HPV infection is associated with a broad spectrum of diseases ranging from benign warts or papillomas to invasive cancer. Although most HPV infections are cleared successfully, there is a large body of evidence suggesting that persistent infection with certain "high risk" types of HPV leads to development of cervical cancer. The "high risk" HPV types most commonly associated with cervical cancer (HPV16 and 18) are sexually transmitted. Therefore, a vaccine delivered in childhood, and capable of inducing long lasting protective immunity against HPV would have a significant impact on the incidence of cervical cancer.

Critical breakthroughs in technology and immunology in the early 1990s resulted in the first HPV vaccine (Gardasil) licensed by the FDA in June 2006. A similar vaccine (Cervarix) is expected to be licensed imminently. These vaccines, sold by Merck and GSK respectively, are based on the same technology of synthetic virus-like particles (VLPs). The HPV L1 capsid protein is produced in both yeast or baculovirus expression systems, and spontaneously reassembles *in vitro* to form VLPs that mimic the natural viral capsid structure. VLPs induce neutralising antibodies against epitopes present on the native viral capsid. The VLPs are safe because, unlike the natural virus, they do not contain any oncogenic viral DNA.

The development of HPV VLP vaccines has been extensively covered in other reviews (Frazer, 2006), so it will not be described here, but it is important to comment on the efficacy of the vaccines. The VLPs have been shown to be highly immunogenic when delivered intramuscularly. Antibody titres following immunisation with VLPs are much higher than those seen after natural infection. Importantly, the VLP technology provides the potential to protect against several HPV types by incorporating mixtures of type-specific VLPs. For example, Gardasil contains VLPs from the HPV types most commonly associated with cervical cancer (HPV16 and 18) and genital warts (HPV6 and 11), and Cervarix contains HPV16 and 18 VLPs.

The efficacy of VLP vaccines in protection against viral challenge had been shown using canine oral papillomavirus (Suzich *et al*., 1995) and cotton tail rabbit papillomavirus models (Breitburd *et al*., 1995). Proof of concept for humans was demonstrated in a landmark study by Koutsky *et al*. (2002). Over 1,500 women were studied in a randomised, double blind study of an HPV16 L1 VLP vaccine. There was almost 100% seroconversion and the vaccine was 100% effective at preventing HPV infection in the vaccinated group during the 17-month follow-up period. Subsequent trials of the two competing vaccines, Gardasil and Cervarix, have tested larger cohorts of women in different age ranges. A recent trial (FUTURE II) of Gardasil (2007) tested more than 12,000 women aged 15–26, who were followed up for 3 years. The main endpoint was the development of HPV16 or 18 preinvasive cervical intraepithelial neoplasia (CIN), the highest grades of which are considered to be the precursors to invasive cancer. The vaccine had an efficacy of 98% against HPV16 and 18 in women who followed the clinical trial protocol, but this dropped to 41% when all trial participants (regardless of HPV status) were considered.

It has been suggested that the decrease in efficacy may result from inclusion of women with previous exposure to HPV

who may already have developed CIN. Another important result from this trial was that vaccine efficacy was only 17% for protection against all CIN lesions (regardless of HPV type). This suggests that this vaccine is not cross-protective against non HPV16 and 18 associated lesions. This is not surprising given that at least 15 HPV types can be associated with cervical cancer, and that a broader spectrum of HPV types can be found in CIN compared to cancer. This study reinforces the notion that the VLP vaccines will be most effective when there has been no previous exposure to HPV, i.e., in children. This age group may also provide the best immunological responses to vaccines (Pedersen *et al*., 2007).

Despite the promising results obtained, the most important question regarding these VLP vaccines cannot be answered in a short-term clinical trial. Namely, can vaccination against HPV prevent the development of cancer? The longest trial follow-up so far has been 5 years and most vaccines against infectious diseases aim to protect for 10–15 years. But cervical cancer is a slow developing disease and cervical screening programs operate for 40 years. Can the HPV vaccines provide protection for this period? This may not be necessary because protection may only be needed for the period when women are most likely to experience multiple HPV infections, during their teens and early twenties.

The development of vaccines to potentially prevent cervical cancer is a remarkable scientific achievement. From initial discovery of the causative agent (high-risk HPV) to full licensing of a vaccine has taken less than 20 years (Zur Hausen, 2002). The implementation of these vaccines is not straightforward and aroused much debate both on sociological issues and the pragmatic issues related to healthcare. Furthermore, the greatest need for these vaccines is not in the countries where this debate is being held, but in the developing countries where 80% of all cervical cancers arise. These countries do not have the economic resources to fund vaccination programs based on these first generation vaccines. They need vaccines that are cheaper to produce, easier to store, and easier to administer. One promising avenue that is currently being explored is to incorporate vaccines into edible plants, e.g., potato, and tomato, that could be grown in developing countries.

The current HPV vaccines have the potential to prevent cervical cancer in the next generation. However, these vaccines are unlikely to impact upon those women with pre-existing infection or disease. Here strong cell-mediated immune responses directed against virally infected cells and early lesions may have a prophylactic effect by preventing viral persistence and development of genetic instability predisposing towards malignancy.

As will be discussed later in this chapter, design of vaccines to treat advanced cancer may be difficult because of problems with overcoming immune suppression. But boosting immune responses in those with early stage disease may be more feasible. For global use, the ideal vaccine may be one that combines a prophylactic component to prevent new infections, and a therapeutic component to induce immune responses against viral proteins expressed in early infection and transformed cells. Such a vaccine has limited commercial value, so it may be left to government and charities to fund development. Basic research in this area is still needed, the human immune response to HPV is still

poorly understood because most studies have analysed systemic rather than local immunity. To maximise the efficacy of vaccines, it is important to identify the immune parameters that most precisely correlate with disease regression/progression, and to continue research into how HPV can evade the immune system.

VACCINES TO PREVENT HEPATITIS B INFECTION AND LIVER CANCER

Hepatitis B virus (HBV) is a double strand DNA virus that causes acute and chronic hepatitis. Most (90–95%) of acutely infected adults recover without further complications, but ~5% will become chronically infected. Although chronic HBV infection can also produce a range of disease states, some individuals will develop cirrhosis and possibly hepatocellular carcinoma (HCC). Chronic HBV carriers have 20–100 fold higher risk of developing primary HCC than uninfected individuals.

HBV is globally important; it has been estimated that there are 300 million carriers of the virus worldwide. Up to 50% of the population in Southern Africa and South East Asia have been infected with HBV. As a result, primary hepatomas are the most common form of cancer worldwide (626,000 cases) and a substantial number of these can be shown to be associated with chronic HBV infection (340,000) (Parkin, 2006).

Prophylactic Vaccines Against HBV

Vaccines against HBV have been used successfully to prevent infection for >20 years. Although not designed with this aim in mind, HBV vaccines can be considered as anti-cancer vaccines. The implementation of a nationwide hepatitis B vaccination program in Taiwan in 1984 reduced the incidence of HBV infection, but was also associated with a decline in the incidence of childhood HCC. Notably, because latter versions of HBV vaccines have used recombinant viral envelope proteins and there has been long term follow-up, they could be models for HPV vaccine development.

Primary immunization campaigns of infants in Sub-Saharan Africa have produced similar conclusions. First, although antibody titres of vaccinated individuals were seen to decline gradually over the course of 14–15 years, a protective response was maintained, with only a 1–31% infection rate. This is noteworthy because only infants were immunised, and there would be ample opportunity for these infants to be infected by nonimmunised teenagers or adults. Because no vaccine boosting was included in these studies, it has been suggested that exposure to natural HBV during follow-up may provide a natural "boosting" effect for vaccinated individuals.

VACCINES TO PREVENT HEPATITIS C INFECTION AND LIVER CANCER

Development of a similar vaccine for Hepatitis C virus (HCV) has been slow, despite the fact that some 150–200 million people are infected world-wide with this virus. HBV and HCV viruses are genetically distinct, HBV is a DNA virus, while HCV is an RNA virus. Chronic infection with HCV

is associated with damage to liver cells, with an increased risk of developing liver cancer. Some 195,000 cases of liver cancer can be attributed to HCV infection (Parkin, 2006).

There are several reasons why there is no prophylactic vaccine available for HCV. First, HCV is a genetically diverse virus, with at least six different genotypes and diverse quasispecies within infected individuals. Secondly, there are no robust tissue culture or small animal model systems to facilitate laboratory research, and testing of candidate vaccines requires use of chimpanzees. There have been several attempts to use viral envelope proteins in vaccines but the results have been mixed; it is difficult to achieve prophylactic immunity in chimpanzees. Nevertheless, there is evidence that HCV infection or vaccination of chimpanzees can reduce viral persistence and severity of subsequent infections. This is supported from clinical observations of IV drug users, suggesting that immunity against viral persistence can be acquired, and together with the experimental results suggests that vaccine development still has value. Perhaps, it might be more realistic to aim vaccine development at preventing viral persistence and development of chronic infection, rather than development of sterilizing immunity. Therefore, vaccines with combined prophylactic/therapeutic properties should be developed. The current vaccine candidates include plasmid DNA, recombinant adenoviruses, and VLPs.

OTHER VIRUSES ASSOCIATED WITH CANCER

Persistent infection with HPV, HBV, and HCV account for the majority of cancers associated with human viruses (> 80%), but it should be noted that there are several other viruses (EBV, HTLV-1, HHV8) that contribute to cancer development which cannot be discussed here because of space constraints. There are no prophylactic vaccines available for these viruses; however, there are intensive efforts on developing therapeutic vaccination approaches, particularly for EBV.

THERAPEUTIC CANCER VACCINES

There are numerous therapeutic cancer vaccines presently undergoing clinical trials. The approaches to direct the immune system to attack established tumors or combining immune-therapy with traditional treatments can be diverse. The requirements for a therapeutic cancer vaccine are similar to those for a preventative vaccine, that is to provide: robust anti-tumor effector immune responses with high levels of antigen specificity, none or negligible autoimmunity, multiple levels of protection to prevent tumor escape, and long-term protective memory. Furthermore, the vaccine should be able to combat cancer-induced immune-modulatory effects when administering it to patients with established tumors. The mainstream approaches are going to be reviewed here, including combination immunotherapy where immunological approaches are applied together with well-established chemo- and radiotherapies.

DENDRITIC CELL VACCINES

Dendritic cells (DC) are professional antigen presenting cells (APC) which, unlike other APC, can migrate into lymph nodes

and prime naïve T cells and are uniquely adept at antigen cross-presentation. They control immunity and tolerance via interactions with both the innate and the adaptive immune systems. DC have three activation levels, such as immature (iDC), intermediate and mature DC (mDC). The three stages can be described clearly by the distinct phenotype and function. Immature DC typically reside in the tissues where they encounter pathogens and take up antigen. Antigen uptake in the presence of microbial products, called pathogen-associated molecular patterns (PAMP), or molecules released by stressed or dying cells (heat shock proteins, HMGB-1, S100 proteins, etc.), called damage-associated molecular patterns (DAMP), trigger DC maturation. During maturation, intermediate DC upregulate MHC Class II and co-stimulatory molecules and chemokine receptor CCR7, the latter guiding them to lymph nodes. The main function of DC in the lymph nodes is antigen presentation to T cells. CD40-CD40L engagement, due to DC-T cell interaction in the lymph node, triggers transient IL-12 production which is the main cytokine necessary for enabling mature DC to prime naïve T cells. DC function can be fundamentally altered by tumors: tumor cells display neither PAMPs nor DAMPs while they produce GM-CSF, TGF-β, IL-10 which negatively influence DC maturation, migration, cytokine production, and T cell stimulatory capacity. These tumor-conditioned DC may even stimulate the proliferation and activation of T regulatory cells (Ghiringhelli, 2005). The aim of DC-based cancer vaccines is to generate a large number of DC *ex vivo*, load them with tumor antigen and mature them for the generation of efficient anti-tumor T cell immunity upon injection into patients. What seems a straightforward idea becomes extremely complex when searching for optimum efficiency, especially as our present understanding of the workings of the immune system in cancer is incomplete. The method of DC generation, the nature of the antigen, the way of loading the antigen, the optimum level of DC maturation, the manner of delivery, are all questions which might be easily answered in preclinical models but require painstaking constant modifications in groups of patients with advanced disease. The main approaches and the present standing of DC vaccines are summarized below.

Ex vivo generation of autologous DC. Large numbers of DC can be generated from peripheral blood cells by different methods. The most frequently used approach utilizes GMCSF and IL-4 for the generation of monocyte-derived DC (MDDC), which takes ~5 days, and can be carried out in a closed culture system. Other methods may differentiate CD34+ hematopoietic progenitors with IL-3, IL-6 and SCF for 6 days or with GMCSF and TNF-α for 12 days. Alternatively, DC can be directly isolated from the blood, requiring no further *in vitro* differentiation. DC are very diverse and all the above methods generate DC with slightly different phenotypic and functional features. There is no systematic study to clarify which DC population is optimal. MDDC are most popular probably because of the homogeneity and relatively stable phenotype of the cells.

Immature DC, generated by any of these methods and loaded with antigens *ex vivo*, as discussed below, have to be matured, as it enables them to migrate to lymph nodes and to present antigen to T cells. Early trials indicated that immature DC are unable

to stimulate T cell responses and may even generate tumor-specific regulatory T cells (Jonuleit *et al*., 2001). However, the strength and complexity of the *ex vivo* provided maturation signal should be finely balanced, as the antigen-loaded DC, injected back into the patients, should be able to migrate to the lymph node but their full maturation should only occur within the lymph node, otherwise T cell priming will not occur. Maturation *ex vivo* is usually induced with Toll-like receptor (TLR)-agonists, such as PAMPs, alone or in combination, or a mixture of cytokines (TNF-α, IL-6, IL-1, PGE, IFN-γ, etc.). Some of these agents, however, are capable of inducing full maturation, including the induction of IL-12 production, which is believed to be undesirable before DC reach their destination *in vivo*.

A recently published "fast-DC" protocol, stimulating monocytes for only 2 days *ex vivo* in the presence of IFN-γ and LPS, reported tumor-peptide-specific responses and decreased tumor volumes in vaccinated breast cancer patients (Czerniecki *et al*., 2007), the mechanism being dependent on a delayed IL-12 burst. Alternatively, maturation can be induced *in vivo* following administration of the antigen-loaded DC with systemically applied antibodies cross-linking stimulatory molecules on DC, such as anti-CD40 antibody.

Antigen loading in vitro. When antigen is loaded onto DC *ex vivo*, the optimal antigen was likely to be chosen based on the following criteria: (1) expressed on the majority of tumor cells in most or all patients with the same type of tumor, (2) not expressed on healthy cells, (3) necessary for the maintenance of tumor growth, antigen escape mutants should not be viable, (4) able to induce robust CD4 and $CD8^+$ T cell responses against the tumor, and (5) immunogenic in several major HLA-haplotypes. Alternatively, when tumor-cell lysates are loaded onto DC, the nature of antigen is not defined. The most frequently used approaches to load DC with tumor-cell antigens are listed below.

Exogenously Loaded Antigen

Tumor cell lysate. This method was used extensively in preclinical models and in clinical trials with some original success in selected melanoma patients (Nestle *et al*., 1998), followed by mixed results in subsequent clinical trials. Potential improvements include the introduction of treatments which would make the tumor cell death more immunogenic. Originally necrotic cell death was thought to be immunogenic while apoptotic was not. These categories are now being replaced by more sophisticated markers of immunogenicity, such as calreticulin surface expression and HMGB1 release. The impact of applying inducers of immunogenic tumor cell death, such as anthracyclins, gamma-irradiation or UVC-induced apoptosis (Obeid *et al*., 2007a, b), to tumor cells before preparing the lysates has yet to be assessed in DC vaccines.

Peptides, proteins and recombinant proteins. With the expanding library of tumor antigens together with that of potential or confirmed T cell epitopes, loading DC with known amount of synthetic peptides became the most popular area of DC vaccines studies. The variation in the approaches included the use of single vs. poly-epitopes, Class I-restricted peptides vs. a mixture of Class I- and Class II-restricted peptides, and short peptides vs. long peptides, etc. Objective clinical

responses in up to 25% of patients were achieved in Phase I/II clinical trials in melanoma, prostate, and bladder cancer patients with metastatic disease. At least one of them was also confirmed by a long term survival study (Fay *et al*., 2006). The conclusion from earlier trials and preclinical experiments is that DC loaded with long peptides, representing poly-epitopes, and including both Class I- and Class II-restricted epitopes are more efficient in generating T cell responses and objective clinical responses.

Using whole tumor antigens has several advantages, the main one being that they are able to generate immune responses against unknown epitopes in any HLA type. However, as they have a rather limited availability at clinical grade, an easier approach is the use of overlapping peptides, spanning the entire length of proteins, synthesized at the required GMP grade. A significant improvement on exogenously loaded antigens is represented by recombinant proteins which deliver DC stimulatory compounds together with the antigen. The best example is Sipuleucel-T (APC8015), where DC are loaded *ex vivo* with a recombinant fusion protein consisting of prostatic acid phosphatase linked to GMCSF. This vaccine is undergoing a phase III randomized placebo-controlled trial. Patients with asymptomatic metastatic hormone refractory prostate cancer (HRPC) who received Sipuleucel-T had a median survival time of 4.5 months longer than those in the placebo arm. The vaccine also demonstrated a 41% overall reduction in the risk of death. In addition, 34% of patients receiving Sipuleucel-T were still alive 36 months after treatment compared to only 11% of patients randomized to receive placebo.

Endogenously Synthesized Antigens

Transfection. The use of tumor antigen-encoding cDNA or mRNA seems attractive as this approach provides unselected endogenous expression of tumor antigens in DC. Interestingly, cDNA-mediated antigen loading has not resulted in T cell responses, while mRNA seems more efficient. One of the advantages of the autologous tumor-derived mRNA approach is that it delivers antigen with the relevant mutations to DCs. Unfortunately, endogenous antigen presentation favors $CD8^+$ T cell stimulation, which results in the lack of CD4 helper responses, thus limiting the usefulness of the method.

Tumor cell: DC hybrids. Finally, the fusion between irradiated tumor cells and DC has been shown to generate immune responses which could eliminate established tumors in mice (Gong *et al*., 1997). Functionally active fusions have also been generated using human cells. They express a broad array of tumor-associated antigens, including yet unidentified ones, and also deliver DC-mediated costimulatory signals. However, unless the tumor cells is autologous to the patient being vaccinated, there is a possibility of invoking a predominant response against allogeneic MHC molecules rather than tumor antigens.

Delivery of DC vaccines. Depending on the site of injection of Ag-loaded DC, their homing pattern, and their ability to generate anti-tumor T cell responses can vary. Prostate cancer patients were injected with DC-enriched blood PBMC, cultured for 2 days *ex vivo* with recombinant mouse prostatic acid phosphatase (PAP), either intradermally (i.d.), intravenously (i.v.) or intralymphatically (i.l., into lymphatic

vessels in the feet). $CD4^+$ T cell proliferative responses were primed by all three treatments, however, i.d. and i.l. vaccination routes were superior to the i.v. route in generating CTL responses (Fong *et al.*, 2001). These observations were confirmed by other studies later, and now the most common route of DC vaccine administration is i.d. or even direct administration into draining lymph nodes.

ADOPTIVE T CELL TRANSFER

There is strong evidence that the number of activated $CD8^+$ T cells infiltrating the tumor has a positive prognostic value (Galon *et al.*, 2006), indicating the direct effect of $CD8^+$ T cells in tumor-immunity. The goal of T cell-based vaccines is to enable large numbers of T cells with the right antigen-specificity and activation status to infiltrate tumor tissues and eliminate tumor cells with a high degree of specificity followed by long lasting protection. The most promising area of T-cell-based vaccines involves the activation of tumor-antigen-specific T cells *ex vivo* and transferring them back into patients, called adoptive T cell transfer (ATC). Significant progress with ATC of cancer was achieved recently by the transfer of *ex vivo* expanded, tumor-antigen-specific T cells into patients after lymphodepleting chemotherapy and high dose IL-2-treatment. The 50% objective response rate in heavily pretreated metastatic melanoma patients (Dudley *et al.*, 2002, 2005) makes ATC in cancer the most promising immunological approach to date. The main elements of this multimodal treatment are discussed below.

Lymphodepletion of recipients. It has been observed in preclinical experiments that treatment of mice with cyclophosphamide before cell transfer increased the rate of regression of established tumors. A similar effect was demonstrated in patients with metastatic melanoma, resistant to standard therapies, who received cyclophosphamide (60 mg/kg for 2 days), followed by fludarabine (25 mg/m^2) for 5 days before T cell transfer. In a cohort of 35 patients, objective clinical responses were observed in 18 including complete remission in 3, patients (Dudley *et al.*, 2005). The effect of lymphodepletion with these drugs may depend on the removal of $CD4^+CD25^+Foxp3^+$ Treg cells, as both cyclophosphamide and fludarabine are known to have anti-Treg effects. Elevated frequencies of Treg cells have been found systemically and in the tumor tissue of cancer patients, and they can inhibit T cell activation in a tumor-antigen-specific manner. Whether their removal alone is sufficient to change a predominantly inhibitory host environment to one which aids the effector function of transferred T cells, has been demonstrated in preclinical models but not in patients. Another possible explanation for the beneficial effect of lymphodepletion is that depleting host T cells in a nonselective manner before the transfer of tumor-specific T cells removes a significant pool of cells (cytokine sink) which would be competing for cytokines necessary for T cell growth and effector function. A third possibility is that lymphodepletion not only spares professional antigen presenting cells of myeloid origin (myeloid DC) but increases their activation and maturation status and simultaneously induces tumor cell apoptosis. These events may lead to

the generation of new T cell responses *via* cross-presentation of tumor antigens, and DC cytokine production may also contribute to the amplification of the *in vivo* effector function of transferred T cells. Ongoing preclinical investigations are going a step further by increasing the intensity of lymphodepletion to a level which causes myeloablation and requires hematopoietic stem cell (HSC) transplantation. The expansion of transferred T cells was supported by the haematopoietic stem cells in these mice in a nonspecific manner.

Expansion of T cells obtained from TIL. The main component of the successful clinical trial by Dudley *et al*. (2005) was the *in vitro* expanded tumor-reactive T cells. These T cells were isolated from the tumor tissue of each patient (autologous system) where high frequencies of tumor-specific T cells are expected to be present. The *in vitro* rapid expansion protocol of these T cells made it possible to obtain sufficiently high cell numbers for transfer ($1.1–16.0 \times 10^{10}$). Interestingly, the protocol providing large numbers of T cells following a relatively short *in vitro* culture period seems to be crucial for the success of the immunotherapy, as T cells expanded this way have a central memory rather than effector phenotype, thus more able to proliferate, migrate, and adapt to the host environment. Another important feature of these T cells was that they were able to infiltrate the tumor tissue.

Transferred cells in early memory stage persisted longer in the host than more differentiated T cells, which correlated with the length of their telomeres at the time of transfer (Zhou *et al*., 2005). The efficient generation of sufficient numbers of tumor-antigen-specific T cells with early memory phenotype is a new goal, as in the past more prolonged *in vitro* cultures were used to obtain large numbers of highly differentiated effector T cells for adoptive transfer. The approaches to generate such T cells include the use of IL-15, IL-7 or IL-21 during *in vitro* T cell expansion rather than IL-2 which drives terminal T cell differentiation. Alternatively, larger numbers of T cells can be obtained for transfer from patients vaccinated with relevant antigens, although these T cells may have already undergone expansion and differentiation in vivo (Powell *et al*., 2006). Genetic modification of T cells with high affinity, tumor-antigen-specific T cell receptors (Morgan *et al*., 2006; Cohen *et al*., 2007; Morgenroth *et al*., 2007) especially at an early stage of differentiation from hematopoietic stem cells (Zhao *et al*., 2007) or reverting effector T cells to a less differentiated state by modulating transcription factors, as reviewed by Gattinoni *et al*. (2006), are some of the ideas presently in experimental phase.

High dose IL-2 co-treatment. The administration of high dose IL-2 to lymphopenic patients receiving adoptive T cell transfer is beneficial for the *in vivo* expansion and effector function of transferred T cells. High dose IL-2 alone (720,000 U/kg every 8 h) can cause tumor regression in some patients with advanced melanoma. However, IL-2 is also able to promote the rapid *in vivo* expansion of $CD4^+CD25^+$ Treg cells. Unfortunately, toxicity (vascular leakage and hypotension) is also a limiting factor in many patients. So, it is possible that IL-2 is not the best cytokine to use in this context. Other cytokines which can support the persistence and activity of transferred T cells without supporting Treg cells, such as IL-15, or

simultaneous blocking or elimination of Treg cells during IL-2 administration may dramatically improve the efficiency of transferred T cells.

Autologous T cell transfer in combination with lymphodepleting chemotherapy and nonspecific adjuvant treatment does not represent an easy off-the-shelf type of treatment, but so far it has provided dramatic evidence for the power of immunotherapy, even in advanced patients who had failed to respond to any previous treatments. Further optimisation of this system, which shows so much promise, will reveal if ATC is a viable approach in the treatment of not only melanoma but also other types of cancers.

PEPTIDE- AND PROTEIN-BASED VACCINES, ADJUVANTS

Unlike cell-based vaccines, synthetic peptides are easy to obtain in large quantities at clinical grade. Peptide vaccines, injected with incomplete Freund's adjuvant (IFA), can induce efficient T cell responses in mice to prevent progression and metastasis of established tumors. The immunogenicity of peptide epitopes can be increased by amino acid modifications, which increase the binding affinity of the peptide to MHC molecules and generate more robust T cell responses cross-reacting with the wild type sequence. Successful modification of a MART-1 peptide, but not that of a WT-1 peptide, to generate cross-reactive T cells has been demonstrated in a small cohort of melanoma patients. Inclusion of Class II-restricted peptides, especially in the form of physical linking of Class-I and Class II-restricted epitopes from the same tumor-antigen, can further improve the antigenicity of peptide vaccines by stimulating T helper responses which support CD8+ T cell function. The limitation of peptide vaccines is due to strict HLA-restriction rules. For the stimulation of T cells with a wide range of HLA Class I and Class II haplotypes, overlapping peptides, representing T cell epitope clusters, can be used (van der Burg *et al*., 2006). Peptide vaccines need to be taken up and processed *in vivo* by DC. Peptides injected alone are unable to trigger DC maturation, and immature DC presenting antigen may generate T cell tolerance or regulatory T cells. Adjuvants, given simultaneously with the peptide vaccines, are required to mature DC *in vivo*, and also to induce cross-presentation of the antigen. In turn, these DC would secure the generation of antigen-specific, long-lived effector T cells, able to migrate to the tumor site. The combination of TLR-agonists and CD40L (see above, in DC vaccines) applied together with a peptide vaccine to mice indeed had a synergistic effect to induce more potent T cell responses; however, it did not lead to tumor eradication, as T cells accumulated in the draining lymph nodes (van der Burg *et al*., 2006). Covalent linking of a TLR agonist to a multiepitope peptide may result in the appropriate T cell stimulation including tumor-infiltration *in vivo*.

Although recombinant proteins are more difficult to generate at a clinical grade, there are promising early phase clinical trials. One example is recombinant NY-ESO-1, a cancer-testis antigen in patients with cancers known to express NY-ESO-1. The recombinant NY-ESO-1 antigen was coinjected with Montanide ISA-51 and the TLR-9-agonist CpG7909 in a water-oil emulsion subcutaneously in 18

patients. The results indicated that specific IgG, produced in all patients, aided the cross-presentation of antigen resulting in the stimulation of CD8 T cell responses (Valmori *et al.*, 2007). This approach needs to be further optimised, such as with increased numbers of vaccinations, the use of multiple TLR agonists, etc.

RECOMBINANT VIRAL VECTOR-VACCINES

Recombinant cancer vaccines consist of tumor antigens encoded by viral vectors. This approach allows antigen to be delivered at a high concentration both endogenously and for cross-presentation, while DC maturation signals are also provided. Good viral vectors can accommodate one or more genes encoding tumor antigens and also costimulatory molecules. Several viruses, such as vaccinia, fowlpox, canarypox, and adenovirus, can be considered as vectors for tumor antigens. Immunological memory against some of these viruses can be limiting because of the presence of preexisting antibodies with the ability to neutralize the recombinant virus particles before they reach their destinations. Vaccinia is becoming an increasingly useful vector, as global immunization with vaccinia has ended in the 1980s. Up to now only Phase I and II clinical trials have been conducted with viral vectors. These trials demonstrated excellent safety and the generation of humoral and cellular immune responses, as summarized by Harrop *et al.* (2006). One of the directions to improve clinical benefit is to include genes for co-stimulatory molecules, such as B7.1, ICAM-1, and LFA-3 (TRICOM) together with that for tumor antigen. Furthermore, a prime-boost regime of vaccine delivery using two different recombinant viruses also improved immunological results. Clinical results of disease stabilization and one complete response have been observed in advanced cancer patients with CEA positive cancers (Marshall *et al.*, 2005) and in prostate cancer patients (Kaufman *et al.*, 2004). However, there is a need to further improve the efficiency of viral vaccines which may be done *via* carefully designed combination with existing treatments and the inclusion of immune response modifiers.

NONSPECIFIC IMMUNE STIMULANTS – IMMUNE RESPONSE MODIFIERS

Nonspecific immune stimulation of cancer patients has been tried for many years. Typically, the adjuvant is injected at the site of the tumor followed by a massive activation of macrophages and release of inflammatory cytokines. These may break immunological tolerance and initiate an avalanche of immunological events which lead to the attack of the tumor cell by the immune system.

Adjuvants

Superficial bladder cancer can be effectively treated with *BCG (Bacillus Calmette-Guerin)* intravesical immunotherapy, by reducing tumor recurrence, disease progression, and mortality. The treatment induces inflammation of the bladder with infiltration of a broad range of cells such as macrophages, T lymphocytes, B lymphocytes, and NK cells. Inflammatory cytokines, such as IL-1, IL-2 and IL-6, IFN-γ, and TNF-α,

can be measured in the urine for many hours after treatment.

CpG-ODN (CpG oligonucleotides). Synthetic oligonucleotides which stimulate cells via TLR9. In humans, TLR9 is expressed on plasmacytoid DC and B cells, while in mice it is also expressed on myeloid DC and monocytes. CpG-ODN activate both innate and adaptive immune responses, stimulate Th1-type immune responses, and mature DC. They also protect immune cells from the damaging effect of chemo- and radiotherapy.

Cytokines, Chemokines

IL-2, when administered in high doses, results in an increased number of T cells B cells and NK cells in the blood, increased NK activity, and increased serum levels of TNF-α, IL-1β, and IFN-γ. There are, however, toxic side effects such as capillary leak syndrome and subsequent severe hypotension. Furthermore, IL-2 has been shown to preferentially expand Treg cells which can suppress effector T cells, preventing them from killing tumor cells. IL–2 is approved for the treatment of metastatic kidney cancer and metastatic melanoma, but requires close monitoring because of the side effects.

IFN-α has an antiproliferative effect on tumor cells, increases the lytic capacity of NK cells, and the expression of MHC class I molecules on various cell types. IFN-α is approved for the treatment of melanoma and AIDS-related Kaposi's sarcoma.

IFN-γ is known to increase the expression MHC Class I and II, adhesion molecules, and molecules associated with antigen processing, as well as activate macrophages, NK cells, T cells, and DC.

GM-CSF and *G-CSF* are used in cancer treatment, primarily not to induce antitumor immune response but to shorten the period of time a patient is neutropenic after chemotherapy. These cytokines stimulate the maturation of granulocyte precursors and the development of monocytes and dendritic cells. Stimulation of the immune system by CSFs may benefit patients undergoing high-dose chemotherapy.

Ligands/Antibodies

Ontak or denileukin diftitox. A recombinant IL-2 – diphteria-toxin (DT) fusion protein. It binds to cells expressing high affinity IL-2R (CD25). It is internalized via receptor-mediated endocytosis and proteolytically cleaved within the endosome liberating the enzymatically active portion of the DT, the A fragment. DT fragment A is released into the cytosol inhibiting the protein synthesis leading to cell death. *In vivo* treatment with Ontak depletes Treg cells significantly, resulting in enhanced Th1-type immune responses and substantial development of antigen-specific CD8 T cells upon vaccination.

Antagonistic CTLA-4 antibody. Engagement of CTLA-4 molecule on T cells by the ligands B7-1 and B7-2 imparts a negative signal to T-cells and results in alteration of T-cell activity and selection. In mice, antibodies to CTLA-4 can promote tumor rejection and tumor immunity. Antibodies to human CTLA-4 have entered clinical trials and demonstrated objective clinical responses for metastatic melanoma.

Recombinant CD40L. CD40L is a strong inducer of DC maturation, stimulating both innate and adaptive immune responses. Interaction with CD40 on DC enables DC to stimulate primary T cell responses. CD40L stimulation may also abrogate the

suppressive effect of Tregs. Interestingly, direct trigger of apoptosis in tumor cells by a poorly understood mechanism has also been implied. CD40L administered to patients as a soluble protein or as trimers is undergoing Phase I trials.

COMBINATION OF CANCER VACCINES WITH CHEMO- AND RADIOTHERAPY

Cancer vaccine trials are often conducted in advanced patients resistant to conventional treatments such as chemo- or radiotherapy. Although early treatment with immunetherapy is not likely to happen soon, well-designed combinations of established treatments with immune therapy would be an important step towards achieving the full potential of cancer vaccines.

Combined Chemoimmunotherapy

Chemotherapy (CT), using cytotoxic agents, destroys dividing cells in a non-specific manner, resulting in a mainly apoptotic elimination of all rapidly dividing cells. The long-held belief that CT is detrimental for not only the tumor but also for the cells of the immune system is not supported by the latest results studying the activation and functional status of T cells in PBMC and tumor-draining lymph nodes during CT (Fattorossi *et al*., 2004; Coleman *et al*., 2005). CT can crucially influence the survival and behavior of immune cells at multiple levels: (1) Tumor cells killed by CT provide a wide range of TAAs for the immune system. (2) Depending on the type of CT, TAA uptake can happen in an immunogenic or a non-immunogenic way. (3) CT can remove immune inhibitory effects produced by tumor cells. (4) CT generates lymphopenia. The latter can create "space" for tumor-specific T cells to expand, and also removes inhibitory host immune cells generated by the tumor. A more detailed analysis of these immunologically beneficial effects of CT, awaiting to be exploited in combined immunological approaches are discussed below.

Antigen release following CT-induced tumor cell death. Whatever is the type of tumor cell death following CT, it is certain that a huge amount of TAA is released from the affected cells. In mice, antigen presenting cells carrying TAA accumulate in draining lymph nodes following CT. High concentration of exogenous antigen can be cross-presented by DC to $CD8^+$ T cells, so TAA released following CT is expected to favor this type of antigen presentation. The nature of TAA is also interesting, as it is likely to represent a very good composition of antigens. Firstly, important, but yet unknown tumor antigens, including tumor-rejection antigens may be released and second, the mix of TAA represents the most complete and relevant array of antigens for immune recognition in an autologous manner.

The type of tumor cell death. CT of bulky solid tumors results mainly in apoptotic cell death but nonapoptotic mechanisms, such as necrosis, autophagy, and mitotic catastrophe, also occur (Okada and Mak, 2004). Apoptotic cells are normally not immunogenic when taken up by macrophages or DC. However, regardless the mode of CT-induced cell death, when it happens on a massive scale and in a highly synchronized manner, the anti-inflammatory default mechanism to clear these cells may easily be overwhelmed. Accumulation of monocytes, B cells, dendritic

cells, and macrophages occurs at the site of tumor cell death, and beside the huge amount and range of TAA taken up by these cells, it is expected that heat shock proteins and HMGB1 (from cells that die by apoptosis) are also released. These molecules represent damage associated molecular patterns (DAMP) which serve as adjuvants to initiate DC maturation. Based simply on this quantitative argument, it would be expected that TAA-specific T cell responses are generated in the draining lymph nodes following CT. A better definition of immunogenic cell death, as mentioned earlier, may enable us to exploit better the wave of CT-induced tumor cell death for immune therapies. The question of immunogenic vs. nonimmunogenic cell death focused for a long time simply on the difference between apoptotic vs. necrotic cell death, is without definitive conclusions. It seems now that the key to immunogenic cell death is the translocation of certain, normally intracellular, molecules on the cell surface during apoptosis. Calreticulin has been indicated as such a molecule and its cell surface expression can be induced by anthracyclins, γ-irradiation, and UVC light (Obeid *et al*., 2007a, b). In mice, a single injection of the anthracyclin mitoxantrone into the tumor was sufficient to cause permanent regression of established tumors, an effect which was only observed in immunocompetent animals. Anthracyclins inhibit DNA and RNA synthesis by intercalating between base pairs of the DNA/RNA strand, thus preventing the replication of cancer cells. They are used to treat a wide range of cancers, including breast, uterine, ovarian, and lung cancers, so it is feasible to consider them for the design of combination chemoimmunotherapy. On the other hand, the recent observation on immunogenic cell death may be followed up by a thorough survey of chemotheraputic drugs exerting similar effects.

Removal of tumor-associated immunosuppressive effects by CT. As most tumors produce TGF-β, IL-10, IL-6, VEGF, and HGF, it can be expected that simply by decreasing the tumor burden the level of these inhibitory factors will fall. Standard, platinum based chemotherapy of ovarian cancer patients decreases the level of Ca125 systemically. Ca125 itself has suppressive effects on NK and maybe on other cell types. Indeed, CT in these patients has been shown to be associated with improved T cell responses (Coleman *et al*., 2005). A similar effect may be responsible for the immune stimulation observed in pancreatic cancer patients treated with gemcitabine. In these patients there was no decrease in the proportion of Treg cells, but the numbers of T cells producing IFN-γ and expressing CD69 increased. Gemcitabine also stimulated TNF-α and IL-2 production in a small group of lung cancer patients, reviewed by Nowak *et al*. (2006).

CT-induced lymphopenia. Earlier in this chapter we discussed the beneficial effects of lymphodepleting chemotherapies for generating a more favorable environment for adoptive T cell transfer. All chemotherapies, not only lymphodepleting drugs, are associated with a certain level of lymphopenia as a side effect which, in the treatment of solid tumors, is usually not symptomatic. The altered immune cell composition in the tumor tissue, draining lymph nodes, or even in the blood during treatment with different agents has not been studied in a systematic manner. Cyclophosphamide and fludarabine have

confirmed anti-Treg cell properties in the blood, but little is known about the effect of these and other drugs on other inhibitory cell subsets such as myeloid suppressor cells or IDO-competent DC. It would be important to determine if routine chemotherapy regimes are sufficient to eliminate inhibitory cell types or a specific combination of drugs should be used to achieve this in chemo-immunotherapy approaches.

Chemo-immunotherapy in the clinic. Combination of standard chemotherapy with therapeutic vaccines or non-specific immune therapy are being tested presently in cancer patients. They are in early phases with small numbers of patients so it is not yet possible to draw conclusions about efficacy.

Combined Radio-Immunotherapy

Radiation therapy (RT) is a successful therapeutic approach in cancer treatment. Besides its cytotoxic effects on tumor cells, RT also has immunomodulatory effects, such as the release of TGF-β in its active form, both *in vivo* or *in vitro*, and the release of histamine during the acute response to radiation. Histamine is able to dysregulate normal DC development generating regulatory DC which support the activation of Treg cells.

The positive immunological effects of ionizing radiation are more numerous, such as upregulating MHC Class I molecules, TAA, adhesion molecules (ICAM-1, PECAM-1 and VCAM-1), heat shock proteins, stimulating IFN-γ-secretion, facilitating the migration of CD8 T cells to the irradiated tissue and increasing the susceptibility of tumor cells to CTL-mediated killing.

The mechanism behind the inhibition of distant tumors after local RT, called abscopal effect, is little understood, but accumulating evidence points towards immunological effector function. Similar to chemotherapy, RT kills tumor cells and as a consequence, releases TAA for uptake by antigen presenting cells, including DC. As discussed in detail earlier, γ-irradiation is able to trigger an immunogenic type of tumor cell death. Another similarity with CT is that repeated cycles of RT cause lymphopenia, which has been used to prepare the host for adoptive cell transfer. The extent and nature of RT-induced lymphopenia have not been studied as well as those caused by CT.

The immunology of radiation therapy is clearly a very understudied area, and before we have a clear understanding regarding effector immune cell behavior in the host undergoing RT, it is difficult to design immune therapeutic approaches other than those that involve adoptive transfer of immune cells. The potential for the success of combination radioimmunotherapy is just as good or even better than for chemoimmunotherapy, given the widespread use of RT and the greater level of standardisation than that in CT.

It is worth mentioning at least one of the promising preclinical experiments which combines the TLR agonist, CpG, with fractionated radiotherapy in mice with established fibrosarcoma. CpG dramatically decreased the dose of radiation needed to achieve a 50% cure rate. Furthermore, mice cured of their tumor were highly resistant to rechallenge. Apart from its immunostimulatory effect, CpG treatment was also shown to be protecting lymphocytes from the damaging effect of radiation. As for CT, combination therapies are in early stages in humans.

MONITORING IMMUNE RESPONSES

The overall aim of therapeutic cancer vaccines is to induce an immune response that results in tumor regression, or stabilizing disease to allow for increased survival times. The immunological mechanisms for tumor regression can be clearly identified in animal models; however, this is not the case for human clinical trials. In these trials investigators measure surrogate immunological endpoints because they believe that these will be of prognostic value or provide an indication of mechanism. The majority of trials have focused on quantitative or qualitative measurement of T cell responses against TAA incorporated into therapeutic cancer vaccines. Continuing technical advances have increased the sensitivity and specificity of assays for measuring T cell responses, in some cases allowing direct *ex vivo* measurements. This section will focus on the different methods used for monitoring T cell responses in therapeutic cancer vaccine trials.

PROLIFERATION ASSAYS

T cells proliferate in response to a variety of stimuli, including specific antigens, mitogens, and cytokines. Effective cancer vaccines should increase the number of T cells responding to specific TAA in the circulation of cancer patients. Thus, when T cells from vaccinated patients are challenged with TAA *in vitro*, there should be an increased proliferative response compared to nonvaccinated patients. However, when there is no response it is not clear whether this reflects an absence of TAA-specific T cells in general or in the circulation, or the presence of TAA-specific T cells that are subject to immunosuppression. Generalized immunosuppression can be tested to some extent by measuring T cell responses against mitogenic stimuli or recall antigens.

The proliferation of T cells can be assessed *in vitro* by measuring the incorporation of radiolabelled tritiated thymidine (^{3}H-Thy) into the DNA of dividing cells. In brief, the assay requires T cells to be incubated in the presence of the antigenic or mitogenic stimulus for 3–7 days, before the addition of ^{3}H-Thy for 6–18 h. The total amount of the radiolabel that was incorporated into the cells in that time period is then measured, which provides a measure of the rate of synthesis of DNA by the entire population of cells. The ideal assay will test a range of concentrations of the stimulating TAA, together with at least one other antigen to act as a negative control to determine the specificity of the response. A mitogenic stimulus is also usually included as a positive control. The absolute counts will depend on several experimental variables; therefore, the results of proliferation assays are usually expressed as a stimulation index (SI), which is the ratio of the scintillation counts (as a result of the incorporated 3H-Thy) obtained in the presence of the test antigen, divided by the counts obtained in the presence of the control antigen (or culture medium alone).

These "traditional" lymphoproliferation assays require several days of cell culture but are reasonably straightforward to set up, providing there are facilities for radioactive work. The major drawback of the thymidine incorporation assay is that it is not directly quantitative, although the degree of proliferation should be proportional

to the number of antigen-specific T cells that were present in the original population. Thymidine incorporation is a good correlate for cell division, but it does not necessarily reflect the overall size of the responding cell population because it only measures the proliferation of cells in the final 18–20 h of the culture period. Cells that proliferated rapidly earlier on and perhaps died will not be detected. Furthermore, no information is available on the phenotype of the responding cells, although it is assumed that the majority of the proliferating cells will be CD4 with helper function. Overall, in terms of immune monitoring for vaccine trials, the thymidine incorporation assay provides a crude measure of T cell response against a given TAA. However, the assay is not suitable for quantitating and comparing antigen-specific T cell responses on samples obtained serially, e.g., following up vaccine responses.

Some of the drawbacks of the ^{3}H-Thy incorporation assay can be circumvented by using the fluorescent dye carboxyfluorescein succinimidyl ester (CFSE) to measure cell proliferation. CFSE is used to label T cells prior to incubation with antigen. As the T cells divide, the dye is diluted equally between the daughter cells such that each cell has half the quantity of dye of the parental cell. Cell proliferation can be visualized by flow cytometry as a series of fluorescent peaks with decreasing signal intensity. Because the starting cell number and the number of divisions are known, the total number of antigen-reactive cells can be estimated. This provides a major advantage over the ^{3}H-Thy-assay and combining this with phenotypic or tetramer analysis (see later) allows precise determination of the cell type that is proliferating. This is a relatively new technique that has not been validated for use in clinical trial monitoring.

CYTOTOXICITY ASSAYS

The chromium release (^{51}Cr) assay has been used for ~40 years as the standard assay to measure the cyototoxic effector function of CD8^{+} T cells (Brunner *et al*., 1968). This assay requires *in vitro* culturing of T cells; multiple rounds of stimulation with TAA (either full-length proteins or peptide) are required to expand T cell numbers sufficiently for testing. Titrated numbers of T cells are then coincubated with a fixed number of "target" cells expressing the TAA. The target cells have been radiolabelled with sodium chromate (Na ^{51}CrO), which is released into the supernatant if the target cells are lysed. After a short period (4–6 h), the amount of ^{51}Cr in the supernatant can be measured to calculate an index for cytotoxicity (% specific lysis). This "bulk" T cell assay allows semi-quantitative or qualitative but not direct quantitative measurement of a cytotoxic T cell response against TAA. Quantitation of T cell responses using the ^{51}Cr-release assay (and proliferation assay) can be achieved using limiting dilution assays (LDA) (Sharrock *et al*., 1990). These assays involve setting up large numbers of micro-cultures in which different concentrations of T cells are stimulated under identical conditions. Thus, the only theoretical variable is the number of TAA responsive T cells. The microcultures are incubated for 7–10 days, then individually assayed for lytic activity against ^{51}Cr labelled target cells. Each micro-culture is scored as being positive or negative

for lysis, and the fraction of negative cultures is calculated for each T cell concentration. This is used to estimate the frequency of precursor T cells specific for any given TAA using equations derived from the Poisson distribution. However, these assays are now rarely used and have been replaced by more sensitive and less cumbersome assays.

Both the "bulk" ^{51}Cr-release and the LDA have made major contributions to immunology research, in particular the demonstration of MHC restriction by virus-specific T cells by Zinkernagel and Doherty (1974). Bulk ^{51}Cr-release or cytotoxic T lymphocyte (CTL) assays have been used successfully to monitor vaccine-induced cytotoxic T cell responses against TAA in several phase I clinical trials (Tsang *et al*., 1995; Adams *et al*., 2001; Borysiewicz *et al*., 1996). Although the CTL assays do not require advanced technology, they are relatively labour intensive, slow, and do require the use of radioactive isotopes and a large amount of blood. For example, in measuring CTL responses against human papillomavirus (HPV) in a clinical trial of a candidate therapeutic vaccine, 50–80 ml of blood was required from each patient, and each assay required a 2 week culture period (Borysiewicz *et al*., 1996).

The major disadvantage of CTL assays is that they are dependent on the ability of CD8 T cells to proliferate during the culture period. This in turn can be affected by the growth conditions (antigens, serum, cytokines, media), which may favor the preferential growth of distinct T cell populations. Therefore, lack of cytotoxicity is not an absolute indicator of lack of response, because it is possible that the TAA-specific T cells induced by a vaccine may have failed to proliferate *in vitro*. Reproducibility of ^{51}Cr-release assays within a laboratory can be readily demonstrated (Nimako *et al*., 1997), but it is very difficult to standardize these assays between laboratories (Scheibenbogen *et al*., 2000). Furthermore, doubt has recently been cast on how appropriate the *in vitro* ^{51}Cr-release assay is as a surrogate marker for cytotoxicity *in vivo*. T cells that are active *in vitro*, as measured by ^{51}Cr-release, may have no activity *in vivo* (Motyka *et al*., 2000), and *vice versa* (Barber *et al*., 2003).

There are several non-radioactive alternatives to ^{51}Cr-release assays for measuring CTL activity, based on flow cytometry. These include assays that measure apoptosis in the target cells through quantitation of fluorescently labelled target cells after coincubation with T cells, or through measurements of caspase activation in target cells. Another type of assay, that has become very popular recently, is the degranulation assay (Betts *et al*., 2003). These assays essentially measure T cell activation in response to a given stimulus in a manner akin to measuring cytokine release. In this case, the capacity of T cells to exert cytotoxic function is measured by cell surface expression of CD107, a protein that is expressed in the membranes of cytotoxic granules. Degranulation (and cell surface expression of CD107) occurs when CD8 T cells are triggered for cytotoxicity. This also coincides with loss of intracellular perforin (Betts *et al*., 2003). Thus, the number of cytotoxic T cells responding to a TAA can be measured on the basis of CD107 expression. CD8 T cells appear to require smaller amounts of antigen to trigger CD107 expression than to trigger cytokine release (Betts *et al*., 2003), which is consistent with previous studies comparing cytotoxicity and cytokine release

effector functions (Valitutti *et al*., 1996; Faroudi *et al*., 2003), and suggests that CD107 assays should be more sensitive than cytokine release assays.

In practical terms, the assay is relatively quick and easy to perform. T cells are stimulated with TAA for 4–6 h in the presence of anti-CD107 antibody and monensin (to facilitate capture of CD107 on the cell surface) before analysis on a flow cytometer. The popularity of the assay stems in part from the simplicity of the protocol, but also from the power of multiparameter analysis of *ex vivo* samples. For example, the phenotype and cytokine profile of responding $CD107^+$ T cells can be determined readily at the population level (Wolint *et al*., 2004). There is also the potential to directly sort TAA-reactive T cells from blood for laboratory analysis or immunotherapy (Rubio *et al*., 2003).

There are some caveats to the sole use of degranulation assays in immune monitoring. First, while demonstrating a T cell response to a vaccine or intervention, and indicating cytotoxic potential, the assay does not directly measure cytotoxicity of the target cell, and certainly cannot predict the efficacy of this effector function *in vivo*. Tumor cells may have mechanisms to evade granule-mediated cytolysis by T cells (Medema *et al*., 2001). Alternatively, it is possible that T cells that do not degranulate in response to tumor cells can mediate anti-tumor effects by direct killing through death receptor pathways (FAS, TRAIL) or indirectly by secretion of cytokines. However, these degranulation assays remain popular and CD107 can be used as part of a panel of markers to investigate the functional heterogeneity of natural and vaccine-induced responses against TAA.

CYTOKINE SECRETION ASSAYS

Cytokine production is an important effector function for both CD4 and CD8 T cells. The balance or ratio of different cytokines produced can influence the outcome of immune responses against tumor cells.

ELISA. The simplest method for detection of secreted cytokines is the enzyme-linked immunosorbent assay (ELISA). ELISAs can be used to detect the concentration of cytokines in serum/plasma samples or tissue culture supernatants of T cells stimulated with antigen. The assays are relatively cheap because they do not involve use of radioactivity or sophisticated equipment, quick and multiple samples can be assayed on a single plate.

ELISAs are usually performed in high protein binding microtitre plates; the test sample or standard is dispensed into the well of a microtitre plate that has been coated with a specific cytokine-capture antibody. The sandwiched target cytokine is quantified by the binding of a second, biotinylated antibody. This binding is detected by a colorimetric reaction based on the activity of an enzyme (avidin alkaline phosphatase or avidin horseradish peroxidase, bound to the second antibody) on a specific substrate. The colored end-product is read by a spectrophotometer and the amount of cytokine determined from extrapolation of the standard curve. Base-line levels of cytokines in body fluids can differ between individuals, but this assay can be used to monitor changes in cytokine levels of individuals during the course of a clinical trial. For T cells, only the cytokines produced by responding T cells will be measured, however, the ELISA may not be sensitive enough to

measure cytokine that is being produced by only a small fraction of cells. Determining whether an individual cell produces cytokine can be determined by the ELISPOT assay (see below) which uses the same principles as the ELISA. A disadvantage of conventional ELISA is that a separate ELISA has to be performed for every cytokine or soluble molecule measured. Recently, multiplex assays have been developed that can measure the presence of multiple cytokines in a sample at a much higher sensitivity than ELISA. Such assays are increasingly being used to measure cytokine responses in serum and whole blood in vaccine trials.

ELISPOT. The enzyme-linked immunospot (ELISPOT) assay is one of a trio of assays, along with intracellular cytokine staining and tetramers, that revolutionised the measurement of T cell responses in the mid 1990s. All three assays allowed direct *ex vivo* quantitation of T cell responses. A series of seminal studies on virus-specific T cell responses demonstrated that previous methods had appreciably underestimated the frequency of antigen specific T cells. The ELISPOT assay depends on the measurement of cytokines (usually IFN-γ) secreted by T cells in response to antigen. To perform the assays, T cells are incubated (6–24 h) with antigen in culture plates whose wells are coated with cytokine-specific antibodies. After incubation, the T cells are washed away and the T cells are further incubated with an enzyme-linked secondary antibody. After developing the plates, the response is visualized in the form of spots that represent captured "cytokine footprint" of individual reactive T cells. Enumeration of spots allows determination of the frequency of responding T cells.

ELISPOT assays are among the most widely used for monitoring human T cell responses, and have been used extensively for monitoring responses to vaccines. Their popularity arises from several features. First, ELISPOT assays are very sensitive and capable of detecting low frequency responses down to the order of 0.01% (1 in 10,000) and so are very useful when patient samples are limiting. Second, these assays do not require specialized equipment (flow cytometers), or use of radioactive isotopes and are quick to perform (results in 1 day). Third, the technique is amenable to standardization between laboratories. Cryopreserved blood samples or assay plates can be sent between laboratories to compare and confirm results. Standardization is discussed in more detail later.

Although ELISPOT assays are capable of detecting low frequency responses directly *ex vivo,* these responses are likely to represent memory T cells with rapid effector function (Lalvani *et al.*, 1997), and may not include central memory T cell responses, which have greater antitumor efficacy than effector memory cells (Klebanoff *et al.*, 2005). Recent studies testing vaccines against malaria and HIV have demonstrated that using ELISPOT assays after culturing T cells with antigen *in vitro* (cultured ELISPOT) increases the sensitivity of detection, and provides correlates for vaccine response. It has been suggested that this is because central memory T cells with proliferative potential are also being detected. The disadvantage of the cultured ELISPOT assay is that the culture period introduces additional variables making it more difficult to standardize between laboratories.

Despite their popularity for immune monitoring, ELISPOTS do have some

disadvantages. First, they only measure a single parameter (the numbers of cytokine secreting T cells). ELISPOTS are often used as surrogates for CTL assays for CD8 T cells, based on the good correlation between cytotoxicity and cytokine secretion. However, care must be taken with terminology particularly when sampling mixed populations of cells from PBMC. Cytokines can be produced by multiple cell types, e.g., IFN-γ by CD4, CD8, NK, γδ T cells, NKT cells, and dendritic cells. Furthermore, there is functional heterogeneity among CD8 T cells, so that multiple effector functions do not always exist in the same cell. The phenotype of responding cells can be determined by presorting responding cells into $CD4^+$ and $CD8^+$ fractions, but this makes the assay more cumbersome and introduces another variable. Another disadvantage of the ELISPOT is that in many studies the numbers of spots have been enumerated by eye, and this can lead to bias and error. Large numbers of spots can be difficult to count, and the spots can differ in size and shape. Many laboratories now use automated or semi-automated plate readers to eliminate these possibilities, and this makes auditing easier in large scale clinical trials.

Intracellular cytokine staining (ICS). ICS is a method used to detect cytokine production at the single cell level by flow cytometry. T cells are stimulated for a short period *in vitro* in the presence of monensin or brefeldin A to block secretion of cytokines, and hence allow the accumulation of cytokines intracellularly. The presence of intracellular cytokine is revealed by staining with fluoresceinated cytokine-specific antibodies, after cell permeabilization.

ICS is a powerful technique because it allows analysis of multiple parameters besides simple cytokine production on a large number of cells. For example, the phenotype (CD4, CD8, memory, activation status, etc) of cytokine secreting cells can be determined, and the secretion of multiple cytokines, cytotoxic markers (CD107, granzyme, perforin) can be analyzed simultaneously. ICS has been used successfully in conjunction with tetramer staining and has been used for longitudinal analysis of clinical trials. In a similar manner to ELISPOT assays, ICS can be used to rapidly map individual peptide epitopes from large pools of peptides from candidate viral and tumor antigens. It is also a technique that is amenable to standardization between laboratories, although a disadvantage of the assay is that multiple parameters need to be optimized for each model system, such as stimulation systems, fixation/permeabilization protocols, reagents/antibodies, controls and gating of cell populations. The last two parameters are intricately linked. Different gating schemes introduced variation in multi-laboratory studies (see standardization section) and influence the percent of T cells defined as positive for cytokine production based on the negative controls. This is important because quite often ICS analyses of mixed populations will produce quite small shifts in fluorescence profiles. Therefore, analysis of multiple cytokines/markers will require a high degree of technical competence with flow cytometry. Conventional ICS kills the T cells to be analyzed, preventing subsequent isolation and *in vitro* culture. This can be overcome through assays that use cell surface capture of cytokines on viable cells, allowing subsequent sorting of cells by flow cytometry or immunomagnetic beads for further analysis or use in adoptive T cell therapy.

TETRAMERS

Fluoresceinated MHC:peptide tetramers or multimers represent the most direct way of enumerating antigen-specific T cells. This is because T cells recognize peptides (derived from pathogens, tumors or self) that are bound to MHC molecules on the surface of target cells or antigen presenting cells. This recognition mediated by clonotypic T cell receptors (TCR) that have specificity for both MHC and peptide. These TCR can also bind to soluble multimerised MHC-peptide complexes, which, when conjugated to fluorochromes, allow identification of antigen-specific T cells, and direct enumeration by flow cytometry. As mentioned earlier, the development of this technology has been paralleled by assays that measure T cell function, and tetramer assays have the greatest utility when functional parameters are studied simultaneously.

MHC class I tetramers were first described in 1996 (Altman *et al*., 1996) and their basic construction has not changed appreciably since that time. They consist of soluble MHC molecules expressed in *E. coli*, that have been engineered with a BirA recognition sequence. These molecules are folded *in vitro* together with peptide and β2 microglobulin to form conformationally correct MHC class I molecules. These molecules are biotinylated by the action of BirA, then coupled *via* biotin to streptavidin that has previously been tagged with fluorochrome. Because each streptavidin molecule has four biotin binding sites, a tetrameric complex is formed containing 4 MHC class I molecules and associated peptides. This complex has greater affinity for TCR than monomeric MHC class I molecules, and the presence of flourochrome allows detection by flow cytometry. In recent years, the term multimers has been proposed based on the realization that not all 4 MHC class I molecules actually bind to TCRs, and that similar reagents based on dimers and pentamers can also be constructed. So far, the majority of studies in viral and tumor immunology have used MHC class I tetramers only, because development of class II tetramers for human studies has been slower and restricted to a few HLA class II alleles e.g., DR1, DR4. This is because MHC class II molecules are inherently less stable than MHC class I molecules, and it has been technically difficult to construct MHC class II tetramers. Furthermore, fluorescent signal intensity of staining with MHC class II appears to be weaker and there are fewer immunodominant epitopes resulting in lower *in vivo* frequencies. For all these reasons, study of CD4 T cell responses against TAA using tetramers has been difficult. The recent development of CD1d tetramers now allows the analysis of NKT cells in anti-tumor responses.

The main advantages of tetramer assays are that they are quick (results in 2 h), specific and sensitive (0.01%), and allow direct *ex vivo* enumeration without *in vitro* culture. As with other assays detecting cell surface markers, T cells that are positive for tetramer staining can be sorted for further use by flow cytometry or magnetic beads. The sensitivity of tetramer assays means that they can also be carried out on lymphocytes extracted from tissue samples. There have been a few demonstrations of direct *in situ* staining with tetramers, although this is technically difficult. At face value the tetramer assay is also amenable to standardization between laboratories because it appears to only

depend on one reagent. For example, the same batch of tetramers could be shared between cooperating laboratories.

The specificity of tetramers is also their biggest drawback, restricting the analyses of T cells to a single specificity. There is a relatively narrow range of tetramers and epitopes based on HLA class I molecules for TAA, so responses generally restricted to CD8 T cells (17 HLA-A+B commercially available). In contrast to human viral antigens, there are few immunodominant epitopes for TAA, so selection of the most appropriate epitopes for analysis requires care. For human studies, the most popular HLA allele studied is HLA-A*0201. This arises from the high frequency of this allele in Caucasian populations (~40%) and the fact that algorithms that predict binding of HLA-A*0201 epitopes are relatively successful. Even so, responses against TAA are often very weak and close to the limits of detection. For many T cell epitopes it is often necessary to culture T cells for a short period (HPV and Melan-A) to obtain significant results. Quantitating rare events with confidence requires a high degree of competence with flow cytometry, and it is easy to obtain false-positives from non-specific uptake of tetramers in mixed cell populations. For example, numerous investigators have gated out cells on the basis of viability, CD14 or CD20 expression to prevent false positive results. Furthermore, tetramers stain functionally heterogeneous cells; not all tetramer positive cells will respond in all functional assays. The issue of correlating tetramer assays with other functional readouts will be covered in the standardizations section.

Tetramers are technically demanding to produce and expensive reagents with a relatively short shelf life (6 months). One recent development that has potential, particularly for monitoring anti-tumor responses, is an assay that uses chip technology to allow analysis with multiple HLA class I tetramers from a single sample. This multiplex approach could allow analysis in human cancers where there are multiple candidate TAAs and could increase the throughput of tetramer assays.

STANDARDIZATION

It is widely acknowledged that monitoring cellular immune responses is important for the rational development of cancer vaccines. Yet there is still no universally accepted and standardized method for measuring immunological endpoints. This is in part an inevitable consequence of the nature of the cancer vaccine field, with a large number of competing laboratories testing different vaccine constructs with different TAA, on small groups of patients with a wide variety of cancers. Invariably each laboratory will have its own immunological endpoint assays, making it difficult to compare between trials even when the vaccines are similar.

Standardization of immune assays in general has been driven by HIV researchers who study immune correlates in large cohorts of HIV-infected individuals. Here, because research is generally funded by government, health organizations or charities, there is a culture of sharing resources between laboratories. This, in turn, allows collective analysis of a large number of samples and the ability to draw statistically significant conclusions regarding the reproducibility of assays both within and between laboratories.

So, what can be learned from these studies? Variation within a laboratory can be controlled by judiciously following standard operating procedures, ensuring batch continuity in reagents, ensuring that any given member of staff can obtain reproducible results, and that similar results can be obtained by different members of the staff. However, there is significant variation between laboratories when analyzing the same patient samples by the same assay. Variation can arise in several ways. First, each laboratory may have different protocols for the ELISPOT assay using different reagents, timings, etc. There may be differences in the skill of operators in performing and counting assays. The ease of transportation of ELISPOT plates means that they can be counted at a single site or counted at multiple sites. Similarly, variation in ICS results can be controlled in part by performing the analysis of results in a single center. In theory, direct staining of T cells *ex vivo* using tetramers should be the easiest to standardize. However, there has been little incentive to carry out such studies. Although tetramers can be used for high throughput assays, they are still relatively expensive and each tetramer can only measure a single MHC:peptide specificity. Furthermore, there are considerable variations in the protocols used for tetramer staining. The first is how laboratories handle samples. Invariably for tumor immunology studies, (and this applies to ELISPOT and ICS) cryopreserved samples are used. There is no consensus on how the samples are cryopreserved, and whether cells are used directly after thawing or transferred into tissue culture briefly before tetramer staining. Individual laboratories also use different gating schemes on flow cytometers to ensure analysis of tetramer positive T lymphocytes.

The importance of assay standardization in cancer vaccine trials is slowly being addressed; in the USA by the Cancer Vaccine Collaborative (http://www.cancerresearch.org//Cancer%20Vaccine%20Collaborative/about.html), funded by the Cancer Research Institute, and in Europe the Monitoring Panel set up by the Association for Immunotherapy of Cancer.

SUMMARY

There are a plethora of available methods for monitoring immune responses to cancer vaccines. The first generation of cancer vaccines was designed purposely to elicit T cell responses, with the simple hypothesis that inducing or boosting a T cell response against TAA will result in tumor regression. Thus, measuring the frequency and activity of T cells against TAA should provide a simple correlate for anti-tumor effects, and this has been the basis for immune monitoring in many vaccine trials.

There are several caveats to using these approaches. The first is that these assays only provide a snapshot of the complex interactions that occur *in vivo* between multiple immune cell types, tumor cells and tumor vasculature. The second is sampling. The frequency of T cells with TAA specificities may differ considerably in peripheral blood from that in the tumor. This discrepancy between localized responses and systemic detection may lead to both false-positive results by detecting circulating TAA-specific T cells that are functionally inactive and/or unable to

penetrate the tumor tissue. False-negative results may be obtained, by not being able to detect T cells, enriched within the tumor tissue, in the circulation. Even detection of high frequencies of TAA-specific T cells in the tumor can be misleading, as these T cells may be functionally inactive *in situ*. These considerations highlight the reasons why quantitation of TAA-specific T cells using tetramers as a single method may be inadequate.

Is there a single best assay for monitoring? The answer is no, the next generation of clinical trials will require multiple assays of function, which in turn will depend on the nature of the vaccine. For example, if full-length TAA is being used in a viral vector, then antibody and T cell responses against the TAA and the vector will need to be monitored. By contrast, if the vaccine consists of peptides, then only T cell response monitoring will be required.

The poor correlation between clinical efficacy and T cell responses against TAAs in 1st generation of cancer vaccines may be in part due to the relatively weak immunogenicity of therapeutic vaccines; T cell responses are at least an order of magnitude weaker than responses against viral antigens in primary viral infection. The 2nd generation of vaccines have taken the knowledge of immune concepts into account by including adjuvants that stimulate TLR or NKT cells, engineered antigens to improve immunogenicity, and improved prime-boost regimens. There has also been an increase in the overall knowledge of cell types in the immune system, particularly of suppressive mechanisms. Ideally, therefore, multiple immune parameters (T and non-T cell associated) should be studied in a manner analogous to microarray expression assays. However, this is not always feasible for resource reasons. A recent review has suggested that protocols for cancer trials should include at least two functional assays for immune monitoring, and that these should be extensively validated in the host laboratory.

For "proof of concept" trials, clear hypothesis driven endpoints must be set to satisfy grant awarding bodies. However, it is clear that increased legislation, particularly in the UK, is increasing the time and expense of setting up clinical trials, so the scientific concepts behind the hypotheses may be out of date by the time the trial starts. Therefore, the trial must be designed so that the maximum amount of information can be obtained from each sample, and that sufficiently large samples should be collected so that retrospective analyses can be performed. It is very important in this regard that technological development continues, particularly in developing assays requiring smaller amounts of clinical material. This will allow sophisticated multiparameter immune monitoring at sites of disease as well as in the peripheral blood. This is vital to understanding the complex interactions of host immunity to tumor regression.

CONCLUSION AND OUTLOOK

There is a large body of evidence supporting the case for developing therapeutic cancer vaccines as part of the arsenal against cancer. We are continuously learning regarding the immune system of cancer patients and eliminating the obstacles from the way of developing successful immune therapies. The enormous complexity of our immune system requires a different approach from the conventional design of drug-target

therapies and also the reevaluation of results achieved in preclinical models. Successful human therapeutic cancer vaccines are likely to include a combination of antigens, adjuvants, inhibitors of immune regulation, and markers for easy monitoring, and will be applied in conjunction with established treatments. Although the first real breakthrough is still being awaited, as at present there is no approved cancer vaccine for therapeutic applications, there are a lot of ongoing early phase and a few phase III trials relentlessly trying to expand our knowledge regarding immunological control in cancer. The website: http://ClinicalTrials.gov contains the most complete and regularly updated list of ongoing cancer vaccine clinical trials. This site currently contains more than 250 cancer vaccine trials which are presently recruiting patients. The studies are sponsored by national agencies or private industry and conducted in >40 countries. The diversity of the ongoing trials reflects the wide array of potential approaches outlined above. There are examples for preventative vaccines, therapeutic vaccines with tumor-cell lysates, modified tumor-cell lysates, DC-vaccines, immune response modifiers, etc. Improvements in technology are enabling us to collect more information than ever regarding immunological parameters in clinical trials. It seems certain that the progress will continue and eventually deliver immunotherapy either as a mainstream treatment of cancer, or as an adjunct to conventional treatment. An eventual aim would be that new biological treatments would extend patients' life sufficiently that cancer could be treated as a chronic manageable disease rather than a fatal one.

REFERENCES

Adams, M., Borysiewicz, L., Fiander, A., Man, S., Jasani, B., Navabi, H., Lipetz, C., Evans, A.S., and Mason, M. 2001. Clinical studies of human papilloma vaccines in pre-invasive and invasive cancer. *Vaccine 19*: 2549–2556.

Altman, J.D., Moss, P.A.H., Goulder, P.J.R., Barouch, D.H., McHeyzer-Williams, M.G., Bell, J.I., McMichael, A.J., and Davis, M.M. 1996. Phenotypic analysis of antigen-specific T lymphocytes. *Science 274*: 94–96.

Barber, D.L., Wherry, E.J., and Ahmed, R. 2003. Cutting edge: rapid in vivo killing by memory CD8 T cells. *J. Immunol. 171*: 27–31.

Betts, M.R., Brenchley, J.M., Price, D.A., De Rosa, S.C., Douek, D.C., Roederer, M., and Koup, R.A. 2003. Sensitive and viable identification of antigen-specific CD8+ T cells by a flow cytometric assay for degranulation. *J. Immunol. Methods 281*: 65–78.

Borysiewicz, L.K., Fiander, A., Nimako, M., Man, S., Wilkinson, G.W.G., Westmoreland, D., Evans, A.S., Adams, M., Stacey, S.N., Boursnell, M.E.G., Rutherford, E., Hickling, J.K., and Inglis, S.C. 1996. A recombinant vaccinia virus encoding human papillomavirus type 16 and type 18, e6 and e7 proteins as immunotherapy for cervical cancer. *Lancet 347*: 1523–1527.

Breitburd, F., Kirnbauer, R., Hubbert, N.L., Nonnenmacher, B., Trin-dinh-Desmarquet, C., Orth, G., Schiller, J.T., and Lowy, D.R. 1995. Immunization with virus-like particles from cottontail rabbit papillomavirus (CRPV) can protect against experimental CRPV infection. *J. Virol. 69*: 3959–3963.

Brunner, K., Mauel, J., Cerottini, J.-C., and Chapuis, B. 1968. Quantitative assay of the lytic action of immune lymphoid cells on 51Cr-labelled allogeneic target cells in vitro; inhibition by isoantibody and by drugs. *Immunology 14*: 181–196.

Cohen, C., Li, Y., El-Gamil, M., Robbins, P., Rosenberg, S., and Morgan, R. 2007. Enhanced antitumor activity of T cells engineered to express T-cell receptors with a second disulfide bond. *Cancer Res. 67*: 3898–3903.

Coleman, S., Clayton, A., Mason, M.D., Jasani, B., Adams, M., and Tabi, Z. 2005. Recovery of CD8+ T-cell function during systemic chemotherapy

in advanced ovarian cancer. *Cancer Res. 65*: 7000–7006.

Czerniecki, B., Koski, G., Koldovsky, U., Xu, S., Cohen, P., Mick, R., Nisenbaum, H., Pasha, T., Xu, M., Fox, K., Weinstein, S., Orel, S., Vonderheide, R., Coukos, G., DeMichele, A., Araujo, L., Spitz, F., Rosen, M., Levine, B., June, C., and Zhang, P. 2007. Targeting HER-2/neu in early breast cancer development using dendritic cells with staged interleukin-12 burst secretion. *Cancer Res. 67*: 1842–1852.

Dudley, M.E., Wunderlich, J.R., Robbins, P.F., Yang, J.C., Hwu, P., Schwartzentruber, D.J., Topalian, S.L., Sherry, R., Restifo, N.P., Hubicki, A.M., Robinson, M.R., Raffeld, M., Duray, P., Seipp, C.A., Rogers-Freezer, L., Morton, K.E., Mavroukakis, S.A., White, D.E., and Rosenberg, S.A. 2002. Cancer regression and autoimmunity in patients after clonal repopulation with antitumor lymphocytes. *Science 298*: 850–854.

Dudley, M.E., Wunderlich, J.R., Yang, J.C., Sherry, R., Topalian, S.L., Restifo, N.P., Royal, R., Kammula, U., White, D.E., Mavroukakis, S.A., Rogers-Freezer, L., Gracia, G., Jones, S., Mangiameli, D., Pelletier, M., Gea-Banacloche, J., Robinson, M.R., Berman, D., Filie, A., Abati, A., and Rosenberg, S.A. 2005. Adoptive cell transfer therapy following non-myeloablative but lymphodepleting chemotherapy for the treatment of patients with refractory metastatic melanoma. *J. Clin. Oncol. 23*: 2346–2357.

Faroudi, M., Utzny, C., Salio, M., Cerundolo, V., Guiraud, M., Muller, S., and Valitutti, S. 2003. Lytic versus stimulatory synapse in cytotoxic T lymphocyte/target cell interaction: manifestation of a dual activation threshold. *Proc. Natl. Acad. Sci. USA 100*: 14145–14150.

Fattorossi, A., Battaglia, A., Ferrandina, G., Coronetta, F., Legge, F., Salutari, V., and Scambia, G. 2004. Neoadjuvant therapy changes the lymphocyte composition of tumor-draining lymph nodes in cervical carcinoma. *Cancer 100*: 1418–1428.

Fay, J., Palucka, A., Paczesny, S., Dhodapkar, M., Johnston, D., Burkeholder, S., Ueno, H., and Banchereau, J. 2006. Long-term outcomes in patients with metastatic melanoma vaccinated with melanoma peptide-pulsed CD34(+) progenitor-derived dendritic cells. *Cancer Immunol. Immunother. 55*: 1209–1218.

Fong, L., Brockstedt, D., Benike, C., Wu, L., and Engleman, E. 2001. Dendritic cells injected via different routes induce immunity in cancer patients. *J. Immunol. 166*: 4254–4259.

Frazer, I. 2006. God's gift to women: the human papillomavirus vaccine. *Immunity 25*: 179–184.

FUTURE 2007. Quadrivalent vaccine against human papillomavirus to prevent high-grade cervical lesions. *N. Engl. J. Med. 356*: 1915–1927.

Galon, J., Costes, A., Sanchez-Cabo, F., Kirilovsky, A., Mlecnik, B., Lagorce-Pagès, C., Tosolini, M., Camus, M., Berger, A., Wind, P., Zinzindohoué, F., Bruneval, P., Cugnenc, P., Trajanoski, Z., Fridman, W., and Pagès, F. 2006. Type, density, and location of immune cells within human colorectal tumors predict clinical outcome. *Science 313*: 1960–1964.

Gattinoni, L., Powell, D., Rosenberg, S., and Restifo, N. 2006. Adoptive immunotherapy for cancer: building on success. *Nat. Rev. Immunol. 6*: 383–393.

Ghiringhelli, F., Puig, P., Roux, S., Parcellier, A., Schmitt, E., Solary, E., Kroemer, G., Martin, F., Chauffert, B., and Zitvogel, L. 2005. Tumor cells convert immature myeloid dendritic cells into TGF-{beta}-secreting cells inducing CD4+CD25+ regulatory T cell proliferation. *J. Exp. Med. 202*: 919–929.

Gong, J., Chen, D., Kashiwaba, M., and Kufe, D. 1977. Induction of antitumor activity by immunization with fusions of dendritic and carcinoma cells. *Nat. Med. 3*: 558–561.

Harrop, R., John, J., and Carroll, M. 2006. Recombinant viral vectors: cancer vaccines. *Adv. Drug Deliv. Rev. 58*: 931–947.

Jonuleit, H., Giesecke-Tuettenberg, A., Tüting, T., Thurner-Schuler, B., Stuge, T., Paragnik, L., Kandemir, A., Lee, P., Schuler, G., Knop, J., and Enk, A. 2001. A comparison of two types of dendritic cell as adjuvants for the induction of melanoma-specific T-cell responses in humans following intranodal injection. *Int. J. Cancer 93*: 243–251.

Kaufman, H., Wang, W., Manola, J., DiPaola, R., Ko, Y., Sweeney, C., Whiteside, T., Schlom, J., Wilding, G., and Weiner, L. 2004. Phase II randomized study of vaccine treatment of advanced prostate cancer (E7897): a trial of the Eastern Cooperative Oncology Group. *J. Clin. Oncol. 22*: 2122–2132.

Klebanoff, C.A., Gattinoni, L., Torabi-Parizi, P., Kerstann, K., Cardones, A.R., Finkelstein, S.E., Palmer, D.C., Antony, P.A., Hwang, S.T., Rosenberg, S.A., Waldmann, T.A., and Restifo, N.P. 2005. Central memory self/tumor-reactive CD8+ T cells confer superior antitumor immunity compared with effector memory T cells. *Proc. Natl. Acad. Sci. USA 102*: 9571–9576.

Koutsky, L.A., Ault, K.A., Wheeler, C.M., Brown, D.R., Barr, E., Alvarez, F.B., Chiacchierini, L.M., and Jansen, K.U. 2002. A controlled trial of a human papillomavirus type 16 vaccine. *N. Engl. J. Med. 347*: 1645–1651.

Lalvani, A., Brookes, R., Hambleton, S., Britton, W.J., Hill, A.V., and McMichael, A.J. 1997. Rapid effector function in CD8+ memory T cells. *J. Exp. Med. 186*: 859–865.

Marshall, J., Gulley, J., Arlen, P., Beetham, P., Tsang, K., Slack, R., Hodge, J., Doren, S., Grosenbach, D., Hwang, J., Fox, E., Odogwu, L., Park, S., Panicali, D., and Schlom, J. 2005. Phase I study of sequential vaccinations with fowlpox-CEA(6D)-TRICOM alone and sequentially with vaccinia-CEA(6D)-TRICOM, with and without granulocyte-macrophage colony-stimulating factor, in patients with carcinoembryonic antigen-expressing carcinomas. *J. Clin. Oncol. 23*: 720–731.

Medema, J.P., de Jong, J., Peltenburg, L.T., Verdegaal, E.M., Gorter, A., Bres, S.A., Franken, K.L., Hahne, M., Albar, J.P., Melief, C.J., and Offringa, R. 2001. Blockade of the granzyme B/perforin pathway through overexpression of the serine protease inhibitor PI-9/SPI-6 constitutes a mechanism for immune escape by tumors. *Proc. Natl. Acad. Sci. USA 98*: 11515–11520.

Morgan, R., Dudley, M., Wunderlich, J., Hughes, M., Yang, J., Sherry, R., Royal, R., Topalian, S., Kammula, U., Restifo, N., Zheng, Z., Nahvi, A., de Vries, C., Rogers-Freezer, L., Mavroukakis, S., and Rosenberg, S. 2006. Cancer regression in patients after transfer of genetically engineered lymphocytes. *Science 314*: 126–129.

Morgenroth, A., Cartellieri, M., Schmitz, M., Günes, S., Weigle, B., Bachmann, M., Abken, H., Rieber, E., and Temme, A. 2007. Targeting of tumor cells expressing the prostate stem cell antigen (PSCA) using genetically engineered T-cells. *Prostate 67*: 1121–1131.

Motyka, B., Korbutt, G., Pinkoski, M.J., Heibein, J.A., Caputo, A., Hobman, M., Barry, M., Shostak, I., Sawchuk, T., Holmes, C.F., Gauldie, J., and Bleackley, R.C. 2000. Mannose 6-phosphate/insulin-like growth factor II receptor is a death receptor for granzyme B during cytotoxic T cell-induced apoptosis. *Cell 103*: 491–500.

Nestle, F., Alijagic, S., Gilliet, M., Sun, Y., Grabbe, S., Dummer, R., Burg, G., and Schadendorf, D. 1998. Vaccination of melanoma patients with peptide- or tumor lysate-pulsed dendritic cells. *Nat. Med. 4*: 328–332.

Nimako, M., Fiander, A.N., Wilkinson, G.W., Borysiewicz, L.K., and Man, S. 1997. Human papillomavirus-specific cytotoxic T lymphocytes in patients with cervical intraepithelial neoplasia grade III. *Cancer Res. 57*: 4855–4861.

Nowak, A., Lake, R., and Robinson, B. 2006. Combined chemoimmunotherapy of solid tumours: improving vaccines? *Adv. Drug Deliv. Rev. 58*: 975–990.

Obeid, M., Panaretakis, T., Joza, N., Tufi, R., Tesniere, A., van Endert, P., Zitvogel, L., and Kroemer, G. 2007a. Calreticulin exposure is required for the immunogenicity of gamma-irradiation and UVC light-induced apoptosis. *Cell Death Differ. 14*: 1848–1850.

Obeid, M., Tesniere, A., Ghiringhelli, F., Fimia, G., Apetoh, L., Perfettini, J., Castedo, M., Mignot, G., Panaretakis, T., Casares, N., Métivier, D., Larochette, N., van Endert, P., Ciccosanti, F., Piacentini, M., Zitvogel, L., and Kroemer, G. 2007b. Calreticulin exposure dictates the immunogenicity of cancer cell death. *Nat. Med. 13*: 54–61.

Okada, H., and Mak, T. 2004. Pathways of apoptotic and non-apoptotic death in tumour cells. *Nat. Rev. Cancer 4*: 592–603.

Parkin, D.M. 2006. The global health burden of infection-associated cancers in the year 2002. *Int. J. Cancer 118*: 3030–3044.

Pedersen, C., Petaja, T., Strauss, G., Rumke, H.C., Poder, A., Richardus, J.H., Spiessens, B., Descamps, D., Hardt, K., Lehtinen, M., and Dubin, G. 2007. Immunization of early adolescent females with human papillomavirus type 16 and 18 L1 virus-like particle vaccine containing AS04 adjuvant. *J. Adolescent Health 40*: 564–571.

Powell, D., Dudley, M., Hogan, K., Wunderlich, J., and Rosenberg, S. 2006. Adoptive transfer of

vaccine-induced peripheral blood mononuclear cells to patients with metastatic melanoma following lymphodepletion. *J. Immunol. 177*: 6527–6539.

Rosenberg, S.A., Yang, J.C., and Restifo, N.P. 2004. Cancer immunotherapy: moving beyond current vaccines. *Nat. Med. 10*: 909–915.

Rubio, V., Stuge, T.B., Singh, N., Betts, M.R., Weber, J.S., Roederer, M., and Lee, P.P. 2003. Ex vivo identification, isolation and analysis of tumor-cytolytic T cells. *Nat. Med. 9*: 1377–1382.

Scheibenbogen, C., Romero, P., Rivoltini, L., Herr, W., Schmittel, A., Cerottini, J., Woelfel, T., Eggermont, A., and Keilholz, U. 2000. Quantitation of antigen-reactive T cells in peripheral blood by IFNgamma-ELISPOT assay and chromium-release assay: a four-centre comparative trial. *J. Immunol. Methods 244*: 81–89.

Sharrock, C., Kaminski, E., and Man, S. 1990. Limiting dilution analysis of human T cells:-it's relevance to clinical immunology. *Immunol. Today 11*: 265–299.

Suzich, J.A., Ghim, S.J., Palmer-Hill, F.J., White, W.I., Tamura, J.K., Bell, J.A., Newsome, J.A., Jenson, A.B., and Schlegel, R. 1995. Systemic immunization with papillomavirus L1 protein completely prevents the development of viral mucosal papillomas. *Proc. Natl. Acad. Sci. USA 92*: 11553–11557.

Tsang, K., Zaremba, S., Nieroda, C., Zhu, M., Hamilton, J., and Schlom, J. 1995. Generation of human cytotoxic T cells specific for human carcinoembryonic antigen epitopes from patients immunized with recombinant vaccinia-CEA vaccine. *J. Natl. Cancer Inst. 87*: 982–990.

Valitutti, S., Muller, S., Dessing, M., and Lanzavecchia, A. 1996. Different responses are elicited in cytotoxic T lymphocytes by different levels of T cell receptor occupancy. *J. Exp. Med. 183*: 1917–1921.

Valmori, D., Souleimanian, N., Tosello, V., Bhardwaj, N., Adams, S., O'Neill, D., Pavlick, A., Escalon, J., Cruz, C., Angiulli, A., Angiulli, F., Mears, G., Vogel, S., Pan, L., Jungbluth, A., Hoffmann, E., Venhaus, R., Ritter, G., Old, L., and Ayyoub, M. 2007. Vaccination with NY-ESO-1 protein and CpG in Montanide induces integrated antibody/Th1 responses and CD8 T cells through cross-priming. *Proc. Natl. Acad. Sci. USA 104*: 8947–8952.

van der Burg, S., Bijker, M., Welters, M., Offringa, R., and Melief, C. 2006. Improved peptide vaccine strategies, creating synthetic artificial infections to maximize immune efficacy. *Adv. Drug Deliv. Rev. 58*: 916–930.

WHO 2003. "World Cancer Report", IARC, Lyon.

Wolint, P., Betts, M.R., Koup, R.A., and Oxenius, A. 2004. Immediate cytotoxicity but not degranulation distinguishes effector and memory subsets of CD8+ T cells. *J. Exp. Med. 199*: 925–936.

Zhao, Y., Parkhurst, M., Zheng, Z., Cohen, C., Riley, J., Gattinoni, L., Restifo, N., Rosenberg, S., and Morgan, R. 2007. Extrathymic generation of tumor-specific T cells from genetically engineered human hematopoietic stem cells via Notch signaling. *Cancer Res. 67*: 2425–2429.

Zhou, J., Shen, X., Huang, J., Hodes, R., Rosenberg, S., and Robbins, P. 2005. Telomere length of transferred lymphocytes correlates with in vivo persistence and tumor regression in melanoma patients receiving cell transfer therapy. *J. Immunol. 175*: 7046–7052.

Zinkernagel, R., and Doherty, P.C. 1974. Immunological surveillance against altered self components by sensitized T lymphocytes in lymphocytic choriomenigitis. *Nature 251*: 547–548.

zur Hausen, H. 2002. Papillomaviruses and cancer: from basic studies to clinical application. *Nat. Rev. Cancer 2*: 342–350.

9
New Insights into the Role of Infection, Immunity and Apoptosis in the Genesis of the Cancer Stem Cell

Peter Grandics

INTRODUCTION

Understanding the pathomechanism of cancer is of primary interest in medical research (Trosko and Rauch, 1998; Bjerkvig *et al*., 2005). In the past century, several mechanisms were proposed. It was hypothesized that cancer arises from a single cell that loses its differentiated state through sequential mutations. This initiation-promotion-progression concept explains the steps in a sequential process. Later, this hypothesis led to the mutagenic and recently the oncogenic theories, which hypothesize that defects in tumor suppressor genes are responsible for the development of cancer. The impairment of cell-to-cell communication as a cause of cancer has also been postulated.

Environmental effects, such as chemical carcinogens or life style factors, such as alcohol or tobacco consumption or drug abuse, could also cause mutations and other genetic abnormalities observed in cancer cells. The discovery of the cancer stem cell lent support to the theory that cancer may develop from a single cell, and raised the question of cancer stem cells arising from normal stem cells. Indeed, if normal stem cells could undergo the type of mutations observed in tumor cells, this would potentially compromise the genetic stability of the organism. Therefore, the likelihood that normal stem cells are very well protected is demonstrated by their resistance to radiation and toxins (Dean *et al*., 2005).

One fascinating finding is that immunosuppressive cytotoxic antineoplastic therapies may, on occasion, cause the regression of a clinically established cancer. At first, applying this as a therapeutic strategy may seem counterintuitive, considering the fundamental role of the immune system in protecting the body against infectious organisms and aberrant cells. In addition, cancer itself is frequently immunosuppressive, so exacerbating a pre-existing immunosuppression may not seem like a rational strategy.

In this light, it appears paradoxical that the same degree of immunosuppression that is lethal in a bacterial or fungal infection actually benefits cancer suppression. In other words, the deletion of the T cell compartment that accompanies cytotoxic antineoplastic therapies may facilitate cancer regression (Mackall, 2000). This suggests that cancer itself may arise from the immune system, potentially from the

T cell compartment, which would explain why the suppression of cellular immunity could also lead to the suppression of the disease. Another observation is that tumor cells are poorly immunogenic, despite the fact that tumor cells are antigenic. Therefore, they do not generate a T cell-mediated immune response, and if so, it is of low intensity (Melief, 2000). If tumor cells were derived from injured lymphocytes, particularly T cells that still share some functional properties with their normal counterparts, an immune tolerance to cancer cells could be explained, as the immune system is not made to attack itself. In pathological situations, T cells do attack self-tissue in a manner reminiscent of the autoreactive nature of cancer cells, which have the ability to attack and invade host tissues. In other words, cancer cells behave like autoreactive lymphocytes. Here, we explore the evidence suggesting that such a mechanism could be at work during cancer development.

The prevalent genetic theories of cancer are built upon observations of genetic abnormalities in tumor cells. These theories do not generally take into account the demonstrated importance of environmental factors in human cancer development. In a previous article, Grandics (2003) has shown that specific dietary deficiencies mimic the effects of chemical or radiation damage to DNA, which we propose plays an important role in human carcinogenesis and tumorigenesis. This observation allows us to consider cancer as a single disease, possibly developing from a single cancer stem cell. Based on this observation, we could assume that the observed genomic abnormalities in cancer cells are an effect rather than the cause of the disease. This idea also points to the direction of upstream events preceding the development of the malignant cell. We propose that identifying these events will be fundamental to understanding the pathomechanism of cancer. By exploring the functional similarities between lymphocytes and cancer cells, we provide an insight into this realm of possible upstream events.

The Exterior Cell Surface Layer (Cell Coat)

The lymphocyte cell coat is a labile structure, and the treatment of cells may lead to the loss of its components (Grandics, 2006a). This material plays an important role in lymphocyte functions including homing, cell mediated immunity, electrophoretic properties and antigen expression; cell surface proteins are thought to be involved in cell propagation and differentiation. After treatment with β-glucosidase, sialidase and trypsin, lymphocytes lose their homing abilities. Cytotoxic lymphocytes transiently lose their cytotoxic ability after a brief papain treatment. Lysis of the cell coat suppresses cell-mediated immunity. Treatment by glycosidases including neuraminidase affects the bodily distribution of lymphocytes and demonstrates alterations in their antigenicity. Treatment with trypsin and neuraminidase reversibly eliminates the mitogenic response of lymphocytes. The cell coat on thymocytes is significantly thicker than on splenic lymphocytes, suggesting a role for the cell coat in T cell function. The cell coat of the lymphocyte cell membrane has been characterized using various stains. These investigations found high acid mucopolysaccharide content with a significant number of acidic amino sugar end groups.

Cancer cells also exhibit an exterior cell surface coat. The similarities between the cell coat of normal and leukemic lymphocytes have been investigated. Pathological lymphocytes (CLL) have a uniformity of staining similar to their normal counterparts, with some differences observed with cationic stains that could be due to a decrease in the sialoprotein of the cell coat of CLL cells. With some similarity to lymphocytes, the tumor cell coat has been suggested to play a role in cell contact and adhesion, cell recognition, as well as the capacity to metastasize.

The tumor cell coat is also sensitive to neuraminidase and can rapidly regrow following treatment with the enzyme. The enzyme treatment also changes the immunological properties of tumor cells. Trypsin and EDTA remove the tumor cell coat. The cell coat is involved in the mechanism by which tumor cells escape cellular immune attack. The degradation of the cell coat by brief hyaluronidase treatment of glioma cells sensitizes them to cytotoxic lymphocyte attack. Although normal human glial cells also produce hyaluronic acid, glioma lines produce significantly more. Hyaluronidase-sensitive coats have been found on a variety of murine sarcoma and carcinoma cell lines. It appears that a mucopolysaccharide coat on tumor cells impedes the successful use of immunotherapy. It was demonstrated that the displacement of the tumor cell coat by charge-functionalized lipids or polycationic substances leads to tumor cell apoptosis and tumor destruction (Kovacs, 1983; Marquez *et al*., 2004).

It has been demonstrated that the cell coat of lymphocytes and tumor cells are functionally significant. The degradation/removal of cell coat significantly impacts the functionality of both tumor cells and lymphocytes; therefore, tumor cell isolation methods could alter the functionality of isolated cells. In other words, with the loss of the cell coat, lymphocytes lose fundamental functions, i.e., cannot attack target cells, while tumor cells also lose cell contact and adhesive properties, as well as the ability to metastasize. In addition, tumor cells become sensitive to apoptosis.

Activation of Coagulation

The activation of coagulation occurs during tissue injury as well as in various pathologies. Infection leads to both an inflammatory reaction and the activation of coagulation, as there is a crosstalk between these functions (Esmon, 2004). Blood coagulation components can inhibit or amplify the inflammatory response. Blood clotting is initiated when pathogenic components, such as endotoxin or inflammatory cytokines, induce synthesis of tissue factor on leukocytes. The coagulation cascade is subsequently triggered. The formation of negatively charged membrane phospholipid surfaces amplifies the coagulation reaction. Natural anticoagulant pathways, such as the protein C anticoagulant pathway, limit the coagulation process, thereby suppressing the inflammatory response, including reducing inflammatory cytokine secretion, decreasing NF-κB signaling, minimizing leukocyte chemotaxis, endothelial cell interactions, and suppressing apoptosis.

Platelets are also involved in the link between inflammation and coagulation. Inflammatory cytokines such as IL-6 or IL-8 increase platelet production, and such platelets are more thrombogenic (Burstein, 1997). In addition, the platelets release the CD40L protein, a potent proinflammatory

mediator, which subsequently induces tissue factor synthesis and amplifies the secretion of proinflammatory cytokines. This, in turn, leads to a progressive cycle that ultimately can produce severe vascular and organ injury.

In 1865, Trousseau first described a cancer-associated condition now called migratory thrombophlebitis in which a spontaneous coagulation of the blood occurs in the absence of inflammatory reactions (Trousseau, 1865). It manifests as migratory thrombosis in the superficial veins of the chest wall and arms, but it can also occur in other sites. This condition is a variant of venous thromboembolism. Thrombosis is a frequent complication of malignancy, and thromboembolic death is the second leading cause of mortality in cancer (Donati, 1995). Malignant cells interact with the blood coagulation system by releasing procoagulant and fibrinolytic substances and inflammatory cytokines (Caine *et al*., 2002). In addition, direct interaction with endothelial cells, monocytes/macrophages, and platelets also leads to localized clotting activation. Similar to normal activated inflammatory cells, malignant cells release tissue factor, which promotes the formation of fibrin deposits in the tumor cell microenvironment.

The fibrin gel matrix, along with other connective tissue components, form the basis for the tumor stroma, a matrix in which tumor cells are dispersed and which provides the vascular supply as well as a barrier against rejection by the cellular immune system. The tumor stroma shares properties with the temporary stroma of a healing wound (Dvorak, 1986). Similar to the fibrin coating on macrophages, the observed fibrin coating of tumor cells is involved in the mechanism by which tumor cells escape destruction by NK cells. Histological evidence suggests that inflammatory lymphocytes are confined to the tumor-host interface, and do not significantly penetrate the tumor (Dvorak *et al*., 1983). Malignant cells secrete inflammatory cytokines such as TNF-α and IL-1β that downregulate the anticoagulant system of vascular endothelial cells (Caine *et al*., 2002). The secretion of IL-8 promotes new blood vessel formation, and the fibrin deposited around tumor cells facilitates angiogenesis.

Tumor cells attach to the vascular endothelium and promote the adhesion of leukocytes and platelets. Monocytes and macrophages also home in on vascular surfaces due to inflammatory stimuli. In response to inflammatory molecules, complement, lymphokines and immune complexes, these cells subsequently secrete procoagulant tissue factor; tumor-associated macrophages express significantly higher levels of tissue factor than control cells. These macrophages also increase their fibrinolytic enzyme production.

Both human and animal cancers cause platelet aggregation *in vitro* and *in vivo* (Hejna *et al*., 1999). The ability of tumor cells to aggregate platelets and secrete plasminogen activator correlates with their metastatic potential. Indeed, thrombocytopenia reduces the metastases of tumors as do compounds capable of reducing platelet aggregation. These include aspirin, prostaglandins and other nonsteroidal (NSAID) anti-inflammatory drugs. A reduced risk of fatal colon cancer has been observed among aspirin users (Thun *et al*., 1991). Administration of heparin and fibrinolysin also reduces the incidence of experimental metastases, while the

administration of anti-fibrinolytic agents increases their incidence.

Cancer treatment by surgery, cytotoxic antineoplastic drugs, and hormonal therapy all contribute to the hypercoagulable state and risk factors for thromboembolism in cancer patients (Caine *et al*., 2002). The risk of fatal pulmonary embolism increases four-fold after surgery in cancer patients. Chemotherapy drugs including cisplatin, mytomicin C and tamoxifen as well as high-dose and multi-drug regimes increase the risk of thrombotic complications. Prophylactic treatment with warfarin reduces this risk. The use of hematopoietic growth factors subsequent to chemotherapy was shown to induce thrombosis in breast cancer patients. Venous thrombosis could also be a marker for an otherwise asymptomatic cancer.

Similarly to a normal inflammatory reaction, activation of coagulation takes place in cancer. The events of tumor stroma development are comparable to wound healing (Dvorak, 1986), and it is possible that tumor formation may be associated with defective wound healing initiated by an inflammatory reaction due to infection and/or tissue injury. Therefore, we believe it is important to investigate potential links between infection, inflammation, and cellular immune response in searching for the origins of the cancer cell.

Infection and Inflammation

The etiological role of infectious agents has been indicated in various cancers (Grandics, 2006a). In 100 cases of human leukemia, *Mycoplasma*, *Salmonella*, *Micropolyspora*, *Mycobacterium*, *Absidia*, pseudorabies virus, and adenovirus antigens were commonly detected in the patient's sera. Hepatotropic viruses (hepatitis B and C) cause hepatic necrosis followed by hepatocellular, B cell and gastric malignancies. Antiviral therapy of hepatitis C infection lead to the regression of virus-associated B cell lymphoma. Adenoviral infection has been associated with childhood leukemia and cytomegalovirus infection with testicular cancer. *Helicobacter pylori* infection is widespread in the population (an estimated 40–80% infected) and is linked to gastric cancer and mucosa-associated lymphoid tissue (MALT) lymphoma. A reversal of lymphoma-induced neutropenia has been observed with the eradication of *H. pylori* infection. Simian virus 40 (SV40) is associated with human brain cancers and non-Hodgkin's lymphoma. Ocular adnexal lymphoma is linked to *Chlamydia psittaci* infection, and the reversal of lymphoma was observed with pathogen-eradicating antibiotic therapy. The list continues: Cervical intraepithelial neoplasia (CIN) is associated with human papilloma virus (HPV) infection with a co-etiological presence of chronic bacterial cervicitis. *Mycoplasma* and HPV association were found to be dominating. The role of mycoplasma in the dysplasia of the uterine cervix and development of CIN has also been demonstrated.

Mycoplasmas are particularly interesting due to their widespread presence in the human population. Although many mycoplasmas are not directly pathogenic in humans, they are associated with many diseases. Mycoplasmas have co-leukemogenic activity, and are found to increase tumor cell invasiveness. In approximately half of the examined cases, mycoplasma DNA was present in ovarian and gastric carcinoma specimens. In gastric, lung, esophageal, breast, and colon cancers as well as glioma

specimens, *Mycoplasma hyorhinis* was detected in 50% of the cases. Mycoplasmas are known to cause chromosomal changes. Mixed *Mycoplasma pneumoniae* and influenza virus infection induce lung cancer in an animal model. The direct role of the AIDS-associated *Mycoplasma fermentans* and *Mycoplasma penetrans* in oncogenesis has been investigated. These mycoplasma strains induce gradual malignant transformations that eventually become irreversible. Besides its direct oncogenic potential, *Mycoplasma fermentans* exhibits a unique cytocidal effect on the undifferentiated myelomonocytic lineage, but not on differentiated myelomonocytic cells. The depletion of immature myelomonocytic cells likely contributes to the functional immunodeficiency present in cancer patients.

In response to pathogens, the host mounts a protective inflammatory response. Immune cells migrate to the area of infection and produce inflammatory messengers called cytokines. Initially, cells of the innate immune system (macrophages, neutrophils, NK cells) become involved, followed by the activation of cells of the adaptive immune system. These include antigen-presenting cells (APCs), T and B cells, which play an important role in propagating the inflammatory response. T cell inflammation plays a major role in antitumor immune responses. Key regulators of T cell-mediated response are the T helper (Th) cells that secrete the cytokines orchestrating this response. The two subtypes Th1 and Th2 cells produce cytokines stimulating cellular and humoral immune responses.

Intracellular pathogens (e.g., viruses and mycoplasmas) use the Toll-like receptor (TLR) signaling mechanism to escape host defenses (Netea *et al*., 2004). Pathogen-associated molecular patterns on the surface of mycoplasmas engage TLRs 1, 2, and 6 on the surface of APCs that lead to a Th2-type polarization of the immune response and the secretion of IL-10, IL-4, IL-5 and IL-13. These cytokines are antagonistic to Th1 type cytokines (TNF-α, IL-2, IFN-γ, IL-6, IL-12); excessive production of either type of cytokine upsets the homeostatic balance needed to maintain a proper mix of cellular and humoral immune responses (Hilleman, 2004). Utilizing this mechanism, mycoplasmas suppress cell-mediated immunity, which allows them to persist and predispose the host for colonization by other pathogens. The observation that leukemia patients were colonized by over half a dozen pathogens besides mycoplasmas (Grandics, 2006a) suggests that suppression of the cellular immune system provides a fertile ground for a variety of pathologies.

Besides regulating innate and adaptive immune responses, cytokines are involved in cell growth and differentiation (Grandics, 2006a). Normally, the secretion of cytokines is of short radius and limited duration, typically regulating self or adjacent cell functions. The activity of cytokines is tightly regulated, and there is evidence that cytokines contribute to inflammatory autoimmune diseases and malignancies. Similar to activated T cells, various tumor cells secrete immune response-polarizing cytokines (IL-10, IL-6, IL-8, IL-13, TGF-β) serving as autocrine and/or paracrine growth factors for the cancer. The progression of the disease and patient survival was correlated with increasing levels of cytokine secretion. This secretion is frequently constitutive, leading to elevated serum levels of cytokines in malignancies including melanoma, non-small cell lung carcinoma,

renal cell carcinoma, and bladder carcinoma. In addition, tumor cells can induce IL-10 in the tumor environment. IL-10, the most potent Th2 polarizing cytokine, suppresses the tumoricidal activity of macrophages, blocks presentation of tumor antigens to professional APCs, and inhibits tumor-specific cytotoxic T cells. However, in cancers both cellular and humoral immune response may be depressed, as in the absence of IL-4 production, IL-10 secretion alone cannot induce a Th2-type response.

It appears that the immune response becomes distorted at multiple levels during the development of cancer. First, infectious agents may act in concert to subvert cellular immunity, thereby upsetting the homeostatic balance of a proper mix of cellular and humoral immune response. This leads to an aberrant cytokine-signaling that results in depressed apoptosis and excessive proliferation (Grandics, 2006a). Cytokines seem to be the key substance of apoptosis of leukemic cells. Abnormal inflammatory cytokine secretion by tumor cells reinforces the existing imbalances and thus promotes disease progression. Similar to T cells, cancer cells use inflammatory cytokines as autocrine and paracrine growth factors, suggesting a functional relationship between cancer cells and cells of the immune system.

Infection, Autoimmunity, and Cancer

Several lines of evidence suggest a direct relationship among infection, autoimmunity, and cancer (Grandics, 2006a). Hepatitis B and C viruses are involved in an autoimmune condition that precedes the development of hepatocellular carcinoma. Data also demonstrate a higher prevalence of B-cell non-Hodgkin's lymphoma in HCV-infected patients with autoimmune manifestations including Sjorgren syndrome, cryoglobulinemia, and systemic lupus erythematosus (SLE). Adenovirus infection is associated with childhood leukemia, and family studies in acute childhood leukemia have shown possible associations with autoimmune disease. Epstein-Barr virus and human T lymphotropic virus type 1 infection are associated with abnormal lymphoproliferation and Hodgkin's lymphoma. Cytomegalovirus infection is linked to autoimmunity and testicular cancer. *H. pylori* infection can lead to autoimmune neutropenia and MALT-lymphoma in addition to its well-established role in the development of gastric cancer. Systemic rheumatic disease has also been linked to lymphoid malignancy. These findings underline a close relationship among infection, autoimmunity, and proliferative disorders, possibly mediated by abnormally functioning cytokine signaling.

Antinuclear antibodies (ANA) were demonstrated in the sera of 19% of patients with malignancies in the absence of overt autoimmune manifestations. In cancer patients, a large number of autoantibodies are observed against tissue-specific antigens, nucleoproteins, membrane receptors, proliferation-associated antigens, tissue-restricted antigens, etc. Autoantibodies to the p53 protein were detected in the sera of cancer patients before the onset of the disease. This raises the possibility that cancer is a specific autoimmune condition. Autoimmune connective tissue disorders are also commonly associated with malignancies. It was reported that gastric atrophy and pernicious anemia carry a risk for gastric carcinoma 18 times that of the population average. It appears that a variety of

infections may induce autoimmune serological features without overt autoimmune disease or organ involvement; however, this condition may progress to clinical autoimmune disease and malignancy if impaired T cell function prevails. Such condition develops at a higher frequency among the elderly.

It was observed 30 years ago that a low percentage of human T cells (3.4%) has the ability to form auto-rosettes with autologous erythrocytes; in breast cancer and melanoma patients, the ratio was elevated to 6.1% and 7.4%, respectively. This observation implied that some level of autoreactivity is normal, confirmed later by studies on T cell tolerance. However, the observation also pointed to an elevated level of autoreactive T cells involved in cancer. The mechanism of activation of an autoreactive T cell response was linked subsequently to bacterial and viral infections through the process of molecular mimicry in which pathogen-derived peptides mimic self-peptides. This phenomenon was studied in animal models and was supported by clinical observations. As a highlight, when lymphocytic choriomeningitis virus (LCV) antigens were expressed in the pancreas of transgenic mice, infection with the virus led to autoimmunity and diabetes.

H. pylori antigens mimic epitopes on H^+,K^+-adenosine triphosphatase in the gastric mucosa, thereby activating cross-reactive gastric T cells. Viral peptides mimic sequences on myelin basic protein, leading to multiple sclerosis. Cytochrome c (cyt c) as an antigen was used to study how self-proteins prime autoreactive T cell responses, as SLE patients possess autoantibodies to cyt c. When non-self cyt c was coadministered with the self-protein, B cells specific for the foreign antigen primed autoreactive T cells caused breaking tolerance to self-cyt c. The same autoimmune phenomenon occurs in the LCV transgenic mice when LCV antigens on pancreatic cells, and the intact virus antigens are copresented to the immune system. Therefore, it is quite likely that autoimmunity spontaneously develops during a variety of infections when antigens on microorganisms mimic self antigens and are presented together, breaking T cell tolerance.

The presence of autoreactive T cells has been observed in healthy persons, which indicates a role for these cells in immune defense (Grandics, 2006a). If autoreactive T cells were always absent in the T cell repertoire, the responsiveness toward foreign antigens that resemble self-antigens would be reduced. This notion is supported by the observation that T cells which recognize variants of self-antigen are of lower avidity than those recognizing a foreign antigen. Also, tolerance to self-antigen reduced T cell variants for these peptides as well as the diversity of T cell receptor α and β-chain sequences of self-specific T cells. It appears that some level of autoreactive T cells is necessary for immune defenses. Clinical autoimmunity may develop when persistent infection provides a continuing high dose of antigenic stimulus, and this situation could predispose patients to the development of proliferative disorders.

Defective Apoptosis

Normal tissue development requires damaged, dangerous or unnecessary cells to be eliminated while healthy cells survive. The survival of harmful or damaged

cells can lead to various pathologies. The evolutionarily conserved mechanism of apoptosis eliminates unwanted or abnormal cell populations (Grandics, 2006a). Lymphocytes require IL-2, IL-4, IL-7, IL-9, and IL-15 for viability, and withdrawal of these cytokines leads to apoptotic cell death. Leukemia patients who went into complete remission following chemotherapy developed a different type of leukemia after being placed on IL-2 therapy. IL-2 is an essential cytokine for the viability of activated T-cells, suggesting a link between the survival of activated T-cells and leukemic cells. Myeloid leukemia cells are also cytokine-dependent and undergo apoptotic cell death following cytokine withdrawal. Various immune response-polarizing cytokines that tumor cells secrete inhibit chemotherapy- or radiation-induced apoptosis. There are myeloid leukemia cell lines that have become independent of an external cytokine supply, but generally cytokines can protect both normal and cancer cells against apoptosis induced by various cytotoxic agents. The persistence of infectious agents and chronic inflammation in cancer patients promotes NF-κB activation and inflammatory cytokine production, thereby contributing to the diminished apoptosis of abnormal cells.

The completion of immune response against pathogenic microorganisms requires the deletion of activated T and B cells that participate in the immune defenses, particularly self-reactive ones (although a fraction of them survive as memory cells). Apoptosis plays an important role in the regulation of peripheral immunity through the Fas/APO-1 cytotoxic pathway. Defective apoptosis can lead to autoimmune disease and cancer. As cancer cells are not immortal, they maintain a program for apoptotic cell death.

The apoptosis marker Fas receptor (FasR) is expressed on numerous cell types, whereas the Fas ligand (FasL) is mainly expressed on T cells. FasL mediates the apoptosis of effector T cells as part of an immune response termination and tolerance development. FasL is also expressed in "immune-privileged" tissues such as the brain, testes, and eyes with the purpose of preventing inflammation. Mutations in Fas or FasL can lead to autoimmune disease. Similar to cytotoxic T cells, various tumor cells also express FasL and use it to induce apoptosis of invading lymphocytes. Breast tumor cells express FasL that can kill Fas-sensitive lymphoid cells. The coexpression of Fas and FasL was observed in brain tumors that can use this mechanism to obtain a proliferating advantage by "counter-attacking" tumor-infiltrating activated Fas-sensitive T lymphocytes. Similar observations have been made in Ewing sarcoma, gastric cancer, cholangiocarcinoma, B cell chronic lymphocytic leukemia (B-CLL), colon adenocarcinoma, head and neck cancer, lung carcinoma, esophageal carcinoma, ovarian carcinoma, lymphoma, pancreatic carcinoma, melanoma, and other malignancies (Grandics, 2006a). Childhood glial tumor cells (but not normal cells) in the brain express the common leukocyte-associated antigen and Fas.

The expression of apoptosis-related molecules on the surface of both neoplastic cells and cytotoxic lymphocytes (CTL) in tumor specimens raises the question of whether neoplastic cells are formed from CTLs by a premature termination of the apoptotic mechanism. Indeed, neoplastic cells behave like CTLs in their expression of FasL and in the induction of apoptotic death of activated T cells, as well as other cancer cells carrying

a functional FasR. In other words, cancer cells continue to act like T cells performing their immune-regulating functions.

Discussion and Therapeutic Implications

Infections by various pathogenic microorganisms are a common occurrence in humans and other animals. In response to invading pathogen(s), an inflammatory reaction develops in the host organism. Initially, the innate immune system becomes involved, followed by the development of an adaptive immune response. Activated leukocytes produce inflammatory cytokines and chemokines as well as other growth factors aimed at clearing up the infection and facilitating tissue healing. The inflammatory reaction at the infection site triggers a variety of physiological responses. Antigen-presenting cells activate T and B cells in response to molecular patterns expressed on the surfaces of pathogenic microorganisms. Intracellular pathogens are overcome by the cellular immune response; in addition, the T cell inflammatory reaction is also key to antitumor immunity. Activated T helper 1 (Th1) cells secrete specific cytokines orchestrating this response.

Pathogenic microorganisms, however, have evolved strategies to evade immune surveillance in order to persist in the host. Several intracellular pathogens including mycoplasmas and viruses deploy molecular patterns on their surfaces that trigger a Th2-type (humoral) immune response and consequently depress cellular immunity. In addition, some infections such as the mycoplasmas remain sub-clinical, and by subverting the cellular immune response, these microorganisms predispose the host for colonization by other pathogens eventually leading to various pathologies.

Molecular mimicry is initiated when viruses integrate host genes within their genome, (Tyler and Fields, 1996) and pathogens with host-like genes may have a survival advantage over those lacking such traits. Animal viruses are capable of fusing with prokaryotic cells that may facilitate gene transfer between distant microbial taxa (Citovsky *et al*., 1988). Influenza virus hemagglutinin A sequences have been located in the p37 protein of *Mycoplasma hyorhinis*, and this protein increases tumor cell invasiveness (Ketcham, 2005). The exchange of genes among various microorganisms (Lawrence, 2006) leads to the development of antibiotic resistance. Gene uptake also occurs by phagocytosis of apoptotic bodies while High Mobility Group (HMG) proteins, commonly associated with human DNA, may facilitate this process in bacteria (Grandics, 2006a).

When antigens from pathogens mimic self-antigens in the process of molecular mimicry, cross-reactive T cells may be generated. The study on breaking T cell tolerance with co-administered foreign and self-cytochrome c is a sobering reminder of just how easy it is to induce autoimmunity. However, evidence also demonstrates that a low level of autoimmunity is normal and necessary to mount an effective immune response to infections. Clinical autoimmunity may develop if a continuing high-dose antigenic stimulus persists, as in cases of chronic infection. In addition, there is also evidence that autoimmunity can lead to proliferative disorders.

As discussed, normal tissue development requires the elimination of dangerous and abnormal cells, and autoimmune T cells belong to this category. With the

completion of the immune response, the evolutionarily conserved mechanism of apoptosis eliminates effector T cells, leading to immune response termination and tolerance development. However, defective apoptosis can lead to autoimmunity and cancer.

We propose that an aberration in the apoptosis process leads to formation of the cancer stem cell from autoreactive T cells. In support of this observation, *Helicobacter*-induced gastric epithelial carcinoma was found to originate from bone marrow-derived cells (Houghton, 2004). This is the direct proof of cancer that does not arise from mutated epithelial cells. Also, the cytotoxic T lymphocyte-associated antigen-4 (CTLA-4), a regulator of the effector function of T cells, is expressed in various leukemias and solid tumors (Contardi *et al*., 2005). This suggests a link between CTLs, hematopoietic neoplasias and solid tumors.

Further evidence: the common acute lymphoblastic leukemia antigen was detected on glioma and melanoma cell lines (Grandics, 2006a). The melanoma-associated PRAME antigen is expressed both in leukemias and some solid tumors. The majority of leukemia and lymphoma cells test positive for the leukocyte common antigen. Seminoma, rhabdomyosarcoma, and some metastatic undifferentiated and neuroendocrine carcinomas have also been found to express CD45. The myeloid antigen Leu-7, typically expressed on natural killer (NK) cells and T cell subsets, was detected on small cell lung carcinoma and a variety of other solid tumors including astrocytoma, neuroblastoma, retinoblastoma, carcinoid tumors, etc. Neoplastic cells of Hodgkin's disease expressing Leu-7 may be related to NK cells or T cells rather than B cells (Grandics, 2006a). We propose that the unexpected presence of some T cell markers on cancer cells may provide an insight into their origins. In addition, the observation that cancer stem cells embedded in an environment of normal host tissue can undergo a differentiation process (during which surface markers of lymphoid origin disappear) explains the absence of leukocyte-derived surface antigens in some solid tumors.

In benign colonic adenomatous polyps and synchronous adenocarcinoma, comparable and very large numbers of genomic alterations (>10,000 events per cell) were found (Stoler *et al*., 1999), demonstrating massive genomic damage characteristic of apoptosis as opposed to sequential mutations. In addition, this demonstrates that genomic instability precedes the development of a malignant state, indicating that malignancy is an effect rather than the cause of genetic abnormalities in cancer cells. It is therefore reasonable to conclude that there is no fundamental difference between benign and malignant tumors, and that possibly a very small difference in the disregulation of proliferative controls leads to a malignant phenotype.

We further propose that the resultant cancer stem cell still preserves some functions of an effector T cell, such as homing in to sites of inflammation such as the inflamed bronchi of a cigarette smoker, the damaged liver of an alcohol abuser, an *H. pylori*-infected gastric mucosa, an HPV-infected uterine cervix, an inflamed colon, etc. The cancer cell retains some capabilities of an effector T cell to secrete inflammatory cytokines (even if in an aberrant, constitutive fashion), thereby distorting local immune responses, disabling cytotoxic T cells and diminishing apoptosis in its environment.

Like normal activated inflammatory cells, cancer cells activate the coagulation system, leading to the formation of the tumor stroma in which tumor cells proliferate. Dvorak (1986) in his paper entitled "Tumors: wounds that do not heal" succinctly described similarities between the formation of the temporary stroma of a healing wound and tumor stroma development. While the cancer cell continues to act as if it participated in a wound healing process, it actually enlarges the wound stroma due to its constitutive secretion of tissue factor, inflammatory cytokines and other growth factors, which also provide stimuli for the propagation of the malignant cells. This leads to an ever-continuing cycle of tumor growth.

Every human cell has the ability to repair itself, and cancer cells retain some of this capacity (Degos, 1992). As cancer stem cells exhibit plasticity similar to normal stem cells, we propose that a cell-to-cell communication between cancer stem cells and surrounding host tissues allows tumor cells to develop varying degrees of differentiated phenotypes resembling cells of normal differentiated tissues. This in turn leads to the emergence of various tumor types and creates the illusion of a great multitude of cancers.

It has been long known that cancer cells, besides growing inside tumors, also circulate in the blood (Griffiths *et al.*, 1973). This is easy to rationalize if cancer cells are indeed damaged autoreactive T cells, and also provides an explanation for metastasis formation. Cancer cells interact with neutrophils, macrophages and platelets that lead to the formation of micrometastases that can remain in the blood for a long time. These aggregates persist even after adjuvant chemotherapy, although in reduced numbers. Larger cell clumps are more effective in promoting metastases than smaller ones (Grandics, 2006a). With the progression of inflammation in cancer patients, the circulating micrometastases find new sites of proliferation that lead to the formation of metastases.

Current cancer therapies are tumor-centric, as tumors are equated with cancerous disease. Main therapeutic modalities include the surgical removal of tumors as well as radiation and chemotherapies. All of these contribute to the hypercoagulable state and risk of thromboembolism, which have a significant negative impact on the morbidity and mortality of cancer patients. If tumor cells did originate from T cells, any therapeutic approach targeting tumor cells will likely diminish T cell function. Cytotoxic antineoplastic therapy represents an extreme situation in this regard, resulting in the deletion of even resting T cells, the reconstitution of which takes several months (Mackall, 2000). This makes the combination of chemotherapy and immunotherapy an unrealistic proposition.

If cancer cells indeed originate from damaged autoreactive T cells, our current views on cancer immunotherapy need to be revised. The immune system was not developed to attack itself, and this is supported by the unresponsiveness of the cellular immune system to cancer even if tumor cells are antigenic. When we attempt to induce an immune response against tumors, we run the risk of developing autoimmune disease (Tirapu *et al.*, 2002) and ultimately, secondary malignancies.

The suppression of the immune system by chemotherapeutic agents and radiation encourages the propagation of microbial and parasitic infections already present in cancer

patients. However, pathogenic microorganisms are intimately involved as coetiological agents in the development of various malignancies via molecular mimicry-induced autoimmunity, and maintain a cytokine milieu that favors proliferation as opposed to apoptosis. Therefore, current immunosuppressive cancer therapies may establish the conditions for disease recurrence as well as the emergence of new primary tumors, which is in fact, a common experience. Also, the cancer patient's system appears to retain a "memory" of the disease as the risk of developing another cancer is higher than those who have never had the disease. This memory could be attributed to autoimmune memory T cells, reactivated by recurrent infections which become cancerous later on as a consequence of defective apoptosis.

The eradication of pathogens could have a favorable effect on the course of malignant diseases, as demonstrated by therapies of HCV, *H. pylori*, and *Chlamydia psittaci* infections (Grandics, 2006a). Mycoplasmas are difficult to eradicate and require high-dose, long-term antibiotic therapies, but even after that the pathogens are found to persist. There are no therapies for many viral infections at this time. With our new understanding of the mechanism of TLR signaling, opportunities have opened for overcoming these types of pathogens. Recently, a therapeutic oral mycoplasma vaccine was described (Szathmary, 2005) the principle of which could be utilized for the therapy of other intracellular infections.

If defective apoptosis of autoreactive T cells leads to the emergence of the cancer stem cell, our research must focus on the physiological events associated with apoptosis. Any therapeutic approach upstream from this step is merely symptomatic, and offers little hope of defeating cancer. A century of accumulated evidence on the use of immunosuppressive cancer therapies supports this observation.

It was demonstrated that the exterior mucopolysaccharide cell surface coat on cancer cells protects them from apoptosis (Gately, 1982). Kovacs has explored this understanding to the greatest degree by synthesizing unsaturated aminolipids capable of displacing the cell coat on tumor cells (Kovacs, 1983). Administration of these compounds led to the apoptotic death of a variety of tumor cells *in vitro* and *in vivo*. Normal lymphocytes are less sensitive to the apoptotic effects of a fatty acid mixture than leukemic cells, although they do show some sensitivity (Otton and Curi, 2005). This observation may explain why the continuing administration of synthetic unsaturated aminolipids led to a diminishing efficacy of the therapy (Kovacs, 2006 personal communication), as normal lymphocytes are also surrounded by an exterior cell surface layer coat essential for their functions.

Endocrine hormonal signaling also affects apoptosis. Corticosteroids facilitate the apoptosis of lymphocytes and exert an immunosuppressive effect when the organism is subject to prolonged stress. Stress also down-regulates the digestive functions of the gut, including those of the stomach and pancreas. This in turn suppresses the uptake of critical nutrients that are essential for genomic stability (Grandics, 2003). It was found that breast cancer patients as a group exhibit a depressed thyroid function, suggesting an etiological role for thyroid deficiency in neoplasia. Thyroid function is profoundly affected by the iodine supply, and thyroid, breast and gastric cancers have been linked

to iodine deficiency (Grandics, 2003). We have also pointed out that critical nutrient deficiencies mimic the effects of chemical or radiation damage to DNA, and suggested that the correction of these deficiencies could reverse the progression of malignant proliferation.

In the past century, insufficient attention was paid to the role of dietary factors in the development and progression of malignant diseases. No Recommended Daily Allowances (RDAs) are available for a number of essential nutrients, and where available, the RDA is of questionable value. Iodine, a vital micronutrient, is an example: the current WHO recommendation for iodine is 0.15 mg/day. However, some Japanese consume as much as 50–80 mg of iodine/day through their seaweed rich diet and exhibit significantly lower rates of the major cancer types than seen in the Western world (Grandics, 2003, 2006a). In addition, iodine supplementation clinical trials with school children have demonstrated that an iodine intake vastly exceeding the RDA (more than 6,000 times higher) was both safe and clinically useful (Benmiloud, 1994). This could not possibly be the case if the RDA for iodine had been correctly determined. Similar clinical observations were made for high-dose administration of folate and vitamin B_{12} (Heimburger et al., 1988) as well as vitamin C (Gonzalez et al., 2005). These findings question the accuracy of dietary RDAs, and suggest that current domestic as well as EU regulatory initiatives aimed at restricting the active ingredient contents in vitamin supplements are based on an erroneous scientific rationale.

It is also important to recognize that vitamin and mineral levels have significantly declined over the past 60 years in our food supply (Worthington, 2002) possibly due to intensive agricultural production methods and industrial food processing. Experience teaches us that in the Western world, despite an abundance of food, people have difficulties in meeting their nutritional needs, demonstrated by now-rampant obesity as well as the historically proven explosion of degenerative diseases including cardiovascular diseases, diabetes and cancer. This suggests that we are still far from understanding the dietary needs of the human organism.

It is known that diabetics develop malignancies at a higher frequency than the population average (Strickler, 2001), which implicates pancreatic dysfunction in the etiology of cancer. Besides secreting digestive enzymes, the pancreas is also a source of hormonal regulators. We hypothesize that a combined effect of adrenal, thyroid and pancreatic dysfunction may predispose patients for neoplasia in a process promoted by dietary deficiencies as well as lifestyle factors including prolonged stress, poor hygiene, smoking, alcoholism and drug abuse, all of which are known to subvert immunity. It appears that we need to make the most important scientific discoveries in the simplest things, i.e., how to conduct our lives in a manner optimal for well-being. Therefore, the main operative principle of health care should be prevention.

To finally defeat cancer, our research needs to focus on the identification of those endocrine-signaling mechanisms that enable CTLs to complete their mission of apoptotic elimination of autoreactive T cells. We must abandon our focus on the tumor cell as far as the development of cancer therapeutics are concerned, as the destruction of cancer itself negatively impacts the immune system, thereby reactivating

the vicious cycle of infection, autoimmunity and malignancy that ultimately dooms cancer patients. By redirecting our focus toward physiological events preceding the formation of the cancer stem cell, we will be able to overcome this scourge that has haunted humanity since time immemorial. A systemic approach described in our previous articles (Grandics, 2003, 2006b) offers an alternative to current cancer therapies that works with the immune system, and which helps to reestablish homeostatic balance in the human body.

SUMMARY

This review explored similarities between lymphocytes and cancer cells based on which we propose a new model for the genesis of human cancer. We suggest that the development of cancer requires infection(s) during which antigenic determinants from pathogens mimicking self-antigens are copresented to the immune system, leading to breaking T cell tolerance. Some level of autoimmunity is normal and necessary for effective pathogen eradication. However, autoreactive T cells must be eliminated by apoptosis when the immune response is terminated. Apoptosis can be deficient in the event of a weakened immune system, the causes of which are multifactorial. Some autoreactive T cells suffer genomic damage in this process, but manage to survive. The resulting cancer stem cell still retains some functions of an inflammatory T cell, so it seeks out sites of inflammation inside the body. Due to its defective, constitutive production of inflammatory cytokines and other growth factors, a stroma is built at the site of inflammation similar to the temporary stroma built during wound healing. The cancer cells grow inside this stroma, forming a tumor that provides their vascular supply and protects them from cellular immune response.

As cancer stem cells have plasticity comparable to normal stem cells, interactions with surrounding normal tissues cause them to give rise to all the various types of cancers, resembling differentiated tissue types. Metastases form an advanced stage of the disease, with the proliferation of sites of inflammation inside the body following a similar mechanism. Immunosuppressive cancer therapies inadvertently reinvigorate pathogenic microorganisms and parasitic infections common to cancer, leading to a vicious cycle of infection, autoimmunity, and malignancy that ultimately dooms cancer patients. Based on this new understanding, we recommend a systemic approach to the development of cancer therapies that supports rather than antagonizes the immune system.

REFERENCES

Benmiloud, M., Chaouki, M.L., Gutekunst, R., Teichert, H.M., Wood, W.G., and Dunn, J.T. 1994. Oral iodized oil for correcting iodine deficiency: optimal dosing and outcome indicator selection. *J. Clin. Endocrinol. Metab. 79*: 20–24.

Bjerkvig, R., Tysnes, B.B., Aboody, K.S., Najbauer, J., and Terzis, A.J.A. 2005. The origin of the cancer stem cell: current controversies and new insights. *Nat. Rev. Cancer 5*: 899–904.

Burstein, S.A. 1997. Cytokines, platelet production and hemostasis. *Platelets 8*: 93–104.

Caine, G.J., Stonelake, P.S., Lip, G.Y.H., and Kehoe, S.T. 2002. The hypercoagulable state of malignancy: pathogenesis and current debate. *Neoplasia 6*: 465–473.

Citovsky, V., Rottem, S., Nussbaum, O., Laster, Y., Rott, R., and Loyter, A. 1988. Animal viruses are able to fuse with prokaryotic cells. Fusion between Sendai or influenza virions and Mycoplasma. *J. Biol. Chem. 263*: 461–467.

Contardi, E., Palmisano, G.L., Tazzari, P.L., Martelli, A.M., Fala, F., Fabbi, M., Kato, T., Lucarelli, E., Donati, D., Polito, L., Bolognesi, A., Ricci, F., Salvi, S., Gargaglione, V., Mantero, S., Alberghini, M., Ferrara, G.B., and Pistillo, M.P. 2005. CTLA-4 is constitutively expressed on tumor cells and can trigger apoptosis upon ligand interaction. *Int. J. Cancer 117*: 538–550.

Dean, M., Fojo, T., and Bates, S. 2005. Tumour stem cells and drug resistance. *Nat. Rev. Cancer 5*: 275–284.

Degos, L. 1992. All-trans-retinoic acid treatment and retinoic acid receptor alpha gene rearrangement in acute promyelocytic leukemia: a model for differentiation therapy. *Int. J. Cell. Cloning 10*: 63–69.

Donati, M.B. 1995. Cancer and thrombosis: from phlegmasia alba dolens to transgenic mice. *Thromb. Haemost. 74*: 278–281.

Dvorak, H.F. 1986. Tumor: wounds that do not heal. *N. Engl. J. Med. 315*: 1650–1659.

Dvorak, H.F., Senger, D.R., and Dvorak, A.M. 1983. Fibrin as a component of the tumor stroma: origins and biological significance. *Cancer Metastasis Rev. 2*: 41–73.

Esmon, T.C. 2004. Interactions between the innate immune system and blood coagulation systems. *Trends Immunol. 25*: 536–542.

Gately, M.K., Glaser, M., McCarron, R.M., Dick, S.J., Dick, M.D., Mettetal, R.W., and Kornblith, P.L. 1982. Mechanisms by which human gliomas may escape cellular immune attack. *Acta Neurochir. 64*: 175–197.

Gonzalez, M.J., Miranda-Massari, J.R., Mora, E.M., Guzman, A., Riordan, N.H., Riordan, H.D., Casciari, J.J., Jackson, J.A., and Roman-Franco, A. 2005. Ascorbic acid and cancer 25 years later. *Integrative Cancer Ther. 4*: 35–44.

Grandics, P. 2003. Cancer: a single disease with a multitude of manifestions? *J. Carcinog. 2*: 9.

Grandics, P. 2006a. The cancer stem cell: evidence for its origin as an injured autoreactive T Cell. *Mol. Cancer. 5*: 6.

Grandics, P. 2006b. Complete remission achieved in a case of adult acute myelogeneous leukemia by a novel nutritional therapy. *J. Altern. Complement Med. 12*: 311–315.

Griffiths, J.D., McKinna, J.A., Rowbotham, H.D., Tsolakidis, P., and Salsbury, A.J. 1973. Carcinoma of the colon and rectum: circulating malignant cells and five-year survival. *Cancer 31*: 226–236.

Heimburger, D.C., Alexander, C.B., Birch, R., Butterworth, C.E. Jr, Bailey, W.C., and Krumdieck, C.L. 1988. Improvement in bronchial squamous cell metaplasia in smokers treated with folic acid and vitamin B-12. Report of a preliminary randomized, double-blind intervention trial. *JAMA 259*: 1525–1530.

Hejna, M. Raderer, M. and Zelinski, C.C. 1999. Inhibition of metastases by anticoagulants. *JNCI 91*: 22–36.

Hilleman, M.R. 2004. Strategies and mechanisms for host and pathogen survival in acute and persistent viral infections. *Proc. Natl. Acad. Sci. USA 101*: 14560–14566.

Houghton, J, Stoicov, C., Nomura, S., Rogers, A.B., Carlson, J., Li, H., Cai, X., Fox, J.G., Goldenring, J.R., and Wang, T.C. 2004. Gastric cancer originating from bone marrow-derived cells. *Science 306*: 1568–1571.

Ketcham, C.M., Anai, S., Reutzel, R., Sheng, S., Schuster, S.M., Brenes, R.B., Agbandje-McKenna, M., McKenna, R., Rosser, C.J., and Boehlein, S.K. 2005. p37 Induces tumor invasiveness. *Mol. Cancer Ther. 4*: 1031–1038.

Kovacs, A. 1983. Process for the preparations of anti-tumor therapeutics. *Hungarian Patent No. 200093 B*.

Kovacs, A. 2006. Personal communication.

Lawrence, J.G. 2005. Horizontal and vertical gene transfer: the life history of pathogens. *Contrib. Microbiol. 12*: 255–271.

Mackall, C.L. 2000. T-cell immunodeficiency following cytotoxic antineoplastic therapy: A review. *Stem Cells 18*: 10–18.

Marquez, M., Nilsson, S., Lennartsson, L., Liu, Z., Tammela, T., Raitanen, M., and Holmberg, A.R. 2004. Charge-dependent targeting: Results in six tumor cell lines. *Anticancer Res. 24*: 1347–1352.

Melief, C.J., Toes, R.E., Medema, J.P., Van der Burg, S.H., Ossendorp, F., and Offringa, R. 2000. Strategies for immunotherapy of cancer. *Adv. Immunol. 75*: 235–282.

Netea, M.G., Van der Meer, J.W.M., and Kullberg, B-J. 2004. Toll-like receptors as an escape mechanism from host defense. *Trends Microbiol. 12*: 484–488.

Otton, R., and Curi, R. 2005. Toxicity of a mixture of fatty acids on human blood lymphocytes and leukaemia cell lines. *Toxicol. In Vitro 19*: 749–755.

Stoler, D.L., Chen, N., Basik, M., Kahlenberg, M.S., Rodriguez-Bigas, M.A., Petrelli. N.J., and Anderson, G.R. 1999. The onset and extent of genomic instability in sporadic colorectal tumor progression. *Proc. Natl. Acad. Sci. USA 96*: 15121–15126.

Strickler, H.D., Wylie-Rosett, J., Rohan, T., Hoover, D.R., Smoller, S., Burk, R.D., and Yu, H. 2001. The relation of type 2 diabetes and cancer. *Diabetes Technol. Ther. 3*: 263–274.

Szathmary, S. 2005. Immunomodulation of pathogen-host interactions, PhD Thesis, Szent Istvan University, Faculty of Veterinary Medicine, Budapest, Hungary.

Thun, M.J., Namboodiri, M.M., and Heath, C.W. Jr. 1991. Aspirin use and reduced risk of fatal colon cancer. *N. Engl. J. Med. 325*: 1593–1596.

Tirapu, I., Mazzolini, G., Rodriguez-Calvillo, M., Arina, A., Palencia, B., Gabari, I., and Melero, I. 2002. Effective Tumor Immunotherapy: start the engine, release the brakes, step on the gas pedal, and get ready to face autoimmunity. *Arch. Immunol. Ther. Exp. 50*: 13–18.

Trosko, J.E. and Rauch, R.J. 1998. Cell-cell communication in carcinogenesis. *Front. Biosci. 3*: 208–236.

Trousseau, A. 1865. Phlegmasia alba dolens. In: Clinique Medicale de l'Hotel -Dieu de Paris, vol. 3, 2nd edn. Balliere, Paris: 654–712.

Tyler, K.L., and Fields, B.N. 1996. Pathogenesis of viral infections. In: Fields Virology, Fields B.N., Knipe D.M., Howley P.M. Eds. Philadelphia, Lippincott-Raven: 173–203.

Worthington, V. 2002. Analyzing data to compare nutrients in conventional versus organic crops. *J. Altern. Complement Med. 8*: 529–532.

10
Successful Cancer Treatment: Eradication of Cancer Stem Cells

David Dingli and Jorge M. Pacheco

INTRODUCTION

The increasing incidence of cancer in many countries is a consequence of our success as a species. Otherwise, cancer would be a rare event. This is no accident, and its justification can be found at the root of the evolution of multicellular organisms. Indeed, the emergence of multicellular organisms required coordination and cooperation between cells that became increasingly specialized resulting in an overall benefit for the organism. Multicellularity also brings with it the risk of cancer, viewed as the deregulated proliferation of a new and particular cell-type population that can threaten the integrity and survival of the organism (Hanahan and Weinberg, 2000).

Studies during the last 40–50 years have shown that cancer is an acquired genetic disorder due to mutations that activate proto-oncogenes, silence tumor suppressor genes or induce genomic instability (Vogelstein and Kinzler, 2004). Genetic mutations can be due to exogenous genotoxic agents such as ionizing radiation or chemotherapeutic agents that interact with DNA. However, the genome replication machinery is also prone to errors that inevitably result in mutations being incorporated in cells (Kunkel and Bebenek, 2000). Hence, individuals with mutations in DNA-repair enzymes have an intrinsically higher risk of cancer.

TISSUE ORGANIZATION AND STEM CELLS

The path selected throughout evolution to mitigate the risk of persistent mutations in tissues led to a hierarchic architecture where the majority of cells have a limited life-span and are continuously being replaced (Nowak *et al.*, 2003). Tissue integrity is maintained by relatively small populations of long lived cells that replicate at a relatively slow pace. This architectural organization is present in all epithelia (skin, respiratory, and gastrointestinal tract) and in the hematopoietic system (Figure 10.1). These constitute the most common sites for tumor development in humans. Indeed, all tissues exposed to the external environment with its genotoxic agents exhibit high cell turnover. Every tissue is composed of a variety of cell types which together give the tissue its specific structure and function. At the

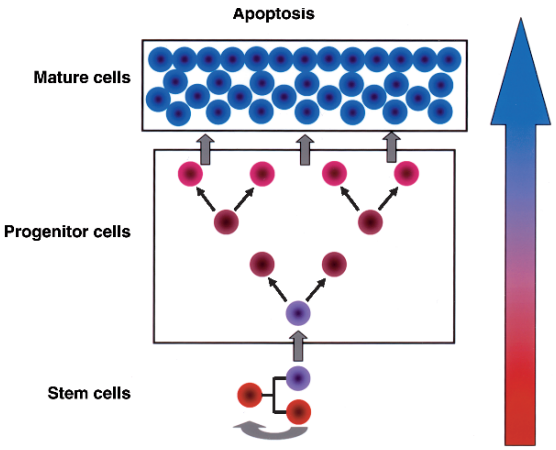

FIGURE 10.1. Normal tissue architecture. The majority of cells in epithelia are short lived and die by apoptosis or are shed. Tissue integrity is maintained by the slow replication of tissue specific stem cells that give rise to progenitor cells that proliferate for a short period of time to produce differentiated cells. Many tumors have a similar hierarchical organization with cancer stem cells responsible for the maintenance of the tumor

root of this tree there is a small population of cells: these are the stem cells (SC). Tissue specific SC are defined by two properties: a capacity for long-term self-renewal to maintain their own population, and their ability to differentiate into various types of specific cells that are found in any given tissue. The best studied SC are those present in the hematopoietic system, although our knowledge regarding skin and gastrointestinal stem cells is increasing rapidly. Stem cells not only provide a mechanism for maintenance of the tissue but are also required for repair after injury (e.g., trauma including surgery, bleeding, chemotherapy, and transplantation).

Tissue specific SC are only a very small fraction of all tissue-specific cell types, being organized within micro environments known as SC niches (Moore and Lemischka, 2006; Scadden, 2006). The niche is a complex structure composed of cytokines and growth factors, extracellular stroma, and supporting cells that, depending on location, may include osteoblasts, fibroblasts and other mesenchymal cells, cells of the monocyte lineage, and immune system cells (Moore and Lemischka, 2006). Stem cell behavior is heavily influenced by the particular niche in which they reside. Current thinking suggests that the interaction between intracellular genetic and epigenetic factors within the SC coupled with extracellular stimulation from the surrounding niche determine the fate of a specific SC, including its rate of replication, (a)symmetry of division and survival. The number of SC present in any given niche is not known and may be variable depending on the site (location) and state (function) of the niche. For example, a colonic crypt has an estimated number between 1 to 10 SC that are responsible for the maintenance of each crypt.

In the absence of an external genotoxic agent, the main cause of genetic mutations is the intrinsic error rate of the DNA replication machinery (Kunkel and Bebenek, 2000). In such a case, a small pool of SC that replicate slowly serve to minimize the risk of acquiring mutations that would persist in the progeny cell population.

EVIDENCE FOR CANCER STEM CELLS

The neoplastic cells that define the origin of the tumor (e.g., epithelial, mesenchymal etc) require the support of a stroma that provides the vascular supply and scaffolding on which the tumor cells grow. Moreover, it is becoming increasingly

clear that even within the neoplastic population, there is an underlying functional hierarchy (architecture) with tumor cells exhibiting various stages of differentiation and survival. Based on this observation, the existence of cancer stem cells (CSC) was initially postulated almost 50 years ago to explain the heterogeneous population of tumor cells. Recent studies using clonogenic assays and flow cytometric cell sorting of established tumor cell lines or human tumors explanted at surgery show that not all cancer cells are created equal. Similar to normal tissues, in any given tumor only a small fraction of cells have long term self-renewal capability and can engraft to form tumor xenografts when implanted into receptive immunodeficient hosts. Tumor cells that have these two capabilities are known as CSC (or cancer initiating cells) and are the subject of intense research (Clarke *et al*., 2006). Initially, CSC were identified in hematopoietic neoplasms such as acute myeloid leukemia (AML) (Lapidot *et al*., 1994). However, to date, CSC have been reported in tumors from the breast (Al-Hajj *et al*., 2003), gastrointestinal tract (O'Brien *et al*., 2007; Ricci-Vitiani *et al*., 2007), lung (Kim *et al*., 2005), prostate (Gu *et al*., 2007), pancreas (Li *et al*., 2007), brain (Singh *et al*., 2004), liver (Suetsugu *et al*., 2006), malignant melanoma (Monzani *et al*., 2007) and multiple myeloma (Matsui *et al*., 2004). Injection of a single breast CSC (LA7) in the foot pad of NOD/SCID mice efficiently induces the growth of mammary tumors in these animal models. The tumors have a complex architecture compatible with differentiation of the progeny cells, and demonstrate both the proliferative potential of these cells as well as the clonal nature of cancer (Zucchi *et al*., 2007). Given the increasing recognition of tumor specific SC, it is not surprising that the current hypothesis is that the majority and perhaps all tumors have CSC at their root to maintain the growing tumor population (Reya *et al*., 2001).

ORIGIN OF CANCER STEM CELLS

A fundamental question in carcinogenesis is the origin of the CSC (Reya *et al*., 2001). In principle, these cells can arise either by the malignant transformation of normal SC, or more differentiated cells can acquire SC – like properties. The favored hypothesis has been that CSC arise due to mutations within the most primitive SC (Wang and Dick, 2005). Because normal SC already have self-renewal capability, a *sine qua non* for the development of the tumor (Hanahan and Weinberg, 2000), CSC originating from mutations of normal SC may free-ride on the self-renewal capacity while expressing the malignant phenotype (Wang and Dick, 2005), and are thus thought to require fewer mutations to reach the malignant phenotype. If the origin of the tumor is within more differentiated progenitor cells, then acquisition of SC-like properties (including unlimited self-renewal) must be an early event in the process of malignant transformation, otherwise the mutant cells would be washed out before significant expansion of the clone could occur. However, there is evidence for the reacquisition of 'SC-like' properties in more committed progenitor cells, depending on the type of tumor and the mutations that drive its evolution and expansion (Huntly *et al*., 2004; Krivtsov *et al*., 2006). It has been

shown that *MOZ-TIF2* expression can confer sustained self-renewal in hematopoietic progenitor cells, but *BCR-ABL* cannot induce long-term self-renewal in the same cell population. However, it is known that chronic myeloid leukaemia (CML) arises by mutation of normal SC. Expression of the *bcr-abl* oncoprotein may be enough to explain the behaviour of the myeloid cells necessary to induce the chronic phase of the disease (Michor *et al.*, 2006). Subsequently, the development of CML blast crisis is associated with the emergence of a new SC that has its origin in CFU-GM cells (Jamieson *et al.*, 2004). In the case of colon cancer, the cell population at risk of neoplastic transformation is thought to be restricted to the (normal) SC that maintain the colonic crypts (Tomlinson *et al.*, 2002). Here mutations in the *APC* gene may be an early event in the path to malignant transformation.

STOCHASTIC DYNAMICS OF CANCER STEM CELLS

It has been the general impression that many of the cancer inducing mutations give an advantage to the tumor (stem) cells by enhancing either proliferation or increasing resistance to apoptosis (Hanahan and Weinberg, 2000; Vogelstein and Kinzler, 2004). In terms of evolutionary dynamics, such mutations give the cell a higher reproductive fitness ($r > 1$) compared to the (normalized to 1) fitness of normal SC. Cells with a higher fitness give rise to a larger number of progeny since they are selected for reproduction more often. If the population of SC were infinite, this would inevitably lead to the extinction of normal SC, that is, invasion of the entire population by CSC. However, given that the size of the SC pool is often small, stochastic effects become relevant. As a consequence, while a mutation that leads to higher reproductive fitness increases the probability that the mutant clone will expand in size and take over the whole population, such an increase does not guarantee invasion. Stochastic considerations show that extinction, latency, or invasion (complete dominance) by the mutant clone is possible during the finite lifetime of the individual (Figure 10.2). It is pointed out that for an infinite lifetime there are only two possible outcomes (absorbing states): either clonal extinction or complete invasion by the mutant cells. However, often these limiting scenarios are not met in practice, because all living systems have a finite lifetime that scales allometrically with mass (Lopes *et al.*, 2007). Even when the relative advantage of CSC is $r = 2$, considered by many to be a very large advantage (Tomlinson *et al.*, 2002), there is a 50% probability that such a clone will die out rather than expand

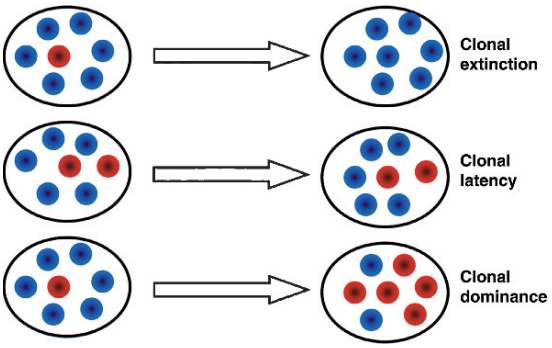

FIGURE 10.2. Stochastic stem cell dynamics. Whenever the pool of stem cells is small, stochastic effects become important. Among the different possible scenarios, three possibilities are detailed, given their experimental realization: extinction of the mutant clone, clonal latency or clonal expansion to cause disease

and take over the compartment where it arises (Dingli *et al*., 2007c). Similarly, it can be shown that a mutation in the SC need not confer a fitness advantage to that cell for the clone to expand. Neutral drift may be enough to expand the population to a size that may be clinically significant (Dingli *et al*., 2007c). This theoretical conclusion may explain several observations in CML where it is thought that the *bcr-abl* oncogene does not give an advantage to the CML SC themselves but only to progenitors further downstream. In such a case, expansion of the CML SC occurs only by neutral drift and perhaps is one reason why the pool of cells driving this disease is so small (Dingli *et al*., 2007b). Moreover, gene expression studies in putative AML SC show that the cells up-regulate two important tumor suppressor genes (interferon regulatory factor 1, IRF-1 and death associated protein kinase, DAPK) that act to suppress proliferation of the malignant SC (Guzman *et al*., 2001b). In other words, these mutations do not necessarily confer to the AML SC an enhanced reproductive fitness. However, they may provide an advantage to downstream progenitors that drive the disease. If this hypothesis is true, it would further support that the number of SC driving a AML is small because their number will increase due to neutral drift as in CML (Dingli *et al*., 2007c). Finally, under stochastic evolutionary dynamics a mutant clone can appear 'stable' for a long time even if the mutation provides a fitness advantage (Dingli *et al*., 2007c). These features are supported by clinical observations from patients with essential thrombocythemia where $JAK2^{V617F}$ clones that remain stable for extended periods of time have been observed (Gale *et al*., 2006).

Stochastic SC dynamics (normal as well as malignant) also show that the time required by a mutant clone to reach a given fraction of the SC pool is highly variable and depends on the fitness provided by the mutation. For any tumor, it is reasonable to assume that the mutant clone must reach a certain fraction for the disease to appear. Simulations of the dynamics of such a population provide data for time probability distributions as a function of fitness. The shapes of such time probability distributions are one humped, but they can be very broad, the width depending on the relative fitness advantage of mutated cells. With increasing fitness advantage these curves become narrower, but the underlying stochastic behavior of these cells (Dingli *et al*., 2007c) will always lead to a range of times during which the process can occur.

Given the widespread impression that cancer inducing mutations give an advantage to the cell, perhaps extinction of tumor SC or tumors would be considered an impossible clinical scenario or simply a theoretical concept. Such conventional wisdom, however, disregards the impact of stochastic effects on the dynamics of SC populations. As discussed before, the probability that a given clone will be eliminated depends on the size it acquires (Dingli *et al*., 2007c). Hence, subclinical clones are more likely to be eliminated while the probability that a clinically evident tumor will undergo spontaneous extinction is small. Again, clinical observations (although rare) show that well established clonal disorders that can threaten the life of the individual can go extinct, even with minimal or no therapy. Perhaps the best example of this is transient myeloproliferative disorder (TMD) seen in patients with Downs' syndrome soon after birth

(Massey *et al*., 2006). Patients with this disease may have very high circulating blast counts (high disease burden that may be life threatening), and yet in almost 85% of these patients, the disorder disappears without recurrence. To date, no explanation has been proposed for this well documented clinical phenomenon, but we propose that stochastic clonal elimination provides the required mechanism. Another example where stochastic tumor extinction may be possible is in the myelodysplastic syndromes where spontaneous resolution has been reported, although this seems to happen quite rarely (Tricot *et al*., 1986).

Stem cells can divide to give rise to two daughter cells that have the same (symmetric division) or different (asymmetric division) fate. A mutation that increases the probability of SC self-renewal, confers a higher reproductive fitness to these cells similar to a scenario where they are selected to reproduce more often. Such mutations (e.g., *adenomatous polyposis coli*, APC) enable the mutant cell to efficiently expand within its environment. An increase in the size of the population of cells at risk increases the probability of acquisition of additional mutations facilitating the full development of the malignant transformation (Dingli *et al*., 2007a).

MARKERS OF CANCER STEM CELLS

As already alluded to, the number of cancer initiating (clonogenic) cells in a given tumor is usually very small, often $< 2\%$ based on flow cytometric cell sorting. The initial screen for these cells is based on their ability to exclude fluorescent DNA binding dyes such as rhodamine or Hoechst 33342. As a result, SC exhibit very low fluorescence with these dyes and appear as negatively stained cells to the side of the majority of cells in a density dot plot; hence, the name 'side population'. Even then, these highly purified cell populations are probably themselves heterogeneous, and it has been shown that acute leukaemia can be induced by the injection of < 100 highly purified cells (Clarke *et al*., 2006). We have recently estimated that for the classic hematopoietic SC disorder CML, perhaps 1–8 active cancer SC may be enough to drive the disease during the chronic phase (Dingli *et al*., 2007b). The small number of cells creates technical difficulties in the identification of cancer SC specific markers that perhaps will be suitable targets for therapy (see below). This notwithstanding, several cell surface markers seem to be over-expressed by these cancer SC. CD133 (prominin-1) recently has been identified on several of the putative cancer SC (Neuzil *et al*., 2007). Prominin-1 is a cell-surface glycoprotein that spans the plasma membrane five times and is expressed in all metazoans. Initially described on hematopoietic SC, it was found to be expressed in normal and malignant SC, although the latter tend to over-express the protein on their surface (Neuzil *et al*., 2007). Another proposed marker is CD44 that is over-expressed by prostate and pancreatic cancer cells as well as leukemic SC (Jin *et al*., 2006). CD44 is a receptor for hyaluronic acid or chondroitin sulfate while variants of this protein can bind to fibronectin, laminin, and collagen (Ponta *et al*., 2003). Prostate cancer SC have the phenotype $CD44^{+}/\alpha_2\beta_1^{hi}/CD133^{+}$ (Collins *et al*., 2005), while brain tumor SC are often $CD133^{+}$/musashi-1^{+}/$nestin^{+}$ (Vescovi *et al*.,

2006). Normal breast SC have the phenotype $Lin^-/CD29^{hi}/CD24^+$ (Shackleton *et al*., 2006), while breast cancer SC have the phenotype $CD44^+/CD24^{-/low}/Lin^-$ (Al-Hajj *et al*., 2003). Pancreatic cancer SC have the phenotype $CD44^+/Cd24^+/ESA^+$ and seem to express CD133, at least at the level of mRNA (Olempska *et al*., 2007).

In the case of tumors derived from the hematopoietic system, characterization of the immunophenotype of putative cancer SC markers has identified several potential antigens. Acute myeloid leukaemia (AML) SC often express CD123, the α chain of the interleukin-3 receptor (Jordan *et al*., 2000). Other putative markers for AML SC include CD33 (Taussig *et al*., 2005) and CD44 (Jin *et al*., 2006), although these are also expressed, albeit at low levels, on normal hematopoietic stem and progenitor cells. There is a growing consensus that AML SC have the phenotype $CD34^+/CD38^-/CD71^-/CD90^-/CD117^-/CD123^+/HLA\text{-}DR^-$ irrespective of the subtype (Jordan, 2002). While some of these markers are shared with normal SC, CD90, CD117, and CD123 are thought to be fairly specific for the malignant cells. More recently, the C-type lectin like molecule-1 (CLL-1) has been identified on AML but not normal hematopoietic stem and progenitor cells (Van Rhenen *et al*., 2007). Injection of $CD34^+/CD38^-/CLL\text{-}1^+$ cells isolated from patients with AML into NOD/SCID mice led to the development of leukaemia, although serial transplantation was not performed. The majority of malignant plasma cells normally do not express CD20, the target for rituximab, but clonogenic cells isolated from highly purified multiple myeloma cell samples express this therapeutically relevant target (Matsui *et al*., 2004).

TREATING CANCER STEM CELLS

Current chemotherapy is often successful in eliminating the bulk of the malignant cell population; however, often the tumor returns. Several, non-mutually exclusive explanations have been proposed to explain disease recurrence including selection for chemotherapy resistant cells (due to mutation) and the presence of cancer SC that are not eliminated by therapy. However, it is also a fact that many patients have been cured of cancer with current chemotherapy alone. Operationally, successful cancer therapy can be defined as long-term survival without evidence of disease recurrence. To our knowledge, no one has shown that curative therapy requires or is associated with complete elimination of all tumor cells from within the body because currently there are no techniques that can reliably prove this point. However, given the present understanding of the importance of CSC for the development and maintenance of the tumor, it makes sense to consider this population of cells as important targets of therapy that could translate into higher cure rates.

Using mathematical models where tumor growth is maintained by a CSC compartment, it was shown that therapy directed at the more differentiated cancer cells will not be able to cure the cancer (Dingli and Michor, 2006). In this theoretical scenario, therapeutic agents that completely stop CSC replication could in principle operationally cure the tumor (but this can take a very long time). It was shown that only agents that actively kill the CSC and the bulk of the tumor cells will effectively cure the disease in a reasonable time frame.

Genomic instability is an important characteristic of cancer that may occur early in the disease process (Bielas *et al*., 2006). A higher mutation rate increases the risk of acquired drug resistance; therefore rapid elimination of the CSC pool seems a desirable goal (Dingli and Michor, 2006).

Problems with Targeting Cancer Stem Cells

There are several hurdles that hinder therapeutic approaches designed to eliminate neoplastic SC. It is likely that the number of cancer SC responsible for tumor growth and maintenance is quite small (Dingli *et al*., 2007b). For example, we estimate that between 1 and 8 cancer SC may be enough to fuel the chronic phase of CML. The small number of these cells and mass action considerations suggest that it is very difficult to effectively reach therapeutically this critically important cell compartment. Often these cells replicate slowly and at any time, the vast majority of them are in G_0 and, therefore, insensitive to all cell-cycle specific agents (Dean *et al*., 2005). It is also becoming increasingly clear that adhesion to the SC niche itself affords protection from the effects of chemotherapy. Moreover, cancer SC, like their normal counterparts, express multi-specific drug efflux pumps on their plasma membrane that effectively protect them from chemotherapeutic and other genotoxic chemicals. Among these membrane proteins, those that belong to the ATP binding cassette (ABC) such as *ABCB1*, also known as *MDR1* or P-glycoprotein, and *ABCG2* seem to be particularly important. These proteins have broad substrate specificities and couple ATP hydrolysis with drug efflux to the outside of the cell against a chemical gradient (Dean *et al*., 2005). Another mechanism of drug resistance is the intrinsic ability of SC to repair DNA damage. Finally, it has been shown that at least in CML, neoplastic SC that harbour the Philadelphia chromosome, do not even express *bcr-abl*, and therefore are not dependent on this mutation for their survival (Holyoake *et al*., 1999). However, such cells cannot be sensitive to imatinib mesylate.

Safe elimination of CSC requires that there is minimal toxicity to non-malignant stem and progenitor cells that maintain normal tissues. Thus, suitable targets must be identified that provide as wide a therapeutic index as possible between the normal and malignant cells. Recent studies suggest that this might be possible. Most of the evidence is based on studies in hematopoietic neoplasms. Primitive AML cells express an active form of the nuclear factor kappa B (NF-κB) independent of their cell cycle status (Guzman *et al*., 2001a). In these cells, NF-κB plays an important role in preventing apoptosis. However, NF-κB is not expressed by normal SC and therefore, provides an exciting target for therapy. There is also encouraging data regarding the role of NF-κB in preventing apoptosis in other neoplasms such as lymphoma and in malignant melanoma, non-small cell lung cancer and pancreatic carcinoma (Jordan, 2002).

Overcoming Drug Resistance

With the recognition of the ABC transporters and their role in drug resistance, several agents have been tested to block the function of these proteins. The calcium channel blocker verapamil was studied in various tumors and did show some activity in patients with breast (Belpomme *et al*., 2000) and non-small cell lung cancer (Millward *et al*.,

1993), although it did not provide any benefit in multiple myeloma (Dalton *et al*., 1995). The drug had low potency and was often poorly tolerated due to hypotension. Cyclosporine A did not improve the efficacy of VAD chemotherapy in patients with advanced multiple myeloma (Sonneveld *et al*., 2001). Moreover, the drug is plagued by a multitude of potentially serious drug-drug interactions as well as nephrotoxicity that limit its use. More recently, several 'second generation' ABC transporter inhibitors have been developed (Dean *et al*., 2005). Some inhibitors such as zosuquidar have been tested in clinical trials and results are awaited.

Evidence for Effective Anti-Cancer Stem Cell Therapy

If we consider that all tumors are maintained by neoplastic SC, then one cannot but conclude that there are occasions when chemotherapy seems to eliminate these cells since many patients with advanced cancer have been cured. There are many examples from acute leukaemia to testicular cancer and Hodgkin and non-Hodgkin lymphoma. All of these diseases are typically advanced when treated with chemotherapy and many patients have been cured. In CML, there are patients that have been treated with interferon alone that not only lost the Philadelphia chromosome but seem to be in remission for many years, even after stopping interferon therapy and perhaps some have been cured. Recently, Van Rhenen *et al*. (2007) showed that patients with AML have a side population of cells that express CLL-1. If chemotherapy leads to eradication of these cells, the patients experience long remissions. However, if these cells are not eradicated by chemotherapy, patients experience very rapid relapse.

Various strategies to eliminate these cells have been implemented or are currently being tested in clinical trials. Experiments in relevant animal models have explored the use of specific targets to eliminate the tumor SC population. Several groups have evaluated the potential use of surface antigens as therapeutic targets for monoclonal antibodies or fusion proteins. Jin *et al*. (2006) showed that a monoclonal antibody directed at CD44, that is often expressed by AML SC, can prevent the development of disease in serially transplanted mice. A monoclonal anti-CD33 antibody, gemtuzumab, is available and has been used in patients with $CD33^+$ AML, but it can have significant toxicity and is associated with marrow suppression probably because even normal hematopoietic SC and recovering progenitor cells express this antigen. Another approach currently under investigation is to target CD123 by a fusion protein between IL-3 and diphtheria toxin (Cohen *et al*., 2005). The initial studies with this agent suggest that therapeutically meaningful serum concentrations can be achieved, although it induced myelosuppression as well as vasculitis in female cynomolgus monkeys.

As discussed before, it appears that malignant SC depend on NF-κB to prevent apoptosis while normal SC do not express this nuclear factor. Intracellular signalling by NF-κB is blocked by the inhibitor of κB (IκB). Thus, prevention of IκB degradation by proteasome inhibition was evaluated in combination with idarubicin. This strategy led to apoptosis of AML SC in culture (Guzman *et al*., 2001a) with a considerable decrease in NOD/SCID repopulating cells (Guzman *et al*., 2002). Importantly, the same treatment did not harm normal SC suggesting that this approach may be effective and safe.

The Future

Despite the lack of efficacy of initial ABC transporter inhibitors, the combined use of second and third generation agents holds promise, because some of these novel agents can block multiple transporters simultaneously and will soon enter clinical trials (for a recent review, see Dean *et al*., 2005). Agents such as Ko143 and GF120918 seem to inhibit both ABCB1 and ABCG2 (Cisternino *et al*., 2004). They may enhance CSC eradication when combined with drugs such as the anthracyclines. Parthenolide is a natural sesquiterpene lactone and the major active component in feverfew, a product of *Tanacetum parthenium*. The drug has broad antitumor activity because it inhibits DNA synthesis, sensitizes tumor cells to other anti-tumor agents and is a potent inhibitor of NF-κB. In addition, it enhances production of reactive oxygen species and interferes with signaling from key tumor associated pathways including signal transducers and activators of transcription 3 (STAT3), and c-Jun N-terminal kinase activation (Jordan, 2007). The drug has potent activity against both blast crisis CML and AML progenitor and SC populations and significantly inhibit NOD/SCID repopulating cell growth. At the same time, the agent had no significant detrimental effect on normal SC and progenitor cells suggesting that it may be fairly specific to tumor cells. A water soluble derivative of this compound is under development. More recently, TDZD-8 was identified as another potent inhibitor of NF-κB with selective activity against AML SC (Jordan, 2007).

Monoclonal antibodies directed against CSC specific markers are also under development and results are expected soon. In one study, the putative myeloma SC is being targeted with rituximab, an anti-CD20 antibody. The advent of antibodies against CLL-1 will surely drive studies for disease eradication in AML. Finally, the last few years have ushered in the era of genomics. The technology is now available for genome wide searches for CSC specific defects that could be the targets of therapy. This approach holds great promise for the development of safe and effective cancer curing therapies. To this end, mathematical models of tumor development incorporating essential realistic features of the neoplasms may prove insightful towards a full understanding of the origin and evolution of these disorders.

It is concluded that curative therapy for any disease relies on a proper understanding of the underlying mechanisms that drive that disorder. During the last few years, our understanding of tumor growth and evolution has been transformed by the discovery of CSC. They are rapidly emerging as the preferential target of antitumor therapy. Cancer stem cell specific markers, either on their surface or within the inner workings of the cell are being identified that will provide many potential therapeutic targets to increase cure rates for this group of diseases.

REFERENCES

Al-Hajj, M., Wicha, M.S., Benito-Hernandez, A., Morrison, S.J., and Clarke, M.F. 2003. Prospective identification of tumorigenic breast cancer cells. *Proc. Natl. Acad. Sci. USA 100*: 3983–3988.

Belpomme, D., Gauthier, S., Pujade-Lauraine, E., Facchini, T., Goudier, M.J., Krakowski, I., Netter-Pinon, G., Frenay, M., Gousset, C., Marie, F.N., Benmiloud, M., and Sturtz, F. 2000. Verapamil increases the survival of patients with anthracycline-resistant metastatic breast carcinoma. *Ann. Oncol. 11*: 1471–1476.

Bielas, J.H., Loeb, K.R. Rubin, B.P., True, L.D., and Loeb, L.A. 2006. From the cover: Human cancers express a mutator phenotype. *Proc. Natl. Acad. Sci. USA 103*: 18238–18242.

Cisternino, S., Mercier, C., Bourasset, F., Roux, F., and Scherrmann, J.M. 2004. Expression, up-regulation, and transport activity of the multi-drug-resistance protein Abcg2 at the mouse blood-brain barrier. *Cancer Res. 64*: 3296–3301.

Clarke, M.F., Dick, J.E., Dirks, P.B., Eaves, C.J., Jamieson, C.H., Jones, D.L., Visvader, J., Weissman, I.L., and Wahl, G.M. 2006. Cancer Stem Cells–Perspectives on Current Status and Future Directions: AACR Workshop on Cancer Stem Cells. *Cancer Res. 66*: 9339–9344.

Cohen, K.A., Liu, T.F., Cline, J.M., Wagner, J.D., Hall, P.D., and Frankel, A.E. 2005. Safety evaluation of DT388IL3, a diphtheria toxin/interleukin 3 fusion protein, in the cynomolgus monkey. *Cancer Immunol. Immunother. 54*: 799–806.

Collins, A.T., Berry, P.A., Hyde, C., Stower, M.J., and Maitland, N.J. 2005. Prospective identification of tumorigenic prostate cancer stem cells. *Cancer Res. 65*: 10946–10951.

Dalton, W.S., Crowley, J.J., Salmon, S.S., Grogan, T.M., Laufman, L. R., Weiss, G.R., and Bonnet, J.D.1995. A phase III randomized study of oral verapamil as a chemosensitizer to reverse drug resistance in patients with refractory myeloma. A Southwest Oncology Group study. *Cancer 75*: 815–820.

Dean, M., Fojo, T., and Bates, S. 2005. Tumour stem cells and drug resistance. *Nat. Rev. Cancer 5*: 275–284.

Dingli, D., and Michor, F. 2006. Successful therapy must eradicate cancer stem cells. *Stem Cells 24*: 2603–2610.

Dingli, D., Traulsen, A., and Michor, F. 2007a. (A)Symmetric stem cell replication and cancer. *PLoS Comput. Biol. 3*: e53.

Dingli, D., Traulsen, A., and Pacheco, J.M. 2007b. Chronic myeloid leukemia: origin, development, response to therapy, and relapse. *Clinical Leukemia* (In Press).

Dingli, D., Traulsen, A., and Pacheco, J.M. 2007c. Stochastic dynamics of hematopoietic tumor stem cells. *Cell Cycle 6*: 441–446.

Gale, R.E., Allen, A.J., Nash, M.J., and Linch, D.C. 2006. Long-term serial analysis of X-chromosome inactivation patterns and JAK2 V617F mutant levels in patients with essential thrombocythemia show that minor mutant-positive clones can remain stable for many years. *Blood 109*: 1241–1243.

Gu, G., Yuan, J., Wills, M., and Kasper, S. 2007. Prostate cancer cells with stem cell characteristics reconstitute the original human tumor in vivo. *Cancer Res. 67*: 4807–4815.

Guzman, M.L., Neering, S.J., Upchurch, D., Grimes, B., Howard, D.S., Rizzieri, D.A., Luger, S.M., and Jordan, C.T. 2001a. Nuclear factor-kappaB is constitutively activated in primitive human acute myelogenous leukemia cells. *Blood 98*: 2301–2307.

Guzman, M.L., Upchurch, D., Grimes, B., Howard, D.S., Rizzieri, D.A., Luger, S.M., Phillips, G.L., and Jordan, C.T. 2001b. Expression of tumor-suppressor genes interferon regulatory factor 1 and death-associated protein kinase in primitive acute myelogenous leukemia cells. *Blood 97*: 2177–2179.

Guzman, M.L., Swiderski, C.F., Howard, D.S., Grimes, B.A., Rossi, R.M., Szilvassy, S.J., and Jordan, C.T. 2002. Preferential induction of apoptosis for primary human leukemic stem cells. *Proc Natl Acad Sci USA 99*: 16220–16225.

Hanahan, D., and Weinberg, R.A. 2000. The hallmarks of cancer. *Cell 100*: 57–70.

Holyoake, T., Jiang, X., Eaves, C., and Eaves, A. 1999. Isolation of a highly quiescent subpopulation of primitive leukemic cells in chronic myeloid leukemia. *Blood 94*: 2056–2064.

Huntly, B.J., Shigematsu, H., Deguchi, K., Lee, B.H., Mizuno, S., Duclos, N., Rowan, R., Amaral, S., Curley, D., Williams, I.R., Akashi, K., and Gilliland, D.G. 2004. MOZ-TIF2, but not BCR-ABL, confers properties of leukemic stem cells to committed murine hematopoietic progenitors. *Cancer Cell 6*: 587–596.

Jamieson, C.H., Ailles, L.E., Dylla, S.J., Muijtjens, M., Jones, C., Zehnder, J.L., Gotlib, J., K. Li, Manz, M.G., Keating, A., Sawyers, C.L., and Weissman, I.L. 2004. Granulocyte-macrophage progenitors as candidate leukemic stem cells in blast-crisis CML. *N. Engl. J. Med. 351*: 657–667.

Jin, L., Hope, K.J., Zhai, Q., Smadja-Joffe, F., and Dick. J.E. 2006. Targeting of CD44 eradicates human acute myeloid leukemic stem cells. *Nat. Med.12*: 1167–1174.

Jordan, C.T. 2002. Unique molecular and cellular features of acute myelogenous leukemia stem cells. *Leukemia 16*: 559–562.

Jordan, C.T. 2007. The leukemic stem cell. *Best Pract. Res. Cl. Ha. 20*: 13–18.

Jordan, C.T., Upchurch, D., Szilvassy, S.J., Guzman, M.L., Howard, D.S., Pettigrew, A.L., Meyerrose, T., Rossi, R., Grimes, B., Rizzieri, D.A., Luger, S.M., and Phillips, G.L. 2000. The interleukin-3 receptor alpha chain is a unique marker for human acute myelogenous leukemia stem cells. *Leukemia 14*: 1777–1784.

Kim, C.F., Jackson, E.L., Woolfenden, A.E., Lawrence, S., Babar, I., Vogel, S., Crowley, D., Bronson, R.T., and Jacks, T. 2005. Identification of bronchioalveolar stem cells in normal lung and lung cancer. *Cell 121*: 823–835.

Krivtsov, A.V., Twomey, D., Feng, Z., Stubbs, M.C., Wang, Y., Faber, J., Levine, J.E., Wang, J., Hahn, W.C., Gilliland, D.G., Golub, T.R., and Armstrong, S.A. 2006. Transformation from committed progenitor to leukaemia stem cell initiated by MLL-AF9. *Nature 442*: 818–822.

Kunkel, T.A., and Bebenek, K. 2000. DNA replication fidelity. *Annu. Rev. Biochem. 69*: 497–529.

Lapidot, T., Sirard, C., Vormoor, J., Murdoch, B., Hoang, T., Caceres-Cortes, J., Minden, M., Paterson, B., Caligiuri, M.A., and Dick, J.E. 1994. A cell initiating human acute myeloid leukaemia after transplantation into SCID mice. *Nature 367*: 645–648.

Li, C., Heidt, D.G., Dalerba, P., Burant,C.F., Zhang, L., Adsay, V., Wicha, M., Clarke, M.F., and Simeone, D.M. 2007. Identification of pancreatic cancer stem cells. *Cancer Res. 67*: 1030–1037.

Lopes, J.V., Pacheco, J.M., and Dingli, D. 2007. Mammalian size and the risk of acquiring hematopoietic stem cell disorders. *Under review*.

Massey, G.V., Zipursky, A., Chang, M.N., Doyle, J.J., Nasim, S., Taub, J.W., Ravindranath, Y., Dahl, G., and Weinstein, H.J. 2006. A prospective study of the natural history of transient leukemia (TL) in neonates with Down syndrome (DS): Children's Oncology Group (COG) study POG-9481. *Blood 107*: 4606–4613.

Matsui, W., Huff, C.A., Wang, Q., Malehorn, M.T., Barber, J., Tanhehco, Y., Smith, B.D., Civin, C.I., and Jones, R.J. 2004. Characterization of clonogenic multiple myeloma cells. *Blood 103*: 2332–2336.

Michor, F., Iwasa, Y., and Nowak, M.A. 2006. The age incidence of chronic myeloid leukemia can be explained by a one-mutation model. *Proc. Natl. Acad. Sci. USA 103*: 14931–14934.

Millward, M.J., Cantwell, B.M., Munro, N.C., Robinson, A., Corris, P.A., and Harris, A.L. 1993. Oral verapamil with chemotherapy for advanced non-small cell lung cancer: a randomised study. *Br. J. Cancer 67*: 1031–1035.

Monzani, E., Facchetti, F., Galmozzi, E., Corsini, E., Benetti, A., Cavazzin, C., Gritti, A., Piccinini, A., Porro, D., Santinami, M., Invernici, G., Parati, E., Alessandri, G., and La Porta, C.A. 2007. Melanoma contains CD133 and ABCG2 positive cells with enhanced tumourigenic potential. *Eur. J. Cancer 43*: 935–946.

Moore, K.A., and Lemischka, I.R. 2006. Stem cells and their niches. *Science 311*: 1880–1885.

Neuzil, J., Stantic, M., Zobalova,R., Chladova, J., Wang, X., Prochazka, L., Dong, L., Andera, L., and Ralph, S.J. 2007. Tumour-initiating cells vs. cancer 'stem' cells and CD133: what's in the name? *Biochem. Biophys. Res. Commun. 355*: 855–859.

Nowak, M.A., Michor, F., and Iwasa, Y. 2003. The linear process of somatic evolution. *Proc. Natl. Acad. Sci. USA 100*: 14966–14969.

O'Brien, C.A., Pollett, A., Gallinger, S., and Dick, J.E. 2007. A human colon cancer cell capable of initiating tumour growth in immunodeficient mice. *Nature 445*: 106–110.

Olempska, M., Eisenach, P.A., Ammerpohl, O., Ungefroren,H., Fandrich, F., and Kalthoff, H. 2007. Detection of tumor stem cell markers in pancreatic carcinoma cell lines. *Hepatobiliary Pancreat. Dis. Int. 6*: 92–97.

Ponta, H., Sherman, L., and Herrlich, P.A. 2003. CD44: from adhesion molecules to signalling regulators. *Nat. Rev. Mol. Cell. Biol. 4*: 33–45.

Reya, T., Morrison, S.J., Clarke, M.F., and Weissman, I.L. 2001. Stem cells, cancer, and cancer stem cells. *Nature 414*: 105–111.

Ricci-Vitiani, L., Lombardi, D.G., Pilozzi, E., Biffoni,M., Todaro, M., Peschle, C., and De Maria, R. 2007. Identification and expansion of human colon-cancer-initiating cells. *Nature 445*: 111–115.

Scadden, D.T. 2006. The stem-cell niche as an entity of action. *Nature 441*: 1075–1079.

Shackleton, M., Vaillant, F., Simpson, K.J., Stingl, J., Smyth, G.K., Asselin-Labat, M.L., Wu, L.,

Lindeman, G.J., and Visvader, J.E. 2006. Generation of a functional mammary gland from a single stem cell. *Nature 439*: 84–88.

Singh, S.K., Hawkins, C., Clarke, I.D., Squire, J.A., Bayani, J., Hide, T., Henkelman, R.M., Cusimano, M.D., and Dirks, P.B. 2004. Identification of human brain tumour initiating cells. *Nature 432*: 396–401.

Sonneveld, P., Suciu, S., Weijermans, P., Beksac, M., Neuwirtova, R., Solbu, G., Lokhorst, H., van der Lelie, J., Dohner, H., Gerhartz, H., Segeren, C.M., Willemze, R., and Lowenberg, B. 2001. Cyclosporin A combined with vincristine, doxorubicin and dexamethasone (VAD) compared with VAD alone in patients with advanced refractory multiple myeloma: an EORTC-HOVON randomized phase III study (06914). *Br. J. Haematol. 115*: 895–902.

Suetsugu, A., Nagaki, M., Aoki, H., Motohashi, T., Kunisada, T., and Moriwaki, H. 2006. Characterization of CD133+ hepatocellular carcinoma cells as cancer stem/progenitor cells. *Biochem. Biophys. Res. Commun. 351*: 820–824.

Taussig, D.C., Pearce,D.J., Simpson, C., Rohatiner, A.Z., Lister, T.A., Kelly, G., Luongo, J.L., Danet-Desnoyers, G.A., and Bonnet, D. 2005. Hematopoietic stem cells express multiple myeloid markers: implications for the origin and targeted therapy of acute myeloid leukemia. *Blood 106*: 4086–4092.

Tomlinson, I., Sasieni, P., and Bodmer, W. 2002. How many mutations in a cancer? *Am. J. Pathol. 160*: 755–758.

Tricot, G., Mecucci, C., and Van den Berghe, H. 1986. Evolution of the myelodysplastic syndromes. *Br. J. Haematol. 63*: 609–614.

Van Rhenen, A., Van Dongen, G.A., Kelder, A., Rombouts, E.J., Feller, N., Moshaver, B., Sigter-van Walsum, M., Zweegman, S., Ossenkoppele, G.J., and Schuurhuis, G.J. 2007. The novel AML stem cell associated antigen CLL-1 aids in discrimination between normal and leukemic stem cells. *Blood* -3-083048.

Vescovi, A.L., Galli, R., and Reynolds, B.A. 2006. Brain tumour stem cells. *Nat. Rev. Cancer 6*: 425–436.

Vogelstein, B., and Kinzler, K.W. 2004. Cancer genes and the pathways they control. *Nat. Med. 10*: 789–799.

Wang, J.C., and Dick, J.E. 2005. Cancer stem cells: lessions from leukemia. *Trends Cell Biol. 15*: 494–501.

Zucchi, I., Sanzone, S., Astigiano, S., Pelucchi, P., Scotti, M., Valsecchi, V., Barbieri, O., Bertoli, G., Albertini, A., Reinbold, R.A., and Dulbecco, R. 2007. The properties of a mammary gland cancer stem cell. *Proc. Natl. Acad. Sci. USA 104*: 10476–10481.

11
Overexposure of Patients to Ionizing Radiation: An Overview

Philip Clewer

INTRODUCTION

Ionizing radiation is very useful in both the diagnosis and treatment of cancer. Roentgen discovered X-rays in 1895 and it was very quickly realised that they could be used to see inside the human body. Clinics opened and used the 'magic rays' before the harmful effects were realised. Today ionizing radiation is widely used in diagnosis and treatment across the world but is subject to much more control.

From time to time patients undergoing a diagnostic X-ray examination, nuclear medicine investigation or radiotherapy may receive a higher radiation dose than necessary – an 'overexposure'. Quite simply, an overexposure is when the patient receives more radiation than was intended. The overexposure factor, the measure of the degree of overexposure, is the ratio of actual dose to the intended dose. It should be noted that, if the patient undergoes the wrong examination and then the correct examination, the actual dose is the sum of the doses from the two examinations.

The word 'dose' can be interpreted in several ways and there are different measures of overexposure. For example, in diagnostic radiology, we can consider overexposure in terms of the dose-area product, entrance surface dose or effective dose. In nuclear medicine the expression 'dose' may be used to describe the administered dose of radioactivity in terms of megaBecquerels (or milliCuries). However, because we are concerned with the detrimental effect on the patient or risk to the patient, it is normal to consider the "effective dose" to the patient as defined by the International Commission on Radiation Units and Measurements (1993) and used in the International Commission on Radiological Protection's 1990 recommendations (1991). In this chapter, I will examine the causes and consequences of overexposures and the requirements for reporting them to the authorities.

JUSTIFICATION AND OPTIMIZATION

The foundations upon which radiation protection philosophy is built are justification, optimization and limitation; these are the principles of the International Commission on Radiological Protection's current recommendations (1991) and the

consultative draft of the replacement recommendations states that they are still applicable. The first two of these principles relate to overexposure of the patient.

Every exposure should be justified. The European Union's Medical Exposures Directive (1997), implemented in 2000, states that "all individual medical exposures shall be justified in advance taking into account the specific objectives of the exposure and the characteristics of the individual involved" and the United Kingdom's Ionising Radiation (Medical Exposure) Regulations 2000 are based on this principle. If the exposure cannot be justified given the clinical information available regarding the patient, there is no good reason to proceed with the exposure and it should not go ahead. If it did, it would be giving an unnecessary radiation dose to the patient. Thus, when a patient that does not need a radiation exposure at all actually receives one, it is an overexposure. Therefore, a failure in the justification process can lead to an overexposure and in this case the overexposure factor is effectively infinity.

Justification of a medical exposure to ionizing radiation is the process of taking the clinical information regarding the patient and deciding if the exposure to radiation will result in a diagnosis that affects the patient's care or, in the case of radiotherapy, will produce a net benefit. If a patient is referred for an examination with the referral simply stating "shoulder pain", this will not be sufficient clinical information to justify an exposure. Once an exposure has been justified by considering the risks of the radiation dose against the risk of not undertaking the examination or treatment, the dose has to be optimised. This is the process of ensuring that, in the case of a diagnostic examination, the patient receives no more radiation dose than is necessary to produce an image of diagnostic quality. In radiotherapy it involves producing a treatment plan for the individual patient to ensure that the target volume receives the appropriate dose, while surrounding organs and tissue receive the minimum possible dose.

So, for the purposes of this discussion, we will consider the definition of an overexposure to include exposure of a patient who should not have received any dose (unintended exposure), a greater than necessary exposure to radiation during a diagnostic exposure, a greater than necessary exposure of a target volume in radiotherapy and overexposure of healthy tissue surrounding a target volume.

UNINTENDED EXPOSURES

When a patient receives a dose of radiation when it should not have been given, this is an unintended exposure. This may happen for several reasons, usually connected with a misidentification; the wrong patient is exposed. For example, a written referral may contain the wrong demographic data, the wrong patient is invited for a radiographic examination and therefore undergoes an unintended exposure. It is possible that the error in identification can take place in the radiology department. The consequences may be less immediate than if the referral was for surgery, but, nonetheless, the patient's risk of a detrimental effect will increase. It could also be that the error is not discovered and so the intended subject of the examination continues with an undiagnosed condition.

OVEREXPOSURE IN RADIOLOGY

There are two categories of overexposure in radiology: those due to equipment failure and those due to human error. Overexposure due to equipment failure can be due to an exposure parameter, for example, applied kilovoltage or tube current, being out of calibration. However, it is more usual that overexposures due to equipment failure are due to a fault in the automatic exposure control (a.e.c.). The a.e.c. performance should be checked regularly as part of the quality assurance programme. If it becomes maladjusted between checks, it can cause patients to receive a greater dose than intended. A back-up system should prevent a gross overexposure but is not designed to mimic the primary a.e.c. device.

Modern technological developments have not necessarily reduced the risk of overexposures. The early computed tomography scanners would typically scan eight slices per minute. Modern multislice scanners, with a rotational speed of 1 s or less, can complete an examination very quickly and by the time the operator realises that something is amiss, the scan is complete. The advent of computed radiography or direct digital radiography is replacing the use of film. With film, the operator had to be reasonably accurate with manually controlled exposures or the a.e.c. had to be well adjusted for automatic exposures. With computed radiography and digital radiography there is more latitude in the exposure and so there is less of a constraint on the operator to be accurate; what would have produced a film too dark for diagnosis can be "windowed" to produce an image of diagnostic quality.

One area where technology is eliminating some overexposures is the electronic referral. Hand written referrals are prone to misreading, perhaps due to poor handwriting. For example, there have been a number of incidents where a referral for a cervical spine examination has been abbreviated to "C spine" and misread by the operator as "L spine", resulting in the patient undergoing a lumbar spine X-ray instead of a cervical spine X-ray and therefore receiving a significantly greater radiation dose.

There is some confusion regarding terminology when a patient undergoes a radiographic examination of the wrong body part. For example, the patient may need a radiographic examination of the right knee but, in error, undergoes an examination of the left knee. It was not intended that the right knee was examined and so this could be regarded as an unintended exposure. However, it was intended that the patient underwent an examination and so it could be argued that, assuming the correct knee is eventually radiographed, the patient is subjected to an overexposure. This is certainly the case if we consider the effective dose received by the patient and it is the effective dose that is used in consideration of the detrimental effect on the patient.

There is one special consideration of overexposure, that of the unborn child. This is when a fetus is irradiated as a result of a justified exposure to the expectant mother. When it is known that a female patient is, or may be pregnant, the justification has to take into account the risk to the fetus as well as the benefit to the mother. It may well be the case that a proper diagnosis of the women's condition by radiographic examination will be of benefit to the unborn child; pregnancy does not automatically prohibit an examination. Occasionally a patient will discover after the examination that she was pregnant

at the time of the exposure. It should be noted that, according to the International Commission on Radiological Protection (2000), the doses involved in diagnostic examinations are well below the threshold at which a termination should be considered; even the dose from a computed tomography examination of the pelvis is not high enough to consider a termination.

Departments should have procedures in place to prevent these unintended exposures and overexposures. The employer who operates the facility should have a system in place to ensure that only authorised persons can refer patients and that referrals are checked as part of the justification process. In addition, in some cases it is appropriate for the person who undertakes the practical aspects of the exposure, the radiographer or technologist, to check the symptoms with the patient. I have known a patient to be referred for a radiographic examination of the knee 2 days after a total knee replacement and the radiographer has proceeded with the X-ray only to find no sign of a replacement knee joint on the image. The patient had undergone a hip replacement. Surely the radiographer should have realized that the lack of any sign of a 2 day old wound indicated an erroneous referral! It should be noted that high skin doses leading to deterministic effects as a result of interventional radiography should not be considered overexposures. These are doses resulting from complex procedures and, although they may be very high, are not greater than intended.

OVEREXPOSURE IN NUCLEAR MEDICINE

The nuclear medicine patient is at risk of similar unintended exposures, related to mis-identification, as radiology patients but is also at risk of other causes of overexposure. Taking the intended dose in terms of administered radioactivity, there are several possible causes of overexposure, mainly related to too much radioactivity being drawn up into the syringe. This could be because the specific activity of the radiopharmaceutical is incorrect, perhaps because of an error by the radiopharmacist or because the wrong volume of liquid is drawn up. These are human errors; there could also be an inaccuracy in the calibration of the isotope calibrator that would result in the wrong radioactivity being administered.

OVEREXPOSURE IN RADIOTHERAPY

Radiotherapy utilizes high doses of ionizing radiation in the form of external beams from linear accelerators or from radioactive materials within the patient. The latter may be temporarily implanted sources in brachytherapy or liquid sources such as the use of iodine-131 for thyroid ablations, administered orally as a drink or a capsule. External beam radiotherapy follows a plan for each individual patient, the result of a complex sequence of imaging and calculation. The process should include a programme of checking to ensure that the risk of errors is minimized, but unfortunately human error can lead to mistakes. Another source of errors occurs when the patient arrives for treatment and the staff can make a mistake in positioning the patient prior to treatment. The treatment is usually given as a number of fractions over a period of a few days or a few weeks. Often an error is identified early in the treatment

and it may be that an overexposure in early fractions can be compensated for in the later fractions, so that the overall dose to the patient is correct.

Sometimes the error is in the form of a 'geographical miss'; the beam or beams have missed the target volume and other organs and tissues have received a much higher dose than was intended. In this case it is not possible to compensate for any error in early fractions by changing later fractions but at least, if discovered, the technique can be corrected. Overexposures in radiotherapy can lead to deterministic effects that are, in these patients, of more concern than the stochastic risk.

In brachytherapy, the insertion of sources is intended to give a localized dose to the target volume. If a remote after-loading device using applicator tubes is used for what is termed 'low dose-rate brachytherapy' taking several hours to deliver the required dose, an unobserved patient can purposefully or inadvertently remove the applicators and leave the source(s) to irradiate healthy tissue. This is particularly likely with patients who are confused. Many such devices have a system for detecting such events and returning the sources to their safe position.

A useful resource for research into radiotherapy incidents is the Radiation Oncology Safety Information System (ROSIS) database on the internet at www.rosis.info. The records cover over 700 radiotherapy incident reports from 19 countries. All information is presented in such a way as to preserve the anonymity of the clinics submitting reports. This is always important in reporting systems in order to encourage an open reporting culture.

AT WHAT LEVEL SHOULD WE BE CONCERNED ABOUT OVEREXPOSURES?

I have already defined the overexposure factor as the ratio of actual dose to intended dose but at what magnitude of overexposure should we become concerned? We can argue that all doses should be as low as reasonably practicable (the ALARP principle) but we have to accept that equipment can fail and humans do make mistakes and so overexposures will always be a fact of life. As a starting point, we will look at practice in the United Kingdom. In general, overexposures are divided into two categories: those that are relatively small and records are kept but not reported to the authorities and those that are larger and are reported to regulatory authorities. The latter category is further subdivided into those that are a result of equipment faults and those that are due to any other reason.

The Health and Safety Executive is the authority responsible for the Ionising Radiations Regulations 1999 and these require that "where a radiation employer suspects or has been informed that an incident may have occurred in which a person while undergoing a medical exposure was, as the result of a malfunction of or defect in radiation equipment under the control of that employer, exposed to ionizing radiation to an extent much greater than that intended, he shall make an immediate investigation of the suspected incident and, unless that investigation shows beyond reasonable doubt that no such incident has occurred, shall forthwith notify the Executive thereof and make or arrange for a detailed investigation of the circumstances of the exposure

and an assessment of the dose received. The Executive has published guidance on what it considers to be "much greater than that intended" (HSE, 1998), and this varies with the intended effective dose. The guideline multiplying factors, above which overexposure must by law be reported to the Health and Safety Executive, were, in 1998: interventional radiology, radiographic and fluoroscopic procedures involving contrast agents, nuclear medicine with intended effective dose > 5 mSv and all CT examinations: three times intended dose; mammography, nuclear medicine with intended effective dose ≤ 5 mSv but > 0.5 mSv, everything else not referred to elsewhere: ten times intended dose; radiography of extremities, skull, dentition, shoulder, chest, elbow, knee and nuclear medicine with intended effective dose ≤ 0.5 mSv: 20 times intended dose; beam radiotherapy and brachytherapy: 1.1 times intended dose for whole course of treatment or 1.2. times intended dose for any fraction; radionuclide therapy: 1.2 times intended dose of any administration.

Therefore, if a fault on an X-ray machine causes a patient undergoing a chest radiograph examination to receive 20 or more times the intended dose, this must be reported to the regulatory authority. In 2006 the Health and Safety Executive revised the overexposure factor for high dose examinations and it was changed to 1.5 times the intended dose.

The Ionising Radiation (Medical Exposure) Regulations 2000, implementing the European Medical Exposures Directive, require where the employer knows or has reason to believe that an incident has or may have occurred in which a person, while undergoing a medical exposure was, otherwise than as a result of a malfunction or defect in equipment, exposed to ionizing radiation to an extent much greater than intended, he shall make an immediate preliminary investigation of the incident and, unless that investigation shows beyond a reasonable doubt that no such overexposure has occurred, he shall forthwith notify the appropriate authority and make or arrange for a detailed investigation of the circumstances of the exposure and an assessment of the dose received. The Department of Health, the regulatory authority for these regulations, stated that they would adopt the same overexposure guidelines for much greater than intended as the Health and Safety Executive's guidelines. However, when the latter reduced the factor for high dose examinations from 3 to 1.5, the Department of Health stated that it would retain the 3 times factor.

In radiotherapy incidents, the dose to surrounding organs is of interest and therefore, in addition to the overexposure factors stated above, the overexposure to critical tissues outside of the treatment volume needs to be assessed, particularly in the event of a geographical miss.

So, in the United Kingdom, if a patient undergoing a chest X-ray receives 19 times the intended dose, i.e., 0.38 mSv, it is not reportable, but an overexposure of 20 times the intended dose, i.e., 0.40 mSv, would be reportable. Taking the International Commission on Radiological Protection's figure of risk for a fatal cancer of 5% per Sievert (ICRP, 1991), this is a risk of ~1 in 53,000 and 1 in 50,000, respectively. These are very small risks compared with the natural lifetime risk of cancer. If a patient undergoing a CT examination of the chest is overexposed, the authorities must be notified if the patient receives a dose of

12 mSv due to equipment malfunction (1.5 times intended dose) or 24 mSv due to other causes (3 times intended dose).

Martin (2005) has published statistics regarding the number of overexposures in radiology or nuclear medicine at a group of hospitals in Scotland. It is normal practice for such incidents to be reported to the local Health Physics or Medical Physics service and a Radiation Protection Adviser or Medical Physics Expert will advise if an incident meets the requirements for reporting to a regulatory authority. Martin's survey found that, of the average 91 patient overexposure incidents in radiology reported to his Health Physics Service per year, four were reported to the regulatory authority under the Ionising Radiation (Medical Exposure) Regulations 2000. For nuclear medicine procedures, the average number of overexposures was seven per year, of which one was reported under the Ionizing Radiation (Medical Exposure) Regulations 2000. Martin concludes that the overexposure rate is ~7 in 100,000 radiology procedures and 30 in 100,000 nuclear medicine procedures. Martin also found that the number of incidents reported per year increased significantly after the year 2000 and it is believed that this is due to a more open, no blame culture and the implementation of the new regulations.

It is normal practice for hospitals and other healthcare institutions to maintain records regarding all accidents and incidents and these should include overexposures of the patient. Analysis of the incident statistics can show areas of activity where the incident rate is higher than might be acceptable and therefore enables the employer to review procedures with a view to reducing the incident rate. However, there is merit in considering where the threshold for reporting to a regulatory authority should lie because to report to an authority involves considerable time and effort. Current United Kingdom guidance indicates that an overexposure that is actually an unintended exposure of a patient who should not have undergone any examination is reportable, regardless of the risk to the patient. So, the unintended exposure of an ankle is just as reportable as an unintended CT scan.

Clewer and Jackson (2006) considered this matter, as far as it relates to diagnostic procedures, and suggested that there should be a simple threshold, set in terms of effective dose, for reporting unintended doses to a regulatory authority. This should be risk-based and would mean that relatively small unintended doses, such as that of an extremity, would be recorded locally and statistics submitted to the authorities annually but that higher unintended doses would be reported to the authorities immediately. Several thresholds were proposed by the authors but they favored a threshold of 2 mSv, equivalent to the risk of a fatal cancer of 1 in 10,000.

At the time of writing, the Department of Health in London is believed to be considering issuing revised guidance on the reporting of overexposures and setting an effective dose threshold for reporting diagnostic overexposures. It is further believed that the reporting thresholds for radiotherapy procedures will be based more on the clinical outcome of the overexposure, apart from errors where the wrong site is exposed; these will automatically require reporting.

In conclusion, patients entering a hospital as inpatients or outpatients, for diagnostic or therapeutic purposes, expect a reasonable level of care. They expect to receive the correct radiation dose commensurate with

the intended purpose. However, accidents can and do happen because human beings are involved in the processes, either in manufacturing the equipment or in operating it. Hospitals should ensure that they have procedures and protocols in place to minimize the risks of overexposing the patient so that, in diagnostic procedures, a satisfactory image is produced with the minimum dose to the patient and, in therapeutic procedures, the target volume is irradiated with minimum dose to the surrounding tissue.

REFERENCES

Clewer, P.R., and Jackson, P.C. 2006. Reporting overexposures and unintended exposures in diagnostic procedures. *Br. J. Radiol. 79*: 866–869.

Council of the European Union 1997. Council Directive 97/43/Euratom of 30 June 1997 on Health Protection of Individuals Against the Dangers of Ionizing Radiation in Relation to Medical Exposure. *OJEU 180*: 0022–0027.

Health and Safety Executive 1998. *Fitness of Equipment Used for Medical Exposure to Ionizing Radiation*. Guidance Note PM77, second edition. HSE Books, Sudbury, UK. ISBN 0 7176 1482 4.

International Commission on Radiation Units and Measurements 1993. *Quantities and Units in Radiation Protection Dosimetry*, ICRU Report 51, ICRU, USA.

International Commission on Radiological Protection 1991. *1990 Recommendations of the International Commission on Radiological Protection*. ICRP Publication 60, Pergamon. ISBN 0 08 041144 4.

International Commission on Radiological Protection 2000. *Pregnancy and Medical Radiation*. ICRP Publication 84, Pergamon. ISBN 008 043 9012.

Martin, C.J. 2005. A survey of incidents in radiology in nuclear medicine in the West of Scotland. *Br. J. Rad. 78*: 913–921.

12
Lung Carcinoma

M.A. Hayat

INTRODUCTION

In developed countries, lung cancer represents the second leading cause of death, exceeded only by cardiovascular diseases. There are ~ 1.2 million new cases of lung cancer diagnosed every year worldwide, and ~ 1.1 million patients die of this malignancy annually. An estimated 213,380 new cases of lung cancer are expected in 2007 in the U.S., accounting for ~ 15% of all cancers diagnosed. An estimated 160, 390 deaths, account for ~ 29% of all cancer deaths occurring in 2007 in the U.S. More women die each year from lung cancer than from breast cancer.

The median age at diagnosis of lung cancer in North America and Europe is ~ 70 years, and the incidence increases with increasing age. The incidence and mortality rates from lung cancer have decreased among persons of 50 years of age and younger, but have increased among those of 70 years and older. However, death rates have continued to decline, reflecting a decrease in smoking rates during the past 3 years.

Non-small cell lung cancer constitutes 80–85% of lung cancer. Small-cell lung cancer (SCLC) makes up the remaining 15–20%. More than 50% of advanced NSCLC are diagnosed in patients older than 65 years of age. Only ~ 15% of patients diagnosed with NSCLC survive after 5 years. Apparently, therapeutic strategies are urgently needed to improve the clinical management of this devastating malignancy.

Lung cancer is the result of a series of genetic and epigenetic alterations in pulmonary epithelial cells. Multiple genetic alterations are required for lung cancer invasion and metastasis. Cycloxygenase-2 (COX-2), the inducible isoenzyme, is constitutively overexpressed in a variety of malignancies, including lung, colon, prostate, gastric, esophageal, breast, and pancreatic. Inhibition of COX-2 leads to lung tumor reduction *in vivo* in animal lung cancer models. Cyclooxygenase-2 activity is detectable throughout the progression of premalignant lesion to the metastatic phenotype. Also, compared with the primary tumor, higher COX-2 expression is observed in lung adenocarcinoma lymph node metastasis. In addition, overexpression of COX-2 is associated with angiogenesis, decreased host immunity, enhanced invasion, metastasis, and poor prognosis.

As stated earlier, multiple genetic alterations are a prerequisite to lung cancer

and because COX-2 can affect multiple mechanistic pathways in this malignancy, this isoenzyme plays a multifaceted role in conferring the malignant and metastatic phenotypes. Cyclooxygenase-2 is thought to play a central role in orchestrating this process. It has been shown that COX-2 dependent pathways contribute to the modulation of E-cadherin expression in NSCLC (Dohadwala *et al*., 2006). This study also demonstrates an inverse relationship between COX-2 and E-cadherin. In addition, treatment of NSCLC cells with exogenous prostaglandin E_2 (PGE_2) decreases the expression of E-cadherin, whereas treatment of cells with celecoxib leads to increased E-cadherin expression. It is known that E-cadherin-catenin complex is critical for intercellular adhesiveness and maintenance of normal tissue architecture. Reduction of E-cadherin is linked to tumor invasion, metastasis, and unfavorable prognosis. It is also known that cell-cell adhesion and extracellular matrix (ECM) represent significant barriers to tumor cell metastasis. This and other evidence indicates that PGE_2 modulates transcriptional repressors of E-cadherin and thereby regulates COX-2-dependent E-cadherin expression at least in NSCLC. Based on this information, blocking of PGE_2 production or activity may contribute to both the prevention and treatment of NSCLC (Dohadwala *et al*., 2006).

Cigarette smoking is casually associated with large numbers of human cancers. Tobacco use is the most widespread link between exposure to known carcinogens and death from cancer. It is emphasized that cigarette smoking without a doubt is the most serious risk factor for lung malignancy. Other factors include occupational and environmental exposure to secondhand smoke, radon, asbestos, ceratin metals, some organic molecules, radiation, air pollution, and a history of tuberculosis (Am. Cancer Soc., 2007). Genetic susceptibility is also a contributing factor in the development of this cancer.

Symptoms of lung cancer include persistent cough, sputum streaked with blood, chest pain, voice change, breathing difficulty, and recurrent pneumonia or bronchitis. A number of approaches are used in attempts to achieve early diagnosis of lung cancer; these efforts include chest X-ray, analysis of cells in sputum, fiberoptic examination of the bronchial passages, low dose spiral computed tomography, and molecular markers in sputum (Am. Cancer Soc., 2007). The objective is to diagnose this cancer at a more operable stage when the chance of survival is better. However, these efforts have shown limited effectiveness. Although lung cancer diagnosis is also attempted using biopsy, this invasive method is associated with some degree of risk.

In technologically-advanced countries we have powerful raw diagnostic tools of unprecedented power with which to interpret normal, benign, and malignant conditions. However, some of these tools are still at an experimental stage, and are not error-proof, and so medical errors in interpreting the results do occur. Indeed, the possibility of errors and disagreements in the diagnosis of malignancies, including lung cancer, cannot be ignored. For example, an error rate of 30% was reported among staff radiologists in their interpretation of chest radiographs (Lehr *et al*., 1976). Herman *et al*. (1975) have also reported that a group of Harvard University radiologists disagreed on the interpretation of chest radiographs as much as 56% of the time. Additional

studies indicate that 26% to 90% of all lung carcinomas were missed by radiologists interpreting chest radiographs (Austin *et al*., 1992). Fortunately, most of the errors are correctable using the utmost care, increased time spent on interpreting the results, additional training and experience, increased consultation with colleagues, decreased volume of cases interpreted per unit of time, and continued efforts at elucidation and correction of other factors involved. Also, because technology has made tremendous advancements, availability of enormous collection of information, knowledge, and experience during the last two decades, error rates have reduced. Recently, Berlin (2007) has reviewed this subject.

The choice of the treatment for lung cancer depends in part on the type of lung cells (non-small cells or small cells) and the stage of cancer. These treatments include surgery, radiation, chemotherapy, and immunotherapy. Combinations of these treatments are also used, especially when the disease has spread. Surgery is the most important curative method of treatment of early-stage (localized) NSCLC. However, only ~ 20–30% of patients are diagnosed at an operable stage.

Although platinum-based dual chemotherapy is the standard treatment for advanced NSCLC, only 30–40% of patient's response with a modest-survival rate increase. Generally, combination chemotherapy is more effective than treatment with a single drug. Median survival (8–10 months) and 1-year survival after first-line chemotherapy are 8–10 months and 30–40%, respectively. It needs to be noted that these regimens are accompanied by considerable toxicity, especially myelosuppression.

Among the new drugs that have been introduced in the treatment of advanced NSCLC after failure of first-line chemotherapy are docetaxel, pemetrexel, and epidermal growth factor receptor (EGFR) tyrosine kinase inhibitors. All of these agents invoke response of >10% with variable degrees of toxicities. Erlotinib shows significant antitumor activity in the first-line treatment of advanced NSCLC, and is a viable alternative to chemotherapy (Giacone *et al*., 2006).

The long term prognosis of patients with lung cancer is poor and the overall survival rate is as low as 11–14%. As stated earlier, although surgical treatment can sometimes be a curative option for lung cancers, the poor diagnosis of such patients depends partially on the relative low sensitivity of this malignancy to both radiotherapy and chemotherapy. Furthermore, a vast majority of lung cancer patients present at an advanced stage at the time of diagnosis. In other words, at the time of diagnosis, the majority of patients already have metastatic disease, and a systemic, palliative treatment is the primary therapeutic option. Even the combined therapy (surgical resection, radiotherapy, and chemotherapy) is not satisfactory for patients in advanced stage. Therefore, in order to improve the prognosis, new therapeutic strategies are needed. One potentially effective strategy is to identify lung tumor specific antigen that can be promising for immunotherapy.

Despite focused research in conventional therapies and significant advances in the understanding of the molecular basis of lung carcinogenesis, the 1-year relative survival rate for lung cancer patients is ~ 45%, while the 5-year survival rate for all stages and localized cancer is ~16% and 40%,

respectively. However, only 16% of lung cancers are diagnosed at an early stage. Most patients suffering from this malignancy eventually succumb to widespread metastasis. Thus, further identification of mechanisms regulating the initiation and progression of lung cancer is needed.

REFERENCES

American Cancer Society: Cancer Facts and Figures, 2007.

Austin, J.H.M., Romney, B.M., and Goldsmith, L.S. 1992. Missed bronchogenic carcinoma: radiographic findings in 27 patients with a potentially respectable lesion evident in retrospect. *Radiology 182*: 115–122.

Berlin, L. 2007. Accuracy of diagnostic procedures: has it improved over the past five decades. *Am. J. Roentgol. 188*: 1173–1178.

Dohadwala, M., Yang, S.C., Luo, J., Sharma, S., Batra, R.K., Huang, M., Lin, Y., Goodglick, L., Krysan, K., Fishbein, M.C., Hong, L., Lai, C., Cameron, R.B., Gemmill, R.M., Drabkin, H.A., and Dubinett, S.M. 2006. Cyclooxygenase-2-dependent regulation of E-cadherin: prostaglandin E(2) induces transcriptional repressors ZEB1 and snail in non-small cell lung cancer. *Cancer Res. 66*: 5338–5345.

Giacone, G., Ruiz, M.G., Le Chevalier, T., Thatcher, N., Smit, E., Rodriguez, J.A., Janne, P., Oulid-Aissa, D., and Soria, J-C. 2006. Erlotinib front-line treatment of advanced non-small cell lung cancer: a phase II study. *Clin. Cancer Res. 12*: 6049–6055.

Herman, P.G., Gerson, D.E., Hessel, S.J., Mayer, B.S., Watrick, M., Blesser, B., and Ozonoff, D. 1975. Disagreement in chestroentgen interpretation. *Chest 68*: 278–282.

Lehr, J.L., Lodwick, G.S., Farrell, C., Braaten, M.O., Virtama, P., and Kolvisto, E.L. 1976. Direct measurement of the effect of film miniaturization on diagnostic accuracy. *Radiology 118*: 257–263.

13
Extra-Pulmonary Small Cell Cancer: Diagnosis, Treatment, and Prognosis

Rabia K. Shahid, Kamal Haider, Amer Sami, Imran Ahmad, Florence Arnold, Sunil Yadav, Kristie Harding, Malcolm Brigden, David Popkin, and Shahid Ahmed

INTRODUCTION

Small cell carcinoma (SCC) is a high grade epithelial cancer of neuroendocrine origin, which is considered to be a distinct cinicopathological entity. It has been reported in the literature by using various terminologies including oat cell carcinoma, anaplastic carcinoma, small cell undifferentiated carcinoma, undifferentiated carcinoma, microcytoma, reserve cell carcinoma, small cell neuroendocrine carcinoma, Kulchitsky cell carcinoma, and carcinoma with amine-precursor uptake and decarboxylase (APUD) cell differentiation. Small cell carcinoma is, however, the recommended pathological term (Beasley *et al*., 2005). It is most commonly of bronchogenic origin and accounts for about 20–25% of all pulmonary malignancies (Hoffman *et al*., 2006). Small cell carcinoma of lung is well recognized for its aggressive clinical behavior and an increased propensity for early metastases. Uncommonly, SCCs can originate in non-pulmonary organs and are collectively known as "extrapulmonary small cell carcinoma" (Remick *et al*., 1987; Remick and Ruckdeschel, 1992).

Extrapulmonary small cell carcinoma (EPSCC) often represents a diagnostic and therapeutic challenge. In 1930, it was first reported in the mediastinal glands without pathologic evidence of primary pulmonary involvement (Duguid and Kennedy, 1930). Since its first description, EPSCC has been reported in virtually all anatomical sites. The primary sites most frequently involved are gynecologic organs, especially the cervix; genitourinary organs, especially the urinary bladder and the prostate gland; the gastrointestinal tract, especially the esophagus, and head and neck region. In addition, SCC has been reported in the breast, thyroid, skin, and thymus gland. If the primary site remains undetected, these tumors are known as small cell carcinoma of unknown primary.

Limited data are available regarding its clinical behavior and outcome. The available literature is predominantly based on reviews of published cases or analysis of institutional data (Remick and Ruckdeschel, 1992; Vrouvas and Ash, 1995). In general, EPSCCs resemble their pulmonary counterparts with respect to purported histogenesis, morphology, and behavior. The clinico-pathological features, diagnosis, and general management of EPSCC are reviewed here, followed by a brief description of

small cell carcinoma specific to the more common sites.

EPIDEMIOLOGY

Small cell carcinoma arising from extrapulmonary sites represents 2–4% of all SCC (Remick and Ruckdeschel, 1992). Approximately, 1,000 cases per year have been reported in the United States, which represents an overall incidence between 0.1% and 0.4% of all cancers. Patients with EPSCC are generally middle-aged or older with more than 70% of patients being older than 50 years. Small cell carcinoma of the cervix is an exception and mainly affects younger females. Both genders are affected and predominance of either gender varies according to the primary site of involvement. For example SCC of esophagus, urinary bladder, and head and neck region are more common in men, whereas female preponderance has been noted in patients with SCC of gallbladder. Specific risk factors for the development of EPSCC have not been identified as yet. Although cigarette smoking appears to be associated with EPSCC especially of the head and neck region, it has not been clearly identified as a risk factor for EPSCC and the role of smoking in the development of this malignancy remains speculative.

PATHOLOGY

Extrapulmonary small cell carcinoma exhibits several neuroendocrine features characterized by the presence of enzymes such as dopa decarboxylase, calcitonin, neuron-specific enolase, chromogranin A, and CD56 (neural cell adhesion molecule). They are morphologically, immunohistochemically, and ultrastructurally indistinguishable from their pulmonary counterparts.

Histogenesis

The pathogenesis of SCC is largely unknown and remains speculative. The earlier theory of origin of SCC from the APUD cells (a group of neuroendocrine cells) has been abandoned in favor of stem cell theory. It is now postulated that SCC originates from totipotent stem cells present in all tissues and capable of divergent differentiation (Frazier *et al*., 2007; Remick and Ruckdeschel, 1992). This theory offers explanation for the tumor heterogeneity and mixed morphology showing an admixture of SCC and various other epithelial cell types. Others have hypothesized that small cell component may arise from more differentiated tumors during the clonal evolution of a carcinoma as a late-stage phenomenon (Shaco-Levy *et al*., 2004). It is possible that there is more than one pathway for the development of these tumors.

Light Microscopic Features

The histologic criteria are the same as those for the pulmonary neoplasm and the light microscopic features of EPSCC are indistinguishable from those of pulmonary SCC. The tumor is composed of sheets and nests of round to spindle-shaped cells with dense nuclei, granular nuclear chromatin, and minimal amounts of cytoplasm (Frazier *et al*., 2007). Nucleoli are absent or inconspicuous. The typical organoid architectural patterns of low-grade neuroendocrine neoplasms such as carcinoid tumor are generally absent. Mitotic rates are high and necrosis of individual malignant cell is common. It

may contain non-SCC elements, varying in type, depending on the location.

Immunophenohistochemistry

The immunophenotype of EPSCC exhibits both epithelial and primitive neuroendocrine differentiation. The malignant cells are immunoreactive for keratin and epithelial membrane antigen in virtually all cases. They may also react with general neuroendocrine markers such as neuron-specific enolase, synaptophysin, neurofilament, leu 7, and chromogranin A (Frazier *et al*., 2007). The malignant cells show a high proliferative rate supported by immunohistochemical staining for MIB-1 and proliferating cell nuclear antigen (PCNA).

Electron Microscopy

Electron microscopy is rarely used but in selected cases may provide additional information for accurate diagnosis (Peydro-Olaya *et al*., 2003). The most consistent ultrastructural feature is the presence of intracytoplasmic dense-core neurosecretory granules of 30–300 nm. These granules are mostly located within cytoplasmic processes or at the periphery of cells. Other characteristic features include the presence of coarse chromatin, inconspicuous nucleoli, and sparse cytoplasmic organells.

Cytogenetics

Despite some similarity in cytogenetics, EPSCCs are not identical to their pulmonary counterparts. Mutations involving deletion of 5q or alterations in chromosome 17 are common to all SCC regardless of their site of origin. However, loss of chromosome 3p, 10q, and deletion in chromosome 13 are common in small cell lung cancer but observed less frequently in EPSCC (Welborn *et al*., 2004).

CLINICAL FEATURES

The clinical presentation is determined by the site of involvement and extent of the disease. Systemic symptoms, such as anorexia and weight loss, are common especially in patients with advanced disease. Focal symptoms are mostly site specific and are usually indistinguishable from those of other neoplasms arising in that anatomical site. Though uncommon, similar to SCC of the lung paraneoplastic syndromes (such as ectopic ACTH) production or inappropriate antidiuretic hormone secretion may be the dominant presenting feature. Eaton-Lambert syndrome, sensory neuropathy associated with "anti Hu", cerebellar cortical degeneration, diffuse uveal melanocytic proliferation, and paraneoplastic retinopathy have also been reported. In addition many patients with EPSCC may have elevated hormones and peptide levels including somatostatin, thyroxin, insulin, glucagons, gastrin, vasoactive intestinal polypeptide, parathyroid hormone-related protein, calcitonin, serotonin, b-melanocyte-stimulating hormone, and progestin-releasing peptide (Frazier *et al*., 2007).

DIFFERENTIAL DIAGNOSIS

The differential diagnosis of EPSCC is broad and includes primary lung SCC, metastatic melanoma, lymphoma, various small round blue cell tumors (small cell osteosarcoma,

rhabdomyosarcoma, mesenchymal chondrosarcoma, Ewing's sarcoma/peripheral neuroectodermal tumor, etc.), poorly differentiated carcinoma and other neuroendocrine tumors. The diagnosis of SCC primarily rests on morphological assessment. However, as described above, immunocytochemistry plays an important role and electron microscopy can be of value in difficult cases.

Small-cell lung cancer (SCLC) is morphologically identical to that of EPSCC. Thyroid transcription factor-1 (TTF-1) immunostaining has been proposed by several investigators to differentiate SCLC from EPSCC; however, TTF-1 expression is not specific for SCC of pulmonary origin and should not be used to distinguish EPSCC from pulmonary SCC. Low grade neuroendocrine tumor, such as typical and atypical carcinoids, can be distinguished from EPSCC by the degree of necrosis, mitosis, and apoptotic activity, whereas the cells of large neuroendocrine carcinoma are generally larger and contain a moderate to abundant amount of cytoplasm. Likewise, Merkel cell carcinoma, a rare neuroendocrine carcinoma of the skin, has morphologic features similar to SCC. Ultrastructurally, the malignant cells differ from EPSCC and contain bundles of intermediate filament in their cytoplasm in a paranuclear distribution (Peydro-Olaya *et al*., 2003). In addition, Merkel cell carcinomas lack TTF-1 immunostaining and display a characteristic perinuclear cytokeratin 20 immunostaining which is very rare in EPSCC outside the salivary glands (Leech *et al*., 2001).

STAGING

Although no specific staging system for EPSCC has been established, most authors have adopted 'Two Stage System' originally introduced by the Veterans' Affairs Lung Study Group (Clark and Ihde, 1998). This staging system consists of two categories: "limited disease" defined as tumor contained within a localized anatomic region, with or without loco-regional lymphadenopathy; and "extensive disease", defined as tumor outside the locoregional boundaries. Information provided by the "Tumor-Node- Metastases (TNM)" staging system may be valuable in certain anatomical sites such as SCC of large bowel.

The diagnosis of EPSCC (other than SCC of esophagus and thymus) requires normal chest radiograph and computed tomography scan of the chest to exclude metastatic pulmonary SCC. Some investigators have suggested routine bronchoscopy, but this is not widely adopted. Abdominal and pelvic computed tomography (CT) scan is a useful test to determine primary site and to assess the extent of the disease. Although there is a lack of data regarding the role of positron emission tomography (PET) scan in the management of EPSCC, it can be a useful tool for the detection of primary tumor in SCC of unknown primary site. In the absence of neurologic symptoms, CT scan of head is not routinely performed. Bone marrow biopsy is indicated if there is cytopenia without other evidence of disseminated disease. Other studies such as endoscopic examination may be performed to assess the affected sites and vary accordingly.

MANAGEMENT

Limited data are available regarding the optimal management of EPSCC. Due to the rarity of the disease, there is a lack of prospective clinical trials to guide treatment. The published series, however, provide

some generalizations regarding the treatment. These recommendations for managing EPSCC have been mostly extrapolated from the retrospective reviews and treatment of pulmonary SCC. As in pulmonary SCC, the survival of untreated patients is poor and the disease is rapidly fatal. Treatment goals for extensive stage and limited stage disease are different and they should be treated differently. Treatment for limited stage disease is potentially curative, whereas that of extensive stage disease is palliative.

Limited Stage Disease

Small cell carcinoma is sensitive to both radiation therapy and chemotherapy. Whereas chemotherapy can induce major regression of localized disease and concurrently treat occult metastases, surgery and/or radiation therapy represent the best option for loco-regional disease control at the majority of the anatomical sites. The unfavorable prognosis and the chemosensitivity of its pulmonary counterpart have led many clinicians to adopt the approach used in the management of SCC of lung. Many patients with limited stage disease are treated with a combined-modality therapy including surgery, radiation and chemotherapy. The response rate varies from 48% to 100% (Lo Re *et al*., 1994; Remick and Ruckdeschel, 1992). The optimal integration of these modalities and precise sequence remains to be defined.

In carefully selected patients with limited stage disease, small tumor volume surgery can be curative. Although the role of adjuvant therapy is not clear, platinum based chemotherapy can be considered to treat micometastases in patients who undergo complete surgical resection given the chemoresponsiveness of the disease and the high rate of systemic recurrence. The possible synergism between chemotherapy and radiotherapy supports combined chemoradiotherapy and for many patients with localized disease at various anatomical sites the combination approach can be an effective and alternate treatment to surgery. The precise incidence of central nervous system recurrence is not known. Hence, cranial irradiation is not routinely used in the management of these patients who achieved a complete response.

Extensive Stage Disease

Patients with extensive stage disease of any site are best managed with systemic chemotherapy, preferably a platinum based regimen. Responses to therapy occur in 60–90% of patients. Unfortunately most responses are partial and of short duration. The use of surgery or radiotherapy in these patients is restricted for palliation of local symptoms.

PROGNOSIS

Extra-pulmonary small cell carcinoma follows an aggressive course with early propensity for metastases. Small cell carcinoma of various anatomical sites behaves differently and outcome varies according to the primary site of the disease involvement. In general, the prognosis of EPSCC is comparable to that of SCC of lung, and the extent of the disease is an important factor predicting survival. Poor performance status and abnormal white blood cell count are the other important variables that correlate with survival (Haider *et al*., 2006).

In reported series, patients with EPSCC are not uniformly treated or comparably staged. The median overall survival of all

patients with EPSCC is 9–15 months and 5-year survival is 10–15%. Patients with limited stage disease have median overall survival of 25–34 months and 5-year survival of 31%, whereas patients with extensive stage disease have a median overall survival of 2–12 months and 5-year survival of 2% (Galanis *et al*., 1997; Haider *et al*., 2006). Despite the generally aggressive behavior of SCC, long term remission or cure may be achieved in selected patients with a tailored therapy.

GENITOURINARY TRACT

Genitourinary tract is among the many sites for the origin of EPSCC. The majority of cases have been observed in the urinary bladder and prostate. Small cell carcinomas of kidneys and renal pelvis are extremely rare.

Urinary Bladder

Although urinary bladder is the most common site of EPSCC in the genitourinary tract, it accounts for <1% of all bladder tumors (Sved *et al*., 2004). Patients are usually between the ages of 40 and 60 years. Small cell carcinoma of urinary bladder is three times more common in men than women. It has been associated with cigarette smoking, bladder calculus, and long-standing cystitis (Shahab, 2007). Small cell carcinoma may coexist with transitional cell carcinoma and other types of bladder tumors. The majority of patients present with locally advanced or disseminated disease. There is no standard therapy for SCC of the bladder. Surgery is generally recommended for patients with localized disease often followed by adjuvant platinum-based chemotherapy. A combination of chemotherapy and radiation has been given concurrently in an effort to preserve the bladder in many cases. The prognosis is poor and the overall median survival of all patients in most reported series is ~2 years.

Prostate

The incidence of prostate SCC is <2% of the total of prostate cancer. The median age of the patients is ~65 years similar to that of patients with adenocarcinoma of prostate. In some cases prostate SCC may present a feature of de-differentiation associated with the evolution of a hormone-refractory adenocarcinoma. In other instances SCC may be the primary histologic diagnosis (Palmgren *et al*., 2007). Approximately, 30% of patients present initially with prostatic adenocarcinoma, 20% present with combined adenocarcinoma and SCC, and 50% of patients present with SCC.

Prostate-specific antigen (PSA) is not elevated in the majority of the patients with prostate SCC. Clinical features favoring the diagnosis of SCC of prostate include rapidly progressive disease, unresponsiveness to hormone therapy, lytic bone lesions, visceral metastases, and disproportionately low PSA levels in the setting of advanced disease. Patients with SCC of prostate respond poorly to antiandrogen therapy. Multimodality treatment provides the best prognosis in patients with localized disease. Most of the patients have advanced disease at diagnosis and median survival is ~15 months. Patients presenting initially with an adenocarcinoma have a median survival of 25 months compared with a median survival of 5 months for patients presenting with SCC.

GYNECOLOGICAL SITES

Small cell carcinoma of female genital tract comprises <2% of all gynecologic malignancies (Crowder and Tuller, 2007). Small cell carcinoma most commonly involves the cervix but may also develop in the endometrium, ovary, vagina, and vulva. In general, SCC of female genital tract has been associated with an aggressive clinical course with a propensity for early hematogenous and lymphatic spread. Mutlimodality therapy is the treatment of choice for most of the patients.

Cervix

Small cell carcinoma represents 0.4–1.4% of all cervical cancers. The cervix should always be considered as the site of origin in a woman with a SCC of unknown primary site. Women with cervical SCC tend to be younger with median diagnostic age of ~ 40–50 year. The prognosis varies with the stage of the disease. In addition, large tumor, deep invasion, smoking history, number of positive lymph nodes, and pure small cell histology have been associated with poor prognosis (Chan *et al*., 2003; Crowder and Tuller, 2007). Treatment includes surgery, radiation, and chemotherapy akin to those regimens used for SCLC. Multimodality therapy is associated with the best results and is the treatment of choice for most patients. Hoskins *et al*. (2003) reported 3-year survival of 60% in patients with primary cervical SCC treated with combination of chemo-radiation.

Endometrium

The mean age at diagnosis is ~60 years (range, 23–78) (Katahira *et al*., 2004). Abnormal vaginal bleeding is the presenting symptom in the majority of cases. In contrast to endometrial adenocarcinoma, most patients with uterine SCC present with advanced-stage disease. The prognosis is poor and long term survival is uncommon. Like other sites multimodality therapy is recommended for localized disease.

GASTROINTESTINAL TRACT

Small cell carcinoma of the gastrointestinal tract has an estimated incidence of 0.1–1% of all gastrointestinal malignancies (Brenner *et al*., 2004, 2007). More than two thirds of these tumors have been reported in the upper gastrointestinal tract with primary SCC; involvement of the esophagus appears to be the most frequently reported site. The second most common location is the large bowel accounting for 20–30% of all digestive tract SCC. Stomach, small intestine, pancreas, ampulla of Vater, gallbladder, bile duct, and liver are the other less common sites. While in extensive stage disease chemotherapy seems to represent the mainstay of treatment, multimodality therapy may offer the best chance for long-term survival in patients with localized disease. Prognosis is poor and median survival is in the range of 6–12 months. Two year survival rate is 25% and long term survival is <10% (Brenner *et al*., 2004, 2007).

Esophagus

Small cell carcinoma of esophagus is rare and its incidence has been estimated to range from 0.8% to 2.4% of all esophageal malignancies (Brenner *et al*., 2004, 2007). Most cases occur between the ages of 50 and 70 years. SCC of esophagus is twice as common in men as compared to women.

Gastroesophgeal reflux disease, achalasia and Barrett's esophagus have been reported to be associated with SCC of esophagus (Medgyesy *et al*., 2000). Most patients with SCC of esophagus who were treated with surgery alone succumbed to disseminated disease soon (Casas *et al*., 1997). The combination of chemoradiotherapy is effective against esophageal SCC and may provide long-term survival benefit in patients with limited disease. Adjuvant systemic chemotherapy, therefore, is recommended following surgery for localized disease. More recently with the recognition of the systemic nature of the disease, surgical resection has been performed as part of multimodality approach and usually considered for residual disease after induction chemotherapy or chemoradiation therapy. Tumor size and type of treatment are known to be important prognostic variables. The reported overall median survival is ~5 months, while the median survival for patients with limited disease is ~8 months, and for patients with advanced disease it is ~3 months (Casas *et al*., 1997). Long-term survival has been reported only in a few cases.

Colon and Rectum

Small cell carcinoma arising in the colon and rectum is comprised of ~0.2% of all colorectal neoplasms. The epidemiology is somewhat similar to that of adenocarcinoma with a slight male predominance. The majority of the cases are diagnosed between the ages of 50 and 70. Within the large bowel, the most frequent site is the rectum, followed by the cecum and sigmoid. Colonic adenoma and ulcerative colitis have been reported in association with SCC of large bowel, and tumors with mixed histology are often present (Brenner *et al*., 2004). The overall prognosis is poor with a median survival of 6 months. Surgery is the primary treatment for localized disease. Adjuvant radiation for local control and systemic chemotherapy to treat micrometastases are recommended. In the absence of clinical trials, the individual contribution of each component to the survival cannot be determined.

HEAD AND NECK REGION

Small cell carcinoma of head and neck region is uncommon but has been reported in nearly all structures associated with the upper aerodigestive tract. Among the SCC of head and neck region, larynx, salivary glands, and the sinonasal region are the principal sites of origin.

Larynx

Although larynx is one of the most common extrapulmonary sites, laryngeal SCC accounts for only 0.5% of all primary laryngeal malignancies. Most patients are between the ages of 60 and 80 years, and there is a male predominance. Smoking, chewing tobacco, and excess alcohol intake have been associated with SCC of the larynx. The supraglottic region is the most commonly reported site. The majority of patients of localized disease have been treated with multimodality of treatment. Although optimal management for these patients is undefined, several investigators have reported that the use of concurrent chemoradiotherapy regimens for limited-stage disease offer potential for long-term survival. Median survival of patients with primary SCC of the larynx, hypopharynx, and trachea is between 7 months and 11 months (Renner, 2007).

Salivary Glands

Small cell carcinoma arises in both major and minor salivary glands. It represents ~1% of all major salivary glands malignancies and 3.5% of all minor salivary glands tumors (Renner, 2007). The median age of diagnosis is 56 years (range, 5–86 year) with a male preponderance. The parotid is the most common site for primary SCC among the major salivary glands. Although the prognosis of the salivary glands SCC is considered to be somewhat better than SCC of other sites, it still has a propensity for development of early metastases. Gnepp *et al*. (1986) have reported the 2-and 5-year survival rates for SCC of the salivary glands of 70% and 40%, respectively. Surgical resection with ipsilateral lymph node dissection is commonly recommended for localized disease. Adjuvant radiotherapy is often suggested and in some cases may be utilized for primary treatment. Chemotherapy is generally considered for large tumors, those with extensive local infiltration and for those with loco-regional recurrence.

BREAST

SCC of breast accounts for <1% of primary breast cancer (Mirza and Shahab, 2007). The median age of diagnosis is 55 years (range, 41–70). The diagnosis of primary SCC of breast is supported by the presence of underlying *in situ* ductal lesion with areas of ductal, lobular, or papillary differentiation with no primary lung lesion (Shin *et al*., 2000). Immunoreactivity for estrogen/progesterone receptors have been observed in two third of patients with primary breast SCC, whereas HER-2/neu expression has not been reported in published series. Primary breast SCC is considered to be an aggressive neoplasm and a multimodality treatment approach including surgery, radiation therapy, and chemotherapy has been recommended for patients with localized or loco-regional disease.

UNKNOWN PRIMARY SITES

The precise incidence of SCC of unknown primary sites is not known. It has been reported to comprise 7–30% of EPSCC (Lobins and Floyd, 2007). The inability to identify a primary lesion can be explained by either the involution of the primary tumor or by the proliferation advantage of subclones over the primary lesion resulting in the development of overt metastases without having a clinically identifiable primary tumor (Abbruzzese *et al*., 1993). Lymph nodes, liver, brain, and bone are the common sites of involvement. The prognosis is based on the location, extent of the disease, and response to therapy. The survival of these patients varies from a few months to several years. Patients with cervical lymph node involvement with unknown primary site regardless of treatment modality are known to have a better prognosis. Platinum based chemotherapy is the primary modality of treatment. In patients with localized disease involving a group of locoregional lymph nodes multimodality treatment may provide long term disease control.

SUMMARY

In summary EPSCCs are uncommon malignancies which are morphologically,

immunohistochemically, and ultrastructurally indistinguishable from their pulmonary counterparts. They are thought to arise either from a multipotential stem cell or as a late-stage phenomenon during the clonal evolution of an organ specific carcinoma. Extrapulmonary small cell carcinomas are aggressive neoplasms and have the tendency for rapid local growth and early distant metastases. The prognosis is in general poor but varies considerably based on the site of involvement and extent of the disease. Using SCC of lung as a therapeutic model, patients with limited stage disease are often treated with combined modality of therapy comprised of locoregional treatment with or without platinum based chemotherapy. Systemic chemotherapy is the mainstay of treatment in patients with extensive stage disease and offers palliation of disease-related symptoms and perhaps modest improvement in survival.

REFERENCES

Abbruzzese, J.L., Lenzi, R., Raber, M.N., Pathak, S., and Frost, P. 1993. The biology of unknown primary tumors. *Semin. Oncol. 20*: 238–243.

Beasley, M.B., Brambilla, E., and Travis W.D. 2005. The 2004 World Health Organization classification of lung tumors. *Semin. Roentgenol. 40*: 90–97.

Brenner, B., Laura, T.H., Klimstra, D.S., and Kelsen, D.P. 2004. Small-cell carcinoma of the gastrointestinal tract: A review. *J. Clin. Oncol. 22*: 2730–2739.

Brenner, B., Tang, L.H., Shia, J., Klimstra, D.S., and Kelsen, D.P. 2007. Small cell carcinomas of the gastrointestinal tract: clinicopathological features and treatment approach. *Semin. Oncol. 34*: 43–50.

Casas, F., Ferrer, F., Farrus, B., Casals, J., and Biete, A. 1997. Primary small cell carcinoma of the esophagus: A review of literature with emphasis on therapy and prognosis. *Cancer 80*: 1366–1372.

Chan, J.K., Loizzi, V., Burger, R.A., Rutgers, J., and Monk, B.J. 2003. Prognostic factors in neuroendocrine small cell cervical carcinoma; a multivariate analysis. *Cancer 97*: 568–574.

Clark, R., and Ihde, D.C. 1998.Small-cell lung cancer: treatment progress and prospects. *Oncology 12*: 47–58.

Crowder, S., and Tuller, E. 2007. Small cell carcinoma of the female genital tract. *Semin. Oncol. 34*: 57–63.

Duguid, J.B., and Kennedy, A.M. Oat cell tumors of mediastinal glands. 1930. *J. Pathol. Bacteriol. 33*: 93–99.

Frazier, S.R., Kaplan, P,A., and Loy, T.S. 2007. The pathology of extrapulmonary small cell carcinoma. *Semin. Oncol.34*: 30–38.

Galanis, E., Frytak, S., and Lioyd, R.V. 1997. Extrapulmonary small cell carcinoma. *Cancer 79*: 1729–1736.

Gnepp, D.R., Corio, R.L., and Brannon, R.B. 1986. Small cell carcinoma of the major salivary glands. *Cancer 58*: 705–714.

Haider, K., Shahid, R.K., Finch, D., Sami, A., Ahmad, I., Yadav, S., Alvi, R., Popkin, D., and Ahmed, S. 2006. Extrapulmonary small cell cancer: a Canadian province's experience. *Cancer107*: 2262–2269.

Hoffman, P.C., Mauer, A.M., and Vokes, E.E. 2006. Lung Cancer. *Lancet 355*: 479–485.

Hoskins, P.J., Swenerton, K.D., Pike, J.A., Lim, P., Aquino-Parsons, C., Wong, F., and Lee, N. 2003. Small-cell carcinoma of the cervix: fourteen years of experience at a single institution using a combined-modality regimen of involved-field irradiation and platinum-based combination chemotherapy. *J. Clin. Oncol. 21*: 3495–3501.

Katahira, A., Akahira, J., Niikura, H., Ito, K., Moriya, T., Matsuzawa, S., Makinoda, S., Oda, T., Fujiwara, K., and Yaegashi, N. 2004. Small cell carcinoma of the endometrium: report of three cases and literature review. *Int. J. Gynecol. Cancer 14*: 1018–1023.

Leech, S.N., Kolar, A.J., Barrett, P.D., Sinclair, S.A., and Leonard, N. 2001. Merkel cell carcinoma can be distinguished from metastatic small cell carcinoma using antibodies to cytokeratin 20 and thyroid transcription factor 1. *J. Clin. Pathol. 54*: 727–729.

Lo Re, G., Canzonieri, V., Veronesi, A., Dal Bo, V., Barzan, L., Zancanaro, C., and Trovo, M. 1994. Extrapulmonary small carcinoma: a single-institution experience and review of literature. *Ann. Oncol. 5*: 909–913.

Lobins, R., and Floyd, J. 2007. Small cell carcinoma of unknown primary. *Semin. Oncol. 34*: 39–424.

Medgyesy, C.D., Wolff, R.A., Putnam, J.B. Jr., and Ajani, J.A. 2000. Small cell carcinoma of the esophagus: The University of Texas M.D. Anderson Cancer Center experience and literature review. *Cancer 88*: 262–267.

Mirza, I., and Shahab, N. 2007. Small cell carcinoma of the breast. *Semin Oncol. 34*: 64–66.

Palmgren J.S., Karavadia S.S., Wakefield M. 2007. Unusual and underappreciated: small cell carcinoma of the prostate. *Semin. Oncol. 34*: 22–29.

Peydro-Olaya, A., Llombart-Bosch, A., Carda-Batalla, C., and Lopez-Guerrero, J.A. 2003. Electron microscopy and other ancillary techniques in the diagnosis of small round cell tumors. *Semin. Diagn. Pathol. 20*: 25–45.

Remick, S.C., Hafez, G.R., and Carbone, P.P. 1987. Extrapulmonary small cell carcinoma. A review of the literature with emphasis on therapy and outcome. *Medicine. 66*: 457–471.

Remick, S.C., and Ruckdeschel, J.C.1992. Extrapulmonary and pulmonary small-cell carcinoma: tumor biology, therapy, and outcome. *Med. Pediatr. Oncol. 20*: 89–99.

Renner, G. 2007. Small cell carcinoma of the head and neck: a review. *Semin. Oncol. 34*: 3–14.

Shahab, N. 2007. Extrapulmonary small cell carcinoma of the bladder. *Semin. Oncol. 34*: 15–21.

Shaco-Levy, R., Manor, E., Piura, B., and Ariel, I. 2004. An unusual composite endometrial tumor combining papillary serous carcinoma and small cell carcinoma. *Am. J. Surg. Pathol. 28*: 1103–1106.

Shin, S.J., DeLellis, R.A., Ying, L., and Rosen, P.P. 2000. Small cell carcinoma of the breast: A clinicopathologic and immunohistochemical study of nine patients. *Am. J. Surg. Pathol. 24*: 715–722.

Sved, P., Gomez, P., Manoharan, M., Civantos, F., and Soloway, M. 2004. Small cell carcinoma of the bladder. *BJU Int. 94*: 12–17.

Vrouvas, J., and Ash, D.V. 1995. Extrapulmonary small cell cancer. *Clin. Oncol. 7*: 377–381.

Welborn, J., Jenks, H., Taplett, H., and Walling, P. 2004. High-grade neuroendocrine carcinomas display unique cytogentics aberrations. *Cancer Genet. Ctyogenet. 155*: 33–41.

14
Magnetic Resonance Imaging of the Lung: Automated Segmentation Methods

William F. Sensakovic and Samuel G. Armato III

INTRODUCTION

Identification and segmentation of structures of interest are necessary steps in the computer-based analysis of medical images. Computer-aided diagnostic (CAD) systems utilize segmentation algorithms to isolate specific structures (represented by 2D or 3D regions in an image or set of images, respectively); conversely, to remove extraneous structures that may introduce errors in the computerized analysis. This step increases both the specificity and sensitivity of the CAD system and decreases computation time by focusing analysis on smaller regions representing the structures of interest. Segmentation of the lung parenchyma is often the first step when computerized analysis focuses on the thorax. High contrast, central positioning, relatively large size in comparison to other thoracic structures, and contiguous to other critical structures (e.g., heart) render the lungs useful as both a target for primary analysis and a reliable starting point for the analysis of other thoracic structures.

Segmentation of lung parenchyma in computed tomography (CT) scans is one of the most extensively researched areas in medical image processing. The low density of lung parenchyma compared with surrounding soft tissue translates into high contrast on CT, which in turn facilitates the use of several image processing techniques such as histogram thresholding, active contours, and seeded region growing. Conversely, multiple factors have limited the clinical utility of thoracic magnetic resonance imaging (MRI) and thus limited the need for lung segmentation in MR scans. Contrast and orientation of magnetic resonance scans are determined by the image acquisition protocol, and thus may require image processing methods specific to each pulse sequence and image orientation. The clinical utility of thoracic MRI is also limited by low resolution and long acquisition times that cause severe image artifacts. Recent improvements in the in-plane resolution, pulse sequences, acquisition time, and contrast media (e.g., hyperpolarized gas), however, have made MR a viable modality for thoracic imaging and have renewed interest in lung segmentation for thoracic MR applications (Eibel *et al*., 2003; Entwisle, 2004; Evans and Gleeson, 2004; Levin *et al*., 2001; Weber *et al*., 2004).

THORACIC MAGNETIC RESONANCE IMAGING AND ACQUISITION ARTIFACTS

A magnetic resonance scanner generates high-contrast soft-tissue images without subjecting a patient to ionizing radiation. First, a patient is placed in a strong magnetic field generated by a superconducting magnet. The nuclei of the hydrogen atoms that compose the tissue of the patient possess a small magnetic moment that causes the nuclei (essentially protons for hydrogen atoms) to align along and precess about the magnetic field. The patient is then subjected to a radio-frequency pulse that causes the hydrogen nuclei to temporarily rotate perpendicular to the axis of the magnetic field. In this alignment, the precessing hydrogen nuclei induce an electric current (signal) in a receiving antenna connected to the magnetic resonance scanner. This signal is then mathematically reconstructed into an image of the patient. The reconstruction maps the signal to a rectangular matrix of numbers, where the position in the matrix corresponds to the physical position of tissue in the patient, and the matrix value (also called gray-level value, brightness, or signal intensity) is proportional to the density of hydrogen nuclei at that specific position in the patient. In general, the greater the density of hydrogen nuclei in the patient, the brighter the gray-level value recorded in the image. The bone and lung parenchyma of a healthy patient produce almost no MR signal due to the low density of hydrogen nuclei. Conversely, thoracic soft tissue and diseases of the lung and pleura (e.g., tumor and effusion) contain a substantially higher density of hydrogen nuclei and thus exhibit high signal intensity. Thus, abnormalities of the lungs in MR images will appear as bright, high-signal tissue on the surrounding dark, low-signal lung parenchyma background. The introduction of intravenous gadolinium contrast further increases the image contrast by increasing the signal of diseased tissue without impacting the signal of normal lung parenchyma.

The promising soft-tissue contrast properties of thoracic MR imaging are mitigated by several acquisition artifacts that reduce image quality and may introduce errors into CAD analysis. Ghosting is the periodic repetition of a structure along the phase-encoding dimension of an image due to motion during image acquisition. In thoracic imaging, several structures (e.g., lungs and heart) exhibit repetitive motion during image acquisition that may result in ghosting (Hashemi *et al*., 2004; Liang and Lauterbur, 2000). Cardiac motion artifacts occur due to the beating of the heart and the pulsation of blood through the major vessels. In transverse MR sections, this artifact manifests as a large column of noise (ghosting) that extends along the anteroposterior dimension of the image (Figure 14.1). This column often masks the underlying lung parenchyma and may mimic disease due to its high signal intensity. Injection of a contrast agent such as gadolinium further increases the signal intensities of the heart and thus exacerbates cardiac motion artifact. Pulmonary motion artifacts are related to respiratory motion and manifest in two ways. First, the expansion and contraction of the thorax may cause ghost contours of the chest wall to form both inside and outside the patient thorax

FIGURE 14.1. Common artifacts occurring in thoracic MR sections. Cardiac motion creates a large column of noise along the anteroposterior direction. Also note the pulmonary motion artifact present as recurring contours of the thorax (white arrows) and lung deformation due to disease (black arrows). (Reprinted with permission from Sensakovic et al., 2006.)

(Figure 14.1). This artifact is especially strong along the anterior portion of the thorax in transverse MR scans. Second, motion of the diaphragm may cause ghosting and partial volume effects that artificially increase the signal intensity in the lung.

AUTOMATED SEGMENTATION METHODS

This section will review automated lung segmentation methods specifically developed and tested on thoracic MR scans. The segmentation methodology and testing results developed in each study will be provided; however, due to the inherent complexity of these methods, the reader is referred to the original studies for specific implementation details.

THRESHOLDING, SHAPE DESCRIPTORS, AND MORPHOLOGICAL OPERATORS

Thresholding (Sonka *et al.*, 1999) is a low-level image processing technique that divides an image into two disjoint sets: (1) pixels with gray-level values greater than the threshold value and (2) pixels with gray-level values less than the threshold value. The threshold may be user defined or automatically derived from the image. The disjoint sets are represented as a binary image (an image with pixels turned "on" if they satisfy the threshold and turned "off" otherwise).

A shape descriptor is a function that takes an image region as input and generates a number that characterizes the morphological shape of the image region. Several such functions are common to medical image processing: area, perimeter, center-of-mass, compactness, and circularity. Area and perimeter are defined in the conventional sense and are computed by counting pixels in the image region or perimeter and then multiplying this count by a scaling factor provided by the magnetic resonance scanner to transform the pixel count into units of mm^2 or mm, respectively. The center of mass defines the balance point of the region, which is mathematically defined as $COM = \sum_i x_i g_i \Big/ \sum_i g_i$ where x_i is the position of the ith pixel within the region and g_i is the corresponding gray-level value. The compactness shape descriptor measures the degree to which a region is elongated. Compactness is defined as: $C = 4\pi * Area/Perimeter^2$ and

ranges from 0 (for a line segment) to 1 (for a perfect circle) (Sonka *et al*., 1999). A shape descriptor similar to compactness is circularity (Giger *et al*., 1988). Circularity measures the degree of similarity between the region and a circle with an equivalent area. Circularity is defined as $Circularity = R_{circle} / R_{total}$, where R_{circle} is the number of region pixels falling within an area-equivalent circle that is centered at the region's center of mass, and R_{total} is the total number of pixels in the region.

Morphological operators (Sonka *et al*., 1999) represent a broad range of image operators that alter the shape of an image region. This discussion will focus on two operators (erosion and dilation) and their combinations (openings and closings). Define the kernel (K) to be a binary set of pixels defined by the user (the most usual choice is a solid disc of user-defined radius). The erosion of a binary image (I) by K is computed in the following manner. For each pixel I_c in I, center the kernel K on I_c. If all "on" pixels in K are also "on" in the corresponding neighborhood of I_c then leave I unaltered. If any pixel is "on" in K but "off" in the neighborhood of I_c then turn "off" I_c. The effect of applying the erosion operator is to thin an image region by turning pixels "off" at the region perimeter. The dilation of I by K is computed in a similar manner. For each pixel I_c in I, center the kernel K on I_c. If all "on" pixels in K are "off" in the neighborhood of I_c then leave I unaltered. If any pixel is "on" in both K and the neighborhood of I_c then turn "on" I_c. The effect of applying the dilation filter is to thicken an image region by turning pixels "on" at the region perimeter.

An opening operation is defined as an erosion followed by a dilation. The result of opening an image is that regions smaller than K will be eliminated from the image and regions larger than K will lose some shape detail at the perimeter (i.e., the perimeter will be smoothed), but otherwise retain the general shape and size of the original region. A closing operation is defined as a dilation followed by an erosion. The result of closing an image is that regions with holes (groups of "off" pixels surrounded by "on" pixels) smaller than K will be filled while the rest of the region and regions without any holes will lose some shape detail at their perimeters similar to the opening operation.

Sensakovic *et al*. (2006) implemented a multi-step method based on thresholding, shape descriptors, and morphological operators to segment the lung parenchyma on a section-by-section basis (Figure 14.2). First, the thorax is segmented from the image background using a threshold derived from the histogram of the section. After application of this threshold to the

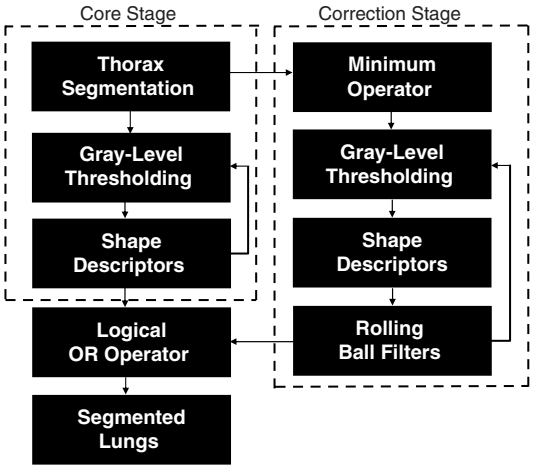

FIGURE 14.2. Block diagram of the automated method for segmentation of lung regions from thoracic MR scans implemented by Sensakovic et al. (2006)

image, the contour of the largest contiguous group of "on" pixels in the resulting binary image is defined as the candidate thoracic contour. All pixels of the original image that lie within the thoracic contour then constitute the candidate thoracic region. Two shape descriptors (area and compactness) are calculated from the candidate thoracic region and compared with predefined minimum values. If the thoracic descriptors are less than their respective minima, then the gray-level threshold is decreased and the process is repeated. If the thoracic descriptor thresholds are satisfied, then a series of opening filters is applied to the candidate thoracic region to smooth the contour. The candidate thoracic region image is then multiplied by the original image to create the thorax-segmented image. This process effectively "stamps out" a thorax-segmented image from the original image using the candidate thoracic region as a template.

Once the thorax-segmented image is established, a histogram-based gray-level thresholding technique is applied to the thorax-segmented image to create a lung-thresholded image. The gray-level histogram of an image is a function f(i), where i is an image gray-level value and f(i) is the number of image pixels with a gray-level value of i. The histogram of a thoracic MR section exhibits a bimodal distribution with a lower peak composed predominantly of the gray-level values of the lung parenchyma regions and an upper peak composed predominantly of the gray-level values of soft-tissue regions. The threshold for lung segmentation is defined as the minimum in the histogram that separates the two histogram peaks of the thorax-segmented image.

Candidate lung contours are defined as the contours encompassing all contiguous groups of "on" pixels in the thresholded image. The candidate lung contours and all enclosed pixels are then defined as candidate lung regions. Shape descriptors (area, compactness, center of mass, and perimeter) are computed for each candidate lung region and are compared to empirically determined shape descriptor thresholds. All regions that fail to satisfy the descriptor thresholds are defined as non-lung regions and are eliminated from the binary image. If any candidate lung region satisfies the shape descriptor thresholds, a lung-segmented image is created; otherwise, the gray-level threshold is decreased and the process is repeated. If the threshold decreases to zero without detecting a lung region, then the initial threshold may have been set too low; the initial threshold is then increased and the process is repeated. If still no lung regions are detected after this final adjustment, then the image is determined to contain no viable lung regions.

The initial segmentation discussed above (referred to from here on as the "core stage" segmentation) is sensitive to the presence of disease and acquisition artifacts, which have the potential to cause substantial segmentation errors. Accordingly, a second stage of segmentation (referred to from here on as the "correction stage" segmentation) is implemented in parallel with the core stage to decrease this sensitivity to disease and artifact and to increase segmentation accuracy. The correction stage is designed to generate a second lung-segmented image that captures valid lung regions that may have been obscured by disease or acquisition artifacts and thus are absent from the lung-segmented image of the core stage. First, a minimum operator (also called a grayscale erosion operator) is applied to

the thorax-segmented image. Acquisition artifacts and disease are typically composed of high gray-level, heterogeneous pixels. The minimum operator lowers the gray-level values of the lung regions masked by acquisition artifacts or disease by assigning to each pixel the minimum gray-level value of its 3×3-neighborhood in the thorax-segmented image. Application of the minimum operator also homogenizes the lung region gray-level values. Gray-level thresholding techniques, morphological filters, and shape descriptors, as described for the core stage, are then applied to the minimum-filtered image to generate a thresholded lung image.

The effect of the minimum operator is indiscriminate and often results in the incorporation of non-lung regions into the thresholded lung image. These non-lung regions are typically composed of soft-tissue pixels immediately adjacent to the actual lung regions. These soft-tissue pixels are included because their gray-level values are artificially lowered by the minimum operator. A series of rolling ball filters (Armato *et al.*, 2001) is applied to the internal aspect of the lung segmentation contours to eliminate these non-lung "protrusions." At each lung contour pixel, a disc of a predefined radius is placed along the inside of the contour with an orientation that yields the greatest amount of overlap between the lung contour and the disc boundary. The segment of lung contour between the two extreme points of contact with the disc boundary is then analyzed. If the length of the lung contour segment exceeds a predefined fraction of the corresponding disc boundary segment length, then a line connecting the two contact points replaces the lung contour segment. If the number of overlapping pixels between the new connecting line and the lung contour exceeds a predefined threshold, then the lung contour is maintained to avoid segmentation error. Thus, these disc-shaped filters locate and eliminate protrusions (usually non-lung regions) in the lung contour based on shape characteristics. The output of the rolling ball filters is the correction stage lung-segmented image.

The application of rolling ball filters to candidate lung contours may incorrectly eliminate protrusions composed of actual lung region pixels. These incorrectly eliminated lung protrusions, however, are often present in the core stage lung-segmented image and thus can be retained by combination of the two lung-segmented images. For each candidate lung region in the correction stage lung-segmented image, circularity is calculated and compared with a predefined threshold. The region is eliminated if it is not within an empirically determined range of circularity values. This process eliminates rinds of non-lung pixels adjacent to the actual lung regions that were incorrectly segmented due to the minimum operator, but not eliminated by the rolling ball. Candidate lung regions from the correction stage lung-segmented image that satisfy the circularity criterion are combined with regions from the core stage lung-segmented image through application of a logical OR operator to construct the final lung-segmented image (Figure 14.3).

A random sample of 101 thoracic MR sections was chosen from a 23-scan, 413-section database of transverse 256×256-pixel T1-weighted spoiled GRASS (SPGR) MR scans. True lung regions were manually delineated by two radiologists through a computer interface (Figure 14.3). Nine of ten patients included abnormalities

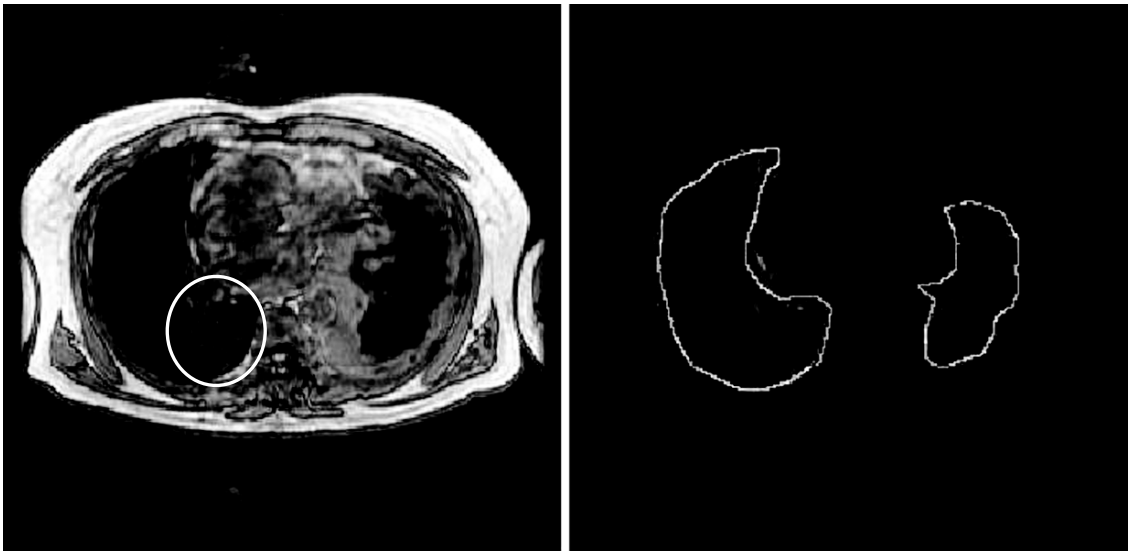

FIGURE 14.3. Example of a typical segmentation result from the automated method. The left image is the original artifact corrupted image and the right is the resulting lung segmentation with a radiologist outline superimposed (white outline). Lung regions severely impacted by cardiac motion artifact have been properly segmented (oval). Note that window and level have been set to illustrate the presence of cardiac motion artifact. (Reprinted with permission from Sensakovic et al., 2006.)

such as mesothelioma, scarring, pleural plaques, enlarged lymph nodes, hydropneumothorax, lung resection, lung nodules, intrathoracic extrapleural fat, and pericardial effusion. Further, only $n=5$ lungs were determined to be free of acquisition artifacts by a radiologist.

An area-of-overlap measure (AOM) was used to compare the true lung regions with lung regions created by the automated method. The AOM measure of two regions, A and B, is defined as the number of pixels contained within the intersection of the regions divided by the number of pixels contained within the union of the regions: $AOM = \frac{(A \cap B)}{(A \cup B)}$. AOM values are contained within the range [0, 1], with a value of 0 corresponding to disjoint regions and a value of 1 corresponding to complete overlap.

The AOM between lung regions delineated by Radiologist 1 (Radiologist 2) and lung regions delineated by the automated method was 0.82 ± 0.16 (0.83 ± 0.13 respectively) when averaged over all lung regions. The AOM values between the lung regions delineated by each radiologist and lung regions delineated by the core stage alone were also calculated. The AOM when averaged over all lung regions was increased when the correction stage was added to the core stage. A paired Student's t-test for differences in means showed that the improved AOM attained by the core and correction stages over the core stage alone was statistically significant ($p<0.01$). In addition to improving the AOM, application of the core and correction stages reduced the number of disjoint lung regions by five for each radiologist when compared with the core stage alone.

Empirically determined shape descriptor thresholds were applied throughout the automated segmentation method. The empirical nature of the shape descriptor thresholds introduces the possibility of reducing robustness of the automated method by over-training the thresholds on a specific data set. The sensitivity of the automated method to each shape descriptor threshold was determined by varying each threshold individually by 30% and calculating the AOM between the automated method (with modified shape descriptor thresholds) and both radiologists for the same 101 randomly selected sections. The maximum deviation in the AOM observed by varying the shape descriptor thresholds was 0.5%, implying that the automated method is insensitive to the specific choices of shape descriptor thresholds. The method was run using unoptimized code written in Matlab 7 on an AMD XP 2500+ with 1 Gigabyte of RAM and the Linux operating system. The average cpu time per section for lung segmentation was 21 s.

MODEL-BASED SEGMENTATION

Model-based segmentation methods (Sonka *et al*., 1999) (also known as template matching and chamfer matching) rely on the creation of an *a priori*, simple, and generally applicable model of the anatomic structures of interest. This model is then "fit" to a target (e.g., the data set under analysis) based on some similarity measure. Once the best fit is achieved, regions of the data set are labeled (segmented) corresponding to the best-fit model. The first step in the application of a model-based segmentation method is the creation of the model. Models are data templates created based on *a priori* characteristics of the structures of interest derived from observation of these structures in some separate training data set. In general, the goal of a model is to capture characteristics (usually shape and positional information) that uniquely identify a structure of interest, but are also general enough that the model is insensitive to minor variations in patient anatomy, data set noise, or acquisition artifacts.

Once defined, the model is fit to the target. Three decisions must be made when determining the model fitting methodology: (1) define the target, (2) define the degrees of freedom for the fit, and (3) define the mechanism (similarity measure) for fitting. The target is usually the data set under analysis; however, it is often advantageous to process the data set to accentuate or suppress certain regions with anticipated improvements in the fitting process. If a processed version of the data set is considered, processing is restricted to transformations that ensure that the best fit of the model to the processed data set is also the best fit of the model to the original data set.

Non-rigid deformation is the most general choice with regard to the degrees of freedom. This deformation essentially treats the model as a rubber sheet allowing non-uniform transformations within the model. Though non-rigid deformation allows for the most general type of fitting, such a method exhibits two major drawbacks. First, computational complexity is substantially increased with each degree of freedom (non-rigid transforms may contain hundreds of degrees of freedom). Second, the more degrees of freedom that exist, the more likely that the model will

fail to fit the data by deforming incorrectly along one of the degrees of freedom. Rigid fitting, conversely, limits transformations to rotations, translations and scalings that globally transform the model. This approach reduces the number of degrees of freedom but does not allow for transformation differences within the model.

Once the degrees of freedom are determined, an appropriate mechanism for fitting the data must be established. A common mechanism for model fitting is to establish an energy potential derived from the data set, which forces the model into the correct position. Once the energy potential is established, the model is iteratively fit to the data set by minimizing (or maximizing) the energy of the model relative to the potential.

Lelieveldt *et al.* (1999) implemented a 3D model-based segmentation method to simultaneously segment two structures of interest: lung parenchyma and thoracic skin boundary. This study implemented a multi–step approach to establish the model. First, an expert manually delineated the surface of each structure of interest on a training data set. Next, a smoothed representation of each structure of interest was derived from the expert-delineated contours. Finally, the smoothed representations were merged to create a single model. The target for fitting was a binary data set where only the pixels lying on the interface between air and soft tissue were retained. Air-tissue interface pixels were identified by applying a histogram-based threshold (similar to the histogram thresholding used in Sensakovic *et al.* (2006)) to identify a gray-level threshold that roughly separated air (extra-thoracic space and lung) from soft tissue. A rigid transformation method that allowed for rotation, translation, and scaling was chosen to limit the degrees of freedom for fitting. This was implemented in a hierarchical manner: (1) fit the thoracic skin boundary, (2) propagate these deformation parameters to the lungs, and (3) fit the lungs individually. The patient position was assumed to be roughly centered in the MR scanner, with the patient supine and feet first; thus, only axial translations were allowed to vary. The scaling was assumed to be equal in all dimensions. Thus, the thoracic skin boundary was only allowed a single scale degree of freedom and a single translational degree of freedom. No such restrictions were imposed on the lungs, thus allowing for all possible rigid deformations. Unlike most model-based segmentation methods, Lelieveldt *et al.* created an energy potential (similarity measure) based on the model and then fit the target to the model (this is in contrast to the usual method of defining the similarity measure on the target and fitting the model to the target). The energy potential applied for fitting was given by

$$E = \begin{cases} 1 & if\ |d(x_i, y_i, z_i)| > \omega \\ \left(d(x_i, y_i, z_i) / \omega \right)^2 & if\ |d(x_i, y_i, z_i)| \le \omega \end{cases}$$

. This assigns a value of 1 to each model pixel (i) that exists a distance (d) greater than ω (set to 10 mm in this study) from a structure-of-interest boundary and a distance-proportional value to each pixel within a distance ω from a structure-of-interest boundary. The energy of a given model fit is determined by summing the energy potential over all points defined by the air-tissue interface pixels of the data set under analysis. The best fit was determined by minimizing the summed energy by applying Levenberg-Marquardt nonlinear minimization.

The model-based segmentation method was applied to 12 ECG-gated thoracic MR scans (8 short axis cardiac MR scans and 4 thoracic scout scans). Computations were carried out on a Sun Ultrasparc 1 workstation, and computation times varied from 2–20 min depending on the size of each image set. The segmentation of each fit was qualitatively evaluated by an expert observer. The segmentation was considered acceptable if the segmented lung boundaries were within 10 mm of the actual lung boundaries. This method resulted in acceptable segmentations in 4 of 8 cardiac scans and 3 of 4 scout scans. This was further improved to 6 of 8 cardiac scans and 4 of 4 scout scans when the model was manually initialized.

PARAMETRIC ACTIVE CONTOURS

A parametric active contour (Kass *et al.*, 1988) is a deformable curve that segments image structures by fitting the curve to structure boundaries. The curve deforms to balance internal and external forces based on the mathematical methods defined by regularization theory and the calculus of variations. In its most basic form, a 2D curve $v(x,y)$ is parameterized by the index $s \in [0,1]$ according to the equation $\vec{v}(s) = [x(s),y(s)]$. The active contour deforms and moves through the image space towards structure boundaries by minimizing its energy functional (E) given by $E = \int E(\vec{v}(s))\, ds$.

The energy functional (E) can be divided into two separate terms based on their sources – an internal energy term and an external energy term. The internal energy is intrinsic to the curve itself and is independent of the image into which the curve is placed. Internal energy acts as a regularizing factor that smoothes the curve and interpolates the curve points in the absence of structure boundary information. The internal energy (E_{int}) is usually defined as $E_{\text{int}} = \frac{1}{2}\left(\alpha \left| \frac{\partial \vec{v}}{\partial s} \right|^2 + \beta \left| \frac{\partial^2 \vec{v}}{\partial s^2} \right|^2 \right)$, where α and β are user-defined scalars. Before explaining the terms of E_{int}, it is first necessary to define how to approximate continuous differential quantities for application to discrete computerized images. The finite difference method is a technique that approximates differential quantities as differences between adjacent points. Thus, given a point s=i on the active contour, the differential $\frac{\partial \vec{v}}{\partial s}$ evaluated at point i can be approximated by the difference $\vec{v}_i - \vec{v}_j$, where j is a neighboring point of i. Given this approximation, it is possible to explain E_{int} in physical terms. Conceptually the active contour can be visualized as a rubber band. The degree of elasticity inherent to the active contour is determined by the first term of E_{int} and the user-defined scalar β. Let s_1 and s_2 be two consecutive points on the curve. The magnitude of the distance between these curve points is $|\vec{v}_2 - \vec{v}_1|$, and from application of finite differences, this magnitude is an approximation of the term $\left| \frac{\partial \vec{v}}{\partial s} \right|$ evaluated at s_2. As the curve expands, this differential increases and causes E_{int} to increase accordingly. Since the curve deforms to minimize its total energy, this term penalizes stretching of the curve with α determining the strength of the penalty.

The degree of stiffness inherent in the active contour is determined by the second term of E_{int} and the user-defined scalar β.

Let s_1, s_2, and s_3 be three consecutive points on the curve and $\vec{d}_{3,2} = \vec{v}_3 - \vec{v}_2 = \vec{v}_1 - \vec{v}_2 = \vec{d}_{1,2}$. If these three points are collinear, then $\left|\vec{d}_{3,2} - \vec{d}_{1,2}\right| = 0$; however, if these points (i.e., vectors) are not collinear so that the line connecting these points is curved, then $|\vec{d}_{3,2} - \vec{d}_{1,2}| > 0$. Similar to the first term, the application of finite differences demonstrates that $|\vec{d}_{3,2} - \vec{d}_{1,2}|$ is an approximation of $\frac{\partial^2 \vec{v}}{\partial s^2}$ evaluated at s_2. As the magnitude of the curvature about this point increases, the term $\frac{\partial^2 \vec{v}}{\partial s^2}$ increases. Thus, the second term increases E_{int} as the curvature of the active contour increases (i.e., the energy penalizes the curve for bending with β determining the strength of the penalty). It should be noted that setting β to zero allows the active contour to attain sharp corners.

The external energy (E_{ext}) is defined by the image into which the active contour is placed. The external energy is derived from the image by application of a user-defined function of the image edges. An edge in an MR image can be visualized as a step in the gray-level values of adjacent pixels. In general, the user-defined external energy must satisfy three conditions: (1) the structure boundary is a subset of the edges within the image, (2) the external energy smoothly increases as the distance to the nearest image edge increases, and (3) the spatial extent of the external energy field should be large enough to impact the entire curve. Conditions 1 and 2 ensure that the correct solution (the structure boundary) exists and that the curve continuously deforms towards it. Condition 3 ensures that the active contour "sees" the external energy field.

Many different external energy fields exist to localize the active contour to structure boundaries; however, this discussion will focus on two fields that have been applied specifically for lung segmentation in MR scans: balloon-distance potential and gradient vector flow. A balloon-distance potential field (Cohen, 1991) is defined as $\vec{F} = k_1 \vec{n}(s) - k_2 \frac{\nabla(-|\nabla I|^2)}{\left\|\nabla(-|\nabla I|^2)\right\|}$, where k_1 and k_2 are user-defined scalars, I is the image, ∇ is the gradient operator, and $\vec{n}(s)$ is the unit vector normal to the active contour at point s. The first term of $\vec{F}$ is a constant force that acts normal to the curve. This term is often referred to as the balloon force since it can be visualized as "blowing up" the active contour with a constant force k_1. The second term detects edges and normalizes them to a constant attractive strength k_2. The field created by the second term does not extend very far from the image edge and thus for the curve to "see" this force, the curve must be initialized close to the actual structure boundary. The first term is applied to extend the "reach" of the force $\vec{F}$. Assuming that the curve is initialized interior to the structure boundary, the first term will cause the curve to expand until it reaches an image edge, at which point the second term counteracts the force of the first term (assuming $k_2 > k_1$) and the contour stops deforming. It should be noted that the first term of $\vec{F}$ should be classified as internal energy since it is dependent on the active contour itself and not on the image; however, it is included as part of the balloon-distance force to illustrate the impact of its interaction with the second term of $\vec{F}$.

The gradient vector flow (GVF) (Xu and Prince, 1998) is currently one of the most widely used external energy fields due to its large capture range and precise localization properties. The first step in

defining the GVF field is to locate edges within the image by applying a derivative of Gaussian filter. The kernels of a derivative of Gaussian filter are defined as $\frac{dG}{dx} = -\frac{x}{\sigma^2} e^{-\frac{x^2+y^2}{2\sigma^2}}$ and $\frac{dG}{dy} = -\frac{y}{\sigma^2} e^{-\frac{x^2+y^2}{2\sigma^2}}$, where σ is the user-defined variance of the Gaussian distribution. Derivative of Gaussian filtering takes the original image as input and produces two derivative images (D_x and D_y) corresponding to edges in the x and y directions. A single edge image (f) is created from D_x and D_y according to $f = \sqrt{D_x^2 + D_y^2}$. The gray-level value of each pixel in f is proportional to edge strength (i.e., how much the gray-level values of the original image pixel change in the neighborhood of the pixel). The advantage of derivative of Gaussian filtering over other edge detection methods is that it simultaneously smoothes the image (to an extent determined by σ) while it detects edges. This smoothing allows the filter to ignore image noise that could otherwise be incorrectly detected as edge pixels.

Once an edge image has been generated by the derivative of Gaussian filter, the GVF field is created by allowing edges to diffuse throughout the edge image. The GVF field $\vec{F}(x, y) = [a(x, y), b(x, y)]$ is a set of two images, a and b, that correspond to the energy field components in the vertical and horizontal directions, respectively. The GVF field is calculated by minimizing the functional $\varepsilon = \iint \mu(a_x^2 + a_y^2 + b_x^2 + b_y^2) + |\nabla f|^2 |\vec{F} - \nabla f|^2 dxdy$ where μ is a user-defined constant controlling the tradeoff between the first and second terms, a_x is the partial derivative of a with respect to x, and f is the derivative of Gaussian generated edge image. When the position is far from an edge in the image, the first term of ε dominates the integral and causes the field to vary slowly. The second term of ε controls GVF field behavior in the neighborhood of an edge. In this case, the second term of the integral is strongest and the field is set to the image edge as defined by ∇f.

The GVF functional (ε) is minimized by applying the techniques derived from the calculus of variations. In the calculus of variations, a functional ε is minimized by solving the Euler equations:

$\mu\nabla^2 a - (a - f_x)(f_x^2 + f_y^2) = 0$

$\mu\nabla^2 b - (b - f_y)(f_x^2 + f_y^2) = 0$. These x and y components of the GVF field (a and b, respectively) are solved by defining the Euler equations as explicit functions of time $\mu\nabla^2 a - (a - f_x)(f_x^2 + f_y^2) = \partial a(x,t)/\partial t$ $\mu\nabla^2 b - (b - f_y)(f_x^2 + f_y^2) = \partial b(x,t)/\partial t$.

The edges diffuse until a steady state is reached when the partial differentials on the right side of these equations are approximately equal to zero. Computationally, the diffusion over time is carried out iteratively by applying the finite difference method to the time-varying differentials of the Euler equations:

$\left[\mu\nabla^2 a - (a - f_x)(f_x^2 + f_y^2)\right]\gamma + b(x, t-1) = a(x,t)$

$\left[\mu\nabla^2 b - (b - f_y)(f_x^2 + f_y^2)\right]\gamma + a(x, t-1) = b(x,t)$.

In this set of equations, γ is a user-defined scalar that controls the time step of the iteration, all quantities on the left side of the equations are evaluated at iteration (time step) t-1, and the current approximation to the GVF field is the pair of images a and b evaluated at iteration t on the right side of the equations.

After the functional forms of the internal and external energy fields are selected, the active contour energy functional E can be minimized using

the same method applied to the GVF functional ε. The Euler equation of E is $\alpha \frac{\partial^2 \vec{v}}{\partial s^2} - \beta \frac{\partial^4 \vec{v}}{\partial s^4} + \vec{F} = 0$, which is then solved by again expressing it as an explicit function of time (with time step ω) and iterating: $\left[\left(\alpha \frac{\partial^2 \vec{v}(x,t)}{\partial s^2} - \beta \frac{\partial^4 \vec{v}(x,t)}{\partial s^4}\right) + \left(\vec{F}\right)\right]\omega + \vec{v}(t-1) = \vec{v}(t).$

Ray *et al.* (2003) implemented a lung segmentation method based on active contours with a modified GVF external energy field. In this implementation, several active contours are initialized within the lung parenchyma of each MR section. Next, the edge image is created and the value at each point corresponding to an initialized contour point is set to the unit normal of that point. The diffusion of the edge image is then performed according to the iterative GVF equations. Once the external energy field is formed, all active contours are simultaneously deformed. The modified GVF field ensures that active contours may become arbitrarily close, but never intersect. Once deformation of all contours is complete, the regions of each MR section defined by each contour are merged by taking their union. This merging results in a single contour for each lung in each section of the MR scan. This method was evaluated on 10 coronal, thoracic MR scans consisting of a total of 118 sections. The true lung boundaries were defined manually by expert radiologists. The true lung regions, defined as the interior of the true lung boundaries, were then compared to the computer segmented lung regions on a section-by-section basis. The segmentation accuracy was quantified by calculating the percent error: $PE = \frac{\sum_{x,y} I_a(x,y) - I_t(x,y)}{\sum_{x,y} I_t(x,y)} * 100$, where I_a is the computer-segmented MR section and I_t is the corresponding MR section with radiologist-defined truth. The active contour method demonstrated a high degree of segmentation accuracy, resulting in a mean percent error (averaged over each scan) between 4.05% and 9.01%.

NEURAL NETWORK/ACTIVE CONTOUR COMBINATION

A neural network (Müller *et al.*, 1995; Sonka *et al.*, 1999) is a system of simple equations that combine multiple inputs to generate an output. The name "neural network" is derived from the idea that each simple equation mimics a single neuron in the human brain. Complex processes can be built from the simple neurons by allowing them to interact with each other (i.e., form a network). Image processing applications based on neural networks usually involve the classification of inputs into predefined sets (e.g., classifying a tumor region as malignant or benign). This discussion will focus on a specific type of neural network that has been previously applied for MR lung segmentation—the multilayer perceptron (MLP).

A multilayer perceptron (MLP) (Minsky and Papert, 1969) is composed of four parts: (1) inputs, (2) weights, (3) activation functions, and (4) outputs (Figure 14.4). The input to a MLP is a set of numbers representative of the object to be classified. Usually inputs are previously calculated features of the image region under analysis. Features most often used as inputs are shape characteristics, texture descriptors, and gray-level values of a local neighborhood of the image region. The interaction among inputs is mediated by a series of weights that define how any two inputs combine. The second

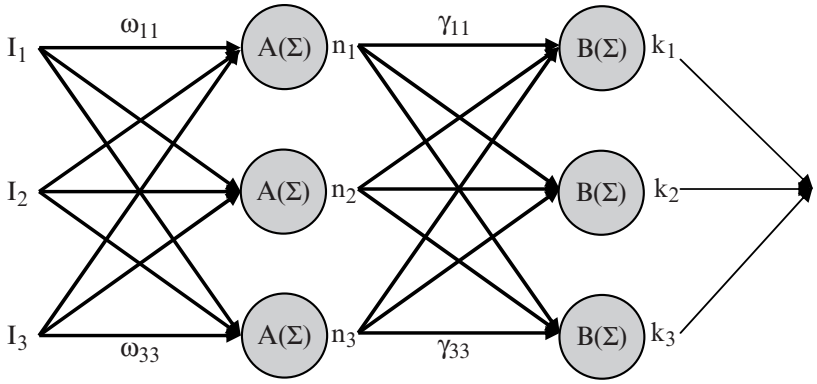

FIGURE 14.4. Block diagram of a multilayer perceptron. Each input (I) is weighted by a value (ω), summed (Σ), and transformed by the activation function (A). Each node value (n) is then weighted by a value (γ), summed, and transformed by the activation function (B). The output values of the second node layer (k) are then combined to generate the final neural network output

layer of the MLP is formed by combining all inputs in all possible combinations according to these weights. For example, given three input values (I_j=I_1, I_2, or I_3), nine possible combinations of inputs exist, each with an interaction weight ω (ω_{ij} = $\omega_{1,1}$, $\omega_{1,2}$, $\omega_{1,3}$, $\omega_{2,1}$, $\omega_{2,2}$, $\omega_{2,3}$, $\omega_{3,1}$, $\omega_{3,2}$, $\omega_{3,3}$). These interactions are grouped into three nodes (n_i) in the second layer by the equation $n_i = A(\sum_j \omega_{i,j} I_j)$ where A is the activation function (Figure 14.4).

This process can be repeated multiple times by adding extra node layers (also called hidden layers) that combine the nodes from the previous layer. Using the previous example, a third layer could be added by defining a second set of weights γ and creating another layer of nodes k using $k_i = B\left(\sum_j \gamma_{i,j} n_j\right)$ where B is a second activation function (Figure 14.4). The addition of node layers increases the flexibility of the neural network when classifying image regions. For a MLP with two node layers (n and k), the first node layer can be viewed as analyzing local knowledge (since its inputs are individual image features), while the second layer analyzes global knowledge (since its inputs are already combinations of image features).

The activation function (A and B in the examples above) is a key element of each node. These functions determine the numerical value of the output of each node (or, in the case of the final layer of nodes, the output of the neural network). These functions traditionally utilize the Heaviside step function, hyperbolic tangent, or other sigmoidal functions. The activation functions allow the output of each node to mimic a neuron by determining if the input values of each node are sufficient to allow the neuron to "fire." The output of the neural network is the output value of the final layer of nodes. For example, to classify a tumor region as malignant or benign, the final layer may use a Heaviside step function as the activation function. If the feature values of the region combine in previous nodes to generate a value greater than the transition value of the Heaviside step function, then the output will be a value of 1 (corresponding to a classification of "malignant"). If the combined

values are below the transition value of the Heaviside step function, then the MLP will generate a value of −1 at output (corresponding to a classification of "benign").

The inputs, outputs, and activation functions implemented for a specific classification task are determined by the network designer based on *a priori* knowledge of the problem to be solved. Weights applied at each set of nodes, however, usually cannot be approximated *a priori*. The weights are instead determined by training the neural network on a known set of data. For classification tasks, the training data usually consists of a set of images with each neighborhood within the image preassigned to a given class (this assignment is usually performed manually by an expert human observer). The training data is analyzed by the neural network and the output of the neural network is compared with the preassigned classes. The weights for each node are then altered, the training data is again analyzed by the neural network, and the output is again compared with the preassigned classes. This process of training is repeated until the output of the neural network is as close as possible to the predefined classifications. The weights for each node that are derived from training are then used when applying the neural network to new data.

Middleton and Damper (2004) applied a combined neural network and active contour method for MR lung segmentation. The first step of this combined method was the application of a multilayer perceptron (MLP). The goal of the MLP was to classify each pixel of an MR section as either "lung boundary" or "not a lung boundary." The inputs to the MLP were the 49 gray-level values that comprise a 7×7-pixel neighborhood of the pixel to be classified. The weights were determined by training on MR sections with lung boundary pixels preassigned semi-automatically by an expert observer.

Unfortunately, the lung boundary that results from application of the MLP often contains gaps or extra contour pixels. These errors are due to false positives (pixels not on the lung boundary that are incorrectly classified as lung-boundary pixels) and false-negatives (lung-boundary pixels that are incorrectly classified as non-lung-boundary pixels) generated by the MLP output. An active contour was applied to the lung boundary output of the MLP to correct these classification problems. A Gaussian-smoothed version of the MLP output was defined as the edge image and the balloon-distance external energy was applied to deform the active contour. The active contours were initialized as two circles encompassing the edges of the right and left lungs. The neural network/active contour method was evaluated on 13 T1-weighted transverse thoracic MR scans consisting of roughly 35 sections per scan. Lung segmentation accuracy was quantified by the precision (P) and recall (R) metrics. Precision is defined as $P = \frac{T_P}{T_P + F_P}$, where T_p is the number of true positives (correctly classified lung-boundary pixels) and F_p is the number of false-positives. Recall is defined as $R = \frac{T_P}{T_P + F_n}$, where F_n is the number of false-negatives. The precision averaged over all sections in a scan ranged from 0.866 to 0.987 for the left lung and from 0.819 to 0.961 for the right lung. Similarly, the recall averaged over all sections in a scan ranged from 0.715 to 0.906 for the left lung and from 0.598 to 0.886 in the right lung.

In conclusion, automated segmentation of lung parenchyma is often the first step in CAD of thoracic MR scans. The presence of disease and acquisition artifacts, however, often confounds simple image processing techniques, thus necessitating the application of complex computerized methods to obtain accurate lung segmentations. The methodology of automated techniques derived from multiple areas of image processing theory was reviewed and the segmentation accuracy of each method was presented. The high levels of accuracy demonstrated by each method imply a potential for research applications and implementation in clinical CAD systems for MR images analysis.

REFERENCES

Armato, S. G., 3rd, Giger, M. L., and MacMahon, H. 2001. Automated detection of lung nodules in CT scans: Preliminary results. *Med. Phys. 28*: 1552–1561.

Cohen, L. 1991. On active contour models and balloons. *Comp. Vision Grap. Image Process 53*: 211–218.

Eibel, R., Tuengerthal, S., and Schoenberg, S. O. 2003. The role of new imaging techniques in diagnosis and staging of malignant pleural mesothelioma. *Curr. Opin. Oncol. 15*: 131–138.

Entwisle, J. 2004. The use of magnetic resonance imaging in malignant mesothelioma. *Lung Cancer 45 Suppl 1*: S69–71.

Evans, A. L., and Gleeson, F. V. 2004. Radiology in pleural disease: State of the art. *Respirology 9*: 300–312.

Giger, M. L., Doi, K., and MacMahon, H. 1988. Image feature analysis and computer-aided diagnosis in digital radiography. 3. Automated detection of nodules in peripheral lung fields. *Med. Phys. 15*: 158–166.

Hashemi, R. H., Bradley, W. G., and Lisanti, C. J. 2004. *MRI*: *The basics*. Philadelphia: Lippincott Williams & Wilkins

Kass, M., Witkin, A., and Terzopoulis, D. 1988. Snakes: Active contour models. *Intern. J. Comp. Vision 1*: 321–332.

Lelieveldt, B. P., van der Geest, R. J., Rezaee, M. R., Bosch, J. G., and Reiber, J. H. 1999. Anatomical model matching with fuzzy implicit surfaces for segmentation of thoracic volume scans. *IEEE Trans. Med. Imag. 18*: 218–230.

Levin, D. L., Chen, Q., Zhang, M., Edelman, R. R., and Hatabu, H. 2001. Evaluation of regional pulmonary perfusion using ultrafast magnetic resonance imaging. *Magn. Reson. Med. 46*: 166–171.

Liang, Z.-P., and Lauterbur, P. C. 2000. *Principles of Magnetic Resonance Imaging: A Signal Processing Perspective*. SPIE Optical Engineering Press: IEEE Press.

Middleton, I., and Damper, R. I. 2004. Segmentation of magnetic resonance images using a combination of neural networks and active contour models. *Med. Engin. Physics 26*: 71–86.

Minsky, M. L., and Papert, S. 1969. *Perceptrons: An Introduction to Computational Geometry*. MIT.

Müller, B., Reinhardt, J., and Strickland, M. T. 1995. *Neural Networks: An Introduction*. Berlin: Springer.

Ray, N., Acton, S. T., Altes, T., de Lange, E. E., and Brookeman, J. R. 2003. Merging parametric active contours within homogeneous image regions for mri-based lung segmentation. *IEEE Trans. Med. Imag. 22*: 189–199.

Sensakovic, W. F., Armato, S. G., 3rd, Starkey, A., and Caligiuri, P. 2006. Automated lung segmentation of diseased and artifact-corrupted magnetic resonance sections. *Med. Phys. 33*: 3085–3093.

Sonka, M., Hlaváč, V., and Boyle, R. 1999. *Image Processing, Analysis, and Machine Vision*. San Francisco: PWS.

Weber, M. A., Bock, M., Plathow, C., Wasser, K., Fink, C., Zuna, I., Schmahl, A., Berger, I., Kauczor, H. U., and Schoenberg, S. O. 2004. Asbestos-related pleural disease: Value of dedicated magnetic resonance imaging techniques. *Invest. Radiol. 39*: 554–564.

Xu, C., and Prince, L. 1998. Snakes, shapes, and gradient vector flow. *IEEE Trans. Imag. Proc. 7*: 359–369.

15
Peripheral Lung Lesions: Diagnosis Using Transcutaneous Contrast-Enhanced Sonography

Christian Görg and Angelique Holland

INTRODUCTION

Diagnostic ultrasound is limited by a nearly complete sound reflexion at the aerated lung. Because of the fundamental limitations of all sonographic modalities, sectional images (e.g., computed tomography (CT) and magnetic resonance tomography [MRT]) are absolutely essential in order to achieve an overview of the entire thorax. Despite this general limitation, sonography has been established as a gold standard diagnosis of pleural effusion in addition to X-ray examination of the thorax (Görg and Bert, 2004a, b). The additional diagnostic potential of sonography in the chest for the diagnosis of peripheral pleural based lung diseases has long been underestimated. The past 20 years have witnessed a large number of original articles that systematically show the potential uses as well as limitations of chest sonography using B mode ultrasound and colour Doppler sonography (Mathis and Lessnau, 2003).

During the last decade ultrasound contrast agents in conjunction with contrast specific imaging techniques are increasingly accepted in clinical use for diagnostic imaging in several organs (Albrecht *et al*., 2004). Based on the dual arterial supply of the lung, this organ is, similar to the liver, suited for evaluation of arterial vascularity by contrast enhanced sonography (Görg *et al*., 2003). Kunz *et al*. (2004) were the first who reported in an abstract regarding the potential use of contrast enhanced sonography in patients with lung disease. Recently, first original articles and a review regarding the value of contrast enhanced sonography for the diagnosis of pleural-based lung lesions were published (Görg *et al*., 2005a, b, 2006a, b).

In the diagnosis of peripheral lung lesions the specific questions raised during sonographic investigation are as follows:

- Criteria to determine the benign or malignant nature of disease
- Image guidance for biopsy
- Whether surgery and resection can be performed
- Controls to monitor therapy
- Imaging vascular complications (Mathis and Lessnau, 2003)

This review will focus on the value of contrast enhanced sonography with a transcapillary second-generation contrast agent (SonoVue®; Braco) (Bokar, 2000) for answering these specific questions. This

pictorial review is based on the experience of 400 contrast enhanced sonographic studies in patients with pleural based lung lesions.

PATHOPHYSIOLOGIC BASICS OF PULMONARY VASCULARITY

Anatomically, the lung is characterized by a dual blood supply. The existence of a systemic *bronchial arterial* supply to the lung, besides pulmonary arteries, was first described by Galen in the second century. The extrapulmonary branches take course to the hila where they form an intercommunicating circular arc around the main stem bronchi from which the true central bronchial arteries radiate. In humans, the bronchial arterial system is invariably related to the bronchial tree and divides with it. Peripheral bronchial arteries lie within the interlobar and interlobular septa and supply the visceral pleura. This system not only provides nutrition to the bronchi, pulmonary vessels, alveoli, interstitial tissue, and visceral pleura, but also functions as a haemodynamic system with anastomoses between bronchial and pulmonary arteries. Anastomoses between the two systems are normally closed. In case of occlusion of pulmonary arteries or during hypoxic conditions in the diseased lung, contraction of smooth muscle in the walls of small blood vessels occurs and therefore, the anastomoses become open and nutrition of this region from bronchial arteries occurs (Babo *et al*., 1979; Turner-Warnick, 1963). From angiographic studies it is known that peripheral lung lesions, like lung cysts, pulmonary abscesses and liquidified pneumonia are predominantly supplied by bronchial arteries (Yuan *et al*., 2002). Even lung cancer is supported by bronchial arteries (Yuan *et al*., 1994).

Pulmonary arterial vessels show a tree-like distribution. The arteries contain relatively little smooth muscle, while the capillaries are free of smooth muscle. Pressures in pulmonary arterial circulation are very low compared to systemic circulation. The circulation is responsible for the gas exchange. In contrast to the hypoxic vasodilatation of the systemic circulation, a hypoxic vasoconstriction is seen in the pulmonary circulation which is called the Euler-Liljestrand mechanism.

Intercostal arteries arise from the aorta, course along the ribs and are supplied to the thoracic wall. They are strictly located within the thoracic wall. Tumorneoangiogenesis arises from bronchial arteries. Pulmonary arteries seem to have no or very low neoangiogenetic capacity (Mitzner *et al*., 2002).

GENERAL CONSIDERATIONS OF CONTRAST-ENHANCED SONOGRAPHY

Contrast-enhanced-sonographic studies in this review were performed immediately after baseline sonography with a contrast-devoted unit (Acuson-Sequoia GI, Siemens medical solution) that had contrast-specific, continuous-mode software. A low mechanical index was used. A sulfur hexafluoride-based microbubble contrast medium (SonoVue®) was injected intravenously within 2 s *via* a 20-gauge cannula. A volume of 2.4 ml was administered, followed by a 5 ml saline flush. This contrast medium containes a low-solubility gas and is therefore suitable for low mechanical index imaging. The low mechanical index technique with low-solubility gas contrast agents permits continuous, real-time imaging of all phases. During clinical studies (Albrecht *et al*., 2004; Bokar, 2000) of

Sonovue®, safety parameters (such as vital signs, electrocardiograph, oxygen saturation, neurologic examination, and clinical laboratory parameters) were monitored and no clinically meaningful change was noted.

Time of enhancement was measured after i.v., space injection and extent of enhancement of pleural lesions were evaluated using the splenic tissue enhancement as an "in vivo" reference (Forsberg *et al*., 1999; Görg and Bert, 2006c). In healthy probands, contrast enhancement appears in the right heart between 1–6 s (indicating the time window of pulmonary arterial vascularity), and between 8–11 s in the left heart after injection (indicating the time window of systemic bronchial arterial vascularity. So a short time of enhancement under 6 s indicates a pulmonary arterial supply and a delayed time of enhancement 6 s may indicate a systemic bronchial arterial supply (Görg *et al*., 2006a) (Figure 15.1). It should be noted that in patients with chronic heart failure and chronic pulmonary disease the values of time to enhancement for pulmonary arterial supply may be longer than 6 s. For distinguishing pulmonary-arterial, from bronchial-arterial vascular supply contrast enhanced sonography of the surrounding chest wall, liver, or spleen is helpful. Time of enhancement of these tissues indicates the time of the systemic arterial supply.

CLINICAL DATA OF CONTRAST-ENHANCED SONOGRAPHY

Pleurisy

Clinical sign of pleurisy is characterized by a breath-dependent localized pleural pain, but the final diagnosis presents a considerable challenge and requires a high degree of clinical suspicion from the attending physician. B-mode sonographic patterns as well as color Doppler sonographic patterns of pleurisy/pleuropneumonia have been described (Görg and Bert, 2004b; Mathis and Lessnau, 2003). In a recent study (Görg *et al*., 2005b), all patients with breath-dependent pain due to pleurisy/pleuropneumonia had a high specific contrast-enhanced-sonographic pattern characterized by a short time of enhancement, indicating a pulmonary arterial supply, and a marked enhancement during the arterial and parenchymal phase (Figure 15.2). The value of contrast enhanced sonography in patients with breath-depending pain and a pleural lesion of unknown cause are characteristic of pleurisy by a short time to enhancement and marked extent of enhancement.

Pulmonary Embolism

With B-mode ultrasound peripheral pleural based lesions may be seen in patients with pulmonary embolism. But these lesions are not specific and a concise exclusion or diagnosis of this embolism requires additional imaging procedures such as ventilation/perfusion scintigraphy (PIOPED, 1990), spiral computed tomography (Baile *et al*., 2000), MRT angiography (Lechleitner *et al*., 2002), and pulmonary angiography (Remy-Jardin *et al*., 1992). First data regarding contrast-enhanced-sonography in patients with confirmed pulmonary embolism have shown no enhancement of the lesions in most cases studied, suggesting the absence of pulmonary arterial blood supply (Figure 15.3). In patients with pulmonary embolism and pleural effusion or chronic pulmonary embolism a mixed enhancement may be observed showing unenhanced infarcted

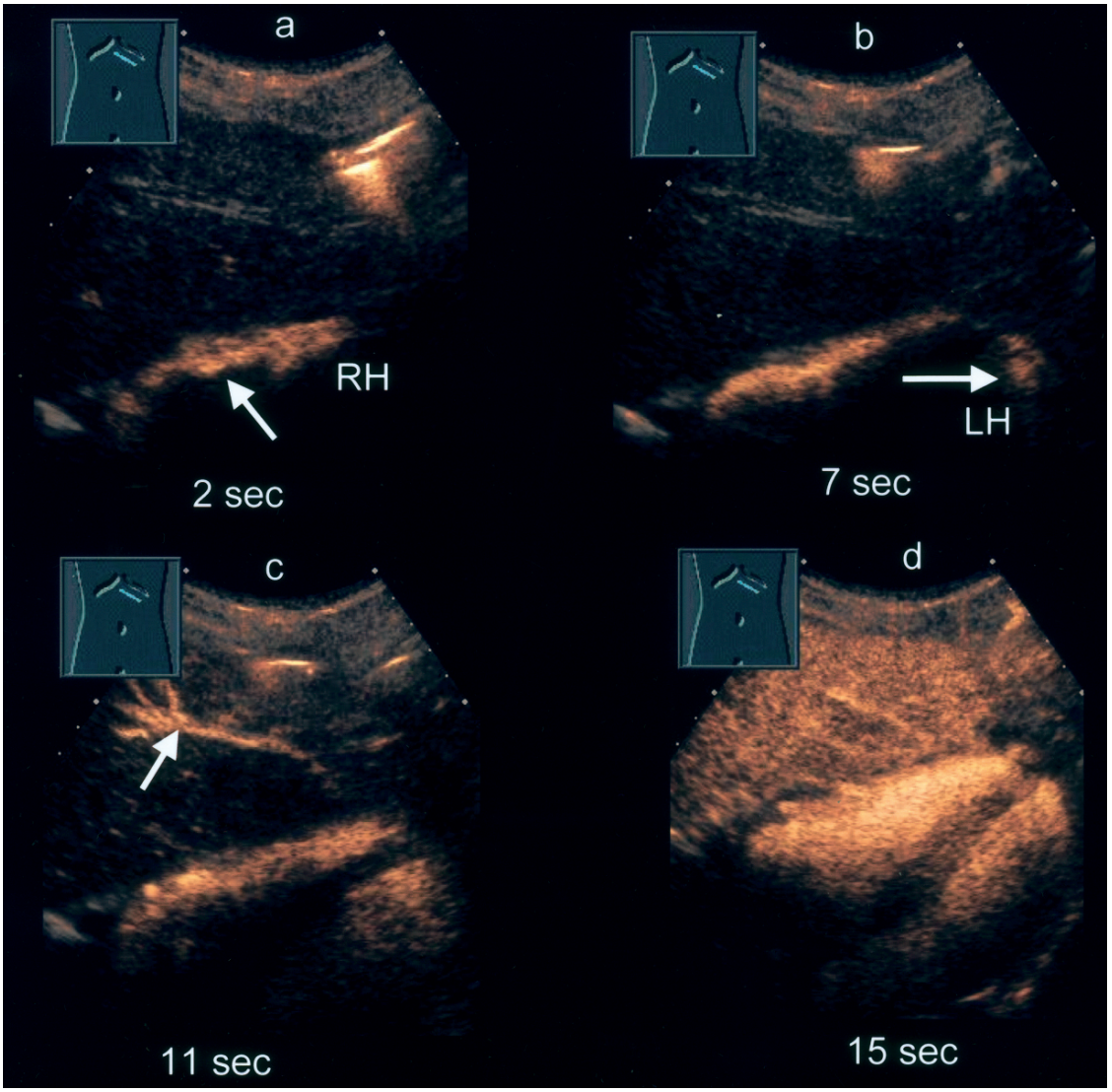

FIGURE 15.1. Subcostal scan through the right and left heart in a healthy young adult with vizualization of the contrast enhancement after contrast medium application into a peripheral vein. (RH = right heart, LH = left heart) A: Contrast enhancement of the right heart appears about 2 s (arrow). B: Contrast enhancement of the left heart appears about 7 s (arrow). C: Arterial contrast enhancement of the liver appears after 11 s (arrow). D: After 15 s a complete enhancement of the liver and the heart is seen.

areas beneath vascularized tissue. In patients with suspected pulmonary embolism and peripheral lesions on B mode ultrasound the complete or partly unenhanced lesion seems to be a characteristic contrast-enhanced-sonographic pattern for pulmonary embolism. In patients with septic embolism the lesion may show a central unenhanced area. There is some evidence that contrast-enhanced-sonography may discriminate

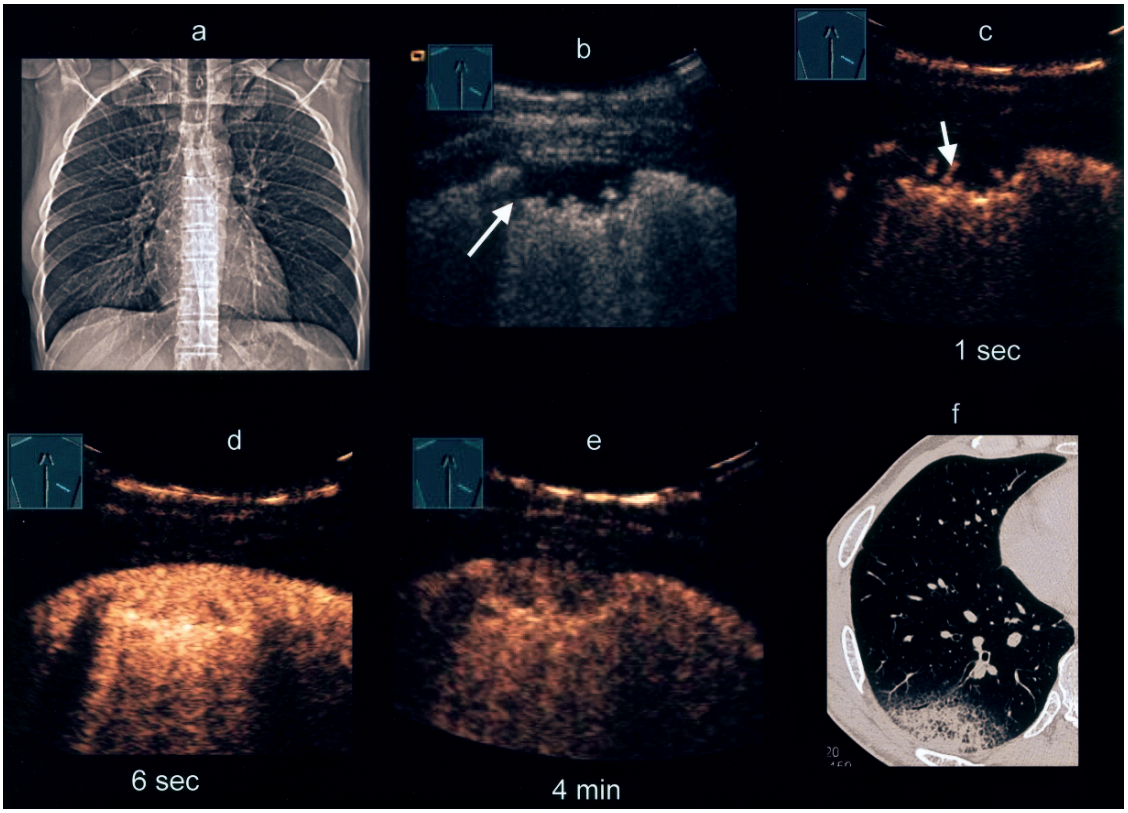

FIGURE 15.2. Thirty-seven year old male patient with breath-dependent right sided pleural pain. Clinical diagnosis of pleurisy was made. A: X-ray of the chest shows no pleural effusion or signs of pleuropneumonia. B: B-mode sonography shows a 2 × 1 cm size irregular delineated hypoechoic pleural lesion (arrow). C: Contrast enhanced sonography shows a short time to enhancement after 1 s (arrow) suggesting pulmonary arterial supply. D: After 6 s a homogeneous enhancement of the lesion is seen. E: After 4 min the lesions shows reduced enhancement. F: Computed tomography confirms diagnosis of pleuropneumonie

peripheral pleural embolism from pleurisy (Görg *et al*., 2005b).

Pleural Based Pulmonary Nodules

Transcutaneous B-mode ultrasound enables visualization of pleural-based pulmonary nodules with a poor correlation to specific pathology. The differential diagnosis of pulmonary nodules includes infectious, malignant, inflammatory, autoimmune, environmental, and vascular causes. Despite the well known value of patient's history, clinical presentation, and radiographic findings for diagnose of pulmonary nodules, aggressive diagnostic procedures for histologic verification as the diagnostic "gold standard" are necessary in all cases of doubt. Based on the dual arterial supply of the lung, contrast-enhanced-sonography is qualified to discriminate pulmonary arterial from bronchial arterial lung vascularity. As shown, quantitative parameters such as

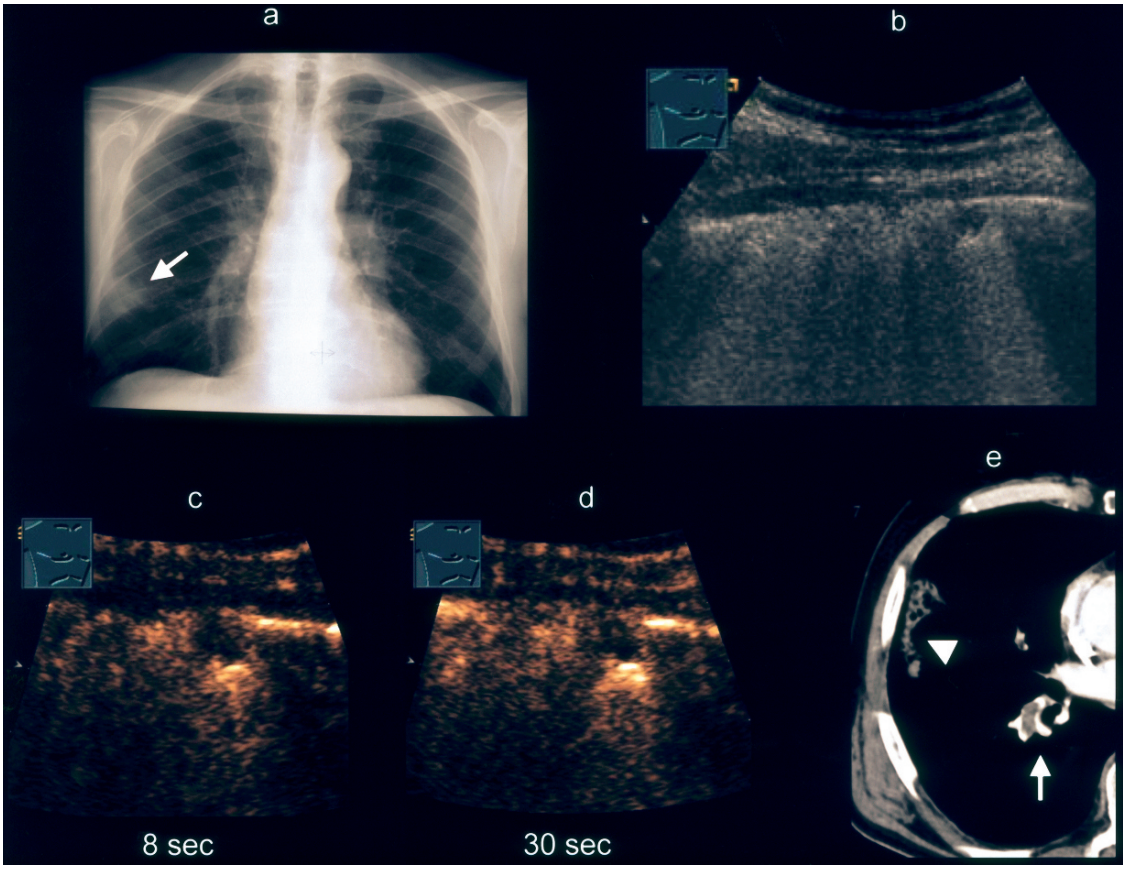

FIGURE 15.3. Sixty-four year old male patient with dyspnea and breath dependent right sided pleural pain. A: X-ray of the chest shows right sided pleural lesion (arrow). B: B-mode sonography shows a small round hypoechoic pleural lesion (arrow). C: Contrast enhanced sonography shows no enhancement after 8 s indicating lost of pulmonary arterial supply. D: After 30 s no enhancement of the lesion is seen indicating absence of bronchial arterial supply. The area of no enhancement suggests evidence of pulmonary embolism. E: Contrast enhanced computed tomography confirms diagnosis of a central pulmonary embolism (arrow) with a peripheral lesion (stick)

time of enhancement and quantitative variables such as extent of enhancement do not enable distinction between benign and malignant pulmonary nodules (Görg *et al*., 2006a). However, in subgroups of patients with pulmonary nodules, contrast-enhanced-sonography identified characteristic patterns for malignant pulmonary nodules, embolic pulmonary nodules, and pneumonic pulmonary nodules (Görg *et al*., 2006a). This indicates only a little value of contrast-enhanced-sonography to reach a diagnostic conclusion in patients with pleural based pulmonary nodules of unknown cause.

Pneumonia

B-mode sonographic as well as color Doppler sonographic patterns of pleural based lesions including pneumonia has been reviewed (Görg *et al*., 2004b; Mathis

and Lessnau, 2003). A concise exclusion or diagnosis of pneumonia requires additional imaging procedures such as X-ray examination of the chest or contrast-enhanced CT. Patients with *pneumonia* and *pleuropneumonia* do have an enhancement by contrast-enhanced-sonography with a specific pattern characterized by a short time of enhancement in the majority of patients, suggesting a pulmonary arterial blood supply (Görg *et al*., 2006a). Additionally, a marked tissue enhancement during the arterial and parenchymal phase was seen in most patients (Figure 15.4). In most patients with pneumonia a reactive marked systemic arterial enhancement of the thickened pleura can be seen. Within the infiltrated parenchyma unen-

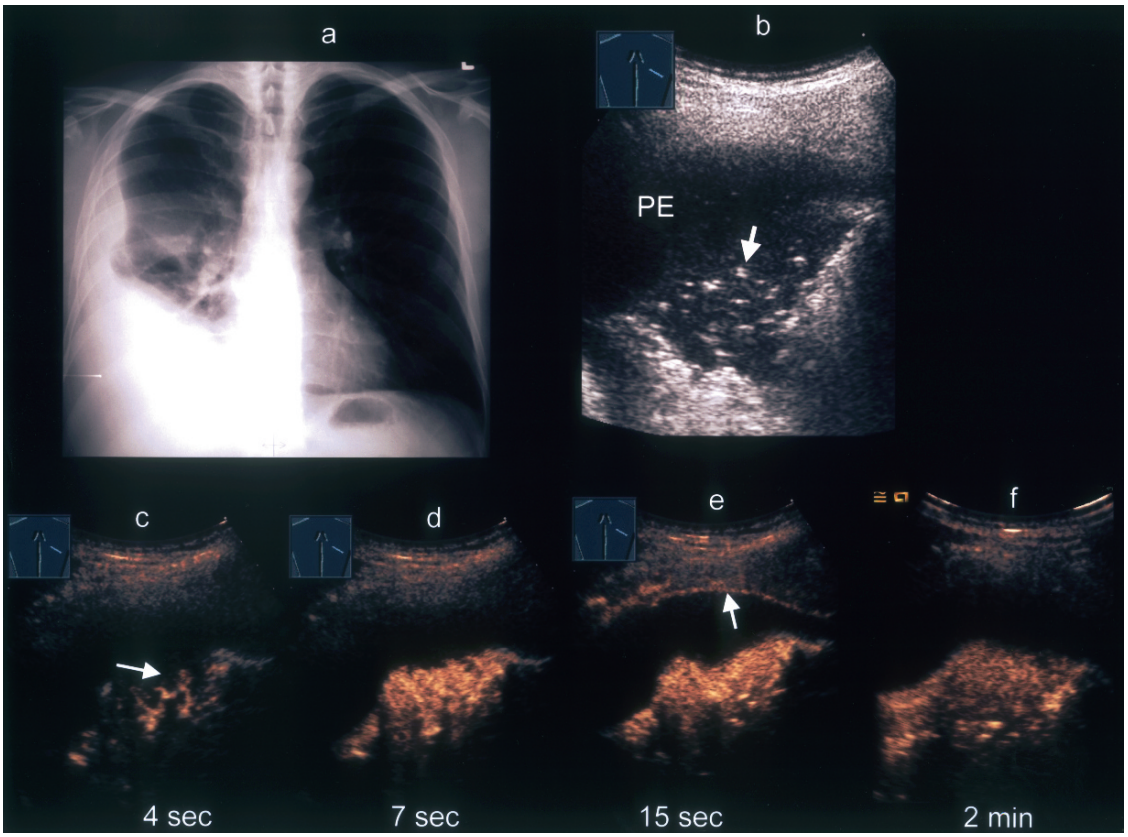

FIGURE 15.4. Forty-three year old male patient with dyspnoea and fever. Diagnosis of pneumonia was made. (PE = pleural effusion). A: X-ray of the chest shows right sided opacification of the lower lobe with a pleural effusion. B: B-mode sonography shows a right-sided pleural effusion with a consolidation of parts of the lung and evidence of an airbronchogram (arrow) suggesting pneumonia. C: Contrast enhanced sonography shows a short time to enhancement (4 s) of the pulmonary infiltration (arrow). This indicates a pulmonary arterial supply. D: After 7 s a homogeneous marked enhancement of the pulmonary infiltration is seen. E: After 15 s an enhancement of the intercostal artery is seen (arrow) indicating the time to systemic arterial supply. F: After 2 min the pulmonary tissue remains enhanced, whereas the thoracic wall shows a wash out phenomenon with no remaining enhancement

hanced areas may be visible and indicates sequestration. Demarcation of echogenic pleural effusion is clearly seen by the contrast-enhanced-sonography. In patients with chronic pneumonia a reduced extent of enhancement may be seen. The well known hypoxic vasoconstriction in the pulmonary circulation may be responsive for this phenomenon. Contrast-enhanced-sonography in patients with pneumonia may be helpful to detect complications such as sequestration or abscess formations, to demarcate surrounding fluid from tissue, and for possible differential diagnosis of infarctpneumonia.

Atelectasis

Atelectasis is defined as the absence of ventilation in portion of the lung or the entire lung and, therefore, can be imaged by sonography. Depending on the origin a distinction is made between compression atelectasis and obstructive (resorption) atelectasis.

As shown in a recent study, patients with atelectasis have a variable contrast-enhanced-sonographic pattern (Görg *et al*., 2006d). In patients with compression atelectasis there was a high specific pattern characterized by a short time to enhancement, indicating a predominant pulmonary arterial vascularisation and a marked enhancement during the arterial and parenchymal phase. In these patients with compression atelectasis the contrast agent apparently remains trapped in the lung tissue after having washed out of the blood pool in comparison to splenic enhancement. In patients with chronic compression atelectasis, a delayed time of enhancement may be seen. This indicates a shift to a bronchial arterial supply. Contrast-enhanced-sonography is helpful to identify unenhanced areas in the atelectated tissue due to necrosis, abscess, or metastasis. In patients with tumor associated obstructive atelectasis, variable contrast-enhanced-sonographic patterns can be seen. This is also seen in patients with a marked extent of enhancement and a short time of enhancement, indicating patent pulmonary arterial supply of the obstructive atelectasis, and in patients with delayed time of enhancement and a reduced extent of enhancement of the obstructive atelectasis, indicating an occlusion of the pulmonary vessels and a shift to a bronchial arterial supply. Transmural tumor growth with intraluminal cell formations in the pulmonary artery branches with consecutive obliteration and occlusions of pulmonary arterial vessels is responsible for this pattern (Kolin *et al*., 1988). This phenomenon is more often seen in chronic obstructive atelectasis or in a patient who already has received radiochemotherapy. The central tumor can be demarcated from the obstructive atelectasis by a delayed time of enhancement and a reduced extent of enhancement. Contrast-enhanced-sonography is helpful to identify unenhanced areas in the infiltrated tissue due to necrosis, abscess or metastasis.

Primary Lung Tumors

Tumors located within the thoracic wall are suited for sonographic imaging. Lung tumors and mediastinal tumors can only be documented on sonography when no aerated tissue hinders echo transmission, and CT is essential in order to overview the entire thorax. Based on color-Doppler-sonographic studies, lesions of the chest wall do have

a systemic intercostals arterial supply. Vascularity may be reduced or marked. Primary lung tumors whether they are benign or malignant are mostly characterized by a reduced vascularity with sparse single vessels (Görg *et al*., 2004a, b). These vessels have been identified as bronchial arteries or intercostal arterial supply in cases of origin in the thoracic wall (Görg *et al*., 2005a). Tumorangiogenesis is regarded as essential for tumor growth, and bronchial arteries play a role in tumor-vascularization. Tumor blood supply of lung cancer depends on tumor size, tumor localization, and tumor histology. In post-mortem angiograms of lung cancers with a size of 4 cm and more, the tumor is characterized by central areas of necrosis and cavities and more and more artery-to-artery anastomoses between bronchial and pulmonary vessels (Müller *et al*., 1978). Regarding the "time of enhancement" peripheral pleural based lung cancer lesions as well as metastasis showed a delayed time of enhancement and a reduced extent of enhancement suggesting a bronchial arterial supply, which plays a major role in the tumorneoangiogenesis of metastasis and growing cancer (Hsu *et al*., 1996, 1998). Central pleural based lung cancer lesions are composed of a central tumor with tumor atelectasis. In this context, pathological anatomical studies in lung cancer are important, which show invasion and destruction of pulmonary arteries in > 90% of cases (Fissler-Eickhoff and Müller, 1994). However, 16% of NSCLC cases show a growth pattern without destruction of the pulmonary vascularity (Pezzella *et al*., 1997). Especially the subtypes of adenocarcinoma and bronchiolo-alveolar carcinoma may be able to grow without neovascularization if they find a suitable pulmonary arterial vascular bed (Görg *et al*., 2002). In these cases with the "alveolar tumor growth pattern", pulmonary arterial supply still remains intact (Fissler-Eickhoff and Müller, 1994).

There is a value of contrast-enhanced-sonography for discrimination the central tumor-lesion from the tumor-atelectasis. Contrast-enhanced-sonography enables discriminating vital from avital tumor tissue, and is a diagnostic tool for correct imaging guided biopsy. Contrast-enhanced-sonography may be helpful to confirm diagnosis of focal cavitation and additionally may allow ultrasound-guided puncture to obtain material for bacteriological investigation in these patients. The value of CES for evaluation of a residual mass at the end of a full course treatment in patients with malignant lesions to the chest to discriminate vital from avital tissue is yet unclear.

In conclusion, contrast-enhanced sonography of the chest is limited to pleural based lesions. This sonography in peripheral lung lesions is feasible and depending on underlying diseases, lesions may show a variable time of enhancement and extent of enhancement. Contrast-enhanced-sonography enables to distinguishing pulmonary arterial supply from bronchial arterial supply by time of enhancement. First experiences with contrast-enhanced-sonography have shown that various peripheral lung lesions do have a characteristic contrast-enhanced-sonographic pattern regarding time of enhancement and extent of enhancement. First clinical data show that there are clinical conditions that may show a diagnostic advantage of contrast-enhanced-sonography in comparison to B-mode ultrasound. Contrast-enhanced-sonography may be helpful to confirm diagnosis of pleurisy, to confirm diagnosis peripheral pulmonary embolism,

to characterize lung opacification due to atelectasis, pneumonia, or tumor, and to assist in interventional procedures.

REFERENCES

Albrecht, T., Blomley, M., Bolondi, L., Claudon, M., Correrai, J-M., Cosgrove, D., Greiner, L., Jäger, K., de Jong, N., Leen, E., Lencioni, R., Lindsell, D., Mertegani, A., Solbiati, L. Thorelius, L., Tranquart, F., Weskott, HP., and Whittingham, T. 2004. Guidelines for the use of contrast agents in ultrasound. *Ultraschall Med. 25*: 249–256.

Babo, v.H., Müller, KMG., Huzky, A., and Bosnjakovic-Buscher, S.1979. Die bronchialarteriographie bei erkrankungen der lunge. *Radiologe 19*: 506–513 (in German).

Baile, E.M., King, G.G., Müller, N.L., D'Yachkova, Y., Coche, E.E., Pare, P.D., and Mayo, J.R. 2000. Spiral computed tomography is comparable to angiography for the diagnosis of pulmonary embolism. *Am. J. Resp. Crit. Care Med. 161*: 1010–1015.

Bokar, D. 2000. Diagnostic efficacy of SonoVue. *Am. J. Cardiol. 86* (suppl.): 196–246.

Fissler-Eickhoff, A., and Müller, K.M.1994. Pathologie der pulmonalarterien bei lungentumoren. *DMW 119*: 1415–1420 (in German).

Forsberg, F., Goldberg, B.B., Liu, B.B., Merton, D.A., Rawool, N.M., and Shi, W.T.1999. Tissue-specific US contrast agent for evaluation of hepatic and splenic parenchyma. *Radiology 210*: 125–132.

Görg, C., Seifart, U., Holzinger, I., Wolf, M., and Zugmaier, G. 2002. Bronchiolo-alveolar carcinoma: sonographic pattern of pneumonia. *Eur. J. Ultrasound 15*: 109–117.

Görg, C., Seifart, U., Görg, K., and Zugmaier, G. 2003. Color doppler sonographic mapping of pulmonary lesions: evidence of dual arterial supply by spectral analysis. *J. Ultrasound Med. 22*: 1033–1039.

Görg, C., and Bert, T. 2004a. Transcutaneous color doppler sonography of lung consolidations review and pictorial essay. Part 1. Pathophysiologic and color doppler sonographic basics of pulmonary vascularity. *Ultraschall Med. 25*: 221–226.

Görg, C., and Bert, T. 2004b. Transcutaneous colour doppler sonography of lung consolidations review and pictorial essay. Part 2. color doppler sonograhic patterns of pulmonary consolidations. *Ultraschall Med. 25*: 285–291.

Görg, C., Bert. T., Görg, K., and Heinzel-Gutenbrunner, M. 2005a. Colour doppler ultrasound mapping of chest wall lesions. *Br. J. Radiol. 78*: 303–307.

Görg, C., Bert, T., and Görg, K. 2005b. Contrast enhanced sonography for differential diagnosis of pleurisy and focal pleural lesions of unknown cause. *Chest 128*: 3894–3899.

Görg, C., Bert, T., Kring, R., and Dempfle, A. 2006a. Transcutaneous contrast enhanced sonography of the chest for evaluation of pleural based pulmonary lesions: experience in 137 patients. *Ultraschall Med. 27*: 437–444.

Görg, C., Kring, R., and Bert, T. 2006b. Transcutaneous contrast-enhanced sonography of peripheral lung lesions. *Am. J. Roentgenol. 187*: 420–429.

Görg, C., and Bert, T. 2006c. Second-generation contrast agent for sonographic differential diagnosis of perisplenic lesions. *Am. J. Roentgenol. 186*: 621–626.

Görg, C., Bert, T., and Kring, R. 2006d. Contrast-enhanced sonography of the lung for differential diagnosis of atelectasis. *J. Ultrasound Med. 25*: 35–39.

Hsu, W.H., Ikezoe. J., Chen, C.Y., Kwan, P.C., Hsu, C.P., Hsu, N.Y., Chiang, C.D., and Ho, W.L. 1996. Color doppler ultrasound signals of thoracic lesions: correlation with resected histologic specimens. *Am. J. Respir. Crit. Care Med. 153*: 1938–1951.

Hsu, W.H., Chiang, C.D., Chen, C.Y., Kwan, P.C., Hsu, J.Y., Hsu, C.P., and Ho, W.L. 1998. Color doppler ultrasound pulsatile flow signals of thoracic lesions: Comparison of lung cancer and benign lesions. *Ultrasound Med. Biol. 24*: 1087–1095.

Kolin, A., and Koutllakis, T. 1988. Role of arterial occlusion in pulmonary scar cancers. *Hum. Pathol. 19*: 1161–1170.

Kunz, A., Blank, W., Gemacher, O., Mathis, G., Schuler, A., Reuss, J., and Wehrle, A. 2004. Echosignalverstärker am thorax- work in progress. *Ultraschall Med. 25*: 37 (abstract).

Lechleitner, P., Riedl, B., Raneburger, W., Gamper, G., Theure, A., and Lederer, A. 2002. Chest sonography in the diagnosis of pulmonary embolism. A comparison with MRI angiography and ventilation perfusion scintigraphy. *Ultraschall Med. 23*: 374–378.

Mathis, G. and Lessnau, K.D. (eds.) 2003. *Atlas of Chest Sonography*. Springer, Berlin, Heidelberg, New York 72–89.

Mitzner, W., Lee, W., Georgukopoulus, O., and Wagner, E. 2002. Angiogenesis in the mouse lung. *Am. J. Pathol. 157*: 93–101.

Müller, K.M., and Meyer-Schwickerath, M. 1978. Bronchial arteries in various stages of bronchogenic carcinoma. *Path. Res. Pract. 163*: 34–46.

Pezzella, F., Pastorino, U., Tagliabue, E., Andreola, S.,Sozzi, G. Gasparini,G., Menare,S., Gatter, K.C., Harris, A.L., Fos, S., Buyse, M., Pilotti, M., Pienotti,M., and Rilke F. 1997. Non-small-cell lung carcinoma tumor growth without morphological evidence of neo-angiogenesis. *Am. J. Pathol. 151*: 1417–1423.

PIOPED Investigators. 1990. Value of the ventilation/perfusion scan in acute pulmonary embolism. Result of the prospective investigation of pulmonary embolism diagnosis. *YAMA 263*: 2753–2759.

Remy-Jardin, M., Remy, J., Wattine, I., and Girand, F. 1992. Central pulmonary thrombembolism: diagnosis with spiral volumetrie CT with the single-breath-hold-technique. Comparison with pulmonary angiography. *Radiology 185*: 381–387.

Turner-Warnick, M. 1963. Systemic arterial patterns in the lung and clubbing of the fingers. *Thorax 18*: 238–245.

Yuan, A., Chang, D.B., Yu, C.J., Kuo, S.M., Luh, K.T., and Yang, P.C. 1994. Color doppler sonography of benign and malignant pulmonoray masses. *Am. J. Roentgenol. 163*: 545–549

Yuan, A., Yang, P.C., Lee, L., Wu, D.H., Kuo, S.H., Luh, K.T., Cheng, W.J., and Liu, F.Y. 2002. Reactive pulmonary artery vasoconstriction in pulmonary consolidation by color doppler ultrasonography. *Ultrasound Med. Biol. 26*: 49–56.

16
Small Pulmonary Nodules: Detection Using Multidetector-Row Computed Tomography

Marco Das

PULMONARY

THE PULMONARY NODULE

Intrapulmonary nodules are one of the most common findings in multidetector row Computed tomography (MDCT) chest examinations. Midthun *et al*. (1993) defined pulmonary nodules as round opacities which are <3 cm in diameter and are usually surrounded by pulmonary parenchyma. Larger lesions are called masses, as they are most likely malignant. Unfortunately most pulmonary nodules are <10 mm in diameter leading to diagnostic difficulties, as differential diagnosis of these nodules is not easy, but may include potentially malignant diseases such as lung cancer and pulmonary metastasis. To differentiate between benign and malignant nodules, image features can be applied, but also sufficient diagnostic workup algorithms are necessary.

DIFFERENTIAL DIAGNOSIS OF PULMONARY NODULES

The differential diagnosis of pulmonary nodules includes a broad spectrum of different entities, including infectious, congenital, neoplastic, and other diseases, which are summarized in Table 16.1. It is well known from lung cancer screening trials (Henschke *et al*., 2001a,b), that more than 90% of pulmonary nodules <5 mm in diameter represent benign disease like granulomas. Unfortunately, the knowledge regarding this is taken from lung cancer screening trials, and less is known regarding pulmonary nodules in oncology patients. In oncology patients every pulmonary nodule may represent pulmonary metastasis.

Granuloma, Harmatomas

A granuloma of the lung is most likely a post-infectious residual from tuberculosis or fungal infection. Less likely, it represents active disease such as in sarcoidosis or Wegener's granulomatosis. Postinfectious granulomas usually do not change their appearance over time. Granulomas are often calcified, and sometimes they show peripheral enhancement and central hypoperfusion. Calcification is the most important characteristic finding for differential diagnosis. If the calcification is homogenous, popcorn like, laminated or diffuse, the lesion can be deemed benign, representing granulomas or harmatomas. Harmatomas are mesenchymal lesions

Table 16.1. Differential diagnosis of small pulmonary nodules detected at MDCT chest examinations.

		Solitary/multiple	Characteristics
Small cell lung cancer (SCLC)	Neoplastic	Solitary	Mostly solid nodule or solid mass
Non small cell lung cancer (NSCLC)	Neoplastic	Solitary	Mostly solid, sometimes with calcification and cavitation
Carcinoid	Neoplastic	Solitary	Endobronchial growth, often very extensive contrast enhancement
Lymphoma	Neoplastic	Multiple	Mostly solid nodules
Metastasis	Neoplastic	Multiple	Mostly solid, peripheral, sometime with calcification
Granuloma	Infectious	Solitary/multiple	Mostly calcified
Abscess/septic embolus	Infectious	Solitary/multiple	Solid or filled with fluid, cavity, air fluid level
Sarcoidosis, Amyloid, Wegener granulomatosis, Infarct	Non-infectious	Multiple	Solid
Harmatoma	Neoplastic	Solitary	Popcorn like calcification
Bronchogenic cyst	Congenital	Solitary	Fluid filled lesion
Ateriovenous malformation	Congenital	Solitary/multiple	Solid

often consisting of calcification, fat, and solid tissue. Popcorn like calcification is characteristic for harmatomas, allowing secure noninvasive diagnosis. If calcification is amorphous, diffuse or eccentric, malignant disease should be assumed.

Lung Cancer

Pulmonary nodules representing lung cancer may include calcification which sometimes also mimics benign disease. Lung cancer in its early stage disease is usually present as a small pulmonary nodule which is mostly solid and sometimes semi-solid. Lung cancer is the most deadly cancer as most of the people who are diagnosed with this cancer are diagnosed with advanced stage of disease. As revised by Mountain(1997), unfortunately the 5 year survival rate decreases dramatically if diagnosed with advanced stage lung cancer. Jemal*et al*. (2004) showed for the year 2004 that 173,700 people in the U.S. were diagnosed with lung cancer and 164,000 will die from the disease. In an interdisciplinary approach to lung cancer, Spira and Ettinger (2004) stated that the 5 year survival rate of stage Ia lung cancer is ~67%, while with locally advanced stage (IIb) 5 year survival rate decreases to <40%.

Lung Cancer is histologically classified either as small cell lung cancer (SCLC) or non-small cell lung cancer (NSCLC). The most common form is NSCLC (~80%). Histologically, NSCLC consists of different types: squamous cell cancer, adenocarcinoma, and large cell lung cancer. NSCLC is often located in the periphery of the lung and is less aggressive than SCLC, as it does not metastasize as early as SCLC. NSCLC often has an appearance as a pulmonary nodule in its early stage, while in advanced stage disease it may not be round shaped and it can infiltrate surrounding structures like bronchi, pleura or the mediastinum. Especially for squamous cell cancer, cavitations can be found. Sometimes calcifications are found within the tumors. Described by Noguchi *et al*. (1995), a special form of adenocarcinoma is bronchioalveolar carcinoma (BAC) which has a diffuse appearance and can present with ground glass opacities and diffuse small consolidations. A different form of adenocarcinoma was described by Kitamura *et al*. (1999), which is called atypical adeno-

matous hyperplasia (AAH), and was found to be a precursor of malignancy.

SCLC is less common (~20%) but more aggressive. Early lymphogenic and hematogenic metastasis is found. The SCLC itself is often represented by a small pulmonary nodule, which may have already extensive mediastinal metastasis. Due to its aggressiveness, SCLC staging is divided into two groups (limited disease and extensive disease). This is especially important for therapy as 5 year survival rate dramatically decreases with extensive disease.

Less common primary lung cancers are carcinoids, that may represent as pulmonary nodule, but are characterized with intensive contrast enhancement, primary pulmonary lymphoma or pulmonary sarcoma.

Metastasis

Pulmonary metastasis represents hematogenic spread of malignant cancers. Pulmonary metastasis usually is bilateral and multiple. Metastasis represents sharply marginated solid pulmonary nodules of different sizes. In rare cases calcification can be included in the nodules. Besides, granulomas pulmonary metastasis is the most common form of intrapulmonary nodule. Chest computed tomography (CT) examinations to rule out pulmonary metastasis are one of the most common indications to perform CT in daily routine practice. Unfortunately less is known of the likelihood of malignancy of small pulmonary nodules in oncology patients. Thus, every detected small pulmonary nodule in oncology patients needs to be considered malignant, and at least short term follow-up should be initialized.

Rare Differential Diagnosis

Besides these most common pathologies, several other pathologies can be found with the appearance of pulmonary nodules. Infectious nodules are especially important. Abscesses can look like pulmonary nodules, e.g., in septic embolism. These nodules are often multiple and show cavities. Typically, these patients are very ill so diagnosis of septic embolism is usually easy to make in combination with the history of the patient. Pulmonary arteriovenous malformations can have the appearance of pulmonary nodules, usually they are located in the periphery. Underlying hereditary hemorrhagic angiomatosis (Osler's disease) is very common. Contrast-enhanced CT usually shows the pathology very well, and pulmonary angiography is only necessary if interventional embolization is performed.

MULTIDETECTOR-ROW COMPUTED TOMOGRAPHY FOR PULMONARY NODULES

Technique

Multidetector-row Computed tomography (MDCT) has become the method of choice for pulmonary nodule detection and characterization. Since the invention of spiral CT in the early nineties, CT technique has made tremendous technical developments regarding spatial and temporal resolution. As Fischbach *et al.* (2003) described, the detection rate of pulmonary nodules is increased significantly with the use of thin sections. Especially the z-axis resolution has increased with the invention of MDCT in the late 1990s, allowing scanning of the entire thorax within a few seconds with

submillimeter slices. The increased spatial resolution produces isotropic voxels which yield the possibility to reconstruct images (multiplanar reformation: MPR) in any dimension with the same image quality as the original dataset. While spatial resolution is necessary to detect even very small pulmonary nodules of < 3 mm, increased temporal resolution allows scanning with less artifacts, which may be caused by breathing or motion of the heart. MDCT scanners allow scanning even of very sick patients usually within 10 s covering a range of ~ 30 cm.

Prior to the examination, the decision has to be made whether to use contrast material or not. If a scan is performed only for the detection of pulmonary nodules, usually no contrast material is necessary and a low dose scan should be performed. But in all other cases especially for additional question for evaluation of the mediastinum or other underlying lung diseases, contrast enhanced scanning should be performed. Initial scanning should be performed with lowest possible collimation, while the pitch (~1) should be adjusted accordingly with respect to dose issues. For the general population a 120 kV tube voltage is appropriate, while for pediatric patients 100 kV or 80 kV protocols should be considered depending on the patient's age, size, and weight.

Low-dose Computed Tomography

Low-dose MDCT refers to low radiation dose settings for chest CT examination. Acquisition parameters include a tube voltage of 120 kV, tube current time setting at least adapted to the patient's weight (weight correlated mAs settings) or even lower tube current time settings of 10–20 mAs. This directly correlates with a decreased radiation dose for the patient (Effective dose: ~1 mSv; DLP ~ 90 mGy; CTDIvol. ~ 2.8 mGy).

Low-dose MDCT has been advocated as the perfect tool for lung cancer screening, e.g., by Sone *et al*. (1998), Swensen *et al*. (2005), and Diederich *et al*. (2004). Although low-dose shows higher image noise, image quality still is high enough to detect small pulmonary nodules < 3 mm and of course delineation of bigger nodules is not problematic. Low-dose MDCT is used in lung cancer screening, usually without administering contrast material or for the detection of pulmonary nodules in unclear findings of chest X-ray. For the detection of pulmonary nodules Valencia *et al*. (2006) suggested the use of additional maximum intensity projections (MIP) for better visualization of vascular structures and thus better delineation of nodules. Using a MIP thickness 5–10 mm also decreases image noise, leading to a better visualization of small pulmonary nodules.

Contrast-Enhanced Computed Tomography

In standard chest CT examinations, usually contrast material is administered through a needle placed in the cubital vein to allow better evaluation of the mediastinum and the vessels. The use of MDCT allows lower contrast material volumes as examination time is significantly decreased. Additionally, the use of a saline chaser after contrast bolus again decreases contrast material volume. In a standard chest CT examination, depending on the patients weight and iodine concentration (300–400 mg/ml), usually ~ 90 ml contrast media are used which are administered ~ 4 ml/s, adding up to an iodine delivery rate of ~ 1.2–1.6 g/s. The use of contrast material also allows evaluation of the abdomen, if necessary, within one examination, without administering additional contrast material. The bolus tracking method is used, placing a bolus tracking into the pulmonary artery trunk. Newest scanner technologies also allow simultaneous evaluation of the

pulmonary arteries, thoracic aorta, and coronary arteries (triple rule out), but this type of examination is not necessary in examinations aimed at oncology staging or nodule evaluation.

Dynamic Computed Tomography

Dynamic CT refers to density changes of a pulmonary nodule after administering contrast material. The contrast enhancement of a pulmonary nodule is directly correlated to its vessel supply. In a growing nodule (e.g., metastasis, cancer) a bigger blood supply is necessary. The increased blood supply directly correlates with contrast uptake and consecutive enhancement in CT densities. Thus, dynamic CT can help to differentiate between benign and malignant pulmonary nodules. This method should be considered if a nodule is either too small for direct biopsy or in patients with less risk for malignancy. Dynamic CT is started with a noncontrast enhanced scan, while the volume of interest can be limited to the pulmonary nodule itself. After the non-contrast enhanced scan, intravenous contrast material is administered. A short spiral scan is performed through the nodule at 1, 2, 3 and 4 min after contrast injection. Time to peak enhancement, net enhancement (subtraction to density value at the non-enhanced scan), and peak enhancement are measured. Yi *et al*. (2004) showed a very high sensitivity for malignant nodules (~99%), while the specificity is relatively low (~54%).

This is especially important as this method yields a high negative predictive value. If a lesion does not show significant increase in density it is very likely to be benign. Usually the cut off value for differentiation has been set to 20 HU, although this remains controversial in the literature, as this value is strongly dependent on the contrast protocol and especially the iodine concentration of the delivered contrast material.

DIAGNOSTIC WORKUP

Detection of Pulmonary Nodules

Even smallest pulmonary nodules can be detected with MDCT chest examination. Still it remains difficult to detect every nodule as with increasing spatial resolution and thinner slice thicknesses the amount of data to be reviewed decreases and thus nodules may be missed. Armato *et al*. (2002) found that this is mainly due to detection failures or to interpretation errors. It is known from the literature that sensitivity for the detection of pulmonary nodules varies greatly between readers. Sensitivity ranges between 50–90% depending on the size of pulmonary nodules, reader experience, and acquisition protocol. In general, the collimation should be as thin as possible and the images should be reconstructed with a slice thickness between 1 mm and 3 mm with a slight overlap to reduce volume averaging effects. Additionally, the images should be analyzed using sliding MIPs with a thickness between 5–10 mm in a dynamic fashion. Fischbach *et al*. (2003) did show the increased detection rate with thin sections and Peloschek *et al*. (2007) could show an increase using MIPs and with the use of volume rendering techniques for nodule detection. The detection of pulmonary nodules is not only influenced by the reader and the image acquisition protocol, but also by the nodule size and its location. Peripheral nodules are detected more easily than nodules located centrally as they can be obstructed by large

branching vessels. Smaller nodules are more frequently missed than large nodules, but even large nodules can be missed. Li *et al*. (2002) reported ~32 missed lung cancers during a lung cancer screening trial. These lung cancers were missed on 39 CT scans. The missed cancers had an average lesion size of 9.8 mm. The authors describe the majority of missed cancers as "small faint nodules, overlapping normal structures or opacities in a complex background of another disease". As detection rate is not yet perfect, computer-based algorithms have been developed to aid the radiologist in the detection of pulmonary nodules and increase sensitivity. These computer-aided detection (CAD) algorithms show promising results in recent studies and will be discussed later.

Nodule Density

Nodule density can be measured easily on CT examination by placing a small region of interest in the detected nodule. Nodules can have different densities related to their histology. They can contain fat, fluid, solid tissue, or calcifications. Unfortunately, only homogenous, lamellated or popcorn like calcifications are associated with benign disease. Nodule density should be measured in the soft tissue settings (typical window settings: C = 80, W = 400).

Recently, newly invented Dual Source CT (DSCT), which allows scanning simultaneously with two X-ray tubes optional with two different kV settings, may allow automated differentiation of nodule histology. But this has yet to be proved. Some nodules have the appearance of ground-glass opacities (semi-solid nodules). These semi-solid nodules are associated with bronchioalveolar carcinoma. Noguchi *et al*. (1995) have shown the relationship of density with malignancy. They demonstrated an increase of malignancy with increasing density.

Nodule Size

The most important characteristic of a pulmonary nodule is size. This is the key factor to decide further diagnostic workup. In an older definition of pulmonary nodules, a nodule is defined as a round-shaped lesion of < 30 mm in size. All lesions bigger than 30 mm are considered masses. But since CT has been performed for lung cancer screening these numbers have changed. It is well known from screening trials as Henschke *et al*. (2001b) demonstrated that likelihood of malignancy dramatically increases for nodules > 10 mm in diameter. This threshold defines a size where further diagnostic workup is justified. Again, we know from screening trials that only 10% of nodules < 10 mm are malignant and only 5% of nodules < 5 mm are malignant. Of course, again these numbers are taken from screening trials and less is known regarding pulmonary nodules in oncology patients, where every nodule could represent intrapulmonary metastasis.

There is a considerable controversy regarding the optimal way of measuring pulmonary nodules. In general, practice manual axial longest diameter according to RECIST criteria is still used. However, Marten *et al*. (2006) reported that this measurement is not optimal as it yields high inter- and intraobserver variability. But accurate and exact measurement are crucial to avoid unnecessary follow-up or invasive workup and most important to assess growth.

Different types of measurements have been suggested, but the most sensitive way of measuring is the assessment of nodule volume as a nodule grows in three dimensions and not only in two dimensions. Thus the volume of a nodule should be measured in addition to the regular two-dimensional measurements. Computer-aided volumetry algorithms allow accurate and objective measurements. MacMahon *et al*. (2005) from the Fleischner Society consensus group recently published a guideline for follow-up recommending measuring the average of nodule length and width.

Nodule Growth

In many cases initial differentiation of benign and malignant pulmonary nodules is not possible as nodules size may be too small or density does not show any typical characteristic. As invasive diagnostic workup is not justified in the broad spectrum of patients and would cause unnecessary side effects, follow-up is usually recommended to assess lesion growth. It is widely accepted that lesion size stability over 2 years can be considered as a sign of a benign nodule. Nodule growth is referred to as doubling time. A wide range of doubling times is known from the literature. In previous studies a doubling time of <7 days was considered benign. Now we know from several CT studies looking at tumor doubling times, that lung cancer may have tumor doubling times between 1 month and 18 months. Unfortunately, slow growing tumors such as adenocarcinoma may also have a doubling time >700 days. This may have impact on the effectiveness of lung cancer screening as follow-up intervals need to be set accordingly. Anyhow, most lung cancers usually grow rapidly. However, less is known about doubling times of metastasis.

As described earlier, unidimensional measurements are usually performed. This yields high inter- and intraobserver variability. Measurements in at least two dimensions should be performed and averaged on two serial images to assess growth according to MacMahon *et al*. (2005). The newest technologies allow volumetric measurements, which are more sensitive to growth changes than diameter only, as they follow the equation for spherical volumes ($4/3*\pi*r^3$). For example, a change in diameter of ~26% would lead to a volume change of ~100%.

For follow-up examinations and assessment of nodule growth, thin sections should be used to reduce volume averaging effects and to be able to use different dimensions with the same image quality. It is important to emphasize that the same image protocol should be used in all follow-up examinations to allow accurate follow-up measurements. Automated measurement tools are most accurate with thin sections between 1 mm and 3 mm and preferably with the same slice thickness at all examinations.

Recommended Workup Algorithms

After detection of a pulmonary nodule which does not have clear benign or malignant characteristics, further diagnostic workup strategies need to be applied. Most of the recommendations in the literature are based on lung cancer screening trials. Prior to the decision of follow-up recommendations an initial risk classification of the patient needs to be done.

It needs to be assessed if the scan was performed for oncology purpose.

If so, every pulmonary nodule needs to be considered as metastasis. Follow-up schemes should be adapted to clinical guidelines depending on the underlying malignant disease. We have to be aware that further research is necessary to know more regarding nodules detected at chest CTs of oncology patients. If a patient was not scanned for oncology purpose and a pulmonary nodule was detected incidentally, further risk classification is justified. A consensus statement of the Fleischner Society (Table 16.2) for the follow-up of incidental pulmonary nodules was published by McMahon *et al*. (2005) classifying patients into low and high risk patients based on their history of smoking and other risk factors for lung cancer. The risk for heavy smokers can be considered ~15–35 times greater than that in nonsmokers.

Additional risk factors for lung cancer include asbestos exposure, radon exposure and lung cancer in first-degree relatives. We also know that increasing patient age increases the risk of malignancy, while in young patients (<40 years) lung cancer is very uncommon. The guidelines do not recommend follow-up only in low risk patients with a nodule size smaller or equal to 4 mm, but all other patients and lesion sizes do require follow-up. It is also a new development that for pulmonary nodules with a diameter (average of length and width) bigger than 8 mm, further workup should be performed using dynamic CT, PET, and/or histological workup. To avoid unnecessary invasive workup best possible biopsy technique should be discussed interdisciplinary considering percutaneous CT guided biopsy, video assisted thoracic surgery, bronchoscopy, or open surgery. A minimally invasive procedure needs to be the goal to reduce unnecessary morbidity and mortality from nodule workup.

LUNG CANCER SCREENING

Since the introduction of spiral CT and further development of MDCT, several research groups have started to use MDCT as the first line screening tool for lung cancer. The goal of screening is to detect precursor or early stage of disease to reduce mortality from the disease. For lung cancer only early detection of the disease allows sufficient treatment and

TABLE 16.2. Suggested workup algorithm for incidentally found pulmonary nodules. (MacMahon *et al*., 2005.)

Size (average of length and width)	Low risk group (non smoker, no other risks)	High risk group (history of smoking or other risks)
≤4 mm	No follow-up	12 months follow-up, no further follow-up if unchanged
>4–6 mm	12 months follow-up, no further follow-up if unchanged	Follow-up after 6 and 12 months, if unchanged further follow-up after 18–24 months
≥6–8 mm	Follow-up after 6 and 12 months, if unchanged further follow-up after 18 and 24 months.	Follow-up after 3–6, 9–12 months and 24 months if unchanged
≥8 mm	Follow-up at 3, 9 and 24 months, dynamic contrast enhanced CT, PET or biopsy	Follow-up at 3, 9 and 24 months, dynamic contrast enhanced CT, PET or biopsy

potential cure. In advanced stage disease the mortality increases and cure is no longer possible. On the other hand, the method needs to be very sensitive for the detection, should not produce too many false positives and should not induce any other disease (related to radiation dose or to invasive nodule workup). These technical prerequisites are given with MDCT. In screening MDCT is performed in a low dose fashion as described by Henschke *et al*. (1999) to reduce radiation exposure to a minimum. In screening an initial baseline examination is performed, usually followed by an annual follow-up examination with the same scan protocol. It is very important to screen a selected cohort, meaning a preselection of participants is necessary to achieve an effective screening. For example, Sone *et al*. (1998) screened the general population (5,483 participants) in Japan and showed the increased sensitivity of CT for lung cancer compared to chest X-ray, but they only found a lung cancer rate of 0.48%, which is too small for an effective economic screening.

Henschke *et al*. (1999, 2006) used a different approach, screening patients older than 60 years with a history of smoking at least a pack/day for 10 years. In this approach they could detect a much higher cancer rate of about 1.6%. In our own screening study the selection was based on asbestos exposure, smoking history and age, resulting in the highest incidence rate of lung cancer of 4.8% in the literature (Das *et al*., 2007). Of course prevalence rate of lung cancer only shows if selection criteria are well performed, but in the follow-up examinations it is of even more importance to detect early lung cancer (early stage of disease) to allow possible cure. In all ongoing screening trials a shift to early stage disease diagnosis is shown, detecting between 60–85% of early stage lung cancer. Still there is an ongoing discussion as to whether these results may justify general recommendation of lung cancer screening with low dose MDCT. The group around Henschke *et al*. (2006) propose the widespread use of lung cancer screening as reduction of mortality could be concluded from their results. Other authors do not share this thought and thus to date no general recommendation for screening was given.

All current screening approaches remain critical as they are cohort studies, without a randomized control arm. Large ongoing screening trials in the US (National Lung Screening Trial = NLST) with more than 40,000 participants, the Nelson trial in Belgium and the Netherlands with more than 24,000 participants and the Depiscan trial in France with ~20,000 participants which will produce new valid results on mortality reduction.

Presently, no general screening recommendation can be given, but smokers over 50–60 years are encouraged to participate in screening trials.

ADVANCED DIAGNOSIS OF PULMONARY NODULES

The diagnosis of pulmonary nodules remains challenging. This is reinforced by the increasing use of MDCT and the consecutive increased data load which has to be reviewed by the radiologists. We have already learned that small pulmonary nodules or even lung cancer may be missed. Thus, computer-aided diagnostic

tools have been advocated to aid the radiologists in decision making (Figure 16.1). With regard to pulmonary nodules CAD helps in several different ways. In the first place, software environments have been developed for enhanced viewing of chest CTs, by allowing MIP, MPR, and VRT viewing of the datasets in comparison with the original dataset. Secondly, computer-aided detection facilitates lesion finding and consecutive nodule quantification. Finally, CAD aids the radiologists with easy follow-up functions.

Computer Aided Detection

The detection performance of radiologists varies greatly, and strongly depends on the experience of the radiologist. Depending on the size of pulmonary nodules, they are frequently missed or misinterpreted. CAD aids the radiologists in pointing out potential malignant lesions (lesion candidates). There are two general concepts for the use of CAD. First, the software is used as a second reader. Using CAD as the second reader allows the radiologist to review the case in the usual way. After he/she has finished reviewing the case the CAD marks (highlights of suspicious regions) are presented to the radiologist to show potential additional lesions which may have been missed initially. Most of the current publications on CAD propose its use in this way, although it might somewhat prolong the reading process. The important advantage is that the radiologist does not change his/her initial way of reading. In the second approach CAD is used as a concurrent reader. Using CAD as a concurrent reader shows the CAD marks directly during the initial read. This might speed up the reading process, but also bears the problem that the radiologist may rely only on the CAD marks, and does not read as carefully as he/she used to.

The sensitivity for the detection of pulmonary nodules for radiologists alone varies between 50–90%. The radiologists tend to miss small and centrally located lesions and perform better on larger and more peripheral lesions. The sensitivity of current CAD algorithms has been tested in several publications such as Rubin *et al.* (2005), varying between 36–73%. CAD performs better on smaller lesions and has no tendency to miss more centrally located lesions. Besides absolute sensitivities, more importantly, the combination of radiologist and CAD as a second reader yields the most promising results as we demonstrated in our own study (Das *et al.*, 2006). Every study that used CAD as a second reader has demonstrated significant increases of nodule detection. Most publications showed a significant increase of nodule detection between 5–30%, and less experienced readers showed the biggest gain in sensitivity increase.

False-positives remain critical in CAD. If the number of false-positives is too high, unnecessary examinations, biopsies and morbidity may be produced, although there is no study which can prove this concern. However, it should be kept in mind that the final decision needs to be made by the radiologist who has to decide from his/her knowledge regarding a true or false-positive finding. In general, CAD has not yet found widespread use in clinical routine work. This is probably due to stand alone solutions, which do not allow fast and quick review of the results. If CAD is integrated into the daily routine workflow, every patient may benefit from the use of CAD.

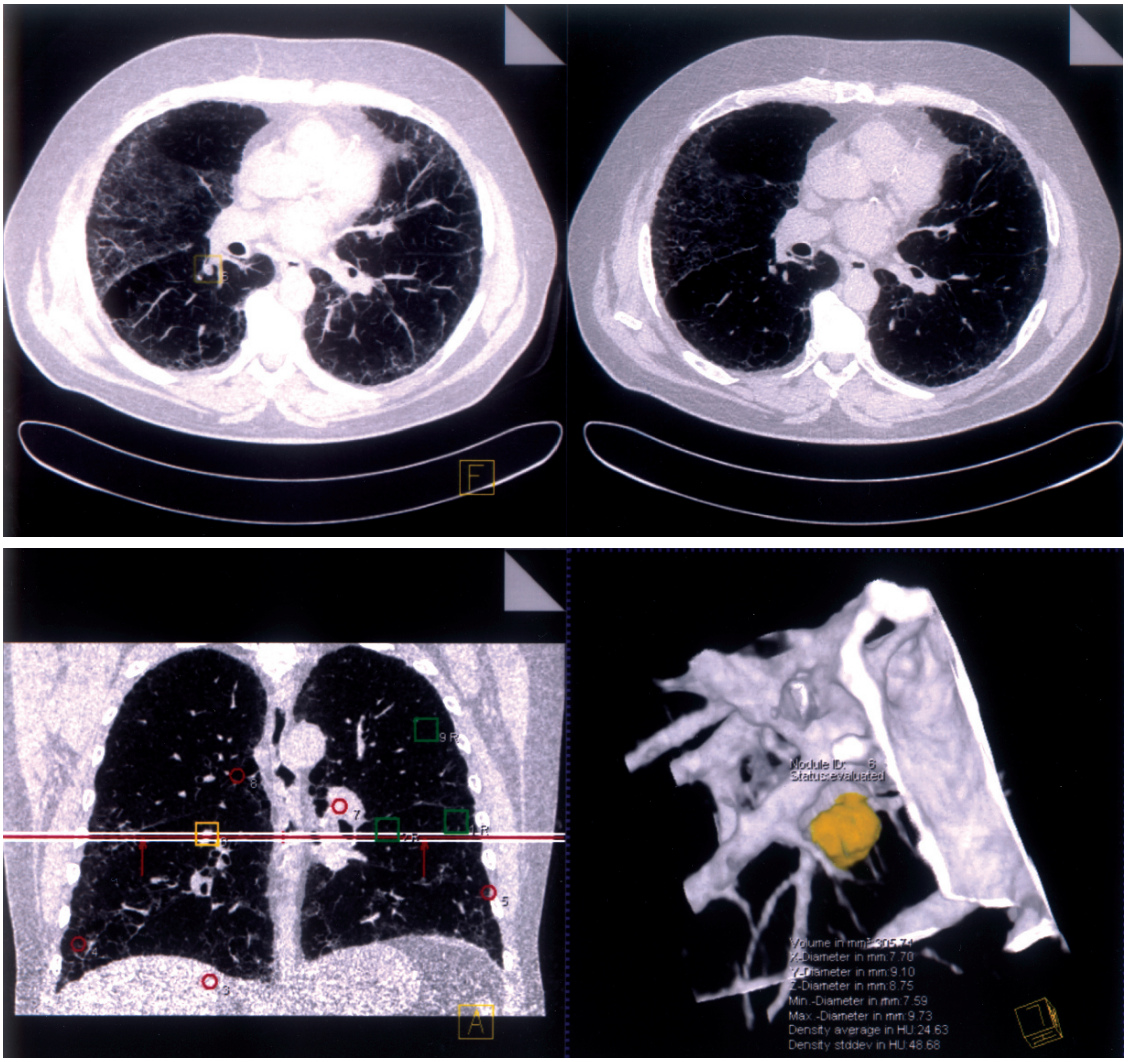

FIGURE 16.1. Advanced analysis of small pulmonary nodules. Graphical user interface of a lung analysis software (LungCare™) for the detection of pulmonary nodules. Left upper window shows thinMips for advanced detection. Right upper window shows the correlated original slices. Left lower window shows an overview of the findings. Red circles indicate CAD marked lesions, which need to be verified by the radiologist. The right lower window shows volumetry results of the pulmonary nodule

Computer Aided Volumetry

Growth assessment is a crucial step in evaluating malignancy of pulmonary nodules and therapy response. As mentioned earlier, axial manual diameter varies greatly between two measurements. Modern guidelines favor the average diameter (average between two perpendicular measurements) as a more reliable measurement. From a mathematical standpoint the most sensitive quantitative measurement is the volume of a spherical lesion. With the

use of thin sections in MDCT, automated measurements have become possible. Thin sections are necessary to reduce volume averaging effects and to generate more reliable measurements. During the past years several CAD algorithms have been developed for automated measurements of all different nodule dimensions. Thus, automatic measurement of diameters, volume, and density has become possible. Additionally, these measurements can be correlated to common measurements such as RECIST and WHO measurements for therapy response control. The usual basic approach to lesion quantification is based on density, which usually varies greatly between the nodule and the surrounding parenchyma. Then, segmentation algorithms, such as threshold based algorithms, region growing algorithms, and fuzzy clustering, are used. In most user interfaces, a 3D rendering of the segmented nodule is presented to the user. Manual editing is usually possible but should not be performed if possible, as this may reduce reproducibility of the measurement. It was shown in several studies such as Das *et al*. (2007) and Goo *et al*. (2005) that nodule size, location, and different acquisition parameters have an influence on nodule volumetry. Therefore, thin sections of <3 mm in a lung window and kernel are recommended for automated volumetry. Pleural lesions and very small lesions (<4 mm) remain challenging for most algorithms and should be analyzed carefully. Besides these critical points, automated nodule volumetry provides reliable reproducible measurements for the broad spectrum of pulmonary nodules and should be used during routine clinical studies to reduce inter- and intrareader variability and for a more sensitive assessment of nodule size and growth.

In conclusion, pulmonary nodules are one of the most common findings in the chest MDCT examinations. The increased use of MDCT has increased the number of indeterminate pulmonary nodules. MDCT has made the detection of pulmonary nodules as small as 1–2 mm possible. CAD algorithms are now able to support the radiologist in detection, characterization, and follow-up of pulmonary nodules. It is crucial to use differentiated workup algorithms for small indeterminate pulmonary nodules.

REFERENCES

Armato, SG., 3rd, Li, F., Giger, ML., MacMahon, H., Sone, S., and Doi, K. 2002. Lung cancer: performance of automated lung nodule detection applied to cancers missed in a CT screening program. *Radiology 225*: 685–692.

Das, M., Mühlenbruch, G., Mahnken, AH., Flohr, TG., Gündel, L., Stanzel, S., Kraus, T., Günther, RW., and Wildberger, JE. 2006. Small pulmonary nodules: effect of two computer-aided detection systems on radiologist performance. *Radiology 241*: 564–571.

Das, M., Ley-Zaporozhan J., Gietema, HA., Czech, A., Mühlenbruch, G., Mahnken, AH., Katoh, M., Bakai, A., Salganicoff, M., Diederich, S., Prokop, M., Kauczor, HU., Günther, RW., and Wildberger, JE. 2007a. Accuracy of automated volumetry of pulmonary nodules across different multislice CT scanners. *Eur. Radiol. 17*: 1979–1984.

Das, M., Mühlenbruch, G., Mahnken, AH., Hering, KG., Sirbu, H., Zschiesche, W., Knoll, L., Felten, MK., Kraus, T., Günther, RW., and Wildberger, JE. 2007b. Asbestos Surveillance Program Aachen (ASPA): initial results from baseline screening for lung cancer in asbestos-exposed high-risk individuals using low-dose multidetector-row CT. *Eur. Radiol. 17*: 1193–1199.

Das, M., Mühlenbruch, G., Katoh, M., Bakai, A., Salganicoff, M., Stanzel, S., Mahnken, AH., Günther, RW., and Wildberger, JE. 2007c. Automated volumetry of solid pulmonary nodules in a phantom: accuracy across different CT scanner technologies. *Invest. Radiol. 42*: 297–302.

Diederich, S., Thomas, M., Semik, M., Lenzen, H., Roos, N., Weber, A., Heindel, W., and Wormanns, D. 2004. Screening for early lung cancer with low-dose spiral computed tomography: results of annual follow-up examinations in asymptomatic smokers. *Eur. Radiol. 14*: 691–702.

Fischbach, F., Knollmann, F., Griesshaber, V., Freund, T., Akkol, E., and Felix, R. 2003. Detection of pulmonary nodules by multislice computed tomography: improved detection rate with reduced slice thickness. *Eur. Radiol. 13*: 2378–2383.

Goo, JM., Tongdee, T., Tongdee, R., Yeo, K., Hildebolt, CF., and Bae, KT. 2005. Volumetric measurement of synthetic lung nodules with multi-detector row CT: effect of various image reconstruction parameters and segmentation thresholds on measurement accuracy. *Radiology 235*: 850–856.

Henschke, CI., McCauley, DI., Yankelevitz, DF., Naidich, DP., McGuinness, G., Miettinen, OS., Libby, DM., Pasmantier, MW., Koizumi, J., Altorki, NK., and Smith, JP. 1999. Early Lung Cancer Action Project: overall design and findings from baseline screening. *Lancet 354*: 99–105.

Henschke, CI., McCauley, DI., Yankelevitz, DF., Naidich, DP., McGuinness, G., Miettinen, OS., Libby, D., Pasmantier, M., Koizumi, J., Altorki, N., and Smith, JP. 2001a. Early lung cancer action project: a summary of the findings on baseline screening. *Oncologist 6*: 147–152.

Henschke, CI., Naidich, DP., Yankelevitz, DF., McGuinness, G., McCauley, DI., Smith, JP., Libby, D., Pasmantier, M., Vazquez, M., Koizumi, J., Flieder, D., Altorki, N., and Miettinen, OS. 2001b. Early lung cancer action project: initial findings on repeat screenings. *Cancer 92*: 153–159.

Henschke, CI., Yankelevitz, DF., Libby, DM., Pasmantier, MW., Smith, JP., and Miettinen, OS. 2006. Survival of patients with stage I lung cancer detected on CT screening. N *Engl. J. Med. 355*: 1763–1771.

Jemal, A., Tiwari, RC., Murray, T., Ghafoor, A., Samuels, A., Ward, E., Feuer, EJ., and Thun, MJ. 2004. American Cancer Society. Cancer statistics, 2004. *C.A.Cancer J. Clin. 54*: 8–29.

Kitamura, H., Kameda, Y., Ito, T., and Hayashi, H. 1999. Atypical adenomatous hyperplasia of the lung. Implications for the pathogenesis of peripheral lung adenocarcinoma. *Am. J. Clin. Pathol. 111*: 610–622.

Li, F., Sone, S., Abe, H., MacMahon, H., Armato, SG., 3rd., and Doi, K. 2002. Lung cancers missed at low-dose helical CT screening in a general population: comparison of clinical, histopathologic, and imaging findings. *Radiology 225*: 673–683.

MacMahon, H., Austin, JH., Gamsu, G., Herold, CJ., Jett, JR., Naidich, DP., Patz, EF. Jr., and Swensen, SJ., Fleischner Society. 2005. Guidelines for management of small pulmonary nodules detected on CT scans: a statement from the Fleischner Society. *Radiology 237*: 395–400.

Marten, K., Auer, F., Schmidt, S., Kohl, G., Rummeny, EJ., and Engelke, C. 2006. Inadequacy of manual measurements compared to automated CT volumetry in assessment of treatment response of pulmonary metastases using RECIST criteria. *Eur. Radiol. 16*: 781–790.

Midthun, DE., Swensen, SJ., and Jett, JR. 1993. Approach to the solitary pulmonary nodule. *Mayo Clin. Proc. 68*: 378–385.

Mountain, CF. 1997. Revisions in the International System for Staging Lung Cancer. *Chest 111*: 1710–1717.

Noguchi, M., Morikawa, A., Kawasaki, M., Matsuno, Y., Yamada, T., Hirohashi, S., Kondo, H., and Shimosato, Y. 1995. Small adenocarcinoma of the lung. Histologic characteristics and prognosis. *Cancer 75*: 2844–2852.

Peloschek, P., Sailer, J., Weber, M., Herold, CJ., Prokop, M., and Schaefer-Prokop, C. 2007. Pulmonary nodules: sensitivity of maximum intensity projection versus that of volume rendering of 3D multidetector CT data. *Radiology 243*: 561–569.

Rubin, GD., Lyo, JK., Paik, DS., Sherbondy, AJ., Chow, LC., Leung, AN., Mindelzun, R., Schraedley-Desmond, PK., Zinck, SE., Naidich, DP., and Napel, S. 2005. Pulmonary nodules on multi-detector row CT scans: performance comparison of radiologists and computer-aided detection. *Radiology 234*: 274–283.

Sone, S., Takashima, S., Li, F., Yang, Z., Honda, T., Maruyama, Y., Hasegawa, M., Yamanda, T., Kubo, K., Hanamura, K., and Asakura, K. 1998. Mass screening for lung cancer with mobile spiral computed tomography scanner. *Lancet 351*: 1242–1245.

Spira, A., and Ettinger, DS. 2004. Multidisciplinary management of lung cancer. *N. Engl. J. Med. 350*: 379–392.

Swensen, SJ., Morin, RL., Schueler, BA., Brown, LR., Cortese, DA., Pairolero, PC., and Brutinel, WM. 1992. Solitary pulmonary nodule: CT evaluation of enhancement with iodinated contrast material–a preliminary report. *Radiology 182*: 343–347.

Swensen, SJ., Jett, JR., Hartman, TE., Midthun, DE., Mandrekar, SJ., Hillman, SL., Sykes, AM., Aughenbaugh, GL., Bungum, AO., and Allen, KL. 2005. CT screening for lung cancer: five-year prospective experience. *Radiology 235*: 259–265.

Valencia, R., Denecke, T., Lehmkuhl, L., Fischbach, F., Felix, R., and Knollmann, F. 2006. Value of axial and coronal maximum intensity projection (MIP) images in the detection of pulmonary nodules by multislice spiral CT: comparison with axial 1-mm and 5-mm slices. *Eur. Radiol. 16*: 325–332.

Yi, C.A., Lee, K.S., Kim, E.A., Han, J., Kim, H., Kwon, O.J., Jeong, Y.J., and Kim, S. 2004. Solitary pulmonary nodules: dynamic enhanced multi-detector row CT study and comparison with vascular endothelial growth factor and microvessel density. *Radiology 233*: 191–199.

17
Secondary Primary Cancer Following Chemoradiation for Non-Small-Cell Lung Cancer

Nagio Takigawa, Yoshihiko Segawa, and Katsuyuki Kiura

INTRODUCTION

Thoracic radiation has been standard treatment for unresectable stage III non-small-cell lung cancer (NSCLC), which accounts for ~35% of all NSCLC (Jemal *et al*., 2004). In the early 1990s, several randomized studies of thoracic radiation versus chemoradiation had been performed. Chemotherapy followed by radiation (sequential chemoradiation) showed significantly superior survival compared to that with radiation alone (Dillman *et al*., 1990; Le Chevalier *et al*., 1994; Sause *et al*., 2000). In a meta-analysis of 22 randomized clinical trials comparing chemoradiation to radiation, chemoradiation resulted in a significant reduction (10%) in the risk of death (Non-small Cell Lung Cancer Collaborative Group,1995). In addition, the cisplatin-based 12 trials showed a benefit of chemoradiation with a significant reduction in the risk of death of 27%. Furthermore, a few randomized trials comparing concurrent cisplatin-based chemoradiation to sequential chemoradiation showed that overall survival was improved by concurrent administration (Fournel *et al*., 2005; Furuse *et al*., 1999; Zatloukal *et al*., 2004). Thus, concurrent cisplatin-based chemoradiation seems the most powerful treatment for the locally advanced NSCLC patients with good performance status. However, long-term follow-up data of the concurrent chemoradiation were not fully analyzed except for some reports.

Meanwhile, cancer survivors have a substantial risk of secondary primary cancer and leukemia and the second malignancy has been recognized in survivors of early NSCLC (Duchateau and Stokkel, 2005). However, secondary primary cancer after chemoradiation for locally advanced NSCLC has not been well recognized because adequate long-term follow-up data are not available.

METHODS

We reviewed long-term results of concurrent chemoradiation and secondary primary cancer in survivors following treatment for NSCLC. In addition, the result of 5-fluorouracil, cisplatin and concurrent thoracic radiation from our group, which is the longest follow-up data of chemoradiation, to our best knowledge, is described.

RESULTS

Long-term follow-up results of concurrent chemoradiation is shown in Table 17.1. Survival rates in the concurrent chemoradiation arms when comparing sequential chemoradiation arms were reported to be 18.6% at 3 years (Zatloukal *et al*., 2004) and 20.7% at 4 years (Fournel *et al*., 2005). In phase II studies, Kubota *et al*. (2000) reported that the 5-year survival rate was 14.8% by a median follow-up of 69 months (range: 2–77 months). Kim *et al*. (2005) reported that the 4-year survival rate in the patients with concurrent chemoradiation was 16.3% by a median follow-up of 498 days (range: 11–2,905 days). Keene *et al*. (2005) also showed that the 5-year survival rate was 23% by a median follow-up of 3 years. The 5-year survival rate of the patients treated with concurrent chemoradiation in a meta-analysis of 9 trials was 8.2% by a median follow-up time of 7.2 years (Auperin *et al*., 2006). The 5-year survival rate of the patients enrolled in 6 Japanese phase II studies including 5 concurrent chemoradiation and 1 alternating chemoradiation was 14.4% by a minimum 3-year follow-up time (Ohe *et al*., 2003). Thus, there is still a minor population but substantial long-term survivors after concurrent chemoradiation for locally advanced NSCLC.

Between July 1994 and November 1996, Okayama Lung Cancer Study Group conducted a phase II study of concurrent chemoradiation for locally advanced unresectable stage IIIA and IIIB NSCLC (Segawa *et al*., 2000). The treatment consisted of three cycles of 5-fluorouracil (500 mg/m^2, day 1–5) and cisplatin (20 mg/m^2, days 1–5), every 4 weeks, and concurrent hyperfractionated thoracic radiation (1.25 Gy twice daily, total dose: 62.5–70 Gy). The interval of initial NSCLC and secondary primary cancer was measured from the initiation of chemoradiation to the diagnosis of secondary primary cancer. Survival rate was calculated using the method of Kaplan and Meier. Fifteen of 50 patients survived more than 5 years and the actual survival rate was 30% at 5-year. The median survival time was 1.6 years (95% confidence interval [CI]: 0.9–2.3 years) at a median follow-up time of 10.4 years (range, 5.2–11.4 years) (Figure 17.1). The median progression-free survival time was 0.75 years (95% CI: 0.12–1.38

TABLE 17.1. Long-term follow-up in stage III NSCLC patients treated with concurrent CRT.

Authors (Year)	Chemotherapy regimen	Follow-up time	Survival
Kubota *et al.* (2000)	MVP	Median: 69 months	14.8 months (MST)
		Range: 2–77 months	14.8% (5 year)
Zatloukal *et al*. (2004)	CDDP/VNB	Median: 39 months	16.6 months (MST)
		Range: 18–62 months	18.6% (3 year)
Kim *et al*. (2005)	CBDCA/PTX	Median: 498 days	16.4 months (MST)
		Range: 11–2,905 days	16.3% (4 year)
Keene *et al*. (2005)	CDDP	Median: 3 years	20.1 months (MST)
			23% (5 year)
Fournel *et al*. (2005)	CDDP/ETP	Median: 4.8 years	16.3 months (MST)
			20.7% (4 year)
Takigawa *et al*. (2006)	CDDP/5-Fu	Median: 10.4 years	19.0 months (MST)
		Range: 5.2–11.4 years	30.0% (5 years)

NSCLC: non-small cell lung cancer; CRT: Chemoradiation; MST: Median survival time; MVP: Mitomycin, vindesine and cisplatin; CDDP: cisplatin, CBDCA: carboplatin, ETP: etoposide; PTX: paclitaxel, 5-Fu: 5-fluorouracil; VNB: vinorelbine.

years) (Figure 17.2). One patient relapsed on the same lobe in the primary NSCLC and had the same histology (adenocarcinoma) 8 years after chemoradiation. In 15 long-term survivors of more than 5 years, 3 patients died due to progression of primary NSCLC, 2 died due to secondary primary cancer (esophageal cancer and bile duct cancer), 1 was lost to follow-up. Overall, 5 patients developed secondary primary cancer (1 NSCLC, 1 small cell lung cancer, 2 esophageal cancer, 1 bile duct), although no patients developed leukemia or myelodysplastic syndrome (Table 17.2). They were all smokers and only one arouse in thoracic radiation field used to treat initial NSCLC.

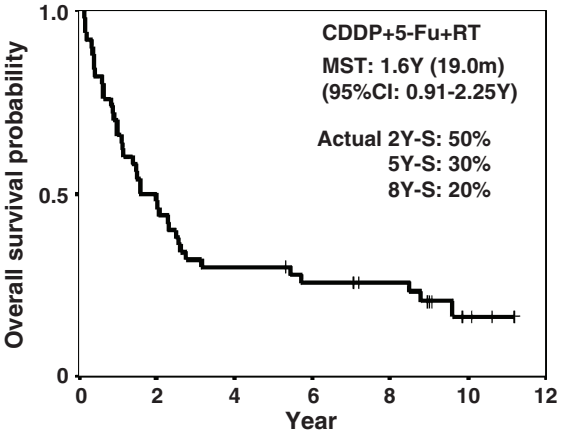

FIGURE 17.1 Overall survival curve from the initiation of 5-fluorouracil, cisplatin and concurrent radiation

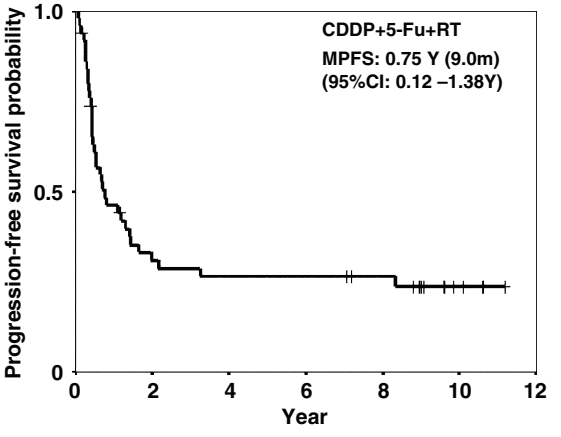

FIGURE 17.2. Progression-free survival curve from the initiation of 5-fluorouracil, cisplatin and concurrent radiation

The incidence of secondary primary cancer depends on the intensity and duration of follow-up and the rate of the survivors after treatment for primary cancer. The rate of secondary primary cancer was usually calculated as the ratio of secondary primary cancer cases over 100 patient-years of follow-up and ranged from 1.7 to 4.3 per 100 patient-years in early stage NSCLC (Table 17.3) (Ginsberg and Rubinstein, 1995; Jeremic *et al.*, 2001; Martini *et al.*, 1995; Thomas and Rubinstein, 1993). Secondary primary cancer in patients with stage III NSCLC was also reported although a variety of chemotherapeutic regimen and thoracic radiation dose and sequence were included (Kawaguchi *et al.*, 2006). Sixty-two of 547 stage III patients treated with chemoradiation between 1985 and 1995 had more than 3-years disease-free survival and 9 patients developed secondary primary cancer. The incidence of secondary primary cancer was estimated at 2.9 per 100 patient-years. The rate of secondary primary cancer in our 2 phase II studies

TABLE 17.2. Characteristics of 5 patients with SPC after FP-RT.

Type of SPC	1st to SPC (years)	Smoking (pack-year)	RT field	Survival after SPC (years)
Esophagus	4.1	30	Outside	7.2+ (alive)
Esophagus	8.3	50	Inside	0.35
Lung (adeno)	8.3	68	Outside	1.5+ (alive)
Bile duct	8.7	40	Outside	0.79
Lung (small)	9.5	75	Outside	1.1+ (alive)

SPC: secondary primary cancer; FP: 5-fluorouracil and cisplatin; RT: radiation.

TABLE 17.3. Frequency of SPC in patients with non-small cell lung cancer.

Authors (Year)	Stage	Number of SPC cases/Number of follow-up cases	Rate of SPC (100 patient-years)
Thomas and Rubinstein (1993)	I	20/308 (6.5%)	2.4–2.6
Ginsberg and Rubinstein (1995)	I	13/247 (5.3%)	1.7
Martini et al. (1995)	I	206/598 (34%)	2.8
Jeremic et al. (2001)	I/II	26/194 (13%)	4.3
Kawaguchi et al. (2006)	III	9/547 (1.6%)	2.8
Takigawa et al. (2006)	III	7/92 (7.6%)	2.4

SPC: secondary primary cancer.

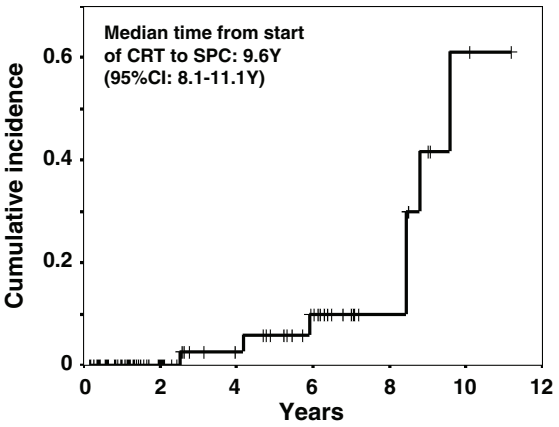

FIGURE 17.3. Cumulative incidence of secondary primary cancer from the initiation of concurrent chemoradiation

was 2.4 per 100 patient-years (95% CI: 1.0–4.9) (Takigawa *et al*., 2006), which is in agreement with the previous studies. The median time from the beginning of chemoradiation to the diagnosis of secondary primary cancer was 9.6 years (95% CI: 8.1–11.1 years) in our study. On the other hand, the cumulative incidence of secondary primary cancer at 5 years was 24% with control arm of the chemopreventive randomized trial of adjuvant retinyl palmitate for resected stage I NSCLC (Pastorino *et al*., 1993). Jeremic *et al*. (2001) reported that the cumulative incidence of secondary primary cancer was 21.8% (standard error: SE, 4.7%) at 5 years and 34.8% (SE, 6.7%) at 10 years in the stage I/II patients treated with thoracic radiation. In our study, the cumulative incidence was 5.8 % (SE, 4.0%) at 5 years and 60.8% (SE, 18.9%) at 10 years (Figure 17.3: reproduced from p1144 of British Journal of Cancer 95, 2006) The difference among the studies may be partially explained by survival difference between early and advanced disease; there were more fatalities due to primary NSCLC during first 5 years in our series.

DISCUSSION

Chemotherapy and thoracic radiation themselves may be carcinogenetic treatments and may have contributed to the occurrence of secondary primary cancer compared to surgery for early NSCLC (Allan and Travis, 2005). Patients with locally advanced NSCLC have still poor prognosis although concurrent cisplatin-containing chemoradiation prolonged the survival. Therefore, the benefit of chemoradiation may still outweigh the risk of secondary primary cancer even if chemoradiation might have contributed to secondary primary cancer.

Chemoprevention trials including β-carotene, α-tocopherol, and retinol have failed to yield substantial evidence

of compounds that can reverse, suppress, or prevent lung cancer progression (Khuri and Cohen, 2004). Although the initial trial of retinyl palmitate in the prevention of secondary primary cancer for resected stage I NSCLC showed effectiveness in reducing secondary primary cancer (Pastorino *et al*., 1993), subsequent trials showed no benefit for intervention with retinoids (Lippman *et al*., 2001; van Zandwijk *et al*., 2000). Trials of cyclooxygenase-2, the ras-signaling pathway through farnesyl transferase inhibitors and the tyrosine kinase/epidermal growth factor receptor pathway have been planned or started (Khuri and Cohen, 2004). Cisplatin is a strong carcinogen in animal models; however, Belinsky *et al*. (1993) reported that cisplatin reduces 4-(methyl nitrosamino)-1-(3-pyridyl)-1-butanone-induced cancer multiplicity. Cisplatin, therefore, has both advantages and disadvantages similar to many other anticancer agents. We previously also reported that (-)-epigallocatechin gallate, celecoxib or gefitinib can inhibit 4-(methyl nitrosamino)-1-(3-pyridyl)-1-butanone-induced lung tumorigensis (a primary lung cancer prevention model) and cisplatin-induced lung tumorigenesis (a secondary lung cancer prevention model) in A/J mice (Kishino *et al*., 2003; Mimoto *et al*., 2000; Okada *et al*., 2003). The combination of chemoprevention or novel agents targeting important cellular signaling pathway based on basic research should be introduced into the clinical trials. In conclusion, occurrence of secondary primary cancer in long-term survivors should be concerned in follow-up. It is important to establish guidelines for follow-up after chemoradiation and to find methods preventing secondary primary cancer in survivors.

Acknowledgments. We thank Okayama Lung Cancer Study Group for their collaborations.

REFERENCES

Non-small Cell Lung Cancer Collaborative Group 1995. Chemotherapy in non-small cell lung cancer: a meta-analysis using updated data on individual patients from 52 randomised clinical trials. Non-small Cell Lung Cancer Collaborative Group. *BMJ 311*: 899–909.

Allan, J.M., and Travis, L.B. 2005. Mechanisms of therapy-related carcinogenesis. *Nat Rev Cancer 5*: 943–955.

Auperin, A., Le Pechoux, C., Pignon, J.P., Koning, C., Jeremic, B., Clamon, G., Einhorn, L., Ball, D., Trovo, M.G., Groen, H.J., Bonner, J.A., Le Chevalier, T., and Arriagada, R. 2006. Concomitant radio-chemotherapy based on platin compounds in patients with locally advanced non-small cell lung cancer (NSCLC): A meta-analysis of individual data from 1764 patients. *Ann. Oncol. 17*: 473–483.

Belinsky, S.A., Stefanski, S.A., and Anderson, M.W. 1993. The A/J mouse lung as a model for developing new chemointervention strategies. *Cancer Res. 53*: 410–416.

Dillman, R.O., Seagren, S.L., Propert, K.J., Guerra, J., Eaton, W.L., Perry, M.C., Carey, R.W., Frei, E.F., 3rd, and Green, M.R. 1990. A randomized trial of induction chemotherapy plus high-dose radiation versus radiation alone in stage III non-small-cell lung cancer. *N. Engl. J. Med. 323*: 940–945.

Duchateau, C.S., and Stokkel, M.P. 2005. Second primary tumors involving non-small cell lung cancer: prevalence and its influence on survival. *Chest 127*: 1152–1158.

Fournel, P., Robinet, G., Thomas, P., Souquet, P.J., Lena, H., Vergnenegre, A., Delhoume, J.Y., Le Treut, J., Silvani, J.A., Dansin, E., Bozonnat, M.C., Daures, J.P., Mornex, F., and Perol, M. 2005. Randomized phase III trial of sequential chemoradiotherapy compared with concurrent chemoradiotherapy in locally advanced non-small-cell lung cancer: Groupe Lyon-Saint-Etienne d'Oncologie Thoracique-Groupe Francais de Pneumo-Cancerologie NPC 95-01 Study. *J. Clin. Oncol. 23*: 5910–5917.

Furuse, K., Fukuoka, M., Kawahara, M., Nishikawa, H., Takada, Y., Kudoh, S., Katagami, N., and Ariyoshi, Y. 1999. Phase III study of concurrent versus sequential thoracic radiotherapy in combination with mitomycin, vindesine, and cisplatin in unresectable stage III non-small-cell lung cancer. *J. Clin. Oncol. 17*: 2692–2699.

Ginsberg, R.J., and Rubinstein, L.V. 1995. Randomized trial of lobectomy versus limited resection for T1 N0 non-small cell lung cancer. Lung Cancer Study Group. *Ann. Thorac. Surg. 60*: 615–622.

Jemal, A., Tiwari, R.C., Murray, T., Ghafoor, A., Samuels, A., Ward, E., Feuer, E.J., and Thun, M.J. 2004. Cancer statistics, 2004. *CA Cancer J. Clin. 54*: 8–29.

Jeremic, B., Shibamoto, Y., Acimovic, L., Nikolic, N., Dagovic, A., Aleksandrovic, J., and Radosavljevic-Asic, G. 2001. Second cancers occurring in patients with early stage non-small-cell lung cancer treated with chest radiation therapy alone. *J. Clin. Oncol. 19*: 1056–1063.

Kawaguchi, T., Matsumura, A., Iuchi, K., Ishikawa, S., Maeda, H., Fukai, S., Komatsu, H., and Kawahara, M. 2006. Second primary cancers in patients with stage III non-small cell lung cancer successfully treated with chemo-radiotherapy. *Jpn. J. Clin. Oncol. 36*: 7–11.

Keene, K.S., Harman, E.M., Knauf, D.G., McCarley, D., and Zlotecki, R.A. 2005. Five-year results of a phase II trial of hyperfractionated radiotherapy and concurrent daily cisplatin chemotherapy for stage III non-small-cell lung cancer. *Am. J. Clin. Oncol. 28*: 217–222.

Khuri, F.R., and Cohen, V. 2004. Molecularly targeted approaches to the chemoprevention of lung cancer. *Clin. Cancer Res. 10*: 4249s–4253s.

Kim, D.W., Shyr, Y., Shaktour, B., Akerley, W., Johnson, D.H., and Choy, H. 2005. Long term follow up and analysis of long term survivors in patients treated with paclitaxel-based concurrent chemo/radiation therapy for locally advanced non-small cell lung cancer. *Lung Cancer 50*: 235–245.

Kishino, D., Kiura, K., Katayama, H., Kuyama, S., Sato, K., Okada, T., Kozuki, T., Hisamoto, A., Nishii, K., Tabata, M., Ueoka, H., and Tanimoto, M. 2003. Gefitinib (Iressa™,ZD1839) can prevent 4-(methylnitrosamino)-1-(3-pyridyl)-1-butanone-induced lung tumorigenesis in A/J mice. *94th Annual Meeting of American Association for Cancer Research*: Abstract #LB-17.

Kubota, K., Tamura, T., Fukuoka, M., Furuse, K., Ikegami, H., Ariyoshi, Y., Kurita, Y., and Saijo, N. 2000. Phase II study of concurrent chemotherapy and radiotherapy for unresectable stage III non-small-cell lung cancer: long-term follow-up results. Japan Clinical Oncology Group Protocol 8902. *Ann. Oncol. 11*: 445–450.

Le Chevalier, T., Arriagada, R., Quoix, E., Ruffie, P., Martin, M., Douillard, J.Y., Tarayre, M., Lacombe-Terrier, M.J., and Laplanche, A. 1994. Radiotherapy alone versus combined chemotherapy and radiotherapy in unresectable non-small cell lung carcinoma. *Lung Cancer 10 Suppl. 1*:S239–S244.

Lippman, S.M., Lee, J.J., Karp, D.D., Vokes, E.E., Benner, S.E., Goodman, G.E., Khuri, F.R., Marks, R., Winn, R.J., Fry, W., Graziano, S.L., Gandara, D.R., Okawara, G., Woodhouse, C.L., Williams, B., Perez, C., Kim, H.W., Lotan, R., Roth, J.A., and Hong, W.K. 2001. Randomized phase III intergroup trial of isotretinoin to prevent second primary tumors in stage I non-small-cell lung cancer. *J. Natl. Cancer. Inst. 93*: 605–618.

Martini, N., Bains, M.S., Burt, M.E., Zakowski, M.F., McCormack, P., Rusch, V.W., and Ginsberg, R.J. 1995. Incidence of local recurrence and second primary tumors in resected stage I lung cancer. *J. Thorac. Cardiovasc. Surg. 109*: 120–129.

Mimoto, J., Kiura, K., Matsuo, K., Yoshino, T., Takata, I., Ueoka, H., Kataoka, M., and Harada, M. 2000. (-)-Epigallocatechin gallate can prevent cisplatin-induced lung tumorigenesis in A/J mice. *Carcinogenesis 21*: 915–919.

Ohe, Y., Ishizuka, N., Tamura, T., Sekine, I., Nishiwaki, Y., and Saijo, N. 2003. Long-term follow-up of patients with unresectable locally advanced non-small cell lung cancer treated with chemoradiotherapy: a retrospective analysis of the data from the Japan Clinical Oncology Group trials (JCOG0003A). *Cancer Sci. 94*: 729–734.

Okada, T., Kishino, D., Kiura, K., Tabata, M., Katayama, H., Kuyama, S., Sato, K., Mimoto, J., Ueoka, H., and Tanimoto, M. 2003. Cyclooxygenase-2 inhibitor prevents cisplatin-induced tumorigenesis in A/J mice dose-dependently. *94th Annual Meeting of American Association for Cancer Research*: Abstract #4920.

Pastorino, U., Infante, M., Maioli, M., Chiesa, G., Buyse, M., Firket, P., Rosmentz, N., Clerici, M., Soresi, E., and Valente, M. 1993. Adjuvant treatment of stage I lung cancer with high-dose vitamin A. *J. Clin. Oncol. 11*: 1216–1222.

Sause, W., Kolesar, P., Taylor, S.I., Johnson, D., Livingston, R., Komaki, R., Emami, B., Curran, W., Jr., Byhardt, R., Dar, A.R., and Turrisi, A., 3rd. 2000. Final results of phase III trial in regionally advanced unresectable non-small cell lung cancer: Radiation Therapy Oncology Group, Eastern Cooperative Oncology Group, and Southwest Oncology Group. *Chest 117*: 358–364.

Segawa, Y., Ueoka, H., Kiura, K., Kamei, H., Tabata, M., Sakae, K., Hiraki, Y., Kawahara, S., Eguchi, K., Hiraki, S., and Harada, M. 2000. A phase II study of cisplatin and 5-fluorouracil with concurrent hyperfractionated thoracic radiation for locally advanced non-small-cell lung cancer: a preliminary report from the Okayama Lung Cancer Study Group. *Br. J. Cancer. 82*: 104–111.

Takigawa, N., Kiura, K., Segawa, Y., Watanabe, Y., Kamei, H., Moritaka, T., Shibayama, T., Ueoka, H., Gemba, K., Yonei, T., Tabata, M., Shinkai, T., Hiraki, S., Takemoto, M., Kanazawa, S., Matsuo, K., and Tanimoto, M. 2006. Second primary cancer in survivors following concurrent chemoradiation for locally advanced non-small-cell lung cancer. *Br. J. Cancer. 95*: 1142–1144.

Thomas, P.A., Jr., and Rubinstein, L. 1993. Malignant disease appearing late after operation for T1 N0 non-small-cell lung cancer. The Lung Cancer Study Group. *J. Thorac. Cardiovasc. Surg. 106*: 1053–1058.

van Zandwijk, N., Dalesio, O., Pastorino, U., de Vries, N., and van Tinteren, H. 2000. EUROSCAN, a randomized trial of vitamin A and N-acetylcysteine in patients with head and neck cancer or lung cancer. For the European Organization for Research and Treatment of Cancer Head and Neck and Lung Cancer Cooperative Groups. *J. Natl. Cancer Inst. 92*: 977–986.

Zatloukal, P., Petruzelka, L., Zemanova, M., Havel, L., Janku, F., Judas, L., Kubik, A., Krepela, E., Fiala, P., and Pecen, L. 2004. Concurrent versus sequential chemoradiotherapy with cisplatin and vinorelbine in locally advanced non-small cell lung cancer: a randomized study. *Lung Cancer 46*: 87–98.

18
Advanced Non-Small Cell Lung Cancer: Second-Line Treatment with Docetaxel

Cesare Gridelli and Paolo Maione

INTRODUCTION

Cisplatin-based chemotherapy is considered standard of care worldwide for patients with advanced non-small-cell lung cancer (NSCLC) (Non Small Cell Lung Cancer Collaborative Group, 1995). Approximately one third of patients obtain an objective response with first-line chemotherapy, and another 20–30% achieve temporary disease stabilization. Unfortunately, all patients ultimately suffer progression. At the time of disease progression, many patients still have a good performance status (PS) and can be considered for further active treatment. Until 2000, there was no evidence supporting the efficacy of second-line treatment, although chemotherapy was often offered to patients in good clinical condition, based on the results of phase II trials of several new drugs showing modest activity in pre-treated NSCLC (Huisman *et al*., 2000). The 1997 guideline of the American Society of Clinical Oncology (ASCO) stated "there is no current evidence that either confirms or refutes that second-line chemotherapy improves survival in patients with advanced NSCLC" (American Society of Clinical Oncology, 1997). In recent years, the efficacy of several drugs in the second-line setting has been demonstrated in phase III trials, and second-line treatment can now be considered a standard of care (Pfister *et al*., 2004; Ettinger *et al*., 2006). Two chemotherapeutic agents, docetaxel and pemetrexed, and the biological drug erlotinib are currently approved for clinical use in this setting.

SECOND-LINE TREATMENT

Patients who experience disease progression during or after first-line treatment for advanced NSCLC have a limited life expectancy. Quality of life is often compromised by disease-related symptoms, by residual toxicity of previous chemotherapy, and by co-morbid diseases. The aims of second-line treatment should be palliation of symptoms, benefit in quality of life and prolongation of survival. The benefits of treatment should outweigh toxicity and inconvenience to the patient. However, the impact of treatment on the natural history of the disease is modest. As shown in a recent review of 19 phase III trials (Hotta *et al*., 2007), in the second-line or later setting, the median objective response rate was 6.8%, and median overall survival was 6.6 months.

Life expectancy of these patients is largely dependent on their clinical condition at the start of second-line treatment. Patients with PS 2, who are considered fit for further treatment may have a *relative benefit* from treatment similar to patients with better PS. However the *absolute* benefit is small, with most studies reporting a median survival of 3–4 months.

In a series of patients enrolled in a randomized trial of second-line chemotherapy, other variables including gender, stage and best response to initial therapy as well as PS were independently associated with survival (Weiss *et al*., 2007). Median survival was better in women, in patients with stage III compared to IV, and in patients who had responded to first-line treatment.

The length of time spent by patients receiving anti-tumor treatment has been increasing recently, due to the availability of new drugs. However, most patients with advanced NSCLC who receive second-line treatment are near the end of life. In a retrospective review of patients treated for advanced NSCLC in a community oncology setting, the mean line of chemotherapy in patients who were receiving active treatment at the time of death was second-line (Murillo and Koeller, 2006). Chemotherapy was given within 1 month and 2 weeks of death to 43% and 20% of patients, respectively. This can be explained in part by the increased demand for additional treatment by patients and their relatives who are unable to accept the futility of further therapy and the inevitability of death from progressive NSCLC. It may also be due to physicians' inability to correctly predict life expectancy of these patients. This emphasizes the importance of identifying predictive markers of response, survival benefit and toxicity in pre-treated NSCLC patients.

DOCETAXEL VERSUS BEST SUPPORTIVE CARE IN THE SECOND-LINE TREATMENT

Docetaxel, 75 mg/m^2 intravenously (i.v.) every 3 weeks, was the first drug to be approved for second-line treatment of advanced NSCLC, based on the results of two phase III trials (Shepherd *et al*., 2000; Fossella *et al*., 2000).

In the TAX317 study (Shepherd *et al*., 2000), docetaxel 100 mg/m^2 every 3 weeks was compared to best supportive care. When interim safety data monitoring identified a significantly higher toxic death rate in the chemotherapy arm, the protocol was amended and the dose was reduced to 75 mg/m^2. About 200 patients were randomized to docetaxel or placebo. Among the 103 patients treated with docetaxel, six (7.1%) achieved partial responses (three patients at each dose level. Time to progression was longer for docetaxel patients than for best supportive care patients (10.6 versus 6.7 weeks, respectively; $p < 0.001$). Median overall survival was significantly longer for patients in the docetaxel arm (7.0 versus 4.6 months; $p = 0.047$). The difference was more significant for docetaxel 75 mg/m^2 patients, compared with corresponding best supportive care patients (7.5 versus 4.6 months; $p = 0.010$; 1-year survival 37% versus 11%; $p = 0.003$). Febrile neutropenia was the most relevant toxicity reported with docetaxel, but was less frequent with the lower dose. In fact, it occurred in 11 patients treated with docetaxel 100 mg/m^2, three of whom died, and in one patient treated with docetaxel 75 mg/m^2. Grade 3 or 4 nonhematologic toxicity, with the exception of diarrhea, occurred at a similar rate in both the docetaxel and best supportive care groups.

Interestingly, all quality of life parameters favoured docetaxel (Dancey *et al*., 2004).

Retrospective pharmaco-economic studies have shown that the cost of second-line docetaxel in NSCLC is in keeping with the cost of second-line treatment in other tumors, and is within an acceptable range for health care interventions (Holmes *et al*., 2004; Leighl *et al*., 2002).

DOCETAXEL VERSUS OTHER CHEMOTHERAPEUTIC AGENTS IN THE SECOND-LINE TREATMENT

In the TAX320 trial (Fossella *et al*., 2000), patients were randomized to receive docetaxel (100 mg/m^2 or 75 mg/m^2, every 3 weeks) or to a control arm of vinorelbine or ifosfamide at the investigator's discretion. A total of 373 patients were randomized. Overall response rates were 10.8% with docetaxel 100 mg/m^2 and 6.7% with docetaxel 75 mg/m^2, each significantly higher than the 0.8% response with vinorelbine or ifosfamide ($p = 0.001$ and $p = 0.036$, respectively). Patients who received docetaxel had a longer time to progression ($p = 0.046$) and a greater progression-free survival at 26 weeks ($p = 0.005$). Although overall survival was not significantly different between the three groups, the 1-year survival was significantly greater with docetaxel 75 mg/m^2 than with the control treatment (32% versus 19%; $p = 0.025$). Prior exposure to paclitaxel did not decrease the likelihood of response to docetaxel, nor did it impact survival. There was a trend toward greater efficacy in patients whose disease was platinum-refractory and in patients with performance status of 0 or 1 versus 2. Patients assigned to docetaxel had more neutropenia and febrile neutropenia compared to the control arm, but the lower dose of docetaxel was generally well tolerated.

Pemetrexed is a multi-targeted antifolate agent. Pemetrexed 500 mg/m^2 was compared to docetaxel 75 mg/m^2 in a phase III trial (Hanna *et al*., 2004). Five hundred seventy-one patients were randomly assigned. Overall response rates were 9.1% and 8.8% for pemetrexed and docetaxel, respectively. Median progression-free survival was 2.9 months for each arm, and median survival time was 8.3 versus 7.9 months (p = not significant) for pemetrexed and docetaxel, respectively. The 1-year survival rate for each arm was 29.7%. Patients receiving docetaxel were more likely to have grade 3 or 4 neutropenia (40.2% versus 5.3%; $p < 0.001$), febrile neutropenia (12.7% versus 1.9%; $p < 0.001$), neutropenia with infections (3.3% versus 0.0%; $p = 0.004$) hospitalizations for neutropenic fever (13.4% versus 1.5%; $p < 0.001$), hospitalizations due to other drug related adverse events (10.5% versus 6.4%; $p = 0.092$), use of granulocyte colony-stimulating factor support (19.2% versus 2.6%; $p < 0.001$) and all grade alopecia (37.7% versus 6.4%; $p < 0.001$) compared with patients receiving pemetrexed. The study was originally designed to test for superiority of pemetrexed, but in an amendment to the protocol a non-inferiority design was adopted. Results were not sufficient to demonstrate the non-inferiority of pemetrexed according to the fixed margin method. However, using the percent retention method, results were adequate to define non-inferiority. Although neither superiority nor non-inferiority for overall survival could be strictly demonstrated according to primary efficacy analysis, comparable response rates and

progression-free survival times supported the conclusion that an effect of pemetrexed on survival was reasonably likely. The trial results led to pemetrexed approval.

Oral topotecan has been compared to standard docetaxel in a phase III study that was designed to test the non-inferiority of oral topotecan (Ramlau *et al*., 2006). One-year survival rates were 25.1% with topotecan and 28.7% with docetaxel, and this difference met the predefined criteria for non-inferiority of topotecan. However, median overall survival was 27.9 weeks with topotecan and 30.7 weeks with docetaxel and the higher survival rate with docetaxel was maintained across the entire treatment period, although the difference did not reach statistical significance. Grade 3/4 neutropenia occurred more frequently with docetaxel, while grade 3/4 anemia and thrombocytopenia occurred more frequently with topotecan. Patients receiving docetaxel had significant advantages in quality of life compared to patients receiving oral topotecan. At the moment, topotecan is not approved for the second-line treatment of advanced NSCLC.

Paclitaxel poliglumex (PP) is a macromolecular drug conjugate that links paclitaxel with a biodegradable polymer (poly-L-glutamic acid). The STELLAR II trial compared PP with docetaxel as second-line therapy in patients with advanced NSCLC (Bonomi *et al*., 2005). Patients assigned to PP experienced significantly less hematological toxicity and less febrile neutropenia. As for non-haematological toxicity, PP was associated with a lower incidence of diarrhea, stomatitis, respiratory symptoms and fatigue, but worse neuropathy. The trial did not demonstrate any survival benefit for PP therapy as compared with docetaxel. Although PP showed comparable efficacy to standard docetaxel, with a favorable tolerability profile, the study was not designed as a non-inferiority trial, and these results cannot be considered sufficient to recommend PP as a standard approach. PP is not yet approved for clinical use in the second-line treatment of advanced NSCLC.

Vinflunine is a new microtubule inhibitor of the vinca alkaloid class with clinical activity in NSCLC. Vinflunine was compared to docetaxel in a phase III trial in pre-treated NSCLC patients (Krzakowski *et al*., 2007). The primary end-point was progression free survival, with a non-inferiority analysis. All efficacy endpoints including median progression free survival, response rate, median and overall survival were similar. Although the toxicity profile of the experimental arm was judged manageable, vinflunine was characterized by higher incidence of grade 3/4 anemia, abdominal pain, constipation and fatigue. Vinflunine is not yet approved by the FDA or EMEA and its use remains experimental.

In first-line treatment of good PS patients, doublet chemotherapy has been shown to be more effective than single-agent, both in terms of response and survival. In the second-line setting, the clinical trials showing efficacy of chemotherapy all tested single-agent treatment. With the aim of obtaining better results, several trials compared a doublet with single agent chemotherapy. Docetaxel was used in the control arms in three of the trials (Takeda *et al*., 2004; Wachters *et al*., 2005; Pectasides *et al*., 2005) whereas other single agents were used in two studies enrolling patients who had already

received docetaxel as first-line treatment (Georgoulias *et al*., 2004; Georgoulias *et al*., 2005). Only one Japanese trial that compared single-agent docetaxel with the combination of docetaxel and gemcitabine had a phase III design (Takeda *et al*., 2004). It was terminated early after the report of an unexpectedly high incidence of interstitial lung disease (ILD) and three treatment-related deaths (5%) due to ILD, seen only in the combination arm. Considering all the trials, combination chemotherapy is characterized by higher toxicity, with some advantage in terms of objective response and progression-free survival, but without a significant difference in overall survival. However, with one exception (Takeda *et al*., 2004), the trials were not designed as comparative phase III trials, but were randomized phase II trials, with a small sample size and inadequate statistical power to exclude potentially relevant differences.

Only patients with clinical and/or radiological evidence of disease progression after or during first-line chemotherapy should be considered for second-line treatment. In patients achieving objective response or disease stabilization with first-line therapy, maintenance treatment with the same or different agents has not definitively been shown to improve overall survival, and should not be considered a standard approach (Westeel *et al*., 2005; Fidias *et al*., 2007). In a recent trial, 307 stable and responding patients were randomized to receive docetaxel either immediately after first-line chemotherapy, or upon disease progression (Fidias *et al*., 2007). Median overall survival showed a trend favouring immediate treatment, but the difference did not reach statistical significance.

DOCETAXEL GIVEN EVERY 3 WEEKS COMPARED WITH WEEKLY SCHEDULE

Although second-line chemotherapy with docetaxel at the dose of 75 mg/m^2, administered once every 3 weeks, has been proven to prolong survival compared to best supportive care, and to improve some quality of life items such as fatigue and pain, myelosuppression with this docetaxel schedule is extremely frequent and severe. Grade 3–4 neutropenia has been reported in 67% of patients in one trial (Shepherd *et al*., 2000) grade 4 in 54% of patients in another (Fossella *et al*., 2000) and febrile neutropenia has been reported in 2% and 8% of cases, respectively (Shepherd *et al*., 2000; Fossella *et al*., 2000).

Weekly scheduling of docetaxel may improve the toxicity profile of the drug in pre-treated NSCLC patients (Hainsworth *et al*., 1998; Lilenbaum *et al*., 2001), without decreasing anti-tumor activity. Particularly, a marked reduction in the occurrence of severe and febrile neutropenia is reported when administering docetaxel in a weekly schedule, as compared to the classic every-3-week administration. On the basis of this evidence, several randomised trials have been conducted, with the aim of comparing the weekly with the standard 3-week schedule of docetaxel in the second-line treatment of advanced NSCLC (Gridelli *et al*., 2004; Gervais *et al*., 2005; Schuette *et al*., 2005; Lai *et al*., 2005; Camps *et al*., 2006). Overall, the studies reported a better toxicity profile for weekly regimen as compared to 3-week schedule with contrasting results in terms of survival. However, sample size of each single trial had insufficient power to detect potentially relevant differences in overall survival.

Di Maio *et al.* (2007) very recently performed a meta-analysis based on individual data from patients enrolled in five randomized trials, aimed at comparing the efficacy of the two different schedules of docetaxel for the second-line treatment of advanced NSCLC. Such a meta-analysis has the advantage of increasing the power of the statistical comparison to detect survival differences.

Systematic reviews and meta-analyses have been increasingly used in recent years, as an important instrument for assessing and interpreting the results from different clinical trials conducted on the same topic. The issue of the comparison between 3-weekly and weekly docetaxel as second-line treatment of NSCLC represents a good topic for this approach, because several underpowered, randomized, and similarly designed trials have been conducted. This individual patient data meta-analysis shows no significant difference in efficacy for weekly schedule of docetaxel compared to standard 3-weekly administration as second-line treatment of patients with advanced NSCLC.

Two of the five assessed trials were phase II randomized trials (Gervais *et al.*, 2005; Lai *et al.*, 2005). Phase II randomized trials should not be planned to formally compare the treatments, but they can be considered when conducting such an individual patient data meta-analysis, because in these studies treatment was assigned randomly, and information on overall survival, i.e. the primary endpoint of the meta-analysis, was collected prospectively.

Weekly schedule was similar in the five studies, with some differences in the docetaxel dose (ranging from 33 and 40 mg/m^2) and in the sequence of weeks with and without treatment. Four of the trials (those conducted in Europe (Gridelli *et al.*, 2004; Gervais *et al.*, 2005; Schuette *et al.*, 2005; Camps *et al.*, 2006) had an identical standard arm (docetaxel given at 75 mg/m^2 every 3 weeks): only the Taiwanese trial (Lai *et al.*, 2005) had a slightly lower dose in the standard arm (66 mg/m^2), because of the higher risk of toxicity when higher doses are administered to Eastern patients. However, all the results of the meta-analysis were completely superimposable even when excluding Taiwanese trial.

Two of the studies were designed with toxicity as the primary end-point (Gervais *et al.*, 2005; Lai *et al.*, 2005). The trial by Gridelli *et al.* (2004) was designed with quality of life as the primary end-point, and planned sample size allowed 80% power to rule out an optimistic 0.67 hazard ratio of death with the weekly schedule. Only the Schuette and the Camps trials were designed with survival as the primary end-point, but with highly optimistic alternative hypotheses. With such a small power for single studies, it is not surprising that results and their interpretation differed among trials. In particular, German authors, discussed a median survival that was longer, although it did not reach a statistical significance, for weekly docetaxel, recommended this treatment as a feasible alternative second-line treatment (Schuette *et al.*, 2005). Italian authors recommended weekly docetaxel as preferable, because of some quality of life advantages, lower toxicity and no evidence of strikingly different effects on survival, but they recognized that no claim could be made about the interpretation of comparison in terms of equivalence (Gridelli *et al.*, 2004). In the Spanish trial on the other hand, survival with weekly schedule was

slightly shorter although not significantly than the standard arm, and the authors did not recommend the weekly schedule, limiting its potential usefulness to patients at high risk of severe neutropenia (Camps *et al*., 2006). Similarly, in the opinion of French authors, the 3-weekly schedule of docetaxel remained the recommended schedule in the second-line setting, while weekly docetaxel administration could be considered as an alternative for patients at high risk of febrile neutropenia (Gervais *et al*., 2005).

Di Maio *et al*. (2007) reported no survival differences between the two schedules, with a hazard ratio estimate of only 1.09 against relevant benefits in terms of toxicity. The absence of significant heterogeneity among the trials, and among subgroups, reinforces these findings and we may be more confident in considering weekly schedule as a valid alternative in all patients who are candidates for second line treatment for advanced NSCLC. Further, patients that have been pre-treated with paclitaxel can receive some benefit from second-line treatment with docetaxel. Pre-treatment with paclitaxel was allowed in four of the five studies, probably based on the evidence of activity of docetaxel in this category of patients in the previous phase III trial of docetaxel versus vinorelbine/ifosfamide (Fossella *et al*., 2000). In these pooled data, 14% of the patients had received prior paclitaxel, and both schedules of docetaxel showed objective responses also in these patients. As for toxicity data, this pooled analysis confirms a significantly different toxicity profile between the two schedules of docetaxel. The most dangerous toxicity with docetaxel is the occurrence of febrile neutropenia, and this meta-analysis confirms that this risk is significantly lower with the weekly schedule. In this analysis, the occurrence of severe non-haematological toxicity was not different between weekly and every-3-week schedule. In conclusion, weekly docetaxel represents a valid alternative to 3-weekly administration for all patients with NSCLC who are candidates for a second-line chemotherapy, based on an advantageous profile of toxicity and no relevant difference in survival.

DOCETAXEL VERSUS TARGETED THERAPIES IN THE SECOND-LINE TREATMENT

Epidermal growth factor receptor (EGFR) expression is common in NSCLC, and the EGFR pathway has been the target of development of new drugs against this disease (Ciardiello *et al*., 2004). Erlotinib and gefitinib are small molecules that inhibit the tyrosine kinase activity of EGFR and have been studied extensively in advanced NSCLC. Erlotinib was compared to placebo in the BR.21 phase III study (Shepherd *et al*., 2005). Patients were randomized in a 2:1 ratio to receive either erlotinib 150 mg orally daily or placebo. Statistically significant and clinically relevant differences were observed for progression-free survival and overall survival. This was the first randomized trial to demonstrate that an EGFR tyrosine kinase inhibitor is able to prolong survival after chemotherapy for advanced NSCLC. Treatment with erlotinib also showed significant benefits in quality of life and lung cancer-related symptoms of cough, dyspnea and pain (Bezjak *et al*., 2007). Based on the results of the BR.21 study, erlotinib was approved

by the FDA in 2004 and is now approved worldwide for the treatment of advanced NSCLC patients failing after previous chemotherapy. Subsequently, gefitinib was compared to placebo in the ISEL phase III trial, for patients with advanced NSCLC who had received one or two regimens of chemotherapy (Thatcher *et al*., 2005). Overall survival did not differ significantly between the groups, neither in the overall population nor among the 812 patients with adenocarcinoma. Due to these negative results, the conditions of gefitinib approval have been restricted, and the drug was relabelled by the FDA for use in patients already receiving it and obtaining a clinical benefit.

Results of a phase III randomized trial comparing gefitinib to docetaxel in patients with advanced NSCLC pretreated with platinum-based chemotherapy have been presented very recently (Douillard *et al*., 2007). This trial, named INTEREST (Iressa NSCLC Trial Evaluating Response and Survival against Taxotere), is the largest reported phase III study comparing targeted therapy (gefitinib) with chemotherapy (docetaxel). Patients with locally advanced or metastatic NSCLC who had progressed or recurred following 1 or 2 prior chemotherapy regimens (at least 1 platinum-based) were randomized to receive gefitinib (250 mg/day orally) or docetaxel (75 mg/m^2 i.v. every 3 weeks). The primary objective was to compare overall survival between gefitinib and docetaxel using a co-primary analysis in both the overall population (non-inferiority), and as a protocol amendment following the emergence of biomarker data, in patients with high EGFR gene copy number (measured by fluorescence in situ hybridization) (superiority). Secondary endpoints were progression free survival, objective response rate, patient-reported functionality, quality of life and safety and tolerability. Approximately, 1,500 patients were randomized to gefitinib or docetaxel. The treatment groups were well balanced in terms of patient demographics and baseline characteristics. In fact, in the gefitinib and docetaxel treatment arms, respectively, 54% and 55% had adenocarcinoma, 36% and 33% were male, and 20% and 21% were never-smokers. Objective tumor response was 9.1% for gefitinib and 7.6% for docetaxel ($p = 0.32$). Median survival was 7.6 months for gefitinib and 8.0 months for docetaxel (HR = 1.020). One-year survival rate was 32% for gefitinib and 34% for docetaxel. These data conclude for non-inferiority of gefitinib in the overall population. Progression-free survival was 2.2 months for gefitinib and 2.7 months for docetaxel (HR = 1.04). Interestingly, median survival results were similar for gefitinib and docetaxel also in patients with high EGFR gene copy number (8.4 months for gefitinib and 7.6 months for docetaxel; HR = 1.09). Safety data showed a better safety profile for gefitinib. In fact, grade 3–4 adverse events occurred in 8.5% and 40.7% of the patients treated respectively with gefitinib and docetaxel. A series of important conclusions can be drawn from this trial. The study met the primary objective of demonstrating non-inferiority of gefitinib relative to docetaxel in terms of overall survival. There was no evidence from the co-primary analysis to support the hypothesis that EGFR FISH positive patients have superior overall survival on gefitinib compared to docetaxel. Progression-free survival, overall response rate and disease-related symptom improvements were similar for gefitinib and docetaxel. Gefitinib had

a more favourable tolerability profile than docetaxel. Significantly more gefitinib-treated patients experienced a clinically important improvement in quality of life compared to docetaxel.

ONGOING STUDIES ON DOCETAXEL

ZD6474 (Zactima) is a multi-target tyrosine kinase inhibitor, inhibiting two key pathways in tumor growth. In fact Zactima is an inhibitor of the tyrosine kinase domain of the vascular endothelial growth factor (VEGF) receptor-2 (VEGFR2) and also inhibits the EGFR tyrosine kinase. Vandetanib showed promising results in randomized phase II trials, both as a single agent (Natale *et al*., 2006) and in combination with docetaxel in the second-line treatment of advanced NSCLC (Heymach *et al*., 2007). Heymach *et al*. (2007) compared in a phase II randomized double-blind study, Zactima in combination with docetaxel to docetaxel plus placebo. The results of this study demonstrated that Zactima combined with docetaxel prolonged progression-free survival compared with docetaxel alone. This phase II trial is the basis of a relevant ongoing phase III randomized double-blind trial that is assessing the efficacy of docetaxel in combination with Zactima versus docetaxel in combination with placebo in patients with locally advanced or metastatic NSCLC after failure of first-line chemotherapy.

REFERENCES

American Society of Clinical Oncology 1997. Clinical practice guidelines for the treatment of unresectable non-small-cell lung cancer. *J. Clin. Oncol. 15*: 2996–3018.

Bezjak, A., Tu, D., Seymour, L., Trajkovic, A., Zukin, M., Ayoub, J., Lago, S., de Albuquerque Ribeiro, R., Gerogianni, A., Cyjon, A., Noble, J., Laberge, F., Chan, R.T., Fenton, D., von Pawel, J., Reck, M., and Shepherd, F.A. 2007. Symptom improvement in lung cancer patients treated with erlotinib: quality of life analysis of the National Cancer Institute of Canada Clinical Trials Group Study BR.21. *J. Clin. Oncol. 24*: 3831–3837.

Bonomi, P., Paz-Ares, L., and Langer, C. 2005. Xyotax versus docetaxel for the second-line treatment of non small cell lung cancer: The STELLAR 2 phase III study. *Lung Cancer 49*: S35.

Camps, C., Massuti, B., Jimenez, A., Maestu, I., Gómez, R.G., Isla, D., González, J.L., Almenar, D., Blasco, A., Rosell, R., Carrato, A., Viñolas, N., Batista, N., Girón, C.G., Galán, A., López, M., Blanco, R., Provencio, M., Diz, P., and Felip, E. 2006. Randomized phase III study of 3-weekly versus weekly docetaxel in pretreated advanced non-small-cell lung cancer: a Spanish Lung Cancer Group trial. *Ann. Oncol. 17*: 467–472.

Ciardiello, F., De Vita, F., Orditura, M., and Tortora, G. 2004. The role of EGFR inhibitors in nonsmall cell lung cancer. *Curr. Opin. Oncol. 16*: 130–135.

Dancey, J., Shepherd, F.A., Gralla, R.J., and Kim, Y.S. 2004. Quality of life assessment of second-line docetaxel versus best supportive care in patients with non-small-cell lung cancer previously based with platinum-based chemotherapy: results of a prospective, randomized phase III trial. *Lung Cancer 43*: 183–194.

Di Maio, M., Perrone, F., Chiodini, P., Gallo, C., Camps, C., Schuette, W., Quoix, E., Tsai, C.M., and Gridelli, C. 2007 Individual patient data meta-analysis of docetaxel administered once every 3 weeks compared with once every week second-line treatment of advanced non-small-cell lung cancer. *J. Clin. Oncol. 25*: 1377–1382.

Douillard, J.Y., Hirsh, E., Mok, V., Socinski, T., Gervais, M., Wu, R., Li, Yi-Long, Sellers, L., and Lowe, M. 2007. Gefitinib (IRESSA) versus docetaxel in patients with locally advanced or metastatic non-small-cell lung cancer pre-treated with platinum-based chemotherapy: a randomized, open-label phase III study (INTEREST). *J. Thorac. Oncol. 2/8 (Suppl. 4)*: S305.

Ettinger, D.S., Bepler, G., Bueno, R., Chang, A., Chang, J.Y., Chirieac, L.R., D'Amico, T.A., Demmy, T.L., Feigenberg, S.J., Grannis, F.W. Jr., Jahan, T., Jahanzeb, M., Kessinger, A., Komaki, R., Kris, M.G., Langer, C.J., Le, Q.T., Martins, R., Otterson, G.A., Robert, F., Sugarbaker, D.J., and Wood, D.E. 2006. Non-small cell lung cancer clinical practice guidelines in oncology. *J. Natl. Compr. Canc. Netw. 4*: 548–582.

Fidias, P., Dakhil, S., and Lyss, A. 2007. Phase III study of immediate versus delayed docetaxel after induction therapy with gemcitabine plus carboplatin in advanced non-small-cell lung cancer: Updated report with survival. *J. Clin. Oncol. 25/18S*: LBA7516.

Fossella, F.V., DeVore, R., Kerr, R.N., Crawford, J., Natale, R.R., Dunphy, F., Kalman, L., Miller, V., Lee, J.S., Moore, M., Gandara, D., Karp, D., Vokes, E., Kris, M., Kim, Y., Gamza, F., and Hammershaimb, L., for the TAX 320 Non–Small-Cell Lung Cancer Study Group. 2000. Randomized phase III trial of docetaxel versus vinorelbine or ifosfamide in patients with non-small cell lung cancer previously treated with platinum - containing chemotherapy regimens. *J. Clin. Oncol. 18*: 2354–2362.

Georgoulias, V., Kouroussis, C., Agelidou, A., Boukovinas, I., Palamidas, P., Stavrinidis, E., Polyzos, A., Syrigos, K., Veslemes, M., Toubis, M., Ardavanis, A., Tselepatiotis, E., and Vlachonikolis, I. 2004. Irinotecan plus gemcitabine vs irinotecan for the second-line treatment of patients with advanced non-small-cell lung cancer pretreated with docetaxel and cisplatin: a multicentre, randomised, phase II study. *Br. J. Cancer 91*: 482–488.

Georgoulias, V., Agelidou, A., Syrigos, K., Rapti, A., Agelidou, M., Nikolakopoulos, J., Polyzos, A., Athanasiadis, A., Tselepatiotis, E., Androulakis, N., Kalbakis, K., Samonis, G., and Mavroudis, D. 2005. Second-line treatment with irinotecan plus cisplatin vs cisplatin of patients with advanced non-small-cell lung cancer pretreated with taxanes and gemcitabine: a multicenter randomised phase II study. *Br. J. Cancer 93*: 763–769.

Gervais, R., Ducolone, A., Breton, J.L., Braun, D., Lebeau, B., Vaylet, F., Debieuvre, D., Pujol, J.L., Tredaniel, J., Clouet, P., and Quoix, E. 2005. Phase II randomised trial comparing docetaxel given every 3 weeks with weekly schedule as second-line therapy in patients with advanced non-small-cell lung cancer (NSCLC). *Ann. Oncol. 16*: 90–96.

Gridelli, C., Gallo, C., Di Maio, M., Barletta, E., Illiano, A., Maione, P., Salvagni, S., Piantedosi, F.V., Palazzolo, G., Caffo, O., Ceribelli, A., Falcone, A., Mazzanti, P., Brancaccio, L., Capuano, M.A., Isa, L., Barbera, S., and Perrone, F. 2004. A randomised clinical trial of two docetaxel regimens (weekly vs 3 week) in the second-line treatment of non-small-cell lung cancer. The DISTAL 01 study. *Br. J. Cancer 91*: 1996–2004.

Hainsworth, J.D., Burris, H.A. 3rd, Erland, J.B., Thomas, M., and Greco, F.A. 1998. Phase I trial of docetaxel administered by weekly infusion in patients with advanced refractory cancer. *J. Clin. Oncol. 16*: 2164–2168.

Hanna, N., Shepherd, F.A., Fossella, F.V., Pereira, J.R., De Marinis, F., von Pawel, J., Gatzemeier, U., Tsao, T.C., Pless, M., Muller, T., Lim, H.L., Desch, C., Szondy, K., Gervais, R., Shaharyar, D., Manegold, C., Paul, S., Paoletti, P., Einhorn, L., and Bunn, P.A. Jr. 2004. Randomized phase III trial of pemetrexed versus docetaxel in patients with non-small –cell lung cancer previously treated with chemotherapy. *J. Clin. Oncol. 22*: 1589–1597.

Heymach, J.V., Johnson, B.E., Prager, D., Csada, E., Roubec, J., Pesek, M., Spásová, I., Belani, C.P., Bodrogi, I., Gadgeel, S., Kennedy, S.J., Hou, J., and Herbst, R.S. 2007. Vandetanib (ZD6474) plus docetaxel in patients with previously treated non-small cell lung cancer: results of a randomized, placebo-controlled phase I/II study. *J. Clin. Oncol. 25*: 4270–4277.

Holmes, J., Dunlop, D., Hemmett, L., Sharplin, P., and Bose, U. 2004. A cost-effectiveness of docetaxel in the second-line treatment of non-small-cell lung cancer. *Pharmacoeconomics 22*: 581–589.

Hotta, K., Fujiwara, Y., Kiura, K., Takigawa, N., Tabata, M., Ueoka, H., and Tanimoto, M. 2007. Relationship between response and survival in more than 50000 patients with advanced non-small cell lung cancer treated with systemic chemotherapy in 143 phase III trials. *J. Thorac. Oncol. 2*: 402–407.

Huisman, C., Smit, E.F., Giaccone, G., Postmus, P.E. 2000. Second-line chemotherapy in relapsing or refractory non-small-cell lung cancer: a review. *J. Clin. Oncol. 18*: 3722–3730.

Krzakowski, M., Douillard, J., and Ramlau, R. 2007. Phase III study of vinflunine versus docetaxel in patients with advanced non-small cell lung cancer previously treated with a platinum-containing regimen. *J. Clin. Oncol. 25/18S*: 7511.

Lai, C.L., Tsai, C.M., Chiu, C.H., Wang, G.S., Su, W.J., Chen, Y.M., and Perng, R.P. 2005. Phase II randomized trial of tri-weekly versus day 1 and 8 weekly docetaxel as a second-line treatment of advanced non-small cell lung cancer. *Jpn. J. Clin. Oncol. 35*: 700–706.

Leighl, N.B., Shepherd, F.A., Kwong, R., Burkes, R.L., Feld, R., and Goodwin, P.J. 2002. Economic analysis of the TAX 317 trial: Docetaxel versus best supportive care as second-line therapy of advanced non-small-cell lung cancer. *J. Clin. Oncol. 20*: 1344–1352.

Lilenbaum, R.C., Schwartz, M.A., Seigel, L., Belette, F., Blaustein, A., Wittlin, F.N., and Davila, E. 2001. Phase II trial of weekly docetaxel in second-line therapy for non-small cell lung carcinoma. *Cancer 92*: 2158–2163.

Murillo, J.R., and Koeller, J. 2006. Chemotherapy given near the end of life by community oncologists for advanced non-small-cell lung cancer. *Oncologist 11*: 1095–1099.

Natale, R.B., Bodkin, D., Govindan, R., Sleckman, B., Rizvi, N., Capo, A., Germonpre, P., Stockman, P., Kennedy, S., and Ranson, M. 2006. ZD6474 versus gefitinib in patients with advanced NSCLC: Final results from a two-part, double-blind, randomized phase II trial. *J. Clin. Oncol. 24/18S*: 7000.

Non-small Cell Lung Cancer Collaborative Group 1995. Chemotherapy in non-small cell lung cancer: a meta-analysis using updated data on individual patients from 52 randomised clinical trials. *BMJ 311*: 899–909.

Pectasides D, Pectasides M, Farmakis D, Kostopoulou, V., Nikolaou, M., Gaglia, A., Koumpou, M., Mylonakis, N., Xiros, N., Economopoulos, T., and Raptis, S.A. 2005. Comparison of docetaxel and docetaxel-irinotecan combination as second-line chemotherapy in advanced non-small-cell lung cancer: a randomized phase II trial. *Ann. Oncol. 16*: 294–299.

Pfister, D.G., Johnson, D.H., Azzoli, C.G., Sause, W., Smith, T.J., Baker, S. Jr., Olak, J., Stover, D., Strawn, J.R., Turrisi, A.T., and Somerfield, M.R. 2004. American Society of Clinical Oncology treatment of unresectable non-small-cell lung cancer guideline: update 2003. *J. Clin. Oncol. 22*: 330–353.

Ramlau, R., Gervais, R., Krzakowski, M., von Pawel, J., Kaukel, E., Abratt, R.P., Dharan, B., Grotzinger, K.M., Ross, G., Dane, G., and Shepherd, F.A. 2006. Phase III study comparing oral topotecan to intravenous docetaxel in patients with pretreated advanced non-small-cell lung cancer. *J. Clin. Oncol. 24*: 2800–2807.

Schuette, W., Nagel, S., Blankenburg, T., Lautenschlaeger, C., Hans, K., Schmidt, E.W., Dittrich, I., Schweisfurth, H., von Weikersthal, L.F., Raghavachar, A., Reissig, A., and Serke, M. 2005. Phase III study of second-line chemotherapy for advanced non-small-cell lung cancer with weekly compared with 3-weekly docetaxel. *J. Clin. Oncol. 23*: 8389–8395.

Shepherd, F.A., Dancey, J., Ramlau, R., Mattson, K., Gralla, R., O'Rourke, M., Levitan, N., Gressot, L., Vincent, M., Burkes, R., Coughlin, S., Kim, Y., and Berille, J. 2000. Prospective randomized trial of docetaxel versus best supportive care in patients with non-small-cell lung cancer previously treated with platinum-based chemotherapy. *J. Clin. Oncol. 18*: 2085–2103.

Shepherd, F.A., Rodrigues, P.J., Ciuleanu, T., Tan, E.H., Hirsh, V., Thongprasert, S., Campos, D., Maoleekoonpiroj, S., Smylie, M., Martins, R., van Kooten, M., Dediu, M., Findlay, B., Tu, D., Johnston, D., Bezjak, A., Clark, G., Santabarbara, P., and Seymour, L. 2005. Erlotinib in previously treated non-small cell lung cancer. *N. Engl. J. Med. 353*: 123–132.

Takeda, K., Negoro, S., and Tamura, T. 2004. Docetaxel versus docetaxel plus gemcitabine for second-line treatment of non-small cell lung cancer: Results of a JCOG randomized trial (JCOG0104). *J. Clin. Oncol. 22/14S*: 7034.

Thatcher, N., Chang, A., Parikh, P., Rodrigues, P.J., Ciuleanu, T., von Pawel, J., Thongprasert, S., Tan, E.H., Pemberton, K., Archer, V., and Carroll, K. 2005. Gefitinib plus best supportive care in previously treated patients with refractory advanced non-small-cell lung cancer: results from a randomised, placebo-controlled,

multicentre study (Iressa Survival Evaluation in Lung cancer). *Lancet 366*: 1527–1537.

Wachters, F.M., Groen, H.J., Biesma, B., Schramel, F.M., Postmus, P.E., Stigt, J.A., and Smit, E.F. 2005. A randomised phase II trial of docetaxel vs docetaxel and irinotecan in patients with stage IIIb-IV non-small-cell lung cancer who failed first-line treatment. *Br. J. Cancer 92*: 15–20.

Weiss, G., Rosell, R., Fossella, F., Perry, M., Stahel, R., Barata, F., Nguyen, B., Paul, S., McAndrews, P., Hanna, N., Kelly, K., and Bunn, P.A. Jr. 2007. The impact of induction chemotherapy on the outcome of second-line therapy with pemetrexed or docetaxel in patients with advanced non-small-cell lung cancer. *Ann. Oncol. 18*: 453–460.

Westeel, V., Quoix, E., Moro-Sibilot, D., Mercier, M., Breton, J.L., Debieuvre, D., Richard, P., Haller, M.A., Milleron, B., Herman, D., Level, M.C., Lebas, F.X., Puyraveau, M., and Depierre, A. 2005. Randomized study of maintenance vinorelbine in responders with advanced non-small-cell lung cancer. *J. Natl. Cancer Inst. 97*: 499–506.

19
Non-Small Cell Lung Cancer with Brain Metastases: Platinum-Based Chemotherapy

Fabrizio Nelli and Luca Moscetti

EPIDEMIOLOGY

Brain metastases are the most common intracranial tumors, occurring in 15–40% of cancer patients with an estimated incidence of 170,000 new cases a year in the United States (Davey, 2002). Lung cancer is the most common primary source of metastases to the central nervous system (CNS), causing brain metastases in 10–64% of patients. Non-small-cell lung cancer (NSCLC) represents 85% of lung cancers, and brain metastases are a frequent finding with an overall incidence of 20–40% of cases during the course of the disease (Langer and Mehta, 2005). The incidence of brain metastases in NSCLC has increased in recent years, probably owing to the longer survival of patients as a result of aggressive treatment of primary tumor and of the improvements achieved in neuroimaging (e.g., magnetic resonance imaging techniques and systematic CNS staging). However, a recent epidemiological study did not confirm this increased incidence (Schouten *et al*., 2002). This discrepancy probably depends on differences in the type of study undertaken (autoptically vs. clinical). A clear relation is known between stage of disease and incidence of brain metastases, and it is interesting to note that 25–30% of new NSCLC cases present with synchronous brain metastases (Sorensen *et al*., 1988).

PROGNOSIS AND TREATMENT OPTIONS

Brain metastases are a major cause of morbidity and mortality in NSCLC patients because two-thirds of them become symptomatic during their lifetime with a serious deterioration in neurological and neurocognitive functions. Often brain metastases are not diagnosed until nonspecific symptoms arise, including headache, changes in mental status, focal or generalized seizures, and focal weakness. The prognosis of NSCLC with brain metastases is, therefore, associated with a poor outcome. Overall, median survival of brain metastases patients is 4 months after whole-brain radiation therapy (WBRT), but it varies based on several prognostic variables (van den Bent, 2001). Factors predicting for better survival include good performance status, age ≤ 65 years, successful control of the primary tumor, absence of extracranial metastases, favorable tumor

histology, and presence of a solitary brain metastasis. Using recursive partitioning analysis (RPA) to identify prognostic variables to group patients into prognostic categories, Gaspar *et al*. (1997) identified a three-tier classification scheme using a database of several Radiation Therapy Oncology Group (RTOG) trials. Median survival ranged from 7.1 months for RPA class 1 patients (all favorable prognostic factors) to 2.3 months for class 3 patients (Karnofsky performance score < 70).

Brain metastases may present as a single lesion or multiple lesions which can be divided into three groups, including solitary metastasis with controlled or controllable primary disease, limited multiple disease (less than three metastases), and multiple metastases.

Whether a patient with brain metastases from lung cancer will be treated with the aim of reducing the number and size of brain metastases depends on several factors including performance status, life-expectancy, patient's expectations, neurological function, previous anti-tumor therapy, number of brain metastases, and status of extra-cranial tumor. For NSCLC, surgical resection in combination with WBRT should be considered in instances of a single brain metastasis when resection is technically feasible (Patchell *et al*., 1990; Mintz *et al*., 1996). Radio-surgery has recently become popular for patients with a single or only a few lesions in the brain (Andrews *et al*., 2004). The major advantage of this approach is the delivery of high-dose radiation therapy (RT) to the brain metastases with sparing of the surrounding brain. Patients with multiple metastatic lesions are generally considered candidates for other approaches. The most commonly administered treatment is WBRT followed by any type of chemotherapy (Khuntia *et al*., 2006). This historical approach of sequential WBRT and chemotherapy might be considered a standard of care in the case of uncontrolled neurological symptoms; however, recent advances could change this practice when brain metastases symptoms are absent or well managed by supportive therapy. In this chapter we will critically evaluate several aspects of newer platinum-based chemotherapy as frontline treatment for patients with brain metastases.

SHIFTING THE PARADIGM OF THE BLOOD-BRAIN BARRIER

Several arguments have been put forward to emphasize the role of the blood-brain barrier as an explanation for lack of efficacy of most cytotoxic compounds in the treatment of brain metastases from lung cancer. The microvasculature of the brain, a relatively isolated site, is lined by a continuous, nonfenestrated endothelium with tight junctions and little pinocytic vesicle activity. This structure, the blood-brain barrier, is moreover covered by the terminal processes of astrocytes that actively contribute to its integrity (Neuwelt, 2004). The blood-brain barrier limits the passage of circulating macromolecules into the brain parenchyma. The passage of macromolecules from the blood is regulated by: (1) passive transport with lipid solubility being the most important determinant of blood-brain barrier permeability, and (2) active transport which affects active efflux pump reducing the penetration of xenobiotics and endogenous substances to the brain. There is a general agreement that

most cytotoxic agents achieve a relatively low concentration in the normal CNS due to the activity of blood-brain barrier. The transport of these compounds over the blood-brain barrier is largely influenced by the physicochemical properties of the latter. For hydrophobic drugs, the transport is mediated by passive diffusion but the efficiency of brain penetration cannot be exclusively predicted by lipophilicity. Especially for hydrophilic drugs including most of cytotoxic agents, transport is limited by the activity of P-glycoprotein, the product of MDR-1 gene which actively extrudes drugs from cell. P-glycoprotein is prominent in the endothelial cells of blood capillaries at the position of blood-brain barrier, and it has been therefore believed to be the most determinant of intrinsic resistance exerted by tumor cell at brain metastases (Doolittle *et al*., 2005). Recent studies have demonstrated that brain metastases from lung cancer, melanoma and breast cancer have a lower expression of P-glycoprotein than normal brain tissue, suggesting that further mechanisms may be involved with chemotherapy resistance (Régina *et al*., 2001; Demeule *et al*., 2001). The growth of metastatic tumor mass at the brain is associated with increased expression of vascular endothelial growth factor, the major determinant in the formation of new vessels at any tumor site. These new vessels lack the properties of normal capillaries found at the same anatomical site and might be involved in the disruption of blood-brain barrier integrity (Fidler *et al*., 2002). A demonstration against the role of blood-brain barrier in brain tumors can be provided by the increased microvascular permeability that leads to brain edema or the accumulation of intravenous contrast during magnetic resonanceimaging (MRI) or computed tomography (CT) scan. Moreover, it has been demonstrated that the level of P-glycoprotein expression in the blood-brain barrier neovasculature of selected brain metastases (NSCLC and melanoma) is similar to the level of P-glycoprotein expression detected in the respective neovasculature of extracranial tumor, suggesting that the histological origin of brain metastases modulates the expression of P-glycoprotein in the neovasculature of the brain tumor (Tóth *et al*., 1996). A major review on this controversial topic by Gerstner and Fine (2007) concluded that brain metastases from primary extracranial tumors with low intrinsic expression of P-glycoprotein (e.g., NSCLC, SCLC, melanoma, and breast cancer) might be more sensitive to cytotoxic agents active against primary histology rather than to lipophilic alkylating drugs that are able to overcome the blood-brain barrier, but quite ineffective against primary tumors. This conclusion would argue: (1) we cannot consider anymore the CNS and brain metastases a pharmacological "sanctuary"; (2) the chance of response to chemotherapy at brain metastases is not different from the response rate expected at extracranial disease; (3) the choice of cytotoxic agents should be guided by the agent's shrinkage potential against the histological origin of the primary tumor that metastasized to the brain.

ROLE OF CHEMOTHERAPY

Until recently, brain metastases have been considered a terminal event of disease even in the group of patients presenting with synchronous brain metastases at first diagnosis, influencing both decision-making process

and treatment selection. In this way, most NSCLC patients with brain metastases were judged not suitable for chemotherapy and addressed to palliative WBRT in order to control or to prevent CNS symptoms (Kelly and Bunn, 1998; Ellis and Gregor, 1998). Because this subset of patients was usually excluded from clinical trials including chemotherapy, few outcome data are currently available on the impact of contemporary chemotherapy regimens, leading to the misleading assumption that chemotherapy does not play any role for this clinical presentation. Although the optimal treatment modality for patients with synchronous brain metastases from NSCLC has not been yet established and no definite algorithm exists regarding the pattern of care, first treatment options is currently driven by clinical status (i.e., CNS symptoms) and local practices (i.e., referred specialist and hospital resources).

With the exclusion of patients with limited brain metastatic involvement suitable for effective local therapy, we cannot discuss the optimal management of NSCLC patients presenting brain metastases as site of recurrence after failing first line chemotherapy, as well as the treatment choice for patients with symptomatic CNS involvement not suitable to be controlled with supportive therapy. In these cases WBRT must be considered a standard of care. Nevertheless, the optimal treatment of previously untreated patients with asymptomatic brain metastases has yet to be defined. In these circumstances, WBRT would represent a standard of care, but even so more than half of the patients die as a result of disease systemic disease progression, and median survival remains <4 months (De Angelis, 1994). If we consider that last decade advances in systemic chemotherapy of advanced NSCLC led to improved survival and defined guidelines, a major challenge, therefore, concerns the role of systemic chemotherapy with current platinum-based regimes in this clinical setting (Bunn, 2003).

PLATINUM-BASED CHEMOTHERAPY: PHASE II TRIALS

The combination of a platinum compound (cisplatin or carboplatin) and a third-generation cytotoxic agent (including gemcitabine, vinorelbine, docetaxel or paclitaxel) is the current standard treatment option for locally advanced stage not suitable for thoracic radiotherapy or metastatic chemïotherapy-naive NSCLC patients (Pfister *et al.*, 2004). Given this assumption, our analysis did not consider those trials employing single-agent therapy such as temozolomide and teniposide designed to cross the blood-brain barrier, neither the studies testing a platinum-based combination with limited efficacy against NSCLC as compared to current combinations. Similarly, we did not consider consistent with the aims of our analysis the studies which enrolled patients with brain metastases from different primary tumors, usually including breast cancer and melanoma. Taken together, results from these phase II trials suggest that although these agents do not definitively improve survival, some of their activity in brain metastases has been observed (Lesser, 1996; Postmus and Smit, 1999).

The activity of platinum-based regimens as up-front treatment for NSCLC with brain metastases has been evaluated in a few and small phase II trials. Two

studies tested the efficacy of three-drug combination of third-generation agents. In the first study by Cortes *et al*. (2003) 26 chemïonaive patients were treated with paclitaxel 135 mg/m^2 and cisplatin 120 mg/m^2 on day 1 with either vinorelbine 30 mg/m^2 or gemcitabine 800 mg/m^2 on day 1–15, every 4 weeks. The intracranial response rate was 38% with a median survival of 21 weeks. In the second study by Bernardo *et al*. (2002) 22 untreated patients received vinorelbine 25 mg/m^2 and gemcitabine 1,000 mg/m^2 with carboplatin area under the concentration-time 5 on day 1–3 of a 3-week cycle. Nine of 20 assessable patients (45%) achieved a partial response at brain metastases with a median survival of 33 weeks. In both trials responses at extracranial sites were consistent with the responses at brain metastases and the median survival time was longer in the group of patients experiencing response at brain metastases. In the study by Quadvlieg *et al*. (2004, only available as abstracted data) 40 consecutive chemïonaive NSCLC patients with synchronous brain metastases received gemcitabine 1,000 mg/m^2 and cisplatin 50 mg/m^2, both delivered on days 1 and 8, every 3–4 weeks. With nine complete responses and 14 partial, the intracranial overall rate surprisingly exceeded 60%, but the authors reported a short median survival of 7 months. The largest prospective phase II trial in which chemotherapy was administered as a primary treatment is the study by Cortot *et al*. (2006), which employed a combination of cisplatin 75 mg/m^2 on day 1 and temozolomide 200 mg/m^2 for 5 consecutive days, with cycles repeated every 28 days. It is worth noting that the unsatisfactory objective response rate of 16% for brain metastases was not different from that observed at extracranial sites of disease. The short median survival of 5 months observed in this prospective and well-conducted phase II trial further suggests that active drugs against brain metastases should be selected on the basis of their intrinsic activity against NSCLC.

PLATINUM-BASED CHEMOTHERAPY: PHASE III TRIALS

The unique and specific phase III study testing standard prime chemotherapy for NSCLC patients with synchronous brain metastases was conducted by Robinet *et al*. (2001). This landmark study compared chemotherapy with cisplatin 100 mg/m^2 on day 1 and vinorelbine 30 mg/m^2 weekly, every 4 weeks with early versus delayed WBRT. The intracranial objective response rate was 27% with chemotherapy alone and was again consistent with response rate at sextracranial sites. Nonetheless, this trial did not find any significant difference between two arms, but showed a poor prognosis for these patients with a median survival of 6 months. This dismal result has been explained by the selection of patients with adverse prognostic factors and the choice of a toxic chemotherapy regimen with a high rate of treatment-related deaths.

The survival rate reported by Robinet *et al*. (2001) confirms the unsatisfactory results observed in previous phase II studies. Nonetheless, these survival figures were not generally consistent with those obtained with standard platinum-based regimens in the subset of patients with brain metastases entered larger phase III studies (Crinò *et al*., 1999; Scagliotti

et al., 2002; Alberola *et al*., 2003). The number of patients with synchronous brain metastases enrolled in these randomized trials per treatment arm ranged from 9 to 31 (Table 19.1). The objective response rate at brain metastases ranged from 30% to 50% and was therefore consistent with the same figure reported by aformentionated trial, but the median survival time for patients with brain metastases exceeded 8 months in all treatment arms. This result is clearly consistent with the median survival times observed with standard platinum-based chemotherapy regimes in the general population affected by advanced NSCLC.

Given this discrepancy, our group conducted a specific survey with the aim to clarify the major opened questions in the subset of NSCLC patients with synchronous brain metastases including the real prognosis of this subset of patients and the efficacy of current chemotherapy regimens on both brain and systemic sites of disease (Moscetti *et al*., 2007). In this survey we compared in a large sample upfront chemotherapy with current platinum-based two-drug regimens versus upfront WBRT followed or not by any type chemotherapy. The results of this survey pointed out relevant messages for the clinical oncologists. The median survival of 11 months and progression-free survival for 6 months observed in the entire cohort were similar to those reported for patients affected by advanced NSCLC without brain metastasis enrolled into major clinical trials. With regard to the pattern of care of symptomatic patients, we highlighted that a symptomatic CNS involvement and a limited disease extension would be the main determinant for choosing WBRT as the more appropriate primary treatment. Conversely, asymptomatic CNS involvement and an elevated burden of metastatic disease would be more appropriately treated with prime systemic chemotherapy. There was no significant difference in our survey between the objective brain or global response rates. The chemotherapy

TABLE 19.1. Selected phase III trials of platinum-based chemotherapy in NSCLC including patients with brain metastasis.

Author	N# of patients		Chemotherapy regimen	Brain response	Median survival (months)
	Total	BMs at first diagnosis			
Crinò *et al*.	155	Not reported	Gemcitabine-cisplatin	41%	8.6
	152	Not reported	Mitomycin-ifosfamide-cisplatin	39%	9.6
Alberola *et al*.	182	9 (5%)	Gemcitabine-cisplatin	29% (overall)	9.3
	188	11 (6%)	Gemcitabine-vinorelbine-cisplatin		8.2
	187	14 (7%)	Vinorelbine-cisplatin		8.1
Scagliotti *et al*.	205	31 (19%)	Gemcitabine-cisplatin	32%	9.8
	201	27 (16%)	Paclitaxel-carboplatin	52%	9.9
	201	24 (15%)	Vinorelbine-cisplatin	25%	9.5
Robinet *et al*.	176	176 (100%)	86 treated with upfront vinorelbine-cisplatin	27%	6

alone appears to produce a 27% response rate in the brain, which was not statistically significant different from the 35% rate obtained in the WBRT cohort where brain response evaluation was performed after two or three cycles of chemotherapy.

The multivariate analysis pointed out interesting data on the clinical significance of brain response. This has shown to be an independent prognostic factor for both median and progression-free survival. A modified RTOG classification (including all but the primary tumor status factors from the class I) was the other independent prognostic factor for survival, which reflects the magnitude of clinical factors such as PS, age and the extension of disease. The activity and efficacy results of our survey would confirm the findings obtained in the subsets of patients with synchronous brain metastases of aforementioned randomized clinical trials.

In conclusion, overall, these result of our survey and few available data from randomized trials should change the inexact opinion for which brain represents an unreachable sanctuary of chemotherapy. Third generation platinum-based regimens are effective treatments for brain metastases from advanced NSCLC, and should be considered an appropriate treatment choice. The optimal treatment strategy for advanced NSCLC with brain metastases remains undefined due to lack of specific randomized trials. To date, treatment choice for these patients should be mainly guided by the pattern of beginning symptoms and the extension of disease. However, primary platinum-based chemotherapy represents an appropriate treatment for asymptomatic patients or those who obtained symptoms control by medical therapies. For these patients the timing and the real need of WBRT remain controversial.

REFERENCES

Alberola, V., Camps, C., Provencio, M., Isla, D., Rosell, R., Vadell, C., Bover, I., Ruiz-Casado, A., Azagra, P., Jiménez, U., González-Larriba, J.L., Diz, P., Cardenal, F., Artal, A., Carrato, A., Morales, S., Sanchez, J.J., de las Peñas, R., Felip, E., and López-Vivanco, G. 2003. Cisplatin plus gemcitabine versus a cisplatin-based triplet versus nonplatinum sequential doublets in advanced non-small-cell lung cancer: A Spanish Lung Cancer Group phase III randomized trial. *J. Clin. Oncol. 21*: 3207–3213.

Andrews, D.W., Scott, C.B., Sperduto, P.W., Flanders, A.E., Gaspar, L.E., Schell, M.C., Werner-Wasik, M., Demas, W., Ryu, J., Bahary, J.P., Souhami, L., Rotman, M., Mehta, M.P., and Curran, W.J. Jr. 2004. Whole brain radiation therapy with or without stereotactic radiosurgery boost for patients with one to three brain metastases: phase III results of the RTOG 9508 randomised trial. *Lancet 363*: 1665–1672.

Bernardo, G., Cuzzoni, Q., Strada, M.R., Bernardo, A., Brunetti, G., Jedrychowska, I., Pozzi, U., and Palumbo, R. 2002. First line chemotherapy with vinorelbine, gemcitabine and carboplatin in the treatment of brain metastases from non small cell lung cancer: a phase II study. *Cancer Invest. 20*: 293–302.

Bunn, P.A. 2003. Treatment of advanced non-small cell lung cancer with two drug combinations. *J. Clin. Oncol. 20*: 3565–3567

Cortes, J., Rodriguez, J., Aramendia, J.M., Salgado, E., Gurpide, A., Garcia-Foncillas, J., Aristu, J.J., Claver, A., Bosch, A., Lopez-Picazo, J.M., Martin-Algarra, S., Brugarolas, A., and Calvo, E. 2003. Front-line paclitaxel/cisplatin-based chemotherapy in brain metastases from non-small-cell lung cancer. *Oncology 64*: 28–35.

Cortot, A.B., Gerinière, L., Robinet, G., Breton, J.L., Corre, R., Falchero, L., Berard, H., Gimenez, C., Chavaillon, J.M., Perol, M., Bombaron, P., Mercier, C., and Souquet, P.J. 2006. Phase II trial of temozolomide and cisplatin followed by whole brain radiotherapy in non-small-cell lung cancer patients with brain metastases: a GLOT-GFPC study. *Ann. Oncol. 17*: 1412–1417.

Crinò, L., Scagliotti, G.V., Ricci, S., De Marinis, F., Rinaldi, M., Gridelli, C., Ceribelli, A., Bianco, R., Marangolo, M., Di Costanzo, F., Sassi, M., Barni, S., Ravaioli, A., Adamo, V., Portalone, L., Cruciani, G., Masotti, A., Ferrara, G., Gozzelino, F., and Tonato, M. 1999. Gemcitabine and cisplatin versus mitomycin, ifosfamide, and cisplatin in advanced non-small-cell lung cancer: A randomized phase III study of the Italian Lung Cancer Project. *J. Clin. Oncol. 17*: 3522–3530.

Davey, P. 2002. Brain metastases: Treatment options to improve outcomes. *CNS Drugs 16*: 325–338.

De Angelis, L.M. 1994. Management of brain metastases. *Cancer Invest. 12*: 156–165.

Demeule, M., Shedid, D., Beaulieu, E., Del Maestro, R.F., Moghrabi, A., Ghosn, P.B., Moumdjian, R., Berthelet, and F., Béliveau, R. 2001. Expression of multidrug-resistance p-glycoprotein (MDR1) in human brain tumors. *Int. J. Cancer 93*: 62–66.

Doolittle, N.D., Abrey, L.E., and Archie Bleyer, W. 2005. New frontiers in translational research in neuro-oncology and the blood brain barrier: report of the tenth annual brain blood barrier disruption consortium meeting. *Clin. Cancer Res. 15*: 421–428.

Ellis, R., and Gregor, A. 1998. The treatment of brain metastases from lung cancer. *Lung Cancer 20*: 81–84.

Fidler, I.J., Yano, S., Zhang, R.D., Fujimaki, T., and Bucana, C.D. 2002. The seed and soil hypothesis: vascularisation and brain metastases. *Lancet Oncol. 3*: 53–57.

Gaspar, L., Scott, C., Rotman, M., Asbell, S., Phillips, T., Wasserman, T., McKenna, W.G., and Byhardt, R. 1997. Recursive partitioning analysis (RPA) of prognostic factors in three Radiation Therapy Oncology Group (RTOG) brain metastases trials. *Int. J. Radiat. Oncol. Biol. Phys. 37*: 745–751.

Gerstner, E.R., and Fine, R.L. 2007. Increased permeability of the blood-brain barrier to chemotherapy in metastatic brain tumors: establishing a treatment paradigm. *J. Clin. Oncol. 25*: 2306–2312

Kelly, K., and Bunn, P.A. 1998. Is it time to re-evaluated our approach to the treatment of brain metastases in patients with non-small cell lung cancer? *Lung Cancer 20*: 85–91.

Khuntia, D., Brown, P., LI, J., and Metha, M. 2006. Whole-brain radiotherapy in the management of brain metastasis. *J. Clin. Oncol. 24*: 1295–1304

Langer, C.J., and Mehta, M.P. 2005. Current management of brain metastases, with a focus on systemic options. *J. Clin. Oncol. 23*: 6207–6219.

Lesser, G.J. 1996. Chemotherapy of cerebral metastases from solid tumors. *Neurosurg. Clin. N. Am. 7*: 527–536.

Mintz, A.H., Kestle, J., Rathbone, M.P., Gaspar, L., Hugenholtz, H., Fisher, B., Duncan, G., Skingley, P., Foster, G., and Levine, M. 1996. A randomized trial to assess the efficacy of surgery in addition to radiotherapy in patients with a single cerebral metastasis. *Cancer 78*: 1470–1476.

Moscetti, L., Nelli, F., Felici, A., Rinaldi, M., De Santis, S., D'Auria, G., Mansueto, G., Tonini, G., Sperduti, I., and Pollera, F.C. 2007. Up-front chemotherapy and radiation treatment in newly diagnosed nonsmall cell lung cancer with brain metastases: survey by Outcome Research Network for Evaluation of Treatment Results in Oncology. *Cancer 109*: 274–281.

Neuwelt, E.A. 2004. Mechanism of disease: the blood brain barrier. *Neurosurgery 54*: 131–142.

Patchell, R.A., Tibbs, P.A., Walsh, J.W., Dempsey, R.J., Maruyama, Y., Kryscio, R.J., Markesbery, W.R., Macdonald, J.S., and Young, B. 1990. A randomized trial of surgery in the treatment of single metastases to the brain. *N. Engl. J. Med. 322*: 494–500.

Pfister, D.G., Johnson, D.H., Azzoli, C.G., Sause, W., Smith, T.J., Baker, S. Jr, Olak, J., Stover, D., Strawn, J.R., Turrisi, and A.T., Somerfield, M.R.. 2004. American Society of Clinical Oncology treatment of unresectable non–small cell lung cancer guideline: update 2003. *J. Clin. Oncol. 22*: 330–363.

Postmus, P.E., and Smit, E.F. 1999. Chemotherapy for brain metastases of lung cancer: a review. *Ann. Oncol. 10*: 753–759.

Quadvlieg, V., Bosquee, L., Gustin, M., and Barthelemy, N. 2004. Frontline gemcitabine and cisplatin based chemotherapy in patients with NSCLC inoperable brain metastases. *J. Clin. Oncol. 22*: 14S (abs 7365).

Régina, A., Demeule, M., Laplante, A., Jodoin, J., Dagenais, C., Berthelet, F., Moghrabi, A., and Béliveau, R. 2001. Multidrug resistance in brain

tumors: roles of the blood-brain barrier. *Cancer Metast. Rev. 20*: 13–25.

Robinet, G., Thomas, P., Breton, J.L., Léna, H., Gouva, S., Dabouis, G., Bennouna, J., Souquet, P.J., Balmes, P., Thiberville, L., Fournel, P., Quoix, E., Riou, R., Rebattu, P., Pérol, M., Paillotin, D., and Mornex, F.. 2001. Results of a phase III study of early versus delayed whole brain radiotherapy with concurrent cisplatin and vinorelbine combination in inoperable brain metastasis of non-small-cell lung cancer: Groupe Francais de Pneumo- Cancerologie (GFPC) Protocol 95-1. *Ann. Oncol. 12*: 59–67.

Scagliotti, G.V., De Marinis, F., Rinaldi, M., Crinò, L., Gridelli, C., Ricci, S., Matano, E., Boni, C., Marangolo, M., Failla, G., Altavilla, G., Adamo, V., Ceribelli, A., Clerici, M., Di Costanzo, F., Frontini, L., and Tonato, M; Italian Lung Cancer Project. 2002. Phase III randomized trial comparing three platinum-based doublets in advanced non-small-cell lung cancer. *J. Clin. Oncol. 20*: 4285–4291.

Schouten, L.J., Rutten, J., Huveneers, H.A., and Twijnstra, A. 2002. Incidence of brain metastases in a cohort of patients with carcinoma of the breast, colon, kidney, and lung and melanoma. *Cancer 94*: 2698–2705.

Sorensen, J.B., Hansen, H.H., Hansen, M., and Dombernowsky, P. 1988. Brain metastases in adenocarcinoma of the lung: frequency, risk groups, and prognosis. *J. Clin. Oncol. 6*: 1474–1480.

Tóth, K., Vaughan, M.M., Peress, N.S., Slocum, H.K., and Rustum, Y.M. 1996. MDR1 p-glycoprotein is expressed by endothelial cells of newly formed capillaries in human gliomas but is not expressed in the neovasculature of other primary tumors. *Am. J. Pathol. 149*: 853–858.

van den Bent, M.J. 2001. The diagnosis and management of brain metastases. *Curr. Opin. Neurol. 14*: 717–723.

20
Non-Small Cell Lung Carcinoma: EGFR Gene Mutations and Response to Gefitinib

Armando Bartolazzi

INTRODUCTION

Lung cancer is the most common cancer in the world and the leading cause of cancer-related mortality (12.6% of all new cancers, 17.8% of cancer deaths). There were an estimated 1.2 million new cases and 1.1 million deaths in the year 2000. The high mortality is mainly due to early development of systemic disease and resistance to currently available chemotherapy. Men have seen declines in incidence and mortality rates in the last ten years, which is associated with reduction in smoking. This is not the case for women, among whom these rates continue to increase. Whether this increase suggests a higher gender-related risk of lung cancer for women or merely reflects changing smoking patterns remains controversial. Almost all lung malignant tumors are carcinomas (other histological types are <1%) broadly divided into small-cell lung cancer (SCLC), comprising 20% of lung carcinomas and non-small-cell lung cancers (NSCLCs), comprising ~80% of lung carcinomas. SCLC is a tumor of neural crest origin whereas NSCLCs originate in bronchial epithelial cells or alveolar and bronchioloalveolar cells and represent a spectrum of histological subtypes including squamous carcinoma, adenocarcinoma, bronchioloalveolar carcinoma, undifferentiated large-cell carcinoma and anaplastic carcinoma. NSCLCs do not represent a single pathological entity but a group of diseases with different '*molecular signatures*,' and consequently different biological features. Genetic models for the development of SCLC and NSCLC have been recently proposed (Yokota and Kohno, 2004; Testa and Siegfried, 1992), and it is becoming clear that the failure of conventional cytotoxic chemotherapy to treat advanced NSCLCs, observed in the last two decades, likely reflects the biological and molecular heterogeneity of these tumors.

Although surgery represents the best therapeutic option with potential for cure in patients with early-stage NSCLCs (~1/3 of the cases), the treatment of metastatic NSCLCs is still a challenge (Tables 20.1 and 20.2). Approximately, 50% of patients with stage IV disease are incurable with currently available chemotherapy. Several chemotherapeutic agents have been developed in the last three decades for the treatment of NSCLCs, but randomized trials of platinum-based combinations seem to reach a therapeutic plateau with an objective response rate of 26–46% and

a median survival time (MST) of 7–11 months for patients with stage IIIB or IV disease (Table 20.2) (Abeloff *et al*., 2004). In general, cytotoxic chemotherapy results in a modest increase in survival at the cost of significant toxicity to the patient.

EPIDERMAL GROWTH FACTOR RECEPTOR AND DOWNSTREAM SIGNALING

The Epidermal growth factor receptor (EGFR) is a transmembrane receptor tyrosine kinase of the ErbB family that is abnormally activated in many epithelial tumors. The family of receptors includes four members: EGFR (ERBB1), HER-2 (ERBB2), HER-3 (ERBB3) and HER-4 (ERBB4) (Mendelsohn and Baselga, 2006; Yarden and Sliwkowski, 2001). Each receptor consists of an extracellular ligand-binding domain, a transmembrane domain, and an intracellular tyrosine kinase domain with a regulatory carboxyl-terminal segment. Ligand binding to EGFR causes receptor dimerization, which can occur also with another member of the ErbB family. Receptor-ligand interaction triggers the tyrosine kinase activity in the receptor intracellular domain, initiating a signal-transduction cascade that regulates cell proliferation and survival (Figure 20.1).

Several mechanisms lead to the receptor's aberrant activation occurring in cancer, these include: (1) receptor overexpression, (2) activating mutations, (3) ligand-dependent receptor dimerization and (4) ligand-independent activation. All of these may induce recruitment and phosphorylation of several intracellular substrates, which, in turn, engage the binding of docking and adaptor molecules to specific phosphotyrosine sites on the receptor molecule, resulting in mitogenic signaling, modulation of the apoptotic program, and other tumor promoting activities. The downstream signaling pathways are not linear but consist of rich multilayered and cross-connected networks, which allow for multi-molecular interactions and consequently multiple combinatorial responses. This may likely explain the variety of biological outcomes to activation of a specific receptor in a specific cell type.

In the recent years, several downstream signaling routes of the ErbB family have been identified (Figure 20.2): Ras-Raf-MAP-kinase pathway (Alroy and Yarden, 1997) that leads to the activation of mitogen-activated protein kinases (MAPKs) ERK1, and ERK2, which regulate transcription of molecules involved in cell proliferation, survival, and malignant transformation. Another important target in EGFR signaling is phosphatidylinositol 3-kinase (Pl3K) and the downstream protein-serine/threonine kinase Akt (Vivanco and

TABLE 20.1. Estimated five years survival following complete surgical resection of NSCLCS. (Modified from Abeloff *et al*., 2004.)

Stage grouping	Estimated survival (%)
0 Tis N0 M0	100
IA T1 N0 M0	75
IB T2 N0 M0	55
IIA T1 N1 M0	50
IIB T2 N1 M0	40
T3 N0 M0	40
IIIA T1-3 N2 M0	15
T3 N1 M0	35
IIIB T1-3 N3 M0	5–10
T4 any N M0	5–10
IV any T any N M1 (solitary M1)	5–10

Sawyers, 2002), which is functionally critical for regulating cell growth and proliferation, cell survival and cell motility. A third route for signaling is represented by the stress-activated protein kinase pathway involving protein kinase C and Jak/Stat, which plays a pivotal role in transcriptional regulation of cell division, survival and apoptosis, invasion, adhesion and DNA repair (Yarden and Sliwkowski, 2001).

Considering the functional role that tyrosine kinase receptors (TKRs) play in regulating cell proliferation, apoptosis, angiogenesis, and tumor growth and progression, these receptors represent, at least theoretically, good candidate molecules for therapeutic targeting in oncology. More then 20 years ago EGFR was proposed as a target for cancer therapy on the bases of its expression in several solid tumors and the inhibitory effects on tumor growth observed *in vitro* and *in vivo* by using a monoclonal antibody able to block EGFR activity (Mendelsohn and Baselga, 2006; Kawamoto *et al*., 1983).

After extensive preclinical and clinical studies these preliminary data were confirmed with two classes of anti-EGFR agents, which demonstrated clinical activity and for this reason were approved for cancer treatment. These are mostly represented by blocking monoclonal antibodies (mAbs) and low-molecular weight (MW) adenosine triphosphate (ATP)- competitive inhibitors of the EGFR tyrosine kinase domain (TKIs).

TABLE 20.2. Randomized trial of platinum-based combinations (Modified from Abeloff *et al*., 2004.)

				Survival	
Author	Treatment	No. patients	Response (%)	Median	1 year (%)
Bonomi	Cis/VP-16	193	12.4	7.6	32
	Cis/Pac	190	25.3	9.5	37
	Cis/Pac (high dose)	191	25.7	10.1	40
Giaccone	Cis/Ten	162	28	9.9	41
	Cis/Pac	155	40	9.7	43
Belani	Cis/VP-16	179	14	9.1	37
	Carbo/Pac	190	22	7.7	32
Crino	Mito/Ifex/Cis	152	26	9.6	34
	Cis/Gem	155	38	8.6	33
Lopez-Cabrerizo	Cis/VP-16	65	21.9	7	26
	Cis/Gem	69	40.6	8.7	32
Kelly	Cis/Vnr	202	28	8.1	36
	Carbo/Pac	206	25	8.6	38
Schiller	Cis/Pac	303	21	7.8	31
	Cis/Gem	301	22	8.1	36
	Cis/Doc	304	17	7.4	31
	Carbo/Pac	299	17	8.1	34
Rodriguez	Cis/Vnr	405	25	9.9	41
	Cis/Doc	408	32	11.3	46
	Carbo/Doc	405	24	10.4	41

Carb: carboplatin; Cis: cisplatin; Doc: docetaxel; Gem: gemcitabine; Ifex: ifosfamide; Mito: mitomycin; Pac: paclitaxel; Ten: teniposide; Vnr: vinorelbine.

EPIDERMAL GROWTH FACTOR RECEPTOR MOLECULAR TARGETED THERAPY FOR NON-SMALL CELL LUNG CARCINOMAS

The advent of a new class of drugs, which specifically target molecules that are critical for cancer, has therefore generated much optimism, given the perception that the limits of conventional chemotherapy have been already reached. Tyrosine kinase inhibitors (TKIs) are an emerging class of anticancer drugs that have shown promising clinical activity. They are directed to specifically inhibit the activity of trans-membrane receptor tyrosine kinases involved in signaling pathways that regulate tumor relevant processes such as cell proliferation, apoptosis, and angiogenesis (Figure 20.1).

On the other hand, expression of EGFR has been demonstrated in several solid tumors, including 40–80% of NSCLCs (Rusch *et al*., 1993). Recently, a retrospective analysis showed EGFR over-expression in 62% of NSCLCs with documented amplification, in some of the cases, of chromosomal region 7p12, where EGFR gene is located (Hirsch *et al*., 2003). Furthermore, the putative EGFR ligands, epidermal growth

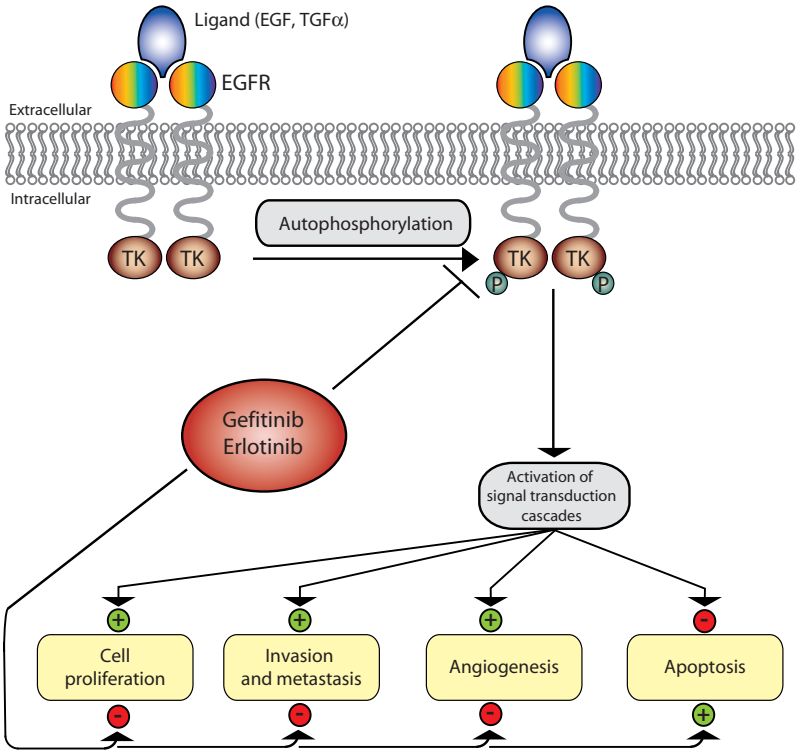

FIGURE 20.1. Schematic representation of EGFR and its mediated functions. The inhibitory effects of gefitinib and erlotinib (TKIs) on downstream EGFR-signaling are also shown

factor (EGF), and transforming growth factorα (TGFα) are frequently detected in NSCLCs and may be responsible of EGFR hyperactivity *via* autocrine loops (Rusch *et al*., 1993). All together these findings provide the molecular rationale for testing EGFR inhibitory strategies at least in a subset of NSCLCs.

A small-molecule inhibitor of EGFR intracellular tyrosine kinase domain (EGFR-TKI) named *gefitinib* (Iressa, AstraZeneca) was approved by the FDA for the third-line treatment of patients with advanced NSCLCs in May 2003. A functionally similar compound worded *erlotinib hydrochloride* (also named OSI-774 or CP-358774, Tarceva OSI/Pharmaceuticals/Genentech/Roche) was approved by the FDA in November 2004 for the treatment of advanced NSCLCs after the failure of conventional chemotherapy. Both drugs are reversible inhibi-

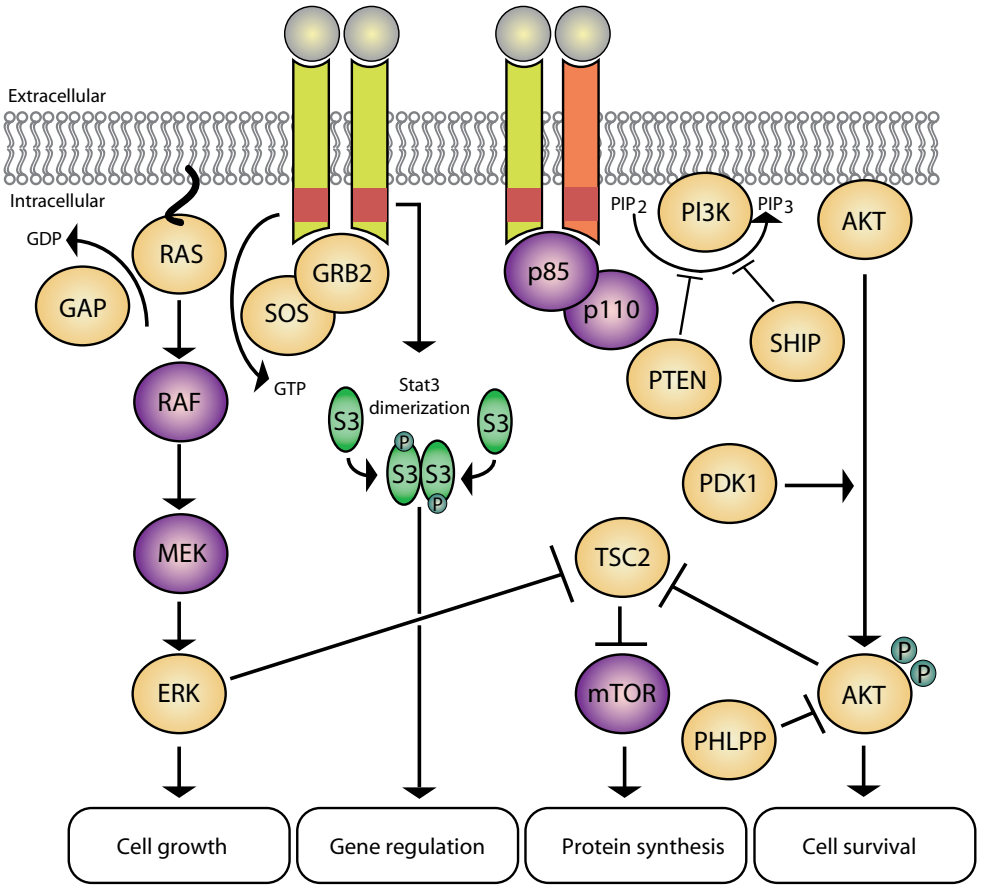

FIGURE 20.2. Cell-proliferation and cell-survival pathways downstream of activated TK-receptor. Three different signaling pathways are indicated along with some of the key constituent signaling molecules. (Footnotes: ERK, extracellular signal-regulated kinase; GRB2, growth factor receptor-bound protein 2; mTOR, mammalian target of rapamycin; SOS, son of sevenless). (Modified from Sharma *et al*., 2007.)

tors of the EGFR kinase designed to play as competitive inhibitors of ATP-binding at the active site of EGFR-TK domain (Figure 20.1).

Several clinical trials, which use these compounds alone or in combination with platinum-based chemotherapy, have been recently conducted. Although survival was significantly longer in patients with advanced NSCLCs treated with EGFR-TKIs compared to the control groups, results were modestly encouraging. A partial response was observed in ~10% of the patients (Fukuoka *et al*., 2003; Shepherd *et al*., 2005). However, it was soon clear that it was not possible to predict EGFR-TKIs tumor sensitivity by using EGFR expression analysis determined by immunohistochemistry or immunoblotting on target tumors. The factors that determined NSCLCs sensitivity to EGFR targeted therapy have long been an enigma.

EPIDERMAL GROWTH FACTOR RECEPTOR MUTATIONS AND THEIR CLINICAL RELEVANCE

EGFR mutations were first reported by Lynch *et al*. (2004), Paez *et al*. (2004), and Pao *et al*. (2004); and the most interesting finding was that NSCLCs harboring these genetic alterations showed a striking response to EGFR-TKIs. Data from 1,170 patients showed that 70% of NSCLCs with EGFR mutations respond to EGFR-TKIs, whereas only 10% of tumors expressing wild-type EGFR do so. This finding is contributing to the development an impressive research activity directed to identify mutationally activated kinases, which may potentially represent crucial anticancer drug targets. At the same time at least some of the reasons that sustain EGFR-TKIs insensitivity will be elucidated, opening new avenues for tailored and molecular targeted therapies for cancer (Greulich *et al*., 2005). Figure 20.3 shows EGFR kinase domain mutations clusterized in four exons 18–21, which encode part of the tyrosine kinase intracellular domain (Sharma *et al*., 2007). These are generally "activating mutations" that result in increased EGFR kinase activity. However, different mutations may be functionally different resulting in a partial activation or fully constitutive activation of the receptor (Sordella *et al*., 2004; Kobayashi *et al*., 2005a, b). In fact, it has been reported that the response rate of gefitinib was higher for patients with deletional EGFR mutations than for those with other types of mutations involving the motif L858R (Mitsudomi *et al*., 2005). Furthermore, partially activated EGFR mutants can be rendered fully ligand-independent (constitutively activated) by a second site substitution in EGFR gene such as the T790M mutation in exon 20 (Kobayashi *et al*., 2005b).

The observation that sensitivity to gefitinib and erlotinib correlated quite well with newly discovered somatic activating mutations in the EGFR kinase domain, explained the unique subset of drug responsive NSCLCs cases observed in a subgroup of EGFR-TKIs treated patients. Surprisingly, such EGFR activating mutations were predominantly discovered in women of Asian origin, with no history of smoking and adenocarcinoma and bronchioloalveolar histology (Mitsudomi *et al*., 2006; Haneda *et al*., 2006). Lung cancer harboring EGFR mutations appear to occur independent of tobacco smoking,

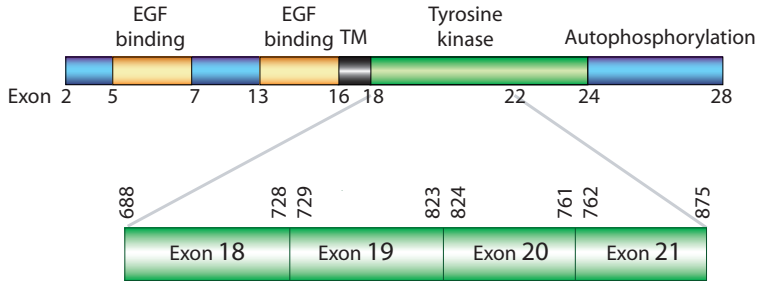

Exon 18	Exon 19	Exon 20	Exon 21
G719C	**ΔE746-A750**	V765A	**L858R (40-45%)**
G719S	ΔE746-T751	T783A	N826S
G719A	ΔE746-A750 (ins RP)	**T790M (50%)***	A839T
V689M	ΔE746-T751 (ins A/I)	D770_N771 (ins NPG)	K846R
N700D	ΔE746-A751 (ins VA)	D770_N771 (ins SVQ)	L861Q
E709K/Q	ΔE746-S752 (ins A/V)	D770_N771 (ins G), N771T	G863D
S720P	ΔL747-E749 (A750P)	V769L	
	ΔL747-A750 (ins P)	S768I	
	ΔL747-T751		
	ΔL747-T751 (ins P/S)		
	ΔL747-S752		
	ΔL747-752 (E746V)		
	ΔL747-752 (P753S)		
	ΔL747-S752 (ins Q)		
	ΔL747-P753		
	ΔL747-P753 (ins S)		
	ΔS752-I759		
	D761Y		

FIGURE 20.3. Gefitinib and erlotinib – sensitizing mutations of EGFR in NSCLC. The involved exons 18, 19, 20, and 21 of the tyrosine kinase domain are depicted. Activating mutations and mutations associated with drug resistance (in red) are listed in the bottom. The most prevalent mutations are in bold. (Modified from Sharma *et al*., 2007.)

whereas the occurrence of lung cancer with wild-type EGFR seems to be dependent on smoking dose.

Although several retrospective studies have shown that patients with EGFR mutations treated with gefitinib live longer than those expressing wild type EGFR (Han *et al*., 2005; Mitsudomi *et al*., 2005), the real impact of this treatment on the overall survival is not defined yet. However, the high response rate to gefitinib in chemotherapy-naïve patients with activating EGFR mutations has been recently confirmed in a prospective phase II study (Inoue *et al*., 2006). The incidence of EGFR mutations is variable in the world. EGFR mutations were detected in ~10% of unselected NSCLC tumors from North America and Western Europe, whereas in patients of East Asian descent it was detected in 30–50% of the cases, and was associated mostly with adenocarcinoma with bronchiolealveolar features (Haneda *et al*., 2006). Clinical studies, supported by molecular analysis showed that good responder patients to EGFR targeted therapy harbored specific EGFR mutations, which play a functional role as *oncogenic* mutations. EGFR kinase domain mutations hyperactivate the kinase domain and

confer a dependence on the activating mutation for proliferation and survival of NSCLC cells. Activating mutations are mostly represented by in-frame deletions of amino-acids 747–750 in EGFR exon 19, accounting for 45% of mutations; exon 21 mutations resulting in L858R substitutions, account for 40–45% of mutations and mutations that involve exons 18 and 20 account for 10% of known mutations, (Figure 20.3). The treatment of sensitive cells with small molecules tyrosine kinase inhibitors such as gefitinib triggers a form of 'oncogenic shock' postulated to result from the differential decay of downstream signals leading to a temporary predominance of apoptotic signals.

Implication of EGFR mutants in NSCLC tumorigenesis has been recently supported by two independent observations in transgenic mice models expressing either exon 19 deletion mutant or the L858R mutant in type II pneumocytes, under the control of doxycycline. Expression of these mutants leads to the development of bronchioloalveolar carcinoma and withdrawal of doxycycline (to downregulate the expression of transgene) or erlotinib treatment results in tumor regression (Ji *et al*., 2006; Politi *et al*., 2006).

The results of these *in vivo* experiments clearly show that persistent EGFR signaling is required for tumor maintenance in NSCLCs expressing EGFR mutants. However, to date, a major confounding factor in NSCLCs mutation analyses is the sensitivity of the mutation detection assay used. Direct Sanger sequencing has been used in the majority of the studies but this technique has a relatively low sensitivity for detection of mutations in routinely available tumor specimens. In fact, results may be obscured by allelic dilution if one copy of the gene is amplified.

Several groups who used more sensitive molecular techniques identified several NSCLCs expressing EGFR mutants, which were undetectable by direct sequencing (Marchetti *et al*., 2005). This fact contributes to the difficulty in any statistical analysis directed to correctly evaluate the real association between EGFR specific mutation and tumor response. The resulting scenario is much more complex if mutations associated with drug resistance are also considered. Greulich *et al*. (2005) reported an insertion mutation (D770insNPG) in exon 20 associated with *in vitro* resistance to erlotinib. Moreover, ~15–20% of NSCLCs, which show a partial response to gefitinib, do not have detectable EGFR mutations raising the question that EGFR mutations are not the sole determinants of TKI response.

ONCOGENE ADDICTION AND GEFITINIB RESPONSE

The concept of oncogene addiction was coined by Weinstein (2002) and provides a strong rationale for molecular targeted therapy in several tumor models. Oncogene addiction describes the phenomenon by which tumor cells, despite the presence of several genetic alterations, become completely dependent on a single oncogenic pathway for proliferation and survival. Implicit in this dependency is the fact that tumor cells should be drastically sensitive to the targeted inhibition of the addicting oncogene. Treatment of some NSCLCs harboring mutant EGFR with gefitinib demonstrates a 50- to 100-fold increase in drug sensitivity compared with tumors expressing wild-type EGFR. Knockdown of wild-type EGFR by using siRNA strategies has minimal impact on

cellular proliferation and survival of the respective tumors. In contrast, in NSCLC cells expressing EGFR-mutants (activating mutations) a comparable knockdown triggers widespread apoptosis (Sordella *et al*., 2004). The abrupt withdrawal of oncogenic mediated critical functions (signaling) may lead to a transient imbalance between downstream apoptotic and antiapoptotic signals, triggering rapid cell death (oncogenic shock). Validation of these recently proposed models would be important to design correctly a tailored molecular targeted therapy for NSCLCs as well as for different solid tumors. Targeted therapies that are based on a strong molecular rationale may potentially reduce toxicity and improve outcomes in a number of cancers. However, benefits of targeted agents are often limited to a subset of patients with particular *molecular signature*, which should be demonstrated and tested *in vitro* in order to predict the therapeutic response to specific treatments. To better understand the mechanistic basis of oncogene addiction represents the most important challenge for modern oncology. It will be essential for ensuring an optimal single or combined therapeutic strategy for tumor killing.

NON-SMALL CELL LUNG CARCINOMA SENSITIVITY TO EPIDERMAL GROWTH FACTOR RECEPTOR TARGETED THERAPY, AND MECHANISMS OF RESISTANCE

Not all EGFR kinase mutations are associated with NSCLC sensitivity to gefitinib. Recently it became clear that only *EGFR-addicted* cancers will respond drastically to EGFR-targeted therapy. The tumor that fails to respond to gefitinib despite the presence of EGFR-activating mutation is likely bear additional genetic lesions, which may also be responsible for acquired resistance in previously sensitive tumors. As reported above, insertion mutations in exon 20 of the EGFR gene (T790M) might render the receptor ~100-fold less sensitive to EGFR-TKIs compared with other sensitizing EGFR mutations (Greulich *et al*., 2005).

EGFR-ligands: Amphiregulin and TGF-α are well known putative ligands of EGFR. The increased expression of these molecules in some NSCLCs has been related with poor response to gefitinib. Recently, it has also been demonstrated that a heregulin-dependent autocrine loop, that activates ERBB2 and ERBB3 signaling pathways, is functionally active in some NSCLCs and is responsible for the observed resistance to EGFR-TKIs. The ADAM 17, a disintegrin and metalloproteinase that controls the cleavage of most EGF-related ligands, has been found upregulated in NSCLCs and correlated with heregulin-mediated ERBB3 activation, leading to gefitinib insensitivity (Zhou *et al*., 2006).

EGFR amplification: Amplification of mutated EGFR gene is quite common in malignant gliomas, but despite the frequency of this genetic alteration, gliomas exhibit very modest responses to gefitinib. These observations suggest that gliomas are less dependent than NSCLCs on EGFR signaling, or alternatively, that different kinase mutations lead to qualitative differences in EGFR-TKIs tumor sensitivity. In NSCLCs, amplification of EGFR involving either wild-type alleles or alleles harboring a kinase mutation has been reported. By using quantitative PCR

analysis (qPCR) Bell *et al*. (2005) showed that only 7% of NSCLCs were found to have significant EGFR amplification, mostly involving a wild-type EGFR allele, although some cases had amplification of a mutant EGFR. EGFR amplification as measured by qPCR was predictive of gefitinib responsiveness, although not as strongly as EGRF mutations. Interestingly, the clinical-epidemiological features of NSCLCs with EGFR amplification were consistently different from those expressing EGFR-TK mutants. EGFR mutations were more common in adenocarcinomas arising in female nonsmokers, whereas tumors with wild-type EGFR amplification were more common in older men and in smokers without association with specific tumor-types (Bell *et al*., 2005).

It seems that although both markers denote alterations in EGFR signaling, they appear to arise in distinct subsets of NSCLCs. The impact of EGFR amplification as a predictor of tumor sensitivity to EGFR targeted therapies is still an open issue. In addition to EGFR gene copy numbers, Cappuzzo *et al*. (2005) reported that ERBB2 amplification is associated with response to gefitinib in EGFR-mutated NSCLCs. The same group also reported that genomic gain for ERBB3 is not a marker for response or resistance to TKIs in patients with advanced NSCLC.

Downstream molecules and "functional receptor shift": Approximately 15–30% of NSCLCs harbor activating mutations in codon 12 and 13 of the *KRAS* gene (Mitsudomi *et al*., 1991). Pao *et al*. (2005) reported that lung carcinomas with *k-ras* mutations are resistant to EGFR-TKIs. None of the nine tumors included in that study responded to EGFR-TKIs, although in a different study some NSCLCs with bronchioloalveolar histology, in which both EGFR activating mutation and KRAS mutation were detected, showed a partial response (Miller *et al*., 2006). Mutant EGFR and KRAS may have overlapping signaling roles in NSCLC etiology, and it is not surprising that KRAS mutations are generally absent in EGFR-TKIs responsive tumors but are almost invariably detected in NSCLCs expressing wild-type EGFR.

As shown in Figure 20.2, Akt is phosphorylated on EGFR activation and mediates a signal transduction pathway, which is critical for cell survival. Tumor cells that are sensitive to gefitinib are characterized by a rapid decrease in Akt activity in response to EGFR-TKIs. The failure to downregulate Akt is a hallmark of drug insensitivity (Sordella *et al*., 2004). It is clear that different molecular mechanisms may be responsible for Akt activation. Of interest are the tumor suppressor phosphatase and tensin homologue PTEN, which regulate indirectly Akt activation. PTEN is frequently lost in human cancer including NSCLCs, and experimental results *in vitro* demonstrate that restoring of PTEN expression in cancer cells is associated with increased sensitivity to gefitinib (Bianco *et al*., 2003).

Although most NSCLCs expressing EGFR–mutants initially respond to EGFR targeted therapy, the vast majority of these tumors become resistant to the drug treatment. This unfavorable event is also common in chronic myelogenous leukemia and gastrointestinal stromal tumors after treatment with BCR-ABL and KIT targeted therapies, respectively. Mechanisms of acquired resistance to kinase inhibitors may include secondary mutations in the kinase itself. As mentioned earlier, in ~50% of NSCLCs, EGFR-TKIs resistance

is due to the occurrence of a secondary mutation (T790M) in EGFR kinase domain, but other mechanisms that contribute to drug resistance may be involved in the remaining tumors. Alternative possibilities include amplification of the target kinase or overexpression of other kinases downstream of the target kinase, as is the case of LYN in chronic myelogenous leukemia.

Very recently, Engelman *et al.* (2007) reported a different and unexpected mechanism of gefitinib resistance, which involves the oncogene MET and ERBB3. MET amplification leads to gefitinib resistance in NSCLCs by activating ERBB3 signaling. In particular, MET amplification (found in a fraction of NSCLCs *in vivo* that becomes resistant to EGFR-TKIs) leads to persistent activation of PI3K/Akt signaling in the presence of gefitinib by maintaining ERBB3 phosphorylation. MET amplification leads to ERBB3 phosphorylation and PI3K activation in an EGFR and ERBB2 independent manner.

This mechanism can be considered a sort of "*functional receptor shift*", which involves activation of EGFR downstream molecules by-passing a direct activation of EGFR itself. MET amplification provides an intriguing example of a resistance mechanism characterized by gene amplification of a kinase that is not a direct or downstream target for gefitinib.

The mitogen-inducible-gene 6 (Mig 6, RALT) is involved in the regulation of receptor TK-activity. Mig 6 deletion causes hyperactivation of EGFR, which triggers downstream signaling through MAPK pathway. This mechanism results in over-proliferation and impaired differentiation of epidermal keratinocytes (Ferby *et al.*, 2006). The potential tumor suppressor activity of Mig 6 in lung carcinoma and other EGFR expressing tumors will be investigated (personal communication). Functional and structural studies will be necessary to better understand the biology of EGFR and to dissect, at least in part, the complex scenario of molecular interactions, which determine tumor sensitivity or resistance to TKIs treatment. Elucidation of these relevant mechanisms will help to provide the rationale for EGFR targeted therapies.

IRREVERSIBLE EPIDERMAL GROWTH FACTOR INHIBITORS AND COMBINATORIAL APPROACHES WITH OTHER TARGETED THERAPIES

As mentioned earlier, gefitinib and the analogous compound erlotinib are reversible inhibitors of EGFR that compete with ATP for binding to the intracellular tyrosine kinase domain of the receptor; thereby, inhibiting EGFR autophosphorylation and blocking downstream signal transduction. Irreversible inhibitors of EGFR have been recently developed to circumvent the acquired drug resistance. These agents, including EKB569 (targeting EGFR) and HKI 272 (that target both EGFR and ErbB2), are similar in their overall structure to the reversible inhibitors but differ in the presence of a motif, which can form a covalent bond with Cys-773 within the catalytic pocket of the receptor (Rabindran *et al.*, 2004). Interestingly, these irreversible inhibitors shared the selective killing of NSCLC cells bearing EGFR-activating mutations, but they are able to maintain a persistent blocking activity against EGFR-mutant cells that had acquired resistance

to gefitinib through the expression of the secondary T790M mutation or alterations in EGFR internalization (Kwak *et al*., 2005). The likely improved reaction kinetics provided by the covalent bond to the EGFR catalytic domain are sufficient to circumvent the reduced drug binding to the T790M-mutated and conformationally altered EGFR. *In vitro* observations raise the possibility that strategies, which use irreversible EGFR inhibitors, may be applied also to target cytoplasmic kinases such as ABL, the gatekeeper residue (codon 315 of BCR-ABL) that represent a hot spot for imatinib resistance in chronic mielocytic leukemia.

Clinical trials aimed to test the efficacy of EKB 569 and HKI 272 in patients with EGFR-mutant NSCLC that have acquired resistance to gefitinib are ongoing. However, the recent discovery that MET amplification leads to gefitinib resistance by activating ERBB3 signaling, suggests that irreversible EGFR inhibitors, which are currently under clinical development, may be ineffective in the subset of NSCLCs with MET amplification, even if they contain an EGFR T790M mutation (Engelman *et al*., 2007). This means that an efficient molecular targeted therapy for cancer killing requires a full understanding of the *molecular signature* of each specific tumor.

FUTURE ADVANCES

During the past ten years a dramatic evolution has taken place in both diagnosis and treatment of cancer. These achievements are mostly due to the improved knowledge of tumor biology, which leads the identification of tumor specific diagnostic and therapeutic targets. Some critical pathways regulating cell growth and death have been defined in several tumors and rearrangements of chromosomes (which can result in novel, tumor specific genes) have been defined in a number of soft tissue tumors such as leukemia and lymphomas. Overexpression of some genes associated with tumor progression or prognosis has been demonstrated in several solid tumors, and mutations in critical genes resulting in deregulated cell-cycle have also been identified. All together these findings provide new opportunities for tumor diagnosis and targeted therapy. Furthermore, it is becoming clear that we are moving toward a personalized molecular medicine for cancer patients, which should replace, in the near future, the conventional chemotherapy.

The rationale of specific targeted therapies will be based on individual tumor molecular profile. Targeted therapy for NSCLCs, as well as for other human malignancies, can potentially reduce toxicity and improve the outcome in a number of cases. However, considering the fact that the benefits of targeted agents are often limited to a subset of patients with particular *molecular signature*, it will be critical to develop an efficient and reliable method for molecular tumor analysis in order to predict the therapeutic response.

For NSCLC, one of the most important emergencies in oncology, mutational analysis of EGFR is already commercially available. Prospective studies will help to correlate specific genetic alterations of EGFR found in these tumors, with the clinical response to EGFR-TKIs. Other genetic or epigenetic factors that may modulate tumor drug response are expected to be identified. The concepts that human tumors may comprise multiple

genetic alterations and that the clinical response to molecular targeted therapy may be limited to a small subset of tumors, will likely have significant implications for the development and testing of new anti-cancer drugs. Nonetheless, specialists involved in the diagnosis and management of cancer will assist in the near future, in drastic changes of their *modus operandi*.

The appropriate use of newly approved and expensive targeted therapies for cancer first depends on the pathologists identifying the target molecule in each tumor sample. Complementary functional approaches *in vitro*, which include the use of short hairpin RNA libraries to identify genes that are essential to cancer cell viability, may also be necessary. The use of expensive targeted therapies should be restricted to pathologically proven indications because truly effective drugs are best applied to those individuals who would most benefit. It follows that in the era of personalized molecular medicine, pathologists, medical oncologists, and scientists should be trained properly for a collaborative clinical work, aimed to optimize and drive the use of molecular targeted therapies.

Several ambitious projects directed to discover and classify all cancer-associated mutations within each histological type are currently in progress in the U.S.A. (US National Institute of Health, Cancer Genome Atlas). When the accurate molecular profiling of each tumor becomes available, new tailored, single or combined targeted therapies, which are based on a strong molecular rationale, will impact consistently on the clinical care and survival of many cancer patients including those with NSCLCs. (see chapter 21 in this volume).

REFERENCES

Abeloff, M.D., Armitage, J.O., Niederhuber, J.E., Kastan, M.B., McKenna, W.J. 2004. Clinical Oncology, vol. 3, Third Ed. pp. 1649–1743. Philadelphia, PA: Ortho Biothec/Excerpta Medica/Elsevier.

Alroy, I., and Yarden, Y. 1997. The ErbB signaling network in embryogenesis and oncogenesis: signal diversification through combinatorial ligand-receptor interactions. *FEBS Lett. 410*: 83–86.

Bell, D.W., Lynch, T.J., Haserlat, S.M., Harris, P.L., Okimoto, R.A., Brannigan, B.W., Sgroi, D.C., Muir, B., Riemenschneider, M.J., Iacona, R.B., Krebs, A.D., Johnson, D.H., Giaccone, G., Herbst, R.S., Manegold, C., Fukuoka, M., Kris, M.G., Baselga, J., Ochs, J.S., and Haber, D.A. 2005. Epidermal growth factor receptor mutations and gene amplification in non-small cell lung cancer: molecular analysis of the IDEAL/INTACT gefitinib trials. *J. Clin. Oncol. 23*: 8081–8092.

Bianco, R., Shin, I., Ritter, C.A., Yakes, F.M., Basso, A., Rosen, N., Tsurutani, J., Dennis, P.A., Mills, G.B., and Arteaga, C.L. 2003. Loss of PTEN/MMAC1/TEP in EGF receptor-expressing tumor cells counteract the antitumor action of EGFR tyrosine kinase inhibitors. *Oncogene 22*: 2812–2822.

Cappuzzo, F., Varella-Garcia, M., Shigematsu, H., Domenichini, I., Bartolini, S., Ceresoli, G.L., Rossi, E., Ludovini, V., Gregorc, V., Toschi, L., Franklin, W.A., Crino, L., Gazdar, A.F., Bunn, P.A. Jr., and Hirsch, F.R. 2005. Increased HER2 gene copy number is associated with response to gefitinib therapy in epidermal growth factor receptor-positive non-small cell lung cancer patients. *J. Clin. Oncol. 23*: 5007–5018.

Engelman, J.A., Zejnullahu, K., Mitsudomi, T., Song, Y., Hyland, C., Park, J.O., Lindeman, N., Gale, C.M., Zhao, X., Christensen, J., Kosaka, T., Holmes, A.J., Rogers, A.M., Cappuzzo, F., Mok, T., Lee, C., Johnson, B.E., Cantley, L.C., and Janne, P.A. 2007. MET amplification leads to gefitinib resistance in lung cancer by activatingERBB3 signaling. *Science 316*: 1039–1042.

Ferby, I., Reschke, M., Kudlacek, O., Knyazev, P., Pante, G., Amann, K., Sommergruber, W., Kraut, N., Ullrich, A., Fassler, R., and Klein, R. 2006. Mig6 is a negative regulator of EGF receptor-

mediated skin morphogenesis and tumor formation. *Nat. Med. 12*: 568–573 (erratum in Nat. Med. 12: 862).

Fukuoka, M., Yano, S., Giaccone, G., Tamura, T., Nakagawa, K., Douillard, J.Y., Nishiwaki, Y., Vansteenkiste, J., Kudoh, S., Rischin, D., Eek, R., Horai, T., Noda, K., Takata, I., Smit, E., Averbuch, S., Macleod, A., Feyereislova, A., Dong, R.P., and Baselga, J. 2003. Multi-institutional randomized phase II trial of gefitinib for previously treated patients with advanced non-small cell lung cancer (The IDEAL 1 Trial). *J. Clin. Oncol. 21*: 2237–2246.

Greulich, H., Chen, T-H., Feng, W., Janne, P.A., Alvarez, J.V., Bulmer, S.E., Zappaterra, M., Frank, D.A., Hahn, W.C., Sellers, W.R., and Meyerson, M. 2005. Oncogenic transformation by inhibitor-sensitive and-resistant EGFR mutants. *PLoS Med. 2*: e313.

Han, S.W., Kim, T.Y., Hwang, P.G., Jeong, S., Kim, J., Choi, I.S., Oh, D.Y., Kim, J.H., Kim, D.W., Chung, D.H., Im, S.A., Kim, Y.T., Lee, J.S., Heo, D.S., Bang, Y.J., and Kim, N.H. 2005. Predictive and prognostic impact of epidermal growth factor receptor mutation in non-small cell lung cancer patients treated with gefitinib. *J. Clin. Oncol. 23*: 2493–2501.

Haneda, H., Sasaki, H., Lindeman, N., Kawano, O., Endo, K., Suzuki, E., Shimizu, S., Yukiue, H., Kobayashi, Y., Yano, M., and Fujii, Y. 2006. A correlation between EGFR gene mutation status and bronchioloalveolar carcinoma features in Japanese patients with adenocarcinoma. *Jpn. J. Clin. Oncol. 36*: 69–75.

Hirsch, F.R., Varella-Garcia, M., Bunn, P.A. Jr., Di Maria, M.V., Veve, R., Bremmes, R.M., Baron, A.E., Zeng, C., and Franklin, W.A. 2003. Epidermal growth factor receptor in non-small cell lung carcinoma: correlation between gene copy number and protein expression and impact on prognosis. *J. Clin. Oncol. 21*: 3798–3807.

Inoue, A., Suzuki, T., Fukuara, T., Maemondo, M., Kimura, Y., Morikawa, N., Watanabe, H., Saijo, Y., and Nukiwa, T. 2006. Prospective phase II study of gefitinib for chemotherapy-naive patients with advanced non-small-cell lung cancer with epidermal growth factor receptor gene mutation. *J. Clin. Oncol. 24*: 3340–3346.

Ji, H., Li, D., Chen, L., Shimamura, T., Kobayashi, S., McMamara, K., Mahmood, U., Mitchell, A., Sun, Y., Al-Hashem, R., Chirieac, L.R., Padera, R., Bronson, R.T., Kim, W., Janne, P.A., Shapiro, G.I., Tenen, D., Johnson, B.E., Weissleder, R., Sharpless, N.E., and Wong, K.K. 2006. The impact of human EGFR kinase domain mutations on lung tumorigenesis and in vivo sensitivity to EGFR-targeted therapies. *Cancer Cell 9*: 485–495.

Kawamoto, T., Sato, J.D., Le, A., Polikoff, J., Sato, G.H., and Mendelsohn, J. 1983. Growth stimulation of A431 cells by EGF: identification of high affinity receptors for epidermal growth factor by an anti-receptor monoclonal antibody. *Proc. Natl. Acad. Sci. USA 80*: 1337–1341.

Kobayashi, S., Boggon, T.J., Dayaram, T., Janne, P.A., Kocher, O., Meyerson, M., Johnson, B.E., Eck, M.J., Tenen, D.G., and Halmos, B. 2005a. EGFR mutation and resistance of non-small cell lung cancer to gefitinib. *N. Engl. J. Med. 352*: 786–792.

Kobayashi, S., Ji, H., Yuza, Y., Meyerson, M., Wong, K.K., Tenen, D.G., and Halmos, B. 2005b. An alternative inhibitor overcomes resistance caused by a mutation of the epidermal growth factor receptor. *Cancer Res. 65*: 7096–7101.

Kwak, E.L., Sordella, R., Bell, D.W., Godin-Heymann, N., Okimoto, R.A., Brannigan, B.W., Harris, P.L., Driscoll, D.R., Fidias, P., Lynch, T.J., Rabindran, S.K., McGinnis, J.P., Wissner, A., Sharma, S.W., Isselbacher, K.J., Settleman, J., and Haber, D.A. 2005. Irreversible inhibitors of the EGF receptor may circumvent acquired resistance to gefitinib. *Proc. Natl. Acad. Sci. USA 102*: 7665–7670.

Lynch, T.J., Bell, D.W., Sordella, R., Gurubhagavatula, S., Okimoto, R.A., Brannigan, B.W., Harris, P.L., Haserlat, S.M., Supko, J.G., Haluska, F.G., Louis, D.N., Christiani, D.C., Settleman, J., and Haber, D.A. 2004. Activating mutations in the epidermal growth factor receptor underlying responsiveness of non-small-cell lung cancer to gefitinib. *N. Engl. J. Med. 350*: 2129–2139.

Marchetti, A., Martella, C., Felicioni, L., Barassi, F., Salvatore, S., Chella, A., Camplese, P.P., Iarussi, T., Mucilli, F., Mezzetti, A., Cuccurullo, F., Sacco, R., and Buttitta, F. 2005. EGFR mutations in non-small cell lung cancer: analysis of a large series of cases and development of a rapid

and sensitive method for diagnostic screening with potential implications on pharmacologic treatment. *J. Clin. Oncol. 23*: 857–865.

Mendelsohn, J., and Baselga, J. 2006. Epidermal growth factor receptor targeting. *Semin. Oncol. 33*: 369–385.

Miller, V.A., Zakowski, M., Riely, G.J., Pao, W., Ladanyi, M., Tsao, A.S., Sandler, A., Herbst, R., Kris, M.G., and Johnson, D.H. 2006. EGFR mutation and copy number, EGFR protein expression and KRAS mutation as predictors of outcome with erlotinib in bronchioloalveolar cell carcinoma (BAC): results of a prospective phase III trial. *J. Clin. Oncol. (meeting abstracts) 24*: 7003.

Mitsudomi, T., Steinberg, S.M., Oie, H.K., Mulshine, J.L., Phelps, R., Viallet, J., Pass, H., Minna, J.D., and Gazdar, A.F. 1991. Ras gene mutation in non-small cell lung cancers are associated with shortened survival irrespective of the treatment intent. *Cancer Res. 51*: 4999–5002.

Mitsudomi, T., Kosaka, T., Endoh, H., Horio, Y., Hida, T., Mori, S., Hatooka, S., Shinoda, M., Takahashi, T., and Yatabe, Y. 2005. Mutations of the epidermal growth factor receptor gene predict prolonged survival after gefitinib treatment in patients with non-small cell lung cancer with postoperative recurrence. *J. Clin. Oncol. 23*: 2513–2520.

Mitsudomi, T., Kosaka, T., Yatabe, Y. 2006. Biological and clinical implications of EGFR mutations in lung cancer. *Int. J. Clin. Oncol. 11*: 190–198.

Paez, J., Janne, P.A., Lee, J.C., Tracy, S., Greulich, H., Gabriel, S., Herman, P., Kaye, F.J., Lindeman, N., Boggon, T.J., Naoki, K., Sasaki, H., Fujii, Y., Eck, M.J., Sellers, W.R., Johnson, B.E., and Meyerson, M. 2004. EGFR mutations in lung cancer: correlation with clinical response to gefitinib therapy. *Science 304*: 1497–1500.

Pao, W., Miller, V., Zakowski, M., Doherty, J., Politi, K., Sarkaria, I., Singh, B., Heelan, R., Rusch, V., Fulton, L., Mardis, E., Kupfer, D., Wilson, R., Kris, M., Varmus, H. 2004. EGF receptor gene mutations are common in lung cancers from "never smokers" and are associated with sensitivity of tumors to gefitinib and erlotinib. *Proc. Natl. Acad. Sci. USA 101*: 13306–13311.

Pao, W., Wang, T.J., Riely, G.J., Miller, V., Pan, Q., Ladanyi, M., Zakowski, M.F., Heelan, R.T., Kris, M.G., and Varmus, H.E. 2005. KRAS mutations and primary resistance of lung adenocarcinoma to gefitinib or erlotinib. *PLoS Med. 2*: e17.

Politi, K., Zakowsky, M.F., Fan, P.D., Schonfeld, E.A., Pao, W., and Varmus, H.E. 2006. Lung adenocarcinomas induced in mice by mutant EGF receptor found in human lung cancer respond to a tyrosine kinase inhibitor or to down regulation of the receptors. *Genes Dev. 20*: 1496–1510.

Rabindran, S.K., Discafani, C.M., Rosfjord, E.C., Baxter, M., Floyd, M.B., Golas, J., Hallett, W.A., Johnson, B.D., Nilakanttan, R., Overbeek, E., Reich, M.F., Shen, R., Shi, X., Tsou, H.R., Wang, Y.F., and Wissner, A. 2004. Antitumor activity of HKI-272, an orally active, irreversible inhibitor of the HER-2 tyrosine kinase. *Cancer Res. 64*: 3958–3965.

Rusch, V., van de Wetering, M.L., Mooi, W.J., Evers, S.G., van Zandwijk, N., and Bos, J.L. 1993. Differential expression of the epidermal growth factor receptor and its ligands in primary non small cell lung cancers and adjacent benign lung. *Cancer Res. 53*: 2379–2385.

Sharma, S.V., Bell, D.W., Settleman, J., and Haber, D.A. 2007. Epidermal growth factor receptor mutations in lung cancer. *Nat. Rev. Cancer 7*: 169–181.

Shepherd, F.A., Rodrigues Pereira, J., Ciuleanu, T., Tan, E.H., Hirsh, V., Thongprasert, S., Campos, D., Maoleekoonpiroj, S., Smylie, M., Martins, R., van Kooten, M., Dediu, M., Findlay, B., Tu, D., Johnston, D., Bezjak, A., Clark, G., Santabarbara, P., and Seymour, L. (National Cancer Institute of Canada Clinical Trials Group). 2005. Erlotinib in previously treated non-small cell lung cancer. *N. Engl. J. Med. 353*: 123–132.

Sordella, R., Bell, D.W., Haber, D.A., and Settleman, J. 2004. Gefitinib-sensitizing EGFR mutations in lung cancer activate anti-apoptotic pathways. *Science 305*: 1163–1167.

Testa, J.R., and Siegfried, J.M. 1992. Chromosome abnormalities in human non-small cell lung cancer. *Cancer Res. 52*: 2702s–2706s.

Vivanco, I., and Sawyers, C.L., 2002. The phosphatydilinositol 3-kinase-Akt pathway in human cancer. *Nat. Rev. Cancer 2*: 489–501.

Weinstein, I.B. 2002. Cancer. Addiction to oncogenes - the Achilles heal of cancer. *Science 297*: 63–64.

Yarden, Y., and Sliwkowski, M. 2001. Untangling the ErbB signaling network. *Nat. Rev. Mol. Cell Biol. 2*: 127–137.

Yokota, J., and Kohno, T. 2004. Molecular footprints of human lung cancer progression. *Cancer Sci. 95*: 197–204.

Zhou, B.B., Peyton, M., He, B., Liu, C., Girard, L., Caudler, E., Lo, Y., Baribaud, F., Mikami, I., Reguart, N., Yang, G., Li, Y., Yao, W., Vaddi, K., Gazdar, A.F., Friedman, S.M., Jablons, D.M., Newton, R.C., Fridman, J.S., Minna, J.D., and Scherle, P.A. 2006. Targeting ADAM-mediated ligand cleavage to inhibit HER3 and EGFR pathways in non-small cell lung cancer. *Cancer Cell 10*: 39–50.

21
Advanced Non-Small Cell Lung Carcinoma: Acquired Resistance to Gefitinib

Katsuyuki Kiura, Nagio Takigawa, and Yoshihiko Segawa

INTRODUCTION

Epidermal growth factor receptor (EGFR) signaling regulates processes essential to tumor progression, including cell motility, cell adhesion, tumor invasion, cell survival, and angiogenesis as well as cell proliferation (Mendelsohn, 2000). Since EGFR is expressed in ~50% of non-small cell lung cancer (NSCLC) tumors (Veale *et al*., 1987), this receptor is a candidate for targeted therapeutics in the treatment of NSCLC. Gefitinib (Iressa: AstraZeneca) is a novel, low-molecular-weight synthetic anilinoquinazoline [4-(3-chloro-4-fluoroanilino)-7-methoxy-6-(3-morpholinopropoxy)-quinazoline] (Ward *et al*., 1994). Its discovery was based on studies designed to characterize the mechanism of catalysis of EGFR tyrosine kinase (TK) inhibition. During the initial phase of the development of gefitinib, researchers aimed at disease control or long-term disease stability. Unexpectedly, however, they experienced a dramatic response to gefitinib in a patient with advanced NSCLC (Fukuoka *et al*., 2003; Fujiwara *et al*., 2003). The marked response observed in this patient, which had never been seen previously in patients with advanced NSCLC impressed physicians who had treated incurable, advanced NSCLC in Japan. Similar dramatic responses to gefitinib were observed in a small but substantial subset of NSCLC patients including those of female gender with adenocarcinoma histology (Fukuoka *et al*., 2003; Kris *et al*., 2003). These patients were nonsmokers and of East Asian ethnicity (Fukuoka *et al*., 2003; Miller *et al*., 2004). However, although gefitinib was employed throughout the world, the mechanisms responsible for its efficacy had remained unclear.

Discovery of Somatic EGFR-TK Mutations

Somatic EGFR-TK mutations were then discovered in a subset of patients who had responded to gefitinib and erlotinib (Lynch *et al*., 2004; Paez *et al*., 2004). The mechanism of action of the EGFR-TK inhibitors was subsequently clarified. Deletion mutations in exon 19 and substitution of arginine for leucine at codon 858 (L858R) account for ~90% of somatic *EGFR* mutations (Kosaka *et al*., 2004; Shigematsu *et al*., 2005). These mutations appear to sensitize cancer cells strongly to the growth-suppressive effects of EGFR-TK inhibitors. It should be noted

that these patients were often females who had never smoked (Kosaka *et al*., 2004; Shigematsu *et al*., 2005). Furthermore, individuals of East Asian ethnicity carry mutations in lung cancer more often than do Caucasians (Shigematsu *et al*., 2005), indicating roles of genetic and/or lifestyle factors in the carcinogenesis of tumors with activating *EGFR* mutations. Patients with activating *EGFR* mutations comprise a distinct clinical entity. Not unexpectedly, activating *EGFR* mutations are oncogenic, and are crucial for maintenance of tumors addicted by EGFR signaling, as shown by transgenic mice studies (Ji *et al*., 2006; Politi *et al*., 2006; Ohashi *et al*., 2007). The activating *EGFR* mutations render EGFR-TK constitutively active, although they still respond to ligands such as EGF (Greulich *et al*., 2005). The reason why EGFR activation arises from such mutations has been determined in recent structural studies. In the absence of ligand binding, EGFR normally remains in an auto-inhibited inactive conformation, which is maintained by intramolecular interaction between the activation loop and the αC helix (Choi *et al*., 2007; Zhang *et al*., 2006). In physiological settings, activation of EGFR is accompanied by ligand-induced homo- or hetero-dimerization with ErbB family members, resulting in active conformation of the kinase domain with phosphorylation on multiple tyrosines in the C-terminal domain. The phospho-tyrosines then act as docking sites for downstream signaling molecules. Given the location of the mutations, *i.e*., within the activation loop (L858R) or adjacent to the αC helix (deletion), auto-inhibition is likely to be disrupted by mutations, resulting in the active conformation.

The dramatic clinical efficacy of EGFR-TK inhibitor in NSCLC patients carrying activating *EGFR* mutations indicates the following: first, the growth and survival of NSCLC cells depend on the signal generated by EGFR, which is abrogated by the treatment of gefitinib, and second, mutated EGFR is more susceptible to inhibitors than wild-type EGFR. Interestingly, binding of erlotinib with EGFR has been shown to be compatible with the active conformation alone (Stamos *et al*., 2002; Zhang *et al*., 2006); this finding may explain the hypersensitivity of mutated EGFR.

Resistance to Gefitinib

Criteria for clinical resistance to gefitinib can be set simply on the basis of the guidelines for evaluating the response to treatment of solid tumors (Therasse *et al*., 2000). When a patient does not exhibit stable disease, partial response, or complete response, his or her tumor is considered resistant to gefitinib. However, it is very difficult to determine whether tumor cells resistant to gefitinib are selected (primary) or undergo mutation (secondary or acquired) during gefitinib treatment, or both. In addition, criteria for resistance to *ex vivo* gefitinib are unclear. Sharma *et al*. (2007) have summarized the sensitivity of NSCLC cell lines to gefitinib and erlotinib as follows: hypersensitive (IC_{50} in the low nM range), to sensitive (IC_{50} in the high nM range), to extremely insensitive (IC_{50} in the high μM range). The hypersensitive cell lines NCI-H3255 and PC-9 harbor the activating *EGFR* mutations L858R and delE746-A750, respectively, which are believed to correspond to dramatic responses observed clinically. The sensitive cell lines NCI-H2170, NCI-H2073, and EBC-2 harbor wild-type EGFR, which is believed to correspond to stable disease. Insensitive cell lines such as NCI-H1975

and NCI-H1650, although harboring the same kinase domain mutations (L858R and delE746-A750), have additional changes such as T790M mutation (NCI-H1975) or loss of phosphatase and tensin homologue (PTEN) (NCI-H1650), and NCI-H460 with *KRAS* mutations are presumed to correspond to primary resistance to gefitinib. Not all EGFR-TK mutations are associated with dramatic response to gefitinib (Shigematsu *et al*., 2006).

Primary Resistance

RAS

The RAS-mitogen-activated protein kinase (MAPK) pathway is another important cell-proliferation pathway downstream of EGFR that is frequently activated in lung cancer. Mutations of *RAS* oncogenes do not appear to coexist with *EGFR* mutations (Kosaka *et al*., 2004). In addition, activation of the RAS-MAPK pathway has not been as well correlated with response to gefitinib and erlotinib (Pao *et al*., 2005a). Furthermore, activated Ras could substitute for most of the upstream EGFR signal in transfection experiments. Thus, mutational activation of targets downstream from the EGFR could induce acquired resistance to gefitinib in cells carrying activating *EGFR* mutations (Uchida *et al*., 2007). However, the majority of patients with activated *RAS* mutations do not have activating *EGFR* mutations. Activated *RAS* mutations might result in primary resistance to gefitinib.

Other Mechanisms

The activation of Akt is indirectly regulated by PTEN, which is frequently lost in human cancers. Although genetic alterations of PTEN are found in $<10\%$ of cases of NSCLC (Kohno *et al*., 1998), the absence of PTEN expression is evident in as many as 70% of cases, and might be mediated by epigenetic mechanisms such as PTEN promoter methylation (Soria *et al*., 2002). In some types of cells, restoration of PTEN expression is associated with increased sensitivity to gefitinib or erlotinib, suggesting that this might modulate sensitivity *in vivo* (She *et al*., 2003). Insulin-like growth factor receptor 1, ERBB3, and activated ERBB2 expression have also been proposed to play roles in mediating resistance to gefitinib.

Acquired Resistance

Although tumors carrying activating *EGFR* mutations display rates of response to gefitinib as high as 75% in most cases of NSCLC, cancer cells eventually become resistant to gefitinib treatment, and the median duration of response is disappointingly short, at only 9–10 months even with first-line gefitinib therapy (Inoue *et al*., 2006; Sutani *et al*., 2006; Asahina *et al*., 2006; Sunaga *et al*., 2007; Table 21.1). In addition, despite dramatic response to gefitinib, patients with *EGFR* mutations rarely achieve complete response. The presence of tumor and continued treatment with gefitinib or erlotinib results in selective pressure for the development of tumor cells with acquired resistance to gefitinib or erlotinib. The mechanisms of this acquired resistance are presently being elucidated. Table 21.2 shows the incidences of mechanisms of resistance to gefitinib confirmed *in vivo*.

Mutation of Threonine 790 to Methionine in EGFR

Tumors from a small number of patients who initially exhibited sensitivity to gefitinib or erlotinib and subsequently

TABLE 21.1. Effects of gefitinib on advanced non-small cell lung cancer patients with activating epidermal growth factor gene mutations.

Authors	Patients	PR (%)	PFS/TTP (months)
Inoue *et al*. (2006)	Untreated NSCLC 16 cases	75	9.7
Sutani *et al*. (2006)	Untreated NSCLC 16 cases	75	8.9
Asahina *et al*. (2006)	Treated/untreated NSCLC 27 cases	78	9.4
Sunaga *et al*. (2007)	Treated/untreated NSCLC 27 cases	76	12.9

NSCLC: non-small cell lung cancer; PFS/TTP: progression-free survival/time to progression; PR: partial response.

TABLE 21.2. Genetic changes in patients whose tumors had developed resistance to gefitinib or erlotinib.

	T790M	D761Y	MET
Balak *et al*. (2006)	44% (7/16)	6% (1/16)	NT
Kosaka *et al*. (2006)	50% (7/14)	0% (0/14)	NT
Engelman *et al*. (2007)	55% (10/18)	0% (0/18)	22% (4/18)
Total	50% (24/48)	2% (1/48)	22%

NT: not tested.

developed acquired resistance have been examined. An additional mutation of threonine 790 in EGFR to methionine (T790M) has been found in specimens with acquired resistance (Kobayashi *et al*., 2005; Pao *et al*., 2005b). A single secondary mutation in *EGFR* exon 20, T790M, is present in a subset of *EGFR*-mutant tumors that recur after an initial response to gefitinib or erlotinib. This finding is analogous to those observed for Bcr-Abl and Kit kinases in imatinib–resistant chronic myelogenous leukemia and gastrointestinal stromal cell tumors, respectively (Carter *et al*., 2005). Consistent with these findings, EGFR carrying both an activating *EGFR* mutation and T790M mutation in COS-7 cells is resistant to gefitinib (Kobayashi *et al*., 2005) and gefitinib-sensitive NSCLC cell lines can be rendered resistant to gefitinib upon introduction of *EGFR* carrying T790M mutation (Engelman *et al*., 2006: Table 21.3). Furthermore, structural modeling studies have presumed that T790M mutation could abrogate binding of erlotinib with the ATP-binding pocket of EGFR kinase domain (Kobayashi *et al*., 2005). However, Yun *et al*. (2007) recently presented evidence that the resistance induced by T790M mutation may stem from its ability to restore wild-type affinity for ATP, rather than from its steric effects on inhibitor binding as previously supposed (Kobayashi *et al*., 2005). The reasons for this were as follows. First, the T790M mutant remains sensitive to a number of irreversible EGFR-TK inhibitors, including HKI-272, Cl-387,785, and Cl-1033, which are believed to bind in the ATP binding cleft in a manner analogous to that of similar reversible EGFR-TK inhibitors. The steric effects of T790M mutation should also interfere with targeting of the irreversible inhibitors, although T790M does not. Second, substitution of T790M has not been found to sterically

TABLE 21.3. Characteristics of gefitinib-resistant cell lines.

Parent cell line Authors	EGFR gene mutation	Resistant cell line	Selection	RR	T790M	MET
PC-9 Koizumi *et al*. (2005)	Ex 19 delE746-A750	PC-9/ZD	MNNG & Gefitinib	182	NT	NT
PC-9 Ogino *et al*. (2007)	Ex 19 delE746-A750	RPC-9	Gefitinib	>250	Yes	No
H3255 Engelmann *et al*. (2006)	L858R	H3255 GR	Gefitinib	>125	Yes	No
HCC827 Engelman *et al*. (2007)	Ex 19 delE746-A750	HCC827 GR	Gefitinib	>1,000	No	Yes

EGFR: epidermal growth factor receptor; MNNG: N-methyl-N´-nitro-N-nitrosoguanidine; NT: not tested; RR: relative resistance (inhibition concentration 50% [IC_{50}] value of resistant cell line/IC_{50} value of parent cell line).

block gefitinib binding in a direct binding assay. Third, crystal structure of irreversible EGFR-TK inhibitor in complex with the T790M mutant is the same as that expected in the wild-type kinase. Kinetic analysis of the T790M mutant shows that it is ~ fivefold more active than the wild-type kinase, with a similar Km for ATP. Finally, the L858R/T790M double mutant also has a Km for ATP equivalent to that of the wild-type kinase, whereas the L858R and G719S single mutants have markedly impaired affinity for ATP. Since gefitinib must compete with ATP to achieve its intended effect, the effective potency of gefitinib is diminished by enhanced affinity for ATP.

Some studies have also shown that T790M mutation is present before patients are exposed to gefitinib (Toyooka *et al*., 2005). This suggests that this mutation might confer a selective advantage on tumor outgrowth and might be further selected after exposure of the tumor to gefitinib or erlotinib. Recently, T790M mutation was found to be easily induced in two gefitinib-sensitive cell lines following exposure to gefitinib (Engelman *et al*., 2006; Ogino *et al*., 2007; Table 21.3). These findings suggest that T790M mutation might either be present in only a subset of resistant cancer cells, or that it might be present only in a minority of copies of the *EGFR* gene in each tumor cell.

T790M mutation has been found in visceral sites but not in the central nervous system (Balak *et al*., 2006); this observation suggests that the selective pressure for mutations conferring resistance could be different in the central nervous system, where drug levels appear to be lower than in the periphery (Jackman *et al*., 2006). Consistent with this notion, a different mutation (D761Y in exon 19) has been found in a patient with acquired resistance to gefitinib that developed in the brain (Balak *et al*., 2006). However, since D761Y mutation is found in primary refractory lung cancer and functional analysis of it did not indicate gefitinib resistance, the significance of D761Y mutation in gefitinib resistance is still unclear (Tokumo *et al*., 2006).

MET Amplification

In about 50% of cases of resistance to gefitinib and erlotinib, the resistance is due to the occurrence of a secondary

T790M mutation in EGFR (Balak *et al*., 2006; Kosaka *et al*., 2006; Engelman *et al*., 2007). The mechanisms contributing to resistance in the remaining tumors are unknown. Recently, using gefitinib-resistant clones from an *EGFR* mutant lung cancer cell line, amplification of the *MET* oncogene and continuous activation of ERBB3/PI3K/Akt signaling in the presence of gefitinib were found (Engelman *et al*., 2007; Table 21.3). Inhibition of MET signaling in these cells restored their sensitivity to gefitinib in an *ex vivo* experiment. *MET* amplification was detected in 4 of 18 (22%) human lung cancer specimens that had become resistant to gefitinib or erlotinib.

Moreover, *MET* amplification might be related to primary resistance to gefitinib. *MET* mRNA overexpression occurs in approximately 10% of squamous cell carcinomas of the lung (Tsao *et al*., 1998) which overexpress wild-type EGFR. EGFR is phosphorylated by MET in *MET*-amplified cell lines (Lutterbach *et al*., 2007). This suggests that inhibition of wild-type EGFR signaling by gefitinib and supported by MET inhibitors might be effective in treating primary gefitinib-refractory lung cancer as well as lung cancers with *MET*-amplified acquired resistance.

Clinical Factors Affecting Acquired Resistance to Gefitinib

Little is known concerning the clinical factors affecting acquired resistance to gefitinib in NSCLC patients. Segawa *et al*. (2006) reported that brain metastasis is the strongest clinical predictor of the emergence of acquired resistance to gefitinib in a retrospective study focusing on previously treated Japanese patients with advanced NSCLC who had benefited from gefitinib treatment for at least 6 months. In addition, decreased baseline hemoglobin level and administration of more than one chemotherapy regimen before gefitinib treatment are potential predictors of the development of acquired resistance. Although it is unclear why NSCLC patients with brain metastasis tend to develop acquired resistance to gefitinib, any extrathoracic site of disease might portend inferior survival, since patients with extrathoracic lesions such as bone, liver, and adrenal metastases had a poor prognosis in that study.

Overcoming Acquired Resistance to Gefitinib

The recent discoveries of T790M mutation and *MET* gene amplification will alter the strategy used for the treatment of NSCLC patients who become resistant to gefitinib. When T790M mutations are found, irreversible EGFR-TK inhibitors are administered. When *MET* amplifications are found, MET inhibitors should be administered in addition to gefitinib in future clinical trials (Janne, 2007; Figure 21.1).

Many curious findings have been obtained in studies of resistance to gefitinib. We cannot address here how different mechanisms of resistance develop in the same cell line (Koizumi *et al*., 2005; Ogino *et al*., 2007; Table 21.3), how gefitinib induces or selects T790M mutation or *MET* amplification, how rechallenge with gefitinib in patients who initially responded to gefitinib after a rest from gefitinib is sometimes effective (Kurata *et al*., 2004), or how gefitinib restores sensitivity to chemotherapy (Fujiwara *et al*., 2005). If resistance to gefitinib can be overcome, advanced NSCLC patients

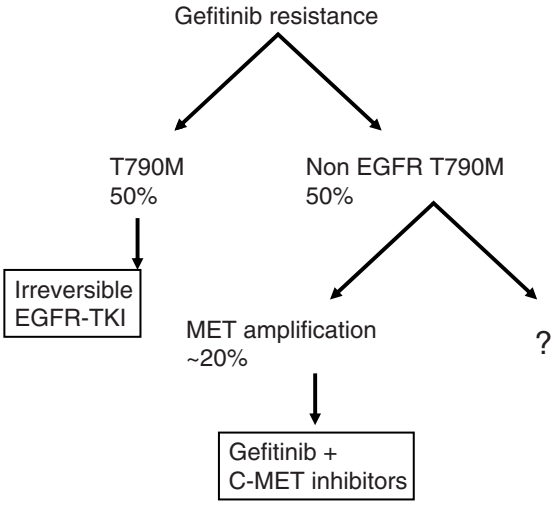

FIGURE 21.1. Treatment strategy for resistance to gefitinib in patients who responded to gefitinib

will be able to survive like those with chronic diseases such as diabetes mellitus and hypertension (see chapter 20 in this volume).

REFERENCES

Asahina, H., Yamazaki, K., Kinoshita, I., Sukoh, N., Harada, M., Yokouchi, H., Ishida, T., Ogura, S., Kojima, T., Okamoto, Y., Fujita, Y., Dosaka-Akita, H., Isobe, H., and Nishimura, M. 2006. A phase II trial of gefitinib as first-line therapy for advanced non-small cell lung cancer with epidermal growth factor receptor mutations. *Br. J. Cancer 95*: 998–1004.

Balak, M.N., Gong, Y., Riely, G.J., Somwar, R., Li, A.R., Zakowski, M.F., Chiang, A., Yang, G., Ouerfelli, O., Kris, M.G., Ladanyi, M., Miller, V.A., and Pao, W. 2006. Novel D761Y and common secondary T790M mutations in epidermal growth factor receptor-mutant lung adenocarcinomas with acquired resistance to kinase inhibitors. *Clin. Cancer Res. 12*: 6494–6501.

Carter, T.A., Wodicka, L.M., Shah, N.P., Velasco, A.M., Fabian, M.A., Treiber, D.K., Milanov, Z.V., Atteridge, C.E., Biggs, W.H. 3rd, Edeen, P.T., Floyd, M., Ford, J.M., Grotzfeld, R.M., Herrgard, S., Insko, D.E., Mehta, S.A., Patel, H.K., Pao, W., Sawyers, C.L., Varmus, H., Zarrinkar, P.P., and Lockhart, D.J. 2005. Inhibition of drug-resistant mutants of ABL, KIT, and EGF receptor kinases. *Proc. Natl. Acad. Sci. USA 102*: 11011–11016.

Choi, S.H., Mendrola, J.M., and Lemmon, M.A. 2007. EGF-independent activation of cell-surface EGF receptors harboring mutations found in gefitinib-sensitive lung cancer. *Oncogene 26*: 1567–1576.

Engelman, J.A., Mukohara, T., Zejnullahu, K., Lifshits, E., Borras, A.M., Gale, C.M., Naumov, G.N., Yeap, B.Y., Jarrell, E., Sun, J., Tracy, S., Zhao, X., Heymach, J.V., Johnson, B.E., Cantley, L.C., and Janne, P.A. 2006. Allelic dilution obscures detection of a biologically significant resistance mutation in EGFR-amplified lung cancer. *J. Clin. Invest. 116*: 2695–2706.

Engelman, J.A., Zejnullahu, K., Mitsudomi, T., Song, Y., Hyland, C., Park, J.O., Lindeman, N., Gale, C.M., Zhao, X., Christensen, J., Kosaka, T., Holmes, A.J., Rogers, A.M., Cappuzzo, F., Mok, T., Lee, C., Johnson, B.E., Cantley, L.C., and Janne, P.A. 2007. MET amplification leads to gefitinib resistance in lung cancer by activating ERBB3 signaling. *Science 316*: 1039–1043.

Fujiwara, K., Kiura, K., Ueoka, H., Tabata, M., Hamasaki, S., and Tanimoto, M. 2003. Dramatic effect of ZD1839 ('Iressa') in a patient with advanced non-small-cell lung cancer and poor performance status. *Lung Cancer 40*: 73–76.

Fujiwara, K., Kiura, K., Gemba, K., Ogata, Y., Hotta, K., Kishino, D., Tabata, M., Ueoka, H., and Tanimoto, M. 2005. Gefitinib ('Iressa', ZD1839) may restore chemosensitivity in NSCLC patients? *Anticancer Res. 25*: 547–549.

Fukuoka, M., Yano, S., Giaccone, G.., Tamura, T., Nakagawa, K., Douillard, J.Y., Nishiwaki, Y., Vansteenkiste, J., Kudoh, S., Rischin, D., Eek, R., Horai, T., Noda, K., Takata, I., Smit, E., Averbuch, S., Macleod, A., Feyereislova, A., Dong, R.P., and Baselga, J. 2003. Multi-institutional randomized phase II trial of gefitinib for previously treated patients with advanced non-small-cell lung cancer (The IDEAL 1 Trial). *J. Clin. Oncol. 21*: 2237–2246.

Greulich, H., Chen, T.H., Feng, W., Janne, P.A., Alvarez, J.V., Zappaterra, M., Bulmer, S.E., Frank, D.A., Hahn, W.C., Sellers, W.R., and Meyerson, M. 2005. Oncogenic transformation by inhibitor-sensitive and -resistant EGFR mutants. *PLoS Med. 2*: e313.

Inoue, A., Suzuki, T., Fukuhara, T., Maemondo, M., Kimura, Y., Morikawa, N., Watanabe, H., Saijo,

Y., and Nukiwa, T. 2006. Prospective phase II study of gefitinib for chemotherapy-naive patients with advanced non-small-cell lung cancer with epidermal growth factor receptor gene mutations. *J. Clin. Oncol. 24*: 3340–2346.

Jackman, D.M., Holmes, A.J., Lindeman, N., Wen, P.Y., Kesari, S., Borras, A.M., Bailey, C., de Jong, F., Janne, P.A., and Johnson, B.E. 2006. Response and resistance in a non-small-cell lung cancer patient with an epidermal growth factor receptor mutation and leptomeningeal metastases treated with high-dose gefitinib. *J. Clin. Oncol. 24*: 4517–4520.

Janne, P. 2007. Targeted therapies for targeted patients: translational research in lung cancer. AACR Annual Meeting April 14–18, 2007, Los Angeles, CA.

Ji, H., Li, D., Chen, L., Shimamura, T., Kobayashi, S., McNamara, K., Mahmood, U., Mitchell, A., Sun, Y., Al-Hashem, R., Chirieac, L.R., Padera, R., Bronson, R.T., Kim, W., Janne, P.A., Shapiro, G.I., Tenen, D., Johnson, B.E., Weissleder, R., Sharpless, N.E., and Wong, K.K. 2006. The impact of human EGFR kinase domain mutations on lung tumorigenesis and in vivo sensitivity to EGFR-targeted therapies. *Cancer Cell 9*: 485–495.

Kobayashi, S., Boggon, T.J., Dayaram, T., Janne, P.A., Kocher, O., Meyerson, M., Johnson, B.E., Eck, M.J., Tenen, D.G., and Halmos, B. 2005. EGFR mutation and resistance of non-small-cell lung cancer to gefitinib. *N. Engl. J. Med. 352*: 786–792.

Kohno, T., Takahashi, M., Manda, R., and Yokota, J. 1998. Inactivation of the PTEN/MMAC1/TEP1 gene in human lung cancers. *Genes Chromosomes Cancer 22*: 152–156.

Koizumi, F., Shimoyama, T., Taguchi, F., Saijo, N., and Nishio, K. 2005. Establishment of a human non-small cell lung cancer cell line resistant to gefitinib. *Int. J. Cancer 116*: 36–44.

Kosaka, T., Yatabe, Y., Endoh, H., Kuwano, H., Takahashi, T., and Mitsudomi, T. 2004. Mutations of the epidermal growth factor receptor gene in lung cancer: biological and clinical implications. *Cancer Res. 64*: 8919–8923.

Kosaka, T., Yatabe, Y., Endoh, H., Yoshida, K., Hida, T., Tsuboi, M., Tada, H., Kuwano, H., and Mitsudomi, T. 2006. Analysis of epidermal growth factor receptor gene mutation in patients with non-small cell lung cancer and acquired resistance to gefitinib. *Clin. Cancer Res. 12*: 5764–5769.

Kris, M.G., Natale, R.B., Herbst, R.S., Lynch, T.J. Jr, Prager, D., Belani, C.P., Schiller, J.H., Kelly, K., Spiridonidis, H., Sandler, A., Albain, K.S., Cella, D., Wolf, M.K., Averbuch, S.D., Ochs, J.J., and Kay, A.C. 2003. Efficacy of gefitinib, an inhibitor of the epidermal growth factor receptor tyrosine kinase, in symptomatic patients with non-small cell lung cancer: a randomized trial. *JAMA 290*: 2149–2158.

Kurata, T., Tamura, K., Kaneda, H., Nogami, T., Uejima, H., Asai, G., Nakagawa, K., and Fukuoka, M. 2004. Effect of re-treatment with gefitinib ('Iressa', ZD1839) after acquisition of resistance. *Ann. Oncol. 15*: 173–174.

Lutterbach, B., Zeng, Q., Davis, L.J., Hatch, H., Hang, G., Kohl, N.E., Gibbs, J.B., and Pan, B.S. 2007. Lung cancer cell lines harboring MET gene amplification are dependent on Met for growth and survival. *Cancer Res. 67*: 2081–2088.

Lynch, T.J., Bell, D.W., Sordella, R., Gurubhagavatula, S., Okimoto, R.A., Brannigan, B.W., Harris, P.L., Haserlat, S.M., Supko, J.G., Haluska, F.G., Louis, D.N., Christiani, D.C., Settleman, J., and Haber, D.A. 2004. Activating mutations in the epidermal growth factor receptor underlying responsiveness of non-small-cell lung cancer to gefitinib. *N. Engl. J. Med. 350*: 2129–2139.

Mendelsohn, J. 2000. Blockade of receptors for growth factors: an anticancer therapy: The Fourth Annual Joseph H. Bacchanal American Association for Cancer Research Clinical Research Award Lecture. *Clin. Cancer Res. 6*: 747–753.

Miller, V.A., Kris, M.G., Shah, N., Patel, J., Azzoli, C., Gomez, J., Krug, L.M., Pao, W., Rizvi, N., Pizzo, B., Tyson, L., Venkatraman, E., Ben-Porat, L., Memoli, N., Zakowski, M., Rusch, V., and Heelan, R.T. 2004. Bronchioloalveolar pathologic subtype and smoking history predict sensitivity to gefitinib in advanced non-small-cell lung cancer. *J. Clin. Oncol. 22*: 1103–1109.

Ogino, A., Kitao, H., Hirano, S., Uchida, A., Takigawa, N., Tabata, M., Takata, M., Kiura, K., and Tanimoto, M. 2007. Emergence of EGFR T790M mutation during chronic exposure to gefitinib in a NSCLC cell line. AACR

Annual Meeting #4005, April 14–18, 2007, Los Angeles, CA.

Ohashi, K., Rai, K., Kiura, K., Osawa, M., Hirano, S., Fujiwara, Y., Yoshino, T., Takigawa, N., Takata, M., and Tanimoto, M. 2007. Transgenic mice with mouse EGFR mutation developed lung adenocarcinoma. AACR Annual Meeting LB-106, April 14–18, 2007, Los Angeles, CA.

Paez, J.G., Janne, P.A., Lee, J.C., Tracy, S., Greulich, H., Gabriel, S., Herman, P., Kaye, F.J., Lindeman, N., Boggon, T.J., Naoki, K., Sasaki, H., Fujii, Y., Eck, M.J., Sellers, W.R., Johnson, B.E., and Meyerson, M. 2004. EGFR mutations in lung cancer: correlation with clinical response to gefitinib therapy. *Science 304*: 1497–1500.

Pao, W., Wang, T.Y., Riely, G.J., Miller, V.A., Pan, Q., Ladanyi, M., Zakowski, M.F., Heelan, R.T., Kris, M.G., and Varmus, H.E. 2005a. KRAS mutations and primary resistance of lung adenocarcinomas to gefitinib or erlotinib. *PLoS Med. 2*: e17.

Pao, W., Miller, V.A., Politi, K.A., Riely, G.J., Somwar, R., Zakowski, M.F., Kris, M.G., and Varmus, H. 2005b. Acquired resistance of lung adenocarcinomas to gefitinib or erlotinib is associated with a second mutation in the EGFR kinase domain. *PLoS Med. 2*: e73.

Politi, K., Zakowski, M.F., Fan, P.D., Schonfeld, E.A., Pao, W., and Varmus, H.E. 2006. Lung adenocarcinomas induced in mice by mutant EGF receptors found in human lung cancers respond to a tyrosine kinase inhibitor or to down-regulation of the receptors. *Genes Dev. 20*: 1496–1510.

Segawa, Y., Hotta, K., Umemura, S., Fujiwara, Y., Shinkai, T., Ueoka, H., Takigawa, N., Tabata, M., Kiura, K., and Tanimoto, M. 2006. Clinical factors affecting acquired resistance to gefitinib in previously treated Japanese patients with advanced non small cell lung cancer. *Cancer 107*: 1866–1872.

Sharma, S.V., Bell, D.W., Settleman, J., and Haber, D.A. 2007. Epidermal growth factor receptor mutations in lung cancer. *Nat Rev. Cancer 7*: 169–181.

She, Q.B., Solit, D., Basso, A., and Moasser, M.M. 2003. Resistance to gefitinib in PTEN-null HER-overexpressing tumor cells can be overcome through restoration of PTEN function or pharmacologic modulation of constitutive phosphatidylinositol 3´-kinase/Akt pathway signaling. *Clin. Cancer Res. 9*: 4340–4346.

Shigematsu, H., Lin, L., Takahashi, T., Nomura, M., Suzuki, M., Wistuba, I.I., Fong, K.M., Lee, H., Toyooka, S., Shimizu, N., Fujisawa, T., Feng, Z., Roth, J.A., Herz, J., Minna, J.D., and Gazdar, A.F. 2005. Clinical and biological features associated with epidermal growth factor receptor gene mutations in lung cancers. *J. Natl. Cancer Inst. 97*: 339–346.

Shigematsu, H., Toyooka, S., and Suzuki, M. 2006. The need for an individual approach to lung cancer treatment. *PLoS Med. 3*: e206.

Soria, J.C., Lee, H.Y., Lee, J.I., Wang, L., Issa, J.P., Kemp, B.L., Liu, D.D., Kurie, J.M., Mao, L., and Khuri, F.R. 2002. Lack of PTEN expression in non-small cell lung cancer could be related to promoter methylation. *Clin. Cancer Res. 8*: 1178–1184.

Stamos, J., Sliwkowski, M.X., and Eigenbrot, C. 2002. Structure of the epidermal growth factor receptor kinase domain alone and in complex with a 4-anilinoquinazoline inhibitor. *J. Biol. Chem. 277*: 46265–46272.

Sunaga, N, Tomizawa, Y., Yanagitani, N., Iijima, H., Kaira, K., Shimizu, K., Tanaka, S., Suga, T., Hisada, T., Ishizuka, T., Saito, R., Dobashi, K., and Mori, M. 2007. Phase II prospective study of the efficacy of gefitinib for the treatment of stage III/IV non-small cell lung cancer with EGFR mutations, irrespective of previous chemotherapy. *Lung Cancer 56*: 383–389.

Sutani, A., Nagai, Y., Udagawa, K., Uchida, Y., Koyama, N., Murayama, Y., Tanaka, T., Miyazawa, H., Nagata, M., Kanazawa, M., Hagiwara, K., and Kobayashi, K. 2006. Gefitinib for non-small-cell lung cancer patients with epidermal growth factor receptor gene mutations screened by peptide nucleic acid-locked nucleic acid PCR clamp. *Br. J. Cancer 95*: 1483–1489.

Therasse, P., Arbuck, S.G., Eisenhauer, E.A., Wanders, J., Kaplan, R.S., Rubinstein, L., Verweij, J., Van Glabbeke, M., van Oosterom, A.T., Christian, M.C., and Gwyther, S.G. 2000. New guidelines to evaluate the response to treatment in solid tumors. European Organization for Research and Treatment of Cancer, National Cancer Institute of the United States, National Cancer Institute of Canada. *J. Natl. Cancer Inst. 92*: 205–216.

Tokumo, M., Toyooka, S., Ichihara, S., Ohashi, K., Tsukuda, K., Ichimura, K., Tabata, M., Kiura, K., Aoe, M., Sano, Y., Date, H., and Shimizu, N. 2006. Double mutation and gene copy number of EGFR in gefitinib refractory non-small-cell lung cancer. *Lung Cancer 53*: 117–121.

Toyooka, S., Kiura, K., and Mitsudomi, T. 2005. EGFR mutation and response of lung cancer to gefitinib. *N. Engl. J. Med. 352*: 2136.

Tsao, M.S., Liu, N., Chen, J.R., Pappas, J., Ho, J., To, C., Viallet, J., Park, M., and Zhu, H. 1998. Differential expression of Met/hepatocyte growth factor receptor in subtypes of non-small cell lung cancers. *Lung Cancer 20*: 1–16.

Uchida, A., Hirano, S., Kitao, H., Ogino, A., Rai, K., Toyooka, S., Takigawa, N., Tabata, M., Takata, M., Kiura, K., and Tanimoto, M. 2007. Activation of downstream epidermal growth factor receptor (EGFR) signaling provides gefitinib-resistance in cells carrying EGFR mutation. *Cancer Sci. 98*: 357–363.

Veale, D., Ashcroft, T., Marsh, C., Gibson, G.J., and Harris, A.L. 1987. Epidermal growth factor receptors in non-small cell lung cancer. *Br. J. Cancer 55*: 513–516.

Ward, W.H., Cook, P.N., Slater, A.M., Davies, D.H., Holdgate, G.A., and Green, L.R. 1994. Epidermal growth factor receptor tyrosine kinase. Investigation of catalytic mechanism, structure-based searching and discovery of a potent inhibitor. *Biochem. Pharmacol. 48*: 659–666.

Yun, C.H., Woo, M.S., Greulich, H., Meyerson, M., Wong, K.K., and Eck, M.J. 2007. EGFR kinase mutations in NSCLC: unexpected structural and kinetic insights into the mechanism of the T790M resistance mutation and its inhibition by irreversible inhibitors including HKI-272. AACR Annual Meeting LB-367, April 14–18, 2007, Los Angeles, CA.

Zhang, X., Gureasko, J., Shen, K., Cole, P.A., and Kuriyan, J. 2006. An allosteric mechanism for activation of the kinase domain of epidermal growth factor receptor. *Cell 125*: 1137–1149.

22
Prognostic Significance of [^{18}F]-Fluorodeoxyglucose Uptake on Positron Emission Tomography in Patients with Pathological Stage I Lung Adenocarcinoma

Hiroaki Nomori

INTRODUCTION

Although patients with stage II or III non-small cell lung cancer (NSCLC) can generally be considered candidates for postoperative chemotherapy, it is still difficult to determine whether it would be useful for patients with stage I after complete resection. To determine the potential usefulness of postoperative adjuvant chemotherapy in patients with stage I NSCLC, it is important to clarify the prognostic factors in these patients.

In recent years, [^{18}F]fluoro-2-deoxyglucose uptake on positron emission tomography (FDG-PET) has been frequently used for diagnosis and staging of lung cancer (Gould *et al*., 2001; Marom *et al*., 2002; Nomori *et al*., 2004a). It has also been reported that FDG uptake on PET can be a prognostic factor in patients with NSCLC (Cerfolio *et al*., 2005; Vansteenkiste *et al*., 1999). However, FDG uptake is dependent on the histological cell type of NSCLC, i.e., FDG uptake by adenocarcinoma is correlated with pathological tumor stage and tumor invasiveness, whereas that of other histological types is not (Nomori *et al*., 2004a; Sagawa *et al*., 2006). Therefore, we consider that the prognostic significance of FDG uptake should be examined in adenocarcinomas, but not in NSCLC including all histological types. Therefore, in the present study, we examined the prognostic significance of FDG uptake in patients with pathological stage I lung adenocarcinoma.

PATIENTS AND METHODS

Between December 2001 and January 2005, FDG-PET was performed for 377 patients with pulmonary nodules. Of these patients, 232 had NSCLC and underwent surgery. Of the 232 patients, 109 had pathological stage I disease. We excluded 6 patients whose tumors were < 1 cm in diameter because the spatial resolution of the PET scanner is 0.7–0.8 cm, making it difficult to image pulmonary nodules that measure < 1 cm (Nomori et al., 2004b). We also excluded 4 patients with

TABLE 22.1. Patient characteristics and number of patients with recurrence.

	Number of patients	Number of recurred patients	Difference
Sex			
Male	56	9	N.S
Female	42	3	
Age (year-old)			
60	64	7	N.S
60	34	5	
Histological grade of differentiation			
Well	47	2	0.036†
Moderately	39	6	
Poorly	12	4	
Surgery			
Pneumonectomy	1	1	N.S.
Lobectomy	80	9	
Segmentectomy	17	2	
Pathologic stage			
IA	63	6	N.S.
IB	35	6	
SUV			
3.3	43	10	0.02
3.3	55	2	

N.S. = not significant

squamous cell carcinoma and 1 patient with carcinosarcoma. As a result, 98 patients with pathological stage I adenocarcinoma, who underwent FDG-PET scanning followed by major pulmonary resection with systematic lymph node dissection, were eligible to participate in this study (Table 22.1). The medical records of each patient were examined with regard to sex, age, operative procedure, tumor stage (stage IA or IB) and histological grade of differentiation. The tumor stages were based on the TNM classification of the International Union Against Cancer (Sobin and Witterkind, 2002). Patients were excluded if they had undergone any chemotherapy or radiotherapy before PET scanning. The histological grade was classified as well, moderate, or poorly differentiated.

PET Data Analysis

The FDG-PET data were evaluated semiquantitatively on the basis of maximum standardized uptake value (SUV). To measure the maximum SUV, a region of interest (ROI) was placed over the tumor after correction for radioactive decay. Then, the maximum activity in the tumor ROI was calculated as tumor activity/injected dose/body weight.

Follow-up and Assessment of Tumor Recurrence

Patients were followed for cancer recurrence. Follow-up data were obtained every 3 months for the first 2 years and every 6 months thereafter. Chest and abdominal CT examinations were performed every 6 months. Each follow-up visit was supplemented by chest radiography, serum biochemistry, tumor marker assay, and any other test required to examine suspected tumor recurrence. In addition, if patients became symptomatic or showed abnormal laboratory findings, appropriate testing (i.e., brain CT and bone scintigraphy) was also performed. Recurrence was defined as any unequivocal occurrence of new cancer foci in a disease-free patient.

Statistical Analysis

Receiver operating characteristic (ROC) curves of SUV for the prediction of recurrence were generated using MedCalc (Medisoftware, Mariakerke, Belgium) by plotting sensitivity versus 1-specificity for varying thresholds of SUV. Patients with recurrence who exceeded the SUV threshold were defined as true-positive and patients without recurrence whose SUVs were less than this were defined as true-negative. Patients with recurrence whose SUVs were below the threshold were defined as false-negative, and patients without recurrence who exceeded the SUV

threshold were defined as false-positive. Sensitivity was calculated as true-positive/true-positive + false-negative, and specificity as true-negative/true-negative + false-positive. The ROC curve was used to determine the cut-off value that yielded the optimal sensitivity and specificity.

The duration of disease-free survival was measured from the date of surgery until the first evidence of recurrence or the last date of follow-up for patients who remained alive and disease-free. The disease-free interval was analyzed according to the Kaplan-Meier method. Univariate analysis with a 2-sided log-rank test for all variables was performed initially to assess the difference in disease-free survival. Variables with the potential for a significant difference between groups on the basis of the results of this analysis were then subjected to multivariate analysis with the Cox proportional-hazards model with both forward and backward stepwise inclusion of factors. Differences at $p < 0.05$ were defined as being statistically significant.

RESULTS

Univariate Analysis

The median follow-up period after surgery in the 98 patients was 31 months (range: 14–50 months). There was no surgical death or loss to follow-up. Twelve patients, i.e., 6 patients each with stage IA and IB, suffered disease recurrence after surgery. The ROC curve showed that the optimal cut-off value for predicting recurrence was 3.3.

Table 22.1 shows the patient characteristics including sex, age (≧60 or <60 years), histological grade of differentiation (well, moderately or poorly differentiated), surgical procedure (pneumonectomy, lobectomy or segmentectomy), and SUV (≧3.3 or <3.3). Sixty-four patients were aged 60 years or older and 34 were younger than 60. There were 56 male and 42 female patients. Surgical procedures included pneumonectomy in 1, lobectomy in 80, and segmentectomy in 17 patients. Histologically, the tumors were well differentiated in 47 patients, moderately differentiated in 39 and poorly differentiated in 12 patients. Sixty-three patients had stage IA disease and 35 had stage IB disease. Forty-three patients had tumors with SUV ≧ 3.3 and 55 patients with SUV < 3.3.

Seventeen (27%) of the 63 patients with stage IA disease and 26 (74%) of the 35 patients with stage IB disease had tumors with SUV ≧ 3.3 (Table 22.2). Among the 12 patients with recurrence, 4 (67%) of the 6 patients with stage IA disease and all (100%) of the 6 patients with stage IB

TABLE 22.2. Correlation between the pathological stage and the cutoff value of FDG uptake.

		SUV	
Stage	Number of patients	3.3	< 3.3
IA	63	17	46
IB	35	26	9
Total	98	44	54

SUV= standardized uptake value

TABLE 22.3. Correlation between the number of patients with recurrence and FDG uptake measured by standardized uptake value

		SUV	
Stage	Number of patients	3.3	3.3
IA	6	4	2
IB6	6	0	
Total	12	10	2

SUV= standardized uptake value

disease had tumors with SUV ≧ 3.3 (Table 22.3). All 9 of the patients with stage IB disease showing SUV < 3.3 (see Table 22.2) had no recurrence.

Univariate analysis showed that patients with SUV ≧ 3.3 and moderately or poorly differentiated adenocarcinomas showed more frequent recurrence than those with SUV < 3.3 and well differentiated tumors (p = 0.020 and 0.036, respectively) (Table 22.1, Figures 22.1 and 22.2). Both of the 2 patients with recurrence of well differentiated adenocarcinoma (Table 22.1) had SUV ≧ 3.3. For both stage IA and IB disease, patients with SUV ≧ 3.3 showed more frequent recurrence than those with SUV < 3.3 (stage IA, p = 0.018, stage IB, p < 0.001). There were no significant correlations between recurrence and other variables including sex, age, surgical procedure, and pathological stage.

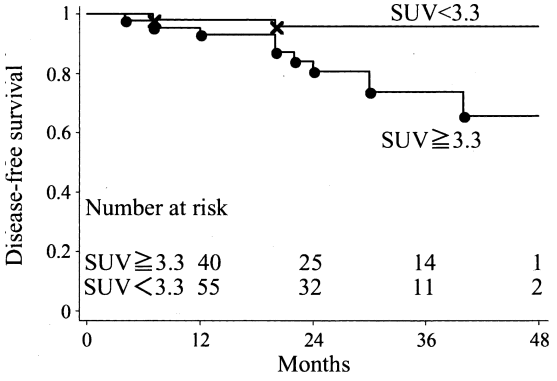

FIGURE 22.1. Disease-free survival of the 98 patients with pathological stage I adenocarcinoma according to the CR of the primary tumor

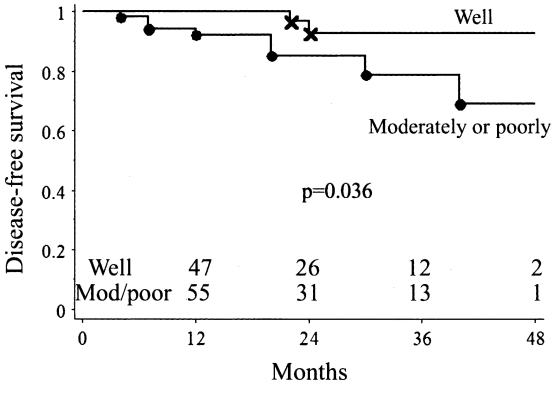

FIGURE 22.2. Disease-free survival of the 98 patients with pathological stage I adenocarcinoma according to the histological grade of differentiation.

Multivariate Analysis

Multivariate analysis showed that while SUV with a cut-off value of 3.3 did not reach significance, it was able to predict tumor recurrence well (p = 0.079). Histological grade of cell differentiation showed no correlation with tumor recurrence (p = 0.28)

DISCUSSION

Although TNM staging is the most important prognostic factor in patients with NSCLC, it is well known that 30% of patients with stage I disease die due to recurrence within 5 years after surgery (Ohtsuka *et al.*, 2004; Pairolero *et al.*, 1984). While some studies have shown that postoperative adjuvant chemotherapy can increase survival in NSCLC patients with stage IB or II disease (Johnson and Rabin, 2005; Kato *et al.*, 2004; Winton *et al.*, 2005), it has been unclear which population would benefit most from adjuvant chemotherapy. In addition, there have been no data to indicate the value of adjuvant chemotherapy for patients with pathological stage IA NSCLC.

We reported that clinical stage IA lung adenocarcinomas with high FDG uptake had more frequent lymph node

metastasis, higher tumor invasiveness, and proliferative activity determined by Ki-67 staining than those with low FDG uptake (Watanabe *et al*., 2006). The present study also revealed that patients with adenocarcinomas showing SUV ≧ 3.3 had poorer disease-free survival than those showing SUV < 3.3, for both stage IA and IB disease. Although further research is needed to further define the usefulness of adjuvant chemotherapy for patients with pathological stage I disease, our data suggest that patients with pathological stage I disease showing SUV ≧ 3.3 could be candidates for adjuvant chemotherapy. We also found that none of the 9 patients with stage IB disease showing SUV < 3.3 suffered disease recurrence. While several studies have reported the benefit of adjuvant treatment for stage IB NSCLC (Johnson and Rabin, 2005; Kato *et al*., 2004; Winton *et al*., 2005), it appears that adjuvant chemotherapy would not be necessary for patients with stage IB lung adenocarcinoma with SUV < 3.3.

While the present study showed that the SUV cut-off value for predicting tumor recurrence was 3.3, Cerfolio *et al*. (2005) and Vansteenkiste *et al*. (1999) reported it to be 10 and 7, respectively. The difference between our results and theirs can be explained as follows: (1) While the previous 2 reports examined NSCLC patients with stage I–IV disease, including patients who were not considered candidates for surgical treatment, we examined only patients with pathological stage I disease treated by complete resection and mediastinal lymph node dissection. (2) While the previous 2 reports examined patients with all histological types of NSCLC, the present study was limited to adenocarcinoma. Because it is reasonable to conclude that patients with advanced disease would have a higher SUV and poorer prognosis than those with early-stage disease, SUV could be an important prognostic factor when examining patients with stage I–IV disease. Cerfolio *et al*. (2005) analyzed their data in detail and reported that NSCLC patients with SUV ≧ 10 had a higher frequency of recurrence than those with SUV < 10 for disease stages IB and II, whereas this difference was not significant for stage IA. In addition, it has been reported that the relationship between FDG uptake and tumor aggressiveness is significant in adenocarcinoma, but not in other histological types of NSCLC (Nomori *et al*., 2004a, b; Sagawa *et al*., 2006). Therefore, we examined the prognostic significance of SUV to determine the potential value of postoperative adjuvant treatment for patients with stage IA and IB adenocarcinoma, and found that the cut-off value was 3.3.

It has been reported that patients with well-differentiated adenocarcinoma generally have a better postoperative prognosis than those with moderately or poorly differentiated adenocarcinoma at pathological stage IA (Noguchi *et al*., 1995). Although the present study also yielded similar results, the prognostic importance of histological grade of differentiation was found not to be significant in multivariate analysis. In fact, both of 2 patients who suffered recurrence of well differentiated adenocarcinoma had tumors with SUV ≧ 3.3. Our results showed that the maximum SUV could be a more reliable factor for predicting recurrence than histological grade of differentiation in patients with pathological stage I adenocarcinoma. We conclude that FDG uptake measured by maximum SUV has potential value as an

independent prognostic factor in patients with stage I lung adenocarcinoma after surgery, and therefore could yield important information for determining the usefulness of adjuvant chemotherapy in such patients.

REFERENCES

Cerfolio, RJ, Bryant, AS, Ohja, B, and Bartolucci, AA. 2005. The maximum standardized uptake values on positron emission tomography of a non-small cell lung cancer predict stage, recurrence, and survival. *J. Thorac Cardiovasc. Surg. 130*: 151–159.

Gould, MK, Maclean, CC, Kuschner, WG, Rydzak, CE, and Owens, DK. 2001. Accuracy of positron emission tomography for diagnosis of pulmonary nodules and mass lesions: a meta-analysis. *JAMA 285*: 914–924.

Johnson, BE, and Rabin, MS. 2005. Patient subsets benefiting from adjuvant therapy following surgical resection of non-small cell lung cancer. *Clin. Cancer Res. 11*: 5022s–5026s.

Kato, H, Ichinose, Y, Ohta, M, Tsubota, N, Tada, H, Watanabe, Y, Wada, H, Tsuboi, M, Hamajima N, and Ohta, M; Japan Lung Cancer Research Group on Postsurgical Adjuvant Chemotheraphy. 2004. A randomized trial of adjuvant chemotherapy with uracil-tegafur for adenocarcinoma of the lung. *N. Engl. J. Med. 350*: 1713–1721.

Marom, EM, Sarvis, S, Herndon, JE, 2nd, and Patz, EF, Jr. 2002. T1 lung cancers: sensitivity of diagnosis with fluorodeoxyglucose PET. *Radiology 223*: 453–459.

Noguchi, M, Morikawa, A, Kawasaki, M, Matsuno, Y, Yamada, T, Hirohashi, S, Kondo, H, and Shimosato, Y. 1995. Small adenocarcinoma of the lung. Histologic characteristics and prognosis. *Cancer 75*: 2844–2852.

Nomori, H, Watanabe, K, Ohtsuka, T, Naruke, T, Suemasu, K, Kobayashi, T, and Uno, K. 2004a. Fluorine 18-tagged fluorodeoxyglucose positron emission tomographic scanning to predict lymph node metastasis, invasiveness, or both, in clinical T1 N0 M0 lung adenocarcinoma. *J. Thorac. Cardiovasc. Surg. 128*: 396–401.

Nomori, H, Watanabe, K, Ohtsuka, T, Naruke, T, Suemasu, K, and Uno, K. 2004b. Evaluation of F-18 fluorodeoxyglucose (FDG) PET scanning for pulmonary nodules less than 3 cm in diameter, with special reference to the CT images. *Lung Cancer 45*: 19–27.

Ohtsuka, T, Nomori, H, Horio, H, Naruke, T, and Suemasu, K. 2004. Is major pulmonary resection by video-assisted thoracic surgery an adequate procedure in clinical stage I lung cancer? *Chest 125*: 1742–1746.

Pairolero, PC, Williams, DE, Bergstralh, EJ, Piehler JM, Bernatz, PE, and Payne, WS. 1984. Postsurgical stage I bronchogenic carcinoma: morbid implications of recurrent disease. *Ann. Thorac. Surg. 38*: 331–338.

Sagawa, M, Higashi, K, Sugita, M, Ueda, Y, Maeda, S, Toga, H, and Sakuma, T. 2006. Fluorodeoxyglucose uptake correlates with the growth pattern of small peripheral pulmonary adenocarcinoma. *Surg. Today 36*: 230–234.

Sobin, LH, and Witterkind, C. 2002. UICC: TNM classification of malignant tumors. New York: Wiley.

Vansteenkiste, JF, Stroobants, SG, Dupont, PJ, De Leyn, PR, Verbeken, EK, Deneffe, GJ, Mortelmans, LA, and Demedts, MG. 1999. Prognostic importance of the standardized uptake value on (18)F-fluoro-2-deoxy-glucose-positron emission tomography scan in non-small-cell lung cancer: An analysis of 125 cases. Leuven Lung Cancer Group. *J. Clin. Oncol. 17*: 3201–3206.

Watanabe, K, Nomori, H, Ohtsuka, T, Naruke, T, Ebihara, A, Orikasa, H, Yamazaki, K, Uno, K, Kobayashi, T, and Goya, T. 2006. [F-18]Fluorodeoxyglucose positron emission tomography can predict pathological tumor stage and proliferative activity determined by Ki-67 in clinical stage IA lung adenocarcinomas. *Jpn. J.Clin. Oncol. 36*: 403–409.

Winton, T, Livingston, R, Johnson, D, Rigas, J, Johnston, M, Butts, C, Cormier, Y, Goss, G, Inculet, R, Vallieres, E, Fry, W, Bethune, D, Ayoub, J, Ding, K, Seymour, L, Graham, B, Tsao, MS, Gandara, D, Kesler, K, Demmy, T, and Shepherd, F; National Cancer Institute of Canada Clinical Trials Group; National Cancer Institute of the United States Intergroup JBR. 10 Trial Investigators. 2005. Vinorelbine plus cisplatin vs. observation in resected non-small-cell lung cancer. *N. Engl. J. Med. 352*: 2589–2597.

23
Non-Small Cell Lung Cancer: Prognosis Using the TNM Staging System

Joachim Pfannschmidt, Heinrich Bulzebruck, and Hendrik Dienemann

INTRODUCTION

The importance of accurate staging according to the international TNM staging system of non-small cell lung cancer for patient management and evaluation of individual prognosis cannot be overemphasized. In the current TNM classification reported by the American Joint Committee on Cancer (AJCC) (2002) and International Union Against Cancer (IUAC) (2002), the primary tumor is subdivided into four categories (T1 to T4) depending on size, site, and local involvement. Lymph node spread has been subdivided into bronchopulmonary (N1), ipsilateral mediastinal (N2), and contralateral or supraclavicular disease (N3). Metastases are absent (M0) or present (M1). The TNM descriptors include clinical as well as pathologic parameters. Using clinical criteria alone, a significant number of tumors are understaged, compared to the stage based finally on the pathologic evaluation of sampled tissues. In non-small cell lung cancer the TNM system has been recognized internationally as the standard for staging disease extension. Four stages of lung cancer have been identified that are associated with significant difference in 5-year survival depending on the stage of disease according to the TNM classification system. It is important to emphasize that the TNM classification and stage grouping should be generally applied also to small cell lung carcinoma (SCLC). The grouping within "limited disease" and "extensive disease" has been widely used to describe staging in SCLC. Nevertheless, the current TNM classification is of significance for prognosis of SCLC and has the advantage of providing a uniform detailed classification of tumor spread.

HISTORY OF TNM

Mountain *et al*. (1974) described the lung cancer staging system for the American Joint Committee for Cancer Staging and End Results Reporting (AJCC) based on the TNM categories devised by Pierre Denoix (1946), who developed the TNM Classification of Cancer Stage. This scheme has been modified and refined over the years. Mountain (1986) presented a new international staging system for lung cancer developed by the AJCC and the Union internationale contre le cancer (UICC) in 1986. Although the staging

system functioned well, several problems became apparent due to differences in survival between subsets of the same stage. Changes included uncommon superficial spreading tumor of any size with its invasive component limited to the bronchial wall, which may extend proximal to the main bronchus. In the 3rd edition of the UICC classification (1982) it was classified as T2 or T3 category but modified in the 4th edition (1987), as T1 tumor. However, several other modifications regarding the importance of pleural fluid, separate tumor nodules found in the same and different lobes, and scalenus and supraclavicular lymph node involvement were introduced subsequently into the TNM staging system. The last revision of the TNM classification system was the 6th edition in 2002 and remained unchanged since the 5th edition (1997), by the International Union against Cancer (UICC) and the AJCC. Modifications included subdivision of stages I and II into A and B categories and the T3N0M0 into stage IIB. Despite the improvements of the 1997/2002 international staging system, there may be marked differences in postoperative 5-year survival rates within each stage. The TNM classification in the publications of the UICC and AJCC is identical, but formulated together in separate books, namely, the UICC TNM Classification of Malignant Tumors (2002) and the AJCC Cancer Staging Manual (2002). The staging system is planned to be updated in the next few years.

TNM DESCRIPTORS

In patients suspected of lung cancer, tissue diagnosis and clinical staging are critical in the planning of treatment strategies and defining individual prognosis. The staging process of patients suspected of having lung cancer should be reproducible and appropriate. Pretreatment clinical classification, designated cTNM is based on evidence acquired from physical examination, imaging, endoscopy, biopsy, surgical exploration, and other examinations. Pathologic postsurgical classification (pTNM) is based on evidence acquired before treatment and additional evidence supplied by surgical resection and histopathology. The pathologic assessment of the primary tumor (pT) entails resection of the primary tumor or biopsy specimen adequate to evaluate the highest pT category.

It was found by Pfannschmidt *et al.* (2007) in a retrospective data base analysis of 2,083 patients after surgical resection for NSCLC within the subgroups of patients according to pT categories, that there was a significant difference in survival between the pT1- and pT2- ($p < 0.001$) or between the pT2 and pT3 categories ($p = 0.005$) (Figure 23.1). However, there was no difference between pT3 and pT4 ($p = 0.573$). Lopez-Encuentra *et al.* (2002) and Tsai *et al.* (2006) discussed if in pT1 and pT2 classification the diameter of the tumor correlates with long-term survival, or if the tumor volume may be of importance.

The pathologic assessment of the regional lymph nodes (pN) entails a systematic hilar and mediastinal lymph node dissection concurrently with all procedures according to the standard systematic lymph node dissection described by Naruke *et al.* (1999) as it enables one to evaluate the highest pN category. The pathologic specimens should be assessed for patterns of tumor spread at pulmonary/hilar (N1) and mediastinal (N2) lymph node stations according to the international guidelines

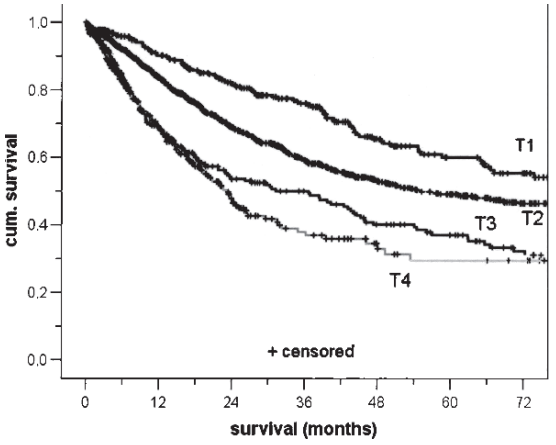

FIGURE 23.1. Survival rates for 2083 patients after complete resection according to pathological T. Differences between groups: T1 (n=344, 5-year survival, 61.3%) versus T2 (n=1298, 5-year survival, 50.7%), p: <0.001; T2 versus T3 (n=238, 5-year survival, 43.3%), p: 0.005; T3 versus T4 (n=203, 5-year survival, 39.4%), p: 0.573.

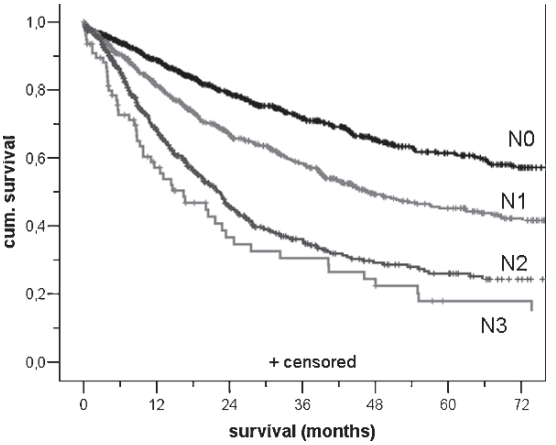

FIGURE 23.2. Survival rates for 2083 patients after complete resection according to pathological N. Differences between groups: N0 (n=1010, 5-year survival, 63.7%) versus N1 (n=584, 5-year survival, 47.3%), p: 0.001; N1 versus N2 (n=431, 5-year survival, 30.2%), p: 0.001; N2 versus N3 (n=58, 5-year survival, 22.5%), p: 0.076.

for the examination of specimens from patients with lung cancer (Myers *et al*., 1995). Information regarding the spread in N1and N2 lymph nodes has to be gathered by the surgeon in addition to the pathology report and lymph node dissection.

In the pN classification, survival rates decrease significantly as stages progress. Accuracy of systematic mediastinal and hilar lymph node dissection and pathologic examination is essential for appropriate staging and should be highly standardized. Chen *et al*. (1993) indicated that the nodal status can be normal with histology, but actually contains occult nodal metastases when sensitive immunohistochemical techniques and specific monoclonal antibodies are utilized. The presence of these previously undetectable nodal metastases were recently associated with shorter survival. Izbicki *et al*. (1998) reported that radical systemic mediastinal lymph node dissection does not influence disease-free or overall survival of patients without overt lymph node involvement. Thus, the extent of lymphadenectomy in the treatment of lung cancer is still under discussion. But without precise lymph node staging a comparison of results from different institutions is questionable.

We have found prognostic significance between pN1 and pN2 disease (Pfannschmidt *et al*., 2007) (Figure 23.2). Between pN2 and pN3 groups there was only a tendency for decreased survival rates in our study; however, this is in contrast with the results published by Naruke *et al*. (2001). The pathologic assessment of distant metastasis (pM) entails microscopic examination.

When appropriate, the following symbols may be used to further characterize staging: the y symbol during or following initial multimodality therapy; the r symbol for recurrent tumors; and the c symbol for validity of classification according to the diagnostic methods employed.

In 60 patients with local complete surgical resection, we found synchronous tumor nodule(s) in different lobes (M1-pulmo) and in 42 patients distant metastatic disease in different organs (M1-distal), with a median survival of 28.7 months (95% CI: 17.1–40.2), and 10.9 months (95% CI: 5.1–16.7), respectively (Pfannschmidt *et al*., 2007). There were significant differences in long-term survival among these two groups (M0 versus M1-pulmo: p = 0.042; M1-pulmo versus M1-distal: p = 0.001) (Figure 23.3).

The tumor status following treatment is described by the residual tumor (R) classification: R0, no residual tumor; R1, microscopic residual tumor; R2, macroscopic residual tumor. The R classification reflects the effects of treatment and influences further treatment planning. Residual tumor may be found in the area of primary tumor and its regional lymph nodes and/or at distant sites.

Size, relationship to surrounding structures, and invasion of contiguous structures by the primary tumor have been categorized by the TNM descriptors (Table 23.1). However, the R classification is a strong predictor of prognosis. Although there exist clear correlations between stage and R classification, the differences in prognosis of R0 versus R1,2 cannot be explained by differences in stage alone (Dienemann *et al*., 1997).

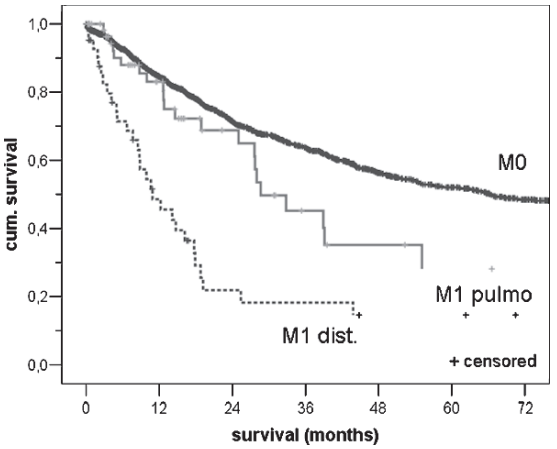

FIGURE 23.3. Survival rates for 2083 patients after complete resection according to pathological M. Differences between groups: M0 (n = 1981) versus M1 (pulmo)(n = 60), p: 0.042; M1 (pulmo) versus M1 (dist.)(n = 42), p: 0.001.

STAGING PROCEDURES

The clinical staging procedures have the primary goal to distinguish between patients with locoregional disease and who are candidates for surgery from those with metastatic disease. Initial evaluation, clinical assessment, and pretreatment evaluation should be followed according to the National Comprehensive Cancer Network (NCCN, 2007): Clinical Practice Guidelines in Oncology.

A thorough family history taken and complete physical examination remain the fundamental steps in the evaluation of a patient with possible lung cancer. Family history and history of tobacco smoking, as well as occupational and environmental exposure deserve special emphasis. Asbestos exposure and exposure to tobacco smoke are known as factors with multiple effects on the risk of the development of lung cancer. Physical examination should focus on symptoms of persistent or recurrent pulmonary infections, hemoptysis, pain, and the overall status of the patient such as evidence of weight loss. Special emphasis should be placed on neurologic signs, lymphadenopathy, paraneoplastic syndromes and other signs indicative of metastatic disease.

Standard imaging procedures encompass chest X-radiograph, CT scanning

Table 23.1. TNM descriptors. (Mountain, 1997)

T-primary tumor	
TX:	Primary tumor cannot be assessed, or tumor proven by the presence of malignant cells in sputum or bronchial washings but not visualized by imaging or bronchoscopy
T0:	No evidence of primary tumor
Tis:	Carcinoma *in situ*
T1:	Tumor 3 cm in greatest dimension, surrounded by lung or visceral pleura, without bronchoscopic evidence of invasion more proximal than the lobar bronchus[a] (*i.e.*, not in the main bronchus)
T2:	Tumor with any of the following features of size or extent: 3 cm in greatest dimension, involves main bronchus, >2 cm distal to the carina, invades the visceral pleura. Associated with atelectasis or obstructive pneumonitis that extends to the hilar region but does not involve the entire lung.
T3:	Tumor of any size that directly invades any of the following: chest wall (including superior sulcus tumors), diaphragm, mediastinal pleura, parietal pericardium; or tumor in the main bronchus, <2 cm distal to the carina, but without involvement of the carina; or associated atelectasis or obstructive pneumonitis of the entire lung
T4:	Tumor of any size that invades any of the following: mediastinum, heart, great vessels, trachea, esophagus, vertebral body, carina; or tumor with a malignant pleural or pericardial effusion,[b] or with satellite tumor nodule(s) within the ipsilateral primary-tumor lobe of the lung
N-regional lymph nodes	
NX:	Regional lymph nodes cannot be assessed
N0:	No regional lymph node metastasis
N1:	Metastasis to ipsilateral peribronchial and/or ipsilateral hilar lymph nodes, and intrapulmonary nodes involved by direct extension of the primary tumor
N2:	Metastasis to ipsilateral mediastinal and/or subcarinal lymph node(s)
N3:	Metastasis to contralateral mediastinal, contralateral hilar, ipsilateral or contralateral scalene, or supraclavicular lymph node(s)
M-distant metastasis	
MX:	Presence of distant metastasis cannot be assessed
M0:	No distant metastasis
M1:	Distant metastasis present[c]

[a] The uncommon superficial tumor of any size with its invasive component limited to the bronchial wall, which may extend proximal to the main bronchus, is also classified T1.

[b] Most pleural effusions associated with lung cancer are due to tumor. However, there are a few patients in whom multiple cytopathologic examinations of pleural fluid show no tumor. In these cases, the fluid is nonbloody and is not an exudate. When these elements and clinical judgment dictate that the effusion is not related to the tumor, the effusion should be excluded as a staging element and the patient's disease should be staged T1, T2, or T3. Pericardial effusion is classified according to the same rules.

Separate metastatic tumor nodule(s) in the ipsilateral nonprimary-tumor lobe(s) of the lung also are classified M1.

of the chest and upper abdomen, liver ultrasound and 99Tc radionuclide bone scan (Silvestri *et al.*, 2003). Magnetic resonance imaging (MRI) scans are used for routine organ scanning to exclude central nervous system metastases or if bone metastases are suspected. MRI is more accurate than CT in evaluating the soft tissue plane, and hence is useful in investigating local invasiveness of superior sulcus tumors, particularly vertebral body invasion, spinal canal, brachial plexus, and subclavian artery involvement (Silvestri *et al.*, 2003). More recently the availability of positron emission tomography (PET) helps to rule out mediastinal or distant metastatic disease (Truong *et al.*, 2004). It was reported by Sihoe and Yim (2004) that there is strong evidence showing the higher accuracy of PET over CT for non-invasive mediastinal staging.

Once an abnormality is detected on CT scan that is suspicious for cancer, additional invasive procedures should be

obtained for establishing tissue diagnosis. The guidelines from the American College of Chest Physicians (ACCP) recommend that further assessment be performed in all patients except those for whom extreme debiliation precludes further treatment (Silvestri *et al*., 2003). Detterbeck *et al*. (2003) reviewed a variety of invasive staging tests that are available for optimal tissue collection. Fiberoptic bronchoscopy with bronchoscopic biopsy, and brushing and washing tissue collection can be performed with minimal morbidity. It enables an excellent visualization of the tracheobronchial tree, and may be used to evaluate enlarged mediastinal lymph nodes by endobronchial ultrasound and transbronchial needle biopsy. Percutaneous fine-needle aspiration biopsies can be performed ultrasonographically guided or CT-guided to obtain material for cytologic or histologic examination (Yasufuku and Fujisawa, 2007). Video-assisted thoracoscopy can be used to obtain a tissue sample of enlarged mediastinal lymph nodes or for resection of peripherally located pulmonary nodules. In assessing the T designator, VATS can provide a visual evaluation of the local invasion by the primary tumor. In mediastinal nodal assessment, VATS provides access to the ipsilateral lymph node station, including paraesophageal and pulmonary ligament stations not accessible through mediastinoscopy. Thoracoscopy with pleural biopsy or percutaneous thoracocenteses with pleural cytology may yield a diagnosis for lung cancer in patients with pleural effusion and M1 disease.

Mediastinoscopy may be indicated if lymph nodes of the upper mediastinal lymph node compartments are larger than 1 cm on CT. Routine application of mediastinoscopy as a staging procedure remains controversial and diagnosis depends on experience and philosophy of the investigator. A multi-institutional study by the Canadian Lung Oncology Group (1995) found that routine mediastinoscopy for all patients has failed to preclude larger numbers of patients from unnecessary thoracotomy than conventional practice. Current ACCP guidelines (Detterbeck *et al*., 2003) advise the use of mediastinoscopy in NSCLC patients with enlarged mediastinal lymph nodes and for patients entering neoadjuvant treatment protocols. Anterior mediastinotomy (Chamberlain procedure) may be prescribed for enlarged lymph nodes at lymph node stations 5 and 6 (aortopulmonary window and along the ascending aorta). Alternatively, if mediastinotomy gives negative results, thoracoscopy may be feasible to obtain tissue diagnosis (Yasufuku and Fujisawa, 2007).

It has been estimated by Miller and Taylor (1965) that up to 75% of NSCLC patients may show N3 nodal metastases at the time of presentation. Scalene node biopsy or fine needle aspiration for palpable lymph nodes is recommended to rule out N3 disease. In patients with nonpalpable cervical lymph nodes modern cervical ultrasound may identify nodes suspicious of harboring metastases (Sihoe *et al*., 2004).

In a small number of cases, diagnostic thoracotomies are still necessary in the diagnosis and staging of lung cancer. Different techniques for biopsies, e.g., true-cut needle, fine-needle biopsy, incisional, and excisional biopsy, with frozen-section examination can yield a diagnosis. In these exceptional cases only intraoperative evaluation can determine the T descriptor and lymph node involvement.

However, selection of a method for invasive staging of lung cancer will depend on the local availability of expertise, and patient-specific anatomic and physiologic considerations.

STAGE GROUPING IN NSCLC

Disease stages were defined according to the 2002 UICC classification (2002). Stage I disease is T1 and T2 tumors with no evidence of lymph node or other distant metastasis. Stage II disease is T1 or T2 lesion with intrapulmonary lymph node or hilar lymph node metastasis. Stage IIIA disease is T1, T2, or T3 lesion with mediastinal lymph node metastasis. T3 lesion without mediastinal lymph node metastasis is also stage IIIA. Stage IIIB disease is primary tumor invasion of the mediastinum and metastasis to the contralateral hilar, contralateral mediastinal, and scalene/supraclavicular lymph nodes. Stage IV disease includes patients with distant metastasis.

IMPLICATIONS OF TNM CLASSIFICATION AND STAGE IN NSCLC

Pretreatment clinical stage of the disease based on clinical acquired parameters helps to select treatment options, and has a direct impact on the survival rate prior to the initiation of therapy. Postsurgical classification hierarchy is important for selection for adjuvant therapy, comparison of data between studies, and prognostic information. For patients with lung cancer, surgery and complete resection of the primary tumor concurrently with a systematic hilar and mediastinal lymph node dissection remain the most effective mode of treatment. Fang *et al*. (2001), Goya *et al*. (2005), Jassem *et al*. (2000), van Rens *et al*. (2000), Naruke *et al*. (2001), and Pfannschmidt *et al*. (2007) reported 5-year postsurgical survival rates in patients with NSCLC between 36% to 52.6%. These data were obtained either at a single institution over a long period (between 14 and 35 years) and with limited numbers (Jassem *et al*., 2000) or in a multi-institutional setting. Goya *et al*. (2005) reported from a multi-institutional series of 6,699 patients in 1994, Jassem *et al*. (2000) reported from a single institution series between 1991 and 1995 of only 586 patients, and Naruke *et al*. (2001) reported from a multi-institutional trial between 1961 and 1995 of 3,043 patients on postoperative 5-year survival rates. We have found in a retrospective data base analysis of 2,376 patients after complete resection for NSCLC at the University of Heidelberg/Thoraxklinik an overall 5-year survival rate of 46.8% (Pfannschmidt *et al*., 2007).

STAGE IA AND IB

Recently reported overall survival rates show a significant better outcome for patients with T1N0M0 lung cancer than for those in the other stages. Analysis of published studies by Naruke *et al*. (2001), Goya *et al*. (2005), Mountain (1997), and Pfannschmidt *et al*. (2006) with 1,000 and more patients reveals that 70.8–72% of patients with clinical stage IA disease are suspected to survive over 5 years after resection of the tumor (Table 23.2). In patients with clinical stage IB tumors reported, 5-year postsurgical survival rates were 44–59.8%. In a collection of patients treated both

Table 23.2. Clinical 5-year survival rate according to the 6th edition UICC (2002).

	Pfannschmidt *et al.* (2006)	Goya *et al.* (2005)	Naruke *et al.* (2001)	Mountain *et al.* (1997)
Patients (n)	2,083	6,644	3,043	5,319
Accumulation period (years)	10	1	34	14
	NSCLC	NSCLC	All	NSCLC
IA	72	72.0	70.8	61
IB	59.8	49.9	44	38
IIA	N. def.	48.7	41.1	34
IIB	47.8	40.6	38.8 (T2N1); 32.6 (T3N0)	24
IIIA	45.0	35.9	22.3 (T1-2N2); 22.9 (T3N1-2)	13
IIIB	38.7	28.0	11.7 (anyTN3; 24.3 (T4anyN)	5
IV	N. def.	20.8		1

N. def.: not definite

surgically and non surgically, Mountain (1997) found a 5-year survival rate in clinical stages IA and IB of 61% and 38%, respectively. Goya *et al*. (2005), Naruke *et al*. (2001), and Pfannschmidt *et al*. (2006) included only patients after surgical resection; thus, their fraction represents a selected subgroup of patients with a more favorable prognosis than the cohort analyzed by Mountain (1997).

The difference in survival rate between the stages IA and IB is most statistically significant. Analysis of the data shows an expected 5-year survival of 67–79.9% of the patients with postsurgical-pathologic stage IA and 57–60.1% of those with IB (Table 23.3). These results, according to clinical as well as postsurgical staging, are not related to newly established adjuvant chemotherapy treatment protocols for stage IB. These very recently advocated treatment protocols for stage IB to IIIA may have a further impact on survival data even in the early stage of the disease.

Interestingly the survival rate of pathological stage IA was 79% in the series reported from Japan by Naruke *et al*. (2001) and Goya *et al*. (2005). We observed in our recently retrospective evaluated data base a survival rate of 68.5% (Pfannschmidt *et al*., 2007) and this was comparable to results reported by Mountain (1997), Fang *et al*. (2001), and van Rens *et al*. (2000) with 5-year survival rates between 63% and 72% (Table 23.3). If this difference in survival of ~10% reflects variance in staging methods, e.g., lymph node dissection, or if it represents ethnic characteristics remains unclear.

STAGE IIA AND IIB

In two large retrospective series reported by Bulzebruck and Drings (1998) and Goya *et al*. (2005) the prognosis of stages IIA and IIB showed significant difference in the clinical staging, but in the studies by Naruke *et al*. (2001) and Pfannschmidt *et al*. (2006) the number of patients in the subgroups was too small, so significance was not detected. Difference in prognosis of patients in the pathological stages IIA and IIB was detected in a number of studies (Inoue *et al*., 1998; Goya *et al*., 2005;

Tabl e 23.3. Pathological (postsurgical) 5-year survival rate according to the 6th edition UICC (2002).

	Pfannschmidt *et al.* (2006)	Goya *et al.* (2005)	Naruke *et al.* (2001)	Fang (2001)	Van Rens (2000)	Mountain *et al.* (1997)
Patients (n)	2,083	6,644	3,043	1,905	2,361	5,319
Accumulation period (years)	10	1	34	35	23	14
	NSCLC	NSCLC	All	All	NSCLC	NSCLC
IA	68.5	79.5	79	72	63	67
IB	66.6	60.1	59.7	61	47	57
IIA	55.3	59.9	56.9	32.9	52	55
IIB	49.0	42.2	45	34.5	33	39
IIIA	35.8	29.8	23.6	22.6	19	23
IIIB	35.4	19.3	16.5	15.9	–	–
IV	–	20.0	5.1	7.1	–	–

Mountain, 1997; van Rens *et al*., 2000) with 5-year survival rates for patients with cT1N1M0 tumors of 55–59.9% and those with cT2N1M0 or cT3N0M0 tumors of 45–33%. However, differences between these subgroups were not seen by Fang *et al*. (2001), Jassem *et al*. (2000), and Pfannschmidt *et al*. (2007). This may be due to the infrequent presentation in T1N1M0 disease.

The end result of reporting based on the surgical-pathologic examination showed that a larger portion of IIA occurred in the surgical treatment population than was identified in the pretreatment population. This represents considerable stage migration from the other clinical stages. The finding of no significant difference in pathological stages IB and IIA has been reported in several large series by Goya *et al*. (2005), Naruke *et al*. (2001), Pfannschmidt *et al*. (2006), and van Rens *et al*. (2000). This may be due to the dependence of statistical power on the limited number of patients in stage IIA disease. However, Asamura *et al*. (2006) suggested the fusion of these stages into the same category.

STAGE IIIA AND IIIB

Four TNM categories, the T3N1M0, T1N2M0, T2N2M0, and T3N2M0 were designated as stage IIIA. Clinical stage IIIA is used to identify local intrathoracic disease that has the potential for complete resection. Selected patients with stage IIIA NSCLC are candidates for surgery. For patients with histologically proven mediastinal lymph node involvement, N2 disease, neoadjuvant chemotherapy may improve long term survival. The cT2N2M0 group represents the majority of patients within the cN2 category, as compared to cT3N2M0 and cT1N2M0.

T3 clinically classified tumors with invasion of the chest wall or diaphragm or a central tumor involving the mediastinum or pericardium are amenable to definitive surgical treatment.

Goya *et al*. (2005) and Naruke *et al*. (2001) reported on significant difference in long term survival between clinical stage IIIA and IIIB, with survival rates between 22.7–35.9%, in stage IIIA and 20.1–28.0% in stage IIIB (Table 23.2).

In most series, as reported by Fang *et al.* (2001), Goya *et al.* (2005), Naruke *et al.* (2001), and Pfannschmidt *et al.* (2007), end result studies showed statistical significance between stages IIB and IIIA 5-year survival rates. The results in pathological stages IIIA and IIIB reported by Goya *et al.* (2005), Naruke *et al.* (2001), and Jassem *et al.* (2000) with 23.6–29.8% in stage IIIA and 16.5–19.3% in stage IIIB, were somewhat lower than in our published series (Pfannschmidt *et al.*, 2007) with 35.8% and 35.4%, respectively (Table 23.3). This may reflect the evolvement in pretreatment evaluation, surgical staging by systematic lymph node dissection, pathologic reporting, and newer standards in neoadjuvant and adjuvant treatment regimen during the last decade. Between pathological stages IIIA and IIIB we (Pfannschmidt *et al.*, 2006), like Jassem *et al.* (2000) and Inoue *et al.* (1998), could not find significant difference in long-term survival; this may demonstrate the impact of patient selection for surgery as well as advances in adjuvant treatment regimen.

The stage IIIB category, including T4 and N3 TNM groups, was developed in 1986 for the International Staging System recommendations (UICC, 1987). Mountain (1997) reported that within stage IIIB categories a histologically validated N3-status evidently shows a survival disadvantage to patients with the possibility for local complete resection of a T4 primary tumor status. A significant number of patients shows a stage migration between the clinical stage IIIA and IIIB into pathologic postsurgical IIB, which reflects the demand of preoperative staging methodology in particular for the N-descriptor (Pfannschmidt *et al.*, 2006). At present CT is the most effective noninvasive method widely available to assess the enlargement of mediastinal lymph nodes. Because CT predicts actual metastatic involvement of mediastinal lymph nodes with a sensitivity of 60–80% and a specificity of 60–90%, histologic evaluation must always be performed if the finding of metastatic nodal involvement would determine inoperability. ^{18}FDG-PET may have additional value over CT in monitoring patients with stage N2 NSCLC. Both examinations are complementary because visual correlation with the anatomic information on CT improves the reader's ability to discriminate between hilar and subaortic mediastinal lymph node FDG uptake, and between paramediastinal tumor versus tracheobronchial mediastinal FDG uptake. Thus, PET may reduce the need for invasive surgical staging. The strength of ^{18}PET-FDG imaging lies in its very high negative predictive value and increased sensitivity.

However, with a positive **^{18}**PET-FDG scan result, further diagnostic procedures should be pursued in order to avoid overstaging and allow better surgical patient selection (Poncelet *et al.*, 2001). Patients within clinical stage IIIA or IIIB being considered for surgery MRT may offer advantages such as the assessment of chest-wall involvement or mediastinal involvement in patients in whom CT remains equivocal (Schaefer-Prokop and Prokop, 2002).

STAGE IV

Stage IV disease is treated primarily palliative with nonsurgical modalities such as chemotherapy and radiotherapy. It has been discussed if patients with intrapulmonary metastases in different lobes may

fit the same M1 category as patients with metastatic disease localized in other organs than the lungs. We have found that postoperative prognosis of patients with totally resected M1 pulmonary disease and no other distant metastases at the time of the operation are comparable with those in patients with postsurgical T3–T4 and with stage IIIA, respectively (Pfannschmidt *et al*., 2007). Satellite nodules associated with lung cancer were indicative of locally advanced and/or premetastatic disease. In 60 patients with local complete surgical resection we found tumor nodule(s) in different lobes (M1-pulmo) and in 42 patients distant metastatic disease in different organs (M1-distal), with a median survival of 28.7 months (95% CI: 17.1–40.2), and 10.9 months (95% CI: 5.1–16.7), respectively. There were significant differences in long-term survival among these two groups (M0 versus M1-pulmo: $p = 0.042$; M1-pulmo versus M1-distal: $p = 0.001$) (Figure 23.3).

Our data concur with the findings of Osaki *et al*. (2003) and Naruke *et al*. (2001) and clearly distinguish pulmonary M1 from metastases localized in other organs than the lung. With regard to pulmonary M1, Osaki *et al*. (2003) and others (Battafarano *et al*., 2002; Nagai *et al*., 2007) conclude that the existence of a solitary intrapulmonary sublesion should not preclude surgical treatment, unless surgery is contraindicated because of other clinical and radiologic findings. The relatively favorable survival data for patients with histologic postsurgical M1 pulmonary disease and patient selection in stage IV may explain the long-term survival data for patients with stage IV disease. Even in patients with operable brain metastases 5-year survival can correspond to that in the customary stage IIIA (Furak *et al*., 2005). However, in most patients M1 disease would determine inoperability, and long-term survival is very limited.

STAGE REPORTING: FUTURE PERSPECTIVE

Based on recent subgroup analyses there seems to be a need for further revision of the current staging system and to establish a new revised classification system. Clinically, a survival difference was observed even within stage IA status. Several retrospective analyses have focused on tumor size in early stage NSCLC. Port *et al*. (2003) reported that tumor size within stage IA was an important prognostic factor for survival. Gajra *et al*. (2003) reported on a more favorable survival for tumor size < 1.5 cm within stage IA disease. Tsai *et al*. (2006) found a good correlation of tumor volume and survival in patients with early stage lung cancer.

With the increased prevalence of screening programs, lung cancer is more frequently detected in sizes 1 cm or less. This will eventually result in unbalanced patient numbers for each stage. While Watanabe reported in 1991 that 18.9% of patients were diagnosed with stage IA, Takeda *et al*. (2005) reported that in 2005 50% were diagnosed within stage IA, and it is foreseeable that the percentage will continue to rise (Lee *et al*., 2006). In contrast, only a few rise patients were diagnosed within stage IIA.

Mountain (1997), Inoue *et al*. (1998), Naruke *et al*. (2001), and Adebonojo *et al*. (1999) reported on the problem of overlapping prognosis between stages IB and IIA

in either clinical or the pathological staging. This is considered to be an important failure of the current staging system, probably due to lack of small numbers within stage IIA. Thus, it has been suggested that stage IB and IIA are merged into a new stage (Asamura *et al.*, 2006). The optimal management of patients with intrapulmonary metastases from NSCLC remains controversial. Importantly, survival of patients with operable multifocal NSCLC (stage IV) is better than the survival rate reported in the series that formed the foundation for these staging classifications (Battafarano *et al.*, 2002; Furak *et al.*, 2005).

To identify more individual prognosis related criteria, it would be important to include further histologic and biological parameters. Further histologic classification according to the WHO classification (Travis *et al.*,1999) could identify subgroups of patients who show different prognosis. Thus, bronchioloalveolar carcinoma (BAC) of histopathological types A and B should be considered as *in situ* carcinoma whereas types C and D indicate poor prognosis (Goldstein *et al.*, 1999; Noguchi *et al.*, 1995). To identify patients with poor prognosis in stage IA, NSCLC upstaging by histopathologic identification of vessel invasion has been discussed. Adjuvant chemotherapy may be beneficial for patients within stage IA NSCLC upstaged by histopathologic vessel invasion (Tsuchiya *et al.*, 2007).

The value of tumor markers as prognostic parameters in patients with stage I NSCLC has been evaluated by Muley *et al.* (2004). Patients of curatively operated NSCLC in stage I with both elevated CYFRA 21-1 and CEA levels were found to be at a high risk of early death. Recently, the standardized uptake value (SUV) for ^{18}F-FDG as measured by using PET has been evaluated as a predictor of survival independent of pTNM classification (Downey *et al.*, 2007). This and other new parameters of tumor behavior may help to improve the current classification system.

REFERENCES

Adebonojo, S.A., Bowser, A.N., Moritz, D.M., and Corcoran, P.C. 1999. Impact of revised stage classification of lung cancer on survival: a military experience. *Chest 115*: 1507–1513.

American Joint Committee on Cancer (AJCC). 2002. *In*: Greene FL, Page D L, Fleming ID, Fritz A, Balch CM, Haller DG, Morrow M, editors. *Cancer Staging Manual*, 6th ed. Berlin/ Heidelberg/New York: Springer.

Asamura, H., Goya, T., Koshiishi, Y., Sohara, Y., Tsuchiya, R., and Miyaoka, E. 2006. How should the TNM staging system for lung cancer be revised? A simulation based on the Japanese Lung Cancer Registry populations. *J. Thorac. Cardiovasc. Surg. 132*: 316–319.

Battafarano, R.J., Meyers, B.F., Guthrie, T.J., Cooper, J.D., and Patterson, G.A. 2002. Surgical resection of multifocal non-small cell lung cancer is associated with prolonged survival. *Ann. Thorac. Surg. 74*: 988–993; discussion 993–994.

Bulzebruck, H., and Drings, P. 1998. Stage migration and prognostic impact of the 5th edition of the TNM classification for lung cancer. *Lung Cancer 21*: 19.

Canadian Lung Oncology Group. 1995. Investigation for mediastinal disease in patients with apparently operable lung cancer. *Ann. Thorac. Surg. 60*: 1382–1389.

Chen, Z.L., Perez, S., Holmes, E.C., Wang, H.J., Coulson, W.F., Wen, D.R., and Cochran, A.J. 1993. Frequency and distribution of occult micrometastases in lymph nodes of patients with non-small-cell lung carcinoma. *J. Natl. Cancer Inst. 85*: 493–498.

Denoix, P.F. 1946. Enquete permanent dans les centres anticancereaux. *Bull. Inst. Nat. Hyg. 1*: 70–75.

Detterbeck, F.C., DeCamp, M.M., Jr., Kohman, L.J., and Silvestri, G.A. 2003. Lung cancer. Invasive staging: the guidelines. *Chest 123*: 167S–175S.

Dienemann, H., Trainer, C., Hoffmann, H., Bulzebruck, H., Muley, T., Kayser, K., and Vogt-Moykopf, I. 1997. [Incomplete resections in bronchial carcinoma: morbidity and prognosis]. *Chirurg 68*: 1014–1019.

Downey, R.J., Akhurst, T., Gonen, M., Park, B., and Rusch, V. 2007. Fluorine-18 fluorodeoxyglucose positron emission tomographic maximal standardized uptake value predicts survival independent of clinical but not pathologic TNM staging of resected non-small cell lung cancer. *J. Thorac. Cardiovasc. Surg. 133*: 1419–1427.

Fang, D., Zhang, D., Huang, G., Zhang, R., Wang, L., and Zhang, D. 2001. Results of surgical resection of patients with primary lung cancer: a retrospective analysis of 1,905 cases. *Ann. Thorac. Surg. 72*: 1155–1159.

Furak, J., Trojan, I., Szoke, T., Agocs, L., Csekeo, A., Kas, J., Svastics, E., Eller, J., and Tiszlavicz, L. 2005. Lung cancer and its operable brain metastasis: survival rate and staging problems. *Ann. Thorac. Surg. 79*: 241–247.

Gajra, A., Newman, N., Gamble, G.P., Abraham, N.Z., Kohman, L.J., and Graziano, S.L. 2003. Impact of tumor size on survival in stage IA non-small cell lung cancer: a case for subdividing stage IA disease. *Lung Cancer 42*: 51–57.

Goldstein, N.S., Mani, A., Chmielewski, G., Welsh, R., and Pursel, S. 1999. Prognostic factors in T1 NO MO adenocarcinomas and bronchioloalveolar carcinomas of the lung. *Am. J. Clin. Pathol. 112*: 391–402.

Goya, T., Asamura, H., Yoshimura, H., Kato, H., Shimokata, K., Tsuchiya, R., Sohara, Y., Miya, T., and Miyaoka, E. 2005. Prognosis of 6644 resected non-small cell lung cancers in Japan: a Japanese lung cancer registry study. *Lung Cancer 50*: 227–234.

Inoue, K., Sato, M., Fujimura, S., Sakurada, A., Takahashi, S., Usuda, K., Kondo, T., Tanita, T., Handa, M., Saito, Y., and Sagawa, M. 1998. Prognostic assessment of 1310 patients with non-small-cell lung cancer who underwent complete resection from 1980 to 1993. *J. Thorac. Cardiovasc. Surg. 116*: 407–411.

International Union Against Cancer. 1982. TNM Classification of Malignant Tumours. *In*: Harmer MH, editor. *TNM Classification of Malignant Tumors*, 3rd ed. Geneva.

International Union Against Cancer. 1987. *In*: Sobin L, Wittekind C, editors. *TNM Classification of Malignant Tumors*, 4th ed. Berlin/Heidelberg/New York: Springer.

International Union Against Cancer. 1997. *In*: Sobin L, Wittekind C, editors. *TNM Classification of Malignant Tumours*, 4th ed. New York: Wiley-Liss.

International Union Against Cancer. 2002. *In*: Sobin L, Wittekind C, editors. *TNM Classification of Malignant Tumours*, 6th ed. New York: Wiley-Liss.

Izbicki, J.R., Passlick, B., Pantel, K., Pichlmeier, U., Hosch, S.B., Karg, O., and Thetter, O. 1998. Effectiveness of radical systematic mediastinal lymphadenectomy in patients with resectable non-small cell lung cancer: results of a prospective randomized trial. *Ann. Surg. 227*: 138–144.

Jassem, J., Skokowski, J., Dziadziuszko, R., Jassem, E., Szymanowska, A., Rzyman, W., and Roszkiewicz, A. 2000. Results of surgical treatment of non-small cell lung cancer: validation of the new postoperative pathologic TNM classification. *J. Thorac. Cardiovasc. Surg. 119*: 1141–1146.

Lee, P.C., Korst, R.J., Port, J.L., Kerem, Y., Kansler, A.L., and Altorki, N.K. 2006. Long-term survival and recurrence in patients with resected non-small cell lung cancer 1 cm or less in size. *J. Thorac. Cardiovasc. Surg. 132*: 1382–1389.

Lopez-Encuentra, A., Duque-Medina, J.L., Rami-Porta, R., de la Camara, A.G., and Ferrando, P. 2002. Staging in lung cancer: is 3 cm a prognostic threshold in pathologic stage I non-small cell lung cancer? A multicenter study of 1,020 patients. *Chest 121*: 1515–1520.

Miller, W.E., and Taylor, A.M. 1965. Biopsy of scalene and supraclavicular lymph nodes: value in diagnosis. *Cleve. Clin. Q. 32*: 205–209.

Mountain, C.F. 1986. A new international staging system for lung cancer. *Chest 89*: 225S–233S.

Mountain, C.F. 1997. Revisions in the international system for staging lung cancer. *Chest 111*: 1710–1717.

Mountain, C.F., Carr, D.T., and Anderson, W.A. 1974. A system for the clinical staging of lung cancer. *Am. J. Roentgenol. Radium. Ther. Nucl .Med. 120*: 130–138.

Muley, T., Dienemann, H., and Ebert, W. 2004. CYFRA 21-1 and CEA are independent prognostic factors in 153 operated stage I NSCLC patients. *Anticancer Res. 24*: 1953–1956.

Myers, J., Askin, F., and Yousem, S. 1995. Recommendations for the reporting of resected primary lung carcinomas: Association of Directors of Anatomic and Surgical Pathology. *Hum. Pathol. 26*: 937.

Nagai, K., Sohara, Y., Tsuchiya, R., Goya, T., and Miyaoka, E. 2007. Prognosis of resected non-small cell lung cancer patients with intrapulmonary metastases. *J. Thorac. Oncol. 2*: 282–286.

Naruke, T., Tsuchiya, R., Kondo, H., Nakayama, H., and Asamura, H. 1999. Lymph node sampling in lung cancer: how should it be done? *Eur. J. Cardiothorac. Surg. 16*: 17–24.

Naruke, T., Tsuchiya, R., Kondo, H., and Asamura, H. 2001. Prognosis and survival after resection for bronchogenic carcinoma based on the 1997 TNM-staging classification: the Japanese experience. *Ann. Thorac. Surg. 71*: 1759–1764.

NCCN. 2007. Clinical Practice Guidlines in Oncology. Available at http:// www. nccn.org/professionals/physician_gls/PDF/nscl.pdf. accessed June7, 2007.

Noguchi, M., Morikawa, A., Kawasaki, M., Matsuno, Y., Yamada, T., Hirohashi, S., Kondo, H., and Shimosato, Y. 1995. Small adenocarcinoma of the lung. Histologic characteristics and prognosis. *Cancer 75*: 2844–2852.

Osaki, T., Sugio, K., Hanagiri, T., Takenoyama, M., Yamashita, T., Sugaya, M., Yasuda, M., and Yasumoto, K. 2003. Survival and prognostic factors of surgically resected T4 non-small cell lung cancer. *Ann. Thorac. Surg. 75*: 1745–1751.

Pfannschmidt, J., Muley, T., Hoffmann, H., Bulzebruck, H., and Dienemann, H. 2006. Prognosis after complete surgical resection for non-small cell lung cancer based on the staging classification. *Dtsch. Med. Wochenschr 131*: 2643–2648.

Pfannschmidt, J., Muley, T., Bulzebruck, H., Hoffmann, H., and Dienemann, H. 2007. Prognostic assessment after surgical resection for non-small cell lung cancer: experiences in 2083 patients. *Lung Cancer 55*: 371–377.

Poncelet, A.J., Lonneux, M., Coche, E., Weynand, B., and Noirhomme, P. 2001. PET-FDG scan enhances but does not replace preoperative surgical staging in non-small cell lung carcinoma. *Eur. J. Cardiothorac. Surg. 20*: 468–474.

Port, J.L., Kent, M.S., Korst, R.J., Libby, D., Pasmantier, M., and Altorki, N.K. 2003. Tumor size predicts survival within stage IA non-small cell lung cancer. *Chest 124*: 1828–1833.

Schaefer-Prokop, C., and Prokop, M. 2002. New imaging techniques in the treatment guidelines for lung cancer. *Eur. Respir. J. Suppl. 35*: 71s–83s.

Sihoe, A.D., and Yim, A.P. 2004. Lung cancer staging. *J. Surg. Res. 117*: 92–106.

Sihoe, A.D., Lee, T.W., Ahuja, A.T., and Yim, A.P. 2004. Should cervical ultrasonography be a routine staging investigation for lung cancer patients with impalpable cervical lymph nodes? *Eur. J. Cardiothorac. Surg. 25*: 486–491.

Silvestri, G.A., Tanoue, L.T., Margolis, M.L., Barker, J., and Detterbeck, F. 2003. The noninvasive staging of non-small cell lung cancer: the guidelines. *Chest 123*: 147S–156S.

Takeda, S., Fukai, S., Komatsu, H., Nemoto, E., Nakamura, K., and Murakami, M. 2005. Impact of large tumor size on survival after resection of pathologically node negative (pN0) non-small cell lung cancer. *Ann. Thorac. Surg. 79*: 1142–1146.

Travis, W., Colby, T., Corrin, B., Shimosato, Y., and Brambilla, E. 1999. Histological Typing of Lung and Pleural Tumours. *World Health Organization*, 3rd ed. Berlin: Springer.

Truong, M.T., Munden, R.F., and Movsas, B. 2004. Imaging to optimally stage lung cancer: conventional modalities and PET/CT. *J. Am. Coll. Radiol. 1*: 957–964.

Tsai, C.H., Lin, C.M., Hsieh, C.C., Hsu, W.H., Wang, H.W., and Wang, L.S. 2006. Tumor volume is a better prognostic factor than greatest tumor diameter in stage Ia non-small cell lung cancer. *J. Thorac. Cardiovasc. Surg. 54*: 537–543.

Tsuchiya, T., Akamine, S., Muraoka, M., Kamohara, R., Tsuji, K., Urabe, S., Honda, S., and Yamasaki, N. 2007. Stage IA non-small cell lung cancer: vessel invasion is a poor prognostic factor and a new target of adjuvant chemotherapy. *Lung Cancer 56*: 341–348.

Van Rens, M.T., de la Riviere, A.B., Elbers, H.R., and van Den Bosch, J.M. 2000. Prognostic assessment of 2,361 patients who underwent pulmonary resection for non-small cell lung cancer, stage I, II, and IIIA. *Chest 117*: 374–379.

Watanabe, Y., Shimizu, J., Oda, M., Hayashi, Y., Iwa, T., Nonomura, A., Kamimura, R., and Takashima, T. 1991. Proposals regarding some deficiencies in the new international staging system for non-small cell lung cancer. *Jpn. J. Clin. Oncol. 21*: 160–168.

Yasufuku, K., and Fujisawa, T. 2007. Staging and diagnosis of non-small cell lung cancer: invasive modalities. *Respirology 12*: 173–183.

24
Differentiation Between Malignant and Benign Pleural Effusions: Methylation Specific Polymerase Chain Reaction Analysis

Susana Benlloch, José Marcelo Galbis-Caravajal, and Bartomeu Massutí

Summary Normally, very small amounts of pleural fluid are present in the pleural spaces, and this fluid is not detectable by routine methods. When certain disorders occur, excessive pleural fluid may accumulate and cause pulmonary signs and symptoms. Pleural effusions occur when the rate of fluid formation exceeds that of fluid absorption. Once a symptomatic, unexplained pleural effusion arises, a diagnosis needs to be established. The clinical importance of pleural effusions ranges from incidental manifestations of cardiopulmonary diseases to symptomatic inflammatory or malignant diseases requiring evaluation and treatment. An exact diagnosis of pleural effusions is difficult; in 40% of malignant effusions, a cytological examination of pleural fluid does not detect tumor cells and the diagnosis of malignant pleural effusions often requires combined procedures. The differentiation between malignant and benign effusions requires a technique which is both more sensitive and more specific. So, the diagnostic value of using methylation-specific polymerase chain reaction (MSP) of several genes for establishing methylation profiles for discrimination has been investigated in pleural effusions collected from patients in whom diagnosis was confirmed with cytological and/or histological examinations and clinical evolution. Pleural effusions were classified as malignant and benign.

INTRODUCTION

The pleura is the serous membrane lining the thoracic cavity. The pleural cavity normally contains ~1 ml of fluid not detectable by routine methods, which is the balance between hydrostatic and oncotic forces in the visceral and parietal pleural vessels and lymphatic drainage. Pleural effusions result from a disruption of this balance, and the rate of fluid formation exceeds that of fluid absorption. The clinical importance of pleural effusions ranges from incidental manifestations of cardiopulmonary diseases to symptomatic inflammatory or malignant diseases requiring evaluation and treatment (Ang *et al*., 2001). Once a symptomatic, unexplained pleural effusion arises, a diagnosis needs to be established. An exact diagnosis of pleural effusions is difficult;

in 40% of malignant effusions, a cytological examination of pleural fluid does not detect tumor cells (Light, 1995; Miedouge *et al*., 1999), and the diagnosis of malignant pleural effusions often requires combined procedures (Demmy *et al*., 2005).

Changes in DNA methylation are among the most common molecular alterations in human neoplasia (Baylin and Herman, 2000; Jones, 1996). CpG islands are regions in DNA where there are a large number of cytosine and guanine adjacent to each other in the backbone of the DNA (i.e., linked by phosphodiester bonds). Aberrant hypermethylation in cancer usually occurs at those CpG islands, most of which are unmethylated in normal somatic cells, and the resulting changes in chromatin structure (such as histone hypoacetylation) effectively silence transcription. Genes involved in cell-cycle regulation, tumor cell invasion, DNA repair, chromatin remodelling, cell signalling, transcription and apoptosis are known to become aberrantly hypermethylated and silenced in nearly every tumor type (Baylin *et al*., 1998). This provides tumor cells with a growth advantage, increases their genetic instability (allowing them to acquire further advantageous genetic changes), and allows them to metastasize. In tumors with a well-defined progression, such as colon cancer, aberrant hypermethylation is detectable in the earliest precursor lesions, indicating that it directly contributes to transformation and is not a late event that arises from genetic alterations (Robertson, 2005). The reciprocal relationship between the density of methylated cytosine residues and the transcriptional activity of a gene has been widely documented (Jones, 1999)

Tumor suppressor genes such as *RARβ* (Lu *et al*., 1997), *RASSF1A* (Dammann *et al*., 2000), *p16/INK4a* (Sherr, 1996) and *DAPK* (Kissil *et al*., 1997) are strong biomarker candidates for the early detection of cancer (Soria *et al*., 2002), and are involved in important cellular regulatory pathways, apoptosis, and ras signal transduction (Belinsky *et al*., 2002). These genes have been found to harbor hypermethylated promoters in 15–45% of solid tumors (Tsou *et al*., 2002), and hypermethylation changes may be excellent tumor markers (Baylin *et al*., 2000). Circulating cell free DNA extracted from bodily fluids has been shown to be a surrogate for neoplastic cells and the presence of promoter hypermethylation of various genes in bodily fluids, including serum (Ramirez *et al*., 2003, 2005), bronchoalveolar lavage of lung cancer patients (Topaloglu *et al*., 2004), sputum (Palmisano *et al*., 2000) and pleural fluid (Brock *et al*., 2005) has been studied.

Methodologically speaking, the analysis of DNA methylation was revolutionized by the introduction of the sodium bisulphite conversion of genomic DNA. The designing of the PCR primers for the amplification of bisulphite converted DNA has to take some important factors into account: (i) they are not self-complementary when designed to amplify the top strand, (ii) they should cover several cytosines that are not part of CpG dinucleotides in the original sequences, and are therefore converted to uracils by bisulphite and (iii) they can be designed to anneal specifically with either the methylated or unmethylated version of bisulphite-converted sequence (MSP) (Laird, 2003).

Methylation-Specific Polymerase Chain Reaction (MSP) technique is highly sensitive, as it is able to detect 0.1% tumor DNA from a heterogeneous cell population

(Herman *et al*., 1996). It has been widely used and is relatively inexpensive. Other techniques are arising such as quantitative MSP (Eads *et al*., 2000), a high-throughput DNA methylation analysis that uses MALDI-TOF mass spectrometry analysis of base-specifically cleaved amplification products (Ehrich *et al*., 2005) and pyrosequencing that has been used in retrospective studies and has potential in a diagnostic setting (Shames *et al*. 2006).

Recently, three studies have been published in which the hypermethylation patterns of three different panels of genes from cell-free DNA obtained from samples of pleural fluid have been studied (Benlloch *et al*., 2006; Brock *et al*., 2005; Katayama *et al*., 2007). In this chapter we will focus on discussing the role of hypermethylation as a marker for differentiating between malignant and benign pleural effusions in patients with pleural effusion as well as on methodology.

MATERIALS AND METHODS

Patients

In three studies, patients with pleural effusion were evaluated. All patients gave their signed informed consent, and the study was approved by each hospital ethics committee. Effusions were considered malignant if one of the following criteria was met: demonstration of malignant cells by cytological examination or in biopsy specimen; or histologically proven primary malignancy with exclusion of any other cause known to be associated with pleural effusion. All pleural effusions were studied by cytological examination, pleural biopsy and/or thoracoscopy with biopsy of visually identified abnormal areas of the pleura. Results of conventional cytology and methylation analyses of the pleural fluids from patients were compared with respect to the definitive diagnosis established by either a tissue biopsy or through clinical follow-up in the case of patients with benign disease. Pleural invasion was defined as the invasion of a tumor through either the parietal or visceral pleura. Patients with non-malignant effusions were clinically free of any cancer at the time of pleural fluid collection, and chest radiographs showed no evidence of lung cancer or lung metastases from other primary cancer. Patients with potentially precancerous cytologic findings such as dysplasia or metaplasia were excluded from methylation analysis.

Collection and Processing of Pleural Fluid Samples and DNA Extraction

Pleural fluid was obtained either via needle during thoracentesis, a chest tube during thoracostomy or by aspiration through a 1 cm incision at the very beginning of a thorascopic pleurodesis procedure. In the patients who underwent thorascopy, the pleural fluid was obtained through only one small incision in the chest located in the fifth intercostals space and mid to anterior axillary line. In all studies, the pleural fluid was collected after 15 min centrifugation at 1,600 g and stored in 1 ml aliquots at –20°C until DNA extraction. DNA was purified from 400 µl/1 ml of pleural fluid by using DNA QIAmp Blood Mini Kit (Qiagen, Valencia, CA) according to the manufacturer's instructions or extracted by standard methods using a simplified proteinase K digestion method.

Methylation-Specific Polymerase Chain Reaction (MSP)

At least 100 ng of sample DNA, mixed with 1 µg of salmon sperm (Sigma Chemical Co., St. Louis, MO), were submitted to chemical modification following the method described by Herman *et al*. (1996). Briefly, DNA was denatured with 2 M of NaOH, followed by treatment with 10 mM of hydroquinone and 3 M of sodium bisulfite (Sigma Chemical Co., St. Louis, MO) at 55°C for 16 h. After purification in a Wizard SV Plus kit column (Promega, Madison, WI), the DNA was treated with 3 M of NaOH and precipitated with three volumes of 100% ethanol, a one-third volume of 10 M NH4OAc, and 20 µg of glycogen (Roche Molecular Biochemicals) at −20°C. The precipitated DNA was washed with 70% ethanol and dissolved in distilled water. This process can also be performed using commercial DNA modification reagent kits such as CpGenome DNA Modification Kit (Intergen, NY), Epitec bisulfite (Qiagen, Valencia, CA) or EZ DNA methylation Gold (Zymo Research) following the manufacturer's instructions.

Polymerase Chain Reaction (PCR) was conducted with primers which were specific for either methylated or unmethylated versions of the gene promoter regions. The 25-µl total reaction volume contained modified DNA, all four dNTPs (each at 300 µM), 3 mM of MgCl2, 0.75 µM of PCR primers, and 1 unit of Hot Start DNA polymerase (Qiagen, Valencia, CA). In their study, Brock *et al*. (2005) performed a multiplex, nested methylation specific PCR. DNA was substituted for water as a negative control. DNA from peripheral blood lymphocytes and either genomic DNA (Roche Molecular Biochemicals, Mannheim, Germany) or placental DNA treated *in vitro* with SssI methyltransferase (New England Biolabs Inc., Beverly MA) were used as positive controls for the methylated reaction. However, both DNA from cancer cell lines, which have promoter methylation of tested genes, can be used as a positive control for the methylated form as can commercial, enzymatically prepared methylated DNA from Zymo Research (Orange, CA) or Chemicon (Millipore, Billerica, MA). DNA from peripheral blood lymphocytes, placental and genomic DNA (Roche Molecular Biochemicals, Mannheim, Germany) were used as positive controls for the unmethylated reaction. PCR products were separated on agarose or nondenaturing 6% polyacrylamide gels and visualized under ultraviolet illumination after staining with ethidium bromide. Results were confirmed by repeating MSP analysis in duplicate/triplicate for all samples.

Statistical Analysis

Sensitivity, specificity, positive predictive values and negative predictive values of both MSP and conventional cytology as well as of the combination of both techniques were calculated in relation to the definitive diagnosis of the patients in the study. Summary receiver operating characteristic curves, which can analyze the accuracy of a single test in a single population, could not be employed because the specificity of both the cytology and methylation tests was 100%. The X^2 or Fisher's exact test was used to test the association between categorical variables. The Pearson correlation coefficient was used to evaluate the association between the numbers of hypermethylated genes in

pleural fluid. Statistical significance was set at $p < 0.05$.

RESULTS

The promoter methylation patterns of three different panels of genes were tested in samples of pleural fluid taken from two groups of patients presenting pleural effusion with or without malignancy by three different laboratories. To investigate the tumor-specific methylation of the panels of genes, different groups of cancer patients and cancer-free patients were compared as to the frequency of hypermethylation in each of their promoter regions. Conventional cytology of pleural effusion was performed in most patients.

As seen in Table 24.1, different percentages of methylated DNA were detected in the pleural fluid of cancer patients. Benlloch *et al*. (2006) and Brock *et al*. (2005) observed no aberrant methylation in pleural fluid DNA samples from the nonmalignant group. However, although Katayama *et al*. (2007) detected no cases among non-malignant effusions of methylated DNA in pleural fluid for MGMT or p16INK4a either, they did find 2.9% for RASSF1A, 26.5% for DAPK, and 17.6% for RARβ.

The accuracy of the MSP-based detection of promoter hypermethylation in pleural fluid was assessed by calculation of sensitivity, specificity, positive predictive value and negative predictive value (Table 24.2). In the Benlloch *et al*. (2006) study, 58% of the pleural fluid samples had methylation in at least one of the four genes with 100% specificity, while all 34 control samples were negative for methylation in these four genes. Conventional cytology of pleural effusion samples revealed neoplastic cells in 17 out of 48 cancer patients (39.1% sensitivity) with 100% specificity (Table 24.2). When both conventional cytology of pleural effusion and detection of hypermethylation in pleural fluid were combined, the sensitivity increased to 69.8% with 100% specificity (Table 24.2). In the Brock *et al*. (2005) study, conventional cytology alone detected the presence of neoplastic cells in 15 out of 24 patients (63% sensitivity), whereas no malignant cells were isolated from the pleural fluid of benign patients (100% specificity). Using the eight genes in the panel, the pleural fluid was ascertained as methylation positive if two or more genes were strongly methylated. Using this criterion, aberrant methylation analysis alone identified 16 patients as being positive for the presence of malignant DNA in their pleural fluid (67% sensitivity) while no patient with benign disease had a positive test of their pleural fluid

TABLE 24.1. Frequency of methylation in five genes in pleural effusion samples (%).

	Malignant pleural effusion					Non-malignant pleural effusion				
	DAPK	P16/ INK4a	RASS-F1A	RARß	MGMT	DAPK	P16/ INK4a	RASS F1A	RARß	MGMT
Benlloch et al.	18.9	37.7	15.1	20.8	ND	0	0	0	0	ND
Katayama et al.	29.8	17	27.7	40.4	6.4	26.5	0	2.9	17.6	0

ND: non determined; *DAPK*: death-associated protein kinase; *RASSF1A*: ras association domain family 1A; *RARβ*: retinoic acid receptor ß; and *MGMT*: O6-methylguanine-DNA methyltransferase.

TABLE 24.2. Accuracy of MSP-based detection of promoter hypermethylation in pleural fluid, as assessed by calculation of sensitivity, specificity, positive predictive value and negative predictive value.

	Brock *et al*. (2005)				Benlloch *et al*. (2006)				Katayama *et al*. (2007)			
	S (%)	Sp (%)	PPV	NPV	S (%)	Sp (%)	PPV	NPV	S (%)	Sp (%)	PPV	NPV
Cytology	63	100	100	44	39.1	100	100	54.1	ND	ND	ND	ND
Aberrant methylation detected	67	100	100	47	58.5	100	100	62.1	59.6	79.4	80	ND
Positive cytology or aberrant methylation detected	87.5	100	100	78	69.8	100	100	68.0	ND	ND	ND	ND

S: sensitivity; Sp: specificity; PPV: positive predictive value; NPV: negative predictive value; ND: not determined.

(100% specificity). If conventional cytology and aberrant methylation were considered together, the two techniques showed complementarity increasing the sensitivity to 87.5% while maintaining 100% specificity in discriminating between benign and malignant disease. The positive predictive value for methylation alone, cytology alone, as well as the combination of both techniques was 100%. The negative predictor values of cytology and methylation tests alone were 44% and 47%, respectively. The combination of both techniques increased the negative predictor values to 78%. In the Katayama *et al*. (2007) study, when the methylation status of at least one of the four genes was found to be positive, the sensitivity, specificity, and positive predictive values for the diagnosis of malignant effusions were 59.6%, 79.4%, and 80.0%, respectively.

DISCUSSION

To date, three studies investigating the possibility of differentiating between malignant and benign pleural effusions by performing a methylation specific PCR analysis have been published (Benlloch *et al*., 2006; Brock *et al*., 2005; Katayama *et al*., 2007). For this purpose, in the three studies, we have included patients with suspected malignant pleural effusions. The average life expectancy for these patients is low. A major factor in the high mortality rate of cancer patients is the presence of metastatic tumors in approximately two-thirds of these patients at the time of diagnosis (Wingo *et al*., 1999). The ability to determine the malignancy or benignity of the pleural effusion is thus very useful both for prognosis and for clinical management.

Several methods are currently used for the diagnosis of pleural effusion. The most informative laboratory procedure is thoracocentesis and cytology. Several factors influence the accuracy of cytological diagnosis, mainly the primary tumor (Light, 1995). If cytological results are negative, the next step is a new thoracocentesis, pleural biopsy and thoracoscopy. Thoracoscopy provides a tissue diagnosis in 80.3% of patients with recurrent

effusions not diagnosed after thoracocentesis, pleural biopsy and bronchoscopy (Ang *et al*., 2001).

Changes in the status of DNA methylation are among the most common molecular alterations in human neoplasia (Jones, 1996). Several genes are involved in the pathogenesis of cancer and are frequently inactivated by aberrant promoter methylation (Kim *et al*., 2004). The potential prognostic and therapeutic values of DNA methylation in cancer have been studied in various types of neoplasia (Wong *et al*., 2004; Yanagawa *et al*., 2003; Takahashi *et al*., 2004). The presence of promoter methylation of various genes in bronchoalveolar lavage (Kim *et al*., 2004; Topaloglu *et al*., 2004) and serum (Ramirez *et al*., 2003, 2005) has been shown to be a surrogate for methylation of the same genes in tumors. Moreover, circulating DNA found in serum harbors the same genetic characteristics as paired tumor DNA as has been reported by several authors (Esteller *et al*., 1999; Ramirez *et al*., 2003, 2005). As tumoral DNA was detected in bodily fluids it was hypothesized that in patients in whom conventional cytology may not be enough to detect malignant cells in the pleural fluid, free-floating, aberrantly hypermethylated DNA would be present quantities sufficiently large enough to be detected, and that the sensitivity of this approach would improve the overall diagnostic sensitivity of conventional cytology. In two of the three studies, aberrant methylation of some of the genes tested was detected in patients with malignant tumors, but there was 0% frequency found in fluids tested in the control group. The hypermethylation of several genes in the bronchial epithelium and sputum of cancer-free subjects (Kim *et al*., 2004) could be related to the direct exposure of epithelial cells to the carcinogenic factor cells; however, it seems that hypermethylation in pleural fluid may be limited to patients with metastases in the pleural cavity. In the three studies, the gene panel was successful in detecting neoplastic DNA with a sensitivity between 58.5–67% in pleural fluid depending both on the number of genes tested and whether conventional MSP or nested MSP was used, whereas the sensitivity of cytology was between 39.1–63%. We all agree that the prevalence of methylation helps to increase the sensitivity of conventional cytology. In all cases, methylation increased the sensitivity in a single sample to 69.8–87.5%, obviating the need for surgical procedures except in specific situations. In addition to helping in the diagnosis of malignant pleural effusions, methylation can also be beneficial in the post-treatment monitoring of the disease's progress.

The role of hypermethylation as a marker of malignant pleural effusions has been demonstrated. This is accomplished by detecting neoplastic methylated DNA in pleural effusions, even in patients with negative results on cytological analysis and even for multiple tumor types, and with a limited cohort size (Table 24.3).

When a panel of eight genes and a multiplex, nested MSP technique is employed the sensitivity increases (Brock *et al*., 2005) when compared with a panel of a smaller number of genes and conventional MSP (Benlloch *et al*., 2006; Katayama *et al*., 2007). It has been observed previously that a single methylation marker is invariably insufficient to characterize fully malignancies from many organ sites, and that a panel of epigenetic markers is essential to provide a spectrum wide enough to detect all types of malignancies (Brock *et al*., 2005).

TABLE 24.3. Diagnosis of patients with pleural effusions.

	Benlloch *et al.* (2006)	Brock *et al.* (2005)	Katayama *et al.* (2007)
Malignant pleural effusion	**53**	**24**	**47**
Lung	23	13	37
Breast carcinoma	10	3	–
Digestive adenocarcinoma	10	1	–
Ovarian carcinoma	3	–	–
Mesothelioma	1	1	10
Other	6	6	–
Non-malignant pleural effusion	**34**	**7**	**34**
Emphysema	12	–	–
Cardiac failure	9	–	–
Tuberculous pleurisy	8	–	22
Pulmonary embolism	1	–	–
Liver disease-cirrhosis	3	–	–
Pneumonia	–	–	12
Hypoproteinemia	1	–	–
Total	**87**	**31**	**81**

The three gene panels successfully detected almost all types of solid tumors included in the study although some of the tumors (Table 24.2) remained undetected. There are several possible explanations for this result, including the specific characteristics in the progression of each tumor, and/or the quantity and quality of the DNA template extracted from bodily fluids. It is likely that the quality of this differs from that of the original tumor tissue due to the time of collection, the content of DNase, and the DNA integrity before and after the bisulfate modification among other factors. It is possible that none of the genes selected in the panel is methylated in the primary tumor, so no methylation would be detected in bodily fluids. On the contrary, it is possible that the primary tumors harbor some methylated genes in the panel but we were not able to detect them in the fluids. Maybe we have to design separate gene panels for tumors originating from specific organs. Epigenetic profiles of tumors from different organs do seem to be different. Although we all confirm that it is possible to detect malignant DNA from a variety of neoplasms, providing complementarity with cytology, and improving the diagnostic yield of the current standard examination of pleural fluid, it is clear that there are limitations to this technology. Besides those already discussed, in no study was there any corresponding epigenetic profiling being performed on the primary tumor from each patient in the study. These results may have added internal validity if the primary tumors had similar methylation profiles to the malignant pleural fluid. A parallel epigenetic study of the primary tumors would also have been useful for interpreting the pleural fluids of patients with only one MSP methylated gene.

Therefore, further studies are warranted to improve the sensitivity of the assay by verifying the minimum number of markers required to identify solid tumors that can metastasize to the pleural cavity. If

these studies conclude that a large number of markers are needed, high-throughput approaches other than MSP will have to be implemented such as the one commercialized by SEQUENOM that utilizes base-specific cleavage of nucleic acids. Samples are analyzed by matrix-assisted laser desorption ionization time-of-flight mass spectrometry (MALDI-TOF MS). This method permits the high-throughput identification of methylation sites and their semiquantitative measurement at single or multiple CpG positions and, therefore, achieves objectives mutually exclusive in many other currently used methods (Ehrich *et al*., 2005). The quantitative analysis of methylation in multiple CpG sites by pyrosequencing with Pyro Q-CpG from Biotage is available, in which single-stranded DNA templates by synthesizing complementary strand are analyzed. The four nucleotides (A, T, C, and G) are added sequentially by a Pyrosequencing instrument to the DNA templates. For every successful nucleotide incorporation, pyrophosphate (PPi) is released. Enzyme-catalysed reactions convert PPi to drive light emission in a quantity that is proportional to the number of incorporations (England, 2005). These kind of high-throughput methodologies will enable us to study a great number of genes and samples.

From the three studies discussed we can conclude that the detection of cell-free methylated DNA in pleural fluid can be performed in patients with neoplastic malignancy by means of a single extraction by thoracocentesis and adequate management, allowing for a rapid and reliable diagnosis in patients with pleural effusion suspected of malignancy without the need for other invasive procedures.

Acknowledgements. Supported by a grant from the Spanish Ministry of Health (FIS 01/3080) and a grant from SEOM (Spanish Society of Medical Oncology). Susana Benlloch is the recipient of a research contract from the Spanish Ministry of Health.

REFERENCES

Ang, P., Tan, E. H., Leong, S. S., Hoh, L., Eng, P., Agasthian, T., and Cheah, F. K. 2001. Primary intrathoracic malignant effusions: a descriptive study. *Chest 120*: 50–54.

Baylin, S. B., and Herman, J. G. 2000. DNA hypermethylation in tumorigenesis: epigenetics joins genetics. *Trends Genet. 16*: 168–174.

Baylin, S. B., Herman, J. G., Graff, J. R., Vertino, P. M., and Issa, J. P. (1998). Alterations in DNA methylation: a fundamental aspect of neoplasia. *Adv. Cancer Res. 72*: 141–196.

Baylin, S. B., Belinsky, S. A., and Herman, J. G. 2000. Aberrant methylation of gene promoters in cancer–concepts, misconcepts, and promise. *J. Natl. Cancer Inst. 92*: 1460–1461.

Belinsky, S. A., Palmisano, W. A., Gilliland, F. D., Crooks, L. A., Divine, K. K., Winters, S. A., Grimes, M. J., Harms, H. J., Tellez, C. S., Smith, T. M., Moots, P. P., Lechner, J. F., Stidley, C. A., and Crowell, R. E. 2002. Aberrant promoter methylation in bronchial epithelium and sputum from current and former smokers. *Cancer Res. 62*: 2370–2377.

Benlloch, S., Galbis-Caravajal, J. M., Martin, C., Sanchez-Paya, J., Rodriguez-Paniagua, J. M., Romero, S., Mafe, J. J., and Massuti, B. 2006. Potential diagnostic value of methylation profile in pleural fluid and serum from cancer patients with pleural effusion. *Cancer 107*: 1859–1865.

Brock, M. V., Hooker, C. M., Yung, R., Guo, M., Han, Y., Ames, S. E., Chang, D., Yang, S. C., Mason, D., Sussman, M., Baylin, S. B., and Herman, J. G. 2005. Can we improve the cytologic examination of malignant pleural effusions using molecular analysis? *Ann. Thorac. Surg. 80*: 1241–1247.

Dammann, R., Li, C., Yoon, J. H., Chin, P. L., Bates, S., and Pfeifer, G. P. 2000. Epigenetic inactivation of a RAS association domain family protein from the lung tumour suppressor locus 3p21.3. *Nat. Genet. 25*: 315–319.

Demmy, T. L., Nwogu, C. H., Sabiston, and Spencer. 2005. Malignant pleural and pericardical effusions. Surgery of the Chest. *In*: *Surgery of the Chest* (Ed., Sabiston and Spencer), pp. 450, vol. 7 Elsevier, Philadelphia, PA.

Eads, C. A., Danenberg, K. D., Kawakami, K., Saltz, L. B., Blake, C., Shibata, D., Danenberg, P. V., and Laird, P. W. 2000. MethyLight: a high-throughput assay to measure DNA methylation. *Nucleic Acids Res. 28*: E32.

Ehrich, M., Nelson, M. R., Stanssens, P., Zabeau, M., Liloglou, T., Xinarianos, G., Cantor, C. R., Field, J. K., and van den Boom, D. 2005. Quantitative high-throughput analysis of DNA methylation patterns by base-specific cleavage and mass spectrometry. *Proc. Natl. Acad. Sci. USA 102*: 15785–15790.

England, R. 2005. Pyro Q-CpG™: quantitative analysis of methylation in multiple CpG sites by pyrosequencing. *Nature Methods 2*: 1–2.

Esteller, M., Sanchez-Cespedes, M., Rosell, R., Sidransky, D., Baylin, S. B., and Herman, J. G. 1999. Detection of aberrant promoter hypermethylation of tumor suppressor genes in serum DNA from non-small cell lung cancer patients. *Cancer Res. 59*: 67–70.

Herman, J. G., Graff, J. R., Myohanen, S., Nelkin, B. D., and Baylin, S. B. 1996. Methylation-specific PCR: a novel PCR assay for methylation status of CpG islands. *Proc. Natl. Acad. Sci. USA 93*: 9821–9826.

Jones, P. A. 1996. DNA methylation errors and cancer. *Cancer Res. 56*: 2463–2467.

Jones, P. A. 1999. The DNA methylation paradox. *Trends Genet. 15*: 34–37.

Katayama, H., Hiraki, A., Aoe, K., Fujiwara, K., Matsuo, K., Maeda, T., Murakami, T., Toyooka, S., Sugi, K., Ueoka, H., and Tanimoto, M. 2007. Aberrant promoter methylation in pleural fluid DNA for diagnosis of malignant pleural effusion. *Int. J. Cancer 120*: 2191–2195.

Kim, H., Know, Y. M., Kim, J. S., Lee, H., Park, J. H., Shim, Y. M., Han, J., Park, J., and Kim, D. H. 2004. Tumor specific methylation in bronchial lavage for the early detection of non-small-cell lung cancer. *J. Clin. Oncol. 22*: 2363–2370.

Kissil, J. L., Feinstein, E., Cohen, O., Jones, P. A., Tsai, I. C., Knowles, M. A., Eydmann, M. A., and Kimchi, A. (1997). DAP-Kinase loss of expression in various carcinoma and B-cell lymphoma cell lines: possible implications for role as tumour suppressor gene. *Oncogene 15*: 403–407.

Laird, P. W. 2003. The power and the promise of DNA methylation markers. *Nat. Rev. Cancer 3*: 253–266.

Light, R. 1995. Malignant pleural diseases. *In* T. Edition, ed., Pleural diseases. Williams & Williams (3rd edition), Baltimore, MD.

Lu, X. P., Fanjul, A., Picard, N., Pfahl, M., Rungta, D., Nared-Hood, K., Carter, B., Piedrafita, J., Tang, S., Fabbrizio, E., and Pfahl, M. 1997. Novel retinoid-related molecules as apoptosis inducers and effective inhibitors of human lung cancer cells in vivo. *Nat. Med. 3*: 686–690.

Miedouge, M., Rouzaud, P., Salama, G., Pujazon, M. C., Vincent, C., Mauduyt, M. A., Reyre, J., Carles, P., and Serre, G. 1999. Evaluation of seven tumors markers in pleural fluid for the diagnosis of malignant effusions. *Br. J. Cancer 81*: 1059–1065.

Palmisano, W. A., Divine, K. K., Saccomanno, G., Gilliland, F. D., Baylin, S. B., Herman, J. G., and Belinsky, S. A. 2000. Predicting lung cancer by detecting aberrant promoter methylation in sputum. *Cancer Res. 60*: 5954–5958.

Ramirez, J. L., Sarries, C., de Castro, P. L., Roig, B., Queralt, C., Escuin, D., de Aguirre, I., Sanchez, J. M., Manzano, J. L., Margeli, M., Sanchez, J. J., Astudillo, J., Taron, M., and Rosell, R. 2003. Methylation patterns and K-ras mutations in tumor and paired serum of resected non-small-cell lung cancer patients. *Cancer Lett. 193*: 207–216.

Ramirez, J. L., Rosell, R., Taron, M., Sanchez-Ronco, M., Alberola, V., de Las Penas, R., Sanchez, J. M., Moran, T., Camps, C., Massuti, B., Sanchez, J. J., Salazar, F., and Catot, S. 2005. 14-3-3sigma methylation in pretreatment serum circulating DNA of cisplatin-plus-gemcitabine-treated advanced non-small-cell lung cancer patients predicts survival: The Spanish Lung Cancer Group. *J. Clin. Oncol. 23*: 9105–9112.

Robertson, K. D. 2005. DNA methylation and human disease. *Nat. Rev. Genet. 6*: 597–610.

Shames, D. S., Minna, J. D., and Gazdar, A. F. 2006. Methods for detecting DNA methylation in tumors: from bench to bedside. *Cancer Lett.*: 187–198.

Sherr, C. J. (1996). Cancer cell cycles. *Science 274*: 1672–1677.

Soria, J. C., Rodriguez, M., Liu, D., Lee, J., Hong, K. M., and Mao, L. 2002. Aberrant promoter

methylation of multiple genes in bronchial brush samples from former cigarette smokers. *Cancer Res. 62*: 351–355.

Takahashi, T., Shivapurkar, N., Riquelme, E., Shigematsu, H., Reddy, J. L., Suzuki, M., Miyajima, K., Zhou, X., Bekele, N., Gazdar, A. F., and Wistuba, I. 2004. Aberrant promoter hypermethylation of multiple genes in gallbladder carcinoma and chronic cholecystitis. *Clin. Cancer Res. 10*: 6126–6133.

Topaloglu, O., Hoque, M. O., Tokumaru, C. Y., Lee, J., Ratovitski, E., Sidransky, D., and Moon, C. 2004. Detection of promoter hypermethylation of multiple genes in the tumor and bronchoalveolar lavage of patients with lung cancer. *Clin. Cancer Res. 10*: 2284–2288.

Tsou, J. A., Hagen, J. A., Carpenter, C. L., and Laird-Offiga, I. A. 2002. DNA methylation analysis: a powerful new tool for lung cancer diagnosis. *Oncogene 21*: 5450–5461.

Wingo, P. A., Ries, L. A., Giovino, G. A., Miller, D. S., Rosenberg, H. M., Shopland, D. R., Thun, M. J., and Edwards, B. K. (1999). Annual report to the nation on the status of cancer 1973 – 1996. *J. Natl. Cancer Inst. 91*: 675–690.

Wong, T. S., Kwong, D. L., Sham, J. S., Wei, W. I., Kwong, Y. L., and Yuen, A. 2004. Quantitative plasma hypermethylated DNA markers of undifferentiated nasopharyngeal carcinoma. *Clin. Cancer Res. 10*: 2401–2406.

Yanagawa, N., Tamura, G., Oizumi, H., Takahashi, N., Shimazaki, Y., and Motoyama, T. 2003. Promoter hypermethylation of tumor suppressor and tumor-related genes in non-small cell lung cancers. *Cancer Sci. 94*: 589–592.

25
Pathological Distinction of Pulmonary Large Cell Neuroendocrine Carcinoma from Small-Cell Lung Carcinoma Using Immunohistochemistry

Kenzo Hiroshima

INTRODUCTION

For many years, only two major categories of pulmonary neuroendocrine tumors were recognized: the carcinoid tumor and small-cell lung carcinoma (SCLC). In 1972, Arrigoni *et al*. (1972) proposed pathologic criteria for the atypical carcinoid tumor. Atypical carcinoids have more evident cytologic atypia, cellularity, focal necrosis, and increased mitotic activity (between 5 and 10 mitoses per 10 high-power fields) than typical carcinoid tumors, and the clinical aggressiveness of atypical carcinoid is less than that of SCLC. Since then, neuroendocrine tumors of the lung have been classified into three categories: typical carcinoid, atypical carcinoid, and SCLC. In recent years, it has become apparent that a large variety of pulmonary neuroendocrine tumors exist and that some tumors cannot be easily classified into one of these three categories. Several new categories have been proposed such as neuroendocrine carcinoma of intermediate sized cells, large-cell neuroendocrine tumor of the lung, peripheral small-cell carcinoma of the lung resembling carcinoid tumor, and non-small cell lung carcinoma (NSCLC) with neuroendocrine features. In 1991, large cell neuroendocrine carcinoma (LCNEC) was proposed for the fourth high-grade neuroendocrine tumor of the lung (Travis *et al*., 1991).

The World Health Organization classification in 1999, which has been further refined with associated molecular and genetic associations, describes LCNEC as a variant of large cell carcinoma, and tumors of the lung with neuroendocrine morphology have three grades of low-grade typical carcinoid, intermediate-grade atypical carcinoid, and high-grade LCNEC and SCLC. In this lung tumor classification schema, large cell carcinomas are classified into four types based on neuroendocrine morphology as determined by light microscopy, and neuroendocrine differentiation demonstrable by immunohistochemistry and/or electron microscopy as follows: (1) LCNEC has both neuroendocrine morphology and evidence of neuroendocrine differentiation with immunohistochemistry and/or electron microscopy; (2) large cell carcinoma with neuroendocrine differentiation (LCCND) lacks neuroendocrine

morphology but has neuroendocrine markers with immunohistochemistry and/or electron microscopy; (3) large cell carcinoma with neuroendocrine morphology (LCCNM) has neuroendocrine morphologic features but lacks neuroendocrine markers with immunohistochemistry and/or electron microscopy; (4) classic large cell carcinoma (CLCC) lacks neuroendocrine morphology or differentiation. Iyoda *et al*. (2001a) sought to define the clinical characteristics of these four categories. They examined 119 cases of pulmonary large cell carcinoma. Fifty cases (42.0%) were classified as LCNEC, 9 (7.6%) as LCCND, 13 (10.9%) as LCCNM, and 47 (39.5%) as CLCC. They found that overall and disease-free survival for patients with carcinomas with neuroendocrine features, which included LCNEC, LCCND, and LCCNM, were significantly lower than for patients with CLCC.

SMALL-CELL LUNG CARCINOMA

Clinical Presentation

Small-cell lung carcinoma is a histologic subtype of lung cancer with a distinct biology and clinical course. This cancer has a rapid doubling time and a more aggressive clinical course than NSCLC, and it often disseminates at presentation. Small-cell lung carcinomas respond remarkably to chemotherapy initially, but they frequently relapse and metastasize. Govindan *et al*. (2006) reported on the incidence of SCLC using the surveillance, epidemiology and end results database. The incidence of SCLC as a percentage of the number of patients diagnosed with all types of lung cancer decreased from 17.26% in 1986 to 12.95% in 2002. Possible explanations for the decreased incidence include the decrease in the percentage of smokers and the change to low-tar filter cigarettes. However, one of the reasons for the decreased incidence of SCLC may be how pathologists distinguish between SCLC and NSCLC.

Pathologic Features

Architectural patterns include nesting, trabecular, peripheral palisading, and rosette formation. Sheet-like growth without these neuroendocrine morphologic patterns is common. Tumor cells of SCLC are round, oval, or spindle-shaped; they usually are less than the size of three small resting lymphocytes and have scant cytoplasm, finely granular chromatin, and absent or inconspicuous nucleoli (Figure 25.1). The cells have a high mitotic rate that averages over 60 mitoses per 2 mm^2. Necrosis is common and often extensive. Basophilic staining of vascular walls due to encrustation by DNA from necrotic tumor cells is frequent in areas of necrosis. The cell size of surgical specimens of SCLC often appears larger than typically seen in SCLC from bronchoscopic biopsy specimens. Once tumor cells with conspicuous nucleoli or pleomorphic giant tumor cells are identified, they are interpreted as large cell carcinoma elements; and when they constitute 10% or more of the tumor volume, the tumor is diagnosed as combined small cell and large cell carcinoma (SC/LC) (Nicholson *et al*., 2002).

Tumor cells in the tumor shown in Figure 25.2 are polygonal with a small amount of cytoplasm. The nuclei are relatively large, and the nuclear to cytoplasmic ratio is high. The nuclear chromatin is coarsely granular or vesicular. The nucleoli are usually observed but are small or

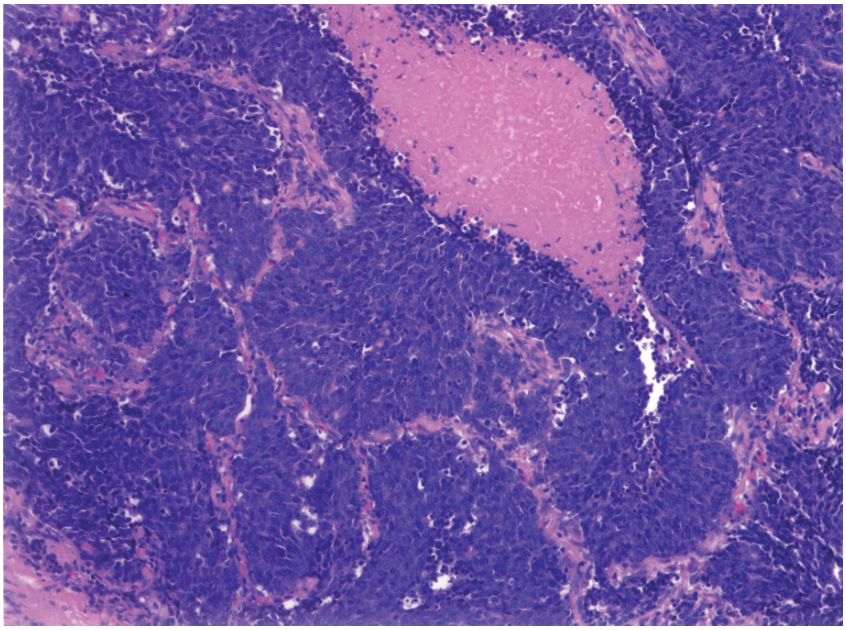

FIGURE 25.1. Small cell carcinoma. Cell size is small. Tumor cells have scant cytoplasm so the cellularity is high. The nuclei are round or oval. The chromatin of the nucleus is finely granular, and nucleoli are inconspicuous

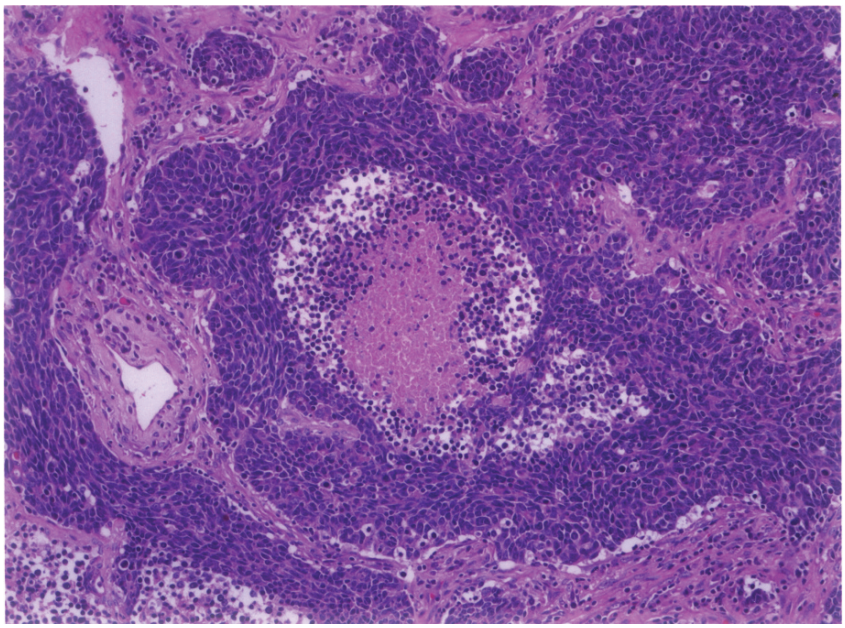

FIGURE 25.2. Small cell carcinoma. Cell size is larger than in Figure 25.1, but smaller than in Figure 25.3. Tumor cells are polygonal and have a moderate amount of cytoplasm. Rosette-like structures are present. The chromatin of the nucleus is vesicular, and nucleoli are seen. Necrosis is present.

inconspicuous. The mitotic rate is high. The tumors have organoid, trabecular, and palisading patterns, and a rosette-arrangement is common. We tentatively diagnose this tumor as SCLC. Nicholson *et al*. (2002) diagnosed the tumor as SCLC that had similar histological findings.

When patients receive treatment for SCLC, morphology different from the original tumor appears such as combined SC/LC or the addition of NSCLC. Whether these morphologic variations were present at the pretreatment stage of the disease or are due to the chemotherapeutic treatment cannot be determined.

Pelosi *et al*. (2005) studied bronchial biopsies from seven patients with typical carcinoid and atypical carcinoid that had been over-diagnosed as SCLC based on evaluation of bronchial biopsy specimens. Carcinoid tumors were composed of tumor cells that had granular and sometimes coarse nuclear chromatin patterns, high levels of chromogranin A/synaptophysin immunoreactivity, and a low (<20%) Ki-67 labeling index. In contrast, SCLCs had finely dispersed nuclear chromatin, lower levels of chromogranin A/synaptophysin immunoreactivity, and a high (>50%) Ki-67 labeling index. The authors concluded that there was an over-diagnosis of the carcinoid tumor as SCLC in small crushed bronchial biopsy specimens.

LARGE CELL NEUROENDOCRINE CARCINOMA

Clinical Presentation

The incidence of LCNEC is very low. It was reported to range from 2.4% to 3.1% in resected lung cancers that have been histologically confirmed to be LCNEC (Iyoda *et al*., 2001a; Takei *et al*., 2002). Patients with LCNEC are predominantly male (Iyoda *et al*., 2001a; Asamura *et al*., 2006), older, and heavy smokers (Iyoda *et al*., 2001a; Takei *et al*., 2002).

All-stage 5-year overall survival for LCNEC ranges from 15% to 57% (Iyoda et al., 2007). The prognoses for LCNEC are comparable to those for SCLC (Iyoda *et al*., 2002; Asamura *et al*., 2006). Iyoda *et al*. (2006a) analyzed 335 cases of pathologic stage Ia NSCLC treated by complete resection, and found that patients with LCNEC had worse prognosis than patients with non-neuroendocrine NSCLC. Therefore, surgical resection alone represents insufficient treatment for LCNEC, even for pathologic stage Ia disease.

Dresler *et al*. (1997) reported that there was no prolongation of survival in patients with LCNEC who received adjuvant therapy compared with those who did not, even in Stage I. However, in a retrospective study, Iyoda *et al*. (2001b) reported that adjuvant chemotherapy prolonged survival in early stage LCNEC but not in stage II or III disease. They recently reported a prospective study that found that adjuvant chemotherapy, consisting of cisplatin and VP-16, after surgery appears promising for the improvement of the prognosis for patients with completely resected LCNECs (Iyoda *et al*., 2006b). The study by Rossi *et al*. (2005) clearly confirms the role of a SCLC-based chemotherapy in an adjuvant setting even for stage I disease.

Pathologic Features

Large cell neuroendocrine carcinoma has histological features such as organoid nesting, trabecular, palisading, and rosette-like

patterns. The tumor cells of LCNEC are generally large and polygonal with moderate to abundant cytoplasm; nuclear chromatin is coarsely granular and nucleoli are prominent (Figure 25.3). Mitotic counts are typically 11 or more (average 75) per 2 mm^2 of viable tumor. A large infarct-like zone of necrosis is commonly present. Confirmation of neuroendocrine differentiation is required using immunohistochemistry or electron microscopy.

MORPHOMETRY

Tumor cells of SCLC are usually smaller than the size of three small resting lymphocytes. However, cell size in SCLC tends to be larger in large, well-fixed specimens, and some samples of SCLC contain scattered or clustered multinucleated tumor giant cells (Nicholson *et al*., 2002). Morphometry studies found a considerable overlap in nuclear size in the high-grade neuroendocrine neoplasms. Marchevsky *et al*. (2001) reported that they morphometrically evaluated H&E-stained sections from 16 SCLCs and 12 LCNECs. The nuclear size of the tumor cells and normal resting lymphocytes was measured using a SAMBA 4000 image analysis system. Approximately one-third of the SCLCs had considerable numbers of neoplastic cells that were larger than three normal lymphocytes, and 4 of 12 LCNECs had a predominant number of small cells. Hiroshima *et al*. (2006) measured the nuclear diameter of the tumor cells and lymphocytes in LCNEC and SCLC with a CAS 200 cellular imaging system, and reported that the average tumor nuclear diameter/lymphocyte size ratios were 3.22 for LCNEC and 2.75 for SCLC. The peak

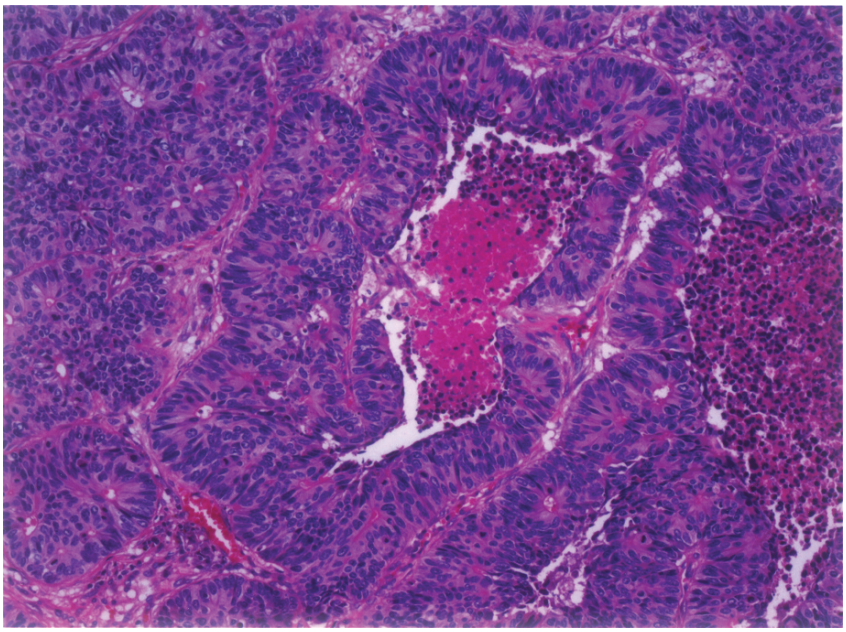

FIGURE 25.3. Large cell neuroendocrine carcinoma. This tumor has organoid nesting and a rosette-arrangement. Tumor cells have abundant eosinophilic cytoplasm, coarsely granular chromatin, and prominent nucleoli. Tumor cells with larger nuclei are observed. Necrosis is present

of tumor nuclear diameter/lymphocyte size ratios was between 3 and 4 for LCNEC and between 2 and 3 for SCLC.

MOLECULAR BIOLOGY

Recently, a genome-wide high-resolution search for loss of heterozygosity (LOH) was completed on SCLC and NSCLC cell lines. These studies found that some losses were common to both SCLC and NSCLC subtypes, whereas others were subtype specific. There are contradictory reports regarding the differences of genetic changes between SCLC and LCNEC. Some studies suggest that LCNECs are more akin genetically to SCLC than NSCLC. Przygodzki *et al.* (1996) reported that both SCLCs and LCNECs have mutations in *p53* exon 5, 7, or 8. They also performed sequence analysis for c-*raf*-1 and K-*ras*-2 in SCLCs and LCNECs; however, no point mutations in these oncogenes were found. LOH at 3p, 5q, 11q, 13q, and 17p was present in both SCLC and LCNEC (Onuki *et al*., 1999). Gugger *et al.* (2002) reported that c-*myc* amplification was observed with a similar frequency in SCLC (20%) and LCNEC (23%). Jones *et al.* (2004) reported that SCLC and LCNEC were indistinguishable with gene expression profiles, and high-grade neuroendocrine carcinoma of the lung can be classified into two groups independent of SCLC and LCNEC.

However, there are reports suggesting that there are abnormalities common to SCLC and LCNEC, but also different genetic changes in these two subtypes. Ullmann *et al.* (2001) reported that both SCLC and LCNEC shared several chromosomal aberrations, especially losses of 3p, 4q, 5q, and 13q and gains of 5p demonstrated by comparative genomic hybridization. However, they suggested that these aberrations could be found in nearly all high-grade lung carcinomas. They also showed that a gain of 3q and a loss of 10q and 17p were observed frequently in SCLC but not in LCNEC, and a gain of 6p occurred more frequently in LCNEC. Peng *et al.* (2005) examined SCLCs and LCNECs by using array-based comparative genomic hybridization method. The most frequent chromosomal alterations were observed with similar frequencies in both subtypes. However, significant differences between these tumors in terms of the frequencies and combinations of alterations were also observed. Losses at 3p26–22, 4q21, 4q24, and 4q31 were detected at significant levels in SCLC, whereas gains at 2q31, 2q32.2, and 2q33 and a loss at 6p21.3 were significantly correlated with LCNEC. Hiroshima *et al.* (2004) found that the frequency of LOH at 3p and 13q was high in LCNEC and SCLC, it was higher at 5q and 17p in SCLC than in LCNEC, and it was higher at 9p in LCNEC than in SCLC. Methylation of the *p16* gene was observed more frequently in LCNEC than in SCLC.

IMMUNOHISTOCHEMISTRY

The most useful markers for the diagnosis of neuroendocrine tumors are chromogranin A, synaptophysin, and CD56. Chromogranins A and B are glycoproteins originally detected in the adrenal medulla. These proteins are also present in a variety of neuroendocrine cells. Synaptophysin is a 38 kDa molecule that is associated with the synaptic vesicles of neurons and cells with neuroendocrine or neuroectodermal characteristics.

Guinee *et al*. (1994) examined the distribution of staining of biopsy specimens of SCLC with a panel of neuroendocrine markers. They found that chromogranin A was the most frequent neuroendocrine marker (60% in open-lung biopsy and 47% in transbronchial biopsy), followed by neuron-specific enolase (60% and 33%), CD57 (40% and 24%), and synaptophysin (5% and 19%). Nicholson *et al*. (2002) reported that 46 of 80 (58%) SCLCs were positive for chromogranin A; they were predominantly focal in distribution but strong in stain intensity. Forty-one of 72 (57%) SCLCs were positive for synaptophysin with a wider distribution of staining but generally less intense staining. Seventeen of 64 (27%) SCLCs were positive for CD57. Hiroshima *et al*. (2006) reported that chromogranin A was positive in 8 of 22 (36%) and synaptophysin was positive in 13 of 23 (57%) SCLCs. Specimens are commonly positive for neuron-specific enolase, but it has proven to be a less specific marker because up to 80% of NSCLCs will stain positive for it.

Guinee *et al*. (1994) reported that there was no staining for all neuroendocrine markers in as many as 25% of cases with SCLC. Nicholson *et al*. (2002) reported that there was no staining for neuroendocrine markers in 9 of 61 (15%) cases. These reports support the idea that negative staining results for neuroendocrine markers should not exclude a diagnosis of SCLC. Some poorly differentiated SCLCs may fail to express overt neuroendocrine differentiation to a degree detectable by our current methods.

Neuroendocrine differentiation must be confirmed by the use of immunohistochemistry (chromogranin A, synaptophysin, or CD56) or electron microscopy for the diagnosis of LCNEC. The positive staining rate for chromogranin A in LCNEC ranges from 59% to 82% (Takei *et al*., 2002; Hiroshima *et al*., 2006), and that of synaptophysin from 40% to 91% (Travis *et al*., 1991; Takei *et al*., 2002).

CD56

CD56 (neural cell adhesion molecule) is a cell-membrane protein that has a role in the cohesion of cells in the peripheral and central nervous systems. CD56 is found in natural killer cells and is distributed among neuroendocrine and neuroectodermal cells and tumors. It is reported that the antibody against CD56 diffusely stained most of an SCLC sample with a strong membranous pattern, and the staining intensity was not diminished in areas with crush artifacts or after decalcification (Kontogianni *et al*., 2005: 100%; Hiroshima *et al*., 2006: 96%; Nitadori *et al*., 2006: 100%). The positive staining rate for CD56 in LCNEC ranges from 53% to 100% (Casali *et al*., 2004; Hiroshima *et al*., 2006; Nitadori *et al*., 2006).

hASH1

Achaete-scute homolog-1 (termed Mash1 in rodents, hASH1 in humans) is a basic helix-loop-helix transcription factor important in early development of neural and neuroendocrine progenitor cells in multiple tissues, including the central nervous system, autonomic nervous system, adrenal medulla, thyroid, lung, and prostate. It is reported that hASH1 is expressed selectively in normal pulmonary neuroendocrine cells. hASH1 expression is strongly increased in lung cancers with neuroendocrine features, especially in SCLC. The frequency of expression of hASH1 is higher in SCLC than in LCNEC. Jiang

et al. (2004) reported that the frequency of expression of hASH1 is 71.8% in SCLC and 56.7% in LCNEC, and Hiroshima *et al*. (2006) reported 87% in SCLC and 59% in LCNEC.

TTF-1

The thyroid transcription factor-1 (TTF-1) is a nuclear transcription factor protein that mediates cell determination and differentiation in thyroid, lung, and brain. It is expressed in thyroid follicular cells, human fetal lung, and alveolar Type II epithelial cells after birth. TTF-1 regulates the expression of surfactant protein production. TTF-1 was detectable in pulmonary adenocarcinomas, SCLC, LCNEC, and CLCC but not in pulmonary squamous cell carcinomas. TTF-1 immunoreactivity occurs with a variable frequency in carcinoid tumors (Folpe *et al*., 1999); 18 of 51 (35%) typical carcinoids, all of 9 (100%) atypical carcinoids; (Kaufmann and Dietel, 2000); 4 of 9 (44%) typical carcinoids, 2 of 3 (67%) atypical carcinoids), or is absent (Sturm *et al*., 2000); 0 of 27 (0%) typical carcinoids, 0 of 23 (0%) atypical carcinoids; Hiroshima *et al*. (2006): 0 of 7 (0%) typical carcinoids, 0 of 2 (0%) atypical carcinoids). Because it is also expressed in extrapulmonary SCLCs and in extrapulmonary LCNECs, TTF-1 cannot be used to distinguish a primary versus metastatic lung tumor (Kaufmann and Dietel, 2000).

The frequency of expression of TTF-1 was reported to range from 80% to 95% in SCLCs (Folpe *et al*., 1999; Jerome Marson *et al*., 2004), whereas it ranged from 49% to 75% in LCNECs (Folpe *et al*., 1999; Sturm *et al*., 2002). Hiroshima *et al*. (2006) reported that 13 of 23 (57%) SCLCs and 4 of 17 (24%) LCNECs were immunoreactive for TTF-1. Nitadori *et al*. (2006) reported positive immunostaining in 6 of 14 (43%) SCLCs and 9 of 39 (23%) LCNECs. All cited studies found that the frequency of expression of TTF-1 is higher in SCLC than in LCNEC. The last two reports (Hiroshima *et al*., 2006; Nitadori *et al*., 2006) evaluated immunostaining in Japanese patients with high-grade neuroendocrine carcinomas, and the positive rates were lower compared with other reports. This may be due to the difference of race, the method of selection of the cases, or the interpretation of the results. The frequency of expression of TTF-1 was low in the neuroendocrine tumor shown in Figure 25.2 in our study (Kenzo Hiroshima, 2006 unpublished data).

Cytokeratins

Because differential diagnosis of SCLC includes lymphoma, cytokeratins (CKs) are often used to identify epithelial origin for the diagnosis of SCLC. Lymphoid lesions are keratin-negative and positive for lymphoid markers. Broers *et al*. (1987) tested for the presence of different subtypes of CKs in lung cancers. They found that the presence of CKs could be detected in 86% of SCLCs using pKer (several CKs), and in 92% of SCLCs using CAM5.2. Nicholson *et al*. (2002) reported that pancytokeratin (AE1/3LP34) was positive in 100% of the 70 SCLCs studied. The distribution of the staining was variable; however, a majority of the cases were stained strongly and diffusely throughout. Jerome Marson *et al*. (2004) studied different staining patterns of CKs in SCLC and LCNEC. Diffuse or membrane staining with CK7 was observed in 70% of LCNECs. In SCLCs, CKs were

absent or weakly expressed. CK19 was expressed intensely and diffusely by most NSCLCs, but a predominant or exclusive 'dot-like' pattern was suggestive of high-grade neuroendocrine carcinoma. Recently, Nitadori *et al*. (2006) reported that LCNECs had diffuse, strong expression of CK7 and CK18, as opposed to focal and weak expression in SCLCs.

p53, Rb, Bcl-2

Rusch *et al*. (1996) characterized patterns of expression of several molecular markers in pulmonary neuroendocrine tumors. They discovered that LCNEC and SCLC have higher rates of proliferation based on Ki-67 staining, abnormal p53, and absent Rb staining in comparison to typical carcinoid and atypical carcinoid, which have lower rates of proliferation, absent p53, and normal staining for Rb. Jiang *et al*. (1996, 1999) reported that Bcl-2 protein was detected in 104 of 111 (94%) SCLCs, and in 24 of 26 (92%) LCNECs. Iyoda *et al*. (2002) reported that immunohistochemical staining for p53 was comparable in LCNEC (12 of 20 (60%)) and CLCC (10 of 13 (77%)); however, immunohistochemical staining for Bcl-2 was significantly higher in LCNEC (11 of 20 (55%)) than CLCC (0 of 13 (0%)). These reports showed that LCNEC has identical cell cycle protein abnormalities and high antiapoptotic activity similar to SCLC and that these markers cannot differentiate LCNEC from SCLC.

CD117

The proto-oncogene c-*kit,* mapping to 4q11-q12 and encoding a cell-surface tyrosine kinase (CD117), acts as growth factor receptor involved in cell differentiation and proliferation. Sekido *et al*. (1991) demonstrated with Northern blot analysis that most SCLC tumors and cell lines expressed c-*kit* transcripts, whereas NSCLC tumors and cell lines did not. Araki *et al*. (2003) reported that c-kit protein was over-expressed in 55% of the LCNEC tumor cells and 46% of the SCLC tumor cells. Casali *et al*. (2004) found that the c-kit protein is frequently expressed in LCNEC (20 of 33 (61%)) and its expression is a negative prognostic factor. Pelosi *et al*. (2004) reported that membrane CD117 immunoreactivity occurred in 77% of LCNECs and 67% of SCLCs; whereas cytoplasmic labeling was seen in 44% of LCNECs and 70% of SCLCs. The different prevalences of CD117 may be explained in part by the different selection criteria for assessing immunoreactivity. The results of these reports suggest that CD117 cannot differentiate LCNEC from SCLC.

DIFFERENTIAL DIAGNOSIS

Large cell neuroendocrine carcinoma and SCLC can be easily distinguished from one another in some cases. The distinction of SCLC and LCNEC should not rest on cell size alone but should incorporate additional features including nuclear to cytoplasmic ratio, nuclear chromatin, nucleoli, nuclear molding, cell shape (fusiform versus polygonal), and hematoxylin vascular staining (Travis *et al*., 1991). Some of the disagreements regarding identification might occur due to different pathologists' perceptions of size and shape of tumor cells. Most patients with SCLC have greater than stage I disease and are not surgical candidates; and in >90% of cases,

the diagnosis is reliably established based on small biopsy or cytology specimens (Nicholson *et al*., 2002). Disagreement over the distinction of SCLC and NSCLC among expert lung cancer pathologists may occur in up to 5% of cases.

Few studies address the histologic features of SCLC based on surgical biopsy or resected tumors. Nicholson *et al*. (2002) found that the histologic appearance of SCLC in surgical biopsies or resected tumors is quite different from small biopsy specimens. Cell size in surgical biopsy specimens appears larger than in bronchoscopic biopsy specimens, and occasional cells may show prominent nucleoli and vesicular nuclear chromatin. Frequent combinations with NSCLC (28%) are sources of considerable diagnostic difficulty. Thickly cut sections and overstaining with hematoxylin may obscure conspicuous nucleoli and truly vesicular chromatin, and in this situation NSCLC is easily misinterpreted as SCLC.

In a study by Travis *et al*. (1998), 40 neuroendocrine tumors were independently evaluated by five lung pathologists and classified as typical carcinoid, atypical carcinoid, LCNEC, or SCLC. There was unanimous diagnostic agreement on 70% of SCLCs and 40% of LCNECs in surgically resected neuroendocrine tumors of the lung. Most of the disagreements concerned the distinction between SCLC and LCNEC. The authors stated that the results indicated a need for more careful definition and application of criteria for SCLC versus LCNEC. Takei *et al*. (2002) reported that, after reviewing retrospectively SCLC diagnoses according to the histological criteria of the World Health Organization classification, 24 of 55 (44%) diagnoses of SCLC were converted to LCNEC. These studies suggest that there is overlap in the pathologic findings of SCLC and LCNEC and the separation of the two categories is difficult in some cases.

Small-cell lung carcinoma and LCNEC have similar neuroendocrine markers, cell cycle protein abnormalities, and similar genetic alterations as determined by LOH analysis. It is difficult to differentiate LCNEC from SCLC with immunostaining one marker. One possible marker may be CD56. Most SCLCs have strong positive membranous staining for CD56 and most LCNECs have negative or focal staining. However, there are some LCNECs that have strong positive membranous staining similar to that of SCLCs.

Some suggested that in daily practice the tumors should be combined into a single group as a high-grade neuroendocrine carcinoma (Marchevsky *et al*., 2001). However, LCNEC and SCLC should be kept separate, because the optimal therapy for LCNEC is different from that for SCLC. Although it is not clear how patients with LCNEC should be treated, surgery is advocated for the treatment of patients with LCNEC. Recent reports suggest that patients with LCNEC may respond to SCLC chemotherapy regimens (Iyoda *et al*., 2001b, 2006b; Rossi *et al*., 2005).

Difficulty of diagnosis of high-grade neuroendocrine carcinoma is thought to be due to a variety of reasons, including the existence of high-grade neuroendocrine carcinomas that have a mixture of small and large cells (Travis *et al*., 1998), the continuum of cell size and morphology between SCLC and LCNEC, and the poor sampling and tissue artifacts due to small crushed biopsy specimens, ischemic changes, poor fixation, and poor histologic sections (Travis *et al*., 1991). It is reported that there are bor-

derline cases between LCNEC and SCLC in high-grade neuroendocrine carcinoma (Asamura *et al*., 2006). We propose that another reason may relate to how pathologists diagnose tumors as shown in Figure 25.2. We tentatively diagnosed this tumor as SCLC because the nuclear to cytoplasmic ratio is high and the cytoplasm is not abundant. However, some pathologists may diagnose this same case as LCNEC because the shape of the tumor cell is polygonal, the nuclear diameter is larger than that of typical SCLC, and nucleoli are observed. The average tumor nuclear diameter/lymphocyte size ratio in the tumors shown in Figure 25.2 is 2.91, which is significantly larger than that in a typical SCLC (2.62) (Kenzo Hiroshima, 2006 unpublished-data). Most of the tumors shown in Figure 25.2 are CD56 positive, hASH1 positive, chromogranin A negative, and synaptophysin negative. However, methylation of the *p16* gene, which is not observed in a typical SCLC, is observed in half of the tumors and the frequency of the expression of TTF-1 (which is often expressed in SCLCs) is low. The LOH analysis showed that genetic changes in this tumor are close to those in SCLC. These facts suggest that this tumor has the characteristics of both LCNEC and SCLC. Additional studies in a larger series are needed to elucidate the molecular and immunohistochemical characteristics of these tumors and analyze the biological behavior including sensitivity to chemotherapeutic agents.

REFERENCES

Araki, K., Ishii, G., Yokose, T., Nagai, K., Funai, K., Kodama, K., Nishiwaki, Y., and Ochiai, A. 2003. Frequent overexpression of the c-kit protein in large cell neuroendocrine carcinoma of the lung. *Lung Cancer 40*: 173–180.

Arrigoni, M.G., Woolner, L.B., and Bernatz, P.E. 1972. Atypical carcinoid tumors of the lung. *J. Thorac. Cardiovasc. Surg. 64*: 413–421.

Asamura, H., Kameya, T., Matsuno, Y., Noguchi, M., Tada, H., Ishikawa, Y., Yokose, T., Jiang, S.X., Inoue, T., Nakagawa, K., Tajima, K., and Nagai, K. 2006. Neuroendocrine neoplasms of the lung: a prognostic spectrum. *J. Clin. Oncol. 24*: 70–76.

Broers, J.L., Rot, M.K., Oostendorp, T., Huysmans, A., Wagenaar, S.S., Wiersma-van Tilburg, A.J., Vooijs, G.P., and Ramaekers, F.C. 1987. Immunocytochemical detection of human lung cancer heterogeneity using antibodies to epithelial, neuronal, and neuroendocrine antigens. *Cancer Res. 47*: 3225–3234.

Casali, C., Stefani, A., Rossi, G., Migaldi, M., Bettelli, S., Parise, A., and Morandi, U. 2004. The prognostic role of c-kit protein expression in resected large cell neuroendocrine carcinoma of the lung. *Ann. Thorac. Surg. 77*: 247–252.

Dresler, C.M., Ritter, J.H., Patterson, G.A., Ross, E., Bailey, M.S., and Wick, M.R. 1997. Clinicalpathologic analysis of 40 patients with large cell neuroendocrine carcinoma of the lung. *Ann. Thorac. Surg. 63*: 180–185.

Folpe, A.L., Gown, A.M., Lamps, L.W., Garcia, R., Dail, D.H., Zarbo, R.J., and Schmidt, R.A. 1999. Thyroid transcription factor-1: immunohistochemical evaluation in pulmonary neuroendocrine tumors. *Mod. Pathol. 12*: 5–8.

Govindan, R., Page, N., Morgensztern, D., Read, W., Tierney, R., Vlahiotis, A., Spitznagel, E.L., and Piccirillo, J. 2006. Changing epidemiology of small-cell lung cancer in the United States over the last 30 years: analysis of the surveillance, epidemiologic, and end results database. *J. Clin. Oncol. 24*: 4539–4544.

Gugger, M., Burckhardt, E., Kappeler, A., Hirsiger, H., Laissue, J.A., and Mazzucchelli, L. 2002. Quantitative expansion of structural genomic alterations in the spectrum of neuroendocrine lung carcinomas. *J. Pathol. 196*: 408–415.

Guinee, D.G. Jr, Fishback, N.F., Koss, M.N., Abbondanzo, S.L., and Travis, W.D. 1994. The spectrum of immunohistochemical staining of small-cell lung carcinoma in specimens from transbronchial and open-lung biopsies. *Am. J. Clin. Pathol. 102*: 406–414.

Hiroshima, K., Iyoda, A., Shibuya, K., Haga, Y., Toyozaki, T., Iizasa, T., Nakayama, T., Fujisawa,

T., and Ohwada, H. 2004. Genetic alterations in early-stage pulmonary large cell neuroendocrine carcinoma. *Cancer 100*: 1190–1198.

Hiroshima, K., Iyoda, A., Shida, T., Shibuya, K., Iizasa, T., Kishi, H., Tanizawa, T., Fujisawa, T., and Nakatani, Y. 2006. Distinction of pulmonary large cell neuroendocrine carcinoma from small cell lung carcinoma: a morphological, immunohistochemical, and molecular analysis. *Mod. Pathol. 19*: 1358–1368.

Iyoda, A., Hiroshima, K., Toyozaki, T., Haga, Y., Fujisawa, T., and Ohwada, H. 2001a. Clinical characterization of pulmonary large cell neuroendocrine carcinoma and large cell carcinoma with neuroendocrine morphology. *Cancer 91*: 1992–2000.

Iyoda, A., Hiroshima, K., Toyozaki, T., Haga, Y., Baba, M., Fujisawa, T., and Ohwada, H. 2001b. Adjuvant chemotherapy for large cell carcinoma with neuroendocrine features. *Cancer 92*: 1108–1112.

Iyoda, A., Hiroshima, K., Baba, M., Saitoh, Y., Ohwada, H., and Fujisawa, T. 2002. Pulmonary large cell carcinomas with neuroendocrine features are high-grade neuroendocrine tumors. *Ann. Thorac. Surg. 73*: 1049–1054.

Iyoda, A., Hiroshima, K., Moriya, Y., Sekine, Y., Shibuya, K., Iizasa, T., Nakatani, Y., and Fujisawa, T. 2006a. Prognostic impact of large cell neuroendocrine histology in patients with pathologic stage Ia pulmonary non-small cell carcinoma. *J. Thorac. Cardiovasc. Surg. 132*: 312–315.

Iyoda, A., Hiroshima, K., Moriya, Y., Takiguchi, Y., Sekine, Y., Shibuya, K., Iizasa, T., Kimura, H., Nakatani, Y., and Fujisawa, T. 2006b. Prospective study of adjuvant chemotherapy for pulmonary large cell neuroendocrine carcinoma. *Ann. Thorac. Surg. 82*: 1802–1807.

Iyoda, A., Hiroshima, K., Nakatani, Y., and Fujisawa, T. 2007. Pulmonary large cell neuroendocrine carcinoma: its place in the spectrum of pulmonary carcinoma. *Ann. Thorac. Surg. 84:* 702–707.

Jerome Marson, V., Mazieres, J., Groussard, O., Garcia, O., Berjaud, J., Dahan, M., Carles, P., and Daste, G. 2004. Expression of TTF-1 and cytokeratins in primary and secondary epithelial lung tumours: correlation with histological type and grade. *Histopathology 45*: 125–134.

Jiang, S.X., Kameya, T., Sato, Y., Yanase, N., Yoshimura, H., and Kodama, T. 1996. Bcl-2 protein expression in lung cancer and close correlation with neuroendocrine differentiation. *Am. J. Pathol. 148*: 837–846.

Jiang, S.X., Kameya, T., Shinada, J., and Yoshimura, H. 1999. The significance of frequent and independent p53 and bcl-2 expression in large-cell neuroendocrine carcinomas of the lung. *Mod. Pathol. 12*: 362–369.

Jiang, S.X., Kameya, T., Asamura, H., Umezawa, A., Sato, Y., Shinada, J., Kawakubo, Y., Igarashi, T., Nagai, K., and Okayasu, I. 2004. hASH1 expression is closely correlated with endocrine phenotype and differentiation extent in pulmonary neuroendocrine tumors. *Mod. Pathol. 17*: 222–229.

Jones, M.H., Virtanen, C., Honjoh, D., Miyoshi, T., Satoh, Y., Okumura, S., Nakagawa, K., Nomura, H., and Ishikawa, Y. 2004. Two prognostically significant subtypes of high-grade lung neuroendocrine tumours independent of small-cell and large-cell neuroendocrine carcinomas identified by gene expression profiles. *Lancet 363*: 775–781.

Kaufmann, O., and Dietel, M. 2000. Expression of thyroid transcription factor-1 in pulmonary and extrapulmonary small cell carcinomas and other neuroendocrine carcinomas of various primary sites. *Histopathology 36*: 415–420.

Kontogianni, K., Nicholson, A.G., Butcher, D., and Sheppard, M.N. 2005. CD56: a useful tool for the diagnosis of small cell lung carcinomas on biopsies with extensive crush artefact. *J. Clin. Pathol. 58*: 978–980.

Marchevsky, A.M., Gal, A.A., Shah, S., and Koss, M.N. 2001. Morphometry confirms the presence of considerable nuclear size overlap between "small cells" and "large cells" in high-grade pulmonary neuroendocrine neoplasms. *Am. J. Clin. Pathol. 116*: 466–472.

Nicholson, S.A., Beasley, M.B., Brambilla, E., Hasleton, P.S., Colby, T.V., Sheppard, M.N., Falk, R., and Travis, W.D. 2002. Small cell lung carcinoma (SCLC): a clinicopathologic study of 100 cases with surgical specimens. *Am. J. Surg. Pathol. 26*: 1184–1197.

Nitadori, J., Ishii, G., Tsuta, K., Yokose, T., Murata, Y., Kodama, T., Nagai, K., Kato, H., and Ochiai, A. 2006. Immunohistochemical differential diagnosis between large cell neuroendocrine carcinoma and small cell carcinoma by tissue microarray analysis with a large antibody panel. *Am. J. Clin. Pathol. 125*: 682–692.

Onuki, N., Wistuba, I.I., Travis, W.D., Virmani, A.K., Yashima, K., Brambilla, E., Hasleton, P., and Gazdar, A.F. 1999. Genetic changes in the spectrum of neuroendocrine lung tumors. *Cancer 85*: 600–607.

Pelosi, G., Masullo, M., Leon, M.E., Veronesi, G., Spaggiari, L., Pasini, F., Sonzogni, A., Iannucci, A., Bresaola, E., and Viale, G. 2004. CD117 immunoreactivity in high-grade neuroendocrine tumors of the lung: a comparative study of 39 large-cell neuroendocrine carcinomas and 27 surgically resected small-cell carcinomas. *Virchows Arch. 445*: 449–455.

Pelosi, G., Rodriguez, J., Viale, G., and Rosai, J. 2005. Typical and atypical pulmonary carcinoid tumor overdiagnosed as small-cell carcinoma on biopsy specimens: a major pitfall in the management of lung cancer patients. *Am. J. Surg. Pathol. 29*: 179–187.

Peng, W.X., Shibata, T., Katoh, H., Kokubu, A., Matsuno, Y., Asamura, H., Tsuchiya, R., Kanai, Y., Hosoda, F., Sakiyama, T., Ohki, M., Imoto, I., Inazawa, J., and Hirohashi, S. 2005. Array-based comparative genomic hybridization analysis of high-grade neuroendocrine tumors of the lung. *Cancer Sci. 96*: 661–667.

Przygodzki, R.M., Finkelstein, S.D., Langer, J.C., Swalsky, P.A., Fishback, N., Bakker, A., Guinee, D.G., Koss, M., and Travis, W.D. 1996. Analysis of p53, K-ras-2, and C-raf-1 in pulmonary neuroendocrine tumors. Correlation with histological subtype and clinical outcome. *Am. J. Pathol. 148*: 1531–1541.

Rossi, G., Cavazza, A., Marchioni, A., Longo, L., Migaldi, M., Sartori, G., Bigiani, N., Schirosi, L., Casali, C., Morandi, U., Facciolongo, N., Maiorana, A., Bavieri, M., Fabbri, L.M., and Brambilla, E. 2005. Role of chemotherapy and the receptor tyrosine kinases KIT, PDGFRalpha, PDGFRbeta, and Met in large-cell neuroendocrine carcinoma of the lung. *J. Clin. Oncol. 23*: 8774–8785.

Rusch, V.W., Klimstra, D.S., and Venkatraman, E.S. 1996. Molecular markers help characterize neuroendocrine lung tumors. *Ann. Thorac. Surg. 62*: 798–810.

Sekido, Y., Obata, Y., Ueda, R., Hida, T., Suyama, M., Shimokata, K., Ariyoshi, Y., and Takahashi, T. 1991. Preferential expression of c-kit protooncogene transcripts in small cell lung cancer. *Cancer Res. 51*: 2416–2419.

Sturm, N., Rossi, G., Lantuejoul, S., Papotti, M., Frachon, S., Claraz, C., Brichon, P.Y., Brambilla, C., and Brambilla, E. 2002. Expression of thyroid transcription factor-1 in the spectrum of neuroendocrine cell lung proliferations with special interest in carcinoids. *Hum. Pathol. 33*: 175–182.

Takei, H., Asamura, H., Maeshima, A., Suzuki, K., Kondo, H., Niki, T., Yamada, T., Tsuchiya, R., and Matsuno, Y. 2002. Large cell neuroendocrine carcinoma of the lung: a clinicopathologic study of eighty-seven cases. *J. Thorac. Cardiovasc. Surg. 124*: 285–292.

Travis, W.D., Linnoila, R.I., Tsokos, M.G., Hitchcock, C.L., Cutler, G.B. Jr, Nieman, L., Chrousos, G., Pass, H., and Doppman, J. 1991. Neuroendocrine tumors of the lung with proposed criteria for large-cell neuroendocrine carcinoma. *Am. J. Surg. Pathol. 15*: 529–553.

Travis, W.D., Gal, A.A., Colby, T.V., Klimstra, D.S., Falk, R., and Koss, M.N. 1998. Reproducibility of neuroendocrine lung tumor classification. *Hum. Pathol. 29*: 272–279.

Ullmann, R., Petzmann, S., Sharma, A., Cagle, P.T., and Popper, H.H. 2001. Chromosomal aberrations in a series of large-cell neuroendocrine carcinomas: unexpected divergence from small-cell carcinoma of the lung. *Hum. Pathol. 32*: 1059–1063.

26
Differentiation Between Pleuropulmonary Desmoid Tumors and Solitary Fibrous Tumors: Role of Histology and Immunohistochemistry

Dani S. Zander and Loren E. Clarke

INTRODUCTION

Pleuropulmonary desmoid tumors (DTs) are extremely rare tumors that can histologically resemble other neoplasms more common to the lungs and pleura. Differentiating between desmoid tumors and solitary fibrous tumors (SFTs) can be particularly difficult. Other entities that may also be considered in the differential diagnosis include desmoplastic malignant mesothelioma, fibrosarcoma and variants, other spindle cell sarcomas, inflammatory myofibroblastic tumor, schwannoma, scar, and the capsule surrounding another process. Although the clinical and radiographic presentations of DTs and SFTs differ somewhat, and therefore clinical information can favor one diagnosis or the other, ultimately histological distinction is crucial.

Intrathoracic desmoid tumors typically arise in the chest wall and can protrude or extend into the pleural cavity secondarily. Rare cases, however, have been described that appear to represent true primary pleural or pulmonary neoplasms (Winer-Muram *et al*., 1994; Wilson *et al*., 1999; Iqbal *et al*., 2001; Andino *et al*., 2006). SFTs, on the other hand, have been reported in most organ systems, but most commonly arise in the pleura, forming well-circumscribed and sometimes polypoid or pedunculated pleural-based masses. Although defined histopathologic criteria exist to separate these tumors microscopically, these features may not be apparent in small or less representative samples. Fortunately, as reviewed by Andino *et al*. (2006) and Wilson *et al*. (1999), immunohistochemistry can aid in the distinction between primary pleuropulmonary DTs and SFTs, while also providing insight into the pathogenesis of these unusual neoplasms.

GROSS AND MICROSCOPIC PATHOLOGY

Gross Features

Grossly, DTs and SFTs typically have a broad-based or sometimes polypoid appearance with a smooth surface. Infiltrative edges may be apparent in some cases. Both types of neoplasms range in size and can measure up to 16 cm. As reviewed in the World Health Organization classification of tumors (Travis *et al*., 2004), SFTs most often arise in the visceral pleura, but can also originate in the parietal pleura or lung

parenchyma. Origin from the parietal pleura, conversely, appears to be more common with DTs. On the cut surface, both entities have a white or tan appearance and SFTs can have a whorled or myxoid appearance. Necrosis or hemorrhage can be seen in some SFTs and raises the question of malignancy, as does large size. Sampling of these neoplasms should be generous in order to microscopically evaluate for malignant features.

Microscopic Features

Microscopically, pleuropulmonary DTs and SFTs resemble those arising in other locations (Granville *et al*., 2005). DTs show relatively low cellularity, and usually consist of slender spindle-shaped and stellate cells with normochromatic nuclei and small, inconspicuous nucleoli (Figure 26.1A–D). The cells are relatively evenly spaced and are arranged both randomly and in long, ill-defined fascicles. Mitotic activity is variable. Typical DTs have a loose collagenous stroma, but occasional examples contain collagen that is keloid-like or hyalinized (Figure 26.1D). Myxoid stroma may also be seen in some cases (Figure 26.1B). Ectatic, thin-walled 'hemangiopericytoma-like' vessels are a common feature of DTs.

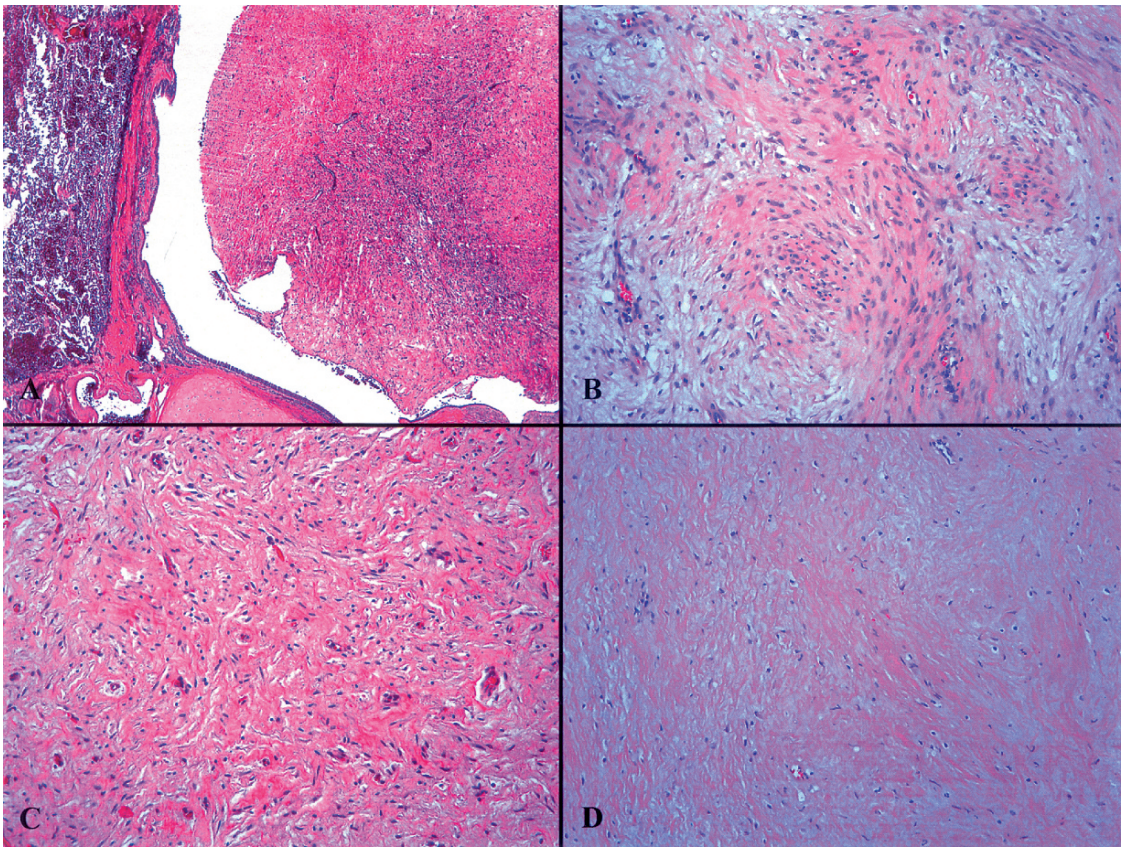

FIGURE 26.1. *Desmoid tumor histology*. (A) This polypoid intrabronchial desmoid tumor caused near total airway obstruction. (B) The neoplastic cells are slender and spindle shaped, and the stroma demonstrates collagenization and myxoid change. (C) The cytologically bland spindle cells are accompanied by more extensive collagenization. (D) Portions of this tumor have a relatively hypocellular appearance, with abundant dense and focally hyalinized collagen

SFTs tend to be more cellular than DTs and consist of plump ovoid or spindled cells with scant cytoplasm and normochromatic nuclei with finely dispersed chromatin (Figure 26.2A–D). Short fascicles or storiform arrangements, a "patternless pattern," (Figure 26.2A) or hemangiopericytoma-like architectural patterns (Figure 26.2C) can be seen, sometimes varying from area to area in an individual lesion. As with DTs, keloidal-type collagen, stromal hyalinization and branching thin-walled vessels are common (Figure 26.2B). Myxoid stroma is not uncommon, similar to DTs. Multinucleated stromal cells and mast cells may be encountered in occasional cases. Mitotic activity is variable, but mitotic figures usually number less than 3 per 10 high-power fields. Malignant SFTs are composed of similar types of cells and stroma as their benign counterparts, and exhibit the same range of architectural patterns. However, they tend to be more cellular, with increased pleomorphism and necrosis, and show mitotic rates greater than four mitoses per 10 high-power fields. As reviewed by Guillou *et al*. (2002), some examples of otherwise benign-appearing SFTs exhibit abrupt transition to frankly malignant areas. Like DTs, malignant SFTs may have an infiltrative growth pattern.

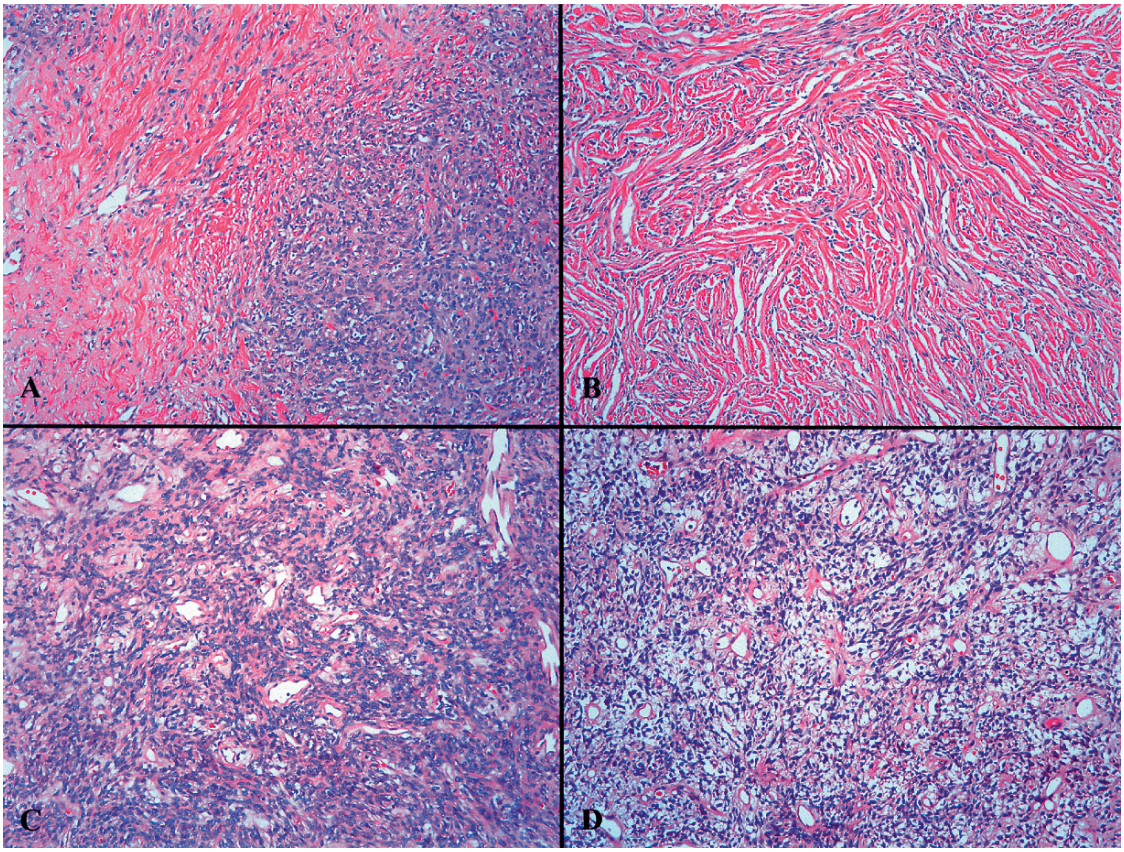

FIGURE 26.2. *Solitary fibrous tumor – histology*. (A) This tumor displays a heterogeneous histologic appearance with a "patternless pattern". Tumor cellularity and collagen deposition vary widely from region to region. (B) This example has abundant dense collagen with interspersed slender spindle cells. (C) A hemangiopericytomatous pattern is conspicuous. (D) Cells with clear cytoplasm are present in this tumor, which also has hemangiopericytomatous features

IMMUNOHISTOCHEMISTRY

Conventional Antibodies

A comprehensive panel that will assist in differentiation between the main pleuropulmonary entities in the differential diagnosis includes the following primary antibodies: smooth muscle actin (SMA), muscle-specific actin (MSA), CD34, bcl-2, S100, pankeratin, and ALK1. The size of the panel can be reduced in some cases depending upon the specific histology and the probabilities of individual diagnoses, but these antibodies have proven useful for distinguishing between the diagnostic possibilities (Andino *et al*., 2006). Similar patterns of immunoreactivity have been noted in examples of these lesions arising in other anatomic sites (Weiss and Goldblum, 2001).

For differentiating between pleuropulmonary DTs and SFTs, SMA, MSA, CD34, and bcl-2 are most useful (Table 26.1). DTs characteristically show intermediate or high degrees of immunoreactivity with SMA (Figure 26.3B), but no reactivity with CD34 (Figure 26.3D). Conversely, over 90% of SFTs, including benign and malignant SFTs, demonstrate immunoreactivity with CD34 (Figure 26.4D), while SMA is usually (although not invariably) negative (Figure 26.4B). Similarly, MSA usually shows intermediate or high levels of immunoreactivity with DTs (Figure 26.3C), while most SFTs do not stain (Figure 26.4C). Desmin is less helpful, showing immunoreactivity in more DTs than SFTs, but with lower frequencies of staining than SMA and MSA, in DTs. Bcl-2 is also worthwhile to use in assessing these tumors, because it is reactive with over 90% of SFTs but not with DTs. Vimentin is immunoreactive with virtually all DTs and SFTs (Figures 26.3A and 26.4A), so it is therefore of no value for distinguishing between the two processes.

Although S100, pancytokeratin, and ALK1 do not aid in distinguishing between DTs and SFTs, these antibodies have utility for assessing the likelihood of other entities in the differential diagnosis. S100 is useful for differentiating DTs and SFTs (immunonegative) from schwannoma (immunopositive). Pankeratin is helpful for distinguishing DTs and SFTs (immunonegative) from malignant mesotheliomas, spindle cell carcinomas, and synovial sarcomas (usually immunopositive). ALK1 expression is valuable for supporting a diagnosis of inflammatory myofibroblastic tumor, but expression is absent in DTs and SFTs. This antibody can be particularly important in evaluating pulmonary DTs vs. inflammatory myofibroblastic tumors, since both express muscle markers.

TABLE 26.1. Typical immunohistochemical reactivities of desmoid tumors and solitary fibrous tumors.

	SMA	MSA	Desmin	CD34	Bcl-2	S100	Pankeratin	ALK1	Vimentin
Desmoid tumors	+	+	+/−	−	−	−	−	−	+
Solitary fibrous tumors	−	−	−	+	+	−	−	−	+

SMA: smooth muscle actin; MSA: muscle-specific actin; +: positive; −: negative; +/−: positive or negative with similar frequencies.

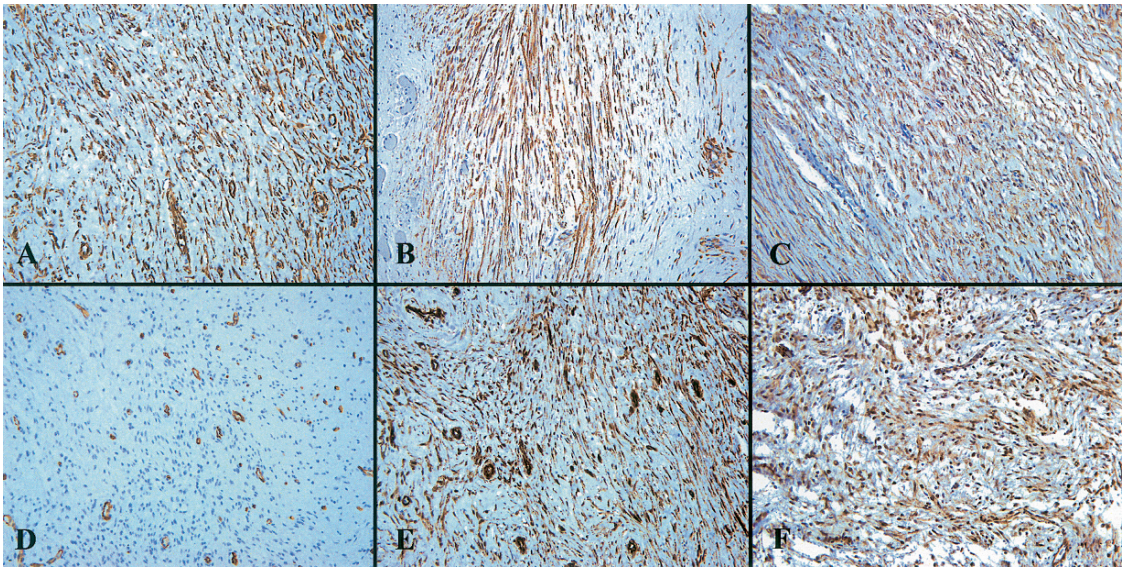

FIGURE 26.3. *Desmoid tumor – immunohistochemistry*. Staining for vimentin (A), smooth muscle actin (B), and muscle-specific actin (C) are characteristic of desmoid tumors. CD34, on the other hand, is negative (D). Nuclear and cytoplasmic staining for β-catenin (E) and cyclin D1 (F) are also shown

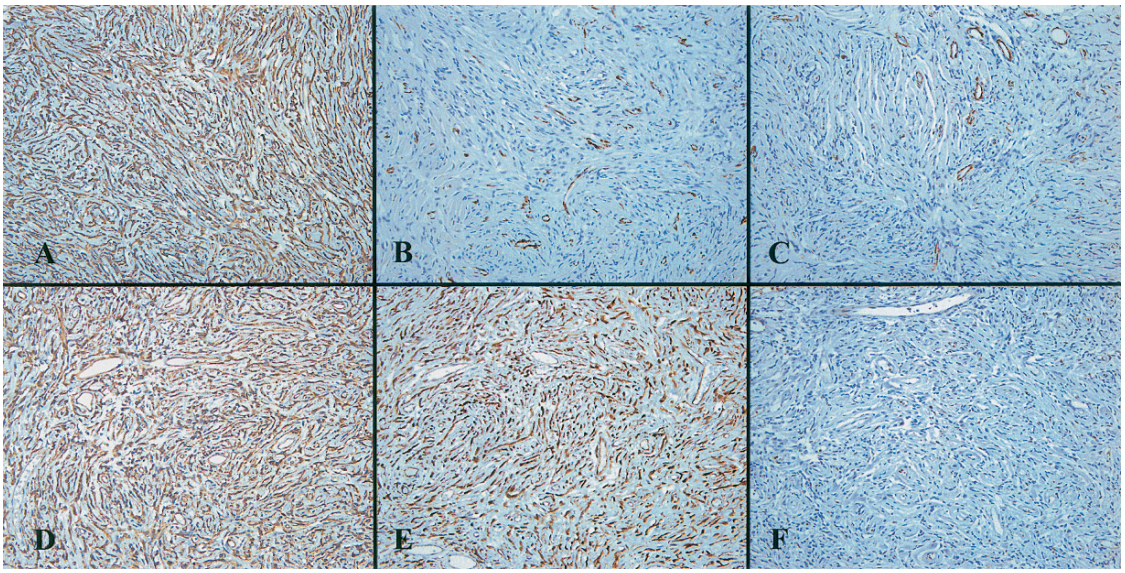

FIGURE 26.4. *Solitary fibrous tumor – immunohistochemistry*. Like desmoid tumors, staining for vimentin (A) is characteristic, but unlike desmoid tumors, tumor cells do not express smooth muscle actin (B) and muscle-specific actin (C). CD34, however, is usually positive (D). Nuclear and cytoplasmic staining for β-catenin (E) is more pronounced than for cyclin D1 (F), which is weakly expressed in scattered tumor cells

β-Catenin and Cyclin D1

Mutations in the *adenomatous polyposis coli (APC)* and β-*catenin* genes are frequently found in sporadic DTs and familial adenomatous polyposis–associated fibromatosis, resulting in nuclear accumulation of β-catenin (Tejpar *et al.*,1999, 2005; Abraham *et al.*, 2002; Alman *et al.*, 1997). β-catenin, a participant in the winglesstype (Wnt) transduction pathway, associates with transcription factors leading to transcription and expression of multiple target genes including *c-myc, c-jun, Fra,* and *cyclin D1*. Saito *et al.* (2001) found that nuclear expression of β-catenin correlated with cyclin D1 overexpression in sporadic DTs, and overexpression of cyclin D1 was also observed in an intrathoracic desmoid tumor with a β-catenin mutation of exon 3, as described by Tajima *et al.* (2006).

In the series of pleuropulmonary DTs and SFTs evaluated by Andino *et al.* (2006), diffuse, moderate or strong, β-catenin staining was characteristic of DTs and SFTs, including histologically benign and malignant SFTs. However, differences were apparent in the subcellular localization of β-catenin staining. Nuclear and cytoplasmic β-catenin staining was typically observed in DTs (Figure 26.3E) and histologically benign SFTs (Figure 26.4E), while cytoplasmic staining without coexisting nuclear staining was more common in histologically malignant SFTs. Nuclear and cytoplasmic reactivity for cyclin D1 was typical of DTs (Figure 26.3F) as well as histologically benign and malignant SFTs (Figure 26.4F), with no significant differences in cyclin D1 expression between the DTs and the SFTs. These results suggest that the APC/ β-catenin pathway and cyclin D1 dysregulation may play a role in the pathogenesis of pleuropulmonary desmoid tumors and SFTs.

Similarly, Ng *et al.* (2005) reported prominent nuclear β–catenin staining in 71% of DTs and 40% of SFTs. Bhattacharya *et al.* (2005) suggested that the nuclear distribution of β–catenin expression in deep fibromatoses is useful for distinguishing these lesions from low-grade fibromyxoid sarcoma, leiomyosarcoma, other fibrosarcoma variants, myofibroma/myofibromatosis, nodular fasciitis, and scars, which display only cytoplasmic β-catenin accumulation. Rakheja *et al.* (2005) found nuclear β–catenin staining in four of 12 SFTs and membranous or mixed membranous and cytoplasmic staining in the other neoplasms; the single histologically malignant SFT studied demonstrated a mixed membranous and cytoplasmic pattern of staining for β-catenin.

Cyclin D1 amplification or overexpression occurs in many neoplasms including mantle cell lymphoma, breast cancer, colon cancer, prostate cancer, lymphoma, melanoma, and parathyroid adenoma. Saito *et al.* (2001) noted cyclin D1 overexpression in 59.1% of 22 sporadic DTs evaluated, and found a significant correlation between cyclin D1 overexpression and nuclear staining for β–catenin. Cyclin D1 expression in SFTs has been described in rare reports of atypical or infiltrative SFTs (Miracco *et al.*, 2001; Cassarino *et al.*, 2003).

In conclusion, immunohistochemistry is a valuable tool for the evaluation of cytologically bland spindle cell proliferations arising in the pleura or lung. Although rare, DTs can arise in these locations, and can resemble the more common solitary fibrous tumor as well as other benign and malignant neoplasms. Careful attention to histologic features and

appropriate use of commercially available immunohistochemical stains can facilitate accurate diagnosis of these lesions.

REFERENCES

Abraham, S.C., Reynolds, C., Lee, J.H., Montgomery, E.A., Baisden, B.L., Krasinskas, A.M., and Wu, T.T. 2002. Fibromatosis of the breast and mutations involving the APC/beta-catenin pathway. *Hum. Pathol. 33*: 39–46.

Alman, B.A., Li, C., Pajerski, M.E., Diaz-Cano, S., and Wolfe, H.J. 1997. Increased beta-catenin protein and somatic APC mutations in sporadic aggressive fibromatoses (desmoid tumors). *Am. J. Pathol. 151*: 329–334.

Andino, L., Cagle, P.T., Murer, B., Lu, L., Popper, H.H., Galateau-Salle, F., Sienko, A.E., Barrios, R., and Zander, D.S. 2006. Pleuropulmonary desmoid tumors: immunohistochemical comparison with solitary fibrous tumors and assessment of beta-catenin and cyclin D1 expression. *Arch. Pathol. Lab. Med. 130*: 1503–1509.

Bhattacharya, B., Dilworth, H.P., Iacobuzio-Donahue, C., Ricci, F., Weber, K., Furlong, M.A., Fisher, C., and Montgomery, E. 2005. Nuclear beta-catenin expression distinguishes deep fibromatosis from other benign and malignant fibroblastic and myofibroblastic lesions. *Am. J. Surg. Pathol. 29*: 653–659.

Cassarino, D.S., Auerbach, A., and Rushing, E.J. 2003. Widely invasive solitary fibrous tumor of the sphenoid sinus, cavernous sinus, and pituitary fossa. *Ann. Diagn. Pathol. 7*: 169–173.

Granville, L., Laga, A.C., Allen, T.C., Dishop, M., Roggli, V.L., Churg, A., Zander, D.S., and Cagle, P.T. 2005. Review and update of uncommon primary pleural tumors: a practical approach to diagnosis. *Arch. Pathol. Lab. Med. 129*: 1428–1443.

Guillou, L., Fletcher, J.A., Fletcher, C.D.M., and Mandahl, N. 2002. Extrapleural solitary fibrous tumor and heamangiopericytoma. In: Fletcher, C.D.M., Unni, K.K., Mertens, F., eds. *Pathology and Genetics of Tumours of Soft Tissue and Bone*. Lyon, France: IARC, pp. 86–88.

Iqbal, M., Rossoff, L.J., Kahn, L., and Lackner, R.P. 2001. Intrathoracic desmoid tumor mimicking primary lung neoplasm. *Ann. Thorac. Surg. 71*: 1698–1700.

Miracco, C., de Santi, M.M., Pacenti, L., Schurfeld, K., Laurini, L., Pirtoli, L., Luzi, P., and Ninfo, V. 2001. Telomerase activity, Ki-67, cyclin D1 and A expression, and apoptosis in solitary fibrous tumors: additional features of a predictable course? *Pathol. Res. Pract. 197*: 475–481.

Ng, T.L., Gown, A.M., Barry, T.S., Cheang, M.C., Chan, A.K., Turbin, D.A., Hsu, F.D., West, R.B., and Nielsen, T.O. 2005. Nuclear beta-catenin in mesenchymal tumors. *Mod. Pathol. 18*: 68–74.

Rakheja, D., Molberg, K.H., Roberts, C.A., and Jaiswal, V.R. 2005. Immunohistochemical expression of beta-catenin in solitary fibrous tumors. *Arch. Pathol. Lab. Med. 129*: 776–779.

Saito, T., Oda, Y., Tanaka, K., Matsuda, S., Tamiya, S., Iwamoto, Y., and Tsuneyoshi, M. 2001. Beta-catenin nuclear expression correlates with cyclin D1 overexpression in sporadic desmoid tumours. *J. Pathol. 195*: 222–228.

Tajima, S., Hironaka, M., Oshikawa, K., Bando, M., Ohno, S., Saito, K., Sohara, Y., and Sugiyama, Y. 2006. Intrathoracic sporadic desmoid tumor with the beta-catenin gene mutation in exon 3 and activated cyclin D1. *Respiration 73*: 558–561.

Tejpar, S., Nollet, F., Li, C., Wunder, J.S., Michils, G., dal Cin, P., Van Cutsem, E., Bapat, B., van Roy, F., Cassiman, J.J., and Alman, B.A. 1999. Predominance of beta-catenin mutations and beta-catenin dysregulation in sporadic aggressive fibromatosis (desmoid tumor). *Oncogene 18*: 6615–6620.

Tejpar, S., Michils, G., Denys, H., Van Dam, K., Nik, S.A., Jadidizadeh, A., and Cassiman, J.J. 2005. Analysis of Wnt/Beta catenin signalling in desmoid tumors. *Acta. Gastroenterol. Belg. 68*: 5–9.

Travis, W.D., Churg, A., Aubry, M.C., Ordonez, N.G., Tazelaar, H., Pugatch, R., Manabe, T., and Miettinen, M. 2004. Mesenchymal tumours. In: Travis, W.D., Brambilla, E., Muller-Hermelink, H.K., Harris, C.C., eds. *Pathology and Genetics of Tumours of the Lung, Pleura, Thymus, and Heart*. Lyon, France: IARC, pp. 142–143.

Weiss, S.W., and Goldblum, J.R. 2001. *Enzinger and Weiss's Soft Tissue Tumors*. 4th ed. St. Louis, MO: CV Mosby.

Wilson, R.W., Gallateau-Salle, F., and Moran, C.A. 1999. Desmoid tumors of the pleura: a clinicopathologic mimic of localized fibrous tumor. *Mod. Pathol. 12*: 9–14.

Winer-Muram, H.T., Bowman, L.C., and Parham, D. 1994. Intrathoracic desmoid tumor: CT and MRI appearance. *South. Med. J. 87*: 1007–1009.

27
Non-Small Cell Lung Cancer with Brain Metastasis: Role of Epidermal Growth Factor Receptor Gene Mutation

Edmond S.K. Ma and Chris L.P. Wong

INTRODUCTION

In April 2004, two groups of investigators in Boston reported that activating mutations of the epidermal growth factor receptor (*EGFR*) gene present in a subset of non-small cell lung carcinoma (NSCLC) were highly correlated with treatment response to *EGFR* tyrosine kinase inhibitor (TKI) gefitinib (Lynch *et al*., 2004; Paez *et al*., 2004). Not long afterwards the same observation was confirmed for erlotinib, another TKI targeting *EGFR*, as well as gefitinib (Pao *et al*., 2004). Since then, a huge amount of information has accumulated on the role of *EGFR* gene mutations in lung cancer. These mutations occur at the tyrosine kinase domain of the *EGFR* gene and preferentially involve a subset of lung cancers characterized by female sex, non-smoker, adenocarcinoma histology, and East Asian ethnicity (Mitsudomi *et al*., 2006).

Histopathological Correlation

The histopathological features of *EGFR* gene mutated lung cancer have been studied extensively. Just prior to the reports on the discovery of *EGFR* gene mutation, bronchioloalveolar carcinoma (BAC) subtype and never smokers were found to predict sensitivity to gefitinib (Miller *et al*., 2004), although it may be difficult to distinguish true BAC from adenocarcinoma with prominent BAC pattern or mixed subtype adenocarcinoma based on strict definition. Moreover, mucinous BAC does not show *EGFR* mutations. It is now clear that *EGFR* mutations are specifically involved in a subset of adenocarcinoma deriving from the terminal respiratory unit (Yatabe *et al*., 2005), the development of which is regulated by the thyroid transcription factor-1 (TTF-1) gene. The *EGFR* mutation is most probably acquired in the parenchymal epithelial cells that constitute the terminal respiratory unit and are the only cells in the body, which function in gaseous exchange. This may explain the tissue specificity of *EGFR* mutations, which are rarely found in adenocarcinoma of other organs (Lee *et al*., 2005). Molecular genetics study also confirms the clustering of *EGFR* mutation with lung adenocarcinoma defined on the basis of gene expression profile data (Takeuchi *et al*., 2006). Taken together, the cellular lineage in which *EGFR* mutation occurs is likely to be adenocarcinoma derived from the terminal respiratory unit or peripheral adenocarcinoma. In contrast, bronchial epithelial associated lung cancer is more

common in male smokers with frequent *K-RAS* and p53 mutation as well as *RB* inactivation. *EGFR* and *K-RAS* mutations have in fact been shown to occur in a mutually exclusive fashion (Tam *et al*., 2006). This is in line with biological or molecular classification of tumor where the putative cell origin remains the center of attention. Approximately 20% of NSCLC harbor activating mutations in codons 12 and 13 of the *K-RAS* gene. *K-RAS* mutations, more common in smokers, are almost always found in NSCLC with wild-type *EGFR* allele, and predict for resistance to gefitinib and erlotinib (Pao *et al*., 2005; Massarelli *et al*., 2007).

Epidermal Growth Factor Receptor Gene Mutation

The EGFR is a transmembrane protein with an extracellular domain, a transmembrane domain, and an intracellular domain. Activation of EGFR stimulates the kinase activity of the protein and mediates a series of signaling cascades *via* phosphorylation that culminate in various cellular processes that include resistance to apoptosis, proliferation, angiogenesis, and metastatic or invasive behavior. Ligand engagement of EGFR causes either heterodimerization or homodimerization that leads to receptor activation. Downstream signaling occurs through the Ras-Raf-MEK-ERK1&2, PI3K-Akt, and STAT3-STAT-5 pathways, with some evidence pointing towards predominant activation of the latter two pathways in the presence of EGFR mutant.

EGFR mutations involve the adenosine triphosphate (ATP)-binding pocket of the receptor tyrosine kinase domain, clustering at exons 18–21 of the *EGFR* gene (Lynch *et al*., 2004; Paez *et al*., 2004; Pao *et al*., 2004). The types of mutations include in-frame deletions, in-frame insertions/duplications and point mutations. Two hotspots namely deletion at exon 19 and point mutation L858R at exon 21 constitute ~ 90% of all mutations. Other less common aberrations, mostly point mutations, are scattered in the kinase domain. Exon 19 deletions that involve the LREA motif and L858R have been shown to be oncogenic in both cell lines and transgenic mouse models (Politi *et al*., 2006). These mutations increase the kinase activity of EGFR, leading to the heightened activation of downstream pathways that favor cell survival, and hence confer oncogenic property on EGFR. The end effect is a selective growth advantage to the cell, which becomes 'addicted' to this mechanism of oncogene activation for maintenance of the malignant phenotype (Weinstein and Joe, 2006), and hence amendable to inhibition through tyrosine kinase inhibitor (TKI) therapy. Small molecular inhibitors, such as erlotinib and gefitinib, penetrate the cellular membrane and bind to the ATP binding site of the receptor. This action prevents homodimer autophosphorylation, which is necessary for inducing a conformational change in the intracellular structure of EGFR that exposes a binding site for signaling proteins. These TKI, therefore, prevent downstream signaling events involving other kinases and adaptor proteins, thereby causing malignant cells to lose their survival and proliferative potential. NSCLC with exon 19 deletion seems to respond better to gefitinib and erlotinib than with L858R (Riely *et al*., 2006). Of note, three mutations D761Y, T790M, and insertions at exon 20 are resistant to TKI therapy (Kobayashi *et al*., 2005; Sasaki *et al*., 2007). It should also be pointed out that, as ~ 10–20% of patients with no detectable mutation show a partial response to gefitinib, absence of *EGFR* gene mutations does not preclude

TKI response (Bell *et al*., 2005; Takano *et al*., 2005; Cappuzzo *et al*., 2005a).

Epidermal Growth Factor Receptor Gene Amplification

Amplification of the *EGFR* gene, besides mutation, is also encountered in lung cancer and detectable by fluorescence *in-situ* hybridization (FISH) (Cappuzzo *et al*., 2005b) or quantitative polymerase chain reaction (Q-PCR) (Bell *et al*., 2005). *EGFR* gene amplification may also be associated in varying extents with clinical response to TKI therapy (Bell *et al*., 2005; Hirsch *et al*., 2005; Cappuzzo *et al*., 2005a). The inconsistency between different studies may arise from differing criteria of amplification and inadequate distinction between specific amplification of the *EGFR* gene locus versus increase in gene copy number due to polysomy of chromosome 7 on which the gene is located. The relationship between *EGFR* gene mutation and amplification is intriguing. In one study (Takano *et al*., 2005) that examined 66 NSCLC, 13 (20%) harbored high *EGFR* gene amplification of ≥ six copies and all of them showed *EGFR* gene mutation, raising the possibility that amplification may be a subset of tumors with gene mutation. While confirmation is needed, it is plausible that amplification of the mutant allele may occur as a secondary event to the mutation and testify to the contention of oncogene addiction.

MATERIALS

1. Template DNA: purified human DNA from micro-dissected tumor tissues of lung cancer patients (with or without brain metastasis).
2. Sense and antisense oligonucleotide primers (MIL, Hong Kong) directed against EGFR exons 18, 19, 20 and 21 (Lynch *et al*., 2004). The oligonucleotide sequence should be as follows: (EGFR first round PCR) 5′CAAATG AGCTGGCAAGTGCCGTGTC3′ for EGFR/Exon 18 sense, 5′GAGTTTC CCAAACACTCAGTGAAAC3′ for EGFR/Exon 18 antisense, 5′GCAA TATCAGCCTTAGGTGCGGCTC3’ for EGFR/Exon 19 sense, 5′CATAG AAAGTGAACATTTAGGATGTG3′ for EGFR/Exon 19 antisense, 5′CCA TGAGTACGTATTTTGAAACTC3′ for EGFR/Exon 20 sense, 5′CATATC CCCATGGCAAACTCTTGC3′ for EGFR/Exon 20 antisense, 5′CTAAC GTTCGCCAGCCATAAGTCC3′ for EGFR/Exon 21 sense 5′GCTGCGA GCTCACCCAGAATGTCTGG3′ for EGFR/Exon 21 antisense (EGFR second round PCR) 5′CAAGTGCCGTG TCCTGGCACCCAAGC3′ for EGFR/ Exon 18 sense, 5′CCAAACACTCA GTGAAACAAAGAG3′ for EGFR/ Exon 18 antisense, 5′CCTTAGGTGC GGCTCCACAGC3′ for EGFR/Exon 19 sense, 5′CATTTAGGATGTGGAG ATGAGC3′ for EGFR/Exon 19 antisense, 5′GAAACTCAAGATCGCAT TCATGC3′ for EGFR/Exon 20 sense, 5′GCAAACTCTTGCTATCCCAGGA G3′ for EGFR/Exon 20 antisense, 5′C AGCCATAAGTCCTCGACGTGG3′ for EGFR/Exon 21 sense, and 5′CATC CTCCCCTGCATGTGTTAAAC3’ for EGFR/Exon 21 antisense. GenBank accession no. NM005228.3.
3. EGFR PCR Mixture: 50 µl reactions containing 50–200 ng purified human DNA, 2 units AmpliTaq Gold DNA polymerase (Applied Biosystems,

Foster City, USA), 0.5 µM each of sense and antisense EGFR-primers, 200 µM each of dATP, dGTP, dCTP, dTTP (Roche Diagnostics GmbH, Mannheim, Germany), and 1.5 mM MgCl2, and 1x Buffer II (Applied Biosystems, Foster City, USA) in thin-walled 0.2 ml PCR tubes (Axygen Scientific, USA), 2 µl first round PCR product is used as template for the second round PCR.

4. Agarose gel, 2%: dissolve 2 g PCR agarose (Bio-Rad Laboratories, USA) in 100 ml 1x TBE buffer under heat, cool down, and cast the gel.
5. 1x Tris-borate EDTA buffer (TBE): dilute 100 ml 10x stock (Bio-Rad Laboratories, USA) with 900 ml distilled water, 1x working buffer contains 89 mM Tris, 89 mM boric acid, 2 mM EDTA (pH 8.3).
6. 6x Orange loading dye solution (Fermentas Life Sciences, Canada): 6x stock contains 0.2% orange G, 0.05% xylene cyanol FF, 60% glycerol and 60 mM EDTA.
7. O'RangeRuler 50 bp DNA Ladder (Fermentas International Inc, Canada).
8. Genomic DNA Extraction-QIAamp DNA Mini Kit (QIAGEN GmbH, Hilden, Germany): contains Buffer ATL, Buffer AL, Buffer AW1 (reconstitute with absolute ethanol), Buffer AW2 (reconstitute with absolute ethanol), Buffer AE, Proteinase K, and QIAamp spin columns.
9. PCR Product Purification-QIAquick PCR Purification Kit (QIAGEN GmbH, Hilden, Germany): contains Buffer PB, Buffer PE (reconstitute with absolute ethanol), Buffer EB, and QIAquick spin columns.
10. Sequencing Mixture: 20 µl reaction contains 3.5 µl 5x Sequencing Buffer (Applied Biosystems, Foster City, USA), 1 µl BigDye Terminator v3.1 Ready Reaction Mix (Applied Biosystems, Foster City, USA), 0.16 µM of sense or antisense primer, and 10 ng purified second round PCR product in thin-walled 0.2 ml PCR tubes.
11. 3130xl Genetic Analyzer Polymer: POP-7 Polymer for DNA sequencing and fragment analysis (Applied Biosystems, Foster City, USA).
12. Highly Deionized (Hi-Di) Formamide (Applied Biosystems, Foster City, USA).
13. GeneScan 500 ROX Size Standard (Applied Biosystems, Foster City, USA).
14. Sequencing Product Purification-DyeEx 2.0 Spin Kit (QIAGEN GmbH, Hilden, Germany): contains DyeEx 2.0 spin columns.
15. SuperFrost Plus slides (Menzel-Gläser, Germany).
16. 10% Buffered Formalin Fixative: dissolve 45 g sodium dihydrogen orthophosphate dehydrate and 65 g di-sodium hydrogen orthophosphate in 8 L distilled water, bring to 9 L. Mix with 1 L 40% formaldehyde solution.
17. Haematoxylin, Eosin Stain and DePeX Mounting Medium (BDH, VWR International Ltd., England).
18. Sterile Disposable Scalpels No. 11 (Swann-Morton, Sheffield, England).
19. SALSA Multiplex Ligation-Dependent Probe Amplification (MLPA) Kit P171 Gain1 (MRC-Holland bv, the Netherlands): contains P171 Gain1 probemix, SALSA MLPA Buffer,

Ligase-65 buffer A, Ligase-65 buffer B, Ligase-65, SALSA PCR buffer, SALSA PCR primer mix, SALSA polymerase, SALSA enzyme dilution buffer.

20. 1x Genetic Analyzer Running Buffer: mix 5 ml 10x stock (Applied Biosystems, Foster City, USA) with 45 ml distilled water.
21. Fluorescence in situ hybridization (FISH) microscope filters (Vysis, Abbott Molecular Inc., USA): Spectrum Green, Spectrum Orange, DAPI, Triple Bandpass filter.
22. FISH Pretreatment Solution (Vysis, Abbott Molecular Inc., USA): contains 1 N sodium thiocyanate.
23. 2,500–3,000 U/mg Protease, lyophilized (Vysis, Abbott Molecular Inc., USA).
24. Protease Buffer II (Vysis, Abbott Molecular Inc., USA): contains 0.2 N HCl.
25. 20x Standard saline citrates (SSC): dissolve 132 g 20x SSC powder (Vysis, Abbott Molecular Inc., USA) in 400 ml distilled water, adjust the pH to 5.3 with 12 N HCl, bring to 500 ml.
26. Nonidet P-40 (NP-40) (Vysis, Abbott Molecular Inc., USA).
27. 2x SSC/0.3% NP-40: mix 100 ml 20x SSC with 850 ml distilled water and 3 ml NP-40, adjust the pH to 7.0 ± 0.2 with 1 N NaOH, bring to 1 l.
28. DAPI I Counterstain (Vysis, Abbott Molecular Inc., USA).
29. LSI EGFR Spectrum Orange/CEP7 Spectrum Green FISH Probes (Vysis, Abbott Molecular Inc., USA).

Additional material required include various plastic-ware, pipettes, microcentrifuge, GeneAmp PCR System 9700 thermal cycler (Applied Biosystems, Foster City, USA), 3130 × l Genetic Analyzer (Applied Biosystems, Foster City, USA), spectrophotometer e.g. BioPhotometer (Eppendorf AG, Hamburg, Germany), centrifugal vacuum concentrator e.g. Concentrator 5301 (Eppendorf AG, Hamburg, Germany) HYBrite Denaturation/Hybridization System (Vysis, Abbott Molecular Inc., USA), FISH Workstation with bright-field/fluorescence microscope, high performance cool CCD camera, computer system with FISHView analysis and Case Data Manager software (Applied Spectral Imaging GmbH, Germany). All organic solvents were from BDH (BDH, VWR International Ltd., England), unless otherwise stated. Reagents and spin columns used in genomic DNA extraction, PCR product purification and sequencing product purification are included in the kits specified except the absolute ethanol for buffer reconstitution.

METHODS

Tissue Preparation

Collect fresh patient tumor tissue and place immediately in excess 10% buffered formalin fixative overnight, then perform subsequent paraffin embedding according to standard procedure.

DNA template generation for *EGFR* gene PCR and Multiplex Ligation-Dependent Probe Amplification (MLPA) detection

1. Cut 4 µm thick sections of paraffin-embedded tissue, mount the sections onto SuperFrost Plus slides, and dry the sections for 2 h at 65°C. Then deparaffinize and rehydrate the sections, and stain with hematoxylin and

eosin (H&E) stain according to standard procedure.
2. Apply cover slip to one of the stained slides with DePeX mounting medium and review under microscope.
3. Select and highlight area rich in tumor cells (> 30% tumor cells preferred).
4. Microdissect the tumor cells from unmounted slides using sterile disposable scalpel under microscope.
5. Transfer dissected tumor cells into 1.5 ml screw-cap sterile microcentrifuge tube containing 360 µl tissue lysis buffer (Buffer ATL), add 40 µl proteinase K, vortex and incubate at 56°C with occasional shaking until the tissue is completely digested.
6. Briefly centrifuge and add 400 µl Buffer AL, vortex for 15 s and incubate at 70°C for 10 min with occasional shaking, pulse-spin and add 400 µl absolute ethanol, vortex for 15 s and briefly centrifuge to remove drops from inside the cap.
7. Transfer 600 µl of the mixture to the QIAamp spin column, centrifuge at 6,000 × g for 1 min, discard the collection tube containing the filtrate, and repeat the step with a new collection tube.
8. Apply 500 µl reconstituted Buffer AW1 to the spin column, centrifuge at 6,000 × g for 1 min, discard the collection tube containing the filtrate, add 500 µl reconstituted Buffer AW2 to the spin column and centrifuge at 20,000 × g for 3 min, discard the collection tube containing the filtrate, place a new collection tube and centrifuge at 20,000 × g for 1 min to remove residue buffer.
9. Place the spin column in a sterile 1.5 ml microcentrifuge tube, add 50 µl elution buffer (Buffer AE), incubate for 5 min at room temperature, centrifuge at 6,000 × g for 1 min, the DNA is now ready for PCR amplification and MLPA detection, or store at −20°C for future testing.
10. Take an aliquot and measure the DNA concentration and purity (A260/280 ratio) in a spectrophotometer, an A260/280 ratio of ≥ 1.8 indicates a good quality of DNA purity.

EGFR Gene PCR Amplification and Sequencing Analysis

1. Extracted and purified DNA is used as template for amplification of exon18-21 of EGFR gene with flanking intronic sequences. For primary amplification, add template DNA and respective primer-pairs to thin-walled 0.2 ml PCR-tubes, together with the other components of the PCR mixture, bringing to 50 µl with PCR grade water. Amplification should then be performed by using an initial AmpliTaq Gold DNA polymerase activation step at 95°C for 10 min, and then 35 cycles including denaturation at 94°C for 30 s, primer annealing at 58°C for 1 min, and primer extension at 72°C for 1 min, followed by a final extension at 72°C for 7 min.
2. Perform secondary PCR with 2 µl primary amplification product, respective primer-pairs and other components of the PCR mixture, bringing to 50 µl. Amplification should then be performed by using the same condition as for the primary amplification.
3. Analyze the primary and secondary PCR products on 2% agarose gel (primary PCR products: 400 bp for exon 18, 372 for exon 19, 408 bp for exon

20 and 415 for exon 21; secondary PCR products: 381 bp for exon 18, 349 for exon 19, 379 bp for exon 20 and 374 for exon 21), visualize under UV-light.

4. Purify the secondary PCR products using the QIAquick spin columns to remove unincorporated nucleotides, primers and enzyme. Mix 40 µl of the PCR product with 200 µl binding buffer (Buffer PB), transfer the mixture to the QIAquick spin column, centrifuge at 17,900 × g for 1 min, discard the collection tube containing the filtrate, replace with a new collection tube.
5. Apply 750 µl reconstituted Buffer PE to the spin column, centrifuge at 17,900 × g for 1 min, discard the collection tube containing the filtrate, place a new collection tube and centrifuge at 17,900 × g for 1 min to remove residue buffer.
6. Place the spin column in a sterile 1.5 ml microcentrifuge tube, add 30 µl elution buffer (Buffer EB), incubate for 1 min at room temperature, centrifuge at 17,900 × g for 1 min.
7. Take an aliquot and measure the DNA concentration and purity (A260/280 ratio) in a spectrophotometer, dilute the DNA concentration to 10 ng/µl, the sample is ready for cycle sequencing reaction.
8. Add template DNA to sequencing mixture with respective primers in thin-walled 0.2 ml PCR tubes. Cycle sequencing reaction should then be performed by using an initial denaturation step at 96°C for 1 min, and then 25 cycles include denaturation at 96°C for 10 s, primer annealing at 50°C for 5 s, and primer extension at 60°C for 4 min, and keep at 4°C until ready to purify.
9. Spin down the contents of the tubes, and purify the sequencing product using the DyeEx spin columns, removing unincorporated nucleotides, primer and enzyme.
10. Resuspend resin in the spin columns, then loosen the cap and snap off the bottom closure, place in a collection tubes and centrifuge at 750 × g for 3 min, discard the collection tubes containing the filtrate, place the spin columns in sterile 1.5 ml microcentrifuge tubes, apply the sequencing reactions to the gel bed, and centrifuge at 750 × g for 3 min.
11. Dry the purified samples in a vacuum concentrator, resuspend in 10 µl Hi-Di formamide, then denature at 95°C for 3 min, followed by cooling on ice for 5 min.
12. The sequencing products are now ready for capillary electrophoresis and sequence analysis using the genetic analyzer.
13. Exons sequence data is compared with reference sequence from GenBank, sequence variant(s) is described according to the "Recommendations for the Description of Sequence Variants" of the Human Genome Variation Society (HGV).

Fluorescence *in-situ* Hybridization Detection of *EGFR* Gene Amplification and Loss of Heterozygosity

1. Cut 4 µm thick sections of paraffin-embedded tissue, mount the sections onto SuperfFrost Plus slides, air-dry the sections and bake overnight at 56°C. Then deparaffinize sections in

xylene (2 × 10 min) at ambient temperature, and dehydrate the sections in absolute ethanol (2 × 5 min) at ambient temperature, dry the sections on a 45°C slide warmer for 5 min.
2. Prewarm FISH pretreatment solution and protease buffer to 80°C and 37°C, respectively, in water baths before using.
3. Prepare protease solution by adding 250 mg protease to the 37°C protease buffer (62.5 ml), mix gently.
4. Incubate the sections in pretreatment solution at 80°C for 10 min, then immerse in distilled water for 3 min, remove slides from water and drain off excess water by blotting the edges of the slides on a paper towel.
5. Incubate slides in protease solution at 37°C for 20 min, immerse in distilled water, check under microscope for complete exposure of the tumor cell nuclei, re-incubate if protease digestion is not complete, and finally immerse slides in distilled water for 3 min.
6. Remove slides from water and dry the sections on a 45°C slide warmer for 5 min.
7. Fix the slides in ethanol series, 70% ethanol for 1 min, followed by 85% for 1 min, and finally in 100% for 1 min.
8. Air-dry the slides.
9. Prepare the HYBritre Denaturization/ Hybridization system, moisten strips of paper towel with water, and place in the channels along the heating surface of the system, pre-warm the system to 37°C.
10. Mark hybridization areas with a diamond tipped scribe on sample slides.
11. Apply 7 µl EGFR/CEP7 probe mixture to the slides and immediately apply cover slips (18 × 18 mm).
12. Seal cover slip with rubber cement.
13. Place slides on the slots of the HYBrite, and fill empty slots with blank glass slide(s).
14. Close the cover, set the melting temperature to 73°C and melting time to 5 min, set the hybridization temperature to 37°C and hybridization time to 16 h, and start the denaturation /hybridization program.
15. After hybridization, remove slides from HYBrite system and remove rubber cement.
16. Prewarm the wash solution 2x SSC/0.3% NP-40 in a water bath at 73°C.
17. Immerse slides in Coplin jar containing 2x SSC/0.3% NP-40 solution at ambient temperature for 2–5 min to float off the cover slips.
18. Immerse and agitate slides in prewarmed 2x SSC/0.3% NP-40 solution for 3 s, incubate in wash solution at 73°C for 2 min.
19. Immerse and incubate slides in 2x SSC/0.3% NP-40 solution at ambient temperature for 1 min.
20. Remove slides from 2x SSC/0.3% NP-40 solution and drain off the solution by blotting the edges of the slides on a paper towel, air-dry the slides completely.
21. Apply 7 µl DAPI I counter-stain to the target area of slides and apply cover slip (18 × 18 mm).
22. View slides using Spectrum Orange, Spectrum Green and DAPI filters on florescence microscope.
23. Perform signal enumeration for EGFR and CEP7 probes, select areas of good nuclei distribution, and skip those nuclei with weak intensity and ambiguous borders.
24. Calculate the EGFR to CEP7 signal ratio, a ratio of >2 is considered

amplification of EGFR gene, tumor cells with multiple CEP7 signals (polysomy 7) should be interpreted with caution.

25. Nuclei with LOH should be presented with two CEP7 signals and one EGFR signal.

MLPA Detection of *EGFR* Gene Copy Number Changes

1. Dilute purified tumor DNA samples and three normal control DNA samples to 20 ng/μl using sterile PCR grade water.
2. For hybridization of DNA template with MLPA probes, label thin-walled 0.2 ml PCR tubes, transfer 5 μl of working DNA (100 ng) to each tube, spin briefly to collect the DNA at the bottom.
3. Denature the DNA samples at 98°C for 5 min with the thermo cycler, and subsequently cool to 25 °C before opening the thermal cycler.
4. Remove the P171 Gain1 probemix and the MLPA buffer from the −20°C freezer, defrost and vortex briefly. Mix 1.5 μl MLPA buffer with 1.5 μl probemix for each sample, prepare one reaction in excess.
5. While at 25 °C, add 3 μl reaction mix to each tube, mix well by pipetting up and down.
6. Continue the hybridization reaction by with an initial denaturation at 95°C for 1 min, then hybridize at 60°C for 16 h, then hold the samples at 54°C.
7. Remove the Ligase-65 buffer A and Ligase-65 buffer B from the freezer, allow to thaw, then vortex briefly.
8. Prepare the ligation reaction mix, for each reaction mix 3 μl Ligase-65 buffer A, 3 μl Ligase-65 buffer B, and 25 μl sterile PCR grade water, mix briefly, then add 1 μl of Ligase-65 per reaction to the ligase buffer mix, and mix well by vortexing.
9. When the samples are at 54°C, add 32 μl of the ligation reaction mix to each sample and mix well by pipetting up and down.
10. Perform the ligation reaction at 54°C for 15 min, followed by incubation at 98°C for 5 min, and hold at 4°C, the ligation products can be stored at 4°C for up to one week.
11. Thaw the SALSA PCR buffer, SALSA PCR primer mix, and SALSA enzyme, and vortex briefly.
12. Label new set of thin-walled 0.2 ml PCR tubes for subsequent PCR amplification.
13. Prepare a PCR buffer mix for each reaction by combining 4 μl SALSA PCR buffer, and 26 μl PCR grade water, and vortex to mix.
14. Aliquot 30 μl of the PCR buffer mix to each new tube, and then transfer 10 μl of each ligation product to the corresponding PCR tube.
15. Spin briefly to collect the mixture at the bottom.
16. Place the PCR tubes into the thermal cycler, then bring to 60°C and hold.
17. Prepare the PCR reaction mix on ice, mix 2 μl SALSA primer mix, 2 μl SALSA enzyme dilution buffer, and 5.5 μl PCR grade water for each sample, mix well by pipetting up and down, and add 0.5 μl SALSA polymerase, vortex briefly.
18. While at 60°C, add 10 μl PCR reaction mix to each tube sitting in PCR thermal cycler, and mix by pipetting up and down, PCR amplification should then be performed for 35

cycles including denaturation at 95°C for 30 s, primer annealing at 60°C for 30 s, and primer extension at 72°C for 1 min, followed by a final extension at 72°C for 20 min.

19. For separation of the PCR product and analysis using the capillary electrophoresis system (3130*xl* genetic analyzer), prepare the instrument according to the instrument operation manual.
20. Mix 1 µl PCR product, 0.3 µl GeneScan 500 ROX size standard, and 9 µl Hi-Di formamide, then denature at 94°C for 2 min, and cool on ice for 5 min.
21. Load the samples to the genetic analyzer, and perform electrophoresis.
22. Perform PCR product size calling and signal intensity measurement (i.e., copy number of targeted gene) using the GeneMapper software, each MLPA PCR product gives a peak signal at a distinct length.
23. Export the size, signal intensity data in delimited text file format. Then perform step-by-step analysis on exported data using the MRC Coffalyser program (available free from MRC Holland: http://www.mrc-holland.com). The data of normal controls is used as reference for data normalization and data filtering. A 35–50% reduction (a normalized ratio of 0.5–0.65) or increase (a normalized ratio of 1.35–1.5) in relative peak area of the amplification product indicates a deletion or amplification of the gene.

RESULTS AND DISCUSSION

Spectrum of *EGFR* Mutations in Hong Kong Chinese Patients with NSCLC

In the two-year period from September 2005 to September 2007, a total of 197 Hong Kong Chinese patients with NSCLC were analyzed for *EGFR* gene mutation at the Division of Molecular Pathology, Department of Pathology, Hong Kong Sanatorium and Hospital (Table 27.1). Among the 72 patients (36.5%) showed detectable mutation, and double mutations were identified in 12 patients (6.1%), giving a total of 84 mutations. Classical hotspot mutations, namely exon 19 E746-A750del and exon 21 L858R accounted for 26.2% and 35.7% of all detectable mutations. To the best of our knowledge, nine mutations (Table 27.1) all found in single patients were novel, and the clinical response to TKI therapy was uncertain. Two patients harbored *EGFR* gene mutations known to be associated with resistance to TKI therapy, including T790M seen in one patient additional to L858R after two years of gefitinib therapy and isolated exon 20 insertion mutation in another patient without prior exposure to TKI.

Role of *EGFR* Gene Mutation in Brain Metastases from NSCLC

After its discovery, the role of *EGFR* mutation in brain metastases from NSCLC was investigated. A case of stage IV NSCLC patient developing symptomatic leptomeningeal metastases while on erlotinib was reported, who subsequently responded to gefitinib (Choong *et al*., 2006). DNA sequencing of lymph node and cerebrospinal fluid showed double L858R and E884K mutations (Choong *et al*., 2006). Contrary to this, however, another case report from Taiwan described partial erlotinib response following gefitinib failure in a patient who had disseminated adenocarcinoma of lung with craniotomy performed for brain metastasis, in which tumor tissue harbored exon 19 deletion (Chang *et al*., 2007).

TABLE 27.1. Spectrum of EGFR gene mutations in Hong Kong Chinese patients with NSCLC.

(A) Summary of cases

	No. of cases	Age range	Median age	% Positive
Female	96	39–90	63	42/96 (43.8%)
Male	101	33–92	61	30/101 (29.7%)

(B) Summary of mutations

Mutation	Exon	Male	Female	Total
p.Glu709Ala	18	1	0	1
p.Gly719Ala	18	1	1	2
p.Gly719_Ser720delins AlaLeu[a]	18	1	0	1
p.Gly719Ser	18	1	0	1
p.Glu709_Thr710delinsA	18	0	1	1
p.Gly719Cys	18	0	1	1
p.Ile706Thr[a]	18	0	1	1
p.Gly717Ser	18	0	1	1
p.Glu746_Ala750del[b]	**19**	**12**	**10**	**22**
p.Leu747_Ala750delinsPro[a]	19	1	0	1
p.Glu746_Thr751delinsAla	19	1	2	3
p.Leu747_Thr751del	19	1	2	3
p.Ser752_Ile759del	19	1	0	1
p.Glu746_Leu747delins Val746_Pro747[a]	19	0	1	1
p.Lys745_Glu749del	19	0	2	2
p.Leu747_Pro753delinsSer	19	0	1	1
p.Thr790Met[c]	20	1	0	1
p.His773Tyr	20	1	0	1
p.Asp770_Asn771insAsnProTyr[c]	20	1	0	1
p.Val774Met[a]	20	1	0	1
p.Ser768Ile[a]	20	0	1	1
p.Phe795Leu[a]	20	0	1	1
p.Leu858Arg[b]	**21**	**11**	**19**	**30**
p.Leu861Gln	21	2	1	3
p.Lys860Ile[a]	21	0	1	1
p.Leu833Val[a]	21	0	1	1
		37	47	84

(C) Breakdown of mutations according to exon location

Exon	Male %	Female %	Total %
18	4/37 (10.8%)	5/47 (10.6%)	9/84(10.7%)
19	16/37 (43.2%)	18/47 (38.3%)	**34/84 (40.5%)**
20	4/37 (10.8%)	2/47 (4.3%)	6/84 (7.1%)
21	13/37 (35.1%)	22/47 (46.8%)	**35/84 (41.7%)**

Key: [a]Novel mutation/mutation of unknown significance; [b]Mutation hotspots; [c]Mutants known to be associated with drug resistance.

A series from Nagoya, Japan described eight NSCLC patients with brain metastases before the initiation of gefitinib treatment and documented *EGFR* gene mutation status (Shimato *et al*., 2006). Of the eight patients, gefitinib was considered effective

in three and not effective in three. All three gefitinib responders showed *EGFR* gene mutation whereas only one of the three non-responders showed *EGFR* gene mutation. Therefore, similar to the lung and other extracranial sites, there exists a relationship between gefitinib response and the presence of *EGFR* gene mutation.

Brain metastases from NSCLC may show an over-representation of *EGFR* gene mutations. The presence of *EGFR* gene mutation was detected in 12 out of 19 (63%) metastatic NSCLC to brain (Matsumoto *et al*., 2006b), which was higher than reported for the prevalence of the mutation in NSCLC in general, notwithstanding the relatively small patient number. In six patients with *EGFR* gene mutations, the corresponding primary lung tumors also showed the same type of mutation when examined. In two patients out of the six, second metastatic tumors in addition to the first showed the same type of *EGFR* gene mutation. These observations suggested that the *EGFR* gene mutations were not only frequent in brain metastases from NSCLC, but also had occurred preceding the development of metastasis (Matsumoto *et al*., 2006b). Consistent with this, *EGFR* gene mutations were also frequent in early non-invasive bronchioloalveolar carcinoma (Matsumoto *et al*., 2006a).

Molecular Genetic Study of NSCLC with Brain Metastasis

In a patient with NSCLC with solitary brain metastasis, we showed that the homozygous *EGFR* mutation present in both primary lung tumor and brain metastasis (Figure 27.1) was due to a combination of loss of heterozygosity (LOH) through deletion of normal allele resulting in hemizygous state, as well as amplification of the mutant allele (Ma *et al*., 2007). The amplification event was demonstrated by FISH (Figure 27.1) and confirmed by MLPA study (Figure 27.1). We inferred that the mutant rather than the wild-type allele was amplified, because the sequence chromatogram showed mutant signal only. Although most *EGFR* mutations in NSCLC occur in the heterozygous state, analysis of sequence chromatograms in one study suggests that ~40% of cases show amplification of the mutant allele (Shigematsu *et al*., 2005), as evident by the peaks corresponding to the mutant sequence being equal to or greater than the corresponding wild type sequence. Moreover, from the two original studies that first identified *EGFR* mutations (Paez *et al*., 2004; Pao *et al*., 2004), a total of three homozygous in-frame deletions at exon 19 were described. The absence of wild type sequence was attributed to several mechanisms, namely hemizygous or homozygous mutation, selective amplification of mutant allele or that mutations in general may be homozygous, with wild type sequence originating from contaminating DNA from nontumorous cells. Consistent with the contention of oncogene addiction, it is highly probable that the growth of the metastatic tumor cells in our patient was dependent on the mutated and amplified *EGFR* gene. However it remains to be seen whether gene amplification or other genetic events that accompany *EGFR* mutation (Yokoyama *et al*., 2006) contribute to the metastasis potential and whether these markers are useful in predicting TKI response in brain metastasis from NSCLC.

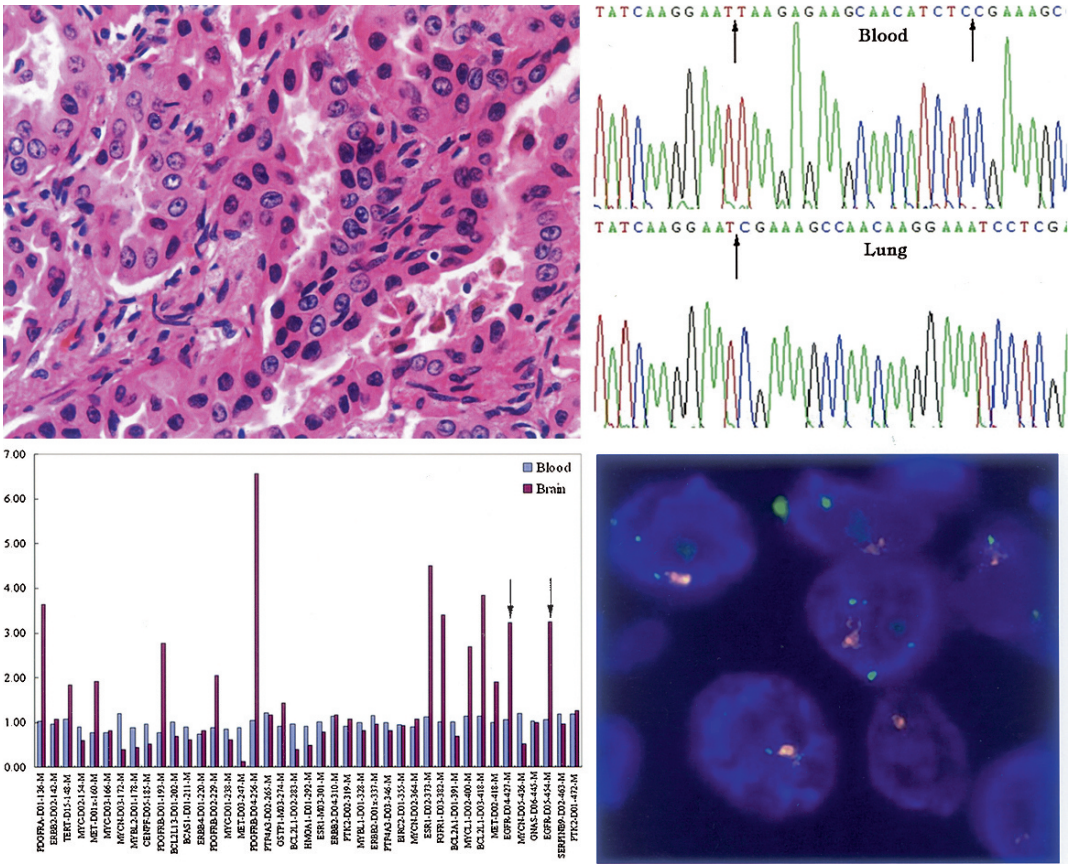

FIGURE 27.1. The figure highlights the successful use of a combination of molecular pathology techniques to interrogate lung cancer cells. Left upper panel: Hematoxylin and Eosin section showing the histology of lung adenocarcinoma. Right upper panel: Sequencing chromatograms revealing the deletion of 18 nucleotides at exon 19 of the *EGFR* gene in lung cancer cells. Right lower panel: FISH study showing amplification of the *EGFR* gene (orange signal) as manifested by one cluster of many signals but loss of the other allele, in association with normal two copies of chromosome 7 (green signal). Left lower panel showing that, with the MLPA assay, a threefold increase in *EGFR* gene dosage is detected in tumor cells by two independent probes, thus confirming *EGFR* gene amplification

Gefitinib Response of Brain Metastases from NSCLC

Brain metastasis is common in patients with NSCLC. While whole brain irradiation is the standard therapy, more invasive approaches such as surgical resection or radio-surgery are indicated in certain patient subsets. Even before the identification of *EGFR* gene mutations, a number of case reports and patient series described clinical response of brain metastases from NSCLC to gefitinib, despite failure of conventional therapy (Cappuzzo *et al*., 2003; Namba *et al*., 2004; Hotta *et al*., 2004; Ceresoli *et al*., 2004). A study from Milan evaluated 41 cases of NSCLC with brain metastases and reported partial response to gefitinib in four patients and stable disease in seven patients, giving an overall

disease control rate of 27%, with a median duration of PR of 13.5 months (Ceresoli *et al*., 2004). Another study from Okayama, Japan reviewed 57 patients with advanced NSCLC on gefitinib (Hotta *et al*., 2004). Out of 14 patients who had brain metastases in this cohort, there was one complete response, five partial responses and eight stable disease states. The median survival and median duration of response were 9.1 and 7.7 months, respectively. This study confirmed the effectiveness of gefitinib for brain metastases as well as extracranial tumors. A third study from Osaka, Japan evaluated 15 NSCLC patients with brain metastases and reported nine patients (60%) showing objective tumor response to gefitinib (Namba *et al*., 2004). The median duration of response was 8.7 months and the median overall survival was 8.3 months. A study from Sapporo, Japan involving 27 NSCLC patients that included 4 with central nervous system (CNS) metastasis showed favorable clinical response to readministration of gefitinib after cessation of therapy in gefitinib responders (Yokouchi *et al*., 2007). Taken together, molecular targeted therapy against EGFR is an option for the treatment of brain metastasis from NSCLC refractory to conventional chemoradiotherapy because TKI has demonstrated a distinct therapeutic potential against brain metastasis when compared with primary lung tumor and extracranial secondary.

Not much data exist on the ability of gefitinib to cross the blood-brain barrier. Against this background, there is reportedly a high incidence of disease recurrence in the brain and the leptomeninges in NSCLC patients after an initial response to gefitinib, regardless of disease control in the lungs (Omuro *et al*., 2005). In a study from the New York Memorial Sloan-Kettering Cancer Center, although 21 out of 139 patients treated by gefitinib achieved a partial response, the CNS was the initial site of recurrence in seven (33%) of the responders, including five brain and two leptomeningeal metastases. Interestingly, four (57%) out of the seven patients with disease recurrence in the CNS had pulmonary disease under control. Besides incomplete CNS penetrance of the drug, other postulated reasons for CNS recurrence were intrinsic resistance of the metastatic clone and longer patient survival for metastasis to manifest (Omuro *et al*., 2005).

In conclusion, the identification of *EGFR* gene mutation in NSCLC and the elucidation of its contribution to carcinogenesis are important in several aspects. First, it illustrates that receptor tyrosine kinase plays a pivotal role in oncology and represents viable therapeutic targets for intervention. Second, it shows that laboratory detection of *EGFR* mutation predicts for treatment response in the subset of patients harboring such aberration. Third, acquired resistance to TKI through acquisition of secondary *EGFR* mutation occurs with treatment and limits the efficacy of these agents. To circumvent the problem, recent developments of molecular targeted therapy in NSCLC focus on abrogation of signaling pathways downstream to the EGFR, though the use of PI3K inhibitors, mTOR inhibitors, and Ras-MAPK inhibitors, either alone or in combination with existing TKI.

Acknowledgment The authors thank Miss Mandy Y.M. Sung for proofreading the manuscript.

REFERENCES

Bell, D.W., Lynch, T.J., Haserlat, S.M., Harris, P.L., Okimoto, R.A., Brannigan, B.W., Sgroi, D.C., Muir, B., Riemenschneider, M.J., Iacona, R.B., Krebs, A.D., Johnson, D.H., Giaccone,G., Herbst, R.S., Manegold, C., Fukuoka, M., Kris, M.G., Baselga, J., Ochs, J.S., and Haber, D.A. 2005. Epidermal growth factor receptor mutations and gene amplification in non-small-cell lung cancer: molecular analysis of the IDEAL/INTACT gefitinib trials. *J. Clin. Oncol. 23*: 8081–8092.

Cappuzzo, F., Ardizzoni, A., Soto-Parra, H., Gridelli, C., Maione, P., Tiseo, M., Calandri, C., Bartolini, S., Santoro, A., and Crino, L. 2003. Epidermal growth factor receptor targeted therapy by ZD 1839 (Iressa) in patients with brain metastases from non-small cell lung cancer (NSCLC). *Lung Cancer 41*: 227–231.

Cappuzzo, F., Hirsch, F.R., Rossi, E., Bartolini, S., Ceresoli, G.L., Bemis, L., Haney, J., Witta, S., Danenberg, K., Domenichini, I., Ludovini, V., Magrini, E., Gregorc, V., Doglioni, C., Sidoni, A., Tonato, M., Franklin, W.A., Crino, L., Bunn, P.A., Jr., and Varella-Garcia, M. 2005a. Epidermal growth factor receptor gene and protein and gefitinib sensitivity in non-small-cell lung cancer. *J. Natl. Cancer Inst. 97*: 643–655.

Cappuzzo, F., Varella-Garcia, M., Shigematsu, H., Domenichini, I., Bartolini, S., Ceresoli, G.L., Rossi, E., Ludovini, V., Gregorc, V., Toschi, L., Franklin, W.A., Crino, L., Gazdar, A.F., Bunn, P.A., Jr., and Hirsch, F.R. 2005b. Increased HER2 gene copy number is associated with response to gefitinib therapy in epidermal growth factor receptor-positive non-small-cell lung cancer patients. *J. Clin. Oncol. 23*: 5007–5018.

Ceresoli, G.L., Cappuzzo, F., Gregorc, V., Bartolini, S., Crino, L., and Villa, E. 2004. Gefitinib in patients with brain metastases from non-small-cell lung cancer: a prospective trial. *Ann. Oncol. 15*: 1042–1047.

Chang, J.W., Chou, C.L., Huang, S.F., Wang, H.M., Hsieh, J.J., Hsu, T., and Cheung, Y.C. 2007. Erlotinib response of EGFR-mutant gefitinib-resistant non-small-cell lung cancer. *Lung Cancer 58*: 414–417.

Choong, N.W., Dietrich, S., Seiwert, T.Y., Tretiakova, M.S., Nallasura, V., Davies, G.C., Lipkowitz, S., Husain, A.N., Salgia, R., and Ma, P.C. 2006. Gefitinib response of erlotinib-refractory lung cancer involving meninges–role of EGFR mutation. *Nat. Clin. Pract. Oncol. 3*: 50–57.

Hirsch, F.R., Varella-Garcia, M., McCoy, J., West, H., Xavier, A.C., Gumerlock, P., Bunn, P.A., Jr., Franklin, W.A., Crowley, J., and Gandara, D.R. 2005. Increased epidermal growth factor receptor gene copy number detected by fluorescence in situ hybridization associates with increased sensitivity to gefitinib in patients with bronchioloalveolar carcinoma subtypes: a Southwest Oncology Group Study. *J. Clin. Oncol. 23*: 6838–6845.

Hotta, K., Kiura, K., Ueoka, H., Tabata, M., Fujiwara, K., Kozuki, T., Okada, T., Hisamoto, A., and Tanimoto, M. 2004. Effect of gefitinib ('Iressa', ZD1839) on brain metastases in patients with advanced non-small-cell lung cancer. *Lung Cancer 46*: 255–261.

Kobayashi, S., Boggon, T.J., Dayaram, T., Janne, P.A., Kocher, O., Meyerson, M., Johnson, B.E., Eck, M.J., Tenen, D.G., and Halmos, B. 2005. EGFR mutation and resistance of non-small-cell lung cancer to gefitinib. *N. Engl. J. Med. 352*: 786–792.

Lee, J.W., Soung, Y.H., Kim, S.Y., Park, W.S., Nam, S.W., Lee, J.Y., Yoo, N.J., and Lee, S.H. 2005. Absence of EGFR mutation in the kinase domain in common human cancers besides non-small cell lung cancer. *Int. J. Cancer 113*: 510–511.

Lynch, T.J., Bell, D.W., Sordella, R., Gurubhagavatula, S., Okimoto, R.A., Brannigan, B.W., Harris, P.L., Haserlat, S.M., Supko, J.G., Haluska, F.G., Louis, D.N., Christiani, D.C., Settleman, J., and Haber, D.A. 2004. Activating mutations in the epidermal growth factor receptor underlying responsiveness of non-small-cell lung cancer to gefitinib. *N. Engl. J. Med. 350*: 2129–2139.

Ma, E.S., Wong, C.L., Siu, D., and Chan, W.K. 2007. Amplification, mutation and loss of heterozygosity of the EGFR gene in metastatic lung cancer. *Int. J. Cancer 120*: 1828–1831.

Massarelli, E., Varella-Garcia, M., Tang, X., Xavier, A.C., Ozburn, N.C., Liu, D.D., Bekele, B.N., Herbst, R.S., and Wistuba, I.I. 2007. KRAS mutation is an important predictor of resistance to therapy with epidermal growth factor receptor

tyrosine kinase inhibitors in non-small-cell lung cancer. *Clin. Cancer Res. 13*: 2890–2896.

Matsumoto, S., Iwakawa, R., Kohno, T., Suzuki, K., Matsuno, Y., Yamamoto, S., Noguchi, M., Shimizu, E., and Yokota, J. 2006a. Frequent EGFR mutations in noninvasive bronchioloalveolar carcinoma. *Int. J. Cancer 118*: 2498–2504.

Matsumoto, S., Takahashi, K., Iwakawa, R., Matsuno, Y., Nakanishi, Y., Kohno, T., Shimizu, E., and Yokota, J. 2006b. Frequent EGFR mutations in brain metastases of lung adenocarcinoma. *Int. J. Cancer 119*: 1491–1494.

Miller, V.A., Kris, M.G., Shah, N., Patel, J., Azzoli, C., Gomez, J., Krug, L.M., Pao, W., Rizvi, N., Pizzo, B., Tyson, L., Venkatraman, E., Ben-Porat, L., Memoli, N., Zakowski, M., Rusch, V., and Heelan, R.T. 2004. Bronchioloalveolar pathologic subtype and smoking history predict sensitivity to gefitinib in advanced non-small-cell lung cancer. *J. Clin. Oncol. 22*: 1103–1109.

Mitsudomi, T., Kosaka, T., and Yatabe, Y. 2006. Biological and clinical implications of EGFR mutations in lung cancer. *Int. J. Clin. Oncol. 11*: 190–198.

Namba, Y., Kijima, T., Yokota, S., Niinaka, M., Kawamura, S., Iwasaki, T., Takeda, Y., Kimura, H., Okada, T., Yamaguchi, T., Nakagawa, M., Okumura, Y., Maeda, H., and Ito, M. 2004. Gefitinib in patients with brain metastases from non-small-cell lung cancer: review of 15 clinical cases. *Clin. Lung Cancer 6*: 123–128.

Omuro, A.M., Kris, M.G., Miller, V.A., Franceschi, E., Shah, N., Milton, D.T., and Abrey, L.E. 2005. High incidence of disease recurrence in the brain and leptomeninges in patients with nonsmall cell lung carcinoma after response to gefitinib. *Cancer 103*: 2344–2348.

Paez, J.G., Janne, P.A., Lee, J.C., Tracy, S., Greulich, H., Gabriel, S., Herman, P., Kaye, F.J., Lindeman, N., Boggon, T.J., Naoki, K., Sasaki, H., Fujii, Y., Eck, M.J., Sellers, W.R., Johnson, B.E., and Meyerson, M. 2004. EGFR mutations in lung cancer: correlation with clinical response to gefitinib therapy. *Science 304*: 1497–1500.

Pao, W., Miller, V., Zakowski, M., Doherty, J., Politi, K., Sarkaria, I., Singh, B., Heelan, R., Rusch, V., Fulton, L., Mardis, E., Kupfer, D., Wilson, R., Kris, M., and Varmus, H. 2004. EGF receptor gene mutations are common in lung cancers from "never smokers" and are associated with sensitivity of tumors to gefitinib and erlotinib. *Proc. Natl. Acad. Sci. USA 101*: 13306–13311.

Pao, W., Wang, T.Y., Riely, G.J., Miller, V.A., Pan, Q., Ladanyi, M., Zakowski, M.F., Heelan, R.T., Kris, M.G., and Varmus, H.E. 2005. KRAS mutations and primary resistance of lung adenocarcinomas to gefitinib or erlotinib. *PLoS Med. 2*: e17.

Politi, K., Zakowski, M.F., Fan, P.D., Schonfeld, E.A., Pao, W., and Varmus, H.E. 2006. Lung adenocarcinomas induced in mice by mutant EGF receptors found in human lung cancers respond to a tyrosine kinase inhibitor or to down-regulation of the receptors. *Genes Dev. 20*: 1496–1510.

Riely, G.J., Pao, W., Pham, D., Li, A.R., Rizvi, N., Venkatraman, E.S., Zakowski, M.F., Kris, M.G., Ladanyi, M., and Miller, V.A. 2006. Clinical course of patients with non-small cell lung cancer and epidermal growth factor receptor exon 19 and exon 21 mutations treated with gefitinib or erlotinib. *Clin. Cancer Res. 12*: 839–844.

Sasaki, H., Endo, K., Takada, M., Kawahara, M., Kitahara, N., Tanaka, H., Okumura, M., Matsumura, A., Iuchi, K., Kawaguchi, T., Kawano, O., Yukiue, H., Yokoyama, T., Yano, M., and Fujii, Y. 2007. EGFR exon 20 insertion mutation in Japanese lung cancer. *Lung Cancer 58*: 324–328.

Shigematsu, H., Lin, L., Takahashi, T., Nomura, M., Suzuki, M., Wistuba, I.I., Fong, K.M., Lee, H., Toyooka, S., Shimizu, N., Fujisawa, T., Feng, Z., Roth, J.A., Herz, J., Minna, J.D., and Gazdar, A.F. 2005. Clinical and biological features associated with epidermal growth factor receptor gene mutations in lung cancers. *J. Natl. Cancer Inst. 97*: 339–346.

Shimato, S., Mitsudomi, T., Kosaka, T., Yatabe, Y., Wakabayashi, T., Mizuno, M., Nakahara, N., Hatano, H., Natsume, A., Ishii, D., and Yoshida, J. 2006. EGFR mutations in patients with brain metastases from lung cancer: association with the efficacy of gefitinib. *Neuro. Oncol. 8*: 137–144.

Takano, T., Ohe, Y., Sakamoto, H., Tsuta, K., Matsuno, Y., Tateishi, U., Yamamoto, S., Nokihara, H., Yamamoto, N., Sekine, I., Kunitoh, H., Shibata, T., Sakiyama, T., Yoshida, T., and Tamura, T. 2005. Epidermal growth factor receptor gene mutations and increased copy numbers

predict gefitinib sensitivity in patients with recurrent non-small-cell lung cancer. *J. Clin. Oncol. 23*: 6829–6837.

Takeuchi, T., Tomida, S., Yatabe, Y., Kosaka, T., Osada, H., Yanagisawa, K., Mitsudomi, T., and Takahashi, T. 2006. Expression profile-defined classification of lung adenocarcinoma shows close relationship with underlying major genetic changes and clinicopathologic behaviors. *J. Clin. Oncol. 24*: 1679–1688.

Tam, I.Y., Chung, L.P., Suen, W.S., Wang, E., Wong, M.C., Ho, K.K., Lam, W.K., Chiu, S.W., Girard, L., Minna, J.D., Gazdar, A.F., and Wong, M.P. 2006. Distinct epidermal growth factor receptor and KRAS mutation patterns in non-small cell lung cancer patients with different tobacco exposure and clinicopathologic features. *Clin. Cancer Res. 12*: 1647–1653.

Weinstein, I.B. and Joe, A.K. 2006. Mechanisms of disease: oncogene addiction–a rationale for molecular targeting in cancer therapy. *Nat. Clin. Pract. Oncol. 3*: 448–457.

Yatabe, Y., Kosaka, T., Takahashi, T., and Mitsudomi, T. 2005. EGFR mutation is specific for terminal respiratory unit type adenocarcinoma. *Am. J. Surg. Pathol. 29*: 633–639.

Yokouchi, H., Yamazaki, K., Kinoshita, I., Konishi, J., Asahina, H., Sukoh, N., Harada, M., Akie, K., Ogura, S., Ishida, T., Munakata, M., Aka-Akita, H., Isobe, H., and Nishimura, M. 2007. Clinical benefit of readministration of gefitinib for initial gefitinib-responders with non-small cell lung cancer. *B.M.C. Cancer 7*: 51.

Yokoyama, T., Kondo, M., Goto, Y., Fukui, T., Yoshioka, H., Yokoi, K., Osada, H., Imaizumi, K., Hasegawa, Y., Shimokata, K., and Sekido, Y. 2006. EGFR point mutation in non-small cell lung cancer is occasionally accompanied by a second mutation or amplification. *Cancer Sci. 97*: 753–759.

28
Prostate Carcinoma

M.A. Hayat

INTRODUCTION

Prostate cancer is the most common non-cutaneous cancer, and the second leading cause of cancer-related deaths among men in the United States. Approximately, 218,890 new cases of prostate cancer are reported each year in the United States, and ~ 27,050 of these patients die (Am. Cancer Soc., 2007). However, death rates have been declining primarily owing to early detection, especially screening with the prostate specific antigen (PSA) blood test (discussed later). Briefly, prostate adenocarcinoma develops as a result of continuous and multiple outpouchings of the epithelium with the formations of small ducts and acini showing cytologic atypia and gradual or abrupt loss of basal cells (Mai *et al*., 2007). High grade prostatic intraepithelial neoplasia is both a precursor of lesions and an accompanying lesion of prostate cancer. The only recognized risk factors for prostate cancer are older age, ethnicity, and family history of the disease. Approximately, 65% of all prostate cancer cases are diagnosed in men 65 years and older; African–American men have the highest incidence rates of this cancer. A diet high in saturated fats and obesity may also be risk factors.

The phenomenon of prostate cancer initiation and progression is slow-advancing and exceedingly complex; some information on the genetic changes, signaling mechanisms, and the roles of the microenvironment and steroid hormones is available. In order to search for an effective prostate cancer therapy, it is necessary to understand molecular strategies responsible for its initiation, progression, and metastasis, which are summarized later.

There are no symptoms of early prostate cancer. At advanced disease stages, symptoms include frequent urination especially at night, weak or interrupted urine flow, inability to urinate or difficulty starting or stopping the urine flow, blood in the urine, and pain or burning feeling during urination. Metastatic stage of prostate cancer may result in pain in the lower back, pelvis or upper thighs. However, it should be noted that many of these symptoms are similar to those caused by benign prostate conditions.

Prostate development is controlled by steroid hormones that induce and maintain a complex interaction between the stromal and epithelial cells (see later). The vast majority of human prostatic cancers arise as adenocarcinomas derived from

the epithelial cells that form the glands and ducts of the prostate. The carcinoma progression is accompanied by phenotypic changes and alterations in gene expression in the adjacent stroma (He *et al*., 2007). The process of prostatic carcinogenesis includes aberrations in the interactions of the prostatic epithelium and its local microenvironment. These changes, in turn, result in reciprocal dedifferentiation of both the emerging carcinoma and the prostatic smooth muscle. Tumor microenvironment supporting the developing tumor includes stromal fibroblasts, infiltrating immune cells, blood, and lymphatic vascular networks. It needs to be noted that alterations in the microenvironment adjacent to the epithelial cells can transform nontumorigenic cells into malignant, while stromal factors can elicit reversion of a malignant teratocarcinoma to a benign phenotype despite genetic changes within the epithelial cells (Hayward *et al*., 2001; Hayashi and Cunha, 1991).

Endogenous variations in estrogens and androgens during the life of a man contribute to causal factors in prostate cancer. Estrogens have been known to be involved in prostate carcinogenesis for more than 2 decades. Estrogen-related genes significantly increase the risk of this cancer through specific polymorphisms. Recently, it was reported that polymorphisms -34T $\rightarrow$ C (CYP17), TTTA repeat (CYP19), V4321 (CYP1B1), and V158M (COMT) in genes are involved in estrogen metabolism pathways, and that these pathways are associated with an elevated risk of prostate cancer or an aggressive disease pattern (Cussenot *et al*., 2007).

Early exposure to estrogens initiates carcinogenesis in the prostate gland, and a decrease of the androgen/estrogen ratio with aging is responsible in part for the carcinogenesis of this cancer (Bosland, 2000; Ho, 2004). It is also known that estrogens, through their receptors or their catechol metabolites, are potential carcinogens in the prostate gland (Rogan and Cavalieri, 2004). Androgen deprivation and administration of estrogens are a recognized therapy for prostate cancer. This and other information suggests new clinical considerations in the management of prostate cancer by targeting the androgen pathways.

Androgen-dependent prostate cancer progressively becomes androgen-independent (androgen refractory), and patients finally succumb to widespread metastases particularly to the bone. One possible mechanism underlying the development of hormone-refractory prostate cancer is upregulation of the IL-6 receptor/JAK1/STAT3 (Tam *et al*., 2007).

Prostate Specific Antigen

Prostate specific antigen (PSA) is a classical tumor marker with high sensitivity but less specificity. It is produced in large quantities by epithelial cells of the prostate and by their derivatives, the prostate cancer cells. PSA leaks into the circulation and eventually the serum level of this antigen is used to monitor the progress of prostate cancer prior to and/or during treatment.

In 1991, Catalona *et al*. (1991) were the first to evaluate the first-line test for prostrate cancer screening, and subsequent studies by Catalona and Smith (1994) reported a multi-institutional trial of PSA-based prostate cancer screening, which led to the U.S. Food and Drug Administration's approval of PSA as an aid to the early detection of this cancer in 1994. It is

estimated that prostate cancer accounts for only 9% of cancer deaths, because of early detection and effective treatment. The more widespread the PSA testing, the less late-stage disease and the lower the prostate cancer-specific rate of death. For prostate screening, it is important to consider age of patient, family history of prostate cancer, ethnicity, urinary voiding symptoms, digital rectal examination, and total and free PSA ratio. It is possible that patients with an initial negative biopsy can show prostate cancer at repeat biopsies (up to 25%).

PSA is regulated by androgens, and cellular effects of androgens are mediated by their receptors. Upon androgen binding to its receptor, a sequence of cellular events occurs, which results in the translation of the androgen receptor into the nucleus, binding to androgen response elements in the promoters of target genes to initiate transcription. Recently, Lai *et al.* (2007) have demonstrated that a single-nucleotide polymorphism may be one of the mechanisms by which PSA expression is altered and predisposes one to prostate cancer. Shain and Boesel (1978) have shown that the total cytoplasmic androgen receptor of hyperplastic canine prostates was four- to sixfold greater than that of normal prostates. Testerone is essential for the development of prostate cancer. The action of testosterone is mediated via its receptors.

The normal cut-off for serum levels of PSA is 4 ng/ml, so any man presenting a PSA above 4 ng/ml is likely to require rectal biopsy, but only ~ 25% of men with serum levels of PSA between 4 ng and 10 ng/ml have cancer (Masters, 2007). Up to 50% of men presenting with prostate cancer have PSA levels within the normal range. It is apparent that screening of prostate cancer using PSA has low specificity, resulting in many unnecessary biopsies, particularly for gray zone values (4 ng–10 ng/ml). The advantages and limitations of PSA in diagnosing prostate cancer were recently reviewed by Hayat (2005). This uncertainty has prompted the application of other approaches to find biological markers for this cancer.

An alternative approach to stratify patients into high-risk or low-risk groups for the development of prostate cancer consists of screening for a set of genes (biological markers) on the basis of their methylation status. According to this approach, urine samples are collected after prostate massage from patients with localized prostate cancer undergoing radical prostatectomy and from control patients. Prostate massage is carried out by digital rectal examination in the operating room to obtain prostate secretion at the external urethral meatus (Rouprêt *et al.*, 2007). The first voided urine after the massage is used to extract DNA for aberrant ten genes using quantitative real-time methylation-specific polymerase chain reaction. Four genes (GSTP1, RASSF1a, APC, and RARB2) showed the greatest statistical difference in aberrant methylation between patients with prostate cancer and controls. The sensitivity and accuracy of the four gene set were 86% and 89%, respectively, and so they could stratify patients into low-and high- risk of having this cancer. However, this test requires validation in a large cohort to determine its specificity, reproducibility, and cost-effectiveness.

Another alternative is the application of proteomics to find a tumor marker that is more sensitive and specific than PSA to diagnose this cancer. Gene expression profiling is limited by the fact that gene expression does not necessarily translate

into protein expression, although molecular profiling is revealing new biomarkers of potential clinical significance. The working end of the human genome is the protein rather than RNA expression (Masters, 2007). Hence, biomarkers for cancer, whether they are in serum, urine, or the tissue, are more reliable. The surface enhanced laser desorption ionization method has been used for identifying prostate cancer biomarkers in serum, urine, and tissues (Banez *et al*., 2005).

The most widely used risk-group classification system for men with prostate cancer is based on clinical T-stage, Gleason score, and pretreatment PSA level. This system can be used to classify low-risk, intermediate-risk, and high-risk prostate cancers (Morgan *et al*., 2007). High-risk patients have significantly higher T-classifications, initial pretreatment PSA levels, and Gleason scores compared with those in the low-risk group. As expected, intermediate-risk and high-risk patients have a greater risk of occult micrometastasis when compared with low-risk patients.

Rate of change (velocity) in PSA level is often higher among men with prostate cancer than that in men without the disease. PSA velocity could be useful for identifying men with potentially life-threatening disease at a time when a cure is still possible with local therapy (surgery or radiation). It is thought that PSA velocity is an indicator of disease that is expected to progress and threaten life. According to D'Amico *et al*. (2007), men with a PSA velocity > 2 ng/ml/year have a significantly higher risk of prostate cancer-specific mortality when compared with men who have any other single high risk factor. They recommend an effective systemic treatment in addition to monotherapy with radical prostatectomy or radiation therapy. These systemic treatments include androgen suppression therapy, docetaxel, and prednisone.

As stated earlier, although baseline PSA value and rate of PSA change are prognostic factors for lethal prostate cancer, they are poor predictors of lethal prostate cancer among patients (with localized prostate cancer) who are managed by watchful waiting (Fall *et al*., 2007). It is difficult to use any PSA curve to substantiate who would develop lethal disease and who would not. Thus, early PSA characteristics are not suitable and safe to determine therapeutic intervention among low-risk patients managed with active monitoring. Progression-free survival of such patients is high, although clinicians lack tools to distinguish lethal cancer from less lethal disease at the time of diagnosis. As a result, many prostate cancer patients undergo aggressive local treatment without any survival benefit. To reduce overtreatment, selective delayed intervention of 2 years under active surveillance has been proposed (Fall *et al*., 2007).

Radiotherapy or prostatectomy is an effective local treatment for prostate cancer. However, PSA levels may increase at an average of 30–40% at 10 years. These data suggest the persistence of local malignancy after these treatments. In other words, biochemical failure indicates that local disease in the prostate remains a problem in some patients after radiotherapy, even among the low-risk patients (Morgan *et al*., 2007). Therefore, prostate biopsy after radiotherapy is recommended to identify patients with local persistence of the disease, so that salvage treatment can be administered before metastasis occurs.

The presence of castration-resistant (i.e., hormone-refractory) metastasis prostate cancer is a serious health problem. The Cancer Care Ontario guidelines for clinical non-hormonal therapy for men with this type of cancer are as follows. Treatment with docetaxel 75 mg/m^2 administered intravenously every 3 weeks plus 5 mg oral prednisone twice daily should be offered to improve overall survival and disease control. Use of estramustine alone or in combination with other cytotoxic drugs is not recommended because of increased risk of toxicities. Other non-hormonal therapies for men with castration-resistant metastatic prostate cancer are available at www.cancercare.on.ca/pdf/pebc14-1f.pdf.

REFERENCES

American Cancer Society Statistics. 2007.

Banez, L.L., Srivastava, S., and Moul, J.W. 2005. Proteomics in prostate cancer. *Curr. Opin. Urol. 15*: 151–156.

Bosland, M.C. 2000. The role of steroid hormones in prostate carcinogenesis. *J. Natl. Cancer Inst. Monogr. 27*: 39–66.

Catalona, W.J., and Smith, D.S. 1994. 5-year tumor recurrence rates after anatomical radical retropubic prostatectomy for prostate cancer. *J. Urol. 152*: 1837–1842.

Catalona, W.J., Smith, D.S., Ratliff, D.S., Dodds, K.M., Coplen, D.E., Yuan, J.J., Petros, J.A., and Andriole, G.L. 1991. Measurement of prostate-specific antigen in serum as a screening test for prostate cancer. *N. Engl. J. Med. 324*: 1156–1161.

Cussenot, O., Azzouzi, A.R., Nicolaiew, N., Fromont, G., Mangin, P., Cormier, L., Fournier, G., Valeri, A., Larre, S., Thibault, F., Giordanella, J-P., Pouchard, M., Zheng, Y., Handy, F.C., Cox, A., and Cancel-Tassin, G. 2007. Combination of polymorphisms from genes related to estrogen metabolism and risk of prostate cancers: the hidden face of estrogens. *J. Clin. Oncol. 25*: 3596–3602.

D'Amico, A.V., Chen, M-H., Catalona, W.J., Sun, L., Roehl, K.A., and Moul, J.W. 2007. Prostate cancer-specific mortality after radical prostatectomy or external beam radiation therapy in men with 1 or more high-risk factors. *Cancer 110*: 56–61.

Fall, K., Garmo, H., Andrén, O., Bill-Axelson, A., Adolfsson, J., Adami, H-O., Johansson, J-E., and Holmberg, L. 2007. Prostate specific antigen levels as a predictor of lethal prostate cancer. *J. Natl. Cancer Inst. 99*: 526–532.

Hayashi, N., and Cunha, G.R. 1991. Mesenchyma-induced changes in neoplastic characteristics of the Dunning prostatic adenocarcinoma. *Cancer Res. 51*: 4924–4930.

Hayat, M.A. 2005. Prostate carcinoma: an introduction. In: *Immunohistochemistry and In Situ Hybridization of Human Carcinomas*, vol. 2 (M.A. Hayat, Ed.), pp. 279–297. Elsevier, San Diego, CA.

Hayward, S.W., Wang, Y., Cao, M., Hom, Y.K., Zhang, B., Grossfeld, G.D., Sudilovsky, D., and Cunha, G.R. 2001. Malignant transformation in a nontumorigenic human prostatic epithelial cell line. *Cancer Res. 61*: 8135–8142.

He, Y., Franco, O.E., Jiang, M., Williams, K., Love, H.D., Coleman, I.M., Nelson, P.S., and Hayward, S.W. 2007. Tissue-specific consequences of cyclin D1 overexpression in prostate cancer progression. *Cancer Res. 67*: 8188–8197.

Ho, S.M. 2004. Estrogens and antiestrogens: key mediators of prostate carcinogenesis and new therapeutic candidates. *J. Cell Biochem. 91*: 491–503.

Lai, J., Kedda, M-A., Hinze, K., Smith, R.L.G., Yaxley, J., Spurdle, A.B., Morris, C.P., Harris, J., and Clements, J.A. 2007. PSA/KLK3 AR EI promoter polymorphism alters androgen receptor binding and its associated with prostate cancer susceptibility. *Carcinogenesis 28*: 1032–1039.

Mai, K.T., Burns, B.F., Stinson, W.A., and Morash, C. 2007. The 3-dimensional structure of isolated and small foci of prostatic adenocarcinoma. *Appl. Immunohistochem. Mol. Morphol. 15*: 50–55.

Masters, J.R. 2007. Clinical applications of expression profiling and proteomics in prostate cancer. *Anticancer Res. 27*: 1273–1276.

Morgan, P.B., Hanlon, A.L., Horwitz, E.M., Buyyounouski, M.K., Uzzo, R.G., and Pollack, A. 2007. Timing of biochemical failure distant metastatic disease for low-, intermediate-, and high-risk prostate cancer after radiotherapy. *Cancer 110*: 68–80.

Rogan, E.G., and Cavalieri, E.L. 2004. Estrogen metabolites, conjugates, and DNA adducts: possible biomarkers for risk of breast, prostate, and other human cancers. *Adv. Clin. Chem. 38*: 135–149.

Rouprêt, M., Hupertan, V., Yates, D.R., Catto, J.W., Rehman, I., Meuth, M., Ricci, S., Lacave, R., Cancel-Tassin, G., de la Taille, A., Rozet, F., Cathelineau, X., Vallancien, G., Hamdy, F.C., and Cussenot, O. 2007. Molecular detection of localized prostate cancer using quantitative methylation-specific PCR on urinary cells obtained following prostate massage. *Clin. Cancer Res. 13*: 1720–1725.

Shain, S.A., and Boesel, R.W. 1978. Androgen receptor content of the normal and hyperplastic canine prostate. *J. Clin. Invest. 61*: 654–660.

Tam, L., McGlynn, L.M., Traynor, P., Mukherjee, R., Bartlett, J.M.S., and Edwards, J. 2007. Expression levels of the JAK/STAT pathway in the transition from hormone-sensitivity to hormone-refractory prostate cancer. *Brit. J. Cancer 97*: 378–383.

29
The Role of Intermediary Metabolism and Molecular Genetics in Prostate Cancer

Renty B. Franklin and Leslie C. Costello

INTRODUCTION

It is estimated that ~ 220,000 males in the U.S. will be diagnosed with prostate cancer (PCa) of which ~ 27,000 will die from this cancer in 2007. African-American males will account for ~ 37% of the prostate cancer cases and ~ 31% of the prostate cancer deaths. Once, the malignancy advances to the androgen-independent and metastatic stages, it is untreatable and results in death. The principal factor in the prevention of deaths and morbidity due to prostate cancer is its early detection. Presently, no simple, non-invasive, and reliable screening test exists for early detection of prostate cancer, and this includes the prevalent use of prostatic specific antigen (PSA) testing. There is neither any protocol for the prevention of prostate cancer nor for the treatment of advanced-stage prostate cancer. A major problem in resolving these issues is the lack of understanding of the cause and factors associated with the pathogenesis and progression of prostate malignancy. Despite the voluminous reports and studies from decades of research, the genetic/molecular/hormonal basis of prostate malignancy remains largely unknown, as is also the case for the environmental and dietary influences.

Among the factors and conditions involved in the development of malignancy, the alteration in cellular intermediary metabolism provides the bioenergetic and synthetic requirements of malignant cells. In the absence of altered metabolism, the neoplastic cell will not manifest its malignant potential and will remain in a dormant state or will die. Such a relationship is represented in the development of prostate cancer. In this chapter we will describe the important role of altered intermediary metabolism of prostate cells in the pathogenesis of prostate adenocarcinoma and the progression of malignancy. We present the overwhelming clinical and experimental evidence that implicates the metabolic transformation of citrate-related metabolism as an essential step in the process of prostate malignancy, and its implications on cellular bioenergetics, cell growth, apoptosis, and lipogenesis. The important role of zinc in the metabolic alteration in malignant cells is also presented. A genetic basis for prostate cancer is evolving based on the metabolic implications in the development of malignant cells. Based on metabolic considerations, new concepts concerning the pathogenesis, diagnosis, and treatment of prostate malignancy are presented.

Unfortunately the metabolism of the prostate has been a seriously neglected and largely ignored area of prostate research. The importance of expanded research into the intermediary metabolism of normal and neoplastic prostate is essential for future significant advances in understanding and dealing with PCa. We refer the reader to our articles (Costello and Franklin, 1997, 2001, 2006; Costello *et al*., 2005; Franklin and Costello, 2007; Franklin *et al*., 2005) that provide extensive and detailed review of the literature concerning the metabolism of normal and malignant prostate. It is not our intention to repeat the presentation of the extensive literature which has been described in our recent publications, and which cite and acknowledge the important contributions of others.

CITRATE PRODUCTION AND THE HUMAN PROSTATE GLAND

The metabolism of all cells is established by the activity of the cells, such as their function, growth, and proliferation. As their cellular activities change, their metabolism must be altered to provide the bioenergetic, synthetic, and catabolic requirements in support of their activities. This relationship is especially applicable to the glandular secretory epithelial cells of the human prostate gland. Human prostate gland is comprised of three regions that include the peripheral zone (~ 75%), the central zone (~ 20%), and the transition zone (~ 5%). The peripheral zone is responsible for the major prostate gland secretory function of producing and secreting extraordinarily high levels of citrate, and is also the principal region for the origin of prostate malignancy. The transition zone is believed to be the origin of hyperplasia that expands into and enlarges the central zone in benign prostatic hyperplasia. Some malignancy also develops in the transition zone.

Because of the functional, anatomical, and embryological diversity of the regions of the prostate gland, one must clearly define the cell type being represented in any relationship that is being addressed. The glandular secretory epithelial cells of the peripheral zone are unique, highly specialized citrate-producing cells of the human prostate. No other cells in the body exhibit this functional and metabolic capability. Clinicians and researchers involved with the prostate must begin to recognize this distinction. The use of any terminology that infers the existence of a common singular secretory epithelial cell type associated with the human prostate is inaccurate and leads to misrepresentations and misconceptions. This especially applies to the description and identification of primary and immortalized prostate epithelial cells in culture as being representative of "normal prostate epithelial cells." A cell that does not express the functional and metabolic characteristics associated with citrate production cannot be identified as being representative of normal secretory epithelial cells of the peripheral zone, and the description of such cells as "normal prostate epithelial cells" is meaningless. To be completely accurate and unambiguous, unless otherwise defined, the following described relationships are applicable only to citrate-producing prostate epithelial cells, which in the human prostate is representative of the peripheral zone secretory epithelial cells.

CITRATE METABOLISM IN NORMAL PROSTATE EPITHELIAL CELLS

The major and unique function of the human prostate gland is the production and secretion of extraordinarily high levels of citrate as shown in Table 29.1. Because the peripheral zone glandular epithelial cells have evolved as highly specialized citrate-producing cells, their intermediary metabolism is dominated by their functional requirement to produce and secrete citrate. This is in contrast to most mammalian cells in which citrate synthesis and oxidation via the Krebs cycle are central to the pathways of intermediary metabolism. The complete oxidation of glucose and fatty acids is achieved through mitochondrial synthesis of citrate and its oxidation via the Krebs cycle. This provides the major supply (~ 80%) of cellular energy (ATP production) by coupled phosphorylation. In addition, the Krebs cycle and the recycling of its intermediates provide major connecting metabolic pathways such as the biosynthesis and degradation reactions of amino acid metabolism. Thus, citrate synthesis and oxidation via an operational Krebs cycle are critical for the normal metabolism, functional capabilities, growth and reproduction, and survival of aerobic mammalian cells. In contrast, the normal prostate cells sacrifice the potential benefits derived from the oxidation of citrate in order to fulfill their specialized function of production and secretion of citrate.

TABLE 29.1. Representative prostate levels.

(Nmols/gram wwt)	Citrate	Zinc
Normal peripheral zone	12,000–14,000	3,000–4,500
Malignant tissue	200–2000	400–800
Other tissues	250–450	200–400
Prostatic fluid	40,000–150,000	8,000–10,000
Blood plasma	100–200	15

M-ACONITASE AND ZINC IN CITRATE PRODUCTION

Although it had long been known that the human prostate gland accumulates very high levels of citrate, the metabolic pathway by which this is achieved has been elucidated more recently. In the prostate secretory epithelial cells, the accumulation and secretion of citrate (which we refer to as "net citrate production") occurs at the expense of citrate oxidation. Instead of being an essential utilized intermediate of cellular metabolism, most of the citrate becomes an end-product of intermediary metabolism. This occurs due to a uniquely limiting mitochondrial (m-) aconitase activity, the initial reaction of citrate oxidation via the Krebs cycle; which inhibits the oxidation of citrate. Therefore, in these cells the operation of the Krebs cycle is aborted prior to any oxidation of the accumulated citrate.

The mechanism of the limiting m-aconitase activity in prostate cells has recently been clarified. The activity of an enzyme can be limited by either decreasing its level and/or by inhibiting its activity. It is now established that the latter is the mechanism involved in limiting m-aconitase activity in the prostate cells. In mammalian cells m-aconitase is generally found in excess and catalyzes the equilibrium reaction:

However, in the prostate cells the m-aconitase activity is inhibited by the presence of high levels of zinc (Costello *et al.*, 1997; Singh *et al.*, 2006) that exist in prostate cells

and mitochondria (to be discussed below). The mechanism of inhibition occurs as follows:

It is important to note that the site of inhibition is at the initiating reaction of conversion of citrate to cis-aconitate. This optimizes the prevention of citrate oxidation through the production of isocitrate. As is evident from the normal equilibrium of m-aconitase, most mammalian cells exhibit a steady-state citrate/isocitrate ratio of ~ 10/1, which is independent of the level of citrate. In contrast, prostate tissue is characterized by a citrate/isocitrate ratio of ~30–40/1, which reflects a limiting m-aconitase reaction. However, the fact that zinc inhibits m-aconitase does not eliminate the possibility that the constituitive level of enzyme might be low in these prostate cells. This consideration is eliminated by several studies that demonstrate that the m-aconitase enzyme level is not uniquely low in prostate cells to account for the limited citrate oxidation; and no difference exists *in situ* between malignant and nonmalignant glands (Singh *et al*., 2006).

GLUCOSE UTILIZATION FOR NET CITRATE PRODUCTION

In the normal operation of the Krebs cycle, citrate is synthesized by the condensation of acetyl coenzyme A (the two-carbon component) with oxalacetate (the four-carbon component). The former is derived from the utilization of glucose through pyruvate oxidation. The latter is obtained by the recycling of oxalacetate that occurs downstream from citrate oxidation. In other words, citrate oxidation via the Krebs cycle results in the loss of two carbons and the conservation of four carbons. Therefore, glucose is the only required replaceable carbon source for continual citrate synthesis and oxidation. However, citrate is an end-product of metabolism in net citrate production and involves the loss of all six carbons that must be replaced for continued citrate production. This is achieved by the combined utilization of glucose for acetyl CoA production, and the utilization of aspartate for oxalacetate production (discussed below).

Human prostate tissue studies (Barron and Huggins, 1944; Huggins, 1946; Muntzing *et al*., 1975) have concluded that prostate tissue exhibits a high aerobic glycolysis. Similarly, the citrate-producing rat ventral prostate gland and isolated epithelial cells also exhibit a high aerobic glycolysis (Harkonen *et al*., 1975; Costello *et al*., 1988). Thus, the available information leads to the likely conclusion that citrate-producing prostate secretory epithelium, including human prostate, exhibits a high aerobic glycolysis. However, direct studies with normal human prostate cells are needed to confirm this expectation. Nevertheless, an important distinction exists between prostate metabolism and the metabolism of most other soft tissues. The latter is characterized by the aerobic utilization of glucose by its complete oxidation via glycolysis and the Krebs cycle. The classical Warburg concept that is often invoked involves the transformation of the tumor cells to a high aerobic glycolysis in which lactate is the major product. The normal prostate epithelial cells require a high "aerobic glycolysis" in order to meet their metabolic function of net citrate production.

One must consider the relationship of aerobic glycolysis to citrate production. The end-product of anaerobic or anoxic (the term that we prefer for mammalian cell metabolism) glycolysis is lactate. If the term "aerobic glycolysis" implies that under aerobic conditions the end-product is lactate as occurs in anaerobic/anoxic glycolysis, this pathway would be inconsistent with the utilization of glucose for citrate production. If the term is meant to imply that lactate is a "major" but not the only end-product of glucose utilization, then some of the glucose utilized becomes available for citrate production. The latter seems to be the case for the citrate-producing prostate cells and can be represented as follows:

This is consistent with the observation that the utilization of glucose by normal prostate epithelial cells results in the production of lactate and citrate as the major end-products (Costello *et al*., 1988; Costello and Franklin, 1989; Harkonen, 1981).

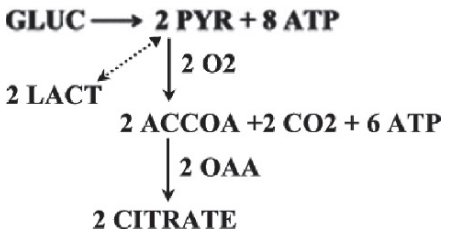

In typical mammalian cell metabolism most of the citrate synthesized remains compartmentalized within the mitochondria until utilized. The mitochondrial inner membrane is highly impermeable to citrate. The export of citrate to the cytosol requires a transporter (e.g., citrate transporter protein), which is normally absent or minimal except in lipogenic/cholesterogenic cells. The cellular concentration of citrate in most mammalian cells is ~ 0.2–0.5 mM. Since most (estimated at ~ 80–90%) of the cellular citrate is compartmentalized in the mitochondria in most mammalian cells, their cytosolic concentration is ~ 0.1 mM or lower. We have estimated that the cellular concentration of citrate in rat ventral prostate cells is ~ 1.2 mM (Franklin *et al*., 1990), and is ~ 10 mM in human prostate cells. Unlike most other mammalian cells, in prostate epithelial cells most of the citrate is exported to the cytosol where it resides for secretion. It would be reasonable to expect that the cytosolic concentration in these cells approximates the cellular concentration, which would be 10- to 100-fold higher than the cytosolic concentration of other cells. This raises an apparent intriguing paradox for the combination of a high rate of glycolysis along with high citrate accumulation in prostate epithelial cells.

A key step in controlling the rate of glycolysis in mammalian cells is the phosphofructokinase (PFK) reaction. The enzyme is negatively modulated by citrate. Conceptually, when the citrate levels rise in mammalian cells a feedback control occurs, which decreases glucose utilization via glycolysis and provides a logical interdependent mechanism to synchronize glycolysis and Krebs cycle activity. For citrate to be a physiological regulator of glycolysis in mammalian cells, its repressive effect on PFK must occur at elevated cellular concentrations. One should then expect that at the very high citrate levels that exist in normal human prostate cells, PFK should be virtually completely inhibited. Glucose utilization via glycolysis should be inhibited, which is in contradiction to the high rate of glycolysis that characterizes citrate-producing prostate cells. This implies that some unique relationship associated with the modulation of PFK and its regulation of glycolysis must exist in these prostate

cells. This paradox is similar to the condition observed in citrate-producing yeast cells, in which citrate-resistant PFK exists (Mlakar and Legisa, 2006).

ASPARTATE AS THE SOURCE OF OXALACETATE FOR CITRATE PRODUCTION

The continual net production of citrate requires an available source of oxalacetate as well as acetyl CoA. In prostate cells, aspartate serves as a source for mitochondrial oxalacetate production, which is achieved via transamination by mAAT. Earlier studies established that the coupling of mAAT and GDH provides an aspartate-glutamate-citrate pathway for the production of oxalacetate as follows:

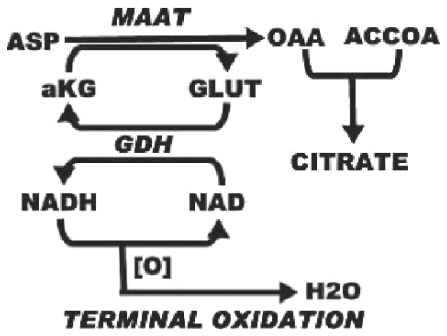

This is unique in that the mAAT reaction in most mammalian cells is in the direction of aspartate production from Krebs cycle generation of oxalacetate. For this reason, aspartate is a non-essential amino acid that is synthesized in most cells. The direction of the reversible mAAT reaction is dictated by the relative levels of the reactants. In prostate cells, the aborted Krebs cycle eliminates the recycling of oxalacetate. In addition, the prostate cells uniquely contain high levels of aspartate, and the combination of low oxalacetate and high aspartate concentrations drives the mAAT reaction in the direction of aspartate conversion to oxalacetate. In addition, alpha ketoglutarate is recycled by the coupled GDH reaction. Also, the oxidation of NADH via terminal oxidation provides the potential for the generation of an additional 3 ATP/citrate produced.

In the specialized prostate cells, aspartate is an essential amino acid that is derived from circulation. As is represented in rat ventral prostate glandular epithelial cells, the cellular concentration of aspartate is maintained at ~ 1.2 mM (Franklin *et al*., 1990). The plasma level of aspartate is ~ 0.03 mM. Therefore, the uptake and accumulation of cellular aspartate occurs against a 40:1 concentration gradient, which results from the existence of high-affinity L-aspartate transporter (Franklin *et al*., 1990; Lao *et al*., 1993; Costello *et al*.; 1993). The transporter has recently been identified as EAAC1, a member of the EAAT (excitatory amino acid transporters) class of X_{AG}^- transporters (Franklin *et al*., 2006). Although EAAC1 is implicated predominantly as a functional glutamate transporter in excitatory cells, it functions as a high-affinity L-aspartate transporter in rat and human prostate cells.

The relationships described above leads to the comparison of the typical metabolic pathway of normal citrate-oxidizing mammalian cells with the metabolic pathway of the highly specialized citrate-producing prostate epithelial cells as illustrated in Figure 29.1.

THE BIOENERGETICS OF NET CITRATE PRODUCTION

One of the important consequences of the net citrate production relates to the bioenergetics of the citrate-producing cells (Figure 29.1).

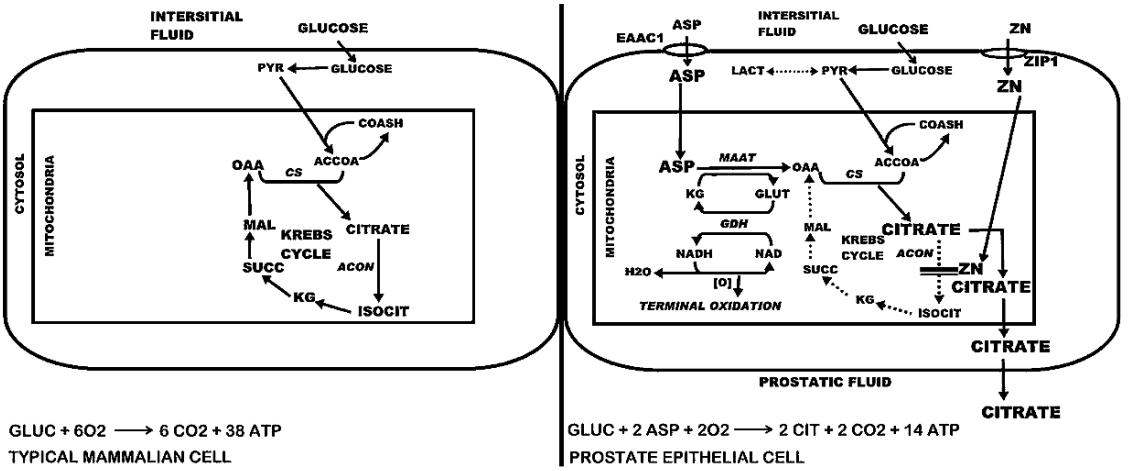

FIGURE 29.1. Comparison of the pathway of complete oxidation of glucose in typical normal mammalian cell metabolism versus the pathway of net citrate production in prostate epithelial cells

The following reactions represent the bioenergetic relationships in the progression of glucose oxidation and citrate production.

(1) Anoxic Glycolytic Pathway:

$$\text{GLUC} \rightarrow 2\,\text{LACT} + 2\,\text{ATP}$$

(2) Normoxic Glycolytic pathway:

$$\text{GLUC} + 6\text{O2} \longrightarrow 2\text{PYR} + 8\text{ATP}$$
$$\hookrightarrow 6\text{CO2} + 30\text{ATP}$$

(3) Net Citrate production:

$$\text{GLUC} + 2\,\text{OAA} + 2\,\text{O2} \rightarrow 2\,\text{CIT} + 2\,\text{CO2} + 14\,\text{ATP}$$

Typically, in most normal mammalian cells under aerobic conditions, the complete oxidation of glucose (reaction 2) results in the production of 38 ATP/glucose oxidized; which includes 6 ATP from the oxidation of glycolytic-produced NADH. Of this amount, the oxidation of citrate results in 24 ATP produced/citrate oxidized. Consequently, net citrate production results in a loss of ~ 63% of the potential ATP production that would result from the complete oxidation of glucose. As described above, the operation of the aspartate-glutamate-citrate pathway could generate additional ATP from the coupled oxidation of glutamate. Nevertheless the net production of citrate is energetically costly. Under similar conditions of impaired citrate oxidation, such as the adverse effects of fluoroacetate inhibition, most mammalian cells do not survive or function well. However, the specialized prostate cells have obviously adapted metabolically to accommodate their function of citrate production and their bioenergetic/synthetic requirements for their maintenance and sustenance. Their high aerobic glycolysis is a likely adaptation that provides accelerated ATP production as well as acetyl CoA for citrate synthesis.

THE CITRATE RELATIONSHIP IN PROSTATE CANCER

In 1946, Huggins (1946) described that the high citrate content of normal human prostatic secretion was dramatically decreased in prostate cancer. It was not until 1959 that Cooper and Imfeld (1959) and subsequent reports (Marberger *et al.*, 1962; Cooper and Farid, 1964; Costello *et al.*, 1978)

determined that the prostate tissue level of citrate was also dramatically decreased in prostate cancer. A major advancement in establishing this relationship in prostate cancer occurred in the 1990s with the development of 1H-magnetic resonance spectroscopy imaging (MRS) for the *in situ* detection of citrate in the prostate gland (described below). MRS conclusively established the dramatic decrease in citrate levels in malignant loci in the peripheral zone.

THE GENETIC/METABOLIC TRANSFORMATION IN MALIGNANT CELLS

The critical issue is the mechanism responsible for the lost ability of the prostate malignant cells *in situ* to accumulate high levels of citrate. It is now evident that the development of prostate malignancy involves the metabolic transformation of the normal citrate-producing epithelial cells to citrate-oxidizing malignant cells. This altered metabolism results from the release of the inhibition of m-aconitase that is the key reaction in the production of citrate in the normal epithelial cells. Whereas the normal epithelial cells accumulate high levels of zinc, the neoplastic malignant cell loses the zinc-accumulating capability. The accumulation of zinc in the normal prostate epithelial cells results from the expression and activity of Zip family zinc uptake transporters, particularly Zip1 and also Zip 2 and Zip3 (Costello and Franklin, 2006; Franklin and Costello, 2007; Desouki *et al*., 2007). However, the expression of these transporters is down regulated in the adenocarcinomatous glands, which eliminates the ability of the malignant cells to accumulate zinc. This accounts for the parallelism between zinc and citrate levels. The concentration of both is always high in normal glandular epithelium, and is always low in malignant tissue. As shown in Table 29.1, the zinc and citrate levels in cancer tissue are decreased by ~ 75% or more as compared to normal peripheral zone tissue values.

The established clinical relationships presented above lead us to propose the concept of the genetic/metabolic transformation involved in the development of prostate malignancy as represented in Figure 29.2. The initiating step in prostate malignancy is the genetic transformation of a normal cell to a neoplastic cell that possesses the potential for manifestation of the malignant process. The normal cell can be defined as a zinc-accumulating citrate-producing epithelial cell due to the expression of hZip1 transporter. Following the initiating genetic transformation, the neoplastic cell still retains the metabolic characteristics of the normal cell. Subsequently, hZip1 gene expression is silenced and the neoplastic cell loses the ability to accumulate zinc and becomes a premalignant cell. The cellular level of zinc decreases, and the inhibitory effect of zinc on m-aconitase activity and on citrate oxidation is released. The cell is now transformed to a citrate-oxidizing malignant cell in which the bioenergetic/synthetic requirements of malignancy can be fulfilled. Additionally, the adverse effects of zinc described below on the malignant cell growth/proliferation and invasive/migration activities are eliminated. In the absence of this metabolic transformation, the neoplastic cell will be arrested in a premalignant stage, and possibly ultimately aborted.

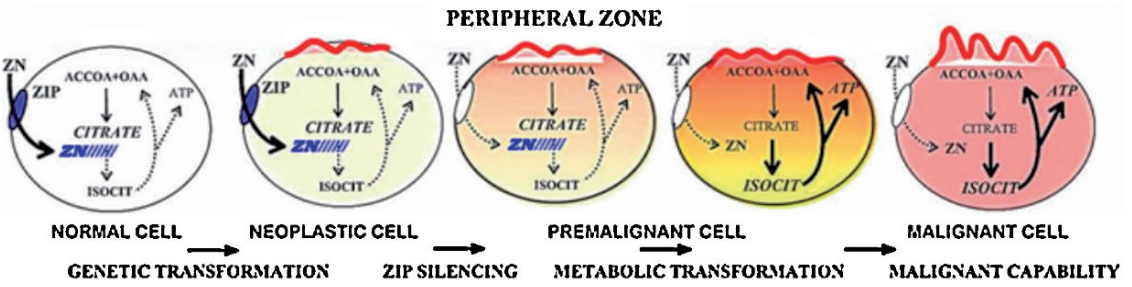

FIGURE 29.2. The relationship of altered intermediary metabolism in the development of prostate malignancy. The normal zinc-accumulating citrate-producing epithelial cells undergo a genetic mutation to a neoplastic cell with malignant potential. hZip1 gene expression is silenced which eliminates the zinc uptake transporter. The cellular level of zinc declines in the premalignant cells. The inhibitory effect of zinc on m-aconitase is eliminated, and the premalignant cell advances to an energy-efficient citrate-oxidizing malignant cell. The malignant cell is bioenergetically and metabolically capable of conducting its malignant activities, and the suppressive effects of zinc on cell proliferation and on invasive capability are eliminated. This concept proposes that hZip1 is a tumor suppressor gene, and zinc is a tumor suppressor agent

IS ZINC A TUMOR SUPPRESSOR IN PROSTATE CANCER?

A suggestion of a tumor suppression agent or gene must have a strong and rational clinical as well as experimental basis. The indisputable clinical evidence consistently reveals that, in contrast to normal prostate glands, zinc and citrate levels are always markedly depleted in malignant glands *in situ*; and malignant glands virtually never exhibit high zinc levels. The citrate decrease is a reflection of the decrease in zinc, which causes the decrease in citrate accumulation. Thus, there is an inherent incompatibility of malignant cells and retention of high zinc accumulation. Zinc exhibits several actions on prostate cells that can be implicated as anti-tumor effects.

1. Metabolic/bioenergetic effects. As already described, zinc accumulation in prostate cells truncates the Krebs cycle and inhibits citrate oxidation. The bioenergetic consequences have already been described in that cells sacrifice ~65% of the potential energy production in order to achieve their function of net citrate production and secretion. Zinc also inhibits terminal oxidation and mitochondrial respiration of prostate cells. This is consistent with the identification of prostate tissue as a "low respiring tissue" (Huggins, 1946). This effect further decreases mitochondrial coupled phosphorylation production of ATP.
2. Growth/proliferation effects. The accumulation of zinc inhibits growth and proliferation of prostate cells (Feng *et al.*, 2000, 2002; Huang *et al.*, 2006). Zinc exhibits a direct effect on the mitochondrial release of cytochrome c, which is followed by activation of the caspase cascade and ultimately induces apoptosis in prostate cells. Zinc treatment also sensitizes malignant prostate cells to apoptosis through its inhibition of NF-kB (Uzzo *et al.*, 2002).
3. Invasive/migration effects. Zinc has also been shown to suppress the invasive capability of malignant prostate cells (Ishii *et al.*, 2001, 2004). Uzzo *et al.*

(2006) reported that the suppressive effect of zinc on the angiogenic and metastatic potentials of cancer cells was also mediated through the inhibition of specific pathways that regulate progression of prostate cancer. These effects of zinc accumulation are inhibitory to and incompatible with the prostate malignant process and can be defined as "tumor suppressor" effects of zinc. The depletion of zinc that occurs in malignant prostate cells *in situ* eliminates these potential anti-tumor effects. The question then arises as to the absence of these adverse effects on the normal glandular epithelial cells *in situ*. Because zinc accumulation is essential to the specialized function of these cells, they must have evolved with conditions that obviate the detrimental effects of zinc. In regard to the bioenergetic consequences, the normal cells compensate by their incorporation of a high aerobic glycolysis. The accelerated glycolysis increases ATP production and increases the generation of acetyl CoA for citrate synthesis. The absence of any significant rate of apoptosis is likely due to anti-apoptotic agents that exist in the normal *in situ* condition. Important research into these relationships is required to understand the mechanisms associated with these transformations.

IS *ZIP1* A TUMOR SUPPRESSOR GENE IN PROSTATE CANCER?

The cellular accumulation of zinc is firstly dependent upon the existence of zinc uptake transporters to extract zinc from external (e.g., interstitial fluid) sources. Once within the cell, the cellular zinc might be subjected to zinc export from the cell, which will alter the cellular level; or the zinc might be sequestered/compartmentalized/tightly-bound, which will alter its bioavailability and reactivity. As described above, hZip1 is a major zinc uptake transporter in prostate cells that is responsible for the cellular accumulation of zinc from circulation. Most importantly, hZip1 gene expression and transporter protein are down regulated in adenocarcinomatous glands along with the depletion of cellular zinc. This provides insight into the genetic/molecular/metabolic relationship associated with lost ability of the malignant cells *in situ* to accumulate zinc. These cells are then released from the tumor-suppressor effects of zinc. On this basis, hZip1 can be characterized as a tumor suppressor gene. More recent studies also identified the presence of hZip2 and hZip3 in normal and BPH prostate glands, which are both down regulated in adenocarcinomatous glands (Desouki *et al*., 2007). Therefore, Zip-family zinc-uptake transporters are associated with zinc accumulation in prostate cells, and consistently down regulated in malignant cells *in situ*. The next important issue that needs to be investigated and resolved is the mechanism responsible for the silencing of these genes in the malignant cells *in situ*.

CITRATE METABOLISM AND *DE NOVO* LIPOGENESIS

Citrate that is synthesized in mitochondria is subject to one of three possible fates (Figure 29.3). In most mammalian cells, citrate is retained predominantly in the mitochondria where it is oxidized via

the Krebs cycle for energy production and for interaction with associated mitochondrial pathways. In normal prostate cells, the citrate is exported to the cytosol and ultimately secreted as a major component of prostatic fluid. Citrate also serves as the source of cytosolic acetyl CoA, the essential precursor for *de novo* lipogenesis/cholesterogenesis, which is essential to the growth and reproduction of cells. The highly specialized normal functional prostate glandular epithelial cells and most other normal specialized mammalian cells are not proliferating cells and do not require *de novo* lipogenesis/cholesterogenesis as a major metabolic activity. However, the malignant prostate cells, like all tumor cells, are parasitic cells that exist as propagating cells. As such, they have a high requirement for lipogenesis/cholesterogenesis as a major metabolic pathway. To achieve this, tumor cells generally will exhibit an increase in citrate production, but will not exhibit an increase in the cellular accumulation of citrate. Instead the citrate will be utilized for and incorporated into the lipogenic/cholesterogenic biosynthetic pathway (Figure 29.3).

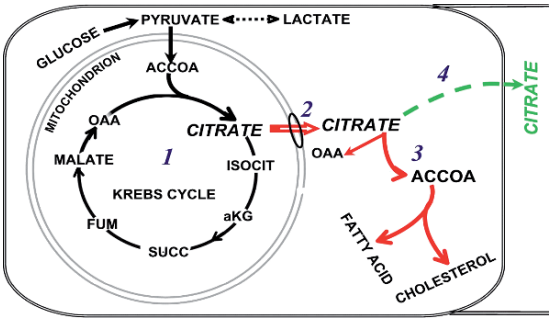

FIGURE 29.3. The fate of citrate in mammalian cells. Typically, in most cells citrate is oxidized via the Krebs cycle. In lipogenic/cholesterogenic cells citrate is exported into the cytosol; and is utilized for acetyl CoA production. In normal prostate cells citrate is exported into the cytosol, and is secreted out of the cell as a major component of prostatic fluid

The essential and common building block for *de novo* lipogenesis/cholesterogenesis is cytosolic acetyl Co, which is derived generally from mitochondrial synthesized citrate. To achieve this, the metabolism of most tumor cells involves metabolic adaptations to permit the export of citrate into the cytosol and its conversion to acetyl CoA. Although the identification of the mitochondrial citrate exporter and the export mechanism requires further study, the up-regulation of the process in tumor cells is well established. Presumably, the increased citrate export results from an increase in expression of CTP (citrate transporter protein) that has been identified in mammalian cells. The concept has evolved that tumor cells exhibit a "truncated Krebs cycle" that results from the increased rapid export of citrate from the mitochondria. However, in the absence of an inhibition of m-aconitase activity, the export of citrate cannot prevent the conversion of citrate by m-aconitase to isocitrate and its oxidation, which exists in most tumor cells. Therefore, it is more likely that some of the mitochondrial citrate pool is exported for lipogenesis/cholesterogenesis and some is oxidized via the Krebs cycle for energy production. Unlike other normal mammalian cells, the normal prostate epithelial cells must posses a high citrate export activity because the citrate must be exported to cytosol in order to be secreted into prostatic fluid. Therefore, up regulation of citrate export would not be an adaptive process in the malignant prostate cells.

Once in the cytosol, the citrate is available as the source of acetyl CoA. This is achieved by the action of ACL (ATP-citrate lyase) that converts citrate to acetyl CoA

+ oxalacetate (Figure 29.3). In non-lipogenic normal mammalian cells the constitutive level of this enzyme is low or absent. Therefore, the up regulation of ACL is an important metabolic transformation in most tumor cells. This includes prostate cells because ACL activity would be incompatible with the function of the normal cells to secrete citrate. That ACL activity is up regulated in malignant prostate cells *in situ* is indicated by the observation that human malignant prostate tissue contained lower citrate and elevated triacylglyceride levels when compared to adjacent nonmalignant tissue (Halliday *et al.*, 1988). However, the mechanism and factors involved in the regulation of ACL in prostate malignancy remain unknown.

THE CONCEPT OF "METABOLIC" GENES

The contemporary development and focus on molecular biology, molecular genetics and proteomics in cancer and other diseases introduces new issues regarding their application in the study of alterations in cellular intermediary metabolism. To address this issue, we have adopted a concept of "metabolic genes". We define "metabolic" genes as a class of genes that express the key enzymes and the transporter proteins that are important in the regulation of pathways of intermediary metabolism. These enzymes and transporter proteins exist in micro-quantities (micro-abundance), and relatively small changes (~ one- to fivefold) in their abundance have pronounced effects on their cellular activity. Macro-abundance of regulatory enzymes and transporter proteins would have little effect on their kinetic maximal cellular activities. Other genes control the expression and biosynthesis of protein products such as structural proteins, secretory proteins, and secretory enzymes, which are produced in relatively large amounts (macro-abundance) in a large range ~tenfold and greater. For discussion purposes, we refer to these genes as "cytokine" genes. However, the present concepts, methodology, application, and interpretation of gene activity and proteomics provide no recognition of the functional difference in their cellular products. Gene products are treated essentially as a homogeneous group of macro-abundant proteins, with no recognition of the special relationship of the proteins that exist as enzymes and transporters involved in cellular intermediary metabolism. This introduces serious consequences and misinterpretations of the role and existence of altered cellular intermediary metabolism based on such genetic and proteomic analysis.

One cannot employ these approaches as substitutes for the "traditional" metabolic/biochemical studies of cellular metabolism (discussed in Costello and Franklin, 2006). Cellular enzyme/transporter activities are dependent on their abundance and the cellular conditions that modify their kinetic activities. The determination of changes in metabolic gene expression and/or the respective protein level do not establish changes and or alterations in the cellular enzyme/transporter activity or the associated metabolic pathways. The prostate m-aconitase relationship described above provides one example of this issue. m-Aconitase enzyme level is relatively unchanged in normal prostate and malignant cells, but the activity of m-aconitase is markedly inhib-

ited in the former and uninhibited in the latter. This accounts for the important metabolic transformation of normal citrate-producing cells to citrate-oxidizing malignant cells. The accumulation or loss of zinc is the critical factor. Gene microarray or proteomic analysis would not detect this metabolic alteration, and this would lead to the misinterpretation that m-aconitase was not an important step in the development of prostate malignancy.

As described above, the specialized metabolic pathway of net citrate production in normal prostate epithelial cells is achieved by several important key enzymes and transporters. The key regulatory enzymes and transporters directly associated with citrate synthesis are pyruvate dehydrogenase E1alpha and mAAT; m-aconitase for regulation of citrate oxidation; hZip1 for regulation of zinc accumulation; and EAAC1 for regulation of aspartate uptake. It is well established that normal prostate citrate production is hormonally controlled by testosterone and by prolactin; both of which stimulate citrate production. Both hormones mediate their effects via the regulation of transcription of the respective genes for these enzymes and transporters (for review of hormonal regulation see Costello and Franklin, 2002). Prolactin regulation of the metabolic genes is directly mediated via a prolactin receptor-PKC-AP1 intracellular signaling pathway. This is independent of and different from the "cytokine" pathway of prolactin regulation of prostate and other cells, which is mediated via "tyrosine kinase"-associated signaling pathways. The PKC pathway provides a direct hormonal regulation of metabolic genes in which the targeted metabolic gene is also the end-point gene for expression of the enzymes and transporters of intermediary metabolism. The "tyrosine kinase" signaling pathway provides a multi-step cascading and amplifying pathway (immediate-early, intermediate, and late acting genes) that recruits multiple downstream end-point genes. Such a system would not be consistent with the regulation of cellular intermediary metabolism. While this dual hormonal regulation of normal prostate citrate metabolism has been revealed, the possible role of prolactin and/or testosterone regulation of the metabolic genes in prostate cancer is unknown.

These genetic/molecular/metabolic relationships highlight the importance of recognizing a distinction between the regulation of the enzymes and transporters associated with changes in intermediary metabolism compared to other cellular activities. In the absence of this understanding, critical issues and identification of the important factors in the role of altered intermediary metabolism in the pathogenesis and progression of prostate cancer and other cancers will be misrepresented.

THE CLINICAL APPLICATION OF PROSTATE CANCER METABOLISM

The elucidation of the pathways of intermediary metabolism of normal prostate epithelial cells versus malignant prostate cells and the factors/conditions associated with the metabolic transformations in malignancy can and will provide an important understanding of the pathogenesis and progression of prostate cancer. Moreover, this information will lead to new approaches in the identification of biomarkers for prostate cancer and for

development of agents for the treatment and, perhaps, prevention of prostate cancer. Some important applications are illustrated in the following examples.

1. *In situ* MRS citrate detection of malignant prostate loci.

   The metabolic transformation of citrate-producing prostate epithelial cells to citrate-oxidizing prostate malignant cells provides the basis for the development of 1H-MRS imaging for the *in situ* identification of malignant loci in the prostate gland. When combined with MRI a "metabolic map" of the prostate gland can be obtained, which reveals important metabolic relationships as shown in Figure 29.4. The normal peripheral zone contains the high concentration of citrate as compared with lower levels of citrate in the central zone. Malignant loci are readily identified by the dramatic decrease and depletion of citrate. One rarely, if ever, finds malignant tissue that retains the high citrate levels that characterize the normal peripheral zone. In contrast to the decrease in citrate, choline levels are increased in malignant loci, which likely reflects the increase in lipogenesis/cholesterogenesis associated with malignant cell activity. The consistency of the MRS imaging of citrate metabolism transformation now provides the most accurate method for the identification, localization, and volume estimation of malignancy, and is even being developed for more accurate guided brachytherapy applications. Also evident is the fact that hyperplastic glands that occupy the central gland in the development of BPH are citrate-producing glands. For extensive reviews of MRS application in prostate cancer see Costello *et al.* (1999) and Kurhanewicz *et al.* (2002).
2. Treatment of prostate malignancy by metabolic inhibitors – Zinc inhibition

   One can employ the metabolic transformation relationships of malignancy as a basis for the development of pharmacologic agents for treatment of prostate cancer. Such agents would have to exhibit a high selectivity and specificity for the prostate cells, with minimal adverse systemic effects. Because zinc exhibits tumor-suppressor effects, it poses a potential agent for the treatment of prostate malignancy. A mouse xenograft study with PC-3 cells that express Zip1 has shown that zinc treatment of the animals inhibits tumor growth (Feng *et al.*, 2003) and shows increased zinc and citrate accumulation in the tumors and increased apoptosis. This response should also occur in human prostate cancer. However, in human prostate cancer, the malignant cells *in situ* are protected from zinc accumulation by the down regulation of hZip transporters. Therefore, the issue involves the development of a vehicle that will deliver zinc into prostate cells *in situ*. Once the *in situ* conditions that induce the epigenetic silencing of hZip1 expression are identified, the possible reestablishment of gene expression in the malignant cells could be possible. In lieu of this approach, other vehicles for zinc delivery can be considered. One might employ the specificity of EAAC1 as an aspartate transporter to deliver zinc in the form of ZnAspartate to the neoplastic/malignant prostate cells. Once in the cell, the relatively low binding affinity will permit the release of zinc for its tumor-suppressor actions. Such approaches now await investigation as

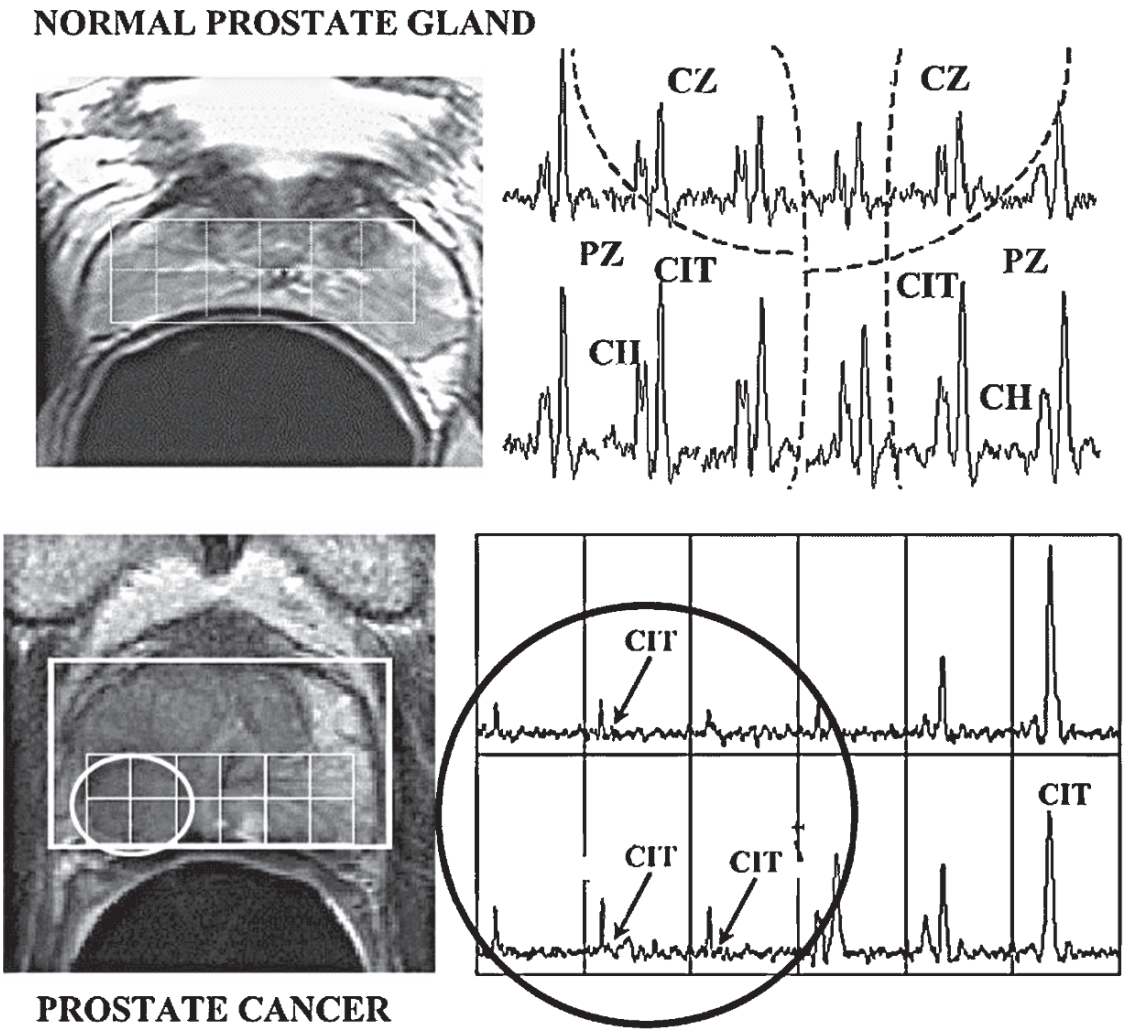

FIGURE 29.4. *In situ* MRS imaging of citrate in the human prostate gland. In the normal gland, citrate is high in the peripheral zone (PZ) and low in the central zone (CZ). In prostate cancer, the malignant locus in the right peripheral zone is depleted of citrate compared to the high citrate in the left peripheral zone. CH = choline peak

improved and expanded understanding of the metabolic relationships of prostate malignancy evolves.

Acknowledgement. The cited studies of LCC and RBF described in this review were supported in part by NIH grants CA71207, CA21097, CA79903, and CA93443.

REFERENCES

Barron, E.S.G., and Huggins, C. 1944. The metabolism of isolated prostatic tissue. *J. Urol. 51*: 630–634.

Cooper, J.E., and Farid, I. 1964. The role of citric acid in the physiology of the prostate. Lactic/citrate ratios in benign and malignant prostatic homogenates as an index of prostatic malignancy. *J. Urol. 92*: 533–536.

Cooper, J.F., and Imfeld, H. 1959. The role of citric acid in the physiology of the prostate: a preliminary report. *J. Urol. 81*: 157–163.

Costello, L.C., and Franklin, R.B. 1989. Prostate epithelial cells utilize glucose and aspartate as the carbon sources for net citrate production. *Prostate 15*: 335–342.

Costello, L.C., and Franklin, R.B. 1997. Citrate metabolism of normal and malignant prostate epithelial cells. *Urology 50*: 3–12.

Costello, L.C., and Franklin, R.B. 2001. The intermediary metabolism of the prostate: a key to understanding the pathogenesis and progression of prostate malignancy. *Oncology 59*: 269–282.

Costello, L.C., and Franklin, R.B. 2002. Testosterone and prolactin regulation of metabolic genes and citrate metabolism of prostate epithelial cells. *Horm. Metabol. Res. 34*: 417–424.

Costello, L.C., and Franklin, R.B. 2006. The clinical relevance of the metabolism of prostate cancer; zinc and tumor suppression: connecting the dots. *Mol. Cancer 5*: 17.

Costello, L.C., Littleton, G.K., and Franklin, R.B. 1978. Regulation of citrate-related metabolism in normal and neoplastic prostate. In: Sharma RK, Criss WE (eds), *Endocrine Control of Neoplasia*. New York, Raven, pp. 303–314.

Costello, L.C., Akuffo, V., and Franklin, R.B. 1988. Net citrate production by isolated prostate epithelial cells. *Enzyme 39*: 125–133.

Costello, L.C., Lao, L., and Franklin, R.B. 1993. Citrate modulation of high affinity aspartate transport in prostate epithelial cells. *Cell. Mol. Biol. 39*: 515–524.

Costello, L.C., Liu, Y., Franklin, R.B., and Kennedy, M.C. 1997. Zinc inhibition of mitochondrial aconitase and its importance in citrate metabolism of prostate epithelial cells. *J. Biol. Chem. 272*: 28875–28881.

Costello, L.C., Franklin, R.B., and Narayan, P. 1999. Citrate in the diagnosis of prostate cancer. *Prostate 38*: 237–245.

Costello, L.C., Feng, P., and Franklin, R.B. 2005. Mitochondrial function, zinc, and intermediary metabolism relationships in normal prostate and prostate cancer. *Mitochondrion 5*: 143–153.

Desouki, M.M., Geradts, J., Milon, B., Franklin, R.B., and Costello, L.C. 2007. hZip2 and hZip3 zinc transporters are down regulated in human prostate adenocarcinomatous glands. *Mol. Cancer 6*: 37.

Feng, P., Liang, J-Y., Li, T-L., Guan, Z-X., Zou, J., Franklin, R.B., and Costello, L.C. 2000. Zinc induces mitochondria apoptogenesis in prostate cells. *Mol. Urol. 4*: 31–36.

Feng, P., Li, T-L., Guan, Z-X., Franklin, R.B., and Costello, L.C. 2002. Direct effect of zinc on mitochondrial apoptogenesis in prostate cells. *Prostate 52*: 311–318.

Feng, P., Li, T.L., Guan, Z-X., Franklin, .R.B., and Costello, L.C. 2003. Effect of zinc on prostatic tumorigenicity in nude mice. *Ann. NY Acad. Sci. 1010*: 316–320.

Franklin, R.B., and Costello, L.C. 2007. Zinc as an anti-tumor agent in prostate cancer and in other cancers. *Arch. Biochem. Biophys*. Mar 16; [Epub ahead of print].

Franklin, R.B., Lao, L., and Costello, L.C. 1990. Evidence for two aspartate transport systems in prostate epithelial cells. *Prostate 16*: 137–146.

Franklin, R.B., Milon, B., Feng. P., and Costello, L.C. 2005. Zinc and zinc transporter in normal prostate function and the pathogenesis of prostate cancer. *Frontiers Biosci. 10*: 2230–2239.

Franklin, R.B., Zou, J., Yu, Z., and Costello, L.C. 2006. EAAC1 is expressed in rat and human prostate epithelial cells; functions as a high-affinity L-aspartate transporter; and is regulated by prolactin and testosterone. *BMC. Biochem. 7*: 10.

Halliday, K.R., Fenoglio-Preiser, C., and Sillerud, L.O. 1988. Differentiation of human tumors from nonmalignant tissue by natural-abundance 13C NMR spectroscopy. *Magn. Res. Med. 7*: 384–411.

Harkonen, P.L.1981. Androgenic control of glycolysis, the pentose cycle and pyruvate dehydrogenase in the rat ventral prostate. *J. Steroid Biochem. Mol. Biol. 14*: 1075–1084.

Harkonen, P., Isotala, A., and Santti, R. 1975. Studies on the mechanism of testosterone action on glucose metabolism in rat ventral prostate. *J. Steroid Biochem. 6*: 1405–1413.

Huang, L., Kirschke, C.P., and Zhang, Y. 2006. Decreased intracellular zinc in human tumorigenic prostate epithelial cells: a possible role in prostate cancer progression. *Cancer Cell Int. 31*: 10

Huggins, C. 1946. The prostatic secretion. *Harvey Lect. 42*: 148–193.

Ishii, K., Usui, S., Sugimura, Y., Yoshida, S., Hioki, T., Tatematsu, M., Yamamoto, H., and Hirano, K. 2001. Aminopeptidase N regulated by zinc in human prostate participates in tumor cell invasion. *Int. J. Cancer 92*: 49–54.

Ishii, K., Otsuka, T., Iguchi, K., Usui, S., Yamamoto, H., Sugimura, Y., Yoshikawa, K., Hayward, S.W., and Hirano, K. 2004. Evidence that the prostate-specific antigen (PSA)/Zn2+ axis may play a role in human prostate cancer cell invasion. *Cancer Lett. 207*: 79–87.

Kurhanewicz, J., Swanson, M.G., Nelson, S.J., and Vigneron, D.B. 2002 Combined magnetic resonance imaging and spectroscopic imaging approach to molecular imaging of prostate cancer. *J. Mag. Reson. Imag. 16*: 451–463.

Lao, L., Franklin, R.B., and Costello, L.C. 1993. A high affinity L-aspartate transporter in prostate epithelial cells which is regulated by testosterone. *Prostate 22*: 53–63.

Marberger, H., Marberger, E., Mann, T., and Lutwak-Mann, C. 1962. Citric acid in human prostatic secretion and metastasizing cancer of prostate gland. *Br. Med. J. 1*: 835–836.

Mlakar, T., and Legisa, M. 2006. Citrate inhibition-resistant form of 6-phosphofructo-1-kinase from Aspergillus niger. *Appl. Environ. Microbiol. 72*: 4515–4521.

Muntzing, J., Varkarakis, M.J., Saroff, J., and Murphy, G.P. 1975. Comparison and significance of respiration and glycolysis of prostatic tissue from various species. *J. Med. Primatol. 4*: 245–251.

Singh, K.K., Desouki, M.M., Franklin, R.B., and Costello, L.C. 2006. Mitochondrial aconitase and citrate metabolism in malignant and non-malignant human prostate tissues. *Mol. Cancer 5*: 14, 4.

Uzzo, R.G., Leavis, P., Hatch, W., Gabai, V.L., Dulin, N., Zvartau, N., and Kolenko, V.M. 2002. Zinc inhibits nuclear factor-kappa B activation and sensitizes prostate cancer cells to cytotoxic agents. *Clin. Cancer Res. 8*: 3579–3583.

Uzzo, R.G., Crispen, P.L., Golovine, K., Makhov, P., Horwitz, E.M., and Kolenko, V.M. 2006. Diverse effects of zinc on NF-{kappa}B and AP-1 transcription factors: implications for prostate cancer progression. *Carcinogenesis 27*: 1980–1990.

30
Array-Based Comparative Genomic Hybridization in Prostate Cancer: Research and Clinical Applications

Franclim R. Ribeiro, Rolf I. Skotheim, Rui Henrique, and Manuel R. Teixeira

INTRODUCTION

It is widely recognized that acquired genomic aberrations, leading to loss of function of tumor suppressor genes or gain of function of protooncogenes, are the driving force behind cellular neoplastic transformation (Hanahan and Weinberg, 2000). The increased knowledge of the human genome and the advances in the field of biotechnology have provided us with powerful tools for high-throughput characterization of these alterations in cancer samples. Novel microarray platforms with genome-wide coverage at escalating resolutions give promise of quickly uncovering the genetic events driving neoplastic transformation, which have previously gone undetected.

For prostate cancer in particular (one of the most frequently diagnosed malignancies and the second cause of cancer-related death among Western men) standard clinical and pathological variables still fail to predict the clinical behavior of most tumors. Uncovering molecular markers with diagnostic and/or prognostic potential is, therefore, of vital importance to improve the detection and management of prostate cancer patients, and considerable effort (and expectations) has been placed on the development of the new array platforms. The technology itself is still relatively young, however, and there are many challenges to overcome.

In this chapter we summarize the state-of-the-art in the fast-evolving field of genomic microarrays, highlighting some of the advantages and pitfalls of different array platforms and analyses techniques. We also review the relative contribution of this new technology to the knowledge of prostate cancer genetics, with an emphasis on its potential use in a clinical setting.

THE METHODOLOGY

Standard cytogenetic analysis is a well-established source of diagnostic and prognostic information for hematological malignancies and sarcomas, but has failed to be informative for most epithelial tumors due to the requirement of fresh tissue for culturing, the low rate of tumor cell proliferation *in vitro*, and the difficulty in interpreting the complex karyotypes often observed (Mitelman, 2000). Thus, other methodologies are needed to be implemented to assess the genomic content of carcinoma samples,

and so comparative genomic hybridization (CGH) was developed to meet the challenge (Kallioniemi *et al*., 1992). This robust screening technique is based on competitive hybridization of tumor and normal DNA, labeled with different fluorochromes, onto a normal DNA template. This template may consist of either metaphase chromosomes from a healthy individual (chromosomal CGH, cCGH) or, with the recent advances in the field, known genomic fragments organized in a microarray format (aCGH, Solinas-Toldo *et al*., 1997; Ylstra *et al*., 2006). CGH will thus detect genomic imbalances (specific gains and/or losses of DNA material) based on the fluorescence ratios measured after hybridization.

A major advantage of this methodology is that it does not require cell culture to be performed, given that tumor DNA can be extracted directly from fresh or archival tissue samples. One downside of DNA copy number analyses is the inability to disclose balanced chromosomal rearrangements (genetic events that do not result in net gain or loss of DNA material). As most carcinomas are known to harbor complex genetic aberrations resulting in gain or loss of genetic material, however, CGH emerges as an excellent approach for their detection, and high-throughput methodologies have been established that can rapidly validate and extend the findings (Kononen *et al*., 1998). Another disadvantage, associated mostly with cCGH, is its lower resolution potential (estimates vary from 3–20 Mb), which makes it necessary to follow up on results with a more selective analysis. With the advent of aCGH, the resolution of the method has been increased by >100-fold, providing a much more sensitive and informative result. Another simplification with the transfer to the array-format is the objective connection of measurements to their genomic location, so karyotyping expertise is no longer a requirement.

Platforms and Methodologies

Genomic microarrays (*i.e*., for the analysis of DNA copy number changes) are normally produced by either spotting or *in situ* synthesis of specific DNA sequences (referred to as "features" or "probes") onto a glass slide (thoroughly reviewed in Tan *et al*., 2007). Generally, spotted microarrays contain DNA fragments of clonal origin, such as complementary DNA (cDNA) clones or bacterial artificial chromosome (BAC) clones, whereas microarrays generated by *in situ* synthesis contain short single stranded sequences (oligonucleotides). Generally, arrays with larger probes provide more intense hybridization signals with lower background noise. The shortcoming is that due to physical constraints fewer probes can be fitted onto a slide, and thus the resolution of the array may decrease.

The type of probe itself will also affect the overall performance of the microarray platform. Complementary DNA arrays (Pollack *et al*., 1999) contain sequences derived exclusively from transcribed regions of the genome (probe sizes usually range from 200 to 2,000 basepairs), resulting in a low locus-specificity due to the fact that the coding-regions of genes often contain sequences that are homologous to loci elsewhere in the genome. In addition to cross-hybridizing with paralogous gene family members and genes encoding the same conserved protein domains, there are often multiple pseudo-genes present for a given gene. Additionally, as the

distribution of coding sequences along the genome is not uniform, there is often an under-representation of gene-poor regions in cDNA arrays, and genomic aberrations occurring within these regions will more likely be missed.

Arrays constructed with BAC clones (Pinkel *et al*., 1998) provide individual measurements from larger segments that include coding and noncoding sequences (the average size of a BAC clone is 100–150 Kbp). Possible effects from unwanted cross-hybridization of individual genes are leveled out due to the larger size of these probes and also to the fact that the main fraction of each BAC consists of intronic and intergenic sequences. As a limitation of these characteristics, BAC probes will often contain repetitive sequences (the human genome is rich in small repetitive elements scattered across all chromosomes) that may generate hybridization noise. This effect is reduced by saturating the template with unlabelled Cot-1 DNA (which is enriched in small repetitive sequences) prior to hybridization. In fact, BAC arrays generally produce less background noise than cDNA arrays. Furthermore, because any known target sequence (of correct size) may be cloned into a BAC probe, BAC arrays can be designed to have an even representation of probes across the genome, or to have a very high (tiling-path) coverage of probes along any specific genomic region.

Finally, at the higher limit of the resolution scale, we have the more recently available oligonucleotide microarrays (Barrett *et al*., 2004), which consist of short single stranded sequences (typically 60 nucleotides long) that are specifically designed and optimized to target unique genomic loci. Interestingly, on an individual basis, these small probes produce less intense and less accurate measurements than individual BACs. However, the high probe density that can be generated on these arrays completely compensates for the increased background noise. Indeed, current oligoarrays may contain several hundred thousand probes, whereas BAC arrays usually contain less than ten thousand individual features. Based on the number of features per genomic length, and on the hybridization accuracy produced by the individual measurements, it is estimated that modern oligoarrays may provide a genome-wide resolution level of ~10 kbp (*i.e*., one reliable measurement every 10,000 bps), whereas BAC arrays may go as low as 100 kbp and cDNA arrays ~ 1 Mbp, which represents at least a tenfold increase when compared to chromosomal CGH (Tan *et al*., 2007).

Establishing and optimizing an in-house facility for genomic microarrays (including manufacturing of custom microarray slides) implicates a vast amount of hands-on work from expert personnel and purchase of expensive equipment. Altogether, this is so costly and time consuming that only a few research facilities worldwide choose this option. Most facilities prefer the more commercial line, purchasing one of the many available hybridization platforms along with the corresponding microarray slides. This is also expensive and requires optimization and expertise. It is thus not surprising that many laboratories are still performing chromosomal CGH on a regular basis, as it remains a fairly good low-cost alternative to the new microarray platforms.

For the sake of completeness, it should be mentioned that some commercial companies have made available (in the last few

years) microarrays for simultaneous detection of single nucleotide polymorphisms (SNPs) along with DNA copy number measurements (Ylstra *et al*., 2006). For semantic interest, these platforms work on a single-channel basis (only one fluorochrome is used), and thus cannot be regarded as *comparative* genome hybridization procedures. However, they do provide competitive whole-genome DNA copy number measurements at a high-resolution scale, and in addition, will also provide information on allele-specificity of the genomic changes, thus enabling high-resolution loss-of-heterozigosity analyses.

Scoring Approaches and Common Pitfalls

One of the important challenges of the microarray methodology concerns the handling and interpretation of the huge amount of data points generated by each individual experiment. Novel bioinformatic tools are being developed and continually optimized to address this issue, and many statistical algorithms exist to automatically process microarray data. Indeed, dozens of microarray software packages are freely available online, and deciding which software to apply is not necessarily a trivial task (Lai *et al*., 2005). Different normalization and scoring methodologies may need to be applied based on factors such as the type of probes in the array, the type of tissue being analyzed, and the fraction of tumor cells in the individual samples. Furthermore, some software packages will perform better during normalization, some provide more reliable scoring algorithms, and some are better for visualizing the results. Thus, using several independent tools on the same dataset is often advisable.

As such, there is currently no consensus on how to analyze genomic microarray data, and usually several good approaches can be applied to each sample set. Many good publications are available in which different statistical methods that can be applied to microarray data are explained, highlighting the advantages and pitfalls of commonly used approaches (Lai *et al*., 2005). It is noteworthy that most software packages function well, and provide comparable results when samples are homogeneous and the hybridization quality is excellent. However, clinical samples often contain nonneoplastic cell populations that reduce the signal amplitudes of copy number changes present in neoplastic cells. Combined with the variability in labeling efficiency and hybridization behavior for different probes, different levels of technical noise/variability are frequently observed that may influence the final results if the software is unable to handle the data correctly. This is particularly evident when fixed thresholds are used to score microarray data that were not segmented or smoothed, as many aberrations are missed or scored only partially (Lai *et al*., 2005). Statistical approaches not dependent on the magnitude of ratio changes, therefore, are recommended to achieve an objective and comparable estimation of copy number levels.

Such an approach will then allow comparison of frequencies of copy number gains and losses for the tumor type under investigation, and subgroups of samples might then be compared to each other. The association of changes at each genomic location to *e.g*., clinical or pathologic parameters may be determined. From genome-wide frequency plots, one can then more easily distinguish commonly

affected genomic segments. The smallest regions of overlapping gains and losses within these regions often contain the protooncogenes and tumor suppressor genes involved in the carcinogenesis of the tumor type in question. Of note, it has been recently shown, using array-CGH, that copy number variants (CNV) are frequent in the genome of healthy individuals. This means that several genomic regions often present duplications/insertions/deletions of varying sizes that do not necessarily carry pathogenic significance. When performing high-resolution DNA copy number analyses to score aberrations linked to tumorigenesis, databases with CNV information (such as http://projects.tcag.ca/variation/) should be taken into account to filter out the variation caused by these polymorphic regions.

TECHNICAL LIMITATIONS OF PROSTATE CANCER SAMPLING

Whereas it is feasible and straightforward to obtain prostate tumor samples from prostatectomy specimens (*i.e.*, after surgical removal of the gland), the clinical usefulness of performing genome analysis on such material would be somewhat limited for the patient whose prostate was removed. The highest clinical potential of the microarray technology should therefore lie on its applicability to prostate needle biopsies, which are routinely collected for diagnostic purposes, before a therapeutic decision is rendered. In fact, histological analysis of prostate biopsies is the main procedure to confirm a suspected diagnosis of prostate cancer, usually following a positive digital rectal examination or abnormal PSA test. These tissue samples may be collected from suspicious hypoechoic regions of the prostate, but more often they are systematically procured from different quadrants of the gland according to well-defined protocols.

Generally, an average of 6–12 tissue cores are sampled from each patient. However, the amount of biopsy tissue available for pathological examination (and thus for genomic analysis) is still a major limitation (Epstein, 2004). Morphologic assessment of tumor grade and extent in these minute samples is difficult and suffers from poor reproducibility, as it is often dependent on the relative occurrence of each histological pattern on the small amount of tissue available, and on the experience of the pathologist (King and Long, 2000). Furthermore, prostate cancer often exhibits a multi-focal and heterogeneous pattern in which several seemingly independent neoplastic foci coexist in the same gland, which leads to the issue of whether a given biopsy sampled a clinically relevant tumor or an indolent one.

Taking these considerations together, it is expected that prostate cancer sampling issues may pose a significant challenge to genomic analysis of primary prostate carcinoma, as opposed to other cancer types from which more homogeneous tumor populations are easier to obtain. Moreover, currently it is not feasible or cost-efficient to perform whole-genome analysis on several biopsy cores from the same patient, and routine microdissection of cancer foci to maximize tumor content can be expensive and difficult to implement on a clinical setting. Thus, it is understandable that most available genetic information on prostate cancer is based on analyses of prostatectomy specimens

(usually early staged tumors), cell lines, or advanced/metastatic tumors, which do not cover the full disease spectrum. Only one study so far has used aCGH on needle biopsies obtained from prostate cancer suspects (Ribeiro *et al*., 2006c).

GENOMIC DATA ON PROSTATE CANCER

Chromosomal CGH has been the most extensively used methodology thus far in the identification of chromosomal regions recurrently affected by genomic imbalances in prostate cancer. Previous cCGH studies have demonstrated that most prostate carcinomas display DNA copy number imbalances (from 50–90% of the samples, depending on tumor stage and grade), and that losses of genomic material are the most frequently observed events, particularly at chromosome arms 8p, 13q, 6q, 10q, 16q, and 18q (recently reviewed by Saramaki and Visakorpi, 2007). Recurrent gains of genetic material are less frequent and are commonly associated with advanced disease stage, occurring mostly at chromosomes 7, 8q, and Xq. To better compare the available studies and derive clinically relevant conclusions, we recently performed a meta-analysis encompassing 294 prostate cancer cases for which individual cCGH and histopathological information were available (Ribeiro *et al*., 2006a).

Statistical analysis of this large dataset provided several interesting conclusions. First, both the frequency of cases with DNA copy number changes as well as genetic complexity itself could be associated with higher pathological grade or clinical stage. This suggests that prostate cancer progression occurs through the accumulation of genetic changes (> 50% of clinically confined cancers do not display copy number changes, whereas up to 89% of metastatic lesions show genomic aberrations). Secondly, several individual changes (such as gains at chromosomal arms 7q and 8q and losses at 6q and 10q) become significantly more frequent as tumors progress from clinically confined to locally invasive and then to metastatic disease (univariate analysis). Third, the specific genomic imbalances 8q gain and 13q loss were associated with extraprostatic disease independently of Gleason score (multivariate analysis).

With this information at hand, we tested the feasibility of performing the same genomic analysis on material obtained from sextant prostate biopsies. We had used cCGH on a retrospective series of 35 biopsy cores taken from patients with confirmed prostate cancer, showing for the first time that the procedure could be successfully and reliably applied to these minute samples (Teixeira *et al*., 2004). We then analyzed a consecutive series of 100 prospectively collected biopsies from prostate cancer suspects (Ribeiro *et al*., 2006b), obtaining a genomic profile similar to that previously described in prostatectomy samples, with some novel regions of loss and amplification. Interestingly, gain of 8q was independently associated with poor disease-specific survival in this dataset, indicating that genetic features could indeed provide additional prognostic information before a therapeutic decision was taken. It should be noted, however, that out of the 71 patients with confirmed cancer in this series, only 61 (85%) presented tumor in the biopsy core used for cCGH, and 16 of these did not have > 25% tumor cells in the sample. Thus, due to technical limitations

of the sampling procedure alone, possible genetic alterations in up to 35% of our tumor samples likely went undetected.

Given this existing cCGH knowledge, what have genomic arrays introduced in the field of prostate cancer genetics? First, it should be noted that few publications can be found regarding whole-genome analysis of prostate tumors, and that many of the studies are based on cell lines. Prostate cancer cell lines are particularly difficult to establish, and the most widely used are derived from metastatic (*e.g.*, LNCaP) and/or hormone-refractory tumors (*e.g.*, DU125 and PC3), thus exhibiting very complex aberrations seldom observed in primary tumors. Nevertheless, they provide good models to study recurrent genomic changes and their corresponding target genes. Clark *et al.* (2003), using cDNA arrays, provided a good genome-wide characterization of the three aforementioned cell lines, uncovering new aberrations that had not been seen using cCGH. Later, Wolf *et al.* (2004), Zhao *et al.* (2005), and Saramaki *et al.* (2006) added to the findings by performing both copy number analysis as well as expression studies on these (and other) prostate cell lines. Using similar cDNA arrays, the three groups demonstrated how low-level copy number changes could impact on the expression profiles of the cancer cells, identifying several candidate genes whose expression was affected by genomic gain and/or loss events. More recently, Watson *et al.* (2007) used a tiling path BAC array to show that seemingly balanced translocations in several prostate cell lines were actually associated with focal losses and/or gains of genetic material, highlighting the fact that lower resolution methodologies may have under-estimated these events.

Regarding clinical tumors, only a few selected studies, which to our knowledge are the most comprehensive and representative, will be addressed here. Paris *et al.* (2003) showed that it was possible to microdissect and extract enough DNA from formalin-fixed, paraffin-embedded prostate tumors to be used for whole-genome analysis. They used a BAC array platform (1.4 Mbp resolution) to report genomic changes in 20 primary carcinomas. As cCGH information was previously available for these tumors, they were able to compare the two CGH methodologies, reporting a 90% concordance between cCGH and aCGH findings. The higher resolution of the latter, however, resulted in a 3.4-fold increase in the detection of copy number changes. This group then proceeded to analyze a larger series of 79 clinical samples (64 primary tumors and 15 metastases), using the same BAC array platform (Paris *et al.*, 2004). They showed that some alterations, such as loss at 8p23 and gain at 11q13, could be associated with advanced disease or progression into metastasis, and provided a list of candidate target genes for these regions. It should be noted that in both of these studies fixed-thresholds were used to score aCGH data without a preceding segmentation/smoothening step. As a result, up to 44% of the alterations consisted of single clone aberrations, requiring careful interpretation and validation steps.

Our group has also used a BAC platform to perform aCGH on prostatectomy and biopsy samples, of which several had previously been assessed using cCGH (Ribeiro *et al.*, 2006c). In our work, 95% of the cCGH changes were confirmed by aCGH, but the latter methodology detected 2.7 times more copy number

aberrations. Six cases for which cCGH failed to detect copy number changes were shown to harbor aberrations upon aCGH analysis. Strikingly, of the aberrations involving DNA segments >10 Mb, 45% had not been scored using cCGH. Small deletions at 5q, 6q, 12p, and 17p were particularly overlooked, which likely reflects the lack of sensitivity of cCGH in detecting low-intensity alterations caused by tumor heterogeneity. Indeed, Hughes *et al*. (2006) used laser-microdissection and a DNA amplification protocol to obtain homogeneous samples from seven prostatic intraepithelial neoplasia (PIN) lesions and eight primary carcinomas. Using a 1 Mbp-resolution BAC array, they showed that all PIN lesions displayed genetic aberrations similar to those seen in primary tumors, such as losses at 8p and 13q, highlighting the advantage of the microdissection protocol in the analysis of this often heterogeneous malignancy.

More recent findings in this field have been produced by the new oligo-array platforms. Liu *et al*. (2006) analyzed 22 primary tumors using a 100 k SNP array (one probe per 24 kb), allowing the authors to provide a list of candidate genes for the recurrent regions of gains and losses. Of particular interest were the homozygous deletions at the *PTEN* locus, and the novel deletions at 21q presumably resulting in the formation of an oncogenic fusion gene (further addressed later). Torring *et al*. (2007) used a similar SNP array to analyze 43 clinical samples microdissected from prostatectomy specimens or from biopsy cores taken during prostatectomy procedures. Several changes were associated with different stage categories, and a putative pathway of prostate carcinogenesis is reported. Interestingly, up to 40% of their biopsy cores (collected from patients with confirmed tumors) did not have tumor cells upon histological analysis.

Finally, Wicker *et al*. (2007) compared the performance of a 1 Mbp-resolution BAC platform with a 100 kb-resolution oligonucleotide platform, using a common series of 19 prostate tumors. The authors concluded that the oligo-array was as reliable as the BAC array for CGH analysis, and further showed that the increased resolution of the oligo-platform resulted in a more sensitive detection of copy number changes (in particular small deletions). As a side note, the authors further suggested that many of the smaller deletions could be scored with the BAC arrays if the raw data were processed using specific segmentation algorithms.

It should be mentioned that several array platforms have also been designed to assess specific genomic regions at tiling path resolution. Watson *et al*. (2004) constructed a BAC array for chromosomal region 16q to refine the breakpoints of deletions in several primary prostate tumors with known losses at this arm. Van Duin *et al*. (2005) used a similar approach to delimit amplified loci at chromosomal region 8q on cell lines, xenografts, and advanced prostate tumors. The full coverage of these arrays allowed both authors to detect different recurrent regions of loss and gain within these chromosomal arms, and several candidate genes were validated. More recently, Vijayakumar *et al*. (2006) constructed a tiling path array for chromosome Y and showed that 44% of the primary prostate tumors tested on this platform carried a deletion at Yp11.2 encompassing the *TSPY* gene, which they validated in cell lines as a tumor-suppressor gene.

Genomic Hotspots in Prostate Cancer

Several recurrent regions of copy number alterations have been mentioned in the previous paragraphs, and we felt it would be interesting to highlight some of the most interesting putative target genes here. We strongly advise the readers to consult the previously cited publications for a much more comprehensive list of all the targets proposed and validated for these genomic regions.

Recurrent Copy Number Gains and Candidate Oncogenes

Even if copy number gains are seen less often than losses in primary prostate carcinomas, they are relatively common at the long arm of chromosome 8. Whereas most of 8q is gained in the majority of cases, two distinct regions can usually be discerned: one at 8q21 and the other at 8q24 (Van Duin *et al*., 2005). Candidate target genes at 8q24 that have been found amplified and overexpressed in prostate cancer include *EIF3S3*, *MYC*, and *PSCA,* whereas a possible target at 8q21 is *TPD52*. Several other loci with high-level amplifications have also been observed, specifically at 6q, 7q, 8p, 11q, 17p, and 19p. Whereas no good candidates stand for many of these regions, putative targets based on their known function are *GTF2* (7q11), *FGFR1* and *BRF2* (8p12), *IL18* (11q22.2–q22.3), *MAPK7* (17p11), and *MLLT1*, *SAFB1* and *VAV1* (19p13.3). Most encode transcription factors that play important roles in normal cellular processes such as cell division, growth, and differentiation. In later staged carcinomas, most often after androgen-ablation therapy, extra copies of chromosomal arm Xq are also a recurrent finding. This region encompasses the androgen receptor (*AR*) locus, and increased expression of this gene is thought to account for the growth of androgen-independent tumor foci that invariably result in patient death.

Recurrent Copy Number Losses and Putative Tumor Suppressor Genes

Recurrent regions of genomic loss have been narrowed down significantly using genomic arrays, but most observed deletions still consist of large DNA segments that cover several hundred genes. Loss at 8p, one of the earliest and most frequent events in prostate cancer and PIN, is one such example. In the available aCGH studies, the minimum region of overlap for 8p losses commonly spans up to 12 Mbp (from 8p21.2 to 8p22), encompassing > 50 genes. *NKX3-1*, a prostate and testis specific androgen-regulated homeobox gene at 8p21, has been proposed as the most prominent target in this region. Targeted disruption of *NKX3-1* in mouse models of prostate cancer leads to prostatic epithelial hyperplasia and dysplasia (Abdulkadir *et al*., 2002), and overexpression of exogenous *NKX3-1* suppresses growth and tumorigenicity in human prostate carcinoma cell lines (Kim *et al*., 2002). Importantly, haploinsufficiency of this gene is enough to significantly alter gene expression patterns in the prostate, reducing the need for the second inactivating event expected in a classic tumor suppressor gene (Abdulkadir *et al*., 2002).

Available aCGH studies have been unable to find homozygous deletions at 8p, suggesting that many genes in this region may be working together on a dosage dependent manner to induce the initial stages of prostate carcinogenesis. Other

candidates at 8p that fit in this concept are *TNFRSF10, TNFRSF10a*, and *TNFRSF10b*, which are members of the tumor necrosis factor receptor superfamily encoding for proteins responsible for triggering apoptosis when activated by specific ligands (Gaur and Aggarwal, 2003). Interestingly, several other genes belonging to this gene family can be found in genomic areas frequently lost in prostate cancer, such as members 1 and 7 (12p13), 6 (10q24), 9 (13q12), 11A (18q22), and 13C (22q13). It is reasonable to hypothesize that prostate cancer cells carrying deletions at these genomic regions may display a reduced number of death receptor proteins, and thus be less responsive to apoptosis. This would result in longer survival, allowing for the sequential acquisition of further genetic changes, eventually leading to increased proliferation and metastatic potential.

Deletions at 5q, 16q, 6q, and 13q were also observed recurrently using aCGH. Whereas several genes known to be involved in other human neoplasias, such as *APC* and *MCC* (5q21), *CTNNA1* (5q31) and *RB1* (13q14), are located in these regions, many fall outside the minimal regions of overlap determined in our and other microarrays studies. Some other candidates in these regions are *ATBF1* (16q22), *CDH13* and *COTL1* (16q24), the latter two involved in cell-cell adhesion and thus proposed to have a significant role in progression towards invasive disease.

Deletions at chromosomal arm 10q are also frequently observed in prostate cancer cells, generally associated with advanced disease. In 12 out of 15 cases with 10q loss in our aCGH series, a common 1 Mbp region at 10q23.31 was affected, with seven of these carcinomas presenting a homozygous deletion (Ribeiro *et al*., 2006c). Paris *et al*. (2004), Liu *et al*. (2006), and Torring *et al*. (2007) reported similar percentages of loss at this locus, and homozygous deletions were indeed observed in several carcinomas (Liu *et al*., 2006). The most prominent candidate target gene for inactivation in this region is *PTEN*, whose expression has already been shown to be reduced in most advanced prostate cancers (Halvorsen *et al*., 2003). Recent studies on mouse models suggest that the absence of functional *PTEN* confers proliferating cells the ability to overlook apoptosis even when subjected to apoptotic stimuli (Kwabi-Addo *et al*., 2001). Haploinsufficiency of *PTEN* also seems to already have a dramatic influence on cellular response to apoptosis (Kwabi-Addo *et al*., 2001). Interestingly, analyses of this multifunctional protein phosphatase generally depict very low mutation frequencies, which suggest that homozygous deletions are in fact the major mechanism of *PTEN* inactivation (Liu *et al*., 2006; Ribeiro *et al*., 2006c; Verhagen *et al*., 2006).

FUSION GENES – NEWLY DISCOVERED PLAYERS

If genomic microarrays are to play a role in the clinical decision process for prostate cancer patients, current and future platforms will perhaps have to acknowledge the recent groundbreaking finding of recurrent fusion genes in prostate cancer. Indeed, chromosomal alterations resulting in the formation of oncogenic fusion genes are well known to drive the development of leukemias, lymphomas, and sarcomas, but they have rarely been detected in epithelial malignancies (Mitelman, 2000).

Tomlins *et al*. (2005) challenged this paradigm by reporting recurrent fusion genes in a large percentage of prostate carcinomas. In particular, members of the erythroblast transformation specific (ETS) transcription factor family, namely *ERG* (40–78% of the samples analyzed) and, to a much lower extent, *ETV1* and *ETV4* (1–4%), were found to be fused with the *TMPRSS2* gene, an androgen-regulated protease constitutively expressed in prostatic epithelium. The *TMPRSS2*-ETS fusion thus resulted in an abnormally high expression of the ETS members involved, triggering their potent transcription activity and concomitant deregulation of normal cellular metabolism (Seth and Watson, 2005).

The reports of recurrent fusion genes in prostate cancer raised a few important questions regarding their clinical significance. Several studies have promptly confirmed the high incidence of the *TMPRSS2-ERG* rearrangement in prostate carcinomas (*ETV1* and *ETV4* fusion events seem to be rare). Importantly, the fusion gene has also been observed in up to 21% of PIN lesions, suggesting that this is a very early event in the development of prostate cancer (Cerveira *et al*., 2006; Perner *et al*., 2007). There are also reports describing some of the molecular mechanisms that give rise to the fusion event (Perner *et al*., 2006) and evaluating its possible clinical relevance (Hermans *et al*., 2006; Iljin *et al*., 2006; Wang *et al*., 2006; Perner *et al*., 2007). However, current data are still insufficient to assess the diagnostic or prognostic significance of ETS fusion products, as well as the relative contribution of chimeric genes and chromosomal imbalances to the pathogenetic mechanisms of prostate carcinogenesis.

It is important to note that both the *TMPRSS2* and *ERG* genes map to the same chromosomal band (21q22), being separated by < 3 Mbp. It has now been demonstrated that in up to 60% of prostate cancers this rearrangement is caused by an interstitial deletion of the DNA segment separating the two genes (Hermans *et al*., 2006; Iljin *et al*., 2006; Perner *et al*., 2006), whereas in the remaining cases the fusion gene is thought to be originated by more complex rearrangements. Irrespective of how the chimeric product is generated, the close genomic location of the two fusion partners prevented standard G-banding techniques, cCGH and most aCGH platforms to detect it, thus explaining why it eluded the scientific community for so long.

Complementary Technologies

Perhaps a more practical way to detect these subtle rearrangements is to use complementary methodologies such as fluorescent *in situ* hybridization (FISH) with probes for the intended DNA segment, or RT-PCR aimed at the corresponding fusion RNA. FISH is a powerful technique that uses nontoxic fluorescent DNA probes to target any given sequence within a nucleus, resulting in colored signals that are detected with a fluorescence microscope. As interphase nuclei from fresh as well as formalin-fixed and paraffin-embedded tissue can be analyzed directly, it provides researchers with a fast and precise screening method over large quantities of cells. This technique is often used to validate candidate targets surfacing from genomic analysis, and when applied to tissue microarrays it becomes a valuable high-throughput validation approach.

A downside of both FISH and RT-PCR is that these reveal information only on the individual aberrations being tested for. For a detailed discussion of the FISH methodology, the reader is referred to the recently published four volume Handbooks (Hayat, 2004–2006).

CONCLUSIONS AND FUTURE PERSPECTIVES

Establishing a microarray facility, with the required equipment and technicians to optimize and handle slide preparation, sample analysis, data processing, and result interpretation is an expensive and time-consuming endeavor. Even commercially available microarray platforms require training and optimization, and are still not cost-efficient and standardized enough as to move from a research setting onto a routine clinical setting. In the particular case of prostate cancer, the additional difficulties in sampling homogeneous and representative tumor populations further hamper the use of genomic microarrays as a diagnostic tool, even if current platforms have been uncovering valuable information regarding the pathogenetic process of prostate carcinogenesis. At present, other technologies such as FISH and/or RT-PCR might be more easily implemented to assess the emerging molecular targets for their potential diagnostic and/or prognostic value.

However, the wealth of information provided by microarray technology ensures a long-term usefulness as a powerful genomic discovery tool, and since their introduction, prices for these analyses have been continuously falling. Indeed, some companies (*e.g.*, Nimblegen) and several microarray core-facilities worldwide are now providing services which include receipt of biological samples, genomic microarray laboratory work, and processing of the raw microarray data. Microarray analyses thus promise to become a feasible alternative for the patients that are willing (and affording) to obtain whole-genome information on their cancer. This opens wide possibilities for personalized patient care, but caution should be taken not to place disproportionate expectations on the potential of these new methodologies.

REFERENCES

Abdulkadir, S.A., Magee, J.A., Peters, T.J., Kaleem, Z., Naughton, C.K., Humphrey, P.A., and Milbrandt, J. 2002. Conditional loss of Nkx3.1 in adult mice induces prostatic intraepithelial neoplasia. *Mol. Cell Biol. 22*: 1495–1503.

Barrett, M.T., Scheffer, A., Ben Dor, A., Sampas, N., Lipson, D., Kincaid, R., Tsang, P., Curry, B., Baird, K., Meltzer, P.S., Yakhini, Z., Bruhn, L., and Laderman, S. 2004. Comparative genomic hybridization using oligonucleotide microarrays and total genomic DNA. *Proc. Natl. Acad. Sci. USA 101*: 17765–17770.

Cerveira, N., Ribeiro, F.R., Peixoto, A., Costa, V., Henrique, R., Jerónimo, C., and Teixeira, M.R. 2006. *TMPRSS2-ERG* gene fusion causing *ERG* overexpression precedes chromosome copy number changes in prostate carcinomas and paired HGPIN lesions. *Neoplasia 8*: 826–832.

Clark, J., Edwards, S., Feber, A., Flohr, P., John, M., Giddings, I., Crossland, S., Stratton, M.R., Wooster, R., Campbell, C., and Cooper, C.S. 2003. Genome-wide screening for complete genetic loss in prostate cancer by comparative hybridization onto cDNA microarrays. *Oncogene 22*: 1247–1252.

Epstein, J.I. 2004. Diagnosis and reporting of limited adenocarcinoma of the prostate on needle biopsy. *Mod. Pathol. 17*: 307–315.

Gaur, U., and Aggarwal, B.B. 2003. Regulation of proliferation, survival and apoptosis by members of the TNF superfamily. *Biochem. Pharmacol. 66*: 1403–1408.

Halvorsen, O.J., Haukaas, S.A., and Akslen, L.A. 2003. Combined loss of PTEN and p27 expression is associated with tumor cell proliferation by Ki-67 and increased risk of recurrent disease in localized prostate cancer. *Clin. Cancer Res. 9*: 1474–1479.

Hanahan, D., and Weinberg, R.A. 2000. The hallmarks of cancer. *Cell 100*: 57–70.

Hayat, MA. Ed. 2004–2006. *Immunohistochemistry and In Situ Hybridization of Human Carcinomas*. Elsevier/Academic, San Diego, CA.

Hermans, K.G., van Marion, R., Van Dekken, H., Jenster, G., van Weerden, W.M., and Trapman, J. 2006. *TMPRSS2:ERG* fusion by translocation or interstitial deletion is highly relevant in androgen-dependent prostate cancer, but is bypassed in late-stage androgen receptor-negative prostate cancer. *Cancer Res. 66*: 10658–10663.

Hughes, S., Yoshimoto, M., Beheshti, B., Houlston, R.S., Squire, J.A., and Evans, A. 2006. The use of whole genome amplification to study chromosomal changes in prostate cancer: insights into genome-wide signature of preneoplasia associated with cancer progression. *B.M.C. Genomics 7*: 65.

Iljin, K., Wolf, M., Edgren, H., Gupta, S., Kilpinen, S., Skotheim, R.I., Peltola, M., Smit, F., Verhaegh, G., Schalken, J., Nees, M., and Kallioniemi, O. 2006. *TMPRSS2* fusions with oncogenic ETS factors in prostate cancer involve unbalanced genomic rearrangements and are associated with *HDAC1* and epigenetic reprogramming. *Cancer Res. 66*: 10242–10246.

Kallioniemi, A., Kallioniemi, O.P., Sudar, D., Rutovitz, D., Gray, J.W., Waldman, F., and Pinkel, D. 1992. Comparative genomic hybridization for molecular cytogenetic analysis of solid tumors. *Science 258*: 818–821.

Kim, M.J., Bhatia-Gaur, R., Banach-Petrosky, W.A., Desai, N., Wang, Y., Hayward, S.W., Cunha, G.R., Cardiff, R.D., Shen, M.M., and Abate-Shen, C. 2002. Nkx3.1 mutant mice recapitulate early stages of prostate carcinogenesis. *Cancer Res. 62*: 2999–3004.

King, C.R., and Long, J.P. 2000. Prostate biopsy grading errors: a sampling problem? *Int. J. Cancer 90*: 326–330.

Kononen, J., Bubendorf, L., Kallioniemi, A., Barlund, M., Schraml, P., Leighton, S., Torhorst, J., Mihatsch, M.J., Sauter, G., and Kallioniemi, O.P. 1998. Tissue microarrays for high-throughput molecular profiling of tumor specimens. *Nat. Med. 4*: 844–847.

Kwabi-Addo, B., Giri, D., Schmidt, K., Podsypanina, K., Parsons, R., Greenberg, N., and Ittmann, M. 2001. Haploinsufficiency of the Pten tumor suppressor gene promotes prostate cancer progression. *Proc. Natl. Acad. Sci. USA 98*: 11563–11568.

Lai, W.R., Johnson, M.D., Kucherlapati, R., and Park, P.J. 2005. Comparative analysis of algorithms for identifying amplifications and deletions in array CGH data. *Bioinformatics 21*: 3763–3770.

Liu, W., Chang, B., Sauvageot, J., Dimitrov, L., Gielzak, M., Li, T., Yan, G., Sun, J., Sun, J., Adams, T.S., Turner, A.R., Kim, J.W., Meyers, D.A., Zheng, S.L., Isaacs, W.B., and Xu, J. 2006. Comprehensive assessment of DNA copy number alterations in human prostate cancers using Affymetrix 100K SNP mapping array. *Genes Chromosomes Cancer 45*: 1018–1032.

Mitelman, F. 2000. Recurrent chromosome aberrations in cancer. *Mutat. Res. 462*: 247–253.

Paris, P.L., Albertson, D.G., Alers, J.C., Andaya, A., Carroll, P., Fridlyand, J., Jain, A.N., Kamkar, S., Kowbel, D., Krijtenburg, P.J., Pinkel, D., Schroder, F.H., Vissers, K.J., Watson, V.J., Wildhagen, M.F., Collins, C., and Van Dekken, H. 2003. High-resolution analysis of paraffin-embedded and formalin-fixed prostate tumors using comparative genomic hybridization to genomic microarrays. *Am. J. Pathol. 162*: 763–770.

Paris, P.L., Andaya, A., Fridlyand, J., Jain, A.N., Weinberg, V., Kowbel, D., Brebner, J.H., Simko, J., Watson, J.E., Volik, S., Albertson, D.G., Pinkel, D., Alers, J.C., van der Kwast, T.H., Vissers, K.J., Schroder, F.H., Wildhagen, M.F., Febbo, P.G., Chinnaiyan, A.M., Pienta, K.J., Carroll, P.R., Rubin, M.A., Collins, C., and Van Dekken, H. 2004. Whole genome scanning identifies genotypes associated with recurrence and metastasis in prostate tumors. *Hum. Mol. Genet. 13*: 1303–1313.

Perner, S., Demichelis, F., Beroukhim, R., Schmidt, F.H., Mosquera, J.M., Setlur, S., Tchinda, J., Tomlins, S.A., Hofer, M.D., Pienta, K.G., Kuefer, R., Vessella, R., Sun, X.W., Meyerson, M., Lee, C., Sellers, W.R., Chinnaiyan, A.M., and Rubin, M.A. 2006. *TMPRSS2:ERG* fusion-associated deletions provide insight into the heterogeneity of prostate cancer. *Cancer Res. 66*: 8337–8341.

Perner, S., Mosquera, J.M., Demichelis, F., Hofer, M.D., Paris, P.L., Simko, J., Collins, C., Bismar, T.A., Chinnaiyan, A.M., De Marzo, A.M., and Rubin, M.A. 2007. *TMPRSS2-ERG* fusion prostate cancer: an early molecular event associated with invasion. *Am. J. Surg. Pathol. 31*: 882–888.

Pinkel, D., Segraves, R., Sudar, D., Clark, S., Poole, I., Kowbel, D., Collins, C., Kuo, W.L., Chen, C., Zhai, Y., Dairkee, S.H., Ljung, B.M., Gray, J.W., and Albertson, D.G. 1998. High resolution analysis of DNA copy number variation using comparative genomic hybridization to microarrays. *Nat. Genet. 20*: 207–211.

Pollack, J.R., Perou, C.M., Alizadeh, A.A., Eisen, M.B., Pergamenschikov, A., Williams, C.F., Jeffrey, S.S., Botstein, D., and Brown, P.O. 1999. Genome-wide analysis of DNA copy-number changes using cDNA microarrays. *Nat. Genet. 23*: 41–46.

Ribeiro, F.R., Diep, C.B., Jeronimo, C., Henrique, R., Lopes, C., Eknaes, M., Lingjaerde, O.C., Lothe, R.A., and Teixeira, M.R. 2006a. Statistical dissection of genetic pathways involved in prostate carcinogenesis. *Genes Chromosomes Cancer 45*: 154–163.

Ribeiro, F.R., Jerónimo, C., Henrique, R., Fonseca, D., Oliveira, J., Lothe, R.A., and Teixeira, M.R. 2006b. 8q gain is an independent predictor of poor survival in diagnostic needle biopsies from prostate cancer suspects. *Clin. Cancer Res. 12*: 3961–3970.

Ribeiro, F.R., Henrique, R., Hektoen, M., Berg, M., Jerónimo, C., Teixeira, M.R., and Lothe, R.A. 2006c. Comparison of chromosomal and array-based comparative genomic hybridization for the detection of genomic imbalances in primary prostate carcinomas. *Mol. Cancer 5*: 33.

Saramaki, O., and Visakorpi, T. 2007. Chromosomal aberrations in prostate cancer. *Front. Biosci. 12*: 3287–3301.

Saramaki, O.R., Porkka, K.P., Vessella, R.L., and Visakorpi, T. 2006. Genetic aberrations in prostate cancer by microarray analysis. *Int. J. Cancer 119*: 1322–1329.

Seth, A., and Watson, D.K. 2005. ETS transcription factors and their emerging roles in human cancer. *Eur. J. Cancer 41*: 2462–2478.

Solinas-Toldo, S., Lampel, S., Stilgenbauer, S., Nickolenko, J., Benner, A., Döhner, H., Cremer, T., and Lichter, P. 1997. Matrix-based comparative genomic hybridization: biochips to screen for genomic imbalances. *Genes Chromosomes Cancer 20*: 399–407.

Tan, D.S., Lambros, M.B., Natrajan, R., and Reis-Filho, J.S. 2007. Getting it right: designing microarray (and not 'microawry') comparative genomic hybridization studies for cancer research. *Lab. Invest. 87*: 737–754.

Teixeira, M.R., Ribeiro, F.R., Eknaes, M., Waehre, H., Stenwig, A.E., Giercksky, K.E., Heim, S., and Lothe, R.A. 2004. Genomic analysis of prostate carcinoma specimens obtained via ultrasound-guided needle biopsy may be of use in preoperative decision-making. *Cancer 101*: 1786–1793.

Tomlins, S.A., Rhodes, D.R., Perner, S., Dhanasekaran, S.M., Mehra, R., Sun, X.W., Varambally, S., Cao, X., Tchinda, J., Kuefer, R., Lee, C., Montie, J.E., Shah, R.B., Pienta, K.J., Rubin, M.A., and Chinnaiyan, A.M. 2005. Recurrent fusion of *TMPRSS2* and ETS transcription factor genes in prostate cancer. *Science 310*: 644–648.

Torring, N., Borre, M., Sorensen, K.D., Andersen, C.L., Wiuf, C., and Orntoft, T.F. 2007. Genome-wide analysis of allelic imbalance in prostate cancer using the Affymetrix 50K SNP mapping array. *Br. J. Cancer 96*: 499–506.

Van Dekken, H., Paris, P.L., Albertson, D.G., Alers, J.C., Andaya, A., Kowbel, D., van der Kwast, T.H., Pinkel, D., Schroder, F.H., Vissers, K.J., Wildhagen, M.F., and Collins, C. 2004. Evaluation of genetic patterns in different tumor areas of intermediate-grade prostatic adenocarcinomas by high-resolution genomic array analysis. *Genes Chromosomes Cancer 39*: 249–256.

van Duin, M., van Marion, R., Vissers, K., Watson, J.E., van Weerden, W.M., Schroder, F.H., Hop, W.C., van der Kwast, T.H., Collins, C., and Van Dekken, H. 2005. High-resolution array comparative genomic hybridization of chromosome arm 8q: evaluation of genetic progression markers for prostate cancer. *Genes Chromosomes Cancer 44*: 438–449.

Verhagen, P.C., van Duijn, P.W., Hermans, K.G., Looijenga, L.H., van Gurp, R.J., Stoop, H., van der Kwast, T.H., and Trapman, J. 2006. The PTEN gene in locally progressive prostate cancer is preferentially inactivated by bi-allelic gene deletion. *J. Pathol. 208*: 699–707.

Vijayakumar, S., Hall, D.C., Reveles, X.T., Troyer, D.A., Thompson, I.M., Garcia, D., Xiang, R., Leach, R.J., Johnson-Pais, T.L., and Naylor, S.L. 2006. Detection of recurrent copy number loss at Yp11.2 involving TSPY gene cluster in prostate cancer using array-based comparative genomic hybridization. *Cancer Res. 66*: 4055–4064.

Wang, J., Cai, Y., Ren, C., and Ittmann, M. 2006. Expression of variant TMPRSS2/ERG fusion messenger RNAs is associated with aggressive prostate cancer. *Cancer Res. 66*: 8347–8351.

Watson, J.E., Doggett, N.A., Albertson, D.G., Andaya, A., Chinnaiyan, A., Van Dekken, H., Ginzinger, D., Haqq, C., James, K., Kamkar, S., Kowbel, D., Pinkel, D., Schmitt, L., Simko, J.P., Volik, S., Weinberg, V.K., Paris, P.L., and Collins, C. 2004. Integration of high-resolution array comparative genomic hybridization analysis of chromosome 16q with expression array data refines common regions of loss at 16q23-qter and identifies underlying candidate tumor suppressor genes in prostate cancer. *Oncogene 23*: 3487–3494.

Watson, S.K., deLeeuw, R.J., Horsman, D.E., Squire, J.A., and Lam, W.L. 2007. Cytogenetically balanced translocations are associated with focal copy number alterations. *Hum. Genet. 120*: 795–805.

Wicker, N., Carles, A., Mills, I.G., Wolf, M., Veerakumarasivam, A., Edgren, H., Boileau, F., Wasylyk, B., Schalken, J.A., Neal, D.E., Kallioniemi, O., and Poch, O. 2007. A new look towards BAC-based array CGH through a comprehensive comparison with oligo-based array CGH. *B.M.C. Genomics 8*: 84.

Wolf, M., Mousses, S., Hautaniemi, S., Karhu, R., Huusko, P., Allinen, M., Elkahloun, A., Monni, O., Chen, Y., Kallioniemi, A., and Kallioniemi, O.P. 2004. High-resolution analysis of gene copy number alterations in human prostate cancer using CGH on cDNA microarrays: impact of copy number on gene expression. *Neoplasia 6*: 240–247.

Ylstra, B., van den Ijssel, P., Carvalho, B., Brakenhoff, R.H., and Meijer, G.A. 2006. BAC to the future! or oligonucleotides: a perspective for microarray comparative genomic hybridization (array CGH). *Nucleic Acids Res. 34*: 445–450.

Zhao, H., Kim, Y., Wang, P., Lapointe, J., Tibshirani, R., Pollack, J.R., and Brooks, J.D. 2005. Genome-wide characterization of gene expression variations and DNA copy number changes in prostate cancer cell lines. *Prostate 63*: 187–197.

31
Prostate Cancer: Role of Vav3 Overexpression in Development and Progression

Shan Lu

INTRODUCTION

Prostate cancer is the most commonly diagnosed cancer and the leading cause of cancer death among men in the United States. Cancer is a polygenic disease. Intensive investigations during last decades have led to identify more gene mutations and chromosomal abnormalities associated with human prostate cancer, such as *p53*, *PTEN*, *myc*, *Ras*, *PI3KCA*, and androgen receptor (*AR*) genes. Recently, it was reported by Dong *et al*. (2006) that DNA oligonucleotide microarray analysis led to the identification of *Vav3* oncogene overexpression in androgen-independent prostate cancer cells compared with their androgen-dependent counterparts. Further analysis revealed that *Vav3* is overexpressed in 32% of human prostate cancer. Given that *Vav3* overexpression enhances ligand-dependent and ligand–independent *AR* activity and stimulates prostate cancer cell growth, these findings suggest a role of *Vav3* overexpression in human prostate cancer.

MULTIPLE FUNCTIONS OF *Vav* FAMILY PROTEINS

Vav gene is an oncogene identified in cell transformation experiments. *Vav* family proteins include three members (*Vav1*, *Vav2*, and *Vav3*) in mammalian cells. *Vav1* is primarily expressed in hematopoietic lineages, while *Vav2* and *Vav3* are more ubiquitously expressed. It was reported by Bustelo (2000, 2001) that *Vav* proteins share a common structure, including a N-terminal calponin homology (CH) domain involved in Ca^{+2} mobilization and transforming activity, an acidic domain (AD) containing three regulatory tyrosines, a Dbl homology (DH) domain with a conserved region that promotes the exchange of GDP for GTP on *Rac*/*Rho* GTPases, a pleckstrin homology (PH) domain binding to PIP_3 that enables its movement to the inner face of the plasma membrane, two Src-homology 3 (SH3) domains interacting with proteins containing proline-rich sequences, and a Src-homology 2 (SH2) domain interacting with the proteins containing phosphorylated tyrosines (Figure 31.1). *Vav* proteins function as guanosine nucleotide

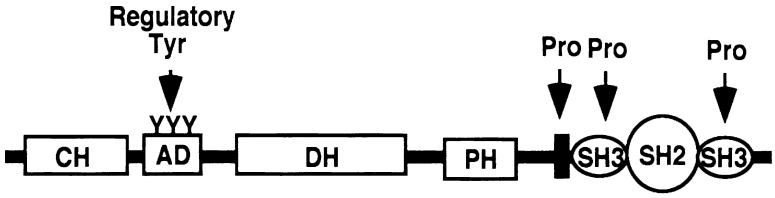

FIGURE 31.1. Functional domains of Vav proteins. (1) A N-terminal calponin homology (CH) domain involved in Ca^{+2} mobilization and transforming activity; (2) An acidic domain (AD) containing three regulatory tyrosines; (3) A Dbl homology (DH) domain with a conserved region that promotes the exchange of GDP for GTP on Rac/Rho GTPases; (4) A pleckstrin homology (PH) domain binding to PIP_3 that enables its movement to the inner face of plasma membrane; (5) Proline-rich (Pro) regions that enable the binding to SH3 containing proteins; (6) Two Src-homology 3 (SH3) domains interacting with proteins containing proline-rich sequences; (7) A Src-homology 2 (SH2) domain interacting with the proteins containing phosphorylated tyrosines

exchange factors (GEFs) for Rho family G proteins. Independent of their GEF activities, *Vav* proteins also function as adapter molecules. It was reported by Moores *et al.* (2000) that tyrosine phosphorylation by receptor or cytoplasmic protein tyrosine kinase is required for activation of *Vav* proteins. In the non-phosphorylation state, *Vav* protein is folded, which is achieved by binding of the tyrosine in the AD domain to the DH domain and binding of the CH domain to the C1 region (Figure 31.1). Upon phosphorylation of the tyrosines in the AD domain, the folding is opened and the DH domain exposes. Thus, *Vav* protein is activated and interacts with substrate proteins, and the PH domain is exposed for PIP_3 binding.

Vav proteins are directly or indirectly activated by receptor protein tyrosine kinase (RPTK) in various signal transduction pathways. For instance, it was reported by Tamas *et al.* (2003) that *Vav2* can be directly activated by RPTK upon activation of epidermal growth factor receptor (*EGFR*). It was also reported by Katzav (2004) that *Vav1* is activated by cytoplasmic tyrosine kinase *ZAP70* upon activation of T cell receptor. For downstream signaling of *Vav* proteins, it was reported by Zeng *et al.* (2000) that upon ligand stimulation of *EGFR*, *Ros*, insulin receptor, and insulin-like growth factor (*IGF*) receptor, *Vav3* is activated and physically associated with a variety of signaling molecules, including *Rac1*, *Cdc42*, *PI3K*, *shc*, *Grb2*, and *PLC-γ*, leading to alteration in cell morphology and cell transformation. Overexpression of *Vav3* leads to *PI3K* activation and focus formation in NIH3T3 cells. It was reported by Sachdev *et al.* (2002) that *Vav3*-induced cell transformation can be blocked by overexpression of *PTEN* or *PI3K* inhibitor LY294002. These findings suggest that *Vav3* overexpression transduces RPTK-elicited signaling and signals via multiple signal transduction pathways contributing to cancer development.

Vav3 IS OVEREXPRESSED IN HUMAN PROSTATE CANCER AND STIMULATES GROWTH OF PROSTATE CANCER CELLS

We have investigated the potential roles of *Vav3* in human prostate cancer. We

found that *Vav3* protein was detected in all human prostate cancer cell lines examined. The expression of *Vav3* was further elevated in androgen-independent human prostate cancer cells in comparison with their androgen-dependent counterpart. Moreover, *Vav3* protein was detected in ~30% of human prostate cancer specimens. *Vav3* overexpression stimulates both androgen-dependent and androgen-independent growth in human prostate cancer cells. Furthermore, *Vav3* overexpression significantly potentiates EGF-stimulated androgen-independent growth.

Vav3 is a well-characterized oncogene in that *Vav3* overexpression and aberrant activation of *Vav3*, such as mutation of tyrosine residues in the AD domain, leads to cell transformation. Biochemically, *Vav3* is a signal molecule involved in multiple signaling pathways. Given the function of *Vav3*, our observations suggest that *Vav3* overexpression stimulates aberrant cell growth in prostate epithelium and may play a critical role in human prostate cancer development. Furthermore, *Vav3* potentiates EGF growth stimulatory activity and stimulates androgen-independent growth in prostate cancer cells. *Vav3* overexpression may contribute to prostate cancer progression to androgen-independent growth.

Vav3 OVEREXPRESSION ENHANCES *AR* TRANSACTIVATION ACTIVITY

Androgen receptor belongs to the steroid/thyroid hormone receptor superfamily. It was reported by McKenna and O'Malley (2002) that steroid/thyroid hormone receptors are ligand-dependent transcription factors. They bind as homodimers or heterodimers to their cognate DNA response elements to modulate transcription of their target genes. In the absence of androgen, *AR*, like other steroid hormone receptors, is located in the cytoplasm of the target cells and associated with cellular chaperones. When bound to androgen, *AR* undergoes conformational change, resulting in the dissociation from cellular chaperones, receptor dimerization, phosphorylation, interaction with coactivators, recruitment of chromatin modifying enzyme activities such as histone acetyl transferase (HAT), ATPase, and methyltransferase activities, DNA-binding at an enhancer element of the target gene, and subsequent recruitment of basal transcription factors to form a stable preinitiation complex (PIC). These events are followed by up- or down-regulation of target gene expression.

Coactivators represent a growing family of proteins, which interact with nuclear receptors in a ligand-dependent manner and enhance the transcriptional activity of nuclear receptors. It was reported by Veogel *et al*. (1998) that *SRC-1* and its related proteins are a family of coactivators containing the homologous bHLH-PAS domain and receptor-interacting domain (RID) with multiple LXXLL motifs or NR boxes, where L is leucine and X is any amino acid. The highly conserved LXXLL motif is critical for nuclear receptor binding. These coactivators possess intrinsic histone acetyl transferase (HAT) activity for remodeling chromatin and stimulating ligand-dependent transactivation. It was reported by Nawaz *et al*. (1999) that *E6-AP*, a multifunction protein, is both a coactivator for nuclear receptor and an E3 ubiquitin-protein ligase. Therefore, these coactivators complex with nuclear receptors at the promoter of the target genes and stimulate the gene expression in nucleus.

Recent findings implicate that *Vav* family proteins also complex with transcription factors and regulate gene expression. It was reported by Houlard *et al*. (2002) that *Vav1* was identified in the component of transcriptionally active nuclear factor of activated T cells (*NFAT*)- and nuclear factor *NFkB*-like complexes. A nuclear localization signal (NLS) in the PH domain is solely responsible for nucleus localization of *Vav1* protein, indicating a role of *Vav* family protein as a transcription coregulator. It was reported by Dong *et al*. (2006) that the DH domain of *Vav3* is responsible for *AR* activation. Sequence analysis revealed that the DH domain of *Vav3* contains three consensus sequences of the LXXLL motifs (Figure 31.2A). It was further reported by Lee *et al*. (2008) from our laboratory that the DH domain of *Vav3* directly binds to *AR*. In addition, homologous analysis of *Vav3* and *Vav1* gene identified a conserved NLS in the PH domain of *Vav3* (Figure 31.2B). Our findings suggest that *Vav3* is a nuclear protein and functions as a coactivator for *AR*. These studies suggest a novel mechanism of *Vav3* overexpression impacting on *AR* signaling axis and support the notion of a critical role of *Vav3* overexpression in prostate cancer development and progression to androgen-independent disease.

THE POTENTIAL IMPACT OF *Vav3* ON NONGENOMIC ANDROGEN RECEPTOR ACTIVITY

The classical *AR* is a ligand-dependent transcription factor to activate transcription of its target genes in nucleus, which is known as genomic *AR* activity (genotropic signal). Recent findings revealed that the classical steroid hormone receptors, including *AR*, associate with cell membrane and mediate cell signaling through kinase cascade, defined as nongenomic (nongenotropic) *AR* activity. It was reported by Freeman (2005) that nongenomic *AR* activity is extremely rapid (in minutes rather than hours) and independent of protein synthesis and gene transcription. Nongenomic *AR* resides in multiprotein complexes in the cytoplasm before ligand binding and nuclear translocation, which allows the

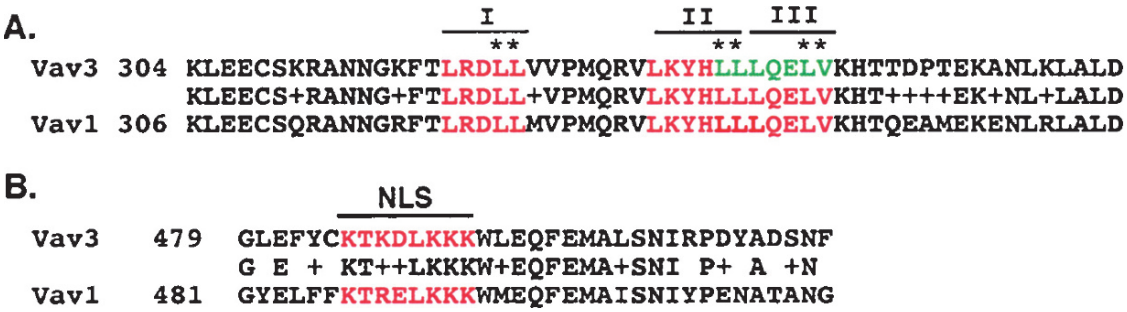

FIGURE 31.2. Alignment of Vav3 and Vav1 amino acid sequence. (A) The consensus sequences of LXXLL motifs I, II, and III in the DH domain of Vav3 were indicated in red. Mutation of LLLQELV sequence (in green) has been shown to abolish GEF activity of Vav3. (B) A consensus sequence of the nucleus localization signal (NLS) in Vav3 was located in the PH domain

productive interaction with molecules, such as Caveolin, *MNAR*, and *Src*, at extranuclear-membrane surfaces.

It was reported by Zhuang *et al.* (2002) that nongenomic *AR* activity contributes to androgen-independent growth in prostate cancer by signaling through the *PI3K-Akt* pathway. It was reported by Lu *et al.* (2001) that *AR* directly interacts with caveolin-1 in the plasma membrane structures called caveolae, an invaginated form of membrane microdomain that are commonly referred to as 'lipid rafts'. Caveolin-1 is a protein marker that is associated with prostate cancer progression and hormone-refractory disease. Membrane associated *AR* was identified within the cholesterol-rich 'lipid raft' membrane fraction to sequester signaling partners in multiple pathways. Nongenomic *AR* also signals cell survival in lipid rafts in the absence of caveolins in human prostate cancer cells. It was reported by Migliaccio *et al.* (2005) that nongenomic *AR* activity contributes to androgen-independent growth in the form of cytoplasmic *Src*/*AR*/*ER* complex. *Src* tyrosine kinase contains SH2 and SH3 domains and is activated by receptor protein tyrosine kinase. It was reported by Guo *et al.* (2006) that Src and *AR* interaction in response to EGF stimulation signals through the *MAPK*-mediated pathway and leads to elevated *AR* phosphorylation and nucleus localization, which is associated with androgen-independent phenotype in prostate cancer cells.

Vav3 oncogene contains the PH domain that binds to PIP_3 and enables its movement to the inner face of the plasma membrane. *Vav3* also contains the SH2 and SH3 domains that anchor *Vav3* with RPTK and activates it by phosphorylation at the intracellular domain of the cell membrane. Recently, we found that *Vav3* is predominantly localized in cytosol (data not shown). Given that *Vav3* contains SH2 and SH3 domains and binds to *AR*, this finding suggests that *Vav3* also interacts with *AR* in the cytoplasm and localizes *AR* to the intracellular domain of the cell membrane. Steroid hormone receptors are localized in cytoplasm in the absence of their ligands. Cytoplasmic *AR* can function as a signaling molecule, a nongenomic *AR* activity rather than a ligand-dependent transcription factor. Therefore, it is reasonable to envision that *Vav3*/*AR* complex can signal androgen-independent growth upon androgen ablation therapy. These findings implicate an underlying molecular mechanism of androgen-independent growth in prostate cancer, which is mediated by the novel nongenomic *AR*/*Vav3*-mediated pathway. We are currently elucidating the underlying molecular mechanisms of *Vav3*-mediated nongenomic *AR* activity in prostate cancer cells.

Vav3 SIGNALING IN PROSTATE CANCER

The *EGFR* family consists of *EGFR*/*ErbB-1*/*HER-1*, *ErbB-2*/*HER-2*/*neu*, *ErbB-3*/*HER-3*, and *ErbB-4*/*HER-4*. These cell surface proteins participate in complex signaling pathways that are initiated by EGF, TGF, neuregulins, and other ligands. Signal transduction via this family is further complicated by its capacity to form functional homodimers and heterodimers, which activate various signaling pathways. Numerous studies have demonstrated that EGF enhances *AR* activity. Overexpression of *HER-2* in prostate cancer cells upregulates *AR* activity and stimulates

androgen-independent growth in prostate cancer cells. Clinical studies also revealed that *HER-2* overexpression is associated with development of hormone refractory prostate cancer. It was reported by Signoretti *et al*. (2000) that *HER-2* is overexpressed in ~ 25% of prostate cancer before androgen ablation treatment and 75% of prostate cancer after failing hormone ablation treatment. These findings suggest that the elevated signaling of the *EGFR*/*HER-2*-elicited pathway enhances *AR* activity and is involved in prostate cancer development and progression to the androgen-independent status. *Vav3* is a downstream signal transducer of *EGFR*/*HER-2*. *Vav3* overexpression can further amplify *EGFR*/*HER-2*-elicited signaling and aberrantly activate *AR* in a ligand-independent manner, implicating a critical role of *Vav3* in androgen-independent growth.

Compelling data showed that the elevated *AR* activity and *PI3K-Akt* signaling play an important role in prostate cancer development and progression. The *PI3K-Akt* pathway is a cell growth and survival pathway. Elevated *PI3K-Akt* signaling, such as mediated by *PTEN* deletion and mutation, contributes to prostate cancer development and progression. It was reported by Wang *et al*. (2003) that prostate-specific deletion of murine *PTEN*, a tumor suppressor gene that shuts off *PI3K-Akt* signaling, induces the prostatic intraepithelial neoplasia lesions, which later progress to invasive prostate cancer in mice. Multiple growth factors and cytokines, including EGF, signal through the *PI3K-Akt* pathway and inappropriately activate *AR* in prostate cancer cells, which can be accomplished by direct *AR* phosphorylation by active Akt. It was reported by Ayala *et al*. (2004) that an elevation of *Akt* phosphorylation is observed in 45.8% of prostate cancer specimens. It was reported by Thomas *et al*. (2004) that a loss of or reduced *PTEN* protein expression occurs in ~ 30% of human prostate cancers. These findings suggest the presence of other mechanisms that activate *PI3K-Akt* signaling in prostate cancer.

It was reported by Lu *et al*. (2006) that the signaling level of the *PI3K-Akt* pathway is elevated in androgen-independent LNCaP-AI cells relative to that in their androgen-independent counterpart LNCaP cells and is critical for their androgen-independent growth. This elevated *PI3K-Akt* signaling in LNCaP-AI cells is not due to *PTEN*, because *PTEN* is mutated in LNCaP cells. We found that overexpression of *Vav3* is at least partially responsible for the elevation of *PI3K-Akt* signaling in LNCaP-AI cells. Our finding implicates that *Vav3* overexpression is an alternative mechanism that leads to an elevated *PI3K-Akt* signaling and *AR* activity in human prostate cancer, which may be of great importance in prostate cancer development and progression to androgen-independent growth (Figure 31.3).

THE ROLE OF *Vav3* IN PROSTATE CANCER BIOLOGY

It was reported by Huggins and Johnson (1947) 60 years ago that the fundamental property of normal prostate epithelium and prostate cancer cells is a requirement of androgen for growth and survival, which led to the hormone ablation therapy as the mainstay treatment for advanced prostate cancer (stage D, local and distant metastasis). Hormone ablation therapy is achieved by bilateral orchiectomy, anti-androgens,

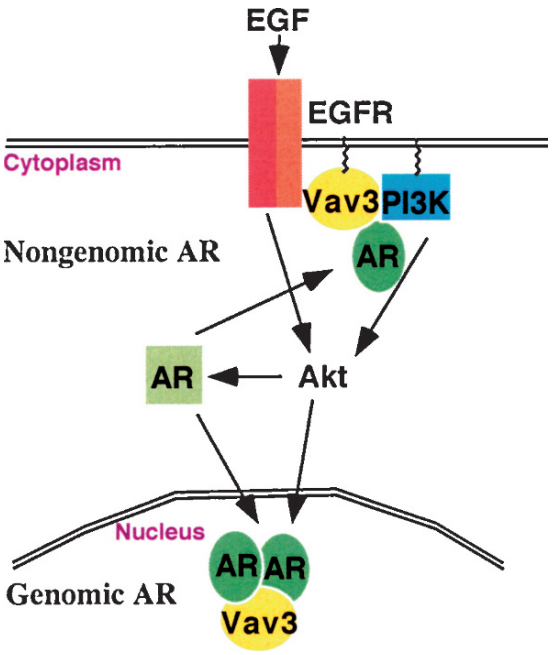

FIGURE 31.3. Vav3 upregulation of AR activity and signaling in prostate cancer. Our data suggest that Vav3 transduces EGFR/HER-2-elicited signaling and enhances both genomic and nongenomic AR activities in prostate cancer cells, which are mediated by at least two potential mechanisms: (1) Vav3 signals through the PI3K-Akt pathway, resulting in an elevated AR phosphorylation and nucleus localization; (2) Vav3 localizes AR to the cell membrane to function as a signaling molecule, known as the nongenomic AR activity

5-alpha-reductase inhibitors, and luteinizing hormone-releasing hormone agonists to compromise *AR* activity. This therapeutic modality is very effective for a short term, but fails in almost all prostate cancers as a consequence of developing androgen-independent disease in 6 to 18 months. There is no effective therapy currently available for androgen-independent prostate cancer.

Androgen receptor is expressed in prostate cancer, and *AR* hypersensitivity plays a critical role in prostate cancer development and progression to the androgen-independent disease. The key question is how *AR* is inappropriately activated. It was reported by Taplin *et al.* (1995) and Visakorpi *et al.* (1995) that *AR* mutation and gene amplification are common alterations associated with prostate cancer progression. Mutations in the ligand binding domain generate a promiscuous *AR*, which is activated by a broad spectrum of ligands, such as estrogen and *AR* antagonist. Overexpression of coactivators, such as *SRC1*, *SRC3*, *TIF-2*, and *ARA55*, was found in prostate cancer. It was reported by Zhou *et al.* (2005) that *SRC-3* is required for prostate cancer cell proliferation and survival in animal models. It was reported by Khan *et al.* (2006) that overexpression of coactivator *E6-AP* significantly enhances *AR* activity simulated by a below physiological level of androgen or by unfavorable ligands. Furthermore, it was reported by Wen *et al.* (2000) that *AR*, as other nuclear receptors, can be activated independent of its ligand by phosphorylation, which is mediated by a variety of signaling pathways, such as by active *Akt*. It was reported by Rochette-Egly *et al.* (2003) that phosphorylation of *AR* facilitates the recruitment of coactivators and chromatin remodellers and modifiers, resulting in a decompact repressive chromatin, response to its ligand, and enhanced expression of its target genes. Therefore, to successfully undergo transition from androgen-dependent to independent growth upon hormonal therapy, development of various mechanisms, including *AR* activation by alternative mechanisms, enhancement of cell survival, and stimulation of cell proliferation by alternative signaling pathways, is essential for prostate cancer cells to survive and proliferate at the below physiological level of androgen.

Our novel finding that *Vav3* overexpression may play a critical role in human prostate cancer is based on the following reasons: (1) *Vav3* is overexpressed in human prostate cancer and in androgen-independent prostate cancer cells; (2) *Vav3* enhances *AR* activity, partially via the *PI3K-Akt* pathway; (3) *Vav3* transduces *HER-2*-elicited signaling and then signals downstream through the *PI3K-Akt* pathway; (4) *Vav3* is a multiple function protein that can impact on multiple signaling pathways, including the SH2 domain interacting with RPTK, the LXXLL motifs responsible for nuclear receptor binding, the PH domain binding PIP3 involved in association with the cell membrane, and the DH domain with GEF activity. *Vav3* overexpression may lead to alteration of multiple signal transduction pathways, resulting in a strong tumorigenesis effect and cancer development. Therefore, *Vav3* overexpression amplifies signaling in the *HER-2* and *PI3K-Akt* pathways, leads to *AR* hypersensitivity, enhances cancer cell growth and survival, and contributes to prostate cancer development and progression to androgen-independent disease.

In conclusion, *Vav3*, a guanosine nucleotide exchange factor (GEF) for the *Rho* family G proteins, is an oncogene. The biochemical properties of *Vav* family proteins are well characterized. However, the role of *Vav3* in human cancer is just beginning to be revealed. We found that *Vav3* is overexpressed in androgen-independent prostate caner cells and in human prostate cancer. *Vav3* interacts with and activates *AR* and stimulates growth in prostate cancer cells. The current chapter has summarized the recent findings in determination of the role of *Vav3* in prostate cancer and potential impacts of *Vav3* overexpression on prostate cancer development and progression.

REFERENCES

Ayala, G., Thompson, T., Yang, G., Frolov, A., Li, R., Scardino, P., Ohori, M., Wheeler, T., and Harper, W. 2004. High levels of phosphorylated form of Akt-1 in prostate cancer and non-neoplastic prostate tissues are strong predictors of biochemical recurrence. *Clin. Cancer Res. 10*: 6572–6578.

Bustelo, X. R. 2000. Regulatory and signaling properties of the Vav family. *Mol. Cell Biol. 20*: 1461–1477.

Bustelo, X. R. 2001. Vav proteins, adaptors and cell signaling. *Oncogene 20*: 6372–6381.

Dong, Z. Y., Liu, Y., Lu, S., Wang, A., Lee, K., Wang, L. H., Revelo, M., and Lu, S. 2006. Vav3 oncogene is overexpressed and regulates cell growth and androgen receptor activity in human prostate cancer. *Mol. Endocrinol. 20*: 2315–2325.

Freeman, M. R., Cinar, B., and Lu, M. L. 2005. Membrane rafts as potential sites of nongenomic hormonal signaling in prostate cancer. *Trends Endocrinol. Metab. 16*: 273–279.

Guo, Z., Dai, B., Jiang, T., Xu, K., Xie, Y., Kim, O., Nesheiwat, I., Kong, X., Melamed, J., Handratta, V. D., Njar, V. C., Brodie, A. M., Yu, L. R., Veenstra, T. D., Chen, H., and Qiu, Y. 2006. Regulation of androgen receptor activity by tyrosine phosphorylation. *Cancer Cell 10*: 309–319.

Houlard, M., Arudchandran, R., Regnier-Ricard, F., Germani, A., Gisselbrecht, S., Blank, U., Rivera, J., and Varin-Blank, N. 2002. Vav1 is a component of transcriptionally active complexes. *J. Exp. Med. 195*: 1115–1127.

Huggins, C., and Johnson, M. 1947. Carcinoma of the bladder and prostate. *JAMA 135*: 1146–1152.

Katzav, S. 2004. Vav1: an oncogene that regulates specific transcriptional activation of T cells. *Blood 103*: 2443–2451.

Khan, O. Y., Fu, G., Ismail, A., Srinivasan, S., Cao, X., Tu, Y., Lu, S., and Nawaz, Z. 2006. Multifunction steroid receptor coactivator, E6-associated protein, is involved in development of the prostate gland. *Mol. Endocrinol. 20*: 544–559.

Lee, K., Liu, Y., Mo, J., Zhang, J., Dong, Z., and Lu, L. 2008. Vav3 oncogene, a quanine nucleotide exchange factor for Rac/Rho GTPases, coactivates nuclear receptors and may play a role in human breast cancer. In Press.

Lu, M. L., Schneider, M. C., Zheng, Y., Zhang, X., and Richie, J. P. 2001. Caveolin-1 interacts with androgen receptor. A positive modulator of androgen receptor mediated transactivation. *J. Biol. Chem. 276*: 13442–13451.

Lu, S., Ren, C. X., Liu, Y., and Epner, D. E. 2006. The PI3K-Akt signaling is involved in regulation of p21WAF/CIP expression and androgen-independent growth in prostate cancer cells. *Int. J. Oncol. 28*: 245–251.

McKenna, N. J., and O'Malley, B. W. 2002. Combinatorial control of gene expression by nuclear receptors and coregulators. *Cell 108*: 465–474.

Migliaccio, A., Di Domenico, M., Castoria, G., Nanayakkara, M., Lombardi, M., de Falco, A., Bilancio, A., Varricchio, L., Ciociola, A., and Auricchio, F. 2005. Steroid receptor regulation of epidermal growth factor signaling through Src in breast and prostate cancer cells: steroid antagonist action. *Cancer Res. 65*: 10585–10593.

Moores, S. L., Selfors, L. M., Fredericks, J., Breit, T., Fujikawa, K., Alt, F. W., Brugge, J. S., and Swat, W. 2000. Vav family proteins couple to diverse cell surface receptors. *Mol. Cell. Biol. 20*: 6364–6373.

Nawaz, Z., Lonard, D. M., Smith, C. L., Lev-Lehman, E., Tsai, S. Y., Tsai, M. J., and O'Malley, B. W. 1999. The Angelman syndrome-associated protein, E6-AP, is a coactivator for the nuclear hormone receptor superfamily. *Mol. Cell. Biol. 19*: 1182–1189.

Rochette-Egly, C. 2003. Nuclear receptors: integration of multiple signalling pathways through phosphorylation. *Cell Signal 15*: 355–366.

Sachdev, P., Zeng, L., and Wang, L. H. 2002. Distinct role of phosphatidylinositol 3-kinase and Rho family GTPases in Vav3-induced cell transformation, cell motility, and morphological changes. *J. Biol. Chem. 277*: 17638–17648.

Signoretti, S., Montironi, R., Manola, J., Altimari, A., Tam, C., Bubley, G., Balk, S., Thomas, G., Kaplan, I., and Hlatky, L., *et al*. 2000. Her-2-neu expression and progression toward androgen independence in human prostate cancer. *J. Natl. Cancer Inst. 92*: 1918–1925.

Tamas, P., Solti, Z., Bauer, P., Illes, A., Sipeki, S., Bauer, A., Farago, A., Downward, J., and Buday, L. 2003. Mechanism of epidermal growth factor regulation of Vav2, a guanine nucleotide exchange factor for Rac. *J. Biol. Chem. 278*: 5163–5171.

Taplin, M. E., Bubley, G. J., Shuster, T. D., Frantz, M. E., Spooner, A. E., Ogata, G. K., Keer, H. N., and Balk, S. P. 1995. Mutation of the androgen-receptor gene in metastatic androgen-independent prostate cancer. *N. Engl. J. Med. 332*: 1393–1398.

Thomas, G. V., Horvath, S., Smith, B. L., Crosby, K., Lebel, L. A., Schrage, M., Said, J., De Kernion, J., Reiter, R. E., and Sawyers, C. L. 2004. Antibody-based profiling of the phosphoinositide 3-kinase pathway in clinical prostate cancer. *Clin. Cancer Res. 10*: 8351–8356.

Visakorpi, T., Hyytinen, E., Koivisto, P., Tanner, M., Keinanen, R., Palmberg, C., Palotie, A., Tammela, T., Isola, J., and Kallioniemi, O. P. 1995. In vivo amplification of the androgen receptor gene and progression of human prostate cancer. *Nature Genet. 9*: 401–406.

Voegel, J. J., Heine, M. J., Tini, M., Vivat, V., Chambon, P., and Gronemeyer, H. 1998. The coactivator TIF2 contains three nuclear receptor-binding motifs and mediates transactivation through CBP binding-dependent and -independent pathways. *Embo. J. 17*: 507–519.

Wang, S., Gao, J., Lei, Q., Rozengurt, N., Pritchard, C., Jiao, J., Thomas, G. V., Li, G., Roy-Burman, P., Nelson, P. S., Liu, and X. Wu, H. 2003. Prostate-specific deletion of the murine Pten tumor suppressor gene leads to metastatic prostate cancer. *Cancer Cell 4*: 209–221.

Wen, Y., Hu, M. C., Makino, K., Spohn, B., Bartholomeusz, G., Yan, D. H., and Hung, M. C. 2000. HER-2/neu promotes androgen-independent survival and growth of prostate cancer cells through the Akt pathway. *Cancer Res. 60*: 6841–6845.

Zeng, L., Sachdev, P., Yan, L., Chan, J. L., Trenkle, T., McClelland, M., Welsh, J., and Wang, L. H. 2000. Vav3 mediates receptor protein tyrosine kinase signaling, regulates GTPase activity, modulates cell morphology, and induces cell transformation. *Mol. Cell. Biol. 20*: 9212–9224.

Zhou, H. J., Yan, J., Luo, W., Ayala, G., Lin, S. H., Erdem, H., Ittmann, M., Tsai, S. Y., and Tsai, M. J. 2005. SRC-3 is required for prostate cancer cell proliferation and survival. *Cancer Res. 65*: 7976–7983.

Zhuang, L., Lin, J., Lu, M. L., Solomon, K. R., and Freeman, M. R. 2002. Cholesterol-rich lipid rafts mediate akt-regulated survival in prostate cancer cells. *Cancer Res. 62*: 2227–2231.

32
Prostate Cancer: Detection and Monitoring Using Mitochondrial Mutations as a Biomarker

Gabriel D. Dakubo, Ryan L. Parr, and John P. Jakupciak

INTRODUCTION

Neoplastic transformation of the prostate gland is one of the leading causes of cancer morbidity and mortality among men in the industrialized world. As an age-associated disease, the incidence of prostate cancer (PCa) will remain on the rise, mirroring the ageing Western population. Similar to other cancers, PCa is debilitating when diagnosed late. Surgical resection of organ-confined tumors is the best available curative method. Therefore, to obtain optimal cure, it is imperative that methods are developed that enable early detection and monitoring of this disease. Epigenetic nuclear gene silencing and alterations in both nuclear and mitochondrial genomes precede histopathologic changes indicative of PCa. Thus, sensitive assays that target the genetic signatures should help with early detection and successful treatment of PCa.

Oxidative stress is strongly implicated in the etiology and pathogenesis of PCa. Inflammatory cells produce and secrete excess reactive oxygen species (ROS), and prostate inflammation is a risk factor of PCa. Proliferative inflammatory atrophy is also identified as a precursor lesion of PCa. Promoter hypermethylation and loss of the antioxidant enzyme, *GSTP1,* is linked to the etiology of PCa and high plasma concentration of antioxidants, such as carotenoid lycopene, reduces the risk of PCa. As a major source of ROS in the cell, it is reasonable to assume an etiologic role for the mitochondrion in PCa. Indeed, the mitochondrial genome is highly susceptible to oxidative damage and due to the inefficient DNA repair mechanisms, it serves as a useful repository of early disease-associated mutations. In contrast to the single nuclear genome, each cell possesses hundreds of mitochondria and several thousands of mitochondrial genomes, suggesting that biomarkers in this molecule will be easier to assay than those in the nucleus. Hence, evaluation of mitochondrial alterations in PCa should be considered as an important complement in patient diagnosis and management.

There are several methods and techniques available for analysis of mitochondrial DNA (mtDNA) mutations in cancer. Amplification by the polymerase chain reaction (PCR) followed by restriction fragment length polymorphism (RFLP) analysis, automated DNA sequencing technologies, and mismatch-dependent

methods of mutation detection are all clinically suitable for diagnosis of mtDNA point mutations, small deletions and insertions. Southern blotting and real time PCR assays enable quantification of large-scale mtDNA deletions or gene rearrangements, copy number, and levels of circulating mitochondrial nucleic acids. This chapter will examine evidence for the involvement of mtDNA mutations in PCa and some methods and technologies for assaying mtDNA mutations. Importantly, because the copy number of mtDNA is high and almost all the methods require genomic amplification, particular emphasis is also placed on strict adherence to quality assurance issues that are mandatory for achieving accurate molecular diagnosis.

MITOCHONDRIAL GENETICS

The mitochondrion is postulated to have evolved from an aerobic bacterium that invaded the primitive eukaryotic cell over a billion years ago. This union enabled the primordial eukaryotic cell to utilize oxygen in energy production via the electron transport chain and oxidative phosphorylation (the respiratory chain). In addition to its primary function of energy production, the mitochondrion has assumed numerous other cellular functions including intermediary metabolism, heme and lipid biosynthesis, metabolism of steroids, iron and nucleotides, calcium homeostasis, integration of cytosolic signaling pathways, and apoptosis. Structurally, this organelle is composed of two distinct membranes, an inter-membrane compartment located between the two membranes and a matrix that is the space inside the inner membrane. Mitochondria are dynamic organelles that undergo frequent cycles of fusion and fission. The density and morphology of mitochondria are related to the cell environment and function.

As an autonomous organism, the aerobic bacterium possessed a complete functional genome. However, during the symbiotic relationship with the primordial eukaryotic cell, the mitochondrion lost a substantial portion of its genome to the nucleus. Some of these ancient nuclear-embedded mitochondrial genes (numts) are neither transcribed nor translated into proteins and therefore remain as pseudogenes, which can confound analysis of authentic mtDNA mutations (Parr *et al*., 2006b). However, more than a thousand of the postulated nuclear-embedded mitochondrial genes retained their capabilities of encoding proteins that are assembled in the cytoplasm and imported into the mitochondria. The remaining human mitochondrial genome is a compact 16,568 bp closed-circular molecule (Anderson *et al*., 1981) that exists as protein-DNA complexes referred to as nucleoids. Structurally, mtDNA is a double stranded molecule with an outer guanine-rich strand referred to as the heavy or H strand and an inner cytosine-rich complementary strand called the light or L strand (Figure 32.1). With the exception of a 1,121 bp (np16024-576) non-coding control region (CR) or displacement loop (D-loop), which houses the *cis* regulatory elements required for the replication and transcription of the molecule, and a 30 bp sequence that contains the light strand origin of replication, the rest of the mitochondrial genome is packed with coding genes that are not punctuated by introns and whose transcripts lack 5′ and 3′ untranslated regions. These genes code for 2 rRNA proteins and 22 tRNA molecules

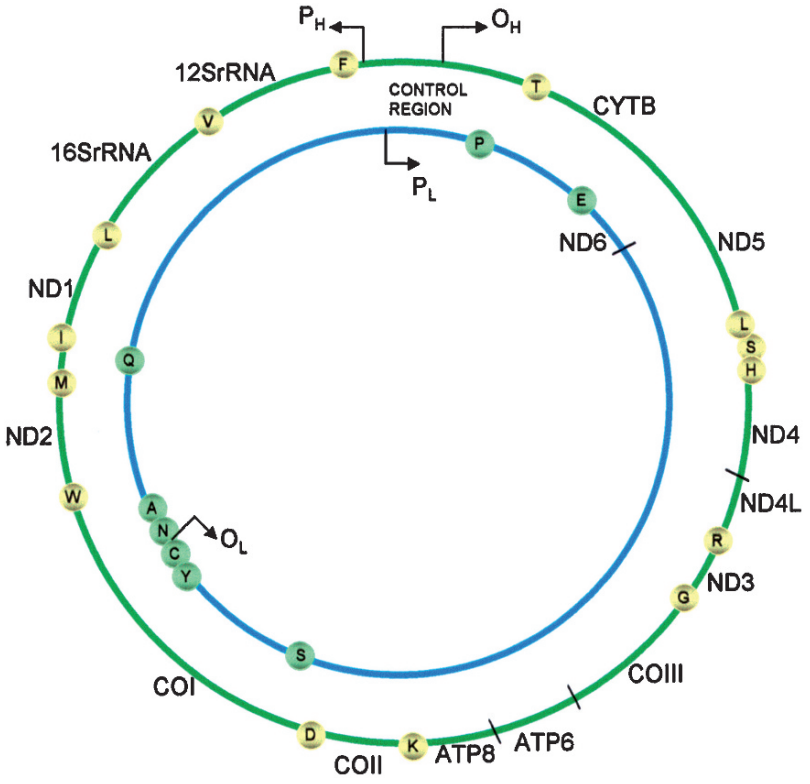

FIGURE 32.1. The human mitochondrial genome. The circular double-stranded mtDNA molecule is organized into the control and coding regions. The genome is packed with 37 genes that are transcribed and translated within the mitochondrion. Transcription factors interact with the heavy strand (P_H) and light strand (P_L) promoters and induce the production of polycistronic transcripts, which are processed into 22 tRNAs, (small circles), 2 rRNAs and 13 proteins. Replication of the molecule starts at the heavy strand origin of replication (O_H) and proceeds in a clockwise direction producing a daughter H-strand molecule. After copying about 2/3rds of the H-strand, the light-strand origin of replication (O_L) is encountered and the parental H-strand is displaced exposing the O_L, which then commences replication in the opposite direction

that are necessary for autonomous mitochondrial protein biosynthesis, as well as 13 polypeptides that critically complement the ~74 nuclear encoded proteins needed for efficient energy production via the respiratory chain.

Mitochondrial genetics differs from classical Mendelian genetics in several aspects. In view of this, phenotypic expressions of mitochondrial diseases are quite variable and unpredictable. Firstly, mitochondria are carried in the ovum and as such are unilaterally transmitted through the maternal line (Giles *et al.*, 1980). Therefore, in contrast to the nuclear genome, transmission of mtDNA is not associated with genetic recombination. This aspect of mtDNA inheritance has proven very useful in evolutionary and genealogical studies as well as forensic applications including identification of missing people and victims of mass disasters. High-throughput methods such as microarray resequencing would improve the identification of degraded samples where the

nuclear genome is inadequate for analysis. Occasionally though, paternal transmission of mitochondrial genomes has been reported and this may have important implications for mitochondrial diseases.

Secondly, mtDNA molecules are not protected by histone and non-histone proteins and also have inefficient DNA proofreading and repair mechanisms, and yet are resident in an organelle that produces most of the nucleic acid-damaging ROS in the cell. Each mitochondrion contains several mtDNA molecules and there are thousands of mitochondrial genomes per cell. In healthy tissues, all mtDNA molecules exist in a state of homoplasmy, whereby all the mitochondrial genomes are identical. MtDNA has a high mutation rate and somatic mutations, which may be early indicators of disease, occur in some but not all genomes, giving rise to the admixture of normal and mutant genomes. This creates a disease phenotype referred to as heteroplasmy. Depending on tissue energy requirements, a minimum number of mutant copies are required for disease manifestation (the threshold effect).

Thirdly, mitochondrial genomes undergo stochastic segregation to daughter cells during cell division (Blok *et al.*, 1997). Mitosis requires that a cell first duplicates its nuclear genetic material, such that following cytokinesis, each daughter cell acquires identical nuclear genomes as the parental cell. Whereas mitosis results in roughly equal distribution of other organelles, mitochondria are randomly segregated to each daughter cell, implying that mitochondria and their genomes will segregate to daughter cells in an unpredictable manner. Thus, in a heteroplasmic state, mutant mtDNA molecules will randomly distribute to daughter cells.

Finally, mutant mitochondrial genomes tend to clonally expand in a fashion that probably depends on the mitotic state of the cell. Expansion of mutant mtDNA might differ between actively dividing and post-mitotic cells. In proliferating epithelial and tumor cells, stochastic segregation can fix mutations resulting in a new homoplasmic genetic signature in some cells, which can then proliferate and lead to expansion of mutant clones. In contrast, clonal expansion of functionally important mtDNA mutations in post-mitotic cells such as cardiomyocytes appears to result from positive selection. In this situation, defective mitochondria preferentially proliferate as a result of nuclear-regulated compensatory mechanisms to overcome the energy deficiency.

MITOCHONDRIAL BIOENERGETICS

The mitochondrial respiratory activity produces most of the energy required for cellular functions (Taylor and Turnbull, 2005). The respiratory machinery, which resides in the inner mitochondrial membrane, is organized into five protein complexes (Figure 32.2). The mitochondrial genome encodes seven (NADH dehydrogenase subunits 1–6 and 4L) of the ~46 subunits of complex I, 1 (cytochrome b) of the 11 subunits of complex III, 3 (cytochrome c oxidase subunits I–III) of the 13 subunits of complex IV and 2 (ATP synthetase subunits 6 and 8) of the ~18 subunits of complex V. Nuclear genes encode all of the four subunits of complex II and the remaining subunits of the other complexes. In addition to the five complexes, ubiquinone (Coenzyme

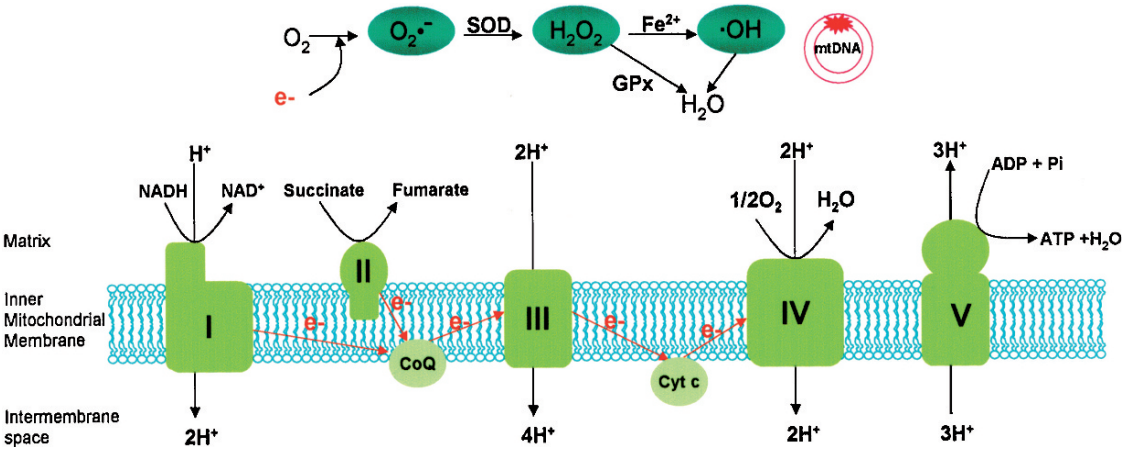

FIGURE 32.2. Mitochondrial bioenergetics and ROS production. ATP production by the respiratory chain complex is associated with the generation of ROS as electrons do leak and interact with oxygen. In normal cells, these deleterious free radicals are quickly removed by various antioxidant mechanisms. However, excess production of free radicals can overwhelm the detoxifying mechanisms leading to damage to the nearby mtDNA molecules

Q10) and cytochrome c participate in electron shuttle through the respiratory chain.

Energy in the form of ATP is generated from calories derived from food. Acetyl CoA from glycolysis and beta-oxidation is oxidized in the Krebs cycle to generate electrons in the form of NADH and succinate ($FADH_2$), which are received by complexes I and II, respectively (Figure 32.2). The electrons are sequentially transported through redox groups to the final acceptor, oxygen, which converts this to water. In the process, protons are pumped from the matrix to the intermembrane space by complexes I, III and IV. Complex V then uses the electrochemical gradient established to pump the protons back into the matrix, and this process is coupled with the synthesis of ATP.

The activities of the respiratory chain are inevitably coupled with the generation of superoxide anion ($O_2^{\bullet -}$), hydrogen peroxide (H_2O_2) and hydroxyl radical ($^{\bullet}OH$) (Figure 32.2). Electrons can leak from the respiratory chain and interact with oxygen to produce the first family member, $O_2^{\bullet -}$, which can be converted to H_2O_2 by superoxide dismutase (SOD). The H_2O_2 generated is usually detoxified by the antioxidant mechanisms such as the activities of cytosolic glutathione peroxidase and perioxismal catalase; however, in the presence of reduced transition metals (e.g., Fe^{2+}), H_2O_2 can be converted to one of the most reactive forms of the free radicals, the $^{\bullet}OH$. Reactive oxygen species (ROS) production increases in conditions of excess electrons such as will occur in states of increased caloric intake and/or defective respiratory chain activity. Thus, functionally important mtDNA mutations in several diseases including cancer are associated with elevated mitochondrial ROS production and a vicious cycle of mtDNA damage.

MITOCHONDRIAL ONCOLOGY

Altered intermediary metabolism, increased oxidative stress, and resistance to apoptosis are key features of cancer cells. Several decades ago, Otto Warburg (1931) observed that in contrast to normal cells that consumed less glucose and produced less lactate when utilizing oxygen to generate energy via the most efficient mode of energy production (the respiratory chain), cancer cells metabolized excess glucose and produced excess lactate. This phenomenon is referred to as aerobic glycolysis or the Warburg effect. In normal cells, pyruvate generated from glycolysis enters the mitochondria and is subsequently oxidized in the Krebs cycle. However, defective cancer cell mitochondria are incapable of removing pyruvate, which therefore accumulates and is converted to lactic acid by lactate dehydrogenase. Excess lactate creates an acidic tumor microenvironment that favors tumor invasiveness. Elucidation of the molecular mechanisms of the Warburg effect is still awaited. This metabolic switch, however, appears to result in part from the inefficient respiratory chain activity, probably from mutations in the mitochondrial genome, and is possibly an adaptive mechanism that permits solid tumors to thrive in adverse environments such as reduced oxygenation.

An important evidence for the involvement of mitochondria in the malignant transformation process came from the discovery that mutations in nuclear genes that encode mitochondrial proteins were associated with some types of human tumors. Uterine leiomyomas and renal cell carcinomas have been linked to mutations in the mitochondrial enzyme, fumarate hydratase, while mutations in succinate dehydrogenase (SDH) subunits B, C or D, three of the four subunits of the respiratory chain complex II, are associated with paragangliomas. Biochemical evidence suggests that mutations in these genes can lead to at least two major defects. Firstly, the reduced metabolism of succinate and fumarate should result in a build-up of these metabolites in the cytosol, which can stabilize the transcription factor, hypoxia inducible factor 1 alpha (HIF-1α) that, in turn, can induce the expression of genes involved in tumor progression. Moreover, tumor hypoxic microenvironment that could also induce expression of HIF-1α, can potentially stimulate the switch of tumor cell metabolism towards aerobic glycolysis. Secondly, the primary function of mitochondrial complex II is to receive and pass electrons from succinate to ubiquinone. Thus, mutations that disrupt the normal functioning of complex II can impede electron flow through the respiratory chain leading to excess electron build-up in the mitochondria. Leakage of electrons from the respiratory chain will reduce oxygen to superoxide anion; thus, initiating the cascade of ROS production (Figure 32.2). Because ROS can initiate and promote tumor growth, alterations in either mitochondrial complex I or II through mutations in nuclear and/or mitochondrial encoded subunits can trigger or enhance tumor development (Baysal, 2006).

The resistance of cancer cells to apoptosis or programmed cell death is one of the intriguing alterations of cancer cell mitochondria. Apoptosis is a homeostatic mechanism by which cells are killed without inducing inflammatory reaction. Intrinsic or mitochondrial apoptotic pathway is

initiated by activation of the mitochondrial permeability transition pore (mtPTP), a complex composed of cyclophilin D, Bcl2, Bax, inner membrane adenine nucleotide translocator and outer membrane voltage-dependent anion channel. Activated mtPTP leads to the release of mitochondrial proapoptotic factors including cytohcrome c, procaspase 9, Smac/Diablo, apoptosis inducing factor (AIF), and endonuclease G into the cytosol. Cytochrome c interacts with Apaf1 and procaspase 9 to form an apoptosome, which then activates the executioner caspase (caspase 3), while Smac/Diablo activates caspase 3 via inhibition of inhibitors of apoptosis (IAPs). Apoptosis inducing factor and endonuclease G, however, translocate into the nucleus to induce DNA fragmentation. An important link between mitochondria and cancer is the finding that mitochondria from cancer cells are resistant to induction of mitochondrial outer membrane permeabilization required for the initiation of apoptosis.

The involvement of the mitochondrial genome in cancer biology has been known for several decades. Clayton and Vinograd (1969) observed mtDNA dimers and higher oligomers in circulating leukocytes of leukemic patients, but not in normal mature human leukocytes. Interestingly, the levels of these abnormal forms of mtDNA molecules declined with chemotherapy. Following this initial report, several groups documented mtDNA alterations in other types of human cancers. However, a direct causal role for mtDNA mutations in cancer was provided by Horton *et al.* (1996) who analyzed renal cell carcinomas and controlled kidney samples that led to the discovery of a 294 bp deletion in NADH dehydrogenase subunit 1. This deletion was present in 50% of the mitochondrial genomes of the tumor and likely to be functionally relevant to the etiology of the tumor because it resulted in truncated protein product that could cause defective respiratory chain activity. Subsequent to this work, the literature on mtDNA mutations in cancer has expanded considerably. Indeed, it has been proposed that cancer should be added to the list of mitochondrial diseases.

MtDNA mutation detection will be important for personalized medicine (Modica-Napolitano *et al.*, 2007). This is because the genetic signature of the disease is different from the individual's inherited genetic signature. The comparison of these signature genomes present within a person is used to determine the mutation load and identify early the presence of personalized disease genotype. For example, the genetic species contained by tumor cells arises from the inherited "native" patient's DNA and is genetically distinct, and that difference is measurable. The intra-genotype comparison of tissues within the same person rules out potential aging-related mutations in the mitochondrial genome.

UNIQUE PROSTATE EPITHELIAL CELL METABOLISM

The prostate gland is composed of three zones; the peripheral, central, and transition zones. The peripheral zone, which makes up the bulk of the gland, is also the origin of many prostate cancers. In contrast to cells in the central zone and other tissues, the secretory epithelial cells of the peripheral zone accumulate substantial amounts of

zinc, which inhibits the activity of mitochondrial aconitase. Reduced m-aconitase activity prevents the complete oxidation of citrate, which therefore accumulates and is secreted (Costello and Franklin, 2006). Thus, in contrast to other cells, normal peripheral zone glandular epithelial cells have a truncated Krebs cycle, low respiration, and low terminal oxidation, and are energy inefficient and presumably generate less ROS. In many other systems, tumorigenesis is associated with metabolic transformation from energy efficient benign cells to energy inefficient tumor cells. In contrast, an early metabolic switch from energy inefficient benign cells to energy efficient tumor cells marks the process of malignant transformation of peripheral zone glandular epithelial cells. An indication of this metabolic switch is the initial downregulation of the zinc uptake transporter, which is followed by marked reduction in zinc levels and therefore activation of m-aconitase, which catalyzes complete oxidation of citrate. The increased generation and donation of electrons to the respiratory chain in mitochondria of transforming prostate cells compared to normal peripheral zone epithelial cells could lead to leakage of excess electrons and an increased ROS production that would damage the naked mtDNA molecules. Consistent with this possible mechanism, the mitochondrial genomes of PCa cells sustain several mutations.

MITOCHONDRIAL DNA MUTATIONS IN PROSTATE CANCER

Mitochondrial genomics and proteomics play an integral role in the pathogenesis of multiple human malignancies including PCa. MtDNA mutations have been demonstrated in almost all cancers of the human body (Jakupciak *et al*., 2006). Several point mutations, small insertions/deletions, and large-scale rearrangements have been reported in PCa. In addition, germline SNPs and population variants are postulated to modulate the risks of developing PCa. Whereas current efforts are directed at unraveling novel mutations and the mechanisms responsible for their causation, the functional importance of these mutations to tumor development are also becoming apparent. Due to the rich population diversity of mtDNA, the search for somatic mutations associated with cancer requires careful comparison between patient blood and matched tumor tissue or non-invasively collected body fluids.

The risk of developing PCa partly depends on the race or ethnicity of the individual. Prostate cancer risk is much higher among men of African descent compared to Europeans and is even much lower in Asian men. This geographic variation in PCa risk could partly be explained by an inherent genetic susceptibility to the disease. In contrast to the nuclear genome, the mitochondrial genome demonstrates considerable geographic and ethnic diversity, and therefore, is an attractive molecule to search for risk conferring genomic biomarkers of PCa.

In a population-based study by Petros *et al*. (2005), it was suggested that men with germline mutations in the mitochondrial COI gene have substantial risk of developing PCa. This conclusion was drawn after extensive epidemiological study of germline and somatic mutations in COI gene. Analysis of COI mutations in 260 PCa patients of European and

African-American descent as well as 54 benign control individuals without cancer revealed over-representation of COI mutations in the PCa group, compared to control individuals without cancer. Further analysis of mtDNA sequences from 1,019 control men found the frequency of COI mutations to be 7.8%, which was much lower than the 12% observed in the PCa cohort. Given that COI polymorphisms are more frequent in African mitochondrial macrohaplogroup L than the rest of the world, data from only Europeans were analyzed and COI mutations in PCa patients were still much higher (11%) than control individuals without cancer (0%) and the general European population (6.5%). The over-representation of COI mutations in PCa patients compared to individuals without cancer implicates mutations in the COI gene as risk factors for developing PCa. In a separate investigation by Booker *et al*. (2006), PCR and restriction digest analysis were used for genotyping 221 white men with confirmed PCa and 246 white controls. An over-representation of mitochondrial haplogroup U was observed in PCa cases. This haplogroup was shown to convey an increased risk for developing PCa, with an odds ratio of 1.95. In another investigation, a specific mtDNA polymorphism (G10398A) that appears to be associated with breast cancer invasiveness in African-American women was found to confer increased risk for PCa in African-American men.

Oxidative stress might be responsible for somatic mtDNA mutations in PCa as indicated by the frequent observation of T-C and G-A base transitions. As reviewed by Dakubo *et al*. (2006), several heteroplasmic and homoplasmic somatic mtDNA mutations have been reported in PCa. Most of these studies focused on the D-loop region that is well known to be a mutational hot spot. Because point mutations in coding and tRNA genes can also be highly pathogenic, we embarked on whole mitochondrial genome sequencing to uncover the complete mutation burden of PCa. Using laser-capture microdissection (LCM), Parr *et al*. (2006a) procured pure population of PCa glands, normal looking adjacent and distant glands for whole genome sequencing using the capillary electrophoresis method. As a control, normal samples from individuals with benign biopsies were also sequenced. DNA template from patient blood and those from their maternal relatives, when available, were sequenced and used as a reference to score somatic mtDNA mutations. Intriguingly, somatic mtDNA mutations were frequent in all prostate samples from a malignant prostate, but very rare in prostate without cancer.

Interestingly, two independent studies suggest that mtDNA mutations in PCa might be linked. Using LCM and mutant-specific PCR methodology, Chen *et al*. (2003) demonstrated that mtDNA mutations in prostate lesions were linked on the same molecule. We cloned and sequenced specific amplicons from patients and observed six linked mutations in one patient sample. It is possible that a burst of mtDNA mutations occurs simultaneously in PCa cells, probably following oxidative stress.

There is evidence to suggest that mutations in the mitochondrial genome occur early in PCa development raising the possibility of early, presymptomatic disease detection. Firstly, identical homoplasmic mtDNA mutations were demonstrated in PCa and corresponding precursor lesion, PIN. Secondly, mtDNA mutations do not

correlate with patient age, Gleason score or tumor stage, suggesting early mutation events that do not modulate with age or disease progression. Finally, mtDNA mutations are present in tumors and the normal-appearing adjacent glands. The presence of mutations in normal cells close to tumor foci is consistent with prostate field cancerization as documented in PCa using several nuclear genetic markers.

A role for mitochondrial ROS in modulation of PCa growth was provided by an interesting experiment conducted by Petros *et al*. (2005). A clinically relevant missense mutation (ATP6 C8932T) in PCa was modeled to uncover the possible functional implications of such mutations in PCa. To achieve this, a well characterized ATP6 mutation (T8993G), that is a few amino acids upstream of the PCa mutation, was used for this study. This mutation is known to generate excess mitochondrial ROS. Enucleated donor cells containing either homoplasmic wildtype (T8993T) or mutant (T8993G) mitochondria were fused to PCa cell line (PC3), depleted of its mtDNA. These transmitochondrial cybrids thus possessed identical nuclear background but different mtDNA genomes. When wildtype and mutant cells were injected into nude mice, it was observed that the mutant cells consistently grew to over sevenfold tumor volume compared to wildtype cells, in a period of approximately 3½ months. Immunohistochemical analysis demonstrated significant superoxide anion generation by the T8993G tumor cells. This finding provides evidence for the potential *in vivo* relevance of mtDNA mutations in promoting prostate tumor growth.

Mitochondrial genome alterations in PCa also appear to reflect at the protein level. Evidence for this was provided by the study of complex IV subunits in PCa by Herrmann *et al*. (2003). Quantitative proteomic analysis of normal, premalignant, and invasive prostate tumor tissues uncovered an increase in the ratio of nuclear encoded mitochondrial subunits IV, Vb, and VIc to mitochondrial encoded subunit I and II in several tumors. More importantly, these protein alterations were observed at the premalignant stage and increased with disease progression to invasive cancer, attesting to the potential usefulness of such proteins as biomarkers for early PCa detection as well as targets for therapeutic intervention

An important aspect of prostate cancer diagnosis and management is the ability to predict tumor behavior, because the majority of PCa patients have favorable outcome. It is encouraging to know that the levels of mitochondrial nucleic acids in circulating blood might have prognostic utility in advanced PCa. In a study by Mehra *et al*. (2007), it was uncovered that advanced PCa patients with high levels of plasma mitochondrial DNA and RNA had a poor 2-year survival compared to those with low levels. Importantly, levels of mitochondrial RNA appear to be an independent predictor of 2-year survival.

In addition to point mutations, the mtDNA molecule is subject to large-scale partial deletions and duplications as a consequence of the numerous direct and indirect repeats that characterize this genome (Jorde *et al*., 2000). Illegitimate recombination at the repeats accounts for the majority (~ 90%) of these deletions, which usually result in the formation of a number of novel rearranged molecules including deletion monomers, dimmers, and multimers. Whereas the mechanism(s) of deletion formation is

not within the scope of the present chapter, it is likely that both intramolecular and intermolecular recombination events are involved in the process.

The first report on mtDNA rearrangement mutations in PCa was issued by Jessie *et al.* (2001), who examined clinical specimens from PCa patients ranging in age from 41 to 81 years. Using long extension PCR, they demonstrated several mtDNA deletions in PCa that appeared to correlate positively with advancing age. The absence of normal tissue controls in this study made it difficult to delineate deletions due to the aging process from those related to the etiology of PCa. We embarked on a comprehensive study of mtDNA deletions in PCa and have identified, characterized, and quantified the levels of a specific deletion that is associated with PCa. This mtDNA deletion also demonstrates PCa field cancerization, and therefore appears to have clinical value in helping resolve false-negative prostate needle biopsy specimens.

Higuchi *et al.* (2006) showed that large-scale mtDNA deletions and mtDNA depletion might confer androgen independence in PCa. The androgen dependent LNCaP cells were demonstrated to harbor less mtDNA deletions than the androgen-independent C4-2 cell line. As a consequence of increased deletions, C4-2 cells also consumed less oxygen than LNCaP cells. The androgen dependence of LNCaP cells was abrogated by depletion of their mtDNA, and this was reversible by reconstitution of the cells with normal mtDNA. Thus, depletion of mtDNA appears sufficient in rendering PCa cells refractory to androgen stimulation, and therefore resistant to apoptosis induced by androgen ablation. Whether these findings are operational in human PCa is unknown.

MtDNA mutations are several-fold more abundant than nuclear mutations, and therefore have been easily detected in body fluids in several other tumors, indicative of the potential clinical utility of non-invasively collected specimens for early pre-symptomatic diagnosis. In an analysis of paired urine and blood samples from PCa patients, Jeronimo *et al.* (2001) observed homoplasmic mutations in tumors and paired blood and urine. It is possible that neoplastic mtDNA can be shed from the prostate epithelium into body fluids, and the high copy number of mutant mtDNA in the tumors offers a detection advantage. Post-digital rectal examination (DRE) collected prostatic fluid (PMF) or urine, contains among other cells, prostate epithelial cells and possibly free nucleic acids from the prostate. If a somatic mutation (or group of mutations) is known to be specific to PCa, PMF will be an excellent minimally invasive sample for analysis. Similarly, methods that enable enrichment of PMF for prostate epithelial cells, or better yet, isolation of pure prostate epithelial cells from these biofluids, will offer great opportunity to use minimally invasive samples for early detection and monitoring of PCa using mtDNA mutations.

SAMPLE PREPARATION FOR MITOCHONDRIAL DNA MUTATION ANALYSIS IN PROSTATE CANCER

The types of clinical samples for mtDNA analysis depend on whether the variant being assayed is a polymorphism or somatic mutation. Any normal tissue, including circulating white blood cells or non-invasively collected saliva or buccal swap (from individuals who do not smoke or have head and

neck tumors), is suitable for SNP and haplotype analysis. Frozen, formalin-fixed, and paraffin-embedded biopsy tissues, PMF, or post-DRE void urine samples enriched for prostate epithelial cells are needed for somatic mutation analysis, while plasma or serum is used for quantitative measurement of circulating nucleic acids.

The recovery of mtDNA from any of these samples can be accomplished by means of commercially available DNA extraction kits. For qualitative analysis, such as sequencing or genotyping, small starting total DNA template can be enriched for mtDNA using the REPLI-g mitochondrial DNA kit from Qiagen. This kit uses high fidelity DNA polymerase in an isothermal reaction to uniformly amplify the entire mitochondrial genome from very small starting material. Typically, 10μg total DNA, which contains nanogram amounts of mtDNA will yield ~4μg mtDNA. A major advantage of this procedure is the enrichment of the sample for mitochondrial genomes that will reduce the likelihood of pseudogene coamplification. Because of the high copy number of mtDNA per cell, it is recommended that appropriate dilution of the starting template is made for quantitative analysis in order to enable resolution between normal and diseased samples. In addition, for each analytical procedure, the recommended template amounts should be used.

ANALYSIS OF MITOCHONDRIAL DNA POINT MUTATIONS IN PROSTATE CANCER

An important aspect of mitochondrial medicine is sensitive detection of heteroplasmy. Low levels of mutant mitochondrial genomes might signal the genesis of disease. Indeed, mutation load as low as 0.1% can be clinically relevant. Given that several mtDNA mutations occur early in PCa, identifying and tracking the accumulation of somatic mtDNA mutant copies could potentially be very useful in early detection and monitoring of PCa. High-throughput and sensitive methods of heteroplasmy detection, which are amenable to automation, should be clinically useful. There is not a specific somatic mutation associated with PCa. However, mutation load is higher in PCa than normal prostate tissue. Thus, analysis of the entire mtDNA for mutation load might seem a reasonable diagnostic approach. PCR-RFLP, traditional dideoxy capillary electrophoresis sequencing, and methods that rely on mismatch heteroduplex formation between mutant and wildtype sequences have been used in analysis of variant mtDNA sequences. However, none of these methods is currently adequate for sensitive heteroplasmy detection, hence the search for newer technologies. Microarray-based resequencing, denaturing high-performance liquid chromatography (DHPLC), and pyrosequencing are newer methods that hold tremendous potential to increase the sensitivity of heteroplasmy detection. We examine methodological considerations and some technologies for analysis of mtDNA point mutations in PCa.

Analysis of haplotype markers, polymorphisms, and known disease mutations is a simple laboratory practice. These mutations often alter or create new restriction sites such that simple PCR amplification of the known region, followed by radioactive or fluorescent RFLP analysis of the amplicon, enable straightforward diagnosis or genotyping. PCR-RFLP analysis

has a sensitivity of 5% for heteroplasmy detection, probably due to heteroduplex species that form after PCR, and therefore interfere with restriction analysis. The traditional capillary electrophoresis sequencing method is a very robust, but insensitive and labor-intensive process that is not easily automated. With a sensitivity of 25% for heteroplasmic detection, low level heteroplasmies will be missed using this method. Other methods including enzymatic and chemical cleavage, denaturing or temperature gradient gel electrophoresis, single-strand conformation polymorphism, allele-specific oligonucleotide probes, ligase-mediated detection, and DHPLC are suitable for mtDNA analysis. However, with the exception of the latter, these methods (most of which depend on heteroduplex formation) are generally time consuming, labor-intensive, not easily adaptable to automation, and require small-sized nucleic acid fragments for detection. GeneChip® resequencing of the entire mitochondrial genome is currently a research tool, but has enormous potential to be translated into clinical practice. Pyrosequencing and other emerging sequencing methods are potentially useful for mtDNA mutation analysis. The utility of some of these newer technologies for mtDNA mutation detection in PCa diagnostics are described.

Microarray resequencing of mitochondrial DNA

The GeneChip® Human mitochondrial resequencing array 2.0 (MitoChip v2.0) is a sensitive, reliable and high-throughput oligonucleotide microarray that is commercially available from Affymetrix. Unlike the first generation MitoChip v1.0 (Maitra *et al*., 2004) that lacks the D-loop, the MitoChip v.2.0 enables bi-directional sequencing of the entire mitochondrial genome. This chip is fabricated using standard Affymetrix photolithography and solid phase DNA synthesis and has a feature size of 8 µm, each of which contains 10^6 copies of 25-mer probes selected from the human revised Cambridge Reference Sequence (rCRS). Eight probes (four for each strand) interrogate each base position. The four features that query a particular base on a strand contain identical 25-mer probes that only differ at the central or 13th base, each of which contains one of the four nucleotides, A, T, C or G. In addition to the 16,568 bases of the human mitochondrial genome, the MitoChip v2.0 contains additional tiling of sequences for 500 of the most common variants in the hypervariable regions I and II of the genome, including single-nucleotide substitutions, insertions, and deletions.

Detailed assay procedures can be found in the Affymetrix GeneChip® CustomSeq® Resequencing Array Protocol. Good assay performance requires the use of high quality template. Depending on the amount and quality of starting material, the entire mitochondrial genome can be amplified using one primer pair in a long extension PCR. Because of polymerase read errors when amplifying long templates, it is recommended that a very high fidelity DNA polymerase is used for whole genome amplification. In many applications, three overlapping primers suffice coverage of the entire mitochondrial genome. However, formalin-fixed and paraffin-embedded clinical samples that usually contain degraded nucleic acids require multiple overlapping primers to cover the entire genome. When more

than one primer pair is used for amplification, equimolar amounts of amplified template should be pooled for subsequent procedures to ensure that equal mtDNA targets are available for each probe set. We have been able to obtain equivalent hybridization and good sequence data using REPLI-g (Qiagen) DNA template. The fragmentation step should be carefully monitored to avoid over or under fragmentation, which otherwise affects assay performance. Over-fragmentation will lead to excessive background and under-fragmentation could interfere with hybridization efficiency.

The Affymetrix GeneChip® CustomSeq® Resequencing Array Protocol suggests using 100 ng of DNA; however, dilution experiments performed at the National Institute of Standards and Technology (NIST) indicate that <1 ng, representing <100 cells is sufficient for obtaining equivalent hybridization to the array (Vallone *et al*., 2007). Once the template is labeled and hybridized, the chips are then washed on an Affymetrix fluidics station using the pre-programmed CustomSeq® Resequencing array wash protocols. After washing, the arrays are scanned and the Affymetrix GSEQ software generates a raw pixel data (.DAT) file, which is automatically converted to a .CEL file for batch analysis.

Batch analysis is performed using RA Tools, a free software available at http://www.dpgp.org. This software is a modified version of ABACUS developed by Cutler *et al*. (2001) for genotype calls using microarray technology. The software uses a statistical algorithm to assign a quality score for each base. Initially, a series of statistical models are developed based on the assumption that various genotypes are present or absent in the sample. For a given genotype, the likelihood of each statistical model is computed independently for each strand and then combined for the overall likelihood of the model. Using these models, a quality score, which is the difference between the log(10) likelihood of the first and second best fitting statistical models for assigning a genotype at any position on the chip, is provided. To make a call, a given base must exceed the total quality score threshold (totThresh), which is empirically determined. Increasing totThresh will result in fewer calls and decreasing it will lead to ambiguous calls. When a base fails to reach this threshold, an "n" is assigned. An important built-in concept of this software is that the quality of base calls improves with multiple uses due to the adaptive nature of the software. Thus, the software uses arrays from multiple runs to factor in the differences in background that occur as a result of unequal levels of cross-hybridizations at each site.

Once batch analysis is complete, the Affymetrix GSEQ software generates a report and .CHP files. In addition to other assay information including quality metrics, these files contain the nucleotide sequences of the samples analyzed as well as the corresponding rCRS nucleotides, making it easy to read and score sequence variants. Pairwise comparison of patient sequences to the rCRS enables polymorphic loci to be scored and haplotype analysis. To identify somatic mutations, the sequences must be compared to known normal maternal mtDNA sequences. Traditionally, sequences from normal peripheral white blood cells of the same individual or a maternal relative suffice for this comparison.

Microarray-based resequencing technology has displayed higher sensitivity and automation capabilities compared with conventional sequencing technologies. In an experiment conducted at the National Institute of Standards and Technology, the MitoChip v2.0 detected heteroplasmy at a level of 1–2%, which is an order of magnitude more sensitive than capillary electrophoretic fluorescent DNA sequencing. MitoChip v2.0 has > 99.99% reproducibility and 99.999% accuracy. Through its development as a rapid and reliable approach to sequencing mtDNA, this array is currently an important research tool. Our preliminary results on the use of the MitoChip to measure the mutation load (the aggregate of genomic mutations in a sample) in non-invasively collected body fluids such as urine, sputum, and nipple aspirate fluids have demonstrated the feasibility of translating the technology into the clinical laboratory.

Denaturing high-performance liquid chromatography

Denaturing high-performance liquid chromatography (DHPLC) is one of the most sensitive methods available for heteroplasmy detection (O'Connell *et al*., 2003). This technique of mtDNA sequence analysis does not allow identification of specific sequence variants; however, it is an excellent method for haplotype analysis and detection of known polymorphisms and mutations associated with specific diseases. Additionally, DHPLC is valuable in screening clinical samples for the total suite of sequence variants or mutation load. Unlike the other mismatch-dependent methods of mutation detection that require small-sized DNA fragments, DHPLC allows mutation detection in larger fragments of up to 1.5 kb. The WAVE® DNA Genetic Analysis System is an automated and cost-effective DHPLC system developed by Transgenomics Inc. This instrument can rapidly screen the entire mitochondrial genome in < 8 h.

The production of template for heteroduplex formation depends on the type of mtDNA mutation or polymorphism being targeted. In nuclear genetic analysis, two separate amplifications of wildtype and mutant sequences are performed and used for heteroduplex formation. For somatic mtDNA mutations, the molecules with pathogenic mutations coexist with normal wildtype genomes in cells and tissues. Therefore, single tube PCR is adequate for obtaining mutant and wildtype products for heteroduplex formation. However, non-pathogenic polymorphisms and haplotype markers are often homoplasmic. For the analysis of such markers in PCa, a known rCRS sequence needs to be amplified separately and used as the wildtype reference sequence for heteroduplex formation. Also, some somatic mtDNA mutations in cancer are homoplasmic and these differ from the germline variant of the individual. Thus, amplification of normal germline mtDNA (e.g., from normal white blood cells) is required for heteroduplex formation. In instances where two separate amplifications have been performed, a ratio of 1:1 wildtype to mutant templates is used for analysis.

The entire mtDNA can be amplified in small fragments with overlapping primers for direct DHPLC analysis. Alternatively, larger fragments encompassing the entire mitochondrial genome can be amplified using multiple overlapping primers, which are then restricted using appropriate restriction sites

to yield smaller-sized fragments for multiplex DHPLC analysis. Because mtDNA demonstrates polymorphisms in individuals, restriction sites could be modified resulting in different end products that could have different melting temperatures. Thus, a gel analysis should be performed on digested PCR products prior to downstream DHPLC analysis. The MitoScreen™ assay kit from Transgenomics Inc., employs 19 primer pairs, the products of 15 of which are restricted prior to analysis. A detailed protocol for using this assay can be found at http://www.transgenomic.com/pd/assaykits/MitoScreen.asp.

The mixed templates are denatured and allowed to cool slowly so that the mtDNA strands reanneal. This process, although simple, is a critical step for accurate mutation detection. Two main types of reannealed products, homoduplex (wildtype and mutant) and heteroduplex species that contain mismatch base pairs will form. Approximately 5–8 μl of the samples are then injected into a flow column of the WAVE system that is filled with alkylated nonporous poly(styrene-divinylbenzene) beads. The flow path has an oven that contains a patented DNASep® Cartridge. The cartridge temperature in the oven is initially set to partially denature the reannealed products. In the presence of triethylamine acetate (TEAA) buffer, the partially denatured templates are anchored to the beads via the interaction of the negatively charged phosphate backbone of the partially denatured DNA to the positively charged ammonium groups in the TEAA, whose hydrophobic parts are anchored to the hydrophobic parts of the beads in the cartridge. The bound mtDNA is then eluted from the column with increasing concentrations of acetonitrile (ACN) at optimized mobile phase temperatures for each mtDNA fragment. The optimal temperatures and ACN gradients can be determined empirically or by means of the Navigator software. Heteroduplexes with internal mismatch base pairing display reduced column retention compared to their homoduplex counterparts, and therefore, elute first followed by homoduplexes. Absorbances of mtDNA fragments are recorded over time as they pass through a UV (or fluorescence) detector. The Navigator software analyzes and records the information as chromatograms. The presence of a single peak means the absence of mutation; however, high percentage heteroplasmic mutations give two peaks, the first peak representing the heteroduplexes and the second one the homoduplexes. Very low percentage heteroplasmy often appears as a small "bump" on the single major peak.

The high sensitivity of DHPLC makes it an attractive method to scan the entire mtDNA for heteroplasmy. The reliability, reproducibility, and sensitivity of DHPLC for mtDNA mutation detection have been demonstrated. Using various mixtures of known percentages of mutant/wildtype mtDNA molecules, DHPCL has been able to resolve heteroplasmies as low 1% (Meierhofer *et al.*, 2005), making it one of the best methods currently available for mtDNA sequence analysis.

Pyrosequencing

Pyrosequencing is another reliable and sensitive DNA sequencing method that has been used to sequence and resolve mtDNA heteroplasmy in clinical samples. This technology allows simultaneous detection and quantification of incorporated nucleotides, and is therefore a very useful method for

analyzing gene copy number and mtDNA heteroplasmy. Pyrosequencing is simply described as DNA sequencing by synthesis (Ronaghi *et al*., 1998). There are two main pyrosequencing techniques: liquid and solid phases.

Liquid phase pyrosequencing uses four enzymes (DNA polymerase, apyrase, ATP sylfurylase, and luciferase) in a reaction cascade during which DNA synthesis is coupled with light emission that is detected and quantified. The template to be sequenced is first amplified by PCR and then an enzymatic template preparation process is used to generate primed single stranded DNA for sequencing. An exonuclease I and nucleotide-degrading enzymes are added to the PCR product and incubated at room temperature. This process removes the nucleotides (nucleotide-degrading enzyme activity) and PCR primers (exonuclease I activity). The sequencing primer is then added to the mixture and heated to inactivate the enzymes. Primed templates are formed by rapidly cooling the mixture.

In solid-phase pyrosequencing, biotinylated PCR products are captured onto streptavidin-coated magnetic beads, followed by washing and alkali denaturation to generate single stranded DNA, which are then primed and used for sequencing. The process employs the same enzymes as liquid phase sequencing except the nucleotide-degrading enzyme, apyrase. Therefore, a washing step is introduced between cycles to remove unincorporated nucleotides.

During the sequencing process, DNA polymerase synthesizes a complementary strand by sequentially adding the correct base. The four nucleotides are added in a defined order, e.g., A, C, T, and G. If the first base, A, added is not the correct complement of the first targeted base in the sequence, it is quickly removed by the DNA-degrading enzyme, apyrase, or washed off. The other bases are sequentially added until the correct base is incorporated. This base-pairing is associated with the release of pyrophosphate (PPi), which is used by ATP sylfurylase to generate energy in the form of ATP. This energy is harnessed by luciferase to oxidize luciferin and in the process, produces light that is measured by a camera and displayed in a Pyrogram as peaks, in conjunction with a record of the incorporated nucleotides. Apyrase then degrades ATP and the other nucleotides and the light switches off. The cycle is repeated several times. The peaks in the Pyrogram are proportional to the number of nucleotides incorporated at a particular position; thereby, allowing some aspects of quantification. The PSQ 96MA system developed by Pyrosequencing AB is an automated instrument and software for simultaneous analysis of 96 samples.

Pyrosequencing is a rapid and robust method of detecting mtDNA point mutations in clinical samples. The technology has successfully been applied in forensics and clinical diagnosis of known disease-associated mtDNA mutations. Whereas pyrosequencing has not yet been used for cancer mtDNA mutation analysis, the ability for this technique to detect and quantify heteroplasmies in formalin-fixed and paraffin-embedded clinical specimens is an obvious advantage for this method to be considered in the clinics for mitochondrial molecular oncology. With a sensitivity and specificity of 100% as well as the capability to detect mtDNA mutations at a 1% heteroplasmic level, this technology holds considerable promise for clinical

translation in analyzing known mtDNA disease mutations.

A major limitation of pyrosequencing is the short read length, due to misincorporation errors and inhibitory substances in the reaction. For whole genome sequencing, a long read length is advantageous because it will permit fewer reactions to cover the entire 16,568 bases of the mitochondrial genome. Thus, complete mitochondrial genome sequencing might require multiple runs. This technology however, appears useful for haplotype and SNP analysis, and because it is fast and cost effective, can prove very useful in clinical diagnostic applications.

Other emerging sequencing technologies

Newer sequencing technologies such as Roche/454 PicoTiterPlate™ device and Illumina/Solexa sequencing will require testing, optimization, and validation before being used in the detection of mitochondrial mutations. These technologies however, could offer some advantages over the current ones for whole mitochondrial genome sequencing.

REAL TIME PCR ANALYSIS OF MITOCHONDRIAL DNA IN PROSTATE CANCER

Large-scale mtDNA deletions are associated with PCa and might be one of the mediators of androgen independence. Furthermore, circulating mitochondrial nucleic acids could potentially hold prognostic value in advanced PCa. Therefore, quantitative measurement of mtDNA deletions and circulating nucleic acids in clinical specimens might be useful in the diagnosis and prognostic evaluation of PCa patients.

Conventionally, Southern blotting is the method of choice used to detect and confirm mtDNA deletions. However, Southern blotting is insensitive, requiring large amounts of template, which are not easily attainable when precious clinical samples such as prostate needle biopsy specimens are used for diagnostic testing. Moreover, low heteroplasmic levels of mtDNA deletions that might still be clinically useful for early detection and monitoring of PCa are not resolved by Southern blotting. Real-time polymerase chain reaction (qPCR) is a sensitive, reliable, and high-throughput method for easy quantification of mtDNA deletions, copy number, and content in clinical specimens.

An important aspect of qPCR analysis of mtDNA deletion is primer and probe design as well as choice of appropriate control targets to be used for normalization and accurate quantification. Three types of primer sets are required for quantification of mtDNA deletions and content alterations: (1) MtDNA deletion-specific primers that will only measure the amount of deleted molecules. This is achieved by designing one primer or probe to span across the deletion junction (bridging primer) and combining this with a downstream or upstream primer to target a small amplicon. Alternatively, flanking primers on either side of the deletion junction that target a very small product can be used, but the qPCR extension time must be reduced to preclude coamplification of wildtype molecules. (2) Primers targeting total mtDNA (both wildtype and deleted mtDNA) molecules. These primers should be located outside the deleted region and preferably

in a region of the mitochondrial genome known to sustain negligible deletions in the tumor. The D-loop can be targeted, however, because this region is highly polymorphic, primer locations should be in the least polymorphic sites. (3) Nuclear primers to control for input template and mtDNA content analysis. In choosing nuclear targets, avoid genes with several homologues (e.g., beta-actin) or multiple copies (18S rRNA). Single copy genes that are not amplified in PCa must be used.

The basic principle of real time PCR is the monitoring of product accumulation during each PCR cycle through the emission of fluorescence. The PCR reaction progresses from initial template detection through an exponential phase and finally non-exponential or plateau phase. Because the choice of chemistry is quite important in qPCR assay design with regards to cost, sensitivity, specificity, and ease of assay performance, we examine the basic chemistries available. Several chemistries for the detection of amplicon accumulation are suitable for mtDNA quantification. These include TaqMan hydrolysis probes, hybridization probes such as molecular beacons and scorpion primer-probe combo, and DNA intercalating dyes such as SYBR green assay.

TaqMan probes have been widely used for mtDNA quantification. These probes are short single-stranded oligonucleotides that are complementary to a sequence in the target amplicon. They contain a fluorescence reporter dye at the 5′ end and a quencher dye at the 3′ end. The close proximity of these two dyes prevents the emission of fluorescence. With the accumulation of amplicons during the PCR cycling process, TaqMan probes anneal to denatured target amplicons, and as the polymerase replicates a template with bound TaqMan probe, the reporter dye is cleaved using its 5′ exonuclease activity, and this releases it from the quencher; thus, resulting in irreversible fluorescence. Because the cleaved reporter dye is irreversible, this introduces background noise in the assay.

Molecular beacon probes are designed such that about six bases at the 5′ and 3′ ends of the single-stranded sequence that contain reporter dye and quencher, are complementary to each other and the middle portion is complementary to the target amplicon. Thus, in an unbound state the complementary ends anneal to form a double-stranded stem, whilst the middle portion remains as a single stranded loop. In this hairpin configuration, the reporter and quencher are in close proximity precluding fluorescent emission. However, the probes are designed to bind to the amplicon at a specified temperature. This interaction, which is thermodynamically more stable than the hairpin structure, leads to destabilization of the stem and thus the emission of fluorescence. Unlike TaqMan probes, molecular beacons produce less background due to the reversibility of the fluorescence at each cycle. This low background makes molecular beacons probably more suitable for multiplex PCR assay designs.

An inherent problem with TaqMan and Molecular beacon probes is that targets with repetitive elements, as is inherent in the mitochondrial genome, may form secondary structures preventing probe interactions. To overcome such problems, Scorpions were developed to combine probe and primer in the same oligonucleotide. Scorpion primers are attached

to Scorpion probes at their 5′ ends. The probes are similar to beacon probes with complementary stem that forms a hairpin structure bringing the reporter and quencher together as well as an intervening loop sequence that is complementary to sequences in the newly synthesized amplicon. Following the first PCR reaction, the newly synthesized amplicon, which is attached to the probe via the primer as a single molecule, will contain complementary sequences to the loop sequence of the probe. An intra-molecular hybridization between the probe and target amplicon occurs during the second PCR cycle of denaturation and annealing. This internal hybridization occurs because denaturation of the hairpin loop requires less energy than the new DNA duplex formed.

Double-stranded DNA intercalating dyes such as SYBR green are less expensive and easy to optimize. These dyes emit fluorescence when bond to double-stranded DNA. As PCR products accumulate, more dye intercalates and more fluorescence emission occurs. SYBR green assays are less specific than the probe-based assays because the dyes interact with any double stranded DNA, including primer dimers. Melting curve analysis, however, allows this to be easily realized. When fully optimized, the inexpensive dye-binding assays perform equally well as hydrolysis and hybridization probe detection methods. Several PCR quantifications of mtDNA levels have relied on TaqMan and SYBR green assays. Many of these assays employ multiple tubes for different targets. However, judicious use of precious clinical material and accurate normalization is achievable with multiplex PCR.

Real time PCR assays often include a passive dye used as an internal reference to normalize or correct for background fluorescence. Rn designates the ratio of emission intensities of reporter dye to passive reference dye. The normalized emission intensity of a reaction containing all reagents and target template is referred to as Rn+ and that of no template control as Rn−. ΔRn is the difference between Rn+ and Rn−. The PCR cycle at which the device software first detects significant reporter fluorescence (Rn+) above threshold is referred to as the cycle threshold (Ct), and this is the critical parameter used for quantification.

Computation of the levels of a target molecule is accomplished using either a standard curve of Ct values obtained from serial dilutions of standard target molecules (absolute quantification) or by comparison of the differences in the Ct between two samples or targets (relative quantification). Relative quantification usually makes several assumptions, which when unfulfilled lead to erroneous results. Moreover, results from relative quantification tend to differ depending on the method and reference target gene chosen. In clinical diagnostics of mtDNA alterations, it is recommended that the "absolute" quantification method is used, and this will be described. "Absolute" quantification aims at accurately measuring the number of target molecules in a sample. Whereas this is a very difficult claim to confirm in many assays, it offers a means of closely measuring target molecules. An important requirement for absolute quantification is that an accurate standard template is prepared. This is achieved by cloning the PCR product of each target sequence into a plasmid vector, followed by sequencing to confirm identity of the cloned fragment. A single clone is then

selected, DNA extracted and quantified by absorbance. The copy number of the target is computed based on the molecular weight of the cloned plasmid DNA.

Target copy number = (cloned plasmid DNA concentration)/(weight of cloned plasmid molecule)

The weight of the cloned plasmid = ($S_{cp} \times 6.6 \times 10^5$ g/mole)/(6.02×10^{23} molecules/mole)

S_{cp} = size of cloned plasmid (plasmid + cloned fragment) in base pairs

6.6×10^5 g/mole = molecular weight of double stranded DNA

6.02×10^{23} molecules/mole = Avogadro's number

For each PCR reaction, serial dilutions of the stock solution are included and the Cts from these are plotted on a standard curve, which shows the target copy numbers and corresponding Cts. This curve is used to compute copy numbers or levels of target molecules in experimental samples using their various Cts. Assay reliability is influenced by the PCR efficiency. It is possible to certify an optical density (OD) value of a quantity of DNA to serve as a standard that can measure the PCR efficiency.

The heteroplasmic levels of deleted mtDNA molecules are determined by computing the ratio of deleted to total mtDNA copies. It is very important to note that this computation is only possible when the primers used to quantify total mtDNA molecules are not within a region of the mtDNA known to be deleted in PCa. The appropriate region can be determined empirically by analysis of a subset of tumor and benign samples with these primers, and ensuring that there is no statistically significant resolution in total mtDNA copies between the two groups. It is equally important to use diluted template for this experiment because concentrated template will shadow any differences, if any, between samples. It is also recommended that two separate primers are used for this quantification. Similarly, mtDNA content (normal, depletion or over-replication) is computed from the ratio of the copies of total mtDNA to nuclear target. Again, it is imperative that this nuclear target is single copy and not amplified in PCa.

QUALITY ASSURANCE ISSUES TO BE CONSIDERED IN MITOCHONDRIAL DNA ANALYSIS

Accurate molecular diagnostics depends on several factors, including instrument performance, assay optimization, training and skill of technicians as well as good sample handling to avoid contamination or mix-up. Sample contamination is a major quality assurance issue in clinical molecular diagnostics. This issue is even of a major concern with regards to mtDNA analysis, given its high copy number per cell. Since many of the methods described above involve genomic amplification, good laboratory practices are required to prevent sample contamination, especially when the same mtDNA fragment is amplified several times. Sample contamination can occur at several levels, beginning with specimen procurement through all the analytical steps. Aerosol means of template spread in the laboratory is one major cryptic mode of contamination. Another important concern when analyzing mtDNA is taking the

necessary precautions to avoid amplifying nuclear embedded mtDNA copies, some of which are 100% homologous to the authentic cytoplasmic DNA. We offer the following minimum recommendations to be observed in clinical molecular diagnostics using mtDNA mutations:

- Instruments used in molecular diagnostics should be maintained and calibrated periodically by trained personnel following the manufacturer's recommendations and an established instrument maintenance standard operating procedure (SOP).
- At least three distinct designated laboratory areas should be used for reagent storage and preparation, DNA extraction and PCR set up as well as PCR amplification and downstream analysis. Each of these areas should have its own dedicated equipment. The PCR amplification and analysis room is a highly contaminated area, and to minimize aerosol spread from this to other rooms; (1) the pressure in this room must be sub-atmospheric, (2) upstream flow of people, equipment and other materials including gowns should be avoided, and (3) surfaces should be decontaminated frequently after work with sodium hypochlorite or UV radiation.
- Assay for each molecular target must be optimized and an SOP developed and followed at all times. For instance, the diagnostics DHPLC quality assurance collaborative group has developed two separate SOPs for instrument operation/maintenance and the detection of a specific mutation using DHPLC (Schollen *et al*., 2005). Similarly, each assay should include a standard reference material with known performance to be used to minimize assay-to-assay variability and to measure assay sensitivity.
- Dedicated gowns and gloves in each room should be worn at all times when handling samples, reagents, equipment and instruments. These should be disposed off, or left in each room before departing.
- Clean reagents, equipments and instruments must be used for sample processing and DNA extraction.
- To prevent pseudogene co-amplification, a BLAST search of mtDNA primers must be performed to ensure lack of homologous nuclear sequences, and these primers then be tested on DNA template from cells lacking mtDNA to confirm lack of pseudogene co-amplification.
- It is also recommended that a high fidelity DNA polymerase is used to prepare template for sequencing, so as to prevent mutation artifacts.
- All analytical steps must include the appropriate controls.
- An important issue with mtDNA analysis is the occasional sample mix-up or cross contamination. In such situations, Short Tandem Repeat (STR) and Phylogenetic analyses should be performed.

In summary, mtDNA mutations are potentially useful for early detection and monitoring, risk assessment, complementary evaluation of prostate needle biopsies and/or prognostic stratification of patients for therapy. Methods discussed here can be used to detect and monitor other cancers (e.g., breast cancer). MtDNA studies should focus on the utility of minimally invasive or noninvasive samples. It should be noted that despite the extensive body of information on the biology of mitochondria and mtDNA mutations in a wide variety of human diseases, an exact role for mtDNA mutations in the etiology of cancer has yet to be established. Mutations

that alter mitochondrial gene structure/function, replication and/or transcription should be considered as significant when evaluating their physiological impact, while silent mutations that are hitchhikers or passengers might be important for assessing mutation load.

REFERENCES

Anderson, S., Bankier, A.T., Barrell, B.G., de Bruijn, M.H., Coulson, A.R., Drouin, J., Eperon, I.C., Nierlich, D.P., Roe, B.A., Sanger, F., Scheier, P.H., Smith, A.J., Staden, R., and Young, I.G. 1981. Sequence and organization of the human mitochondrial genome. *Nature 290*: 457–465.

Baysal, B.E. 2006. Role of mitochondrial mutations in cancer. *Endocr. Pathol. 17*: 203–212.

Blok, R.B., Gook, D.A., Thorburn, D.R., and Dahl, H.H. 1997. Skewed segregation of the mtDNA nt 8993 (T–>G) mutation in human oocytes. *Am. J. Hum. Genet. 60*: 1495–1501.

Booker, L.M., Habermacher, G.M., Jessie, B.C., Sun, Q.C., Baumann, A.K., Amin, M., Lim, S.D., Fernandez-Golarz, C., Lyles, R.H., Brown, M.D., Marshall, F.F., and Petros, J.A. 2006. North American white mitochondrial haplogroups in prostate and renal cancer. *J. Urol. 175*: 468–472.

Chen, J.Z., Gokden, N., Greene, G.F., Green, B., and Kadlubar, F.F. 2003. Simultaneous generation of multiple mitochondrial DNA mutations in human prostate tumors suggests mitochondrial hyper-mutagenesis. *Carcinogenesis 24*: 1481–1487.

Clayton, D.A., and Vinograd, J. 1969. Complex mitochondrial DNA in leukemic and normal human myeloid cells. *Proc. Natl. Acad. Sci. USA 62*: 1077–1084.

Costello, L.C., and Franklin, R.B. 2006. The clinical relevance of the metabolism of prostate cancer; zinc and tumor suppression: connecting the dots. *Mol. Cancer 5*: 17.

Cutler, D.J., Zwick, M.E., Carrasquillo, M.M., Yohn, C.T., Tobin, K.P., Kashuk, C., Mathews, D.J., Shah, N.A., Eichler, E.E., Warrington, J.A., and Chakravarti, A. 2001. High-throughput variation detection and genotyping using microarrays. *Genome Res. 11*: 1913–1925.

Dakubo, G.D., Parr, R.L., Costello, L.C., Franklin, R.B., and Thayer, R.E. 2006. Altered metabolism and mitochondrial genome in prostate cancer. *J. Clin. Pathol. 59*: 10–16.

Giles, R.E., Blanc, H., Cann, H.M., and Wallace, D.C. 1980. Maternal inheritance of human mitochondrial DNA. *Proc. Natl. Acad. Sci. USA 77*: 6715–6719.

Herrmann, P.C., Gillespie, J.W., Charboneau, L., Bichsel, V.E., Paweletz, C.P., Calvert, V.S., Kohn, E.C., Emmert-Buck, M.R., Liotta, L.A., and Petricoin, E.F., 3rd. 2003. Mitochondrial proteome: altered cytochrome c oxidase subunit levels in prostate cancer. *Proteomics 3*: 1801–1810.

Higuchi, M., Kudo, T., Suzuki, S., Evans, T.T., Sasaki, R., Wada, Y., Shirakawa, T., Sawyer, J.R., and Gotoh, A. 2006. Mitochondrial DNA determines androgen dependence in prostate cancer cell lines. *Oncogene 25*: 1437–1445.

Horton, T.M., Petros, J.A., Heddi, A., Shoffner, J., Kaufman, A.E., Graham, S.D., Jr., Gramlich, T., and Wallace, D.C. 1996. Novel mitochondrial DNA deletion found in a renal cell carcinoma. *Genes Chromosomes Cancer 15*: 95–101.

Jakupciak, J.P., Dakubo, G.D., Maragh, S., and Parr, R.L. 2006. Analysis of potential cancer biomarkers in mitochondrial DNA. *Curr. Opin. Mol. Ther. 8*: 500–506.

Jeronimo, C., Nomoto, S., Caballero, O.L., Usadel, H., Henrique, R., Varzim, G., Oliveira, J., Lopes, C., Fliss, M.S., and Sidransky, D. 2001. Mitochondrial mutations in early stage prostate cancer and bodily fluids. *Oncogene 20*: 5195–5198.

Jessie, B.C., Sun, C.Q., Irons, H.R., Marshall, F.F., Wallace. D.C., and Petros, J.A. 2001. Accumulation of mitochondrial DNA deletions in the malignant prostate of patients of different ages. *Exp. Gerontol. 37*: 169–174.

Jorde, L.B., Watkins, W.S., Bamshad, M.J., Dixon, M.E., Ricker, C.E., Seielstad, M.T., and Batzer, M.A. 2000. The distribution of human genetic diversity: a comparison of mitochondrial, autosomal, and Y-chromosome data. *Am. J. Hum. Genet. 66*: 979–988.

Maitra, A., Cohen, Y., Gillespie, S.E., Mambo, E., Fukushima, N., Hoque, M.O., Shah, N., Goggins, M., Califano, J., Sidransky, D., and Chakravarti, A. 2004. The Human MitoChip:

a high-throughput sequencing microarray for mitochondrial mutation detection. *Genome Res. 14*: 812–819.

Mehra, N., Penning, M., Maas, J., van Daal, N., Giles, R.H., and Voest, E.E. 2007. Circulating mitochondrial nucleic acids have prognostic value for survival in patients with advanced prostate cancer. *Clin. Cancer Res. 13*: 421–426.

Meierhofer, D., Mayr, J.A., Ebner, S., Sperl, W., and Kofler, B. 2005. Rapid screening of the entire mitochondrial DNA for low-level heteroplasmic mutations. *Mitochondrion 5*: 282–296.

Modica-Napolitano, J.S., Kulawiec, M., and Singh, K.K. 2007. Mitochondria and human cancer. *Curr. Mol. Med. 7*: 121–131.

O'Connell, C.D., Tully, L.A., Devaney, J.M., Marino, M.A., Jakupciak, J.P., and Atha, D.H. 2003. Renewable standard reference material for the detection of TP53 mutations. *Mol. Diagn. 7*: 85–97.

Parr, R.L., Dakubo, G.D., Crandall, K.A., Maki, J., Reguly, B., Aguirre, A., Wittock, R., Robinson, K., Alexander, J.S., Birch-Machin, M.A., Abdel-Malak, M., Froberg, M.K., Diamandis, E.P., and Thayer, R.E. 2006a. Somatic mitochondrial DNA mutations in prostate cancer and normal appearing adjacent glands in comparison to age-matched prostate samples without malignant histology. *J. Mol. Diagn. 8*: 312–319.

Parr, R.L., Maki, J., Reguly, B., Dakubo, G.D., Aguirre, A., Wittock, R., Robinson, K., Jakupciak, J.P., and Thayer, R.E. 2006b. The pseudo-mitochondrial genome influences mistakes in heteroplasmy interpretation. *BMC. Genomics 7*: 185.

Petros, J.A., Baumann, A.K., Ruiz-Pesini, E., Amin, M.B., Sun, C.Q., Hall, J., Lim, S., Issa, M.M., Flanders, W.D., Hosseini, S.H., Marshall, F.F., and Wallace, D.C. 2005. mtDNA mutations increase tumorigenicity in prostate cancer. *Proc. Natl. Acad. Sci. USA 102*: 719–724.

Ronaghi, M., Uhlen, M., and Nyren, P. 1998. A sequencing method based on real-time pyrophosphate. *Science 281*: 363–365.

Schollen, E., Dequeker, E., McQuaid, S., Vankeirsbilck, B., Michils, G., Harvey, J., van den Akker, E., van Schooten, R., Clark, Z., Schrooten, S., Mattijs, G., and DDQA Collaborative Group. 2005. Diagnostic DHPLC Quality Assurance (DDQA): a collaborative approach to the generation of validated and standardized methods for DHPLC-based mutation screening in clinical genetics laboratories. *Hum. Mutat. 25*: 583–592.

Taylor, R.W., and Turnbull, D.M. 2005. Mitochondrial DNA mutations in human disease. *Nat. Rev. Genet. 6*: 389–402.

Vallone, P.M., Jakupciak, J.P., and Coble, M.D. 2007. Forensic application of the Affymetrix human mitochondrial resequencing array. *For. Sci. Inter. 1*: 196–198.

Warburg, O. 1931. *The metabolism of tumors*. New York: Smith RR.

33
Prognostic Markers in Prostatic Carcinoma

Sonia L. El-Sharkawy, Naglaa F. Abbas, and Nadia G. EL-Hefnawy

INTRODUCTION

Prostatic carcinoma is the most prevalent cancer among men in the Western world. Rates of prostate cancer vary widely across the world, it is least common in South and East Asia, more common in Europe, and most common in the United States. However, these high rates may be affected by increasing rates of detection. Prostate cancer develops most frequently in men over 50 years of age. The incidence of prostate carcinoma increases directly with age; however, it causes death in a relatively small proportion of men. Prostate cancers have several distinctive properties. These tumors often grow very slowly in the prostate. In fact, the majority of men with prostate cancer will not have metastases to other organs and will not die of prostate cancer. Early prostate cancers rarely have the capacity to metastasize. It often takes years or decades for the tumors to develop a series of mutations that allow the cells to form metastases outside of the prostate (Punglia *et al*., 2006).

Preneoplastic lesions, known as prostatic intraepithelial neoplasia (PIN), have been found in men as early as 20 years of age and are commonly observed in men > 50 years of age. Prostatic intraepithelial neoplastic lesions are thought to be precursors of invasive prostate cancer in which incidence significantly increases in the sixth decade of life (Calvo *et al*., 2003). Aging, genetic factors, environmental carcinogens, and steroid hormone levels are factors that have been associated with the development of prostatic cancer. One of the most important unsolved problems in prostate cancer today is finding a way to predict the eventual outcome of an individual's prostate cancer at the time he is first diagnosed. Although the prostate specific antigen (PSA) test has allowed considerable earlier diagnosis of prostate cancer, a positive PSA only shows that there is prostate cancer present. It does not predict what will happen to that cancer in the near future. It is necessary to find prognostic markers that will warn which tumors will stay confined to the prostate over time and which are at risk for metastasis. In prostate cancer, a marker may be considered predictive if it can distinguish between patients who require immediate treatment and patients who can safely be monitored over time without immediate radiation or surgery (Punglia *et al*., 2006).

Regulation and maintenance between cell death and cell proliferation are very

critical for normal and neoplastic tissue homeostasis. Apoptosis is a protective mechanism that operates by removing senescent, DNA-damaged or diseased cells. Inhibition of apoptosis (programmed cell death) may be involved in the pathogenesis of cancer by prolonging cell life and facilitating retention of deleterious mutations. Several inhibitors of apoptosis have been identified, and bcl-2, the most notable inhibitor of apoptosis, has been well characterized in several human malignancies. The bcl-2 oncoprotein prolongs the cell life span by inhibiting apoptosis. It thus increases the risk of acquiring other unfavorable changes such as chromosomal abnormalities and DNA damage, rendering the cells more susceptible to malignant transformation. Moreover, bcl-2 expression has also been in various precancerous and cancerous lesions (Rosaria *et al*., 2006). Apoptotic cell death in prostate has been shown to be accompanied or preceded by elevated expression of the proto-oncogen that can initiate alteration in the synthesis of apoptosis regulating gene products such as bcl-2 family members. However, bcl-2 has been studied in benign prostatic tissues and cancer cell lines with conflicting results in regard to the prognostic variables and clinical outcome (Maffini *et al*., 2001).

The C-erbB-2 proto-oncogene (also called HER-2 or neu) encodes a 185 Kda transmembrane glycoprotein. It has been noted that this protein is closely related, but yet different, to epidermal growth factor receptor (EGF-R) encoded by the C-erbB-2 proto-oncogene. The structural alteration responsible for activation of C-erbB-2 gene is thought to be the result of a single mutation by a single amino acid substitution in the transmembrane domain. Over-expression of the protein product, usually associated with gene amplification, has been demonstrated in a wide range of human adenocarcinomas originating in different organs such as breast and ovaries in which a strong correlation between C-erbB-2 amplification and poor prognosis of the disease has been observed. However, very little is known concerning the roles of growth factors, growth factor receptors or proto-oncogenes in the development and progression of prostatic adenocarcinomas (Myers *et al*., 1994).

Metallothioneins (MTs) belong to a family of cystein-rich, metal-binding intracellular proteins, which have been linked to cell proliferation. They are believed to serve an important role in the homeostasis of essential metals such as Zn and Cu during growth and development, as well as in the detoxification of heavy metals such as Cd and Hg, rendering the MTs important mediators and attenuators of heavy metal-induced toxicity. It was found that MTs are involved in metalloregulatory functions such as cell proliferation, growth, and differentiation. In recent years, MT expression has been linked with carcinogenesis, resistance to cancer therapy, and tumor progression. Immunohistochemically detected MT is not usually found in normal tissues except in myoepithelial cells of the breast, and epithelial cells of the kidney and thyroid. Metallothionein overexpression occurs frequently in human malignant tumors, but the underlying mechanism is unknown. Several lines of evidence suggest that MT may be involved in cell proliferation and differentiation in carcinogenesis. Many studies have shown an association of metallothionein overexpression with tumor type and grade (Surowiak *et al*., 2004).

DNA content measurement has been widely applied in studies of normal and neoplastic cell growth. DNA ploidy has been investigated as a potential prognostic factor for prostate cancer for many years, and in the vast majority of reports, it has been found to be predictive of patient outcome (Pollack *et al*., 2003). Tumor aneuploidy, as determined by image or flow cytometry, correlates both with a higher Gleason score and with local and distant spread. However, there is still no agreement as to whether this technique provides independent information. The Karolinska Institute authors, who have obtained the most impressive results with this technique, believe that the controversies related to its use are largely related to methodologic inadequacies (Falkmer, 1993).

The nucleolus plays a vital role in the control of cell proliferation and protein synthesis, as it is the only part of the nucleus where ribosomal ribonucleic acid (rRNA) is transcribed. The region of the nucleolus that performs this function is the nuclear organizer region (NORs). These NORs are defined as nuclear components containing a set of argyrophilic proteins, which are selectively stained by silver methods. After silver staining, the NORs can be easily identified as black dots exclusively localized throughout the nuclear area, and are called "Ag-NORs". Silver staining of NORs and subsequent quantification by image analysis are used increasingly in human pathological specimens and experimental models as markers of cellular proliferation. Histologic grade of differentiation is a strong prognostic factor for prostate carcinoma. However, most tumors are placed in the intermediate group. Nuclear and nucleolar morphometry and analysis of the argyrophilic nucleolar organizer regions (AgNORs) have been performed to improve prognosis, especially for patients with intermediate histologic grade tumors (Orsea *et al*., 2001).

MATERIALS AND METHODS

Formalin fixed and paraffin embedded tissue blocks from patients with benign prostatic hyperplasia (BPH), prostatic intraepithelial neoplasia (PIN), and prostatic carcinoma (PC) were collected. They were obtained by radical prostatectomy, transurethral resection or prostatic needle biopsy. Normal prostatic tissue adjacent to tumors were included in this study. PIN lesions were classified into low and high grades (Bostwick *et al*., 1993). The Gleason system was used for histological grading of malignant tumors (Gleason, 1977). According to Xiang-Hua *et al*. (1996), the cases were classified as low grade (Gleason score 2–4), moderate grade (Gleason score 5–6) and high grade (Gleason score 7–10).

In this report, we apply the following studies:

Routine histopathological evaluation was done on the hematoxylin and eosin stained slides for histologic grading. Prostatic intraepithelial neoplasia has been divided into three grades depending on the severity of cell crowding and stratification; nuclear enlargement, pleomorphism, chromatin pattern, and nucleolar appearance. These three grades (I, II, and III) are grouped into two categories: low-grade PIN (grade I and II) and high grade (grade III). The key feature in distinguishing high-grade from low-grade PIN is the nuclear (and particularly the nucleolar) appearance (Berman

et al., 2000). The microscopic grading system for prostatic carcinoma is based on the degree of glandular differentiation and the growth pattern of the tumor in relation to the stroma as evaluated on low-power examination as follows:

Stage 1: Single, separate, uniform glands in closely packed masses with a definite, usually rounded, edge limiting the area of tumor

Stage 2: Single, separate, slightly less uniform glands, loosely packed, with less sharp edge

Stage 3a: Single, separate, much more variable glands, may be closely packed but usually irregularly separated; ragged, poorly defined edge

Stage 3b: Like 3a, but very small glands or tiny cell clusters

Stage 3c: Sharply and smoothly rounded masses of papillary or loose cribriform tumor ("Papillary intraduct")

Stage 4a: Raggedly outlined, raggedly infiltrating, fused glandular tumor

Stage 4b: Like 4a, with large pale cells ("hypernephroid")

Stage 5a: Sharply circumscribed, rounded masses of almost solid cribriform tumor, usually with central necrosis ("comedocarcinoma")

Stage 5b: Ragged masses of anaplastic carcinoma with only enough gland formation or vacuoles to identify it as adenocarcinoma

The predominant tumor pattern (referred to as primary) is graded from 1 to 5 (irrespective of its subgrade, as indicated by letter), and the secondary pattern (if present) is graded similarly, with the two numbers being added to obtain the Gleason's score. If the tumor has the same pattern throughout, the number is multiplied by 2 to obtain the final score (Gleason, 1977).

Immunohistochemical study for evaluation of MT, Bcl-2, and C-erbB-2 expression. Streptavidin-biotin technique was used. Tissue samples were fixed in 10% buffered formalin for 24 h. 4 mμ-thick sections were cut. After deparaffinization and hydration of tissue sections, they were incubated for 30 min in 0.3% hydrogen peroxide to quench endogenous peroxidase activity. Antigen retrieval was done by microwave pretreatment for 10 min in 0.01 M citrate buffer. The sections were incubated for 20 min with normal blocking serum to suppress nonspecific binding of immunoglobulin. The tissue sections were incubated at 4°C overnight with the primary antibody. These steps were followed by a 30 min incubation with biotinylated horse anti-mouse antibody at room temperature, avidin-biotin peroxidase complex for 50 min at room temperature and finally diamiobenzidine (DAB) for 3–5 min. The slides were counterstained with hematoxylin, dehydrated, and mounted. Negative control was obtained by omitting the primary antibody. In each staining batch positive control was included.

Bcl-2 was considered positive when sections displayed a distinct cytoplasmic reaction. Staining patterns were assessed semiquantitatively to define the proportion of positive cells; each slide was examined under high power magnification (X400). Ten high power fields were counted and the percentage of cytoplasmic positivity for bcl-2 was graded as follows: low, moderate and high when < 25%, 25–50 % and > 50% of cells were immunoreactive, respectively (Maffini *et al*., 2001). For C-erbB-2, the slides were examined and were

scored based on both the staining intensity and the proportion of stained cells. All cases with membrane staining either alone or associated with cytoplasmic staining were scored positive. Cytoplasmic staining alone was considered negative. If the staining intensity was not greater than that observed in negative controls, the specimen was assigned a score of "none". If the intensity of the stain was low, or if the intensity was strong but limited to less than 50% of the cells, the immunostaining was scored as weak. Strong staining in 50% or more was scored as moderate and strong, respectively (Utrilla *et al*., 1999). Metallothionein immunostaining results were scored 0: no, 1: < 25%, 2–25% to 50% and 3-> 50% staining cells. The results were judged positive if more than 25% of the tissue section stained. Staining intensity was recorded semiquantitatively as mild (+), moderate (++) or strong (+++) according to Somji *et al*. (2001).

DNA content analysis (Feulgen staining): The silver staining reaction specifically stains the DNA to give specific blue staining of the nuclear DNA. Nucleoli and cytoplasm should show no staining. The stained DNA can then be quantified by analysis on the Leica Qwin 500 image analyzer. The stained DNA was quantitated using the Leica Qwin 500 Image Analyzer (LEICA Imaging Systems Ltd, Cambridge, England,) at the Pathology Department, National Research Center. We started by system calibration before each measurement session using the calibration slides provided with the system. We placed the slide to be examined on the stage of the microscope, and focused it at high power magnification (400X). The light source was set to the required level. DNA ploidy analysis was performed on the normal control specimen using the DNA cytometry software. Selection of nuclear boundaries was usually performed automatically by the image analysis system; however, some degree of interaction or editing was usually needed for optimal nuclear selection "Touching" nuclei can be "Cut" from each other, and cellular fragments or extraneous cells can be erased prior to DNA measurements. Only separate, intact nuclei were measured. Care was taken to measure various nuclei representative of the examined lesion, so that measurements were not biased toward the bizarre or anaplastic nuclei. We selected many fields until the desired number of nuclei, 100–150 had been measured. The results were displayed as a frequency histogram on the monitor generated by plotting the DNA content versus the number of nuclei counted. The DNA histograms were classified, according to Danque *et al*. (1993), as diploid, tetraploid and aneuploid based on the amount of DNA relative to the normal control.

AgNORs scoring of silver stained slides: Paraffin-embedded tissues were sectioned at 5 mμ, the sections were stained as previously described (Smith and Veldhu, 1989). No counterstaining was used. In all cases, 50 nuclei per case were counted, using oil-immersion lens at magnification of X100. AgNORs counting and typing was done after sharp focusing on the nuclear membrane and fine granules nuclear matrix in each nucleus. Only individual AgNORs with sharp nonblurred contours in this plane of focus were selected for description. For AgNORs typing we used the typing system as previously proposed (Hansen and Ostergard, 1990).

RESULTS AND DISCUSSION

Prostate cancer occurs when cells of the prostate mutate and begin to multiply out of control. These cells may spread (metastasize) from the prostate to other parts of the body, especially the bones and lymph nodes. Prognostic criteria currently in use cannot fully predict tumor behavior and thus limit the ability to recommend treatment regimens with the assurance that they are the best course of action for each individual patient. The search for better prognostic markers is now focused on the molecular mechanisms, such as altered cell cycle progression, apoptosis, neuroendocrine differentiation, and angiogenesis, which underlay tumor behavior. As the number of potential molecular markers increases, it is becoming evident that no single marker will provide the prognostic information necessary to make a significant improvement in patient care. In addition, it seems likely that traditional methods of assessing the prognostic value of this multitude of new markers will prove inadequate (Montironi *et al*., 2005).

Bcl-2 altered expression has been implicated in the pathogenesis of many epithelial malignancies including prostate, bladder, endometrium and colon. Bcl-2 is normally expressed in the basal cell layer of normal and hyperplastic glands. This result is in agreement with Baltaci *et al*. (2000), and is consistent with the interpretation that the basal cells represent the stem layer in the adult prostate gland, which are resistant to the programmed cell death in contrast to the secretory cells. Bcl-2 immunoreactivity is detected in 12.5% of low-grade PIN lesions. This result is in agreement with Baltaci *et al*. (2000) who were the first to characterize expression of bcl-2 in low-grade PIN in contrast to another study which showed negative bcl-2 expression in these lesions (Bonkhoff *et al*., 1998). However, this low rate of bcl-2 expression in low-grade PIN supports the reports of many pathologists who hold that low-grade PIN corresponds to very mild dysplasia. In the present study, bcl-2 was strongly expressed in 87.5% of high-grade PIN lesions. In the previous study of Stattin *et al*. (1997), strong bcl-2 immunoreactivity was reported in all high-grade PIN, whereas in other studies, only 17–35% of high-grade PIN lesions were bcl-2 positive (Bonkhoff *et al*., 1998). This variation could be attributed to differences in the antibodies used, the relative preservation of antigen epitopes and antigen retrieval by microwave pretreatment, which may increase antigen preservation, resulting in higher bcl-2 positivity. However, the high incidence of bcl-2 protein expression in high-grade PIN lesions supports the theory that high-grade PIN is a precursor of invasive carcinoma. Baltaci *et al*. (2000) suggested that bcl-2 expression, probably by prolonging cell survival, renders the PIN cells more vulnerable to other oncogens that can induce further steps in tumorigenesis. In primary prostatic adenocarcinoma, positive staining of bcl-2 was found in 66.7% of cases. The previously published incidence varies widely at 13.4–69% (Kaur *et al*., 2004). Some of these variations might be related to the threshold level for the positivity population presenting to different institutions. Alternatively, it might also reflect differences in the antibodies used and the relative preservation of antigen epitopes. However, in all studies, bcl-2 staining was

always heterogeneous in the cancer cases. There are conflicting results regarding the relationship between bcl-2 immunoreactivity and tumor grade. In the present study a trend for association of bcl-2 with high-grade prostatic carcinoma in comparison to low-grade (P = 0.06) was found. This was consistent with the previous study by Stattin *et al*. (1997) who showed that bcl-2 expression tended to be higer in high-grade tumors. These results suggest that expression of this anti-apoptotic marker increases during progression of prostatic cancer, a finding that may be relevant to the hormone insensitive phenotype of most advanced adenocarcinoma of prostate (Figure 33.1).

Over-expression of C-erbB-2 protein has been demonstrated in a wide range of human adenocarcinomas orginating in different organs. It was mentioned that this protein is closely related, but yet different, to EGF-receptor encoded by the C-erbB-2 proto-oncogene (Dougall *et al*., 1994). In the present study, there was similarity between low-grade PIN and BPH concerning the pattern, distribution, and intensity of C-erbB-2 immunostaining. Basal cell immunostaining and membranous pattern were frequently observed in both lesions (BPH and low-grade PIN). A similar predominance of basal cell staining has been mentioned in a previous report (Kamoi *et al*., 2000) which indicated localized EGF receptor to the basal cells of BPH. In a further study, it was stated that immunostaining for C-erbB-2 in benign glands was the strongest in basal cells, while it was typically absent or weak in the luminal cells, and the expression was localized to cell membranes. Although the function of prostatic basal cells is unknown, it has been proposed that basal cells give rise to secretory epithelial cells and function as stem cells (Myers *et al*., 1994). The proliferative potential of basal cells and their expression of various growth factor receptors and protooncogene products are consistent with this hypothesis. In our study, moderate immunostaining for C-erbB-2 oncoprotein was observed within the cytoplasm and in the membranes of luminal cells of high-grade PIN and PCs. The cytoplasmic staining in prostate was more coarse than the pattern observed in breast tumors. In the prostate, pure membrane staining was unusual without concomitant cytoplasmic staining. The biological significance of cytoplasmic C-erbB-2 in malignant cells as observed by us and others (Myers *et al*., 1994) remains unknown. Thus, our findings demonstrate similarity in the expression of C-erbB-2 oncoprotein among high-grade PIN and PCs. These findings are consistent with previous reports (Harper *et al*., 1998; Myers *et al*., 1994). In another report, no differences in the three dimensional nuclear size were found between high-grade PIN and prostatic adenocarcinoma (Lopez Beltran *et al*., 2000), and this supports high-grade PIN as a precursor of prostatic adenocarcinoma (Figure 33.2).

Prostatic glands contain heavy metals such as zinc and cadmium, and epidemiological studies showed that both metals have been associated with prostate cancer development. Metallothionein is a low-molecular weight cystein-rich protein, which has the ability to bind and sequestrate heavy metal ions. Its synthesis is induced in a variety of tissues by these metal ions, as well as by endogenous factors such as glucocorticoids, interferon, interleukin-1, and vitamin D. Several lines

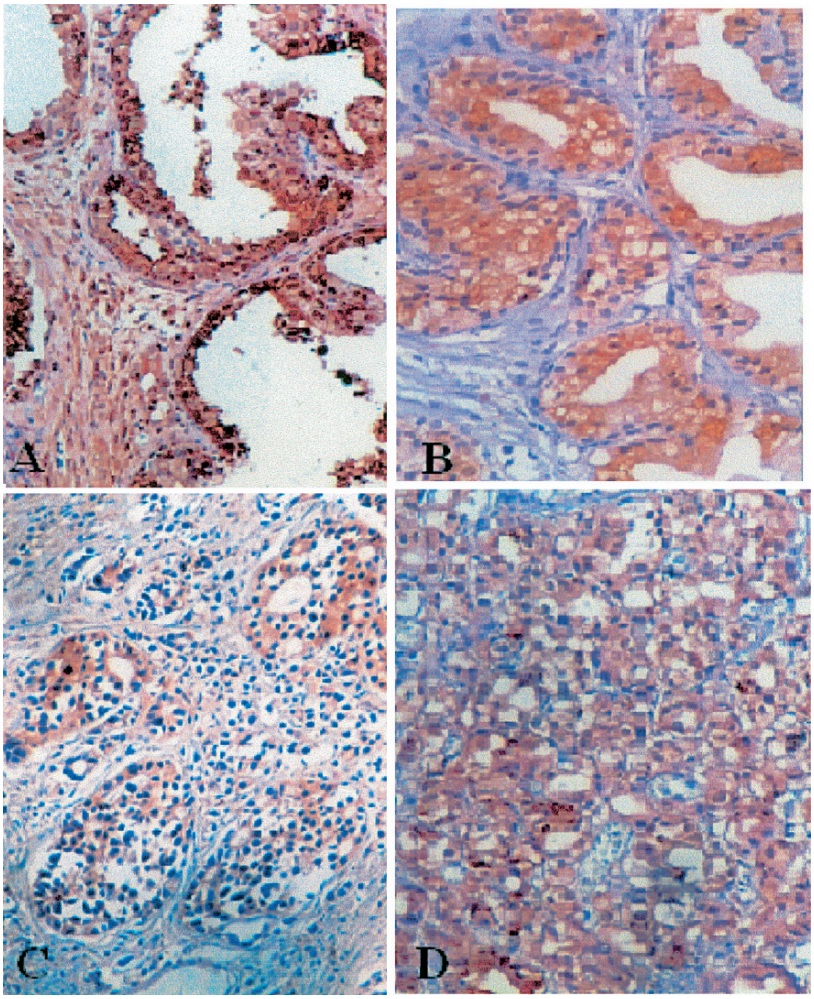

FIGURE 33.1. Bcl-2 immunoreactivity in low-grade (A), and high-grade prostatic intraepithelial neoplasia (B); moderate-grade (C), and high-grade prostatic carcinoma (D). (Immunohistochemical stain X200.)

of evidence have indicated that MT may play a role in carcinogenesis and in drug resistance of tumors (Surowiak *et al*., 2004). A few previous studies have evaluated MT expression in prostatic lesions with conflicting results. The present study aimed to study the expression of MT in benign prostatic hyperplasia (BPH), PIN, and prostatic carcinoma (PC) to evaluate its role in prostatic carcinogenesis. Also, MT expression was correlated with histologic grade of prostatic carcinoma to study its usefulness as an indicator of aggressive behavior of the tumors. In the present study, normal and benign prostatic tissue showed patchy MT staining of epithelial cells. In addition, MT was increased in PIN and further increased in a highly variable fashion in PC. These results were in concordance with the studies by Moussa *et al*. (1997) and Zhang *et al*. (2000). Metallothionein expression was observed in 66.7% of PC. This

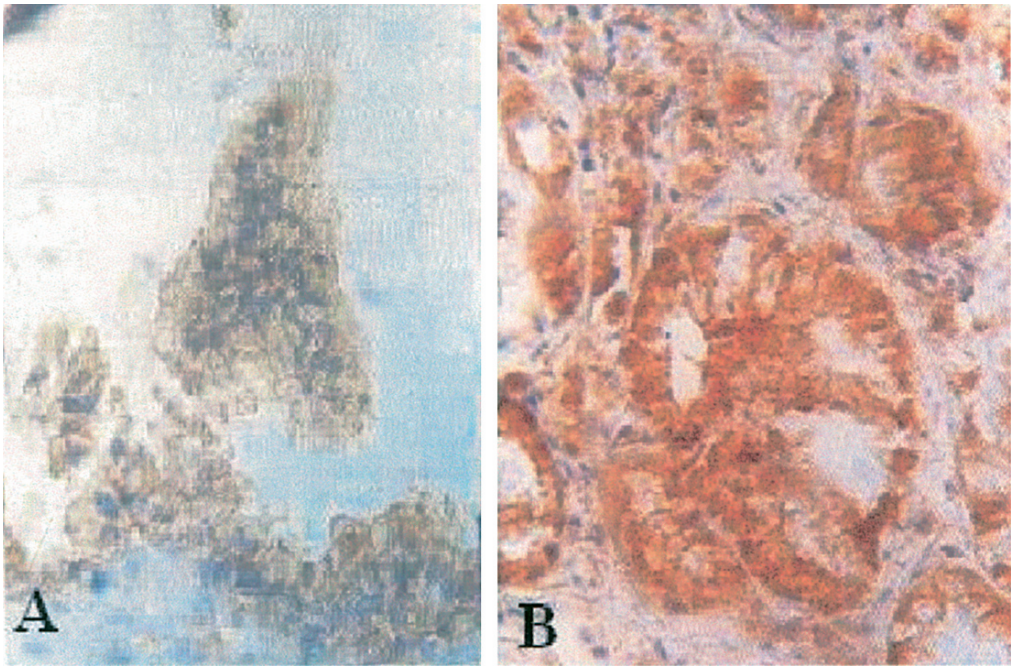

FIGURE 33.2. Immunohistochemical staining of C-erb-2 oncoprotein in low-grade Prostatic intraepithelial neoplasia showing weak and predominant membranous staining in both basal and luminal cells (A), and moderate-grade prostatic carcinoma revealing predominant cytoplasmic staining pattern (B). (Immunohistochemical stain X400.)

result is higher than that shown by Zhang *et al*. (2000) in which MT was expressed in 33.3% only of PC cases. In contrast, Moussa *et al*. (1997) showed that all tumor foci were positively stained for MT. These conflicting results may be explained by the differences in antibodies, methods, and/or interpretation of immunostaining results. Regarding the staining pattern, similar to previous findings by Moussa *et al*. (1997), most cancer cells revealed cytoplasmic and nuclear staining. Although MT is thought to be a cytoplasmic protein, many studies suggest that MT is present in the cytoplasm and nucleus of normal and malignant cells. It is known that subcellular localization of MT is regulated in cells undergoing proliferation, developmental progression, tumorigenesis, and during the cell cycle (Ogra and Suzuki, 2000). In the present study, only 17% of PIN and 25% of PC cases showed positive staining of the basement membrane surrounding the cancer cells; this was in agreement with the study by Zhang *et al*. (2000) where 2 out of 15 cases of PC showed the same finding. It is well known that the glandular epithelial cells (normal cells, particularly the basal cells, or malignant cells) may participate in biosynthesis of the basement membrane. Consequently, this phenomenon may be regarded as an actively secretory result of the cancer cells (Zhang *et al*., 2000). A close correlation of MT expression and high tumor grade and poor prognosis in invasive breast carcinoma and bladder carcinoma has been reported (Zhang *et al*., 2000; Surowiak

et al., 2004). In these studies MT expression was significantly correlated with the histologic grading of PC where its expression increased from low to moderate to high-grade tumors. These results were in accordance with the studies by Zhang *et al*. (2000) and Dutta *et al*. (2002). It was also found that the proportion of positively stained cells significantly correlated with histologic grade of PC. With regard to MT staining intensity in the present study, the epithelial cells were lacking uniformity in immunoreaction where some stained strongly while others stained weakly, and the percentage of strongly stained cells increased from low to high grade PC. This was in agreement with the study by Suzuki *et al*. (1992). Generally, it is believed that anaplastic and aggressive tumors with more cellular metabolic activity may have greater zinc and metallothionein requirements. Therefore, this wide range of lacking uniformity of MT expression may result from changes in zinc or cadmium metallothionein in prostate cancer (Figure 33.3).

DNA ploidy in prostatic carcinoma has been extensively studied and has been found to provide prognostic information independent of histopathologic grade and tumor stage. In the present study, all cases of high grade PIN and 83% of prostatic carcinoma were aneuploid. Previous study showed that aneuploidy can be acquired at preinvasive stage of carcinogenesis in the prostate, and suggested that aneuploid high-grade PIN might be regarded as a precursor of some but not all aneuploid prostatic carcinomas. In the present study it was found that tumor aneuploidy was significantly associated with histologic grades of prostatic carcinoma on comparing low-grade versus high-grade tumors. This is consistent with previous studies which found that tumor aneuploidy, as determined by image or flow cytometry, was correlated both with a higher Gleason score and local and distant spread. However, there is still no agreement as to whether this technique provides independent information (Leiber *et al*., 1995). The Karolinska Institute authors believe that the controversy related to its use is largely related to methodological inadequacies (Leiber, 1993).

Nuclear and nucleolar areas as well as AgNOR counts supplement histologic grading in the prognostic assessment of prostate carcinoma in patients receiving only hormone therapy. AgNOR count also is a prognostic factor for patients with intermediate grade tumors. The combination of histologic grade and proliferative activity allows the stratification of patients into low and high risk groups (Chiusa *et al*., 1997). The grading of PIN has been previously defined (McNeal and Bostwick, 1986), and the WHO grading system for PCs (Mostofi *et al*., 1986) takes nuclear features into account; the total number of AgNORs has been shown to correlate with other methods of analysis of cellular proliferative activity and ploidy such as Ki-67 immunostaining and DNA flow cytometry in breast carcinoma. Also, nuclear DNA ploidy status and AgNORs have been used to predict the biological behavior of prostatic adenocarcinoma (Murad *et al*., 1996). In the present, study we applied the one-step silver nitrate method as previously described (Smith and Veldhu, 1989), to prostatic lesions. We observed a significant difference in AgNORs counts per nucleus, among BPH, PIN, and PCs; this finding is consistent with the studies by other authors (Gillen *et al*., 1990; Hansen and Ostergard

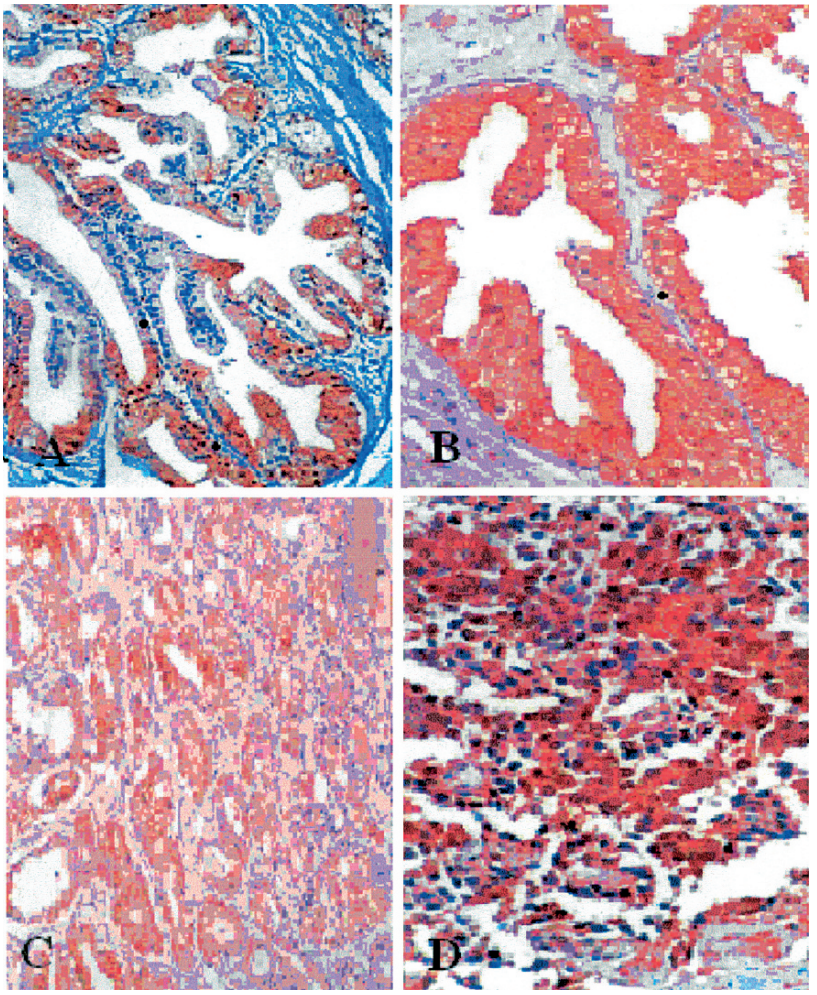

FIGURE 33.3. Immunohistochemical staining of metallothionein in benign prostaic hyperplasia showing patchy cytoplasmic staining (A), prostatic intraepithelial neoplasia revealing diffuse cytoplasmic and focal membranous staining (B), low-grade prostatic carcinoma revealing cytoplasmic staining which lacks uniformity of staining intensity (C), and high-grade prostatic carcinoma showing cytoplasmic staining with high proportion of strongly stained cells (D). (Immunohistochemical stain X300.)

1990). They stated that NORs have prognostic significance in PCs, and found that NORs were significantly increased in malignant prostatic tissue compared to benign tissues. NORs were significantly increased in patients destined to develop metastases. They concluded that AgNORs may be useful as a predictor of disease outcome. Other studies have also reported that AgNOR analysis revealed low values in BPH, moderate values in low-grade carcinomas and high values in PIN as well as high grade carcinomas (Mukherjee *et al*., 1997). The similarities of AgNOR analysis between PIN and high grade carcinomas support the idea that PIN is the precursor of the peripheral prostatic carcinoma. However, in contrast to previous studies,

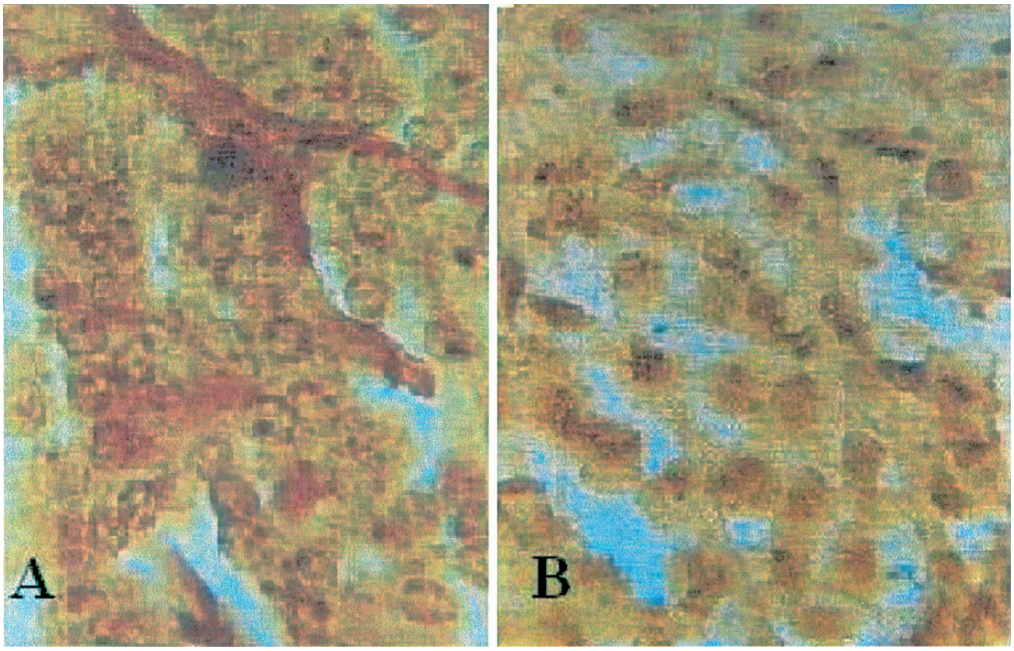

FIGURE 33.4. (A) Low-grade prostatic carcinoma showing type C2 (medium sized coarse to semisolid AgNORs in the nucleoli. (B) High-grade prostatic carcinoma revealing type B2 and scattered satellite AgNORs. (Silver stain X1000.)

others (Cheville *et al.*, 1990) found no significant difference in AgNORs counts in BPH, PIN, and PCs. They concluded that AgNORs counts are of no use in differentiation of these lesions. In our study we also concluded that AgNORs counts are of no use in diagnosis. We applied the typing system as previously proposed (Hansen and Ostergard, 1990). This typing system includes two important features of AgNORs, namely the size as previously pointed out (Ooms and Veldhu, 1989) and the degree of nucleolar disaggregation as stressed in other previous reports (Crocker and Nar, 1987). Satellite AgNORs predominated in BPH, while medium-sized nucleoli with granular AgNORs predominated in PIN lesions. Large nucleoli with granular AgNORs were more frequently seen in PCs. It is concluded that quantitative typing of AgNORs may contribute to the differential diagnosis between benign and malignant prostatic lesions (Figure 33.4).

From our study, overexpression of bcl-2, MT, and C-erbB-2 in high-grade PIN may suggest an association with early prostate tumorigenesis. The significant correlation of their expression with high-grade prostatic carcinoma suggests that they may contribute to tumor cell progression. Also, the finding of high-grade prostatic intraepithelial neoplasia in a biopsy without prostate cancer warrants repeated biopsy because of the risk of concurrent cancer. In addition, qualitative typing of AgNORs may contribute to the differential diagnosis between benign and malignant prostatic lesions, but this needs further analysis. As the number of potential molecular markers

increases, it is becoming evident that no single marker will provide the prognostic information necessary to make a significant improvement in patient care.

REFERENCES

Baltaci, S., Orhan, D., Ozer, G., Tounary, O., and Gegous, O. 2000. Bcl-2 proto-oncogen expression in low and high-grade prostatic intraepithelial neoplasia. *B. J. U. Int., 85*: 155–159.

Berman, D.M., Yang, J., Epstein, J.I. 2000. Foamy gland high-grade prostatic intraepithelial neoplasia. *Am. J. Surg. Pathol. 24*: 140–144.

Bonkhoff, H., Fixemer, T., and Remberger, K. 1998. Relation between bcl-2, cell proliferation and the androgen receptor status in prostatic tissue and precursors of prostate cancer. *Prostate 34*: 251–258.

Bostwick, D.G., Amin, M.B., and Dundore, P. 1993. Architectural patterns of high-grade prostatic intraepithelial neoplasia. *Hum. Pathol. 24*: 298–310.

Calvo, A., Xiao, N., Kang, J., Best, C.J., Leiva, I., Emmert-Buck, M.R., Jorcyk, C., and Green, J.E. 2003. Alterations in gene expression profiles during prostate cancer progression. *Cancer Res. 62*: 5325–5335.

Cheville, J.C., Clanon, G.H., and Robinson, R.H. 1990. Silver-stained nucleolar organizer regions in the differentiation of prostatic hyperplasia, intraepithelial neoplasia and adenocarcinoma. *Mod. Pathol. 3*: 596–600.

Chiusa, L., Galliano, D., Formiconi, A., Di Primio, O., and Pich, A. 1997. High and low risk prostate carcinoma determined by histologic grade and proliferative activity. *Cancer 79*: 1956–1963.

Crocker, J., and Nar, P. 1987. Nucleolar organizer regions in lymphoma. *J. Pathol. 151*: 111–118.

Danque, P.O., Chen, H.B., Patil, J., Jagirdar, J., Orsatti, G., and Paronetto, F. 1993. Image analysis versus flow cytometry for DNA ploidy quantitation of solid tumors: a comparison of six methods of sample preparation. *Mod. Pathol. 6*: 270–275.

Dougall, W.C., Qian, X., and Peterrrson, N.C. 1994. The neu-oncogene, signal transduction pathways, transformation mechanisms and envolving therapies. *Oncogene 9*: 2109– 2123.

Dutta, R., Sens, D.A., Somji S., Sens, M.A., and Garrett, S.H. 2002. Metallothionein isoform 3 expression inhibits cell growth and increases drug resistance of PC-3 prostate cancer cells. *Prostate 52*: 89–97.

Falkmer, U.C. 1993. Methodologic sources of errors in image and flow cytometric DNA assessments of the malignancy potential of prostatic carcinoma. *Hum. Pathol. 23*: 360–367.

Gillen, P., Grace, P.A., and Dervan, P. 1990. Nucleolar organizer regions as predictors of outcome in prostatic carcinoma. *World J. Urol. 8*: 175–178.

Gleason, D.F. 1977. Histological grading and clinical staging of prostatic carcinoma. In: *Urologic Pathology: The Prostate*. Edited by M. Tannenbaum. Philadelphia, PA: Lea & Febiger, Chapter 9, pp. 171–198.

Hansen, A.B., and Ostergard, B. 1990. Nucleolar organizer regions in hyperplastic and neoplastic prostatic tissue. *Virchiv A. pathol. Anat. 417*: 9–13.

Harper, M.E., Glynne-Jones, E., Goddard, L., Mathewa, P., and Nicholson, R.I. 1998. Expression of androgen receptor growth factors in premalignant lesions of the prostate. *J. Pathol. 186*: 169–177.

Kamoi, K., Tronosco, P., and Babaian, R.J. 2000. Strategy for repeat biopsy in patients with high grade prostatic intraepithelial neoplasia. *J. Urol. 163*: 819–823.

Kaur, P., Kallakury, B.V.S., Sheehan, C.E., Fisher, H.A.G., Kaufman, R.P., and Ross, J.S. 2004. Survivin and bcl-2 expression in prostatic adenocarcinomas. *Arch. Pathol. Lab. Med. 128*: 39–43.

Leiber, M.M., Murtaugh, P.A., Farrow, G.M., Myers, R.P., and Plute, M.L. 1995: DNA ploidy and surgically treated prostate cancer. Important independent association with prognosis for patients with prostate carcinoma treated by radical prostatectomy. *Cancer 75*: 1935–1943.

Leiber, U.G. 1993. Methodologic sources of errors in image and flow cytometric DNA assessments of the malignancy potential of prostatic carcinoma. *Hum. Pathol. 23*: 360–367.

Lopez Beltran, A., Artacho Perula, F., Roldan Villa Lobos, R., and Lugue Barona, R. 2000. Nuclear volume estimates in prostatic intraepithelial neoplasia. *Anal. Cytol. Histol. 22*: 37–44.

Maffini, V.M., Ortega, H.H., Stoker, C., Giardina, R.H., Luque, E.H., and Munoz da toro, M.M. 2001. Bcl-2 correlation with ploidy and nuclear morphology in early stage prostate carcinoma. *Pathol. Res. Pract. 197*: 487–492.

McNeal, J.E., and Bostwick, D.G. 1986. Intraductal dysplasia: a premalignant lesion of the prostate. *Hum. Pathol. 17*: 64–71.

Montironi, R., Mazzucchelli, R., Scarpelli, M., Lopez-Beltran, A., and Mikuz, G. 2005. Prostate carcinoma I: prognostic factors in radical prostatectomy specimens and pelvic lymph nodes. *BJU. Int. 97*: 485–491.

Mostofi, F.K., Sesterhenn, I., and Sobin, L.H. 1986. Histological typing of prostate tumours. In: *The International Histological Classification of Tumours, No. 22*. World Health Organization, Geneva.

Moussa, M., Kloth, D., Peers, G., Cherian, M.G., Frei, J.V., and Chin, J.L. 1997. Metallothionein expression in prostatic carcinoma: correlation with Gleason grade, pathologic state, DNA content and serum level of prostate-specific antigen. *Clin. Invest. Med. 20*: 371–380.

Mukherjee, J., Misra, V., Gupta, A.K., and Tandon, S.P. 1997. Argyrophilic nucleolar organizer regions in atypical adenomatous hyperplasia, prostatic intraepithelial neoplasia and prostatic neoplasms. *Urol. Int. 58*: 75–79.

Murad, M., El-Hosseiny, S., Anwar, M., Mosaad, M., Tharwat, W., and Eissa, S. 1996. Value of histologic grading DNA ploidy status and nucleolar organizer regions (AgNORs) count in predicting the biologic behaviour of prostatic adenocarcinoma. *J. of Egyptian Nat. Cancer Inst. 8*: 89–96.

Myers, R.B., Srivastava, S., Oelschlager, D.K., and Grizzle, W.E. 1994. Expression of P 160^{erbB-3} and P 185^{erbB-2} in prostatic intraepithelial neoplasia and prostatic adenocarcinoma. *J. Nat. Cancer Inst. 86*: 1140–1145.

Ogra, Y., and Suzuki, K.T. 2000. Nuclear trafficking of metallothionein; possible mechanisms and current knowledge. *Cell. Mol. Biol. 46*: 357–364.

Ooms, E.C.M., and Veldhu, R.W. 1989. Argyrophilic proteins of nucleolar organizer regions in bladder tumours. *Virchows Arch. (A) 414*: 365–369.

Orsea, S.C., Tomasi, V.H., Schwint, A.E., and Itoiz, M.E. 2001. Modified silver staining of nucleolar organizer regions to improve the accuracy of image analysis. *Biotech. Histochem. 16*: 67–73.

Pollack, D.J., Grignon, K.H., Heydon, E.H., Hammond, C.A., Lawton, J.B., Mesic, K.K., Fu, A.T., Porter, R.A., and Abrams, W.U. 2003. Prostate cancer DNA ploidy and response to salvage hormone therapy after radiotherapy with or without short-term total androgen blockade. *J. Clin. Oncol. 21*: 1238–1248.

Punglia, R.S., D'Amico, A.V., Catalona, W.J., Roehl, K.A., and Kuntz, K.M. 2006. Impact of age, benign prostate hyperplasia and cancer on PSA level. *Cancer 106*: 1507–1513.

Rosaria, R.M., Gianni, A., Alessandro, V., Francesca C., Rossi, D., Gianna, B., Milena, P., and Luigi T.G. 2006. HER-2/neu and bcl-2 in ovarian carcinoma: clinicopathologic, immunohistochemical, and molecular study in patients with shorter and longer survival. *Appl. Immunohistochem. Mol. Morphol. 14*: 181–186.

Smith, E.C.M., and Veldhu, R.W. 1989. Argyrophilic proteins of the nucleolar regions in bladder tumours. *Virchows Arch. (A) 414*: 365–369.

Somji, S., Sens, M.A., Lam, D.L., Garrett, S.H., and Sens, D.A. 2001. Metallothionein isoform 1 and 2 gene expression in the human bladder: evidence for upregulation of MT-1X Mrna in bladder cancer. *Cancer Detect. Preven. 25*: 62–75.

Stattin, P., Damber, J.E., Kalbrg, L., Nordgren, H., and Bergh, A. 1997. Bcl-2 immunoreactivity in prostate tumorigenesis in relation to prostatic intraepithelial neoplasia, grade, hormonal status, metastatic growth and survival. *Urol. Res. 24*: 257–264.

Surowiak, P., Paluchowski, P., Wysocka, T., Wojnar, A., and Zabel, M. 2004. Receptor status, proliferation and metallothionein expression in primary invasive ductal breast cancers. *Pathol. Oncol. Res. 10*: 207–211.

Suzuki, T., Yamanaka, H., Nakajima, K., Suzuki, K., Kanatani, K., Kimura, M., Ohma, C., and Otaki, N. 1992. Immunohistochemical study of metallothionein in human seminal vesicles. *Tohoku J. Exp. Med. 167*: 127–134.

Utrilla, J.C., Lacave, J.M., and San Martin, M.V. 1999. Expression of C-erbB-2 oncoprotein in thyroid tumours. *Histopathology 34*: 60–65.

Xiang-Hua, X.H., Li, J., and Ikumasa, T. 1996. Immunohistochemical localization of metallothionein in human prostate cancer. *J. Urol. 156*: 1679–1681.

Zhang, R., Zhang, H., Wei, H., and Luo, X. 2000. Expression of metallothionein in invasive ductal breast cancer in relation to prognosis. *J. Environ. Pathol. Toxicol. Oncol. 19*: 95–97.

34
Prostate Cancer: Detection of Free Tumor-Specific DNA in Blood and Bone Marrow

Heidi Schwarzenbach and Klaus Pantel

INTRODUCTION

Prostate carcinoma is one of the most frequently diagnosed cancer types in men. If diagnosed at an early stage, prostate cancer is usually treatable. For a patient with a clinically localized tumor, the primary treatment alternatives are surgery and radiotherapy. Conversely, if this cancer entity is identified at a late stage and metastases are identified, complete remissions are rare by the current medical therapies. To identify prostate cancer, Gleason grading score, serum markers, and clinical staging are important factors which are related to tumor volume, zonal origin of the tumor, and spread into the gland and surrounding tissues. Diagnostic standard tools, such as the measurement of prostate-specific antigen (PSA) and standard transrectal ultrasound-guided biopsies, lack sufficient specificity and sensitivity for detection of all prostate cancer cases, and therefore, every fourth prostate tumor remains undiagnosed. In particular, a rise of PSA level in blood is not specific enough to distinguish between malignant and benign lesions including benign prostatic hypertrophy (BPH) and prostatitis. A low PSA value does not guarantee a disease-free outcome, and an elevated value is frequently associated with negative biopsies (Algaba *et al*., 2007).

Thus, better markers are urgently needed. In this context, the detection and characterization of cell-free DNA in the peripheral blood from tumor patients have attracted great interest in biomedical research. During the past ten years, more than a hundred articles on quantification of circulating blood DNA derived from patients with various tumor entities and the analysis of its genetic and epigenetic pattern have been published (Fleischhacker and Schmidt, 2007). Until now, only few studies have been conducted to explore the diagnostic value of cell-free DNA in relationship to prostate cancer. However, the presence of elevated cell-free DNA concentrations could also be confirmed in blood from prostate cancer patients (Chun *et al*., 2006; Hanley *et al*., 2006). Additionally, the size distribution of circulating DNA in blood from these patients was measured (Boddy *et al*., 2006). Recent research data on genetic and epigenetic alterations of the extracelluar blood DNA emphasize the utility of this new noninvasive approach as a diagnostic tool for prostate cancer.

GENETICS AND EPIGENETICS OF PROSTATE TUMORS

The broad application of cytogenetic and molecular genetic methods has led to the identification of numerous tumor-associated chromosomal regions playing a role in the tumorigenesis of prostate cancer. The development of prostate cancer is associated with such genetic and epigenetic alterations accumulating during tumor growth and disease progression.

Altered gene expression levels in neoplastic cells relative to their normal, non-transformed counterparts were identified in these tumors. DNA alterations of numerous chromosomal regions and down-regulation of genes coding molecules involved in cell adhesion, cell cycle or apoptosis, are associated with prostate progression (Saric *et al*., 1999). Allele typing and CGH (comparative genomic hybridization) analyses have detected DNA deletions at diverse chromosomal loci to be of importance in prostate cancer initiation and progression, and may contribute to understanding and treatment of prostate carcinomas (Yano *et al*., 2004). Allele typing studies applying microsatellite analysis were able to confirm the results obtained from CGH analyses and further delineated the tumor-associated regions. Cell biological studies on introduction of chromosomal DNA with deleted regions of tumor suppressor genes into a cell line have demonstrated that the lacking regions contain genes playing a substantial role in tumor growth and disease progression of prostate cancer. The systematic use of microcell hybrid clones has identified a number of chromosomal regions which are important for the proliferation of prostate tumor cells (Sanchez *et al*., 1996). Significant stage-specific differences in frequency of allelic losses, such as LOH (loss of heterozygosity), were shown to specify genetic loci involved in early and late stages of prostate carcinogenesis. Incidences of LOH were progressively higher in metastatic lesions than primary prostate tumors (Saric *et al*., 1999). Extensive studies on genetic alterations have shown that allelic losses as well as microsatellite instability (MSI) could be found at diverse chromosomal regions mapping to potential tumor suppressor genes, and are common events in the initiation, progression and metastasis of the prostate tumor.

Prostate carcinogenesis is not only characterized by the accumulation of genetic alterations but also by epigenetic aberrations. Modifications in DNA methylation appear early during the pathogenesis of prostate cancer, and because the nucleotide sequence remains intact, they may be therapeutically reversible. A panel of cancer-related genes inactivated by hypermethylation in prostate cancer has proven to be effective in the detection of prostate cancer (Costa *et al*., 2007).

LIMITATIONS OF USING TUMOR TISSUES FOR GENETIC AND EPIGENETIC ANALYSES

According to the noninvasive and rapid blood sample collection by simple venous puncture and the accumulation of cell-free DNA in blood, plasma or serum may be a convenient source for detection of tumor-specific DNA and have a benefit over tumor tissues. Another important feature is the possibility of taking repeated blood samples

during treatment to trace the changes in genetics and epigenetic of the tumor.

Prostate tumors often arise multifocally and each focal area may harbor various genetic and epigenetic alterations. To obtain general information on these alterations accompanied by tumor growth, demanding examination of several areas of the microdissected tumor tissues have to be carried out. Because free DNA is supposed to be released into the blood circulation by apoptotic and necrotic cells of the primary tumor early during tumorigenesis, blood may constitute an ideal reservoir of differently altered tumor-specific DNA derived from various sources, amongst others from heterogenous areas of the primary tumor. Furthermore, to avoid contaminations with stromal cells, which may mask tumor-specific allelic losses, microdissection of tumor material has to be performed, which is often laborious and time-consuming.

Archival formalin-fixed, paraffin-embedded tumor blocks contain frequently low yields of actually amplifiable DNA leading to false-positive data and causing a poor reproducibility of genetic alterations in repeated experiments (Farrand *et al*., 2002). Among these factors, leading to ineffective amplification, DNA degradation and PCR inhibitors have been mentioned. Usually, the amount of DNA obtained from microdissected tumor tissues has been limited which makes it difficult to analyze several aberrations using the currently available clinical material and with some combinations of primer sets binding to different tumor suppressor genes. This, however, is of importance considering that allelic imbalances and DNA methylation of various tumor suppressor genes accumulate during tumorigenesis.

HISTORY OF DETECTION OF CIRCULATING DNA IN BLOOD

In the year 1948, Mandel and Métais (1948) described the presence of extracellular nucleic acids in the human blood circulation for the first time. At that time the occurrence of cell-free DNA in blood attracted little attention in the scientific community. It went largely unnoticed until nearly two decades later when infectious DNA from the tumor-inducing polyoma virus and pneumococcal-transforming DNA in their biologically active form could be recovered in blood from mice after intraperitoneal injection. In light of these observations, Bendich *et al*. (1965) suggested that the metastatic spread of cancer may be determind by the circulation of tumor-associated DNA in the bloodstream. In the following year, Tan *et al*. (1966) detected DNA in serum from patients with systemic lupus erythematosus using antibodies to DNA. They reported that DNA was of endogenous origin because DNA could be found in serum from diseases associated with tissue destruction, hepatitis, metastatic carcinoma, and miliary tuberculosis.

Approximately ten years later a radioimmunoassay for the measurement of the content of DNA in blood was developed. The level of cell-free DNA in the serum of patients with various types of cancer and in healthy individuals was determined. Normal controls and cancer patients had DNA concentrations of a mean of 13 and 180 ng/ml, respectively (Leon *et al*., 1977). Significantly higher DNA levels were found in the serum of patients with metastatic disease. The end of the 1980s was designated by the isolation and

characterization of the extracellular DNA. Stroun *et al*. (1987, 1989), intensively engaged in these investigations, proposed correlations between presence of DNA in serum from tumor patients and malignancy of their disease. Based on the absence of serum DNA in healthy controls they found that plasma DNA fragments may originate from cancer cells. However, until now, the origin of circulating nucleic acids in blood is not fully clarified. In general, it is accepted that free extracellular DNA enters the blood circulation either actively by tumor cells or passively by necrotic and apoptotic cells (Jahr *et al*., 2001).

In 1994, the importance of circulating nucleic acids was recognized, when the occurrences of mutated K-ras molecules in blood from patients with pancreatic cancer and N-ras gene mutations in patients with myelodysplastic syndrome were described (Sorenson *et al*., 1994; Vasioukhin *et al*., 1994). From that time, the study of cell-free nucleic acids has become a rapidly developing field of research, and at last it has gained the interest of a wide scientific community. Numerous publications have reported the presence of tumor-specific DNA in the blood of patients with different tumor entities, such as lung, head and neck, colon, breast, and prostate carcinomas (reviewed by Fleischhacker and Schmidt, 2007).

Concordance and discordance between the genetic aberrations of the primary tumor and the alterations of the circulating DNA were detected by several groups (Fleischhacker and Schmidt, 2007). However, numerous studies indicated that the DNA aberrations (e.g., LOH and MSI) found in the plasma DNA corresponded to the alterations detected in the analogous microdissected tumor tissue from the same patients (Fleischhacker and Schmidt, 2007). Surprisingly, genetic alterations in patients with small and *in situ* lesions could even be discovered, indicating that DNA is released early into the blood circulation during tumor development (Chen *et al*., 1999).

ELEVATED LEVELS OF CELL-FREE NUCLEIC ACIDS IN PROSTATE CANCER PATIENTS

Measurements of cell-free DNA have been shown to have diagnostic potential in a number of malignant diseases. With respect to these studies dealing with nucleic acid levels in blood from patients with other tumor entities, measurements of cell-free DNA in blood from prostate cancer patients is an emerging area of research. Recent studies recommended elevated levels of circulating DNA to be a noninvasive approach also for early detection of prostate cancer.

In order to adapt cell-free DNA to a routine clinical laboratory test, Allen *et al*. (2004) quantified plasma DNA using real-time quantitative PCR and the beta-globin gene as a template, and reported that quantification of cell-free DNA may have an important diagnostic role in distinguishing malignant from benign prostate disease. Their measurements in genome equivalents (GE) showed that prior to biopsy, the plasma DNA concentration in BPH patients was 936 GE/ml while cancer and prostatic intraepithelial neoplasia (PIN) patients had significantly higher levels of DNA at 1,734 GE/ml and 1,780 GE/ml, respectively. Comparison of plasma DNA concentrations before and

after biopsy showed that 60 min after biopsy the values were significantly higher in both BPH (1,494 GE/ml) and cancer patients (2,758 GE/ml).

The study by Chun *et al.* (2006) investigated whether preoperative plasma levels of cell-free DNA can discriminate between men with localized prostate cancer and BPH. In this report the median plasma DNA concentrations were 267 ng/ml and 709 ng/ml in blood from BPH and prostate cancer patients, respectively. The data underlined plasma DNA levels as highly accurate and informative predictors in uni- and multivariate models for the presence of prostate cancer on needle biopsy.

However, the investigation by Jung *et al.* (2004) comparing the plasma DNA concentrations in patients with different prostate cancer stages and BPH, as well as in healthy persons showed that plasma DNA had limited validity as a tumor marker. Increased plasma DNA levels were found in patients with lymph node and distant metastases and also in BPH patients, whereas men with localized cancer had plasma DNA concentrations within the reference interval. The association between plasma DNA and the survival time was similarly strong as with PSA. Moreover, Wu *et al.* (2002) employing the commonly used QIAamp blood kit (Qiagen) for DNA extraction and the PicoGreen DNA kit for DNA quantification found no correlation between serum cell-free DNA and serum levels of PSA in random specimens from prostate cancer patients. In addition, no correlation between the levels of cell-free DNA and dominant tumor markers except at low concentrations could be observed. The concentration of cell-free DNA also did not increase further with the increase of tumor marker concentration (Wu *et al.*, 2002).

Besides measurements of the total cell-free DNA, the portion of plasma mitochondrial nucleic acids can also be determined. Their quantification by real-time amplification may be used to recognize patients with a poor prognosis. In advanced prostate cancer patients, circulating mitochondrial RNA seems to be the strongest predictor of overall survival and an independent prognostic factor for cancer-related death. Amplification of mitochondrial nucleic acids showed increased sensitivity and specificity over genomic DNA as diagnostic and prognostic marker in blood of prostate cancer patients (Mehra *et al.*, 2007).

Finally, the apoptosis index can be determined by real-time PCR using DNA fragments that biochemically characterize apoptosis and define other cell death entities as templates. Ellinger *et al.* (2007) reported that the apoptosis index was significantly increased in blood serum from prostate cancer patients versus BPH patients and healthy individuals. Concentrations of apoptotic DNA fragments discriminated sensitively and specifically between BPH and prostate cancer patients. A significant correlation between apoptotic DNA fragments or the apoptosis index and PSA recurrence following radical prostatectomy could be observed. These findings indicate that circulating DNA fragments derived from apoptotic origin and the apoptosis index may be promising serum biomarkers for the diagnosis and prognosis of prostate cancer.

Because bone marrow is a common site for prostate cancer recurrence, bone marrow may also provide a viable source for extracellular tumor-specific DNA. Our determinations of the DNA levels demonstrated that the mean concentration in bone

marrow (2,160 ng/ml) was twice higher than that in blood from prostate cancer patients (1,104 ng/ml). The origin of cell-free DNA in bone marrow aspirates is unknown. However, they may presumably consist of DNA derived from disseminated micrometastatic cells. Bone marrow is a frequent site of prostate cancer metastases and may serve as a homing site or reservoir for disseminating tumor cells (Pantel and Brakenhoff, 2004) which may release DNA.

Body fluids other than blood and bone marrow may also deliver circulating nucleic acids for diagnostic investigation. Consequently, urine could be such a source of cell-free DNA. However, molecular biological examination of urine samples can be difficult and exposed to problems such as the significant degradation of nucleic acids by the presence of DNases and RNases in such samples. To detect prostate cancer with greater specificity than PSA, a study tried to identify molecular markers in urine samples. Using the RT-PCR differential display method the group (Bai *et al*., 2007) detected differential expression of mRNA transcripts in urine and blood samples. They demonstrated the principle that specific cDNA probes of frequently differentially expressed mRNA transcripts can be used for the detection of prostate cancer in urine and blood samples.

PLASMA-BASED MICROSATELLITE ANALYSIS

In the tumorigenesis, genetic alterations play a crucial role of switching off the function of particular genes (loss of function) or eliciting new functions (gain of function). The loss of particular sequences coding for tumor suppressors can lead to the loss of a tumor-protective function of the appropriate gene product. For example, a missing or incorrect protein cannot continue its proliferation-inhibitory task any longer and contributes to tumor development. Moreover, such gene defects can have an influence on the cell cycle, as the cells do not enter the G0 phase or suppress the apoptotic cell death. LOH and MSI often occur in regions encoding for tumor suppressor proteins. These DNA losses arise either directly in the coding or regulatory regions or in the proximity of a gene and can then lead to loss of information and a potential aberrant cell growth. In general, analyses of LOH and MSI are performed by using microsatellite DNA.

Microsatellite DNA consists of short, highly-repetitive DNA sequences (2–6 base pairs), and usually occur as repetitions of di-, tri- or tetranucleotides, e.g. $(CA)_n$. They are different from minisatellite DNA, whose repetition units cover 15–70 base pairs. In the genome, microsatellites are widely spread and usually lie in noncoding regions (introns), seldom in exons. Microsatellite DNA in maternal and paternal chromosomes frequently differs in length. Due to the different number of their microsatellites both alleles of a gene can be separated by electrophoresis after amplification with specific primers. Furthermore, the nature of microsatellite DNA with its highly-repetitive sequences can cause an increased error rate during replication. The DNA polymerase can be overstrained by the copying of the repetitions of nucleotides, resulting in loss or gain of microsatellites. The size-dependent shift of the alleles can lead to additional bands during gel electrophoresis.

Despite the publications describing the potential of plasma-based microsatellite analysis to be a new diagnostic marker for various cancer entities, only our laboratory has conducted LOH on cell-free DNA in blood and bone marrow from prostate patients. To investigate the potential significance of genetic aberrations in this cancer type, allelic imbalances of circulating tumor-associated DNA in blood from patients with localized prostate cancer was identified and characterized using a panel of 15 polymorphic microsatellite markers mapping to known tumor suppressor genes. Comparative analyses were performed with a control group of patients with BPH. Besides the higher DNA concentration measured in the blood circulation of prostate cancer patients, LOH was more frequently recorded in the tumor patients (34%) than in BPH patients (22%). These findings indicate that microsatellite analysis using plasma DNA may be an implement for molecular screening of prostate cancer patients (Müller *et al*., 2006).

Genetic aberrations could not only be detected in blood but also in bone marrow plasma from cancer patients. For the first time, the publication of Taback *et al*. (2003) demonstrated tumor-related genetic markers in bone marrow aspirate plasma from early-stage breast cancer patients and provided an approach for assessing subclinical systemic disease progression and the monitoring of breast cancer patients. The subsequent report of Schwarzenbach *et al*. (2007) showed the presence of cell-free tumor-specific DNA in bone marrow of prostate cancer patients and its possible relationship to bone marrow micrometastasis. In this study the validity of allelic imbalance in bone marrow, peripheral blood, and tumor tissues of 57 prostate cancer patients was compared. Comparative analyses were performed with blood plasma of 27 BPH patients. Figure 34.1 shows a representative example of LOH in tumor tissue and bone marrow plasma from a prostate cancer patient. The LOH index (number of LOH of each patient divided by the informative cases) of the respective patients was significantly higher in primary tumors (72%) than in bone marrow (56%) and blood plasma (44%) samples and higher in bone marrow than

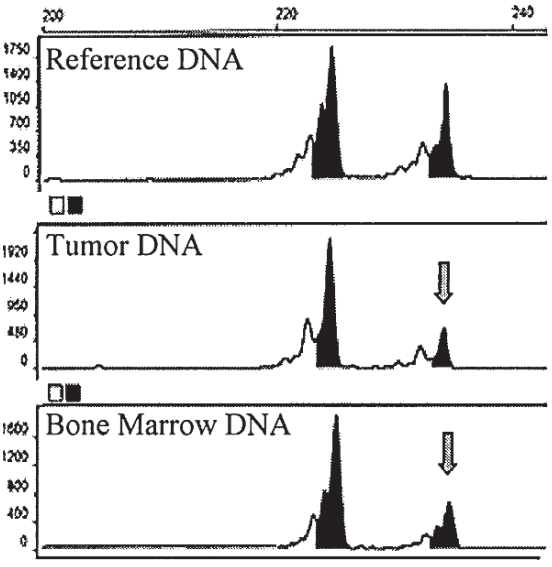

FIGURE 34.1. Example of LOH detected in tumor tissue and BM plasma from a prostate cancer patient.
The fluorescence-labeled PCR products of leukocytes, tumor and bone marrow plasma DNA were separated by capillary gel electrophoresis on a Genetic Analyzer and evaluated with the Gene Scan Analysis program. The abscissa indicates the length of the PCR product, while the ordinate gives information on the fluorescence intensity represented as peaks. The upper diagram shows the leukocytes DNA (reference) and the lower diagrams show tumor and bone marrow plasma DNA. In the lower diagrams the arrows refer to LOH. (Schwarzenbach et al., 2007.)

in blood plasma samples. Figure 34.2 shows the frequency of LOH at 15 different polymorphic microsatellite markers used as described in Table 34.1. The overall frequency of LOH in all analysis was higher in bone marrow plasma (11%) than in the paired blood samples (5%), suggesting that LOH on cell-free DNA may be masked by the prevalence of normal DNA in blood and that free tumor-specific DNA may accumulate in bone marrow of prostate cancer patients. Concordance of LOH identified in the tumor and blood samples was observed in 65% of the informative cases, whereas in 35% of the analyses LOHs were detected in the blood plasma samples but not in the paired tumor samples. LOHs which were identified in the bone marrow plasma samples could be retrieved in 55% of the paired tumor samples. The statistical evaluation of the LOH data revealed a correlation between increasing pathologic Gleason scores, the differentiation grade of the tumor, and LOH at the microsatellite marker D9S1748 in bone marrow and primary tumor. This chromosomal region

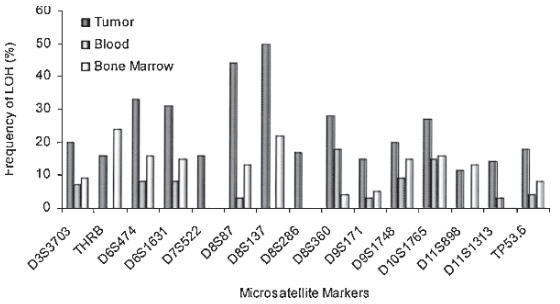

FIGURE 34.2. Comparison of the frequency of LOH at 15 different chromosomal markers detected in tumor tissues, blood and BM samples.
The frequency of LOH was calculated by division of the number of LOHs with the informative cases for each locus (Schwarzenbach et al., 2007).

TABLE 34.1. A selection of microsatellite markers.

Marker	Chromosomal locus	Tumor suppressor gene	PCR product (bp)
D3S1255	3p23	ARVD5 (arrhythmogenic right ventricular dysplasia 5)	156
D3S3703	3q13.3	n.i.	226–244
THRB	3p24	Thyroid hormone receptor ß	197
D6S474	6q21-22	BFD4	151–167
D6S1631	6q16	TAK 1 (Transforming growth factor ß aktivating kinase)	164–182
D7S522	7q31.1	Caveolin 1	217–229
D8S87	8p12	Neuregulin 1	145
D8S137	8p21.1	Dematin	150–162
D8S286	8q13	HNF-4γ	238
D8S360	8p21	n.i.	95
D9S171	9p21-22	CDKN2/p16	158–177
D9S1748	9p21	CDKN2/p16	130
D10S215	10q23	PTEN (phosphatase and tensin homolog)	188 bp
D10S1765	10q23.3	PTEN	166–184
D11S898	11q22	n.i.	140–156
D11S1313	11q12	n.i.	184–204
D13S218	13q12–14	ATOD5	187–195
D16S421	16q22-23	E-cadherin	206–216
D17S250	17q11.2-12	PNMT (phenylethanolamine-N-methyltransferase	151
D17S855	17q21	BRCA1	143
TP53.6	17p13.1	p53	107

n.i.: non identified.

encodes the tumor suppressor product CDKN2/p16, an inhibitor of the cyclin dependent kinase (CDKN2).

Because bone marrow is a major homing site for metastatic cells in prostate cancer (Pantel and Brakenhoff, 2004), the LOH profiles detected in bone marrow were correlated with the presence of disseminated tumor cells in bone marrow. Dissemination of tumor cells into the bone marrow was assessed by a Ficoll density gradient centrifugation and an immunocytological cytokeratin assay. Cytokeratins form a part of the cytoskeleton of epithelial cells, and are at present the most reliable markers for detection of disseminated tumor cells. The immunostaining of the disseminated tumor cells showed that the subset of prostate cancer patients with disseminated tumor cells in their bone marrow tended to have more LOH in their bone marrow than patients who harbored no tumor cells in their bone marrow, indicating that an increase in LOH on cell-free DNA in bone marrow plasma may be associated with the presence of disseminated tumor cells in bone marrow. It is conceivable that the free tumor-specific DNA in bone marrow could be related to the rate of turnover of the disseminated tumor cells, and that the free DNA might originate from both, the disseminated tumor cells and the primary tumor. From recent microarray studies, there is increasing evidence that the metastatic capacity of solid tumors is already determined early in the primary tumor (Pantel and Brakenhoff, 2004). This could explain at least in part the divergent results on the genetic profiles observed between bone marrow and primary tumors in the study (Schwarzenbach *et al*., 2007). The future investigations of the origin and role of cell-free DNA in bone marrow may provide additional insight into metastatic progression. Free DNA may also play an active role in this process because spontaneous passages of DNA from prokaryotic and eukaryotic cells to eukaryotic cells have been described (Anker *et al*., 1999).

PLASMA-BASED SINGLE NUCLEOTIDE POLYMORPHISM ANALYSIS

Conclusively, the low frequency of LOH usually detected in blood samples might also be caused by the limited sensitivity of the used microsatellite marker sets. Therefore, experiments are required to compare the incidence of LOH at the classical microsatellite markers exhibiting length polymorphism with the occurrence of LOH at the SNP (single nucleotide polymorphism) markers that only differ from each other at a single nucleotide using blood from prostate cancer patients. The SNP markers have recently been described to provide reliable and high quality data on a range of different DNA templates and to be suitable for detection of LOH in clinical tissue samples. Unfortunately, only very few reports have presented and compared allelotyping data on multiple chromosomal loci in the same tumor using SNP and microsatellite DNA. In the majority of the types of cancer analyzed in these studies the LOH patterns were concordant, lending validity to both methods (Zheng *et al*., 2005). A recent publication of Hata *et al*. (2006) assessed the accuracy of a fluorescent single-strand conformation polymorphism (SSCP) method for the quantification of SNP alleles, using DNA mixtures that were

composed of tumor and normal DNA at various ratios. The technique could precisely characterize LOH in glioma tumor tissue samples, suggesting that it is applicable to the genetic diagnosis of cancers different from gliomas. Presently, there are no studies on LOH at SNP markers on cell-free DNA in peripheral blood from prostate cancer patients. It might, therefore, be of interest to examine the potential of such markers for recovery of LOH in blood in future studies.

PCR-BASED FLUORESCENCE MICROSATELLITE AND SNP TECHNIQUE USING BLOOD AND BONE MARROW DNA

1. Preparation of plasma and leukocytes from whole blood:
   Centrifuge at 2,500 g for 10 min. The upper phase contains the cell-free blood plasma.
   For isolation of leukocytes supplement the remaining blood up to 50 ml with lysis buffer (0.3 M sucrose, 10 mM Tris-HCl pH 7.5, 5 mM MgCl2 and 1% Triton X100) and incubate for 15 min on ice, followed by two centrifugation steps at 2,500 g, 4°C for 20 min. The leukocyte DNA serves as reference DNA.
2. Preparation of bone marrow plasma:
   Centrifuge bone marrow at 400 g for 5 min. The supernatant contains the cell-free bone marrow plasma.
3. Fluorescence-labeled PCR:
   Amplify 10–20 ng of extracted template DNA with a Taq Gold DNA-Polymerase and primers binding to microsatellite (Table 34.1) or SNP regions. The sense primer is fluorescence-labeled at the 5′ end. Adequate primers can be selected from the public database NCBI. Microsatellites and SNP can be found under www.ncbi.nlm.nih.gov /UniSTS and /SNP, respectively.
4. Detection of the PCR products:
   The fluorescence-labeled PCR products can be separated by capillary gel electrophoresis and detected by a fluorescence laser on a Genetic Analyzer (Applied Biosystems). The 500-ROX size marker serves as an internal standard.
5. Analysis of LOH at microsatellite markers:
   The evaluation of the obtained peaks corresponding to both alleles is performed by the fragment analysis program. The incidence of LOH is calculated by division of the quotient of the peak intensity derived from blood, bone marrow plasma or tumor DNA by the quotient of the peak intensity derived from the matched leukocyte DNA (reference DNA). LOH is interpreted to be present when the intensity ratio of plasma sample alleles differed by > 40–50% from the reference DNA. MSI is defined by the occurrence of a number of additional peaks.
6. Analysis of LOH at SNP markers:
   Analysis is performed by DNA sequencing with additional consideration of the sequenced mixed bases.

LIMITATIONS OF THE BLOOD-BASED LOH ANALYSIS

Although similar plasma-/serum-based methods have been used, a great variability in detection of cell-free tumor-specific DNA

has been reported. Besides the described concordances between allelic imbalances in blood DNA and those in the matched primary tumors, discrepancies were also discovered (Fleischhacker and Schmidt, 2007). The contradictory microsatellite data derived from blood and tumor tissue were explained by PCR artifacts, which may be caused by the low prevalence of tumor-associated DNA in blood. The observation that tumor-associated blood DNA is diluted by normal DNA was discussed for different tumor entities.

Coulet *et al*. (2000) reported that the incidence of microsatellite alterations in the plasma DNA of head and neck squamous cell carcinomas was low and described sensitive mutation detection methods which allow a more precise interpretation of LOH. Moreover, Wang *et al*. (2003) suggested that circulating plasma DNA may not be an accurate reflection of the clinical status of breast tumor activity because the mean proportion of LOH was much lower than that in primary tumors. Diehl *et al*. (2005) revealed that the proportion of mutant APC (adenomatous polyposis coli) DNA fragments in plasma from patients with colorectal cancer was small, averaging only 11% of the total DNA fragments, even in large, metastatic cancers. They explained the low occurrence of the mutant DNA molecules in the plasma by the prevalence of *wild type* DNA fragments which are discharged from necrotic regions besides mutant DNA. These findings point out that apart from killing of neoplastic cells, necrosis may also cause death of the surrounding stromal and inflammatory cells. A model was suggested by these authors wherein hypoxia induces necrosis of tumors, leading to phagocytosis of tumor cells and the subsequent release of digested DNA into the blood circulation (Diehl *et al*., 2005).

The electrophoretic pattern of cell-free DNA showed that cell-free DNA from cancer patients may be fragmented and contains smaller DNA (100 bp) not found in normal cell-free DNA. One study (Wang *et al*., 2004) demonstrated that use of fragmented DNA enhanced the detection rate of circulating mutated k-*ras* DNA from colorectal cancer patients. To enhance assay sensitivity for detection of somatic mutations or epigenetic modifications in circulating DNA, the publication proposed that a method which can preferentially isolate small DNA molecules should be used. A further study measured the variation in length of soluble plasma DNA fragments by electron microscopy and indicated that a significant amount of this DNA is probably derived from apoptotic neoplastic and normal cells (Giacona *et al*., 1998). Moreover, abnormal proliferation of malignant and benign cells was found to be accompanied by an increase in apoptotic cell death and that small, fragmented DNA may accumulate in blood circulation (Schulte-Hermann *et al*., 1995). Necrotic and apoptotic cells that are released into the bloodstream can be digested by macrophages (Choi *et al*., 2005). Dying cells are not only derived from necrotic tumor areas but also from the surrounding stromal and the inflammatory regions of the tumor; blood DNA may consist of tumor-associated and normal DNA of different fragment lengths.

In summary, the bare occurrence of elevated DNA concentrations in blood does not indicate any association with a malignant tumor, because inflammation processes can also release their DNA into the bloodstream. However, many promising investigations have shown that in principle

it is possible to discover tumor-associated alterations in blood from prostate cancer patients, and optimized methods may improve the detection rate.

TECHNICAL CONSIDERATIONS OF THE PLASMA-BASED ANALYSES

Dilution experiments were performed to determine the dilution factor of tumor-specific DNA in blood plasma from prostate cancer patients and accordingly, to assess the lowest portion of tumor-specific DNA which can be detected in the pool of cell-free DNA. Known quantities and proportions of reference DNA and plasma DNA were mixed and amplified. LOH was considered to be present when the intensity ratio of plasma sample alleles differed by > 40% from the reference DNA. An admixture of 5% of normal DNA to plasma DNA was sufficient to reach the cutoff value of 0.6 or the inverse value of 1.67.

To emphasize the high dilution of tumor-associated DNA in blood plasma, a dilution series with DNA derived from microdissected tumor tissue was carried out. A dilution ratio of 20% of reference DNA to tumor DNA caused the transition of LOH to heterozygosity. These findings show that the dilution factor of tumor-specific plasma DNA is fourfold higher than that of DNA derived from tumor tissues, and imply that tumor-specific plasma DNA is largely diluted by normal DNA.

Accurate identification of LOH on cell-free DNA is often restricted by technical limitations such as poor quality and quantity of tumor-specific DNA and contamination by normal DNA. Use of DNA fragments from blood and bone marrow in PCR can result in false-positive data and artificial LOHs displaying either DNA loss at the shorter or longer allele of the same locus and in the same plasma sample. Furthermore, microsatellites consisting of dinucleotide repeats, e.g., CA repeats, frequently form slippage peaks in addition to both alleles. To avoid such shortcomings and fluctuations of the calculated peak ratios, PCR should be repeated at least twice, and the quality and validity of plasma DNA be checked in dilution experiments. Additionally, to stabilize the PCR reaction, 0.1 mM tetramethylammonium chloride (TMAC) can be added to the reaction. Administration of this substance usually results in ~ 20% more PCR product. TMAC can enhance the specificity of the reaction by decreasing primer dimerization, formation of slippage peaks and occurrence of artificial LOHs.

To further optimize the assay conditions, different DNA polymerases should be compared, e.g., the thermostable AmpliTaq Gold and the high fidelity iProof DNA polymerase. Both enzymes differ by their 3′ to 5′ exonuclease activity. The AmpliTaq Gold DNA polymerase possesses a template-independent polymerase activity, which is responsible for adding an additional base, mostly an adenosine, to the end of the newly synthesized strand. In contrast, the iProof DNA polymerase has a 3′–5′ exonuclease activity allowing a DNA proofreading and producing blunt end products. The evaluation of the amplification reactions included the AmpliTaq Gold DNA polymerase that forms additional peaks for the adenosine shoulders besides the two actual alleles. As shown in Figure 34.3A the peaks of the adenosine shoulder can be almost as high as the alleles, and

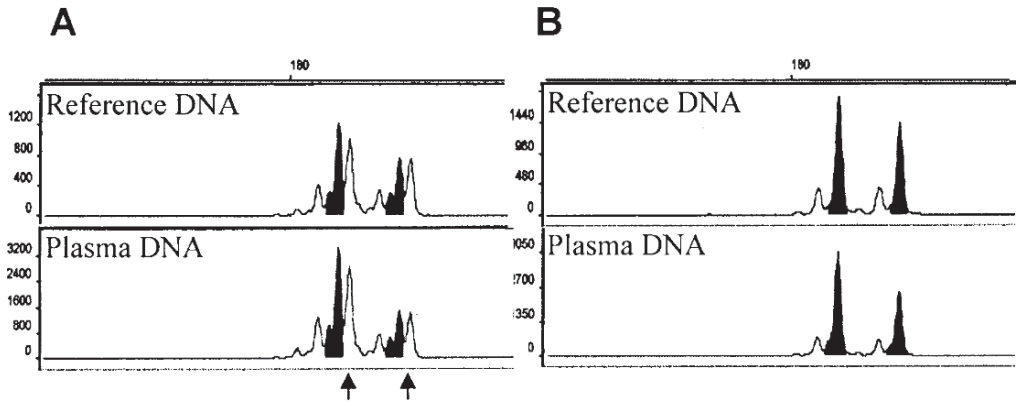

FIGURE 34.3. Comparison of the PCR products with or without adenosine appendage.
Genomic DNA of leukocytes (reference) and circulating plasma DNA were amplified with the AmpliTaq Gold (A) or the iProof DNA-Polymerase (B). The arrows point to the peaks corresponding to the PCR products with the adenosine shoulders

therefore, together with the slippage peaks they may complicate evaluation. However, when the amplification is performed with the iProof DNA polymerase these additional peaks vanish and the remaining peaks can be clearly referred to both alleles (Figure 34.3B).

PLASMA-BASED EPIGENETIC ANALYSIS

Loss of gene expression is not only determined by genetic alterations but also by promoter hypermethylation. The pattern of DNA methylation is primarily generated during vertebrate development and alterations in the created methylation profile occur during the pathogenesis of human tumors. Despite the global DNA hypomethylation observed in various carcinomas, hypermethylated regions leading to transcriptional silencing also occur in malignant cells and particularly map to tumor suppressor and DNA repair genes (Esteller and Herman, 2002). Transcriptional suppression is caused by abnormal methylation of DNA at CpG islands that frequently lie in the promoter regions of these genes. These findings recommend that changes both in DNA hypermethylation and hypomethylation play a crucial role during tumorigenesis. The mounting recognition of the importance of epigenetic alterations in cancer pathogenesis has led to the investigation of methylation of classic tumor suppressor genes. To address this issue, a growing list of candidate tumor suppressor affected by this process was assorted for various tumor entities. The assembled methylation patterns may serve as biomarkers for the particular tumor type and markers for risk assessment, and alleviate early discovery.

Use of bisulfite converted DNA allows detection of tumor suppressor genes transcriptionally repressed by methylation, and cell-free DNA from blood has been shown to be an appropriate source for this screening technique. However, only a limited number of studies concentrated

on the search for new plasma-based tumor markers has been engaged in exploring promoter hypermethylation of tumor suppressor genes in blood from prostate cancer patients (Goessl *et al*., 2000; Papadopoulou *et al*., 2006; Bastian *et al*., 2005; Vis *et al*., 2001). Because promoter hypermethylation of the detoxification gene glutathione-S-transferase P1 (GSTP1) is the most common somatic genome abnormality in prostate tumors, this candidate gene was first analyzed for epigenetic alterations in plasma DNA. In benign or hyperplastic prostate tissue, methylated GSTP1 genes have not been found. With the exception of liver cancer, GSTP1 methylation is also a rare event in other malignancies. GSTP1 promoter hypermethylation has been shown by Goessl *et al*. (2000) to constitute an ideal molecular tumor marker for detection of cell-free tumor-associated DNA in blood from prostate cancer patients. They detected free tumor DNA in all their analyzed plasma or serum samples by retrieval of the methylated GSTP1 gene. Notably, GSTP1 promoter hypermethylation was additionally detectable in a limited number of sperm and urine samples from patients with prostate cancer. Papadopoulou *et al*. (2006) found GSTP1 promotor hypermethylation in 75% of plasma samples obtained from patients with newly diagnosed prostate cancer and in 37% of patients during therapy. The combination of DNA load and promotor methylation status identified ~ 90% of prostate cancer patients. Bastian *et al*. (2005) evaluated circulating cell-free and hypermethylated GSTP1 DNA as a prognostic serum-based biomarker for prostate cancer. In a multivariable analysis including established prognostic factors, the presence of hypermethylated GTSP1 DNA in serum was the most significant predictor of PSA recurrence.

Besides the GSTP1 gene, the methylation of a second gene, namely the adhesion molecule CD44, was of note to be considered. CD44 is an important metastasis-suppressor gene in prostate cancer. Downregulation of the CD44 gene has been attributed to methylation of its promoter. Vis *et al*. (2001) examined the presence of cell-free methylated CD44 fragments as a diagnostic tool in serum from prostate cancer patients using methylation-specific PCR. However, they found that assessment of tumor-derived DNA methylation in serum of cancer patients lacked tissue specificity and seemed not to be applicable in clinical settings due to the physiologic promoter methylation in normal tissues.

DNA METHYLATION ANALYSIS BY THE SODIUM BISULFITE TECHNIQUE

1. Sodium bisulfite conversion:
   For the sodium bisulfite conversion, denature 4 µg DNA in 0.3 mol/l NaOH for 20 min at 42°C. Incubate the denatured DNA in a 600 µl solution of 3 mol/l sodium bisulfite, 0.5 mmol/l hydroquinone, and 1.6 mol/l NaOH (pH 5.0) for at least 16 h at 50°C. Desalt and concentrate the sodium bisulfite-treated DNA by a silica matrix.
2. Methylation-sensitive PCR and DNA sequencing:
   Following precipitation and resuspension, amplify 4 µl modified DNA by methylation-specific primers. The PCR reaction should contain Q-Solution for analyses of CG-rich sequences. For determination of the promoter methyla-

tion patterns, clone the PCR products of bisulfite-treated genomic DNA into the pCR4-TOPO vector using the TOPO TA cloning kit (Invitrogen). Amplify the constructs by primers specific for the M13 sequences flanking the cloning site of the pCR4-TOPO vector, and subsequently sequence the PCR products.

REFERENCES

Algaba, F., Trias, I., and Arce, Y. 2007. Natural history of prostatic carcinoma: the pathologist's perspective. *Recent Results Cancer Res. 175*: 9–24.

Allen, D., Butt, A., Cahill, D., Wheeler, M., Popert, R., and Swaminathan, R. 2004. Role of cell-free plasma DNA as a diagnostic marker for prostate cancer. *Ann. NY Acad. Sci 1022*: 76–80.

Anker, P., Mulcahy, H., Chen, X.Q., and Stroun M. 1999. Detection of circulating tumour DNA in the blood (plasma/serum) of cancer patients. *Cancer Metastasis Rev.18*: 65–73.

Bai, V.U., Kaseb, A., Tejwani, S., Divine, G.W., Barrack, E.R., Menon, M., Pardee, A.B., and Reddy G.P. 2007. Identification of prostate cancer mRNA markers by averaged differential expression and their detection in biopsies, blood, and urine. *Proc. Natl. Acad. Sci. USA 104*: 2343–2348.

Bastian, P.J., Palapattu, G.S., Lin, X., Yegnasubramanian, S., Mangold, L.A., Trock, B., Eisenberger, M.A., Partin, A.W., and Nelson, W. G. 2005. Preoperative serum DNA GSTP1 CpG island hypermethylation and the risk of early prostate-specific antigen recurrence following radical prostatectomy. *Clin. Cancer Res. 11*: 4037–4043.

Bendich, A., Wilczok, T., and Borenfreund, E. 1965. Circulating DNA as a possible factor in oncogenesis. *Science 148*: 374–376.

Boddy, J.L., Gal, S., Malone, P.R., Shaida, N., Wainscoat, J.S., and Harris, A.L. 2006. The role of cell-free DNA size distribution in the management of prostate cancer. *Oncol. Res. 16*: 35–41.

Chen, X., Bonnefoi, H., Diebold-Berger, S., Lyautey, J., Lederrey, C., Faltin-Traub, E., Stroun, M., and Anker, P. 1999. Detecting tumor-related alterations in plasma or serum DNA of patients diagnosed with breast cancer. *Clin. Cancer Res. 5*: 2297–303.

Choi, J.J., Reich 3rd, C.G., and Pisetsky, D.S. 2005. The role of macrophages in the *in vitro* generation of extracellular DNA from apoptotic and necrotic cells. *Immunology 115*: 55–62.

Chun, F.K.H., Müller, I., Lange, I., Friedrich, M., Erbersdobler, A., Karakiewicz, P.I., Graefen, M., Pantel, K., Huland, H., and Schwarzenbach, H. 2006 Circulating tumour-associated plasma DNA represents an independent and informative predictor of prostate cancer. *Br. J. Urol. Int. 98*: 544–548.

Costa, V.L., Henrique R., and Jerónimo, C. 2007. Epigenetic markers for molecular detection of prostate cancer. *Dis. Markers 23*: 31–41.

Coulet, F., Blons, H., Cabelguenne, A., Lecomte, T., Laccourreye, O., Brasnu, D., Beaune, P., Zucman, J., and Laurent-Puig, P. 2000. Detection of plasma tumor DNA in head and neck squamous cell carcinoma by microsatellite typing and p53 mutation analysis. *Cancer Res. 60*: 707–711.

Diehl, F., Li, M., Dressman, D., He, Y., Shen, D., Szabo, S., Diaz, Jr. L.A., Goodman, S.N., David, K. A., Juhl, H., Kinzler, K.W., and Vogelstein B. 2005. Detection and quantification of mutations in the plasma of patients with colorectal tumors. *Proc. Natl. Acad. Sci. USA. 102*: 16368–16373.

Ellinger, J., Bastian, P.J., Haan, K.I., Heukamp, L. C., Buettner, R., Fimmers, R., Mueller, S.C., and von Ruecker, A. 2007. Noncancerous PTGS2 DNA fragments of apoptotic origin in sera of prostate cancer patients qualify as diagnostic and prognostic indicators. *Int. J. Cancer 122*: 138–143.

Esteller, M., and Herman, J.G. 2002. Cancer as an epigenetic disease: DNA methylation and chromatin alterations in human tumours. *J. Pathol.196*: 1–7.

Farrand, K., Jovanovic, L., Delahunt, B., McIver, B., Hay, I.D., Eberhardt, N.L., and Grebe, S.K. 2002. Loss of heterozygosity studies revisited: prior quantification of the amplifiable DNA content of archival samples improves efficiency and reliability. *J Mol. Diagn. 4*: 150–158.

Fleischhacker, M., and Schmidt, B. 2007. Circulating nucleic acids (CNAs) and cancer – a survey. *Biochim. Biophys. Acta 1775*: 181–232.

Giacona, M.B., Ruben, G.C., Iczkowski, K.A., Roos, T.B., Porter, D.M., and Sorenson, G.D. 1998. Cell-free DNA in human blood plasma: length measurements in patients with pancreatic cancer and healthy controls. *Pancreas 17*: 89–97.

Goessl, C., Müller, M., and Miller, K. 2000. Methylation-specific PCR (MSP) for detection of tumour DNA in the blood plasma and serum of patients with prostate cancer. *Prostate Cancer Prostatic Dis. 3 Suppl 1*: 17.

Hanley, R., Rieger-Christ, K.M., Canes, D., Emara, N. R., Shuber, A.P., Boynton, K.A., Libertino, J.A., and Summerhayes, I.C. 2006. DNA integrity assay: a plasma-based screening tool for the detection of prostate cancer. *Clin. Cancer Res. 12*: 4569–4574.

Hata, N., Yoshimoto, K., Yokoyama, N., Mizoguchi, M., Shono, T., Guan, Y., Tahira T., Kukita, Y., Higasa, K., Nagata, S., Iwaki., T., Sasaki, T., and Hayashi, K. 2006. Allelic losses of chromosome 10 in glioma tissues detected by quantitative single-strand conformation polymorphism analysis. *Clin. Chem. 52*: 370–378.

Jahr, S., Hentze, H., Englisch, S., Hardt, D., Fackelmayer, F.O., Hesch, R.D., and Knippers, R. 2001. DNA fragments in the blood plasma of cancer patients: quantitations and evidence for their origin from apoptotic and necrotic cells. *Cancer Res. 61*: 1659–1665.

Jung, K., Stephan, C., Lewandowski, M., Klotzek, S., Jung, M., Kristiansen, G., Lein, M., Loening, S. A., and Schnorr, D. 2004. Increased cell-free DNA in plasma of patients with metastatic spread in prostate cancer. *Cancer Lett. 205*: 173–180.

Leon, S.A., Shapiro, B., Sklaroff, D.M., and Yaros, M.J. 1977. Free DNA in the serum of cancer patients and the effect of therapy. *Cancer Res. 37*: 646–650.

Mandel, P., and Métais, P. 1948. Les acides nucléiques du plasma sanguin chez l'homme. *C. R. Acad. Sci. Paris 142*: 241–243.

Mehra, N., Penning, M., Maas, J., van Daal, N., Giles, R.H., and Voest, E.E. 2007. Circulating mitochondrial nucleic acids have prognostic value for survival in patients with advanced prostate cancer. *Clin. Cancer Res. 13*: 421–426.

Müller, I., Urban, K., Pantel, K., and Schwarzenbach, H. 2006. Comparison of genetic alterations detected in circulating microsatellite-DNA in blood plasma samples of patients with prostate cancer and benign prostatic hyperplasia. *Ann. NY Acad. Sci. 1075*: 222–229.

Pantel, K., and Brakenhoff R.H. 2004. Dissecting the metastatic cascade. *Nat. Rev. Cancer 4*: 448–456.

Papadopoulou, E., Davilas, E., Sotiriou, V., Georgakopoulos, E., Georgakopoulou, S., Koliopanos, A., Aggelakis, F., Dardoufas, K., Agnanti, N.J., Karydas, I., and Nasioulas, G. 2006. Cell-free DNA and RNA in plasma as a new molecular marker for prostate and breast cancer. *Ann. NY Acad. Sci. 1075*: 235–243.

Sanchez, Y., Lovell, M., Marin, M.C., Wong, P. E., Wolf-Ledbetter, M.E., McDonnell, T.J., and Killary, A.M. 1996. Tumor suppression and apoptosis of human prostate carcinoma mediated by a genetic locus within human chromosome 10pter-q11. *Proc. Natl. Acad. Sci. USA 93*: 2551–2556.

Saric, T., Brkanac, Z., Troyer, D.A., Padalecki, S. S., Sarosdy, M., Williams, K., Abadesco, L., Leach, R.J., and O'Connell, P. 1999. Genetic pattern of prostate cancer progression. *Int. J. Cancer 81*: 219–224.

Schulte-Hermann, R., Bursch, W., Grasl-Kraupp, B., Torok, L., and Ellinger, A.M.L. 1995. Role of active cell death (apoptosis) in multi-stage carcinogenesis. *Toxicol. Lett. 83*: 143–148.

Schwarzenbach, H., Chun, F.K.H., Lange, I., Carpenter, S., Gottberg, M., Erbersdobler, A., Friedrich, M.G., Huland, H., and Pantel, K. 2007. Detection of tumor-specific DNA in bone marrow plasma from patients with prostate cancer. *Int. J. Cancer 120*: 1457–1463.

Sorenson, G.D., Pribish, D.M., Valone, F.H., Memoli, V.A., Bzik, D.J., and Yao, S.L. 1994. Soluble normal and mutated DNA sequences from single-copy genes in human blood. *Cancer Epidemiol. Biomarkers Prev. 3*: 67–71.

Stroun, M., Anker, P., Lyautey, J., Lederrey, C., and Maurice, P.A. 1987. Isolation and characterization of DNA from the plasma of cancer patients. *Eur. J. Cancer Clin. Oncol. 23*: 707–712.

Stroun, M., Anker, P., Maurice, P., Lyautey, J., Lederrey, C., and Beljanski, M. 1989. Neoplastic characteristics of the DNA found in the plasma of cancer patients. *Oncology 46*: 318–322.

Taback, B., Giuliano, A.E., Hansen, N.M., Singer, F.R., Shu, S., and Hoon, D.S.B. 2003. Detection

of tumor-specific genetic alterations in bone marrow from early-stage breast cancer patients. *Cancer Res. 63*: 1884–1887.

Tan, E.M., Schur, P.H., Carr, R.I., and Kunkel, H.G. 1966. Deoxyribonucleic acid (DNA) and antibodies to DNA in the serum of patients with systemic lupus erythematosus. *J. Clin. Invest. 45*: 1732–1740.

Vasioukhin, V., Anker, P., Maurice, P., Lyautey, J., Lederrey, C., and Stroun, M. 1994. Point mutations of the N-ras gene in the blood plasma of patients with myelodysplastic syndrome or acute myelogenous leukemia. *Br. J. Haematol. 86*: 774–779.

Vis, A.N., Oomen, M., Schröder, F.H., and van der Kwast, T.H. 2001. Feasibility of assessment of promoter methylation of the CD44 gene in serum of prostate cancer patients. *Mol. Urol. 5*: 199–203.

Wang, M., Block, T.M., Steel, L., Brenner, D.E., and Su, Y.H. 2004. Preferential isolation of fragmented DNA enhances the detection of circulating mutated k-ras DNA. *Clin. Chem. 50*: 211–213.

Wang, Q., Larson, P.S., Schlechter, B.L., Zahid, N., Finnemore, E., de las Morenas, A., Blanchard, R. A., and Rosenberg, C.L. 2003. Loss of heterozygosity in serial plasma DNA samples during follow-up of women with breast cancer. *Int. J. Cancer 106*: 923–929.

Wu, T.L., Zhang, D., Chia, J.H., Tsao, K.C., Sun, C. F., and Wu, J.T. 2002. Cell-free DNA: measurement in various carcinomas and establishment of normal reference range. *Clinica Chimica Acta 321*: 77–87.

Yano, S., Matsuyama, H., Matsuda, K., Matsumoto, H., Yoshihiro, S., and Naito, K. 2004. Accuracy of an array comparative genomic hybridization (CGH) technique in detecting DNA copy number aberrations: comparison with conventional CGH and loss of heterozygosity analysis in prostate cancer. *Cancer Genet. Cytogenet. 150*: 122–127.

Zheng, H.T., Peng, Z.H., Li, S., and He, L. 2005. Loss of heterozygosity analyzed by single nucleotide polymorphism array in cancer. *World J. Gastroenterol. 11*: 6740–6744.

35
Prostate Carcinoma: Evaluation Using Transrectal Sonography

Ahmet T. Turgut and Vikram S. Dogra

INTRODUCTION

Prostate cancer (PC) is a major medical problem as well as a significant public health challenge that has economic effects. At present, it is the most commonly diagnosed visceral cancer affecting the male population. The reported annual incidence rates for the disease vary within the range of 1.9/100,000 for Asian men to 137/100,000 for African-American men. According to 2004 estimates from the American Cancer Society, 230,110 new cases of PC were diagnosed in the United States (American Cancer Society, 2004), which is nearly one-third of all new male cancers.

On the other hand, the annual mortality of the disease varies from 25 to 45/100,000. The American Cancer Society estimates 27,050 deaths in 2007 from PC, which is 9% of all cancer associated deaths, second after lung cancer as the leading cause of male cancer deaths in the United States (American Cancer Society, 2007). Likewise, 12% of all cancer-related male deaths in the United Kingdom were reported to be due to PC. Lifetime risk of developing the disease is approximately 42%, though the relevant risk for having clinically detectable cancer is 18%. It is noteworthy that 86% of currently diagnosed PC is amenable to curative treatment. In this regard, accurate early detection plays a critical role for the management of the disease, though "insignificant cancers," which are not a cause of death, may be detected consequently in addition to the significant ones.

Currently, the diagnosis of PC is based on digital rectal examination, prostate specific antigen (PSA), and transrectal ultrasound. Before the 1990s, the only means for detection of PC was PSA and digital rectal examination with the accompanying manual biopsy. However, digital rectal examination alone is of insufficient sensitivity and positive predictive value to detect most cases of PC, as it only provides access to the tumors in a restricted area of the prostate. Furthermore, digital rectal examination has been reported to miss 44–59% of cancers as it is often occult to the examining finger, whereas the method has an understaging rate of 22–66% for the disease. The heightened interest in the use of PSA tests, on the other hand, caused an exponential increase in the detection of the disease. The reported increase in the prevalence and incidence

of PC resulted in an increased public awareness of the problem, which became a further stimulus to incorporate imaging within the efforts to detect aggressive PC while it is still confined to the prostate gland. This can help plan an optimal treatment strategy and determine the prognosis. In this regard, PSA screening is advocated as it detects the cancer at an earlier stage. However, the tests have a low specificity for PC despite having an associated high sensitivity (Djavan *et al*., 1999). Moreover, the method has a low accuracy, particularly in the intermediate range (4–20 ng/ml) (Wijkstra *et al*., 2004). Although there is controversy about the accuracy and the exact threshold values for serum PSA and its derivatives, such as age- and race-adjusted PSA, PSA velocity, PSA density, and free PSA, their development has strengthened the central role of imaging in the evaluation of PC.

Imaging has a crucial role in the management of PC because the relevant information regarding its detectability as well as its location, size, and aggressiveness is associated with accurate diagnosis and staging of the disease. Furthermore, it plays a critical role not only in the detection and localization of the tumor, but also for guiding the biopsies and treatment of PC. Among the currently available imaging techniques, transrectal ultrasound stands as the fundamental choice for visualizing prostate. Unfortunately, the value of gray scale transrectal ultrasound in the detection of PC is limited, though it has a high accuracy for the anatomic delineation of the prostate gland and the measurement of the prostate size. Therefore, the main role of transrectal ultrasound imaging has for a long time been biopsy guidance to detect PC.

PROSTATE CARCINOMA DIAGNOSIS

Digital rectal examination provides the manual evaluation of the prostate gland, which enables the detection of suspicious findings as nodules, firmness, induration, or asymmetry (Boczko *et al*., 2006). Long ago, PC was only detectable at an advanced stage by means of incidental digital rectal examination. Contrary to digital rectal examination having a lower positive predictive value for the detection of PC and a limited benefit for identifying high-risk patients, PSA has become the main tool for the identification of high-risk individuals. This has resulted in an obvious stage migration with a decrease in the percentage of patients presenting with local spread of the disease beyond the prostate or distant metastasis. Classically, a PSA value of 4 ng/ml has been accepted as the upper limit of normal. Twenty percent of PC with aggressive pathologic features may be accompanied by a PSA level less than 4 ng/ml, though PSA is currently accepted as the best known single screening tool for the disease. Therefore, a combination of a suspicious digital rectal examination finding and/or elevated PSA is advocated to assess the risk of PC. Alternatively, the specificity of PSA is limited, as it is elevated in several other conditions, including acute and chronic prostatitis, benign prostatic hyperplasia, and gland manipulation due to digital rectal examination or biopsy. Moreover, there has been no consensus regarding the upper limit of normal values, which has led to the definition of age-corrected PSA values, ratio of free to total PSA, and development of newer PSA derivatives aimed to better identify high-risk individuals.

TRANSRECTAL ULTRASONOGRAPHY USING ASSESSMENT OF PROSTATE CANCER

The most common indication for transrectal ultrasound examination of the prostate is the evaluation of the suspected PC. The combined use of transrectal ultrasound and needle biopsy, with the capability to direct the biopsy needle precisely into the target region or provide a uniform spatial separation of the biopsy cores improves the detectability of PC compared to digitally guided biopsy.

ANATOMY

The normal prostate in adulthood is conically shaped and weighs 12–20 g. Heavier organs are also considered to be normal, particularly in the over 40 population, as the gland enlarges with aging. The average sized normal prostate measures approximately 4.0–4.5 cm in maximum transverse diameter, 2.5–3.0 cm in anteroposterior diameter, and 3.0–4.0 cm in craniocaudal dimension. Anatomically, the prostate is enclosed by a thin pseudocapsule of fibromuscular stroma that is indistinct from the surrounding fascial planes. It is thin anteriorly and thins as it surrounds the gland laterally and posteriorly. The superior margin of the gland is the base of the prostate abutting the inferior aspect of the urinary bladder. The caudal margin, namely the apex of the prostate, is angled downward and lies slightly anterior, abutting the superior surface of the urogenital diaphragm. The prostatic urethra coursing from the bladder to the prostate through the internal sphincter at the prostatic base exits the gland through the external sphincter at the apex of the prostate where it becomes the membranous urethra.

Lymphatic drainage is completed primarily by obturator and internal iliac nodes. The lateral venous plexus surrounding the prostate, also named neurovascular bundles, is bilaterally paired at the posterolateral margins of the gland and courses from the apex toward the seminal vesicles and urinary bladder. The neurovascular bundles are significant for tumor involvement as they are a major site of capsular weakness, perforating the prostate capsule. The arterial supply of the prostate is mainly from the prostaticovesical arteries, arising from the internal iliac artery on each side. The distal capsular group of prostatic arteries, which are the main feeding arteries of the prostate, supply approximately two-thirds of the total glandular tissue, whereas the urethral group of prostatic arteries supply nearly one-third of the gland (Neumaier *et al*., 1995).

PHYSICS

In ultrasound imaging, sound waves transmitted from a piezoelectronic crystal and propagating through the tissue of interest reflect as they encounter a boundary separating areas of different propagation velocities. The reflected signals received by the piezoelectric device are consequently used to construct a graphic display of the site of interest in the form of an image depicting patterns of regions having different acoustic impedance. These images are used to evaluate the anatomy of the target organ (de la Rosette and Aarnink, 2001).

SONOGRAPHIC ANATOMY

The ultrasound appearance of the normal prostate changes according to age. In younger men the small, normal prostate

has a minimal hyperplastic glandular tissue, whereas in the elderly the inevitable enlargement of the gland due to the development of benign prostatic hyperplasia will cause a different appearance with a more rounded shape. On average, 70% of the prostate is composed of glandular elements, whereas the remaining 30% consists of fibromuscular stroma (Boczko *et al.*, 2006). The glandular portion of the prostate is conventionally divided into an inner gland consisting of a transition zone and periurethral glandular tissue and an outer gland composed of both a peripheral zone and a central zone. The transition zone, shown as a hypoechoic zone on the ventral side of the prostate, is usually discernable from the peripheral zone by transrectal ultrasound. The outer gland of the prostate is homogenous and more echogenic than the inner gland. However, the central zone cannot be differentiated from peripheral zone in the normal male. Although the transition zone, the area where hyperplastic changes develop, comprises inevitably a larger proportion of the prostate in older men, it can account for approximately 20% of PC as well. Additionally, 1–5% of PC originates from the central zone. The outer peripheral zone of the prostate, on the other hand, is the origin of approximately 70% of PC, which can eventually infiltrate into other glandular zones. Furthermore, the peripheral zone is the region that is most affected by chronic prostatitis. It is noteworthy that transition zone cancers are usually difficult to identify by transrectal ultrasound contrary to those located in the peripeheral zone. The fibromuscular stroma, alternatively, is rarely a site of origin for PC.

TECHNIQUES

Transrectal ultrasound was first introduced as a diagnostic tool for PC in the late 1960s. The earliest commercially available endorectal probes were radial scanners placed through a central hole in a chair in which the patient would sit. However, remarkable progress in technical refinements of ultrasound machinery achieved since then have provided multi-axial imaging by wide-band, high-frequency transducers. At present, biplane probes for transrectal prostate scanning combined with an end-viewing or side-viewing transducer allow for multiplanar imaging in semicoronal, axial, and sagittal projections. Compared to the earlier transducers in the 2–4 MHz range, which provided fairly enough depth of penetration, current transducers in the 5–8 MHz range enable the examiner to visualize the gland periphery with a clear resolution, which is critical for targeting during any accompanying biopsy procedure.

The use of a self-administered enema on the morning of the procedure is suggested to evacuate gas and feces, which might impair visibility during scanning. Most examiners prefer that the patient lie in the left lateral decubitis position during the examination as it is well-tolerated. The patient is asked to take a deep breath and relax so that the probe can more easily be inserted into the rectum. A digital rectal examination should be performed before probe insertion to reveal any accompanying physical examination finding correlating with the ultrasound findings. The use of ultrasound gel over a latex condom covering the probe is advocated to eliminate any rectal air artifact. Importantly, the urinary bladder should not be empty so that a clear interface with the prostate base margin can be created.

A systematic approach in the transverse or semicoronal plane, beginning from the level of seminal vesicles above the prostate base, continuing with the demonstration of the central zone, transition zone, and periurethral glandular area and periperhal zone thereafter down to the level of the apex is necessary so that the entire gland can be examined. Scanning from right to left in the sagittal plane is necessary to reveal the presence of any asymmetry or to confirm any suspicious finding detected on axial or coronal scanning. Care should be taken to scan all parts of the prostate and the periprostatic tissue sufficiently. After measuring the dimensions in three planes, the prostate volume can be calculated by using the following ellipsoid formula:

Volume of prostate = 0.52 × td × apd × ccd where *td* represents the transverse diameter of the prostate, *apd* is the anteroposterior diameter of the prostate, and *ccd* is the craniocaudal diameter of the prostate.

Evaluation of suspected PC is the most common indication for ultrasound examination of the prostate. However, men may also present with the confronting symptoms of diminishing bladder outflow or constitutional symptoms of metastatic cancer. Compared to the other routes of ultrasound scanning, transrectal ultrasound provides the clearest visualization of the prostate. In this regard, transrectal ultrasound is a useful tool for various diagnostic and therapeutic interventions for PC (Ukimura *et al*., 2004).

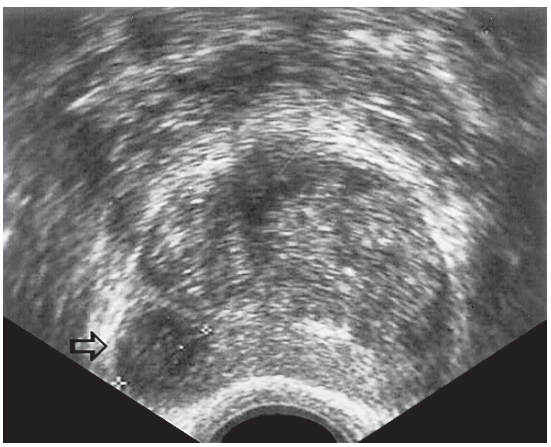

FIGURE 35.1. Transverse transrectal ultrasound image depicting focal nodular (open arrow) pattern of PC

GRAY SCALE ULTRASOUND

Contrary to the neoplasms in other organs, PC does not generally present as a solitary round mass. Instead, most PCs are multifocal. On the other hand, only 30% of the cancers may appear as a focal nodule, whereas 50% present with a nodule having an accompanying infiltrative component, and the remaining 20% with a predominantly infiltrative pattern (Grossfeld and Coakley, 2005) (Figure 35.1). The aforementioned morphological variability of PC is another factor that limits the utility of conventional imaging techniques optimized for well-defined, round tumor masses.

In a previous study, PC was reported to appear hypoechoic (60–70%), isoechoic (40%), or rarely hyperechoic. Rare hyperechoic appearance in some PCs has been attributed to the associated fibrosis. The classic gray scale ultrasound finding of PC, however, is a reduction of the echo density compared to the ordinary tissue of the prostate, resulting in a hypoechoic lesion in the peripheral zone. Microscopically, the loss of normal glandular architecture, particularly for high-grade PC, results in fewer reflective interfaces and reduced echotexture in gray scale ultrasound (Halpern, 2006). Not infre-

quently, the echotexture of the peripheral zone, which is normally either isoechoic or hyperechoic compared to the inner gland, may change to a diffusely hypoechoic pattern suggestive of advanced PC (Figure 35.2). Furthermore, oedema and neovascularity contribute to the hypoechoic appearance of the cancerous tissue.

The differential diagnosis for hypoechoic areas in the peripheral zone include benign prostatic hyperplasia, prostatic atrophy, inflammation, focal areas of acute prostatitis, abscess, hematoma, ductal ectasia, granulomatous prostatitis, tuberculous prostatitis, prostatic intraepithelial neoplasia and lymphoma. Prostatitis is a commonly encountered pathology that may present with either a heterogeneous appearance or hypoechoic peripheral zone lesions (Halpern, 2006). Benign prostatic hyperplasia, affecting primarily the transition zone and harboring associated hyperplastic nodules located close to the surgical capsule, which may protrude into the peripheral zone, is another common prostate pathology. Long ago, Lee *et al.* (1989) reported that positive predictive values for PC diagnosis of a peripheral zone hypoechoic area alone, peripheral zone hypoechoic area with elevated PSA, and peripheral zone hypoechoic area with-elevated PSA and a palpable abnormality were 41%, 52%, and 71%, respectively. Small cancers appear as hypoechoic areas in the peripheral zone, whereas they tend either to be isoechoic or have an inhomogeneous echo pattern as the tumor enlarges (Loch, 2007; Papatheodorou *et al.*, 2005) (Figure 35.3).

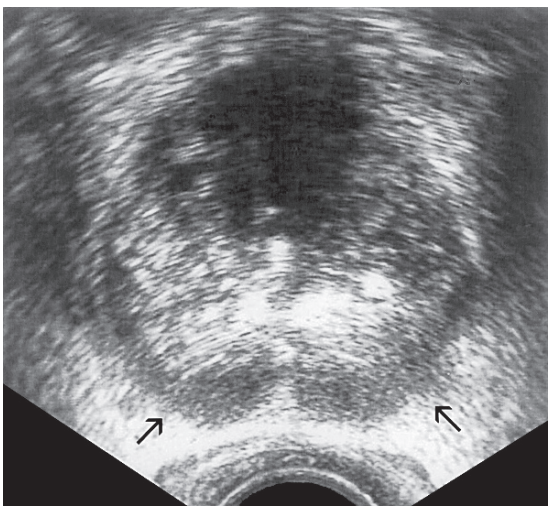

FIGURE 35.2. Normal iso- or hyperechoic appearance of the p has been replaced with a diffuse hypoechoic echotexture (arrows), which was proven, by systematic biopsy, to be adenocarcinoma of the prostate

Importantly, a significant proportion of contemporary PC is isoechoic, which obviates the use of other less specific features for the diagnosis. A very important criterion is the asymmetry of the prostate, which applies both to the echotexture and the margins of the gland. In this regard, a non-specific echo irregularity may be a clue for the diagnosis of PC (Figure 35.4). Likewise, a bulge or irregularity in the outline of the capsule in the dorsal or lateral region or the ventral parts of the apex should be regarded as suspicious for malignancy (Loch, 2007).

The application of transrectal ultrasound alone for the detection of PC harbors some limitations. First, the operator-dependent nature of the technique results in variations among the examiners for the detection of subtle differences in gray scale. Second, the wide range of transducer frequencies presently in use, from 3.5 to 7.5 MHz, causes differences in the ability to delineate prostatic zonal anatomy (Purohit *et al.*, 2003). Additionally, the variability in the sonographic appearances of PC, the low specificity of the ultrasound findings,

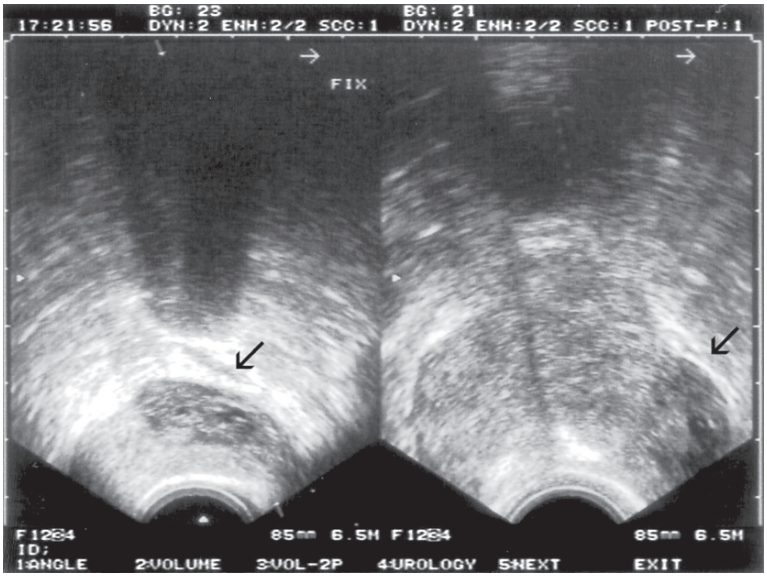

FIGURE 35.3. Transverse and longitudinal transrectal ultrasound scan depicting relatively large, subcapsular lesion with heterogenous echotexture accompanied with a capsular bulge suggestive of an extracapsular extension (arrows) of prostate adenocarcinoma

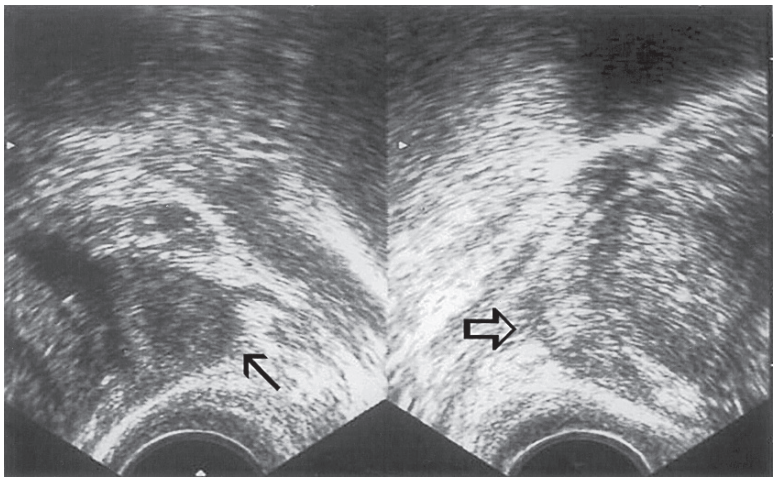

FIGURE 35.4. Transverse transrectal ultrasound scan showing a diffusely heterogenous echotexture of the peripheral zone at the left mid-prostate that was proven to be cancer (arrow). Note that the parenchyma of the peripheral zone on the contralatetal side is homogenously isoechoic, representing benign tissue (open arrow)

multi-focality, and the substantial percentage of isoechoic PCs that cannot be differentiated sonographically from adjacent benign tissues limit the capability of the technique for cancer detection. Another limiting factor is that approximately half of contemporary PCs are not detectable by gray scale ultrasound (Halpern and Strup,

2000). The PSA level correlating with the stage and volume of the tumor is one of several factors limiting the visibility of the tumor by gray scale transrectal ultrasound examination. Benign prostatic hyperplasia, another factor complicating the transrectal ultrasound image, may mask any concurrent cancer because of its mixed echo pattern. Moreover, its compression effect on the peripheral zone where the tumors are best visualized by transrectal ultrasound may be a further limitation for the evaluation of the peripheral zone (Purohit *et al*., 2003).

The ultrasound features of the rarer prostatic tumors have also been described in the literature. Comedocarcinoma, which is the most malignant form of PC, presents with a transrectal ultrasound appearance of stippled multiple small hyperechoic foci within the hypoechoic cancer area. Adenoid cystic carcinoma has been reported to be associated with multiple small cysts of similar size in the prostate. Rhabdomyosarcoma, representing a childhood malignant tumor alternatively, presents as a soft tissue mass infiltrating the bladder and prostate. A case of cystosarcoma phyllodes of the prostate was reported to present radiologically as a large right-sided pelvic mass displacing the bladder. Finally, transrectal ultrasound in lymphoma has been reported to show large hypoechoic masses in both the transition zone and peripheral zone.

As the frequency and metastastic potential of transition zone cancers is lower than those located in the peripheral zone, little attention has been paid to the assessment of hypoechoic areas in the transition zone. Although the clinical features of transition zone cancers are thought to be different than those of peripheral zone cancers, they have not been reported to be associated with specific ultrasound characteristics. Currently, systematic biopsies are the only means for the detection of transisition zone cancers. Although the technique has limited use for staging purposes (Carey, 2005), several transrectal ultrasound findings that are suggestive of extracapsular extension of PC should be investigated as well. In this regard, the exam should search for protuberance and irregularity of the capsule margins, disruption of or hypoechoic strands within the fat planes posterior to the prostate, hypoechoic and posterior thickening, or loss of bulging of the seminal vesicles that may reveal an associated invasion (Figure 35.5). It is noteworthy that extracapsular extension by small microscopic clusters of tumor cells is not detectable by transrectal ultrasound (Purohit *et al*., 2003).

Gray scale transrectal ultrasound alone has a positive predictive value of 6% for PC diagnosis (Coley *et al*., 1997). Similarly, the technique has been reported to have a sensitivity of 44% and a specificity of 74% for the diagnosis of the disease (Halpern and Strup, 2000). In conclusion, gray scale transrectal ultrasound is not accurate enough for PC diagnosis and staging, though it provides an evaluation of the anatomic outline of the prostate and the performance of the biopsies. In addition, the aforementioned isoechoic nature of a significant proportion of contemporary PC has become the main stimulus for further scientific research conducted to improve the accuracy of the technique and incorporate modifications of transrectal ultrasound to image-guided biopsy procedures.

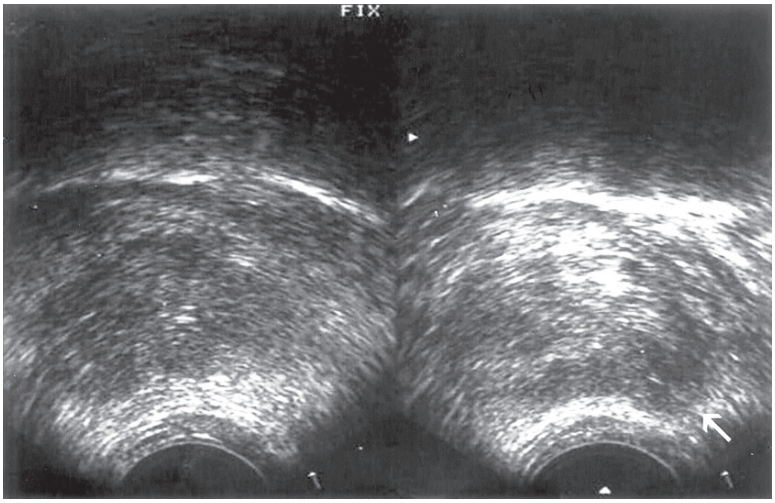

FIGURE 35.5. Different gray scale transrectal ultrasound findings suggestive of extracapsular extension of PC. A hypoechoic tumor in the peripheral zone with capsular bulging and obvious thinning and distortion of periprostatic fat (white arrow)

COLOR DOPPLER ULTRASOUND

Contrary to the conventional gray scale ultrasound showing gray scale brightness used in the target organ, and reflecting changes in local acoustic impedance, Doppler imaging is used to evaluate local blood flow, which is a measure of the tissue function and viability. The idea that tumors need an increased blood supply, demonstrated by changes in the local hemodynamics in an organ, was regarded as the basis for the visibility and detectability of cancerous sites by color Doppler ultrasound.

Regarding the changes in metabolism and perfusion associated with the development of PC, a high degree of glucose consumption correlating with the aggressiveness and the prognosis of the tumor followed by the development of hypoxic areas within the tumor increasing in size was noted (Wijkstra *et al*., 2004). Thereby, angiogenesis and an increase in the capacity of the available blood vessels by vasodilatation are compensatory mechanisms for the increasing needs for nutrients and oxygen.

The growth of cancerous tissue associated with a replication rate that is typically faster than normal tissue necessitates an increased blood supply. Accordingly, the blood flow to the cancerous tissue is increased compared with non-malignant conditions (Frauscher *et al*., 2002). Thereby, color Doppler ultrasound may demonstrate an increased number of visualized vessels having an increased size and irregularity accompanied with an increased flow rate (Frauscher *et al*., 2002). Hence, color Doppler ultrasound suggested as a potential means for the detection of PC, which has been reported to be associated with diffuse, focal, and surrounding patterns of flow, with diffuse flow being the most commonly detected type of flow within the lesion.

In general, an increased blood flow can be depicted either by pulsed wave Doppler imaging displaying spectral waves representing the frequency shift or velocity or by color Doppler imaging showing a spectrum of colors revealing the range of mean frequency shift or velocities of red blood cells within the flowing blood (Jain *et al.*, 1991). Color assignment is associated with the relation of the direction of blood flow and the orientation of the transducer receiving the signal, with the flow towards the transducer represented in shades of red and flow away in shades of blue.

Color Doppler ultrasound can also be used for the evaluation of the vascularity of the prostate and the surrounding structures. Initially, color Doppler ultrasound was shown to provide an increase in the diagnosis of PC, though the associated specificity was low. Moreover, hypoechoic areas and hypervascularity in the peripheral zone may not necessarily correlate as not all tumors show increased vascularity, and hypervascularity is not specific for PC, which is mostly represented by hypoechoic areas. Alternatively, the color Doppler signal has been reported to correlate positively with the stage and the grade of PC and with the post-treatment risk of recurrence. However, the angle dependency of Doppler flow and the inability to detect low flow velocities, as well as the intraprostatic noise mimicking increased blood flow are the main potential limitations for Doppler examination of the prostate.

Earlier, it was reported that up to 85% of men with PC greater than 5 mm were shown to have visibly increased flow in the cancerous site. Moreover, color Doppler ultrasound can identify areas of hypervascularity with isoechoic and hyperechoic appearance. In a previous study by Rifkin *et al.* (1993) conducted on 619 patients, 123 out of 132 cancers (86%) detected by lesion biopsies were shown to have gray scale ultrasound findings and color Doppler abnormalities, whereas nine out of 132 cancers (7%) had abnormal color Doppler ultrasound findings alone. Likewise, they also found that 8 out of 33 inflammatory foci (24%) were associated with findings of abnormal flow without any gray scale finding. A recent study by Halpern *et al.* (2002) evaluated the impact of patient position on increased Doppler flow in healthy subjects. They noted that increased blood flow was detected on the dependent side of the prostate in both right and left lateral decubitis positions and emphasized the necessity of supine position for Doppler examination during prostate biopsies, revealing a symmetrical flow pattern.

In a study by Shigeno *et al.* (2000), the use of a combination of color Doppler ultrasound and gray scale ultrasound was suggested for the detection of PC as it had a relatively higher rate of specificity and positive predictive value compared to gray scale ultrasound alone. In another study Cornud *et al.* (2000), stated that tumors that were detected by color Doppler ultrasound were also visualized by gray scale examination and concluded that the additional information provided by color Doppler ultrasound was only minor. They also added that color Doppler ultrasound may be of use for the differentiation of low-risk, invisible, and hypovascular tumors from high-risk, visible, and hypervascular tumors, as hypervascularity corresponded to a higher rate of Gleason tumor grades compared to hypovascularity (Cornud *et al.*, 2000). In a similar study, they suggested that the behavior and

aggressiveness of PC could be predicted by color Doppler ultrasound, as they found that hypervascular tumors were associated with higher Gleason scores and higher risk of relapse.

The standard use of targeted biopsy solely depending on high-frequency color or power Doppler imaging is not suggested, as it is feared these techniques miss a significant number of cancer cases (Carey, 2005). Halpern and Strup (2000) have emphasized the need for sextant biopsies by considering the relative insufficiency of the associated Doppler findings for cancer detection.

The assessment of blood flow within prostate tumors by color (or power) Doppler can be made either by the evaluation of the distribution of the microvasculature or the quantitative assessment of blood flow within the area. In this regard, PC was reported to exhibit increased microvessel density that was higher in metastatic tumors (Hall *et al*., 1994). The assessment of prostatic microvasculature might be an indicator of the prognosis of the disease, both in the choice of treatment for the cancer and in the follow-up of cancers treated by radiotherapy, as the core biopsy was suspected to underestimate the Gleason score, which is a sign of histological grade (Lissbrandt *et al*., 1997).

Unfortunately, the literature on the utility of color Doppler ultrasound for staging localized disease is scarce. The obscurity of the prostatic capsule in gray scale due to the color signals in color Doppler ultrasound may be a limiting factor for the relevant evaluation. In the aforementioned study by Cornud *et al*. (2000), however, hypervascular tumors were reported to have a higher risk of extraprostatic spread.

POWER DOPPLER ULTRASOUND

Power Doppler ultrasound, which is an amplitude-based technique that is particularly sensitive for the detection of slow flow, is less angle-dependent than color Doppler ultrasound. The technique provides color-coded information about the presence and the intensity of the signals. It can detect small differences in blood flow and alterations in flow in very small tumoral vessels. However, the technique does not give information about the directionality of the flow. Compared to the color Doppler ultrasound alone, the technique has a threefold to fourfold sensitivity.

A study by Unal *et al*. (2000), claimed that power Doppler could discriminate benign prostatic hyperplasia and PC with an accuracy of 81%. In several studies, power Doppler ultrasound was reported to be more useful for the detection of PC (Cho *et al*., 1998), though the technique was rarely reported to provide benefit over color Doppler ultrasound (Halpern and Strup, 2000).

Detection of focal hypervascularity on power Doppler ultrasound increases the likelihood of PC and was felt that power Doppler can help identify the appropriate sites for the biopsy. However, power Doppler was reported to be no superior to color Doppler ultrasound, though it was noted to be useful for targeted biopsies when the number of biopsy passes was limited (Halpern and Strup, 2000). In a study by Okihara *et al*. (2002) the technique was claimed to provide no significant benefit for the efficacy of prostate biopsies. In a separate paper where the added benefit from power Doppler ultrasound was evaluated, it showed a 98% sensitivity and 99% negative predictive value for the detection of PC, which was superior to gray scale transrectal

ultrasound. They added, however, that the 59% positive predictive value in the study was not higher by the former technique. Nevertheless, they concluded that the technique might reduce the number of unnecessary biopsies in patients with abnormally high PSA. However, it should be noted that the combined use of gray scale and color Doppler ultrasound-guided biopsy has been reported to provide no sufficient sensitivity to preclude the need for systematic biopsy.

To the best of our knowledge, no data has been presented in the literature regarding the use of power Doppler ultrasound for the staging of PC.

CONTRAST-ENHANCED ULTRASOUND IMAGING

The proliferation of neovessels in the cancerous tissue of the prostate results in increased microvessel density, which is correlated with the prognosis of the disease. As the microvessels of cancerous tissue are smaller than those of benign prostate tissue, they are associated with a more uniform blood supply. However, these microvessels are below the resolution of conventional Doppler imaging. In this regard, microbubble contrast agents have been proposed as a means for imaging prostatic microvasculature, which would be helpful in enhancing the detection of PC.

Recently developed ultrasound contrast agents with the capability to improve the detection of low-volume blood flow by increasing signal-to-noise ratio between the blood and the surrounding tissues allow a more complete delineation of the neovascular anatomy as they increase the signal strength from microvasculature (Frauscher *et al*., 2002). Most ultrasound contrast agent solutions consist of microbubbles that are free or encapsulated in soft or hard shells. They can easily penetrate the capillary beds as they have a diameter less than 10 μm. Depending on the bubble type, the duration of enhancement lasts from a few seconds to many minutes after the injection. The half-life of contrast agents depends on bubble construction. Unlike radiographic contrast media with the potential to diffuse into the tissue and obscure the microvasculature, microbubble echo-enhancing agents are confined to the vascular lumen, where they persist until they dissolve, which makes them suitable for perfusion imaging techniques. The mismatch between the acoustic properties of the microbubbles and the surrounding blood provides intensified reflections of the ultrasound wave (Wijkstra *et al*., 2004).

The first approach to image microbubble contrast agents is contrast-enhanced Doppler imaging. Approximately 20 s after intravenous injection, the number of ultrasound reflectors increases in the prostatic vasculature resulting in an improvement in Doppler shift signal that provides a higher sensitivity for color and Power Doppler measurements (Wijkstra *et al*., 2004).

In a recent study by Yi *et al*. (2006) in which the usefulness of contrast-enhanced ultrasound for PC detection in patients with an indeterminate PSA level (4–10 ng/ml) and negative digital rectal examination findings was evaluated, the technique was concluded to improve only the sensitivity for cancer detection as far as the biopsy sites were concerned but did not improve the overall diagnostic performance of ultrasound. Pelzer *et al*. (2005), alternatively, reported that the combined use of contrast-enhanced color Doppler ultrasound and

systematic biopsies increased the detection rate of PC in a group of patients with a total PSA of 4–10 ng/ml.

Contrast-enhanced power Doppler ultrasonography is another method for combining the use of contrast agents with Doppler imaging; however, the efficacy of the technique was questioned in a prospective study where 32 patients with digital rectal examination findings suspicious for malignancy and/or a serum PSA level higher than 4 ng/dl were evaluated. Power Doppler ultrasound images before and after sonocontrast (Levovist®, Schering, Berlin, Germany) injection were obtained to characterize the hypoechoic prostate nodules in the peripheral zone detected by transrectal ultrasound. They labeled mixed and penetrating patterns of vascularity as suggestive for malignancy, whereas peripheral and central types of vascularity were thought to be associated with benign prostatic tissue. It was found that both benign and malignant nodules might show hypervascularity and malignant patterns vascularity on power Doppler ultrasound morphologically. Accordingly, they concluded that the use of contrast-enhanced power Doppler ultrasound did not provide a considerable benefit for the detection of PC on a morphological basis, as its specificity was very low despite its relatively higher sensitivity.

In another study, contrast-enhanced three-dimensional (3-D) imaging of prostate vasculature with power Doppler was used to obtain 3-D image reconstructions before and after intravenous administration of Levovist. Afterwards, random and/or directed transrectal ultrasound guided biopsies were performed, and prostatic vasculature was evaluated for symmetry and vessel distribution. They also calculated the sensitivity and specificity of enhanced images at 85% and 80%, respectively, whereas the relevant values for unenhanced images and conventional gray scale transrectal ultrasound were 38% with 80% and 77% with 60%, respectively. On the other hand, Unal *et al*. (2000) proposed the combination of 3-D contrast-enhanced power Doppler ultrasound and PSA levels as the most suitable diagnostic predictor for PC (Unal *et al*., 2000). Importantly, time to peak enhancement was noted as the most predictive parameter for the localization of the major malignant prostate lobe (Wijkstra *et al*., 2004). Based on the inherent potential of 3-D contrast-enhanced power Doppler ultrasound to visualize the lesions with increased microvessel density, Sedelaar *et al*. claimed that the technique could be used for the detection of PC (2001).

Gray scale harmonic imaging further permits low-energy imaging of contrast agents resulting in less bubble destruction and allowing the microbubble agents to progress further into the microvessels for imaging. Contrary to the aforementioned research on contrast-enhanced color Doppler ultrasound, harmonic imaging techniques are associated with the detection of non-linear responses of the bubbles. A recent approach for contrast-enhanced imaging of the prostate is phase inversion (pulse-inversion) technology, which made broad bandwidth harmonic imaging possible contrary to the early ultrasound systems using a narrow bandwidth technology to insonate tissue with a narrow range of fundamental frequencies. The technique improved the detection of the signals reflected by the microbubbles, providing a further improvement for the assessment of tissue perfusion (Wijkstra

et al., 2004). It is noteworthy that narrow bandwidth is associated with a loss of spatial resolution, whereas broad bandwidth harmonic imaging allows gray scale harmonic imaging of ultrasound microbubble contrast agents with high resolution.

Contrast-enhanced color or power Doppler imaging shows primarily the flow in relatively larger vessels owing to the destruction of the microbubbles by Doppler imaging before reaching the neovessels. The parenchymal enhancement relying on the imaging of microbubbles traveling into microvessels is the focus of contrast-enhanced gray scale harmonic imaging. Finally, intermittent imaging, which provides a further improvement in the survival of microbubbles, increases the paranchymal enhancement. The technique of harmonic gray scale imaging incorporated into targeted biopsies of the prostate has several advantages compared to conventional color or power Doppler imaging. First, the harmonic gray scale does not bloom around a vessel. Besides, an inherently higher degree of spatial and temporal resolution, the technique allows accurate placement of the biopsy needle as it is visualized better. Moreover, no color flash artifact that would potentially limit the visibility of the needle penetrating the prostate is seen around the biopsy needle.

In a prospective study, Halpern and Strup (2000) evaluated contrast-enhanced transrectal ultrasound findings in patients undergoing sextant biopsy of the prostate. Thereby, each subject was evaluated with conventional gray scale, harmonic gray scale, and power Doppler ultrasound both before and after the infusion of the contrast agent, and it was found that contrast-enhanced transrectal ultrasound provided a significant improvement in the sensitivity for PC detection without any decrease in specificity (Halpern and Strup, 2000). In a similar study by Halpern *et al*. (2001b), harmonic gray scale enhancement was correlated with sextant biopsy whereby the sensitivity for the detection of PC increased from 38% of baseline examinations to 65% of post-infusion imaging. Moreover, analysis of the histopathological outcome for targeted biopsies of the sites of enhancement in a high degree revealed a significant increase for cancer detection (Halpern *et al*., 2001b). Interestingly, the lesions detected by contrast enhancement were proven to be associated with a higher Gleason score (Halpern *et al*., 2001b).

ELASTOGRAPHY

Elastography (strain imaging) was first introduced in 1991 by Ophir *et al*. (1991). The philosophy of the method is that backscattered US signal changes little in degree if the insonified tissue is slightly compressed and decompressed during the examination. The compressibility of the insonified tissue has an impact on time or space differences between regions of interest having different compression ratios. Technically, the change in the pressure applied to the prostate via the probe during the transrectal ultrasound examination changes the real-time ultrasound image constructed, showing only the changes in local tissue compression (Loch, 2007). Thereby, cancerous tissue can be distinguished from benign tissue by means of its hardness gradient and degree of elasticity loss (Loch, 2007). PC, which is characterized by limited elasticity or compressibility, is depicted sonographically as a dark zone.

Elastography has been suggested as a potential imaging modality for the detection

of PC. An improvement of 20% for positive biopsies was achieved with the combined use of real-time elastography and conventional gray scale transrectal ultrasound compared to the use of the latter technique alone. Recently, Miyanaga *et al.* (2006) reported that the detectability of PC with elastography (93%) was obviously better than digital rectal examination and transrectal ultrasound. Very recently, Pallwein *et al.* (2007) suggested contrast-enhanced ultrasound and elastography as new advances for ultrasound of the prostate as they improve PC detection and may be useful for PC grading and staging as well.

TRANSRECTAL ULTRASOUND-GUIDED PROSTATE BIOPSY

Transrectal ultrasound has dramatically changed the prostate biopsy technique. Currently, transrectal ultrasound-guided prostate biopsy has been accepted as the "gold standard" method for the detection of PC. Each year, approximately 500,000 prostate biopsies are performed in the United States (Soloway, 2003). Apart from the diagnosis of PC, the biological potential of the individual tumor should be detected as it has a significant impact on patient management. In this regard, Gleason grade, a measure of the tumor aggressiveness, should be detected. Accordingly, a Gleason score of less than four represents well-differentiated cancers whereas one greater than seven signifies poorly differentiated, aggressive tumors. In addition to the Gleason score as the most reliable prognostic factor, the number of cores with the disease and the percentage of tumor in each core are considered in the management of the tumor and the assessment of the prognosis. Hence, prostate biopsy plays a pivotal role in the management of PC.

Among the other image-guided biopsies, transrectal ultrasound-guided prostate biopsy is unique in that it is associated with zone-based systematic sampling from the regions of the prostate where the tumors are most likely to be located, rather than being lesion directed. This approach is based on the multicentric nature of the disease and the limited diagnostic ability of transrectal ultrasound for cancer detection. Classically, suspicious digital rectal examination findings and/or a total PSA level exceeding 4 ng/ml are considered to increase the risk for PC. However, there is still no consensus on the upper limit for normal PSA. For better identification of the high-risk individuals who should be referred for biopsy, PSA refinements such as age-adjusted PSA, PSA velocity, and ratio of free PSA/total PSA are considered. As the vast majority (80%) of PCs are located in the peripheral zone and associated with a higher Gleason grade and risk for metastasis compared to inner gland cancers, the sampling strategy of prostate biopsy is directed to the peripheral zone.

In the early 1980s, transrectal ultrasound-guided prostate biopsy was first introduced as targeted biopsies for nodular lesions and was later found to miss a significant number of cancers. The classical sextant sampling protocol was associated with sampling from the cores located halfway between the lateral border and the median plane of the prostate at the levels of the base, mid-gland, and apex. The modification of sextant sampling as modified sextant or extended sampling protocols and saturation biopsies came into use over time as a result of intense efforts aiming to increase the diagnostic yield of the procedure. The

main idea behind these modifications was that increasing the number of cores and directing the cores more laterally would decrease the false-negative rates. However, there has still been no consensus on the optimal sites and the number of cores to be biopsied. PC has been reported to expand mostly in the transverse plane across the posterior capsule surface, followed by the craniocaudal direction. In this regard, it is supposed that shifting of the biopsy cores more lateral to the mid-parasagittal line might enhance the capability to sample the relatively outer peripheral zone rendering most of the cancers. In a study by Eichler *et al*. (2006), biopsy schemes consisting of 12 cores, including laterally directed cores as well as the standard sextant scheme, provided a balance between the rate of cancer detection and the adverse effect associated with the procedure. They added that the rate of detection for the cancer did not increase significantly with 18–24 core schemes (Eichler *et al*., 2006).

The current trend for primary biopsies is not to include the inner gland sampling into the routine protocol due to their low yield of cancer and less aggressive nature of the relevant cancers. In one study performed on 390 men undergoing repeat biopsy, Liu *et al*. (2001) reported that the true rate for cancer detection in inner gland biopsies was around 2%. Additionally they noted that the rate of cancers detected only on inner gland biopsies was around 10%.

REPEAT BIOPSIES

Occasionally, abnormal biochemical parameters persist despite a negative first biopsy. The indications for a repeat biopsy are a persistently high or rising PSA level, an abnormal digital rectal examination, high-grade prostatic intraepithelial neoplasia, or atypical small acinar proliferation. Assuming that the initial biopsy may have missed the cancer because of its small volume or its inner gland location, areas of the prostate not routinely sampled in the initial biopsy such as the anterior horn of the peripheral zone, lateral areas, and the inner gland should be sampled in the repeat biopsy. In addition, the number of cores to be sampled should be increased up to 24 to decrease the need for a future rebiopsy (Boczko *et al*., 2006).

High-grade prostatic intraepithelial neoplasia with the transrectal ultrasound feature of clusters of millimetric hypoechoic foci as well as hypoechoic areas with well-defined margins or heterogeneous echotexture are accepted as precursors for PC (Bostwick, 2000). It is agreed that high-grade prostatic intraepithelial neoplasia cases, especially when accompanied by high PSA or suspicious digital rectal examination findings, should be candidates for repeat biopsies. Besides, high-grade prostatic intraepithelial neoplasia is considered to be concurrent with a remote location. Therefore, a repeat biopsy procedure should sample the whole gland, paying particular attention to the inner gland and high predilection areas of the peripheral zone rather than focusing on the sites with high-grade prostatic intraepithelial neoplasia reported with the initial biopsy. However, a site-specific approach focusing around the suspicious areas is necessary for sampling the cases diagnosed as atypical small gland proliferation in the previous biopsy. This is based on the assumption that the insufficiency of the diagnostic material on the previous biopsy was either because of the small size of the tumor or the biopsy needle passed through the edge of

an adjacent tumor. In cases with a persistent suspicion of PC despite repeated negative biopsies, the use of saturation biopsy techniques with more than 20 cores involving the sampling of the gland evenly without considering any specific zonal pattern is recommended. It is noteworthy that the duration between the previous biopsy and the repeat biopsy should be at least 6 weeks.

COMPLICATIONS

Some minor morbidity may be seen with prostate biopsy by transrectal ultrasound, though major complications are rare and the procedure is generally considered to be well-tolerated and safe. Perineal pain, mild hematuria lasting a few days, hematospermia, mild rectal bleeding, and asymptomatic bacterium or bacteriuria are among the relatively frequent minor complications, at least one of which can be detected in 70% of patients undergoing the procedure (Djavan *et al*., 2002; Lindert *et al*., 2000). Severe complications such as severe rectal bleeding or hematuria, fever, sepsis, urinary infection, urinary retention, periprostatic hematoma or epididymitis are very rare.

Direct compression of the rectal mucosa with a transrectal ultrasound probe might be a conservative measure against severe rectal bleeding; hospitalization may be necessary for severe cases. The discontinuation of aspirin, nonsteroidal anti-inflammatory drugs, and anticoagulants 7–10 days before the biopsy procedure has been suggested to be helpful in minimizing urinary and rectal hemorrhagic complications (Margreiter, 2007). Likewise, intravenous antibiotic therapy against the most commonly encountered responsible microorganisms such as coliforms, anaerobes, and gram positive organisms is considered to be helpful for urinary infection. The agreed preprocedural measure to prevent the development of infectious complications is prophylaxis, mostly with fluorokinolones before, the day of, and after the biopsy procedure, though the optimal regimen has not been defined (Sadeghi-Nejad *et al*., 2006). However, the application of a prebiopsy cleansing rectal enema, which is administered to minimize the infectious complications as well as for obtaining an optimal transrectal ultrasound image, is controversial. Urinary retention, on the other hand, may necessitate catheterization. In general, the rate of complications is reported not to increase with an increase in the number of peripheral zone cores biopsied. However, an increased number of inner gland biopsies has been suggested to be associated with an increase in the rate of urinary retention.

PAIN OR DISCOMFORT

A considerable degree of pain or discomfort expressed by as many as 30% of patients has been reported. Likewise, nearly one-fifth of the patients who underwent the procedure were not biopsied without anesthesia (Irani *et al*., 1997). Moreover, 6% of the patients in the same study declared that it should have been performed under general anesthesia. Irani *et al*., (1997) noted that more than one-fifth of the patients requested sedation if they had to be biopsied again. Our observation during the daily practice regarding the necessity of anesthesia concurred with the literature data. The increasing number of patients undergoing prostate biopsy as

well as the high percentage of patients requiring repeat biopsy, reminding them of unpleasant memories from the previous biopsy, and associated with the increased number of inner gland cores sampled reinforce the significance of pain related to prostate biopsies. In addition, an age-dependent pattern for pain experienced by younger patients expressing a higher discomfort rate intensifies the need for anesthesia. Rather than the insertion of the probe and the maneuvers aiming to visualize the gland extensively and to align the biopsy needle for the sampling procedure, penetration of the prostate capsule by the biopsy needle through the rectal wall causing the stimulation of the sensory receptors located in the capsule is considered to be the main factor for the pain associated with the procedure.

ANESTHESIA

Apart from the rarely applied methods such as nitrous oxide inhalation or general anesthesia, periprostatic nerve block under transrectal ultrasound guidance has been the most popular and effective method of anesthesia for increasing patient tolerance during the prostate biopsy. The technique involves the penetration of the Denonvilier's fascia at the posterolateral aspect of the base of the prostate by a 22G needle and the infiltration of the anesthetic agent (lidocaine without epinephrine) to the lateral aspect of the prostate seminal vesicle junction around the neurovascular bundle. It has been reported that a combination of short- and long-term anesthetics would be useful for avoiding rebound pain. Fewer in number and amount of injections of the potentially contaminated anesthetic agent is advised to lessen the associated complications, though no consensus has been reached yet on the exact site, amount, and number of injections. The mean visual analogue score reported in the literature for the efficiency of the periprostatic anesthetic infiltration, the overwhelming majority of which is less than four, corresponds to a mild degree of discomfort and signifies an improvement in patient comfort (Irani *et al*., 1997; Turgut *et al*., 2006; Alavi *et al*., 2001).

Periprostatic block might have some potential complications, such as the need for repeat injections, lidocaine toxicity, urinary incontinence due to the theoretical risk of relaxation of the external sphincter, distortion or artifact formation on the transrectal ultrasound image, periprostatic infection, and erectile dysfunction (Stirling *et al*., 2002; Vaidya and Soloway, 2001). Besides, the operator dependent nature and inefficiency of the pain due to probe insertion are among the disadvantages of the technique. Moreover, poor improvement for patient comfort in the presence of risk factors such as patient anxiety, repeat biopsies, or increased anal tone due to hemorrhoids and anal fissure are limitations of periprostatic anesthesia.

Recently, we conducted a prospective study to evaluate the efficacy of conscious sedation, an accepted method proven to be useful for lessening patient discomfort related to interventional radiological procedures, and to compare it with periprostatic anesthesia (Turgut *et al*., 2006). Thereby, the mean visual analogue scores of 1.4 and 2.0 for the subgroups of patients receiving conscious sedation with intravenous midazolam and periprostatic lidocaine injection, respectively, were lower than the mean discomfort score of 4.7 for those receiving no anesthetic (Turgut *et al*., 2006). Moreover, we noticed that the

number of patients with scores exceeding four, corresponding to moderate to severe discomfort, which we believe to be the target population for the measures aimed to relieve the discomfort, were significantly lower in the sedation subgroup compared to the other two (Turgut *et al*., 2006). Accordingly, we concluded that sedation would be an alternative to increase patient comfort in the presence of risk factors for the lower degree of benefit from periprostatic anesthesia (Turgut *et al*., 2006).

THERAPEUTIC APPLICATIONS OF TRANSRECTAL ULTRASOUND FOR PROSTATE CANCER

Several reports in the literature have focused on the potential utility of real-time transrectal ultrasound guidance for surgical precision during laparoscopic radical prostatectomy. Ukimura *et al*. (2004) reported that real-time intraoperative transrectal ultrasound monitoring during the operation using gray scale, power Doppler, and 3-D imaging would be helpful for mapping important periprostatic structures such as neurovascular bundle, bladder neck, seminal vesicle, vas deferens, rectal wall, and membranous urethra as well as for the depiction of a bulging prostatic nodule. In another study, Ukimura *et al*. (2006) reported that the rate of positive surgical margins was significantly lower in patients undergoing laparoscopic radical prostatectomy with intraoperative real-time transrectal ultrasound navigation compared to those who underwent the operation without intraoperative transrectal ultrasound imaging.

Utility of contrast-enhanced utlrasound during radio frequency ablation of the prostate as a mode of minimally invasive treatment for PC has been evaluated. A new therapeutic strategy for the treatment of PC, with radio frequency ablation under contrast-enhanced pulse inversion harmonic imaging has been proposed.

TRANSRECTAL ULTRASOUND IN THE EVALUATION OF LOCAL RECURRENCE AFTER RADICAL PROSTATECTOMY

Currently, the detection of locally recurrent PC is based on the combined use of digital rectal examination, transrectal ultrasound, and transrectal ultrasound -guided prostate biopsy. Gray scale transrectal ultrasound examination alone is not sufficient for the differentiation of postoperative fibrosis from the recurrence of PC. Transrectal ultrasound -guided prostatic fossa biopsy, on the other hand, remains the most efficient method for the diagnosis of local recurrence after radical retropubic prostatectomy. Earlier, the application of Doppler imaging during transrectal ultrasound-guided biopsy of the prostatic fossa was reported to increase the sensitivity and specificity of gray scale findings. In a recent study by Tamsel *et al*. (2006), power Doppler examination facilitating the identification of hypervascular areas during transrectal ultrasound-guided prostate biopsy has been suggested to be helpful for the earlier detection of local recurrent tumors with the typical finding of increased vascularity within the tumoral tissue.

REFERENCES

Alavi, A.S., Soloway, M.S., Vaidya, A., Lynne, C.M., and Gheiler, E.L. 2001. Local anesthesia for ultrasound guided prostate biopsy: a prospective randomized trial comparing 2 methods. *J. Urol. 166*: 1343–1345.

American Cancer Society 2004. Cancer facts and figures. American Cancer Society, Atlanta.

American Cancer Society 2007. Cancer facts and figures. American Cancer Society, Altanta.

Boczko, J., Messing, E., and Dogra, V. 2006. Transrectal sonography in prostate evaluation. *Radiol. Clin. North Am. 44*: 679–687.

Bostwick, D.G. 2000. Prostatic intraepithelial neoplasia. *Curr. Urol. Rep. 1*: 65–70.

Carey, B.M. 2005. Imaging for PC. *Clin. Oncol. (R. Coll. Radiol.) 17*: 553–559.

Cho, J.Y., Kim, S.H., and Lee, S.E. 1998. Diffuse prostatic lesions: role of color Doppler and power Doppler ultrasonography. *J. Ultrasound Med. 17*: 283–287.

Coley, C.M., Barry, M.J., Fleming, C., and Mulley, A.G. 1997. Early detection of prostate cancer: part I prior probability and effectiveness of tests. *Ann. Intern. Med. 126*: 394–406.

Cornud, F, Hamida, K., Flam, T, Helenon, O., Chretien, Y., Thiounn, N., Correas, J.M., Casanova, J.M., and Moreau, J.F. 2000. Endorectal color doppler sonography and endorectal MR imaging features of nonpalpable PC: correlation with radical prostatectomy findings. *AJR Am. J. Roentgenol. 175*: 1161–1168.

De la Rosette, J.J., and Aarnink, R.G. 2001. New developments in ultrasonography for the detection of PC. *J. Endourol. 15*: 93–104.

Djavan, B., Zlotta, A., Kratzik, C., Remzi, M., Seitz, C., Schulman, C.C., and Marberger, M. 1999. PSA, PSA density, PSA density of transition zone, free/total PSA ratio, and PSA velocity for early detection of PC in men with serum PSA 2.5 to 4.0 ng/mL. *Urology 54*: 517–522.

Djavan, B., Remzi, M., Schulman, C.C., Marberger, M., and Zlotta, A.R. 2002. Repeat prostate biopsy: who, how and when? A review. *Eur. Urol. 42*: 93–103.

Eichler, K., Hempel, S., Wilby, J., Myers, L., Bachmann, L.M., and Kleijnen, J. 2006. Diagnostic value of systematic biopsy methods in the investigation of PC: a systematic review. *J. Urol. 175*: 1605–1612.

Frauscher, F., Klauser, A., Halpern, E.J., Horninger, W., and Bartsch, G. 2001. Detection of PC with a microbubble ultrasound contrast agent. *Lancet 357*: 1849–1850.

Frauscher, F., Klauser A., and Halpern E.J. 2002. Advances in ultrasound for the detection of PC. *Ultrasound Q*. 18: 135–142.

Grossfeld G.D., and Coakley F.V. 2000. Benign prostatic hyperplasia: clinical overview and value of diagnostic imaging. *Radiol. Clin. North Am. 38*: 31–47.

Hall, M.C., Troncoso, P., Pollack, A., Zhau, H.Y., Zagars, G.K., Chung, L.W., and von Eschenbach, A.C. 1994. Significance of tumor angiogenesis in clinically localized prostate carcinoma treated with external beam radiotherapy. *Urology 44*: 869–875.

Halpern, E.J., and Strup, S.E. 2000. Using gray-scale and color and power Doppler sonography to detect prostatic cancer. *AJR Am. J. Roentgenol. 174*: 623–627.

Halpern, E.J., Frauscher, F., Rosenberg, M., and Gomella, L.G. 2001a. Directed biopsy during contrast-enhanced sonography of the prostate. *AJR Am. J. Roentgenol. 178*: 915–919.

Halpern, E.J., Rosenberg, M., and Gomella, L.G. 2001b. PC: contrast-enhanced us for detection. *Radiology 219*: 219–225.

Halpern, E.J., Frauscher, F., Forsberg, F., Strup, S.E., Nazarian, L.N., O'Kane, P., and Gomella, L.G. 2002. High-frequency Doppler US of the prostate: effect of patient position. *Radiology 222*: 634–639.

Halpern, E.J. 2006. Contrast-enhanced ultrasound imaging of prostate cancer. *Rev. Urol. 8*: S29–37.

Irani, J., Fournier, F., Bon, D., Gremmo, E., Dore, B., and Aubert, J. 1997. Patient tolerance of transrectal ultrasound-guided biopsy of the prostate. *Br. J. Urol. 79*: 608–610.

Jain, S.P., Fan, P.H., Philpot, E.F., Nanda, N.C., Aggarwal, K.K., Moos, S., and Yoganathan, A.P. 1991. Influence of various instrument settings on the flow information derived from the power mode. *Ultrasound Med. Biol. 17*: 49–54.

Lee, F., Torp-Pedersen, S., Littrup, P.J., McLeary, R.D., McHugh, T.A., Smid, A.P., Stella, P.J., and Borlaza G.S. 1989. Hypoechoic lesions of the prostate: clinical relevance of tumor size,

digital rectal rectal examination, and prostate-specific antigen. *Radiol. 170*: 29–32.

Lindert, K.A., Kabalin, J.N., and Terris, M.K. 2000. Bacteremia and bacteriuria after transrectal ultrasound guided prostate biopsy. *J. Urol. 164*: 76–80.

Lissbrandt, I.F., Stattin, P., Damber, J.E., and Bergh, A. 1997. Vascular density is a predictor of cancer-specific survival in prostatic carcinoma. *Prostate 33*: 38–45.

Liu, I.J., Macy, M., Lai, Y.H., and Terris, M.K. 2001. Critical evaluation of the current indications for transition zone biopsies. *Urology 57*: 1117–1120.

Loch, T. 2007. Urologic imaging for localized PC in 2007. *World J. Urol. 25*: 121–129.

Miyanaga, N., Akaza, H., Yamakawa, M., Oikawa, T., Sekido, N., Hinotsu, S., Kawai, K., Shimazui, T., and Shiina, T. 2006. Tissue elasticity imaging for diagnosis of PC: a preliminary report. *Int. J. Urol. 13*: 1514–1518.

Neumaier, C.E., Martinoli, C., Derchi, L.E., Silvestri, E., and Rosenberg, I. 1995. Normal prostate gland: examination with color Doppler US. *Radiology 196*: 453–457.

Okihara, K., Miki, T., and Babaian, R.J. 2002. Clinical efficacy of PC detection using power doppler imaging in American and Japanese men. *J. Clin. Ultrasound 30*: 213–221.

Ophir, J., Cespedes, I., Ponnekanti, H., Yazdi, Y., and Li, X. 1991. Elastography: a quantitative method for imaging the elasticity of biological tissues. *Ultrason. Imaging 13*: 111–134.

Ozden, E., Yaman, O., Gogus, C., Ozgencil, E., and Soygur, T. 2003. The optimum doses of and injection locations for periprostatic nerve blockade for transrectal ultrasound guided biopsy of the prostate: a prospective, randomized, placebo controlled study. *J. Urol. 170*: 2319–2322.

Pallwein, L., Mitterberger, M., Gradl, J., Aigner, F., Horninger, W., Strasser, H., Bartsch, G., zur Nedden, D, and Frauscher, F. 2007. Value of contrast-enhanced ultrasound and elastography in imaging of PC. *Curr. Opin. Urol. 17*: 39–47.

Papatheodorou, A., Ellinas, P., Tandeles, S., Takis, F., Poulias, H., Nikolaou, I., and Batakis, N. 2005. Transrectal ultrasonography and ultrasound-guided biopsies of the prostate gland: how, when, and where. *Curr. Probl. Diagn. Radiol. 34*: 76–83.

Pelzer, A., Bektic, J., Berger, A.P., Pallwein, L., Halpern, E.J., Horninger, W., Bartsch, G., and Frauscher, F. 2005. PC detection in men with prostate specific antigen 4 to 10 ng/ml using a combined approach of contrast enhanced color Doppler targeted and systematic biopsy. *J. Urol. 173*: 1926–1929.

Purohit, R.S., Shinohara, K., Meng, M.V., and Carroll, P.R. 2003. Imaging clinically localized PC. *Urol. Clin. North Am. 30*: 279–293.

Rifkin, M.D., Sudakoff, G.S., and Alexander, A.A. 1993. Prostate: techniques, results, and potential applications of color Doppler US scanning. *Radiol. 186*: 509–513.

Sadeghi-Nejad, H., Simmons, M., Dakwar, G., and Dogra, V. 2006. Controversies in transrectal ultrasonography and prostate biopsy. *Ultrasound Q. 22*: 169–175; 386–388.

Sedelaar, J.P., van Leenders, G.J., Hulsbergen-van de Kaa, C.A., van der Poel, H.G., van der Laak, J.A., Debruyne, F.M., Wijkstra, H., and de la Rosette, J.J. 2001. Microvessel density: correlation between contrast ultrasonography and histology of PC. *Eur Urol. 40*: 285–293.

Shigeno, K., Igawa, M., Shiina, H., Wada, H., and Yoneda T. 2000. The role of colour Doppler ultrasonography in detecting PC. *BJU Int. 86*: 229–233.

Soloway, M.S. 2003. Do unto others - why I would want anesthesia for my prostate biopsy. *Urology 62*: 973–975.

Stirling, B.N., Shockley, K.F., Carothers, G.G., and Maatman, T.J. 2002. Comparison of local anesthesia techniques during transrectal ultrasound-guided biopsies. *Urology 60*: 89–92.

Tamsel, S., Killi, R., Apaydin, E., Hekimgil, M., and Demirpolat, G. 2006. The potential value of power Doppler ultrasound imaging compared with grey-scale ultrasound findings in the diagnosis of local recurrence after radical prostatectomy. *Clin. Radiol. 61*: 325–330.

Turgut, A.T., Ergun, E., Kosar, U., Kosar, P., and Ozcan, A. 2006. Sedation as an alternative method to lessen patient discomfort due to transrectal ultrasonography-guided prostate biopsy. *Eur. J. Radiol. 57*: 148–153.

Ukimura, O., Gill, I., Desai, M., Steinberg, A., Kilciler, M., Ng, C., Abreu, S., Spaliviero, M.,

Ramani, A., and Kaouk, J. 2004. Real-time transrectal ultrasonography during laparoscopic radical prostatectomy. *J. Urol. 172*: 112–118.

Ukimura, O., Magi-Galluzzi, C., and Gill, I.S. 2006. Real-time transrectal ultrasound guidance during laparoscopic radical prostatectomy: impact on surgical margins. *J. Urol. 175*: 1304–1310.

Unal, D., Sedelaar, J.P., Aarnink, R.G., van Leenders, G.J., Wijkstra, H., Debruyne, F.M., and de la Rosette, J.J. 2000. Three-dimensional contrast-enhanced power Doppler ultrasonography and conventional examination methods: the value of diagnostic predictors of PC. *BJU Int. 86*: 58–64.

Vaidya, A., and Soloway. M.S. 2001. Periprostatic local anesthesia before ultrasound-guided prostate biopsy: an update of the miami experience. *Eur. Urol. 40*: 135–138.

Wijkstra, H., Wink, M.H., and de la Rosette, J.J. 2004. Contrast specific imaging in the detection and localization of PC. *World J. Urol. 22*: 346–350.

Yi, A., Kim, J.K., Park, S.H., Kim, K.W., Kim, H.S., Kim, J.H., Eun, H.W., and Cho, K.S. 2006. Contrast-enhanced sonography for PC detection in patients with indeterminate clinical findings. *AJR Am. J. Roentgenol. 186*: 1431–1435.

36
Prostate Cancer: 16β-[^{18}F] Fluoro-5α-Dihydrotesterone (FDHT) Whole-Body Positron Emission Tomography

Pat Zanzonico

INTRODUCTION

Prostate cancer (PC) is the second most common cause of cancer-related mortality in the United States, with over 40,000 deaths per year (Horst *et al*., 1995; Jemal *et al*., 2003). This cancer exhibits a complex, temporally varying natural history (Visakorpi *et al*., 1995; Fenton *et al*., 1997; Craft *et al*., 1999), and metastatic PC is difficult to treat effectively. Virtually all PCs are initially sensitive to androgen receptor (AR)-mediated signaling and respond to AR blockade or androgen withdrawal. Medical or surgical suppression of androgen action is thus standard first-line therapy for non-resectable PC, and most commonly focuses on androgen ablation, that is, reducing the production of testosterone. Testosterone is converted in the prostate to dihydrotestosterone (DHT), which in turn binds to and activates the AR. The activated receptor regulates the transcription of a number of target genes which support and stimulate the growth of prostatic tissue. The clinical benefits of castration depend on the degree to which the tumor is dependent on androgens for growth and survival, but it is not a curative strategy; the disease will eventually alter its biology, becoming hormone-independent (i.e., castration-resistant) and will continue to grow despite ongoing androgen suppression (Agus *et al*., 1999). In the clinical state model of PC progression (Scher and Heller, 2000), patients who have failed such therapy are distinguished as either non-castrate or castrate based on measured testosterone concentrations in blood, with castration-resistance representing the lethal variant of the disease.

THE POTENTIAL ROLE OF ANDROGEN-RECEPTOR IMAGING IN PROSTATE CANCER

A number of aberrant metabolic and signaling pathways contribute to the development of the metastatic phenotype, and the emergence of castration-resistant (i.e., hormone-independent), progressing PC leads inexorably to the death of the patient.

Pathological and molecular analyses of progressing PC show evidence of mutant but still-functional AR expression, the presumptive cause of androgen-independent (i.e., promiscuous) AR activation (Fenton *et al*., 1997). Alternative, non-mutually exclusive mechanisms of castration resistance include increased tumoral levels of wild-type ARs (Visakorpi *et al*., 1995), increased intra-tumoral levels of adrenal androgens, and ligand-independent activation by growth factors such as receptor-linked tyrosine kinases and cytokines (Kelloff *et al*., 2005). To systematically study the biology of PC and its progression and to develop therapies that effectively target ARs require methods of assessing receptor expression and functional status. However, such analyses are problematic in that PC predominantly metastasizes to bone, a site which is difficult to biopsy. Furthermore, the biology of metastatic PC can differ from that of the primary tumor and can vary among metastatic lesions. Sampling of the primary tumor or of individual metastases therefore does not necessarily reflect the AR status of the metastatic disease generally, likely accounting for the poor correlation between AR positivity and clinical response to androgen withdrawal (Barrack and Tindall, 1987). The development of whole-body molecular imaging techniques for the assessment of the AR signaling pathway in PC would thus provide a clinically more meaningful representation of the overall AR status of the disease.

Except for treatment with AR-binding anti-androgens (Neri, 1989), AR imaging could be performed over the entire course of hormonal treatment, as androgen-ablative therapies such as orchiectomy and administration of estrogenic therapies leave the ARs unoccupied. Such biologic (i.e., functional) imaging of cancer, particularly of signaling pathways and other molecular features leading to resistance to specific therapies and disease progression, would dramatically impact clinical decision-making and potentially eliminate the need for invasive and sample-limited (i.e., undersampled) biopsies. In PC, characterization of AR functionality would allow the clinician to switch a patient's therapy in a timely manner from androgen withdrawal once the disease has become hormone-unresponsive and would therefore progress despite effective androgen suppression. In addition, AR imaging may eventually illuminate the basic biology of PC by providing a noninvasive assay of receptor levels in vivo.

POSITRON EMISSION TOMOGRAPHY

A "tomogram" is literally a picture of a slice. Tomography may be characterized as either transmission or emission tomography, depending on the origin of the radiation. In transmission tomography (i.e., computed tomography [CT]), x-rays are transmitted through the patient whereas in emission tomography, X- or γ-rays are emitted from within the patient. Emission tomography can be further characterized on the basis of the nature of the emitted radiation. Single photons, such as γ-rays associated with isomeric transition and X-rays associated with electron capture or internal conversion, form the basis of single-photon emission computed tomography (SPECT) (Zanzonico, 1995). The two 511-keV annihilation photons simultaneously emitted following positron emission and the subsequent positron-negatron annihilation form the basis of positron

emission tomography (PET) (Zanzonico, 2004).

Positron emission tomography (PET) is based on the annihilation coincidence detection (ACD) of these two co-linear 511-keV γ-rays. When signals from the two coincidence detectors simultaneously trigger the coincidence circuit, an output, or coincidence event, is generated by this circuit. The event is localized to the volume (or "line of response") between the opposed coincidence detectors. State-of-the-art PET scanners employ a series of rings of discrete, small-area detectors encircling the patient and typically spanning a distance of 10–20 cm in the patient's longitudinal direction. By longitudinal motion of the patient through the detector gantry, scans can be acquired at discrete bed positions, and then merged (or "knitted") into a whole-body scan – typically in 30–40 min. The distinctive features of PET among radionuclide imaging modalities include excellent spatial resolution – of the order of 5 mm (expressed as the full-width half-maximum of the line spread function) and high sensitivity – 100 to 1,000-fold higher than that of SPECT. In contrast to SPECT, accurate attenuation and scatter correction and therefore accurate quantitation of radiotracer activities in situ are achievable with PET. Radiotracer activity concentrations are often expressed as the standard uptake value (SUV), kilobecquerel found/gram of tissue per kilobecquerel injected/gram of body mass.

The major manufacturers of medical imaging instrumentation now market multi-modality scanners, combining high-performance state-of-the-art PET and CT scanners in a single device (Schoder *et al.*, 2003; Townsend *et al.*, 2004). These instruments provide near-perfect registration of images of *in vivo* function (PET) and anatomy (CT). Such scanners are already having a major impact on clinical practice, particularly in oncology, and are currently outselling "PET-only" systems 2 to 1. Although generally encased in a single seamless housing, the PET (or SPECT) and CT gantries in such devices are separate; the respective fields of view are separated by a distance of the order of 1 m and the PET and CT scans are actually performed sequentially.

The pertinent properties of radionuclides for PET include: the physical half-life ($T_{1/2}$), the branching ratio (i.e., the percentage of total decays resulting in positron emission), and the maximum positron energy (E_{max}), corresponding maximum extrapolated range (R_{max}), and root-mean-square (rms) range (R_{rms}). Many positron-emitting radioisotopes also emit significant numbers of high-energy prompt γ-rays, and such γ-rays may be in cascade with each other or with the positrons. These can result in radiations scattered into the 511-keV photopeak energy window (~350–750 keV) typically used in PET, and therefore spurious, erroneously positioned coincidence events occur (Zanzonico, 2004). Although such events degrade overall quality and quantitative accuracy, isotopes such as copper-62 (^{62}Cu), gallium-66 (^{66}Ga), gallium-68 (^{68}Ga), bromine-75 (^{75}Br), rubidium-82 (^{82}Ru), yttrium-86 (^{86}Y), and iodine-124 (^{124}I) have nonetheless been used effectively in PET (Pentlow *et al.*, 1996, 2000).

The overall spatial resolution of PET scanners results from a combination of instrumentation and physical factors, including the positron range. For positron emitters used to date in PET, the maximum energies (E_{max}) vary from 0.58 to 3.7 MeV and the corresponding extrapolated ranges (R_e) from 2 to 20 mm, and

the root-mean-square (rms) ranges (R_{rms}) from 0.2 to 3.3 mm (Zanzonico, 2004). Although the finite positron range acts to blur PET images (i.e., degrade spatial resolution), the range-related blurring is mitigated by the spectral distribution of positron energies for a given radioisotope as well as the characteristically tortuous path positrons travel. These effects are reflected by that the fact the rms positron ranges are nearly ten-fold shorter than the extrapolated positron ranges (Derenzo, 1986; Levin and Hoffman, 1999). The perpendicular distance the positron travels (which actually impacts imaging resolution) is thus considerably shorter than the actual path length it travels. For example, the positron range degrades spatial resolution by only ~0.1 mm for fluorine-18 (E_{max} = 640 keV) and ~0.5 mm for oxygen-15 (E_{max} = 1,720 keV). These values are much closer to the respective rms positron ranges, 0.2 and 0.9 mm, than to the respective extrapolated positron ranges, 2.3 and 8.0 mm (Derenzo, 1986; Levin and Hoffman, 1999).

PRE-CLINICAL STUDIES OF ANDROGEN RECEPTOR RADIOLIGANDS

Androgen receptor (AR) ligands have been radiolabeled with the positron-emitting nuclides fluorine-18 and carbon-11 and with radioisotopes of bromine, iodine, and selenium (Liu *et al*., 1992a; Bonasera *et al*., 1996). ^{18}F-labeled radioligands are, for a number of reasons, particularly attractive as probes for AR imaging. ^{18}F can be produced in large amounts on "standard" (i.e., relatively low-beam energy) medical cyclotrons. It has a favorable half-life of 1.8 h, long enough for off-site production and radiotracer synthesis at a regional facility and subsequent transport to the clinical site (as is now commonly done for ^{18}F-labeled fluoro-deoxyglucose (FDG)). In contrast, the 20-min half-life of ^{11}C is prohibitively short for off-site production. At the same time, it is short-lived enough to allow short-term repeat administration and imaging and to minimize organ doses and mitigate other radiation protection issues. ^{18}F is also readily adaptable to no-carrier-added radiosyntheses of high-specific activity receptor-binding radiotracers. Finally, its high positron branching ratio (~1) and low-energy (E_{max} = 640 keV), short-range (R_{rms} = 2 mm) positron are very favorable for PET.

Collaborators at Washington University (St. Louis, MO) and University of Illinois (Urbana, IL) were the first to synthesize and evaluate a series of fluorinated androgens – 16β-fluorine-substituted testosterone and 5α-dihydrotestosterone, 16β- and 20-fluorine-substituted mibolerone, 16α- and 16β-fluorine-substituted 7α-methyl-19-nortestosterone, and 20-fluoro-R1881 (metribolone) – with high in vitro affinity for the AR (Liu *et al*., 1991; 1992a, b). (As noted, dihydrotestosterone (DHT), which results from intra-prostatic reduction of testosterone, is the native AR-binding ligand.) In biodistribution studies in diethylstilbestrol-treated male rats, high selective uptake by the prostate was observed – 0.39–1.21% injected dose per gram (%ID/gm) at 1 h and 0.20–0.60 % ID/gm at 4 h – with prostate-to-blood and prostate-to-muscle ratios of 3.3–9.5 at 1 h and 4.1 to 35 at 4 h. The more rapidly metabolized of these compounds showed lower prostate uptake but higher uptake

ratios at 4 h. Compounds with a 16-β-fluorine substituent showed extensive metabolic de-fluorination, resulting in ~ 50% of the administered activity localizing in bone at 4 h.

Importantly, the foregoing radiofluorinated AR ligands differ substantially in their binding affinities for the progesterone receptor (PgR) and for sex-hormone binding globulin (SHBG) (Liu *et al.*, 1992b; Bonasera *et al.*, 1996). Because PC expresses PgRs (Kumar *et al.*, 1990), binding of an AR imaging agent to PgRs would confound the assessment of AR levels in prostate tumors. SHBG is a blood-borne steroid-binding glycoprotein found in primates (including humans), but not rats. While SHBG binding of AR radioligands was originally thought to reduce the bioavailability and thus the AR binding of such ligands *in vivo*, it now appears that SHBG protects androgens from metabolic degradation and also facilitates their transport from blood into AR-expressing tissues. Thus, besides a high uptake (i.e., %ID/gm) in prostatic tissue and high prostate-to-non-prostate ratios, a low binding affinity for the PgR and a high binding affinity for SHBG are desirable properties of a prospective AR imaging agent.

Based on these criteria, Bonasera *et al.* (1996) selected three of the radiofluorinated AR ligands, 16β-[18F]fluoro-5α-dihydrotestosterone ([18F]FDHT), 16β-[18F] fluoro-mibolerone (16β-[18F]Fmib), and 20-[18F]fluoro-mibolerone (20-[18F]Fmib), for further evaluation in male baboons by PET and blood sampling. Unlike rats, but like other primates, baboons have high levels of circulating SHBG. Imageable prostate activities were observed and uptakes were comparable for all three 18F-labeled AR ligands. At 60 min pi, [18F]FDHT achieved the highest prostate-to-peri-prostatic tissue ratios, 6.5–7.5 compared to 4.0–5.5 and 2.5–3.0 for 16β- and 20-[18F]Fmib, respectively. Prostate-to-blood (3.0–3.5) and prostate-to-bone (3.5–6.5) ratios for [18F]FDHT were also slightly higher than those for 16β-and 20-[18F]Fmib. Prostate uptake was dramatically reduced by coadministration of non-radioactive testosterone and was thus shown to be AR-mediated. [18F]FDHT, with a 100-fold greater binding for SHBG than either 16β- or 20-[18F]Fmib, had the highest level of parent (i.e., unmetabolized) radioligand in blood up to 45 min, as determined by thin-layer chromatography of the ethanol-extractable fraction of plasma. It achieved a 37-fold greater prostate-to-bone ratio at 2 h in baboons than in rats; presumably as a result of the protective effect against metabolic degradation of SHBG binding. Although all three of these radiofluorinated ligands can potentially be used for AR imaging, [18F]FDHT was selected for clinical evaluation based on its more specific prostate uptake and greater stability *in vivo*.

CLINICAL STUDIES OF 16β-[18F]FLUORO-5α-DIHYDROTESTERONE

Larson *et al.* (2004) performed the initial feasibility study of clinical assessment of AR expression by [18F]FDHT-PET, measuring its *in vivo* tumor targeting and pharmacokinetics in patients with metastatic PC. Seven patients with progressing clinically metastatic PC and castrate levels of testosterone underwent [18F]FDG- and [18F]FDHT-PET scans in addition to

conventional imaging studies (i.e., CT or MRI and ^{99m}Tc-methylene diphosphonate bone scans) (Figure 36.1). Three of the seven patients had their studies repeated 1 month later, two while on testosterone therapy and the third after treatment with 17-allylamino-17-demethoxygeldanamycin (17-AAG). High-pressure liquid radiochromatography (HPLC) was used to separate [^{18}F]FDHT from its radiolabeled metabolites in blood. Lesion-by-lesion comparisons of the [^{18}F]FDG, [^{18}F]FDHT, and conventional imaging studies were performed. Metabolism of [^{18}F]FDHT was rapid, with 80% or greater conversion within 10 min of injection to non-AR binding metabolites (Figure 36.2). Tumor uptake was rapid and retention was prolonged. Conveniently, therefore, [^{18}F]FDHT-PET can be conveniently performed anytime from ~30 min to ~2 h post-injection. Fifty-nine lesions (49 in bone, 10 in soft tissue) were identified by conventional imaging methods. [^{18}F]FDG-PET was positive in 57 of 59 lesions (97%), with an average maximum standardized uptake value (SUV(max)) of 5.2. [^{18}F]FDHT-PET was positive in 46 of 59 lesions (78%), with an average SUV(max) of 5.3 among [^{18}F]FDHT-positive lesions. As expected, treatment with testosterone resulted in diminished tumor uptake of [^{18}F]FDHT (Figure 36.3).

In a subsequent clinical study, Dehdashti *et al*. (2005) further evaluated the feasibility of specific AR imaging by [^{18}F]FDHT-PET in PC patients. Twenty patients with advanced PC were studied, all except one of whom had histological and/or radiological confirmation of metastatic disease. Conventional imaging

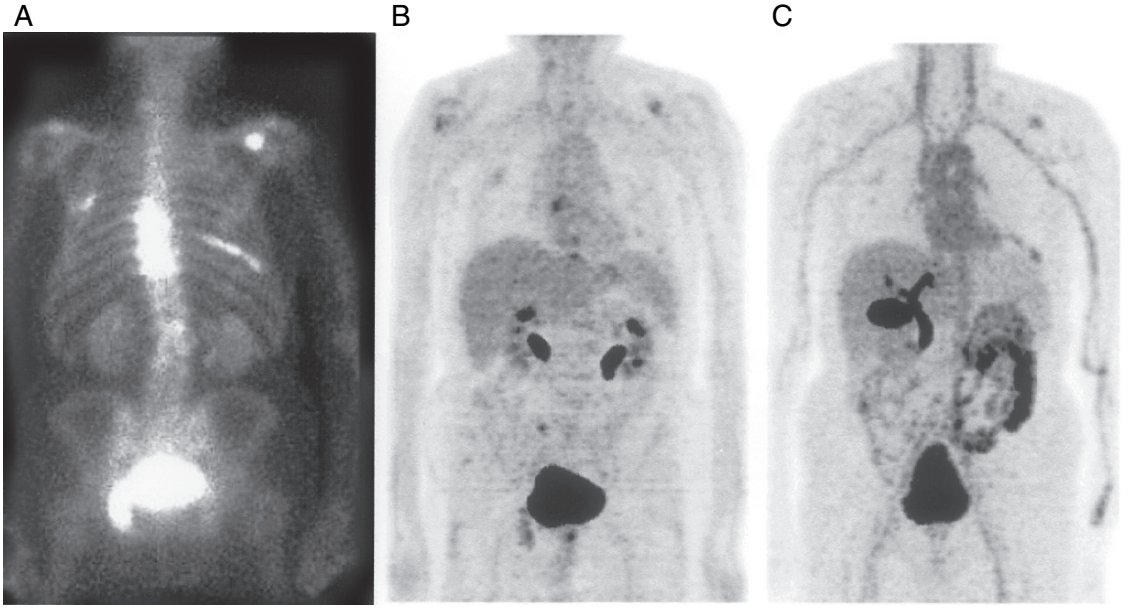

FIGURE 36.1. Comparative whole-body images of a 75-year-old man with progressive PC metastatic to bones of the thoracic spine, left rib cage, and scapula. (A) Planar gamma camera image of ^{99m}Tc-methylene di-phosphonate (MDP). (B) Coronal PET image of [^{18}F]FDG. (C) Coronal PET image of [^{18}F]FDHT. (Adapted from Zanzonico *et al*., 2004 by permission of the authors.)

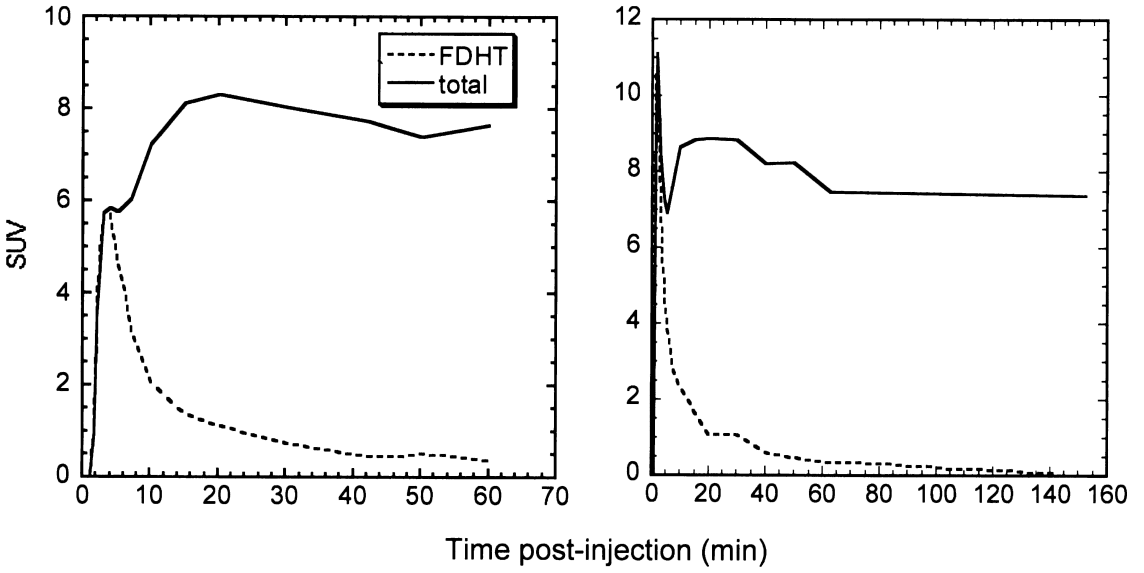

FIGURE 36.2. Time-activity curves for blood-borne [18F]FDHT-derived activity, in terms of the SUV of total activity and of intact [18F]FDHT, in two patients with progressing PC. These graphs illustrate the rapid metabolism of [18F]FDHT in vivo. (Adapted from Larson *et al.*, 2004 by permission of the authors.)

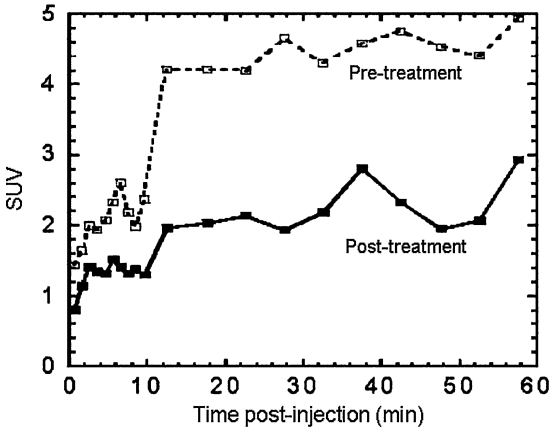

FIGURE 36.3. PET-derived time–activity curves (average of three metastases in a single PC patient) for [18F]FDHT before (dashed line) and after (solid line) treatment with non-radioactive testosterone. This graph illustrates the testosterone-induced suppression of lesion uptake of 16β-[18F]FDHT, presumably as a result of the saturable, AR-mediated basis of this uptake. (Adapted from Larson *et al.*, 2004 by permission of the authors.)

demonstrated very widespread metastatic lesions in two patients and 43 lesions in the remaining 17 patients. [18F]FDHT-PET was positive in 12 of 19 patients (63%), including the two patients with widespread lesions, and detected 24 of 28 known lesions (86%) in the remaining ten patients. Additionally, 17 unsuspected lesions were detected in five of these ten patients. To assess the AR specificity of [18F]FDHT, all 12 patients positive on [18F]FDHT-PET underwent a repeat PET study after receiving the AR antagonist flutamide for 1 day (250 mg × 3). In all cases, there was a decrease in tumor [18F]FDHT uptake after flutamide – the SUV and tumor-to-muscle ratio (mean ± standard deviation) decreased significantly ($p = 0.002$) from 7.0 ± 4.7 and 6.9 ± 3.9 to 3.0 ± 1.5 and 3.0 ± 1.6, respectively – indicating that tumor uptake was receptor-mediated. Furthermore, the mean

PSA in patients positive on [^{18}F]FDHT-PET was significantly higher ($p = 0.006$) than that in patients negative on [^{18}F]FDHT-PET, suggestive of an association between positivity of [^{18}F]FDHT-PET and tumor burden.

RADIATION DOSIMETRY OF 16β-[^{18}F]FLUORO-5α-DIHYDROTESTERONE

Using the PET-derived pharmacokinetic data from the study of Larson *et al*. (2004) (which included ten PET scans and blood sampling in seven patients with advanced PC), Zanzonico *et al*. (2004) derived normal-tissue absorbed dose estimates for [^{18}F]FDHT. Activity concentrations in plasma and red marrow (assuming a plasmacrit of 0.58, an extracellular fluid (ECF) fraction of 0.4, and equilibration of activity between plasma and marrow ECF) were measured ex vivo from a peripheral blood sample. Liver, spleen, urinary bladder contents, and total body activities were measured by region-of-interest (ROI) analysis of serial quantitative whole-body PET scans. Total organ activities and residence times (i.e., cumulated activities) were calculated from the respective PET scan-derived activity concentrations assuming Standard (70-kg) Man organ masses. Urinary excretion was corrected for hepatobiliary excretion (liver activity) and a first-order adjustment was made for the bladder-wall mass based on the patient's total-body mass. Mean organ absorbed doses were calculated with the MIRD formalism (Zanzonico, 2000) and the Standard-Man model using the *MIRDOSE III* computer program. The absorbed doses (mean ± standard deviation) ranged from 0.021 ± 0.010 cGy/37 MBq to spleen to 0.32 ± 0.19 cGy/37 MBq to the bladder wall (voiding intervals: 1–2 h) and the effective dose equivalent (Zanzonico, 2000) was 0.059 ± 0.006 cSv/37 MBq. The maximum absorbed dose among all tissues in all ten studies, 0.56 cGy/37 MBq, occurred for the urinary bladder wall. To ensure that the maximum normal tissue absorbed dose is kept below the recommended maximum permissible dose of 5 cGy per single administration, a maximum administered activity of 333 MBq (9 mCi) was therefore recommended for [^{18}F]FDHT.

In conclusion, consistent with the results of extensive pre-clinical studies in rats and in non-human primates, [^{18}F]FDHT-PET is feasible in patients with advanced PC with castrate levels of testosterone. There is AR-mediated, high-contrast uptake of [^{18}F]FDHT in the majority of metastatic lesions detected by conventional imaging. The clinical data to date suggest that [^{18}F]FDHT-PET will be very useful for characterizing the global AR status of advanced PC and, therefore, for determining the likelihood of the therapeutic effectiveness of AR blockade and, ultimately, for elucidating the biology of PC progression.

REFERENCES

Agus, D. B., Cordon-Cardo, C., Fox, W., Drobnjak, M., Koff, A., Golde, D. W., and Scher, H. I. 1999. Prostate cancer cell cycle regulators: response to androgen withdrawal and development of androgen independence. *J. Natl. Cancer Inst. 91*: 1869–1876.

Barrack, E. R., and Tindall, D. J. 1987. A critical evaluation of the use of androgen receptor assays to predict the androgen responsiveness of prostatic cancer. *Current Concepts and Approaches to the Study of Prostatic Cancer*. D. S. Coffey (ed.). New York, Allan R Liss: 155–187.

Bonasera, T. A., O'Neil, J. P., Xu, M., Dobkin, J. A., Cutler, P. D., Lich, L. L., Choe, Y. S., Katzenellenbogen, J. A., and Welch, M. J. 1996.

Preclinical evaluation of fluorine-18-labeled androgen receptor ligands in baboons. *J. Nucl. Med. 37*: 1009–1015.

Craft, N., Shostak, Y., Carey, M., and Sawyers, C. L. 1999. A mechanism for hormone-independent prostate cancer through modulation of androgen receptor signaling by the HER-2/neu tyrosine kinase. *Nat. Med. 5*: 280–285.

Dehdashti, F., Picus, J., Michalski, J. M., Dence, C. S., Siegel, B. A., Katzenellenbogen, J. A., and Welch, M. J. 2005. Positron tomographic assessment of androgen receptors in prostatic carcinoma. *Eur. J. Nucl. Med. Mol. Imaging 32*: 344–350.

Derenzo, S. E. 1986. Mathematical removal of positron range blurring in high-resolution tomography. *IEEE Trans. Nucl. Sci. NS-33*: 565–569.

Fenton, M. A., Shuster, T. D., Fertig, A. M., Taplin, M. E., Kolvenbag, G., Bubley, G. J., and Balk, S. P. 1997. Functional characterization of mutant androgen receptors from androgen-independent prostate cancer. *Clin. Cancer Res. 3*: 1383–1388.

Horst, T., Meyer, B., and Taplin, S. 1995. Screening, health promotion, and prevention in men. *Prim. Care 22*: 679–695.

Jemal, A., Murray, T., Samuels, A., Ghafoor, A., Ward, E., and Thun, M. J. 2003. Cancer statistics, 2003. *CA Cancer J. Clin. 53*: 5–26.

Kelloff, G. J., Krohn, K. A., Larson, S. M., Weissleder, R., Mankoff, D. A., Hoffman, J. M., Link, J. M., Guyton, K. Z., Eckelman, W. C., Scher, H. I., O'Shaughnessy, J., Cheson, B. D., Sigman, C. C., Tatum, J. L., Mills, G. Q., Sullivan, D. C., and Woodcock, J. 2005. The progress and promise of molecular imaging probes in oncologic drug development. *Clin. Cancer Res. 11*: 7967–7985.

Kumar, V. L., Wadhwa, S. N., Kumar, V., and Farooq, A. 1990. Androgen, estrogen, and progesterone receptor contents and serum hormone profiles in patients with benign hypertrophy and carcinoma of the prostate. *J. Surg. Oncol. 44*: 122–128.

Larson, S. M., Morris, M., Gunther, I., Beattie, B., Humm, J. L., Akhurst, T. A., Finn, R. D., Erdi, Y., Pentlow, K., Dyke, J., Squire, O., Bornmann, W., McCarthy, T., Welch, M., and Scher, H. 2004. Tumor localization of 16beta-18F-fluoro-5alpha-dihydrotestosterone versus 18F-FDG in patients with progressive, metastatic prostate cancer. *J. Nucl. Med. 45*: 366–373.

Levin, C. S., and Hoffman, E. J. 1999. Calculation of positron range and its effect on the fundamental limit of positron emission tomography system spatial resolution. *Phys. Med. Biol. 44*: 781–799.

Liu, A. J., Katzenellenbogen, J. A., VanBrocklin, H. F., Mathias, C. J., and Welch, M. J. 1991. 20-[18F]fluoromibolerone, a positron-emitting radiotracer for androgen receptors: synthesis and tissue distribution studies. *J. Nucl. Med. 32*: 81–88.

Liu, A., Dence, C. S., Welch, M. J., and Katzenellenbogen, J. A. 1992a. Fluorine-18-labeled androgens: radiochemical synthesis and tissue distribution studies on six fluorine-substituted androgens, potential imaging agents for prostatic cancer. *J. Nucl. Med. 33*: 724–734.

Liu, A., Carlson, K. E., and Katzenellenbogen, J. A. 1992b. Synthesis of high affinity fluorine-substituted ligands for the androgen receptor. Potential agents for imaging prostatic cancer by positron emission tomography. *J. Med. Chem. 35*: 2113–2129.

Neri, R. 1989. Pharmacology and pharmacokinetics of flutamide. *Urology 34*: 19–21; discussion 46–56.

Pentlow, K. S., Graham, M. C., Lambrecht, R. M., Daghighian, F., Bacharach, S. L., Bendriem, B., Finn, R. D., Jordan, K., Kalaigian, H., Karp, J. S., Robeson, W. R., and Larson, S. M. 1996. Quantitative imaging of iodine-124 with PET. *J. Nucl. Med. 37*: 1557–1562.

Pentlow, K. S., Finn, R. D., Larson, S. L., Erdi, Y. E., Beattie, B. J., and Humm, J. L. 2000. Quantitative imaging of yttrium-86 with PET: the occurrence and correction of anomalous apparent activity in high density regions. *Clin. Positron Imaging 3*: 85–90.

Scher, H. I., and Heller, G. 2000. Clinical states in prostate cancer: toward a dynamic model of disease progression. *Urology 55*: 323–327.

Schoder, H., Erdi, Y., Larson, S., and Yeung, H. W. D. 2003. PET/CT: a new imaging technology in nuclear medicine. *Eur. J..Nucl..Med..Mol. 30*: 1419–1437.

Townsend, D. W., Carney, J. P., Yap, J. T., and Hall, N. C. 2004. PET/CT today and tomorrow. *J. Nucl. Med. 45 Suppl 1*: 4S–14S.

Visakorpi, T., Hyytinen, E., Koivisto, P., Tanner, M., Keinanen, R., Palmberg, C., Palotie, A., Tammela, T., Isola, J., and Kallioniemi,

O. P. 1995. In vivo amplification of the androgen receptor gene and progression of human prostate cancer. *Nat. Genet. 9*: 401–406.

Zanzonico, P. 1995. Technical requirements for SPECT: instrumentation, data acquisition and processing, and quality control. *Clinical SPECT Imaging*. E. Kramer and J. Sanger (eds.). New York, Raven: 7–41.

Zanzonico, P. 2004. Positron emission tomography: a review of basic principles, scanner design and performance, and current systems. *Semin. Nucl. Med. 34*: 87–111.

Zanzonico, P. B. 2000. Internal radionuclide radiation dosimetry: a review of basic concepts and recent developments. *J. Nucl. Med. 41*: 297–308.

Zanzonico, P. B., Finn, R., Pentlow, K. S., Erdi, Y., Beattie, B., Akhurst, T., Squire, O., Morris, M., Scher, H., McCarthy, T., Welch, M., Larson, S. M., and Humm, J. L. 2004. PET-based radiation dosimetry in man of 18F-fluorodihydrotestosterone, a new radiotracer for imaging prostate cancer. *J. Nucl. Med. 45*: 1966–1971.

37
Effects of Standard Treatments on the Immune Response to Prostate Cancer

Nancy J. Nesslinger, Howard H. Pai, Charles M. Ludgate, and Brad H. Nelson

INTRODUCTION

Prostate cancer is the most frequently diagnosed cancer in North American men and, despite improvements in early detection due to prostate-specific antigen (PSA) screening, it remains the second leading cause of cancer-related death among men. Standard treatment for localized disease includes radical prostatectomy, external beam radiation therapy (EBRT), and brachytherapy, which are often combined with hormone therapy in high risk patients. These treatments are successful in controlling organ-confined disease; however if tumors recur, the disease is typically systemic and hormone therapy remains the only treatment option. While hormone therapy is initially efficacious, patients eventually progress to androgen-independent disease, which is incurable. Immune-based treatments such as cancer vaccines are emerging as a treatment option for those patients with hormone-refractory disease, however the results to date from clinical trials, while promising, do not yet warrant the adoption of immunotherapy as standard of care. Further progress will require a deeper understanding of the interactions between the immune system and prostate cancer. Although we have some understanding of the natural host response to prostate cancer at the time of diagnosis, far less is known regarding the state of tumor immunity at the completion of standard treatments and beyond, despite the fact that this is the immunological context in which immune-based treatments must operate if the goal is to prevent or delay recurrence. One can imagine that standard treatments, by causing tumor cell death in an inflammatory context, must have an impact on the host immune response. Do standard treatments enhance or inhibit host immunity to prostate cancer? Does host immunity have a significant influence on clinical outcomes? If standard treatments fail, does this in part reflect a failure of the immune system? And finally, how can we best enhance the immune response to tip the balance in favor of tumor stabilization or rejection? We begin this discussion by reviewing the concepts, technical issues, and evidence concerning the effect of standard treatments on tumor-specific immunity in prostate cancer.

There is considerable evidence that the immune system recognizes prostate tumors in a significant proportion of patients. McNeel *et al*. (2000) demonstrated the

presence of serum antibody responses to PSA, prostatic acid phosphatase (PAP), p53, and HER2/neu in patients with prostate cancer. In addition, serological screening has revealed serum antibody responses to antigens such as T21 (Miles *et al*., 2007), MAD-CT-1 and MAD-CT-2 (Hoeppner *et al*., 2006), KU-CT-1 (Okada *et al*., 2006), NY-BR-1 (Jager *et al*., 2005), NY-ESO-1, Lage-1 and Xage-1 (Fossa *et al*., 2004), and PARIS-1 (Zhou *et al*., 2002) in prostate cancer patients. Screening of a peptide library with serum from prostate cancer patients demonstrated that antibody responses are very common at the time of diagnosis and are directed against a diverse set of antigens (Wang *et al*., 2005). In fact, the authors of the latter study proposed that serum antibodies could potentially serve as novel biomarkers for prostate cancer screening. The presence of tumor-infiltrating lymphocytes (TIL) provides additional evidence that prostate tumors are recognized by the immune system. In a series of 325 prostatic adenocarcinomas with long-term follow-up, Vesalainen *et al*. (1994) found that tumors with lower densities of TIL were associated with higher risk of tumor progression and poor prognosis.

In an attempt to enhance the immune response to prostate cancer, several clinical vaccine trials have been conducted using a variety of strategies, including viral vaccines, whole-tumor cell vaccines, and dendritic cell (DC) vaccines. The concept behind viral vaccines is to expose the patient's immune system to tumor-associated antigens (TAAs) in the highly immunogenic context of viral infection, with the goal of eliciting antitumoral T cell responses. Recent studies have demonstrated the efficacy of a prime-boost strategy in which patients are initially vaccinated with recombinant vaccinia vaccine to prime T cell responses, and then boosted with a recombinant fowlpox vaccine. This dual vaccine strategy is referred to as Prostvac-VF (Therion Biologics) and utilizes PSA as the target antigen. To improve the immunogenicity of the vaccines, a gene construct encoding three costimulatory molecules, LFA-3, ICAM-1, and B7.1 (collectively referred to as TRICOM; Therion Biologics) was added to both recombinant viruses (Kaufman and Divgi, 2005). A number of trials have been conducted using Prostvac-VF with or without TRICOM, as well as with or without different immunologic adjuvants such as low-dose IL-2 or GM-CSF (Kaufman *et al*., 2004; Gulley *et al*., 2005a, b; DiPaola *et al*., 2006). In these trials, the majority of patients have demonstrated immunological responses such as increased numbers of PSA-reactive T cells, but clinical responses have been limited to PSA stabilization, and only in a minority of patients.

A second type of vaccine currently in clinical trials involves the use of whole tumor cells. An initial investigation utilized autologous irradiated tumor cells that were engineered to secrete GM-CSF (Simons *et al*., 1999). In this trial, vaccination was found to activate new T-cell and B-cell immune responses against prostate cancer antigens, however due to the difficulty in preparing autologous cells; focus has since shifted to the use of allogeneic cells derived from established prostate cancer cell lines. An example of this type of vaccine is GVAX (Cell GeneSys), an admixture of the prostate cancer cell lines LNCaP and PC-3 modified to secrete GM-CSF. Several Phase I and II clinical trials have been conducted using repeated

GVAX vaccinations in hormone refractory metastatic prostate cancer patients. Results from these trials have been encouraging with some treated patients showing transient reductions in serum PSA or decreased PSA progression (Simons and Sacks, 2006). There was also an overall tendency of extended time to progression, prompting the development of two phase III trials which are currently open for recruitment (Small *et al*., 2007a).

A third type of prostate cancer vaccine involves antigen-loaded DCs. The sources of antigen attempted to date include peptides, recombinant proteins and mRNA to such tumor-associated antigens as prostate-specific membrane antigen (Lodge *et al*., 2000), PSA (Heiser *et al*., 2002), TERT (Vonderheide *et al*., 2004), and PAP (Burch *et al*., 2000). To date, the most successful DC-based vaccine is Provenge (sipuleucel-T; APC8015), an autologous DC vaccine loaded with a PAP-GM-CSF fusion protein (Dendreon Corporation). In a phase III trial, Provenge induced PAP-specific T cell responses and significantly increased 3-year overall survival in patients randomized to APC8015 compared to placebo (25.9 versus 21.4 months, $p = 0.01$), representing the first survival advantage attributed to an immunotherapy product in prostate cancer (Small *et al*., 2006).

Despite this progress with immune-based therapies for prostate cancer, there is little information available on whether standard treatments, such as hormone therapy and radiation therapy, might also induce tumor-specific immune responses. We became interested in this issue based on clinical observations at our cancer centre that high risk prostate cancer patients who were treated with hormone therapy prior to radiation therapy had much better clinical outcomes than those treated with radiation therapy alone (Ludgate *et al*., 2005). Indeed, the combined use of hormone therapy with radiation therapy has become standard treatment for high-risk prostate cancer, based on the improved outcomes seen in several trials (Bolla *et al*., 2002; Laverdiere *et al*., 2004; Heymann *et al*., 2007). The basis for this apparent synergism remains poorly understood. As discussed below, recent data from multiple laboratories make a compelling case for the potential involvement of the immune system.

Radiation therapy induces tumor cell necrosis and apoptosis, which when accompanied with inflammatory or other "danger" signals, could potentially provide both antigen and maturation signals to DCs and other antigen presenting cells, leading to the induction of T cell responses (Demaria *et al*., 2005a). Radiation therapy has been shown to up-regulate a number of immunoregulatory molecules, including chemokines; inflammatory cytokines; Fas/CD95 and other death receptors; MHC molecules; B7 and other co-stimulatory molecules; adhesion molecules; heat shock proteins; and tumor-associated antigens (McBride *et al*., 2004; Demaria *et al*., 2005a; Garnett *et al*., 2004; Chakraborty *et al*., 2003). *In vitro* studies have shown that radiation can increase the antigenicity of tumor cells through enhanced degradation of existing proteins, enhanced protein translation, and the induced expression of new antigens that are processed and presented by MHC class I molecules (Reits *et al*., 2006). *In vivo* studies in mice have shown that localized radiation can increase TAA presentation by tumors; this was associated with an increased number of tumor-infiltrating lymphocytes

that secreted IFN-γ and lysed tumor target cells (Lugade *et al*., 2005).

Hormone therapy too could potentially influence tumor-specific immune responses. To begin with, hormone therapy can cause changes in circulating lymphocyte populations. In normal mice, hormone therapy in the form of castration has been shown to cause a dramatic increase in naïve IgM+ splenic B cells (Wilson *et al*., 1995). In humans, hormone therapy can induce thymic renewal in older patients, which in turn may increase the diversity of the T cell repertoire and hence the pool of antigens that can potentially be recognized by the immune system (Aragon-Ching *et al*., 2007). In one study, 77% of patients receiving hormone therapy showed increased numbers of circulating lymphocytes within the first month of treatment (Oliver *et al*., 1995).

The effect of hormone therapy on T cell mediated immunity has been investigated most extensively in mouse models. Roden *et al*. (2004) demonstrated that androgen deprivation in tumor-free male mice increased the absolute number of T cells residing in peripheral lymphoid tissues. Furthermore, androgen deprivation led to transient increases in T cell proliferation in response to T cell receptor stimulation. In a second study, Drake *et al*. (2005) created a transgenic mouse that expressed a model antigen, influenza hemagglutinin (HA), under the control of a prostate-specific probasin promoter (Pro-HA). These mice were then crossed with TRAMP mice, which express the SV40 T antigen under the control of the probasin promoter. The resulting bitransgenic mice developed spontaneous prostate tumors that expressed the HA antigen. The authors found that, in tumor-free Pro-HA mice, naïve HA-specific CD4+ T cells generally ignored the normal prostate gland. In contrast, in tumor-bearing, double transgenic mice, naïve HA-specific CD4+ T cells proliferated, yet eventually became tolerized. Intriguingly, when tumor-bearing mice were subjected to androgen deprivation therapy, immunological tolerance was broken and T cells then mounted strong functional responses to vaccination.

In humans, hormone therapy has been shown to induce profuse T cell infiltration of benign prostate glands and tumors. Mercader *et al*. (2001) performed a prospective study in which patients with low risk localized prostate cancer were randomized to receive 0, 7, 14, 21 or 28 days of androgen ablation therapy before radical prostatectomy. They found that the number of CD3+ T cells in both the benign gland and tumor tissue were significantly higher in those patients receiving hormone therapy compared to those who did not, with the greatest density of intratumoral T cells present at 21 days post androgen deprivation. Further analysis revealed that the infiltrate contained predominately CD4+ T cells compared to CD8+ T cells. Analysis of the CD3+ rich infiltrate with additional markers revealed high expression of IFN-γ, the proliferation marker Ki-67, the activation marker CD25, and the cytotoxic marker TIA-1. Thus, androgen deprivation promotes infiltration of prostate tumors by CD4+ T cells that are activated, proliferating and polarized toward IFN-γ production. Finally, androgen ablation resulted in increased numbers of intratumoral antigen presenting cells, including macrophages and DCs, along with increased expression of the costimulatory molecules B7.1 and B7.2 (Mercader *et al*., 2001).

Collectively, the above studies support the concept that radiation therapy and hormone therapy can trigger immune responses by causing the release of tumor-associated antigens while at the same time generating local inflammatory or "danger" signals that promote antigen presentation to T and B cells. While this model has conceptual appeal, until recently there was little evidence that the above phenomena do in fact result in *bona fide* antigen-specific immune responses. Indeed, it is possible that the T cell infiltrates described by Mercader *et al*. (2001) involve bulk populations of T cells with little specificity for tumor antigens, in which case the clinical relevance of such observations would be in question. While cellular infiltrates are a good measure of innate immune responses, adaptive immune responses involving B cells and T cells are best measured using specific antigens. Several methods have been developed to identify tumor antigens recognized by T cells, such as the T cell epitope cloning method developed by van der Bruggen *et al*. (1991). The difficulty with these approaches lies in their complexity and their reliance on established T cell and tumor lines, conditions that are very difficult to meet in the case of human prostate cancer where tissue specimens are often limited or unavailable. Measurement of antibody (i.e., B cell) responses using serological methods such as SEREX (serological analysis of recombinant cDNA expression libraries) has a number of advantages over T cell cloning methods. First, serological methods are relatively easy and fast. Second, only limited amounts of serum and tumor tissue are required. Importantly, the presence of a mature IgG antibody response implies an underlying CD4+ T helper response, which means the humoral antibody repertoire can be considered a reflection of the CD4+ T cell repertoire. Furthermore, tumor antigens recognized by patient antibodies can also be recognized by CD8+ cytotoxic T cells, at least in the case of NY-ESO-1 and p53 (Jager *et al*., 1998; Hoffmann *et al*., 2002). Thus, SEREX provides a rapid and convenient method to identify human tumor antigens, which can then be further evaluated as CD4+ and CD8+ T cell antigens.

Based on this rationale, we chose to use serological methods, including SEREX, to evaluate the effects of standard treatments on antigen-specific immune responses to prostate cancer. We assembled a cohort of 73 prostate cancer patients representing all stages and grades of disease. Patients underwent a variety of local treatments, including external beam radiation therapy, brachytherapy, radical prostatectomy, and hormone therapy, alone or in combination. Serum samples were collected before, during and after treatment for up to 3 years. The cohort also included patients who chose watchful waiting *in lieu* of treatment and hence served as untreated controls. Fifty age-matched men without a diagnosis of prostate cancer or other cancers served as additional controls. Pre-treatment and post-treatment serum samples were evaluated by Western blot and SEREX antigen arrays for the detection of treatment-associated autoantibody responses. As discussed below, with these methods we were able to show for the first time that hormone therapy and radiation therapy induce antigen-specific antibody responses in a significant proportion of prostate cancer patients (Nesslinger *et al*., 2007).

METHODOLOGY

Western Blotting Assay

This Western blotting protocol has been adapted for the use of serum from patients or controls as primary antibody, followed by IgG secondary detection.

Materials for Cell Culture

1. LNCaP or other prostate cancer or tumor cell line (American Type Culture Collection).
2. RPMI 1640 media (with L-glutamine) supplemented with 10% FBS, 2% Penicillin-Streptomycin (10,000 units; 10,000 µg stock), 2% L-glutamine (all components from Invitrogen).
3. Trypsin-EDTA (Invitrogen).
4. Phosphate-buffered saline (PBS): 10× contains 87.68 g NaCl, 4.56 g NaH_2PO_4, 23.0 g Na_2HPO_4. Add dH_2O to 1 L, adjust to pH 6.8.
5. General tissue culture supplies including: T75 tissue culture flasks, sterile plastic pipettes, sterile glass pipettes, sterile disposable 15 ml and 50 ml centrifuge tubes, sterile 1.5 ml microfuge tubes.

Materials for Protein Lysate Preparation and Quantification

1. RIPA buffer: Combine 5 ml 1 M Tris pH 7.5, 3 ml 5 M NaCl, 5 ml 20% NP-40 stock, 5 ml 10% sodium deoxycholate stock, 1 ml 10% SDS stock. Add dH_2O to 100 ml. Store at 4°C.
2. BSA protein standard at 1 mg/ml concentration.
3. BCA Assay components: Bicinchroninic Acid Solution, Copper (II) Solution (Sigma).
4. General supplies and equipment including ice, vortex, high-speed refrigerated micro-centrifuge, general purpose 96-well plate with lid, 37°C incubator, plate reader, multi-channel pipettor, solution basin.

Materials for Western Blotting Assay

1. XCell SureLock™ Mini-Cell with XCell II™ Blot Module (Invitrogen).
2. NuPAGE® Novex 4–12% 2D Bis-Tris gels (Invitrogen).
3. NuPAGE® Antioxidant, NuPAGE® Sample Reducing Agent (10×), NuPAGE® LDS Sample Buffer (4×), NuPAGE® MES SDS Running Buffer (all from Invitrogen).
4. Protein Standard: PageRuler Protein Ladder (10–250 kDa) (Fermentas Life Sciences).
5. Transfer Buffer: for 20× stock use 40.8 g Bicine, 52.4 g Bis-Tris, 3 g EDTA and add dH_2O to 500 ml. Aliquot into 50 ml volumes and store at 4°C. To prepare transfer buffer combine 100 ml 20× stock, 200 ml methanol, 2 ml NuPAGE® Antioxidant and 1,698 ml dH_2O in a 2 L bottle. Store at room temperature.
6. NitroBind Pure Nitrocellulose, 0.45 µM (GE Water + Process Technologies).
7. Whatmann 3 mm filter paper.
8. Criterion size extra thick blot paper (BioRad).
9. Ponceau S Solution (Sigma).
10. Tris-buffered Saline (TBS): for 4 L 10× stock, mix 242.2 g Tris base with 350.6 g NaCl and add dH_2O to 4 L. Adjust to pH 8.0 with HCl.
11. TBST: Combine 200 ml 10× TBS and 10 ml 20% Tween-20. Add dH_2O to 2 L.
12. Blotto: Mix 25 g skim milk powder with 2.5 ml 20% Tween 20 and 50 ml 10× TBS. Add dH_2O to 500 ml. Store at 4°C.

13. Patient serum. Collect blood in no additive tubes. Allow blood to clot for 30 min – 2 h. Spin at 2,500 rpm for 20 min at 4°C. Transfer the serum into 2 ml cryovials and store at −80°C.
14. MiniProtean II Multiscreen Apparatus (BioRad).
15. Goat anti-Human IgG (H+L), HRP-conjugated secondary antibody (Jackson ImmunoResearch).
16. ECL Reagent: Prepare 250 mM stock Luminol (4.43 g 3-aminophthalhydrazine in DMSO) and 90 mM stock para-coumaric acid (0.74 g in DMSO). To prepare 500 ml ECL Solution 1: combine 222 ml dH_2O, 2.5 ml Luminol, 1.1 ml p-coumaric acid and 25 ml 1 M Tris pH 8.5. Wrap the bottle in foil to prevent exposure to light. To prepare 500 ml ECL Solution 2: combine 225 ml dH_2O, 25 ml 1 M Tris pH 8.5 and 0.155 ml 30% H_2O_2. Store both at 4°C.
17. Whatmann Absorbent Protector Sheets.
18. Kodak GBX Developer and Replenisher; Kodak GBX Fixer and Replenisher.
19. Kodak BioMax Light Film.

Additional materials required include various glass and plasticware, pipettors, a heat block at 95°C, an orbital shaker and a rocking shaker.

Protocol for Cell Culture, Protein Lysate Preparation and Quantification

1. Grow LNCaP cells (or other cells of interest) in RPMI+10% FBS+ antibiotics at 37°C, 5% CO_2. Follow standard tissue culture practices to expand the cells. Depending on the quantity of protein that is desired, grow 6–12 T75 flasks to ~ 80% confluency.
2. Harvest the cells using trypsin-EDTA. Spin the cells at 4°C, 1,000 rpm for 10 min to pellet. Resuspend the cells in 1 ml sterile PBS. Transfer the cells into a 1.5 ml microfuge tube. Spin the cells in a micro centrifuge at 1,000 rpm for 10 min. Remove the PBS and keep the cells on ice. At this point the cell pellet can be frozen and kept at −80°C until protein lysate preparation is performed. Alternatively, protein lysates can be prepared immediately.
3. Prepare the protein lysate by estimating the volume of cells in the pellet. Add an equal volume of cold RIPA buffer. Vortex the cells. Place the tube on ice for 30 min, vortexing every 2–3 min. Spin the cells at 10,000 rpm for 20 min at 4°C. Transfer the supernatant, containing the whole cell lysate to a fresh microfuge tube. Store the protein lysate at −80°C.
4. To determine the concentration of protein in the lysate, perform a modified BCA assay. Prepare a standard curve using stock 1 mg/ml BSA protein. Dilute the BSA to concentrations of 0 (blank), 0.2, 0.4, 0.6, 0.8 and 1.0 mg/ml in a 10 µl volume, using RIPA buffer as diluent. Add each known concentration in triplicate to wells (10 µl/well) of a 96-well plate. Dilute the protein sample(s) to be tested 10, 20, and 40 fold in RIPA buffer. Add 10 µl of each dilution in triplicate to the 96-well plate. Prepare the BCA reagent (enough for 200 µl per well) by adding 1 part Copper (II) Solution into 50 parts Bicinchroninic Acid Solution. Add 200 µl per well, cover the plate and incubate for 30 min at 37°C. Read the plate at 562 nm on a plate reader (such as the Molecular Devices Versamax microplate reader) to determine the protein concentration.

Protocol for Western Blotting

We use the XCell SureLock™ Mini-Cell with XCell II™ Blot Module with Novex pre-cast gels from Invitrogen. The methodology may be adapted to other manufacturer's equipment.

1. Follow standard Western blotting protocol established for the type of equipment being used to run the Westerns, using 400 µg protein lysate of interest.
2. Boil the protein samples for 5 min at 95°C.
3. Using a gel with one large well and one small one for the protein ladder, load 10 µl protein ladder into the single marker well. Load the entire 400 µg protein sample into the large well.
4. Run the gel at 200 V for 50 min.
5. Set up the transfer and run according to the manufacturer's directions.
6. Once the transfer is complete, stain the membrane with a small amount of Ponceau stain to visualize the transferred protein. Mark the left and right edges of the protein; this will help align the multi-channel apparatus later. Wash off the Ponceau stain with water and 1× TBST.
7. Block the membrane in Blotto for 1 h on an orbital shaker.
8. In the meantime, prepare the serum samples. Choose samples from several patients from which a pre-treatment and post-treatment sample is available. The slot blot will allow loading of 14 different serum samples on one membrane. Thaw an aliquot of the serum samples of interest. Dilute each serum sample 1 in 500 by adding 1.5 µl serum to 750 µl Blotto. Keep the diluted serum samples at 4°C until ready to load.
9. Place the membrane in the multi-screen apparatus. Line up the channels such that they fall between the marked edges. Screw down until just finger tight. Prop the top edge of the apparatus on a microfuge tube rack, such that the entire apparatus is on an incline. Add 600 µl of each diluted serum sample to consecutive channels, loading from the bottom of each channel. Once completely loaded, place the apparatus flat and leave for 1 h at room temperature.
10. Using a vacuum, aspirate the serum from the bottom of the channel. Wash each channel twice with 1× TBST, aspirating between each wash. Remove the membrane from the apparatus and wash once in 1× TBST for 10 min and once in 1× TBS for 5 min on an orbital shaker.
11. Remove the TBS wash and add a 1:10,000 dilution of HRP-conjugated goat anti-human IgG secondary antibody in Blotto to the membrane. Place on a rocker for 1 h.
12. Remove the secondary antibody and wash the membrane twice with 1× TBST and once with 1× TBS for 10 min each on the orbital shaker.
13. Measure out 3 ml ECL Solution 1 and Solution 2 into separate 15 ml disposable centrifuge tubes. Remove the final wash from the membrane. Combine ECL Solutions 1 and 2. Pour on the membrane. Leave for 1 min. Remove the ECL and blot off excess with a Kimwipe. Place the membrane on a piece of absorbent protector sheet and wrap in plastic wrap.
14. Expose the membrane to X-ray film for 30 s. Develop the X-ray and determine if longer or shorter exposure times are required.

SEREX Screening

This protocol has been used successfully to identify antigens underlying treatment-induced autoantibody responses in prostate

cancer patients. We describe both the primary screening strategy, as well as the use of antigen arrays to evaluate autoantibody responses across a panel of serum samples.

Materials for cDNA Library Construction

1. mRNA from prostate cancer cell lines or prostate tissue.
2. Kanamycin (7.5 mg/ml stock), tetracycline (10 mg/ml stock), ampicillin (100 mg/ml stock).
3. ZAP cDNA Synthesis kit (includes XL1-Blue MRF' and SOLR bacterial strains) (Stratagene).
4. Stock plates of XL1-Blue MRF' cells streaked for single colonies on an LB + tetracycline and SOLR cells streaked for single colonies on an LB + kanamycin. Streak a fresh plate of cells every 1–2 weeks.
5. DEPC-treated dH_2O.
6. Alkaline agarose gel reagents:

   2× Loading Buffer: for 1 ml, add 200 µl glycerol, 46 µl bromophenol blue, 5 µl NaOH, 750 µl dH_2O.

   10× Alkaline Buffer: for 100 ml, add 6 ml 5 M NaOH, 4 ml 0.5 M EDTA, 90 ml dH_2O.

7. SYBR green (Invitrogen).
8. 10× STE: for 10 ml, add 2 ml 5 M NaCl, 2 ml 1 M Tris-HCl pH 7.5, 2 ml 0.5 M EDTA, 4 ml dH_2O.
9. Ultrapure agarose (Invitrogen).
10. TAE: for 50× stock- combine 242.2 g Tris base, 57.1 ml Glacial acetic acid, 23.8 g EDTA. Add dH_2O to 1 L.
11. Gel Loading Dye: Combine 0.125 g bromophenol blue, 0.125 g xylene cyanol, 15 g glycerol. Add dH_2O to 50 ml. Aliquot into 1.5 ml microfuge tubes.
12. 1 kb ladder (Invitrogen).
13. Ethidium bromide (Sigma).
14. Qiaquick Gel Extraction Kit (Qiagen).
15. LB broth and agar plates: 10 g NaCl, 10 g tryptone, 5 g yeast extract, add dH_2O to 1 L. For plates add 20 g bacto-agar per litre broth. Autoclave.
16. LB + supplements: To 1 L autoclaved LB broth, add 10 ml 1 M $MgSO_4$ and 3 ml 2 M maltose.
17. NZYCM top agar: 11 g NZYCM powder, 3.5 g agarose, dH_2O to 500 ml. Autoclave.
18. NZYCM agar plates: 22 g NZYCM powder, 20 g bacto-agar, dH_2O to 1 L. Autoclave, cool to 50°C and pour into petri plates (~20 ml per plate).
19. SM Buffer: 5.8 g NaCl, 2.0 g $MgSO_4$, 50 ml 1 M Tris pH7.5, 5.0 ml 2% gelatin, dH_2O to 1 L.
20. X-gal and IPTG.

Materials for SEREX Screening

1. Nitrocellulose circles (for cDNA library screening): 0.45 µm HATF membranes, 82 mm (Millipore).
2. NitroBind Pure Nitrocellulose (for antigen arrays, cut to size of array plate): 0.45 µM, 30 cm × 3 m (GE Water + Process Technologies).
3. 1 M IPTG.
4. Uncoupled Gel Wash: 1 mM HCl-41.3 µl concentrated HCl in 500 ml.
5. Borate Buffer: 12.4 g boric acid, 19.07 g borax, dH_2O to 1 L.
6. Basic Wash: 50 ml 1 M Tris pH 8.5, 50 ml 5 M NaCl, dH_2O to 500 ml. Adjust to pH 8.5.
7. Acidic Wash: 16.67 ml 3 M sodium acetate, 50 ml 5 M NaCl, dH_20 to 500 ml. Adjust to pH 4.5 with concentrated HCl.

8. Tris Buffered Saline (TBS): for 4 L 10× stock, mix 242.2 g Tris base with 350.6 g NaCl and add dH_2O to 4 L. Adjust to pH 8.0 with HCl.
9. 1× TBST: Combine 200 ml 10× TBS and 10 ml 20% Tween-20. Add dH_2O to 2 L.
10. 1× TBS/1% BSA: combine 100 ml 10× TBS and 10 g BSA. Add dH_2O to 900 ml. Store at 4°C.
11. Mouse anti-human IgG (H+L), AP-conjugated secondary antibody (Jackson ImmunoResearch).
12. Colour Developing Solution (for NBT/BCIP developer): 100 ml 1 M Tris-HCl pH 9.5, 20 ml 5 M NaCl, 5 ml 1 M $MgCl_2$, dH_2O to 1 l.
13. NBT: 0.5 g in 10 ml 70% dimethylformamide.
14. BCIP: 0.5 g in 10 ml 100% dimethylformamide.
15. CNBr-activated resin (Pharmacia).
16. Micro Bio-Spin Chromatography Columns (BioRad).
17. Qiagen Qiaprep Miniprep kit.
18. KpnI and SacI (NEB).

Additional materials required include various glassware, plasticware and pipettors, including square petri dishes with grids used for antigen arrays. General equipment required includes agarose gel box and power supply, UV transilluminator, spectrophotometer and cuvettes, shaking incubator, 37°C incubator, water bath, refrigerated centrifuge, probe sonicator (such as the Branson Sonifier 450), orbital shaker and rocker.

Protocol for cDNA Library Construction

The cDNA library was constructed using a total of 5 µg mRNA from three different prostate cancer cell lines: LNCaP, PC-3 and DU-145. Library construction followed the Stratagene ZAP cDNA Synthesis kit manufacturer's directions, except for the cDNA size fractionation step, which was conducted as follows:

1. Prepare a 1% agarose gel by adding 0.75 g Ultrapure agarose to 75 ml 1× TAE. Microwave for 1–2 min to dissolve agarose. Cool to ~50°C and pour into a gel tray with a 15-well comb. Let set for at least 30 min.
2. Prepare the cDNA samples (in a 10 µl volume) by adding 2 µl gel loading dye.
3. Load the gel with a 1 kb ladder at each end and two empty wells separating all the samples.
4. Run the gel at 75 V for 90 min.
5. Cut the 1 kb ladder off the gel and stain in an ethidium bromide solution (20 µl ethidium bromide in 100 ml dH_2O) for 20 min on an orbital shaker. Destain in dH_2O for 20 min.
6. Piece the gel back together. Visualize the 1 kb ladder on a UV transilluminator. Cut out the cDNA lane from just below 1 kb to ~8 kb. Place the gel slice in a microfuge tube. Discard the remaining gel.
7. Use the Qiaquick Gel Extraction Kit (Qiagen) to purify the cDNA from the gel slices, using the manufacturer's directions.
8. Precipitate the eluted cDNA by adding 1/10 volume 3 M NaOAc and 2 volumes 100% ethanol. Leave samples to precipitate overnight at −20°C.
9. Spin the precipitated cDNA at 4°C for 60 min. Wash the pellet in 500 µl 70% ethanol. Spin 10 min at 4°C and remove as much ethanol as possible with a pipettor. Air-dry the pellet in a fume hood for a few minutes and resuspend the pellet in 3.5 µl sterile dH_2O.

10. Continue the cDNA library construction as outlined in the ZAP cDNA Synthesis kit directions.

Protocol for Pre-clearing Serum Samples

To reduce background during the SEREX screening, serum samples should be pre-cleared of antibodies that might cross-react with XL1-Blue bacterial proteins. To further reduce background, serum samples should also be pseudo-lifted at least twice against phage plaques containing a non-recombinant clone.

Day 1:

1. Grow an overnight culture of XL1-Blue MRF' cells by adding 15 µl 10 mg/ml tetracycline to 10 ml LB + supplements. Pick an isolated XL1-Blue MRF' colony and grow the culture overnight at 30°C, 250 rpm.

Day 2:

1. Use 500 µl of the overnight culture to seed 200 ml LB + supplements + 300 µl tetracycline. Grow the culture at 37°C until the OD_{600} = 0.5, ~3h. Spin the culture at 5,000 rpm for 10 min to pellet. Resuspend the pellet in 10 ml borate buffer.
2. Cut a 50 ml Falcon tube down to ~25 ml. Transfer the resuspended bacteria to the cut-off tube. Set up a sonicator with a ½ inch diameter probe, setting 8, 50% duty cycle. Keeping the tube on ice, sonicate the bacteria for 4 min, keeping the probe submerged about half-way and not touching the sides of the tube.
3. Quantify the XL1-Blue MRF' protein using the modified BCA protein assay outlined above in the Cell Culture and Protein Lysate Preparation methods, step 4.
4. Prepare the CNBr-activated resin. 1 gram of resin equals ~3.5 ml. Use 1 gram of resin per 50 ml tube. Wash the resin 5 × 50 ml with 1 mM HCl, mix and spin 2 min at 2,000 rpm between each wash. Remove the last wash completely, leaving the resin in the bottom of the 50 ml tube. Add 5–10 mg of XL1-Blue MRF' protein per ml of resin.
5. Rotate the resin/protein mixture on a rotator overnight at 4°C or for 2 h at room temperature.

Day 3:

1. Wash the cross-linked resin/protein mix. Fill the resin/protein tube with blocking buffer (0.1 M Tris pH 8.0). Rotate at room temperature for 2 h.
2. Spin the tube at 2,000 rpm for 2 min. Remove the blocking buffer. Wash the resin with the basic and acidic wash, alternating between the two, 4 times each. Spin 2 min, 2,000 rpm between each wash. Remove the last acid wash completely. Fill the tube with TBS pH 7.5 + 0.05% thimerazol. Store at 4°C until ready to use to pre-clear patient serum.

In general, for each serum sample, a total of 250 µl serum should be cleared for cDNA library screening and 100 µl serum should be cleared for antigen array screening.

Day 1:

1. An equal volume of XL1-Blue cross-linked resin and patient serum is required. Mix the tube of crosslinked resin and fill the appropriate number of 1.5 ml tubes (equal to the number of serum samples being cleared). Allow the resin to settle and remove the buffer. Repeat by adding more cross-linked resin to each tube until the appropriate

volume of resin is reached (equal to the volume of serum to be cleared).
2. Add the volume of patient serum to be cleared to the resin. Mix by inverting the tube several times. Rotate the tubes overnight at room temperature.

Day 2:

1. Recover the pre-cleared serum by pipetting the resin/serum into a Micro Bio-Spin Chromatography column, one column per sample.
2. Place the column in a 1.5 ml microfuge tube with the lid cut off. Spin 3,000 rpm, 1 min. Transfer the eluate (containing the pre-cleared serum) to a fresh 1.5 ml tube.
3. Wash the column with 1× TBS, using a volume equal to the original amount of serum. Spin at 3,000 rpm for 1 min. Pool the wash eluate with the serum eluate.
4. Dilute the serum 1:20 in 1× TBS + 0.05% thimerazol in a 15 ml tube. For example, for 10 ml of a 1:20 dilution, add 500 µl precleared serum, 100 µl 5% thimerazol and 9.4 ml 1× TBS.
5. Store the diluted precleared serum samples at 4°C.

Protocol for SEREX Screening

Day 1:

Grow an overnight culture of XL1-Blue MRF' by adding an isolated colony from a fresh XL1-Blue MRF' plate to 50 ml LB + supplements + 75 µl tetracycline. Grow the culture overnight at 30°C at 250 rpm.

Day 2:

1. Prepare the bacteria by spinning the overnight culture at 1,000 × g for 10 min. Resuspend the pellet in 25 ml 10 mM $MgSO_4$. Take an OD_{600} reading and dilute the cells with 10 mM $MgSO_4$ to get an $OD_{600} = 0.5$.
2. Pre-warm the NZYCM plates at 37°C for 1–2 h.
3. Prepare the nitrocellulose membranes by soaking them in IPTG. This will induce protein expression and is required for both the cDNA library screening and antigen array. The membranes used for pseudo-lifts do not require soaking in IPTG. Prepare the IPTG by combining 20 ml sterile dH_2O and 200 µl 1 M IPTG in a sterile petrie dish. Set up a number of Petri dishes, depending on the number of membranes that need to be soaked. Submerge the membrane in the IPTG for a minimum of 5 min, but not longer than 25 min. Air-dry the membranes on 3 mm filter paper for at least 45 min. Label the membranes.
4. Combine the library titre that will give well-separated, distinct plaques (~1,000–2,000 plaques per plate) with 200 µl XL1-Blue MRF' cells at $OD_{600} = 0.5$ (from step 1 above) in a snap-cap tube, preparing one tube per plate to be screened.
5. Incubate the tubes in a 37°C water bath for 15 min.
6. Add 3 ml top agar (cooled to 50°C) to each tube and immediately pour on to the pre-warmed NZYCM plates. Ensure that the top agar completely covers the plate and that there are no bubbles. Let the top agar set for 10 min.
7. Incubate the plates (face down) at 37°C for 3–4 h until plaques just begin to appear.
8. Once the plates have been incubated for 3–4 h, place the IPTG-soaked membrane face-down on top of the agar. Mark the orientation with asymmetrical needle sticks through the membrane and the agar.
9. Incubate the plates face-down, overnight at 37°C.

Protocol for Analyzing SEREX Antigen Arrays

Perform Steps 1–3 as described under "Protocol for SEREX Screening"

4. Design an antigen map, on which each antigen is assigned a specific position (using a 96-well plate as a template). Each antigen should be placed on the map in duplicate and in non-adjacent positions. Include a positive control (e.g. human IgG) and a negative control (e.g. a non-recombinant clone). Prepare each antigen in a 96-well plate, following the designed antigen map. Dilute 1 µl of freezer stock for each antigen in 200 µl SM buffer in the appropriate well. The antigen array can be kept at 4°C and used for several assays.
5. Add 300 µl XL1-Blue MRF' cells at OD_{600} = 0.5 to 4 ml top agar and pour immediately onto prewarmed NZYCM square plates. Let the agar set for 10 min.
6. Spot 0.6 µl of each antigen on the plate, using a multi-channel repeat pipettor, carefully following the antigen map. Let the plates dry for 10 min then add the IPTG-soaked membrane to each plate face-down.
7. Incubate the plates face-down in a 37°C incubator overnight.

NOTE: If the serum requires pseudo-lifts, prepare the pseudo-lift plates (2 per serum sample) at the same time as the screening plates. Follow the directions as above; however instead of plating the library or array, plate a non-recombinant phage clone at a titre that will produce 100–300 plaques per plate.

Day 3:

1. Carefully peel the membranes off the plates, placing each face up in a clean petri dish, including membranes meant for pseudo-lifting (if necessary). Wash the membranes twice in 1× TBST and once in 1× TBS for 5 min each. Make sure to wrap the plates and store them at 4°C.
2. Block all the membranes with 1× TBS/1% BSA for 60 min on an orbital shaker.
3. Before using precleared serum as primary antibody, the serum should be pseudolifted twice against plaques containing non-recombinant clones. This will help reduce background against any antibodies in the serum that might crossreact nonspecifically with phage proteins. To perform pseudolifts, add the serum, which has been diluted to 1:200 in TBS/1% BSA, to the membranes containing only non-recombinant clones (one serum sample per membrane). Leave 60 min on the orbital shaker. To perform the second pseudolift, remove the TBS/BSA block from the second set of non-recombinant membranes and pour the serum from the first set of pseudolift plates onto these membranes. Leave for 60 min on the orbital shaker.
4. Pour off the TBS/BSA block from the library membranes to be screened and add 10 ml pre-cleared and twice pseudolifted serum at a 1:200 dilution to each. Place plates on rocker overnight at room temperature.

Day 4:

1. Pour the serum from each plate back into a labeled 15 ml tube. Keep at 4°C as the serum can be reused up to four times for screening.
2. Wash the membranes twice in 1× TBST for 5 min each and once in 1× TBS for 5 min on an orbital shaker.
3. Block the membranes in 1× TBS/1% BSA for 60 min on an orbital shaker.

4. Prepare the secondary antibody by adding 1 µl mouse anti-human AP-conjugated IgG antibody to 10 ml 1× TBS/1% BSA in a 15 ml tube (one per plate). Remove the blocking buffer from the plates and add the prepared secondary antibody. Place the plates on the rocker for 60 min at room temperature.
5. Pour off the secondary antibody and wash the membranes twice in 1× TBST and once in 1× TBS for 5 min each on an orbital shaker.
6. Prepare the NBT/BCIP developer by adding 20 ml sterile dH_2O to a Petri dish. Add 200 µl NBT and 100 µl BCIP to the dH_2O. Each dish of developer will develop 4 membranes consecutively. Place a single membrane in the dish of developer and leave 5 min. Wash the membrane in dH_2O for 15 min. Dry the membranes between 2 sheets of 3 mm filter paper.

For the cDNA library screening, positive clones will appear as purple spots on the membrane whereas negative clones should be white. Once a positive clone has been identified, the membrane can be superimposed on the original plate to identify the positive plaque. The plaque can be cored using a 1,000 µl pipette tip and the core transferred into 500 µl SM buffer + 20 µl chloroform. The cores can be stored at 4°C. A secondary screen should be performed to ensure the clone is positive and to choose a well isolated clone. The phage clone can then be converted to plasmid and sent for sequencing.

Protocol for Purifying Phage Clones

Day 1:

1. Grow 50 ml overnight cultures of XL1-Blue MRF' in LB + supplements + tetracycline and SOLR in LB + supplements + kanamycin. Incubate the cultures at 30°C, 250 rpm.

Day 2:

1. Spin the XL1-Blue MRF' and SOLR cells at 1,000× g for 10 min to pellet. Resuspend each pellet in 25 ml 10 mM $MgSO_4$. Measure the OD_{600} and adjust the concentration of cells to $OD_{600} = 1.0$ with 10 mM $MgSO_4$.
2. Combine 200 µl XL1-Blue MRF' at $OD_{600} = 1.0$ with 250 µl phage stock (from the cored positive clone) and 1 µl ExAssist helper phage in a snap-cap tube. Incubate the tube at 37°C for 15 min. Add 3 ml LB + supplements and incubate at 37°C with shaking for 2.5–3 h.
3. Heat the tube at 70°C for 20 min to lyse the phage particles and cells. Spin the tube at 1,000× g for 15 min to pellet the cell debris. Decant the supernatant into a fresh tube.
4. Make a 10^{-2} and 10^{-3} dilution of the phage supernatant.
5. Add 200 µl SOLR cells at $OD_{600} = 1.0$ to two 1.5 ml microfuge tubes. Add 100 µl of the 10^{-2} and 10^{-3} phage supernatant dilutions from above to each tube. Incubate the tubes at 37°C for 15 min. Plate 200 µl of each dilution on LB + ampicillin plates. Incubate the plates overnight at 37°C.

Day 3:

1. Choose 2 isolated colonies from each transformation and inoculate separate tubes containing 5 ml LB + amp. Grow overnight at 37°C, 250 rpm.

Day 4:

1. Perform mini-preps on the overnight cultures using the Qiagen Qiaprep Miniprep kit and following the manufacturer's directions.

2. Digest the plasmid DNA with SacI and KpnI to check the size of the insert, using 5 µl of plasmid DNA (inserts are cloned in pBluescript, vector size = 3.0 kb).
3. Plasmids containing cloned antigens are now ready for sequencing.

RESULTS AND DISCUSSION

We first used Western blotting to broadly assess whether standard treatments induce immune responses to tumor antigens. Briefly, patient serum samples were used to probe whole-cell lysates from the allogeneic cell line LNCaP, as described in the Methodology section. Of 24 patients receiving hormone therapy, 7 (29.2%) showed the emergence of new seroreactivities during hormone therapy, as evidenced by the appearance of one or more immunoreactive bands by Western blot. Five patients with a hormone therapy-associated response went on to receive EBRT. In all but one case, the autoantibody response induced by hormone therapy persisted or even intensified with EBRT. EBRT also induced *de novo* seroreactivities in four of 29 (13.8%) patients, some whom had received prior HT. Similar results were seen with patients receiving brachytherapy as an alternative to EBRT: five of 20 patients (25%) showed the emergence of new seroreactivities during or after brachytherapy, three of whom had received prior hormone therapy.

Fourteen patients on the study were treated by radical prostatectomy, and intriguingly, none showed any serological changes with a follow-up ranging from 5 to 20 months. Similarly, nine patients who underwent watchful waiting instead of treatment showed no serological changes over a 5–30 month interval. Twenty-seven cancer-free individuals from which two to three serial blood draws were available were also evaluated. Two of the 27 controls showed a serologic change over a 5–10 month interval, whereas the rest did not. Thus, the serologic changes seen by Western blot can also occur with low frequency in cancer-free individuals (although the possibility of occult cancer was not ruled out in these two subjects). Importantly, the frequency of responses in patients treated with hormone therapy and/or radiation therapy (28.8%; 15 of 52) is significantly higher than that seen in cancer-free controls (2 of 27, 7.4%; $p = 0.028$, $\chi 2$ test) and prostate patients treated surgically (0 of 14, 0%; $p = 0.22$, $\chi 2$ test), and approaches significance in patients undergoing watchful waiting (0 of 9, 0%; $p = 0.064$, $\chi 2$ test), indicating that the responses are indeed induced by hormone or radiation treatments (Nesslinger *et al.*, 2007). Note that the serological assays were performed against an allogeneic cell line (LNCaP) and hence would not be expected to detect antibody responses to patient-specific antigens. Thus, the true frequency of treatment-induced antibody responses may be greater than we observed.

We considered which clinical factors might influence the development of treatment-induced immune responses. We found no obvious differences in the hormone therapy drug regimens between those patients who developed a serological response and those who did not. We were not able to comment on radiation dose effect on serological response, as all patients received the same dose. In addition, there was no obvious correlation with disease severity, as autoantibody responses were equally prevalent in low-risk, intermediate risk and high risk patients.

In additional unpublished experiments, we attempted to determine whether treatment of LNCaP cells with radiation or androgen withdrawal might unmask other antigens that were recognized by patient autoantibodies. This experiment was based on the well-documented finding that stressed cells commonly express so-called "stress proteins", including heat shock proteins and MICA, many of which can be recognized by the immune system (Javid *et al.*, 2007). For the radiation experiment, LNCaP cells were grown in culture to ~ 60% confluency, at which time they were treated with either 2 or 8 Gy radiation and harvested 24 h later. To mimic androgen withdrawal, cells were grown in charcoal-stripped (androgen depleted) serum for either 3 or 7 days before harvesting. Unmanipulated LNCaP cells served as controls. Western blots were performed with protein lysates from each of the treatment groups as well as unmanipulated control cells using 16 serum samples from the 73 patient cohort. Eight of the tested serum samples had previously shown treatment-induced immune responses against lysates from unmanipulated LNCaP cells. However, despite the cellular stress caused by radiation and androgen deprivation, we saw the same pattern of seroreactivities that were originally observed with unmanipulated LNCaP cells, suggesting that stress-induced antigens are not a major target of treatment-induced antibody responses (Figure 37.1A).

Which tumor antigens are involved in treatment-induced immune responses? To address this, we used SEREX immunoscreening to clone a subset of the antigens underlying the autoantibody responses seen by Western blot (Nesslinger *et al.*, 2007). SEREX screening was performed using a cDNA expression library constructed from three human prostate cancer cell lines. Additional screening was performed against a library derived from testis tissue in an attempt to identify antigens of the cancer-testis class. The antigens identified in the primary SEREX screens were then placed on an antigen array which in turn was probed with sera from 50 patients. For those sera that showed seroreactivity to one of the arrayed antigens, samples drawn from serial time points were then tested to determine whether the autoantibody response was induced by treatment. In four patients, we observed antigen-specific autoantibody responses that developed during treatment. In one patient, PC011, an autoantibody response arose against SDCCAG1 after EBRT (Figure 37.1B). In a second patient, PC015, an autoantibody response to PARP1 became evident after 4 months of hormone therapy and intensified during subsequent EBRT. In a third patient, PC036, autoantibody responses arose to two antigens, ZNF707+PTMA and CEP78, after 7 months of hormone therapy. In a fourth patient, PC001, hormone therapy was associated with the disappearance of autoantibodies to two antigens, KTN1 and RALBP1, whereas EBRT induced an autoantibody response to a third antigen, ODF2.

The results seen in this human study were independently confirmed in a mouse model. We used the Shionogi mammary carcinoma model (SC-115), which has been used extensively to study the progression of androgen-dependent tumors to androgen-independence. When implanted Shionogi tumors reached ~8 mm in diameter, mice were castrated, which precipitated apoptosis and regression of the

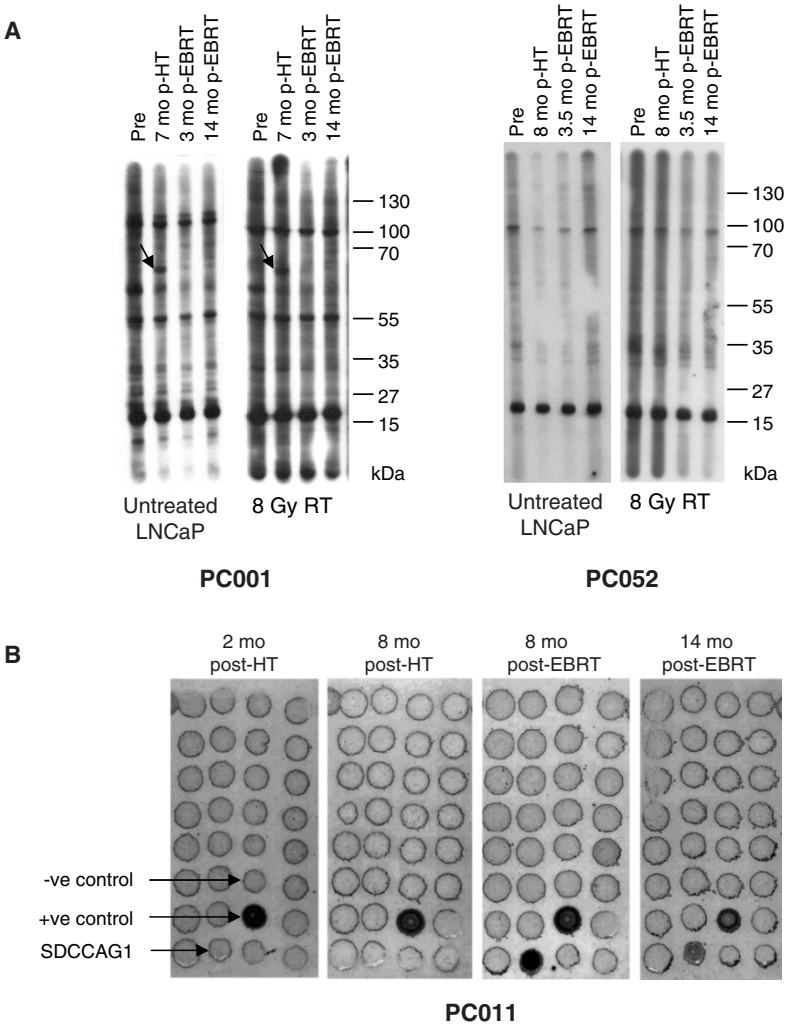

FIGURE 37.1. Analysis of treatment-induced autoantibody responses by Western blot and SEREX antigen arrays. (A) Western blot analysis of serum from two patients who were treated with hormone therapy (HT) and external beam radiation therapy (EBRT). Serum from serial time points was probed against LNCaP protein lysate from untreated cells or cells treated with 8 Gy radiation and harvested 24 h later. In patient PC001, a novel serological response to a ~ 65 kDa protein was transiently induced after HT and diminished after EBRT. These responses were seen in both the untreated LNCaP lysate and the 8 Gy-treated LNCaP lysate. In patient PC052, no serological changes were seen over time and throughout treatment with either protein lysate. (B) SEREX antigen array analysis of pre-treatment and post-treatment sera in a prostate cancer patient demonstrating treatment-associated changes in seroreactivity. Patient PC011 was treated with hormone therapy (HT) and external beam radiation therapy (EBRT), and serum was analyzed 2 and 8 months post-HT and 8 and 14 months post-EBRT. The patient was negative for autoantibodies to SDCCAG1 in the post-hormone therapy samples, but became seroreactive after EBRT. "+ve control", positive control consisting of an IgG clone; "−ve control", negative control consisting of a non-recombinant λ clone

tumor, as occurs with hormone therapy in human prostate cancer patients. Pre-castration and post-castration sera were analyzed by immunoblot against Shionogi tumor protein lysate. Five of ten mice (50%) showed the emergence of an autoantibody response to a ~ 40 kDa tumor protein within 3 weeks of castration. We are currently cloning this antigen using SEREX methodology to facilitate studies of the underlying T cell response. Thus, androgen withdrawal can induce autoantibody responses to tumor antigens in both mice and humans.

How can our findings be interpreted in the broader context of tumor immunology and cancer therapy? As described in the Introduction, there is mounting evidence that standard treatments for prostate cancer trigger T and B cell responses. Radiation and hormone therapy not only cause the release of antigens due to direct killing of tumor cells, but also create an inflammatory milieu that is favorable for antigen presentation to B and T cells. In addition, hormone therapy can induce systemic changes in circulating lymphocyte populations that may promote tumor immunity. The study by Mercader et al. (2001) showed that hormone therapy induces T cell infiltration of human prostate tumors, together with functional hallmarks such as expression of IFN-γ, Ki-67, CD25, and TIA-1. As for B cell responses, we have now shown that hormone therapy and radiation therapy induce antigen-specific autoantibody responses in 25–30% of prostate cancer patients (Nesslinger et al., 2007). Having demonstrated that standard treatments do indeed induce antigen-specific immune responses, we believe it is now imperative to understand the underlying immunological mechanisms and to assess the contribution of such immune responses to clinical outcomes.

Using the SEREX immunoscreening method, we were able to identify the antigens underlying treatment-induced antibody responses in four patients. We identified a total of five antigens, namely SDCCAG1, PARP1, ZNF707+PTMA, CEP78, and ODF2. These results are typical of SEREX experiments, in that each patient appeared to recognize one or more unique antigens, and most of the antigens were of unknown functional significance with respect to prostate cancer. Further study will be required to understand why these particular antigens became immunogenic as patients underwent treatment, however a plausible mechanism exists for PARP1. PARP1 has previously been identified as an autoantigen in colorectal cancer (Scanlan *et al*., 1998) and autoimmune conditions such as systemic lupus erythematosus (Lim *et al*., 2002). It is a well-known target for cleavage by caspase-3 during apoptosis and necrosis (Casiano *et al*., 1998). Therefore, we speculate that PARP1 might become immunogenic by virtue of caspase-3-mediated cleavage in apoptotic tumor cells, resulting in the generation of a truncated neoantigen. The recent discovery of novel gene fusions in prostate cancer suggests that other antigens remain to be discovered in this disease, some of which may prove to be of functional importance (Tomlins *et al*., 2007).

The combined use of hormone and radiation therapy has dramatically improved clinical outcomes in prostate cancer. Our results and others suggest there may be an immunological basis for this synergy. Hormone therapy eliminates tumor cells by apoptosis and in so doing initiates tumor-

specific autoantibody responses and infiltration of tumors by predominantly CD4+ T cells (Nesslinger *et al*., 2007; Mercader *et al*., 2001). Autoantibodies and CD4+ T cells play important roles in autoimmune disease, and therefore could conceivably mediate an anti-tumor effect in prostate cancer. However, anti-tumor responses are generally more potent when CD8+ cytolytic T cells are involved, which may be where the synergistic effects of radiation therapy come into play. Radiation therapy not only causes apoptosis and necrosis, but also creates an inflammatory environment that promotes maturation of local antigen presenting cells (McBride *et al*., 2004). A recent study by Apetoh *et al*. (2007) has determined that the "danger" signal emitted by dying tumor cells is the release of the HMGB1 protein, a ligand for toll-like receptor 4. In turn, they showed that toll-like receptor 4 expression by dendritic cells is a prerequisite for efficient cross-presentation of tumor antigens supplied by dying cells during radiotherapy. Other studies have shown that inflammation, type 1 interferons, heat shock proteins and uric acid enhance the ability of DCs to cross-present antigens on MHC class I to CD8+ T cells (Le Bon *et al*., 2003; Heath *et al*., 2004; Melero *et al*., 2006). Based on this premise, we propose that hormone therapy may initiate humoral, Th2-like responses, whereas subsequent radiation therapy may promote conversion to cytolytic, Th1-like responses that provide greater tumor control (Figure 37.2). We are currently testing this hypothesis using the Shionogi mouse model described above.

Several combination radiation therapy and immunotherapy approaches have been attempted in preclinical models, all demonstrating varying degrees of synergism between the two modalities. For example, Tsai *et al*. (2006) used intratumorally expressed IL-3 in combination with fractionated local radiation therapy in the murine TRAMP prostate cancer model in an attempt to enhance tumor immunity. They found that, while each therapy alone caused a modest delay in tumor growth, the combined treatment was synergistic, with 50% of mice being cured and developing long-term, tumor-specific immunity. The combination of vaccine therapy and radiation therapy has been extensively investigated, especially in preclinical models, with the overall conclusion that the two modalities are synergistic (Ciernik *et al*., 1999; Chakraborty *et al*., 2004; Newcomb *et al*., 2006). For example, Kudo-Saito *et al*. (2005) showed in a murine model that vaccination and anti-CD25 mAb therapy could trigger antigen-specific immune responses, but elimination of established tumors required the addition of radiation therapy. These preclinical studies led to the establishment of a Phase II clinical trial in which vaccination with a poxviral vaccine encoding PSA was combined with standard radiotherapy for patients with clinically localized prostate cancer. Thirteen of 17 patients receiving the combined therapy had at least 3-fold increases in PSA-specific T cells compared to no detectable increases in the patients receiving only radiation therapy (Gulley *et al*., 2005a). It remains to be seen whether this combination of treatments will result in improved clinical outcomes.

The addition of immune modulatory agents to standard treatments is a promising area of investigation. For example, in preclinical studies, Flt3 ligand was shown to enhance the abscopal effect of radiation therapy in a T cell dependent manner (Demaria *et al*., 2004). In these experi-

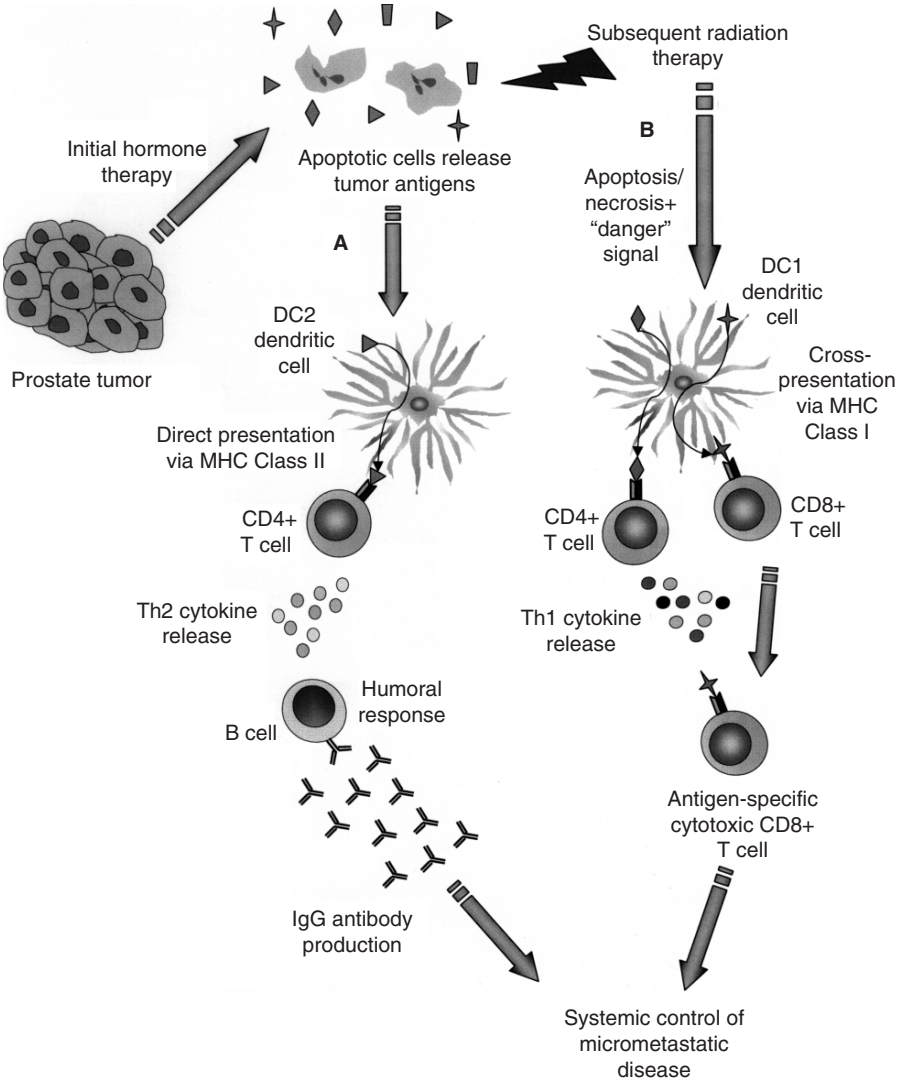

FIGURE 37.2. Proposed immunological model to explain the synergistic effects of hormone and radiation therapy. (A) Treatment of prostate cancer tumors with hormone therapy causes tumor cell death by apoptosis and initiates a humoral response through direct presentation of tumor antigens by DC2 dendritic cells via MHC class II, activating CD4+ T cells and a Th2 response. (B) Subsequent radiation therapy causes further apoptosis/necrosis of residual tumor cells in an inflammatory context, providing the necessary "danger" signals to promote effective cross-presentation of tumor antigens by DC1 dendritic cells to CD8+ T cells. In addition, CD4+ T cells are activated and release Th1 cytokines, allowing maturation of CD8+ cytotoxic T cells. The combination of tumor-specific autoantibodies and CD8+ cytotoxic T cells leads to systemic control of micrometastatic disease

ments, mice bearing two 67NR mammary carcinoma tumors were treated with radiation to one tumor only, with or without systemic administration of Flt3 ligand. RT alone led to delayed growth of the irradiated tumor. However, when RT was combined with Flt3 ligand, growth of the non-irradiated tumor was also delayed, which was not observed when Flt3 ligand was used alone nor when the treatment was given

to T cell deficient nude mice (Demaria *et al*., 2004). Another immunomodulatory strategy that could potentially have clinical impact when used in combination with standard therapy is CTLA-4 blockade. In a mouse mammary carcinoma model, the combination of RT with CTLA-4 blockade was shown to be superior to either treatment modality alone (Demaria *et al*., 2005b). Although it has yet to be tested in combination with RT in humans, CTLA-4 blockade alone has shown promise in the setting of prostate cancer. Specifically, in a recent clinical trial, patients with metastatic hormone refractory prostate cancer received a single dose of the anti-CTLA-4 antibody Ipilimumab. Two of 14 patients showed a PSA decline of ≥ 50%, with no significant clinical autoimmunity observed (Small *et al*., 2007b).

Although much progress has been made toward the development of cancer vaccines and other forms of immunotherapy, many of these approaches remain impractical for clinics outside of a research setting. Recent findings from our laboratory and others demonstrate that standard cancer treatments are an alternative means to induce B and T cell responses. One can argue that standard treatments represent a form of *in situ* vaccination that could potentially contribute to clinical outcomes. Importantly, the immune responses induced by standard treatments involve the antigen repertoire present in individual tumors, including patient-specific sequence alterations that might otherwise be difficult to identify and target. The prevalence, magnitude, and nature of such responses could potentially be enhanced by administration of immunomodulatory agents. By optimizing the immunological effects of standard treatments, it may be possible to create a cost-effective and clinically practical alternative to personalized cancer vaccines.

REFERENCES

Apetoh, L., Ghiringhelli, F., Tesniere, A., Obeid, M., Ortiz, C., Criollo, A., Mignot, G., Maiuri, M.C., Ullrich, E., Saulnier, P., Yang, H., Amigorena, S., Ryffel, B., Barrat, F.J., Saftig, P., Levi, F., Lidereau, R., Nogues, C., Mira, J.P., Chompret, A., Joulin, V., Clavel-Chapelon, F., Bourhis J., Andre, F., Delaloge, S., Tursz, T., Kroemer, G., and Zitvogel, L. 2007. Toll-like receptor 4-dependent contribution of the immune system to anticancer chemotherapy and radiotherapy. *Nat. Med. 13*: 1050–1059.

Aragon-Ching, J.B., Williams, K.M., and Gulley, J.L. 2007. Impact of androgen-deprivation therapy on the immune system: implications for combination therapy of prostate cancer. *Front. Biosci. 12*: 4957–4971.

Bolla, M., Collette, L., Blank, L., Warde, P., Dubois, J.B., Mirimanoff, R.O., Storme, G., Bernier, J., Kuten, A., Sternberg, C., Mattelaer, J., Lopez Torecilla, J., Pfeffer, J.R., Lino Cutajar, C., Zurlo, A., and Pierart, M. 2002. Long-term results with immediate androgen suppression and external irradiation in patients with locally advanced prostate cancer (an EORTC study): a phase III randomised trial.[comment]. *Lancet 360*: 103–106.

Burch, P.A., Breen, J.K., Buckner, J.C., Gastineau, D.A., Kaur, J.A., Laus, R.L., Padley, D.J., Peshwa, M.V., Pitot, H.C., Richardson, R.L., Smits, B.J., Sopapan, P., Strang, G., Valone, F.H., and Vuk-Pavlovic, S. 2000. Priming tissue-specific cellular immunity in a phase I trial of autologous dendritic cells for prostate cancer. *Clin.Cancer Res. 6*: 2175–2182.

Casiano, C.A., Ochs, R.L., and Tan, E.M. 1998. Distinct cleavage products of nuclear proteins in apoptosis and necrosis revealed by autoantibody probes. *Cell Death Differ. 5*: 183–190.

Chakraborty, M., Abrams, S.I., Camphausen, K., Liu, K., Scott, T., Coleman, C.N., and Hodge, J.W. 2003. Irradiation of tumor cells up-regulates Fas and enhances CTL lytic activity and CTL adoptive immunotherapy. *J. Immunol. 170*: 6338–6347.

Chakraborty, M., Abrams, S.I., Coleman, C.N., Camphausen, K., Schlom, J., and Hodge, J.W. 2004. External beam radiation of tumors alters phenotype of tumor cells to render them susceptible to vaccine-mediated T-cell killing. *Cancer Res. 64*: 4328–4337.

Ciernik, I.F., Romero, P., Berzofsky, J.A., and Carbone, D.P. 1999. Ionizing radiation enhances immunogenicity of cells expressing a tumor-specific T-cell epitope. *Int. J. Radiat. Oncol. Biol. Phys. 45*: 735–741.

Demaria, S., Ng, B., Devitt, M.L., Babb, J.S., Kawashima, N., Liebes, L., and Formenti, S.C. 2004. Ionizing radiation inhibition of distant untreated tumors (abscopal effect) is immune mediated. *Int. J. Radiat. Oncol. Biol. Phys. 58*: 862–870.

Demaria, S., Bhardwaj, N., McBride, W.H., and Formenti, S.C. 2005a. Combining radiotherapy and immunotherapy: a revived partnership. *Int. J. Radiat. Oncol. Biol. Phys. 63*: 655–666.

Demaria, S., Kawashima, N., Yang, A.M., Devitt, M.L., Babb, J.S., Allison, J.P., and Formenti, S.C. 2005b. Immune-mediated inhibition of metastases after treatment with local radiation and CTLA-4 blockade in a mouse model of breast cancer. *Clin. Cancer Res. 11*: 728–734.

DiPaola, R.S., Plante, M., Kaufman, H., Petrylak, D.P., Israeli, R., Lattime, E., Manson, K., and Schuetz, T. 2006. A phase I trial of pox PSA vaccines (PROSTVAC-VF) with B7-1, ICAM-1, and LFA-3 co-stimulatory molecules (TRICOM) in patients with prostate cancer. *J. Transl. Med. 4*: 1.

Drake, C.G., Doody, A.D., Mihalyo, M.A., Huang, C.T., Kelleher, E., Ravi, S., Hipkiss, E.L., Flies, D.B., Kennedy, E.P., Long, M., McGary, P.W., Coryell, L., Nelson, W.G., Pardoll, D. M., and Adler, A.J. 2005. Androgen ablation mitigates tolerance to a prostate/prostate cancer-restricted antigen. *Cancer Cell 7*: 239–249.

Fossa, A., Alsoe, L., Crameri, R., Funderud, S., Gaudernack, G., and Smeland, E.B. 2004. Serological cloning of cancer/testis antigens expressed in prostate cancer using cDNA phage surface display. *Cancer Immunol. Immunother. 53*: 431–438.

Garnett, C.T., Palena, C., Chakraborty, M., Tsang, K.Y., Schlom, J., and Hodge, J.W. 2004. Sublethal irradiation of human tumor cells modulates phenotype resulting in enhanced killing by cytotoxic T lymphocytes. *Cancer Res. 64*: 7985–7994.

Gulley, J.L., Arlen, P.M., Bastian, A., Morin, S., Marte, J., Beetham, P., Tsang, K.Y., Yokokawa, J., Hodge, J.W., Menard, C., Camphausen, K., Coleman, C.N., Sullivan, F., Steinberg, S.M., Schlom, J., and Dahut, W. 2005a. Combining a recombinant cancer vaccine with standard definitive radiotherapy in patients with localized prostate cancer. *Clin. Cancer Res. 11*: 3353–3362.

Gulley, J.L., Todd, N., Dahut W., Schlom, J., and Arlen, P. 2005b. A phase II study of PROSTVAC-VF vaccine, and the role of GM-CSF, in patients with metastatic androgen insensitive prostate cancer (AIPC). *J. Clin. Oncol. 23*: Supplement, 2504.

Heath, W.R., Belz, G.T., Behrens, G.M., Smith, C.M., Forehan, S.P., Parish, I.A., Davey, G.M., Wilson, N.S., Carbone, F.R., and Villadangos, J.A. 2004. Cross-presentation, dendritic cell subsets, and the generation of immunity to cellular antigens. *Immunol. Rev. 199*: 9–26.

Heiser, A., Coleman, D., Dannull, J., Yancey, D., Maurice, M.A., Lallas, C.D., Dahm, P., Niedzwiecki, D., Gilboa, E., and Vieweg, J. 2002. Autologous dendritic cells transfected with prostate-specific antigen RNA stimulate CTL responses against metastatic prostate tumors. *J. Clin. Invest. 109*: 409–417.

Heymann, J.J., Benson, M.C., O'Toole, K.M., Malyszko, B., Brody, R., Vecchio, D., Schiff, P.B., Mansukhani, M.M., and Ennis, R.D. 2007. Phase II study of neoadjuvant androgen deprivation followed by external-beam radiotherapy with 9 months of androgen deprivation for intermediate- to high-risk localized prostate cancer. *J. Clin. Oncol. 25*: 77–84.

Hoeppner, L.H., Dubovsky, J.A., Dunphy, E.J., and McNeel, D.G. 2006. Humoral immune responses to testis antigens in sera from patients with prostate cancer. *Cancer Immun. 6*: 1.

Hoffmann, T.K., Donnenberg, A.D., Finkelstein, S.D., Donnenberg, V.S., Friebe-Hoffmann, U., Myers, E.N., Appella, E., DeLeo, A.B., and Whiteside, T.L. 2002. Frequencies of tetramer+ T cells specific for the wild-type sequence p53(264–272) peptide in the circulation of patients with head and neck cancer. *Cancer Res. 62*: 3521–3529.

Jager, D., Karbach, J., Pauligk, C., Seil, I., Frei, C., Chen, Y.T., Old, L.J., Knuth, A., and Jager, E.

2005. Humoral and cellular immune responses against the breast cancer antigen NY-BR-1: definition of two HLA-A2 restricted peptide epitopes. *Cancer Immun. 5*: 11–17.

Jager, E., Chen, Y.T., Drijfhout, J.W., Karbach, J., Ringhoffer, M., Jager, D., Arand, M., Wada, H., Noguchi, Y., Stockert, E., Old, L.J., and Knuth, A. 1998. Simultaneous humoral and cellular immune response against cancer-testis antigen NY-ESO-1: definition of human histocompatibility leukocyte antigen (HLA)-A2-binding peptide epitopes. *J. Exp. Med. 187*: 265–270.

Javid, B., MacAry, P.A., and Lehner, P.J. 2007. Structure and function: heat shock proteins and adaptive immunity. *J. Immunol. 179*: 2035–2040.

Kaufman, H.L., and Divgi, C.R. 2005. Optimizing prostate cancer treatment by combining local radiation therapy with systemic vaccination. *Clin. Cancer Res. 11*: 6757–6762.

Kaufman, H.L., Wang, W., Manola, J., DiPaola, R.S., Ko, Y.J., Sweeney, C., Whiteside, T.L., Schlom, J., Wilding, G., and Weiner, L.M. 2004. Phase II randomized study of vaccine treatment of advanced prostate cancer (E7897): a trial of the Eastern Cooperative Oncology Group. *J. Clin. Oncol. 22*: 2122–2132.

Kudo-Saito, C., Schlom, J., Camphausen, K., Coleman, C.N., and Hodge, J.W. 2005. The requirement of multimodal therapy (vaccine, local tumor radiation, and reduction of suppressor cells) to eliminate established tumors. *Clin. Cancer Res. 11*: 4533–4544.

Laverdiere, J., Nabid, A., De Bedoya, L.D., Ebacher, A., Fortin, A., Wang, C.S., and Harel, F. 2004. The efficacy and sequencing of a short course of androgen suppression on freedom from biochemical failure when administered with radiation therapy for T2-T3 prostate cancer. *J. Urol. 171*: 1137–1140.

Le Bon, A., Etchart, N., Rossmann, C., Ashton, M., Hou, S., Gewert, D., Borrow, P., and Tough, D.F. 2003. Cross-priming of CD8+ T cells stimulated by virus-induced type I interferon. *Nat. Immunol. 4*: 1009–1015.

Lim, Y., Lee, D.Y., Lee, S., Park, S.Y., Kim, J., Cho, B., Lee, H., Kim, H.Y., Lee, E., Song, Y.W., and Jeoung, D.I. 2002. Identification of autoantibodies associated with systemic lupus erythematosus. *Biochem. Biophys. Res. Commun. 295*: 119–124.

Lodge, P.A., Jones, L.A., Bader, R.A., Murphy, G.P., and Salgaller, M.L. 2000. Dendritic cell-based immunotherapy of prostate cancer: immune monitoring of a phase II clinical trial. *Cancer Res. 60*: 829–833.

Ludgate, C.M., Bishop, D.C., Pai, H., Eldridge, B., Lim, J., Berthelet, E., Blood, P., Piercy, G.B., and Steinhoff, G. 2005. Neoadjuvant hormone therapy and external-beam radiation for localized high-risk prostate cancer: the importance of PSA nadir before radiation. *Int. J. Radiat. Oncol. Biol. Phys. 62*: 1309–1315.

Lugade, A.A., Moran, J.P., Gerber, S.A., Rose, R.C., Frelinger, J.G., and Lord, E.M. 2005. Local radiation therapy of B16 melanoma tumors increases the generation of tumor antigen-specific effector cells that traffic to the tumor. *J. Immunol. 174*: 7516–7523.

McBride, W.H., Chiang, C.S., Olson, J.L., Wang, C.C., Hong, J.H., Pajonk, F., Dougherty, G.J., Iwamoto, K.S., Pervan, M., and Liao, Y.P. 2004. A sense of danger from radiation. *Radiat. Res. 162*: 1–19.

McNeel, D.G., Nguyen, L.D., Storer, B.E., Vessella, R., Lange, P.H., and Disis, M.L. 2000. Antibody immunity to prostate cancer associated antigens can be detected in the serum of patients with prostate cancer. *J. Urol. 164*: 1825–1829.

Melero, I., Arina, A., Murillo, O., Dubrot, J., Alfaro, C., Perez-Gracia, J.L., Bendandi, M., and Hervas-Stubbs, S. 2006. Immunogenic cell death and cross-priming are reaching the clinical immunotherapy arena. *Clin. Cancer Res. 12*: 2385–2389.

Mercader, M., Bodner, B.K., Moser, M.T., Kwon, P.S., Park, E.S., Manecke, R.G., Ellis, T.M., Wojcik, E.M., Yang, D., Flanigan, R.C., Waters, W.B., Kast, W.M., and Kwon, E.D. 2001. T cell infiltration of the prostate induced by androgen withdrawal in patients with prostate cancer. *Proc. Natl. Acad. Sci. USA. 98*: 14565–14570.

Miles, A.K., Rogers, A., Li, G., Seth, R., Powe, D., McArdle, S.E., McCulloch, T.A., Bishop, M.C., and Rees, R.C. 2007. Identification of a novel prostate cancer-associated tumor antigen. *Prostate 67*: 274–287.

Nesslinger, N.J., Sahota, R.A., Stone, B., Johnson, K., Chima, N., King, C., Rasmussen, D., Bishop, D., Rennie, P.S., Gleave, M., Blood, P., Pai, H., Ludgate, C., and Nelson, B.H. 2007. Standard

treatments induce antigen-specific immune responses in prostate cancer. *Clin. Cancer Res. 13*: 1493–1502.

Newcomb, E.W., Demaria, S., Lukyanov, Y., Shao, Y., Schnee, T., Kawashima, N., Lan, L., Dewyngaert, J.K., Zagzag, D., McBride, W.H., and Formenti, S.C. 2006. The combination of ionizing radiation and peripheral vaccination produces long-term survival of mice bearing established invasive GL261 gliomas. *Clin. Cancer Res. 12*: 4730–4737.

Okada, T., Akada, M., Fujita, T., Iwata, T., Goto, Y., Kido, K., Okada, T., Matsuzaki, Y., Kobayashi, K., Matsuno, S., Sunamura, M., and Kawakami, Y. 2006. A novel cancer testis antigen that is frequently expressed in pancreatic, lung, and endometrial cancers. *Clin. Cancer Res. 12*: 191–197.

Oliver, R.T., Joseph, J.V., and Gallagher, C.J. 1995. Castration-induced lymphocytosis in prostate cancer: possible evidence for gonad/thymus endocrine interaction in man. *Urol. Int. 54*: 226–229.

Reits, E.A., Hodge, J.W., Herberts, C.A., Groothuis, T.A., Chakraborty, M., Wansley, E.K., Camphausen, K., Luiten, R.M., de Ru, A.H., Neijssen, J., Griekspoor, A., Mesman, E., Verreck, F.A., Spits, H., Schlom, J., van Veelen, P., and Neefjes, J.J. 2006. Radiation modulates the peptide repertoire, enhances MHC class I expression, and induces successful antitumor immunotherapy. *J. Exp. Med. 203*: 1259–1271.

Roden, A.C., Moser, M.T., Tri, S.D., Mercader, M., Kuntz, S.M., Dong, H., Hurwitz, A.A., McKean, D.J., Celis, E., Leibovich, B.C., Allison, J.P., and Kwon, E.D. 2004. Augmentation of T cell levels and responses induced by androgen deprivation. *J. Immunol. 173*: 6098–6108.

Scanlan, M.J., Chen, Y.T., Williamson, B., Gure, A.O., Stockert, E., Gordan, J.D., Tureci, O., Sahin, U., Pfreundschuh, M., and Old, L.J. 1998. Characterization of human colon cancer antigens recognized by autologous antibodies. *Int. J. Cancer 76*: 652–658.

Simons, J.W., and Sacks, N. 2006. Granulocyte-macrophage colony-stimulating factor-transduced allogeneic cancer cellular immunotherapy: the GVAX vaccine for prostate cancer. *Urol. Oncol. 24*: 419–424.

Simons, J.W., Mikhak, B., Chang, J.F., DeMarzo, A.M., Carducci, M.A., Lim, M., Weber, C.E., Baccala, A.A., Goemann, M.A., Clift, S.M., Ando, D.G., Levitsky, H.I., Cohen, L.K., Sanda, M.G., Mulligan, R.C., Partin, A.W., Carter, H.B., Piantadosi, S., Marshall, F.F., and Nelson, W.G. 1999. Induction of immunity to prostate cancer antigens: results of a clinical trial of vaccination with irradiated autologous prostate tumor cells engineered to secrete granulocyte-macrophage colony-stimulating factor using ex vivo gene transfer. *Cancer Res. 59*: 5160–5168.

Small,E.J.,Rini,B.,Higano,C.,Redfern,C.,Nemunaitis, J., Valone, F., Kylstr, J., and Schellhammer, P.F. 2003. A randomized, placebo-controlled phase III trial of APC8015 in patients with androgen-independent prostate cancer (AiPCa). *Proc. Am. Soc. Clin. Oncol. 22*: 382–388.

Small, E.J., Schellhammer, P.F., Higano, C.S., Redfern, C.H., Nemunaitis, J.J., Valone, F.H., Verjee, S.S., Jones, L.A., and Hershberg, R.M. 2006. Placebo-controlled phase III trial of immunologic therapy with sipuleucel-T (APC8015) in patients with metastatic, asymptomatic hormone refractory prostate cancer. *J. Clin. Oncol. 24*: 3089–3094.

Small, E.J., Sacks, N., Nemunaitis, J., Urba, W.J., Dula, E., Centeno, A.S., Nelson, W.G., Ando, D., Howard, C., Borellini, F., Nguyen, M., Hege, K., and Simons, J.W. 2007a. Granulocyte macrophage colony-stimulating factor–secreting allogeneic cellular immunotherapy for hormone-refractory prostate cancer. *Clin. Cancer Res. 13*: 3883–3891.

Small, E.J., Tchekmedyian, N.S., Rini, B.I., Fong, L., Lowy, I., and Allison, J.P. 2007b. A pilot trial of CTLA-4 blockade with human anti-CTLA-4 in patients with hormone-refractory prostate cancer. *Clin. Cancer Res. 13*: 1810–1815.

Tomlins, S.A., Laxman, B., Dhanasekaran, S.M., Helgeson, B.E., Cao, X., Morris, D.S., Menon, A., Jing, X., Cao, Q., Han, B., Yu, J., Wang, L., Montie, J.E., Rubin, M.A., Pienta, K.J., Roulston, D., Shah, R.B., Varambally, S., Mehra, R., and Chinnaiyan, A.M. 2007. Distinct classes of chromosomal rearrangements create oncogenic ETS gene fusions in prostate cancer. *Nature 448*: 595–599.

Tsai, C.H., Hong, J.H., Hsieh, K.F., Hsiao, H.W., Chuang, W.L., Lee, C.C., McBride, W.H., and Chiang, C.S. 2006. Tetracycline-regulated intra-

tumoral expression of interleukin-3 enhances the efficacy of radiation therapy for murine prostate cancer. *Cancer Gene Ther. 13*: 1082–1092.

van der Bruggen, P., Traversari, C., Chomez, P., Lurquin, C., De Plaen, E., Van den Eynde, B., Knuth, A., and Boon, T. 1991. A gene encoding an antigen recognized by cytolytic T lymphocytes on a human melanoma. *Science 254*: 1643–1647.

Vesalainen, S., Lipponen, P., Talja, M., and Syrjanen, K. 1994. Histological grade, perineural infiltration, tumour-infiltrating lymphocytes and apoptosis as determinants of long-term prognosis in prostatic adenocarcinoma. *Eur. J. Cancer 30A*: 1797–1803.

Vonderheide, R.H., Domchek, S.M., Schultze, J.L., George, D.J., Hoar, K.M., Chen, D.Y., Stephans, K.F., Masutomi, K., Loda, M., Xia, Z., Anderson, K.S., Hahn, W.C., and Nadler, L.M. 2004. Vaccination of cancer patients against telomerase induces functional antitumor CD8+ T lymphocytes. *Clin. Cancer Res. 10*: 828–839.

Wang, X., Yu, J., Sreekumar, A., Varambally, S., Shen, R., Giacherio, D., Mehra, R., Montie, J.E., Pienta, K.J., Sanda, M.G., Kantoff, P.W., Rubin, M.A., Wei, J.T., Ghosh, D., and Chinnaiyan, A.M. 2005. Autoantibody signatures in prostate cancer. *N. Engl. J. Med. 353*: 1224–1235.

Wilson, C.A., Mrose, S.A., and Thomas, D.W. 1995. Enhanced production of B lymphocytes after castration. *Blood 85*: 1535–1539.

Zhou, Y., Toth, M., Hamman, M.S., Monahan, S.J., Lodge, P.A., Boynton, A.L., and Salgaller, M.L. 2002. Serological cloning of PARIS-1: a new TBC domain-containing, immunogenic tumor antigen from a prostate cancer cell line. *Biochem. Biophys. Res. Commun. 290*: 830–838.

38
Vinorelbine, Doxorubicin, and Prednisone in Hormone Refractory Prostate Cancer

Samer Kalakish and Frank M. Torti

INTRODUCTION

Prostate Cancer is the most common non-skin cancer affecting men in the United States. The National Cancer Institute estimates that ~218,890 new cases and 27,050 deaths will be attributed to this disease in 2007. During the course of the disease, roughly 30–50% of patients will have metastatic progression (Gittes, 1991). In the mid 1980s, androgen deprivation by bilateral orchiectomy or luteinizing hormone-releasing hormone (LHRH) agonists showed tumor stabilization or regression in 80–95% of patients (Parmar *et al*., 1985). These therapies ultimately fail and these patients progress to a hormone refractory disease state in a median of 18–36 months (Aragon-Ching and Dahut, 2007).

Invariably, all patients with metastatic disease progress despite androgen ablation. Various chemotherapeutic regimens (single agent or combination therapy) have been employed in attempts to achieve prolongation of survival, better pain control, and improvement of quality of life. However, major adverse effects such as myelosuppression, cardiac toxicity, alopecia, neuropathy and gastrointestinal toxicity with chemotherapy make a risk and benefit analysis paramount when considering any chemotherapeutic intervention for a hormone refractory prostate cancer (Mike *et al*., 2006).

Vinorelbine tartrate is a semisynthetic drug that belongs to the vinca alkaloid family that interferes with microtubule assembly. When used alone, vinorelbine has response rates that range from 13% to 17% (Fields-Jones *et al*., 1999; Oudard *et al*., 2001; Morant *et al*., 2002). Smith *et al*. (2000) and Sweeney *et al*. (2002) report that when vinorelbine was combined with estramustine in phase II trials, higher rates, ranging from 24% to 71% were achieved. Other phase II studies have combined vinorelbine with prednisone: Robles *et al*. (2003) report favorable toxicity profile and encouraging PSA response rate and pain control. Using the same regimen, Tralongo *et al*. (2003) have observed > 50% PSA reduction in 36% of patients with pain reduction in 44% of patients in another phase II trial.

Doxorubicin is an anthracycline antibiotic that intercalates with DNA with antitumor activity against a wide range of cancers. It has been investigated as a chemotherapeutic drug for hormone refractory prostate cancer as single agent or in combination in studies that span 3 decades. O'Bryan *et al*. (1977) showed a dose-response relationship

between doxorubicin and prostate cancer. Concurrently, DeWys *et al.* (1977) in the Eastern Cooperative Oncology Group proved that doxorubicin at 60 mg/m^2 had a greater partial response (25%) compared to 5% with 5-fluorouracil. In more recent studies by various authors, doxorubicin in combination regimens showed responses from 46% to 58% of treated patients. For example, Small *et al.* (1996) combined cyclophosphamide and granulocyte colony stimulating factor with doxorubicin, while Haas *et al.* (2000) investigated adding estramustine to doxorubicin.

Weekly doses of doxorubicin have yielded promising results in earlier studies. When compared to 3-weekly dosing, weekly doxorubicin revealed tumor response, improved pain and performance scores, and substantially reduced acute toxicity (Torti *et al.*, 1983a; Raghavan, 1988). Von Hoff *et al.* (1979) and Torti *et al.* (1983b) published that cardiotoxicity was also lower with the weekly dosing regimen. When patients were randomized to receive doxorubicin with prednisone or prednisone alone, there was an improved subjective response and longer stable disease in the combination arm (Rangel *et al.*, 1992). Therefore, weekly dosing of doxorubicin provides therapeutic benefit with less toxicity.

Glucocorticoids have been used in the treatment of prostate cancer since the 1950s (Miller and Hinman, 1954). Tannock *et al.* (1989) reported that 38% of patients treated with steroids had pain improvement together with better quality of life. Further investigations demonstrated the significant pain control and quality of life benefits derived from prednisone (Osoba *et al.*, 1999; Tannock *et al.*, 1996). Moreover, several phase III trials documented decrease of PSA levels >50% in 21–24% of patients receiving prednisone alone (Tannock *et al.*, 1996; Gregurich, 2000; Fosså *et al.*, 2001). Hence, prednisone has been used extensively as an adjunct in various regimens with a limited toxicity profile.

Although the recent use of taxanes with corticosteroids has been a major treatment advance, there remains a pressing need for new chemotherapy regimens to treat AIPC (Tannock *et al.*, 2004). Furthermore, because bone pain is a particularly debilitating symptom in patients with metastatic prostate cancer, improved palliation and quality of life become important parameters to consider in assessing the effectiveness of these regimens. Given the individual benefits of vinorelbine, doxorubicin, and prednisone, a phase II trial to evaluate clinical efficacy and quality of life (QOL) impact using vinorelbine, doxorubicin, and prednisone (NAP) in patients with advanced AIPC was conducted at Wake Forest University Health Sciences.

ELIGIBILITY

A protocol was submitted and approved by the Institutional Review Board. Patients were considered to have AIPC once they failed hormonal therapy (LHRH or orchiectomy) and antiandrogen withdrawal documented as an increasing PSA, new bone metastasis or new soft tissue disease. For the purpose of the trial, patients could receive secondary hormone manipulations but no new hormonal therapies were allowed within 4 weeks of enrollment. Patients who had radiation therapy or surgery could be enrolled unless therapy was within 1 or 4 weeks of enrollment, respectively. Exclusion criteria included prior immunotherapy, chemotherapy, or therapeutic radiopharmaceuticals.

Patients enrolled had an ECOG performance status of 0 or 1 with a life expectancy greater or equal to 3 months, a creatinine less than or equal to 2 mcmol/l, bilirubin less than or equal 2 mcmol/l with adequate hematologic function (granulocytes > = 1,000/mcl; platelet count > = 100,000/mcl; hemoglobin > = 10 g/dl), and cardiac function (ejection fraction > = 50%). Exclusion criteria included another malignancy within 5 years, known brain metastases, active uncontrolled infection, psychiatric illness or other conditions that impeded informed consent.

TREATMENT PLAN

This trial is a phase II single arm study. Signed informed consent was obtained from all patients. Baseline studies obtained included PSA, bone scans, chest X-rays, multiple gated acquisition (MUGA) scans. Quality of life was assessed using the Functional Assessment of Cancer Therapy-Prostate (FACT-P) and FACT-General (FACT-G) evaluation tools as well as the Brief Pain Inventory (BPI) and a Narcotic Pain Medication Logbook. Computed tomography and magnetic resonance imaging were performed if clinically indicated.

The treatment regimen consisted of a 3-week cycles of (NAP) as follows:

- Vinorelbine tartrate (Navelbine®; Glaxo-Smith-Kline-Welcome, Research Triangle Park, NC) at 20 mg/m^2 every week for 3 weeks with medication vacation on the fourth week.
- Doxorubicin at 20 mg/m^2 every week for 3 weeks with a medication vacation on the fourth week.
- Oral prednisone 5 mg twice a daily.

EVALUATION

The primary endpoints of the study were response to therapy, time to progression (time from study enrollment to PSA rise or progression of disease at any site), and survival. Quality of life was followed using the FACT-P, FACT-G, and BPI scales in addition to Narcotic Pain Medication Logbook. Patients were automatically re-evaluated with PSA, chest X-rays, and bone scans after 3 cycles of NAP or with clinical disease progression. According to the clinical situation, CT or MRI studies were ordered. Partial response was defined as a decrease > 50% in PSA from baseline with a confirmatory PSA level at the next patient encounter without bone scan progression. Complete response was defined as normalization of PSA levels with evidence of resolution of measurable disease in soft tissue and by bone scan. Progressive disease was designated as an increase in PSA > 50% from PSA nadir.

Three cycles of NAP were considered adequate therapeutic intervention. Patients responding to therapy or with stable disease were continued on more cycles. Patients were withdrawn from the study if significant toxicity developed or if disease progressed. Patients were followed till death; early death or early progression was not a criterion to exclude the patient from statistical evaluation. Evaluating QOL was done at baseline, after the second cycle, third cycle, and 1 month after completing the third cycle of NAP employing the FACT-P scale (which includes FACT-G subscale). The BPI and the Narcotic Pain Medication Logbook were inspected at the end of each 3 week cycle. Morphine equivalents were calculated for the various narcotics used as previously described (Lacy *et al.*, 2003).

The Expanded Common Toxicity Criteria version 2.0 was employed in the evaluation of toxicity. During the study, the doses of vinorelbine and doxorubicin could be altered depending on the clinical situation. Blood transfusions and various growth factors were allowed in addition to growth factors according to established guidelines from the American Society for Clinical Oncology. Patients while on the protocol could not receive palliative radiation.

STATISTICAL ANALYSIS

Kaplan-Meier methods were utilized in the analysis of events (survival, relapse, etc.). Mixed-model regression for the longitudinal FACT-G and FACT-P scores were used to correlate measurements within individuals. Means were calculated at baseline, 1 month, 2 months, and 3 months, and regression analysis was used to calculate P values and average changes per month. Student t tests were used to study the BPI response from enrollment to the end of the third month.

RESULTS

Forty six patients with hormone-refractory prostate cancer participated in the study between 1998 and 2002. The median age was 68 years (50–82), with ECOG performance status of 0 in 22 (48%) and 1 in 24 (52%). The mean and median of the PSA were 395 and 144 (ng/ml), respectively with a range of 9–4379 (ng/ml). Baseline bone scans showed that all but 2 patients had bone metastases (96%). The mean cardiac ejection fraction of the patients at the beginning of the study was 61%. Prior therapies included prostatectomy (43%), radiation therapy (46%), orchiectomy (37%), LHRH agonists (61%), antiandrogens (83%), and ketoconozale/steroid (13%). Other therapies included cryosurgery (2%), cytadren (2%), herbal medications (2%), and bisphosphonates (9%).

Among the 46 patients enrolled, 36 (78%) completed 3 cycles of NAP, an adequate therapeutic intervention. The proportions of patients that completed 6, 9, and 12 cycles were 46%, 20%, and 11%, respectively. All 46 patients had a median follow-up of 13.4 months. The median survival rate was 57 weeks (36–76 weeks [95% CI]). The partial response in PSA among the patients that completed 3 cycles was 42% (26–59% [95%CI]) with a median time of 7 weeks (3–39 weeks) to achieve PR. In the entire study population, there was disease progression in 39 patients (85%); median time to progressive disease was 17 weeks (11–24 weeks). One patient continued to show no progression of disease at 11.5 months on NAP. Three patients refused further therapeutic intervention and 3 died prior to restaging.

Quality of life was assessed at baseline and every month for 3 months. FACT-P and FACT-G subscales were evaluated and there was a statistically significant improvement in both scale scores with an average increase of 1.2 points per month for the FACT-G score ($P = 0.03$) and 2.8 points per month for the FACT-P score ($P = 0.0006$). There was a concomitant decline in the use of pain medication associated with the improved quality of life. Approximately 30% of patients were off narcotics by the end of cycle 1. This percentage remained stable till the end of the third cycle. In addition, in patients who continued to require narcotics, the median morphine equivalents

were lower at the end of each cycle compared to baseline. Moreover, improvement in pain control was evident by the BPI questionnaire. There was a 33% decrease in average pain ($P = 0.005$) and a 26% decrease in worst pain ($P < 0.001$) when nadir pain scores were compared to baseline pain scores. There was also strong correlation between pain measurements in the BPI and the FACT questionnaires. When either the worst pain or the average pain in the BPI questionnaire was compared to the pain question in the FACT scale, there was a strong correlation ($P < 0.001$).

Forty six patients received a total of 261 cycles of treatment; toxicity was assessed for all patients. The number of cycles ranged from 1 to 16 with a median of 4 cycles. Neutropenia was common, with 28 (61%) patients out of 46 showing various degrees of toxicity. Only 6 patients (13%) suffered grade 4 neutropenia; 3 patients required admission for antibiotics therapy. Withdrawal from the protocol due to neutropenia occurred in 1 patient (2%). Unlike neutropenia, thrombocytopenia was not a common occurrence. Severe hyperglycemia (grade 3 and 4) occurred in 11 patients (24%) while on treatment; most of these patients had preexisting diabetes. Adequate blood glucose control was reached by oral regimens and only 1 patient had to stop prednisone due to refractory hyperglycemia.

Congestive heart failure did not develop in any of the treated patients. Doxorubicin was discontinued in 5 patients (11%) due a decrease in cardiac ejection fraction to < 50%; none had clinical symptoms of congestive heart failure. At the time of termination of doxorubicin, the reported ejection fraction in those patients as determined by MUGA scans were 44%, 46%, 48%, 48%, 49% with corresponding cumulative doses of 336 mg/m^2, 750 mg/m^2, 140 mg/m^2, 482 mg/m^2, and 239 mg/m^2, respectively. Pulmonary emboli developed in 3 patients with subsequent fatal myocardial infarction in 2 patients. Because these events are not established toxicities of the NAP regimen drugs, it is not clear whether they are treatment related or a result of the patients' advanced cancer or other illnesses.

Other grade 3 and 4 adverse effects were documented but infrequent. There was an episode of angioedema with stridor and facial swelling occurring after infusion of vinoblastine and doxorubicin in 1 patient. The patient recovered completely with epinephrine and corticosteroids. Other adverse effects included deep vein thrombosis, fatigue, depression, and anorexia, each occurring in 1 patient. There was another patient who started having parasthesias after 12 cycles of therapy prompting cessation of treatment. Two patients had elevation in liver function tests, and 3 patients suffered dyspnea. Two patients on anticoagulation with normal platelet counts suffered bleeding episodes; 1 had a gastrointestinal bleeding while another had a subdural hematoma. Among grade 1 and 2 toxicities, fatigue (61%) was most common. The gastrointestinal adverse effects were nausea and vomiting (48%), anorexia (28%), and diarrhea (20%).

DISCUSSION

Androgen independent prostate cancer continues to challenge physicians despite the recent advances in therapy. Further delay in disease progression as well as improved palliation of symptoms represent important goals. Pain from bone metastases is often debilitating and frequently affects the quality of life. Malaise, fatigue, and

cachexia are also common. Therefore, the balance between drug efficacy and cancer symptom palliation of the therapeutic agents is often critical for patients. In this chapter, we review our initial report of the therapeutic regimen (NAP) that was explored to determine its antineoplastic efficacy as well as impact on quality of life (Borden *et al*., 2006).

One of the major benefits of this regimen was the improvement in the quality of life. This was demonstrated using the FACT scales, BPI scale and the patient's narcotic log book. The FACT questionnaires are among the most widely accepted and validated tools in assessing quality of life in the cancer patients undergoing therapy. The NAP regimen showed significant improvement in the FACT-P scores which was mirrored in improved pain scores using the BPI scale and lower narcotic requirement. Although any Phase II study is limited in the inferences that can be drawn, our study shows the feasibility of quality of life assessment in Phase II trials. Multiple assessments reinforced the finding of palliative benefit.

Another interesting observation of the study is relatively rapid time to achieve palliation of pain as well as the rapid decline of PSA in responding patients. Among the patients who had partial response in PSA, 33% of them experienced the partial response in the first month. In parallel with the PSA response, pain scores improved. At the end of the first cycle, 30% of the patients who were on pain medications at enrollment were medication free. This percentage remained stable throughout the study. Furthermore, in patients who still had some cancer pain, there was decline in narcotic requirements by the end of the first cycle. Overall, rapid symptomatic relief was observed and was sustained in responding patients.

The adverse effect profile related to the NAP regimen was modest. Neutropenia was relatively common, but was controllable. There were 3 patients (6%) with neutropenia who were admitted for antibiotics, and in 1 patient (2%), neutropenia was a contributing factor to withdraw from the protocol. Hyperglycemia was also a frequent occurrence due to prednisone. Most patients with hyperglycemia were preexisting diabetics, and glucose was controlled without major difficulty. Decreased cardiac ejection fraction dropped below 50% in 5 patients (11%). None of the patients developed clinical symptoms of congestive heart failure, in keeping with earlier reports of diminished cardiotoxicity with weekly doxorubicin dosing. The NAP regimen was designed before recent studies that incorporated taxotere into therapy were published. However, the quality of life impact with substantial palliation remains notable, and the trial design which emphasizes quality of life assessment in a Phase II study represents a useful paradigm for further drug development.

REFERENCES

Aragon-Ching, J.B., and Dahut, W.L. 2007. Chemotherapy in androgen-independent prostate cancer (AIPC): What's next after taxane progression? *Cancer Ther. 5A*: 151–160.

Borden, L.S. Jr., Clark, P.E., Lovato, J., Hall, M.C., Stindt, D., Harmon, M., Mohler, R., and Torti, F.M. 2006. Vinorelbine, doxorubicin, and prednisone in androgen-independent prostate cancer. *Cancer 107*: 1093–1100.

DeWys, W.D., Bauer, M., Colsky, J., Cooper, R.A., Creech, R., and Carbone P.P. 1977. Comparative trial of adriamycin and 5-fluorouracil in advanced prostatic cancer - progress report. *Cancer Treat. Rep. 61*: 325–328.

Fields-Jones, S., Koletsky, A., Wilding, G., O'Rourke, M., O'Rourke, T., Eckardt J., Yates, B., McGuirt, C., and Burris, H.A. 3rd. 1999. Improvements in clinical benefit with vinorelbine in the treatment of hormone-refractory prostate cancer: a Phase II trial. *Ann. Oncol. 10*: 1307–1310.

Fosså, S.D., Slee, P.H., Brausi, M., Horenblas, S., Hall, R.R., Hetherington, J.W., Aaronson, N., de Prijck, L., and Collette, L. 2001. Flutamide versus prednisone in patients with prostate cancer symptomatically progressing after androgen-ablative therapy: a Phase III study of the European Organization for Research and Treatment of Cancer Genitourinary Group. *J. Clin. Oncol. 19*: 62–71.

Gittes, R.F. 1991. Carcinoma of the prostate. *N. Engl. J. Med. 324*: 236–245.

Gregurich, M. 2000. Phase III study of mitoxantrone/low-dose prednisone versus low-dose prednisone alone in patients with asymptomatic hormone-refractory carcinoma of the prostate. *Proc. Am. Soc. Clin. Oncol. 18*: 1440–1450. Abstract.

Haas, N.B., Manola, J., Hudes, G., Citrin, D.L., Kies, M.S., and Davis, T.E., Eastern Cooperative Oncology Group Study PH882. 2000. Phase II pilot study of combined chemohormonal therapy with doxorubicin and estramustine in metastatic prostate cancer. *Am. J. Clin. Oncol. 23*: 589–592.

Lacy, C.F., Armstrong. L.L., and Goldman, M.P. 2003. Narcotic Agonists Comparative Pharmacokinetics. Drug Information Handbook, 11th ed. Hudson, OH: Lexi-Comp.

Mike, S., Harrison, C., Coles, B., Staffurth J., Wilt, T.J., and Mason, M.D. 2006. Chemotherapy for hormone-refractory prostate cancer. *Cochrane Database Syst. Rev. 18(4)*: CD005247.

Miller, G.M., and Hinman, F. Jr. 1954. Cortisone treatment in advanced carcinoma of the prostate. *J. Urol. 72*: 485–496.

Morant, R., Hsu Schmitz, S.F., Bernhard, J., Thürlimann, B., Borner, M., Wernli, M., Egli, F., Forrer, P., Streit, A., Jacky, E., Hanselmann, S., Bauer, J., Hering, F., Schmid, H.P. 2002. Vinorelbine in androgen-independent metastatic prostatic carcinoma - a Phase II study. *Eur. J. Cancer 38*: 1626–1632.

O'Bryan, R.M., Baker, L.H., Gottlieb, J.E., Rivkin, S.E., Balcerzak, S.P., Grumet, G.N., Salmon, S.E., Moon, T.E., and Hoogstraten, B. 1977. Dose response evaluation of Adriamycin in human neoplasia. *Cancer 39*: 1940–1948.

Osoba, D., Tannock, I.F., Ernst, D.S., Neville, A.J. 1999. Health-related quality of life in men with metastatic prostate cancer treated with prednisone alone or mitoxantrone and prednisone. *J. Clin. Oncol. 17*: 1654–1663.

Oudard, S., Caty, A., Humblet, Y., Beauduin, M., Suc, E., Piccart, M., Rolland, F., Fumoleau, P., Bugat, R., Houyau, P., Monnier, A., Sun, X., Montcuquet, P., Breza, J., Novak, J., Gil, T., and Chopin, D. 2001. Phase II study of vinorelbine in patients with androgen-independent prostate cancer. *Ann. Oncol. 12*: 847–852.

Parmar, H., Phillips, R.H., Lightman, S.L., Edwards, L., Allen, L., and Schally, A.V. 1985. Randomized controlled study of orchiectomy versus long-acting D-trp-6-LHRH microcapsules in advanced prostate carcinoma. *Lancet 2*: 1201–1205.

Raghavan, D. 1988. Non-hormone chemotherapy for prostate cancer: principles of treatment and application to the testing of new drugs. *Semin. Oncol. 15*: 371–389.

Rangel, C., Matzkin, H., and Soloway, M.S. 1992. Experience with weekly doxorubicin (Adriamycin) in hormone-refractory Stage D2 prostate cancer. *Urology. 39*: 577–582.

Robles, C., Furst, A.J., Sriratana, P., Lai, S., Chua, L., Donnelly, E., Solomon, J., Sundaram, M., Feun, L., and Savaraj, N. 2003. Phase II study of vinorelbine with low dose prednisone in the treatment of hormone-refractory metastatic prostate cancer. *Oncol. Rep. 10*: 885–889.

Small, E.J., Srinivas, S., Egan, B., McMillan, A., and Rearden, T. P. 1996. Doxorubicin and dose-escalated cyclophosphamide with granulocyte colony-stimulating factor for the treatment of hormone-resistant prostate cancer. *J. Clin. Oncol. 14*: 1617–1625.

Smith, M.R., Kaufman, D., Oh, W., Guerin, K., Seiden, M., Makatsoris, T., Manola, J., and Kantoff, P.W. 2000. Vinorelbine and estramustine in androgen-independent metastatic prostate cancer: a Phase II study. *Cancer 89*: 1824–1828.

Sweeney, C.J., Monaco, F.J., Jung, S.H., Wasielewski, M.J., Picus, J., Ansari, R.H., Dugan, W.M., and Einhorn, L.H. 2002. A Phase

II Hoosier Oncology Group study of vinorelbine and estramustine phosphate in hormone-refractory prostate cancer. *Ann. Oncol. 13*: 435–440.

Tannock, I., Gospodarowicz, M., Meakin, W., Panzarella, T., Stewart, L., and Rider, W. 1989. Treatment of metastatic prostatic cancer with low-dose prednisone: evaluation of pain and quality of life as pragmatic indices of response. *J. Clin. Oncol. 7*: 590–597.

Tannock, I.F., Osoba, D., Stockler, M.R., Ernst, D.S., Neville, A.J., Moore, M.J., Armitage, G.R., Wilson, J.J., Venner, P.M., Coppin, C.M., and Murphy, K.C. 1996. Chemotherapy with mitoxantrone plus prednisone or prednisone alone for symptomatic hormone-resistant prostate cancer: a Canadian randomized trial with palliative end points. *J. Clin. Oncol. 14*: 1756–1764.

Tannock, I.F., de Wit, R., Berry, W.R., Horti, J., Pluzanska, A., Chi, K.N., Oudard, S., Théodore, C., James, N.D., Turesson, I., Rosenthal, M. A., and Eisenberger, M.A.; TAX 327 Investigators. 2004. Docetaxel plus prednisone or mitoxantrone plus prednisone for advanced prostate cancer. *N. Engl. J. Med. 351(15)*: 1502–1512.

Torti, F.M., Aston, D., Lum, B.L., Kohler, M., Williams, R., Spaulding, J.T., Shortliffe, L., and Freiha, F.S. 1983a. Weekly doxorubicin in endocrine-refractory carcinoma of the prostate. *J. Clin. Oncol. 1*: 477–482.

Torti, F.M., Bristow, M.R., Howes, A.E., Aston, D., Stockdale, F.E., Carter, S.K., Kohler, M., Brown, B.W. Jr., and Billingham, M. E. 1983b. Reduced cardiotoxicity of doxorubicin delivered on a weekly schedule. Assessment by endomyocardial biopsy. *Ann. Intern. Med. 99*: 745–749.

Tralongo, P., Bollina, R., Aiello, R., Di Mari, A., Moruzzi, G., Beretta, G., Mauceri, G., and Conti, G. 2003. Vinorelbine and prednisone in older cancer patients with hormone-refractory metastatic prostate cancer. A Phase II study. *Tumori 89*: 26–30.

Von Hoff, D.D., Layard, M.W., Basa, P., Davis, H.L. Jr., Von Hoff, A.L., Rozencweig, M., and Muggia, F.M. 1979. Risk factors for doxorubicin-induced congestive heart failure. *Ann. Intern. Med. 91*: 710–717.

39
Locally Advanced Prostate Cancer Biochemical Recurrence after Radiotherapy: *Use of Cyclic Androgen Withdrawal Therapy*

Juanita Crook

INTRODUCTION

Following conventional radiotherapy for prostate cancer, 30–40% of men with favorable to intermediate risk disease will suffer recurrence and up to 75–80% of those with locally advanced disease or unfavorable risk factors (Pilepich *et al*., 2001; Bolla *et al*., 2002). Dose escalation and the combination of hormone therapy with radiotherapy have reduced recurrence rates substantially. However, in the prostate specific antigen (PSA) era, biochemical monitoring following treatment continues to detect failures in asymptomatic men with a lead time of many months to years. Because a biochemical failure may incur further treatment or intervention, it is important to have a PSA-based definition of failure that correlates with subsequent clinical failure.

Since its incorporation into clinical practice in the early 1990s, PSA has become the standard measure of disease recurrence after radical prostatectomy, external beam radiotherapy, and brachytherapy. Assessment after radical prostatectomy is relatively clear-cut, as the removal of all PSA-producing tissue should reduce the PSA to undetectable within a few weeks. However, radiotherapy functions through a slower process of tumor cell kill, producing a gradual decline in PSA to an eventual nadir in 2–5 years. The prolonged time to radiation-induced prostate cancer cell death, and the acceptance of variable amounts of normal PSA–producing epithelium as being compatible with cure, has lead to a long and difficult search for a PSA–based definition of cure following radiotherapy (Thames *et al*., 2003; Kuban *et al*., 2004). A declining or stable value has generally been accepted as a favorable sign.

In 1997 the American Society for Therapeutic Radiology and Oncology (ASTRO) consensus conference grappled with a definition of biochemical failure after radiotherapy and, recognizing the unsuitability of a single numeric threshold and the importance of stability of PSA values, chose the widely-accepted "three consecutive rising values spaced at least 3–6 months apart" with back-dating of failure to midway between the nadir and the first rise (Cox *et al*., 1997). Although this definition provided a solution for uniformity of reporting of clinical results of external

beam radiotherapy, it was often inappropriately applied to populations who had other forms of treatment, including brachytherapy, or hormonal therapy combined with radiation (Pickles, 2006). In addition, with experience, it became evident that backdating of failures severely biased Kaplan Meier estimates of disease free survival. Because of these problems, the situation was re-examined at the 2005 RTOG-ASTRO Phoenix consensus conference. These deliberations lead to the "Houston" or "Phoenix" definition, a compromise for sensitivity and specificity which defined biochemical failure as a PSA reading of more than 2 ng/ml over the nadir (Roach *et al*., 2006). Both the original ASTRO and the subsequent Phoenix definition were based on pooled date from men treated with external beam radiotherapy but the more recent "nadir+2" definition can be applied to men treated with a combination of hormones and external radiotherapy with fewer "false calls" of failure (Pickles, 2006).

It is not uncommon for PSA to rise temporarily following treatment, and then decline spontaneously. This can mimic a biochemical failure and lead to inappropriate intervention. These so-called PSA bounces are common after prostate brachytherapy and have no adverse clinical significance. However, after external radiotherapy, either alone or combined with neoadjuvant hormonal therapy, PSA fluctuations can also occur. In the scenario of neoadjuvant hormonal therapy (HT), the temporary rise in the PSA seen a few months after radiotherapy is attributed to the effect of testosterone recovery on residual PSA-producing tissue (Zietman *et al*., 2005; Pickles, 2006). Without the use of HT, the etiology of a PSA bounce after external radiotherapy is unclear. However, unlike the situation after brachytherapy, such "bounces" after external radiation have been reported to be an independent predictor of subsequent biochemical failure (Feigenberg *et al*., 2006; Horwitz *et al*., 2006). Rates of 20–25% have been reported, but it may be seen in over 50% of men treated with combined external beam and neoadjuvant HT.

Uniform criteria for reporting biochemical failure facilitate the reporting of results, the comparison of different treatment modalities or regimens, and the establishment of end-points for clinical trials. The criteria do not elucidate the site of failure (local vs. distant) nor do they address the timing, indications, or form of subsequent intervention. Many controversies remain concerning the optimal time to initiate hormonal therapy (early vs. late), ideal treatment schedules (cyclic vs. continuous), and the optimal agents or combinations of agents (anti-androgen, LHRHa, 5α-reductase inhibitor). This chapter addresses the use of cyclic or intermittent administration of androgen suppression (IAS) in men with established biochemical recurrence following radiotherapy.

LABORATORY BASIS FOR HUMAN STUDIES

Sandford *et al*. (1984) first reported the phenomenon of hormonally-regulated successive waves of apoptotic regression and subsequent regrowth in the rat prostate. Castration resulted in a 35-fold increase in apoptotic bodies within 3 days, with testosterone replacement enabling reconstitution of a histologically normal gland within 10 days.

Subsequent experiments with both the androgen-dependent Shionogi mouse mammary tumor and the human prostate cancer cell line LNCaP (Rennie *et al*.,

1990; Akakura *et al*., 1993) similarly demonstrated successive waves of apoptotic regression and regeneration following cyclic androgen withdrawal and replacement. The Shionogi tumor normally progresses to androgen independence after 50 days of continuous androgen deprivation, showing a 500-fold increase in androgen-independent stem cells. If, after castration of the host and a period of regression the tumor is transplanted into the testosterone-containing hormonal milieu of an intact host, it regrows with differentiated tumor cells that retain the potential for further hormonal response. Four cycles of castration and transplantation resulted in a 3-fold increase in the duration of the period of hormonal responsiveness. Sato *et al*., (1996) demonstrated similar results using the LNCaP cell line in a single host mouse achieving cyclical exposure to testosterone through removal and replacement of testosterone implants.

MECHANISMS OF PROGRESSION TO ANDROGEN INDEPENDENCE

Although normal prostate cells will not regrow in the absence of androgens, prostate cancer cells develop the androgen independent phenotype, often within the relatively short span of 2–3 years of continuous androgen deprivation. Although multiple mechanisms may be involved, even within the same patient, explanations involve at least two theories: clonal selection and molecular adaptation.

Clonal Selection

Of the 3 types of cells in the prostate epithelium, only the secretory epithelium has surface androgen receptors and undergoes apoptosis with androgen deprivation. Neither the basal cell layer nor the small population of neuro-endocrine cells contain androgen receptors, and are thus androgen-independent. Continuous complete androgen deprivation may allow the androgen-independent basal cell clones to predominate (Isaacs and Coffey, 1981).

Molecular Adaptation

Androgen independence may also result from molecular pathways involving the androgen receptor (Feldman and Feldman, 2001; Debes and Tindall, 2004) or cell survival pathways independent of the androgen receptor. Pathways involving the androgen receptor include both gene amplification that makes the receptor responsive to much smaller concentrations of androgen, as well as mutations of the receptor that make it responsive to other molecules such as anti-androgens originally designed as receptor blockers (the so-called "promiscuous activation"). In addition, the function or expression of receptor co-activators such as insulin-like growth factor and cytokines may be altered. These altered survival pathways may bypass the androgen receptor, by means such as deregulation of apoptotic genes such as Bcl-2 (Debes and Tindall, 2004)

RATIONALE FOR INTERMITTENT ADMINISTRATION OF ANDROGEN SUPPRESSION IN CLINICAL PRACTICE

The preclinical evidence on cyclical withdrawal and replacement of androgens in the management of androgen responsive

tumors such as the Shionogi mouse mammary tumor offered the intriguing possibility of prolongation of the duration of hormone responsiveness for men afflicted with incurable prostate cancer. If borne out clinically, this could potentially transform incurable recurrent prostate cancer from a fatal disease to a chronic condition. Although this optimism has not yet been realized in the currently available clinical data, the approach has been shown to be feasible; the details of appropriate patient selection and optimization of treatment schedules are still being determined.

Even if ultimately shown not to offer a survival advantage when compared to continuous hormonal regimens, IAS may significantly alter the toxicity profile of continuous androgen withdrawal. The androgen deprivation syndrome is protean, including not only sexual dysfunction and loss of libido, but also anemia (Strum *et al*., 1997), altered lipid profiles, weight gain, loss of muscle mass, decreased bone density (Maillefert *et al*., 1999; Daniell *et al*., 2000), cognitive dysfunction (Green *et al*., 2002) and mood alterations including depression. Periods of return to the normal male hormonal milieu have the potential to ameliorate or reverse many aspects of this syndrome and improve quality of life.

A final consideration is the tremendous burden of cost of these agents on health care. Prostate cancer is the most common cancer in men in Western civilization, and the second most common cause of cancer death. If even only one third of men initially diagnosed with prostate cancer eventually require hormonal therapy after failure of their primary treatment, the potential cost saving of an intermittent approach to androgen withdrawal is considerable.

PHASE II CLINICAL STUDIES

Many Phase II studies demonstrate the safety and efficacy of IAS (Table 39.1). We will concentrate on those of Bruchovsky *et al*. (2006) and Malone *et al*. (2007) which report a large experience with mature follow up.

TABLE 39.1. Selected phase II trials of intermittent androgen suppression.

Author year	Local/PSA	D1/D2	Prior RT	Total n	Time on	Time off Cycle 1	PSA to restart
Goldenberg *et al*. (1999)	56	31	21	87	6+ (to nadir)	15	10–20 ng/ml
Higano *et al*. (1996)	12	10	13	22	9–12	8	variable
Tunn (1996)	20		0	20	9	9	>3 ng/ml
Oliver *et al*. (1997)	13	7		20	3–18	9–42	variable
Theyer and Hamilton (1998)	15	37	0	52	9	7	4 local 20 mets
Horwich *et al*. (1998)		16		16	5–8	8	Any ↑
Strum *et al*. (2000)	43	9		52	16 (med)	15.5	5 ng/ml
Grossfeld *et al*. (2001)	61			61	8(med)	9	Variable
De La Taille *et al*. (2003)	136	10	74	146	14.8 (med)	10.1	>4 ng/ml
Bruchovsky *et al*. (2006)	103		103	103	9	15.5	>10 ng/ml
Malone *et al*. (2007)	35	60	73	95	8.5	10	>10 ng/ml

Local/PSA: local failure or PSA elevation only
D1/D2: stage D1 or D2
Prior RT: previous radiotherapy

The Canadian Prospective Trial

Bruchovsky *et al's*. (2006) Phase II Canadian Prospective Trial was conducted in 4 centers between 1995 and 2001. This was a prospective, open-label trial for men with a rising PSA in the absence of distant metastases at least 6 months following external beam radiotherapy for prostate cancer. Initial stage T1–T3 tumors were included with no limits on PSA or Gleason score. At trial, entry patients had a PSA > 6.0 ng/ml and normal testosterone (6.3–27 nmol/l), and could not have had prior HT other than neoadjuvant for a maximum of 3 months. Transrectal ultrasound-guided prostate biopsies, as well as staging abdominal/pelvic CT scan, bone scan and chest X-ray were required. The treatment protocol began with a lead-in with cyproterone acetate, 100 mg bid for 4 weeks, followed by leuprolide acetate 7.5 mg IM monthly for 8 doses. The cyproterone acetate was continued at the same dose for 2 weeks after the start of the leuprolide injections and then reduced to 50 mg po twice daily. Serum PSA and testosterone were monitored monthly. If the PSA was < 4.0 ng/ml at both 24 and 32 weeks, with a constant or decreasing slope, the patient was eligible for an off- treatment period. PSA and testosterone continued to be monitored every 4 weeks and therapy was resumed when the PSA was ≥ 10.0 ng/ml.

One hundred and nine men were registered to the trial; 4 withdrew prior to completing the first treatment interval and 2 others were ineligible for the first off treatment period, leaving 103 evaluable. Characteristics of the population are given in Table 39.2. The median number of cycles per patient was 2.3 (range: 1–5). In total 277 cycles were initiated and 218 completed. At the completion of the study 42 men were still on-study, undergoing active treatment. None was still in their first cycle, but were equally divided between the off-treatment periods of cycles 2, 3 and 4, with 5 men in cycle 5. The mean duration of the off-treatment interval for cycles 1 through 5 for men completing a cycle without progression (n) decreased progressively being 68 weeks for cycle 1 (n = 68), 51 weeks for cycle 2 (n = 55), 38 weeks for cycle 3 (n = 31), 28 weeks for cycle 4 (n = 14) and 26 weeks for cycle 5 (n = 2). However, a significant proportion of the men in cycles 2–5 were still in their off-treatment phase, having neither completed it nor progressed. Their exclusion from the calculation of the duration of the off-treatment intervals for each cycle clearly results in a decrease of the mean duration. Neither biopsy status nor Gleason score predicted for the duration of the off-treatment intervals. At the end of 6 years of follow-up, 38.5% of the men were still being actively treated as per protocol, 24% had had disease progression and had been withdrawn, 15.6% had died (2 of prostate cancer, 13 from other causes, and 2 of unknown cause).

Bruchovsky *et al*. (2007) performed a detailed analysis of PSA and testosterone kinetics through the treatment cycles of the Canadian Prospective Trial. Mean serum PSA at the beginning of cycle 1 was 18.5 ng/ml, 10.5 ng/ml in cycle 2, 11.5 ng/ml in cycle 3, and 11.9 ng/ml in cycle 4. The mean reduction in PSA through each of the treatment periods was 95.2%. A plateau in the PSA level was reached after 20–24 weeks of treatment in cycle 1 but only after 36–40 weeks in cycles 2–4. When patients were stratified according to PSA at the start of each cycle (4–10 ng/ml, 10.1–20 ng/ml or >20 ng/ml), the mean

reduction in each treatment cycle remained constant. This translates into a 3-fold difference in nadir values amongst the 3 strata of entry PSA levels. Cycle 1 PSA nadir is a significant predictor for progression free survival ($p < 0.001$) in multivariate analysis, while age, initial stage, Gleason score, interval since radiotherapy, and PSA and testosterone at trial entry were not. An additional important observation was that men who began the IAS trial with a PSA in the 4–10 ng/ml range had a 2.3 times longer off-treatment interval in cycle 1 than men with a PSA > 20 ng/ml. This observation is presumably due to the smaller tumor burden associated with a lower PSA and suggests that IAS should ideally be started before the PSA reaches 10 ng/ml.

The mean serum testosterone levels at the beginning of each cycle were 12.8 nmol/l in cycle 1, 9.2 nmol/l in cycle 2, 8.2 nmol/l in cycle 3, and 7.2 nmol/l in cycle 4. Testosterone was reduced by an average of 95.3% in each treatment cycle indicating a reproducible inhibitory effect on testicular function through repeated treatment cycles. However, the trend towards a reduced baseline level of testosterone at the start of each subsequent cycle suggests a declining ability of the testicle to recover with repeated treatment cycles.

The Ottawa Phase II Intermittent Androgen Suppression Experience

Malone *et al*. (2007) reported on a single institution phase II trial of IAS conducted between 1993 and 2000. This was a prospective, open-label trial for men with incurable prostate cancer, either a rising PSA following external beam radiotherapy in the presence or absence of distant metastases, or newly diagnosed patients with metastatic disease at presentation. Those with metastatic disease could have involvement of lymph nodes, lung or other soft tissue, or a maximum of 6 sites on bone scan. At trial entry patients had a PSA > 10.0 ng/ml, and normal testosterone (6.3–27 nmol/l), and could not have had prior HT other than neoadjuvant for a maximum of 3 months. Staging abdominal/pelvic CT scan, bone scan, and chest X-ray were required at baseline evaluation. The treatment protocol began with nilutamide, 100 mg tid for 2 weeks, followed by leuprolide acetate 7.5 mg IM monthly for 8 doses. The nilutamide was continued at the same dose for 2 weeks after the start of the leuprolide injections and then reduced to 150 mg po daily. Serum PSA and testosterone were monitored monthly. If the PSA was < 4.0 ng/ml after 8 months with no clinical or radiological evidence of progression, the patient was eligible for an off- treatment period. Prostate specific antigen (PSA) and testosterone continued to be monitored every 4 weeks and therapy was resumed when the PSA was ≥ 10.0 ng/ml. Those who failed to meet the criteria for an off-treatment period at the completion of any cycle were taken off study and continued on androgen blockade, either with a change in anti-androgen or a trial of anti-androgen withdrawal.

Ninety-five men were registered to the trial; 23% (n = 22) were ineligible for the first off-treatment period because of progression, leaving 73 men who moved on into cycle 2 and beyond. Characteristics of the population are given in Table 39.2. The median number of cycles per patient was 2.2 (range: 1–7). In total, 187 cycles were completed. At the completion of the study 10 men were still on-study, undergoing active treatment. None was still in their first cycle, but were dispersed through

TABLE 39.2. Comparison of characteristics of the study populations in the Canadian prospective trial and the Ottawa trial.

Characteristic	Bruchovsky *et al.* (2006)	range	Malone *et al.* (2007)	Range
Age (years)	73.3	45–89	66	49–80
Gleason 7–10	46.5%		35%	
Prior RT	100%		77%	
Distant/regional	0%		63%	
Local failure	84%		16%	
Entry PSA	21.2 ng/ml	5–229 ng/ml	27 ng/ml	16% > 50 ng/ml
Mo since RT	54		41	3–126
Mean number of cycles/pt	2.3	1–5	2.2	1–6

RT: radiotherapy
Mo: months
Pt: patient

cycles 2–7. The median time to withdrawal from the trial from the time of initiation of the first cycle was 37 months (1–110). Sixty-three per cent withdrew because of disease progression, 3% because of toxicity and 9.5% died without evidence of progression.

The median duration of off-treatment intervals for all cycles was 8.5 months (1.7–60). Similar to results from the Canadian Prospective Trial, the median duration of the off-treatment interval decreased progressively through sequential cycles, being almost 10 months in cycle 1, just over 8 months in cycles 2 and 3, 7 months in cycle 4, and 6 months in cycle 5. However, when each patient is used as his own control and the duration of each off-treatment interval is examined as a proportion of the length of the first off-treatment interval for that patient, the length of the off-treatment interval is seen to be well preserved through subsequent cycles for the individual. The Ottawa trial studied a much less homogenous population than the Canadian Prospective Trial. Although 77% had received prior external radiotherapy, many had failed with metastatic disease and 23% of the population had metastases at diagnosis. In multivariate analysis of predictors for shorter duration of off treatment intervals, only the presence of distant metastases was significant.

Similar to the Canadian Prospective Trial findings, the Ottawa trial reported that men successfully completing the first cycle of therapy achieved a lower PSA nadir (0.1 ng/ml) at an earlier time (3.9 months) compared to 0.3 ng/ml at 5.3 months for those progressing. Median nadir for successful completion of cycles 2–4 was higher and took longer to achieve, 0.2 ng/ml at 4.6–5.6 months. Furthermore, a higher baseline PSA predicted for progression within cycle one ($p = 0.006$).

Side Effects of Treatment

The Ottawa trial also reported on the long-term side effects of IAS. Testosterone recovery was reported during off treatment intervals in 61% of cycles, with a median time to normalization of 23 weeks (range: 4–61 weeks). Prior to study entry only 32% of men reported normal potency. For these individuals, sexual function recovered in 47% of cycles. Mild anemia was reported in 33%, 44%, and 66% of cycles 1,2, and 3. Of men developing anemia, only 20% had a hemoglobin < 120 gm/l and 7% <110 gm/l. Hemoglobin and testosterone recovery are related in that anemia was observed in 47% of off-treatment intervals when testosterone did not recover vs 14% when there was recovery of testosterone ($p = 0.001$). There was no significant change in body mass Index

(BMI) through the duration of the study. In only 13% of patients did weight gain during the study period result in an increase of BMI > 10%. The mean and median overall weight change form the first to last evaluation in the study (median follow-up 44 months; range 9–92) was −0.6 kg and −0.1 kg suggesting that the weight gain usually observed in association with continuous androgen deprivation is corrected during the off treatment intervals. Emerging evidence on the association of the metabolic syndrome and early cardiac death with use of androgen deprivation (Keating *et al*., 2006) suggests that this adverse effect is seen with as little as 3 months of androgen deprivation (D'Amico *et al*., 2007). As such, it appears unlikely that an intermittent approach will lesson the cardiac impact on predisposed men.

Bone Density

Malone *et al*. (2005) assessed bone mineral density (BMD) in 41 of their 95 patients at a mean of 43 months after protocol entry and found that 37% had osteoporosis in at least one of 4 sites tested, the most common site being the distal radius. Unfortunately baseline measurements were not part of the protocol.

Higano *et al*. (2004) studied BMD prospectively in 19 men commencing on an IAS regimen. Two were osteopenic at baseline. In the remainder, a 9-month period of androgen deprivation resulted in a mean decrease in BMD in the lumbar spine of 4.5% and in the hip of 2.5%. The subsequent 8-month off treatment interval, did not result in a return to baseline values, although improvement was seen, especially in the lumbar spine (1.5%).

PHASE III CLINICAL STUDIES

Sufficient Phase II data exist to demonstrate that IAS is clinically feasible in a variety of clinical scenarios. Both the efficacy and the most appropriate regimen may vary according to the scenario. The optimal entry PSA may be different for a patient who has failed after radical prostatectomy, or after external radiotherapy, or who is newly diagnosed with metastatic disease. The optimal duration of the on-treatment intervals may also vary according to the burden of disease. Phase III trials are exploring each of these different clinical situations.

The particular scenario of the rising PSA after external radiotherapy, has been explored in a large phase III inter-group trial lead by the National Cancer Institute of Canada (NCIC PR7) with participation by SWOG (Southwest Oncology Group JPR7), the Medical Research Council and the Cancer Trials Support Unit (CTSU). The trial opened in 1999 with a planned accrual of 1,340. Men with a rising PSA following external beam radiotherapy, in the absence of clinically evident metastatic disease, were randomized to either continuous or intermittent androgen ablation. The endpoints of the trial are overall survival, time to hormone resistance, and quality of life. The trial was initially sponsored by Hoescht Roussel (later Aventis and then Sanofi-Aventis) and used 8 month cycles of nilutamide (anti-androgen) and buserelin (2 month depot LHRHa), but was subsequently opened to the use of other anti-androgen-LHRHa combinations. Monotherapy with an LHRHa was also acceptable, with anti-androgen use limited to the initial blockage of flare, according to the

investigator's choice. Eligibility criteria included an entry PSA ≥ 3.0 ng/ml and higher than the post radiotherapy nadir, and a serum testosterone ≥ 6.0 nmol/l (age-adjusted normal). Prior hormone therapy in conjunction with radiotherapy was permissible as either neoadjuvant, concurrent or adjuvant, provided that the total duration was < 12 months and it was completed > 12 months prior to trial entry. Following an 8 month treatment cycle, individuals were eligible for an off-treatment period of variable length provided their PSA was under 4.0 and stable or decreasing. The next treatment cycle was commenced when the PSA reached 10 ng/ml.

Accrual took 7 years to complete but closed in 2005 with 1386 men randomized. The median age was 74 years. Radiotherapy was completed > 3 years previously in 78% and 1–3 years previously in 22%; only 21% had a palpable local failure. Prior hormone therapy (neoadjuvant, adjuvant or concurrent) had been used in 39%, and 11% had had a prior radical prostatectomy, salvage radiotherapy and then subsequent biochemical failure. Baseline PSA was 3–15 ng/ml in 77% and > 15 ng/ml in 23%. As of April 2008 there have been 288 deaths. Analysis is planned after 400 deaths. This trial will provide much needed answers concerning both the efficacy of IAS with respect to continuous androgen deprivation, as well as its effect on quality of life. In the intermittent arm valuable data on the duration of off-treatment periods, the time to testosterone recovery, and recovery of potency will be available. Furthermore, optimal patient selection factors such as Gleason score, entry PSA and interval since RT will be clarified.

IS THERE AN ACCEPTED STANDARD REGIMEN OF INTERMITTENT ANDROGEN SUPPRESSION?

Although most IAS protocols have employed treatment cycles of 8–9 months with variable length off-treatment intervals, this duration was chosen empirically based on the kinetics of the PSA decrease in response to androgen ablation (Gleave et al., 1996). Both the Canadian Prospective Trial (Bruchovsky *et al*., 2006) and the Ottawa trial (Malone *et al.,* 2007), observed that the PSA plateau in the first cycle of treatment was achieved after approximately 20 weeks of therapy, well before the 8 month cycle was finished. In subsequent treatment cycles, a longer period of androgen ablation was needed to achieve a PSA nadir, 36–40 weeks in the Canadian Prospective Trial and 4.5–5.5 months in the Ottawa trial. This would suggest that a variable length treatment interval based on the time to PSA nadir may be more appropriate than treatment cycles of a fixed duration.

Calais da Silva *et al*. (2003) and the South European Urology Group (SEUG) conducted a Phase III trial of IAS for primary management of locally advanced or metastatic prostate cancer, randomizing 626 men to either continuous androgen ablation or 3 month treatment cycles using depot leuprolide and cyproterone acetate. Despite the relatively short treatment interval used in this trial, off-treatment intervals of > 52 weeks were seen in 50% of men, and 29% had off-treatment intervals > 36 months. The Ottawa trial (Malone *et al.,* 2007), using 8 month treatment cycles

reported that 42% of men had at least one off treatment interval >52 weeks in length. This would suggest that longer treatment intervals of 8–9 months may not provide longer off-treatment periods. The optimal duration of the treatment interval in IAS needs to be explored in a randomized trial.

SUMMARY AND CONCLUSIONS

The IAS approach for men with locally advanced prostate cancer and a rising PSA after external radiotherapy is a treatment strategy for which there is considerable preclinical evidence and phase II clinical experience. To date, empirically developed treatment schedules, with close monitoring during off-treatment intervals, have allowed patients to go through multiple cycles of treatment with apparent safety. The median number of cycles per individual is 2–3 but hormone responsiveness may be retained through 5–8 cycles. The duration of the first off-treatment period can be used to predict the duration of subsequent off-treatment intervals for the individual and is well maintained through sequential cycles until development of hormone resistance. In any study population, men with shorter off treatment periods will move more rapidly through cycles, while those with long off treatment periods will linger in the early cycles. Median cycle duration can only be an accurate reflection of cycle dynamics if all patients have completed all cycles.

Intermittent androgen suppression has the potential to ameliorate the side effects of androgen ablation by reestablishment of the normal male hormonal milieu during the off treatment intervals. Testosterone recovery, however, is not universally seen, and despite the intervals off treatment, anemia and loss of BMD become more common in later cycles.

Lessons learned from phase II experience would suggest that men with a lower tumor burden, those with local recurrence after radiotherapy, and those with an entry PSA < 10 ng/ml are more likely to achieve a lower PSA nadir in the first cycle and enjoy a longer off treatment period. Gleason score, however, does not appear to predict the duration of the off treatment interval. Forthcoming results from the NCIC Inter-group (JPR 7) trial will help to clarify appropriate selection factors for an intermittent approach, such as interval since radiotherapy, Gleason score and entry PSA. Furthermore, the optimal duration of treatment cycles and the threshold for restarting treatment have not been determined, although it seems evident that treatment should continue until PSA nadir is achieved.

The combination of IAS with the use of bisphosphonates to lesson the impact of androgen deprivation on BMD has not been fully investigated. Similarly, the use of 5-alpha reductase inhibitors to decrease intra-prostatic dihydro-testosterone (DHT) and perhaps lengthen the duration of off-treatment intervals remains experimental. The ultimate effect of IAS on overall survival and on quality of life as measured by validated instruments remains to be determined. Until results from Phase III trials provide answers to these questions, IAS remains an investigational approach. For men with intolerable side effects from androgen ablation, or those with a strong desire to preserve potency, an intermittent approach could be considered, adhering to the treatment schedule and monitoring

of an established protocol such as JPR-7, provided the patient is aware of the investigational nature of this approach.

REFERENCES

Akakura, K., Bruchovsky, N., Goldenberg, S. L., Rennie, P. S., Buckley, A. R., and Sullivan, L. D. 1993. Effects of intermittent androgen suppression on androgen-dependent tumors. Apoptosis and serum prostate-specific antigen. *Cancer 71*: 2782–2790.

Bolla, M., Collette, L., Blank, L., Warde, P., Dubois, J. B., Mirimanoff, R. O., Storme, G., Bernier, J., Kuten, A., Sternberg, C., J. Mattelaer, Lopez Torecilla, J., Pfeffer, J. R., Lino Cutajar, C., Zurlo, A., and Pierart, M. 2002. Long-term results with immediate androgen suppression and external irradiation in patients with locally advanced prostate cancer (an EORTC study): a phase III randomised trial. *Lancet 360*: 103–106.

Bruchovsky, N., Klotz, L., Crook, J., Malone, S., Ludgate, C., Morris, W. J., Gleave, M. E., and Goldenberg, S. L. 2006. Final results of the Canadian prospective phase II trial of intermittent androgen suppression for men in biochemical recurrence after radiotherapy for locally advanced prostate cancer: clinical parameters. *Cancer 107*: 389–395.

Bruchovsky, N., Klotz, L., Crook, J., and Goldenberg, S. L. 2007. Locally advanced prostate cancer–biochemical results from a prospective phase II study of intermittent androgen suppression for men with evidence of prostate-specific antigen recurrence after radiotherapy. *Cancer 109*: 858–867.

Calais da Silva, F., Bono, A., Whelan, P., Brausi, M., Queimadelos, M., Portillo, J., Kirkali, Z., and Robertson, C. 2003. Intermittent androgen deprivation for locally advanced prostate cancer. Preliminary experience from an ongoing randomized controlled study of the South European urooncological group. *Oncology 65*: 24.

Cox, J. D., Grignon, D. J., Kaplan, R. S., Parsons, J. T., and Schellhammer, P. F. 1997. Consensus statement: guidelines for PSA following radiation therapy. *Int. J. Radiat. Oncol. Biol. Phys. 37*: 1035–1041.

D'Amico, A. V., Denham, J. W., Crook, J., Chen, M. H., Goldhaber, S. Z., Lamb, D. S., Joseph, D., Tai, K. H., Malone, S., Ludgate, C., Steigler, A., and Kantoff, P. W. 2007. Influence of androgen suppression therapy for prostate cancer on the frequency and timing of fatal myocardial infarctions. *J. Clin. Oncol. 25*: 2420–2425.

Daniell, H. W., Dunn, S. R., Ferguson, D. W., Lomas, G., Niazi, Z., and Stratte, P. T. 2000. Progressive osteoporosis during androgen deprivation therapy for prostate cancer. *J. Urol. 163*: 181–186.

De La Taille, A., Zerbib, M., Conquy, S., Amsellem-Ouazana, D., Thiounn, N., Flam, T. A., and Debre, B. 2003. Intermittent androgen suppression in patients with prostate cancer. *Int. Br. J. Urol. 91*: 18–22.

Debes, J. D. and Tindall, D. J. 2004. Mechanisms of androgen-refractory prostate cancer. *N. Engl. J. Med. 351*: 1488–1490.

Feigenberg, S. J., Hanlon, A. L., Horwitz, E. M., Uzzo, R. G., Eisenberg, D., and Pollack, A. 2006. A prostate specific antigen (PSA) bounce greater than 1.4 ng/mL Is clinically significant after external beam radiotherapy for prostate cancer. *Am. J. Clin. Oncol. 29*: 458–462.

Feldman, B. J. and Feldman, D. 2001. The development of androgen-independent prostate cancer. *Nat. Rev. Cancer 1*: 34–45.

Gleave, M. E., Goldenberg, S. L., Jones, E. C., Bruchovsky, N., and Sullivan, L. D. 1996. Biochemical and pathological effects of 8 months of neoadjuvant androgen withdrawal therapy before radical prostatectomy in patients with clinically confined prostate cancer. *J. Urol. 155*: 213–219.

Goldenberg, S. L., Gleave, M. E., Taylor, D., and Bruchovsky, N. 1999. Clinical experience with intermittent androgen suppression in prostate cancer: minimum of 3 years' follow-up. *Mol. Urol. 3*: 287–292.

Green, H. J., Pakenham, K. I., Headley, B. C., Yaxley, J., Nicol, D. L., Mactaggart, P. N., Swanson, C., Watson, R. B., and Gardiner, R. A. 2002. Altered cognitive function in men treated for prostate cancer with luteinizing hormone-releasing hormone analogues and cyproterone acetate: a randomized controlled trial. *BJU Int. 90*: 427–432.

Grossfeld, G. D., Chaudhary, U. B., Reese, D. M., Carroll, P. R., and Small, E. J. 2001. Intermittent

androgen deprivation: update of cycling characteristics in patients without clinically apparent metastatic prostate cancer. *Urology 58*: 240–245.

Higano, C. S., Ellis, W., Russell, K., and Lange, P. H. 1996. Intermittent androgen suppression with leuprolide and flutamide for prostate cancer: a pilot study. *Urology 48*: 800–804.

Higano, C.S., Shields, A., Wood, N., Brown, J., and Tangen, C. 2004. Bone mineral density in patients with prostate cancer without bone metastases treated with intermittent androgen suppression. *Urology 64*: 1182–1186.

Horwich, A., Huddart, R. A., Gadd, J., Boyd, P. J., Hetherington, J. W., Whelan, P., and Dearnaley, D. P. 1998. A pilot study of intermittent androgen deprivation in advanced prostate cancer. *Br. J. Urol. 81*: 96–99.

Horwitz, E. M., Levy, L. B., Thames, H. D., Kupelian, P. A., Martinez, A. A., Michalski, J. M., Pisansky, T. M., Sandler, H. M., Shipley, W. U., Zelefsky, M. J., Zietman, A. L., and Kuban, D. A. 2006. Biochemical and clinical significance of the posttreatment prostate-specific antigen bounce for prostate cancer patients treated with external beam radiation therapy alone: a multiinstitutional pooled analysis. *Cancer 107*: 1496–1502.

Isaacs, J. T. and Coffey, D. S. 1981. Adaptation versus selection as the mechanism responsible for the relapse of prostatic cancer to androgen ablation therapy as studied in the Dunning R-3327-H adenocarcinoma. *Cancer Res. 41*: 5070–5075.

Keating, N. L., O'Malley, A. J., and Smith, M. R. 2006. Diabetes and cardiovascular disease during androgen deprivation therapy for prostate cancer. *J. Clin. Oncol. 24*: 4448–4456.

Kuban, D. A., Thames, H. D., and Levy, L. B. 2004. PSA after radiation for prostate cancer. *Oncology 18*: 595–609.

Maillefert, J. F., Sibilia, J., Michel F., Saussine, C., Javier, R. M., and Tavernier, C. 1999. Bone mineral density in men treated with synthetic gonadotropin-releasing hormone agonists for prostatic carcinoma. *J. Urol. 161*: 1219–1222.

Malone, S., Perry G., Segal R., Dahrouge S., and Crook J. 2005. Long-term side-effects of intermittent androgen suppression therapy in prostate cancer: results of a phase II study. *Int. Br. J. Urol. 96*: 514–520.

Malone, S., G. Perry, L. Eapen, Segal, R., Gallant, V., Dahrouge, S., Crook, J., and Spaans, J. N. 2007. Mature results of the Ottawa phase II study of intermittent androgen-suppression therapy in prostate cancer: clinical predictors of outcome. *Int. J. Radiat. Oncol. Biol. Phys. 68*: 699–706.

Oliver, R. T., Williams, G., Paris, A. M., and Blandy, J. P. 1997. Intermittent androgen deprivation after PSA-complete response as a strategy to reduce induction of hormone-resistant prostate cancer. *Urology 49*: 79–82.

Pickles, T. 2006. Prostate-specific antigen (PSA) bounce and other fluctuations: which biochemical relapse definition is least prone to PSA false calls? An analysis of 2030 men treated for prostate cancer with external beam or brachytherapy with or without adjuvant androgen deprivation therapy. *Int. J. Radiat. Oncol. Biol. Phys. 64*: 1355–1359.

Pilepich, M. V., Winter, K., John, M. J., Mesic, J. B., Sause, W., Rubin, P., Lawton, C., Machtay, M., and Grignon, D. 2001. Phase III radiation therapy oncology group (RTOG) trial 86–10 of androgen deprivation adjuvant to definitive radiotherapy in locally advanced carcinoma of the prostate. *Int. J. Radiat. Oncol. Biol. Phys. 50*: 1243–1252.

Rennie, P. S., Bruchovsky, N., and Coldman, A. J. 1990. Loss of androgen dependence is associated with an increase in tumorigenic stem cells and resistance to cell-death genes. *J. Steroid Biochem. Mol. Biol. 37*: 843–847.

Roach, M., 3rd, Hanks, G., Thames, H., Jr., Schellhammer, P., Shipley, W. U., Sokol, G. H., and Sandler, H. 2006. Defining biochemical failure following radiotherapy with or without hormonal therapy in men with clinically localized prostate cancer: recommendations of the RTOG-ASTRO Phoenix Consensus Conference. *Int. J. Radiat. Oncol. Biol. Phys. 65*: 965–974.

Sandford, N. L., Searle, J. W., and Kerr, J. F. 1984. Successive waves of apoptosis in the rat prostate after repeated withdrawal of testosterone stimulation. *Pathology 16*: 406–410.

Sato, N., Gleave, M. E., Bruchovsky, N., Rennie, P. S., Goldenberg, S. L., Lange, P. H., and Sullivan, L. D. 1996. Intermittent androgen suppression delays progression to androgen-independent regulation of prostate-specific antigen gene in the LNCaP prostate tumour model. *J. Steroid Biochem. Mol. Biol. 58*: 139–146.

Strum, S. B., McDermed, J. E., Scholz, M. C., Johnson, H., and Tisman, G. 1997. Anaemia associated with androgen deprivation in patients with prostate cancer receiving combined hormone blockade. *Br. J. Urol. 79*: 933–941.

Strum, S. B., Scholz, M. C., and McDermed, J. E. 2000. Intermittent androgen deprivation in prostate cancer patients: factors predictive of prolonged time off therapy. *Oncologist 5*: 45–52.

Thames, H., Kuban, D., Levy, L., Horwitz, E. M., Kupelian, P., Martinez, A., Michalski, J., Pisansky, T., Sandler, H., Shipley, W., Zelefsky, M., and Zietman, A. 2003. Comparison of alternative biochemical failure definitions based on clinical outcome in 4839 prostate cancer patients treated by external beam radiotherapy between 1986 and 1995. *Int. J. Radiat. Oncol. Biol. Phys. 57*: 929–943.

Theyer, G. and Hamilton, G. 1998. Current status of intermittent androgen suppression in the treatment of prostate cancer. *Urology 52*: 353–359.

Tunn, U. W. 1996. Intermittent endocrine therapy of prostate cancer. *Eur. Urol. 30*: 22–25; discussion 38–39.

Zietman, A. L., Christodouleas, J. P., and Shipley, W. U. 2005. PSA bounces after neoadjuvant androgen deprivation and external beam radiation: impact on definitions of failure. *Int. J. Radiat. Oncol. Biol. Phys. 62*: 714–718.

Index